PIERS 2009 Moscow

Progress In Electromagnetics Research Symposium

Abstracts

August 18–21, 2009

Moscow, RUSSIA

www.emacademy.org
www.piers.org

PIERS 2009 Moscow Abstracts

Published by

The Electromagnetics Academy
777 Concord Avenue, Suite 207
Cambridge, MA 02138

www.emacademy.org
www.piers.org

ISSN: 1559-9450
ISBN: 978-1-934142-09-7

Progress in Electromagnetics Research Symposium
August 18–21, 2009
Moscow, RUSSIA

PIERS 2009 MOSCOW ORGANIZATION

PIERS Founding Chair

J. A. Kong, MIT, USA

PIERS Chair

L. Tsang, University of Washington, USA

PIERS 2009 Moscow General Chair

A. B. Samokhin,
Moscow Technical University of Radio Engineering, Electronics and Automatics, Moscow, RUSSIA

PIERS 2009 Moscow General Vice Chair

Y. V. Shestopalov, Karlstad University, Karlstad, SWEDEN

K. Kobayashi, Chuo University, Tokyo, JAPAN

PIERS 2009 Moscow International Advisory Committee

V. S. Buldyrev	A. Büyükaksoy	W. C. Chew	A. S. Dmitriev
N. Engheta	V. Freilikher	Y. V. Gandel	Y. V. Gulyaev
T. Habashy	M. Idemen	A. S. Ilinski	A. Ishimaru
A. A. Kirilenko	G. Kristensson	A. N. Lagarkov	K. J. Langenberg
L.-W. Li	K.-M. Luk	D. S. Lukin	Y. Miyazaki
Z. T. Nazarchuk	S. A. Nikitov	P. Pampaloni	A. Priou
J. W. Ra	M. Raugi	H. W. Schürmann	L. Shafai
A. S. Sigov	A. Sihvola	P. D. Smith	M. Tateiba
A. V. Tikhonravov	P. Y. Ufimtsev	P. M. van den Berg	J. Vrba
K. Yasumoto	V. A. Zernov	W. X. Zhang	

PIERS 2009 Moscow Technical Program Committee

A. Altintas	S. Barmada	W. M. Boerner	D. Censor
V. V. Chebyshev	H. Chen	K.-S. Chen	F. Gunes
S. Helhel	Q. Jiang	A. Komiyama	V. F. Kravchenko
A. S. Kryukovsky	V. Eu. Kunitsyn	M. Kuroda	M. A. Lyalinov
F. Molinet	V. I. Naidenko	A. Osipov	A. V. Popov
S. L. Prosvirnin	L. X. Ran	A. K. Sarychev	A. H. Serbest
V. Serov	X.-Q. Sheng	Y. G. Smirnov	R. Talhi
K. Tanaka	M. Tanaka	O. A. Tretyakov	S. Tretyakov
B.-I. Wu	G. Xie	V. V. Yakovlev	T. Yamasaki
A. Yarovoy	N. P. Yashina	N. Y. Zhu	

PIERS 2009 Moscow Organization Committee

V. V. Cherdincev	I. E. Fedotov	A. S. Ivanov	Q. Jiang
K. Kobayashi (Vice Chair)	S. P. Koulikov	D. B. Kuryliak	B. A. Lagovsky
O. V. Mikheev	D. V. Rastyagaev	A. B. Samokhin (Chair)	A. S. Samokhina
Y. V. Shestopalov (Vice Chair)	V. N. Spivac	A. A. Voroncov	B.-I. Wu

PIERS 2009 MOSCOW SESSION ORGANIZERS

I. Abdulhalim
M. E. Belkin
D. J. Bergman
K. Y. Bliokh
L. Capineri
J. Colinas
C. de Mello Gallep
A. S. Dmitriev
A. Eroglu
N. S. Erokhin
P. Febvre
Y. K. Fetisov
A. H. J. Fleming
L. Gammaitoni
E. Gescheidtová
M. Gorkunov
A. D. Grigoryev
Z.-H. Gu
M. Hasler
D. Huang
A. S. Ilinskiy
S. Kar
K. Kobayashi
V. F. Kravchenko
A. S. Kryukovsky
V. E. Kunitsyn
J. Li
J. G. Lin
D. V. Louzguine-Luzgin
D. S. Lukin
G. S. Makeeva
G. Manara
V. A. Markel
R. C. McPhedran
M. I. Mishchenko
E. Mishina
F. Molinet
S. Nakamura
Y. Okuno
M. Oristaglio
A. I. Panas
L. V. Panina
M. Pardavi-Horvath
V. A. Permyakov
M. Piat
A. B. Samokhin
Y. V. Shestopalov
Y. G. Smirnov
G. Srinivasan
S. O. Starkov
Y. Strelniker
R. Talhi
L. Tang
E. E. Tyrtyshnikov
J. Vrba
S. Wabnitz
C. G. Windsor
C.-J. Wu
G. Xie
V. V. Yakovlev
T. Yamasaki
P. Yang
T.-J. Yang
H. O. Zhang
A. P. Zhukov

PIERS 2009 MOSCOW EXHIBITOR

- CST (www.cst.com)

PIERS 2009 MOSCOW SPONSORSHIP

- Moscow State Institute of Radio Engineering, Electronics and Automation
- Russian New University
- NVK “VIST”
- Russian Foundation for Basic Research
- Russian Academy of Science
- Scientific Research Institute of Automatic Equipment n.a. acad.V.S.Semenihina
- VIMPEL Interstate Corporation
- Zhejiang University
- The Electromagnetics Academy at Zhejiang University
- MIT Center for Electromagnetic Theory and Applications/Research Laboratory of Electronics
- The Electromagnetics Academy

PIERS 2009 SESSIONS

Session 2P1
Remote Sensing, RADAR Imaging & Detection

Experimental Study of Shadow Region Imaging Algorithm with Multiple Scattered Waves for UWB Radars

Shouhei Kidera[1], **Takuya Sakamoto**[2], **and Toru Sato**[2]

[1]Department of Electronic Engineering, University of Electro-Communications, Japan
[2]Graduate School of Informatics, Kyoto University, Japan

Abstract— Ultra-wide band (UWB) radar holds high range resolution in the near field sensing, and is thus applicable to security systems designed to identify a human body even in invisible situations. Although Synthetic Aperture Radar (SAR) creates a stable and accurate target image for such applications, it often suffers from increased shadow regions in the case of complex or multiple targets. On the contrarily, a multiple scattered wave has the potential to make a shadow region visible because it propagates a path, that differs from that of a single scattered wave. While various time reversal algorithms with multiple scattered waves have been developed, these require a priori information of the surroundings or a target model [1, 2]. This paper proposes a shadow region imaging algorithm based on the aperture synthesis of multiple scattered waves, that can directly increases the visible area and is applicable to arbitrary target shapes. This algorithm reconstructs a target image by synthesizing a double scattered wave according to its propagation path. Further details of the experimental investigation of this method are given bellow. Fig. 1 shows the experimental setup with both cylindrical and rectangular targets. The UWB pulse with a 10 dB-bandwidth of 2.0 GHz and a center wavelength λ of 93.75 mm is used. The pair of the transmitting and receiving antennas is scanned on the $z = 0.0\lambda$ plane. The left and right hand sides of Fig. 2 show the estimated images viewed at $y = 0.0\lambda$ using the SAR and the proposed method, respectively. The S/N of the double scattered wave is around 25 dB. The image obtained using the SAR depicts only the bottom part of the target boundaries, whereas the proposed method reconstructs the sides of the rectangular target as well, since many of the double scattered waves are focused on this region. This result verifies that the proposed method effectively enlarges the visible area on target surfaces even in a real environment.

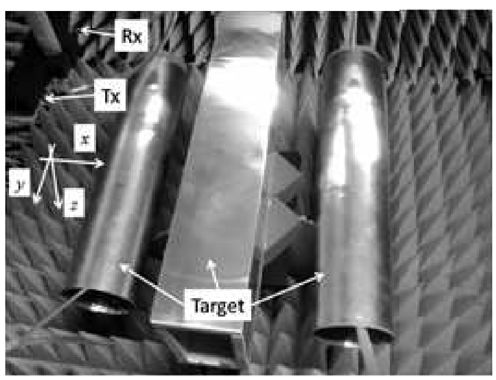

Figure 1: Arrangement of the cylindrical and rectangular targets in the experiment.

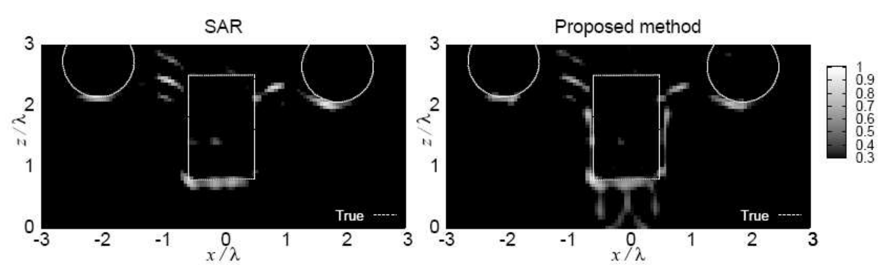

Figure 2: Estimated images at $y = 0.0\lambda$ with the SAR (left) and the proposed method (right) in the experiment.

REFERENCES

1. Lehmanm, S. K. and A. J. Devaney, *Acoust. Soc. Am.*, Vol. 113, No. 5, May 2003.
2. Moura, J. M. F. and Y. Jin, *IEEE Trans. on Signal Process.*, Vol. 55, No. 1, 187–201, Jan. 2007.

Frequency and Polarization Dependence of Scattering in Bi-continuous Random Media Model with Application to Snow

Xiaolan Xu and Leung Tsang
Department of Electrical Engineering, University of Washington
Box 352500, Seattle, WA 98195-2500, USA

Abstract— The multi-frequency measurements are widely used in the microwave remote sensing applications. The Snow and Cold Land Process (SCLP) satellite mission has been recommended by the Decadal Study in the US and the Cold Regions Hydrology Highresolution Observatory (CoReH2O) was proposed to the European Space Agency. Both satellite missions SCLP and CoReH2O include a dual-frequency synthetic aperture radar. Careful studies of frequency dependence of the scattering coefficient are important to understand the radar response at different frequencies. It is also useful for developing the retrieval algorithm of the key properties of snowpacks.

In the past, the dense media model is based on discrete scatterers and using the quasicrystalline approximation and numerical solutions of Foldy-Lax equations. Recently, we proposed a new method to solve the scattering problem of media with discrete permittivities. Instead of using particles, the mathematical formalism of bi-continuous medium is applied in this study to simulate the morphologies of random porous structures such as snow. The model is based on a continuous representation of interfaces between inhomogeneities within the medium. The random structure is then defined by setting a level on this Gaussian random process according to the required volume fractions of inhomogeneities.

Maxwell equations have been applied to the defined structure and solved numerically. The numerical method is based on the volume integral equation. The discrete dipole approximation (DDA) is used and the result matrix equation is solved by CGS-FFT (Conjugate Gradient Squared method accelerated by the Fast Fourier Transform technique). The extinction, scattering and absorption coefficient has been calculated for different frequencies. The numerical solutions indicate that the frequency dependence is related to the setup level of the bi-continuous random media. When the volume fraction of snow increases, the frequency dependence of scattering coefficient can be much weaker than the independent scattering. Numerical results are illustrated and compared with previous dense media models model, QCA (Quasi-crystalline Approximation model) and NMM3D (Numerical Maxwell Model of three-dimensional sphere simulations). We also studied the polarization dependences of scattering. The results are demonstrated.

Monitoring Surface Deformations over Siberian Gas Deposit Areas Using ALOS PALSAR Interferometry

Makoto Maruya[1], **Seiji Yoshimoto**[1], **Masanori Miyawaki**[2], **Shino Yamaguchi**[2], **Evgeniy Kiselevskiy**[3], **Peter Korviakov**[4], **Dmitry Sergeev**[4], **Yuriy Baranov**[5], **Goro Ando**[6], **and Masaki Kawai**[6]

[1]NEC Corporation, Japan
[2]NEC Aerospace Systems, Japan
[3]Gazprom, Russia
[4]Gazprom Space Systems, Russia
[5]Gazprom VNIIGAZ, Russia
[6]ERSDAC, Japan

Abstract— Japan and Russia cooperated in performing a study to monitor ground surface deformations over gas deposit areas in Siberia using the phased array type L-band synthetic aperture radar (PALSAR) of the Advanced Land Observation Satellite (ALOS). The studied areas had permafrost and surface subsidence due to gas extraction, both of which would affect gas facilities and infrastructure.

The observation sites were located in a tundra that had widespread permafrost, bogs, and a thin layer of mosses and lichens. Therefore, phased array type L-band synthetic aperture radar was used instead of C-band or X-band radar to minimize the effects of vegetation, snow, and the atmosphere on interferometry analysis.

Differential interferometry (DInSAR) analysis was conducted independently by both NEC and GASPROM Space Systems using PALSAR data observed by ERSDAC on June 9, 2006 (data A), July 25, 2006 (data B), and September 14, 2008 (data C). The DInSAR analysis clearly showed widespread ground subsidence with block structures over the past two years. Also, small hills and dips apparently formed by permafrost were detected by high resolution (25 m) interferometry analysis.

This study demonstrates that L-band SAR observation using a satellite provides a wide area instrumental technique for gathering information to support field and pipeline operation and for observing the resulting impact on the environment. The results also show the technical and economic efficiency of surveying and performing geodesic monitoring of gas field areas using ALOS PALSAR.

Over the Horizon Sky-wave Radar: Coordinate Registration by Sea-land Transitions Identification

F. Cuccoli[1], **L. Facheris**[2], **D. Giuli**[2], **and F. Sermi**[1]

[1]U.O. CNIT, c/o Dipartimento di Elettronica e Telecomunicazioni, Università di Firenze
Via di Santa Marta, 3, 50139 Firenze, Italy
[2]Dipartimento di Elettronica e Telecomunicazioni, Università di Firenze
via di Santa Marta, 3, 50139 Firenze, Italy

Abstract— Non-homogeneous structure and time-dependent behavior of the Ionosphere led to a substantial uncertainty in the standard Coordinate Registration (CR) procedure for Over The Horizon Sky-Wave Radar (OTHR sw) systems. Such uncertainty propagates to every radar measurements and the estimated position of an eventually detected target can results heavily inaccurate.

Although OTHR transmission channel is extremely hard to model and requires continuous ionospheric soundings, the surveillance area geo-morphological structure can be easily employed as geographic reference. In this paper we propose an approach to OTHR real time CR task based on the a-priori knowledge of the sea-land transitions location within the radar coverage area.

We basically mark the above-mentioned sea-land transitions in order to build a static reference binary clutter mask. An estimate of the actual ionospheric equivalent reflection height (h_{eq}) and consequently of the radar footprint position, is achieved by cross-correlating the received radar pulse echoes and the clutter mask, for different values of h_{eq}, and evaluating the cross-correlation maxima.

The proposed method consists then in a backwards procedure that allows an OTHR sw pulse to geographically place the received echo footprint within the surveillance area, independently from any external information. Only required inputs are in fact the radar pulse echo and the reference mask.

Significant differences between backscattering coefficient values of sea and land ($\Delta\sigma_0$) in HF band should guarantee discrimination of the two different area contributes in the received OTHR echo.

In order to prove the reliability of the method and determine under which hypothesis (minimum value of $\Delta\sigma_0$) it is achieved, we designed a simplified model of the OTHR scenario where noise and clutter distribution are modeled on the base of two independent statistical processes (Gaussian for the noise and Rayleigh for the clutter models).

Simulations have been performed under different geographic scenarios and their results have been discussed in order to provide a performance analysis of the proposed method. Preliminary indications on the minimum values of $\Delta\sigma_0$ and of the clutter to noise ratio are summarized referring to the error estimate of heq and consequently of the radar footprint location.

Complex Permittivity Measurement of Ores and Rocks by Two Coaxial Methods

Sixin Liu, **Junjun Wu**, **and Hang Dong**
College of Geo-exploration Science & Technology, Jilin University, Changchun 130026, China

Abstract— The complex permittivity measurement and analysis is a very important aspect for high-frequency Electromagnetic geophysical prospecting, such as Ground Penetrating Radar, Borehole Radar, and EM Logging. The enough large difference between target ores and the surrounding rocks in Electromagnetic parameters is the pre-condition for Surface and Borehole Radar reflection imaging.

Two coaxial methods for permittivity measurement are used to measure the complex permittivity of many ore and rock samples from a metal mine. The first one is the open-ended coaxial probe technique. The probe is touched to a rock sample sheet which is backed by a perfect conducting background during the measuring. The probe is connected to a Network Analyzer E5071B which measures only the S_{11} parameter in this situation. The complex permittivity is inverted by comparing the forwarded reflection coefficient and the measured one. The second method is the transmission/reflection coaxial one, which consists of a coaxial sample holder. The impedance of the sample determined the values of S_{11} and S_{21} parameters. The NRW algorithm is used to calculate the complex permittivity from S parameters.

We compare these two methods and find that they can give similar measured results in many situations. Considering the sample fabrication, the sheet-shaped samples for the first method are easy to be fabricated; however, the hollow circular cylinder sample making for the second method is difficult because the rock is often friable. On the other hand, the open-ended coaxial probe senses very small local volume while the transmission/reflection coaxial one measures the whole volume of a rock sample. As the sample is homogeneous, two methods show similar results. As the rock sample becomes inhomogeneous, the first method shows various values as we move the position of the probe on the sample. We analyze the measured data and find they are optimistic for mineral exploration.

A Radar's Electronic Protection from ARM Attack Using an Active Decoy

Joong-Soo Lim
Baekseok University, Korea

Abstract— To defense radar from Anti-Radiation Missile (ARM) attack, a lot of methods are used. It is a very effective method to use an active decoy which is used to simulate radar signals. But new ARM has a capability that selects the radar signal from decoy signals. Therefore, decoy signal should be made finely and transmitted on amplitude.

When we use an active decoy to defense an ARM, the Position of decoy from radar is important and the amplitude of decoy signal is also important comparing with radar's. In this paper, we simulate the power density of radar signal and decoy signal at ARM RF front-end according to radar frequencies and distances. Radar signal is radiated with direction with antenna beam pattern, but decoy signal is radiated with omni-direction.

In particular, the sum of radar's main-lobe signal and decoy signal is calculated, and the sum of radar's side-lobe signal and decoy signal also. These results can be used to decide the decoy distance. Fig. 1 display the effect of decoy signals when ARM track the radar's main-lobe, and Fig. 2 display the effect of decoy signals when ARM track the radar's side-lobe.

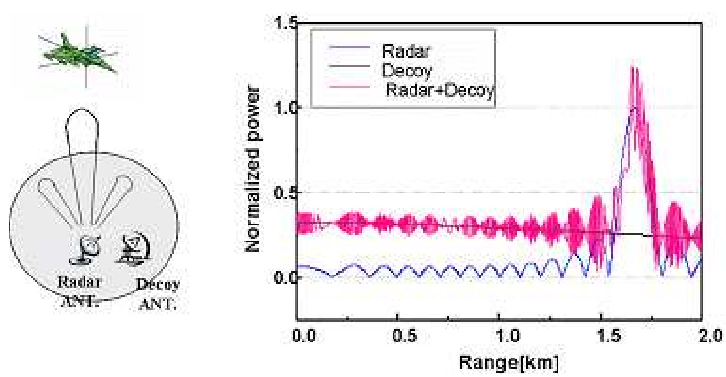

Figure 1: Decoy signal and radar's main-lobe signal at RF front end of ARM. For the simulation radar frequency = 1.0 GHz, decoy distance from radar = 110 m, phase difference between radar signal and decoy signal = 90 degree.

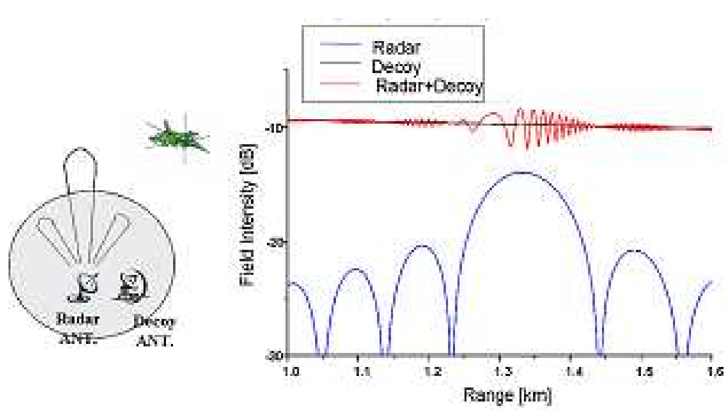

Figure 2: Decoy signal and radar's side-lobe signal at RF front end of ARM. For the simulation radar frequency = 1.0 GHz, decoy distance from radar = 110 m, phase difference between radar signal and decoy signal = 90 degree.

Radar Target Imaging from Ramp Responses Using Low Frequency Extrapolation

J. Chauveau, N. de Beaucoudrey, and J. Saillard

IREENA, Fédération CNRS Atlanstic, Université de Nantes
La Chantrerie, Rue C. Pauc, BP 50609, 44306 Nantes Cedex 3, France

Abstract— Low frequency imaging in radar domain is useful to characterize stealthy or buried targets. Indeed, the use of lower frequency bands permits to counter the stealthiness obtained with composite materials absorbing electromagnetic waves in usual radar frequency bands. In the same way, Ground Penetrating Radar (GPR) systems operate in low frequency bands for the characterization of buried targets, since the wave attenuation in most soil increases with the frequency. These low frequency bands correspond to the Rayleigh region and the resonance region for object dimensions respectively small and of the same order compared to electromagnetic wavelengths. Unlike high frequency imaging, low frequency methods cannot bring high resolution, i.e., details on the target, but they provide information on the overall dimension and the approximate shape of the target.

Three dimensional (3D) microwave imaging by high frequency inverse scattering methods (diffraction tomography) requires a considerable number of look angles for image reconstruction. On the contrary, the low frequency method, proposed by Young [1] and known as "the ramp response technique", needs no more than three viewing angles to generate an image. The ramp response, $h_r(t)$, first suggested by Kennaugh and Moffatt [2] for radar identification, is the far zone backscattered time domain response resulting from the illumination of the target by a plane electromagnetic wave with a time domain ramp waveshape. $h_r(t)$ is directly related to the "profile function" of the target, which is the transverse cross-sectional area of the target as a function of the distance along the line-of-sight [2]. The 3D reconstruction of the target shape is then performed with three such profile functions, using approximate limiting surfaces [1]. This ramp response imaging technique is applied to electromagnetic scattering [3] as well as to acoustic imaging of underwater objects [4].

To obtain a valid estimate of profile functions of a radar target, it is necessary to be in the upper Rayleigh region and the resonance region of the target, i.e., with electromagnetic wavelengths included between $D/2$ and $200D$, where D is the characteristic dimension of the target in the incident direction. The corresponding frequency band is $f = [1.5\,\mathrm{MHz}/D; 60\,\mathrm{MHz}/D]$ with D in meter. For example, for $D = 1.5\,\mathrm{m}$, $f = [1\,\mathrm{MHz}; 400\,\mathrm{MHz}]$.

However, such low frequency bands are not always available in experiments. That is why we propose to extrapolate the frequency response of targets, taking advantage of its behaviour in f^p in the Rayleigh region, with p depending on the target shape (for example, $p = 2$ for a conducting sphere). For $D = 1.5\,\mathrm{m}$, such extrapolation allows to increase the low limit of the frequency band to 70 MHz.

We will explain the reconstruction process of the target image and we will compare results with and without such frequency extrapolation.

REFERENCES

1. Young J. D., "Radar imaging from ramp response signatures," *IEEE Trans. Antennas Propagat.*, Vol. 24, 276–282, May 1976.
2. Kennaugh E. M. and D. L. Moffat, "Transient and impulse response approximations," *Proc. IEEE*, Vol. 53, 893–901, Aug. 1965.
3. Chen, C.-C. and L. Peters Jr., "Radar scattering and target imaging obtained using ramp-response techniques," *IEEE Antennas and Propagat. Mag.*, Vol. 49, No. 3, 13–27, June 2007.
4. Zhang, X. M., W. Lib, and G. R. Liu, "A new technique in ramp response for acoustic imaging of underwater objects," *Applied Acoustics*, Vol. 63, 453–465, 2002.

Infrared Signature Studies of Aircraft and Helicopters

S. P. Mahulikar, G. A. Rao, H. R. Sonawane, and H. S. S. Prasad
Department of Aerospace Engineering, Indian Institute of Technology, Bombay, India

Abstract— The infrared (IR) seekers have exploited techniques to passively acquire and intercept airborne targets, by detecting their IR energy [1]. The basic principle of IR detection is the discrimination of target's IR radiance in the detector's wavelength band with the background IR radiance (atmospheric emission / solar radiation) [2]. In an aircraft, the internal sources include plume and surface emissions; and power-plant is the major and reliable source. The aircraft rear fuselage skin of a typical military aircraft is heated by the flow of hot combustion products in the embedded engine [3]. The solid angle subtended by the rear fuselage skin is an order of magnitude larger than that of the tailpipe [4]. Therefore, its contribution is significant especially in the 8–12 micron band; in which, IR-detection is possible also due to external sources, e.g., earthshine and skyshine reflection [5].

Unlike surfaces of solids, gases emit and absorb radiation only at discrete wavelengths associated with specific rotational and vibrational frequencies. These frequencies depend on the particular type of molecule, temperature, pressure, and molecular concentration of radiation participating species [6]. The atmosphere limits the use of the IR spectrum to specific bands called as *atmospheric windows*; and has a crucial role, which includes that of transmission and background radiance [7]. For reducing detection by IR-guided missiles, aircraft and helicopters use IR Signature Suppression (IRSS) techniques. A well-designed IRSS system can drastically reduce IRSL by restricting the visibility of hot parts and by matching the visible radiance with the background [8]. Their effect in reducing target's susceptibility (P_{H}) can be gauged by models that relate *the two*. Due to significant advancements in the performance of IR-detectors, modern missiles are generally constrained by their burnout range rather than their lock-on range. The 'lethal range' is a function of target's lock-on range, target's velocity, missile velocity, missile burnout range, missile's guidance logic and blast kill radius; and it is a superior estimate of P_{H} [9].

REFERENCES

1. Rao, G. A. and S. P. Mahulikar, "Integrated review of stealth technology and its role in airpower," *The Aeronautical Journal*, Vol. 106, No. 1066, 629–641, Dec. 2002.
2. Mahulikar, S. P., H. R. Sonawane, and G. A. Rao, "Infrared signature studies of aerospace vehicles," *Progress in Aerospace Sciences*, Vol. 43, Nos. 7–8, 218–245, Oct.–Nov. 2007.
3. Mahulikar, S. P., P. S. Kolhe, and G. A. Rao, "Skin temperature prediction of aircraft rear fuselage with multi-mode thermal model," *AIAA Journal of Thermophysics* & *Heat Transfer*, Vol. 19, No. 1, 114–124, Jan.–Mar. 2005.
4. Mahulikar, S. P., S. K. Potnuru, and P. S. Kolhe, "Analytical estimation of solid angle subtended by complex well-resolved surfaces for infrared detection studies," *Applied Optics*, Vol. 46, No. 22, 4991–4998, Aug. 2007.
5. Mahulikar, S. P., S. K. Potnuru, and G. A. Rao, "Study of sunshine, skyshine, and earthshine for aircraft infrared detection," *Journal of Optics A: Pure* & *Applied Optics*, Vol. 11, No. 4, art. No. 045703, 10, Apr. 2009.
6. Mahulikar, S. P., G. A. Rao, S. K. Sane, and A. G. Marathe, "Aircraft plume infrared signature in non-afterburning mode," *AIAA Journal of Thermophysics* & *Heat Transfer*, Vol. 19, No. 3, 413–415, Jul.–Sep. 2005.
7. Rao, G. A. and S. P. Mahulikar, "Effect of atmospheric transmission and radiance on aircraft infrared signatures," *AIAA Journal of Aircraft*, Vol. 42, No. 4, 1046–1054, Jul.–Aug. 2005.
8. Mahulikar, S. P., H. S. S. Prasad, and S. K. Potnuru, "Infrared signature suppression of helicopter engine duct based on 'conceal and camouflage'," *AIAA Journal of Propulsion* & *Power*, Vol. 24, No. 3, 613–618, May–Jun. 2008.
9. Rao, G. A. and S. P. Mahulikar, "New criterion for aircraft susceptibility to infrared homing missiles," *Aerospace Science* & *Technology*, Vol. 9, No. 8, 701–712, Nov. 2005.

Attitude Determination for Geostationary Satellite Using Optimized Real Time Image Registration Algorithm

Mohamed A. Hebaishy, **Osama A. Elsayed**, **and Ahmed Farag**
Egyptian Space Program, NARSS, Cairo, Egypt

Abstract— Attitude determination system for satellites is indispensable part of satellite control system and is used to both measure and control the spacecraft orientation, we try to use image registration on geostationary satellite to make attitude determination which need a huge volume of data. It consumes few minutes to align two images together. Therefore, registration may take few hours to register huge data. So there is a need for optimized software running on a high speed platform.

In this work, we present image registration techniques survey, then we select the suitable registration algorithm based on the type of image difficulties during acquisition of Satellite images. We make hardware platforms survey then select Blackfin DSP processor low cost, low power for this task. An optimized algorithms for feature selection based on DCT and IDCT on Blackfin DSP Microprocessor is implemented. The results show that reduction in time is more than 50% between the optimized and non-optimized algorithms that reduce the computation time of image registration to a fraction of a second.

Session 2P2a
Anisotropic and Liquid Crystals Optics

An Analytic Method for Computing the Time-Dependent Electromagnetic Fields in Anisotropic Crystals

V. G. Yakhno[1] **and T. M. Yakhno**[2]

[1]Electrical and Electronics Engineering Department, Dokuz Eylul University, Turkey
[2]Computer Engineering Department, Izmir University, Turkey

Abstract— The mathematical models of electric and magnetic waves motions in anisotropic crystals are related to the time-dependent Maxwell's system containing tensors of the dielectric permittivity $\mathcal{E} = (\varepsilon_{ij})_{3\times 3}$ and magnetic permeability $\mathcal{M} = \mu\mathbf{I}$ (see, for example, [1]), where μ is a positive constant, $\mathbf{I}$ is the identity matrix.

The time-dependent electric and magnetic fields in homogeneous non-dispersive electrically anisotropic materials are governed by the following Maxwell's system (see, [1, 2])

$$\begin{aligned} curl_x\mathbf{H} &= \mathcal{E}\frac{\partial \mathbf{E}}{\partial t} + \mathbf{j}, \quad & curl_x\mathbf{E} &= -\mathcal{M}\frac{\partial \mathbf{H}}{\partial t}, \\ div_x(\mathcal{M}\mathbf{H}) &= 0, & div_x(\mathcal{E}\mathbf{E}) &= \rho, \end{aligned}$$

where $x = (x_1, x_2, x_3)$ is a space variable from R^3, t is a time variable from R, $\mathbf{E} = (E_1, E_2, E_3)$, $\mathbf{H} = (H_1, H_2, H_3)$ are electric and magnetic fields, $E_k = E_k(x, t)$, $H_k = H_k(x, t)$, $k = 1, 2, 3$; $\mathbf{j} = (j_1, j_2, j_3)$ is the density of the electric current, $j_k = j_k(x, t)$, $k = 1, 2, 3$; ρ is the density of electric charges.

In the present paper a new analytic method for computing the time dependent electric and magnetic fields in anisotropic crystals is suggested. This method essentially uses matrix symbolic calculations in MATLAB and allows us to compute explicit formulae of electric and magnetic fields. These formulae are used for generating images of electric and magnetic fields in different homogeneous non-dispersive anisotropic crystals. Electric and magnetic fields images generated by a pulse dipole with a fixed polarization are presented. The present paper continues the study of [3, 4].

REFERENCES

1. Kong, K. J., *Electromagnetic Wave Theory*, John Wiley and Sons, New York, 1986.
2. Ramo, S., J. R. Whinnery, and T. Duzer, *Fields and Waves in Communication Electronics*, John Wiley and Sons, New York, 1994.
3. Yakhno, V. G., T. M. Yakhno, and M. Kasap, "A novel approach for modelling and simulation of electromagnetic waves in anisotropic dielectrics," *International Journal of Solids and Structures*, Vol. 43, 6261–6276, 2006.
4. Yakhno, V. G. and T. M. Yakhno, "Modelling and simulation of electric and magnetic fields in homogeneous non-dispersive anisotropic materials," *Computers and Structures*, Vol. 85, 1623–1634, 2007.

All-optically Tunable Photonic Structures Infiltrated with Liquid Crystals

A. Miroshnichenko[1], **E. Brasselet**[2], **W. Krolikowski**[1], **and Y. Kivshar**[1]

[1]Australian National University, ACT, Australia
[2]Université Bordeaux 1, CNRS, France

Abstract— We study all-optical reorientational effects in one-dimensional periodic structures with a single homeotropic nematic liquid crystal defect [1]. The strong enhancement of the light excitation at defect modes leads to the spectral modulation of the optical Fréedericksz transition threshold within the photonic bandgap region with drastic threshold reduction at the defect mode wavelengths. Under a linearly polarized light field, the very nature of the optical Fréedericksz transition can be changed from the second to the first-order and multistability can be achieved [1]. We show that such changes occur due to a "defect mode boost mechanism" that corresponds to a transient optical field enhancement inside the liquid crystal defect during the reorientation process. By suppressing the critical slowing down near the reorientation threshold, it becomes possible to achieve fast defect mode switching without high input powers as it is necessary using the low-frequency electrically tunable periodic structure analogue. In addition, the all-optical switching hysteresis width can be almost 100%, with the minimal power required to sustain the switch in the "on" state being several orders of magnitude below the classical Fréedericksz transition threshold. We also report the first experimental verification of these predicted effects [2, 3]. In addition to this we have considered the role of dye-dopants, which may alter the above-mentioned results for pure nematics [4].

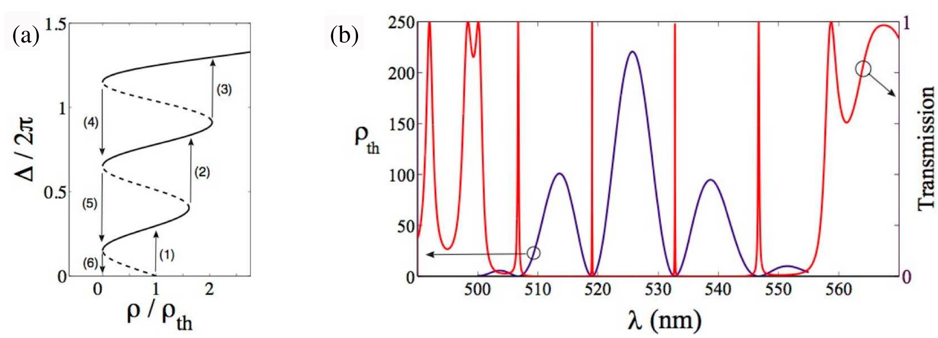

Figure 1: (a) Multistable reorientation diagram for positive detuning; (b) Transmission spectra of the unperturbed system (red) and normalized Freedericksz threshold (blue).

REFERENCES

1. Miroshnichenko, A., E. Brasselet, and Y. Kivshar, *Appl. Phys. Lett.*, Vol. 92, 253306, 2008.
2. Laudyn, U. A., A. E. Miroshnichenko, W. Krolikowski, D. F. Chen, Y. S. Kivshar, and M. A. Karpierz, *Appl. Phys. Lett.*, Vol. 92, 203304-3, 2008.
3. Brasselet, E., A. E. Miroshnichenko, W. Krolikowski, D. F. Chen, and Y. S. Kivshar, *Opt. Lett.*, Vol. 34, 488, 2009,
4. Miroshnichenko, A. E., E. Brasselet, and Y. S. Kivshar, *Phys. Rev. A*, Vol. 78, 053823, 2008.

Design of Wide Band Tunable Birefringent Filters with Liquid Crystals

Ofir Aharon and I. Abdulhalim
Department of Electro Optic Engineering, Ben Gurion University, Beer Sheva 84105, Israel

Abstract— Liquid crystals (LC) tunable filters have been in use for the last years in many fields like digital displays, optical telecommunications, and optical imaging. The design of an optical filter is against two major parameters. First the bandwidth, defined by the full width at half maximum (FWHM) of its main output peak and the free spectral range (FSR), these two parameters are very desirable for wavelength filtering and tuning. We demonstrate LC tunable filters oriented for integration into biomedical optical imaging systems and can be utilized to many other areas. Most widely used methods of primary narrowing of the emission spectra employs various modifications of the birefringent filter proposed by Lyot, commonly referred to as Lyot filter. Our work improved the Lyot filter output spectrum in several ways. Modification of sets of Lyot filters controlled by different sets of external electric field allowed us to eliminate unwanted orders. Different approach is integrating an additional thinner liquid crystal cell (retarder) between crossed polarizers to eliminate one order of the Lyot filter and by that widening the FSR. The presentation includes a novel set of retarders similar to the Lyot filter in its principle but yet different in its polarizers position and mathematical analysis of its odd increase in the retarders thickness, which we call Jump filter. Nevertheless the ***Jump filter*** stands by its own, we show new algorithm for combining it with Lyot filter to increase the FSR and decrease the FWHM at the same time. Experimental results will be presented along with the theoretical design.

Assessment of Guided Mode Resonant Structures for Sensing

Olga Krasnykov, **Mark Auslender**, **and I. Abdulhalim**
Department of Electrooptic Engineering, Ben Gurion University of the Negev
Beer Sheva 84105, Israel

Abstract— Guided mode resonant (GMR) structures consist of grating coupled waveguide structure that exhibits a sharp resonant reflection peak when the wave vector of the first order wave coincides with the effective waveguide mode wave vector. This resonance location shifts as the refractive index of the top dielectric medium varies due to the interaction with the evanescent field inside the top dielectric medium. Considering water as the top dielectric medium (analyte), variations of its index due to pollutants shifts the resonance and hence the GMR can act as a sensor. On the other hand having a low index of 1.33 for water compared to the waveguide layer reduces the evanescence region thus reducing the sensitivity. Results and the design procedure to obtain optimum sensor will be presented using rigorous electromagnetic simulations.

Session 2P2b
Geometric Phases and Transport in Polarization and Singular Optics

Exploiting the Optical Berry Phase for Quantum Logic Using Cavity QED

T. D. Ladd[1, 2] **and Y. Yamamoto**[1, 2]

[1]National Institute of Informatics, 2-1-2 Hitotsubashi, Chiyoda-ku, Tokyo 101-8430, Japan
[2]Edward L. Ginzton Laboratory, Stanford University, Stanford, California 94305-4088, USA

Abstract— Recent experiments on single charged quantum dots reveal the ability for ultrafast optical pulses to rotate single electron spins by large angles on timescales much faster than the Larmor frequency [1]. The enabling phenomenon is the rapid AC-Stark shift of a quantum dot Zeeman level controlled by the off-resonant optical pulse.

Existing experiments may be understood by treating the electromagnetic field as a rapidly varying parameter in the Hamiltonian. However, future potential uses of these effects include quantum logic of multiple electron spins mediated by optical fields in one or more modes of an optical microcavity or extended microcavity/waveguide structure. These proposals employ the Berry phases of the cavity modes which accrue as they are driven and subsequently emptied by a combination of interference and cavity leakage [2]. For the successful design of devices to realize these proposals, the detailed evolution of dynamic and geometric phases accrued by both the electron spins and the cavity modes must be carefully modeled. Here we discuss these modeling efforts in view of current experimental capabilities. Driving conditions are optimized using semiclassical Maxwell-Bloch equations in the dispersive limit (employing adiabatic elimination of excited quantum dot states), but the ultimate potential performance is modeled via complete quantum master-equation simulations. In both cases, the electromagnetic field is modeled using eigenmodes of realistic microcavity geometries coupled to broadband waveguides.

We find that for appropriately optimized optical pulses and microcavities, the electromagnetic field may be driven through closed paths of phase space that achieve Berry-phase-driven controlled-phase logic gates between pairs of electron spins, while revealing negligible amounts of information about the quantum state of those electron spins when photons incoherently leak from the cavity. This enables high-fidelity quantum logic in future high-speed quantum computers driven by ultrafast light in nanophotonic structures [2].

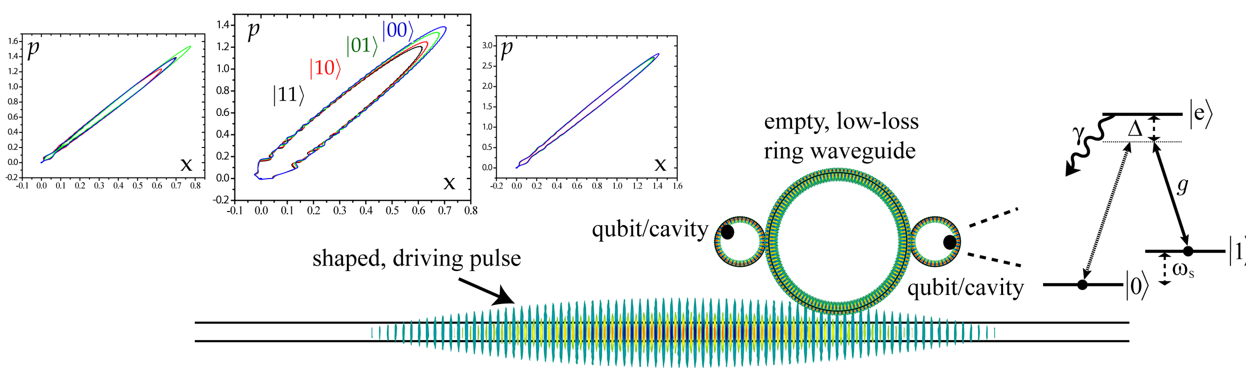

Figure 1: Example scheme in which a shaped pulse drives the modes of two microdisk cavities coupled to a single ring waveguide. The coupled modes traverse closed phase space paths which depend on the states of electron spins in two quantum dots [2].

REFERENCES

1. Press, D., T. D. Ladd, B. Zhang, and Y. Yamamoto, "Complete quantum control of a single quantum dot spin using ultrafast optical pulses," *Nature*, Vol. 456, No. 7219, 218–221, 2008.
2. Clark, S. M., K.-M. C. Fu, T. D. Ladd, and Y. Yamamoto, "Quantum computers based on electron spins controlled by ultrafast off-resonant single optical pulses," *Phys. Rev. Lett.*, Vol. 99, No. 4, 040501, 2007.

Beam Propagation Effects in Goos-Hanchen and Imbert-fedorov Shifts

Andrea Aiello[1,2] **and J. P. Woerdman**[2]

[1]Max Planck Institute for the Science of Light, Erlangen, Germany
[2]Huygens Laboratory, Leiden University, Leiden, The Netherlands

Abstract— It is known that the behavior of bounded beams of light reflected from and transmitted through a planar interface differs from that exhibited by plane waves, the latter being ruled by Snell's law and the Fresnel equations [1]. For bounded beams diffractive corrections occur, the most prominent of which are the so-called Goos-Hänchen (GH) [2] and Imbert-Fedorov (IF) shifts [3] of the beam, occurring in the directions parallel and perpendicular to the plane of incidence, respectively. In principle, both reflected and transmitted beams are subject to such shifts. A great deal of literature exists about experimental and theoretical demonstrations of both GH and IF shifts (see, e.g., [4, 5] and references therein) but generally the effects of beam propagation are not accounted for. A notable exception is a recent paper by Hosten and Kwiat [6] where the authors report, among other issues, on a dramatic signal enhancement technique ($\sim 100\times$) for a *quantum* version of the IF shift, the spin Hall effect of light (SHEL), based on beam propagation. The theoretical discussion in [6] uses the quantum formalism of weak measurements [7], although the authors note that the *beam propagation enhancement* (BPE) is essentially a classical phenomenon.

The purpose of this presentation is to show a purely classical analysis of the BPE [1]; this is useful since a classical description will make this important technique, which allows sub-nm sensitivity [6], better accessible to the metrology community. In particular, we derive the polarization-dependent displacements parallel and perpendicular to the plane of incidence, for a Gaussian light beam reflected from a planar interface, taking into account the propagation of the beam. It results that beam propagation may greatly affect both Goos-Hänchen and Imbert-Fedorov shifts when the incident beam is focussed.

REFERENCES

1. Born, M. and E. Wolf, *Principles of Optics*, 7 edition, Cambridge University Press, Cambridge, UK, 2003.
2. Goos, F. and H. Hanchen. "Ein neuer and fundamentaler versuch zur total reflection," *Ann. Phys. (Leipzig)*, Vol. 1, 333, 1947.
3. Costa de Beauregard, O. and C. Imbert, "Quantized longitudinal and transverse shifts associated with total internal reflection," *Phys. Rev. Lett.*, Vol. 28, No. 18, 1211, 1972.
4. Pillon, F., H. Gilles, and S. Girard, "Experimental observation of the Imbert-Fedorov transverse displacement after a single total reflection," *Appl. Opt.*, Vol. 43, No. 9, 1863, 2004.
5. Bliokh, K. Y. and Y. P. Bliokh, "Conservation of angular momentum, transverse shift, and spin Hall effect in reflection and refraction of an electromagnetic wave packet," *Phys. Rev. Lett.*, Vol. 96, 073903, 2006.
6. Hosten, O. and P. Kwiat, "Observation of the spin Hall effect of light via weak measurements," *Science*, Vol. 319, 787, 2008.
7. Aharonov, Y., D. Z. Albert, and L. Vaidman, "How the result of a measurement of a component of the spin of a spin-1/2 particle can turn out to be 100," *Phys. Rev. Lett.*, Vol. 60, No. 1351, 1988.
8. Aiello, A. and J. P. Woerdman, "Role of beam propagation in Goos-Hänchen and Imbert-Fedorov shifts," *Opt. Lett.*, Vol. 33, No. 13, 1437–1439, 1986.

Singularities in Single Photon Fields

E. J. Galvez, L. E. Coyle, E. Johnson, and B. Reschovsky
Department of Physics and Astronomy, Colgate University, USA

Abstract— T optical singularities, and in particular optical vortices, are topics of fundamental and applied research in the context of classical optics. Their study and use at the photon level has potential for use in quantum information and quantum imaging.

In this work, we report on experimental studies with correlated photon pairs produced via parametric down conversion and detected in coincidence. Optical vortices are imparted on one or both photons by passive optical components. We study the interference patterns that are produced with these light forms, where optical singularities may be present in one or both photons.

In a series of experiments presently under way we study the singularities carried by single photons. Heralded single photons are sent to a Mach-Zehnder interferometer where in one of the arms a spiral phase plate imparts to the light a phase singularity with a topological charge of 1. This puts the light in a helical mode, where the phase advances as a function of angle in a transverse plane. These types of modes are represented by Laguerre-Gauss functions. The mode of the light in the other arms is the fundamental spatial mode. The light leaving the interferometer thus consists of photons interfering with themselves in two modes. In these experiments we study the images by either scanning detectors or scanning apertures. Preliminary results show evidence of optical vortices carried by single photon via the changing images that are produced when the relative phase imparted by the interferometer is varied, consistent with the expectations.

Spin-to-orbital Light Angular Momentum Coupling in Homogeneous Uniaxial Media

E. Brasselet[1], **Y. Izdebskaya**[2], **V. Shvedov**[2,3],
A. S. Desyatnikov[2], **W. Krolikowski**[2], **and Y. S. Kivshar**[2]

[1]Centre de Physique Moléculaire Optique et Hertzienne
Université Bordeaux 1, CNRS, Talence Cedex 33405, France
[2]Nonlinear Physics Centre and Laser Physics Centre, Research School of Physics and Engineering
The Australian National University, Canberra ACT 0200, Australia
[3]Department of Physics, Taurida National University, Simferopol 95007 Crimea, Ukraine

Abstract— We report on the detailed dynamics of spin-to-orbital light angular momentum coupling for mono- and polychromatic Gaussian beams propagating in homogeneous uniaxial media. Three situations are explored for crystal slabs having their optical axis perpendicular to its facets. Namely, (i) the normal incidence case for circularly polarized light where the light propagates along the optical axis of the crystal, which leads to the generation of charge two optical vortex (ii) the normal incidence case with linearly polarized light, which leads to the generation of a topological quadrupole, and (iii) the oblique incidence case with linearly polarized light that can give rise to an isolated single-charge vortex centered on the beam axis for a specific incidence angle that depends on the crystal thickness and birefringence. In all cases, we developed a simplified matrix formulation of the problem in the limit of small birefringence that quantitatively supports all the experimental observations, which include power coupling efficiency between orthogonally polarized light field components and optical vortices trajectories.

Spin Hall Effect of Light and the Geometrical Phase

S. Murakami[1, 2]

[1]Tokyo Institute of Technology, 2-12-1 Ookayama, Meguro-ku, Tokyo 152-8551, Japan
[2]PRESTO, Japan Science and Technology Agency, Kawaguchi, Saitama 332-0012, Japan

Abstract— By applying an electric field in a solid, a flow of electron spins (spin current) perpendicular to the field is induced [1]. This effect is called spin Hall effect (SHE). The SHE is theoretically proposed to occur by an intrinsic mechanism due to the Berry phase (geometrical phase) in k-space. This intrinsic SHE can be regarded as a consequence of wave interference. Therefore, this effect occurs in various wave phenomena such as light.

In my talk, we present our study on the SHE of light [2–4]. In the vacuum, this effect brings about a transverse shift when the light is refracted at a gradual spatial change of refractive index. This shift is calculated via the Berry phase and is independent of the details such as the beam profile [2, 3]. If the spatial change of the refractive index becomes abrupt, the effect reduces to the Imbert shift in interface refraction. In this limit, we cannot use the Berry phase and the shift depends on details [3, 4].

In condensed materials, the effect is enhanced by lattice periodicity of the crystal. Therefore the similar enhancement is expected for the SHE of light as well. In contrast with the Imbert shift which is smaller than the wavelength, the shift in the photonic crystal can be much larger than the wavelength, if we tune the photonic band structure [2].

REFERENCES

1. Murakami, S., N. Nagaosa, and S.-C. Zhang, "Dissipationless quantum spin current at room temperature," *Science*, Vol. 301, 1348, 2003.
2. Onoda, M., S. Murakami, and N. Nagaosa, "Hall effect of light," *Phys. Rev. Lett.*, Vol. 93, 083901, 2004.
3. Onoda, M., S. Murakami, and N. Nagaosa, "Geometrical aspects in optical wave-packet dynamics," *Phys. Rev. E*, Vol. 74, 066610, 2006.
4. Bliokh, K. Yu. and Yu. P. Bliokh, "Conservation of angular momentum, transverse shift, and spin hall effect in reflection and refraction of an electromagnetic wave packet," *Phys. Rev. Lett.*, Vol. 96, 073903, 2006.

Dynamics of the Reflection and Transmission Processes of a Light Beam Carrying the Orbital Angular Momentum at a Plane Interface

V. G. Fedoseyev
Institute of Physics, University of Tartu
Riia 142, 51014 Tartu, Estonia

Abstract— The light beams carrying the orbital angular momenta (OAMs), for instance, the Laguerre-Gaussian beams, are the important objects of singular optics. We consider the dynamical aspects of the reflection and transmission processes of such beams at a plane interface of two isotropic transparent media.

The ratios of the intrinsic OAMs to the electromagnetic energies for the incident, reflected and transmitted beams (the quantities $\Sigma^{(i)}$, $\Sigma^{(\rho)}$, and $\Sigma^{(\tau)}$, respectively) have been calculated. The following relations have been obtained: $\Sigma^{(\rho)} = -\Sigma^{(i)}$, and $\Sigma^{(\tau)} = 0.5(\cos\theta^{(i)}/\cos\theta^{(\tau)} + \cos\theta^{(\tau)}/\cos\theta^{(i)})\Sigma^{(i)}$, where $\theta^{(i)}$ and $\theta^{(\tau)}$ are the angles of incidence and transmission, respectively, ([1], see also [2]). The physical meanings of these relations are explained. Owing to these relations, the normal-to-interface component of the total intrinsic OAM changes after the reflection and the transmission of the beam. However, the normal component of the Minkowski OAM is the invariant of the process under consideration [1, 2]. It is shown that the change of the normal component of the total intrinsic OAM is compensated by the appearance of the normal component of the total extrinsic OAM, which is generated by the shifts of the centers of gravity of the secondary packets in the transverse, i.e., perpendicular to the plane of incidence, direction [1–3].

It is shown that the above-mentioned process is accompanied by the appearance of the transverse power flow. The relation between this effect and the transverse shifts of the centers of gravity of the reflected and transmitted packets is established.

REFERENCES

1. Fedoseyev, V. G., *J. Phys. A: Math. Gen.*, Vol. 41, 505202, 2008.
2. Bliokh, K. Yu., I. V. Shadrivof, and Yu. S. Kivshar, arXiv:0810.2855v1 [physics.optics] (2008); *Opt. Lett.*, Vol. 34, 389, 2009.
3. Fedoseyev, V. G., *Opt. Commun.*, Vol. 193, 9, 2001.

Spin-orbit Interactions of Light at Nano-scales

K. Y. Bliokh[1,2]

[1]Nonlinear Physics Centre, Research School of Physics and Engineering
Australian National University, Canberra ACT 0200, Australia
[2]Institute of Radio Astronomy, 4 Krasnoznamyonnaya St., Kharkov 61002, Ukraine

Abstract— Spin and orbital degrees of freedom of light are independent of each other as the wave propagates freely in vacuum. However, they become coupled by various perturbations of the medium, such as inhomogeneity, anisotropy, or non-linearity. This produces spin-orbit coupling within the Maxwell equations, which leads to the spin-to-orbital angular momentum conversion and spin-dependent transport of light (spin Hall effect). The transport effects are typically small (proportional to the wavelength) and negligible in classical optics, but they might be crucial for operating light at nano-scales — e.g., in photonic and plasmonic system. I will give an overview of recent theoretical and experimental studies of fine spin-induced phenomena upon the light propagation and scattering in inhomogeneous media. The spin-orbit interactions are characterized by a fundamental duality of dynamical (particle) and geometrical (wave) aspects. On the one hand, the spin-orbit coupling can be attributed to the Coriolis effect and angular momentum dynamics. On the other hand, it is described in terms of the Berry phases and interference of partial plane waves in the wave packet. We anticipate that, akin to electron spintronics, spin-induced wavelength-scale phenomena in the evolution of light will form a promising avenue in nano-optics.

Session 2P3a
Systems and Components, Electromagnetic Compatibility

Design of Composite Electromagnetic Wave Absorber Made of Fine Aluminum Particles Dispersed in Polystyrene Resin by Controlling Permeability

K. Sakai, **Y. Wada**, **Y. Sato**, **and S. Yoshikado**
Department of Electronics, Doshisha University, Japan

Abstract— Development of an electromagnetic wave absorber suitable for frequencies above 10 GHz is required with the increasing use of wireless telecommunication systems. In this study, the frequency dependences of the relative complex permeability μ_r^*, the relative complex permittivity ε_r^* and the absorption characteristics for composite electromagnetic wave absorbers made of fine aluminium particles dispersed in polystyrene resin were investigated in the frequency range from 1 to 40 GHz. In addition, the control of μ_r^* was also discussed because the frequency dependences of μ_r^* is important factor to determine the absorption of electromagnetic waves. In particular, μ_r', the real part of μ_r^*, must be less than unity to satisfy the non-reflective condition at frequencies above 10 GHz. When an electromagnetic wave of high frequency enters an aluminum particle, an eddy current flows on the particle surface and a reverse magnetic moment appears. Thus, μ_r' becomes less than unity. To examine this phenomenon, μ_r' and μ_r'', the imaginary part of μ_r^*, were calculated theoretically. In the case of calculating μ_r', the eddy current which flows inside aluminum particle was calculated strictly from the Maxwell's equation and μ_r' was obtained from this eddy current. The results of calculation showed the values of $1 - \mu_r'$ increase proportional to the volume mixture ratio V of aluminum particle in the high frequency range, at which the eddy current can be considered to flow in the thin layer of particle surface. Meanwhile, in the low frequency range at which the skin depth is close to the particle size of aluminum, $1 - \mu_r'$ decreased with decreasing frequency. In addition, calculated values of μ_r'' is proportional to V and inversely proportional to particle size of aluminum. These calculated results almost agreed with the measured values of μ_r' and μ_r'' for the composite made of aluminum and polystyrene when V and particle size of aluminum were varied. Therefore, μ_r' and μ_r'' can be estimated by theoretical calculation and can be controlled independently each other by adjusting V and particle size of aluminum to satisfy the non-reflective condition. Moreover, the control of μ_r' and μ_r'' was also proposed from above results if the aluminum particles of different sizes were dispersed in the polystyrene resin. The composite made of aluminum and polystyrene absorbed more than 99% of electromagnetic wave power in the frequency range from 1 to 40 GHz and the absorption of electromagnetic waves at frequencies above 40 GHz is expected by controlling μ_r' and μ_r''.

On the Passivation of AlGaN/GaN MSM 2-DEG Varactor and Its Electromagnetic Pulse Protection Application

Liann-Be Chang[1], **Yi-Cherng Ferng**[1], **Chien-Yeu Chen**[1], **Atanu Das**[1], **Chien-Fu Shih**[1], **Hsien-Chin Chiu**[1], **Ray-Ming Lin**[1], **Ming-Jer Jeng**[1], **and Ta-Wei Soong**[2]

[1]Department of Electronic Engineering & Green Technology Research Center
Chang Gung University, 259, Wen-Hwa 1st Road, Kwei-Shan, Tao-Yuan 333, Taiwan, R.O.C.
[2]Department and Institute of Electronic Engineering, Minghsin University of Science and Technology
1, Xinxing Road, Xinfeng, Hsinchu 30401, Taiwan, R.O.C.

Abstract— This thesis focuses on the discussion of the cascaded electromagnetic pulse protection circuit with a series AlGaN/GaN varactor and its behavior before and after a sulfidizing process. The cascaded electromagnetic pulse protection circuit comprises of a gas discharge tube (GDT) and a fast response (nano-second grade) electromagnetic pulse protection device and by using an AlGaN/GaN metal/semiconductor/metal (MSM) varactor in between as a connector. Thereby, the proposed novel electromagnetic pulse protection configuration can effectively protect front-end communication electronic devices against LEMP, ESD (electrostatic discharge) and other special electromagnetic pulses with fast rise time. The MSM varactor with two dimension electron gas (2-DEG) characteristic consists of two back-to-back Schottky contacts. Due to the AlGaN/GaN MSM 2-DEG varactor behavior, the capacitance changes according to the voltage input. During normal operating mode, the varactor has large capacitance which allows small signal to pass through with low insertion loss. However, when overvoltage surge induces to the varactor, the capacitance will reduce rapidly and will have high insertion loss, therefore it guarantees the surge pulse not going to the next stage to damage the electronic device. The AlGaN/GaN MSM 2-DEG heterostucture was grown on sapphire substrate by our MOCVD system. The carrier concentration is $3.6 \times 10^{13}\,\mathrm{cm}^{-2}$ and the electronic mobility is $600\,\mathrm{cm}^2/\mathrm{V{\cdot}s}$, respectively. The device processing steps began with mesa isolation, performed by argon sputtering and followed by Ni/Au metal pad deposition. Finally, a sulfidizing process, with (P_2S_5 + NH_4S_2) or NH_4S_2 solution, was carried out and the correspondent capacitance variation is reported. The varactor's capacitive transition ratio $C_{\max}/C_{\min}$ is found to be improved. A cascaded electromagnetic pulse protection configuration with a varactor cascaded to the signal path is proposed and simulated. With the (P_2S_5 + NH_4S_2) or NH_4S_2 sulfidizing process, the cascaded electromagnetic pulse protection configuration will have better protection performance.

Investigation of Coupling of EMC Disturbances in Doubly Fed Induction Generators

S. Schulz, R. Doebbelin, and A. Lindemann
Institute of Electric Power Systems, Otto-von-Guericke-University Magdeburg, Germany

Abstract— In recent years, the exploitation of renewable energy has significantly increased with a major contribution of wind and water energy. One intent of energy production is high yield as achievable by variable speed operation. This requires the use of a converter. However, the high-frequency and fast changing output voltage of the converter can cause conducted emissions and system perturbation. In power plants (especially in water-power plants and wind farms) doubly fed induction generators (DFIG) are used, in which the stator of the generator is directly connected to the mains, whereas the rotor of the machine is supplied by a converter. The converter for the rotor is only rated for slip power which is about 30% of the nominal power of the DFIG. Thus, this topology can inherently decrease the EMI level because of the lower power rating of the rotor converter compared to a converter for full rated power in conventional systems.

In DFIG the applied rotor converters are designed as indirect power converter with DC link or as cycloconverters. Electromagnetic compatibility aspects concerning system perturbation (up to 2 kHz) and conducted emissions (9 kHz to 30 MHz) of power converters are regulated in grid connection regulations of the transmission system operator, and furthermore in EN 61000, EN 61800-3 and EN 50160. The emission limits given by these standards correspond with limits of the fundamental EMC standard EN 55011.

The harmonics and conducted emissions produced by the rotor converter are compensated by an input filter of the converter. The focus of this investigation is on system perturbation and conducted emissions in the usually non-regulated (2 kHz to 9 kHz) range of the switching frequency of rotor converters. The paper deals with the interaction of rotor and stator winding in a DFIG. High-frequency harmonics caused by the pulsed output of rotor power converters are transmitted into the stator current and cause conducted emissions. This high-frequency harmonics have to be considered, taking into account that harmonics — which can be limited by filters — will also be transmitted into the stator. In most generator systems with rotor converters line inductors instead of line filters are implemented in the rotor circuit. The paper gives an overview about topologies to reduce these harmonics.

With the increase of power plants with DFIG — without line filters of the rotor circuit or system filters — also EMC disturbances increase. These high frequency harmonics influence the mains, transformers and line filters of other systems connected to the mains. As a consequence malfunction and damage of electronic equipment can occur.

The reason for this behavior can be found in the single-phase equivalent circuit of a doubly fed induction machine which corresponds to the equivalent circuit of a transformer. Harmonics in rotor voltage caused by the converter will produce harmonics in rotor and stator currents. Therefore, mains current of the DFIG is a superposition of a sinusoidal current with high-frequency harmonics. The conducted emissions and harmonics depend on the pulse pattern of the rotor converter, frequency, the rotor filter and the line filter of the system.

Figure 1 shows several possibilities for the emergence and propagation of conducted emissions in the considered system: High-frequency pulsed rotor voltages cause harmonics of the rotor

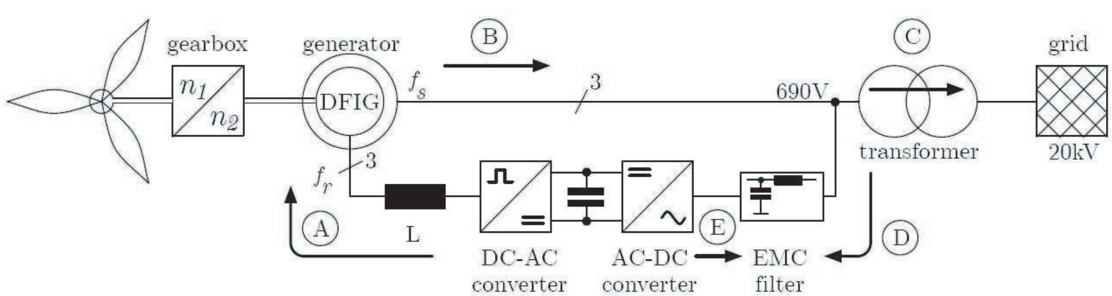

Figure 1: Possibilities for the emergence and propagation of conducted emissions in wind power systems with DFIG.

currents (A) which are transferred to the stator current (B); considering the slip of the generator, interharmonics will occur. The stator current supplies the transformer, thus the harmonics and interharmonics will proceed to the grid (C). The implemented EMC filter is mostly intended to reduce the additional conducted emissions of the rotor converter (E) on transformer side (D). Emissions of the stator current are hardly affected by this filter.

Inductive Coupling between Wires in Cables with a Grounded Conductor

Bernd W. Jaekel
Siemens AG, Sector Industry, EMC-Center, Germany

Abstract— Modern low voltage power installations are carried out as TNS power networks with separate neutral and protective earth conductors. This type of network prevents that any operational currents flow outside of the phase and neutral conductors and ensures that there is no stray current in the protective earth system. Actually a TNS power network should not have any common mode currents theoretically. But there are some mechanisms to be considered which do nevertheless worsen the situation with respect to the occurrence of such common mode voltages and currents. This is due to the mutual inductance between the phase conductors and the protective earth conductor in a twisted power cable. The mechanism can be explained by the details and a schematic illustration of a twisted power cable as given in Figure 1.

Figure 1 shows a power cable with twisted phase conductors and a protective earth (PE) conductor 1(b). The conductors are physically arranged as helical structures with a twist length (pitch) l and a core (helix) radius **a** 1(a). The PE conductor is connected to the protective earth (PE) system resulting in a loop 1(c).

Each of the phase conductors has a defined mutual inductance with respect to the PE-conductor and the PEloop connected with it. And each of those conductors therefore induces a voltage in the protective earth conductor loop. The individual induced voltages overlap and a power net frequency voltage results which amplitude and phase depends on the different values of the superimposed mutual inductances.

In order to understand the situation a coordinate transformation might be helpful by which the helical arrangement of the conductors is transformed into a linear one. This can be established by introducing a helical coordinate system. From the cross-section of the entire configuration with the phase conductors, the protective earth conductor and the resulting loop in the protective earth system it can easily be seen that there is no total symmetry when looking at the three mutual inductances between the phase conductors and the protective earth loop in case of a four-conductor cable. Hence a net mutual inductance results leading to a net induced common mode voltage in the entire arrangement and consequently a common mode current.

An analytical approach to this situation might be elegant but represents a very difficult task as already the determination of magnetic field strengths around a twisted cable can be looked at as a bonanza for Bessel functions. Therefore, in order to investigate this situation quantitatively, numerical simulations as well as experimental investigations were performed.

Numerical simulations were carried out for a power cable of type NYM 4×25 with a cross section of $25\,\mathrm{mm}^2$ for each of the four conductors. A twist length of 0.4 m was considered. The cable was modelled by means of four helical structures representing the different conductors. Three conductors of this model were excited by means of a three-phase current source leading to a balanced three-phase current. The fourth conductor is connected to further wires which represent the PE loop. The simulations were performed by means of a computer program which bases on the numerical procedure of the method of moments (MoM).

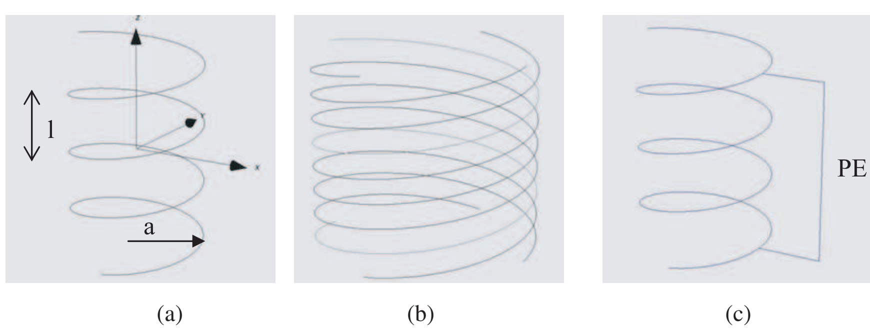

Figure 1: Schematic structure of a low voltage power cable, (a) helical conductor (twist length l and core radius **a**), (b) twisted phase and protective earth conductors, (c) protective earth conductor connected to grounding system building up a loop (phase conductor not shown).

Measurement of Corona Characteristics and Electromagnetic Environment of ±800 kV HVDC Transmission Lines under High Altitude Condition

Zheng Zhang, **Rong Zeng**, **and Zhanqing Yu**
State Key Lab of Control and Simulation of Power Systems and Generation Equipments
Department of Electrical Engineering, Tsinghua University, Haidian District, Beijing 100084, China

Abstract— In recent years, the rapid economic development in China has called for great needs in electricity. Under such circumstances, the ultra high voltage DC power transmission technique, which could realize power delivery in larger capacity and longer distance, is developing rapidly in accordance with the nation's energy policy. The construction of a brand new ultra high voltage test base, funded by China Southern Power Grid Co., Ltd., has recently been completed near Kunming, a famous tourist city in southwest China with an altitude of over 2000 meters. Measurement of the corona performance characteristics including radio interference, audible noise, electric field and ion current density is carried out under a 800 meters long bipolar HVDC test line with the nominal voltage of ±800 kV, a pole spacing of 22 meters and a minimum height of 18 meters in the base. The lateral profiles of radio interference, audible noise, electric field and ion current density are measured at the center of the midspan under the nominal voltage. The measurement results are compared to those calculated by internationally recognized empirical formulas. The comparison shows calculated RI and AN are lower than the measurement result under such a high voltage and altitude level. It is necessary therefore to further research and acquire improved empirical formulas that can be used under such circumstances. Measurement of those characteristics is also carried out under other three voltage levels: ±500 kV, ±600 kV and ±950 kV. Value and distribution differences in the corona characteristics under different voltage levels are compared and analyzed. Monopolar tests have also been conducted by energizing one pole with the other grounded, and the results are compared with the bipolars'. Comprehensive research is still needed to disclose the corona mechanism more than 2000 m altitude.

Session 2P3b
Numerical and Semi-analytic Modelling of Photonic Crystals

Envelope-Function-Based Asymptotics of Photonic Crystal Waveguides

S. Mahmoodian[1], **K. B. Dossou**[2], **C. G. Poulton**[2], **R. C. McPhedran**[1], **L. C. Botten**[2], **and C. M. De Sterke**[1]

[1]IPOS, CUDOS, School of Physics, University of Sydney, Australia
[2]CUDOS, School of Mathematical Sciences, University of Technology, Sydney, Australia

Abstract— Photonic crystal (PC) waveguides provide a mechanism to guide light using a PC bandgap [1]. PC waveguide modes have been thoroughly analysed numerically [2], however little analytic insight exists into how waveguide modes behave, particularly close to the band-edge. Previous analytic treatments based on envelope functions have been reported [3], but they assumed that the perturbation used to create the defect is slowly varying limiting the applicability of the approach. Here we make no such assumption, and only require that the perturbation is periodic and causes a small change in electric energy in a given period.

Our asymptotic treatment for PC waveguides is based on that of Luttinger and Kohn (L-K) developed for solid state physics [4]. Here we are considering a shallow periodic perturbation in an infinite 2D PC in E_z polarisation, forming a PC waveguide. The modes of this structure are quasi-periodic in the direction of propagation, say x, and are composed of a product of a Bloch mode and an envelope function in the direction orthogonal to the PC waveguide, y. This is denoted $f(y)\psi_{k_x,k_{Ly}}(x,y)$, where $\psi_{k_x,k_{Ly}}(x,y)$ is the Bloch mode on the projected band-structure edge with Bloch wavevector k_x. This approach enables us to derive a differential equation governing the envelope function $f(y)$ and frequency of the waveguide ω_{k_x}, with Bloch wavevector, k_x as a parameter,

$$\omega^2_{k_x,-i\frac{d}{dy}} f(y) = \omega^2_{k_x}\left[1+\frac{\Omega}{\mathcal{E}_{kx}\Delta}\int_{C_0}\delta\epsilon(\mathbf{r})|\psi_{k_x,k_{Ly}}(\mathbf{r})|^2 dx\right] f(y). \tag{1}$$

Here, Δ is the periodicity of the perturbation forming the waveguide, Ω is the area of the unit cell of the unperturbed PC and $\mathcal{E}_{kx}$ is the electric energy of the projected band-edge Bloch mode. $\omega^2_{k_x,-id/dy}$ is the 1D modified L-K operator given by

$$\omega^2_{k_x,-i\frac{d}{dy}} = \left[\omega^2(k_x,k_{Ly}) - \frac{\omega(k_x,k_{Ly})}{C_{Ly}(k_x)}\frac{d^2}{dy^2}+\ldots\right], \tag{2}$$

where C_{Ly} is the curvature of the projected band-structure edge in the orthogonal direction and $\omega(k_x,k_{Ly})$ is the frequency along the projected band-structure edge. Equation (1) is solved by replacing the perturbation with one which gives rise to a uniform change in electric energy over the perturbed region, while preserving the total change in electric energy. This leads to a small distortion in the solutions of the envelope function, $f(y)$, inside the perturbation, but preserves the change in frequency since $\delta\omega$, to first order, depends only on changes in electric energy [5]. By applying the boundary conditions on the edge of the perturbation we obtain for the frequency

$$\omega_{kx} = \omega(k_x,k_{Ly}) - \frac{C_{Ly}(k_x)}{8}\left(\frac{\omega(k_x,k_{Ly})\Omega}{\Delta}\right)^2\left(\frac{\delta\mathcal{E}_{kx}}{\mathcal{E}_{kx}}\right)^2. \tag{3}$$

From this we note that the mode does have a cutoff unless $\delta\mathcal{E}_{kx}\neq 0$, where $\delta\mathcal{E}_{kx}$ is the total change in electric energy at a particular band-edge value of k_x. The quadratic dependence of ω_{kx} on $\delta\mathcal{E}_{kx}$ is indicative of 1D systems. Finally, we have observed excellent agreement between (3) and numerical calculations.

REFERENCES

1. Joannopoulos, J. D., et al., *Molding the Flow of Light*, Princeton University Press, 2008.
2. De Sterke, C. M., et al., *Opt. Lett.*, Vol. 29, No. 12, 1384–1386, 2004.
3. Charbonneau-Lefort, M., et al., *Phys. Rev. B*, Vol. 65, No. 12, 2002.
4. Luttinger, J. M. and W. Kohn, *Physical Review*, Vol. 97, No. 4, 869–883, 1955.
5. Johnson, S. G., et al., *Phys. Rev. E*, Vol. 65, No. 6, 2002.

Accurate Semi-analytic Modelling of Finite Cluster Defects in Photonic Crystals

K. B. Dossou[1], R. C. McPhedran[2], L. C. Botten[1], C. G. Poulton[1], S. Mahmoodian[2], and C. Martijn de Sterke[2]

[1]CUDOS, Department of Mathematical Sciences, University of Technology Sydney, NSW 2007, Australia
[2]CUDOS, School of Physics, University of Sydney, NSW 2006, Australia

Abstract— We have developed a semi-analytic treatment for symmetric composite defects in two-dimensional photonic crystals (PCs). Our approach exploits the rotational periodicity of these structures to reduce the analysis to a single unit cell. The matrix eigenproblems are solved elegantly by using known results for the eigenvalues of block circulant matrices. This allows us to investigate the modal properties of finite cluster defects (dispersion relations, cutoff, degeneracy, mode symmetry, fundamental modes).

Composite defect structures, see Fig. 1(a), consisting of multiple defect cavities, such as photonic crystal ring resonators [1], are "a promising design" for the realisation of integrated photonic circuits. Multiple defects are difficult to model because they can comprise a large number of cavities and near a band-edge (shallow defects) their fields are arbitrarily extended. In this work, we study cluster defects as their frequencies evolve from the vicinity of a band-edge into a band gap (loose binding limit). The main results about the spectral properties of the defect modes are based only on the structure of the matrices and can be generalized to the tight binding formulation.

Our semi-analytic method generalizes to multiple defects the asymptotic method we have developed for an isolated defect [2]. Near each defect cylinder C_j, for $j = 1, \ldots, N$, a defect mode $\psi(\boldsymbol{r})$ is approximated as a superposition of the Bloch modes $\psi_L(\boldsymbol{k}_L, \boldsymbol{r})$ at the band edge; for the case of a non-degenerate band edge we then have $\psi(\boldsymbol{r}) \approx B^{(j)}\psi_L(\boldsymbol{k}_L, \boldsymbol{r})$ near C_j. By applying Green's Theorem, together with a leading order estimate for the Green function near the gap edge [2], we can derive a matrix equation $\boldsymbol{MB} = \boldsymbol{B}$ or $(\boldsymbol{M} - \boldsymbol{I})\boldsymbol{B} = \boldsymbol{0}$. It follows from the rotational invariance of the problem (see Fig. 1(a)) that $\boldsymbol{M}$ is block circulant matrix [3] consisting of the submatrices $\boldsymbol{M}^{(l)}$ for $l = 0, \ldots, N_e - 1$ (N_e is the number of edges of the polygon defined by the composite defect). The eigenvectors of a block circulant matrix are [3] $\boldsymbol{B} = \left[\boldsymbol{w}, \rho_m\boldsymbol{w}, \ldots, \rho_m^{N_e-1}\boldsymbol{w}\right]^T$ where $\boldsymbol{w}$ is an eigenvector of $\boldsymbol{T}_m = \sum_{l=0}^{N_e-1} \rho_m^l \boldsymbol{M}^{(l)}$ and ρ_m is a root of unity: $\rho_m = e^{2\pi i m/N_e}$. A pair of conjugate roots correspond to a doubly degenerate mode of $\boldsymbol{M}$ while a real root generally gives a non degenerate mode. Fig. 1(b) shows that for a weak perturbation, there is a good agreement between the asymptotic results (dashed curve) and a full numerical calculation. The derivation can be extended to the case of degenerate band edge.

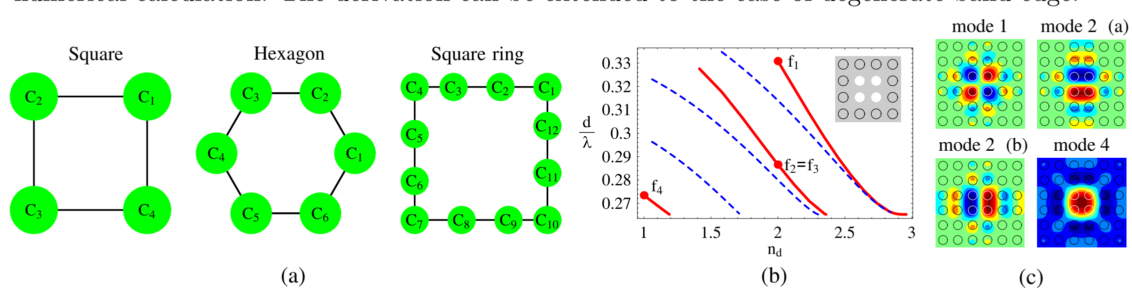

Figure 1: (a) Rotationally symmetric structures. (b) Evolution of the resonance frequency with the defect index n_d. (c) Field plot of the modes at the resonance frequencies f_m in panel (b).

REFERENCES

1. Qiang, Z., W. Zhou, and R. Soref, "Optical add-drop filters based on photonic crystal ring resonators," *Opt. Express*, Vol. 15, No. 4, 1823–1831, 2007.
2. Dossou, K. B., L. C. Botten, R. C. McPhedran, C. G. Poulton, A. A. Asatryan, and C. M. de Sterke, "Shallow defect states in two-dimensional photonic crystals," *Phys. Rev. A*, Vol. 77, No. 6, 063839, 2008.
3. Tee, G., "Eigenvectors of block circulant and alternating circulant matrices," *Res. Lett. Inf. Math. Sci*, Vol. 8, 123–142, 2005, www.massey.ac.nz/wwiims/research/letters.

Revision of the Plane Wave Expansion Method of 2D Photonic Crystals Using Complex Fourier Factorization

Roman Antos
Faculty of Math. & Phys., Institute of Physics, Charles University, Czech Republic

Abstract— The plane wave expansion method treating electromagnetic modes in photonic crystals have been the subject of extensive development for about twenty years, following optical research on diffraction gratings. In the case of discontinuous structures the method suffered from poor convergence properties until the discovery of the correct Fourier factorization principles. Those rules have then been successfully applied to anisotropic or slanted patterns, arbitrary reliefs, two-dimensional (2D) periodic structures, etc., and are also used for other (nonperiodic) applications. As regards 2D structures, however, considerable troubles appeared in the case of cylindrical elements for which Lifeng Li's zig-zag integration method was not convenient. For this purpose some authors created modification by treating independently the tangential and normal components of fields on the edges of the circular profiles of periodic elements. However, these approaches always dealt with linear polarizations and thus ignored the fact that the transformation matrix of polarization became discontinuous at some points of space, which slows down the convergence of calculations in some configurations. In this presentation, the theory is reformulated by introducing the complex Fourier factorization (CFF) method, which avoids the points of discontinuity of the polarization transformation by employing generally elliptical polarization bases, simply by using complex-valued Jones matrices. A brief description of the theory is provided, demonstrating the technique of calculation of optics in 2D periodic structures as well as the photonic band structures. The results of calculations employing the CFF method are compared with the previously demonstrated approaches with respect to the convergence properties, exhibiting the considerable improvement of the new method. The comparison is carried out for several samples of 2D structures made of various materials. It is also shown that for most practical purposes (e.g., when we are studying the tendency of the optical quantities while some parameter is varied, or for comparison with experiment affected by measurement errors) the new method provides sufficient precision for the maximum of Fourier harmonics retained inside the periodic medium being 4 (or less in some configurations), which considerably saves the computer memory and the time of calculations. It is worth pointing out that the essential difference between the CFF method and the previous Fourier factorization implementations is (from the mathematical viewpoint) the fact that the matrix transformation of polarization in the former method just contains complex-valued elements, so that this generalization is surprisingly simple.

Numerical Modelling of Multiple-scattering Problems in Periodic Media

J. Coatléven and P. Joly
INRIA Rocquencourt, France

Abstract— This work concerns time-harmonic multiple-scattering problems in periodic media. We show that one can solve exactly this problem by reducing computations to the union of bounded domains surrounding the scatterers, via the factorisation of a Robin-to-Robin operator.

Introduction: Our model equation is the Helmholtz equation in $\mathbb{R}^2$, where the medium $n(x) \in \mathbb{R}$ differs from a periodic medium in a finite union of small bounded regions Ω_j i.e.,:

$$-\Delta u - n^2\omega^2 u = f \quad \text{in } \mathbb{R}^2, \quad \mathit{supp}\ f \cup \mathit{supp}\ (n^2 - n_{ref}^2) \ \subset\ \cup_{i=1}^{N}\Omega_i,$$

where $n_{ref}(x) \in \mathbb{R}$ is a biperiodic function (the unperturbed medium). A natural idea is to restrict the computational domain to the Ω_j's, expressing the boundary conditions through Robin-to-Robin (RtR) operators, noted Λ, on the artificial boundaries $\partial\Omega_j$ $j = 1, \ldots, N$ ($\alpha \in \mathbb{R}$, $\beta \in i\mathbb{R}$):

$$\Lambda_{ij}\ :\ \varphi_j = (\alpha\tfrac{\partial u}{\partial n} + \beta u)_{|\partial\Omega_i} \quad\longmapsto\quad \psi_i = (\alpha\tfrac{\partial u}{\partial n} - \beta u)_{|\partial\Omega_i}, \quad \Lambda = (\Lambda_{ij})_{1\le i,\, j\le N}$$

Main Results: We generalize a property known for a homogeneous reference medium (see [3] or [2]): the solution u, outside the union of the Ω_j's, can be uniquely written as the sum of single scatterer exterior problems

$$\exists\,!\ (\widetilde{u}_j) \text{ such that } u = \sum \widetilde{u}_j \text{ and } -\Delta\widetilde{u}_j - n_{ref}^2\,\omega^2\,\widetilde{u}_j = 0 \quad \text{in } \mathbb{R}^2 \setminus \overline{\Omega_j}$$

The existence and uniqueness proof is based on the propagation operators:

$$\Theta_{ij}\ :\ \varphi_j = (\alpha\tfrac{\partial\widetilde{u}_j}{\partial n} + \beta\widetilde{u}_j)_{|\partial\Omega_j} \quad\longmapsto\quad \psi_i = (\alpha\tfrac{\partial\widetilde{u}_j}{\partial n} + \beta\widetilde{u}_j)_{|\partial\Omega_i}, \quad \Theta = (\Theta_{ij})_{1\le i,j\le N}$$

From this result, we deduce the factorization : $\Lambda = \widetilde{\Lambda}\cdot\Theta^{-1}$, where $\widetilde{\Lambda} = (\widetilde{\Lambda}_{ij})_{1\le i,j\le N}$ is the "decoupled scatterers" RtR operator :

$$\widetilde{\Lambda}_{ij} : \varphi_j = (\alpha\frac{\partial\widetilde{u}_j}{\partial n} + \beta\widetilde{u}_j)_{|\partial\Omega_j} \quad\longmapsto\quad (\alpha\frac{\partial\widetilde{u}_j}{\partial n} - \beta\widetilde{u}_j)_{|\partial\Omega_i},$$

The interest of this decomposition is that, for well chosen Ω_j's, the operators Λ and Θ can be decomposed using the solution of single scatterer problems computed with the method of [1].

Conclusion: We have reduced the computation of the multi-scattering RtR operator to the computation of several one-scatterer RtR operators. Numerical results will be presented at the conference.

REFERENCES

1. Fliss, S. and P. Joly, "Exact boundary conditions for time-harmonic wave propagation in locally perturbed periodic media," *Appl. Num. Math.*, doi:10.1016/j.apnum.2008.12.013, 2008.
2. Potthast, R. and F. Ben Hassen, and J. Liu, "On source analysis by wave splitting with applications in inverse scattering of multiple obstacles," *Journal of Computational Mathematics*, Vol. 25, No. 3, 266–281, 2007.
3. Grote, M. J. and C. Kirsch, "Dirichlet-to-Neumann boundary conditions for multiple scattering problems," *Journal of Computational Physics*, Vol. 201, 630–650, 2004.

Diffraction by Slanted Lamellar Gratings

S. Campbell[1], **R. C. McPhedran**[1], **L. C. Botten**[2], **and C. M. de Sterke**[1]

[1]IPOS, CUDOS, School of Physics, University of Sydney, Australia
[2]CUDOS, School of Mathematical Sciences, University of Technology, Sydney, Australia

Abstract— Modal methods are of interest in electromagnetic scattering theory because they permit highly accurate reference solutions to particular classes of problems, and because they may also give deeper insight into the mechanisms for striking diffraction effects. The method we describe here is a generalization of the familiar Kronig-Penney model from the quantum theory of the solid state to electromagnetic diffraction by dielectric or metallic (ideal orlossy) lamellar gratings, able to treat lamellae inclined at a general angle to the axis of periodicity [1, 2].

The method relies on expanding fields in modes in the grating region. The modes are in trigonometric form, and each explicitly obeys boundary and quasiperiodicity conditions, as long as their propagation constant satisfies a transcendental equation. They are set up for individual slices of the profile, and then are coupled together at interfaces between slices, taking into account the displacement of one slice to the next due to the grating slope. The result of a limiting procedure with the number of slices going to infinity is an expression for the transfer matrix $\mathcal{T}$ going from the bottom to the top of the grating:

$$\mathcal{T} = \exp(h\mathbf{M}), \quad \mathbf{M} = i\mu + \tan(\theta)\mathbf{M}_{as}. \tag{1}$$

Here, μ is a diagonal matrix containing propagation constants of modes in the unslanted grating, h is the grating thickness and θ is the slope angle of the lamellar grating. $\mathbf{M}_{as}$ is a matrix containing inner products giving the change of the modes to first order due to a displacement along the axis of periodicity. To complete the solution of the grating scattering problem, the fields above and below the grating are expressed as appropriate plane wave expansions, and coupled using the transfer matrix $\mathcal{T}$. We discuss here the case of classical incidence of light, but the method also has been generalized to conical incidence.

We comment on how the method is implemented, and how completeness of the truncated set of modes may be established in practice, even in the difficult and important case of gratings made up of metamaterials. We give examples showing that the method works well, even up to slant angles approaching 90°, where the lamellae are very close to being parallel to the grating periodicity axis (see Figs. 1 and 2). As is evident from Fig. 1(d), as the slant angle tends to 90°, the diffraction grating approaches a stack of thin films, and indeed its reflectance can be predicted accurately by homogenisation theory.

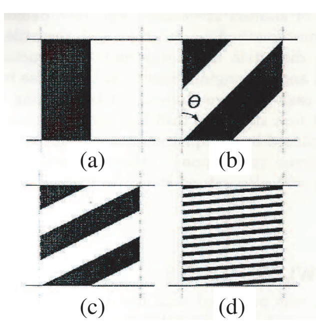

Figure 1: Schematic periods of slanted lamellar gratings for (a) no slant, (b) $\theta = 45°$, (c) $\theta = 63.4°$, (c) $\theta = 85.2°$.

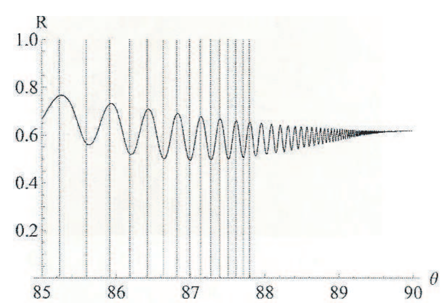

Figure 2: Energy reflected from a lamellar grating under normal incidence and E_z polarization versus slant angle for a mark-space ration of 0.5, refractive index contrast of 5 : 1, $\lambda/d = 1.1$ and $h/d = 0.5$. Angles where $\tan\theta$ increases by one are shown as vertical lines.

REFERENCES

1. Campbell, S., et al., *J. Opt. Soc. Am A.*, Vol. 25, 2415, 2008.
2. Foresti, M. and A. V. Tishchenko, *Proc. SPIE*, Vol. 6182, 61821G1-10, 2006.

Session 2P4
Electromagnetic Field in the Metamaterials and Dispersion Design of Cloaks and Photonic Crystals 1

No Maxwell Electromagnetic Wavefield Excited inside Cloaked Concealment and Broadband GL Cloaks

Jianhua Li, **Ganquan Xie**, **Lee Xie**, **and Feng Xie**
GL Geophysical Laboratory, USA

Abstract— For the point source located outside of the cloak, the 3D Global and Local field (GL) EM modeling method [1–3] has been used to simulate the 3D full EM wave field propagation through the cloaks. Our simulations and theoretical analysis in [1] verify the ideal cloak functions [4]. The EM wave field propagation outside of cloak does not penetrate into the concealment and never be disturbed by the cloaks. There are several papers to simulate the plane wave propagation through the cloak from outside of the cloak. The plane wave is excited by plane source which can not be located inside of the cloak or concealment. The cloak simulation of the point sources and the local sources inside of the cloak is lack in the published papers. The GL modeling simulations of the EM wave field through cloak and excited by the nonzero local sources inside of the cloak is presented in this paper. Moreover, by GL EM method simulation of the nonzero local sources inside of the concealment, we discover a phenomenon that **there is no Maxwell EM wave field can be excited by nonzero local sources inside of the cloaked concealment**. The phenomenon is proved by the GL method theoretical analysis and the EM integral equation [1–3]. Any EM field divorced from the Maxwell equation governing will be vanished or become an irregular chaos. The high frequency EM chaos field will hurt the health of the Human and damaged and shut down the EM devices and equipments working in the concealment. Therefore, the cloaked concealment will be dark hole or an EM chaos hazard area. By using the GL Meter Carlo inversion [5], we created a class of new GL cloaks to overcome the serious difficulty.

Our GL method is fully different from conventional methods for cloak and physical and science simulations. It has advantages over the conventional methods. The GL method consistent combines the theoretical analytical and numerical method together. In the GL modeling, there is no big matrix equation to solve and no absorption condition on artificial boundary to truncate infinite domain. The method is a significant physical scattering process. The finite inhomogeneous domain is divided into a set of small sub domains. The interaction between the global field and anomalous material polarization field in the sub domain causes a local scattering wave field. The local scattering wave field updates the global wave field by an integral equation. Once all sub domains are scattered, the wave field in the inhomogeneous anomalous materials will be obtained. Therefore, the GL method can be used to both of theoretical analysis and numerical simulation for physical and chemical phenomena and process. The GL EM modeling and inversion software are patented by GLGEO. This full paper is submitted to PRL.

REFERENCES

1. Xie, G., J. Li, F. Xie, and L. Xie, "Global and local electromagnetic modeling for simulation of the EM cloaks," submitted to *PRE* on 12/29/08.
2. Xie, G., F. Xie, L. Xie, and J. Li, *Progress In Electromagnetics Research*, PIER 63, 141–152, 2006.
3. Xie, G., J. Li, L. Xie, and F. Xie, *Acta Mathematicae Application Sinica*, Vol. 23, No. 2, 391–404, 2008.
4. Pendry, J. B., D. Schurig, and D. R. Smith, *Science*, Vol. 312, 1780, 2006.
5. Xie, G., J. Li, L. Xie, and F. Xie, *JEMW*, Vol. 20, No. 14, 1991–2000, 2006.
6. Chen, H., B. Wu, B. Zhang, and A. Kong, *PRL*, Vol. 99, 063903, 2007.
7. Cummer, S. A., et al., *Phys. Rev. E*, Vol. 74, 036621, 2006.
8. Argyropoulos, C., Y. Zhao, and Y. Hao, arXiv:0805.2050v1, 2008.

Design Rules for a Multilayer Fabry-Perot Narrow Band Transmission Filter Containing a Metamaterial Negative-index Defect

Heng-Tung Hsu[1], **Tzong-Jer Yang**[2], **and Chien-Jang Wu**[3]

[1]Department of Communication Engineering, Yuan Ze University, Chungli 320, Taiwan
[2]Department of Electrical Engineering, Chung Hua University, Hsinchu 300, Taiwan
[3]Institute of Electro-Optical Science and Technology, National Taiwan Normal University
Taipei 116, Taiwan

Abstract— In this work, we theoretically study the optical properties of a multilayer Fabry-Perot narrow band transmission filter containing a metamaterial negative-index defect. As in the usual Fabry-Perot filter design, the negative-index defect is sandwiched by two quarter-wave dielectric mirrors. Some useful design rules on selecting value of the negative-index of the defect have been numerically elucidated. Such narrow band transmission filtering is achieved when the refractive index of defect is either a negative integer if the thickness is taken as a quarter of design wavelength; or a negative odd integer if the thickness is taken as a half of design wavelength. Finally, the effect of loss in the metamaterial defect on the filtering feature is also investigated.

Scattering Field Interactions and Surface Plasmon Resonance in a Coupled Silver Nanocapsule

Yuan-Fong Chau[1] **and Tzong-Jer Yang**[2]

[1]Department of Electronic Engineering, Ching Yun University, Jung-Li 320, Taiwan, R.O.C.
[2]Department of Electrical Engineering, Chung Hua University, Hsinchu 300, Taiwan, R.O.C.

Abstract— Scattering field interactions and surface plasmon resonance (SPR) in a coupled silver nanocapsule (a silver nanosphere pair connected by a silver nanobar) are simulated by using the finite-element method, which includes the influences of near field enhancements of electric field by the width of silver nanobar in capsule as well as the polarizations of the incident wave. The proposed structures exhibit a red-shifted that can be tuned by varying the width of silver nanobar. Implications for surface-enhance Raman scattering and nano-optics are discussed in three-dimensional models. The evolution of SPR and nano-photonic device with the structural variations can be designed in a controlled manner.

Sub-wavelength Microwave Guiding on a Periodically Corrugated Metal Wire

Jin-Jei Wu[1], **Tzong-Jer Yang**[1], **and Linfang Shen**[2]

[1]Department of Electrical Engineering, Chung Hua University, Hsinchu 300, Taiwan, R.O.C.
[2]Department of Information Science and Electronic Engineering
Electromagnetic Academy, Zhejiang University, Zhejiang Province, Hangzhou 310027, China

Abstract— Guiding microwave on a periodically corrugated wire with the outer radius of sub-wavelength size is theoretically studied. The groves of the corrugated wire are filled in a high-permittivity dielectric material, and the strong field confinement of spoof surface plasmon polaritons (SPPs) is found even at frequencies smaller than the asymptotic frequency at which the SPP losses are quite low. In such wire structure, the sub-wavelength microwave guiding is shown to be available for a certain frequency range.

ACKNOWLEDGMENT

This work has been partially supported by NSC of Republic of China.

Microwave Equipment for Investigations of Metamaterials

I. A. Karpov and M. R. Trunin
Institute of Solid State Physics of RAS, Russia

Abstract— In this moment we develop new original experimental equipment for research of properties and measuring of performance for SHF metamaterial. This equipment enable control behaviour of electromagnetic SHF stream in outskirts of metamaterial product with predetermine step into polar coordinates. It's enable reconstruct image of electromagnetic SHF field in space around metamaterial product.

Measuring chamber of this equipment consist of two plane-parallel horizontal copper disks. In gap between these disks be situated a investigated metamaterial product. SHF radiation come in measuring chamber from SHF generator by waveguide megaphone, which be directed to metamaterial specimen. This metamaterial specimen be located in centre of measuring chamber. Magnitude of SHF field in space around a investigated specimen be analysed by antenna probe. This antenna probe to represent coaxial cable with vertical plane wire loop on their tip. This wire loop move by two stepping motor, which govern by computer. Antenna probe move along arc of circle as well as radial direction. It's enable lead measuring of SHF field inside measuring chamber into polar coordinates with predetermine step. Values of SHF field, which be measured by antenna probe, be transmited to SHF complex plane analyzer, which be connected to computer. On screen of this computer by special processing program form colored image of SHF field amplitude in space around investigated metamaterial specimen. Color of this image predetermine correspond with a magnitude of SHF field.

Thus this measuring equipment enable see on screen of computer a spatial image of magnitude of SHF field in surrounding metamaterial specimen space. This image is possible receive with some predetermine step, which it's possible change at every investigation within some range.

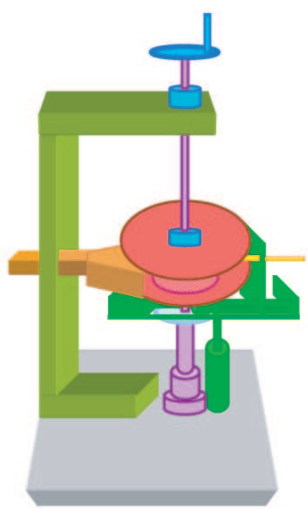

Surface Waves Suppression in a Biaxially Anisotropic Metamaterial Grounded Slab

Salma Mirhadi and Manoochehr Kamyab Hessari
Department of Electrical Engineering, K. N. Toosi University of Technology, Tehran, Iran

Abstract— In this paper, we have investigated specific conditions for the suppression of transverse electric (TE) and transverse magnetic (TM) surface waves in a biaxially anisotropic metamaterial grounded slab. Some recent publications have dealt with the surface wave suppression in an isotropic metamaterial grounded slab [1, 2]. However, the left handed media (LHM) that have been made are actually anisotropic because the realization of 3D isotropic artificial left handed (LH) structures may be difficult [3, 4]; therefore, it is important to investigate suppression of surface waves in an anisotropic grounded slab.

We have studied conditions that ensure the absence of surface modes in a biaxially anisotropic grounded slab and shown that the suppression of entire surface modes can occur only in the anisotropic metamaterial grounded slab. Ordinary and evanescent surface waves, which evanescent only in the air and both in the air and inside the slab respectively, are considered for TE and TM polarizations. On the basis of the graphical solution of dispersion equations, we have presented conditions which surface waves are eliminated. Consequently, this structure may be useful as a substrate for planar antennas. We have shown that the suppression of surface waves in this structure is greatly dependent on the tensor components of the constitutive parameters, height of slab and operating frequency.

REFERENCES

1. Baccarelli, P., P. Burghignoli, F. Frezza, A. Galli, P. Lampariello, G. Lovat, and S. Paulotto, "Fundamental modal properties of surface waves on metamaterial grounded slabs," *IEEE Trans. Microwave Theory Tech.*, Vol. 53, No. 4, 1431–1442, 2005.
2. Baccarelli, P., P. Burghignoli, G. Lovat, and S. Paulotto, "Surface-wave suppression in a double-negative metamaterial grounded slab," *IEEE Antennas Wireless Propag. Lett.*, Vol. 2, No. 19, 269–272, 2003.
3. Hudlicka, M., J. Machac, and I. S. Nefedov, "A triple wire medium as an isotropic negative permittivity metamaterial," *Progress In Electromagnetic Research*, PIER 65, 233–246, 2006
4. Sliveirinha, M. G. and C. A. Fernandes, "Homogenization of 3-D-connected and nonconnected wire metamaterials," *IEEE Trans. Microwave Theory Tech.*, Vol. 53, 1418–1490, 2004.

Localisations and Perfect Lensing: GRIN Modelling in LHM (Part 2)

Philip Ingrey
Department of Applied Mathematics, University of Nottingham
University Park, Nottingham, NG7 2RD, United Kingdom

Abstract— Recently [1] we investigated analytically the novel electromagnetic effects caused by a smooth transition of refractive index confined to a thin interfacial layer between bulk rightand left handed media with indices $n = +1$ and $n = -1$ respectively. The inhomogeniety causes a significant localization of the field that within the layer which affects the transmission properties if the bulk LHM is dissipative. The substantial implications of this model for the resolving power of a slab of lefthanded media with imperfect boundaries that are described by these inhomogeneous layers is discussed in the present paper.

This paper is principally concerned with the layers' effect on evanescent modes which are required for the enhanced resolution properties of the 'perfect lens'. The localizations are manifested by steep gradients in the field. Consequently those modes whose component of the wavenumber parallel to the interface is large compared with reciprocal of the layer width will dissipated anomalously if the LHM is lossy, and this have an enhanced and detrimental effect on the resolution.

The resolving capacity of the lens as a function of the layer thickness is quantified for different values of the loss in the bulk medium. The effect of the layers is qualitatively similar to a LHM lens with perfect surfaces but with a nonlinearly enhanced loss. Indeed, until such time that losses $\sim 10^{-5} - 10^{-6}$ can be attained by improved materials science methods, it will be shown that the quality of the lens' boundaries will be vitally important to the recovery of evanescent modes.

REFERENCES

1. Ingrey, P. C., K. I. Hopcraft, E. Jakeman, and O. French, "Between right and left handed media," *Opt. Commun.*, Vol. 5, 282, 2009.

Almost Complete Absorption of Light in Nanostructured Metallic Coatings: Blackbody Behavior

V. G. Kravets, F. Schedin, and A. N. Grigorenko
Department of Physics, University of Manchester, M13 9PL, Manchester, UK

Abstract— Blackbody surfaces are of increasing importance in many fields of science and modern technologies. One of the most promising applications of the blackbody coatings is in the field of photothermal and photoelectrical conversion of the solar energy, where they could considerably increase the effectiveness of solar cells. In this work we experimentally demonstrate plasmonic "blackbody" based on deep diffraction gratings made of extremely thin and robust gold films deposited on Poly-methyl-methacrylate (PMMA) nanostripes. By "blackbody" in this work we imply an object which strongly absorbs light in a wide spectral and angle range demonstrating blackbody-like behavior. We demonstrate that plasmonic structures consisting of gold stripes combined with PMMA stripes exhibit almost complete wide-angle absorption over a broad spectral range in visible spectrum important for solar cell operation. This behavior is recorded over a wide optical wavelength range (240–550 nm) and for a broad range of angles of light incidence (0–75°) for samples with metal thickness of just 90 nm. The strong absorption at a level of 97–99% is observed for one light polarization and is attributed to excitation of localized plasmons coupled to incident light waves. We found that polarization and periodicity (grating geometry) play key roles in determining the optical characteristics of the one-dimensional refractory metallic coatings. It was shown that for the gold stripes the reflection totally vanishes for the light with electric vector perpendicular to the stripes in the spectral region 240–550 nm while the reflection for the other polarization is analogous to that from the plain gold film. We also found that the reflection and transmission spectra in uv and visible range can be controlled by adjusting the width of the gold nanostripes which can be useful for device applications.

We observe the absence of reflection at some angle of incidence (Brewster-like effect) for reflection of both p- and s- polarized waves. Significant birefringence indicates the potential usefulness of a deep metallic sub-wavelength grating as a reflection polarizer. The reflection and transmission spectra of the gold stripes were interpreted using the effective-medium approximation. This theory confirms blackbody-like behavior and provides satisfactory qualitative description of the optical response of the studied system.

Theoretical Studies on Wired-based Metamaterials and Its Application in Spatial Beam-Splitter Design

Ruey-Bing Hwang[1] **and Song-Tsuen Peng**[2]

[1]Department of Communication Engineering, National Chiao-Tung University
Hsinchu, Taiwan, R.O.C.
[2]Department of Communication Engineering, Yuan-Ze University
Chung-Li, Taiwan, R.O.C.

Abstract— Metamaterials are mostly artificially engineered structures that are synthesized by embedding specific inclusions, such as periodic structures, in a host medium. Recently, a rich variety of periodic structure has been reported to exhibit extraordinary phenomena, such as negative refraction, and the effective medium and equivalent-circuit models were proposed to explain their physical mechanism. In contrast to the approximated approach described previously, in this work, we employed the rigorous mode-matching method incorporating the Floquet-Bloch theorem to analyze the propagating characteristics in a two-dimensionally (2D) metallic periodic structure. Specifically, the effective refractive index can be rigorously determined from the phase relation. The structure under study consists of an array of 2D metallic rods of square cross-section, arranged in a square-lattice pattern and embedded in metallic parallel plates. The numbers of metallic rods along the x- and y-direction are both 6. The periods along the x- and y-direction are both 15 mm. Each of the square metallic rods has the width 2.36 mm. The distance from the edge of the metamaterial to that of the metal plate is 30 mm. The structure is fed by a coaxial probe with its center conductor extending into the parallel-plate region. We first synthesized a metamaterial having effective refractive index smaller than unity, shown in Fig. 1(a). The largest circle represents the phase relation of wave propagating in the air with $n_{eff} = 1$, while the others, with the operational frequency attached, are those for $n_{eff} < 1$. From Snell's law, we know that the wave propagating from a medium with $n_{eff} \ll 1$ into the air tends to be normal to the interface between the two media, forming a quasi plane-wave. After guiding those waves into each of the flared openings, we could obtain four directional beam patterns along respective directions. In addition to the phase relation, we also calculated the Poynting vector distribution within the structure, depicted in Fig. 1(b). To verify the theoretical results, we measured the pattern of radiation from the source of excitation, as shown in Fig. 1(c). Apparently, the measured results are in an excellent agreement with that obtained by the numerical simulation based on the time-domain finite integration method.

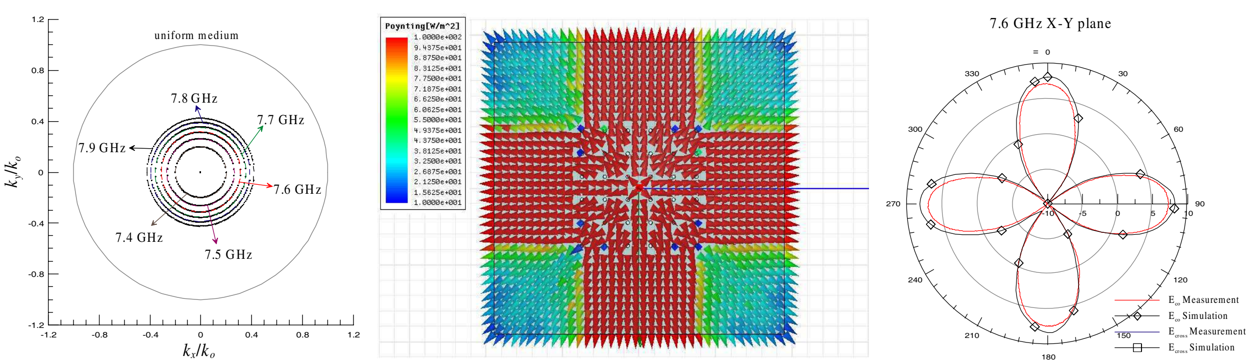

(a) (b) (c)

Effects of Array Dimensions on the Resonance Characteristics of SRR Type Metamaterial Arrays with Small Sizes: Simulations and Experiments

E. Ekmekci[1,2], **K. Topalli**[1], **T. Akin**[1], **and G. Turhan-Sayan**[1]

[1]Department of Electrical and Electronics Engineering
Middle East Technical University, Ankara, Turkey
[2]Department of Electronics and Communication Engineering
Suleyman Demirel University, Isparta, Turkey

Abstract— The SRR (Split Ring Resonator) is a commonly used magnetic resonator, which shows negative values of effective permeability over a certain frequency band around its resonance frequency. It has been discussed in various studies that two dimensional periodical arrays of SRRs with large array sizes have wider stop bandwidths and lower transmission magnitudes around their resonance frequencies as compared to the single SRR unit cell. In this paper, effects of array dimensions on the resonance parameters are investigated in more detail especially for small sized arrays as various applications reported in literature makes use of one or two dimensional SRR arrays of very small sizes. In this work, it is experimentally demonstrated that increasing the array size in one dimension only as opposed to both dimensions has different effects on the widening of the bandwidth and on the depth of resonance curve.

The SRR unit cell and the SRR arrays used in experiments are fabricated at METU MEMS Center Fabrication Facilities with 100 Å/0.5 µm Ti/Au patterned with lithography on a 4″ glass substrate having a thickness of 500 µm and relative permittivity of 4.6 with a loss tangent of 0.01. For the experimental procedure, the samples are placed in an X-band waveguide and the transmission characteristics (i.e., the S_{21} spectra) are measured by Agilent 8720D network analyzer using TRL calibration. The experimental observations are found in very good agreement with the results of the full wave HFSS simulations.

A Novel Dual-band Metamaterial Structure

E. Ekmekci[1,2] and G. Turhan-Sayan[1]

[1]Department of Electrical and Electronics Engineering
Middle East Technical University, Ankara, Turkey
[2]Department of Electronics and Communication Engineering
Suleyman Demirel University, Isparta, Turkey

Abstract— The conventional SRR (Split Ring Resonator) and SR (Spiral Resonator) are well-known metamaterial topologies providing negative values of effective permeability over a bandwidth around a certain resonance frequency, which is determined by the geometrical parameters and the material properties used in the magnetic resonator design. In this paper, we propose a novel metamaterial structure having magnetic resonances at two different frequencies and hence providing negative effective permeability values over two separate bandwidths. A periodical array of this dual-band magnetic resonator structure can be easily combined with an array of thin wires to obtain an effective left-handed medium offering unusual properties such as negative refractive index, negative Doppler effect, and negative Vavilov-Cerenkov effect over two distinct frequency bands.

The metamaterial unit cell topology to be introduced in this paper is made of a single loop of conducting strip printed over a dielectric substrate with the special winding geometry as shown in the figure below. Transmission and reflection spectra (i.e., S_{21} and S_{11} parameters versus frequency) of this unit cell are simulated using the Ansoft's HFSS software to observe its resonance frequencies. Then, the effective permeability (μ_{eff}) and effective permittivity (ε_{eff}) curves are retrieved from the already computed complex S-parameters to demonstrate the presence of two distinct negative permeability bandwidths. The results clearly show that this novel structure can be a very useful alternative to the ordinary SRR and SR structures especially when a dual band operation is needed.

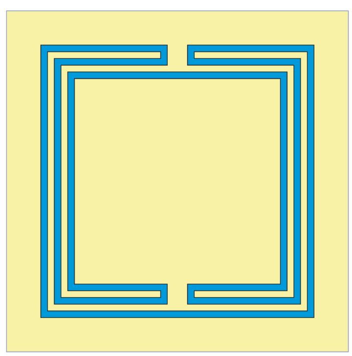

Figure 1: The unit cell topology for the suggested dual-band metamaterial.

The Effect of TEM in Generation of Earthquake Associated with Geological Engineering

Alireza Bayat[1], **H. Ghafori Fard**[2], **and Abolfazl Taherpour**[3]

[1]Communication Eng. Department, Imam Khomeini International University, Iran
[2]Electrical Eng. Department, Imam Khomeini International University, Iran
[3]International Institute of Earthquake Engineering and Seismology, Iran

Abstract— In this paper, the authors is explaining a new method of phenomena of earth quick; due to creation of electromagnetic fields which is owing to the strong negative charged clouds near the surface of earth that in turn form a closed loop circuit with volume charge density of earth. Critical angles & Brewster angles should also be taken into account (1). The effect of vertical polarization regarding to the geology engineering and sounds in the fault which is indicative of earthquake, should be considered as well.

The connection between clouds and earthquake faded from view after 1985. Zhanglao has predicted earthquake since June 20, 1990, when he observed a long line shaped cloud with a tail pointing in the North West direction, 18 hours later, a magnitude 7.7 Richter earthquakes struck Iran and killed and injured so many people (2). One of the authors observed some dark clouds very close to the surface of the earth about 8 to 10 hour before occurrence of the earthquakes at the Alamut zone on 2004 in Iran, which has been occurred. About 8 to 10 hours before the earthquake on Alamut area, there was emission of TEM waves; which was due to the interaction of earth magnet and charged cloud near the surface of earth.

Authors believed according to data collected, that some relations between the emissions of TEM waves and created sound in the inner layers of the earths and space exists. Of course, in earthquake the created sounds and fault depends on the permeability and permittivity of the earth. So with different angle of emission of TEM waves critical angles will be created. Gathering of highly charged clouds near the surface of earth and transferring energy in to earth a closed loop of magnetic flux density will be formed, so changing the behavior of animals before occurring earthquake (8 to 10 hours before occurrence of earthquake). Therefore created TEM waves will polarize the animals blood, and some eventuation can be taken in to account that existence of TEM waves will irritate animals prior to Earthquake.

Localisations and Perfect Lensing: GRIN Modelling in LHM (Part 1)

Philip Ingrey
Department of Applied Mathematics, University of Nottingham
University Park, Nottingham, NG7 2RD, United Kingdom

Abstract— In manufacturing lefthanded media (LHM) the interfaces will never be perfect; roughness, manufacturing faults and other disturbances to interfaces are unavoidable. We recently [1] reported results from an analytical model for a diffuse or nonperfect boundary between rightand lefthanded media. This model characterises these boundaries as a gradedindex change from one medium to the next for which a fullwave analytical solution to Maxwell's equations can be obtained. The gradedindex profile used is one where the change in refractive index is represented as a linear transition between the media with the addition of a discontinuity at a point within the transitional region to encapsulate rapid changes in the refractive index.

This model accounts for smooth changes of permittivity and permeability across a diffuse boundary between bulk rightand lefthanded metamaterials. A fullwave, exact analytical solution to this problem leads to a strong localisation of the field in the transition region whilst being fully transmissive to the radiation. This localisation has a positive exponential dependence on the layer width. In the lossy case the strong localisation is removed and a reflected wave then exists. If the layer contains a discontinuity in the refractive index profile, then the qualitative features of the lossless case are restored. In all cases it is possible to analytically quantify the reflected and transmitted wave properties.

The reason for the localization in the layer is the constructive interference of evanescent modes that are stimulated whenever $|n| < \sin(\theta)$. It should be stressed that these modes are not a conventional plasmon mode which is generated by a discontinuous change in the refractive index. Rather, they are a volume effect caused by the coherent addition of a plasmon and an antiplasmon throughout the region of the metamaterial for which $|n| < \sin(\theta)$.

The effect of the localizations on a slab of LHM in terms of the resolving power of a perfect lens is discussed in an accompanying paper. Practical applications of this model include extending the graded index approach, of modelling surface roughness as a graded index change, to include magnetic and lefthanded materials. Also, since the solution contains the polarizationstate of the wave the approach can be used to investigate, for example, the emission polarization effects of infrared radiation, from lefthanded media. Other applications include further polarization effects, such as the Brewster angle, and to analyse how superlensing properties are sensitive to the polarization state and by roughness of the lens surfaces.

REFERENCES

1. Ingrey, P. C., K. I. Hopcraft, E. Jakeman, and O. French, "Between right and left handed media," *Opt. Commun.*, Vol. 5, 282, 2009.

Session 2P5
Novel Mathematical Methods in Electromagnetics 1

RCS of a Finite Parallel-plate Waveguide with Four-layer Material Loading

E. H. Shang[1], **J. P. Zheng**[2], **and K. Kobayashi**[3]

[1]Japan Radio Co., Ltd., Japan
[2]Panasonic R&D Center China Co., Ltd., China
[3]Chuo University, Japan

Abstract— The analysis of electromagnetic scattering by open-ended metallic waveguide cavities has received much attention recently in connection with the prediction and reduction of the radar cross section (RCS) of a target. Various diffraction problems involving two- and three-dimensional cavities have been analyzed thus far based on high-frequency techniques and numerical methods. However, the solutions obtained by these methods may not be uniformly valid for arbitrary cavity dimensions.

In this paper, we shall consider a finite parallel-plate waveguide with four-layer material loading as a canonical geometry that can form cavities, and analyze the plane wave diffraction for both E and H polarizations using the Wiener-Hopf technique. The geometry of the waveguide is shown in Fig. 1, where ϕ^i is the incident field of E or H polarization, and the waveguide plates are infinitely thin, perfectly conducting, and uniform in the y-direction. The material layers I ($D_1 < z < D_2$), II ($D_2 < z < D_3$), III ($D_3 < z < D_4$), and IV ($D_4 < z < D_5$) are characterized by the relative permittivity/permeability (ε_m, μ_m) for $m = 1, 2, 3,$ and 4, respectively. A rigorous Wiener-Hopf analysis is carried out and efficient solutions valid for the waveguide length large compared with the incident wavelength are explicitly obtained. Illustrative numerical examples of the RCS are presented for various physical parameters, and the far field scattering characteristics of the waveguide are discussed in detail. Main results of this paper are published in [1–4].

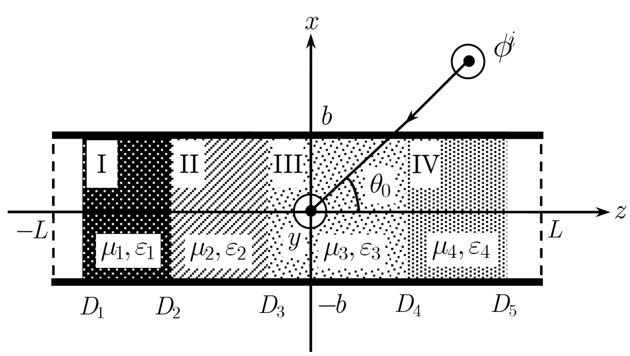

Figure 1: Geometry of the waveguide.

REFERENCES

1. Zheng, J. P. and K. Kobayashi, "Plane wave diffraction by a finite parallel-plate waveguide with four-layer material loading: Part I — the case of E polarization," *Progress In Electromagnetics Research B*, Vol. 6, 1–36, 2008.
2. Shang, E. H. and K. Kobayashi, "Plane wave diffraction by a finite parallel-plate waveguide with four-layer material loading: Part II — the case of H polarization," *Progress In Electromagnetics Research B*, Vol. 6, 267–294, 2008.
3. Shang, E. H., "Radar cross section analysis of parallel-plate waveguides with material loading," Ph.D. Dissertation, Chuo University, Tokyo, March 2009.
4. Zheng, J. P., "Wiener-Hopf solutions of canonical, two-dimensional scattering problems," Ph.D. Dissertation, Chuo University, Tokyo, March 2009.

H-Polarized Plane Wave Diffraction by a Semi-Infinite Parallel-Plate Waveguide with Sinusoidal Wall Corrugation

J. P. Zheng and K. Kobayashi
Chuo University, Japan

Abstract— In microwave and optical engineering, there are many devices with periodic structures including resonators, filters, and couplers composed of gratings as well as reflector antennas. Therefore the analysis of the scattering by periodic structures is an important subject in electromagnetic theory and optics. Various analytical and numerical methods have been developed thus far and the diffraction phenomena have been investigated for a number of periodic structures. However, there are only a few treatments of the diffraction by periodic structures using rigorous function-theoretic methods. In the previous paper [1], we have considered a semi-infinite parallel-plate waveguide with sinusoidal wall corrugation, and solved the E-polarized plane wave diffraction using the Wiener-Hopf technique combined with the perturbation method. The same diffraction problem has been analyzed for the H-polarized plane wave incidence by Chakrabarti and Dowerah [2] following a method similar to that developed in [1]. However, the analysis presented in [2] is incorrect from a mathematical point of view.

In this paper, we shall reconsider the problem solved by Chakrabarti and Dowerah [2], and analyze the H-polarized plane wave diffraction by a semi-infinite parallel-plate waveguide with sinusoidal wall corrugation using the method established in our previous paper [1]. The geometry of the problem is shown in Fig. 1, where ϕ^i is the incident field of H polarization. The surface of the waveguide plates is assumed to be infinitely thin, perfectly conducting, and uniform in the y-direction, being defined by $x = \pm b + h \sin mz \, (z < 0)$, where m and h are positive constants. Assuming that the corrugation amplitude $2h$ is small compared with the wavelength, the original problem is replaced by the problem of diffraction by a flat, semi-infinite parallel-plate waveguide with an impedance-type boundary condition. Introducing the perturbation series expansion of the scattered field and taking the Fourier transform of the Helmholtz equation, the problem is formulated in terms of the zero- and first-order Wiener-Hopf equations by application of the approximate boundary condition. The Wiener-Hopf equations are solved via the factorization and decomposition procedure leading to the exact solution. The scattered field inside and outside the waveguide is evaluated analytically by taking the inverse Fourier transform and applying the saddle point method. Numerical examples of the scattered far field are presented, and the scattering characteristics of the waveguide are discussed in detail.

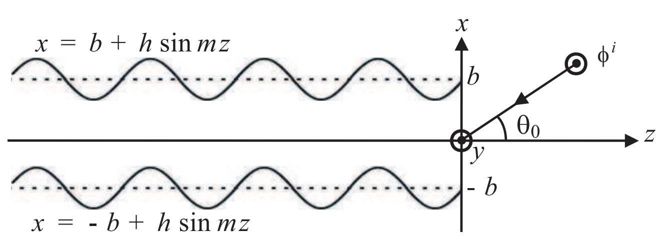

Figure 1: Geometry of the problem.

REFERENCES

1. Zheng, J. P. and K. Kobayashi, "Diffraction by a semi-infinite parallel-plate waveguide with sinusoidal wall corrugation: Combined perturbation and Wiener-Hopf analysis," *Progress In Electromagnetics Research B*, Vol. 13, 75–110, 2009.
2. Chakrabarti, A. and S. Dowerah, "Traveling waves in a parallel plate waveguide with periodic wall perturbations," *Can. J. Phys.*, Vol. 62, 271–284, 1984.

Analytical Regularization Approach to Solve MPIE for Axially Symmetrical Strip-like Surface

Fatih Dikmen, Hüseyin Yiğit, and S. Sinan Başer
Electronics Engineering Department, Gebze Institute of Technology
41400 Çayırova Gebze/Kocaeli, Turkey

Abstract— The set of diffraction problems that can be solved in mathematical rigor and with numerical efficiency by the establishment of Analytical Regularization (AR) is presented in [1]. In [2] basic steps to the AR approach that is related to its application to the considered problem can be found. The formulation of the Magnetic Potential Integral Equation (MPIE) in context of this paper is similar to one explained in [3]. It involves solution of the boundary value problem (BVP) by expressing the classical magnetic vector potential and electric scalar potential on the perfectly electrically conductive boundary of the smooth axially symmetrical strip-like open surface (Figure 1) which leads us to classical MPIE. The concerning formulation will be given on orthogonal coordinates presenting the generalization possibility of the method used. The canonical integral equation pair including free-constants (1) is met in production of final algebraic system. Representing the terms in (1) by their Fourier-Chebyshev expansions lead to an algebraic system of the first kind subject to AR. Here free-constants A and B to be determined by the edge condition of the normal to strip-edge component of the surface current vector, emerge from the homogenous solution part (that is particularly represented through $\Phi^{([1,2]\pm)}(u)$ in (1)) of the inhomogeneous Helmholtz-like equation that scalar potential satisfies on S. In (1) $K_{1,2}(u,v)$ are functions continuous up to their second derivatives and first mixed derivative.

$$\begin{aligned}
&\int_{-1}^{1}\left[\left\{-\frac{1}{\pi}\ln|u-v|+K_1(u,v)\right\}z_1(v)+K_2(u,v)\,z_2(v)\right]dv\\
&=b_1(u)+A\Phi^{1+}(u)+B\Phi^{1-}(u)\,,\ u\in[-1,1]\\
&\int_{-1}^{1}\left[-K_1(u,v)\,z_1(v)+\left\{-\frac{1}{\pi}\ln|u-v|+K_2(u,v)\right\}z_2(v)\right]dv\\
&=b_2(u)+A\Phi^{2+}(u)+B\Phi^{2-}(u)\,,\ u\in[-1,1]
\end{aligned}\tag{1}$$

Under any excitation that is given through $b_{1,2}(u)$, having the BVP reduced equivalently to an algebraic system of the second kind by using relevant AR based on [2], the Fourier-Chebyshev coefficients for tangential and normal to the strip-edge components of surface current vector appearing through $z_{1,2}(v)$ in MPIE can be retrieved. Then near and far fields can be constructed using those currents as very well-known [4].

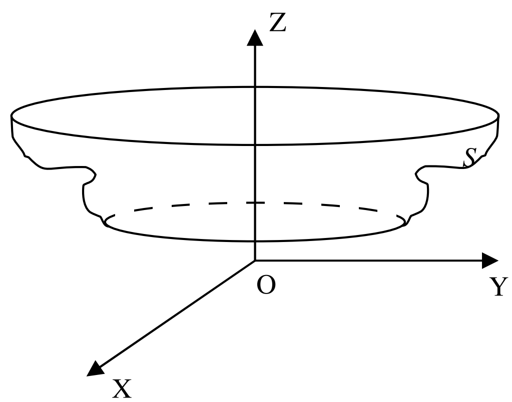

Figure 1.

REFERENCES

1. Poyedinchuk, A. Ye., Yu. A. Tuchkin, and V. P. Shestopalov, "New numerical — Analytical methods in diffraction theory," *Mathematical and Computer Modeling*, Vol. 32, 1029–1046, 2000.
2. Tuchkin, Y. A., E. Karaçuha, and F. Dikmen, "Scalar wave diffraction by perfectly conductive infinitely thin circular ring," *Elektrik, Turkish Journal of Electrical Engineering and Computer Science*, TUBITAK Doga Series, Vol. 9, No. 2, 199–220, 2001.
3. Zakharov, E. V. and Yu. V. Pimenov, *Numerical Analysis of Radio Waves (in Russian)*, Radio i Sviaz' Publishing House, Moscow, 1982.
4. Balanis, C. A., *Advanced Engineering Electromagnetics*, John Wiley & Sons, 1989.

Improving the Absorbing Boundary Condition in a 3D Maxwell's Equation Solver

F. Assous
Ariel University Center, Ariel 40700, Israel

Abstract— The numerical solution of time-dependent Maxwell's equations in a unbounded domain requires the introduction of artificial absorbing boundary conditions (*ABCs*) designed to minimize the amplitude of the parasitic waves re ected by the artificial frontier of the domain of computation. In [1], a P^1-conforming finite element method for the time-dependent three dimensional Maxwell equations was proposed. Particular attention was paid on a correct account of the divergence constraints on the electric and magnetic fields, in view of coupling this method with a particle approximation of the Vlasov equation. The applications we had in mind dealt with electron beam propagation, hyperfrequency vacuum devices, etc.... However, the method proved to be also worthwhile in pure electromagnetic wave propagation problems like radar problems. Nevertheless, the *ABC* implemented in the code was of the first order. So, there was a need in improving it in order to apply the code in pure electromagnetic context.

To construct *ABCs* which lead to a well-posed problem (from a mathematical point of view), and to a stable algorithm (from a numerical point of view), often needs to a rigourous mathematical and numerical analysis. In a previous study, Joly et al. [2] have proposed a new second order *ABC* for the Maxwell's equation in dimension 3, that is particularly well-adapted to a finite element formulation. In this approach, this can be viewed as an alternative to the famous Beranger condition.

The aim of this paper is to present how to apply this second-order *ABC* in the framework of our finite element method. A first question is to verify the stabilty of this condition expressed in the context of our formulation. Then it is necessary to derive the new variational formulation. Afterwards, the problem of the implementation in a finite element 3D code, based on a Taylor-Hood method of approximation, has to be addressed.

Our paper will be organized as follows. After a brief recall of the expression and of the properties of the *ABC*, we will show an efficient way to include it in a finite element approach. Finally, numerical results will be shown to illustrate the feasibility and the accuracy of this method.

REFERENCES

1. Assous, F., P. Degond, E. Heintze, P. A. Raviart, and J. Segré, "On a finite-element method for solving the three-dimensional Maxwell equations," *J. Comput. Phys.*, Vol. 109, 222, 1993.
2. Joly, P. and B. Mercier, "A new second order absorbing boundary condition for the Maxwell's equation in dimension 3," INRIA Res. Report, 1047, 1989.

Parallel Power Grid Analysis Using Sensitivities

A. Korobkov, **W. Au**, **L. Yang**, **and V. Subramanian**
Sun Microsystems Inc., USA

Abstract— Design and analysis of on-chip power distribution network are extremely important to ensure the reliable and fully functional product. Growing chip size and complexity makes power network analysis a very challenging task, where the traditional methods such as parasitics level time domain circuit simulation of the entire design does not work. In this paper, we propose an efficient power network simulation method for extremely large scale processor design with tens of millions devices. We present a new technique designed to partition power distribution network into the smaller clusters, and to determine current locality shell size for each cluster using sensitivity analysis, such that each shell can be simulated independently in multiple threads taking advantage of the modern CMT (Chip MultiThreading) processor architecture. In order to improve simulation performance we employ "divide and conquer" approach by partitioning a sparse vector of current sources representing a current drawn from the power network by MOSFET devices, into the set of subvectors according to the order created by linear solver. Then we construct a dependency graph of state variables representing a voltage drop at the network nodes using a symbolic representation of the lower triangular part of linear circuit matrix and a subvector of current sources. Finally, we identify a locality shell associated with each subvector of current sources using worst case sensitivity analysis, to further reduce the number of variables within a partition. Forward and backward substitution are performed independently in parallel within a linear solver for each partition, due to the the known variables interdependency and locality effect. The method is scalable with the number of parallel threads, and we have demonstrated an impressive performance improvement over the conventional single thread transient simulation, when applied to the UltraSparc power network design.

Diffraction of a Waveguide Mode in a Nanowire

V. G. Bordo
NanoSYD, Mads Clausen Institute, University of Southern Denmark, Denmark

Abstract— Despite recent progress in fabrication and investigation of submicron-sized optical fibers known as nanowires or nanofibers, the lack of theory which could describe their optical response adequately prevents from fundamental understanding of experimental results. Although diffraction in a nanowire can be calculated numerically, such an approach does not allow comprehensive analysis of the problem.

In the present talk, the rigorous theory of reflection and diffraction of a waveguide mode at the end of a semi-infinite dielectric circular cylinder is developed. The theory assumes an arbitrary ratio between the cylinder radius and the wavelength and hence it can be used for the description of the nanowire optical properties. An exact solution of this problem is found by the use of fictitious electric and magnetic current sheets located at the end of the cylinder. The solution has the form of the Fourier integral along the integration path in the complex plane of propagation constants. Deforming this path, one obtains either the field reflected from the nanowire end or the diffracted field in the outer space. The case when the incident wave is a TM or TE waveguide mode is analyzed in detail. It is shown that the polarization of the electromagnetic field is not changed upon reflection and its amplitude is zero in the far-field limit.

The extension of this approach to the case of a nanowire of a finite length is also discussed. The normal modes of such a resonator which are analogs of the Fabry-Pérot modes dictate possible wavelengths of nanolaser generation.

Nonlinear Time Series Analysis of the Ionospheric Measurements

Victor A. Eremenko and Natalia I. Manaenkova
Institute of Terrestrial Magnetism, Ionosphere and Radio Wave Propagation (IZMIRAN)
Troitsk 142190, Moscow Region, Russia

Abstract— The tools of nonlinear time-series analysis have been applied to the ionospheric measurements, obtained by modern digital high-precision ionosonde "Parus", created at IZMIRAN. We examine small-scaled structure of the electron density N_e at F-region of ionosphere by exploring time-series of the observable of reflected HF radio wave, corresponding to not perturbed day ionograms.

Nonlinear time series analysis has been developed for the study of data sets of physical observable, whose dynamics exhibits chaotic behavior. For forced, dissipative systems the low-dimensional chaotic dynamics is often associated with the presence of a strange attractor in the system phase space. The various methods provide to estimate properties of the attractor such as the correlation dimension D_2 (lower estimation of the fractal dimension D); the K_2-entropy (estimation of the Kolmogorov entropy), the spectrum of Lyapunov exponents. Estimation of the fractal dimension D allows us to determine the number of effective degrees of freedom, or dimension of the system ionosonde-ionosphere.

In order to avoid the spuriously low estimate of dimension we have examined large enough data sets, using not only Grassberger and Procaccia's algorithm of calculation D_2, K_2, but J. Theiler's modification of standard algorithm, depending of the autocorrelation time.

Reliability of the estimations was confirmed by applying to data sets the test of time-separation.

In order to distinguish low-dimensional dynamics from stochastic processes, it is useful to consider the stochastic surrogate signals obtained by inverting a power spectrum exactly equal to that of the signal under study and random, independent and uniformly distributed Fourier phases. Analysis of the surrogate data and calculation of the largest Liapounov exponent $\lambda_{\max}$ were employed. It is well-known, that $\lambda_{\max} \approx K_2$. A positive $\lambda_{\max}$ does not constitute, by itself, convincing evidence of low-dimensional chaos, since random signals are also known to yield $\lambda_{\max} > 0$. $\lambda_{\max}$ for a deterministic system is expected to increase, when the dimensionality of the embedding space is reduced, as the attractor occupies a larger "portion" of available space. For our time series: $\lambda_{\max} \approx 0.008$ for $n > 15$; for $n = 7$, $\lambda_{\max} = 0.016$ and for $n = 3$, $\lambda_{\max} = 0.029$. This behavior is quite distinct from what is observed for a random signal.

For low-dimensional chaos there are well-known numerical techniques for constructing nonlinear predictive model directly from time series. For example, there is the method of constructing short-term predictors of Farmer and Sidorowich, so-called "method of nearest neighbors". To predict $X(t+T)$ for time-series $\{X(t_i)\}, i = 1, \ldots, N$, we make local first-order linear approximation, using only K neighboring points. Simple formulae $T_{\max} = 1/K_2 \ln(1/\varepsilon)$ clear up, that maximum time of reliable prediction of investigated parameter is limited. $T_{\max}$ is defined by the value of $K_2(D_2)$ and the accuracy ε of data measurements or computations of the corresponding ionosphere parameters.

Born-Infeld Non-linear Electrodynamics and String Theory

S. V. Ketov
Tokyo Metropolitan University, Japan

Abstract— Born-Infeld electrodynamics is the particular non-linear generalization of Maxwell electrodynamics. The well known remarkable features of the Born-Infeld electrodynamics include (i) its invariance under (Dirac) electric-magnetic duality, (ii) absence of dichroism, and (iii) existence of solitonic solutions. In addition, the Born-Infeld electrodynamics arises as the low-energy effective action of open strings, and as part of the world-volume effective action of D3-branes (string solitons). I describe an $N = 1$ supersymmetric generalization of the Born-Infeld action, and its physical significance as the Nambu-Goldstone-type action associated with partial spontaneous supersymmetry breaking, $N = 2$ to $N = 1$, in a 4-dimensional spacetime.

Computer System to Assist Selecting Models, Methods and Solution Algorithms for Problems in Electrodynamics

A. S. Samokhina and E. A. Trahtengerz
Institute of Control Sciences, Moscow, Russia

Abstract— Major steps while solving electromagnetic problems:

1. to describe the problem (to construct the physical model),
2. to formulate the problem (to construct the mathematical model),
3. to write down the problem in differential or integral equations. To determine boundary conditions for differential equations,
4. to estimate parameters of the mathematical model and criterions for choosing optimal solution,
5. to solve electromagnetic problem by using analytical or numerical methods,
6. to analyze the solution.

At the each step of solving we face the need to make a choice, be it choosing the correct and optimal physical and mathematical model, or choosing the numerical (analytical) method and the algorithm of the solution. Thus the construction of Computer System to Support Choosing the models, methods and algorithms of solving mathematical physics problems, incl. electromagnetic problems, is of dire importance.

In general case mathematical physics problems may be described as the boundary value problem of determining the solution $u(x)$ for the equation:

$$(Lu)(x) = f(x), \quad x \in D,$$

where variables $x = (x_1, \ldots, x_n)$ belong to the domain D and $u(x)$ satisfy at the boundary S of the domain D (or of its part) the boundary conditions:

$$(Bu)(y) = \varphi(y), \quad y \in S.$$

Boundary value problem is correctly formulated if the solution exists, is unique and continuously depends on the input data of the problem. Correctness of the problem formulation is bounded with the type of the operator L, the form of the boundary S and the operator of boundary conditions B. Operators B and L may be wrote down as algebra functions. These values may be formalized and elaborated by the Computer System with the help of experts-mathematicians needed to classify problems of mathematical physics and brought in while building up the System to Support Choosing so that later in while formulating the concrete problem the user could be assisted to correctly construct and write down the mathematical description of the problem.

For many problems also applies the alternate formulation in integral equations. In this case boundary conditions are considered in the core of integral equation.

Therefore, the System to Support Choosing is intended for the correct formulating of the problem by integral or differential equations with defined boundary conditions and for choosing the numerical method of the solution.

The Virtual Resonator in Embedding Method of Horn Array Antennas

P. V. Filonov and V. L. Kuznetsov
Moscow State Technical University of Civil Aviation, Russia

Abstract— In our publication in PIERS in Beijing 2007, we considered the application of embedding method to problem of computing the transparency and reflection coefficients of horn array antennas (HAA). The imbedding equations basics on the virtual resonator with "semitransparent" mirror could be written down:

$$\begin{aligned} T_{n+1} &= t_{n+1} M_n^{-1} T_n \\ R_{n+1} &= r_{n+1} + t_{n+1} M_n^{-1} R_n t_{n+1} \\ M_n &= I + R_n r_{n+1} \end{aligned}$$

here T_n, R_n — transparency and reflection matrices of HAA, t_n, r_n — transparency and reflection matrices of "semitransparent" elemental layer, M_n^{-1} — matrix which describe the virtual resonator. It could be easily shown what elementary layer could be consider as grating lattice consist of ideal conductive rectangle section skids with small height. As we are using the iteration procedure to compute the solution, to good accuracy we must produce high requirements to computing of t_n and r_n.

In classical solution of diffraction problem on skids lattice (considered in Shestopalov's works) we have to distribute the fields by two different basis's with different periods. Such kind of procedure must be done because usually the equations on metal and on slot are considering separately. And they exists only on a part of the period. In this work, we use method which allow us to consider both equations as a one and distribute the fields on all period of lattice. Such approach allow to connect filed in slot with filed in free space.

The are a lot of numerical experiments show a better accuracy of new method in individual problem and in computing the parameters of HAA. The method is also good with inhomogeneous waves falling from free space. The pointing theorem was used to check the accuracy.

Numerical Calculation of Diffracted Field by a Circular Disk of Perfect Conductor Using Multiple Precision Arithmetic

Takashi Kuroki[1], **Toshihiko Shibazaki**[1], **and Teruhiro Kinoshita**[2]

[1]Tokyo Metropolitan College of Industrial Technology, Japan
[2]Tokyo Polytechnic University, Japan

Abstract— The electromagnetic diffraction by a circular disk of a perfect conductor has been analyzed rigorously by Nomura and Katsura [1]. The numerical data of the diffracted field using their analysis method have been reported in the case that the radius of the disk is smaller than 3 wavelengths [2]. This is why calculation error increase, while the radius of the disk become larger.

The purpose of this study is to obtain numerical data of current distribution on the disk with the radius larger than 3 wavelengths using multiple precision arithmetic and to calculate the diffracted field.

In our calculation, the center of a circular disk of a perfect conductor is put at the origin of the rectangular coordinate system laying on x-y plane ($z = 0$). And a plane wave, whose electric field is polarized to x direction, is coming along the z axis from positive infinity to the origin.

Figure 1 shows the current distribution on the disk calculated at $a/\lambda = 3.99, 4.00, 4.01$ with double precision using FORTRAN code for the normal incidence ($\varphi = 0°$). Parameter φ is the angle from x axis to the observer. The horizontal axis indicates the distance r normalized by the wavelength λ from the center of the disk to the observer. The vertical axis indicates y component of the current normalized by the incident magnetic field $\mathbf{H}^{(i)}$.

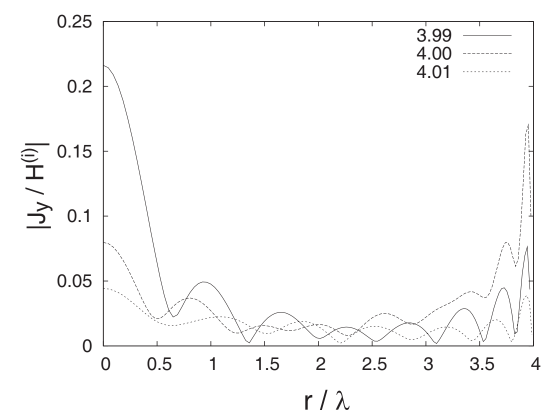

Figure 1: Current distribution at $a/\lambda = 3.99$, 4.00, 4.01 with double precision using FORTRAN code.

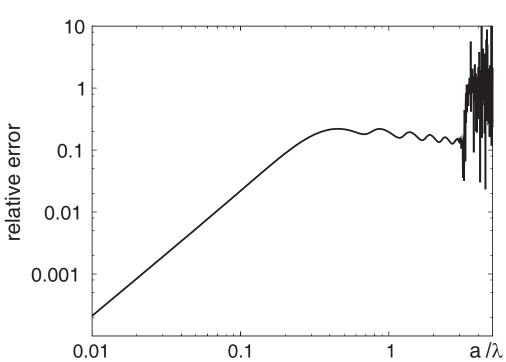

Figure 2: Energy error with double precision.

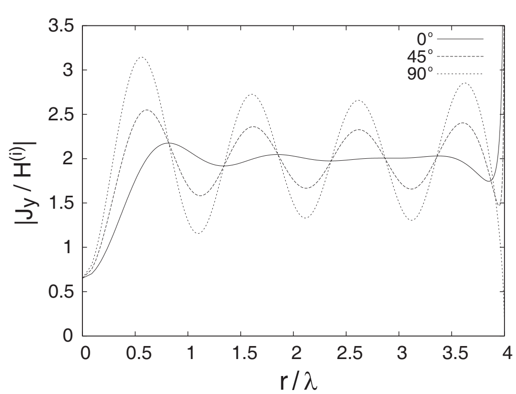

Figure 3: Current distribution at $a/\lambda = 4.0$ with 128-bit precision.

In Fig. 1, the current distribution changes greatly, as a/λ changes slightly. Also, the value at the center ($r = 0$) is less than 2 estimated by physical optics and all data are unstable.

Figure 2 shows the energy error based on the optical theorem with double precision. The horizontal axis indicates the radius of the disk a normalized by the wavelength λ. The vertical axis indicates the relative energy error. After approximately $a/\lambda = 3.0$, an unstable large error is occurred, as a increase. From this result, there is a necessity to calculate the current distribution with the another method at more than $a/\lambda = 3.0$.

Figure 3 shows the current distribution in the same case with 128-bit precision. The expected result is obtained. This means that the current distribution can be calculated more accurately by increasing the calculation precision in the circular disk larger than 3 wavelengths radius.

Based on the above discussion, we will calculate the diffracted field hereafter.

REFERENCES

1. Nomura, Y. and S. Katsura, "Diffraction of electormagnetic waves by circular plate and circular hole," *J. Physical Society of Japan*, Vol. 10, No. 4, 285–304, Apr. 1955.
2. Ando, M., T. Murasaki, and T. Kinoshita, "Elimination of false singularities in GTD equivalent edge currents," *IEEE Proc. H*, Vol. 138, No. 4, 289–296, Aug. 1991.

Fourier Solution of the 2D Dirichlet Problem for the Helmholtz Equation

D. Caratelli[1], **P. Natalini**[2], **and P. E. Ricci**[3]

[1]Delft University of Technology, The Netherlands
[2]Roma Tre University, Italy
[3]Sapienza University of Rome, Italy

Abstract— Many applications of Mathematical Physics and Engineering are connected with the Laplacian. However, the most part of boundary-value problems (*BVPs*) relevant to such operator are solved in explicit form only in domains having a very special shape (e.g., intervals, circles) or particular symmetries [1].

In recent papers [2–4], the classical Fourier method for solving the Dirichlet problem for the Laplace equation in canonical domains has been extended in order to address the same differential problem in a starlike domain, i.e., a domain $\mathcal{D}$ which is normal with respect to a suitable polar coordinate system, so that $\partial\mathcal{D}$ can be interpreted as *an anisotropically stretched unit circle*, centered at the origin. In this way closed-form solutions can be obtained by using suitable quadrature rules, so avoiding cumbersome numerical techniques such as finite-difference or finite-element methods [5].

In this contribution, a suitable technique useful to compute the coefficients of Fourier-type expansions representing solutions of boundary-value problems for the classical Helmholtz equation in complex planar domains is presented. In particular, the boundaries of the considered domains are defined by the so called "superformula" introduced by J. Gielis [6].

In order to verify and validate the relevant technique, a suitable numerical procedure based on the computer algebra system Mathematica© has been developed. By using such procedure, a point-wise convergence of the Fourier-series representation of the solution in regular points of the boundary, with Gibbs-like phenomena potentially occurring in singular points, has been observed. The obtained numerical results are in good agreement with the theoretical findings by L. Carleson [7].

ACKNOWLEDGMENT

This research has been partially carried out under a grant by Italian PRIN/2006 Cap. 7320.

REFERENCES

1. Andrews, L. C., *Special Functions of Mathematics for Engineers*, Oxford University Press, Oxford, New York, 1998.
2. Caratelli, D. and P. E. Ricci, "The Dirichlet problem for the Laplace equation in a starlike domain," *Proceedings of 2008 International Conference on Scientific Computing*, 160–166, Las Vegas, Nevada, July 2008.
3. Caratelli, D., B. Germano, M. X. He, and P. E. Ricci, "Solution of the Dirichlet problem for the Laplace equation in a general cylinder," (submitted).
4. Caratelli, D., P. Natalini, and P. E. Ricci, "The Dirichlet problem for the Helmholtz equation in a starlike planar domain," (submitted).
5. Bondeson, A., T. Rylander, and P. Ingelstrom, *Computational Electromagnetics*, Springer Science, Texts in Applied Mathematics, New York, 2005.
6. Gielis, J., "A generic geometric transformation that unifies a wide range of natural and abstract shapes," *Amer. J. Botany*, Vol. 90, 333–338, 2003.
7. Carleson, L., "On convergence and growth of partial sums of Fourier series," *Acta Math.*, Vol. 116, 135–157, 1966.

Session 2P6a
Applicators for Medical and Industrial Applications of EM Field

Rigorous Electromagnetic Analysis of Domestic Induction Heating Appliances

G. Cerri, **S. A. Kovyryalov**, **V. Mariani Primiani**, **and P. Russo**
Università Politecnica Delle Marche — DIBET, Via Brecce Bianche, Ancona 60100, Italy

Abstract— Domestic induction cookers become more and more popular because of their high efficiency, safety and ease in use. Induction cookers consist of an inductor, some ferrite bars below the coil screened by aluminum and the load (pot) above the coil (see Fig. 1). The inductor usually is winded using a Litz-wire and fed by a medium-frequency (20–100 kHz) power source, producing an alternating magnetic field. According to Faraday's law the alternating magnetic field induces eddy currents in the metal pan and, additionally in ferromagnetic materials, produces magnetic hysteresis. Both phenomena heat up the pan. In spite of many works and papers dedicated to the analysis of induction heating systems, there are still some problems to be investigated and solved such as hysteresis influence on the system operation, Litz-wire characterization (its complex geometry, skin and proximity effects, analytical description), non-linearity of the load, safety aspects and far-field radiation. The objective of the present work is to develop accurate analytical electromagnetic model of domestic induction heating applicator. The model was built up assuming equivalent electric and magnetic currents flowing in each planar element of the structure of Fig. 1: the load disk representing the pan steel bottom (electric J_S and magnetic J_{mS} currents), the copper inductor (electric current J_C), ferrite flux conveyor (magnetic current J_{mF}) and the aluminum shield (electric current J_A). The following equation system was then obtained enforcing the boundary conditions on each element of the structure for the electric and magnetic fields, produced by the equivalent currents. E_0 is the source field established by the power generator across the gap feeding the source inductor. σ_S is the conductivity of the steel, μ_{rS} is the relative permeability of the steel, σ_C is the copper conductivity, σ_A is the aluminum conductivity and μ_{rF} is the relative permeability of the ferrite.

$$\begin{cases} 0+\bar{E}(\bar{J}_C)+\bar{E}(\bar{J}_S)+\bar{E}(\bar{J}_{mS})+\bar{E}(\bar{J}_{mF})+\bar{E}(\bar{J}_A)=\dfrac{\bar{J}_S}{\sigma_S} & (1) \\ 0+\bar{H}(\bar{J}_C)+\bar{H}(\bar{J}_S)+\bar{H}(\bar{J}_{mS})+\bar{H}(\bar{J}_{mF})+\bar{H}(\bar{J}_A)=\dfrac{\bar{J}_{mS}}{j\omega\mu_0(\mu_{rS}-1)} & (2) \\ \bar{E}_0+\bar{E}(\bar{J}_C)+\bar{E}(\bar{J}_S)+\bar{E}(\bar{J}_{mS})+\bar{E}(\bar{J}_{mF})+\bar{E}(\bar{J}_A)=\dfrac{\bar{J}_C}{\sigma_C} & (3) \\ 0+\bar{H}(\bar{J}_C)+\bar{H}(\bar{J}_S)+\bar{H}(\bar{J}_{mS})+\bar{H}(\bar{J}_{mF})+\bar{H}(\bar{J}_A)=\dfrac{\bar{J}_{mF}}{j\omega\mu_0(\mu_{rF}-1)} & (4) \\ 0+\bar{E}(\bar{J}_C)+\bar{E}(\bar{J}_S)+\bar{E}(\bar{J}_{mS})+\bar{E}(\bar{J}_{mF})+\bar{E}(\bar{J}_A)=\dfrac{\bar{J}_A}{\sigma_A} & (5) \end{cases}$$

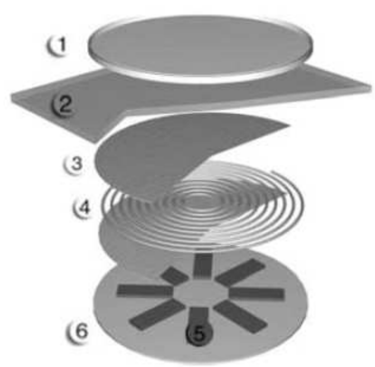

Figure 1: Inductor system structure: (1) pot, (2) cooking surface, (3) electric insulation, (4) winding, (5) flux conveyor and (6) shielding.

The numerical solution of the system is a matrix equation with a known voltage vector in the left-hand side, and product of impedance coefficients matrix and electric and magnetic currents vector in the right-hand side. Since the feeding voltage is known, and impedance coefficients are calculated using of geometry and material parameters, currents vector can be also calculated. Thus, the whole model is solved and it gives a detailed picture of currents distribution in the system, which in its turn allows to analyze heating process in the load. Moreover, considering the fact that modern inductors are usually winded of Litz-wire, the calculation of impedance coefficients matrix becomes more interesting because of complexity of its geometry. The proposed model gives detailed accurate analytical characterization of Litz-wire winded heating coil. The characterization of Litz-wire is developed from parametrical description of trajectory's curves of each strand in it. Each step of developing of the model was verified by appropriate experimental measurements. Achieved results give a possibility to analyze and develop improvements in order to increase efficiency, safety and to reduce the cost. More then that, Litz-wire analysis gives the unique analytical model of its geometry which makes possible to analyze other types of wires in different frequencies and areas of using.

Vibrations of Electrically Polar Structures in Biosystems Give Rise to Electromagnetic Field: Theories and Experiments

M. Cifra[1, 2], J. Pokorný[2], F. Jelínek[2], and O. Kučera[2, 3]

[1]Department of Electromagnetic Field, FEE, Czech Technical University in Prague, Czech Republic
[2]Institute of Photonics and Electronics, Academy of Sciences of the Czech Republic, Czech Republic
[3]Department of Circuit Theory, FEE, Czech Technical University in Prague, Czech Republic

Abstract— Fundamental principle of generation of electromagnetic field in living cells is mechanical vibration of electrically polar structures. Proteins are electrically polar structures which are ubiquitous in biological cells. Vibrations may be excited in the protein structures provided that energy is supplied. The spectrum of vibrations may span from low kHz up to THz region. The existence of endogenous biological electromagnetic field may have deep consequences in possible interaction with exogenous electromagnetic field.

The most likely candidate for the generation of electromagnetic field in a cell is cytoskeleton. Amount of energy supplied to the cytoskeleton is estimated regarding possible sources: dynamic instability, motor protein movement and wasted energy from mitochondria.

There are various theories which have been postulated regarding the generation of electromagnetic field in biological systems and its possible organizational role. Transformation of thermal vibrations to coherent vibrations has been postulated by Fröhlich. Nonlinear conditions allowing this transformation have been assumed. Only recent experimental findings show that there is a high static electric field due to mitochondria activity which may be that necessary condition for the nonlinear behavior.

Overview of the experiments showing existence of the vibrations on the cellular level by measurements with various techniques is given: vibrations of the cell membrane have been measured up to tens of Hz by optical techniques, measurement of kHz membrane oscillations have been measured by AFM by various authors. Various author also attempted to measure coherent oscillations of living cells by Raman spectroscopy. Crucial points of the success and failures of this kind of experiments are elucidated. Some of the recent experiments of the author's group are also presented.

A Value-added Method to Design a Compact and Low Cost Hairpin Line Microstrip Bandpass Filter for Communication Systems

Jagdish Shivhare[1] **and S. B. Jain**[2]

[1]Department of Electronics and Communication, Institute of Technology and Management
Sector-23 A, Gurgaon, Haryana, India
[2]Department of Electronics and Communication
Indira Gandhi Institute of Technology, Indraprashth University Campus, Delhi, India

Abstract— A value-added design method has been discussed for a multi-section Hairpin line microstrip bandpass filter at microwave frequencies.The design method may be used from a few hundred MHz to 10 GHz to serve the very basic purpose of reducing the overall size of the hairpin line band pass filters. Hairpin line resonator filters are relatively simple to design and build and are compact and low in cost. Two hairpin line microstrip band pass filters have been designed by using this value-added method. Simulation and optimization have been done by using Agilent-make software ADS 2005. These hairpin line filters have been fabricatyed by using very low cost metallized ABS-plastic substrate in place of very high cost RT-Duroid substrates. Finally these hairpin line bandpass filters have been tested on Vector Network Analyzer HP8510 (HP-make).

Analytical Model of Resonant Dryer Textile

Jan Vrba and Marika Pourova
Department of Electromagnetic Field, FEL, CTU, Czech Republic

Abstract— In cooperation with Research Institute of Textile Machines Liberec we developed applicator for microwave drying of textile in manufacturing, which is working on the open resonator principle at working frequency 2.45 GHz. In this contribution we would like to describe our new analytic model of microwave applicator for drying textile. The purpose of the present work is to investigate influence of distribution of the electric field strength on the dielectric properties of textile materials. We have numerical simulation and the analyses of the electric field strength in the plate of textile.

Our new model is created by several cells. Every cell has own magnetron which is source of electromagnetic energy. Magnetron is situated in the waveguide which is ended with funnel. All the cells are placed on one reflective plate.

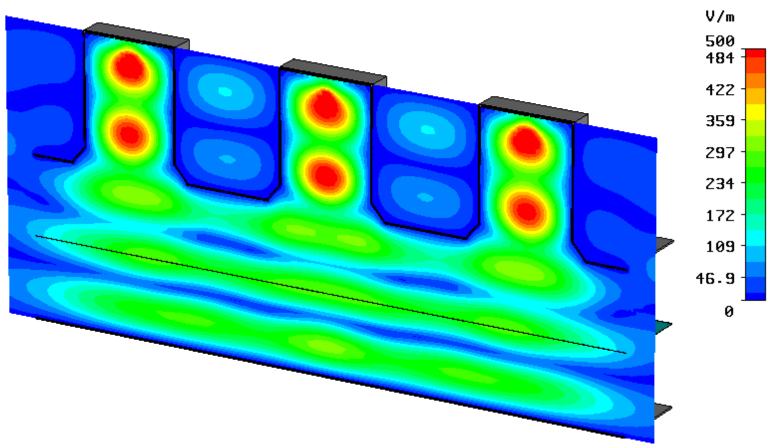

Figure 1: Distribution of electric field strength in applicator.

Conclusions: New results in optimization of microwave textile dryer based on analytical model are described in this paper. These results will enable us to increase efficiency of microwave drying machine.

TEM Applicators with Enlarged Effective Aperture

Jan Vrba, Jaroslav Vorlíček, and Jan Borovka
Department of Electromagnetic Field, FEE, CTU in Prague
Technicka 2, 166 27, Czech Republic

Abstract— This contribution describes new types of applicators for microwave hyperthermia with large effective aperture, which are used for Head and Neck cancer treatment.

Introduction: The addition of Hyperthermia in the treatment of Head and Neck tumors has been shown in several randomized clinical studies. Because of specific tumor's localization, it is very convenient to have a small applicator with a large effective aperture. Goal of our project was to develop new types of applicators with a large effective aperture. Its effective aperture has been compared with cases of Waveguide and EMW (Evanescent Mode Waveguide) applicator.

We have compared four (2 new types and 2 well known) microwave applicators operating at frequency 434 MHz. 1) SH (Stripline Horn) applicator, 2) SME (Stripline with Magnetic Excitation) applicator, 3) EMW (Evanescent Mode Waveguide) applicator, 4) Waveguide applicator. We have designed and optimized these applicators by aid of numerical models based on FDTD. Vector analyzer based on sixport measured the radiation matching. The SAR distribution has been measured on muscle equivalent biological tissue by using the matrix of thermistory probes.

SH applicator is an applicator (Fig. 1) with aperture dimensions 10×12 cm, which is filled by distilled water. The impedance matching was performed by capacity screw and it is shown on the Fig. 2. Both lateral walls are made of dielectric material. It was studied that it increases the effective aperture.

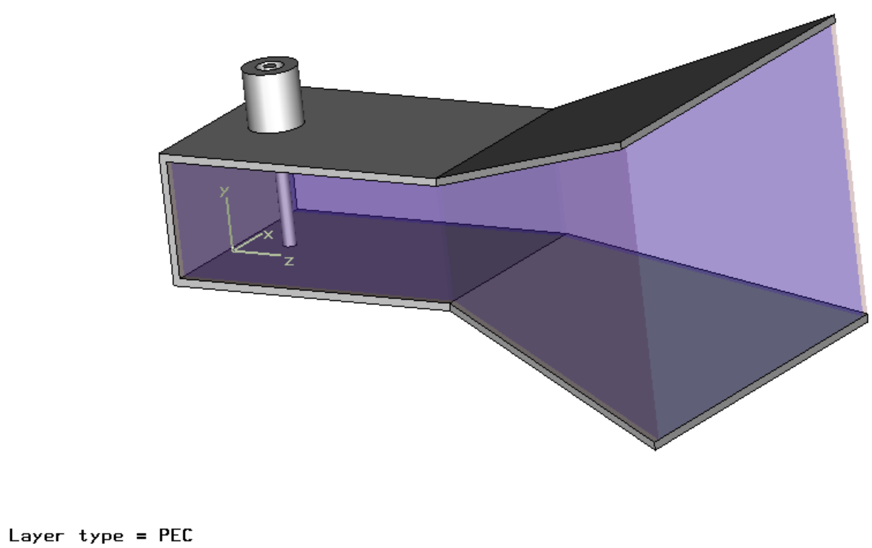

Figure 1: Stripline horn applicators, Prague, 2003.

Evaluation of Microwave Applicators for Medical Applications

Jan Vrba and Ladislav Oppl
Department of EM Field, Czech Technical University in Prague
Technická 2, Prague 16627, Czech Republic

Abstract— Paper deals with our new results in the field of waveguide and intracavitary applicators used for microwave thermotherapy, like e.g., cancer treatment, physiotherapy, benign prostatic hyperplasia (BPH) treatment, etc.

Introduction: In our contribution we describe waveguide and intracavitary applicators working at 70, 434 and 2450 MHz see Refs. [1–6]. These applicators were used here in Prague for the treatment of more then 500 cancer patients with superficial or subcutaneous tumors (up to the depth of approximately 4 cm). Now, following new trends in this field, we continue our research in important direction of deep local and regional applicators.

Evaluation of Microwave Applicators: Evaluation of hyperthermia applicators in the water phantom means to measure the electromagnetic field power distribution in front of the aperture of this applicator. The E-field distribution can be measured by the dipole antenna. The length of this antenna must be smaller than $\lambda/4$ (λ is the wavelength of measured field in this media). The voltage induced in this antenna supply the LED. The optical signal from the LED is leaded by the optical fiber outside the phantom to the optical detector. The scheme of the described system for microwave applicators evaluation is shown in the Figure 1.

The output voltage from the optical detector is measured by the voltmeter or is converted by the ADC to the digital form and processed by the computer.

Conclusions: Microwave thermotherapy is successfully applied in clinics in the Czech Republic. Technical support is at present from the Czech Technical University in Prague. Our goal for the next technical development is:

- improve the theory of the local and intracavitary applicator design and optimisation,
- innovate the system for the applicator evaluation (mathematical modelling and measurements),
- develop system for regional treatment.

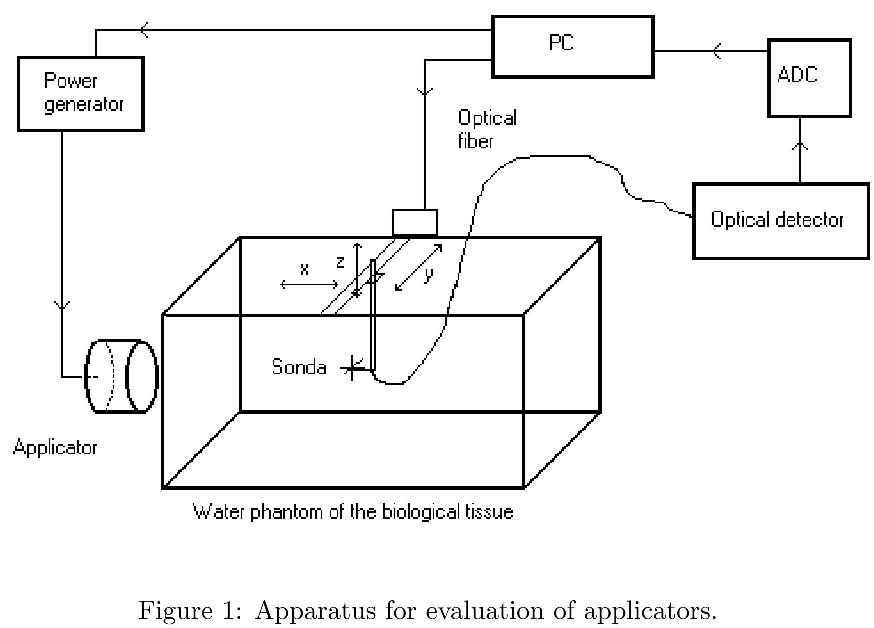

Figure 1: Apparatus for evaluation of applicators.

Session 2P6b
Medical Electromagnetics, RF Biological Effect

Influence of Weak Combined Static and Low-frequency Alternating Magnetic Fields on Tumor Growth of Ehrlich Ascites Carcinoma in Mice

V. V. Novikov, G. V. Novikov, V. O. Ponomarev, V. V. Kuvichkin, and E. E. Fesenko
Institute of Cell Biophysics, Russian Academy of Sciences
Pushchino, Moscow region 142290, Russia

Abstract— It has been shown that the ultralow-frequency extremely weak alternating component of combined magnetic fields (MFs) exhibits a marked antitumor activity. The parameters of this component have been found (frequency 1, 4.4, 16.5 Hz or the sum of these frequencies; intensity 240, 80, 160 nT, respectively) at which this MF in combination with a collinear static MF of 42 μT inhibits or suppresses the growth of Ehrlich ascites carcinoma (EAC) in mice. It was shown that the exposure of mice with EAC to combined MFs causes structural changes in some organs (liver, adrenal glands), which are due probably to the total degradation of the tumor tissue. In mice with transplanted EAC, the tumor tissue after the exposure to weak MFs was practically absent, as distinct from control animals in which the invasion of the tumor into the adipose tissue surrounding the kidneys, mesenteric lymph nodes, and spermatic appendages was observed.

Based on the results of the study, it can be concluded that normal tissues of the organism, as distinct from tumor tissues, are not susceptible to the damaging action of superweak AC of the nanotesla intensity range. Conversely, this field component has an activating effect on the immune tissue, which manifests itself, for example, in enhanced production of TNF by macrophages isolated from the mouse abdomen. Presumably, the difference in the responses of immune and tumor tissues to superweak AC is due to the features of the metabolism of macrophages and tumor cells. It is known that, in tumor cells, anaerobic processes, in particular glycolysis, prevail. In cells of the immune system, the oxidative phosphorylation processes predominate. It is likely that it is the difference in the type of their metabolism that determines the difference in their responses to AC. It would be tempting to suggest that, if this is the case, then the stimulation of ROS production by the action of superweak AC MF with the characteristics specified in our study may lead to the activation of the cells of the immune system and simultaneously to the disturbance of the metabolism in tumor cells.

Closed-loop Inductive Link for Wireless Powering of a Retinal Prosthesis

D. C. Ng[1], **S. Bai**[2], **J. Yang**[2], **N. Tran**[2], **and E. Skafidas**[1]

[1]Victoria Research Laboratory, National Information & Communication Technology Australia
University of Melbourne, Victoria 3010, Australia
[2]Department of Electrical & Electronic Engineering, The University of Melbourne, Australia

Abstract— A retinal prosthesis intended for rehabilitation of vision impaired patients will require continuous power transmission in order to achieve real-time moving images [1]. However, reliable transmission of power is a major performance-limiting factor for successful implementation of such a prosthetic device. In this paper, we discuss the various technologies required to develop and realize a closed-loop inductive link module to transmit power to a batteryless retinal prosthesis implanted inside the eye. This involves design of inductive link circuit architecture (Fig. 1), simulation of electromagnetic field distribution in and surrounding the eye and, fabrication and testing of the coils *in vivo*.

We estimate that a high density electrode array with more than 1000 electrodes will consume about 45 mW of power. The supply of power to the retinal prosthesis is difficult due to many factors. Apart from the need to deliver power wirelessly to eliminate the risk of infection through exposed tethers, constant motion of the implant results in variation of magnetic coupling between the transmit and receive inductive coils. Furthermore, the electrode-tissue impedance is likely to change over time from initial implantation due to tissue growth over the foreign object. In order to maintain optimal operation of the link, a closed-loop operation is proposed.

The front end of the wireless power module, the coil, needs to be small compared to the size of the eye. We use 10 MHz as the operating frequency, which is optimal for electromagnetic propagation through the eye [2]. We estimate that the wireless module will operate in the reactive near-field region due to the small separation between transmit and receive coils, compared to their size and corresponding operating wavelengths. Adaptive control using back-telemetry of the induced voltage on the secondary side can close the power supply loop and result in optimum power transfer by boosting the supply voltage on the primary side when load is high and reducing this voltage when load is small. In this work, we integrate the circuit together with microfabricated coils to realize the wireless module.

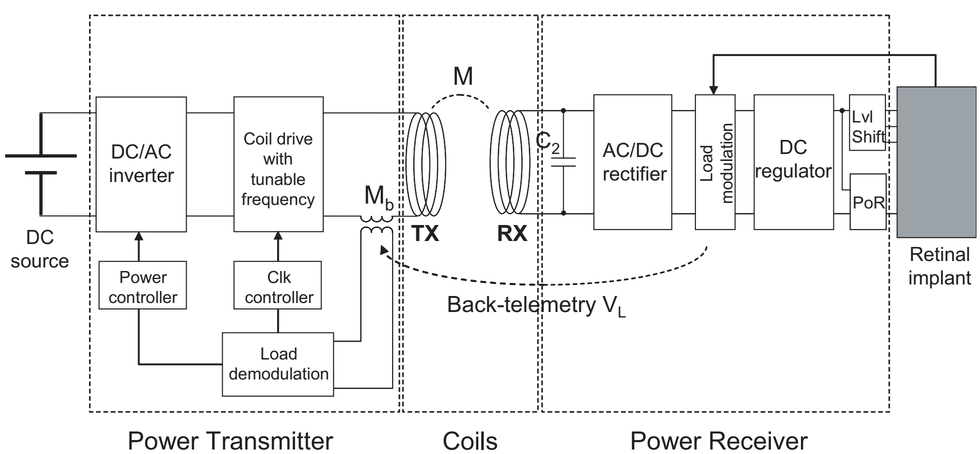

Figure 1: Schematic of the inductive link power supply.

REFERENCES

1. Weiland, J. D., W. Liu, and M. S. Humayun, "Retinal prosthesis," *Annu. Rev. Biomed. Eng.*, Vol. 7, 361–401, 2005.
2. Vaillantcourt, P., A. Djemouai, J. F. Harvey, and M. Sawan, "EM radiation behaviour upon biological tissues in a radio-frequency power transfer link for a cortical visual implant," *Proc. IEEE Int. Conf. Engineering in Medicine and Biology*, 2499–2502, Vancouver, Canada, Oct. 1997.

Merger of Two Different Dosimetry Rationales

S. Perov[1], **Q. Balzano**[2], **and N. Kuster**[3]

[1]RAMS Research Institute of Occupational Health, Moscow, Russia
[2]Department of Electrical and Computer Engineering, University of Maryland, Maryland, USA
[3]Foundation for Research on Information Technologies in Society, Zurich, Switzerland

Abstract— At the present time there are two basic scientific rationalizations of radiofrequency dosimetry. Finding the possible correlations between the measured parameters of the two different scientific approaches is one of the main obstacles to global safety (hygienic) standard harmonization. One approach is based on the measure or estimate of specific absorption rate which is the power absorbed per unit weight of an object. The other relies on the measure of the time integrated radiofrequency power density incident on an object. Development of a common science-based dosimetric approach may be possible by taking into account the exposure time. Time is the "key" factor, which is used both in the specific absorption rate and the power density definitions. Finding the correlations between the specific absorption rate and the power density of an exposure depending on time duration might make possible the creation of a common estimate of electromagnetic field biological action. It can help to find the correlation between power density and specific abortion rate for near and far field of radiofrequency sources.

Safety standard harmonization is much more complicated than just harmonizing dosimetric criteria. Safety standard setting involves the mediation of various concerns and interests, such as political, economic, technological, etc. However a necessary common ground is one dosimetric approach with accurate substantiation of measurement methodologies. It will consist in finding a homogeneous bioeffect data base for the two current science-based dosimetric approaches.

Microwave Effect on Proteins in Solution — Fluorescence Polarization Studies

I. Barak, M. Golosovsky, and D. Davidov
The Racah Institute of Physics, The Hebrew University of Jerusalem
Jerusalem 91904, Israel

Abstract— The use of low-power microwaves in chemistry and biology is rapidly growing [1]. From the theoretical standpoint, whether or not microwave irradiation can exert a nonthermal effect on biomolecules is a controversial issue [2–4]. While several experimental studies [5–7] barely show any irreversible changes in proteins after mw irradiation, there are a few studies reported a specific microwave effect on biomolecules [8–11]. In this work we focused on the effects occurring under irradiation of biomolecules with microwaves with a well-defined orientation. We studied the Enhanced Green Fluorescent protein (EGFP) in aqueous solution [12] whose fluorescence is a good "reporter" of its structure and environment. We measured EGFP fluorescence intensity, spectrum, and polarization before, under and after 250 mW microwave irradiation in a TE_{011} microwave cavity operating at 9.5 GHz. We carefully distinguished between the alleged specific microwave effect and the temperature-dependent effects arising from the microwave absorption in the solvent. We estimated temperature rise in solution through the change in EGFP fluorescence intensity and spectrum while the possible specific microwave effect was observed through the fluorescence polarization. We observed that in the spectral range of 500–540 nm, the microwave-induced variation of the EGFP fluorescence polarization is similar to that achieved by conventional heating, while in the spectral range of 540–560 nm, the microwave-induced effect is different from that resulting from the conventional heating.

REFERENCES

1. Kappe, C. O. and A. Stadtler, *Microwaves in Organic and Medicinal Chemistry*, Wiley-VCH, Weinheim, 2005.
2. Foster, K. R., *IEEE Trans. Plasma Sci.*, Vol. 28, 15, 2000.
3. Laurence, J. A., D. R. McKenzie, and K. R. Foster, *J. Theor. Biol.*, Vol. 222, 403, 2003.
4. Adair, R. K., *Bioelectromagnetics*, Vol. 24, 39, 2003.
5. Weissenborn, R., K. Diederichs, W. Welte, G. Maret, and T. Gisler, *Acta Crystallogr.*, Sec. D, Vol. 61, 163, 2005.
6. Aslan, K. and C. D. Geddes, *Anal. Chem.*, Vol. 77, 8057, 2005.
7. Olapinski, M., S. Manus, N. Fertig, and F. C. Simmel, *Biosensors and Bioelectronics*, Vol. 23, 872, 2008.
8. Bohr, H. and J. Bohr, *Phys. Rev. E*, Vol. 61, 4310, 2000.
9. Hamad-Schifferli, K., J. J. Schwartz, A. T. Santos, S. G. Zhang, and J. M. Jacobson, *Nature*, Vol. 415, 152, 2002.
10. Copty, A. B., Y. Neve-Oz, I. Barak, M. Golosovsky, and D. Davidov, *Biophys. J.*, Vol. 91, 1413, 2006.
11. George, D. F., M. M. Bilek, and D. R. McKenzie, *Bioelectromagnetics*, Vol. 29, 324, 2008.
12. Zimmer, M., *Chem. Rev.*, Vol. 102, 759, 2002.

Ion Cyclotron Bioresonance in Regenerative Medicine

Alberto Foletti[1] **and Settimio Grimaldi**[2]

[1]BITitalia, Milan, Italy
[2]Institute of Neurobiology and Molecular Medicine, CNR, Rome, Italy

Abstract— The prometheus myth, is a fitting model for regenerative medicine. As punishment for giving fire to humanity, Zeus ordered Prometheus chained to a rock and sent an eagle to eat his liver each day. However, Prometheus' liver was able to regenerate itself daily, enabling him to survive. Today, we hope to make the legendary concept of regeneration into reality by developing therapies to restore lost, damaged, or aging cells and tissues in the human body. Electromagnetic therapy is a treatment method in which an electromagnetic or magnetic stimulus is used to achieve physiological changes in the body. The specific aim of the present work concerns the effectiveness of low frequency electromagnetic fields treatment (tuned at Calcium cyclotron energy resonance) to modify biochemical properties and trigger cells differentiation in a pituitary cells line (AtT20). Cells were exposed to a 7 Hz electromagnetic field (B_o field 9.2 μT) a commercially available wave generator (Vega Select 719), the cyclotron frequency were calculated by the following equation

$$f_c = \frac{q}{2\pi m} B_o$$

where f_c is the cyclotron frequency, q and m are the charge and mass of the ion, and B_o is the vector of the geomagnetic field (DC field) parallel to the component of the applied electromagnetic field (B sin). In our case since the geomagnetic component (B_o) parallel to the applied B sin is 9.2 μT, the calculated f_c for calcium is 7 Hz. Here, we report that 50 Hz 2 mT ELF-EMF on rat anterior pituitary derived AtT20 D16V cells produces a sudden increase in the intracellular calcium level, followed by the reorganization of the cytoskeletal network via the polymerization of the actin and the differentiation of the proteins expression. These findings demonstrate that exposure to cyclotron resonance can transfer biological information on pituitary cells, supporting the relevance of low frequency electro-magnetic field as a therapeutic agent, thus suggesting the potential use of cyclotron resonance in nerve regeneratrion.

A Definition of Thermophysiological Parameters of SAM Materials for Temperature Rise Calculation in the Head of Cellular Handset User

S. I. Al-Mously[1] **and M. M. Abousetta**[2]

[1]Department of Electrical and Computer Engineering
School of Applied Sciences and Engineering, Academy of Graduate Studies, Tripoli, Libya
[2]Department of Electrical and Electronics Engineering, Faculty of Engineering
Al-Fateh University, Tripoli, Libya

Abstract— Both of the physical and CAD models of the Specific Anthropomorphic Mannequin (SAM) are used to measure and compute the specific absorption rate (SAR) in the head of cellular handset user, respectively. This standard phantom was developed by the IEEE standards Coordinating Committee 34, Sub-Committee 2, Working Group 1 (SCC34/SC2/WG1), and has also been adopted by other different committees, commissions and associations. Basically, SAM was designed to produce a conservative SAR for a significant majority of persons during normal use of handset. SAM is a lossless plastic shell and ear spacer, where the shell is filled with a homogeneous fluid having the average electrical properties of head tissues at the test frequencies. A SAM CAD model is also available to compute the SAR due to cellular handsets using different methods, e.g., Finite Element, Finite-Difference Time-Domain and Method of Moment. The investigators have used computational RF dosimetry to compare the SAR in SAM to that in anatomically correct models of the human head.

Physically, it is impossible to fill the SAM lossless shell with a fluid having the averaged thermophysiological parameters of the natural human head tissues, as some parameters such as the heat generation rate and the blood perfusion rate have no existence. This is why the SAM is not used as a standard model to measure the temperature rise due to the exposure to the EM radiation. Consequently, only SAM CAD model with certain thermophysiological parameters may be adopted to compute the temperature rise.

Although the SAM is a homogeneous model, where the computed inside-temperature rise associated with handset RF emissions may not indicates the temperature rise in every distinguished natural head tissue, it is possible to compute the temperature rise in the entire head. It is essential to have a standard phantom with standard thermophysiological parameters to compute the temperature rise in the entire head of cellular handset user, as many anatomically correct head models are available for different sexes, ages, resolutions and number of tissues, with different thermophysiological parameters, which as a result give different temperature rise induced by the cellular handset.

Why Plants Do Not Suffer From Cancer

Ahmad Majd[1] and Azita Shabrangi[2]

[1]Islamic Azad University, Tehran North Branch, Iran
[2]Department of Biological Sciences, Faculty of Science
Tehran Tarbiat Moallem University, Iran

Abstract— In spite of reporting harmful effects of electromagnetic fields (EMFs) on live tissues, many researchers believe in EMFs therapy.

Cancer is a special kind of adaptation to energetic overload, characterized by multiplication and mutation of genomic DNA (generation of new biomolecules which enhance the probability of survival under harmful conditions) and by chiral alterations (reduction of entropy by entrapping energy) Therefore genetic alterations are probably secondary changes. Cancer serves to dissipate energy in a type of developmental process but the results are harmful to the whole organism [2]. It is assumed that entropy production rate of cancer cell is always higher than healthy cell. The entropy flow from cancer to healthy cell takes along the harmful information of cancerous cell, propagating its toxic action to healthy tissues. Therefore a lowfrequency and low-intensity electromagnetic field may increase the entropy production rate of a cell in normal tissue than that in cancer, consequently reverse the direction of entropy current between two kinds of cells. So, the biological tissue under the irradiation of electromagnetic field can avoid the propagation of harmful information from cancer cells [3].

We believe this phenomenon happens naturally in plants. The entropy flow is always from apical meristem cells and secondary meristem cells toward differentiated cells. Therefore differentiated cells would not be overload energized and their entropy entrapped by the entropy flow from meristem cells.

Battley reported that entropy of organic substances can be determined experimentally, using low-temperature calorimeter and the second Law of thermodynamic in yeast [1].

Deducing all these information, it would be possible in collaboration with biochemists, biophysicists and biologists to determine experimentally entropy production of different kinds of cells (meristem, differentiated cells and crown gall cells as a tumor in plants provided by Agrobacterium tumefaciens).

REFERENCES

1. Battley, E. H. and J. R. Stone, "A comparison of values for the entropy and the enthalpy of formation of selected organic substances of biological importance in the solid states, as determined experimentally or calculated empirically," *Thermochimica Acta*, Vol. 349, 153–161, 2000.
2. Hauptmann. S, "A thermodynamic interpretation of malignancy: Do the genes come later?," *Medical Hypotheses*, Vol. 58, No. 2, 144–147, 2002.
3. Luo, L. F., "Entropy production in a cell and reversal of entropy flow as an anticancer therapy," arXiv:0802.0048v1 [q-bio.CB], 2008.

Session 2P7
Antenna and Array: Theory and Design

A Class of Broadband Planar Traveling-wave Antennas and Their Latest Applications

Johnson J. H. Wang
Wang Electro-Opto Corporation (WEO), Marietta, Georgia 30067, USA

Abstract— Classical antenna theory often ignores the practical problem of platform mounting, which can have deadly impact on antenna performance. This is an unavoidable problem since an antenna is invariably inseparable from a transceiver or platform, which the antenna is connected with or mounted on. In the worst scenario, the main radiator is the platform or transceiver, not the antenna per se. The slot antenna and the microstrip patch antenna provide a narrowband solution to this problem. For broadband needs, a class of planar traveling-wave (TW) antennas, as depicted in Figure 1, and TW phased arrays employing such TW elements, emerged in the past two decades [e.g., 1], offering a satisfactory solution. This paper addresses the fundamental theory for this class of planar TW antennas.

A common feature of these patented designs is a ground plane placed very close to a planar broadband TW structure, which is preferably a self-complementary surface. The TW is characterized by a radial component of propagation to and from the geometrical center of the planar TW structure. The conducting ground plane on the back side of the antenna enables the antenna to be conformally mounted on any platform, with minimal EMC/EMI problems as well as a stable radiation property fairly independent of the mounting platform. In addition to an octaval bandwidth of 10 : 1 or more, this class of broadband planar TW antenna offers features such as dual-polarization and multifunction rarely available in other antennas.

Applications include ultra-wideband conformal body-wearable antennas, air/sea/ground vehicle antennas, handset antennas, planar phased arrays, etc. A recent application is in high-performance low-cost GNSS antennas that cover all three GNSS services (GPS/GLONASS/Galileo), requiring a wide frequency bandwidth of 1.164–1.610 GHz. The TW structure in this design is a planar four-arm spiral, which has an inherently stable phase center nearly independent of spatial and frequency variations. Such a performance is not achievable by conventional GNSS antenna approaches such as the patch antenna and other broadband antennas. Its phase center stability versus frequency and spatial angle is primarily limited by its manufacturing tolerance and the excitation accuracy of its feed network.

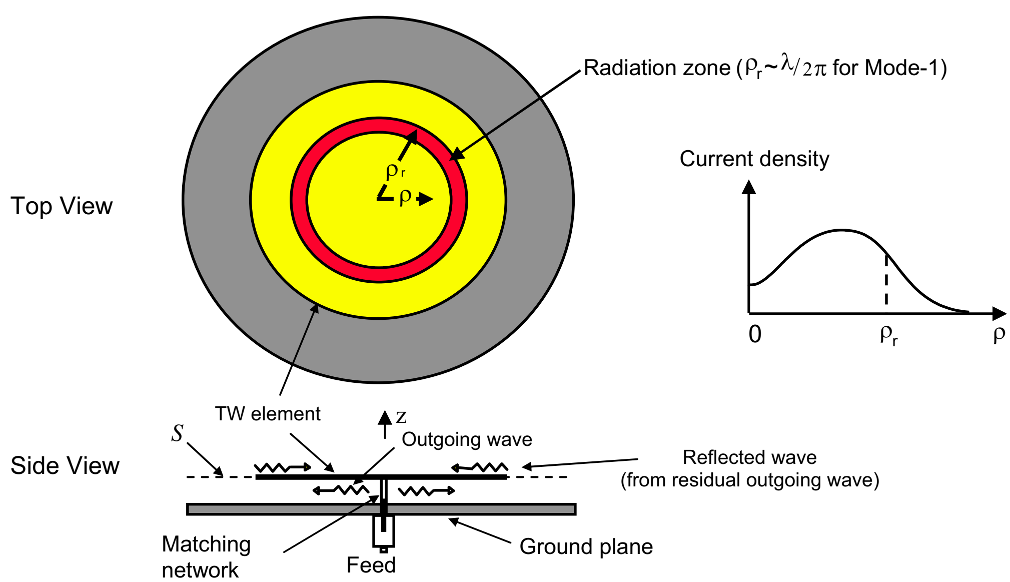

Figure 1: The planar TW antenna.

REFERENCES

1. Wang, J. J. H., D. J. Triplett, and C. J. Stevens, "Broadband/Multiband conformal circular beam-steering array," *IEEE Trans. Antennas and Prop.*, Vol. 54, No. 11, November 2006.

Phase-only Synthesis of the Radiation Pattern of an Antenna Array with Quantized Phase Shifters

Alexander S. Kondratiev
Moscow Power Engineering Institute (Technical University), JSC Altair, Russia

Abstract— At present, solution of many radar and communication problems requires application of antennas with shaped radiation patterns and/or pattern nulls or deep gaps in prescribed directions. Antenna arrays, which have many controllable elements, are most suitable candidates for formation of such patterns. In many arrays, only the phases of the amplitude-phase distribution over the array elements can be controlled. In this case, formation of an array pattern with prescribed properties requires solution of the so-called phase-only synthesis problem [1].

Phase-only synthesis problems are inherently nonlinear and, generally, are solved with the use of numerical methods [2, 3]. The most reliable methods are those based on reduction of the initial synthesis problem to the problem of minimization of a nonlinear nonnegative definite function of desired phases and application of numerical optimization techniques to finding the minimum of this function. (In general, the minimum is local and the obtained solution is only approximate.)

In most cases, the element excitation phases are controlled with quantized phase shifters that change the excitation phases only stepwise. The value of phase increment $\Delta\psi$ is usually determined from the formula

$$\Delta\psi = 2\pi/2^K, \tag{1}$$

where K is the number of binary digits.

In this case, it is desirable to solve the problem in the domain of discrete values of the desired phases [2, 3]. This approach, in particular, allows formation of deep nulls in prescribed directions.

In formation of a shaped pattern, it is often desirable to ensure near uniform approximation of the desired shape. This approximation can be attained with the use of the Chebyshev metric or an approximation of this metric for the difference between the desired and the synthesized patterns.

Here, an approach to solution of the phase-only pattern synthesis problem is proposed that involves

(i) formation of the objective function with the use of a power approximation of the Chebyshev metric and

(ii) iterative minimization of this objective function by means of finite search over discrete phase values at each iteration.

A version of this approach is described below.

Let us specify the desired radiation pattern by its values at M angular directions F_m^0, $m = 1, \ldots, M$.

Then, the phase-only synthesis problem is reduced to solution of the following set of equations:

$$\sum_{n=1}^{N} F_n^e\left(\theta_m, \varphi_m\right) \cdot A_n \cdot \exp(j\psi_n) \cdot \exp\left(j\left(kx_n\kappa_{xm} + ky_n\kappa_{ym} + kz_n\kappa_{zm}\right)\right) = F_m^0, \quad m = 1, \ldots, M, \tag{2}$$

where $F_n^e(\theta_m, \varphi_m)$ is the radiation pattern of the nth array element in the mth angular direction (θ_m, φ_m) in the spherical coordinate system;

A_n and ψ_n are the amplitude and phase of the excitation of the nth array element;

kx_n, ky_n, and kz_n are the Cartesian electric coordinates of the nth array element;

$k = 2\pi/\lambda$ and λ is the wavelength.

Amplitudes A_n are fixed and system (2) is solved for desired phases ψ_n taking discrete values according to formula (1). Since the solution domain of this system of nonlinear equations is

generally unknown, system (2) is solved approximately by reducing it to the objective function

$$Q = \sum_{m=1}^{M} W_m \Bigg| \sum_{n=1}^{N} F_n^e(\theta_m, \varphi_m) \cdot A_n \cdot \exp(j\psi_n) \cdot \exp(j(kx_n\kappa_{xm} + ky_n\kappa_{ym} + kz_n\kappa_{zm})) - F_m^0 \exp(j\alpha_m)\Bigg|^l, \quad (3)$$

where α_m are the phase values whose values are specified during iterative minimization of this objective function [3] and $l \geq 2$ is a positive even integer number.

The minima of objective function (3) are the approximate solutions to system (2).

Analysis of objective function (3) shows that, along each phase ψ_n, function (3) is periodic with a period divisible by $2\pi/l$. This feature is used to develop a simple iterative minimization technique in which objective function (3) is successively minimized along coordinates ψ_n. If $l=$ 2, the minimum along each coordinate can be found analytically [2, 3]. If $l > 2$, the minimum at each iteration is found numerically by means of the search over a finite number of phase values determined by formula (1) within the period $[0,\, 2\pi]$. The advantages of this synthesis procedure are the simplest selection of the search direction and a limited search interval at each iteration.

This procedure can be further improved by replacing the coordinatewise search method with one of faster methods, for example, the well-known conjugate gradient method [4]. However, direct application of this method is impossible because phases ψ_n can take only discrete values determined by formula (1). If the phase values are considered continuous and formula (1) is applied to the solution found with continuous phases, this operation may result in substantial deterioration of the obtained solution, which is most pronounced for the null synthesis problems.

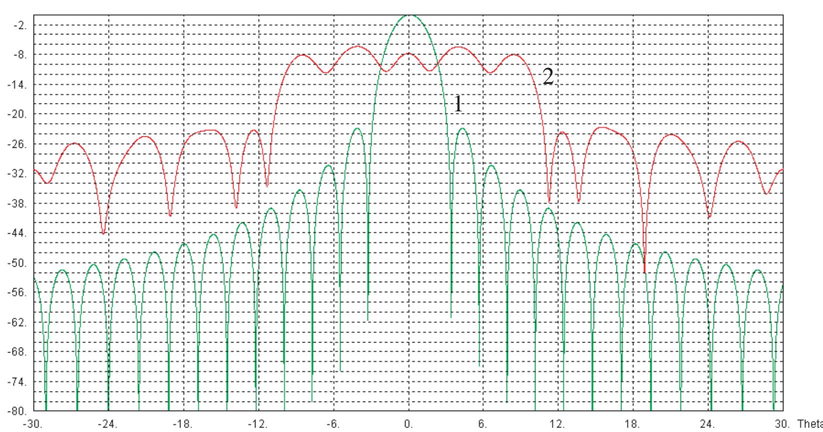

Figure 1: Initial and synthesized patterns for $l = 2$.

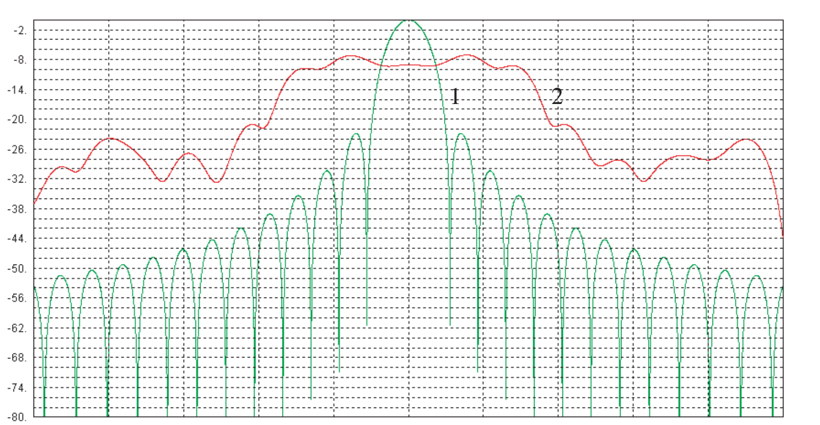

Figure 2: Initial and synthesized patterns for $l = 4$.

To return the linear search performed at each iteration to the search over only the allowed phase values, one can use a technique in which the search direction is adjusted so that the components of the original search vector are approximated by the values that are the multiples of phase increment $\Delta\psi$. A normalization procedure is used to set the maximum vector component to 2π. At each iteration, objective function (3) is simultaneously minimized along the coordinates changed according to the above algorithm and the steps along coordinates ψ_n take only the discrete values specified by formula (1). In practice, this is a stepwise approximation of the original search direction.

An example of application of the coordinatewise version of the proposed method is shown below for the synthesis of a linear equispaced array of 50 isotropic radiators with a flat-top pattern. The synthesis results are shown in Figs. 1 and 2. In all figures, curves 1 correspond to the initial array pattern and curves 2 correspond to the synthesized patterns for $l = 2$ (Fig. 1) and 4 (Fig. 2), respectively.

As seen from the results in Figs. 1 and 2, the synthesized patterns depend on power l. Changing this parameter, it is possible to flatten the ripples on the top of the synthesized pattern.

REFERENCES

1. Cheng, D. K., "Optimization techniques for antenna arrays," *Proc. IEEE*, Vol. 59, 1664–1674, 1971.
2. Kondrat'yev, A. S., "Method for phase synthesis of antenna arrays with additional requirements on the shape of the directivity pattern taken into account," *Soviet J. Communications Technol. Electron.*, Vol. 36, 94–102, 1991.
3. Kondrat'yev, A. S. and A. D. Khzmalyan, "Phase-only synthesis of antenna arrays for a given amplitude radiation pattern," *J. Communications Technol. Electron.*, Vol. 41, 859–866, 1996.
4. Fletcher, R. and C. M. Reeves, "Function minimization by conjugate gradients," *Computer J.*, Vol. 7, 149–154, 1964.

Stage-by-stage Testing Technique of Active Phased Array

M. V. Markosyan, **V. H. Avetisyan**, **and S. G. Eyremjyan**
Yerevan Telecommunication Research Institute, Yerevan, Republic of Armenia

Abstract— Manufacturing and bringing of the active phased array (APhA) to a readiness for operation (with the goal of reception of the parameters inserted at the APhA designing) demand significant zeal and expenses. At production the step-by-step assembly of component units of the APhA to entire antenna system is carried out. The basic element of APhA is transceiver module (TM), which combines the electronic-controlled discrete attenuator, phase-shifter, switches, power amplifier and low-noise amplifier; N pieces of TM are combined in a cell; M pieces of cells are combined in group; K pieces of groups are combined in subarray and F pieces of subarraies are combined in entire system of the APhA. At assembling of new unit it is possible to disturb an operability of one or more component units. On each stage of such sequential enlargements it is important to eliminate of faulty component units from process of following assembly for avoiding of additional expenditures.

With this goal in given article the technique of stage-by-stage testing and electric alignment of the APhA component units is offered at the described assembly process. In the beginning of everyone specifically-observed stage the checking (according to the developed techniques) of the final assembly units of the previous stage is provided. Note, the final assembly units of the previous stage are the component units of the specifically-observed stage unit, which should be tested. The mentioned checking of each final assembly unit of the previous stage is carried out in mode of in-phase and amplitude uniform excitations of its component units. The check testing defines operability of the previous stage assembly units and also deviations of their amplitude and phase transmission characteristics. On the basis of the received data about deviations for each of tested units, the corrections by amplitude and phase are defined for inserting of additional attenuations and phase-shifts, which necessary for their in-phase and amplitude uniform excitations in composition of the observed stage assembly unit. Such excitation condition of the observed stage component unit is final result of its electronic alignment. After that, the correctness of executed electric alignment of the tested unit is checked by corresponding measurements and its certificate on required parameters is made out. It is an end of the specifically-observed stage.

Process of the TM testing is carried out on the basis of radiator far-field measurements by means of the developed automatic measurement system, which determines also polarization characteristics of its radiated wave. Testing of groups, subarraies and whole APhA is carried out by the offered near-field automatic measurement system.

The offered stage-by-stage testing technique allows clearly and reliably to carry out a process of bringing of the APhA to a readiness for operation in accordance with requirements on its electric parameters.

Experimental Investigations of Adaptive Reactance Parasitic Antenna Dipole Array

M. O. Shuralev[1,2], **A. L. Umnov**[1,2], **A. Mainwaring**[3], **M. A. Sokolov**[1,2], **and A. U. Eltsov**[1,2]

[1]Nizhny Novgorod State University, Nizhny Novgorod 603950, Russia
[2]Intel Corporation, Nizhny Novgorod, Russia
[3]Intel Research Laboratory at Berkeley, CA 94704, USA

Abstract— This work explores the theory and practice of low-cost beam steering antennas for WiFi, specifically high-gain arrays of interest for long-distance point-to-point and point-to-multipoint links based on WiFi technology operating at 2.4 GHz. The antenna systems are constructed on a basis of tunable impedance mirrors, named as reflectarrays, assembled from periodic array of passive scatterers illuminated by a single, driven RF element, placed at 2.5 wave-lengths from the center of the reflectarray. Although this approach avoids energy losses and unwanted influence between the passive elements through surface wave interactions, the close spacing of the elements leads to mutual coupling. This complicates the theoretical analysis and modeling of these antennas, but these complications can be resolved through a combination of simulation and experiment. Four key aspects of this work are presented: (1) the careful balancing of the amplitude-phase characteristics of the passive scatteres with using special experimental schemes, taking into account most mutual coupling effect, (2) the development of multilayer structures and array assemblies, intended for widening of phase range of the reflected RF radiation from the mirror, (3) an examination of the bandwidth, and (4) experimental measurement of antenna directivity diagrams and pattern integrity. Our results demonstrated that highly directional patterns can be realized while controlling beam orientation in both azimuth and elevation. Prototype antennas achieve 19 to 22 dBi of gain across an operational 120 degrees of azimuth and 20 degrees in elevation, using an array with an aperture of 100 cm $\times$ 65 cm (5 rows of 100 elements each).

Planar Array Antenna with Parasitic Elements for Beam Steering Control

M. T. Ali[1], **T. A. Rahman**[2], **M. R. Kamarudin**[2], **M. N. Md Tan**[1], **and R. Sauleau**[3]

[1]Faculty of Electrical Engineering, Universiti Teknologi Mara (UiTM)
Shah Alam, Selangor, Malaysia
[2]Wireless Communication Center (WCC), Universiti Teknologi Malaysia
81310 UTM Skudai, Johor, Malaysia
[3]Institut d'électronique et de télécommunications de Rennes, (IETR)
UMR CNRS 6164, University of Rennes 1, France

Abstract— A new antenna structure is formed by combining the concept of a reconfigurable planar array antenna with the parasitic elements technique to improve the beam steering. The integration of PIN diode switches to the antenna has enabled to steer the antenna beams in the desired direction. This can be done by changing the switches mode to either switch it ON or OFF. In this work, a number of reflectors have been proposed namely parasitic elements and were placed between the patches which aimed to increase the steering beam angle. By having such configuration, the main beam of the array can be titled due to the effect of mutual coupling between the driven elements and the parasitic elements (reflectors). The unique property of this antenna design is that instead of fabricating all together in the same plane, the antenna's feeding network is separated from the antenna radiating elements (the patches) by an air gap distance. This will allow the interferences from the feeding line to be minimized. The optimization results for the resonant frequencies of the antennas with variable air gap heights were also studied. The comparison results between antenna with and without parasitic elements were investigated in this paper. The simulation results for the antenna will be compared with measurements, to show that the beam can be steered by controlling the switches mode. Experimental results are presented to demonstrate the excellent performance of this antenna.

Multiband MIMO Antenna with a Band Stop Matching Circuit for Next Generation Mobile Applications

Min-Seok Han and Jaehoon Choi
Division of Electrical and Computer Engineering, Hanyang University
17 Haengdang-dong, Seongdong-gu, Seoul 133-791, Korea

Abstract— Next generation mobile systems have to satisfy the requirements of high data rates and flexible interfaces for different communication system standards. MIMO (Multiple Input Multiple Output) technology has been regarded as one of practical approaches to accommodate such requirements by increasing wireless channel capacity and reliability. However, it is usually a big challenge to place multiple antennas within a small and slim mobile handset while maintaining the good isolation between antenna elements since the antennas are strongly coupled with each other and even with the ground plane by sharing the surface currents distributed on it.

In this paper, a multiband MIMO antenna with a band stop matching circuit for next generation mobile applications is proposed. The proposed multiband MIMO antenna consists of two dual-band PIFAs which provide wideband characteristics. In order to improve the isolation characteristic at the LTE band, a band stop matching circuit was inserted at the corner of each antenna element. The inserted band stop matching circuit is to suppress the surface currents at the specific frequency band and to generate two additional resonances in the 760 MHz band to cover LTE operation and in the 860 MHz band to cover GSM850 operation. In addition, the band stop matching circuit reveals minimal effect on the upper band performance. The proposed MIMO antenna can cover LTE, GSM850, GSM900, GSM1800, GSM1900, WCDMA and M-WiMAX services, simultaneously. Design considerations and experimental results of the multiband MIMO antenna with a band stop matching circuit are presented.

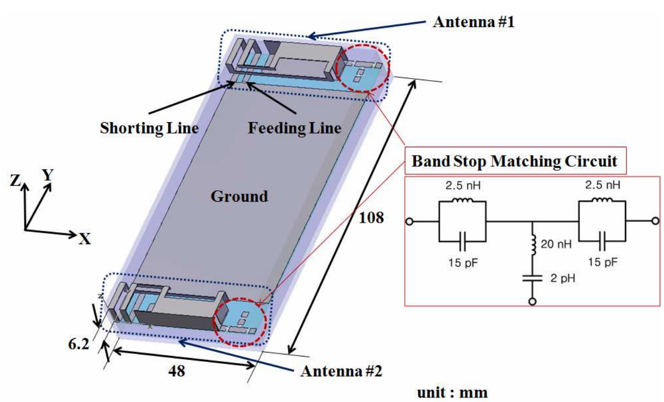

Figure 1: Geometry of the proposed multiband MIMO antenna.

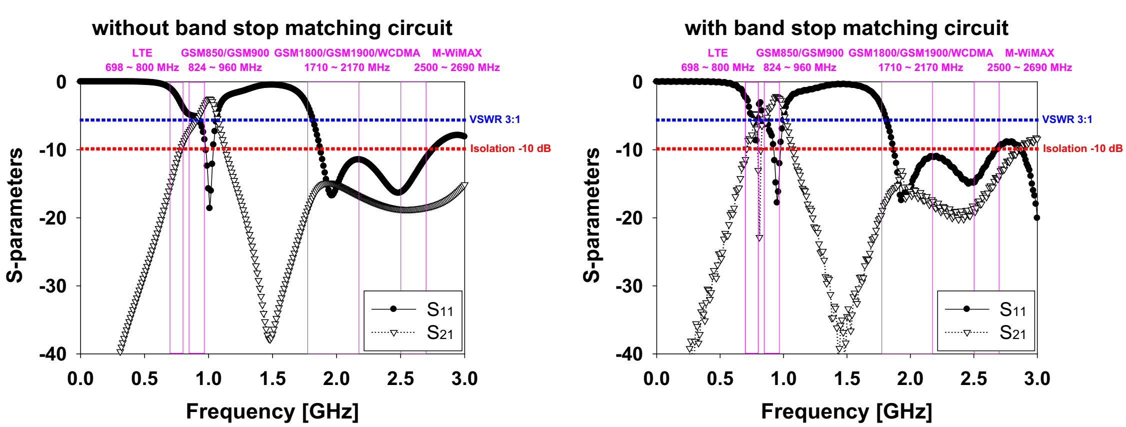

Figure 2: Simulated S-parameter characteristics without and with band stop matching circuit.

Dual ISM Band Mircostrip Antenna for Satellite Internet Service

Byoungchul Kim[1], **Sangwoon Lee**[1], **Joongyu Ryu**[2],
Hosung Choo[3], **Hojin Lee**[2], **and Ikmo Park**[1]

[1]Department of Electrical and Computer Engineering, Ajou University
5 Wonchun-dong, Youngtong-gu, Suwon 443-749, Korea
[2]Broadcasting and Telecommunications Convergence Research Laboratory, ETRI
161 Gajeong-dong, Yuseong-gu, Daejeon 305-700, Korea
[3]School of Electronics and Electrical Engineering, Hongik University
72-1 Sangsu-dong, Mapo-gu, Seoul 121-791, Korea

Abstract— In recent years, satellite internet has received much attention for wireless internet applications on high-speed trains. The Korean high-speed train (KTX) network requires antennas that operate at both the 2.4 GHz and 5.8 GHz industrial, scientific, and medical (ISM) bands for simultaneous transmission and receiving of data. Additionally, it should have nearly equal gain with similar radiation patterns in both bands for optimum communication. Microstrip patch antennas have been used in many applications due to their low cost, light weight, low profile, and ease of fabrication. Dual-frequency operation can be obtained by making slots on the microstrip patch, or by placing shorting pins at appropriate locations on the microstrip patch. However, when the higher frequency band is more than twice that of the lower frequency band, the radiation pattern of the higher resonant frequency becomes distorted due to the higher order resonant modes. In this paper, a dual-band microstrip antenna with nearly equal gain and similar radiation patterns at the 2.4 GHz and 5.8 GHz ISM bands is described. The proposed antenna, shown in Fig. 1, has two Y-shaped slots on the microstrip patch. It is fabricated on an RO4003 substrate, which has a dielectric constant of 3.38 and a thickness of 0.508 mm. The size of the antenna is $50 \times 47.5 \times 6.5\,\mathrm{mm}^3$, and it is fed by a coaxial cable. The measured bandwidth of the antenna is 2.376–2.492 GHz and 5.425–6.055 GHz for VSWR < 2. The measured gain is 8.37 dB and 8.38 dB for the 2.4 GHz and 5.8 GHz ISM bands, respectively.

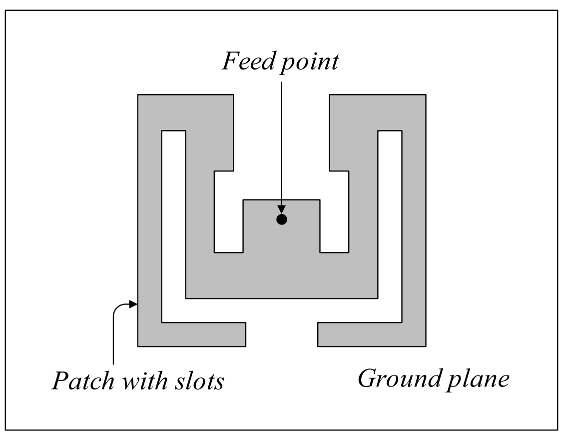

Figure 1: Antenna structure.

Directional GPS Antenna for Indoor Positioning Applications

Kerem Özsoy[1, 2] **and Ibrahim Tekin**[1]

[1]Electronics Engineering, Sabancı University, Istanbul, Turkey
[2]Vestek Electronic Research & Development Corp., Istanbul, Turkey

Abstract— In this paper, a directional GPS antenna for L1 frequency — 1575 MHz — with RHCP and a high directive gain is proposed for indoor positioning applications. The proposed antenna is made of a standard off the shelf GPS patch antenna with an additional conical reflector to enhance the gain and the beamwidth of the antenna. The angle of the cone reflector is optimized by HFSS 11 software. Finally, the cone is fabricated, integrated with the patch antenna and measured. The measurement results show that the antenna with the reflector has a 9 dBi gain and a beamwidth of 60 degrees with an axial ratio of 1 dB which agrees well with simulation results.

Introduction: The Civil Global Positioning System (GPS) has become very popular in recent years and it has wide usage in many areas. With the latest technological advances such as Differential GPS (DGPS), Assisted GPS (AGPS), civil GPS receivers are able to locate themselves with an error of 1–3 meters outdoors [1]. Although GPS is very successful in outdoor areas, it is hard to decode GPS signals indoors due to the additional signal loss caused by the buildings. For indoors, signals go through additional loss of 10–30 dB [2], in which case, signal levels are too low for an off-the shelf GPS receiver to detect the satellite signal. In order to solve indoor coverage problem, we plan to build an indoor positioning system that uses the GPS infrastructure. This indoor positioning system consists of GPS pseudo-satellites (pseudolite) and a GPS receiver with improved positioning algorithms. A pseudolite should be able to pick up the satellite signal only from a given direction in the sky and transmit the amplified signals to an indoor area. There are several ways to design a directional antenna such as Yagi-Uda, horn, log periodic, reflector and parabolic antenna or phased array systems [3]. Along these antennas, a reflector antenna type is chosen since these antennas are simple to manufacture, and also compact and robust in performance and low cost.

In this paper, we propose a directional GPS antenna for L1 frequency — 1575 MHz — with RHCP and a high directive gain. A standard off the shelf GPS patch antenna is used in the design, and directivity increase is achieved through the use of a conical reflector. Off-the-shelf microstrip patch antenna has a gain of 4 dBi. When the conical reflector is placed around the microstrip antenna, gain of the microstrip antenna is increased while the beamwidth of the antenna decreases. The cone is optimized by running simulations on HFSS 11 software tool. Finally, the cone is fabricated and integrated with patch antenna and measured. The measurement results show that the antenna has a 9 dBi gain which is 5 dB higher than the original patch antenna and a beamwidth of 60 degrees with an axial ratio of 1 dB. In the conference, design of the conical reflector, the simulation results and the measurements obtained in an anechoic chamber will be presented.

REFERENCES

1. Liu, H., H. Darabi, P. Banerjee, and J. Liu, "Survey of wireless indoor positioning techniques and systems," *IEEE Transaction on Systems, Man, and Cybernetics*, Vol. 37, No. 6, 1067–1077, November 2007.
2. Peterson, B. B., D. Bruckner, and S. Heye, "Measuring GPS signals indoors," *Proceedings of the Institute of Navigation's ION GPS-2001*, September 2001.
3. Balanis, C. A., *Antenna Theory, Analysis and Design*, 2nd ed., Wiley, New York, 1997.

Printed Dipole Array Fed with Parallel Stripline for Ku-band Applications

M. Dogan[1,3], **K. Özsoy**[1,2], **and I. Tekin**[1]

[1]Electronics Engineering, Sabanci University, Istanbul, Turkey
[2]Vestek Electronic Research & Development Corp., Istanbul, Turkey
[3]TUBITAK, UEKAE, Kocaeli, Turkey

Abstract— This paper presents the design procedure of a printed dipole antenna and 1D array configurations of the single dipole element in the Ku-Band with its metallic reflector plane parallel to the array plane. The proposed antenna has a natural beam tilt which is useful for some specific applications. Several array configurations in 1D are simulated and tested. The effect of mutual coupling among each array elements is also investigated. Required modifications on the individual array element and the feed structures due to the effect of mutual coupling are examined. The single dipole and array of dipole has measured VSWR values smaller than 2 in the Ku-Band with simulated gains of 5.7 dBi and 12 dBi, respectively.

Introduction: Recent studies are highly focused on antenna design in Ku-Band. Since the Ku-band has enough available bandwidth for satellite links, Ku-band systems are widely used in satellite communications, especially in the mobile antenna systems used in vehicles. There are also other application areas of Ku-band systems such as weather radars and fire detection radars. These sort of systems needs highly directive antennas with a very wide frequency band covers the all Ku-Band to transmit signals to the receiver with equal power in the whole frequency range and an automatic tracking systems to capture the maximum power incident from the satellite while the time and place of the receiver changed. In order to provide good tracking system, one can use digital phase shifter technology or mechanical systems to tilt the beam of the receiver both in azimuth and elevation to the specified direction which will increase the cost of the system or decrease the accuracy of the tracking system respectively. In this paper, a printed dipole antenna which operates in the Ku-Band with high gain and tilted beam is proposed. Since the proposed antenna has a tilted beam in elevation, it will be used in mobile satellite communication systems to eliminate the mechanical or digital needs at least in one direction to tilt the beam of the system. Also, arrays of these printed dipoles will be investigated and the gain of the arrays will be both simulated and measured.

Simulation & Measurement Results: The single printed dipole element designed in ADS-2006A has a VSWR < 2 in the 10.7 GHz–13.1 GHz range. The measurement results show that it has $S_{11} < -10$ dB in between 9 GHz–14 GHz. The simulated gain of the single element printed dipole antenna is 5.7 dBi at 11.5 GHz. The characteristics of 1×2 printed dipole array is also measured and the preliminary results show us that the array has VSWR < 2 in the Ku-band.

We have also simulated 1×8 dipole array in Ku band, and results show that the array return loss is less than -10 dB in 10.7–12.7 GHz band. Simulated gain changes between 10–12 dBi in the band of interest. The beam is tilted from the broadside direction such that only azimuthal rotation is necessary for a mobile antenna system. The measurement results and the simulated results of the single dipole element and 1×2 and 1×8 dipole arrays will be presented at the conference.

A Circular Disc Monopole UWB Antenna Fed with a Tapered Microstrip Line on a Circular Ground

Yangjun Zhang, **Masahiro Shimasaki**, **and Toyokatsu Miyashita**
Department of Electronics & Informatics, Ryukoku University
Seta, Ohtsu 520-2194, Japan

Abstract— The printed disc monopole antenna is considered a good candidate for 3.1 to 10.6 GHz UWB systems [1, 2]. This paper presents a miniature circular disc monopole UWB antenna implemented on a FR-4 substrate ($\varepsilon_r = 4.4$). The antenna was miniaturized by using a tapered microstrip feed line on a circular ground, as shown in Fig. 1. The total size of antenna is $40 \times 30\,\mathrm{mm}^2$, and the diameter of radiation disc is 12 mm. The results of measured and simulated return loss are shown in Fig. 2. It indicates there are differences between the simulated and measured return loss, but both the simulated and measured results show that good impedance matching has been obtained as the -10 dB return loss bandwidth covers the whole UWB band from 3.1 to 10.6 GHz.

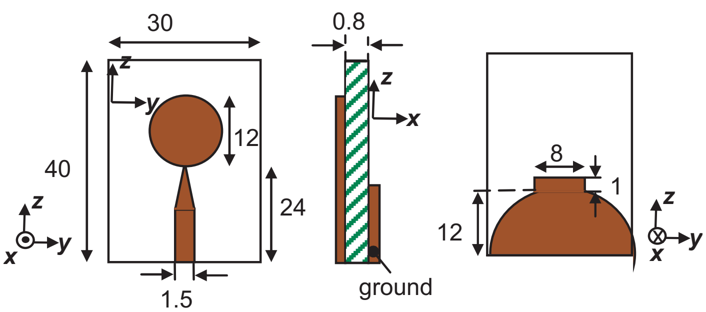

(a) Top view (b) Side view (c) Back view

Figure 1: The UWB antenna configuration.

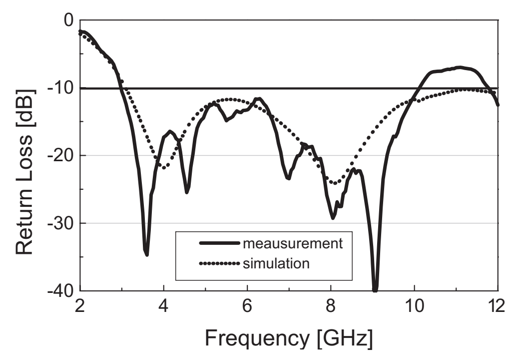

Figure 2: Measured and simulated return loss.

The radiation patterns of the proposed antenna over the UWB frequency band have been measured. The results at 8 GHz are shown in Fig. 3. It is noticed that the measured and simulated radiation patterns agree well, and the omnidirectional pattern was shown at x-y-plane. The time-domain performance of the UWB antenna is shown in Fig. 4, where the group delay of the two UWB antennas placed with a distance of 36 cm was given. Within the frequency range from 3 to 9 GHz, the group delay is about 2 ns.

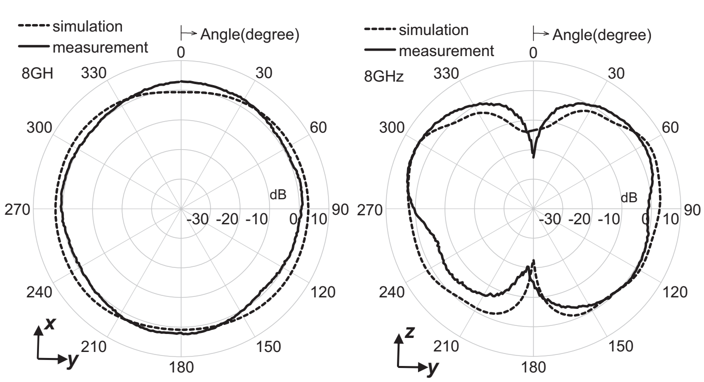

(a) x-y-plane (b) y-z-plane

Figure 3: Measured and simulated radiation patterns at 8 GHz.

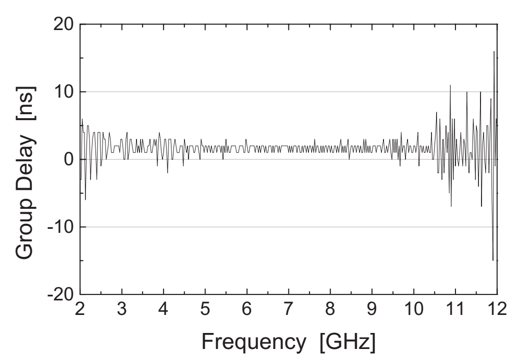

Figure 4: Measured group delay.

REFERENCES

1. Cho, Y. J., K. H. Kim, D. H. Choi, S. S. Lee, and S.-O. Park, "A miniature UWB planar monopole antenna with 5-GHz band-rejection filter and the time-domain characteristics," *IEEE Trans. on Antennas and Propagation*, Vol. 54, No. 5, 1453–1460, 2006.
2. Guo, L., J. Liang, C. C. Chiau, X. Chen, C. G. Parini, and J. Yu, "Performances of ultra-wideband disc monopoles in time domain," *IET Microwave Antennas Propag.*, Vol. 1, No. 4, 955–959, 2007.

Improved Tapered Slot-line Antennas Loaded by Grating

Peng Zhang, Shu Jun Tang, and Wen-Xun Zhang
State Key Laboratory of Millimeter Waves, Southeast University
Nanjing, Jiangsu 210096, China

Abstract— The tapered slot-line antenna (TSA) has been used widely as element of phased arrays, feed of reflector or reflectarray, UWB radiator for time-domain systems. It is a travelling-wave end-fire antenna with advantages of wideband, uni-directive beam, and thin-sheet structure. However, its gain is less than a broadside antenna with the similar sizes; the cost of enhancing gain will be sharply extending its length; the bandwidth depends on the taper ratio (max./min. of the slot-width) and the length of taper too. Hence, a risen question is how to further improve the performance of Gain or Bandwidth based on a fixed structural frame? The answer should be to utilize sufficiently the frame-space, one scheme is just setting proper grating inside the zone of tapered slot. Correspondingly, two kinds of samples are designed, simulated, and tested with good results as expected.

One is a gain enhanced TSA with grating load and symmetric linear taper. It increases gain 2 dB up over the frequency range of $6.0 \sim 9.5$ GHz (45.2%); or 3 dB up over $8.0 \sim 9.5$ GHz (17.1%). However, the bandwidth for VSWR $\leq 2.0:1$ was slightly decreased from $5.7 \sim 11.2$ GHz (65.1%) to $5.3 \sim 9.6$ GHz (57.7%). In addition, the beam-width in E- and H-planes approaches to the same.

Another is a bandwidth broaden TSA with grating load and asymmetric exponential (Vivaldi) taper. It expands the bandwidth $2.0 \sim 6.0$ GHz for VSWR $\leq 2.0:1$, and also $3.0 \sim 6.0$ GHz (75%) for vertical shaping pattern satisfying the specifications of base-station in mobile communication system. Especially, the VSWR $\leq 1.5:1$ is over both two WiMAX bands of $3.3 \sim 3.8$ GHz and $5.1 \sim 5.8$ GHz; while the service coverage efficiencies are higher than 69.5% and 73.2% respectively; about 1 dB gain enhancement, and also improved radiation patterns with lower back-lobe and downward null-filling are achieved.

Both samples keep planar structure with complete printed technology in fabrication, and maintain the frame sizes.

ACKNOWLEDGMENT

This work was supported by the National High-Tech Project (No. 2007AA01Z264).

Using High Impedance Ground Plane for Improving Radiation in Monopole Antenna and Its Unusual Reflection Phase Properties

S. M. Abootorabi, M. Kaboli, S. A. Mirtaheri, and M. S. Abrishamian
K. N. Toosi University of Technology, Iran

Abstract— In this paper improving radiation characteristics of monopole antenna on a high impedance ground plane has been investigated. For this purpose the properties of periodic electromagnetic band gap (EBG) structures have been used [1, 2].

As we know conductors are used as reflectors or ground plane in many antenna situations. Surface waves or surface currents are bound to the interface of metal and air. Recent researches have dealt with the suppression of surface wave to improve radiation characteristics of monopole antenna

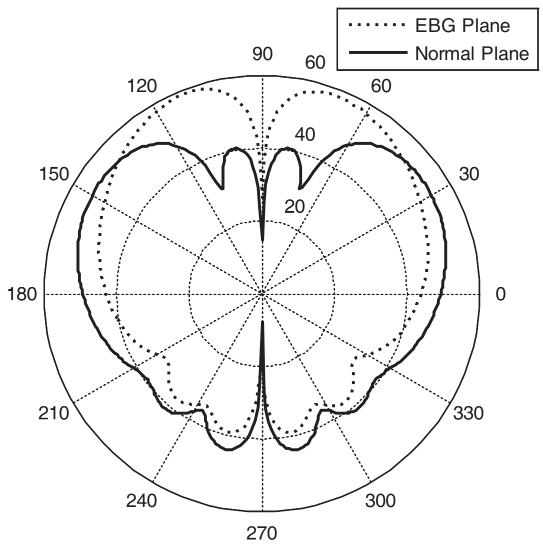

Figure 1: Comparison of radiation patterns on EBG ground plane and normal ground plane using HFSS simulation.

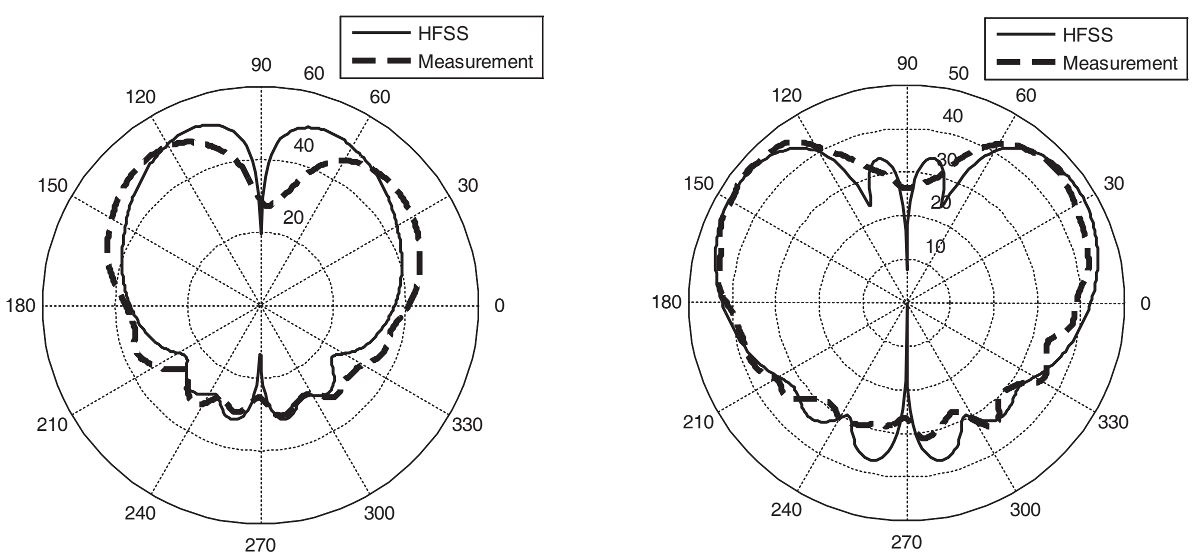

(a) (b)

Figure 2: Comparison of measurement and HFSS simulation, (a) EBG ground plane, (b) Normal metal ground plane.

using high impedance ground plane (HIGP) in high frequencies such as 35 GHz with hexagonal patches on substrate [3, 4]. In this study high Impedance surface (HIS) as ground plane for monopole antenna at lower frequencies such as 6 GHz with square patches in shape have been used. Due to suppression of surface waves in the band gap, a significant amount of power that is wasted in back lobes reduces about 8 dB, also radiation power in forward direction increases about $10 \sim 25$ dB in some directions. Comparison of patterns on normal metal ground plane and HIGP which are obtained by HFSS simulation could be seen in Figure 1. There are good agreements with measurement and simulation results as shown in Figure 2, in 6 GHz frequency.

Effect of the ground plane dimension and number of square patches have also been investigated and it has been observed that a bigger ground plane and more number of metal patches will have a better effect of improving radiation pattern.

Another property that is confined to EBG structures is their unusual reflection phase which is changing continuously from +180 to −180 [5]. We changed the length of monopole antenna from 0.245λ to 0.27λ and it found that where the monopole antenna has a good return loss is very close to points that the reflection phase has a quantity between $90° \pm 45°$.

Consequently this HIS may be very useful in a variety of electromagnetic problems and antenna structures.

REFERENCES

1. Xu, H.-J., Y.-H. Zhang, and Y. Fan, "Analysis of the connector section between K connector and microstrip with Electromagnetic Band Gap (EBG) structure," *Progress In Electromagnetic Research*, PIER 73, 239–247, 2007.
2. Pirhadi, A. and M. Hakkak, "Using electromagnetic band gap superstrate to enhance the bandwidth of probe-fed microstrip antenna," *Progress In Electromagnetic Research*, PIER 61, 215–230, 2006.
3. Sievenpiper, D., L. Zhang, R. F. Jimenez Broas, N. G. Alexopolous, and E. Yablonovitch, "High-impedance electromagnetic surfaces with a forbidden frequency band," *IEEE Transactions on Microwave Theory and Technique*, Vol. 47, No. 11, November 1999.
4. Sievenpiper, D., "High-impedance electromagnetic surfaces," PhD Dissertation, UCLA, 1999.
5. Yang, F. and Y. Rahmat Samii, "Microstrip antennas integrated with Electromagnetic Band-Gap (EBG) structures: A low mutual coupling design for array applications," *IEEE Transactions on Antennas and Propagation*, Vol. 51, No. 10, October 2003.

The Impact of New Feeder Arrangement on RDRA Radiation Characteristics

A. S. Elkorany, A. A. Sharshar, and S. M. Elhalafawy
Department of Electronics and Electrical Comm., Faculty of Electronics Eng.
Menoufia University, Menouf, Menoufia 32952, Egypt

Abstract— Dielectric resonator antennas (DRAs) have been extensively investigated after the first paper published by Long et al.. Recently one of the major topics in DRA research is to enhance the impedance bandwidth. The techniques that have been used to widen the impedance bandwidth include, inserting air gap between the dielectric and the ground plane, using different dielectric geometries, using strip fed, using hybrid configuration, and using multi-segment configuration.

Rectangular dielectric resonator antenna RDRA with an air gap that inserted between the dielectric and ground plane was previously proposed, and an achievement in the impedance bandwidth in the order of 31% between 4.5 GHz and 6.2 GHz has been obtained. In this work, a further development in the antenna structure has been suggested to get further improvement in the antenna impedance bandwidth. A new feeder arrangement has been proposed and its effect on the impedance bandwidth has been recorded. This is done by inserting a small rectangular metallic patch within the air gap between the ground plane and the dielectric. The metallic batch is connected to the inner of the coaxial probe feeder. This technique was used successfully in a previous work with microstrip patch antenna, in which two metallic patches with different shapes were inserted between the patch and ground plane. In the present research the dimensions of inserted patch have been changed and the impact of that on the impedance bandwidth has been examined. The dielectric that is used is FR4 with $\varepsilon_r = 4.5$, and its dimensions is $20\,\mathrm{mm} \times 12\,\mathrm{mm} \times 5\,\mathrm{mm}$, the probe diameter is 1.25 mm, and its height is 2.5 mm, the inserted patch height is 1 mm, all theses parameters are held constant in all cases. Unexpected ultrawide impedance bandwidth has been obtained. Some results are recorded here to show the effect of this new feeder on the antenna impedance bandwidth. An impedance bandwidth of about 2.55 : 1 between 10.2 GHz and 26 GHz is achieved when the patch dimensions were $9\,\mathrm{mm} \times 4\,\mathrm{mm}$, while the bandwidth extends from 16 GHz up to a value behind 34 GHz is achieved when the patch dimensions was $16\,\mathrm{mm} \times 3\,\mathrm{mm}$. The maximum radiation is in the broadside direction and is obtained with a suitable cross polarization level.

Session 2P8
Electromagnetic Probing of Atmosphere and Ionosphere

Vector Diffraction Integrals for Solving Inverse Problems of Radio-holographic Sensing of the Earth's Surface and Atmosphere

A. G. Pavelyev
IRE RAS, Moscow Region 141120, Russia

Abstract— Vector relationships between the fields on a certain surface confining an inhomogeneous three-dimensional volume and the fields inside this volume are obtained by the Stratton-Chu method developed for the case of homogeneous media. The vector relationships allow us to solve the direct and inverse problems of determining the fields inside an inhomogeneous medium given the field on its boundary. The vector equations take into account the polarization changes of direct and inverse waves propagated in an inhomogeneous medium. In the case of a two-dimensional homogeneous medium, the vector equations reduce to the previously obtained scalar equations used in the approximation of spherical symmetry to describe the process of backward wave propagation during the atmospheric and ionospheric radio-occultation monitoring. It is shown that the Green's function of the scalar wave equation in an inhomogeneous medium should be used as the reference signal for solving the inverse problem of radio-occultation monitoring. This validates the method of radio-holographic focused synthetic aperture method (RHFSA) previously used for high-accuracy retrieval of the vertical refractive-index profiles in the ionosphere and atmosphere. In this method, the reference-signal phase was determined from a model which describes with sufficient accuracy the radiophysical parameters of a refracting medium in the region of radio-occultation sensing. Zverev's diffractive integral is used to compare the canonical transform (CT), back propagation (BP), and RFSA methods. For comparison, a general inverse operator (GIO) is introduced. The CT and BP transforms can be obtained by application of the GIO transform to Zverev's diffractive integral. The CT method can resolve physical rays in multipath situations under an assumption of the global spherical symmetry of the atmosphere and ionosphere. The RHFSA method can account for the multipath in the case when the global spherical symmetry is absent by using the appropriate model of the refractivity and has a promise to be effective for operational data analysis. The obtained equations can be used for the high-accuracy solving of inverse problems of radio-holographic remote sensing of the Earth's atmosphere and surface by highly-stabilized signals of radio-navigation satellites.

Identification and Localization of Layers in the Atmosphere and Ionosphere Based on Observing Variations in the Phase and Amplitude of Radio Waves along the Satellite-to-satellite Path

A. G. Pavelyev[1], **Y. A. Liou**[2], **J. Wickert**[3], **and A. A. Pavelyev**[1]

[1]IRE RAS, Moscow, Russia
[2]CSRSR, NCU, Chung-Li 320, Taiwan
[3]GFZ-Potsdam, Potsdam, Germany

Abstract— The phase acceleration of radio waves is fundamentally important to the analysis of radio occultations (RO) data and plays the same role as the Doppler frequency and phase path excess. Phase acceleration technique allows one to convert the phase path excess or Doppler frequency changes measured in RO experiments into the refraction attenuation variations. From these derived refraction attenuation and amplitude data one can estimate the integral absorption of radio waves. This is important for future RO missions when measuring the water vapor and minor atmospheric gas constituents concentrations because the difficulty of removing the refraction attenuation effect from the amplitude data can be avoided. It is important also that the contribution in RO signal from layered structures in the atmosphere and ionosphere can be separated from that one of the irregularities and turbulence by comparison and/or correlation of the refraction attenuations found from the phase and amplitude data. The advantages of the phase acceleration/intensity technique are validated by analyzing the RO data from the Challenging Minisatellite Payload (CHAMP) and the FORMOSA Satellite Constellation Observing Systems for Meteorology, Ionosphere, and Climate missions (FORMOSAT-3/COSMIC). The technique locates the turning point, where the gradient of the refraction index is perpendicular to the ray trajectory and the influence of the layered structure on the parameters of radio waves is maximal. The technique was verified by measuring the turning point on the ray trajectory in a neutral gas in the atmosphere. The position for inclined plasma layers was determined and the electron density distribution was found for the considered radio occultation sessions.

Peculiarities and Perspectives of Network Digital Ionospheric Station "PARUS"

Alexander L. Karpenko, Ljudmila N. Leshchenko, and Natalia I. Manaenkova
Institute of Terrestrial Magnetism, Ionosphere and Radio Wave Propagation (IZMIRAN)
Troitsk, Moscow Region 142190, Russia

Abstract— The commonly used method of remote diagnostic of the space distribution and the time behavior of so complex media as ionosphere is based on the using of special devices — so called ionosondes. The Digital Ionosonde "Parus", first created at IZMIRAN almost twenty years ago, is developing successfully and now it is advanced modern high-precision inexpensive instrument.

Digital ionosonde "Parus" is constructed on two-processor basis: IBM PC + DSP ADSP2189. Signal processor performs the most complicated part of calculations with incoming data stream: signal accumulation, analysis, extraction from noise, digital conversion of signal in the case of using pseudo-random modulation. Signal processor module is fulfilled as PCI slot.

PC processor controls the total sounding process: radio receiving/transmitting, time synchronization. It performs final data storing, dynamic graphical presentation of results, interaction with operator. Ionosonde "PARUS" provides standard regime of ionospheric station with the possibility of self-acting every 5, 15, 30 minute. Minimum time of ionogram registration is near 6 seconds (for 500 transmitted frequencies).

The measurements, obtained by digital ionosonde are time-series of the observables of reflected HF radio wave. In order to use these data and make ionosphere monitoring, HF radio wave propagation forecasts and other researches it had been necessary to create suitable interface.

Ionosonde "Parus" is accompanied by special software — "Integrated multiwindow Data Processor". Wide capabilities of this Data Processor allow to direct data proceeding, including actions with data base of measurements, generating day F-H-graphics, month accounts; generating archive of row and processed ionograms. "Graphic Editor" produces interactive scaling of ionogram. As a result of processing of row ionogram by so-called "Graphic Editor" it is possible to receive all main ionospheric parameters and characteristics, corresponding URSI standard, to digitize any ionosphere layer, to generate output file in SAO-format.

Software of Ionosonde "Parus" didn't contain automatic data processing, but it is not so serious disadvantage. Manual data processing of single ionogram need at less than 5 minutes, but precision of all ionospheric parameters and characteristics are perfect. It is well-known, that inaccuracy of automatic data processing may reach 30%. But for scientific investigations of ionosphere high precision is more preferable than time-delay.

As regards HF radio wave propagation forecast, software of Ionosonde "Parus" contains so-called "Clearance procedure" of row ionogram. This procedure may simplify automatic finding of main ionospheric parameters of each, unique ionogram. This will be new way, different from mean square approximation to the parameters of "nearest" ionograms of Digital Ionogram DataBase, which is provided for general use at Software of "Digisonde".

At IZMIRAN during period 2002–2009 years Data Base of processed ionograms and accounts are accumulated. Now Ionospheric Data of Ionosonde "Parus" are regularly sent to World Data Centers in Moscow. There is not enough Interactive Ionosperic Data Resource in Russia. That is why nearest future plan is to add all available digital ionospheric data stored by network Ionosphere Stations "Parus" into existing Information Systems of Ionospheric Data.

Active Space Experiments with the Use of the Transport Spacecraft "Progress" and Irkutsk IS Radar

Alexander P. Potekhin[1], **Vitaly V. Khakhinov**[1,2], **Andrey V. Medvedev**[1], **Dmitry S. Kushnarev**[1], **Valentin P. Lebedev**[1], **and Boris G. Shpynev**[1]

[1]Institute of Solar-Terrestrial Physics of Siberian Branch of Russian Academy of Sciences
664033, Lermontov St. 126a, p/o Box 291, Irkutsk, Russia
[2]Irkutsk State University of Railway Engineering, Irkutsk, Russia

Abstract— A sequence of active space experiments was carried out in 2007–2009. Orbital maneuvering subsystem (OMS) engines of the transport spacecraft (TSC) "Progress" were used as a source of disturbances for ionospheric and radar signature characteristics. The TSC orbit altitude was about 340 km. Amount of the OMS engine exhaust products was relatively small.

In order to perform this experiment, the Irkutsk Incoherent Scatter Radar of ISTP SB RAS was used. Each burn took place exactly over the radar. Exhaust directions and amount of injected products changed for each flight. High precision measurements of TSC coordinate and reflecting characteristics as well as space-time disturbances of plasma parameters were executed during experiments. Multiple radar beams allowed us to observe the modified and unmodified ionosphere simultaneously. The data analysis showed that relatively small exhaust products caused considerable changes in the electron concentration profile and TSC radar cross-section (RCS) value.

The following parameters of the radar signal were analyzed to study radar TSC signatures: amplitude, range, beam velocity, azimuth, and elevation as a function of two half-horns of the radar antenna phase difference. Range and beam velocity reacted to the engine burn very insignificantly. When the exhaust was directed towards the radar, the amplitude, azimuth and elevation changed significantly.

Results of the experimental data processing allow us to conclude that artificial ionospheric disturbances, associated with the "Progress" OMS engine burn, produce significant changes in ionospheric and radar signatures even for a relatively small amount of exhaust product. Changes in ionospheric and radar characteristics strongly depend on geometry of the experiment. The most significant changes are observed when the OMS engine burn is directed towards the radar. Electron density depression ("hole") reaches up to $\sim$20%–30%. The hole life-time is about 10–15 minutes. Angular characteristics and RCS are the most sensitive radar parameters.

Influence of Ionospheric Disturbances on HF Propagation

V. I. Kurkin
Institute of Solar-Terrestrial Physics, Siberian Branch of Russian Academy of Sciences, Irkutsk, Russia

Abstract— Vertical and oblique-incidence sounding (VIS&OIS) data obtained from ionosounders located in the north-eastern region of Russia have been used to study ionospheric disturbances and influence of ones on HF propagation. Prolonged experiments on 24-hour basis for 30 days were carried out using OIS for Magadan-Irkutsk and Norilsk-Irkutsk paths at all seasons for 2005–2008. Spectrums of multi-scale variations were derived from that the data. We used the spectral analysis based on a modified Fourier transform with varying upper limit. It was shown that disturbances with a periods ~1–4 hours occurred during main phase of the moderate storms. These disturbances produce the changes in the height of F2 layer maximum ~40–100 km and in the critical frequency ~1.5–2.0 MHz. Similar wave disturbances may be caused by a generation AGW in auroral zone and their propagation to equatorial latitudes. These disturbances affect on the variations of maximal observed frequency (MOF) on investigated paths. The second type of ionospheric disturbances is associated with the response of ionosphere to the geomagnetic storm and manifests as the strong decrease of ionization in daytime. These are the typical negative disturbances. In the recovery storm phase in the afternoon and evening hours the abrupt decreases of electron concentration (falls of foF2 diurnal variation) associated with the shift of the main ionospheric trough to the low latitudes are observed. These abrupt decreases of ionization in the F2-layer also distort the characteristics of ionospheric radio channel. The spectral analysis of OIS data revealed stable fluctuations of MOF with 7–8 days the periods around autumnal equinoxes and with 2–3 days periods around vernal equinoxes. These periods are characteristic for planetary waves. According to vertical sounding data in the extensive spatial area of the north-eastern region of Russia similar change of some parameters of the ionosphere was marked. This variations can serve as the experimental evidence of planetary waves penetration up to ionosphere heights and their influence on distribution of electronic concentration.

ACKNOWLEDGMENT

This work was supported by Russian Foundation for Basic Research (grant 08-05-00658).

Detection of Heating Effects Due to Powerful Radiowaves Propagation by Irkutsk Complex for Passive Doppler Sounding of the Ionosphere

O. I. Berngardt, **V. G. Abramov**, **V. I. Kurkin**, **and G. A. Zherebtsov**
Institute of Solar-Terrestrial Physics, SB RAS, Russia

Abstract— Irkutsk Complex for Passive Doppler Sounding of the Ionosphere (ICPDSI) was created in Institute of Solar-Terrestrial physics SB RAS (ISTP SB RAS). The ICPDSI complex includes the system for simultaneous four-channel receiving of 1–30 MHz radiosignals with the ability of program frequency control and the three-position receiving system for estimating radiowaves propagation azimuth.

Doppler measurements in ISTP SB RAS was started a long time ago, but solving the task of making regular measurements in continuous monitoring mode for different propagation paths becomes possible only recently due to increasing of technical abilities.

In the talk, we have presented the data of observations of the signals generated by the heaters SURA (Russia, October 20–22, 2008) and Tromsø (Norway, March 4–12, 2009) in Irkutsk. The main peculiarities of the observations are long propagation distance almost along the latitude over the midlatitude (SURA-Irkutsk) and subpolar (Tromsø-Irkutsk) paths. The source generating the radiowaves is lengthy and located at ionospheric heights (near the F2 maximum).

In the talk the variations of frequency and amplitude of the received signals are presented. The observations of spectral broadening of the signals, received at the basic heating frequency, are demonstrated. The preliminary estimations of azimuthal characteristics of the received signals are presented and discussed.

Numerical simulations of long propagation of radiosignals, arising as a result of propagation of powerful radiowaves in the ionosphere, are made. The estimation of the conditions for successful observations of the heater facilities signals is done.

Qualitative interpretation of the observations is made.

It is shown that Irkutsk Complex for Passive Doppler Sounding of the Ionosphere is an instrument effective enough for detecting the effects caused by the heating facilities functioning and for investigating the propagation conditions for radiowaves, generated during the heating of the ionosphere by powerful radiowaves.

Ionosphere Wave Packets Excited by the Solar Terminator: AGW or MHD origin?

E. L. Afraimovich, **S. V. Voyeikov**, **I. K. Edemskiy**, **and Yu. V. Yasyukevich**
Institute of Solar-Terrestrial Physics SB RAS, Russia

Abstract— We analyzed the dynamic and spectral characteristics of the medium-scale travelling ionospheric disturbances (MS TID) in the form of travelling wave packets (MS TWP). We used total electron content (TEC) measurements from the global network of GPS receivers (up to 1500 stations) in 1998–2007 and the dense Japanese network GPS/GEONET (1220 stations) in 2008–2009. Diurnal, seasonal, spectral and spatial-temporal MS TWP characteristics are determined by the solar terminator (ST) dynamics and do not depend on the solar or geomagnetic activity. In the time field, TWPs are narrow-band TEC oscillations of duration of about 1–2 hours with oscillation periods of 10–20 minutes. In winter, TWPs in the northern hemisphere are observed 3–4 hours after the morning ST passage, when the TEC time derivative achieves his maximum. In summer, TWPs are recorded 1.5–2 hours before the evening ST occurrence at the point of observations, but at the moment of the evening ST passage in the magneto-conjugate area. The TWP spatial structure is of a high degree of anisotropy and coherence at the distance of more than 10 wavelengths; the TWP wavelength is about 100–300 km. Both the high Q-factor of oscillatory system and synchronization of TWP occurrence with solar terminator passage at the point of observations and in the magneto-conjugate area testify the MHD nature of ST-excited TWP generation. The obtained results are the first experimental evidence for the hypothesis for the ST-generated ion sound waves (Huba et al., GRL, 2000, 27, 19, 3181).

Radio Probing and Tomographic Imaging of the Ionosphere

V. E. Kunitsyn[1], **E. D. Tereshchenko**[2], **E. S. Andreeva**[1], **I. A. Nesterov**[1], **and M. O. Nazarenko**[1]

[1]M. Lomonosov Moscow State University, Moscow, Russia
[2]Polar Geophysical Institute RAS, Murmansk, Russia

Abstract— Results are presented of radio tomography (RT) and radio sounding of the ionosphere in different latitudinal and longitudinal sectors during quiet and disturbed time intervals. Methods are considered for ionospheric radio tomography employing radio transmissions from low-orbital satellite systems (LORT) such as the Russian "Tsikada" or American "Transit". Radio tomographic technique based on high-orbital satellite systems (HORT) like GPS/GLONASS is discussed. LO and HO RT imaging of the ionosphere reveal various ionospheric structures including different forms of ionospheric trough, equatorial anomaly, traveling ionospheric disturbances, blobes, ionospheric traces of precipitation, wavelike structures, etc. Manifestations of anthropogenic impact (rocket launching, industrial explosions, HF heating) upon the ionosphere are illustrated by RT images. Determination of ionospheric plasma fluxes from a series of successive LORT cross-sections is described. Ionospheric effects related to the Earth's rotation that are observed consecutively at corresponding sites in the eastern and western hemispheres are discussed. Specificity of HORT technique, application of this method to the ionospheric research and results obtained so far are described. Due to low angular velocity of GPS satellites it becomes essential in HORT to take into account temporal variations in the ionosphere during the period of reconstruction, which necessarily results in the 4D statement of RT problem (three spatial coordinates and time). Another problem ensues from uneven coverage of the Earth by GPS ground receivers, therefore, unlike in 2D LORT, here an additional procedure is required to interpolate the found solutions into regions of missing data. Examples are given of 4D ionospheric RT imaging during periods of disturbed and quiet geophysical conditions. HORT results are compared with other ionospheric measurements including radar and ionosondes data. Examples of LORT comparison with HORT are shown. Spatial resolution of HORT is much worse than that of LORT. It is shown that combination of LORT and HORT provides best quality ionospheric imaging. LORT and HORT results obtained in different latidudinal and longitudinal sectors are compared with corresponding model data. Scenarios for RT with elements of radio occultation technique are described. Problem of RT data assimilation is discussed.

Intercomparison between Different Schemes of Electromagnetic Probing

E. S. Andreeva, **S. A. Kalashnikova**, **and V. E. Kunitsyn**
M. Lomonosov Moscow State University, Moscow, Russia

Abstract— The upper atmosphere is known to respond to both external influences, such as solar variations, and internal motions originating in the atmosphere near the Earth's surface. The Global Ultraviolet Imager (GUVI) [http://guvi.jhuapl.edu/] is used to determine energy inputs from the sun into a region of the upper atmosphere where ultraviolet light ionizes the atoms and molecules. GUVI is one of four instruments constituting the TIMED (Thermosphere Ionosphere Mesosphere Energetics and Dynamics) [2] spacecraft, which has 625 kilometer circular orbit with the inclination 74.1 degrees from the equator. It is a far-ultraviolet (115 to 180 nm), scanning imaging spectrograph that provides horizon-to-horizon images in five selectable wavelength intervals, or "colors". These colors (HI 121.6 nm, OI 130.4 nm, OI 135.6 nm, and N2 Lyman-Birge-Hopfield bands 140 to 150 nm and 165 to 180 nm) are chosen in order to produce the GUVI key parameters. The DMSP (Defense Meteorological Satellite Program) satellites fly in sun-synchronous, 99-degree inclination orbits at 840 km altitude with orbital periods of about $\sim$ 101 min [3]. The Precipitating Energetic Particle Spectrometer (SSJ/4) aboard the DMSP spacecraft measures electrons and ions in 20 energy channels ranging from 30 eV to 31.3 keV at sweep rate of once per second. The sensors are oriented such that their look direction is within a few degrees of the local vertical. Thus at 840 km in the auroral zone, the instruments are always looking within the loss cone. Detailed description of the SSJ/4 sensors can be found in [4]. In this study, vertical TEC data obtained with Radio Tomography technique [1] along the chain in Alaska region and the Russian chain Moscow-Spitsbergen during the period of an extra strong geomagnetic storm in October 2003 are compared with GUVI data, and with the fluxes of ionizing particles measured by DMSP satellites. GUVI data allows, in the case of coincidence of the ground projection of the satellite path with adjusted region, to get average intensity for 5 colors of 2 types (types are rectified, unrectified). The tracks of DMSP satellites are close to the orientation of receivers chain but still can pass aside. In the comparison only nearby tracks were considered. The analysis shows the qualitative correspondence of ionization along the chains both between latitudinal distribution of precipitations and intensity.

REFERENCES

1. Kunitsyn, V. E. and E. D. Tereshchenko, *Ionospheric Tomography*, Springer-Verlag, 2003.
2. Thermosphere Ionosphere Mesosphere Energetics and Dynamics, A Guide to the Mission, the Spacecraft and the Mission Team, Johns Hopkins University Applied Physics Laboratory, 2006.
3. Lilensten, J. and M. Galand, "Proton-electron precipitation e.ects on the electron production and density above EISCAT (Tromso) and ESR," *Ann. Geophysicae*, Vol. 16, 1299–1307, 1998.
4. Hardy, D. A., et al., "Precipitating electron and ion detectors (SSJ/4) on the block 5D/Flights 6-10 DMSP satellites: Calibration and data presentation," Rep. AFGL-TR-84-0317, Air Force Geophys. Lab., Hanscom Air Force Base, Mass., 1984.

Theoretical Investigation of the Ultrawideband FMCW Signal Propagation through Ionospheric Radiochannel

Nikolay V. Ilyin[1] **and Vitaly V. Khakhinov**[1,2]
[1]Institute of Solar-Terrestrial Physics of Siberian Branch of Russian Academy of Sciences, Irkutsk, Russia
[2]Irkutsk State University of Railway Engineering, Irkutsk, Russia

Abstract— The central objective in the FMCW theory is to solve the problem of ionospheric propagation of HF ultrawideband signals. The well known approaches to solving this problem are the following. The earlier approach was reported in [1]. The principle of the method is that the radiated FMCW signal is divided into narrow-band components using the theory of ionospheric propagation of narrow-band pulses. Another approach has been reported in [2]. The transfer function of the ionospheric radiochannel was represented as a set of transfer functions, each of which was expanded into a Taylor series in the neighborhoods of central frequencies; the passing of the transmitted signal through each transfer function was considered separately.

The approach used in this paper was suggested in [3], and differs fundamentally from those mentioned above. It is based on a consistent formal examination of the influence results exerted by the ionospheric radiochannel and the chirpsounder receiver devices on the FMCW signal. Subsequent transformations of the formal expression obtained for the recorded spectrum are carried out by using the main functional and technical characteristics of the chirpsounder receiver. It is shown that the recorded spectrum of the received signal sample is similar to the response of the ionospheric radiochannel to the narrow-band signal with the envelope, which is an exact replica of the form of the window's spectral function.

Digital methods applied to chirp signal processing considerably expand its ability to adaptively reverse signal distortion in the dispersive ionospheric radiochannels and correct the phase-frequency characteristic of the radiochannel. This paper presents a technique that analyses the FMCW signal at the output of the IF filter to reconstruct the radiochannel transfer function of the ionospheric path.

REFERENCES

1. Phillipp, N. D., N. Sh. Blaunshtein, L. M. Eruhimov, V. A. Ivanov, and V. P. Uryadov, *Modern Methods Investigation of Dynamical Process in Ionosphere*, Shtiinca, Kishinev, 1991.
2. Lunborg, B. and M. Lungren, "On the spectral width of chirpsounder signals," *J. Atmos. Terr. Phys.*, 54, 1992.
3. Ilyin, N. V., V. V. Khakhinov, V. I. Kurkin, V. E. Nosov, I. I. Orlov, and S. N. Ponomarchuk, "The theory of chirp-signal ionospheric sounding," *Proc. Int. Symp. Anten. & Prop.*, 3, Chiba, Japan, 1996.

Session 2P9
Theory and Methods of Digital Signal and Image Processing

Nongaussian Kravchenko-Rvachev Distributions in Radio Physical Applications

V. F. Kravchenko[1], **O. V. Kravchenko**[2], **and A. R. Safin**[1]

[1]Kotel'nikov Institute of Radio Engineering and Electronics of RAS, Russian Federation
[2]Bauman Moscow State Technical University, Russian Federarion

Abstract— Nongaussian distributions [1] both stationary and nonstationary random processes in respect of digital signal and image processing (DSIP) different physical nature are considered. This approach based on the theory of atomic functions (AF) [2] received from strict solving of functional differential equation the following kind:

$$Lf(x) = \lambda \sum_{k=1}^{M} c(k) f(ax - b(k)), \quad |a| > 1, \tag{1}$$

where L is a linear differential operator with constant coefficients. If $a = 1$ and $b(k) \equiv 0$ ($k = 1; M$) (1) becomes an ordinary differential equation.

The following questions are examined.

1. Variate transformations:
   (a) transformation by addition constant;
   (b) transformation by multiplication on constant;
   (c) general transformation.
2. Conditional density.
3. Statistical independence.
4. Mixed expressions.
5. Main theorem about mathematical expectation.
6. Characteristic functions.
7. Limit theorems.

It should note that construction a new nongaussian Kravchenko-Rvachev distribution based on cumulant analysis (semi-invariant) principles. This approach make it possible to increase class of problems associated with two-dimensional and N-dimensional probability densities with regard to independent random processes. A new theory application on a concrete physical problems is considered. A numerical experiment and comparison with gaussian (normal) distribution shown efficiency as well as reliability of developed and founded approach.

REFERENCES

1. Maurice, G. and M. A. Kendall, *The Advanced Theory of Statistics*, Vol. 1, Second Edition, Charles Griffin & Company Limited, London, 1945.
2. Kravchenko, V. F., "Lectures on the theory of atomic functions and their applications," *Radiotekhnika*, Moscow, 2003.

The Theory of Spectral Estimation of Signals and Generalized Kravchenko-Kotel'nikov-Levitan Theorems

V. F. Kravchenko and D. V. Churikov
Kotel'nikov Institute of Radio Engineering and Electronics of RAS, Russian Federatian

Abstract— In this report, the theory of spectral estimation of signals on based of generalized two-dimensional (2D) Kravchenko-Kotel'nikov-Levitan theorems is considered. In the first part the 2D weight functions with support area of the complex shape on the basis of R-functions are constructed. Two-dimensional weight functions are constructing by means the folowing expression: $W(x,y) = w(1 - \Omega(x,y))$. Here, $w(x)$ is one dimensional prototype and $\Omega(x,y)$ is the normalized R-function [1]. The Kravchenko-Kotel'nikov (KK) and Kravchenko-Levitan (KL) weight functions are constructed on basis of atomic functions [2]. One dimensional Kravchenko-Kotel'nikov weight functions (windows) are defined by the following expression $w_{KK}(x) = \prod\limits_{j=1}^{M} \operatorname{sinc}\left(\frac{\pi}{\Delta a^{j-1}}x\right)$. Its behavior is influenced with three parameters: M, a, and Δ. One dimensional Kravchenko-Levitan weight functions (windows) are defined like this $w_{KL}(x) = \prod\limits_{j=1}^{M} \left(\operatorname{sinc}\left(\frac{\pi}{\Delta 2^{j-1}}x\right)\right)^{2r+2}$. Weight functions $w_{KL}(x)$ as well as $w_{KK}(x)$ depend on the following three parameters: M, r, and Δ. So, 2D weight functions $W_{KK}(x,y)$ and $W_{KL}(x,y)$ are depend on more than three parameters. In the second part the 2D Kravchenko-Kotel'nikov-Levitan theorems are formulated. In the third part, it's application for spectral estimation, filtering and correction of 2D signals and images. As the examples the problems of noise reduction, scaling and also spectral properties improvement of images are submited. The numerical experiment and physical analysis of 2D signal processing results are show efficiency of new 2D kernels construction of sampling theorems.

REFERENCES

1. Kravchenko, V. F. and V. L. Rvachev, *Boolean Algebra, Atomic Functions and Wavelets in Physical Applications*, Fizmatlit, Moscow, 2006.
2. Kravchenko, V. F., *Digital Signal and Image Processing in Radio Physical Applications*, Fiznatlit, Moscow, 2007.

Application of the Theory of R-functions to the Analysis and Synthesis of Multidimensional Signals

D. V. Churikov
Kotel'nikov Institute of Radio Engineering and Electronics of RAS, Moscow, Russian Federation

Abstract— In this report application of the theory of R-functions for construction of two-dimensional (2D) digital filters (DF) is considered. It is known that 2D DF are synthesized in time or frequency space on some support areas which geometry has significant importance. The form of support area influences physical characteristics of 2D DF. Known methods allow to synthesize 2D DF only on the elementary support areas [1, 2]. Theory of R-functions (Rvachev functions) [3] allows to describe at analytical level the equation of support area of the complex shape. Procedure of construction of 2D DF includes some stages. At first the ideal frequency characteristic of the filter on the support area set in the form of R-function as following $H(\omega_1, \omega_2) = \begin{cases} 1, & \Omega(\omega_1, \omega_2) \geq 0, \\ 0, & \Omega(\omega_1, \omega_2) < 0 \end{cases}$. Here, $\Omega(\omega_1, \omega_2)$ is the R-function. Then coefficient of the infinite pulse characteristic of filter are computed by $h_0[n_1, n_2] = \frac{1}{4\pi^2} \int\limits_{-\pi}^{\pi} \int\limits_{-\pi}^{\pi} H_0(\omega_1, \omega_2) e^{j(\omega_1 n_1 + \omega_2 n_2)} d\omega_1 d\omega_2$. At a following stage for improvement of convergence of series the coefficients $h_0[n_1, n_2]$ should be multiplied on finite 2D weight function (WF) $h[n_1, n_2] = w[n_1, n_2] \cdot h_0[n_1, n_2]$. Here, $w[n_1, n_2] = w^*[-n_1, -n_2]$ is the real-valued function. As the examples the problems of noise reduction and spectral properties improvement of images are submitted. The numerical experiment and physical analysis of 2D signal processing results are show efficiency of new 2D digital filters.

REFERENCES

1. Dudgeon, D. E. and R. M. Mersereau, *Multidimensional Digital Signal Processing*, Prentice-Hall, Inc., 1984.
2. Shirmana, J. D., *Radio-electronic Systems: Bases of Construction and the Theory*, The directory, Radio engineering, Moscow, 2007.
3. Kravchenko, V. F. and V. L. Rvachev, *Boolean Algebra, Atomic Functions and Wavelets in Physical Applications*, Fizmatlit, Moscow, 2006.

An Application Generalized Kravchenko-Kotel'nikov Theorem on Atomic Functions $fup_N(t)$ to Interpolation Nonstationary Random Processes

O. V. Kravchenko[1] **and A. R. Safin**[2]

[1]Bauman Moscow State Technical University, Russian Federarion
[2]Kotel'nikov Institute of Radio Engineering and Electronics of RAS, Russian Federation

Abstract— Signal interpolation problem (restoration) on it's discrete values is important both in signals with finite spectrum theory and theory of random processes. In report methods and interpolation algoritms of nonstationary random processes with finite spectrum on discrete samples with Kravchenko-Kotel'nikov theorem using are considered. In the capacity of interpolation kernels atomic function [1] Fourier transforms $\mathrm{fup}_n(\mathrm{t})$ are used in it. This approach allows of obtain convergence acceleration constructed serieses in comparison with Whittaker-Kotelnikov-Shannon serieses. Questions associated with finite number of samples in constructed serieses, choice of optimal filters transmission band, interpolation random processes with infinite spectrum are analyzed. A carried out numerical experiment and comparison with Whittaker-Kotelnikov-Shannon theorem shown efficiency of introduced approach with a view to mean square error minimum. This affect is reached by using complicated (in comparison with ideal) low-pass filters which could be easily to do using digital processing methods on a modern microprocessors and microcontrollers.

REFERENCES

1. Kravchenko, V. F., *Lectures on the Theory of Atomic Functions and Their Applications*, Radiotekhnika, Moscow, 2003.

Atomic Functions in Problems of Analysis and Synthesis of Optimal Discrete Recievers

O. V. Kravchenko[1] **and A. R. Safin**[2]

[1]Moscow State Technical University, Russian Federarion
[2]Kotel'nikov Institute of Radio Engineering and Electronics of RAS, Russian Federation

Abstract— In this report, a synthesis approaches of optimal discrete receivers use of Kravchenko-Kotel'nikov theorem on atomic functions fup_n [Victor F. Kravchenko. Lectures on the theory of atomic functions and their applications, Moscow, Radiotekhnika, 2003.] are considered. A choice of interpolation filter minimizing a relative mean square error restoration continuous signal on its discrete samples in terms of Kravchenko-Kotel'nikov theorem [Victor F. Kravchenko and Ansar R. Safin. Atomic Functions and N-D Whittaker-Kotel'nikov-Shannon Theorem, Moscow, An International Journal Electromagnetic Waves and Electronic Systems, 2008, Vol. 13, No. 12, pp.31–44] is discussed on the first step. Comparison to the theorem Wittaker-Kotel'nikov-Shannon is carried out (for ideal low-pass filters). On the step stage concrete analysis and synthesis optimal discrete signal receivers methods are suggested. The following questions are researched in terms of this approach:

1. Discrete representation of signals with finite spectrum in terms of Kravchenko-Kotel'nikov theorem.
2. Signals with finite spectrum through quadripole with time-dependent parameters. Narrow-band and wide-band oscillation.
3. Transient responce with time-dependent parameters. Consider the following channel models:
   (a) image channel;
   (b) dispersion channel;
   (c) mixed channel.
4. Signals reception with and without an estimate of parameters (concrete circuitry).
5. Optimal narrow and wide-band signal receivers.

Numerical experiments shown efficiency and validity using approach proposed in the problems of discrete signal reception.

Construction of New Kravchenko-Kotel'nikov-Chebyshev-Legendre Spectral Kernels and Their Application in Digital Multidimensional Signals Processing

D. V. Churikov
Kotel'nikov Institute of Radio Engineering and Electronics of RAS, Russian Federation

Abstract— In this report, the new approach based on combination of Kravchenko-Kotel'nikov weight functions (WF) (windows) with Chebyshev and Legendre polynomials as spectral kernels is proposed. Shown that obtained structures have some advantages in comparison with spectral wave analysis of multidimensional signals. The new approach based on application of spectral kernels to problems of digital signal processing is considered. In theory of communication the signals are represented in the form of a linear combination of elementary functions. The Kravchenko-Kotel'nikov (KK) WF are constructed on basis of atomic functions [1]. Kravchenko-Kotel'nikov WF are defined by the following expression: $w_{KK}(x) = \prod_{j=1}^{M} \operatorname{sinc}\left(\frac{\pi}{\Delta a^{j-1}} x\right)$. Its behavior is influenced with three parameters: M, a, and Δ. The new constructions of spectral kernels are obtained in form of direct product of KK WF with Chebyshev and Legendre polynomials. Application of spectral analysis of multidimensional signals in basis of digital functions in comparison with the spectral harmonious analysis gives certain advantages. Optimal processing in spectral area in comparison with the time possesses has advantages on application of numerical algorithms. Spectral signal processing possesses a high noise stability in noise condition which eigen basis differs from eigenfunctions of a signal. The physical characteristics and analysis of numerical experiment confirm efficiency of new spectral kernels and also WA-systems on their basis in tasks of spectral estimation and digital multidimensional signal processing.

REFERENCES

1. Kravchenko, V. F., *Digital Signal and Image Processing in Radio Physical Applications*, Moscow, Fizmatlit, 2007.

Short Range Radar with MIMO Antenna System and Multifrequency Sounding Signal

V. V. Chapursky, **S. I. Ivashov**, **I. A. Vasiliev**, **and A. V. Zhuravlev**
Bauman Moscow State Technical University, Russia

Abstract— New direction of radiolocation systems (RLS) development is application of principles of spatially multichannel construction at continuous radiation of orthogonal sounding signals (SS). In radio communication systems and in recent publications on radiolocation such construction is designated by abbreviation MIMO (Multiple Input-Multiple Output) [1]. The MIMO radar assumes the use of transmitting and receiving antenna systems (AS) consisting of spatially distributed elements of low directivity, radiating mutually orthogonal SS. One of the first radars of the given class is French long range system RIAS [2]. Similar RLS are studied also in Russia and China [3–5]. Application of MIMO radar principles is perspective also at creation of short range radars for detection of people behind radiotransparent obstacles since allows to apply energetically more favourable continuous multifrequency SS. At continuous radiation and the greater number of MIMO AS elements the greater signal accumulation takes place. That is equivalently to antenna gain increase. The low level of side lobe of system signal function on spatial coordinates is reached also. Such approach does not demand the application of a complex antenna element phase control system and allows to make the space surveillance in digital vector signals processing system fed from outputs of simple receiving elements of AS.

In the given work the test mockup of short range MIMO radar was created and algorithms of digital vector signals processing system fed from outputs of AS simple receiving elements are developed at radiation by transmitting AS elements the orthogonal multifrequency SS. The problem of allocation of inactive objects (people) on a background of motionless local objects was solved. Thus there was expedient a refusal of the target speed resolution. The following variants of local objects suppression are offered: 1) coherent processing of quadrature signals on each of partial frequencies in receiving channels of AS on a basis of rejection filters bank with the subsequent performance of coherent focusing algorithms on spatial coordinates; 2) spatial focusing on two or several surveillance periods at the subsequent coherent or noncoherent subtraction for registration of changes on these surveys. In the report the technological view of MIMO RLS breadboard model from eight-elements transmitting and eight-elements receiving linear antenna arrays in length accordingly 0.9 m and 1.2 m is submitted at radiation of 16 orthogonal frequency SS components in a frequency range from 1.45 GHz up to 1.75 GHz. Modeling the offered processing algorithms is carried out and the results of laboratory experiments with detection of slowly moving object as a metal plate on a background of local objects and indoors interferences are submitted. The received experimental results as a whole have confirmed efficiency of a breadboard model and the chosen algorithm of the targets selection on a background of local object reflections.

REFERENCES

1. Fishler, E., A. Haimovich, R. Blum, D. Chizhik, L. Cimini, and R. Valenzuela, MIMO radar: An idea who's time has come," *Proceedings of the IEEE Radar Conference*, 71–78, April 26–29, 2004.
2. Dorey, J., G. Garnier, and G. Auvray, "RIAS, radar a impulsion et antenne syntetique," *Colloque International sur le Radar*, 556–562, Paris, April 1989.
3. Kucherov, J. S. and V. V. Chapursky, "Antennae arrays with super fast beam scanning," *A Radio Engineering and Electronics*, 1562–1569, 1994.
4. Vovshin, B. M., "UWB radar-tracking systems," *Progressive Directions of Radio-electronic Complexes and Systems Development Proceedings*, Part 1, 139–149, 30-anniversary of TZNI-IRES, Moscow, September 12–14, 2001.
5. Wu, J., K. Jiang, and R. He, "Researches of a new kind of advansed meter wave radar," *Proceedings of International Radar Conference*, 71–75, Beijing, China, October 2001.

A Wavelet Technique to Extract the Backscatter Signatures from SAR Images of the Sea

S. Zecchetto[1], **F. De Biasio**[1], **and P. Trivero**[2]

[1]Istituto Scienze dell'Atmosfera e del Clima, Italy
[2]Università di Alessandria, Italy

Abstract— Synthetic Aperture Radar (SAR) images of the sea often show backscatter structures linked to the horizontal structure of the Marine Atmospheric Boundary Layer (MABL) at the interface with the sea surface. In general, their dimensions are spread over a wide range of length scales; furthermore, they may present spatial periodicity as well as intermittence. Standard techniques, as the two-dimensional Fourier analysis, are unsuitable when it is of interest both to detect intermittent phenomena and to analyze the spatial pattern of the backscatter structures imaged by SAR. With the aim to isolate such backscatter structures, the two-dimensional continuous wavelet transform (CWT2) analysis has been applied to SAR images of the sea.

CWT2 has been computed using the Mexican Hat mother wavelet, which has the property of capturing the fine scale structure of the data and is suitable for the continuous wavelet transform because it is non-orthogonal. Other wavelets tested, i.e., the Morlet and Paul4, produce similar but less accurate results.

The choice of the continuous instead of the Discrete Wavelet Transform (DWT), computationally more efficient, is done to explore in detail a region roughly from 0.8 to 2.5 km, where the cells produced by the wind are expected to lie. This would be impossible with the DWT: with pixel size of about 150 m, the only scales explored in this range are 1.2 km and 2.4 km.

The SAR images have been compressed to get a pixel size of about 150 m: this narrows the radiometric confidence interval of the radar backscatter intensity estimate, and smears out the effects of the variable geometry of the scattering surface. It also filters out geophysical phenomena at scales shorter than 150 m as, for instance, sea gravity waves, without hiding the backscatter structures related to the atmosphere dynamics.

The images have to be preprocessed before the CWT2 analysis, to mask the land and to mitigate the effects introduced by the variation in range of the radar incidence angle. Preprocessing is needed to avoid that structures on the inner part of the image, where the radar incidence angle is smaller and the radar backscatter higher, prevail on the outer ones.

The scales range is very important because it defines the geophysical phenomena to study. In this work we focus on the spatial range from 300 m to 4 km in both the x and the y directions. The scales have been obtained dividing logarithmically the range of interest in seven intervals, corresponding to eight scales. Thus, 64 maps have been computed for each SAR image.

Through the evaluation of the wavelet variance map, which ideally corresponds to the two-dimensional Fourier spectrum, it has been possible to infer the scales of the maximum energy.

SAR-like maps, obtained adding the wavelet coefficient maps at scales around the position of the maximum value of the wavelet variance map, have permitted to highlight the backscatter cells associated to the structure of MABL. These cells have been statistically characterized by the frequency distributions of the length of the cells maximum and minimum axes, of the orientation of the maximum axis and of their area. The results indicate that backscatter cells have an elliptic shape, with the major axis along the wind roll direction; the average axes ratio is of 2.5. The frequency distribution of the cells area is almost continuous without significant gaps. The cells major axis indicates the aliased wind direction.

The technique developed is the background for several applications: it has been used to compute the wind fields without any a priori information (Zecchetto et al., 2008), as well as to study the inner structure of the Langmuir atmospheric circulation (Zecchetto et al., 2002). Other applications could be on the detection of sea surface oil slicks.

Some example of results obtained analyzing hundreds of SAR images will be shown.

Orthogonal Kravchenko Wavelets in Digital Signal and Image Processing

Y. Y. Konovalov and A. V. Yurin
Bauman Moscow State Technical University, Moscow, Russia

Abstract— A new class of orthogonal Kravchenko WA-systems [1] is discussed. These wavelets are based on multiresolution analysis construction with the using of atomic functions. As there are many different classes of atomic functions, so a new class of wavelets contains a wide set of functions. Each of them has its own properties: localization both in time and frequency; decomposition and reconstruction filters; uncertainty constants. Their common properties are smoothness and symmetry. The comparison of new Kravchenko wavelets with the well known ones is presented. It demonstrates the advantage of new WA-systems. The numeric experiment shows the efficiency of new Kravchenko wavelets in model problems of digital signal and image processing.

REFERENCES

1. Kravchenko, V. F., O. S. Labunko, A. M. Lerer, and G. P. Sinyavsky, *Computing Methods in the Modern Radio Physics*, Fizmatlit, 2009.

Radar-target Identification Using Exponential Single-pulse Synthesis

Juan D. Morales León[1], **David Blanco**[2], **Diego P. Ruiz Padillo**[2], **and María C. Carrión**[2]

[1]Telefónica España, Spain
[2]Applied Physics Department, Sciences Faculty, University of Granada, Spain

Abstract— New contributions to non-cooperative radar-target discrimination using only the scattered response $r(t)$ of conductive objects are presented in this paper. The technique studied is the single-pulse (S-pulse), which makes use of natural resonances as discrimination features [1–4]. These technique uses the structure of the late-time response of the target to design a filter, the S-pulse, such the convolution between the S-pulse and the scattered signal $r(t)$, in the late time, is a damped sinusoid when the target used in the design of the filter and the one that scattered the signal are the same. The S-pulse expansion using complex exponential functions as basis functions is proposed, obtaining new S-pulse with characteristics completely different from those in the literature. Due to the increase in the number of free parameters, an adjustable spectrum can be designed to achieve our goal, i.e., to improve discrimination capability. Specifically, a weighting factor is added to modulate the exponential frequency. On the other hand, in order to find the optimum discrimination, a non-linear optimum process is required. These optimization processes can be done using the SIMPLEX method. This is a non-linear optimization method that just needs the evaluation of the cost function, but not the gradient or the hessian. This last property is specially important in this case, since the cost function does not possess an analytical form, and its derivatives can not be obtained. Numerical results achieved in the discrimination between thin straight wires of different lengths show that the proposed exponential S-pulse improve the discrimination results with respect to other types of S-pulse in the literature.

REFERENCES

1. Chen, K. M., D. P. Nyquist, E. J. Rothwell, L. L.Webb, and B. Drachman, "Radar target discrimination by convolution of radar return with extinction-pulses and single-mode extraction signals," *IEEE Trans. Antennas and Propagat.*, Vol. 34, 896–904, July 1986.
2. Gallego, A., M. C. Carrión, D. P. Ruiz, and J. A. Morente, "Improved S-pulse automated scheme using subsectional polynomial basis functions," *IEEE Trans. Antennas and Propagat.*, Vol. 44, 859–862, Junio, 1996.
3. Baum, C. E., E. J. Rothwell, K. M. Chen, and D. P. Nyquist, "The singularity expansion method and its application to target identification," *Proc. IEEE*, Vol. 79, 1481–1492, Oct. 1991.
4. Morales, J. D., D. Blanco, D. P. Ruiz, and M. C. Carrión, "Radar-target identification via exponential extinction-pulse synthesis," *IEEE Trans. Antennas and Propagat.*, Vol. 54, No. 5, 1577–1585, 2007.

Signal Processing and Time Delay Resolution of Noise Radar System Based on Retrodirective Antennas

V. V. Chapursky[1], **V. A. Cherepenin**[2], **and V. I. Kalinin**[2]

[1]Bauman Moscow State Technical University, Russia
[2]Institute of Radioengineering and Electronics, Moscow, Russia

Abstract— One of the most interesting self-steering technologies for radar and wireless communication environments is based on retrodirective antenna [1]. A self-phased or retrodirective antenna automatically sends a received signal back to the direction of its originating source. Thus, the retrodirective antenna continuously adapts its phase response to track incoming waveform without prior knowledge of the source detection. Implementation of retrodirective antennas allows increasing spatial directivity and also to improve power efficiency and security (low interception) of radar systems [2, 3].

In recent years, investigations for the target observation method using wideband noise radar with recirculation antennas have been resumed. The surveillance is performed owing to recirculation of a noise signal in the spatial feedback loop. The loop is closed by means of combining a portion of the received radar signal with the current signal of the transmitter and radiation of the obtained sum signal toward the target. Although the application of retrodirective antennas have advanced greatly in the past years, the determination of great potential, spatial resolution, uniqueness for an antennas with spatial recirculation of wideband noise signals is still an unsolved problem, which, certainly, is of interest for theory and practice.

The purpose of this study is to fill this gap in the theory and to perform comparative estimation the resolution of noise radar in the presence and in the absence of spatial recirculation. This report presents theoretical comparison results of basic noise signal processing methods for one channel retrodirective noise radar system: 1) Cross-correlation processing with delayed reference signal of noise transmitter generator; 2) double spectrum processing of received recirculation noise signal; 3) cross-correlation processing with reference noise signal in special design recirculator based on various reference time delays. For basic processing methods it is obtained analytically expressions for output correlation functions as reference time delay is changed. It is theoretically demonstrated that first and second methods give completely identical results for spatial (or delay time) resolution of reflected target. But third correlation method allows obtaining spatial resolution that is bigger in several times as first and second methods with the same frequency band of noise signal. Third method of correlation signal processing is characterized by ultra high spatial (delay time) resolution of radar measurement. It is expected that noise waveforms recirculation will not only increase the delay resolution but will also enhance the angular resolution for the same dimensions of the antenna.

REFERENCES

1. Pon, C. Y., "Retrodirective array using the heterodyne technique," *IEEE Trans. Antennas and Propagation*, Vol. 12, 176–180, Mar. 1966.
2. Gupta, S. and E. R. Brown, "Noise-correlating radar based on retrodirective antennas," *IEEE Trans. Aerospace and Electronic Systems*, Vol. 43, No. 2, 472–479, Apr. 2007.
3. Kalinin, V. I. and V. V. Chapursky, "Ultrawideband noise radar based on antenna arrays with signal recirculation," *Journal of Communications Technology and Electronics*, Vol. 53, No. 10, 1195–1205, 2008.

Fractal Properties, Structural Entropy and Color of Printed Circuits Boards Processed by Laser Treatment

B. Varga[1], **Sz. Nagy**[2], **and I. Mojzes**[3]

[1]Temic Telefunken Microelectronic Hungary Kft., H-1106 Budapest, Napmátka u. 6., Hungary
[2]Department of Telecommunications, Széchenyi István University, H-9026 Győr, Egyetem tér 1., Hungary
[3]Department of Electronics Technology, Budapest University of Technology and Economics
H-1111, Budapest, Goldmann Gy. tér 3., Hungary

Abstract— Printed circuits boards (PCB) are sufficient parts of electronic and electronics appliances. Mass production of these devices requires identification of these products both during the technological steps (Traceability) and the services. The most effective way for marking these plates is to form data matrix code (DMC) on the surface and/or in-depth profiling of the solder masks up to the metallization. This is the first step in the surface mounted technology. In the course of the present work different PCB's were analysed originating from 12 manufacturers. The data matrix was formed using Nd:YAG and CO_2 lasers with different power and duration.

Two types of PCB samples were investigated. In the first group, only discoloration of the solder mask appeared, which was caused by the laser beam penetrating into the layer only down to a depth of several ms (coloring). In the second case, the solder mask is completely removed up to the copper layer, according to the pattern of data matrix code (engraving). The marking process of the first case with CO_2 laser is much different from the removal of layer with Nd:YAG laser. The different wavelength causes different marking solution. Coloring requires a low energy laser pulse in contrast to the engraving.

In our paper we present the results of laser parameter optimization for two laser types. A new coloring measure system was developed for the PCB's identification, namely measuring the coloring in XYZ-color system. The XYZ values of solder mask layers are measured, and a software was developed for calculating automatically the color coordinates x and y and the brightness value L. The formed data matrices were analyzed using fractal mathematics, some pictures showed fractal behavior. The line sharpness of the data matrices were also determined by using a structural entropy based method, which is able to derive the type of grid distributions.

Weak Signals Detection, Recovery Algorithms and Real Time Processing

Li-Ping Chen and Xiao-Juan Zhang
Institute of Electronics, Chinese Academy of Sciences, Beijing 100080, China

Abstract— The weak signals in the nature can represent some very important information like the rate of breathe and heartbreak of human beings, the health situation of some machines and huge buildings etc. And weak signals detection and recovery technologies have been studied for years and are growing fast. There are two detection methods: contact way using sensor to translate the vibration signals into electronic signals and process it, the other way is non-contact way using microwave or laser. However, the weak signals processing is essential and very important in the whole detection system. In order to improve the SNR of the signals in the output of the system, digital signals processing algorithm is frequently used. In this paper, the writer emphasized on the weak signals detection and recovery technologies based on a non-contact microwave detection system. In the base-band of the microwave receiver, we studied some algorithms that can separate the weak signals from the noise.

In the base-band of the detection system, based on a digital signal processing card and a notebook, we finished a platform that can process the signals in real time. Especially for the weak speech signals, we describe a modified single channel speech enhancement algorithm based on a spectral gain derived from MMSE-LSA and a minimum noise estimation approach. The proposed method does not need a voice activity detector to estimate the noise and renew the noise estimation in every frame to track varying level noise. Considering the properties of clean speech signal, we modified the spectral gain derived from MMSE-LSA. Extensive testing has shown that this algorithm can be implemented in real time and excellent noise suppression is achieved, while avoiding the musical residual noise phenomena and leading weak speech distortion.

Session 3AP
Poster Session 1

Effective Constitutive Model of Grain-oriented Fe-Si Laminations Core under Orthogonal Magnetization

Zhengrong Jiang[1,2], **Zhengxi Li**[1], **and Dehui Sun**[1]

[1]Department of Electric & Machinery Engineering
North China University of Technology, Beijing 100041, China
[2]State Key Lab of Power Systems, Department of Electrical Engineering
Tsinghua University, Beijing, China

Abstract— The mechanism of variable inductor based on orthogonal magnetization was discussed. The experiment and simulation showed that the dc bias field makes the hysteresis loop "shearing" and reduces the enclosed area. Hence the effective permeability decreases with increasing dc bias field. By comparing the shearing hysteresis caused by orthogonal magnetization with escalator, an effective anisotropic energy has been incorporated into the existing isotropic model equations. It has proved that effective constitutive model can adequately described the hysteresis and harmonic characteristic caused by orthogonal magnetization.

Prototype Design, Hardware and Construction of Compact and Tuneable X-band Pre-bunched Free Electron Maser

Fareq Malek[1], **James Lucas**[2], **Yi Huang**[2], **R. Badlishah Ahmad**[1], **Badr Muhammad Abdullah**[3], **and Azlan Awang**[4]

[1]Universiti Malaysia Perlis (UniMAP), Malaysia
[2]The University of Liverpool, United Kingdom
[3]King Fahd University of Petroleum and Minerals (KFUPM), Kingdom of Saudi Arabia
[4]TELECOM Bretagne, France

Abstract— We are developing prototype free electron maser (FEM) that is compact, tuneable and efficient for potential industrial use. Therefore we define the characteristics for the construction of a novel X-band rectangular waveguide pre-bunched free electron maser (PFEM). Our device operates at 10 GHz and employs two rectangular waveguide cavities (one for velocity modulation and the other for energy extraction). The electron beam used in this experiment is produced by thermionic electron gun which can operate at 3 kV and up to 50 μA. The resonant cavity consists of a thin gap section of height 1.5 mm which reduces the beam energy required for beam wave interaction. The prototype design, hardware and construction process are reported in this paper.

A Novel Electro-magnetic Transient Analysis Method Based on Orthogonal Projection Approach

Heng-Xu Ha[1], **Yu-Zhen Tan**[1], **Bo Chen**[2], **and Z. Q. Bo**[3]

[1]Shandong University of Technology, Zibo 255049, China
[2]Dispatching Center, Shaanxi Electric Power Company, 710045, China
[3]AREVA T&D UK Limited, UK

Abstract— The Electro-magnetic transient analysis for power system, which is the basis of the transient protection, fault analysis, transient computation, etc., plays an important role in the area of protective relaying. Modern Electro-magnetic transient analysis techniques are all based on the "characteristic method", in which the analysis firstly proceeded in frequency domain by Laplace transformation and the time domain solution is obtained by taking the inverse Laplace transform. The mathematics involved in this process is tedious and the complexity increases in non-linear circuits due to the convolution in each time interval, which needs a large amount of historic data.

Recently, several methods have been proposed to deal with this drawback and to avoid time domain convolution. The Finite Element Method requires the line to be subdivided into a finite number of regions. This allows the telegraph equations to be converted into a one-dimensional differential vector equation related to variable t and the recursive formulas of each element can be obtained. Waveform relaxation techniques avoid time domain convolution by solving the transmission line equations in the frequency domain and using the faster Fourier transform (FFT) to transform the results back and forth between time and frequency domain at each iteration. However, this requires many data points in order to avoid aliasing effects when very fast signals have to be studied. Recently, growing attention has been devoted to wavelets in applied electromagnetic, mainly for the solution of Galerkin-like problems and as shape functions in the moment method to obtain sparse matrices.

This paper presents a novel technique of transient analysis for power system, which based on a new principle, the orthogonal projection method. According to the approximation principle, signals can be approximated by the linear combination of a set of orthogonal basis, in which the set of coefficients of the linear combination are also called "projection to the basis". Certainly the voltage and the current at each point on the line can be approximated to be the linear combination of a certain set of orthogonal basis, for example, the Daubiechies basis. The differential functions of the current and voltage are also approximated by the linear combination of a set of projection values with the orthogonal basis. After projection onto orthogonal bases, which map to a function space relates to time variable t over a given resolution, the differential equations related to the voltage and current of transmission line transform to algebraic vector equations, based on which the projected equivalent models of each unit can be obtained. Then, the transients of the transmission system can be computed in the projection domain accordingly. EMTP simulation tests are presented which validate the method described.

Analytical Expressions of the Magnetic Field Created by Tile Permanent Magnets of Various Magnetization Directions

R. Ravaud and G. Lemarquand
LAUM, UMR CNRS 6613, Universite du Maine, Ave Olivier Messiaen, Le Mans 72085, France

Abstract— This paper presents a thorough study of the magnetic field created by tile permanent magnets in air. To do so, we use the coulombian model for determining the analytical expressions of the three magnetic field components created by tile magnets. Moreover, various magnetization directions are considered. Indeed, the direction of the magnetization can be axial, radial, uniform, tangential or intermediate between radial and tangential. Thus, this analytical study encompasses all the magnetization possibilities generally encountered in electrical engineering applications. According to the coulombian model, the magnets are represented by fictitious magnetic charge densities. For each configuration studied, both the surface and volume densities are taken into account for the analytical calculations. Consequently, our analytical calculations have been performed without using any simplifying assumption. It has to be noted that such analytical calculations are enabled because the tile permanent magnets considered are in air and the structures using these tile magnets are always ironless. Then, special functions such as elliptic integrals of the first, second and third kind are used to express analytically the components of the magnetic field. The case of the tile permanent magnet tangentially magnetized can be performed without any special functions. As a result, the given expressions allow the calculation of the three magnetic field components at any point in the space, may it be outside the magnet as well as inside it. Furthermore, the computational cost is very low and so, parametric optimizations can be carried out. Indeed, tile permanent magnets can be assembled in very various ways depending on the intended application. For example, radially magnetized tiles can be assembled to form a radially magnetized ring magnet and axially magnetized ring magnets can also be achieved in a similar way with axially magnetized tiles. Finally, tile permanent magnets of different magnetizations can be associated for the design of Halbach structures and ring permanent magnets can be stacked for the design of magnetic bearings. By using such analytical expressions, the magnetic field created by such assemblies can always be determined accuratly and structures using such tile permanent magnets can also be rapidly optimized with regard to criteria applying to the magnetic field values and its spatial variations.

Calculation of DC Grounding Electrodes with Open-boundary Domain by the FEM with Hemispherical Kelvin Transformation

Fang Zhang[1], **Jiansheng Yuan**[1], **and Zong Wei**[1]

[1]Dept. of Electrical Engineering, Tsinghua University, Beijing 100084, China
[2]Dept. of Electrical and Electronic Eng., North China Electric Power Univ., Beijing 102206, China

Abstract— Great progress in calculation of grounding system has been made. However, most of the approaches are limited in parallel conductive soil layersor the calculation domain is finite. Actually, the soil domain is infinite large and the conductivity of soil near the grounding body may vary greatly. The FEM is capable of solving the problems with heterogeneous soils. Choosing a finite domain is the application prerequisite of the FEM, which may influence the solution accuracy. A space transformation approach can solve this problem, which transforms the infinite open-boundary domain to a finite closed one that can be solved by a transmuted FEM. The FEM combined with the hemispherical Kelvin transformation is presented in this paper. This approach is ideal for any soil structure, such as heterogeneous or even anisotropic material, so that the grounding electrode in different shapes of soil structure can be solved.

The procedure of the presented approach is: (1) divide the semi-infinite domain into two parts V_1 and V_2, then discretize V_1 and V_2 separately, as shows in Fig. 1; (2) transform the boundary-value problem into its equivalent variational problem, and then obtain the final FEM equation in matrix form basing the discretized domains above.

Examples were computed by the approach. Through analyzing a sphere grounding body in different soil conditions such as one-layer, two-layer vertically and horizontally, the approach was verified. Fig. 2 shows the results of two-layer vertically soil. The result is agreed with its analytical solution. A small quantity of nodes and element is enough to get a precise result. Some other examples are also computed, such as ring shaped grounding body.

Several factors affect the accuracy of the calculation, such as the discretization of domains, the sphere radius of Kelvin transformation, the depth of the grounding body, which will be introduced in the full paper.

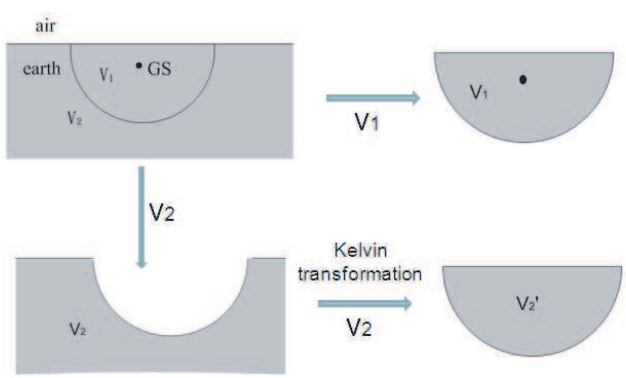

Figure 1: Two domains of soil division.

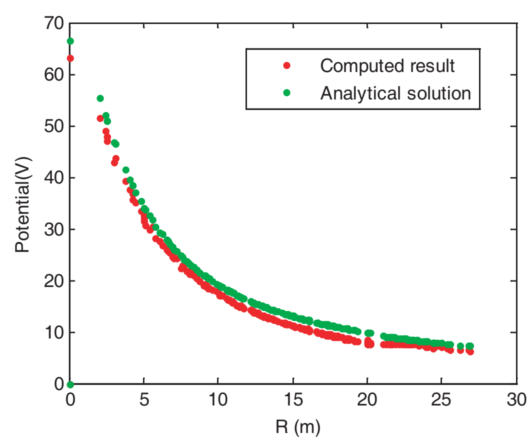

Figure 2: Potential distribution in the earth surface.

A New Electromagnetic Parameter Model of Giant Magnetostriction Material

Liyi Li, **Baiping Yan**, **and Chengming Zhang**
Department of Electrical Engineering, Harbin Institute of Technology, Harbin, China

Abstract— This paper presents a new electromagnetic parameter model that use parameter of permeability and mechanical compliance denote the conversion between the energy of magnetic and mechanical. Based on the parameter exchange of initial magnetic, mechanical equation, we clearly expressed the micro-model of magnetostriction. Additionally, Raise an inter-uniformity assumption between the parameter of permeability, mechanical compliance and the magnetization of material. Through analyze the equations of dynamic micro-energy, educe a result that the of stress coefficient of permeability and magnetic field of mechanical compliance is the most important factors of output response. The validity of the electromagnetic parameter model is illustrated by experiment, and the data of parameters exchange can clearly express the relation of magnetization and output response.

Introduction: The linear constitutive piezomagnetic equations of giant magnetostriction material (GMM) describe the conversion between the magnetic and mechanical energy of material through the parameter of magnetoelastic coupling coefficients. But the analyze of magnetoelastic coupling coefficients is just in the phase of concept, and have no carefully study in the space of the energy exchange between the magnetic and mechanical, Additionally, the piezomagnetic equations can't express the micro-model and inner mechanism of material, restrict the used of material in precision mechanical process, micro-orientation system, etc.

The parameter of permeability and mechanical compliance is the most intuitionistic expression of the material magnetization, we can analyze these two parameters exchange to investigate the magnetization of material and output response. This paper studies the relation between permeability, mechanical compliance and input parameters, analyze the electromagnetic parameter model of material, illuminate the veracity of the model and parameter assumption.

Analysis of Electromagnetic Parameter Model: Based on the initial magnetic and mechanical equation, this paper indicate an Equation (1) of electromagnetic parameter model.

$$\begin{cases} \varepsilon = S(\sigma,\, H) \cdot \sigma_i \\ B = \mu(\sigma,\, H) \cdot H_e \end{cases} \tag{1}$$

In these relations, σ_i and H_e denote the inner stress and the effective field of material, $S(\sigma, H)$ and $\mu(\sigma, H)$ denote permeability and mechanical compliance, which is influence by parameters of stress and field. Equation (1) distribute the contribution of input stress and magnetic field to every parameter, use the exchange of the permeability and mechanical compliance to replace the energy conversion, which is denoted by magnetoelastic coupling coefficients.

With the micro-energy of material, educe a relation of parameters in the process of magnetostriction, which express in the Equation (2), and get the result that compare with the simple energy conversion in magnetic or mechanical, the energy conversion between magnetic and mechanical is the most important factor of magnetization and output response.

$$\frac{1}{\sigma_i}\frac{\partial \mu(\sigma,\, H)}{\partial \sigma_i} = \frac{1}{H_e}\frac{\partial S(\sigma,\, H)}{\partial H_e} \tag{2}$$

Experimental: We explain the electromagnetic parameter model through the experimental data, and clearly explain the relation between permeability, mechanical compliance and different input parameters in the process of magnetostriction, the validity of the assumption of magnetization parameter is illustrated.

Conclusion: This paper presents a new electromagnetic parameter model. Base on this, analyze the relation between the parameters, get a result of the truly intuitionistic output response which is express by parameters.

Clausius-Mossotti Relations for Monolayer with Spatial Dispersion

A. A. Tishchenko, M. I. Ryazanov, and M. N. Strikhanov
Moscow Engineering Physics Institute, State University, Moscow, Russia

Abstract— Clausius-Mossotti relations join the microscopic and macroscopic properties of a substance and they are well known and widely used in the optics, spectroscopy of condensed media and many other fields of physics. Usually, these relations take into account only frequency dispersion, not the spatial one. The effects of frequency and spatial dispersions are caused by the nonlocal properties of response functions in time and in space, correspondingly.

Except for some special cases, like electrons in plasma, effects of frequency dispersion are much more considerable than that of spatial dispersion. But sometimes, despite their smallness, the latter may play a vital part. For example, one should take the spatial dispersion of dielectric function into account to describe the gyrotropy (natural optical activity) of some materials, optical anisotropy of nongyrotropic cubic crystals, and so on [1]. The spatial dispersion of dielectric function may change the number of the roots of the dispersion equation. Therefore, taking into account of the spatial dispersion may give us the additional, new types of electromagnetic waves, which are absent in the medium without spatial dispersion [2].

Clausius-Mossotti relations for 2D-structure (monolayer of particles with arbitrary dielectric properties) were obtained in Refs. [3, 4]. Here we present the results for monolayer of particles with arbitrary dielectric properties for the case of spatial dispersion. Thereby, the general theory of dielectric monolayers is created. The analytical properties of responses functions are discussed. There are two of responses functions that are obtained: the one describing the response of the monolayer to the field of external sources, and the second one describing the response to the field of eigenmodes. It should be noticed that the free electrons, existing between the particles (like conduction electrons in the metals and semiconductors) are not taken into consideration, which reduces the degree of generality the results obtained. Nevertheless, the 2D systems considered seem to be good enough to describe all the spectrum of electromagnetic phenomena in the monolayers that consist of metal or dielectric particles, including nanoparticles.

REFERENCES

1. Agranovich, V. M. and V. L. Ginzburg, *Spatial Dispersion in Crystal Optics and the Theory of Excitons*, Wiley-Interscience, New York, 1966.
2. Ryazanov, M. I., *Electrodynamics of Condensed Matter*, Nauka, Moscow, 1984 (in Russian).
3. Ryazanov, M. I. and A. A. Tishchenko, *JETP*, Vol. 103, 539, 2006.
4. Ryazanov, M. I. and A. A. Tishchenko, *ZhETF*, Vol. 130, 621, 2006.

Local Field Effects for Dielectric Function of Semi-infinite Dielectric Covered with a Monolayer of Other Particles

M. I. Ryazanov, A. A. Tishchenko, and M. N. Strikhanov
Moscow Engineering Physics Institute, State University, Moscow, Russia

Abstract— The well known fact is that the average field acting on a molecule differs from the macroscopic field. The usual way is to call the field obtained by averaging the solution to the microscopic Maxwell equations over the quantum states of atomic electrons and the thermal motion of nuclei — to call it by *macroscopic field* [1], and to call average field acting on a single molecule by *local field*. The effects resulting from the difference between the local and macroscopic fields are called local field effects. Relations between the external field, the macroscopic field and the local field lead to the Clausius-Mossotti formula; for three-dimensional systems this can be obtained by using a pair distribution function for molecules [2].

In this paper, the Clausius-Mossotti relation have been obtained for half-infinite medium with the monolayer of other particles on its surface. The interaction between a molecule and an electromagnetic field is analyzed in the dipole approximation, which is good approximation at wavelengths much longer than the intermolecular distance. For the three limits the results couincide with ones obtained before: i) the case of infinite medium give us the standard, well-known Clausius-Mossotti relation [3]; ii) the case of half-infinite medium without surface monolayer. Here Clausius-Mossotti relation is obtained with corrections due to limitation in one direction. The divergence is considerable near the surface and vanishes far from it [4]; iii) the case of a monolayer only, without the substrate — this limit gives the expressions obtained in Ref. [5]. It should be mentioned that in this work the relations between the local and macroscopic field are only treating; to find a relation between the local field and a field of external sources in 3D case is more difficult problem, and it is not dealt with here. The effects of spatial dispersions are also not considered.

REFERENCES

1. Ginzburg, V. L., *Application of Electrodynamics in Theoretical Physics and Astrophysics*, Gordon and Breach, 1989.
2. Dolgov, O. V. and E. G. Maksimov, *Usp. Fiz. Nauk*, Vol. 135, 441, 1981.
3. Ryazanov, M. I., *Electrodynamics of Condensed Matter*, Nauka, Moscow, 1984 (in Russian).
4. Ryazanov, M. I., *JETP*, Vol. 83, 529, 1996. [*ZhETF*, Vol. 110, 959, 1996].
5. Ryazanov, M. I. and A. A. Tishchenko, *JETP*, Vol. 103, 539, 2006. [*ZhETF*, Vol. 130, 621, 2006].

The Equivalence between Time Reversed Means and Employment of Left Hand Materials to Overcome the Diffraction Limit

J. M. Velázquez-Arcos, **J. Granados-Samaniego**,
J. L. Fernández-Chapou, **and A. L. Rodríguez-Soria**
Departamento de Ciencias Básicas, División de Ciencias Básicas e Ingeniería
Universidad Autónoma Metropolitana, Unidad Azcapotzalco
Av. San Pablo 180, Azcapotzalco 02200 D. F., México

Abstract— From microwave spectra time reversed reported experiments, we find that it is possible to observe how the necessary conditions to recover the evanescent fields can be provided by a quite different kind of method that at first sight seems to be completely unrelated to the most common one. That is, we make a discussion of the analogies between the general properties of the so called Left Hand Materials (LHM) that allow us to rescue the evanescent waves and the detailed process of time reversed techniques applied to electromagnetic waves. As we know, both ways make possible the breakdown of the diffraction limit. We recall some results from Time Reversed Acoustics that can be easily used in the electromagnetic case in order to perform some kind of mapping from one frame to the other. We hope that our analysis will be useful in designing a wide class of devices which require the breakdown of the aforementioned limit.

Hertz Tensor, Current Potentials and Their Norm Transformations

J. L. Fernández Chapou, **J. Granados Samaniego**,
C. A. Vargas, **and J. M. Velázquez Arcos**
Departamento de Ciencias Básicas, División de Ciencias Básicas e Ingeniería
Universidad Autónoma Metropolitana, Unidad Azcapotzalco
Av. San Pablo 180, Azcapotzalco, 02200 D. F., México

Abstract— In unified tensorial form, we develop the Hertz and Current super potentials. We are doing, also, a detailed study of associated Norm Transformations demonstrating that if an electromagnetic field (EM) can be represented in a Hertz Tensor, for a given choice of current potentials, then exist another current potentials for which the representation of the same field EM is expressed like the new Hertz super potential transformed by means of a Norm Transformation.

Far-field Spectral Characteristics of a Broad Band Light Source for One Side Movable Single Slit

Pin Han
Institute of Precision Engineering, National Chung Hsing University
250 Kuo Kuang Road, Taichung 402, Taiwan, R.O.C.

Abstract— The far-field spectral characteristic for a broad-band Gaussian spectrum diffracted by one side moveable single slit is studied. The red shift and blue shift of the peak of the diffracted spectra is found as well as the spectral switches phenomenon. It is found that the spectral switches can be easily controlled by moving the one side of the slit. This control mechanism has the benefit of easier implementation than other previous schemes which modulate some properties of the light source such as the spectrum width or the spatial coherence to achieve it.

Electrostatics of a New Type of Pyroelectric Accelerator — The Pyroelectric Channel Accelerator

V. Sandomirsky[1], **A. Butenko**[1], **Y. Schlesinger**[1], **and R. Levin**[2]

[1]Department of Physics, Bar-Ilan University, Ramat-Gan 52900, Israel
[2]The College of Judea and Samaria, Ariel 44837, Israel

Abstract— Pyroelectric accelerators (PEA) for charged particles, and for generation of X-rays and neutrons attracted recently increasing attention, due to their simple construction, light weight, compact size and low cost. The main efforts concentrate on enhancing the yield of the PEA. Commercial PE X-ray source are available and laboratory models of PEA for neutron generation are being investigated. The presently attained yield reaches $\sim 10^5$ neutrons/heating-cooling cycle. We proposed recently [1] a channel PEA (CPEA) differing essentially from the presently investigated PEAs. We present here, the electrostatic characteristics of such device: mapping of potential, electric field and lines-of-force.

The basic element of CPEA is an ~ 1 cm long PE-cylinder with a channel along it's axis parallel to the polarization direction. Varying the PE's temperature (ΔT), the depolarizing electric field appears inside, as well as outside the PE. For a good PE (e.g., $LiTaO_3$, $LiNbO_3$) and $\Delta T \approx 50$ K, the electric field is $\sim 10^5$ V/cm. Thus, the energy increment of a charged particle in a single channel will be $\sim 10^5$ eV, as reached in the current, design models, of PEA. Using several sections of CPAs provides more versatility, and an increase of energy. We calculated the electrical field and the lines-of-force for single, two and three cylinder configurations. The trajectories of charged particles have been calculated for a number of cases.

Variations of the CPEA concept, such as a CPEA-"collider" (consisting of a pair of axially aligned PEA's with opposite polarization) or special geometry channels creating strongly inhomogeneous field (allowing to accelerate electrically neutral polarized particles) are also analyzed.

REFERENCES

1. Sandomirsky, V., Y. Schlesinger, and R. Levin, *J. Appl. Phys.*, Vol. 100, 113722, 2006.

Near Field Coupling with Small RFID Objects

Arnaud Vena and Pascal Roux
R&D Department, ACS Solutions France SAS, France

Abstract— This paper presents a study on the coupling between a reader and a contactless object in order to define some good working rules to deal with objects with small antennas (NFC mobile phones, key fobs...). Today, the working group in charge of ISO/IEC14443 standard is defining new antenna classes smaller than the very popular "Class 1" [1]. We will study such classes and analyze their compatibility with existing readers. In transportation sector, contactless validators use antennas with a typical size of 10 cm by 10 cm to assure a good reading range. But with smaller classes of contactless object, the magnetic coupling factor (and therefore the reading range) tends to reduce.

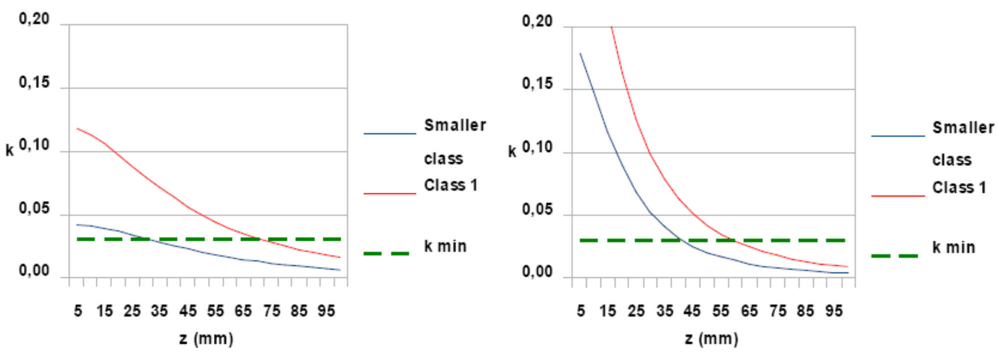

(a) (b)

Figure 1: Coupling factor as a function of distance z, (a) 6.5 cm radius circular loop, (b) 3 cm radius circular loop.

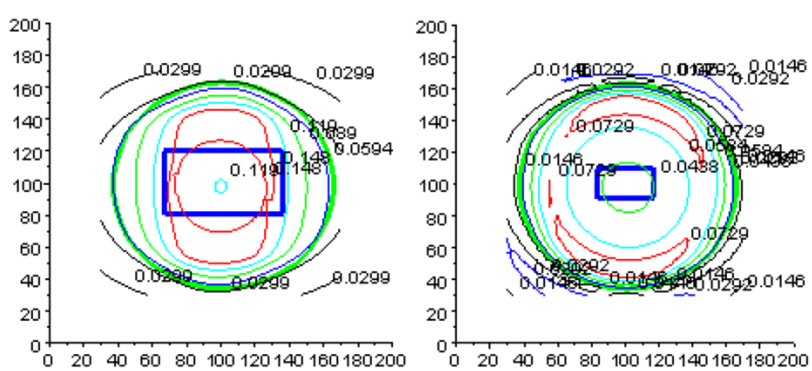

(a) (b)

Figure 2: Coupling factor 2D map at a distance z of 5 mm, between a 6.5 cm radius circular loop (green loop) and a rectangular loop (blue loop), (a) Class 1, (b) Smaller class. Note: The coupling factor is maximum in the red zone.

For the study, we will define a model representing the magnetically coupled system composed of the reader, the object and their coupling factor. The coupling factor variation according to reading distance and antennas shapes is a must to predict the overall system performance. To calculate the coupling factor, we have to define each antenna loop self inductance and the mutual inductance between them. To deal with any antenna shape we will use Von Neumann formula:

$$M = \frac{\mu 0}{4\pi} \oint_{C1} \oint_{C2} \frac{dr1 \cdot dr2}{|r1 - r2|} \tag{1}$$

To obtain an approximate value of the self inductance [2], the method used is to take $C2 = C1 + \Delta z$, this means that the $C2$ path is located on the wire boundary, to avoid any singularities. This formula can be processed with numerical methods [3] to obtain a 2D or 3D magnetic coupling map.

In Figure 1, we can see the coupling factor theoretical value k as a function of distance z between the reader and the object when their antennas axes are aligned. A 6.5 cm radius reader antenna assures a better reading distance than a 3 cm radius reader antenna but only with Class 1 contactless objects.

In Figure 2, we can observe the coupling factor evolution at a distance z of 5 mm when the reader antenna is a 6.5 cm radius circular loop and the object antenna is either a Class 1 or a smaller class.

The study will validate the model by experimental measurements and will analyze the near field coupling between readers and objects with various antenna shapes.

REFERENCES

1. ISO/IEC 14443-1, 2008.
2. Traité d'électricité, T3 Electromagnétisme Fred Gardiol.
3. Numerical Method in Engineering with Matlab.

Chirality of the Electromagnetic Field and Its Spectroscopic Significance

Yiqiao Tang[1] **and Adam E. Cohen**[2]

[1]Department of Physics, Harvard University, USA
[2]Department of Chemistry and Chemical Biology and of Physics, Harvard University, USA

Abstract— It has long been known that chiral objects interact asymmetrically with chiral fields. For example, chiral molecules of a single handedness are excited at slightly different rates when exposed to left- and right-circularly polarized light (CPL). This circular dichroism is widely used to characterize organic and biological compounds.

Chiroptical effects are typically small, due to a mismatch between the wavelength of light and the size of most molecules. To quantify the interaction of chiral fields with chiral molecules, we invented a time-even pseudo-scalar quantity which measures the local density of chirality, or twistiness, of the electromagnetic (EM) field. We call this quantity the "electromagnetic chirality":

$$C \equiv \frac{\epsilon}{2}\langle E \cdot (\Delta \times E)\rangle$$

where ε is the permittivity of the medium, and E the electric field; the brackets indicate an average over time. By applying quantum perturbation theory, we found that the EM chirality couples to molecular rotatory strength, i.e., enhancement of either one boosts the asymmetry of interaction between a chiral molecule and chiral electromagnetic fields.

The formulation of chiroptical effects in terms of the electromagnetic chirality allows us to calculate the response of a chiral molecule in an arbitrary time-periodic electromagnetic field. We found several simple solutions to Maxwell's equations with surprising chiroptical properties:

1) fields in which the ratio of EM chirality to optical intensity is enhanced up to several hundred fold, in some regions of space, relative to a circularly polarized plane wave;
2) fields which are everywhere linearly polarized but which are nevertheless chiral and show circular dichroism; and
3) fields which are circularly polarized in some regions of space but are completely achiral and show no circular dichroism.

The EM chirality is fundamentally different from the well known helicity of the electromagnetic field, which is normally used to describe polarization of the fields. While helicity describes the motion of the electric field in a single plane, chirality is related to the three-dimensional structure of the field.

Mutual Inductance Calculation between Circular Coils with Lateral and Angular Misalignment

Slobodan I. Babic, **Cevdet Akyel**, **and Mohamed-Mehdi Mahmoudi**
École Polytechnique de Montréal, Montréal, Québec, Canada

Abstract— The magnetically coupled coils are important in magnetically controllable devices and sensors, in modern medicine and telemetric systems applied in biomedical engineering (long-term implantable devices such as pacemakers, cochlear implants, defibrillators, instrumented orthopedic implants), in conventional medical MRI systems, tokamaks, superconducting coils. In all these applications it is necessary to calculate or measure the mutual inductance of magnetically coupled coils. The problem of the accurate and fast calculation of the mutual inductance of circular coils in air has a long history in the electrical engineering. The mutual inductance of circular coils can be obtained by analytical, semi-analytical and numerical methods. The purpose of this paper is to present a relatively easy approach for the 3D calculation of the mutual inductance between circular coils with lateral and angular misalignment. The filament method and Grover's formula for the mutual inductance between filamentary circular coils with parallel and inclined axes are used in this approach. The circular coils of the rectangular cross section either with lateral or with angular misalignment have been taken into consideration. The semi-analytical formulas of the mutual induction given in the integral form cover all possible coil configurations and lead to very accurate and fast results. The simple numerical integration is required to integrate the kernel functions expressed over the complete elliptical integrals of the first and second kind. This easy and lucid approach is suitable either for microcoils or large coils so that one does not need to use modern numerical methods such as FEM and BEM frequently employed in such calculations. Computed mutual-inductance values obtained by the proposed approach, by the software FastHenry (based on FEM) and by already published data are in a very good agreement.

Optimization Research on Electric Field of 500 kV Standard Capacitor

Shizuo Li[1] **and Shiyu Kang**[2]

[1]Institute of Electrical Engineering, Guangxi University, Nanning 530004, China
[2]Guangxi Vocational & Technical Institute of Industry, Nanning 530001, China

Abstract— Capacitance stability of high voltage standard capacitor is very important to testing result, and the main factor to stability of capacitance is air ionization. Usually, in the interior of capacitor, SF6 gas which has good isolation is filled and the electric field is even, no gas ionization will occur. But on the out of capacitor, medium is air and the electric field is asymmetry, air ionization may occur in the zone which electric field intension is very high to a certain limit. Electric field distribution of standard capacitor is needed to calculate accurately and the structure of is needed to optimize to reduce the maximum of electric field intension.

Now finite element method is used to calculate the electric field of standard capacitor, but this method have some shortcoming, it is not suit for infinite field firstly, then it use potential as solving variable, the quantities such as charges density and electric field intensity need to differentiate with respect to the potential, and will lead to more error. Lastly, more triangle elements and calculation time must be needed to get an accurate result.

Surface charge density method is presented in this paper. Height of nether voltage balance ring is selected as maximizing variable to reduce the maximum of electric field intension.

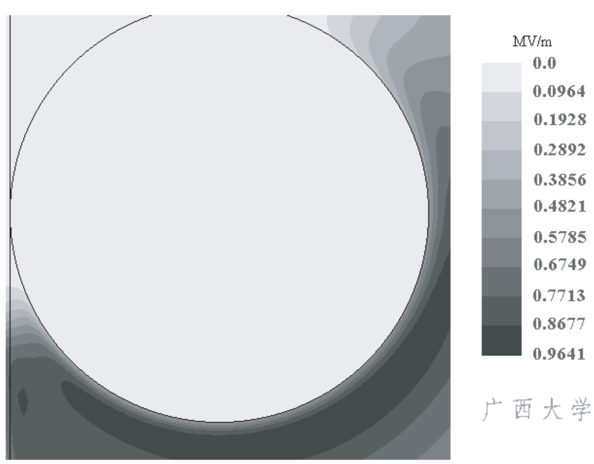

Figure 1: Distribution of electric field intension near nether voltage balance ring.

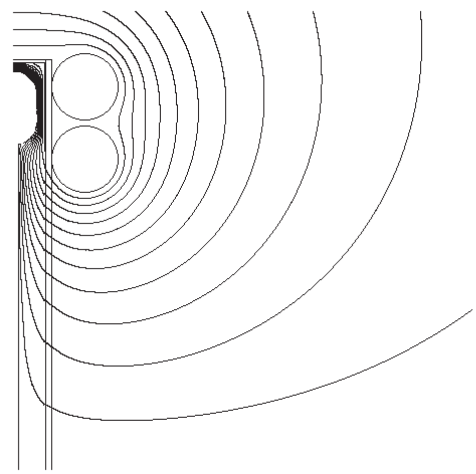

Figure 2: Equipotential line distribution.

On Analog Approach for Current Lissajous Undulator

S. Micloş[1], D. Savastru[1], and V. I. R. Niculescu[2]

[1]National Institute of R&D for Optoelectronics INOE-2000
09 Atomistilor Str., POB MG-5, Magurele, Ilfov, Romania
[2]National Institute of R&D for Lasers, Plasma and Radiation Physics INFPLR
409 Atomiştilor Str., POB MG-36, Magurele, Ilfov, Romania

Abstract— In free-electron laser (FEL) research and development one of the main trends is the elaboration of the compact devices. The undulator is the principal component where the phenomenon of coherent radiation take place. A new theoretical model of an undulator for free electron lasers in a modified Lissajous magnetic field is presented. The undulator is a stack of wires which are described in xy plane by modified Lissajous equations. Analogic simulation is more intuitive and also enables a validation of the numerical simulation. The modified Lissajous, comprizing a Lissajous portion and a linear, is implemented using analog gates controlled by gate signals.

Analysis for Squarely V-shaped Groove Guide

Yinqin Cheng[1], **Guojian Li**[1], **Shuwen Wang**[1], **Binzhao Cao**[2], **and Fuyong Xu**[2]

[1]Northwest University for Nationalities, China
[2]Lanzhou University, China

Abstract— The squarely V-shaped groove guide has been studied by using the method of moment. The cut-off and dispersion characteristics of the dominant mode have been gotten and discussed. It is of important values in theoretical studies and practical engineering applications of V-shaped groove guide for millimeter waves.

Study on Trapezoidal Groove Guide with Arbitrary Inclination Angle

Yinqin Cheng[1], **Guojian Li**[1], **Shuwen Wang**[1], **Binzhao Cao**[2], **and Fuyong Xu**[2]

[1]Northwest University for Nationalities, China
[2]Lanzhou University, China

Abstract— The trapezoidal groove guide with arbitrary inclination angle has been studied with method of moment. The transmission properties of the dominant mode have been obtained and discussed. It is of important values in theoretical studies and practical engineering applications of arbitrarily trapezoidal groove guide for millimeter waves.

An Efficient Algorithm for Combining Linear Lumped Networks with the FDTD Method

Hsin Hsiang Su[1], **Chih Wen Kuo**[1], **and Toshihide Kitazawa**[2]

[1]Department of Electrical Engineering, National Sun Yat-Sen University, Kaohsiung 804, Taiwan
[2]Department of Electrical and Electronic Engineering, Ritsumeikan University
Kusatsu 525-8777, Japan

Abstract— In this study, an efficient approach is presented for processing two terminal networks consisting of arbitrary linear lumped elements into a single grid of FDTD (finite difference time domain) method. The relation of the node voltage to current of the networks can be expressed as a rational function (transfer function) in frequency domain. Field-updating equations and the rational function can be combined together into a new rational function since a single FDTD grid can be regarded as a Norton (or Thevenine) equivalent circuit. The proposed method is based o n control theory and the resulting rational function with an explicit updating algorithm efficiently. A six-order circuit terminated with a transmission line is simulated to demonstrate the accuracy and efficiency of the proposed method. The simulation time of the proposed methods are about 30% less than a similar configuration using the equivalent current source (ECSM) method. Simulation results agree well with data from the ECSM and Agilent's commercial software ADS.

Distribution of Magnetic Field in the Working Space of the Superconductor HGMS

Antoni Cieśla
Department of Electrical Engineering, University of Science and Technology, Poland

Abstract— The subject of this paper is field distribution in a magnetic separator containing ferromagnetic matrix where the magnetic field is generated by a dc superconducting magnet. To develop invariable conditions for the extraction of particles from the slurry in a filter matrix, it is necessary to create a homogenous magnetic field within the working space of the device. The source of the field is usually a solenoidal coil winding with superconducting wire and, in order to achieve the design objective of field uniformity, various configurations have been considered using optimization techniques.

The author proposes considering other possibilities of windings for magnetic field excitation in HGMS, which promises improved homogeneity of the magnetic field in the working space of the separator. Two of the possible improved designs are presented in Fig. 1. Field distributions for the designs of Fig. 1 have been predicted numerically using finite elements modeling.

Figures 2 and 3 present distribution graphs of a relative value of z component of magnetic flux density on the symmetry axis for $z = \pm 150$ mm for the two proposed new designs.

The author proposes the shaping of the magnetic field using the construction from Fig. 1(b), where the coil is divided into small sections with different current density. This solution leads to both technical and economical considerations. The technical aspect consists in a good usage of superconductor. From the economical point of view, the variable cross-section method makes it possible to minimize the volume of the superconductor used. However, there may be a problem of supplying different currents to different sections, as in the case of using the superconductor this would require using several current leads. This could cause an increase in liquid helium evaporation from the cryostat.

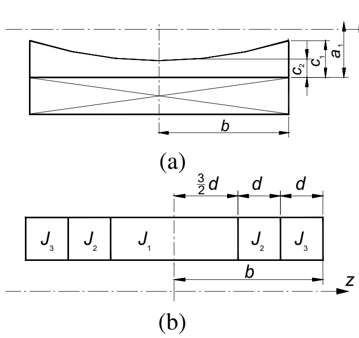

Figure 1: Proposed designs: (a) coil with additional turns of the winding, (b) coil with variable current density in the cross-section (J_1, J_2, J_3); $\beta_1 = L_e/(a_1 - c_1)$, $\beta_2 = L_e/(a_2 - c_2)$.

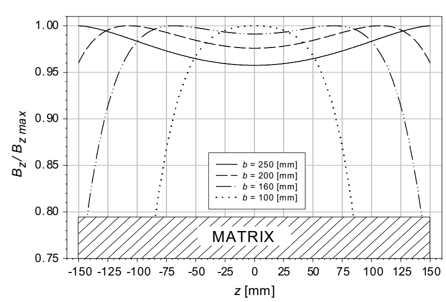

Figure 2: Distribution of B_z (z component of the magnetic flux density) for $r = 0$ for the design from Fig. 1(a); ($\beta_1 = 5$ and $\beta_2 = 3.75$).

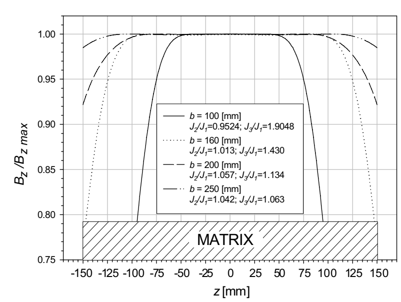

Figure 3: Distribution of B_z (z component of the magnetic flux density) for $r = 0$ for the design from Fig. 1(b).

Dispersion Characteristics of Dielectric Loaded V Ridge-Trough Waveguide

Guojian Li[1], **Shuwen Wang**[1], **Yinqin Cheng**[1], **and Fuyong Xu**[2]

[1]Northwest University for Nationalities, China
[2]Lanzhou University, China

Abstract— A new kind of V ridge-Trough waveguide is presented in this paper. The transmission problem is solved by edge element for the first time. The field patterns of the waveguide for different values of dielectric constant have been presented. Variations of the cutoff wavelength with the ridge dimensions for different values of dielectric constant are investigated in detail. The results will be of practical significance in designing waveguide components in microwave and millimeter wave engineering.

Analysis of the Pulse-Modulated Microwave Propagation into 3D Anisotropic Heart Model by SIE Method

L. Nickelson[1], **S. Asmontas**[1], **R. Martavicius**[2], **and V. Engelson**[3]

[1]Semiconductor Physics Institute, A. Gostauto 11, Vilnius, Lithuania
[2]Electronic System Department, Gediminas Technical University, Vilnius, Lithuania
[3]Linkoping University, SE-58183, Linkoping, Sweden

Abstract— A human heart may be under influence of the microwave radiation for the medical examination of patients or because of hazardous environment [1].

Here we represent the electrodynamical analyses of 3D anisotropic heart model for the first time. The electrodynamical rigorous solution of Maxwell's equations related to the microwave pulse propagation in a three-dimension heart model with anisotropic and isotropic media is presented here. The myocardium tissue media is the anisotropic media and blood is the isotropic media. The boundary problem was solved by using the singular integral equations' (SIE) method [2–4]. Our solution, obtained by our SIE method, is electrodynamically rigorous. The false roots do not appear and the boundary conditions have to be satisfied only the surfaces dividing different materials.

We formulated our electrodynamical problem like this: an antenna radiates a microwave pulse into a 3D heart model. The heart model has an intricate shape and it limited by a non-coordinate shape surfaces. The surfaces of the 3D heart model with an antenna were created in the 3D Studio MAX. This tool exports the surfaces as a set of triangles with a normal vector on certain surface points. The heart model consisted of cardiac muscle and the right and left atriums with ventricles cavities which were filled with blood. In our calculations the cavities were filled with blood and the walls of the heart consisted of myocardium tissue. The width of our heart model was 9 cm, the length b was 13 cm and the depth was 8 cm. We also assumed that a microwave point source was placed at the tip of the antenna. We assumed the monochromatic carrier microwave with the frequency 2.45 GHz was modulated with a triangular video pulse. We calculated for several on-off time ratios. In our calculations we fixed the time $t = \text{const}$ and we investigate the electric field distribution of the microwave pulses in different planes of the heart in the same time moment at the coordinate $y = 0$. The pulse durations were always equal to 20 μs and the on-off time ratio is 100.

It is important to note five factors which determine the microwave pulse propagation:

1) the modulating signal which is a video pulse we describe by formula as a sum of harmonics; 2) a number of harmonics which approximate the modulating video pulse is chosen proportional to the on-off time ratio of the pulse; 3) a number of harmonics depends on the form of a video pulse; 4) harmonics of the microwave signals can reflect repeatedly from the interior and external heart model surfaces; 5) the harmonics interference occurs inside of the heart model.

We investigated microwave electric field distributions at several cross-sections of a 3D anisotropic heart model. We have compared the electric field distribution of anisotropic and isotropic 3D heart models. We found that the pictures of the electric field distribution of the anisotropic heart model became asymmetrical and the electric field peaks became larger.

REFERENCES

1. Kubacki, R., "Biological interaction of pulse-modulated electromagnetic fields and protection of humans from exposure to fields emitted from radars," *Conf. Proc. of 17th Intern. Conf. on Microwaves, Radar and Wireless Communications, MIKON-2008*, Vol. 2, 360–366, Wrocław, Poland, May 19–21, 2008.
2. Nickelson, L. and V. Shugurov, *Singular Integral Equations' Methods for the Analysis of Microwave Structures*, 348, VSP Brill Academic Publishers, Leiden-Boston, 2005.
3. Nickelson, L., S. Asmontas, V. Shugurov, R. Martavicius, V. Malisauskas, and V. Engelson, "SIE method of analysing microwave fields of a 3D heart model," *Journal of Electromagnetic Waves and Applications*, Vol. 20, No 2, 193–206, 2006.
4. Nickelson, L., S. Asmontas, R. Martavicius, and V. Engelson, "Singular integral method for the pulse-modulated microwave electric field computations in a 3D heart model," *Progress In Electromagnetics Research*, PIER 86, 217–228, 2008.

Analysis of Slow and Fast Modes of Lossy Ceramic SiC Waveguides

L. Nickelson[1], **S. Asmontas**[1], **T. Gric**[2], **and R. Martavicius**[2]

[1]Semiconductor Physics Institute, A. Gostauto 11, Vilnius, Lithuania
[2]Electronic System Department, Gediminas Technical University, Vilnius, Lithuania

Abstract— SiC waveguides operating at the microwave range are presently being developed for advantageous use in high-temperature, high-power, and high-radiation conditions. SiC waveguides can operate in high-corrosion environment.

The SiC waveguides can act as separate devices. The SiC material can be used for improvement of characteristics of some devices. For example, it can be applied for improved high-voltage switching, for energy savings in some public electric power distribution and electric vehicles, for more powerful microwave electronics, for radars, for sensors, for cleaner-burning more fuel-efficient jet aircraft and automobile engines [1, 2].

Here we are going to present an electrodynamical analysis of the circular and rectangular SiC rod waveguides. We present dispersion characteristics of the SiC waveguide concerning the fact that the longitudinal propagation constant $h = h' - ih''$ is the complex number. The solution of the Maxwell's equations has been carried out by method of singular integral equations [3] and partial areas method [4, 5]. For searching of complex roots of dispersion equation we use the modified Muller method. We carried out a test of the algorithm stability and made the algorithm regularization when the material losses were quite large. We analyzed the value h', losses h'' as well as the electric and magnetic components of slow and fast modes of SiC rod waveguides. Here we are going to present the pictures of the electric field strength lines and electric field intensities of the investigated modes. We have created a computer algorithm with **3D** graphical visualization in the MATLAB language.

REFERENCES

1. Pandraud, G., P. J. French, and P. M. Sarro, "PECVD silicon carbide waveguides for multi-channel sensors," *IEEE Sensors 2007 Conference*, 395–398, 2007.
2. Neudeck, P. G., "Progress towards high temperature, high power SiC devices," *Institute of Physics Conf. Series 141: Compound Semiconductors 1994*, paper presented at *21st Int. Symp. Compound Semiconductors*, 1–6, San Diego CA, 1994.
3. Nickelson, L. and V. Shugurov, *Singular Integral Equations' Methods for the Analysis of Microwave Structures*, 348, VSP Publ., Leiden-Boston, 2005.
4. Nickelson, L., T. Gric, S. Asmontas, and R. Martavicius, "Electrodynamical analyses of dielectric and metamaterial hollow-core cylindrical waveguides," *Electronics and Electrical Engineering*, Vol. 82, No. 2, 3–8, 2008.
5. Nickelson, L. and T. Gric, "Dispersion characteristics and electric field distributions of modes propagating in the open electrically gyrotropic semiconductor rod waveguide," *Proceedings of 17th Intern. Conf. on Microwaves, Radar and Wireless Communications, MIKON-2008*, Vol. 2, 577–580, Wrocław, Poland, May 19–21, 2008.

Mathematical Model of an Infinite Periodic Open Ended Slot Lines Array Antenna

Andrey A. Prilutskiy
Scientific Research Institute of Long Distance Radio Communication
Buhvostova 1-st Str., 12/11, Moscow 3107258, Russia

Abstract— The decision of an electrodynamics problem of radiation of the array antenna representing infinite periodic structure, generated of the open ends of the coupled slot lines is offered. In a E-plane slot lines are divided by metal half plans. The mathematical problem is shown to the decision of the integral equation concerning unknown fields in the aperture of a slot line within one the Flocke cell. The integral equation dares a method of the moments (MoM). The numerical analysis of influence of array antenna parameters on characteristics of radiation — reflection coefficient and pattern.

Mathematical Model of an Infinite Periodic Open Ended Waveguide Array Antenna with Multilayered Dielectric Filling in a Cross Section

Andrey A. Prilutskiy
Scientific Research Institute of Long Distance Radio Communication
Buhvostova 1-st Str., 12/11, Moscow 3107258, Russia

Abstract— The decision of an electrodynamics problem of radiation of the array antenna representing infinite periodic structure, generated of the open ends of waveguides with multilayered dielectric filling of cross-section is offered. The mathematical problem is shown to the integral equation concerning unknown fields in the aperture of a waveguide within one the Floquet cell. The integral equation dares a method of the moments (MOM). The numerical analysis of influence of parameters of filling on characteristics of radiation of an array antenna is carried out. The behavior of an interconnection in an array antenna is studied.

On the Preconditioning of the Algebraic Linear Systems Arising from the Discretization of the EFIE

G. Angiulli, P. Quattrone, and S. Tringàli
DIMET, Univ. Mediterranea, via Graziella 1, Loc. Feo di Vito, Reggio Calabria 89122, Italy

Abstract— The integral equations involved in electromagnetics are discretized by subdomain or entire domain-type Method of Moments (MoM). These eventually result into complex algebraic linear systems, whose size depends on both the meshing fineness and the electrical dimensions of the structures at hand. So the overall performance of the numerical method is dramatically affected by the availability of efficient matrix solvers. Though at times we can still think of employing direct factorization, as far as the structures are small or the mesh is coarse, this approach is useless in practice, as the size of the discretized problem grows. Then the only concrete alternative is the use of Krylov Subspace methods. However, when dealing with systems produced by discretization of EFIE by MoM, Krylov methods are known to converge very slowly or not at all. This behavior is caused by unfavorably spectral properties of the impedance matrix **Z**. Therefore, it is crucial to use an iterative method in conjunction with an efficient preconditioner. In technical literature, researches relevant preconditioning have been mainly directed toward the design of algebraic preconditioners as AINV, SPAI and ILUT [1]. In this work, we consider a simple pre-conditioner based on the skew Hermitian component **S** of the **Z** impedance matrix. This choice is justified by the observation that **S** is expected to dominate (in some sense) the Hermitian part **H** of **Z** causing a localization of the spectrum of the preconditioned system around the point (1; 0) of the complex plane. It is well-known that this condition causes an enhancement of the convergence rate of Krylov Subspace Methods.

REFERENCES

1. Chew, W. C., et al., *Fast and Efficient Algorithms in Computational Electromagnetics*, Artech House Inc., 2001.
2. Saad, Y. and M. H. Schultz, "GMRES: A generalize minimal residual algorithm for solving nonsymmetric linear systems," *SIAM J. Sci. Stat. Comput.*, Vol. 7, 856–869, 1986.
3. Canning, F. X., "Physical and mathematical structure determine convergence rate of iterative techniques," *IEEE Trans. on Magnetics*, Vol. 25, No. 4, 2825–2827, 1997.
4. Bai, Z. Z., G. Golub, and M. K. Ng, "Hermitian and skew-hermitian splitting methods for non hermitian positive definite linear systems," *SIAM J. Matrix. Anal. Appl.*, Vol. 24, 603–626, 2003.

The Effective 3D Modeling of Electromagnetic Waves' Evolution in Photonic Crystals and Metamaterials

A. V. Zakirov[1] **and V. D. Levchenko**[2]

[1]Moscow Institute of Physics and Technology, Russia
[2]Keldysh Institute of Applied Mathematics, Russia

Abstract— Up-to-date artificial optical devices and materials such as photonic crystals, metamaterials (Left-Handed Materials), streamlined surfaces are usually very complicated structures. Analytical calculations for propagation of electromagnetic waves in this media are possible only in simplest cases. On application of computational algorithms the difficulties appear due to large dimentions of calculation area. It results in necessity of effective algorithm development and realization for this calculations. "Effective" algorithm means such one, that has real rate coming up to theoretical. In the work, the implementation of such algorithm is offered for Maxwell's equations' modeling.

In the capacity of difference scheme, the Finite-difference time-domain method (FDTD) is used. For method of cell rounding (sequence of calculations) the Local-recursive nonlocal-anisochronous algorithm (LRnLA) is used, which makes possible to reach the high rate of program's effectiveness. The computational area contains of many Yee cells, that form the rectangular parallelepiped. This area is rounded from 5 faces by Perfectly Matched Layer (PML). So we can set absorbtion boundary conditions. In many cases, it is the necessary requirement for limited areas studying. At the 6th face there are the source and reflecting boundary conditions. In addition, the reflecting or periodic boundary conditions are available to set at the any face. It is developed the methods for modeling of the following media:

- The simple undispersion materials with real permittivity ε and magnetic permeability μ, whish are depened only on the position in space.
- The media with dispersion described by Drude model, where $\varepsilon = 1 + \frac{e^2}{m}\sum\frac{N_k}{\omega_k^2-\omega^2+i\gamma_k\omega}$. The Negative Index Media (NIM, same as LHM) are under this model too.
- Anisotropic media.
- Nonlinear media.

The optimization the software package makes possible to use the advantages of modern processors for acceleration of calculations and allows to use many cores or processors in single calculations without descending of rate. The rate of calculations in all cases is nevertheless than 40% beside the theoretical estimation on the assumption of CPU clock and doesn't depend on capacity of analized data that is the computational area. Due to the such results we can use the existent program for modeling of many electrodynamics problems of today.

Transient Response Analysis of Conducting Bodies by Combination of MoM/AWE and Vector Fitting Techniques

D. Wójcik and M. Surma
Silesian University of Technology, Gliwice, Poland

Abstract— To perform transient analysis of high resonant structure by using of direct time-domain methods long lasting computations are usually required. The analysis can be carried out applying frequency domain integral equation method, such as method of moments (MoM), combined with inverse fast Fourier transform (IFFT). However, the approach is very ineffective, especially when electrically large structures over wide frequency range are analyzed, because of a huge number of samples required by IFFT. To speed-up fre- quency domain calculations, MoM combined with asymptotic waveform evaluation (AWE) technique [1] and complex frequency hopping (CHF) algorithm [2] can be successively employed. AWE is based on rational approximation of current over wide frequency range from relatively small number of discrete frequency and frequency derivatives samples, while CFH algorithm is very helpful to locate frequency points which derivatives are calculated for. As a result one obtains frequency response as a form of a set of rational functions: each function describes the frequency behavior of observable on certain frequency subrange. If the frequency response is described by one rational function covering the whole frequency range, time (transient) response will be obtained analytically by using of inverse Laplace transform. In this paper, to obtain one rational representation from the set of rational functions vector fitting (VF) technique is employed. VF is a robust macromodeling tool that circumvents ill-conditioning problems which usually occur in high order rational approximations [3]. VF method ensures also stability and passivity of the response, which is not guaranteed by AWE algorithm.

To exam efficiency and accuracy of proposed approach (AWE + VF) a numerical example is considered. The structure under investigation consists of three parallel wires located above perfect conducting plane (see Figure 1). The structure was excited by voltage generator in the form of the derivative of Gaussian pulse. Observable is a time response of the current at feeding point. As one can notice in the Figure 1, the accuracy of the results obtained using AWE + VF are quite good compared to conventional MM + IFFT approach. Time of analysis using MM + IFFT and AWE + VF is 6240 and 1604 seconds, respectively. For electrically large structures the ratio of time of analysis using MM + IFFT to time of analysis with AWE + VF can be much greater then in presented example. In the final paper, more numerical examples and more precise analysis of the AWE + VF technique will be presented.

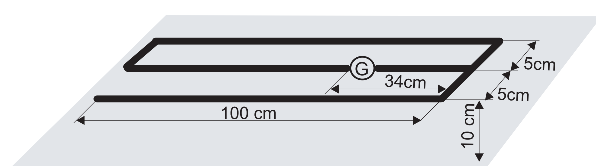

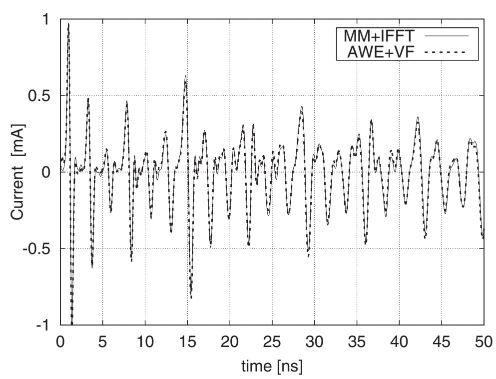

Figure 1: The structure under investigation and the transient response of current at feeding point.

REFERENCES

1. Cockrell, C. R. and F. B. Beck, "Asymptotic waveform evaluation (AWE) technique for frequency domain electromagnetic analysis," *NASA Technical Memororandum 110292*, November 1996.
2. Kolbedhari, M. A., M. Srinirasan, M. S. Nakhla, Q. J. Zhang, and R. Achor, "Simultaneous time and frequency domain solutions of em problems using finite element and CFH technique," *IEEE Trans. Microwave Theory Tech.*, Vol. 49, No. 8, 1419–1430, 2001.
3. Gustavsen, B. and A. Semley, "Ratonal approximation of frequency domain responses by vector fitting," *IEEE Trans. Power Deliv.*, Vol. 14, No. 3, 1052–1061, 1999.

The Numerical Solution of the Three-dimensional Helmholtz Equation with Sommerfeld Boundary Conditions

Géza Hegedűs
Department of Georgikon Faculty, Pannon University, Deák F. u. 16, H-8360, Keszthely, Hungary

Abstract— Many physical phenomena such as acoustics, optics and electromagnetic waves are governed by the scalar wave equation. In the frequency-domain, the wave equation is called Helmholtz equation. In this study, we start with the 3D Helmholtz equation.

In this paper, we look for the solution of the Helmholtz equation discretized by using finite difference discretizations, in a rectangular domain. We approximate the Laplacian with the second order accurate 7-point finite difference stencil. The discretizaion results in a system of linear equation. The system matrix is a large but sparse matrix with complex values. In order to obtain an accurate numerical solution, the number of gridpoints per wavelength should be sufficiently large. As result, the linear system becomes extremely large.

In this work, method is presented to generate a solution to the problem. Through informatics solution I was trying to minimalise runtime. Efforts were made to place the most valuable data possible into the memory to be made processable with the fastest operations.

The linear equation system describing the studied wave-range is composed of seven diagonal matrices, which can be transformed into seven matrices containing seven valuable lines. This is, however, still too big to be kept in the memory simultaneously. To reduce the memory capacity, a work-window of optimum size should be defined to go into the main memory — and regarding its organization — it should demand the minimum possible data-pouring over the whole matrix. Within the work — window a direct procedure was used — based on the Gauss-elimination. Considering all that, — depending on the capacity of the main memory — we can achieve good calculation capacity when determining the wave-range with the optimum selection of the valuable data-segment in the memory, the rate and organization of the working variable.

The effectiveness of the presented method is investigated by the means of numerical example of the beam propagation from an aperture in a homogeneous medium (Fig. 1).

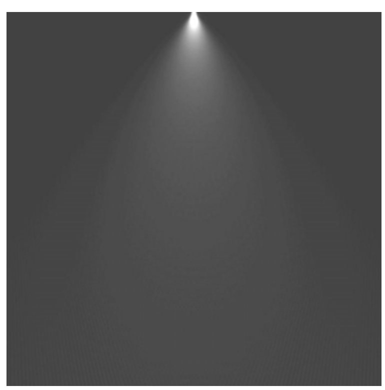

Figure 1.

Analysis of Complex Radiating Structures by Hybrid FDTD/MoM-PO Method

A. Noga, T. Topa, and D. Wójcik
Silesian University of Technology, Gliwice, Poland

Abstract— This paper is devoted to numerical modelling of antennas radiating in the presence of both electrically large conducting objects and inhomogeneous lossy dielectric bodies. For this class of structures the hybrid FDTD/MoM-PO method is proposed. The algorithm starts with subdivision of the structure into three regions: FDTD region contains all dielectric objects, while the antenna and electrically large platforms constitute the MoM and PO regions, respectively. In the first step, calculations in MoM and PO regions are carried out omitting the influence of dielectric scatterer. The problem is formulated analytically in terms of the electric field integral equation (EFIE) for current in the MoM-region, whereas current in the PO-region is obtained through the physical optics approximation [1]. In the second step, computations are carried out in FDTD region illuminated by the fields from MoM and PO regions. Then, MoM-PO algorithm is again employed for evaluating the current on the antenna due to new excitation, taking into account back-scattered steady-state FDTD fields. The procedure is repeated until a specified convergence criterion is met [2].

To exam efficiency and accuracy of proposed approach a numerical example is considered. A testing structure is shown in Figure 1. A monopole antenna is attached to the centre of a square con- ducting ground plane. The antenna and the shaded part of the plate constitute the MoM region, whereas the remaining part of the platform is assigned to PO region. The antenna is coupled to a rectangular box of lossy dielectric ($\varepsilon_r = 41$, $\sigma = 1.3\,\mathrm{S/m}$). Figure 1 shows also the horizontal gain pattern for the operating frequency 300 MHz. The numerical results obtained by the discussed approach (denoted by FDTD/MoM-PO) are compared to the commercial software CST MWS [3] as well as the classical FDTD (in-house). As can be seen, the gain functions obtained by the FDTD/MoM-PO method compare well with the reference waveforms. Proposed approach offers reasonable accuracy that seems to be fully acceptable for practical purposes, limiting about three times memory requirements (in comparison to both FDTD and CST) and time of computations (four and three times in comparison to FDTD and CST, respectively).

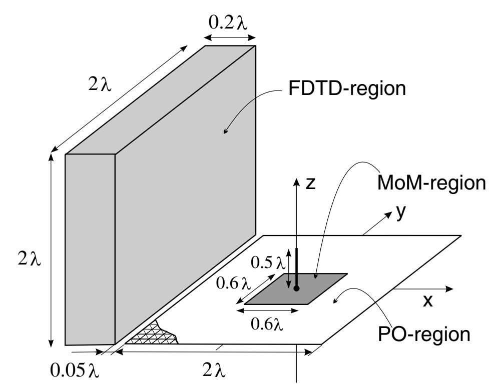

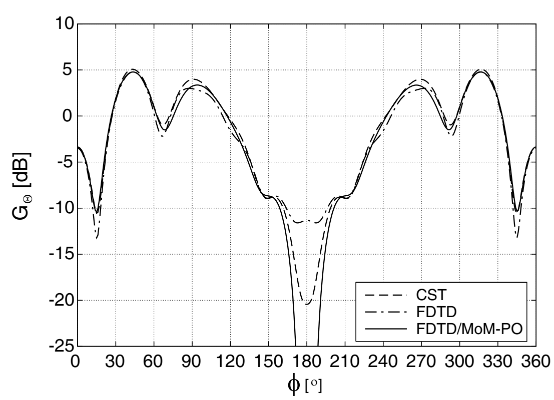

Figure 1: The structure under investigation and its gain pattern ($\theta = 90°$).

REFERENCES

1. Jakobus, U. and F. M. Landstorfer, "Improved PO-MM hybrid formulation for scattering from three-dimensional perfectly conducting bodies of arbitrary shape," *IEEE Trans. Antennas Propagat.*, Vol. 49, No. 2, 162–169, 1995.
2. Abd-Alhameed, R. A., P. S. Excell, and A. M. Mangoud, "A hybrid computational electromagnetics formulation for simulation of antennas coupled to lossy dielectric volumes," *IEEE Trans. Broadcast.*, Vol. 50, No. 3, 253–259, 2004.
3. http://www.cst.com.

On the Relationship between Nonuniqueness of Electromagnetic Scattering Integral Equations and Krylov Subspace Methods

G. Angiulli, P. Quattrone, and S. Tringàli
Dimet, Univ. Mediterranea, via Graziella 1, Loc. Feo di Vito, 89122 Reggio Calabria, Italy

Abstract— Some relevant operator equations appearing in the study of physical phenomena are characterized by critical values of one or more parameters (on which they are dependent), that make them *degenerate*. In the particular instance of the electric (EFIE) and magnetic (MFIE) integral equations used to model direct scattering of a time-harmonic electromagnetic field from perfect conducting bodies [1, 2], this corresponds to the existence of some set of frequencies such that the null space of the underlying linear operator $\mathcal{L} : X \to Y$ is no longer trivial, provided that X and Y, respectively, are suitable topological vector spaces of (even generalized) functions (e.g., separable Banach or Hilbert spaces), standing for the domain and codomain of $\mathcal{L}$. It is common in the literature to refer to such frequencies as the *resonances*, due to their subtle relationship with the physical resonances of the interior problem. Actually one can still think of introducing the notion of a generalized solution in order to bypass the pathological behavior of the degenerate model via the pseudo-inverse of $\mathcal{L}$ (at least as far as $\mathcal{L}$ is Fredholmian and X and Y are locally convex spaces). Then solving the original problem is the same as optimizing some nonnegative auxiliary functional $F : X \to \mathbb{R}$, on condition that F can be proved to have one optimum point — which is likely in many interesting cases where an ordinary solution would even fail to exist. But practice is not so comfortable as theory. In fact, the problem deals numerically with the computation of the so-called Moore-Penrose pseudo-inverse [3] of a large and generally dense square matrix $A \in \mathbb{C}^{n,n}$ resulting by the discretization of the integral model via the Method of Moments and its consequent approximation (in the sense of the uniform operator limit) by means of a linear system of algebraic equations like $Ax = b$. Ultimately this involves computing the singular value decomposition (SVD) of A, that is a very time-consuming task, in order to filter the noisy effects introduced on the unknown current by the almost-singularity of A when EFIE or MFIE are applied in the neighborhood of a resonance [4]. Then the question raises naturally: is it possible to solve the system $Ax = b$ in such a way that one avoids distinguishing between the case when A is regular and the case when A is (numerically) singular? In this paper, we try to give an answer and provide theoretical motivations and numerical evidence to prove it should be the right one, relying on the inherent capability of some Krylov subspace methods to extract the minimum norm solution to the linear system $Ax = b$ to the extent that b lies in the range of A (even if A is singular).

REFERENCES

1. Cho, S. K., *Electromagnetic Scattering*, Springer-Verlag, 1990.
2. Colton, D. and R. Kress, *Integral Equation Methods in Scattering Theory*, John Wiley & Sons, 1983.
3. Groetsch, C. W., *Generalized Inverses of Linear Operators*, Pure and Applied Mathematic 37, Marcel Dekker, 1977.
4. Bagby, J. S., "Reduction of cavity resonances in MoM solutions of EM problems," *IEE Electronics Letters*, Vol. 32, No. 18, 1652–1653, 1996.

Finite-difference Time-domain Simulation with Higher-order Difference Scheme

Y.-P. Chiou[1,2] **and C.-H. Du**[1]

[1]Graduate Institute of Photonics and Optoelectronics, National Taiwan University
Taipei 10617, Taiwan
[2]Department of Electrical Engineering, National Taiwan University
Taipei 10617, Taiwan

Abstract— A higher-order finite-difference formulation based on generalized Douglas scheme is adopted. Centered mesh is adopted instead of the commonly used Yee's mesh. The accuracy of spatial derivative is enhanced by two orders. The numerical dispersion can be reduced. Simulation shows the grid size can be larger for the same accuracy.

Field Dependence of Complex Permittivity of LDPE Filled with PZT

S. N. Tkachenko, O. S. Gefle, and S. M. Lebedev
High-Voltage Research Institute, Tomsk Polytechnic University, Tomsk, Russia

Abstract— Study results of the field dependence of the complex permittivity of low density polyethylene filled with a ferroelectric ceramic powder are presented in this paper. It is obvious that local field is increase at the interface polymer/filler in composite polymeric materials (CPMs) filled with a ferroelectric ceramic. The local Lorentz field for low density polyethylene filled with $C = 40$ vol. % of a ferroelectric ceramic powder lead zirconate titanate are estimated. In this case the local field in a non-polar matrix is increased by a factor of 3 compared with the external electric field E_0. It can result in the local breakdown of a dielectric in the high field. In this reason change in the specific volume resistivity ρ_v and permittivity ε of a dielectric due to introduction of modifying agents and additives at the external electric field $E_0 \leq 10^4$ V/m can give incorrect information concerning a possible behaviour of CPMs in the high electric field.

Thus, the study of influence of an external electric field on the real ε' and imaginary ε'' parts of the complex permittivity of LDPE filled with PZT and an establishment of interrelation between parameters of a dielectric relaxation spectrum and breakdown strength of CPMs was the aim of this work.

The relation between ε'' and ε' on the complex plane below and above the critical voltage V_{0c} (at which non-linear change of the relation $\varepsilon'' = f(\varepsilon')$ begins) may be approximated by two functions, namely: a linear function at $V \leq V_{0c}$, and the Debye function at $V > V_{0c}$. The direct line crosses a semi-circle in two points. Coordinates of these points can be estimated by field dependences of ε' and ε''. The first crossing point corresponds to the critical voltage V_{0c}, and the second point corresponds to the voltage V_c at which maximal values of $\varepsilon''_{\max}$ or $\tan\delta_{\max} = \varepsilon''_{\max}/\varepsilon'_{cs}$ are observed. V_{0c} corresponds to the beginning voltage of ionization processes in CPMs which caused by the local field increase at the interface polymer/filler. The value V_c is the critical voltage at which the dielectric breakdown occurs.

The estimation of parameters both in linear and non-linear regions of the dielectric relaxation spectrum allows the dielectric strength for CPMs to be predicted at the confidence level not less than 95% without HV tests.

Polymeric Blends and Compositions with High Permittivity

S. N. Tkachenko, O. S. Gefle, and S. M. Lebedev
High-Voltage Research Institute, Tomsk Polytechnic University, Tomsk, Russia

Abstract— Electric and thermophysical properties of composite materials with high permittivity on the basis of low density polyethylene (LDPE) and polyvinylidene fluoride (PVDF) were studied in this work. The first group of materials on the basis of non-polar LDPE-matrix includes blends with various content of chlorocosane. The second group of materials on the basis of LDPE filled with a lead zirconate titanate (PZT). The third group of materials on the basis of polar PVDF-matrix includes compositions: PVDF + 45 vol% TiO_2 and PVDF + 30 vol% PZT.

Methods of dielectric spectroscopy in frequency domain and differential scanning calorimetry allow both electrical properties and fields of application of filled polymeric dielectrics with high permittivity to be established.

Adding chlorocosane into the LDPE-matrix results in the appearance of the complex permittivity dispersion at the infra-low frequency range. Blends on the basis of LDPE modified by chlorocosane can be applied as insulating materials in the frequency range from 10^1 to 10^6 Hz.

Compositions on the basis of LDPE filled with ferroelectric ceramics PZT can be applied as insulating materials in the frequency range from 10^{-2} to 10^3 Hz because the relaxation maximum of dielectric losses for these compositions is observed in the high frequency range from 10^4 to 10^7 Hz.

Compositions on the basis of PVDF filled with ferroelectric ceramics PZT are suitable for usage in the frequency range from 10^0 to 10^5 Hz because they do not possess dispersion of the complex permittivity in this frequency range.

The higher permittivity can be achieved for polymeric compositions on the basis of a polar matrix and polar filler due to the high interphase interaction between a polymeric matrix and filler.

Magnetic Field Created by Thin Wall Solenoids and Axially Magnetized Cylindrical Permanent Magnets

G. Lemarquand[1], **V. Lemarquand**[1], **S. Babic**[2], **and C. Akyel**[3]

[1]Laboratoire d'Acoustique de l'Universite du Maine, UMR CNRS 6613, Le Mans, France
[2]Departement de Genie Physique, Ecole Polytechnique Montreal, Canada
[3]Departement de Genie Electrique, Ecole Polytechnique Montreal, Canada

Abstract— This paper presents calculations of the magnetic field created by circular systems which are constituted either of coils or of permanent magnets in air. Indeed, these are the two usual natural sources of magnetic field. Furthermore, numerous applications contain no iron and this is what allows analytical formulations for the magnetic field. Then, two visions or modellings are found in the literature: the Amperian model and the Coulombian one. The Amperian model corresponds to a representation of the sources of the magnetic field that uses coils. Of course, it is the obvious one for coils but it applies to magnets too. Besides, the Coulombian model represents the field source with surface and volume magnetic charge densities and can be used for both kinds of sources too.

The presented cases have analogous geometries and purposes, but are nevertheless quite different when one looks at the applications they come from. Indeed, the co-authors have different backgrounds and approaches. On one hand, Babic and Akyel calculate the magnetic field created by coils and thus inductances and mutual inductances. On the other hand, Lemarquand and al. calculate the magnetic field created by ring or tile permanent magnets and the forces exerted between them. However, the point is that even though the initial problems are different and the approaches to solve them, depending on the choice of model, are different too, the problems to solve become the same and the formulations obtained are the same as well.

Self-inductance is a fundamental electrical engineering parameter for a coil that can be computed by applying the Biot-Savart law directly or using alternate methods. Moreover, the case of thin circular air-core coil is considered here, which can be separated in two sub-cases: thin-wall solenoids and disk coils. The accurate self-inductance and mutual inductance expressions are given. Indeed, the results are obtained in an analytical form (thin-wall solenoids) and in an analytical/numerical form (disk coils) over complete Jacobian elliptic integrals of orders I and II and Heumann's Lambda function and some members, which have to be solved numerically using the single integration. Furthermore, the singular cases have been avoided and the integral kernels are continuous functions on intervals of interest.

The corresponding geometry when considering permanent magnets is the ring and two magnetization directions are investigated. Indeed, an analytical formulation of the magnetic field created by an axially magnetized ring permanent magnet is given. The approach uses a Coulombian model of the magnet which is represented by magnetic charge surface densities on the plane faces of the magnet. The field can be compared to the one created by two concentric thin-wall solenoids. Then, a 3D analytical formulation of the field created by a radially magnetized ring is given. The magnet is modelled by charge surface densities on the inner and outer faces of the ring and the charge volume density corresponding to the magnetization divergence is taken into account. Different fully analytical formulations can be considered and are discussed, depending on the influence of the volume charge density. Indeed, for large radii and/or thin rings the latter can be neglected, whereas for small radii and/or thick rings it can't. Furthermore, the field created by a thick ring can be compared to the one created by a disk coil. Moreover, the calculation difficulty encountered for the disk coil inductance is of the same kind as the taking into account of the volume charge density. Besides, the forces between ring magnets can be analytically formulated.

Method for Calculating Interference Protection Ratio of ATSC System from Mobile WiMAX System

Sung Woong Choi[1], **Wang Rok Oh**[2], **and Heon Jin Hong**[1]

[1]Broadcasting & Telecommunications Convergence Research Lab., ETRI, Korea
[2]Division of Electrical & Computer Engineering, Chungnam National University, Korea

Abstract— According to the rapid development of the digital technology, the broadcasting environments are changing into the digital television transmission of the high quality and high-efficiency from the existing analog television transmission. Due to the high efficiency characteristics of digital television, the unprecedented amount of spectrum that will be freed up in the switchover from analog to digital terrestrial TV is known as the Digital Dividend. Most of countries in the world collect the digital dividend frequency generated by the analog television broadcasting switch off and plan to use that frequency in the different service like the next generation mobile communication, and etc. At that time, it must be considered that interference effect between Digital TV and new service in order to introduce the new services in the digital dividend.

Until now, it is general that the field test data are used for setting up the Protection ratio(PR) to analyze the interference between the different systems. But it needs much time and cost in order to collect and analyze the field test data. Therefore, by drawing method for setting up the PR based on the computational simulation, it is easy to calculate the PR about the corresponding system.

In this paper, we proposed the method for calculating the Protection Ratio (PR) of the Advanced Television Systems Committee (ATSC) broadcasting system from the Mobile WIMAX system through the computational experiment. For this, the transmitter/receiver of the ATSC system and transmitter of the Mobile WiMAX system were modeled. By integrating those, the computational simulator for setting up the PR of the ATSC system from the Mobile WiMAX system was implemented. The ATSC TV signal was regarded as the desired one and the Mobile WiMAX signal was regarded as the interfering one. In order to simplify the simulation complexity, it was modeled sending/receiving signals in the Intermediate Frequency (IF) band instead of those in the RF band.

Electric Field Calculation of High Voltage Transmission Line

Yong Lu
Guangxi Electric Power Institute of Vocational Training, Nanning 530007, China

Abstract— Electric field around the high voltage transmission line is needed to calculate accurately for design and environment evaluation. Now, three are two calculation methods as following.

(1) Equivalent charges method. This method assumes that the charge of transmission line is concentrating on the centre line of the splitting conductors, and can not give the maximums of surface charges density and electric field intensity.
(2) Finite element method. This method is not suit for infinite field firstly, then it use potential as solving variable, the quantities such as charges density and electric field intensity need to differentiate with respect to the potential, and will lead to more error. Lastly, surface of the splitting conductors is very difficult to dissect into small triangle element, more triangle elements and calculation time must be need.

Surface charges method for calculating electrostatic field around the high voltage transmission line is given in this paper. This method supposes that the charges of transmission line distribute continuously on the surface of the splitting conductors, and the surface of every splitting conductor is divided into many arc segments, linear interpolation is used to express the charges density of every arc segment. The surface charges density of the splitting conductors is calculated, and maximums of surface charges density and electric field intensity can be determined. Example shows the advantage and the precision of this method.

Also, partial capacitors between two phases are introduced to substitute the concept of every phase average capacitor which is used in power transmission design currently, and the arrangement of the phase conductors is researched to improve imbalance of the partial capacitor.

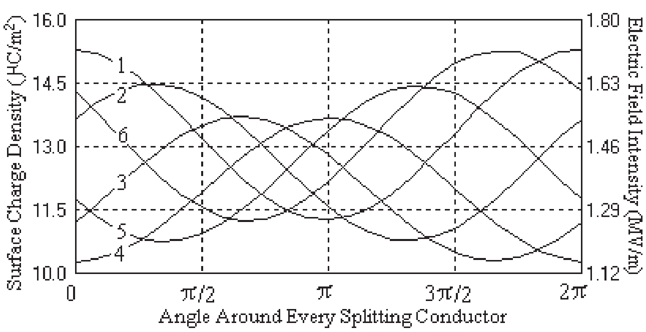

Figure 1: Surface charges density.

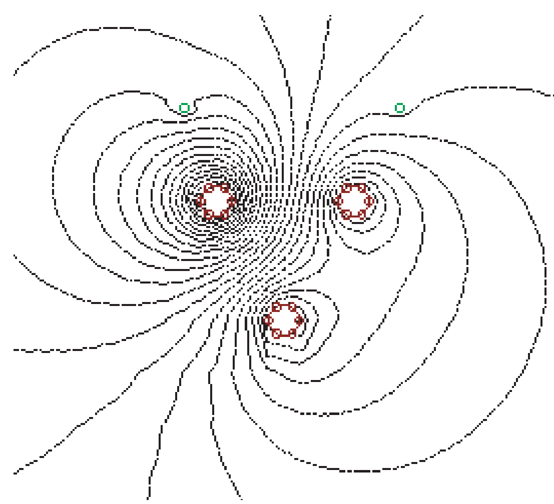

Figure 2: Equipotential line distribution.

Investigation of Dispersion Characteristics of the Open Complicated Shape Rod with a Channel Iside

L. Nickelson[1], **D. Zylkov**[1], **S. Asmontas**[1], **and R. Martavicius**[2]

[1]Semiconductor Physics Institute, A. Gostauto 11, Vilnius, Lithuania
[2]Electronic System Department, Gediminas Technical University, Vilnius, Lithuania

Abstract— Complicated shape rod waveguides widely are used in microelectronics and opto-electronics [1]. Integrated microfluidic devices can be created on the base of comb rod waveguide with channels [2, 3].

Here we are going to present the dispersion characteristic analysis of the open silica rod waveguide having one or two combs and channels inside of the waveguides. The solution of the Maxwell's equations has been carried out by our method of singular integral equations [4]. Our solution, obtained by the SIE method, is electrodynamically rigorous. The false roots do not appear and the boundary conditions have to be satisfied only the surfaces dividing different materials.

We are going to present the behavior of the main and the two first higher modes dependent on the sizes of channel and combs. We observed the unusual dependences on the location of the waveguide channel. We have created a computer program in the C# language.

REFERENCES

1. Park, J.-H., Y.-J. Choi, and J.-G. Park, "Evolution of nanowires, nanocombs, and nanosheets in oxide semiconductors with variation of processing conditions," *Journal of the European Ceramic Society*, Vol. 25, 2037–2040, 2005.
2. Erickson, D. and D. Li, "Integrated microfluidic devices," *Analytica Chimica Acta*, Vol. 507, 11–26, 2004.
3. Poenr, D. P., C. Iliescu, M. Carp. Ah. J. Pang, and K. J. Leck, "Glass-based microfluidic device fabricated by parylene wafer-to-wafer bonding for impedance spectroscopy," *Sensors and Actuators*, Vol. A 139, 162–171, Elsevier, 2007.
4. Nickelson, L. and V. Shugurov, *Singular Integral Equations' Methods for the Analysis of Microwave Structures*, 348, VSP Publ., Leiden-Boston, 2005.

Coupling onto the Two-wire Transmission Line Enclosed in Cavities with Apertures

Ying Li, **Gu-Yan Ni**, **Jian-Shu Luo**, **Ji-Yuan Shi**, **and Xu-Feng Zhang**
College of Science, National University of Defense Technology
Changsha 410073, China

Abstract— In this paper, we consider the field penetration through apertures and their coupling with a two-wire transmission line. By the Modal Green's Function with the method of moment (MoM) and Baum-Liu-Tesche (BLT) equation, a semi-analytical solution is obtained for the load response of the two-wire transmission line in the cavity.

Surface Mounting Packaging of SAW Low-loss High Stop-band Rejection Filter

Peng Fu and Xiaoqin Hao
Nanjing Research Institute of Electronic Technology, China

Abstract— The assembly technology which is used in SAW filter with surface mounting package in this paper. The problem of the stop-band response's decay is simulated in HFSS and solved. A harmless test fixture for the SMD mass-production was also designed and manufactured. This experiment is important for the enhancement of SAW filter's post-packaging stop band rejection feature, and valuable for miniaturization for receiver on antenna.

An LTCC Dual-band Filter Based on Two Different Mechanisms

Guo-Shu Huang and Chun Hsiung Chen
Department of Electrical Engineering and Graduate Institute of Communication Engineering
National Taiwan University, Taipei 106, Taiwan

Abstract— A dual-band filter is presented by properly designing the associated trisection filter and the parallel-plate-mode-based filter within the low-temperature co-fired ceramic (LTCC) substrate. The substrate has a dielectric constant of 7.8 and its loss tangent is 0.005 at 10 GHz. The multilayer structure has seven metal layers and the thickness of each metal layer is 13 μm. The thickness of each substrate between two metal layers is 50 μm. The trisection filter is composed of three broadside-coupled stripline resonators, which are fed by the conductor-backed coplanar waveguide (CBCPW) at the input/output ports to form the first passband (f_1). The three coupled stripline resonators are separately located at third and fifth metal layers, and the CBCPW is formed by the first and seventh metal layers. The top ground plane of the substrate is shorted to the one on the bottom by using the via holes. Specifically, the feeding structure is realized by the CBCPW-to-stripline transition designed as a part of the bandpass filter to provide the necessary external quality factor (Q_{ext}) in the filter design. Besides, due to the presence of the parallel-plate-mode propagation within the CBCPW, this mode may be utilized to form the second passband (f_2), which can be controlled by adjusting the position of the middle two via holes in the filter structure. Specifically, the wider the separation of two via holes, the higher the second passband frequency can be achieved.

The dual-band filter shows good selectivity due to the introduction of one transmission zero between two passbands. Thanks to the three dimensional (3-D) multilayer technology, the implemented filter structure can be made compact and the overall size of the filter, without the input/output feeding CBCPW lines, is $5.074 \times 3.05\,\text{mm}^2$. Measured results are presented and compared to those simulated by Ansoft's High Frequency Structure Simulator (HFSS) software package. The measured insertion losses near the center frequencies of the first (f_1) and second (f_2) passbands are 3.76 dB and 3.1 dB with the fractional bandwidths of 5.49% and 6.82%, respectively. Good agreement between simulated and measured results is observed, validating the dual-band design concept with the LTCC substrate integration technology.

Design of the 2.4 GHz Band-pass Filter for Flexible Appliance

Jin-Sup Kim and Kyu-Bok Lee
Wireless Communication Research Center, Korea Electronics Technology Institute, Korea

Abstract— The 2.4 GHz filter is proposed and implemented using flexible substrate, aiming at bending the substrate. It is composed of slot line resonators and CPW (Coplanar Waveguide) feeding line. After optimization of this filter, a good bandpass behavior with transmission poles is theoretically realized and experimentally confirmed. Suppose the PCB substrate is flexible and it can be bent toward arbitrary angles. Two configurations of the same band-pass filter are shown in Figure 1. To validate the above design approach, the proposed filter was fabricated on a flexible substrate with relative dielectric of 2.17 and thickness of 5 mil. The overall size of the filter is 32.2×24.3 mm. The frequency response is specified with a pass band of 2.4–2.5 GHz, and with less than 1 dB insertion loss and more than 12 dB return loss in the pass band. Good agreement between the measured and simulated results has been observed.

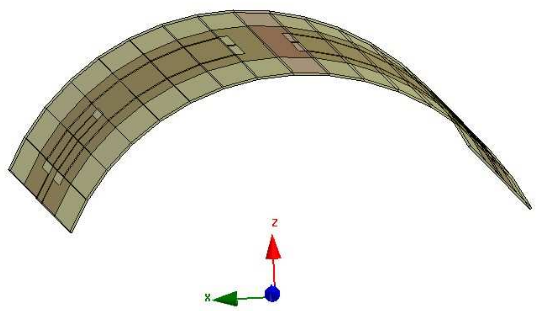

Figure 1: Bandpass filter using flexible PCB.

REFERENCES

1. Yu, S., "Embedded wide-band filter on rigid/flex. multilayer PCB for SiP," *IEEE MTT-S Int. Microw. Symp. Dig.*, June 2006.
2. Kim, J. S., N. S. Kim, W. G. Moon, S. G. Byeon, and H. S. Shin, "A novel broadband suspended substrate stripline filter using resonators with T-shaped open-circuited stubs," *IEEE MTT-S Int. Microw. Symp. Dig.*, 917–920, June 2007.

Design of a Compact Narrow Band Pass Filter Using the Rectangular CSRRs

Dong-Muk Choi, **Dang-Oh Kim**, **and Che-Young Kim**
School of Electrical Engineering and Computer Science, Kyungpook National University
Sankyuk-dong, Puk-gu, Daegu 702-701, Korea

Abstract— In this paper, a design method of the compact narrow band pass filter on the microstrip board is proposed using the complementary split-ring resonators (CSRRs). The design technique of this filter is based on cascading filter stages consisting of the combination of rectangular CSRRs, capacitive gaps between patches, and inductive grounded stubs with the meander configuration. The first design key is the introduction of the shunt connected wire in the structure, which allows us to improve frequency selectivity and the out-of-band rejection of the filter. The second feature makes an addition of gap capacitance resulting in the desired phase shift.

By these means, it was possible to get the nearly symmetric frequency responses, adjustable bandwidths, and compact sizes. And also excellent characteristic of the out-of-band rejection is achieved in contrast to the conventional filter design technique. The frequency selectivity at both band edges is high enough with approximately symmetric transition bands. Cell lengths are smaller than the signal wavelength realizing a compact filter size. The results of the frequency response measured on the fabricated band pass filter substrate show satisfactory agreement with the simulated frequency responses by the HFSS in the region of interest. The newly proposed filter by this article can be found its application on the design of compact filters with planar circuit technology.

Quad Flat Non-lead Package Characterization and Circuit Modeling

M. Sigalov[1,2,3], **D. Regev**[2], **E. Kabatsky**[3], **and R. Shavit**[1]

[1]Department of Electrical and Computer Engineering, Ben-Gurion University of the Negev
Beer-Sheva 84105, Israel
[2]Elipse-RFIC Array Devices, Kfar Neter 40593, Israel
[3]Department Electrical and Electronics Engineering, Sami Shamoon College of Engineering
Beer-Sheva 84100, Israel

Abstract— The increasing demand for faster data transmission is pushing the communication systems toward higher microwave frequencies and more complex integrated radio frequency circuits (RFICs). At such high frequencies, the electrical parasitics of the packages become so evident that they significantly degrade the performance of RFICs. One way to improve the functionality and performance of the RFIC devices is to develop accurate broadband electrical circuit models of the packages. Obtaining accurate electrical models of a miniaturized package such as a chip scale (CS) package is not a trivial task. The purpose of this work is an electrical modeling of CS quad flat no-lead (QFN) packages by utilizing three-dimensional electromagnetic (EM) numerical simulation and extraction of parasitic elements of an equivalent circuit model based on the physical structure of the package.

The QFN package is a CP leadless package where electrical contact to the printed circuit board (PCB) is made by soldering the leads on the bottom surface of the package to the PCB, instead of the conventional formed leads. The bottom-lead package structure is able to provide good electrical interconnections to the PCB. The exposed die paddle on the bottom of the chip efficiently conducts the heat to the PCB and provides a stable ground for the bonds. The small size and weight with excellent thermal and electrical performance [1, 2] make the QFN package an ideal choice for handheld portable applications such as cell phones or any other application where size, weight and package performance are required. There are currently two general types of QFN packages in the market; an air-cavity QFN and a plastic-molded QFN. The air-cavity QFN is usually made up of 3 parts; a copper leadframe, plastic-molded body (open, and not sealed), and either a ceramic or plastic lid. In contrast, the plastic-molded QFN is usually composed of just two parts, a plastic compound and a copper leadframe, and usually are less expensive.

In this work we will concentrate our attention to the characterization and circuit modeling of a fully encapsulated plastic-molded QFN package. The equivalent wideband (up to 20 GHz) electrical circuit model of the package that accounts for the high-frequency parasitic effects, such as resonance, coupling, and frequency-dependent losses will be presented. Dependence of the model on the different QFN topologies and the geometrical parameters (such as the number of leads and wires, angle between wires, distance between leads and so on) were studied and will be presented.

REFERENCES

1. Chen, N., K. Chiang. T. D. Her, Y. L. Lai, and C. Chen, "Electrical characterization and structure investigation of quad flat non-lead package for RFIC applications," *Solid-State Electronics*, Vol. 47, 315, 2003.
2. Kühnlein, G., "A design a manufacturing solution for high-reliable, non-leaded CSPs like QFN," *Proc. 51st Electron. Comp. Technol. Conf.*, 47, 2001.

A V-band Amplifier with Negative Resistance Using 0.13-μm CMOS Process

Jeng-Han Tsai[1], **Fang-Yao Kuo**[1], **and Fu-Hung Cheng**[2]

[1]Dept. of Communication Engineering, Yuan Ze University, Chung-Li, Taoyuan 320, Taiwan, R.O.C.
[2]Dept. of Electrical Engineering and Graduate Institute of Communication Engineering
National Taiwan University, Taipei 106, Taiwan, R.O.C.

Abstract— A miniature V-band amplifier with negative resistance using 0.13-μm standard MS/RF CMOS technology is presented in this paper. To solve the problem of significant matching loss of passive components at MMW frequency, a negative resistance for gain boosting technique is adopted. A small inductance L_g is added at the gate of common-gate stage of the cascade device to extend the gain performance. With the negative resistance, this four-stage thin-film microstrip amplifier MMIC achieves a peak gain of 17 dB at 67 GHz with a compact chip size of 0.49 mm^2. The supply voltage of the amplifier is 2.8-V with total current of 38 mA. The measured output 1 dB compression point is 1.18 dBm at 64 GHz.

A New Bandstop Cascaded Defected Microstrip Structure (CDMS) Filter with 10 GHz Symmetrical Bandwidth

M. Kazerooni[1], **A. Cheldavi**[1], **and M. Kamarei**[2]

[1]College of Electrical Engineering, Iran University of Science and Technology, Tehran, Iran
[2]Faculty of Electrical and Computer, University of Tehran, Tehran, Iran

Abstract— This paper presents a new bandstop filter to obtaining the broad-bandwidth rejection in microstrip transmission line. This structure is a cascaded defected microstrip structure (CDMS). To this property, two defects with similar directions and connecting line between them is designed and simulated. Then, its performance is investigated and discussed.

A Planar Yagi-Uda Antenna with High Input Resistance for Continuous-wave Terahertz Photomixer

Kyungho Han[1], **Troung Khang Nguyen**[1], **Haewook Han**[2], **and Ikmo Park**[1]

[1]Department of Electrical and Computer Engineering, Ajou University
5 Wonchon-dong, Youngtong-gu, Suwon 443-749, Korea
[2]Department of Electrical and Computer Engineering, POSTECH
San-31 Hyoja-dong, Nam-gu, Pohang 790-784, Korea

Abstract— Recent advances in terahertz (THz) technology have made possible many applications. However, the virtual absence of practical and compact solid-state continuous-wave (CW) THz sources has limited the widespread use of THz technologies. Some fundamental CW THz sources have been developed, such as quantum cascade lasers and p-Ge lasers, but these quantum-effect sources can only operate at cryogenic temperatures. Photomixers are attractive CW THz sources due to their compactness, wide tuning range, and ability to operate at room temperature. In a THz photomixer, a DC-biased electrode gap, fabricated on an ultrafast photoconductor, is illuminated by two single-mode lasers at frequencies ω_1 and ω_2 to modulate photocurrent at the THz difference frequency $|\omega_1 - \omega_2|$. As a current source, the photomixer drives an antenna to radiate THz waves into free space. The resistance of the photomixer is usually much larger than that of the antenna; this impedance mismatch severely limits the THz output power and yields the thermal dissipation problem for high output power. Consequently, it is expected that THz output power is nearly proportional to the antenna resistance for the large impedance mismatch. Several efforts have been made to design the antennas with high input resistance characteristics, such as the dual dipole, dual slot, and folded dipole antennas. However, the input resistances of those antennas are only several hundred ohms at best, so the severe impedance mismatching problem still remains. In this paper, we describe the design of a planar Yagi-Uda antenna on a very thin substrate that achieves much better impedance matching with a photomixer by using a U-shaped full-wavelength dipole as a driver element.

A Fast Approximate Method for Analyzing the Spurious Emissions from a Mitered Microstrip Bend Circuit

Han-Chang Hsieh[1], **Jay-San Chen**[2], **Chi-Hsueh Wang**[1], **Cheng-Nan Chiu**[3], **Ming-Shing Lin**[4], **and Chun Hsiung Chen**[1]

[1]Department of Electrical Engineering and Graduate Institute of Communication Engineering
National Taiwan University, Taipei 106, Taiwan
[2]Bureau of Standards, Metrology and Inspection (BSMI), Ministry of Economic Affairs, Taiwan
[3]Department of Electrical Engineering, Da-Yeh University, Changhua 515, Taiwan
[4]Department of Electrical Engineering
National Yunlin University of Science and Technology, Yunlin 640, Taiwan

Abstract— A fast approximate method for analyzing the spurious emissions from a microstrip circuit on printed circuit board (PCB) with mitered bend is proposed. By combining the transmission-line theory, the Green-function technique, and the equivalent circuit of microstrip bend, one may develop a simple method for analyzing the radiated electric field of microstrip circuit with arbitrary-angle bend. In this method, the microstrip line currents are formulated in terms of the source voltage and impedance. This method is very useful in handling the microstrip circuit with arbitrary-angle bend structures on PCB. In this study, the computer codes associated with the proposed method are developed and implemented in MATLAB, from which one may quickly calculate the radiated electric field from the mitered microstrip bend circuit. Simulated and measured results, for right-angle bend and mitered 135° bend, are compared and good agreement among the results is observed, validating the usefulness of the proposed method in characterizing the mitered microstrip bend circuit.

For validation, the radiated emissions are measured in several configurations. Specifically, the PCB circuit under test is placed on a 1.2 m high holder inside a fully anechoic chamber. The signal source is generated by the Anritus MG3692A signal generator. The emissions are received by the R&S FSP spectrum analyzer equipped with the wide-band antennas (Emco 3115 and Schwarzbeck UHALP 9107). Several ferrite cores are arranged on the coaxial cable (near the PCB) to minimize the common-mode current induced on the cable. The distance between the antenna and the DUT is 3.0 m.

The proposed method is very efficient and its simulation time is much lesser than that of the numerical simulator software EMSIM, which is developed by IBM. For instance, to obtain the data for the microstrip circuit with mitered 135° bend, which consist of 39 frequency points separated by approximately 50 MHz, our method using the personal computer only takes a couple of seconds in simulation, while the EMSIM software using the AIX, IBM P570 server needs more than hundreds of seconds to give the same results.

A BOR-FEM/Mode Expansion Analysis Based on the Helmholtz Weak Form

Hongchao Wu
Key Laboratory of Antenna & Microwave Technonlogy
Nanjing Research Institute of Electronics Technology, Nanjing 210096, China

Abstract— Millimeter wave systems have many distinct advantages, such as miniaturizing system components, increasing frequency bandwidth, providing higher detectability, and so on. The main work of the paper is solving the complicated electromagnetic boundary value problems in the actual project, mastery of the key technique, design and manufacture of the 3 mm Mono-Pulse Antenna.

Firstly, a combination approach of the mode expansion method and BOR-FEM (finite element method) is approached, which is based on the weak form of Helmholtz equation. Mode expansion is used other than PML to truncate the computing space of finite element. This approach has many advantages.

Secondly, using this approach, a W-band Mono-Pulse Cassegrain Antenna feeded by a combination of five rectangular waveguides is analyzed and manufactured, which is a electrical-large structure. Calculated results are shown and compared to those in experiments. Good agreements have been observed.

Radiated Emissions from Microstrip Ultra-Wideband Bandpass Filters

Chung-Hwa Wu, **Han-Chang Hsieh**, **and Chun Hsiung Chen**
Department of Electrical Engineering and Graduate Institute of Communication Engineering
National Taiwan University, Taipei 106, Taiwan

Abstract— With increasing operating frequency up to several gigahertz, the radiated emissions from microstrip circuits become significant and should be seriously dealt with. To address this problem, a fast simulation model based on the electric field integral equation formulation containing dyadic Green's function is utilized to analyze the radiated emissions form microstrip circuits such as the ultra-wideband (UWB) bandpass filter. First, the current distribution on each microstrip line element is evaluated and expressed in terms of two-terminal voltages and currents. Then, by applying the microstrip current distribution and the associated dyadic Green's function into the electric field integral equation, one may establish a fast model for estimating the electric field intensity radiated from each microstrip element. Finally, by combining the contributions from each element, one may consequently obtain the resultant radiation from the microstrip UWB bandpass filter.

Among various UWB filter topologies, the 11th-order optimum distributed highpass filter structure consisting of microstrip shorted stubs and connecting lines is adopted as an example to examine the corresponding radiated emission. From the simulated results, it is found that the radiated emission form this UWB bandpass filter is about 85 dBμV/m within the passband (3.1 GHz∼10.6 GHz), and the radiated emission in its spurious passband (16.8 GHz∼24.3 GHz) is 20 dB larger than that in the filter passband. By comparison with the FCC indoor emission mask, it is observed that the radiated emission in the spurious passband (16.8 GHz∼24.3 GHz) is unfortunately beyond the required limit and thus needs further reduction.

To solve this problem, the examined microstrip UWB filter should be modified so as to improve the out-of-band rejection level. For improvement, two microstrip lowpass filters are introduced in conjunction with the UWB bandpass filter. Specifically, the out-of-band rejection level of the lowpass filters is designed better than 30 dB for meeting the FCC indoor mask. By this modification, the undesired spurious emission from the microstrip UWB bandpasss filter can quickly be estimated by using the fast model based on the electric field integral equation formulation. The simulated results reveal that the radiated emission in spurious passband has effectively been reduced within the FCC indoor mask by the introduction of lowpass filters.

Design and Simulation of a Wideband Dualpolarized Conical Doubleridged Horn Antenna

M. Moshiri, H. Abiri, and A. A. Dastranj
ECE Department, Shiraz University, Shiraz, Iran

Abstract— Dual-polarized antennas are widely used in many fields including measurements, equipments, electromagnetic compatibility tests, electronic warfare, etc. These antennas in pyramidal horn shape have been investigated before. In this paper, the design and analysis of a dual polarized conical double-ridged horn antenna with dual polarization, high gain and low cross polarization for wideband applications is presented. These antennas have higher gain and lower side lobe level than pyramidal antennas. The designed antenna has a voltage standing wave ratio (VSWR) less than 2.5 for the frequency range of 8–18 GHz. Moreover, the proposed antenna exhibits a very good dual polarization, low cross polarization, low side lobe level, high gain, and stable far-field radiation characteristics in the entire operating bandwidth. Quad-ridged horn antennas also can produce dual polarization but these antennas have two input ports and have hard manufacturing processes. In this paper, a five layers slant linear polarizer is used. Five layer polarizer has lower VSWR than other multilayer polarizer. In order to achieve dual polarizations, the strips width, spacing between two adjacent strips and dielectric layers thickness are optimized. Dielectric material between layers is Styrofoam $|[\epsilon|_{\downarrow}r = 1.03)$. The proposed antenna is simulated with commercially available packages, such as CST Microwave Studio (Sax Software Corp.) and Ansoft HFSS (Ansoft Corp.), in the operating frequency range. Excellent agreement is observed between two simulation results. The best result is achieved for $\frac{\lambda}{4}$ strips spacing where λ is the wave length at the mid frequency. simulation results agree with the theoretical results. Simulation results for the VSWR, radiation patterns, and gain of the designed antenna over the frequency band 8–18 GHz are presented and discussed.

Beam Steering Capability Based on Microstrip CRLH Transmission Line

Mostafa Barati, Manouchehr Kaamyab, and Ali Azimi Fashi
Electrical Engineering Department, K. N. Toosi University of Technology (KNTU)
Tehran, Iran

Abstract— In this paper an improved version of Leaky Wave (LW) antenna with capability to scan the pattern continuously versus frequency is presented. The LW transmission line is consisting of 10 cells, each cell is made in the form of 8 finger interdigital capacitor and a shorted stub to the ground through a via. The antenna is printed on Taconic TLY5 substrate. The radiation pattern scans from left to right depending on the excitation frequency at input port. Property of leaky wave antenna using transmission line with left hand materials has been studied recently and results are represented in literature [1, 2]. In this paper we focus on Composite Right Left Hand (CRLH) effects to study the leaky wave antenna. We are able to obtain a pattern that moves from backward to forward as we increase operating frequency. The side lobe of antenna is negligible and its gain is higher considerably comparing to previous structures represented in literatures [2]. The frequency range for the implemented structure is from 1.5 GHz to 3.6 GHz; scanning for backwards occurs from 1.5 GHz to 2.3 GHz, the forward scanning is performed from 2.4 GHz to 3.5 GHz and for 2.3 to 2.4 GHz the pattern oriented almost broadside.

Leaky wave transmission line using metamaterial structures have received lots of attention in recent years, this kind of antennas have capability of pattern steering which have extensive applications in communication and radar systems. This kind of antenna for beam scanning against frequency was first presented in [1] where it was indicated that for CRLH, propagation constant, β, is negative for lower frequencies which implies backward radiation (LH), $\beta = 0$ for broadside radiation and $\beta > 0$ for higher frequencies resulting in forward radiation (RH). The theory of CRLH structures is extensively discussed in [2, 4–6] , there are some equivalent circuit for a unit cell of the antenna which accomplished earlier in [3]. It is shown that return loss is not appropriate enough in literature [2]; In this paper it will be indicated that the return loss for proposed structure is reduced significantly in comparison to [2]. Due to the modifications which have been done on the proposed antenna, gain of the antenna is much better than other similar structures in previous studies [2]. Beam scanning array can be performed by using active feed network containing varactor diodes which add to complexity in the structure of designed array [7, 8], this kind of antenna can provide tunable radiation angle electronically, scanning in this case is based on the biasing of the elements but it should be noted that such structures require biasing and the range of the scanning angle is too much lower than frequency scan.

The proposed antenna in this paper shows reduction in return loss (based on simulation and experimental results) in comparison to the structure presented in [1, 2]. The antenna shows reasonable gain in LH area (lower frequencies, Gain > 2 dB) however the structure proposed in [1] and confirmed in Chapter 6 of [2] shows low gain (Gain < -5 dB) for backward radiation. So the antenna can have similar performance in different point of space and frequencies. The simulation and measurement results in [1–3] show that the pattern in LH, Broadside and RH has some undesired side lobes, but as it is indicated in this paper, side lobes in most of the frequencies are much smaller than the main lobe and can be neglected; It is confirmed in this paper by comparing simulation (with Ansoft HFSS and CST Microwave Studio) and experimental results which are in good accordance with each other.

REFERENCES

1. Liu, L., C. Caloz, and T. Itoh, "Dominant mode (DM) leaky-wave antenna with backfire-to-endfire scanning capability," *Electron. Lett.*, Vol. 38, No. 23, 1414–1416, Nov. 2002.
2. Caloz, C. and T. Itoh, "Electromagnetic metamaterials: Transmission line theory and microwave applications," Copyright 2006 by John Wiley & Sons, Inc.
3. Caloz, C. and T. Itoh, "Novel microwave devices and structures based on the transmission line approach of meta-materials," *IEEE-MTT Int'l Symp.*, Vol. 1, 195–198, Philadelphia, PA, June 2003.
4. Sanada, A., C. Caloz, and T. Itoh, "Characteristics of the composite right/left-handed transmission lines," *IEEE Microwave Wireless Compon. Lett.*, Vol. 14, No. 2, 68–70, Feb. 2004.

5. Caloz, C. and T. Itoh, "Application of the transmission line theory of left-handed (LH) materials to the realization of a microstrip LH transmission line," *Proc. IEEE-AP-S USNC/URSI National Radio Science Meeting*, Vol. 2, 412–415, San Antonio, TX, June 2002.
6. Lai, A., C. Caloz, and T. Itoh, "Composite right/left handed transmission line metamaterials," *IEEE Microwave Mag.*, Vol. 5, No. 3, 34–50, Sept. 2004.
7. Lim, S., C. Caloz, and T. Itoh, "Metamaterial-based electronically-controlled transmission line structure as a novel leaky-wave antenna with tunable radiation angle and beamwidth," *IEEE Trans. Microwave Theory Tech.*, Vol. 53, No. 1, 161–173, Nov. 2004.
8. Lim, S., C. Caloz, and T. Itoh, "Electronically scanned composite right/left handed microsrtip leaky-wave antenna," *IEEE Microwave and Wireless Components Lett.*, Vol. 14, No. 6, June 2004.

A Novel Dual-frequency Planar Inverted-F Antenna

Jian-Wu Zhang and Yi Liu
Department of Telecommunication, Hangzhou Dianzi University, China

Abstract— The planar inverted-F antenna (PIFA) is one of the most popular antennas for various wireless communication systems due to its high radiation efficiency, compact size and simple structure. However, the resonant characteristics of a PIFA limit the operation bandwidth, making the antenna not suitable for wideband applications. A number of techniques for PIFA have been reported to achieve a wider bandwidth or a smaller size. These include adding a parasitic resonant element, patterning the ground plane to achieve multiple resonances for bandwidth enhancement, spatially bending the radiating element, and capacitive feeding and loading for a more compact size. In general, bandwidth enhancement and size reduction are not achieved at the same time, especially for resonant structures such as PIFA.

The antennas must work in several frequencies in multi-frequency systems, and the size must be compact enough. Based on it, a new dual-frequency (GSM/DCS) planar inverted F antenna (PIFA) is presented and studied. Antenna radiation tablets, short-circuit wall and antenna ground all use the 0.25 mm copper, the ground size of 40 mm × 40 mm, radiation-chip size of 33 mm × 15 mm, short-circuit wall size of 1 mm × 7 mm. A single coaxial feed is implemented in this antenna, inner conductor connects to the radiation patch antenna, and the outer conductor connects to the back of antenna ground. Through match-conditioning the feeding point, that is, to optimize the design, to realize the impedance matching, to reduce return loss, and to improve gain to meet the bandwidth requirements. The antenna features are that to open a U-shaped slot and a square shaped slot in the radiation-chip, as well as through appropriate design of the radiation patch and short-circuit wall's height and width, and the location and size of U-shape slot, and to optimize the feed location, which can obtain 2 operating frequencies that is GSM 900 MHz and DCS 1800 MHz, and the bandwidth in every band are also ideal. Simulated results are computed by Ansoft's HFSS10.0 antenna simulation software, which in the low frequency band S_{11} below -10 dB frequency range is 870 MHz–930 MHz, in high frequency band S_{11} below -10 dB frequency range is 1720 MHz–1920 MHz. And, if the size of U-shaped slot is adjust appropriately, the operating frequencies will change.

ACKNOWLEDGMENT

The work is supported by Zhejiang provincial Natural Science Foundation of China under grant number R105473.

Influence of the Human Head in the Radiation of a Mobile Antenna

P. Pinho[1, 2] **and J. Casaleiro**[1]

[1]Instituto Superior de Engenharia de Lisboa (ISEL), Portugal
[2]Instituto de Telecomunicações, Portugal

Abstract— The big proliferation of mobile communication systems has caused an increased concern about the interaction between the human body and the antennas of mobile handsets. A lot of research studies have been carried out based on this interaction [1–3], dealing generally with two aspects. The first aspect is the mobile phone antenna influence on the human body in particular on the head. In fact, when a cellular phone works, the transmitting antenna is placed near to the user's head where a substantial part of radiated power is absorbed. It's important to characterize and quantify the distribution of the electromagnetic fields and the energy levels absorbed by the human tissues. In order to characterize the absorbed radiation by the human body, we use the Specific Absorption Rate (SAR) that represents the levels which is absorbed by a mass unit of tissue. The second aspect is the influence of the user's body on radiation properties of the mobile phone, which is significant from the antenna design point of view. Antenna characteristics that are mostly affected by the presence of the human body are radiation pattern, input impedance and radiation efficiency [4]. The presence of the human body (and more specifically of the head) close to the handset causes (generally) degradation of its performance in comparison with the operation of the handset alone. The measure of this performance is the radiation efficiency of its antenna.

In order to study the problem, first a multiband antenna was designed to operate over two frequency sub bands 900 and 1800 MHz, because those are the typical frequencies for mobile communications systems nowadays.The project of this antenna was obtained using the FDTD [5, 6], and a prototype of the final version was fabricated and measured and a good agreement was obtained. The next step was to simulate the same antenna in the presence of a human head and analyse the head's influence. Based on theoretical and experimental results, the influence of the human head on the radiation efficiency of the antenna has been investigated as a function of the distance between the head and the handset and with the inclination of the antenna. The considered distances were 1.6 mm, 4.4 mm and 9.6 mm. The antenna's inclinations were 0°, 45°, and 90°. Furthermore, the relative amount of the electromagnetic power absorbed in the head has been obtained, calculating the SAR for the two frequencies. As a starting point of our research an anatomically-realistic model of the human head has been used. It is as most approximate to real heterogeneous human head as prescribed in safety standards. In the next figure, we show some of the results obtained in this investigation. In the left we present the simulated results of the return loss for an antenna distance of 1.6 mm from the head to the handset, and for handset's inclinations of 0°, 45°, and 90°. In right, we present the simulated results for an inclination's antenna of 45° and distances of 1.6 mm, 4.4 mm and 9.6 mm.

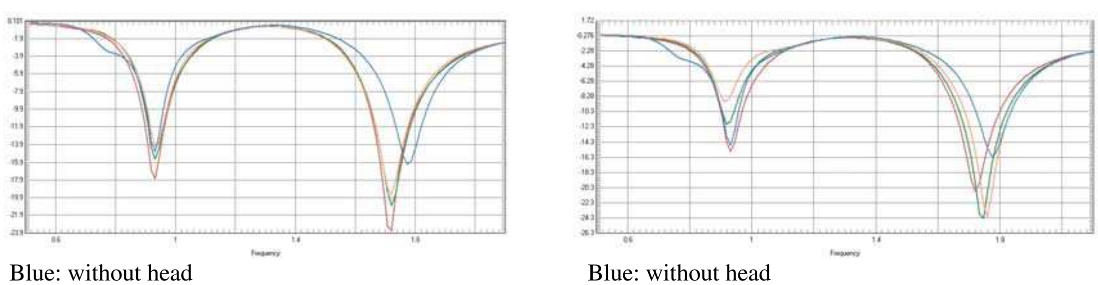

Blue: without head
Red: with head at 0º; Green: with head at 45º
Salmon: with head at 90º

Blue: without head
Red: with head at 1.6mm; Green: with head at 4.4mm
Salmon: with head at 9,6mm

Figure 1: Return loss of multiband antenna with or without head.

REFERENCES

1. Zervos, T., A. Alexandridis, V. Petrović, K. Dangakis, B. Kolundžija, D. Olcan, A. Dordević, and C. Soras, "Accurate measurements and modelling of interaction between the human head and the mobile handset," *Proc. 7th WSEAS Int. Multiconf. CSCC*, 2003.

2. Alexandridis, A., V. Petrović K. Dangakis, B. Kolundžija, P. Kostarakis, M. Nikoliić, T. Zervos, and A. Dordević, "Accurate modelling and measurements of a mobile handset EM radiation," *Proc. 2nd Intern. Workshop on Biol. Effects of Electromagnetic Fields*, 251–259, 2002.
3. Jensen, M. A. and Y. Rahmat-Samii, "EM interaction of handset antennas and a human in personal communications," *Proc. IEEE*, Vol. 83, 7–17, 1995.
4. Pedersen, G., M. Tartiere, and M. Knudsen, "Radiation efficiency of handheld phones," *Proc. IEEE Vehicular Technology Conf.*, 1381–1385, Tokyo, Japan, May 2000.
5. Yee, K. S., "Numerical solution of initial boundary value problems involving Maxwell's equations in isotropic media," *IEEE Trans. Antennas and Propagation*, Vol. 14, 302–307, April 1966.
6. Taflove, A. and S. Hagness, *Computational Electrodynamics — The Finite-Difference Time-Domain Method*, Artech House, 2005.
7. Gabriel, C., "Compilation of the dielectric properties of body tissues at RF and microwave frequencies," Brooks Air Force Technical Report, AL/OE-TR-1996-0037, 1996.

A Novel Small Resonant Antenna Using the Meta-materials Array

Ali Azimi Fashi, Manoochehr Kamyab, and Mostafa Barati
Electrical Engineering Department, K. N. Toosi University of Technology (KNTU)
Seyedkhandan, Dr. Shariati Ave, Tehran, Iran

Abstract— A novel resonant antenna array based on the transmission line (TL) approach of meta-materials is presented in this paper. The composite right/left-handed (CRLH) architecture is used to implement this antenna. When the CRLH transmission line forms an open-ended resonator, it resonates when $\beta = n\pi/L$, where L is the physical length of the resonator and n is the mode number. The CRLH TL can resonate at the zeroth-order mode ($n = 0$) with an infinite wavelength [1, 2, 6]. Since the resonant frequency of the zeroth-order resonator (ZOR) antenna is determined not by the physical resonator length, the antenna size can be arbitrary regardless of the operation frequency and, therefore, there is a freedom in radiation pattern and directivity design. There are some equivalent circuits for a unit cell of the resonant antenna which accomplished earlier in [1, 2, 5].

The array structure includes two open-ended parallel 5-cell elements that each cell consists of 8 finger interdigital capacitor and a shunt meander line connected to a virtual ground patch. The design is implemented on Taconic TLY5 substrate. In this paper, it is mainly focused on CRLH effects for antenna effective area reduction and on array structure for antenna gain enhancement. When number of cells is increased, directivity increases with no change in the operation frequency. The structure is designed to have a minimum effective area size in two dimension with an acceptable directivity. The operation frequency for the implemented structure is 3.94 MHz and maximum gain of the antenna is about 6.5 dB. The size of array radiating part is almost 26 mm × 20 mm that compared with a conventional array, about 57% effective area reduction is achieved. Due to the array structure, gain of the antenna is much better than other similar structures in previous studies, compared with results for gain reported earlier in [1, 2], our proposed antenna has reasonable gain in ZOR. In this paper, it is shown that two simulation results using Ansoft HFSS and CST Microwave Studio agree well with measured results. For proposed structure measured return loss is −12.5 dB which is better than the previously reported design [1] and radiation pattern is desired with no undesired side lobes.

REFERENCES

1. Sanada, A., M. Kimura, I. Awai, C. Caloz, and T. Itoh, "A planar zeroth-order resonator antenna using a left-handed transmission line," *2004 European Microwave Conference*, Vol. 3, 1341–1344, Oct. 2004.
2. Caloz, C. and T. Itoh, *Electromagnetic Metamaterials: Transmission Line Theory and Microwave Applications*, John Wiley & Sons, Inc., Copyright 2006.
3. Zhu, Q. and H. Liao, "Design of printed antenna with left-handed array," *2005 Asia-Pacific Microwave Conference (APMC) Proceedings*, Vol. 4, 3, Dec. 2005.
4. Caloz, C. and T. Itoh, "Novel microwave devices and structures based on the transmission line approach of meta-materials," *IEEE-MTT Int'l Symp.*, Vol. 1, 195–198, Philadelphia, PA, Jun. 2003.
5. Caloz, C. and T. Itoh, "Application of the transmission line theory of left-handed (LH) materials to the realization of a microstrip LH transmission line," *Proc. IEEE-AP-S USNC/URSI National Radio Science Meeting*, Vol. 2, 412–415, San Antonio, TX, Jun. 2002.
6. Lee, C.-J., K. M. K. H. Leong, and T. Itoh, "Composite right/left-handed transmission line based compact resonant antennas for RF module integration," *IEEE Trans. on Antennas and Propagation*, Vol. 54, No. 8, Aug. 2006.

Radar Cross Section Measurements and Simulations of a Model Airplane in the X-band

I. M. Martin[1,2], M. A. Alves[1], G. G. Peixoto[1,3], and M. C. Rezende[1,3]

[1]Instituto Tecnológico de Aeronáutica, ITA-CTA, Brazil
[2]Universidade de Taubaté, UNITAU, Brazil
[3]Instituto de Aeronáutica e Espaço, Divisão de Materiais, IAE-CTA, Brazil

Abstract— The objective of this study was to illustrate how different methods of obtaining the Radar Cross Section (RCS) of an object may produce different results. RCS diagrams of an airplane model (Boeing 777) was obtained in three different ways: a) measurements in an anechoic chamber; b) measurements with a Lab-Volt RCS; and c) simulations using the commercial electromagnetic simulation software CADRCS. Both the anechoic chamber experimental setup and the LabVolt system consisted of inverse synthetic aperture radars designed to operate at close range. The airplane model is 0.64 m long ($\sim 20\lambda$) and its outer surface is completely metallic (aluminum coating). The measurements and simulations were carried out at the radar frequency of 9.4 GHz with the radar operating in a quasi-monostatic configuration, and using vertically polarized radar waves. Both types of measurements and simulations were performed in a near-field situation (distance target-radar, 6.5 m), and the simulations mimicked the experimental setup (distance between antenna and target, wave polarization, quasi-monostatic configuration). The resulting RCS diagrams show that although there was a good correspondence of the main features in the RCS diagrams, some differences can still be observed. The RCS diagram is a one-dimensional representation of a three-dimensional object, and as such, it can hide or exaggerate certain aspects of the RCS of the target related to its shape and reflecting characteristics. The use of different techniques and methods in the study of the RCS of an object serves to highlight these differences and, at the same time, help with the identification of particular features of the object being studied.

A Medium Open Range Radar Cross Section Facility in Brazil

G. G. Peixoto[1,2], **M. A. Alves**[1], **I. M. Martin**[1,3], **and M. C. Rezende**[1,2]

[1]Instituto Tecnológico de Aeronáutica, ITA-CTA, Brazil
[2]Instituto de Aeronáutica e Espaço, Divisão de Materiais, IAE-CTA, Brazil
[3]Universidade de Taubaté, UNITAU, Brazil

Abstract— The modernization of the Brazilian aeronautical industry requires that a better knowledge of the reflecting properties of aircraft and other flying objects be acquired. In order to understand and predict the response to radar waves of several types of objects, and fill a void in this area of technology, a medium range facility for the measurement of the radar cross section (RCS) has begun operating in Brazil. To the best of our knowledge, this is the first-of-a-kind facility in Brazil and Latin America. The main features of this facility are a square-section, 8-m high support pylon made of reinforced concrete with a rotating support table at its top with a load capacity of 2 ton, and radars operating in the X-, C- and S-bands. The radar antennas in this setup are movable parabolic dishes 1.5 m in diameter, approximately. The transmitted radar pulse is produced by a synthesized microwave generator coupled to 20-W power amplifier. The received signal is collected by an antenna coupled to a low-noise amplifier; the amplified signal is then sent to a spectral analyzer for visualization or recording. The distance between the pylon and the antennas is about 240 m, which, for example, allows measurements in the far-field condition at 18 GHz and 2 GHz of objects measuring 1.4 m and 4.2 m, respectively. It is planned that RCS measurements of small- and medium-size targets (up to 3 m in length) will be carried out in this facility. In this paper, we present results of the first measurements obtained in this facility; simple-geometry objects (a metallic square plate and a metallic dihedron) and complex-geometry targets (decommissioned air-to-air missile).

Suppression of Antenna's Radiation Sidelobes Using Particle Swarm Optimisation

Nik Noordini Nik Abd Malik, **Mazlina Esa**,
Sharifah Kamilah Syed Yusof, **and Jayaseelan Marimuthu**
Faculty of Electrical Engineering, Universiti Teknologi Malaysia
81310 UTM Skudai, Johor, Malaysia

Abstract— The presence of large sidelobe radiation beam levels of an antenna is undesirable as the antenna performance and efficiency will be greatly degraded. Antenna structures especially in array arrangements have the capability to provide interference reduction, improvement of the channel capacity and expanding the range of a signal's coverage. In this paper, Particle Swarm Optimization (PSO) is utilized to optimize the inter-element position of even-element linear antenna arrays (LAA). The objective is to produce as close to a desired radiation pattern as possible that exhibits sidelobe level (SLL) suppression. The PSO algorithm can be successfully used to locate the optimum element positions based on symmetric and even-element LAAs of isotropic radiators. The results obtained showed that the PSO algorithm is capable of finding the optimal solution in most cases with superior performance over conventional method.

A New and Innovative Conformal Dipole Configuration Very Close to a Ground Plane

Bin Zhou, James Breakall, Kyle Labowski, and Guizhen Lu
Communication University of China, China

Abstract— A new and innovative conformal dipole configuration that can be very close to a ground plane is presented. An open-sleeve concept has been used in an optimization to obtain 50 ohms input impedance as opposed to extremely low impedance that normally occurs. The gain approaches 10 dBi broadside to the ground plane.

Small Size and Multiband Monopole F-shaped Antenna Configuration for Wireless Communications Applications

Fawwaz J. Jibrael and Majd F. Yuhanna
Electrical and Electronic Engineering Department, University of Technology, Baghdad, Iraq

Abstract— The performance and analysis of a small size and multiband monopole F-antenna (MFA) are introduced. The proposed antenna design, analysis and characterization are performed using the Method of Moments (MoM) technique. The radiation characteristics, VSWR, reflection coefficient, input impedance, gain, and polarization of the proposed antenna are described and simulated using 4NEC2 software package. The proposed antenna operates at higher than frequency band (3 or 4 bands) depending on dimensions of the antenna.

Design and Manufacturing the Balance Amplifier Using the Lange Coupler in X-Band

Mohammad Nikfal Azar, **Manochehr Kamyab**, **and Mehrdad Djavid**
K. N. Toosi University of Technology, Iran

Abstract— In this paper we demonstrate and manufacturing the balance amplifier with 10 GHz central frequency using the microelectronic technology. we designed this structure in the range of 8 to 12 GHz frequency and utilize a lange coupler as an input and output port which has 17 dBm returned power. The coupler has been designed in HFSS as well as IE3D software and a substrate which is for this coupler is TMM6.

Electrostatic Single-probe Manipulation of a Conductive/Dielectric Micro-particle

Shigeki Saito
Tokyo Institute of Technology, Japan

Abstract— In this study, we report the possibility of electrostatic single-probe manipulation of a conductive/dielectric micro-particle. The manipulation system consists of three objects: a conductive probe as a manipulating tool, a conductive plate as a substrate, and a conductive/dielectric particle that dubs as a micro-particle. For a conductive particle, the micromanipulation technique by applying accelerating and decelerating voltage with high switching rate is developed for low impact deposition from the probe onto the plate. We theoretically determine the desired voltage as the function of time by boundary element method so that the total work to the particle given by external electrostatic force can be minimized; besides, we experimentally demonstrate the voltage effectively works with a 30-micrometer-in-diameter solder particle. For a dielectric particle having small conductivity on the surface (e.g., polystyrene particle), the micromanipulation technique by applying a single-pulse voltage with a certain pulse duration is developed. We experimentally determine the desired pulse duration through the observation of a "micro-dribble" phenomenon in which the polystyrene micro-particle going back and forth between the probe-tip and the plate even when just the constant voltage is applied, because the phenomenon can be modeled as a resistor-capacitor (RC) circuit in terms of electric characteristic that determines the frequency of the "micro-dribble". Furthermore, we also experimentally demonstrate the voltage effectively works with a 60-micrometer-in-diameter polystyrene particle. Although the techniques still need to be improved in the viewpoint of the success rate of the demonstrations, the study shows the techniques could be applied to the industrial applications such as MEMS assembly or next-generation IC packaging technology in the future.

A New Microwave Bandstop Filter Using Defected Microstrip Structure (DMS)

M. Kazerooni[1], **N. P. Gandji**[1], **A. Cheldavi**[1], **and M. Kamarei**[2]

[1]College of Electrical Engineering, Iran University of Science and Technology, Tehran, Iran
[2]Faculty of Electrical and Computer, University of Tehran, Tehran, Iran

Abstract— This paper presents a new bandstop filter by creation of some slots on the strip. These slots perform a serious LC resonance property in certain frequency and suppress the spurious signals. In the high frequencies applications, the board area is seriously limited, so using this filter; the circuit area is minimized. The proposed filter is very suitable for high density MMIC circuits.

Retrodirective Array Composed of Two-port Dual Polarized Elements

The Nan Chang and Jui-Shuan Wu
E. E. Department, Tatung University, Taipei, Taiwan

Abstract— To design a retrodirective array, two major types of fields are unavoidably coupled together to yield a ripple-like total field if no special strategy is taken. The first one is scattered directly from antenna elements and their supporting structure (such as grounded substrate); the second one is transmitted from antennas that are re-arranged through connecting transmission lines.

In this paper, planar retro-directive linear and circular polarized arrays have been implemented using stripline-coupled dual polarized two-port patch antenna elements. We validate that this structure is catered for both linear and circular polarizations by simulation with IE3D and by experiments. When the structure is used to retro-direct a circular polarized wave, both transmitting and receiving antenna can be of the same polarization state (either both of RHCP or both of LHCP). The ground reflection can automatically be rejected from reception as its polarization state is orthogonal to that of the transmitting antenna. When this structure is used to retro-direct a linearly polarized wave, polarization states of transmitting and receiving antenna are orthogonal.

Simulations and experiments were conducted at 5 GHz and 10 GHz for 2D linear and circularly polarized array. The measured 10 dB beamwidth at 5 GHz for linear polarization is 140°, and the measured 10 dB beamwidth at 10 GHz for circular polarization is 130°, both of them are much wider than the beam width of reflection from metal sheet with the same size.

Comparing Effects of Electromagnetic Fields (60 Hz) on Seed Germination and Seedling Development in Monocotyledons and Dicotyledons

Azita Shabrangi[1] **and Ahmad Majd**[2]

[1]Department of Biological Sciences, Faculty of Science
Tehran Tarbiat Moallem University, Tehran, Iran
[2]Islamic Azad University, North Branch, Tehran, Iran

Abstract— Various biological effects of exposure to extremely low frequency electromagnetic fields (ELF-EMFs) have been documented so far, but very little work has been carried out on plants. Monocotyledons are assumed to be more evolved than dicotyledons in phylogenic trends. In this research two states of seeds (wet, dry) of *Brassica napus L.* (dicot) and *Zea mays L* (monocot) were exposed to pulsed EMFs (15 min on, 15 min off) by magnitude of 1 to 7 mT in steps of 2 mT and the highest intensity was 10 mT for 1 to 4 hours in steps of 1 h. Exposure to EMFs was performed by a locally designed EMF generator. The electrical power was provided by a 220 V, AC power supply with variable voltages and currents. This system consisted of one coil, cylindrical in form, made of polyethelen with 12 cm in diameter and 50 cm in length. The number of turns is 1000 of 0.5 mm copper wire. A fan was employed to avoid the increase of temperature ($22 + 1°$C). Three replicates, with 30 seeds in each one were used. They were placed in germinator with 23°C temperature after treatment. The number of germinated seeds was registered on the 2nd day after moisturizing in *Brassica napus* and 6th day after moisturizing in *Zea mays*. Developmental growth characteristics including: root and shoot length, fresh and dried biomass weight and leaf surface of 7 days seedlings were measured. The variance analyses ANOVA and DUNCAN tests were used to calculate the level of differences of all measured traits among EMFs, duration of exposure and their interaction ($P < 0.05$).

Seedlings grown from dry pretreated seeds of *Brassica napus* showed the most significant increase in developmental growth at 10 mT and seedlings grown from wet treated seeds showed the most significant decrease in developmental growth at 10 mT comparing to control ($p < 0.05$) we observed an overall stimulating effects of EMFs in *Zea mays* with respect to developmental growth characteristics and the most significant increase observed at 10 mT ($p < 0.05$).

Authors believe these differences between two kinds of species depend on not only the genotype of species, but also hardness of seeds and stored polysaccharides in seeds which cover embryo.

All experimental data suggested Monocotyledons are more resistant than Dicotyledons against EMFs as an abiotic stress.

Effect of AC and DC Magnetic Fields on Seed Germination and Early Vegetative Growth in Brassica Napus L

Ahmad Majd[1], **Azita Shabrangi**[2], **Mahmood Bahar**[3], **and Soheilla Abdi**[3]

[1]Islamic Azad University, Tehran North Branch, Tehran, Iran
[2]Department of Biological Sciences, Faculty of Science
Tehran Tarbiat Moallem University, Tehran, Iran
[3]Physic Department, Islamic Azad University, Tehran North Branch, Tehran, Iran

Abstract— Because of the important role of plants on the earth, studying about the environmental factors which affect on plant growth is essential. Nowadays effects of electric and magnetic fields have attracted considerable attention. In this research we studied the effects of different intensities (3.7 mT and 4.5 mT) of DC magnetic fields ,different intensities (2.7 mT and 3.5 mT) of AC magnetic fields and duration of exposure (30, 60 and 90 min) on seed germination and seedlings primary growth of *Brassica napus L.* Seeds were divided into four sets and each set to three replicates. The treated and untreated seeds were then germinated under an identical condition of the waterbedded Petri-dish in a temperature and relative humidity. The growth factors were measured every day in the same time for a week.

Results indicated that the magnetic fields have no significant effect on seed germination of *Brassica napus* ($P < 0.05$) The roots length increased about 1.1 times in low intensity of AC magnetic field (without diode) and 1.1–1.2 times in high intensity of DC magnetic field (with diode) comparing with the untreated seeds. The growth of hypocotyls increased about 1.1 times in the intensity of 2.7 mT (AC) in all exposure times compared with control ($P < 0.05$). However an inhibitory effect about 10% to 40 on hypocotyls growth were observed in the case of AC and DC magnetic fields and the maximum inhibitory effect were observed in the intensity of 3.7 mT. The number of axillary roots increased about 25% in the intensity of 4.5 mT compared with untreated seeds.

All the results suggested that AC and DC magnetic fields, which were used in this research, have no significant effect on seed germination of *Brassica napus*. However magnetic fields can affect the primary growth of seedlings and these effects are altered in different intensities and duration of exposure, and also in different states of seedlings growth and differentiation.

Radio Studies of Ionospheric Sporadic E (1950–1960)

Ernest K. Smith
ECE Department, University of Colorado at Boulder, USA

Abstract— In the spring of 1950, as a young graduate student, I entered the office of Prof. Henry G. Booker, recently from Cambridge. I was his first thesis student at Cornell University. I asked for a masters thesis topic. "Sporadic E or spread F", he replied "Take your pick". I chose sporadic E whereupon he picked up a large manila envelope from his desk. "These are over 400 reports of reception of television stations at distances of 500 to 1600 miles sent to me by Hugo Gernsback of Radio Electronics magazine. They are due to sporadic-E propagation. See if you can prove it". I did so successfully in my masters thesis with the result that Booker took me on as a Ph.D. student. My Ph.D. thesis was published in 1957 by the National Bureau of Standards as "Worldwide Occurrence of Sporadic E", Circular 582, perhaps the first macroscopic study of the subject. The title soon showed up in the New Yorker magazine under the category "Irrelevant and Wasteful Government Publications".

Sporadic E (not yet known by that name) was identified by Sir Edward Appleton in 1930 based on the observation that the otherwise Chapman-like E layer showed occasional irregularities. These irregularities came to be known as sporadic E, abbreviated Es. During the International Geophysical year (IGY, 1957–1959), more definitions came into vogue including a listing of 8 types of sporadic E. The number of ionosonde stations (vertical-incidence sweep-frequency radars) reached a peak during the IGY and a more detailed set of world Es maps became possible (see [1]). By then, there was a plethora of radio techniques and rocket observations. But explanations for the cause, structure and temporal behavior of sporadic E were still unsatisfactory at the end of the IGY. (e.g., see [2]). However, at the 1960 URSI General Assembly, it was reported that Prof. J. D. Whitehead had just developed a windshear theory for sporadic E. This started a new era of sporadic-E studies. Post-1960 research is described in [3].

REFERENCES

1. Leighton, H. I., A. H. Shapley, and E. K. Smith, *Maps and Es Types in Ionospheric Sporadic E*, E. K. Smith and S. Matsushita, Eds., 166–177, Pergamon Press, 1962.
2. Thomas, J. A. and E. K. Smith, "A survey of present knowledge of sporadic-E ionization," *JATP*, Vol. 13, 295–314, 1959.
3. Whitehead, J. D., "Recent work on midlatitude and equatorial sporadic E," *JATP*, Vol. 51, 401, 1989.

Analysis of Beam Efficiency in Multiple Beam Reflector Antennas

José Alberto Bava[1,2], **Alberto Maltz**[3], **and Mario Garavaglia**[2,4]

[1]Departamento de Electrotecnia, Facultad de Ingeniería
Universidad Nacional de La Plata, Calle 1 y 47, 1900 La Plata, Argentina
[2]Centro de Investigaciones Opticas (CIOp),
Camino Centenario y 506, 1897 Gonnet, La Plata, Argentina
[3]Departamento de Matemática, Facultad de Ciencias Exactas
Universidad Nacional de La Plata, Calle 50 y 115, 1900 La Plata, Argentina
[4]Departamento de Física, Facultad de Ciencias Exactas
Universidad Nacional de La Plata, Calle 49 y 115, 1900 La Plata, Argentina

Abstract— Over the last few years there has been a significant growth in the use of multiple beam reflectors for radiometric satellite applications. Beam efficiency proven to be an important characterizing variable in the performance of these reflector antennas. High beam efficiency is required to achieve the detection of brightness variation in a specific field of view on earth. This paper presents an analysis of beam efficiency using feeder illumination tapers on the reflector's edge as a variable. Analytical results of central beam from a prototype reflector antenna, including the comparison with computed values are shown. A particular case of multiple beams is also examined.

Separating Dielectric and Conductor Loss for Rough Striplines in Printed Circuit Boards

M. Y. Koledintseva[1], A. Koul[1], P. K. R. Anmula[1], J. L. Drewniak[1], S. Hinaga[2], E. Montgomery[3], and K. N. Rozanov[4]

[1]Missouri University of Science and Technology, Rolla, MO, USA
[2]Cisco Systems, San Jose, CA, USA
[3]Simclar Interconnect Technologies, Springfield, MO, USA
[4]Institute for Theoretical and Applied Electromagnetics, Russian Academy of Sciences
Moscow, Russia

Abstract— Knowledge on dielectric constant and loss tangent of printed circuit boards (PCB) in a wide frequency range from a few MHz to tens GHz is important for modern high-speed digital design. Dielectric properties can be determined from S-parameters of a test line measured using either vector network analyzer or time-domain reflectometer. Accurate measuring of dielectric parameters requires separation of conductor loss from dielectric loss. The existing models of conductor loss in rough conductors (e.g., the most widely used empirical Hammerstad's formula [1]), have been developed for the design of microwave planar transmission line structures that require extremely smooth conductors (r.m.s. roughness $\ll 1\,\mu$m). However, an amplitude of conductor roughness in PCBs is principally on the order of 1–10 µm, and Hammerstad's formula is not applicable. The conductor loss is represented as $\alpha_c = a_{c0}(1+r)$, where $\alpha_{c0} \propto \sqrt{\omega}$ is loss in a smooth conductor, and r is the roughness term, which may be a complicated function of frequency and geometry. Loss in the corresponding smooth conductor can be calculated as $\alpha_{c0} = \beta_0\eta_0\delta_s/(4PZ_c)$, where δ_s is skin depth, Z_c is the characteristic impedance of the transmission line, η_0 is the free-space impedance, β_0 is the propagation constant in free space, and P is the actual cross-sectional perimeter of the smooth conductor [2].

The ***objective of this work*** is to accurately take into account surface roughness in the stripline structure within a PCB and separate conductor loss from dielectric loss. One of the ways of accounting for surface roughness is to use Sanderson's approach [2] of electromagnetic wave propagation along a corrugated surface. The rough surface function is represented as a periodic function of coordinate of propagation and expanded into Fourier series to get spatial harmonics. In [3], different periodic surface roughness functions have been considered: sinusoidal, rectangular, and saw tooth. We have considered a peak-like periodic function, too. It turns out that the resultant conductor loss substantially depends on amplitude and period of the surface roughness function, but not on its shape. In this work, we have also analyzed random surface roughness function based on "white noise" and "Gaussian noise" formulations [2]. It is shown that random surface roughness models may substantially overestimate actual conductor loss in PCBs, especially at frequencies over 10 GHz. Also, for correct computations while using random surface roughness models, data on power spectral density, or corresponding correlation functions for surface roughness should be available through surface imaging techniques [4].

Herein, ***a new approach*** to analyze surface roughness loss has been proposed. It is assumed that surface roughness forms a high-loss composite dielectric shell around a smooth conductor. Effective permittivity of the shell is calculated using an appropriate effective medium model, e.g., Bruggeman or Maxwell Garnett rule with aligned inclusions [5]. Then the corresponding surface roughness term that depends on ε''_{eff} is added to the characteristic impedance and propagation constant. ***Another approach*** of separating dielectric and conductor loss proposed in this work is a differential technique, which can be called "redistribution". It can be applied only if two boards with the same dielectric properties, but different conductor roughness are available. Total loss on each board α_{t1} and α_{t2} are extracted from the measured S-parameters, and the difference should be only due to the different conductor loss. In the processing algorithm, it is assumed that the conductor loss is $\alpha_{c0} = a\sqrt{\omega}$, and the dielectric loss is $\alpha_d = b\omega + c\omega^2$, which corresponds to a causal dielectric response, according to Kramers-Kroenig relations [6]. Then a curve-fitting algorithm (e.g., a genetic algorithm, or regression analysis) is applied to retrieve the coefficients a, b, and c. However, representation $\alpha_{c0} = a\sqrt{\omega}$ will result in only smooth-surface conductor loss, so that the actual conductor loss would be underestimated, while dielectric loss would be overestimated. Hence, for two boards, the calculated dielectric loss will differ, which contradicts the fact that the dielectric is the same. This urges a redistribution, which is done by introducing weight coefficients, inversely proportional to the amplitudes of surface roughness of the boards, $\nu_1/\nu_2 = A_2/A_1$, so

that $\nu_1 + \nu_2 = 1$. Then the corresponding dielectric loss for the two boards becomes equal, $\alpha_d = \nu_1\alpha_{d1} + \nu_2\alpha_{d2}$, and the corrected conductor loss is calculated as $\alpha_{c1} = \alpha_{t1} - \alpha_d$ and $\alpha_{c2} = \alpha_{t2} - \alpha_d$.

REFERENCES

1. Hammerstad, E. O. and F. Bekkadal, *Microstrip Handbook*, ELAB Report STF44 A74169, The Electronics Research Laboratory, University of Trondheim, Norway, Feb. 1975.
2. Sanderson, A. E., "Effect of surface roughness on propagation of the TEM mode," *Advances in Microwaves*, Vol. 7, 1–57, Academic Press, Cambridge, MA, USA, 1971.
3. Sundstroem, S., "Stripline Models with Conductor Surface Roughness," Master of Science Thesis, Helsinki University of Technology, Finland, Feb. 2004.
4. Braunisch, H., X. Gu, A. Camacho-Bragado, and L. Tsang, "Off-chip rough-metal-surface propagation loss modeling and correlation with measurements," *IEEE Electronic Components and Technology Conf.*, 785–791, 2007.
5. Sihvola, A., *Electromagnetic Mixing Formulas and Applications*, 67–68, The IEE, London, UK, 1999.
6. Landau, L. D., E. M. Lifshitz, and L. P. Pitaevskii, *Electrodynamics of Continuous Media*, 2nd Edition, Pergamon Press, 1984.

Research on THz Frequency Selective Surface

Xiao-Qiu Li[1] **and Jin-Song Gao**[2]

[1]Key Laboratory of Antenna & Microwave Technology
Nanjing Research Institute of Electronics Technology, Nanjing 210033, China
[2]Changchun Institute of Optics, Fine Mechanics and Physics, Chinese Academy of Sciences
Changchun 130033, China

Abstract— A two-dimensional periodic array of patch or aperture element is called a frequency selective surface (FSS) because of the frequency filtering property suggested by this structure. It is impossible to fabricate filters in THz range traditional thin film deposition method, but using frequency selective surface technology can easily come true.

In this paper, our goal is as follows: firstly, based on the spectral domain method, the THz frequency selective surface is researched. The formulation is based on constructing an integral equation for a single unit cell. The integral equation is modified for periodic cells by the application of Floquet's theorem such that the continuous convolution integral is converted to an infinite summation with each summand being a product of the spectral Green's function and the spectral equivalent surface current. The frequency response characteristics of THz frequency selective surface can be obtained by moment method. Secondly, the method is used to simulate and analyze the frequency response characteristics of THz frequency selective surface for the crosse-dipole aperture element frequency selective surface. The frequency response characteristics mainly include center frequency and bandwidth. The rusults show that, the length of the cross-dipole mainly influence the center frequency, with the length increase the center frequency decrease; the space between the elements mainly influence the bandwidth,with the space increase the bandwidth decrease; the center frequency of FSS decrease along with the dielectric loading; the center frequency of the cross-dipole element frequency selective surface shifts drastically when incoming waves have large incident angles, because the incident direction is oblique to the broadside of the cross-dipole, which will not resonate effectively, depending on the incident angles, because the projected length of the cross-dipole in the incident direction is now less than a half-wavelength.

Mesh Termination Condition Based on Two-component Version of Discretized Boundary Equation for Two-dimensional Scattering Problems

Kan Wang
Nanjing Research Institute of Electronics Technology, Nanjing 210013, China

Abstract— Recently, the discretized boundary equation (DBE) method involved two-component or one-component version has been introduced for two-dimensional scattering problems [1]. The On-surface DBE based on the former was derived for the solution of scattering by perfect electric conducting (PEC) cylinders, and further incorporated with asymptotic waveform evaluation technique to improve its efficiency, which was actually a fast spatial sweep technique [2]. The latter used as termination conditions of a finite difference (FD) or finite element mesh was validated through the numerical results for scattering by cylinders with various material properties. In this paper, a new mesh termination condition as an application of the two-component version is presented to determine the scattering problems together with FD method.

For scattering by PEC cylinders, the two components are the longitudinal electric and transverse magnetic component of the scattered field on the object surface in TM case, while they denote the transverse electric and longitudinal magnetic one in TE case. Theoretically, they satisfy the first derivation, and substituting the derivation into the two-component formulation of DBE can generate the new mesh termination condition.

In the termination condition based on the one-component version in [1] or the measured equation of invariance, the great condition numbers of both the matrix to generate coefficients and the overall sparse matrix constrain their applications. The formulation in this paper will eliminate the ill-condition phenomenon so as to significantly improve the efficiency and accuracy. Numerical results are presented to demonstrate the validity and efficiency of the proposed method.

REFERENCES

1. Xu, Y.-S. and K. Wang, "Discretized boundary equation method for two-dimensional scattering problems," *IEEE Trans. Antennas Propag.*, Vol. 55, No. 12, 3550–3564, Dec. 2007.
2. Wang, K. and Y.-S. Xu, "Application of asymptotic waveform evaluation technique in the on-surface discretized boundary equation method," *Microw. Opt. Technol. Lett.*, Vol. 51, No. 1, 67–70, Jan. 2009.

Optimization Technique on Filling Impedance Matrix in Moment Method

Guodong Han[1], **Yuhu Pan**[1], **and Changqing Gu**[2]

[1]Key Laboratory of Antenna & Microwave Technology
Nanjing Research Institute of Electronic Technology, Nanjing 210013, China
[2]College of Information Science and Technology
Nanjing University of Aeronautics & Astronautics, Nanjing, 210016, China

Abstract— Moment method and the relative fast algorithms such as fast multiple method are widely used for analyzing the electromagnetic scattering caused by three dimension objects. In traditional proceedings, the first step is to partition the surface into many triangular meshes. And the surface integral equations including EFIE, MFIE and CFIE are usually employed. The RWG basis function is chosen to discrete these integral equations in order to produce impedance matrix. And the ordinary matter of filling impedance matrix is based on the common edges. That is to define the source points and observing points on the common edges. Each common edge has interaction with other edges besides itself. The mutual effect result is expressed as the element of impedance matrix. The filling time is relevant to the square of total number of common edges.

In this paper, we propose a novel technique to fill the impedance matrix based on triangular patches. Every pair of the triangular patches has 9 common edges at most. There are some common parts in integral equation between every pairs of common edges if these edges locate on a pair of triangular patches. So we can elicit the common parts in integral equations between the different triangular patches, and distribute the values over the interaction between the relative common edges. In this case, if the object has a closed geometry shape, this matter to form the elements of impedance matrix can lead to save 4/9 filling time than the conventional way at least. Several examples show that numerical results educed from the novel technique agree very well with that from the traditional methods.

Use of TDR to Determine the Dielectric Constant of Vermiculite

G. Fontgalland[1], **S. E. Barbin**[2,3], **and I. F. Dos Anjos**[1]

[1]Electrical Engineering Department
Federal University of Campina Grande — UFCG
Campina Grande, PB, Brazil
[2]Department of Telecommunication and Control Engineering
Polytechnic School of Engineering University of São Paulo, SP, Brazil
[3]Center for Information Technology Renato Archer, Campinas, SP, Brazil

Abstract— The determination of water content in bulk soil using Time Domain Reflectometry (TDR) exhibited substantial advances in the last two decades. TDR has the advantage of enabling the accurate measurement of a material permittivity and, as a consequence, its water content. In fact, as early as 1939, geologists and other scientists recognized the existence of a close relationship between both quantities. However, at that time scientists lacked of the necessary instruments to make reliable experiments and make full use of this property.

Relying on the fact that the propagation velocity of a wave traveling in a medium depends on its permittivity, TDR became increasingly popular enabling the accurate determination of the travel time of an electronic pulse in a probe inserted in the soil. Topp et al. present a method for determining travel times in TDR probes fitting tangent lines to the waveforms of the reflected signals [1]. Nowadays, after the advent of automatic wave acquisition systems, collecting several waveforms in a single measurement campaign is possible and automatic interpretation of these waveforms became common in finding travel times, through the use of computer codes.

The equation proposed by Topp et al. [1] is described by the following single polynomial function

$$\theta = \left(-530 + 292\varepsilon - 5.5\varepsilon^2 + 0.043\varepsilon^3\right) \times 10^{-4}$$

where θ is the water content and ε the relative permittivity. As a reference, the relative permittivity of mineral substances in soil varies between 3 and 5 and the relative permittivity of water is about 80, depending on temperature. Air, which may take up to 45% of the soil volume, has negligible influence [2].

In this study, TDR is employed for the determination of the dielectric constant and water content of raw vermiculite [3, 4]. This is very important for better selection and classification of the raw material.

Through an accurate characterization of raw vermiculite it is possible to model and develop microwave industrial furnaces and efficiently produce expanded vermiculite. We will demonstrate that an increased amount of expanded vermiculite can be obtained per batch and that the use of microwaves significantly improves the related industrial process, through better control, production of a final mineral with higher added value and reduction of waste materials. A low cost reflectometer will be used in the experiments.

REFERENCES

1. Topp, G. C., J. L. Davis, and A. P. Annan, "Electromagnetic determination of soil water content: Measurements in coaxial transmission lines," *Water Resour. Res.*, Vol. 16, No. 3, 574–582, 1980.
2. Dasberg, S. and F. N. Dalton, "Time domain reflectometry field measurements of soil water content and electrical conductivity," *Soil Sci. Soc. Am. J.*, Vol. 49, 293–297, 1985.
3. Topp, G. C., M. Yanuka, W. D. Zebchuk, and S. Zegelin, "Determination of electrical conductivity using time domain reflectometry: Soil and water experiments in coaxial lines," *Water Resour. Res.*, Vol. 24, 945–952, 1988.
4. White, I., J. H. Knight, S. J. Zegelin, and G. C. Topp, "Comments on 'Considerations on the use of time-domain reflectometry (TDR) for measuring soil water content,'" by W. R. Whalley, *European J. Soil Sci.*, Vol. 45, 503–508, December 1994.

Planar Inductor for RFICs Surrounded by Metallic Vias Forming a Cavity-backed Structure Improving Isolation from the Circuitry

L. C. Kretly[1] **and S. E. Barbin**[2, 3]

[1]University of Campinas, Campinas, São Paulo, Brazil
[2]Department of Telecommunications and Control, Polytechnic School of Engineering
University of São Paulo, Brazil
[3]Center for Information Technology Renato Archer, Brazil

Abstract— Planar Inductors are very useful devices for high performance RFICs. There are several methods to increase their Quality Factors and Inductance to values required by the designer in many cases. However, due to specific silicon properties and electromagnetic fields interactions with the substrate, several undesired effects between those devices and the CMOS circuitry arise.

This work presents a new structure that surrounds the planar inductor core using via holes and N+ sinkers aiming at shielding it effectively and using the same additional strategies employed for improving the Q and expand the L values.

Shielding planes (polysilicon and n+ buried layer) are placed vertically in the structure connecting these two types of feed-through to a guard ring located at the uppermost surface providing an efficient current path between the ground pads. The overall shape looks like a cavity-backed configuration.

An interesting study carried out by Kouzaev [1] introduces a semi-analytical electromagnetic model of a ground square-pad via-hole based on previous cavity theory. This model can be extended or adapted to the n+ sinker. The vertical configuration associated with the via-holes and N+ sinkers has a second order influence on the inductor Q and L but these effects must be experimentally verified.

The figure below shows the general schematic layout of the planar inductor, via-hole and N+ sinker for simulation purposes. This work presents also the simulation results of the cavity-backed planar inductor compared to the basic planar device, and the modeling and design guide lines for RFICs designers.

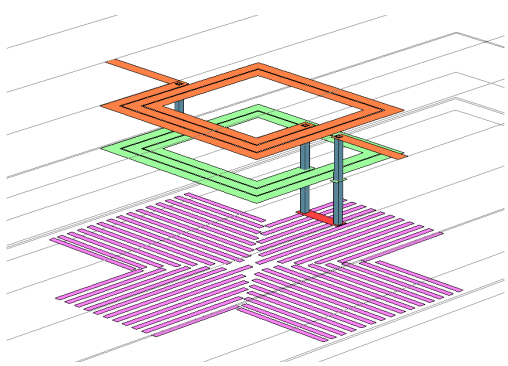

Figure 1: Planar inductor with shielding structure-vertical n+ sinker and vias create a cavity-backed structure.

REFERENCES

1. Kouzaev, G. A., "Cavity models of planar components grounded by via-holes and their experimental verification," *IEEE Trans. on MTT*, Vol. 54, No. 3, March 2006.

Experimental Characterization of Electromagnetic Properties of ASPHALT Material

O. Louhichi[1], **D. Bechevet**[1], **and S. Tedjini**[2]

[1]MIND, Archamps, Haute Savoie, France
[2]LCIS, Grenoble-INP, Valenc, France

Abstract— This communication describes an applicable method to dielectric permittivity and losses factor measurement. It is used to determine the "asphalt" electromagnetic properties.

Introduction: Studies of electromagnetic propagation environment are increasing with the expansion of wireless communications. Electromagnetic waves propagation model in different materials is not possible without the knowledge of their permittivity. Thus permittivity and permeability measurements are required in numerous applications for a large variety of materials, at a given frequency. Most widely used techniques for characterization are: cavity resonators, free space and open-ended coaxial probe and transmission line.

Method of Characterization: There exist several measurements used to study dielectric material characteristics such as techniques in transmission/reflection, guided propagation and in free space. To study asphalt electromagnetic characteristics, we chose resonant cavity method. It is one of the oldest technique for measuring the permittivity. In term of accuracy this method is very powerful.

Complexity of electromagnetic analysis depends on cavity shape and the easiest one is the rectangular one. The operating principle of a resonant cavity is based on resonance of electromagnetic waves phenomenon. Formulas below summarize how to recover the value of the dielectric constant [1, 3]:

$$fr_{TE_{mnp}} = \frac{1}{2\sqrt{\mu\varepsilon}} \cdot \sqrt{\left(\frac{m}{a}\right)^2 + \left(\frac{n}{b}\right)^2 + \left(\frac{p}{d}\right)}, \tag{1}$$

where a, b and d are the width, the height and the length of the cavity, $fr_{TE_{mnp}}$ represent the resonance frequency of an Electrical Transverse Mode of the cavity and μ_r and ε_r respectively permeability and permittivity of material filling the cavity.

Results: Different simulations with CST Microwave Studio software were made to validate the principle of the characterization by electromagnetic resonant cavity. Next graph shows two results of transmission coefficient versus frequency. The first one (green line) is for an empty cavity and the second one (red line) is for a cavity filled with bitumen (similar to asphalt). We used some bitumen because its dielectric characteristics are known [2] ($\varepsilon_r = 2.41$ and $\tan\delta = 0.0043$ at $f = 1\,\text{GHz}$).

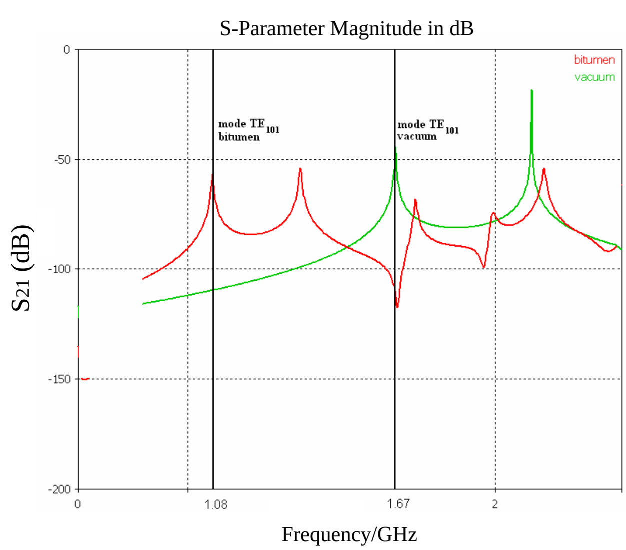

Figure 1: Two simulation results, S_{21}(dB) vs f(GHz) with empty cavity and filled with bitumen.

The aim is to deduce characterization of a material with this method. If we use results on Figure 1, we obtain a fixed resonance frequency at 1.08 GHz on the first mode ($TE_{mnp} = TE_{101}$) through the bitumen. Using formula (1) and known parameters leads to bitumen's permittivity.

Application for a cavity with $a = 100$ mm (width), $b = 26$ mm (height) and $d = 200$ mm (length):

$$\begin{aligned}\varepsilon_r &= \frac{c^2}{4 \cdot f^2} \cdot \left(\frac{m^2}{a^2} + \frac{n^2}{b^2} + \frac{p^2}{d^2}\right)\\ &= \frac{(3 \times 10^8)^2}{4 \times (1.08 \times 10^9)^2} \cdot \left(\frac{1^2}{(100 \times 10^{-3})^2} + \frac{0^2}{(26 \times 10^{-3})^2} + \frac{1^2}{(200 \times 10^{-3})^2}\right) = 2.41\end{aligned}$$

This result validates the method. We would use it on practical test to characterize asphalt with the cavity and a Vector Network Analyzer (VNA).

Conclusions: This work is intended to validate, test and develop the measurement technique (electromagnetic resonance cavity). This allows characterization of dielectric properties of civil engineering materials, especially asphalt material in the ISM frequencies band and specially UHF. The final paper will include more details on the analysis behind this measurement approach. It will include some simulation results thanks to CST Simulator. Some experimental date will also be included and discussed.

REFERENCES

1. Bechevet, D., "Contribution to the development of RFID tags in UHF and microwaves ranges, on plastic materials,".
2. Adous, M., "Caractérisation électromagnétique des matériaux traités du génie civil dans la bande de fréquence 50 MHz–13 GHz,".
3. Collin, R. E., *Foundations for Microwave Engineering (2nd Edition)*, John Wiley & Sons, 2001.

Session 3A1
New Applications of Ground Penetrating Radar for Non-destructive Testing 1

Three-dimensional Views of Buried Objects from Holographic Radar Imaging

M. Inagaki[1], **C. G. Windsor**[2], **T. Bechtel**[3], **E. Bechtel**[3], **S. Ivashov**[4], **and A. Zhuravlev**[4]

[1]Walnut Ltd, Japan
[2]116, New Road, East Hagbourne, OX119LD, UK
[3]Enviroscan Inc, USA
[4]Remote Sensing Laboratory, Bauman Moscow State Technical University, Russia

Abstract— Conventional pulsed radar produces an image along an underground vertical section. The radar scan delineates layer boundaries. Holographic radars — like the Rascan system — produce a plan view in a grey scale. It operates at 5 discrete frequencies from 3.6 to 4.0 GHz with two receiving antennae in parallel and cross polarizations relative to the transmitter. As a result, we obtain 2 sets of 5 images. The incident wave is not a pulse but a continuous wave. The recorded signal is strong when the reflected wave from a subsurface target is well correlated with the incident wave, Since the phase of the reflected wave is dependent upon target depth, the correlation varies with depth. When a target is gradually deepened, positive and negative correlations appear periodically. For instance, scans over an inclined aluminium plate using the Rascan system produce a radar image with repeated black and white stripes - dubbed the "zebra effect".

If an object is large enough (around the size of the wavelength in the soil), the zebra stripes recognizably appear over the object. Each stripe corresponds to a contour line that traces the same depth from the radar antenna. We prepared a pyramid-shaped test object, with 300 mm square base and 100 mm height. A thin aluminium film was placed on the pyramid surface. Holographic images have been recorded in four different angles with the apex directly up, to 30 degrees from vertical. The resulting radar images show zebra stripes that look very similar to simulated contour maps in any angular position. Topographic contour lines on a map depict height above sea level. However, similar to unlabelled topographic contour lines, the zebra stripes without independent depth information entail concavo-convex ambiguity. In further testing, Rascan produced concentric circle zebra stripes over a hemispherical steel bowl. From a single Rascan image, we can recognize the hemispherical shape, but cannot tell whether the bowl lies up or down. However, when viewing the 5 images from differing frequencies frame-by-frame, we can see pseudo-animated view. In this animation, the widths of the stripes shorten with increasing frequency. Thus, the zebra stripes produced by the inclined aluminium plate appear to move in the animation — creating a "zebra shift".

The bowl animation reveals that if the concentric circles expand outwards, the bowl lies concave up. If the stripes shrink inwards, the bowl lies concave down. Thus, we have found that the animation of multiple frequency images is an effective way to determine relative heights of zebra stripes on image by observing the zebra shift.

Actual buried objects will not always provide such simple geometry, the burial medium may have differing water content, and there may be clutter objects as well. All of these could distort the zebra stripes. However, this testing demonstrates that Rascan images contain information, similar to topographic contour maps, that could produce a three-dimensional view of buried objects.

Diagnostics of Mediums and Line Objects, Probing with Ultra-wideband Short-pulse Signals

A. Yu. Grinev[1], **A. V. Andriyanov**[2], **D. V. Bagno**[1], **V. S. Temchenko**[1], **E. V. Ilyin**[1], **and D. V. Nikishov**[1]

[1]Moscow Aviation Institute (State Technical university), Russia
[2]"Tenzor" Co. Ltd., Russia

Abstract— The results of design of multifunctional ground penetrating radar (GPR) are presented. The new multi-channel architecture of the GPR has been elaborated for search of metallic and dielectric objects in soil down to 1.2 meters depth. Multi-channel architecture allows to inspect 1 m width strip of ground surface simultaneously. The following items are consequently discussed: the block diagram of the GPR, its structural parts and features, the software. Both numerical and experimental results are presented.

The radar uses ultra-wideband (UWB) short-pulse signal. GPR structure is based on time-domain reflectometer. The multi-channel operation is realized by sequential connection of one of seven antennas and a single calibration channel to the reflectometer output. Stroboscopic method is used for reception of UWB short-pulse signals.

The GPR consists of receiver/transmitter module, SHF multichannel switchboard, antenna module, controlling notebook computer which are mounted on four-wheel carriage. Detailed technical characteristics are presented: outgoing waveform — a single period of sine wave, pulse width -1 ns, pulse repetition rate -1 MHz, amplitude -25 V. Operating frequency bandwidth -1.4 GHz (0.6, …, 2.0 GHz), power budget -100 dB. Antenna module is array of seven elements, element type is screened T-horn with dielectric filling, SWR is $2:1$ or less in operating frequency band, power gain of a single antenna element -5 dBi at 1 GHz.

The radar software provides graphic user interface, controls transmitter/receiver module and receives the data from it, visualizes B- and C-scans, forms 2D and 3D radio images of subsurface objects. As well, software includes modules for estimation of geometry and electrophysical parameters of subsurface medium and objects inside of it. The following procedures have been integrated at present time: forming of radio images using reverse projections method and range migration method; measurement of geometrical and electrophysical parameters for plane-layered subsurface medium using Computational Diagnostics Method (CDM); identification of typical subsurface objects using CDM and radio images analysis.

The CDM solves a reverse problem of restoration of geometrical and electrophysical parameters of mediums and objects by their UWB electromagnetic waves scattering properties. These parameters of objects and their scattering properties are related by operator equation of the first kind. In general case, the CDM brings the solution in form of absolute extremum search of smoothing functional on the frequency grid within some frequency band. The first summand is the function of discrepancy between numerically calculated scattering and measured scattering. The second summand in CDM functional is stabilizing add-on which includes *a priori* information about the medium or the object. The functional is non-convex and multi-extremal, and genetic algorithm is implemented for global extremum search.

To provide correct measuring of objects' scattering, the main artifacts should be taking into account which distort both the sounding and the scattered UWB signals. The most essential are the artifacts caused by vector effective height (VEH) of transmitting and receiving antennas as well as by radio frequency channels of transmitter and receiver. The following methods are used for account of antenna VEH: method of decomposition of electromagnetic field by a finite number of elementary plane waves; method of approximation of the real antenna by a dipole; method of virtual source. Method of decomposition is based on measurement (or numerical calculation) of the electric field component on the plane surface close to the transmitting antenna; field approximation by the superposition of elementary E and H plane waves; determination of antenna VEH; estimation of sufficient number of plane waves which is necessary for finding reflection function of the medium; transformation of scattered field back to the receiving antenna port.

Experimental results are discussed including restoration of plane layered medium parameters, forming of radio images of line objects (pipes and places of their intersections), estimation of geometrical parameters of pipes and other objects of simple shape.

Multi-frequency Full-polarized Subsurface Holographic Radar with Quadrature Receiver

A. V. Zhuravlev, **S. I. Ivashov**, **V. V. Razevig**, **and I. A. Vasiliev**
Remote Sensing Laboratory, Bauman Moscow State Technical University, Russia

Abstract— The current modification of subsurface holographic radar RASCAN features amplitude detector and five preset operational frequencies allowing for a target to be visible at least on one frequency. Ten grayscale images (5 frequencies $\times$ 2 polarizations) reflect phase shifts between the reference harmonic signal and the signal reflected by a buried object. This technique works well enough at shallow depths and on lossy media as high attenuation of a medium suppresses interferential side lobes on radar images resulting in good reproduction of buried object shape by its interference pattern. Among the drawbacks of this technique one can mention the dependence of object contrast on its depth, obscure images formed by the interference pattern when signal attenuation is relatively small and the depth to the buried object increases, necessity to observe several images in the search for the best representative, and the lack of a depth estimation technique. On the way to eliminate the above mentioned drawbacks and increase capabilities of the system, a new modification was designed. The generator is build around an integral frequency synthesizer in the frequency band 1.6–1.95 GHz, which provides software selection of an arbitrary frequency set. The quadrature receiver allows phase measurements of reflected signal on each frequency and polarization. The earlier version of the radar had a single transmit stub antenna and two mutually orthogonal receive antennas. In such a configuration the receive antenna that is orthogonal to the transmitter antenna registered depolarization effect while the current modification has two pairs of transmit and receive antennas, with each receive antenna responding to its codirectional transmit antenna. Such an implementation of antennas suggests that both these symmetric polarizations can be used in signal processing. The described modification of the radar significantly expands its potential. For example, such problems as medium dielectric constant estimation and hologram reconstruction become feasible.

Testing of the Theoretical Model for a Wideband Pulse Propagation in the Oil-Gas Collector Media

V. L. Mironov and K. V. Muzalevskiy
Kirensky Institute of Physics, SB RAS, Krasnoyarsk, Russia

Abstract— In our paper [1] there was developed a theoretical model for propagation of a superbroadband pulse radiated by a point electric dipole placed in an oil-bearing rock which is bordering on a water-bearing one, both representing the media characteristic for oil-gas collectors. A spherical wave field emitted by the dipole was represented as a superposition of plane waves propagating through an absorbing and frequency dispersive medium. In the propagation model of [1], there was used the refractive mixing dielectric spectrum model earlier proposed in [2]. Recently [3], there were conducted experiments on propagation and reflection of quasi-plane pulse waves in the oil-gas collector media similar to those used for simulation in [1]. The results of work [3] can be applied to testing the theoretical model proposed in [1] and estimating the errors caused by the approximations accepted in [1], regarding both the propagation theory and dielectric model.

The methodology of [1] was applied to develop a theoretical models corresponding to the experiments of [3]. As a result, the time shapes of the transmitted and reflected pulses were calculated, as well as energy flow density attenuation coefficients and analytical signal envelope amplitudes pertaining to the propagating pulse. Finally, the error of theoretical simulations for these characteristics were obtained. The standard deviation of the simulated values from those measured appeared to be of 11.5% and 8.2%, concerning the time shapes of pulses transmitted through oil saturated layer and reflected from the system of oil and water saturated layers bordering on each other, respectively. In the case of oil-saturated layer, the error of the simulated transmission coefficient relative to the one measured was found to be of 11.9% and 3.7%, as determined through the pulse energy flow and the analytical signal envelope amplitude, respectively.

The good correlation between the simulated and measured characteristics given above has to be limited to the short propagation distances in the studied media of only 5 cm. Because for the absorbing and frequency dispersive media, these results can not be extended over longer propagation distances. Therefore, the further experimental test for the model of [1] are currently carried out.

REFERENCES

1. Epov, M. I., V. L. Mironov, S. A. Komarov, and K. V. Muzalevskiy, "Ultrabroadband electromagnetic wave propagation in hydrocarbon reservoirs in the presence of an oil-water interface," *Russian Geology and Geophysics*, Vol. 50, No. 1, 46–52, Jan. 2009.
2. Epov, M. I., V. L. Mironov, S. A. Komarov, and K. V. Muzalevskiy, "Nanosecond electromagnetic sounding of a fluid-saturated layered formation," *Russian Geology and Geophysics*, Vol. 48, No. 12, 1054–1060, 2007.
3. Epov, M. I., O. V. Yakubov, E. D. Telpukhovsky, V. L. Mironov, and V. P. Yakubov, "The method of ultrawideband radiowave logging horizontal wells," *Izvestiya Vuzov. Phizika*, Vol. 51, No. 9, 63–71, 2008 (in Russian).

A Single Display for RASCAN 5-frequency 2-polarisation Holographic Radar Scans

C. G. Windsor[1], **A. Bulletti**[2], **L. Capineri**[2], **P. Falorni**[2], **S. Valentini**[2], **G. Borgioli**[2], **M. Inagaki**[3], **T. Bechtel**[4], **E. Bechtel**[4], **A. Zhuravlev**[5], **and S. Ivashov**[5]

[1]116, New Road, East Hagbourne, OX11 9LD, UK
[2]Dipartimento Elettronica e Telecomunicazioni, Università di Firenze, Firenze, Italy
[3]Walnut Ltd, 4-2-54 Sakaecho Tachikawa 190, Japan
[4]Enviroscan Inc, 1051 Columbia Avenue, Lancaster, PA 17603, USA
[5]Remote Sensing Laboratory, Bauman Moscow State Technical University, Russia

Abstract— The RASCAN holographic radar system has been developed by the Remote Sensing Laboratory of Bauman Moscow Technical University. The present design uses five frequencies and two polarisations to give 10 distinct images from a single scan of buried objects. The images display an interference signal between a reflected and reference beam that has sinusoidal phase variations which depicted in gray scale on each image. The phase images vary in a complicated fashion between the different frequencies and polarizations, with the different images each containing some important information on the subsurface objects. This work describes an investigation into the possibility of an optimal presentation of the 10 images as a single composite image. The objective is to display in one image as much as possible of the information present in the original individual images. The solution presented here is to sum the absolute values of the background-corrected amplitude over both the five frequencies and the two polarizations. The method is justified using an experiment in which nine US pennies, and 9 metal washers, were buried in sand at increasing depths in the range 0 to 56 mm, in a sand box test bed. The raw multi-image (i.e., multi-frequency, multi-polarisation) display was difficult to interpret as the pennies were sometimes light and sometimes dark, and appeared to vary almost randomly in amplitude between images. The algorithm chosen took the form of a summation over all frequencies f and polarisations p of the form $\Sigma_p \Sigma_f |A_{fp}(x) - B_{fp}|$ where $A_{fp}(x)$ is the amplitude at frequency f, polarisation p and position x, and B_{fp} is the background at frequency f. In some situations the two polarisation directions give important extra information and in such cases they may be separately viewed. In other cases, such as the pennies experiment, the two polarisations give essentially the same information and may be summed. Several results are described. In the pennies experiment all the nine pennies and washers are seen in a single image. The result is compared with two other possible algorithms: a summed background-subtracted amplitudes squared, and summed absolute differences between the amplitudes at each frequency and that at the one below. Neither gave significant improvement. Other examples are shown. One is a floor scan of historic Fackenthal Hall at Franklin & Marshall College, Lancaster, PA, USA. This was over a concrete floor with electrical conduits, metal reinforcing mesh and metal pan decking; all of which appear clearly in the composite image. These various floor elements even appear with proper relative apparent depth. Another example composed of four simulated land mines was taken in a sand pit at the University of Florence, Italy. All four landmine simulant objects, as well as a piece of wire "clutter" were satisfactorily represented on the single composite image.

TDR Calibration for Soil Moisture Measurements Using a Spectroscopic Dielectric Model

V. L. Mironov, L. G. Kosolapova, and K. V. Muzalevskiy
Kirensky Institute of Physics, SB, RAS, Krasnoyarsk, Russia

Abstract—

Introduction: Time Domain Reflectometry has become popular as a method to measure soil moisture of the topsoil. The TDR method applied to measure soil moisture needs a calibration relationship linking the measured time delay of sounding pulse to soil moisture. Usually, the TDR calibration is a laborious process that must be conducted for every individual type of soil at an assigned temperature. For example, such calibration has been realized in [1]. In this paper, for a given TDR device, which corresponds with the certain pulse waveform, the regression calibration plots were acquired for a broad variety of soil type. In this paper, a new calibration methodology for TDR moisture measurements is developed. It is based on the theory of broadband pulse propagation through the moist soils which textures are known, thus allowing to exclude laborious calibration measurements.

Methodologies Applied: Our approach applies the mineralogy based soil dielectric model (MBSDM) [2] that provides the complex dielectric constant of moist soil as a function of moisture, frequency, and clay content as a soil texture parameter. The propagation of a step like pulse of 0.1 ns duration was modeled according to the method proposed in [3]. The electric current distribution along an ideally conducting rod of finite length immersed in moist soil was calculated using an integral equation method to finally yield a current of reflected pulse as a function of time induced at the rod feeding input.

Analysis of Pulse Propagation: As a result, the calibration plots for the time delay of reflected pulse were obtained as a function of moisture, with the clay content of soil being a parameter. These calibration relationships were used to derive moistures from the pulse time delays measured in [1] for a set of soils with clay contents varying from 0 to 62%. The moistures thus determined were correlated with the ones measured in the process of calibration in [1]. The linear correlation coefficient between the moistures measured and derived with proposed methodology and standard deviation of the measured ones from those derived appeared to be 0.99 and $0.02\,\mathrm{cm}^3/\mathrm{cm}^3$, respectively, regarding the range of moistures from 0 to $0.6\,\mathrm{cm}^3/\mathrm{cm}^3$.

REFERENCES

1. Miyamoto, T. and J. Chikushi, "Time domain reflectometry calibration for typical upland soils in Kyushu," *JARQ*, Vol. 40, No. 3, 225–231, Japan, 2006. http://www.jircas.affrc.go.jp.
2. Mironov, V. L., L. G. Kosolapova, and S. V. Fomin, "Dielectric model accounting for contribution of bound water spectra through clay content," *PIERS Online*, Vol. 4, No. 1, 31–35, 2008.
3. Epov, M. I., V. L. Mironov, S. A. Komarov, and K. V. Muzalevskiy, "Ultrabroadband electromagnetic wave propagation in hydrocarbon reservoirs in the presence of an oil-water interface," *Russian Geology and Geophysics*, Vol. 50, No. 1, 46–52, Jan. 2009.

Comparison of UWB Impulse, FMCW, and Noise Radar for Through-wall Bioradiolocation with Finite Difference Time Domain Simulations

Lanbo Liu[1], **Sergey Ivashov**[2], **Timothy Bechtel**[3], **and Lorenzo Capineri**[4]

[1]School of Engineering, University of Connecticut, Storrs, CT 06269-2037, USA
[2]Remote Sensing Laboratory, Bauman Moscow State Technical University, Moscow, Russia
[3]Department of Earth and Environmental Science, University of Pennsylvania, Philadelphia, PA, USA
[4]Department of Electronics and Telecommunications, University of Florence, Florence, Italy

Abstract— Using the finite difference time domain (FDTD) method we have conducted bioradiolocation simulation to assess the effectiveness of remote monitoring of the cardiorespiratory parameters of human behind opaque obstacles by radar. The radiation source types under study are ultra-wide band (UWB) impulse, frequency modulated continuous wave (FMCW), and random electromagnetic noises. The impulse radar demands the most sophisticated hardware source modulation but minimal in software for imaging process. In contrast to the impulse radar, the FMCW radar possesses the advantage of much less demand on high sampling rate electronics, thus reduces the cost of high rate A/D converters, and achieves the similar resolution as the impulse radar but with lower cost on hardware. The noise radar approach possesses the major advantages of the FMCW radar, with the addition of low probability of intercept, and the ability of being immune from interference when multiple noise radars operate in the same frequency band in the vicinity.

This paper will present the simulation results for the 3 types of radar detection of human cardiorespiratory parameters and discuss the pros and cons of each of these radar techniques and recommend the approaches for a number of detection scenarios, including the multiple moving human targets within the radar antenna beam.

Session 3A2
Light Scattering and Radiative Transfer: Theories and Applications 1

Dissecting the Transition Zone between Cloud and Clear Sky Using Shortwave Spectrometers

Warren Wiscombe[1], **Alexander Marshak**[2], **and Christine Chiu**[2]

[1]Brookhaven National Lab, USA
[2]NASA Goddard Space Flight Center, USA

Abstract— The transition zone between cloud-free and cloudy air is studied using spectral measurements of zenith and nadir radiances around cloud edges obtained from the ARM's Shortwave Spectrometer (surface) and Moderate-resolution Imaging Spectroradiometer (satellite), respectively.

Studies on aerosol direct and indirect effects require a precise separation of cloud-free and cloudy air. However, such a separation is ambiguous when remotely-sensed measurements are used. The transition zone in the regions around clouds often stretches out tens of km; these regions are neither precisely clear nor precisely cloudy. As a result, in satellite retrievals, aerosol optical depth may be underestimated because of biases towards unambiguously cloud-free environments; this in turn will underestimate aerosol direct radiative forcing.

We study the transition zone between cloud-free and cloudy air using spectral measurements of zenith and nadir radiance around cloud edges obtained from the ARM Shortwave Spectrometer (SWS), a surface-based instrument, and the MODerate-resolution Imaging Spectroradiometer (MODIS), a satellite instrument, respectively. The width of transition zones from SWS data is in the range of 50–500 m, which differs from the width in satellite observations (1–10 km).

The ARM SWS looks straight up and measures zenith radiance at 418 wavelengths ranging between 350 and 2200 nm. Its 1-sec sampling resolution provides a unique opportunity to study the transition zone between cloudy and clear sky areas. As an example, we show a remarkable linear relationship between the sum and difference of radiances at 870 and 1640 nm wavelengths. The intercept of the relationship is determined primarily by aerosol properties, and the slope by cloud properties. We then discuss how this linearity can be predicted from simple radiative transfer considerations.

We also analyzed a large set of MODIS observations to determine the effect of 3D radiative interactions between clouds and cloud-free areas. We show that 3D radiative effects are responsible for a large portion of the observed increase in nadir radiances, extending about 15 km from clouds. Finally, we describe a simple model that estimates the cloud-induced enhanced reflectances of cloud-free areas in the vicinity of clouds. The enhancement is assumed to be due entirely to Rayleigh scattering; thus it is bigger for the shorter wavelengths creating a so-called "bluing" of aerosols in remote sensing retrievals.

FDTD Algorithm for Arbitrary EM Beam's Interaction with Arbitrary Dielectric Surface

Wenbo Sun[1] **and Gorden Videen**[2]

[1]Science Systems and Applications, Inc., Hampton, Virginia 23666, USA
[2]Army Research Laboratory, 2800 Powder Mill Road, Adelphi, MD 20783, USA

Abstract— We present a new FDTD algorithm that allows us to incorporate an arbitrary source term, which can be used to study the electromagnetic wave's interaction with arbitrary particles or surfaces. In order to eliminate scattered waves inside the dielectric medium space, a new set of perfectly absorbing boundary conditions were derived for the source term. Such modifications allow us to consider the EM light scattered by a number of different systems. The algorithm was designed especially to consider arbitrary surfaces illuminated by arbitrary beams at arbitrary angles of incidence. We will present initial results calculated using this new algorithm.

Optical Properties of Non-spherical Dust Aerosols from Mie Theory for Radiative Flux Calculations

Qiang Fu
Department of Atmospheric Sciences, University of Washington Seattle
WA 98195, USA

Abstract— The shapes of dust aerosols are exclusively nonspherical. It is well recognized that the scattering phase functions of nonspherical dust aerosols are vastly different from those of equivalent spheres based on the Mie theory. It is thus critically important to take into account the nonspherical effect when retrieving dust aerosol optical and microphysical properties from the measurements of solar radiances.

It is a common practice to use the Mie theory to approximate the single-scattering properties of dust aerosols in the radiative flux calculations. But so far there is no systematic assessment of the application of equivalent spheres to dust aerosols in the solar radiative flux calculations. This talk will address the following questions. What are the errors in the solar radiative fluxes associated with solar reflectivity and absorptivity of a dust layer by using the extinction coefficient, single-scattering albdeo, and scattering phase function from the Mie theory? How accurate is the Henyey-Greenstein (HG) function to represent the scattering phase function of dust aerosols in the radiative flux calculations? The HG scattering phase function that is based on a single parameter, the asymmetry factor, is exclusively used in the radiative flux calculations in the climate models. And how do errors related to the use of equivalent spheres and the HG function compare to errors due to the delta-two- and delta-four-stream radiative transfer schemes that are widely used in climate models?

Single Particle Scattering Calculations with a Discontinuous Galerkin Method

R. Lee Panetta, Guanglin Tang, and Ping Yang
Department of Atmospheric Sciences, Texas A&M University, College Station, TX 77843, USA

Abstract— A significant challenge in climate modeling and in remote sensing is to understand the interactions of radiation fields and atmospheric particulates. The problem is complex on two levels: the interaction of a radiation field with individual particles (i.e., the so-called singlescattering process), and multiple scattering by an ensemble of particles. Our interest here is the single-scattering problem for particles with size parameters in the range 50–100, a regime that is known to be computationally quite demanding in the case of non-spherical particle geometries. We therefore are interested in computationally efficient methods that lend themselves to parallelization. Pseudo-spectral Galerkin methods, which reduce PDE's to coupled systems of ODE's for spectral amplitudes, have definitely attractive properties (e.g., excellent representation of phase velocities and highly accurate calculation of derivatives) and in the case of a linear problem like ours do not suffer from the "non-locality" and aliasing complications that arise in non-linear problems. These methods essentially interpolate solution values at gridpoints using trigonometric polynomials that are defined over the entire domain and the associated grid only requires two gridpoints per wavelength. But such methods are most effective for problems where periodicity assumptions are natural, boundaries are geometrically simple, and neither material properties nor features of the solution change abruptly in space. More suited to our scattering problem is a related method, the discontinuous Galerkin (DG) method, which combines the accuracy advantages of Galerkin methods with the geometric flexibility of the finite element and finite volume methods, methods that by design allow for complex geometries and abrupt spatial changes.

In the DG method, the computational domain is divided into a large number of subdomains (not in general rectangular) called elements, and solutions are represented in terms of locally defined polynomials of any desired order on the individual elements, polynomials that interpolate solution values at conveniently chosen nodal points within the elements. As in spectral methods, the PDEs involved in Maxwell's curl equations are reduced to a system of ODE's for nodal amplitude coefficients; the resulting system of ODEs can be written in a matrix form for which the matrices, because of the localized nature of the elements, are much easier to invert than their analogues in the finite element method. Communication between elements is mediated by fluxes chosen in the manner of finite volume methods.

We outline the key ideas of the DG method and, with a view to applications to scattering from ice particles in the atmosphere, we present results from two-dimensional calculations for circular and hexagonal cross sections. Results will be discussed in terms of the trade-off between mesh refinement and order of approximation on elements, and comparisons will be made with the exact solution for a circular cross-section and with the finite difference counterpart obtained for a hexagonal cross-section.

Light Scattering by Preferentially Oriented Ice Crystals

A. Borovoi and N. Kustova
Institute of Atmospheric Optics, Rus. Acad. Sci., Tomsk, Russia

Abstract— Cirrus clouds consisting mainly of ice crystals play an important role in radiative budget of the Earth. Consequently, their radiative properties are needed to incorporate in up-to-date numerical models of climate prediction and change. These radiative properties have been calculated by a lot of authors in the assumption that the crystals are 3D randomly oriented. However, experimental data obtained from both the ground and satellites prove that the ice crystals often reveal their preferentially horizontal orientation. For such crystals, the radiative properties are poor studied yet both theoretically and experimentally. In this contribution, certain theoretical results concerning this problem are presented. We divide the light scattered by preferentially oriented ice crystals into two parts: specular and diffuse components. Both components reveal their specific features and, consequently, they are calculated by different methods.

Specular Component: The specular component is seen as a bright narrow dot or a line on the background of a fuzzy wan diffuse component. Its angular structure is governed by two physical phenomena: particle flutter and diffraction of light. We have shown that the total bidirectional phase matrix for the specular component is reduced to a convolution of two separate functions responsible for either flutter or diffraction. Because of simplicity of analytical equations for the specular component, there are a number of promising procedures allowing anybody to retrieve either flutter parameters or crystal sizes from the specular component. Some of the procedures will be discussed in details.

Diffuse Component: The diffuse component averaged over ice crystal orientation within the framework of the preferential orientation is less sensitive to diffraction as compared to the specular cousin. Therefore we calculate the bidirectional phase matrix for the diffuse component by use of conventional codes corresponding to geometric optics. In nature, the ice crystal flutter is often small. In this case, the phase matrix is reduced to smoothed halo patterns well known in atmospheric optics for perfectly horizontal orientation of the crystals. A scheme for creating a data base for the diffuse component will be discussed.

Optical Characterization of Surfaces Based on the Study of the Linear Polarization Degree

P. Albella, **J. M. Saiz**, **F. Gonzlez**, and **F. Moreno**
Departamento de Fsica Aplicada, Grupo de Óptica, Facultad de Ciencias
Universidad de Cantabria, Avda de los Castros SN, Santander 39005, Spain

Abstract— During the last two decades, research involving metallic nanoparticles (NPs) has grown very fast in part because the need of different technological industries to inspect, monitor and characterize materials, looking for particulate contaminants, roughness, and other defects in the subwavelenght limit [1]. Near-field microscopy enables to image such phenomena well beyond the diffraction limit [2, 3]. In a previous work [4], we presented a surface inspection method based on optical spectroscopy, where a silver nanoparticle acting as a sensor was scanned over a surface, and by studying the plasmonic shifts induced by the substrate we were able to predict and characterize the existance of inhomogeneities on it. Following this research line we present a new optical characterization method based on the study of the linear polarization degree (P_L at normal incidence, defined as $(I_s - I_p)/(I_s + I_p)$ and measured at 90°, where I_s and I_p are the intensities with polarization perpendicular and parallel to the plane of incidence, respectively (see Fig. 1). The system under study consists of a silver nanoparticle with cubic shape acting as a sensor and located close to a dielectric substrate, both illuminated with a plane wave linearly polarized in either the scattering plane or orthogonal to it, thus producing I_s and I_p (see Fig. 1). This combined measurement can be very useful for profilometry and surface characterization, as it is sensitive to the NP-Substrate distance and to the refractive index of the substrate.

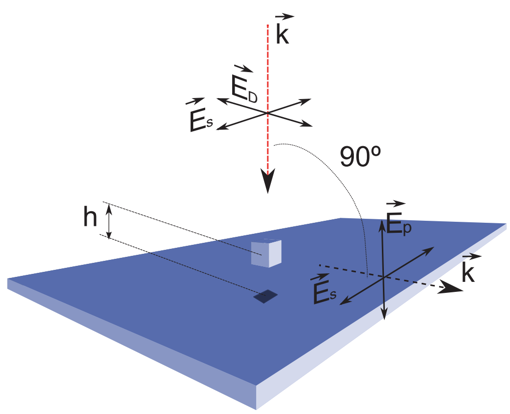

Figure 1: Experimental setup.

ACKNOWLEDGMENT

This research has been supported by the Ministry of Education of Spain under project #FIS2007-60158 and USAITC-A through R&D 1275-PH-01. The authors thankfully acknowledge the computer resources provided by the RES node at Universidad de Cantabria. P. Albella thanks the Ministry of Education for his FPI grant.

REFERENCES

1. Davies, A. G. and J. M. T. Thompson, *Advances in Nanoengineering: Electronics, Materials and Assembly*, Imperial College Press, 2007.
2. Frey, H. G., S. Witt, K. Felderer, and R. Guckenberger, "High-resolution imaging of single fluorescent Mole cules with the optical near-field of a metal tip," *Phys. Rev. Lett.*, Vol. 93, No. 20, 200801, 2004.
3. Kalkbrenner, T., U. Håkanson, A. Schädle, S. Burger, C. Henkel, and V. Sandoghdar, "Optical microscopy via spectral modications of a nanoantenna," *Phys. Rev. Lett.*, Vol. 95, 200801, 2005.
4. Albella, P., F. Moreno, J. M. Saiz, and F. González, "Surface inspection by monitoring spectral shifts of localized plasmon resonances," *Opt. Express*, Vol. 16, 12872–12879, 2008.

T-matrix Light Scattering Calculation for Extreme Particle Shapes

J. Hellmers[1] **and T. Wriedt**[2]

[1]University of Bremen, Germany
[2]Institute of Materials Science, Germany

Abstract— Over the years the **T**-matrix method for light scattering simulation became quite popular. Unfortunately the underlying Nullfield Method to calculate the **T**-matrix shows a limited numerical stability for non-spherical particles. Hereby we would like to demonstrate how to improve the numerical stability and to get results also for particles with extreme shapes like fibers or discs with high aspect ratios or concavities.

Introduction: Waterman's Nullfield Method (NFM) [1], which is usually used to calculate the **T**-matrix, can be applied to (nearly) spherical particles only. This is due to the fact, that the computation of the **T**-matrix requires the numerical inversion of another matrix which contains the field expansions for the incident field. In short, there is the rule that the more non-spherical the geometry of the studied particle is the more the elements in this matrix differ. As a result the numerical inversion gets susceptible to round-off errors and thereby instable [2].

Improving the Numerical Stability: One method to improve the numerical stability of the NFM is to use a higher numerical precision (e.g., by choosing the computer numbering format 'quad') for the variables within the corresponding program code. In another recent development the use of distributed discrete sources for the field expansion into spherical vector wave functions leads to an improved numerical stability in general [3].

With a computer program based on this advanced Nullfield Method with Discrete Sources (NFM-DS) it is possible to calculate light scattering by particles with non-spherical geometries like elongated fibers [4], oblate discs [5], biconcave discs [6] or peanut-shaped nanoparticles [7]. To demonstrate the effectiveness of the NFM-DS, simulation results for such particles will be presented together with comparative results gained by other light scattering theories like Discrete Dipole Approximation (DDA) or Finite Difference Time Domain (FDTD). This enables to estimate accuracy and calculation speed of the NFM-DS compared to other methods.

REFERENCES

1. Waterman, P., "Matrix formulation of electromagnetic scattering," *Proc. IEEE*, Vol. 53, 805–812, 1965.
2. Mishchenko, M., L. Travis, and A. Lacis, *Scattering, Absorption and Emission of Light by Small Particles*, Cambridge University Press, Cambridge, 2002.
3. Doicu, A., T. Wriedt, and Y. Eremin, *Light Scattering by Systems of Particles*, Springer, Berlin/Heidelberg/New York, 2006.
4. Pulbere, S. and T. Wriedt, "Light scattering by cylindrical fibers with high aspect ratio using the Null-Field Method with discrete sources," *Part. Part. Syst. Charact.*, Vol. 21, No. 10, 213–218, 2004.
5. Hellmers, J., T. Wriedt, and A. Doicu, "Light scattering simulation by oblate discspheres using the Nullfield Method with discrete sources located in the complex plane," *J. Mod. Opt.*, Vol. 53, 267–282, 2006.
6. Hellmers, J., E. Eremina, and T. Wriedt, "Simulation of light scattering by biconcave Cassini ovals using the Nullfield Method with discrete sources," *J. Opt. A*, Vol. 8, 1–9, 2006.
7. Hellmers, J., N. Riefler, T. Wriedt, and Y. Eremin, "Light scattering simulation for the characterization of sintered silver nanoparticles," *JQSRT*, Vol. 109, 1363–1373, 2008.

General Derivation of the Total Electromagnetic Cross Sections for an Arbitrary Particle

M. J. Berg[1], **A. Chakrabarti**[2], **and C. M. Sorensen**[2]

[1]U. S. Army Research Laboratory, USA
[2]Kansas State University, USA

Abstract— This work concerns a common problem in electromagnetic scattering and radiative transfer theory; calculation of the total scattering, extinction, and absorption cross sections for an arbitrary particle. Typical expressions for the cross sections are obtained in terms of the vector spherical wave function expansions for the incident and scattered waves. This is done with the assumption that the incident wave is monochromatic and linearly-polarized and that the particle resides in vacuum. The unique aspect of this work is that the derivation is carried out specifically without use of the far-field zone approximation. To do this, integral expressions for the particle's cross sections are analytically evaluated in the particle's near-field zone. The Wronskian relations describing the linear independence of the various spherical Bessel functions occurring in the vector spherical wave function expansions are used to simplify the near-field cross sections. The resulting expressions, which are valid at any distance, exactly match those obtained from use of the far-field zone approximation. This demonstrates that the cross sections are independent of the distance from the particle at which they are calculated. This conclusion is expected since the cross sections collectively account for the redistribution and conservation of energy, neither of which should depend on some assumed far-field distance from the particle. Numerical simulations of the near and far-field zone energy flows for a homogeneous spherical particle are presented to illustrate several implications of this result. A brief discussion will be presented regarding the specific implications of this result regarding the traditional explanation of the so-called extinction paradox.

Light Fields in a Horizontally Inhomogeneous Cloud-aerosol Layer

L. P. Bass[1], **O. V. Nikolaeva**[1], **V. S. Kuznetsov**[2], **and A. A. Kokhanovsky**[3,4]

[1]Keldysh Institute of Applied Mathematics, Russian Academy of Science, Moscow, Russia
[2]Research Scientific Center "Kurchatov Institute", Moscow, Russia
[3]Institute of Remote Sensing, Bremen University, Germany
[4]Institute of Physics, National Academy of Sciences of Belarus, Minsk, Belarus

Abstract— Horizontal changes in microphysical and optical properties of atmosphere (for example, vertical boundary of a cloud) lead to horizontal variations in reflected and transferred intensity of solar light, which are due to horizontal transport of photons and appear as brightening and shadowing effects. We study these mechanisms basing on radiation balance relation.

Quasi one-dimensional IPA (Independent Pixel Approximation) model produces large errors in the calculated reflected and transmitted light intensities in the vicinity of a cloud vertical edge and multi-dimensional models should be used to simulation of light fields in this case. Development of other one-dimensional models for radiation transfer simulations in the horizontally inhomogeneous media is an urgent problem.

We present such a model [1, 2] based upon one-dimensional transport equations for each spatial coordinate. This model gives an opportunity to estimate rapidly sizes of sub-regions, where the influence of the horizontal inhomogeneity on light intensity is essential, and obtain horizontal spatial distributions of reflected and transmitted radiation. We present numerical examples derived using this model.

ACKNOWLEDGMENT

This work was supported by Presidium of Russian Academy of Science via research program N2.

REFERENCES

1. Nikolaeva, O. V., "Simplified 1D model to 2D transport equation," *Proc. of 20th International Conference on Transport Theory*, Obninsk, 2007.
2. Bass, L. P., T. A. Germogenova, O. V. Nikolaeva, A. A. Kokhanovsky, and V. S. Kuznetsov, "Numerical simulation of boundary effects in aerosol and cloud optics," *Atmospheric and Oceanic Optics*, Vol. 22, No. 1, 102–107, 2009.

Session 3A3
Plasmonics, Metamaterials, and Magneto-Optics 1

Transforming Light and Cloaking with Photonic Metamaterials

Vladimir M. Shalaev, **Alexander V. Kildishev**, **Vladimir P. Drachev**,
Uday K. Chettiar, **and Wenshan Cai**
School of Electrical and Computer Engineering and Birck
Nanotechnology Center Purdue University, USA

Abstract— We review recent progress in developing metamaterials for the optical part of the spectrum as well as the new emerging field of transformation optics. A new paradigm of engineering space for light with transformation optics and its applications for cloaking and "super-imaging" will be also discussed.

Fabricating Plasmonic Structures via Lithographic and Imprint Techniques

Alexandra Boltasseva[1], **Paul West**[1], **and Rasmus B. Nielsen**[2]

[1]Birck Nanotechnology Center, Purdue University West Lafayette, IN 47907, USA
[2]Technical University of Denmark, DTU Building 343, DK-2800 Kongens Lyngby, Denmark

Abstract— Different fabrication approaches for realization of plasmonic components and optical metamaterials will be discussed. For applications in integrated optical systems, large-scale photolithography-based fabrication of low-loss surface plasmon polariton (SPP) waveguides and waveguide components will be reported. Profiled metal surfaces (V-grooves and wedges) used as plasmonic waveguides with subwavelength confinement will also be discussed. For plasmonic waveguides, nanoimprint-based fabrication techniques that offer mass-production compatibility and wafer-scale parallel fabrication of plasmonic components will be presented. Electron-beam-lithography based fabrication of different arrangements of surface nanoscatterers for efficient in-plane manipulation of SPPs will also be outlined. Controlled fabrication of metal nanoparticles will be discussed for optical nanoantennae realization.

Employing Epsilon-near-zero Material in Cloaking

A. P. Vinogradov[1], **A. V. Dorofeenko**[1], **E. O. Liznev**[1], **H. Liu**[3], **and S. Zouhdi**[2]

[1]Institute for Theoretical and Applied Electromagnetics, RAS
Izhorskaya 13, Moscow 125412, Russia
[2]Laboratoire de Génie Electrique de Paris LGEP-Supélec Plateau de Moulon 91192
GIF-SUR-YVETTE CEDEX, France
[3]Department of Electrical & Computer Engineering, National University of Singapore
4 Engineering Drive 3, Singapore 117576, Singapore

Abstract— Recently new approaches of anti-radar coatings have been proposed, which are usually referred to as cloaking. More specifically, there are three methods of cloaking. The first one, suggested by J. B. Pendry and U. Leonhardt, is based on a well-known phenomenon of mirage. It has been shown that by a proper choice of space distribution of permittivity and permeability one can force the light rays go perfectly around the object. The second approach elaborated by the team of Prof. S. A. Tretyakov, growth out from the first one and consists in designing a network of waveguides terminated by impedance-matched with free space antennas. This system enables the field propagation from free space to the network and vice versa. Thus, the incident waves are transmitted through the waveguides bending the cloaked object. The third approach, so-called, plasmonic cloaking, is aimed at decrease of the dipole response of the object and is based on the solution to the Hashin-Strikman problem. The cloak in this case reduces to a uniform shell covering the object.

In this communication, we show that the key point of all these approaches is the employment of a material, whose permittivity is nearly equal to zero, so-called epsilon-near-zero metamaterial (ENZM). The first approach demands ENZM because it is the interface with ENZM that prevents propagation of the light into the cloaked volume because normal components of both electric and magnetic inductions are equal to zero at this interface. Recently the team of Prof. N. Engheta has shown that a waveguide made of ENM material can support waves' traveling even if the cross section of this waveguide is very small. Thus, the ENZM waveguides may work in accordance with the second cloak method. In this communication it is also shown in a quasi-static approach that the perfect plasmonic cloak of aspherical object is asymptotically possible by employing ENZM.

The permittivity that is equal to zero may be observed for natural material whose permittivity is temporal dispersive (e.g., silver). Certainly the real part of permittivity can be equal to zero at a unique frequency. To make an ENZM we suggest to design an artificial composite material, which is a dielectric matrix filled with nano-sized multy-shell spherical inclusions. It is obvious that there are many ways to design a ENZV changing the structure of the inclusions and their concentration. We have carried out a comparative analysis of losses in such composites.

Fast Light and Focusing in 2D Photonic Quasicrystals

Y. Neve-Oz[1], **T. Pollok**[2], **Sven Burger**[2], **Michael Golosovsky**[1], **and Dan Davidov**[1]

[1]The Racah Institute of Physics, The Hebrew University of Jerusalem
Jerusalem 91904, Israel
[2]Zuse Institute, Takustrasse 7, Berlin 14195, Germany

Abstract— We report on microwave focusing by a plano-concave lens based on planar array of dielectric rods arranged in a crystalline or quasicrystalline (QC) configuration.

We designed a 2D photonic crystal superlattice made of dielectric rods of two different diameters for the operation in the microwave range. The composite unit cell of the superlattice results in a narrow transmission subband inside the photonic stop-band. Due to Brillouin zone folding in the superlattice, this transmission band is characterized by a negative refractive index. This was verified experimentally by constructing a plano-concave lens that focused the microwave radiation into a subwavelength spot [1, 2].

Another way to achieve focusing by the plano-concave lens is to use aperiodic, quasicrystalline arrangement of the dielectric rods. We studied microwave propagation in such arrays using JCM-Wave software that is based on a time-harmonic, adaptive, higher-order finite-element method. We found that in specially designed dielectric rod arrays based on Penrose tilings with 5- and 10-fold symmetry there is light localization, resulting from multiple scattering. This results in a very small refractive index (fast light). We showed by numeric simulations that a plano-concave lens built from such material exhibits focusing (Figure 1).

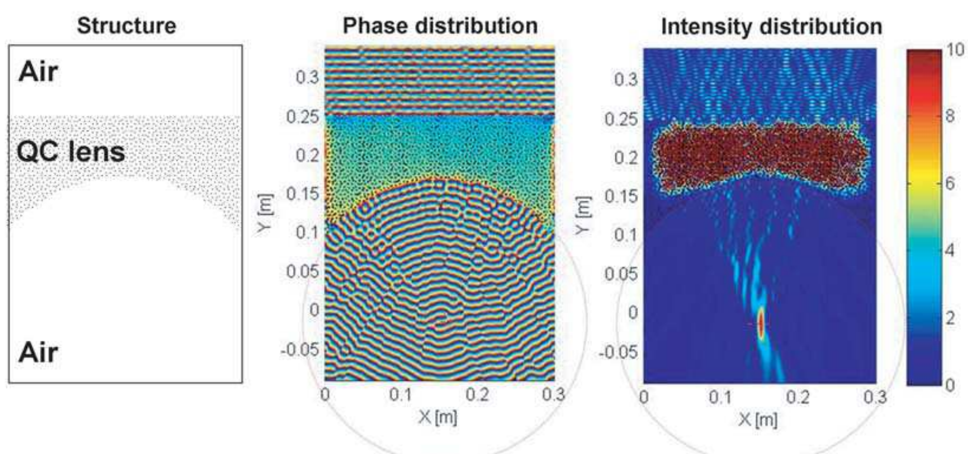

Figure 1: A plano-concave quasicrystalline lens. The phase distribution shows almost constant phase inside the lens and a uniform phase front on the concave face. The intensity distribution shows focusing.

REFERENCES

1. Saado, Y., Y. Neve-Oz, M. Golosovsky, D. Davidov, and A. Frenkel, *J. Appl. Phys.*, 104, 2008, in press.
2. Neve-Oz, Y., M. Golosovsky, A. Frenkel, and D. Davidov, *Phys. Stat. Sol. (A)*, Vol. 204, 3878–3885, 2007.

Negative Radiation-pressure Response of a Left-handed Plasmonic Metamaterial

Henri J. Lezec[1] **and Kenneth J. Chau**[1,2]

[1]Center for Nanoscale Science and Technology, National Institute of Standards and Technology
Gaithersburg, MD 20899, USA
[2]School of Engineering, University of British Columbia
Okanagan, Kelowna, B. C. V1V 1V7, Canada

Abstract— Four decades ago, V. Veselago derived the electromagnetic properties of a hypothetical material having simultaneously-negative values of electric permittivity and magnetic permeability [1]. Such a material, denominated "left-handed", was predicted to exhibit a negative index of refraction, as well as a number of other counter-intuitive optical properties. For example, it was hypothesized that a perfect mirror illuminated with a plane wave would experience a negative radiation pressure (pull) when immersed in a left-handed medium, as opposed to the usual positive radiation pressure experienced when facing a dielectric medium such as air or glass. Since left-handed materials are not available in nature, considerable efforts are currently under way to implement them under the form of artificial "metamaterials" — composite media with tailored bulk optical characteristics resulting from constituent structures which are smaller in both size and density than the effective wavelength in the medium.

Here we show how surface-plasmon modes propagating in a stacked array of metal-insulator-metal (MIM) waveguides can be harnessed to yield a volumetric left-handed metamaterial characterized by an in-plane-isotropic index of refraction which is negative over a broad frequency range spanning the blue and green. By sculpting this metamaterial with a focused-ion beam, we realize micro-cantilevers which we use to demonstrate, for the first time, a negative radiation pressure. Direct imaging of cantilever oscillation dynamics, using a scanning electron microscope (SEM), reveals that a flat slab of metamaterial experiences a pull when illuminated at normal-incidence by an electromagnetic plane wave of free-space wavelength between 450 and 600 nm. We also predict and experimentally verify a negative "super-pressure" of magnitude significantly greater than the largest photon pressure achievable under normal circumstances — that experienced by a perfect mirror.

REFERENCES

1. Veselago, V., "The electrodynamics of substances with simultaneously negative values of ε and μ," *Sov. Phys. Usp.*, Vol. 10, 509–514, 1968.

Optics of Active Metamaterials

A. K. Sarychev
Institute for Theoretical and Applied Electrodynamics
Moscow Institute of Physics and Technology, Russia

Abstract— Light is in a sense "one-handed" when interacting with atoms of conventional materials. This is because out of the two field components of light, electric and magnetic, only the electric "hand" efficiently probes the atoms of a material, whereas the magnetic component remains relatively unused because the interaction of atoms with the magnetic field component of light is normally weak. Metamaterials, i.e., artificial materials with rationally designed properties, can enable the coupling of both of the field components of light to meta-atoms, enabling entirely new optical properties and exciting applications with such "two-handed" light.

For example, specifically shaped metal nanoantennas can exhibit strong magnetic properties in the optical spectral range due to excitation of the magnetic plasmon resonance. A case in which a metamaterial comprising such meta-atoms can demonstrate both left handiness and negative permeability in the optical range is discussed. We show that high losses predicted for optical left-handed materials can be compensated in the gain medium. Gain allows achieving local generation in magnetically active metamaterials. The possibility for the metamaterial to exhibit optical ferromagnetism is discussed.

We propose a plasmonic nanolaser, where the metal nanoantenna operates in a fashion similar to a resonator. The size of the proposed plasmonic laser is much smaller than the light wavelength. Therefore, it can serve as a very compact source of coherent electromagnetic radiation and can be incorporated in future plasmonic devices. We consider various collective phenomena like superradiance in an array of nanolasers when phases of all nanolasers are synchronized and they radiate as one superlarge atom.

The Effect of Metamaterials on Anderson Localization

A. A. Asatryan[1], **L. C. Botten**[1], **M. A. Byrne**[1], **V. D. Freilikher**[2], **S. A. Gredeskul**[3], **I. V. Shadrivov**[5], **R. C. McPhedran**[4], **and Y. S. Kivshar**[5]

[1]Centre for Ultrahigh-bandwidth Devices for Optical Systems (CUDOS)
Department of Mathematical Sciences
University of Technology, Sydney, NSW 2007, Australia
[2]Department of Physics, Bar-Ilan University, Ramat-Gan 52900, Israel
[3]Department of Physics, Ben Gurion University of the Negev, Beer Sheva 84105, Israel
[4]CUDOS and School of Physics, University of Sydney, NSW 2006, Australia
[5]Nonlinear Physics Centre, Australian National University, ACT 0200, Australia

Abstract— Recently, we have shown that the combination of disorder (refractive index disorder) and meta-refraction, can substantially suppress Anderson localisation [1]. In this work, we have extended the previous study to investigate the effects of both refractive index and layer thickness disorder. We have derived a simple elegant formula that describes the localization length as a function of wavelength for both a mixed stack as well as for a homogenous stack. The localization length in the low reflection limit is determined by three quantities: the average of the reflection of a single layer $< r >$, the average of the square of the transmission $< t^2 >$ and average of the logarithm of the transmission $< \ln t >$.

$$\frac{l}{d} = -\left[\frac{< \ln t_l > + < \ln t_r >}{2} + \frac{A_r A_l}{1 - B_r B_l} + \frac{A_l^2 B_r + A_r^2 B_l}{2(1 - B_r B_l)}\right]^{-1},$$

where $A_\tau =< \ln t_\tau >$, $B_\tau =< t_\tau^2 >$ for the left and right handed slabs respectively denoted by types $\tau = l$, r (left hand or right hand layer). In the case of a homogeneous stack made up of right handed layers only, this reduces to

$$\frac{l}{d} = -\mathrm{Re}\left[< \ln t > + \frac{< r >^2}{1 - < t^2 >}\right]^{-1}.$$

The localisation length has been simulated numerically and we show that it is excellent agreement with the analytic result for both the homogenous stack and for mixed stacks, given both refractive index and thickness disorder are present (See Fig. 1). While at short wavelengths the localization length is the same for mixed stacks and homogenous stacks, the localization length is longer for the stacks composed of mixed layers compared with stacks composed of homogenous layers in the long wavelength limit.

The effect of absorption on the localisation length in such systems has also been studied, with both numerical simulation and the theoretical analysis being in excellent agreement.

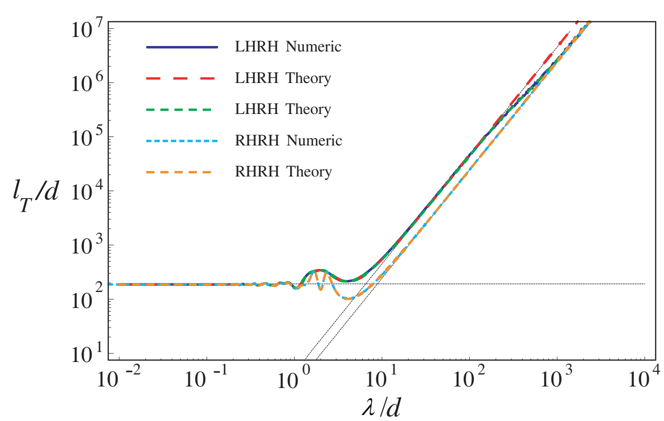

Figure 1: Localization length versus wavelength.

REFERENCES

1. Asatryan, A. A., L. C. Botten, M. A. Byrne, V. D. Freilikher, S. A. Gredeskul, I. V. Shadrivov, R. C. McPhedran, and Y. S. Kivshar, *Phys. Rev. Lett.*, Vol. 99, 193902, 2007.

Magnetophotonic Crystals with Various Designs

Seung Min Baek[1], **Taichi Goto**[1], **Alexander V. Baryshev**[1], **Alexander M. Merzlikin**[2], **Kazuo Yayoi**[1], **and Mitsuteru Inoue**[1]

[1]Toyohashi University of Technology, Toyohashi, Aichi, Japan
[2]Institute for Theoretical and Applied Electromagnetics, Moscow, Russia

Abstract— Within the last two decades progress in nanotechnology has allowed creating with high accuracy structures composed of dielectric materials with different refractive indices, known as photonic crystals (PCs) and shown to manipulate the flow of light [1–3]. For magnetophotonic crystals (MPCs), in which the constitutive elements exhibit magneto-optical (MO) response, there exists an additional degree of freedom to operate the photonic band structure, diffraction patterns, and the state of polarization of light, i.e., their characteristics can be influenced by magnetic fields [4–6].

In this work we demonstrate that tailoring of surfaces of PCs provides a new approach to engineer responses of known materials. 1D MPCs with structures of $(SiO_2/Ta_2O_5)^5/(Bi:YIG/SiO_2)^5$ and $(SiO_2/Bi:YIG)^5/Au$ were fabricated onto quartz substrates using sputtering. Parameters of these multilayers were chosen such that they supported spectrally narrow localized surface states, the so-called optical Tamm states (OTSs) [7]. Calculations show that the distribution of the electric field amplitude is remarkably high at the interface between $(SiO_2/Ta_2O_5)^5$ and $(Bi:YIG/SiO_2)^5$ {or $(SiO_2/Bi:YIG)^5$ and Au film, for the second sample} and falls exponentially away from the interface. Such a distribution confirms the formation of the OTS. All the maxima of the OTS's amplitude are spatially located within (or close to) the Bi:YIG layers. The OTSs were spectrally located within photonic band gaps and were associated with a sharp transmission peak in measured spectra of the MPCs. Substantial enhancement of the Faraday rotation for the wavelength of OTS was experimentally observed and attributed to strong light coupling to Bi:YIG constituents of the MPCs.

Another representatives of MPCs under our study were autocloned $(Bi:YIG/SiO_2)^7$ multilayers with a quasi-2D structure. They were fabricated via sputtering onto e-beam lithography patterned substrates. Diffraction experiments and polarization-resolved transmission spectra showed that light coupling happened due to superimposition of three gratings existing in these multilayers. Structural parameters were such that two spectrally neighboring stop bands (band 1 and band 2) were observed at normal incidence. Moreover, the long-wavelength edge of band 1 intersected the shortwavelength one of band 2, i.e., the band crossing was realized. Enhancement of Faraday rotation was observed for wavelengths corresponding to the short-wavelength edges of both stop bands. Faraday rotation of the quasi-2D multilayer was significantly larger than that of the conventional 1D multilayer fabricated simultaneously, for reference, onto the non-patterned area of the same substrate. Interestingly, the large reverse rotation was observed in the spectral range of the crossing. Thus, we can state that light coupling to the quasi-2D multilayer is more effective. As for the sign of rotation, it is likely governed by an amplitude-phase relationship between beams emerging from the multilayer.

REFERENCES

1. Joannopoulos, J. D., R. Meade, and J. Winn, *Photonic Crystals*, Princeton University Press, Princeton, 1995.
2. Lopes, C., *Adv. Mater.*, Vol. 15, 1679, 2003.
3. Lourtioz, J.-M., H. Benisty, V. Berger, et al., *Photonic Crystals: Towards Nanoscale Photonic Devices*, Springer, Berlin, 2005.
4. Inoue, M., R. Fujikawa, A. Baryshev, et al., *J. Phys. D: Appl. Phys.*, Vol. 39, R151, 2006.
5. Khanikaev, A. B., A. V. Baryshev, M. Inoue, et al., *Phys. Rev. B*, Vol. 72, 035123, 2005.
6. Vinogradov, A. P., A. V. Dorofeenko, S. G. Erokhin, et al., *Phys. Rev. B*, Vol. 74, 045128, 2006.
7. Goto, T., A. V. Dorofeenko, A. M. Merzlikin, et al., *Phys. Rev. Lett.*, Vol. 101, 113902, 2008.

Influence of the Shapes of Holes or Islands on the Surface Plasmon Resonances and on the Light Transmission though a Metallic Film: Theory and Experiment

Yakov M. Strelniker[1], **David J. Bergman**[2], **Anna O. Voznesenskaya**[3], **David G. Stroud**[4], **Yafit Fleger**[1], **and Michael Rosenbluh**[1]

[1]Department of Physics, Bar-Ilan University, IL-52900 Ramat-Gan, Israel
[2]Raymond and Beverly Sackler School of Physics and Astronomy
Faculty of Exact Sciences, Tel Aviv University, IL-69978 Tel Aviv, Israel
[3]St. Petersburg State University of Information Technologies, Mechanics and Optics
St. Petersburg 197101, Russian Federation
[4]Department of Physics, The Ohio State University, Columbus, Ohio 43210, USA

Abstract— The light transmission through metallic films with different types of micro-structures was studied both theoretically [1–4] and experimentally. It is shown, analytically, numerically and experimentally, that the positions of the surface plasmon resonances depend on micro-structural details. This leads to a strong dependence of the amplitude of the light transmission, as well as the polarization of the transmitted light and other optical properties (e.g., Faraday and Kerr rotations) on those details. Two complementary situations are considered: a metal film with dielectric holes and a dielectric film with metallic islands. Two different possibilities for manipulating the light transmission are considered: One is based upon application of a static magnetic field, (actually, this is equivalent to changing the micro-structure in a transformed configuration space) the other is based upon using liquid crystals as one of the constituents of a micro-structured film.

REFERENCES

1. Strelniker, Y. M. and D. J. Bergman, "Transmittance and transparency of subwavelength-perforated conducting films in the presence of a magnetic field," *Phys. Rev. B*, Vol. 77, No. 20, 205113, 2008.
2. Strelniker, Y. M. and D. J. Bergman, "Optical transmission through metal films with a sub-wavelength hole array in the presence of a magnetic field," *Phys. Rev. B*, Vol. 59, No. 20, R12763–R12766, 1999.
3. Strelniker, Y. M. and D. J. Bergman, "Anisotropic ac electrical permittivity of a periodic metal-dielectric composite film in a strong magnetic field," *Phys. Rev. Lett.*, Vol. 80, No. 4, 857–860, 1998.
4. Strelniker, Y. M., D. G. Stroud D, and A. O. Voznesenskaya, "Control of extraordinary light transmission through perforated metal films using liquid crystals," *Eur. Phys. J. B*, Vol. 52, No. 1, 1–7, 2006.

Session 3A4
Electromagnetic Field in the Metamaterials and Dispersion Design of Cloaks and Photonic Crystals 2

Global and Local Field EM Modeling and Novel GL Double Layered Electromagnetic Cloaks

Ganquan Xie, **Jianhua Li**, **Feng Xie**, **and Lee Xie**
GL Geophysical Laboratory, USA

Abstract— Recent years, the electromagnetic metamaterials cloak and LHM materials are hot research projects. The EM cloak is anisotropic inhomogeneous dispersive materials. The exterior EM wavefield propagation through the cloak never be disturbed by the cloak and the EM wavefield can not penetrate into the cloak. Therefore, the cloak can be invisibility materials. In almost EM cloak simulations, only the plane wave is used to be incident field, the plane wave is excited by infinite plane sources. The plane sources can not be located inside of the cloak domain and can not be located inside of the cloaked concealment. These cloak simulation research papers only reported the exterior EM field propagation through cloak. They did not study the difficult cases that the local sources polarization excitation inside of the cloak and its concealment. They did not know what happen of the EM radiation excited by local sources inside of cloaked concealment. Our 3D GL EM modeling can simulate all cases that the point or local sources to excite EM wave field through the cloaks. The local and point source can be located I in any where in 3D space. We obtained excellent simulations of the EM wave propagation through the cloaks, the EM wave field are excited by the point source outside of the cloak, inside of cloak, and in side of the cloaked concealment. **We discovered that there is no Maxwell electromagnetic wavefield excited by nonzero local sources inside of a concealment**. In this paper, a Global and Local field modeling is proposed to simulate the electromagnetic wave propagation in the inhomogeneous anomalous materials, in particular, in the cloak metamaterials. The method is a significant physical scattering process. The finite inhomogeneous domain is divided into a set of small sub domains. The interaction between the global field and anomalous material polarization field in the sub domain causes a local scattering wave field. The local scattering wave field updates the global wave field by an integral equation. Once all sub domains are scattered, the wave field in the inhomogeneous anomalous materials will be obtained. We call the method as the Global and local field method, i.e., GL method which is fully different from the traditional numerical methods. The GL method combines the analytical and numerical method consistently together. There is no big matrix to solve in it. The GL method does not need artificial boundary and absorption boundary condition to truncate infinite domain. The GL method is suitable for any frequency band and isotropic and anisotropic materials. Many 3D electromagnetic cloak simulations show that the GL method is effective to simulate the electromagnetic wave propagation through the anomalous materials and cloak metamaterials. The theoretical analysis of the 3D electromagnetic cloakis presented in this paper.

Isotropic Metamaterial Based on Dielectric Cubes

M. A. Odit and I. B. Vendik
Microwave Microelectronics Department
St. Petersburg Electrotechnical University "LETI", Russia

Abstract— Artificial materials with negative effective permittivity and permeability (metamaterials) became extremely popular because of possibility to design perfect lens [1] and cloaking covers [2]. For these devices the isotropy of metamaterial is of high importance. Spherical dielectric particles with two different diameters can be used to manufacture isotropic metamaterial [3]. The resonance behavior of smaller and bigger spheres provides negative effective permeability and permittivity response. Unfortunately electric resonance (TM-mode) is weakly pronounced in comparison with magnetic resonance (TE-mode), so double negative behavior is hardly to observe. Additionally, the manufacturing process for spherical particles is rather complicated. That is why it was suggested to use cubic dielectric resonators to replace spherical particles. The cubic resonators are easier to manufacture and arrange.

The basic idea of the cubic-particle based metamaterial is the same as the case of spherical particles. The magnetic type resonance (first Mie-resonance) appears in the cubes of smaller dimensions and the electric type resonance (second Mie resonance) appears in the cubes of higher dimensions [4]. The dimensions of cubes can be adjusted so that both resonances have the same frequency. Electric and magnetic dipoles in different cubes on the frequency below the resonance provide effective negative magnetic and electric response. The isotropy of the structure is provided by the cubic symmetry in dielectric resonators arrangement.

The structure consisting of dielectric cubes with permittivity $\varepsilon = 80$ arranged in host material ($\varepsilon = 1$) was modeled analytically. Dimensions of cubes were 1 mm and 1.36 mm. The result of modeling shows existing of resonant stop band near frequency 30 GHz in case if only big or only small cubes were considered. The stop band appears because of existence of imaginary part of the wave vector above the resonance frequency, where permittivity or permeability is negative. At the same time, if both particles are considered together, pass band appears where the frequencies of two types of resonances coincide. This implies real, but negative value of wave vector in case when both permittivity and permeability are negative at the same time.

The isotropic media with negative permittivity and permeability have negative refractive index — the main characteristics of metamaterial.

REFERENCES

1. Pendry, J. B., "Negative refraction makes a perfect lens," *Phys. Rev. Lett.*, Vol. 85, 3966, 2000.
2. Pendry, J. B., D. Schurig, and D. R. Smith, "Controlling electromagnetic fields," *Science*, Vol. 312, 1780–1782, 2006.
3. Odit, M., I. Vendik, and O. Vendik, "3D isotropic metamaterial based on dielectric resonant spheres," *Metamaterials 2007 — Proceedings of the Conference*, 2007.
4. Zhao, Q., L. Kang, B. Du, H. Zhao, Q. Xie, X. Huang, B. Li, J. Zhou, and L. Li, "Experimental demonstration of isotropic negative permeability in a three-dimensional dielectric composite," *Physical Review Letters*, PRL 101, 027402, 2008.

Electromagnetic Dispersion of Waveguide Based on Periodic Structures

S. Bouali and T. Aguili
National Engineering School of Tunis, ENIT, Tunisia

Abstract—

Introduction: This paper presents a study of electromagnetic dispersion of waveguide based on periodic structure using the transmission line approach and the theorem of Floquet. The waveguide structure discussed in this paper is made of an infinite repetition of layers in one dimension. The structure is modeled as an infinite repetition of unit cell, by defining the matrix chain of the unit cell and using Floquet's theorem, we obtain the equation of dispersion of the structure. This structure produces a set of allowed and forbidden frequency bands which are plotted and discussed, the width of these band depends on many parameter of the structure, the results of this analysis are presented.

Modeling of the Structure: The structure shown in Figure 1 is considered as waveguide formed by periodic variation of permittivity dielectric. By using the transmission line approach we consider the structure as a succession of transmission line. The unit cell consists of a succession of three part network one half of the transmission line ($a/2$), a transmission line (b) and another half ($a/2$) of the transmission line, the total line length is l ($l = a + b$).

The so-called **ABCD** matrix can be obtained by cascading three sections: One half ($a/2$) of the transmission line, transmission line (b) and another half ($a/2$) of the transmission line. Therefore, the matrix of the unit cell is given by: $C_T = C_{a/2} \cdot C_b \cdot C_{a/2}$. Using the Floquet theorem we obtain two equation of dispersion of the structure.

Simulation and Conclusion: There are two equation of dispersion with condition, the first equation with varying attenuation constant α_p and fixed phase constant β_p, for this equation if $ch(\alpha_p(a+b)/2) > 1$, the periodic structure supports a propagation waves, else $(ch(\alpha_p(a+b)/2)) < 1)$ no wave can propagate along the periodic structure. The second equation without attenuation constant $\alpha_p = 0$ and the phase constant is varying, for this equation if $\cos(\beta_p(a + b)/2)$ is included between -1 and $+1$ the periodic structure supports a propagation waves, else no wave can propagate along the periodic structure. We simulated these equations using MATLAB. The results reveal the presence of stop band and pass band, by varying some parameters of the structure we can commend the stop and the pass band.

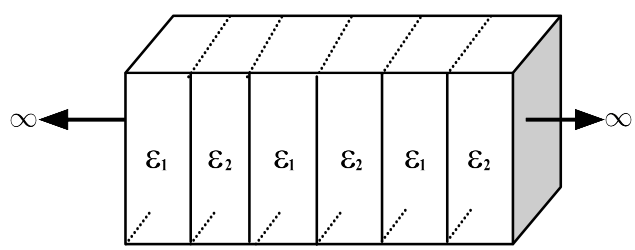

Figure 1: Schema of the structure of waveguide formed by periodic variation of permittivity.

REFERENCES

1. Gao, J. and L. Zhu, "Guided-wave characteristics of CPW transmission line metamaterials: Effective per-unit-length parameters," *IEEE International Workshop Antennas Technology: Small Antennas and novel Metamaterials, IWAT 2005*, IEEE, 2005.
2. Massaoudi, S., A. Lustrac, and T. Denidni, "Study of dielectric and metallic photonic band gap material at micro-waves frequencies: Calculation and experimental verification," *Antennas and Propagation Society International Symposium 2006*, IEEE, 2006.
3. Bouali, S. and T. Aguili, "The study of electromagnetic dispersion in the periodic structures," *MMS*, Syria, October 14–16, 2008.

Cloaking of the Matter Waves under the Global Effect

D. H. Lin[1] **and P. G. Luan**[2]

[1]Department of Physics, National Sun Yat-sen University, Kaohsiung, Taiwan
[2]Department of Optics, National Central University, Chung-Li, Taiwan

Abstract— We discuss the Aharonov-Bohm effect of a magnetic flux for its influence on a two-dimensional (2D) quantum cloak. It is shown that the efficiency of quantum cloak is unaltered even when there is a magnetic flux inside the clocked region. Owing to the perfect nature of cloaking matter waves, the cloak provides an ideal setup to test the pure physical effects of a single flux, and possibly other nonlocal global effects in physics.

Introduction of a New Class of Materials Called Double Zero Media Having the Real Parts of Epsilon and Mu Equal to Zero

Homayoon Oraizi[1], **Ali Abdolali**[1], **and Noushin Vaseghi**[2]

[1]Department of Electrical Engineering, Iran University of Science and Technology
Tehran 1684613114, Iran
[2]Department of Electrical Engineering, K. N. Toosi University of Technology
Tehran 16315-1355, Iran

Abstract— Various uncommon materials such as metamaterials [1–4] have been recently the subject of intensive research. In this paper, we introduce a new class of materials called double zero material (DZR) having the real parts of both its epsilon and mu equal to zero and investigate the electromagnetic wave propagation in them [5, 6], particularly the propagation constant k and intrinsic impedance η. We investigate the reflection and transmission coefficients from multilayer structures [7, 8] made of DZR material located in various media. It is shown that the DZR constants namely k and η and also the reflection and transmission coefficients from the multilayer structures are all real quantities. Several numerical examples are provided for both dispersive and nondispersive DZR materials.

REFERENCES

1. Veselago, V. G., "The electrodynamics of substances with simultaneously negative values of ε and μ," *Soviet Physics Uspekhi*, Vol. 10, No. 4, 509–514, Jan.–Feb. 1968.
2. Caloz, C. and T. Itoh, *Electromagnetic Metamaterials, Transmission Line Theory and Microwave Applications*, Wiley-IEEE Press, Hoboken, NJ, 2005.
3. Marques, R., F. Martin, and M. Sorolla, *Metamaterials with Negative Parameters Theory, Design, and Microwave Applications*, 1st Edition, Wiley, 2008.
4. Smith, D. R., W. J. Padilla, D. C. Vier, S. C. Nemat-Nasser, and S. Schultz, "Composite medium with simultaneously negative permeability and permittivity," *Phys. Rev. Lett.*, Vol. 84, No. 18, 4184–4187, May 2000.
5. Oraizi, H. and A. Abdolali, "Design and optimization of planar multilayer antireflection metamaterial coatings at Ku band under circularly polarized oblique plane wave incidence," *Progress In Electromagnetics Research C*, Vol. 3, 1–18, 2008.
6. Kong, J. A., "Electromagnetic wave interaction with stratified negative isotropic media," *Progress In Electromagnetics Research*, PIER 35, 1–52, 2002.
7. Oraizi, H. and A. Abdolali, "Mathematical formulation for zero reflection from multilayer metamaterial structures and their notable applications," *IET Microwaves, Antennas & Propagation Journal*, to be published.
8. Cory, H. and C. Zach, "Wave propagation in metamaterial multilayered structures," *Microwave and Optical Technology Letters*, Vol. 40, No. 6, 460–465, Mar. 2004.

Ultra Wide Band Radar Absorbing Materials

Ali Abdolali[1], **Homayoon Oraizi**[1], **and Ahad Tavakoli**[2]

[1]Department of Electrical Engineering, Iran University of Science and Technology, Tehran, Iran
[2]Department of Electrical Engineering, Amirkabir University of Science and Technology, Tehran, Iran

Abstract—

Introduction: Radar absorbing materials (RAMs) have been studied for stealth technology, which have different characteristics and many applications [1]. Salisbury plates and Dallenbach layers [2] have been developed for narrow frequency band. However, multilayer structures such as Jaumann absorbers were developed for the wide frequency band reduction of radar cross section (RCS) [3, 4]. In the investigation of RAM, the dispersion properties of materials may first be ignored to acquire a general understanding of their behavior. However, available physically realizable dispersion relations may be adopted and their parameters may be determined to devise a RAM suitable for an application [5].

In this paper, we follow a procedure to obtain the permittivity ε and permeability μ of a material at several discrete frequencies in a band width. Then, any particular dispersion function may be fitted to the data to determine its parameters. This procedure of not limiting to and not assuming any particular dispersion, leads to a drastic reduction of RCS and reflected power in an ultra wide frequency band. The Genetic Algorithm [6] has been used for the optimization process and the generalized Fourier series has been used to fit a continuous function to the data.

Problem Configuration, Formulation and Numerical Implementation: Consider a perfect electric conductor (PEC) plate covered by two layers of lossy materials as in Fig. 1.

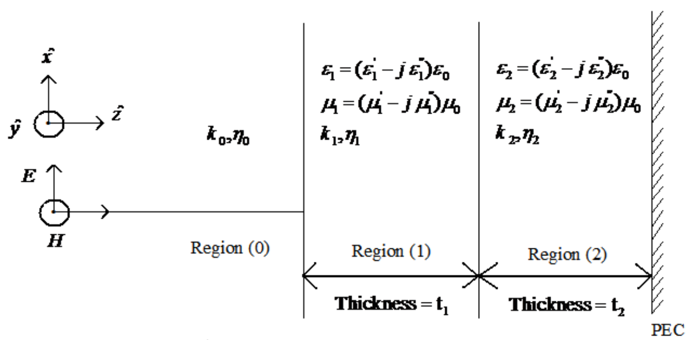

Figure 1: Problem configuration.

A plane wave is normally incident on the structure. The forward and backward traveling plane waves are considered in the three regions [7]. The reflection coefficient R may be determined by imposing the boundary conditions

$$R = f\left(t_1, t_2, \in_1', \in_1'', \mu_1', \mu_1'', \in_2', \in_2'', \mu_2', \mu_2''\right) \tag{1}$$

It is a function of layer thicknesses (t_1, t_2) and the parameters of their permittivities and permeabilities. We may assume some constraints on the layer thicknesses, we fix them at some values.

$$t_1 = 2\,\mathrm{mm}, \quad t_2 = 1.9\,\mathrm{mm} \tag{2}$$

We now construct an error function to minimize the reflection from this structure as [8]

$$Error = |R|^2 \tag{3}$$

This error function is minimized with respect to the parameters of layers denoted in (2). At first the error function is minimized at single frequencies $f = 10$, 20, 30, 40 GHz. The values of parameters for each frequency are given in Table 1.

Then the magnitude of reflection coefficient is calculated for each case over the frequency band 8–40 (GHz) and drawn in Fig. 2. It is seen that in each case, R has a very low value at the related frequency, but its magnitude changes between 20–100 dB in the frequency range.

Table 1: The optimum values of the real and imaginary parts of ε and μ for each layer at frequencies $f = 10$, 20, 30, 40 GHz.

Frequency (GHz)	Re($\in_{r1}$)	Im($\in_{r1}$)	Re(μ_{r1})	Im(μ_{r1})	Re($\in_{r2}$)	Im($\in_{r2}$)	Re(μ_{r2})	Im(μ_{r2})
10	0.7645	1.2817	0.2890	1.7108	0.6648	0.1866	0.5734	105051
20	0.7989	0.9926	0.8311	0.9538	0.6242	0.4201	0.3318	1.5175
30	0.8023	0.9255	0.8576	0.9420	0.5851	0.6942	0.3190	1.5537
40	0.8485	0.8956	0.8622	0.9233	0.5547	0.8559	0.3117	1.5932

Then, the minimization of the error function is carried out in a wide frequency band width in the range 8–40 (GHz) at discrete frequencies at steps of 0.5 GHz. We assume dispersion relations as various functions such as $a + bf + cf^2$ and $d + \frac{e}{f} + \frac{g}{f^2}$ for the real part and the imaginary part of ε and μ. The generalized Fourier series is used to determine the constants in the dispersion relations. Then the magnitude of R is evaluated with the dispersion relations in the frequency band 8–40 (GHz) and drawn in Fig. 2. It is seen that the magnitude of reflection coefficient has actually reduced more than 40 dB. The realization of these dispersion relations should be the subject of further research.

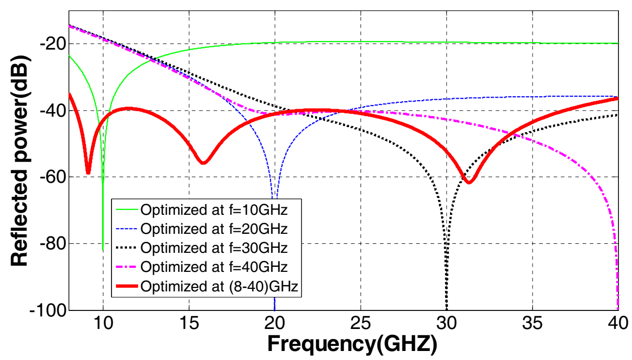

Figure 2: Reflected power (dB) versus frequency from a PEC plate coated with two layers with thicknesses $t_1 = 2$ mm, $t_2 = 1.9$ mm and optimum real and imaginary parts of ε and μ after minimization at single frequencies $f = 10$, 20, 30, 40 GHz and in a wide frequency band width in the range 8–40 (GHz).

REFERENCES

1. Vinoy, K. J. and R. M. Jha, *Radar Absorbing Materials: From Theory to Design and Characterization*, Kluwer Academic Publishers, Norwell, Massachusetts, 1996.
2. Jaggard, D. L. and N. Engheta, "Chiroshield: A salisbury/dallenbach shield alternative," *Electron. Lett.*, Vol. 26, No. 17, 1332–1334, August 1990.
3. Berenger, J. P., "A perfectly matched layer for the absorption of electromagnetic waves," *Journal of Computational Physics*, Vol. 114, 185–200, 1994.
4. Chew, W. C., J. M. Jin, and E. Michielssen, "Complex coordinate stretching as a generalized absorbing boundary condition," *Microwave Opt. Technol. Lett.*, Vol. 15, 363–369, August 1997.
5. Oraizi, H. and A. Abdolali, "Design and optimization of planar multilayer antireflection metamaterial coatings at Ku Band under circularly polarized oblique plane wave incidence," *Progress In Electromagnetics Research C*, Vol. 3, 1–18, 2008.
6. Michielssen, E., J. M. Sajer, S. Ranjithan, and R. Mittra, "Design of lightweight, broad-band microwave absorbers using genetic algorithms," *IEEE Trans. Microwave Theory Tech.*, Vol. 41, No. 67, 1024–1031, 1993.
7. Kong, J. A., *Theory of Electromagnetic Waves*, EMW Pub., New York, 2005.
8. Oraizi, H., "Application of the method of least squares to electromagnetic engineering problems," *IEEE Antenna and Propagation Magazine*, Vol. 48, No. 1, 50–75, 2006.

A Theorem for the Reflection and Transmission of Electromagnetic Waves from a Slab Made of Common Materials and Metamaterials

Homayoon Oraizi and Ali Abdolali
Department of Electrical Engineering, Iran University of Science and Technology
Tehran 1684613114, Iran

Abstract— Consider a planar slab made of a double positive (DPS) material located between two half spaces as shown in Fig. 1.

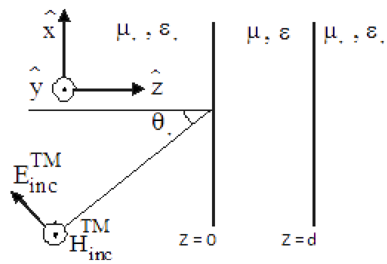

Figure 1: Geometry of the problem: oblique TM wave interaction with one slab.

A TM polarized plane wave is obliquely incident on the slab. The transverse field components in the three religions are [1, 2]

$$region(l) : \begin{cases} H_{ly} = \left(A_l e^{+jk_l \cos\theta_l z} + B_l e^{-jk_l \cos\theta_l z}\right) e^{-jk_{lx}x} \\ E_{lx} = \eta_l \cos\theta_l \left(A_l e^{+jk_l \cos\theta_l z} - B_l e^{-jk_l \cos\theta_l z}\right) e^{-jk_{lx}x} \end{cases} ; \quad l = 0, 1, 2 \tag{1}$$

$$k_l = \omega\sqrt{\mu_0\varepsilon_0\mu_l\varepsilon_l}, \quad \eta_l = \sqrt{\frac{\mu_0\mu_l}{\varepsilon_0\varepsilon_l}}, \quad k_{lx} = k_l \sin\theta_l = k_{l+1}\sin\theta_{l+1} = k_0 \sin\theta_0; \quad l = 0, 1, 2 \tag{2}$$

where A_ℓ, B_ℓ are the amplitudes of forward and backward traveling waves. The reflection and transmission coefficients are defined as

$$R = \frac{B_0}{A_0}, \quad T = \frac{A_2}{A_0} \tag{3}$$

The boundary conditions at the two planes of the slab may be written in a matrix equation

$$\begin{bmatrix} +1 & -1 & -1 & 0 \\ p & +1 & -1 & 0 \\ 0 & a & 1/a & -b \\ 0 & a & -1/a & -pb \end{bmatrix} \begin{bmatrix} R \\ A_1 \\ B_1 \\ T \end{bmatrix} = \begin{bmatrix} -1 \\ p \\ 0 \\ 0 \end{bmatrix} \tag{4}$$

where

$$a = e^{-jk_1 \cos\theta_1 d}, \quad b = e^{-jk_0 \cos\theta_0 d}, \quad p = \frac{\eta_0 \cos\theta_0}{\eta_1 \cos\theta_1} \tag{5}$$

Then the reflection and transmission coefficients may be determined

$$R^{TM} = \frac{-1 + a^2 + p^2 - a^2p^2}{2p + 1 + 2a^2p - a^2 + p^2 - a^2p^2} \quad \& \quad T^{TM} = \frac{4pa}{b\left(2p + 1 + 2a^2p - a^2 + p^2 - a^2p^2\right)} \tag{6}$$

Now, the DPS media in the three regions are replaced by symmetrical double negative (DNG) media, according to the following relations [3–5]

$$\begin{cases} \varepsilon_{DPS} = \varepsilon' - j\varepsilon'' \\ \mu_{DPS} = \mu' - j\mu'' \end{cases} \Rightarrow \begin{cases} \varepsilon_{DNG} = -\varepsilon' - j\varepsilon'' \\ \mu_{DNG} = -\mu' - j\mu'' \end{cases} \tag{7}$$

Consequently, the wave numbers and intrinsic impedances are obtained according to the rules given in [2, 6]

$$\begin{cases} k_{DPS} = k' - jk'' \\ \eta_{DPS} = \eta' \pm j\eta'' \end{cases} \Rightarrow \begin{cases} k_{DNG} = -k - jk'' = -k^*_{DPS} \\ \eta_{DNG} = \eta' \mp j\eta'' = \eta^*_{DPS} \end{cases} \Rightarrow \begin{cases} a_{DNG} = a^*_{DPS} \\ b_{DNG} = b^*_{DPS} \\ p_{DNG} = p^*_{DPS} \end{cases} \tag{8}$$

These relations are substituted in Eq. (5), which lead to the following relations

$$R^{TM}_{DNG} = R^{TM*}_{DPS}, \quad T^{TM}_{DNG} = T^{TM*}_{DPS} \tag{9}$$

Therefore, the reflected powers, $P_r = RR^* = |R|^2$ and the transmitted powers $P_t = TT^* = |T|^2$ in the two cases are equal.

Now, in a practical situation that the half spaces in the two cases are filled with the same media, but the material in the slab is interchanged ($DPS \leftrightarrow DNG$), then only the reflection coefficients become complex conjugates of each other, but the transmissions coefficients are not and do not have a simple relationship. As an example, consider a slab of thickness $d = 5\,\text{mm}$ composed of DPS material with characteristics $\varepsilon = 7 - j0.3$ and $\mu = 1 - j0.1$, which is placed in free space. Then consider this slab to be composed of a dual DNG metamaterial with symmetrical characteristics $\varepsilon = -7 - j0.3$ and $\mu = -1 - j0.1$. A plane wave is obliquely incident on these two dual slabs. The real and imaginary parts of the reflection coefficients are computed and drawn as a function of frequency in Fig. 2. It is observed that Re(R) for the two dual cases are equal but Im(R) are symmetrical. This example verifies the above theorems.

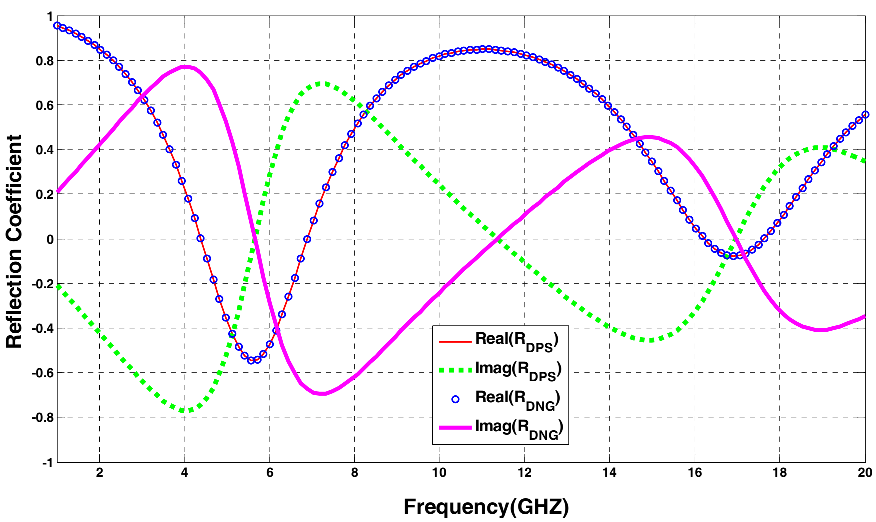

Figure 2: The real and imaginary parts of reflection coefficients from a DPS and DNG layer in free space with parameters specified in the text.

REFERENCES

1. Kong, J. A., *Theory of Electromagnetic Waves*, EMW Publishing, 2005.
2. Oraizi, H. and A. Abdolali, "Design and optimization of planar multilayer antireflection metamaterial coatings at ku band under circularly polarized oblique plane wave incidence," *Progress In Electromagnetics Research C*, Vol. 3, 1–18, 2008.
3. Smith, D. R., W. J. Padilla, D. C. Vier, S. C. Nemat-Nasser, and S. Schultz, "Composite medium with simultaneously negative permeability and permittivity," *Phys. Rev. Lett.*, Vol. 84, No. 18, 4184–4187, May 2000.
4. Ziolkowski, R. W. and E. Heyman, "Wave propagation in media having negative permittivity and permeability," *Phys. Rev. E, Stat. Phys. Plasmas Fluids Relat.*, Vol. 64, No. 5, 617–625, 2001.
5. Kong, J. A., "Electromagnetic wave interaction with stratified negative isotropic media," *Progress In Electromagnetics Research*, PIER 35, 1–52, 2002.
6. Oraizi, H. and A. Abdolali, "Mathematical formulation for zero reflection from multilayer metamaterial structures and their notable applications," *IET Microwaves, Antennas & Propagation Journal*, to be published.

About Energy, Linear Momentum and Mass Transfer by Electromagnetic Wave in Negative Refraction Media

V. G. Veselago[1,2]

[1]A. M. Prokhorov General Physics Institute, Moscow 119991, Russia
[2]Moscow Institute of Physics and Technology, Dolgoprudny 141700, Russia

Abstract— With the advent in scientific language the terms "negative refraction coefficient" or "negative refraction" as well as related terms, researchers put some questions, which generally speaking have a much broader significance than the above words. The notion of "negative refraction coefficient" was shown for the first time probably in our early work [1]. However, we have shown [2] that a simple substitution of negative values n in some formula of electrodynamics and optics often leads to grave mistakes. Moreover, if the phase and group velocity are antiparallel, you must be very careful with some other formulas, which are not directly included value of n. This applies, for example, to the very well known formula $P = hk$, linking the value of the photon linear momentum with its wave vector. It is obvious that in the case of negative wave vector k, this formula gives a negative value for the photon linear momentum, and thus in case of the light absorption light pressure should be replaced by light attraction. This is all the more imperative that, strangely enough, the value of the photon linear momentum, even for the usual matter with positive n case is a subject of debate for over 100 years [3]. This discussion is based on the existence of two completely different energy-momentum tensors for electromagnetic fields, namely tensors in Minkowski form and in the form of Abraham. They give different expression for the forces in the transparent body by passing it through the electromagnetic radiation. Interesting to note that the tensor of Abraham in fact is not a tensor, because it is not a relativistic invariant. As to the Minkowski tensor, its use leads to some unusual expression $M = E/v_{gr}v_{ph}$ for the masses, transferred by the radiation from the emitter to the receiver (values v_{ph} and v_{gr} are phase and group velocities accordingly). From this expression becomes clear, that in the case of negative refractive index the mass is transferred not from the radiator to the receiver, but in opposite direction from the receiver to the radiator.

ACKNOWLEDGMENT

This work was supported by Russian Foundation for Basic Research, grants No. 06-02-16830-a and 07-02-00233-a.

REFERENCES

1. Veselago, V. G., "Electrodynamics of substancies with simultaneosly negative values of electric and magnetic permeabilities," *Sov. Phys. Usp.*, Vol. 10, 509–514, 1968.
2. Veselago, V., L. Braginsky, V. Shklover, and C. Hafner, "Negative refractive index materials," *Journal of Computation and Theoretical Nanoscience*, Vol. 3, 1–30, 2006.
3. Pfeifer, R. N., T. A. Nieminen, N. R. Heckenberg, and H. Rubinsztein-Dunlop, "Momentum of an electromagnetic wave in dielectric media," *Rev. Mod. Phys.*, Vol. 79, 1197–1216, 2007.

High Reflection Coatings with Negative and Positive Refractive Indexes

C. Sabah[1] **and S. Uckun**[2]

[1]Johann Wolfgang Goethe-University, Physikalisches Institut
D-60438, Frankfurt am Main, Germany
[2]Electrical and Electronics Engineering Department
University of Gaziantep, Gaziantep, Turkey

Abstract— In this paper, we intend to create a stratified structure comprised of negative and positive refractive indexes, NRI and PRI, coatings to achieve high reflection. The coatings and all computations are performed and determined using the theory of transfer matrix method. Generally, quarter wave length longs of alternately high and low refractive index media are applied to the substrate to form NRI-PRI multilayer stacks. By choosing the proper indexes, the various reflected wave fronts can be made to interfere gainfully to generate a well-organized reflector. The reflectance peak depends on the ratio of refractive indexes of two media, as well as the number of stack pairs. Increasing either increases the reflectance. The larger ratio means a wider high reflectance region. Furthermore, the coatings are effective for both parallel and perpendicular polarization components, and can be designed for a wide frequency range. A structure containing several identical pairs of NRI-PRI stacks is demonstrated to maximize the reflection for the high frequency range. It is found that for NRI-PRI high reflection structures, the pass band is larger and the effect of angle of incidence and polarization is less dominant as compared to the all PRI structures. Moreover, these structures display no ripples but a monotonous quasi symmetric rise in the transmittance to the left and to the right of operation frequency is observed. In addition to all results found, this paper also provides to be able to decrease/increase the frequency range to the desired band and to make size reduction in the number of stacks.

Session 3A5
Novel Mathematical Methods in Electromagnetics 2

Electromagnetic Forces on Charged Particles

Zi-Hua Weng
School of Physics and Mechanical & Electrical Engineering
Xiamen University, Xiamen 361005, China

Abstract— The gravitational field and electromagnetic field both can be demonstrated by the algebra of quaternions, meanwhile their quaternion spaces will be combined together to become the octonion space. In other words, the characteristics of gravitational field and electromagnetic field can be described with the octonion space simultaneously, including the property of applied force density in the case for coexistence of the electromagnetic field and gravitational field.

The applied force density is defined from the quaternion linear momentum, which is one function of the field sources. The applied force density includes the gravity density, inertial force density, Lorentz force density, interacting force density between electromagnetic strength with magnetic moment, and some new terms. Most new terms are very tiny by contrast with the above parts of forces, except for one new term of force which direction is along the magnetic field line.

The new term of force described by the quaternion can draw out some conclusions about the movement of charged particle. It will cause a charged particle to move parallel to the magnetic field line. It means that, in the Lorentz force experiment, the velocity of the charged particle will vary in the direction of magnetic field line. But the reason for the varying velocity has never been investigated before. Varying velocity this way does not violate any principle of physics.

It can explain why the charged particles will drift in a perpendicular direction when they move in a circle around magnetic field lines. But the drift distance is small due to a tiny time and zero initial velocity. In a narrow spatial extension, it may be difficult to find the drift phenomenon in a short time. However, in the astronomical surveying, the magnetic field can speed up or slow down a solar wind along open magnetic field lines in an interplanetary space or coronal hole on the sun.

ACKNOWLEDGMENT

The author is grateful for the financial support from the National Natural Science Foundation of China under grant number 60677039.

TM-Electromagnetic Guided Waves in a (Kerr-) Nonlinear Three-layer Structure

K. A. Yuskaeva[1], **V. S. Serov**[2], **and H. W. Schürmann**[1]

[1]University of Osnabrück, Germany
[2]University of Oulu, Finland

Abstract— The propagation of TM (transverse-magnetic) guided waves in a lossless and non-magnetic three-layer structure, consisting of a film, characterized by a local Kerr-like tensorial nonlinearity, situated between two semi-infinite linear and isotropic media is considered.

Maxwell's equations are reduced to an exact differential equation leading to a first integral that relates the two field components so that one component can be eliminated. Hence the other one can be found by integration. The resulting integral combined with the boundary conditions is used to derive the exact dispersion relation establishing a link between the parameters of the problem (in particular between the thickness of the film, the propagation constant, and the field intensity at the interface between the substrate and the film). Numerical results for focusing and de-focusing Kerr-nonlinearity are presented.

Hierarchical Tensors for Fast Field Evaluation in Micromagnetics

A. V. Goncharov[1], **G. Hrkac**[1], **J. Dean**[1], **S. Bance**[1], **and T. Schrefl**[1,2]

[1]Department of Engineering Materials, The University of Sheffield, Sheffield, S13JD, UK
[2]St. Poelten University of Applied Science, St. Poelten, Austria

Abstract— Large scale problems in micromagnetics result in huge matrix systems for the magnetostatic field computations. To deal with these huge matrix systems, various methods have been developed for data compression. Such methods include Fast Multipole Method (FMM), H-matrices etc [1, 2]. In this work we report on application of the hierarchical tensor structure to the pointwise demagnetizing tensor, discretized on a tensor product grid with dimensions $N \times N \times N$. Hierarchical tensor can be seen as a hierarchical matrix on a tensor product grid where each matrix block is represented in a tensor form and admissible blocks are stored in the Kronecker format. The Kronecker format approximation for potentials on a tensor product grid is described in [3, 4]. The Advantage of this type of approximation compared to other techniques is its superlinear compression property. If a block has N cells in one dimension then a total number of cells in the block is N^3. Standard algorithms for a full tensor will scale with a total number of cells squared giving N^6. With large scale simulations the required storage and CPU time is not affordable even at modern computers. Kronecker compression applied to the block lowers the storage requirement to $O(N^2)$ elements. The total memory consumption in the hierarchical tensor is hence asymptotically proportional to $O(N^2 \log N^3)$. When magnetization and magnetostatic field vectors are stored in compressed forms, a superlinear speed-up of a field evaluation is also gained.

The Kronecker approximation of admissible blocks was obtained by applying the canonical decomposition (sum of rank-1 tensors or triads) [5]. This was achieved in two steps: the 3D ACA algorithm [6] was used to obtain a rank-R Tucker decomposition, then the core tensor was decomposed into the canonical form using Levenberg-Marquardt (LM) minimization. Multiplication of tucker matrices and canonical factors of the core lead to the full trilinear decomposition of the tensor block. Magnetization and field vectors were also compressed into canonical forms using the ALS algorithm. Using compressed data, magnetostatic energy was calculated for cubes discretized with 1 nm computational cells and with sizes ranging from 10 nm (10^3 cells) to 100 nm (10^6 cells). Corresponding full problem sizes range from 13 Mb to approximately 7.6 Tb of RAM. Absolute error in the computed value of the magnetostatic energy was between 1.e-5 to 1.e-2. It is worth to note that for the 10 nm cube the absolute error introduced by the discretization method itself is around 1.e-5, which was estimated using full matrix-vector multiplication.

REFERENCES

1. Greengard, L. and V. Rokhlin, *Acta Numerica*, Vol. 6, 229–269, 1997.
2. Hackbush, W., et al., *Mathematica Bohemica*, Vol. 2, 229–241, 2002.
3. Tyrtyshnikov, E., *Linear Algebra and Its Applications*, Vol. 379, 423–437, 2004.
4. Hackbush, W. and B. N. Khoromskij, *Computing*, Vol. 76, 177–202, 2006.
5. Harshman, R. A., *UCLA Working Papers in Phonetics*, Vol. 16, No. 10,085, 1–84, University Microfilms, Ann Arbor, Michigan, 1970.
6. Oseledets, I., D. Savostianov, and E. Tyrtyshnikov, *SIAM J. Matrix Anal. & Appl.*, Vol. 30, No. 3, 939, 2008.

Quantum Electro Dynamical Mechanisms of Combined Magnetic Fields Action on Water Solution of Amino Acids

Mikhail Zhadin
Institute of Cell Biophysics of RAS, Moscow Region 142290, Russia

Abstract— In 1985, Liboff and Blackman et al. discovered different biological effects of combined action of weak ($\sim 10^{-5}$ T) static and alternating magnetic fields (SMF and AMF) at cyclotron frequency of AMF). Later (Novikov, Zhadin, 1994; Zhadin et al., 1998) an effect of action of extremely weak ($\sim 10^{-8}$ T) AMF combined with parallel weak ($\sim 10^{-5}$ T) SMF on conductivity of aqueous solutions of some amino acids (AA) was revealed. This effect manifested itself in short-time resonance increase of solution conductivity at cyclotron frequency of AMF. The theoretical analysis (Zhadin, 1998; Zhadin, Barnes, 2005) showed that such phenomena could appear only at solution viscosity much less than real water viscosity that seemed absolutely impossible from the viewpoint of Classical Physics. However, the reproduction of the abovementioned experiments in other laboratories (Del Giudice et al., 2002; Pazur, 2004: Comisso et al., 2005; Giuliani et al.) confirmed our results. Inevitable conclusion about very low viscosity in microvolumes of aqueous solution had obtained support in modern Quantum ElectroDynamics (Preparata, 1995). In concordance with this branch of Theoretical Physics, the aqueous medium consists of two components: the coherent one contained into spheres with diameters of about 0.1 microns which is called "coherence domains" (CD), and the incoherent one surrounding CDs which corresponds to classical presentations of water. At room temperature the whole volume of CDs is equal to about 40% of the total volume of aqueous medium. Inside CD the viscosity of water is much lower than viscosity of incoherent water and diffusion is much quicker than in incoherent water. This theory explained a lot of strange qualities of water. From these positions we (Zhadin, Giuliani, 2006; Zhadin, 2008) explained the main unusual features of resonance effects in aqueous amino acid solutions: 1) the mechanism of an amino acid ion transition from incoherent medium into CD; 2) the metamorphosis of ion forms and mechanism of resonant acceleration of the amino acid ion within CD under the influence of combined SMF and AMF; 3) the escape of the ion from CD into the incoherent component; 4) the generation of short resonant peak in the current through the incoherent component and the recovery processes in the solution.

A Generalized Signals and Systems Theory Scheme and Its Applications in the Description of Electromagnetic Problems

E. Gago-Ribas and A. Serroukh
Electrical Engineering Department, University of Oviedo, Spain

Abstract— Signals and systems theory plays a fundamental role in electrical engineering, as well as in other scientific areas, but the usual way of presenting this theory avoids treating some important concepts that may lead to later conceptual and practical problems; then a generalization of basic signals and systems theory is required, specially to clarify the connection between this theory and the mathematical representation of physical problems — electromagnetic problems seen as a particular case.

A kind of generalization of the signals and systems theory is presented in this work. This generalization may be summarized as follows. First, infinite dimensional function vector spaces of arbitrary variable — continuous or discrete — becomes a fundamental step in this generalization in order to represent and classify signals; the definition of an algebra structure on these spaces — usually determined by the distance, norm and scalar product — plays a fundamental role on the generalization. Also, the systems are characterized by operator theory — in particular, differential operators when dealing with wave problems. With these fundamental ideas in mind, it is possible to introduce a representation in terms of a general linear combination operator; depending on the problem under analysis, this operator will reduce to continuous summations different forms of integral operators such as Riemman or Lebesgue integration or to discrete summations. This concept leads also to a general interpretation of a transformation and the corresponding analysis of a system under a particular transform — usually referred as the spectral analysis of a system. This scheme requires also of a generalized representation of subspaces sets of functions within the initial vector space. Finally, the connection of this scheme with the theory of distributions becomes a fundamental point in this procedure in order to provide with a general structure capable to unify the regular function analysis and the generalized function theory. This point becomes extremely important when trying to clearly understand and generalize the Green's function theory, for instance. Some particular problems associated to this generalization procedure will be also presented to clarify the importance of this scheme; for instance, the spectral characterization of linear non invariant systems that plays a fundamental role in the spectral characterization with respect to the spatial coordinates of electromagnetic radiation and scattering problems.

An important extension of this generalized scheme is concerned with the possibility of its extension to study complex variable signal spaces or complex signal theory. The practical application of these results is concerned with the analysis of electromagnetic radiation and scattering problems when time and/or space coordinates are continued into complex ones.

Finally, a more powerful connection between the algebra of regular functions and the theory of distributions is currently under investigation through the Rigged Hilbert Spaces (RHS) theory and its utility in the representation of electromagnetic problems.

Method of Analytical Regularization: New Approaches and Perspectives

Yu. A. Tuchkin[1, 2]

[1]GIT, Gebze Institute of Technology, P. K. 141, Gebze/Kocaeli 41400, Turkey
[2]IRE NASU, Institute for Radiophisics and Electronics of National Academy of Science of The Ukraine
12 Akademika Proskury St., Kharkov 310262, Ukraine

Abstract— Analytical Regularization Method is historically an extension of the so-called semi-inversion procedure, which is known in diffraction theory more than 40 years and is originated in [1]. The essential extension of this procedure has been suggested in papers [2] and [3], and they are known as the first examples and samples for Analytical Regularization usage in diffraction theory.

A big set of diffraction problems has been solved during the last two decades by Analytical Regularization Method or, better to say, by means of the set of various methods joined by common philosophy, which is firstly explained in details in book [4].

Now, after more than the twenty years experience, it is clear that Analytical Regularization Method is powerful tool for relevant (i.e., mathematically strong and numerically stable) solving of huge amount of theoretical and practically necessary problems in diffraction theory.

In the same time, it came to be clear that the method requires its generalization for solving more complicated, especially — three dimensional, problems.

The ability of Analytical Regularization Method, its main qualitative and numerical features, as well as its last time generalizations will be demonstrated with problems of wave diffraction by arbitrary shaped screen of revolution (see [5]), and with periodic wavy metal screen, and with dielectric layer or half-space having wavy surfaces (see [6]). As well, efficient simulation of hollow waveguides will be considered. Much attention will be paid to the problems of numerical implementation of the method.

REFERENCES

1. Agranovich, Z. S., V. A. Marchenko, and V. P. Shestopalov, "Electromagnetic wave diffraction by plane metal grating," *Zhurnal Tekhnich*, Vol. 32, No. 4, 381–394, Fiziki, 1962 (in Russian).
2. Tuchkin, Y. A., "Wave scattering by unclosed cylindrical screen of arbitrary profile with Dirichlet boundary condition," *Soviet Physics Doklady*, Vol. 30, 1027–1030, 1985.
3. Tuchkin, Y. A., "Wave scattering by unclosed cylindrical screen of arbitrary profile with Neumann boundary condition," *Soviet Physics Doklady*, Vol. 32, 213–216, 1987.
4. Shestopalov, V. P., Y. A. Tuchkin, A. Y. Poyedinchuk, and Y. K. Sirenko, "Novel methods for solving of direct and inverse problems of diffraction theory," *Analytical Regularization of Electromagnetic Boundary Value Problems*, Vol. 1, Publishing house "Osnova", Kharkov, 1997 (in Russian).
5. Tuchkin, Y. A., "Scalar wave diffraction by axial symmetrical screen. Analytical regularization method," *Proceedings of International Workshop on Direct and Inverse Wave Scattering*, Gebze, Turkey, 2000.
6. Tuchkin, Y. A., "Analytical Regularization method for electromagnetic Wave diffraction by periodic wavy obstacles: Perfectly conductive screen and two media boundary surface," *Proceedings of ICEAA'05 — 9-th International Conference on Electromagnetics in Advanced Applications*, 911–914, Torino, Italy, 2005.

Session 3A6a
Power Electronics

Matrix Converter Output Voltage Control with Overmodulation

J. Lettl and S. Fligl
Department of Electric Drives and Traction, Faculty of Electrical Engineering
Czech Technical University in Prague, Czech Republic

Abstract— In the paper special attention is paid to the indirect space vector modulation, which is based on the virtual DC link concept. The entire converter is interpreted as a series connection of two matrix converters (rectifying and inverting virtual matrix converter). Thanks to this insight, it is possible to compose the modulation strategy for the entire matrix converter from the inverter and rectifier part modulations.

Achievement of the maximum available output voltage was defined as the main goal. Based on the indirect space vector modulation, an overmodulation with square wave output is introduced. It enables to increase the transfer ratio from the common 0.866 to the value of 0.955. It is also presented that the output voltage level can be adjusted continuously in an easy way, even in overmodulation. The obtained voltage and current waveforms are presented.

Matrix converters provide an all-silicon solution to the problem of converting AC power from one frequency to another, offering almost all the features required of an ideal static frequency changer. They possess many advantages compared to the conventional voltage or current source inverters. A matrix converter does not require energy storage components as a bulky capacitor or an inductance in the DC link. It enables the bi-directional power flow between the power supply and load. The most of the contemporary modulation strategies are able to provide practically sinusoidal waveforms of the input and output currents with negligible low order harmonics, and to control the input displacement factor. The solution is advantageous especially with regard to the above mentioned reactive component reduction.

Basis of the realized control system consists of two common personal computers. The first one should be equipped with any multitasking operating system and the MatLab programme must be installed on it. It serves for compiling of the target real-time applications and for monitoring purposes only, such as downloading and displaying of measured waveforms, commands entry, etc. One serial port of the RS232 standard and one parallel port enabling operation in the ECP mode are inevitable. The second personal computer works in real time and the matrix converter control programme is processed on it only. The most important component of this personal computer is the Multi I/O PCI card containing A/D and D/A converters and digital inputs and outputs. All the signals are reprocessed and adjusted in interface cards situated in the control rack. Here is also placed the IGBT's switch pulses generating card based on a FPGA device. To make the work easy, the firmware for the second personal computer and the monitoring programme for the first personal computer were prepared. The firmware consists of the libraries set programmed in the ASSEMBLER and C language enabling faster algorithm implementation and testing. It has the real-time kernel with 50–200 microseconds period and contains synchronisation, communication, and I/O card specific routines. The monitoring programme consists of the set of the mutually communicating programmes programmed in the MatLab, JAVA, and C languages. However, from the user sight it seems to be one application only. This software is very important for easy control application developing.

The results obtained on the built-up experimental test bed have proved validity of the designed pulse width modulation strategy and matrix converter control system conception, proper function of the developed control hardware and software, and high level of the matrix converter energy conversion electromagnetic compatibility as concerns both the input phase displacement and the current and voltage harmonic content.

A Passivity-Based Control for Power Electronics Converter in a DFIG Wind Turbine

Y. B. Qu and H. H. Song
Department of Electrical Engineering and Automation, Harbin Institute of Technology, China

Abstract— Utilization of the power electronics converter in a doubly-fed induction generator wind turbine, thus decoupling mechanical and electrical frequencies and making variable-speed operation possible, can vary the electrical rotor frequency. This paper addresses the circumstances of no matter either capacitor voltage or inductor current is chosen as the output in a converter, the zero dynamics is not both stable for two power flow direction cases. A passivity-based controller for back-to-back converter is presented to avoid this problem in wind power generation. Based on the port-controlled hamiltonian model of the converter, the skew-symmetric matrix and the damp matrix are collocated and the desired equilibrium is approached rapidly. Simulation studies are carried out in Matlab/Simulink and the results show that the new control method enables to avoid instability for a bidirectional use of the power converter in DFIG wind turbine.

Computerized Calculation of Leakage Inductance Values of Transformers

R. Doebbelin, C. Teichert, M. Benecke, and A. Lindemann
Institute of Electric Power Systems, Otto-von-Guericke-University Magdeburg, Germany

Abstract— Power transfer and its limitation caused by internal losses or voltage drops are important aspects in all applications of power transformers. This is true in the case of mains-frequency operated transformers and is even more relevant in medium- or high-frequency transformers. As is well-known, the design of a transformer with special focus on the windings has a big impact on internal losses and voltage drops of the transformer. Copper losses are influenced by the cross-section and (because of the skin and proximity effect with influences of frequency and field distribution) also by the arrangement of windings. Imperfect magnetic coupling occurring in each real transformer is expressed by the term "leakage" and represented by leakage inductances in equivalent circuits of transformers. This way, the operation of electrical equipment including transformers can be investigated by means of calculation and simulation. Whereas in most power transformer applications particularly low leakage inductance values are desirable, there are certain power electronic arrangements (e.g., resonant topologies and power sources for laser beam generation) which require first of all a defined leakage inductance value of the applied transformer.

In the case of existing transformers, leakage inductance can be determined by measurements. However, more often it is necessary to predict the leakage inductance of a transformer in the design phase, especially if circuit simulation is intended. This can be done applying certain approximation methods in which geometry parameters of the transformer are used to calculate its leakage inductance. The most common method is the method of ROGOWSKI which is based on the consideration of the energy of the leakage magnetic field. The formulas for leakage inductance calculation which are given in contemporary technical literature are usually predicated on this method but often slightly simplified resulting in a decrease of accuracy. As a precondition for the application of the method of ROGOWSKI the windings of the considered transformer must be arranged on the same leg and they should have the same height in the case of concentric windings and the same width in the case of pie windings. According to deviations in these dimensions, inaccuracies of the calculation results occur. The leakage inductance is calculated using the formula $L_S = \mu_0 \cdot N_1^2 \cdot l_m \cdot \lambda \cdot k_\sigma$ with L_S — leakage inductance, μ_0 — absolute permeability, N_1 — number of primary turns, l_m — mean length per turn for whole arrangement of windings, λ — relative leakage conductance, k_σ — Rogowski factor. The relative leakage conductance and the Rogowski factor have to be calculated related to the specific arrangement of windings.

Alternatively to the method of ROGOWSKI, leakage inductance calculation can be performed by the method of PETROV. Also in this method the windings of the considered transformer have to be arranged on the same leg. Thus, both methods can advantageously be used to ascertain the leakage inductance of shell-type transformers. However, in the case of the method of PETROV the dimensions concerning height and width of the windings can be different what makes the method more universal. Due to the following formula, two leakage inductance constituents have to be calculated, which have to be summed up to the final leakage inductance.

To determine the K_c-factors related to the portions of the coils inside and outside the core window, the cross-sections of the coils have to be reflected at the adjacent or surrounding core surface lines. The calculation of the K_c-factors is based on the method of mean geometric distances by J. C. MAXWELL considering the cross-sections of the coils and their mirror images.

If windings of a transformer are arranged on different legs like in the case of core-type transformers, leakage inductance can be calculated by means of another approximation method which has been established by LEBEDEV.

The mentioned approximation methods enable the direct calculation of the leakage inductance related to one couple of coils of a transformer. In the case of transformers with a complex design of interleaved windings which is often used to minimize the total leakage inductance, generally the leakage inductance values of the respective couples of single coils have to be merged together into the total transformer leakage inductance using certain combination formulas. This results in a high number of single leakage inductance calculation procedures. Using computerized calculation after implementing the algorithms of the approximation methods into appropriate calculation software (e.g., MATLAB®), it is possible to determine the relevant leakage inductance values

of a transformer within the short computational time of a PC. Thus, efficient investigations of transformer concepts with different geometry of windings can be performed. Nowadays, usually CAD systems are used for transformer design. Therefore, the required geometry parameters are available and can be transferred to the leakage inductance calculation program. Beside computerized calculation due to the mentioned approximation methods, computer-based numerical finite elements method (FEM) calculations can be used for leakage inductance determination. Considering several transformer specimens which vary in their design, in the paper, the results of the different methods for leakage inductance calculation shall be discussed and compared with the results of leakage inductance determination by measurement.

$$L_{Sx} = \frac{\mu_0}{2\cdot\pi}\cdot N_1^2 \cdot l_{mx} \cdot \ln\left(K_{Cx}\cdot\frac{g_{12}^2}{g_1\cdot g_2}\right)$$

$x = in$ (for portion inside core window)
$x = out$ (for portion outside core window)

with

L_{Sx} - leakage inductance portion
K_{cx} - correction factor for consideration of the influence of the core on leakage inductance
g_{12} - mean geometric distance between the cross-sections of the coils 1 and 2
g_1, g_2 - mean geometric distance of the cross-sections of a coil to itself

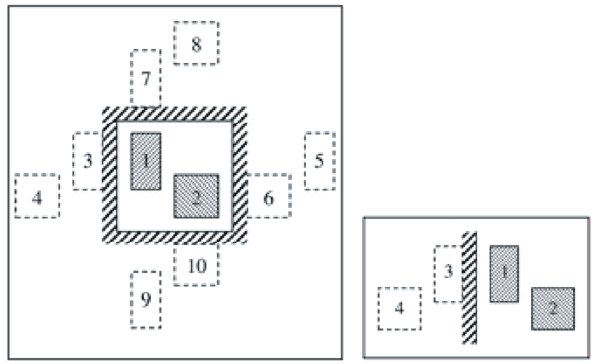

Figure 1: Formation of mirror images of the coils required for determination of the correction factor K_c for the leakage inductance portion inside core window (left) and for the leakage inductance portion outside core window (right).

The Simplifying for PEEC Model of DC Bus Based on Parameter Sensitivity Analysis

Fangzheng Li, **Xudong Sun**, **Lipei Huang**, **and Jianguo Jiang**
Country State Key Lab of Power Systems, Department of Electrical Engineering
Tsinghua University, Beijing, China

Abstract— The electromagnetic interference (EMI) caused by di/dt and dv/dt on switching transient of converters propagates mainly through DC bus, passive components, output circuit and so on. The power DC bus is the predominant link of the propagation path and can significantly influence the EMI character of converters. The equivalent circuit model of the bus is usually constructed for analyzing the commutation process and EMI performance of converters.

However, it may be difficult even impossible to construct the lumped-circuit model of DC bus, especially large size bus with complex structure in high capacity converters. Partial element equivalent circuit (PEEC) technology provides an approach for the problem. It subdivides large scale continuous conductor into partial elements and constructs the equivalent circuit of the conductor with the parasitic parameter of all elements.

Our former paper had constructed the PEEC model of the DC bus for an H-bridge power unit. Experiment and simulation proved that the equivalent circuit is accurate and effective. The equivalent circuit is composed of more than 20 resistor components, more than 50 capacitor components and more than 20 inductor components with complicated circuit topology. It is necessary to simplify the model for simple and convenient.

Based on parameter sensitivity analysis, the PEEC model was simplified. Taking the positive variation rate of bus current as specification, sensitivities to all partial parameters are calculated with Pspice. The simplified model with legible topology was gotten by ignoring the non-sensitive components. The transient process simulation demonstrates the accuracy of the simplified model. Simultaneously, the PEEC model of the bus can be regarded as a two-port circuit. Admittance parameters (Y Parameters) analysis illustrate that the circuit characteristic of the simplified model agree well with the original one.

Session 3A6b
RF and Wireless Communication

ICI Suppression Method for the DFT-spread OFDM Communication System with Phase Noise

Sang Burm Ryu and Heung-Gyoon Ryu
Chungbuk National University
12 Kaesin-dong, Chungbuk 361-763, Korea

Abstract— 3GPP (3rd generation partnership project) adopted the SC-FDMA based on DFT-spread method for the standard technique of LTE (long term evolution) for the uplink. SC-FDMA is to resolve the PAPR problem for the uplink. DFT-Spread OFDM has the properties of low PAPR, good spectral efficiency, commonality in design and coexistence with OFDM technique. However, DFT-Spread OFDM produces more interference components of ICI (inter-subcarrier interference) and SCI (self channel interference) than ordinary OFDM because of the DFT (Discrete Fourier Transform) spreading effect and phase offset mismatch caused by random phase noise. Furthermore, much cost is required to solve these problems for high speed data in uplink data transmission.

In this paper, we analyze the effect of phase noise considering the back-off amount of high power amplifier. And we propose the equalizer of advanced PNS (phase noise suppressing) algorithm to remove the ICI component effectively. This equalizer has similar form of SD-FDE and the equalization process is based on PNS algorithm, which removes the ICI component by phase noise. Through the result of simulation, proposed method can be achieved about 2.5 dB back-off gain comparing the performance with 7 dB back-off due to remove the ICI using proposed equalization algorithm.

Comparison of Wideband Channel Sounding Techniques

Xiao Hong Mao, Yee Hui Lee, and Boon Chong Ng
School of Electrical and Electronic Engineering, Nanyang Technological University, Singapore

Abstract— This paper compares two wideband channel sounding techniques; The spread spectrum sliding correlator sounding technique and; The frequency domain channel sounding technique. Two groups of wideband channel measurements using the two different sounding techniques are performed along a lift shaft in the university environment, at a frequency of 255.6 MHz as shown in Fig. 1. For the measurements, a 1023-bit pseudorandom noise sequence with a bandwidth of 20 MHz is applied for the spread spectrum sliding correlator sounding technique, while a 1601 continuous tone is transmitted over a 300 MHz wide bandwidth using the vector network analyzer for the frequency domain channel sounding. The impulse responses from both sounding techniques are compared in detail. By examining the power contained in the power delay profile (PDP), it is observed that the decreases in power level as separation between the transmitter and the receiver increases are nearly the same for both techniques. Furthermore, the coherence bandwidths for the multipath channel are found to be similar even though different spread bandwidths are used for the different sounding techniques. It is also concluded that the coherence bandwidth decreases as the transmitter to receiver separation increases. This conclusion is consistent for both the techniques. Comparisons on the system complexity, spread bandwidth or resolution, channel information and noise immunity between the two sounding techniques are also included in this paper. The paper then presents the advantages and disadvantaged of the two techniques. For a relatively simple environment with big obstacles where high resolution is not required, the spread spectrum sliding correlator technique is recommended. For a relatively complex environment where fine resolution is required, the frequency domain channel sounding is recommended. However, each method has their own constrains to be taken care of.

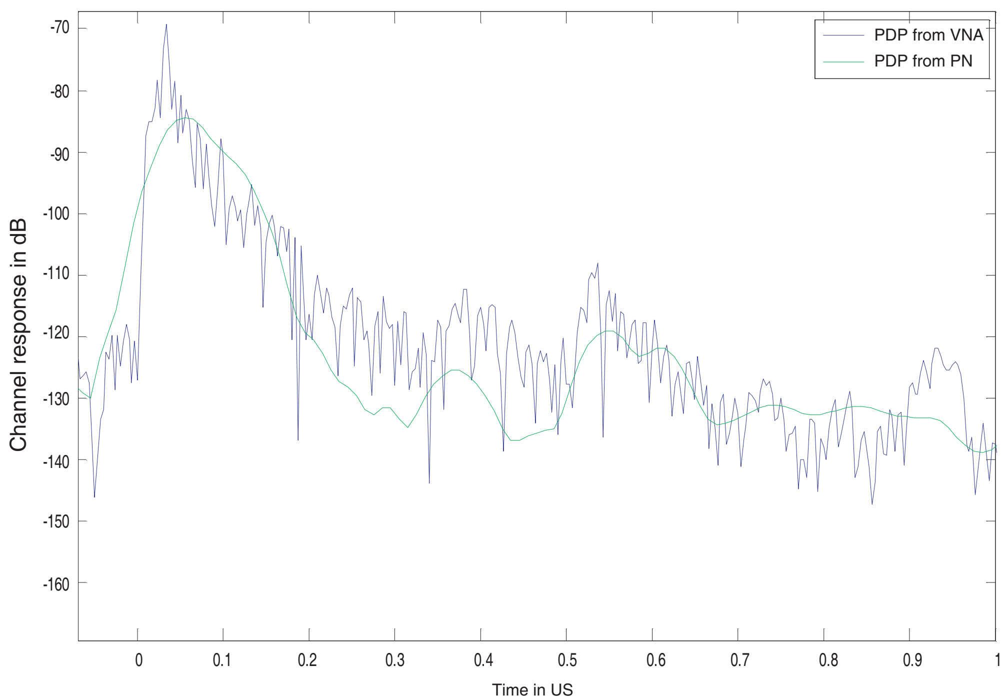

Figure 1: Power delay profile for two wideband sounding techniques.

T-DVB Services Coexistence with IMT-advanced Service

Z. A. Shamsan and T. A. Rahman
Wireless Communication Centre, Universiti Teknologi Malaysia (UTM), Malaysia

Abstract— Due to spectrum scarcity and emerging various wireless applications, coexistence and spectrum sharing between wireless systems become a recently critical issue. At World Radiocommunication Conference 2007 (WRC-07), 790–862 MHz is allocated for the coming fourth generation (4G) or IMT-Advanced on a co-primary basis along with existing Terrestrial-Digital Video Broadcasting (T-DVB). Therefore, coexistence and sharing requirements such as separation distance and frequency separation coordination must be achieved in terms of both co-channel and adjacent channel frequencies. The two coexisted systems are analyzed by Spectral Emission Mask (SEM) model and Interference to Noise ratio (I/N) of -6 dB as a standard coexistence criterion for the interference coming from broadcasting base station into base station of IMT-Advanced represented by mobile Worldwide Interoperability for Microwave Access (WiMAX) as a candidate technology for 4G. Finally, possible intersystem interference mitigation techniques are suggested.

Wireless Tiny Mass Sensor System Based on FBAR

W. W. Cheng, Y. Han, S. R. Dong, X. X. Han, S. H. Zhao, and H. J. Zhang
Department of Information Science and Electronic Engineering
Zhejiang University, Hangzhou, Zhejiang 310027, China

Abstract— A new-type wireless tiny mass sensor circuit based on film bulk acoustic resonators (FBARs) with dual-path and a receiver to test the sensor circuit are designed, fabricated and tested. A pair of differential inputs of the sensor circuit, one is for sensing and the other is for reference, sense the increase of mass loading respectively and simultaneously in the same environment. Therefore, the sensor circuit can measure tiny mass on the FBAR accurately without effect of temperature. Further, the measuring results are sent to a receiver wirelessly to display a visual value to remote users.

Investigation of Low Altitude Air-to-Ground Channel over a Tropical Sea Surface at C Band

Yee Hui Lee and Yu Song Meng
School of Electrical and Electronic Engineering, Nanyang Technological University, Singapore

Abstract— Due to the rapid increase in aircraft density, the current air traffic control (ATC) system that operates at VHF band is fast becoming saturated. Therefore, an alternative frequency band is introduced for traffic control communication systems in order to satisfy this increasing demand. At present, C band is assigned for Microwave Landing System (MLS) in aviation navigation. In order to optimize the MLS performance at C band, thorough air-to-ground channel measurements and characterizations are important. In our previous studies [1, 2]; C band channel characterization at a small airport [1], and air-to-ground channel investigation over a sea surface at high airborne altitude (20 kft to 40 kft) [2], was investigated. In this study, air-to-ground channel measurements are conducted over the sea surface at low airborne altitudes of 1.2 kft, 3 kft and 6 kft. These measurements are conducted at 5.69 GHz over the South China Sea. Two identical directional antennas with a beamwidth of 20° in azimuth and 25° in elevation as shown in Fig. 1(a) are used to create diverse receptor as shown in Fig. 1(b). The reception site, as shown in Fig. 1(c) is directly at the coast. The site is selected in order to ensure mainly propagation over the sea surface and to avoid any blockage of the propagation signal. From the measurement results obtained, it is found that, unlike the air-to-ground channel for the high airborne altitude reported in [2], the propagation channel cannot be assumed as a free space channel. The effects of both the sea surface reflection and the evaporation duct over the sea surface become prominent for the low airborne altitudes. From this study, spatial diversity at the reception is found to be a possible good solution for the improvement of communication links.

(a) Close view of the antenna (b) Far view of the spatial diversity (c) Landscape in front of antennas

Figure 1: View of the directional antenna, spatial diversity, and environment.

REFERENCES

1. Meng, Y. S., Y. H. Lee, and Y. H. Heng, "Channel characterization and modeling in C band for a small airport," *Proceedings of Eleventh URSI Commission F Triennial Open Symposium on Radio Wave Propagation and Remote Sensing*, 113–117, Rio de Janeiro, Brazil, October–November 2007.
2. Lee, Y. H., Y. S. Meng, and Y. H. Heng, "Experimental characterizations of an air to land channel over sea surface in C band," *Proceedings of XXIXth URSI General Assembly*, Chicago, Illinois, USA, August 2008.

Session 3A7
Antenna Theory and Radiation 1

Realization of Ramp and Stair-step Patterns from the Rectangular Wave-guide Arrays

A. Sudhakar[1] **and Y. V. Narayana**[2]

[1]Department of ECE, RVR & JC College of Engineering, Chowdavaram, Guntur-522019
Andhra Pradesh, India
[2]Tirumala Engineering College, Jonnalagadda (PO), Narasaraopet-522601, Guntur (Dist)
Andhra Pradesh, India

Abstract— Antenna arrays are highly useful for the generation of narrow beams and other desired beam shapes. Any pattern obtained from antenna array consists of one major lobe followed by number of minor lobes. When an array is sufficiently large enough, the width of main beam becomes very small and is useful in point to point communication. However, it is required to design such arrays to produce the shaped beams in terms of beam width, side lobe levels. Different approaches like space distribution, amplitude control and phase excitations are employed in order to obtain the desired beam shapes. The amplitude control method can be used to produce desired beam shapes but it is not found to be suitable for fast scanning applications. Although, Fourier transform method, Chebyshev and Woodward methods are common techniques, they yield only approximate patterns. The space controlled technique also used to produce the same but it is not possible to obtain precise space functions. The phase only controlled technique is found to be the most suitable to produce optimized beam shapes and for scanning purposes with digital phase shifters. In view of the above considerations, the phase only control method is proposed to be used in the present work for obtaining any desired beam shape. In the present technique, a low side lobe narrow beam is converted into a ramp and stair-step patterns by introducing additional non-linear phase distribution which allows a fast scanning of the beam without moving antenna structure. Pencil beams are widely used for point to point communications as well as high resolution radars. Ramp patterns have the applications similar to those of pencil beams. Stair-step patterns are popularly used to identify more than one target moving in different altitudes and different angular regions. In this paper, ramp and stair-step patterns are generated from arrays of rectangular waveguides. The data on the variation of field strength as a function of $u(\sin\theta)$ for both small and large arrays over specified angular sectors is computed.

Field Statistics of the Circular Aperture Antenna

Y. S. Shifrin and V. V. Dolzhikov
Kharkov National University of Radio Electronics, 14 Lenin Av.,Kharkov 61166, Ukraine

Abstract— The field statistics of the circular aperture antenna in the presence of the phase fluctuations in its aperture is considered. Main expressions are formulated in the invariant form with respect to the focal point location. This enables one to use them at the analysis of the field statistics of antennas focused to the Fresnel zone, as well as when investigating the field statistics of "ordinary" (that is focused to infinity) circular aperture antennas both in their Fresnel zones and, what is especially interesting, in their far zones. Formulas for mean and fluctuation field characteristics and plots illustrating these characteristics vs parameters of phase fluctuations (their dispersions and correlation radii) and vs location of their focusing and observation points are given. Main attention is paid to studying both the field mean intensity distribution (MID) and the fluctuations of the field amplitude and phase on the focal sphere and along the focal axis. For these two important particular cases, there are investigated changes in shapes of MID curves vs parameters of the phase fluctuations, the MID curves broadening at the half-power level, as well as displacement of locations and levels of extremes (maxima and minima) in MID. Features of MID along the focal axis at shallow and deep focusing are noted. In conclusion, formulas for the fluctuations of the field maximum intensity point in longitudinal and broadside directions are derived. The latter in particular characterizes the drift of the main maximum direction (MMD) for the ordinary unfocused circular antenna with phase errors in its aperture. In the paper, significant attention is paid to a comparison of the results for the field statistics of the circular aperture antenna with the corresponding earlier results obtained by the authors for the field statistics of the linear antenna. It is noted that qualitatively, the statistical effects in these two radiating systems are similar. However, quantitatively, at small correlation radii of the phase fluctuations, the statistical field characteristics for the circular aperture antenna and for the linear system are quite different. The difference degrades as the fluctuation correlation radius increases. The results for antennas with circular and square apertures are compared as well. This is mutually useful when studying the field statistics of these types of two-dimensional radiating systems. The latter is illustrated by an example of the problem concerning the MMD fluctuations in two-dimensional radiating systems in the presence of sources' fluctuations in its aperture.

Resonant Effect at the Coordination of Spatial Structures of Spiral Aerials and Environments of Distribution of Electromagnetic Waves

V. I. Kuzmin, **V. D. Kazakov**, **and A. V. Krishtopov**
Moscow State Institute of Radio Engineering, Electronics, and Automation, Russia

Abstract— The Basic direction of modern researches is connected to development of the technologies based on properties of open systems, functioning in interactions with environment.

In the Essential parameter influencing efficiency of aerials, their form is. For check of a basic opportunity of realization of a resonance due to a choice of the form it is expedient to stop on logarithmic spiral widely distributed in a nature. For a logarithmic spiral a ratio of distances of polar radiuses up to consecutive coils and a corner are constant. We shall determine value of a corner a logarithmic spiral, proceeding from the theory of critical levels of development of natural systems [1]. We shall choose for check critical constant e^e, as a ratio of polar radiuses up to consecutive coils of a spiral, also we shall receive a corner $66°33'$.

The additional corner to the received value is equal $23°27'$. This value corresponds to a corner between an axis of rotation of the Earth and her orbit. This corner is really well shown in characteristics of natural and man-made systems.

For experimental researches equiangular spiral aerial were chosen. The purpose of experiment was research of characteristics of the coordination of three breadboard models of aerials of the specified structure having the maximal size of radiating cloth $D = 21.1\,\mathrm{sm}$ and a corner of spirals $20°$, $23°27'$ and $27°$. Besides that aerials differed only a corner spirals should have a corner of divergence of metal strips equal $90°$.

Measurements were carried out in a range of frequencies 1.4???. The results of measurements show, that in a researched range character curves is identical.

The aerial with a corner spirals $23°27'$ has more uniform characteristic in comparison with other breadboard models which have been built up from it on a corner of a spiral on $\pm 3.5°$, with other things being equal. It means, that the given aerial in a researched range of frequencies can be more effective.

REFERENCES

1. Zhirmunskij, A. V. and V. I. Kuzmin, *Critical Levels in the Development of Natural Systems*, Springer-Verlag, Heidelberg, London, Paris, New York, Tokyo, 1988.

On the Design of CPW-fed Appollian Gasket Fractal Antenna

Anupam Tiwari[1] **and Raj Kumar**[2]

[1]Department of Applied Mathematics, Defence Institute of Advanced Technology (DU)
Girinagar, Pune-411 025, India
[2]Microwave and MM Wave Antenna Lab., Department of Electronics Engineering
Defence Institute of Advanced Technology (DU), Girinagar, Pune-411 025, India

Abstract— This paper presents Appollian gasket CPW-fed monopole fractal antenna. The Antenna has been designed on FR4 substrate $\varepsilon_r = 4.3$ and thickness 1.53 mm. The antenna has been fabricated and tested using by VNA. The experimental result shows the multiband behavior with the centre frequencies of 1.265 GHz, 4.66 GHz and 7.8 GHz with bandwidth of 50%, 17.5% and 15% respectively. The shift in first resonant frequency of antenna also reveals the size reduction in comparison of solid equilateral triangular patch resonant frequency 2.394 GHz. This antenna can be used for Cellular, GSM, LAN, WAN and Micro air vehicular Radar applications.

Summary of Work: The progress in wireless and dramatic development of a variety of wireless applications have remarkely increases the demand of multiband/wideband antennas with smaller dimensions than conventionally possible. It has been reported in literature that if the size of planar antenna decreases less than $\lambda/2$, the efficiency, bandwidth, gain and polarization purity decrease. With growing development of small devices, the research for compact, wide bandwidth antenna has attracted researchers. Fractals, owing to their geometrical properties, has been reported in literature for miniaturization of antenna as well as for multiband and wider bandwidth. Puente et al. has reported the Sierpinski gasket multiband fractal monopole antenna with probe feed. With probe fed, the matching of second and third band is better than first band because current does not reach properly at the top of sierpinski gasket. This paper reports the appollian based gasket compact fractal antenna with CPW-fed. The advantages of CPW-fed antenna are that radiating element and ground plane are at same side, no need for via. In result, CPW-fed improves the matching at the first band with wider bandwidth in comparison to conventional feed.

Design and Experimental Results: Appollian based Gasket fractal antenna has been designed on FR4 substrate of height 1.53 mm and $\varepsilon_r = 4.3$. Antenna is fed by CPW-fed of dimension 2 mm wide, 25 mm length, 0.2 mm gap. Dimension of one tip to another at base is 40 cm and vertical height 32 mm. Appollian Gasket Fractal antenna with CPW-fed monopole has been shown in Fig. 1. The antenna has been fabricated and tested using VNA. The experimental result of antenna i.e., return loss versus frequency reveals the multiband with centre frequencies of 1.265 GHz, 4.66 GHz and 7.8GHs respectively as shown in Fig. 2. The shift in the 1st resonant frequency in comparison to same dimension solid triangular patch indicates the size reduction around 50%. The bandwidth of the first, second and third band is 570 MHz, 830 MHz and 1160 MHz respectively. This antenna also exhibits the wider bandwidth from 4.25 to 14 GHz with return loss of −5 dB. The radiation pattern of fractal antenna at 1.188 GHz is shown in

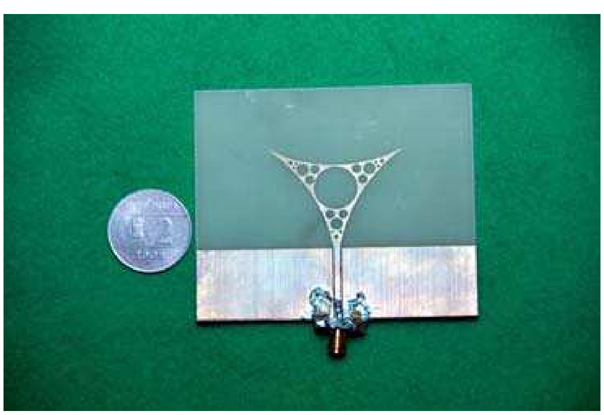

Figure 1: Appollian gasket CPW monopole fractal antenna.

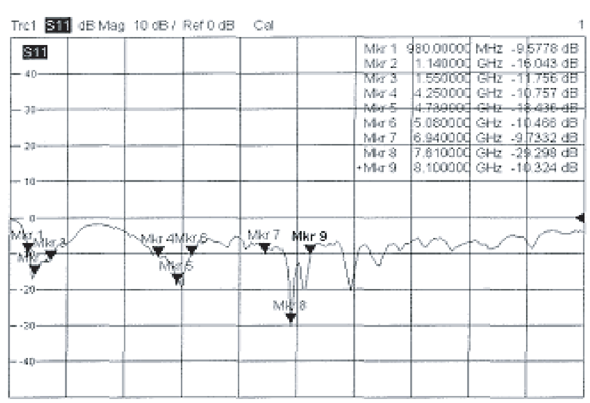

Figure 2: Experimental results of appollian gasket fractal antenna.

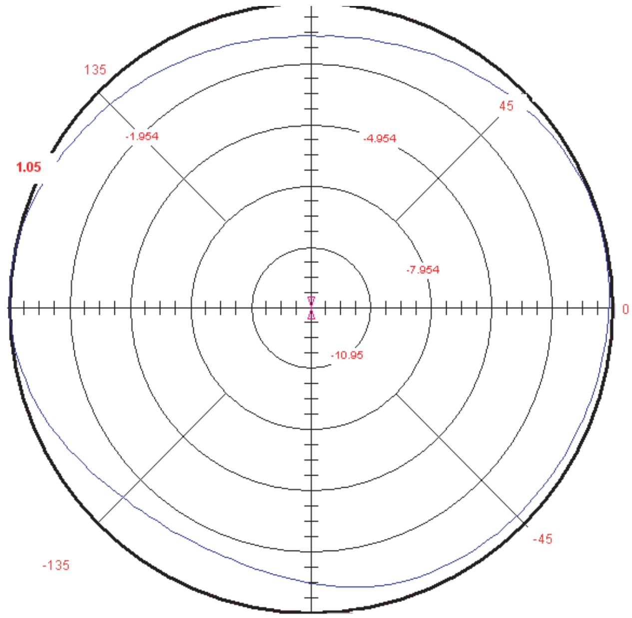

Figure 3: Radiation pattern of appollian gasket fractal antenna at 1.188 GHz.

Fig. 3. The gain for this antenna at 1.188 GHz is 1.05 dB. Such type of antenna can be useful Cellular and LAN applications.

A Y-Y-shaped Slot Antenna Design for an RFID Tag Designed for Metallic Tag Applications

Sung-Lin Chen and Ken-Huang Lin
Department of Electrical Engineering, National Sun Yat-Sen University, Taiwan

Abstract— The radio Frequency Identification (RFID) technology, which is used for object identification, is finding an increasing number of applications in a wide variety of industries. There are some natural limitations when applying RFID technology in the steel industry, because the tags do not function well in metallic environments. Even though some commercial RFID metal tags are available in the market, they are found to be too expensive by steel companies. This paper proposes a Y-Y-shaped slot antenna for UHF RFID applications which use the metallic substrate as label carrier. The proposed metallic RFID tag directly presses out a Y-Y-shaped slot on the metallic foil to form an RFID tag antenna. The design methodology, simulation and measurement results of the proposed metallic RFID tag antenna are also presented in this paper. The maximum read range of the prototype metallic RFID tag can reach about 4.7 m, measured with 2.0 W EIRP radiation power of RFID reader system. The low profile and low cost features make the design more suitable and applicable to metallic tag labeling system which RFID technology needs to be integrated. In addition, a practical application for wire-rod products tracking in steel industry applied Y-Y-shaped slot metallic RFID tag is also demonstrated.

On the Problem of Dielectric Coated Thin Wire Antenna

A. Adekola[1], **A. I. Mowete**[1], **and A. Ogunsola**[1,2]

[1]Department of Electrical and Electronics Engineering, Faculty of Engineering, University of Lagos
Lagos, Nigeria
[2]Parsons Group International, Rail Treansit Divison, London, United Kingdom

Abstract— It is shown in this paper that when the thin dielectric shell that insulates coated thin-wire antennas is modeled by Schelkunuff.s volume equivalent currents, such that the problem essentially reduces to that of specifying the electric field in the dielectric region, a quasistatic moment-method solution applies. First, the paper demonstrates that solutions earlier proposed by Richmond and Newman [1] on one hand, and Lee and Balmain [2] on the other, apply only when it may be assumed that the wire antenna is of infinite extent; and second, it further reveals that a modification of the solution, as proposed by Adekola and Mowete [3], is incomplete. The paper then provides a quasi-static moment method analysis applicable for the solution of the problem of thin-wire antenna structures coated with thin dielectric shells. Numerical data obtained from a computer simulation of the analytical results suggest that this approach constitutes a significant improvement over the three earlier referred to in the foregoing.

REFERENCES

1. Richmond, J. H. and E. H. Newman, "Dielectric coated wires antennas," *Radio Science*, Vol. 11, No. 1, 13–20, January 1976.
2. Lee, J. P. Y. and K. G. Balmain, "Wire antennas coated with electrically and magnetically lossy materials," *Radio Science*, Vol. 14, No. 3, 437–445, May–June 1978.
3. Adekola, S. A. and A. I. Mowete, "A quasi-static moment-method analysis of dielectric-coated thin-wire antennas," *Proc. SATCAM 2000*, Paper Number 14 (AP/BEM), University of Stellenbosch, Cape Town, South Africa, July 2000.

Leaky-wave Antenna Based of EBG Structures

S. E. Bankov
Institute of Radio Engineering and Electronics of Russian Academy of Science, Russian Federation

Abstract— A leaky-wave flat antenna on the base of EBG structures is considered. The antenna contains a system of coupled EBG waveguides with array of radiating slots and an exciter that feeds this array. The exciter is considered in two variants: planar double layered EBG mirror with a planar horn and EBG waveguide with leaky wave.

At the first stage mentioned above elements of the antenna are studied theoretically and numerically. Eigen modes of an infinite array of infinite EBG waveguides formed by metal cylinders placed inside a parallel plate waveguide are analyzed with help of known compensating sources technique (CST). EBG waveguides have longitudinal radiating slots in the upper screen of parallel plate waveguide. The array is considered in the regime of quasi-periodical excitation. Method CST combined with a method of transversal resonance allows one to obtain in analytical form approximate dispersion equation relatively a complex propagation constant of the array eigen mode. Imaginary part of the propagation constant describes loss of energy radiated into the free space through slots. Its real part determines angle of radiation of the array. Dependence of the propagation constant on the array parameters is studied numerically.

EBG waveguide with leaky wave is considered theoretically also with help of CST. EBG waveguide is a channel inside a periodical EBG structure. The structure is an array of metal cylinders located inside parallel plate waveguide. Waveguide mode may radiate energy through EBG structure if it has a finite number of layers of cylinders. Practically it should have one layer. In this case waveguide mode is a leaky-mode that forms inside parallel plate waveguide a wide wave beam that excites described above array of EBG waveguides. As in the previous case CST combined with a method of transversal resonance gives us a dispersion equation relatively leaky-wave complex propagation constant.

The second type of the array exciter is a planar double layered mirror. In this case our antenna has two layers: down and upper. Planar mirror is excited by a planar horn that is located at the down layer. The horn forms inside down parallel plate waveguide a wave with a cylindrical phase front. This wave incidents on the mirror which is a curved EBG structure with a coupling slot which is curved along the same line. This slot is cut in the common wall of upper and down parallel plate waveguides and it connects both waveguides. Thus planar mirror fulfils two functions. It transforms cylindrical wave of planar horn into plane wave and at the same time it transmits energy from down layer to upper one. Thus plane wave propagates inside upper parallel plate waveguide while cylindrical wave propagates along down waveguide. This plane wave excites array of EBG waveguides. Planar mirror is studied numerically with help of HFSS simulation. Numerical calculations allow one to study different operating regimes of the planar mirror and to optimize it. They demonstrate that the mirror may be well matched in a wide frequency range.

The last stage of the antenna theoretical investigation is a complex analysis of waveguide array together with exciter. This analysis allows us to calculate antenna radiation pattern, gain, operating frequency range etc. Type of the exciter has a sufficient influence at antenna parameters. For example antenna with planar mirror radiates energy along waveguides with slots. At the same time radiation pattern of antenna with waveguide exciter is tilted relatively radiating waveguides.

Some results of antenna with planar mirror experimental investigation are presented. The antenna is studied in frequency range 9–11 GHz. Experimental and theoretical results are compared. Some details of antenna design and fabrication are discussed.

Beam Forming Networks on the Base of Coupled Waveguides for Multi-beam Hybrid Antennas

S. E. Bankov, V. A. Kaloshin, and E. V. Frolova
Institute of Radio Engineering and Electronics of Russian Academy of Science, Russian Federation

Abstract— Proposed and investigated a new class of beam forming networks (BFN) for multi-beam antennas (MBA). The proposed N-port BFN forms together with an optical system (OS) N narrow beams crossed at the high level close to -3 dB. Ports of the BFN are well matched and isolated. The main part of the BFN is a system of coupled waveguides. The following types of BFN are considered theoretically, numerically and experimentally: one-dimensional (linear) BFN with identical coupled waveguides and fixed phase shifters, BFN with different coupled waveguides (without phase shifters), two-dimensional BFN with rectangular cell, identical waveguides and phase shifters, two-dimensional BFN with rectangular cell and different waveguides, two-dimensional BFN with hexagonal cell, identical waveguides and phase shifters.

All the proposed BFN are analyzed in approach of theory of coupled waves. Solutions for one and two-dimensional systems of identical and non-identical coupled waveguides are obtained and studied analytically and numerically. Phase and amplitude distributions at the output ports of BFN and corresponding radiation patterns are obtained analytically for linear BFN and numerically for two-dimensional BFN. Numerical analysis demonstrates that a correct choice of waveguide propagation constant β, coupling coefficient C and phase shift $\Delta\varphi$ allows one to have in linear BFN with $2N$ waveguides N isolated and matched input ports. BFN produces N identical beams with radiation patterns close to sector type radiation patterns. Such a shape of beam produces optimal conditions for illumination of OS. In case of two-dimensional BFN with rectangular or hexagonal cells BFN with $4N$ waveguides has N input ports.

Coefficient of BFN efficiency which takes into account MBA gain degradation because of imperfect phase-amplitude distribution in aperture of OS and loss of energy radiated out of OS is introduced. BFN are optimized to obtain maximum efficiency. Optimal BFN have coefficient of efficiency from -0.25 dB for one-dimensional BFN to -0.75 dB for two-dimensional BFN. Optimization gives optimal values of coupling coefficient C for all types of BFN and values of phase shifts for BFN with fixed phase shifters and propagation constants of waveguides for BFN with non-identical waveguides. Two-dimensional BFN are optimized for two shapes of OS: rectangular and circular.

BFN based on waveguides in EBG structure (EBG waveguides) are presented. Infinite arrays of mentioned above waveguides are theoretically and numerically studied in regime of periodical excitation. Eigen modes propagation constants are studied to obtain generalized parameters: propagation constant of uncoupled waveguide and coupling coefficient. Electrodynamic solution allows one to find dependence of generalized parameters on geometrical parameters of coupled waveguides.

BFN with EBG waveguides is studied and optimized numerically with help of HFSS. Results of HFSS simulation are compared with results obtained applying analytical-numerical method of compensated sources and coupled waves theory. Sample of BFN with EBG waveguides studied experimentally in frequency range 8–9 GHz. Experimental and theoretical results are compared.

Results of mirror antennas with BFN modeling are presented. Radiation patterns in far zone of parabolic antennas and field distributions in focal plane of elliptic mirror are calculated numerically and discussed. It is shown that application of coupled waveguide linear BFN allows one to obtain a system of narrow beams crossing at -4 dB level.

Application of Imbedding Method to the Problem of Nanosecond Impulses Distortion

P. V. Filonov and V. L. Kuznetsov
Moscow State Technical University of Civil Aviation, Moscow, Russia

Abstract— In this work, we consider hypothesis about the reasons of nanosecond impulse distortion in process of radiation by antenna system and ways of eliminating effect. By our opinion, the main reason of distortion could be the non-linear dependence of phase shift on spectrum of radiated signal. This could be caused by Wood's cross resonances concerning with overradiation of lattice elements. We consider modification of signal as a filter which could be present as a matrix operator $K(\omega) = A(\omega)e^{i\Phi(\omega)}$, there $\Phi(\omega)$ — phase shift for different elements of spectrum. This distortion could be presented as non-linear dependence near the points of Wood's resonances (Fig. 1). We suppose that non-linear regions of $\Phi(\omega)$ have periodic structure. The description of this anomalies look naturally in imbedding method.

In this work, we consider the truncated horn area antenna (HAA). For computing the transparency and reflection coefficients the iteration embedding equations are using. The results of numerical experiments which confirm periodical structure of anomalies on phase shift are considered. The methods used in this work could be easily applied to antenna systems with different geometry. The transition from endless periodical to finite lattice also shown.

The recommendation about form and parameters of impulses are adducted. This recommendations allow to reduce the distraction of hypershort impulses and save where properties.

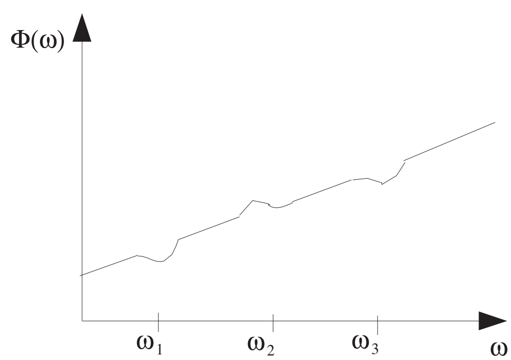

Figure 1: Nonlinear regions of phase shift.

Near-field Microwave Detection of a Spherical Object: Theory and Application

M. A. Galin and A. N. Reznik
Institute for Physics of Microstructures, RAS, GSP-105, N. Novgorod 603950, Russia

Abstract— Near-field (NF) diagnostics is an emerging technology to study an electrodynamic response of materials on length scales much smaller than the wavelength λ. Such small scales are due to a NF interaction between a probe and a sample in the near zone of the size $D << \lambda$ (D is the aperture size of the probe). The scale D determines the space resolution, which yields submicron values for modern devices ($D/\lambda \sim 10^{-5}$–10^{-6}). Such microscopes are applied now in microelectronics. Probes of a middle resolution $\sim$ 0.1–1 cm ($D/\lambda \sim 10^{-1}$–10^{-3}) are also promising for application, because their sounding depth is about several centimeters. Such characteristics are of interest, for example, in medical diagnostics.

Although there is a wide variety of designs and applications of NF probes, an adequate theory of NF sounding has not been yet developed completely. This is explained by rather complicated electrodynamics of the interaction between the NF probe and a 3D nonuniform medium around the probe. We have solved the above problem for a particular case of spherical object detection. Our model addresses a NF probe as an electrically small antenna with the Gaussian-like current distribution, the single characteristic length scale of which is D. An electrodynamic response of an antenna is determined by its complex impedance Z. We represented Z using Green functions in the form of space spectral transforms for electric and magnetic fields generated by a point-like dipole. The key element of our model is the solution of the diffraction problem for a sphere located in the antenna near zone. This solution represents the diffraction fields as a series of electric and magnetic multipole radiation (dipoles, quadrupoles, etc.). In contrast to the classical Mie theory we took into account quasi-static fields, both incident and diffracted. From this common solution we determined the number of radiated multipoles which should be taken into account in calculation of Z. This number depends on geometric and electrodynamic parameters of the probe-sample system. We also determined the conditions for applicability of the small-particle approximation (the Rayleigh approximation) to the considered problem. Two-dimensional spatial distributions recorded by the NF probe during scanning of the object were calculated. Specific features related to the excitation of the wave fields were discovered in these distributions. It is shown that the NF probe response as a function of the antenna-object distance is characterized by two scales: the quasi-static scale h_q and the wave scale h_w; besides $h_w > h_q$. We found that the probe resolution can be 2–3 times increased, if the correct informative parameter is chosen.

We used the developed theory to study the prospects of detection of 3D contrast formations (tumors) in a human body. It is shown that tumors as small as 0.7–1 cm and located at a depth of up to 2 cm can be detected at optimized parameters of the NF device. For experimental study we used a resonant probe with $D = 1.5$ cm and the operating frequency ~ 500 MHz. We modeled the tumor as a contrast object which was immersed in water. The probe resonant curve was measured during scanning of the water surface. Sharp images of the object were obtained at a depth of up to 1.5 cm.

Session 3A8
Nonlinear Dynamics in Electromagnetics, Electronics and Animate Nature

Electric and Magnetic Spinor Particles — The Electromagnetic Source of Gravitation, Theory and Experiments

Robert Sizov
Individual researcher, Moscow, Russia

Abstract— The universally known gravitational field is electromagnetic in its nature and, under natural conditions, is generated by EM atomic and nucleonic shells. Immediate elementary sources of GF are provided by eddy EM quasi-particles (s-gravitons) which contain electric and magnetic fundamental particles, both material and physical-vacuum ones.

The s-gravitons constitute the so-called compensated EM density and populate atomic or nucleonic orbits in accordance with the refined Pauli principle for EM shells (see the entry for Pauli principle in the Glossary).

The existing theoretical contention that atoms in the normal (unexcited) state do not emit., anything is profoundly erroneous. Atoms in any state continuously generate a gravitational EM fields constitutive, for example, the Earth gravity field. As to excited atoms, they emit photons (known from spectra of atomic emission) in the pulsed mode in addition to atomic gravitational radiation. Note that the emission of photons appears to be, generally speaking, exotic against the background of steady generation of GF by atoms.

It is worthy of note that the gravitational field, which is simple to perceive, as well as to technically implement, remains an unrealizable dream and a cause for endless theoretical variations until the magnetic particles are recognized by scientists and engineers and until controlled MC currents are involved in experiments and technical projects.

Atomic gravitational fields may be both vector (axially vector) and tensor ones. Condensed media (liquids and solids) for the most part radiate a tensor GF field. In particular, the Earth gravity field is a tensor one. Mutual repulsion or displacement of one film by the other takes place between the vector and tensor gravitational fields. Such interactions manifest themselves in the effects of volatility of light atoms (molecules) of gases, for example, gaseous hydrogen.

Continuous generation (radiation) of gravitational field by atomic EM shell made up of electrons and magnetons presumes the mandatory existence of the World fundamental field medium; in the processes of interaction with this medium, the fundamental particles show their "capacity" to generate fields which correspond to their nature. Regarded as such medium in the present book are fields of physical vacuum (PV). Under conditions of interaction of electrons and magnetons with PV field medium, they "act" as continuously operating converters of initial PV fields into electric or magnetic fields corresponding to these particles. The very capacity of electrons and magnetons for such transformations is perceived as their charge.

The geometric direction of flow of transformation of PV field medium by fundamental particles may apparently serve as explanation for a sacramental notion such as spin vector of particles. If the fundamental particles involved in the processes of foregoing transformations perform a rotational motion and, in so doing, the rotation axis coincides with the direction of flow of transformation of PV into respective fields, the word *spin* will correspond to the universally accepted opinion of spin as intrinsic rotational moment of movement of particles. However, in this case, the notion of spin of fundamental particles acquires a physical content which shows up as its correlation with the processes of transformation of initial PV fields into electric and magnetic fields.

The part played by the spin of fundamental particles is not limited to defining the direction of flow of transformation of PV fields. The modulus of the spin vector $|\mathbf{S}|$, which corresponds to the angular rotational velocity of particle, defines the rate of efflux of the flow of fields being transformed, i.e., the rate of propagation of intensity of electric and magnetic fields and, in the end, the velocity of light in the medium.

Given in the book is the author's assumption as to the nature of the charge of fundamental particles (electric or magnetic), which may be defined by the direction of rotation of particles (counterclockwise or clockwise). These directions of rotation may be introduced into electrons and magnetons during their production by respective left or right neutrinos.

REFERENCES

1. Sizov, R. A., *Electric, and Magnetic Spinor Particle — Structure-forming Component Mass and Electromagnetic Source of Gravitation*, Moscow, 2008.

Generation of the Microwave Chaotic Oscillations by CMOS Structure

Artem Yu. Nikishov[1,2]

[1]Moscow Institute of Physics and Technology, Russia
[2]Kotel'nikov Institute of Radioengineering and Electronics of RAS, Russia

Abstract— Application of ultrawideband (UWB) signals is actively investigated in communications. In particular, UWB signals are adopted in wireless personal area networks (WPANs) that are developed within the limits of IEEE 802.15.4a standard. One of the signal types that are recommended for use in UWB WPANs as an information carrier is chaotic signals.

A promising approach to UWB communications is direct chaotic communication scheme when generation of chaotic carrier, its modulation and demodulation by information signal are performed in microwave band.

Effective sources of UWB chaotic signals are necessary for implementation of such systems. These sources must have a simple structure, form a chaotic signal in a necessary frequency band and provide uniform power spectral density. The main requirements to the sources are: low weight and size, reliability, low power consumption, etc.

One of classes of such sources are ring microwave chaotic oscillator based on the microchip amplifiers. These devices allow receiving a chaotic signal in a wide range of frequencies.

However, possibility of their implementation as complementary metal-oxidesemiconductor (CMOS) integrated microcircuit could become the most attractive property of such devices.

In this report, CMOS structure capable to generate ultrawideband microwave chaotic signal with uniform power spectral density is proposed.

The CMOS structure represents ring self-oscillatory system. This system realized as an integrated microcircuit on 180 nm CMOS technology and consists of three microwave amplifiers and a frequency selective circuit (one RC-, and some LC-sections) connected in series in a closed loop, on which parameters the range and bandwidth of oscillations frequencies depends.

In this case, oscillator with two LC-sections in the feedback loop is considered. RC- and LC-sections in oscillator are high-pass filters and it is distinctive feature of the oscillator. Therefore using given sections and microwave amplifiers it is possible to generate highfrequency ultrawideband microwave chaotic oscillations.

Amplifiers are small-signal microwave amplifiers with amplification gain 10 to 2 dB in frequency band 1 to 10 GHz. Each amplifiers used in oscillator consists of two cascades. The first cascade is an inverter (common-source circuit) with negative feedback. The second cascade is a buffer (common-drain circuit).

Simulation results of the oscillator circuit, topology and its experimental realization are presented. Basic oscillation mode dynamics is described, the fact of the chaotic generation is shown. Bifurcation phenomena are analyzed. It is proved that chaotic oscillations are excited on the basis of mechanism of two-frequency oscillation mode destruction.

The described CMOS oscillator can be used in different wireless communication applications as a compact device for ultrawideband microwave chaotic signal generation.

Avalanche Dynamics of Single Photon Sensitive Avalanche Photodiode

Josef Blazej and Ivan Prochazka
Czech Technical University, Prague, Czech Republic

Abstract— We are presenting the results of the study of the Single Photon Avalanche Diode (SPAD) pulse response risetime and its dependence on several key parameters. We were investigating the unique properties of K14 type SPAD with its high delay uniformity of 200 μm active area and the correlation between the dynamics of the avalanche buildup time and the photon number involved in the avalanche trigger. The detection chip was operated in a passive quenching circuit with active gating. This setup enabled us to monitor the diode reverse current using an electrometer, a fast digitizing oscilloscope, and using a custom design dual comparator circuit. The electrometer reading enabled to estimate the photon number per detection event, independently on avalanche process. The avalanche dynamics was recorded on the oscilloscope and processed by custom designed waveform analysis package. The correlation of avalanche build up to the photon number, bias above break, photon absorption location, optical pulse length and photon energy was investigated in detail. The experimental results are presented. The primary application of our research is the laser ranging where it is highly desirable to have a detector, which detects both single photon and multi photon signals with picoseconds stability.

Forming and Receiving Ultra Low-energy Electromagnetic Signals

A. S. Dmitriev
Kotel'nikov Institute of Radio Engineering and Electronics of RAS, Russia

Abstract— Communication revolutions of last decades radically changed principles of people interaction from company level to interpersonal contacts. The process is continuing and one of its main directions is expansion of wireless communication possibilities over smaller geometrical scales, mass use for local diagnostics and control of environment, different home applications. Such systems as wireless sensor networks, wireless personal networks and smart houses become widespread. Wireless technologies with typical communication range from several to tens of meters are developed for these applications. Energy-per-bit parameter in these systems equals 1 to 100 nJ.

Transition to smaller operation range (1 cm to several meters), less emitted energy per information bit (1 to 100 pJ) and smaller transceiver dimensions requires solution of physical problems in the field of ultralow-energy signal generation, putting data into these signals and developing methods of their reception. Forming ultralow energy signals, putting data in them and receiving signals in systems with ultralow energy consumption are nonlinear dynamical processes.

Some of the above questions are considered in the report.

First of all we determine link margin for typical communication distances. For these distances optimal frequency bands are evaluated. The main question here is relationship between communication distance and appropriate frequency band. For smaller distances we must use higher frequencies because of transceiver dimensions and CMOS technology restrictions (e.g., size of passive components). On the other hand, maximum frequency value is restricted by f_T, boundary frequency of concrete CMOS process.

Then, the questions of energy-effective generation of oscillations and use of super-regenerative receiver for ultralow-power communications are discussed. As is shown, power consumption in such systems can be below 100 μW, i.e., approximately 1000 times less than in typical personal area wireless systems, such as Wi-Fi or Bluetooth.

Chaotic Oscillators

N. A. Maksimov
Institute of Radio Engineering and Electronics, Russian Academy of Sciences
Mokhovaya St. 11, GSP-3, Moscow 103907, Russia

Abstract— An approach to design of chaotic oscillators with controlled bandwidth in different frequency bands is proposed. Mathematical models of the oscillator and simulation results are considered. Implementations of microwave chaotic oscillators and experimental results are demonstrated.

In the report, we propose approach to design of chaotic oscillators with controlled bandwidth in different frequency bands. The approach is based on principles of scale invariance and structure hierarchy.

A harmonic oscillator whose dynamic is described by a second-order ordinary differential equation (i.e., a system with one degree of freedom) can be used as the base — the active oscillator.

A passive oscillator is the second element of the structure. It can contain both linear and nonlinear reactive elements and it has frequency-selective response in the corresponding frequency range. In general, we shall imply that passive oscillator is a resnant circuit consisting of several simpler oscillating systems, whose number of freedom degrees essentially exceeds 2. In particular this pertains to distributed systems exploited in microwaves.

The third element of the structure is the connection between active and passive oscillators, providing their self-consistent interaction. Power spectrum of chaotic oscillations, arising in this system, is restricted to the bandwidth of resonant response of the passive oscillator.

An approach to chaotic oscillator design with prescribed and controlled bandwidth in different frequency ranges was verified by means of simulation and experiments. Microwave ultrawideband generator, designed using this approach, represents a structure consisting of topologically similar interacting chaotic oscillators connected as a whole in required frequency range.

Transistor Generator of Microwave Chaotic Oscillations with Single External Reactive Component

N. A. Maksimov
Institute of Radio Engineering and Electronics, Russian Academy of Sciences
Mokhovaya St. 11, GSP-3, Moscow 103907, Russia

Abstract— One of the simplest-structure transistor chaotic generators is a capacitive three-point circuit (Colpitts circuit). With three reactive elements this circuit has 1.5 freedom degrees and it can produce chaotic oscillations for certain parameter values. The scheme of this generator can be treated as a RLC low-pass filter activated by bipolar transistor. Consequently, power distribution over the spectrum and upper spectrum bound are determined by the amplitude-frequency response of this filter.

In this report, the results of design of ultrawideband chaotic generator with the band 0.5–8 GHz (at -10 dB level) are presented. In microwaves, the values of inductors and capacitors are measured in units of nH and pF, respectively, and capacitances of *p*-*n* junctions and parasitic inductances of transistors start making influence. The effect of inter-electrode capacitances leads to oscillations in the circuit even in the absence of external capacitors. In this case, the collector-emitter feedback is implemented with inner capacitance of this transistor junction. In Si-Ge transistor BFP620F, which was used in simulation as well as in generator testbeds, this capacitance was $C_{CE} \sim 0.2$ pF. Capacitances of the other junctions of this transistor were $C_{CB} = 0.12$ pF, $C_{EB} = 0.45$ pF.

By design of chaotic generator only one external reactive component was used in the generator circuit, namely, an inductor which, in combination with capacitances of transistor *p*-*n* junctions, made a frequency-selective circuit. To decrease Q-factor of this circuit, which was necessary for wideband oscillations, an external resistor was used. Generator testbed was made and its modes were investigated for various values of external inductor L. At $L = 1$ nH at the output of the generator, loaded at 50 Ohm, stable chaotic oscillations in the band 0.5–8 GHz were observed.

Forest Fire Localization Using Distributed Algorithms in Wireless Sensor Networks

A. Khadivi, **L. Georgopoulos**, **and M. Hasler**
School of Computer and Communication Sciences
Ecole Polytechnique Fédérale de Lausanne (EPFL), Switzerland

Abstract— Wireless sensor networks are an emerging technology that opens new possibilities for monitoring in environmental sciences, engineering and biology [1]. In this paper, we address a few questions arising in the application of wireless sensor networks in forest fire detection and localization.

One of the specificities of forest fire monitoring is that as the fire progresses part of the network is destroyed. Therefore, the information about the fire cannot be concentrated on a single node of the network, but must be distributed over the whole network. Accordingly, we propose to use a discrete-valued consensus algorithm to detect the outbreak of a fire and a continuous-valued consensus algorithm for its localization by a circle. For both, after a short time to reach approximate convergence, the information is available at each sensor node and can be read out e.g., by a mobile device.

We have simulated the functioning of such a wireless sensor network, using as input data produced by the fire simulator software FARSITE [2] and as a communication systems simulator CASTALIA [3]. The result is a rapid reaction to the fire outbreak, a good representation of the fire location by a circle, and a good agreement with MATLAB simulations that do not take model any details of the communication system.

Distributed consensus algorithms need a certain number of iterations to reach consensus at a given precision. Each iteration takes time and consumes energy. Since consensus reaching has to be repeated at regular time intervals in the presence of a fire, it is important to reduce the number of iterations, i.e., to speed up the convergence. In the literature, this question is addressed, but normally only the asymptotic speed of convergence is considered [4]. However, initially the speed of convergence is higher than asymptotically, and networks that have higher asymptotic speed of convergence not necessarily also have higher initial speed of convergence. Depending on the size of the network and the desired precision of consensus, the initial speed of convergence may be more important to optimize than the asymptotic one. We shall illustrate this fact and present a nonlinear consensus algorithm that actually exploits this property.

REFERENCES

1. Culler, D., D. Estrin, and M. Srivastava, "Overview of sensor networks," *IEEE Computer*, Vol. 37, No. 8, 41–49, August 2004.
2. http://www.firemodels.org.
3. http://castalia.npc.nicta.com.au.
4. Xiao, L., S. Boyd, and S.-J. Kim, "Distributed average consensus with least-mean-square deviation," *J. Parallel Distrib. Comput.*, Vol. 67, 33–46, 2007.

Information Transmission between Neuron-like Elements

A. S. Dmitriev[1] **and A. I. Ryzhov**[2]

[1]Institute of Radio Engineering and Electronics of RAS, Mokhovaya st., 11/7, Moscow 125009, Russia
[2]Moscow Institute of Physics and Technology, Institutskiy pereulok, 9, Dolgopruniy 141700, Russia

Abstract— There is a question about information processes organization in neuron systems and it attracts scientists' attention for a long time. A. L. Hodgkin and A. F. Huxley were the founders in the area of dynamic neuron model and they managed to give rather powerful incentive to the development of this trend in their classical paper. Later a number of other mathematical models describing neuron behavior were created by different experts. However, Hodgkin-Huxley model is still vital.

At once question about information transmission principles and its interpretation is still opened. In this report we are not trying to answer this question directly, but we reformulate this question from pragmatic point of view: what does neuron represent if treated like information transmitter or receiver in communication theory? How can information flow transmission be organized with the help of neuron-like elements using conventional bit streams? What are the characteristics of communication channel between neurons and what do they depend on?

Communication system using neuron-like elements as transmitters and receivers is considered in this report. Also this system includes a former of rectangular pulse stream acting on the input of transmitting neuron, a "communication channel" that transfers spikes from neuron-transmitter to neuron-receiver and a decoding device that transforms spike streams into binary pulse sequence.

If this decoding device restores correctly the bit sequence generated by pulse former, then the information bit stream is considered like successfully transmitted with the help of "neuron communication channel".

Modeling results showed that neuron-transmitter is able to produce spike sequence corresponding to a certain binary sequence generated by information source (pulse former). Moreover, this spike sequence can be recognized correctly by neuron-receiver, so that its output after decoding will be similar to the initial binary sequence.

Thereby, system of two neurons described by Hodgkin-Huxley equations is considered in this report in terms of communication channel organization for digital information transmission. It is shown that such system does form communication channel with quite good characteristics in terms of classic communication theory.

Session 3A9
Microwave and Millimeter Wave Circuits and Devices, CAD

Temperature-dependent Microwave Reflection-and-Transmission Narrowband Filter in a Type-II Superconducting Bilayer in the Mixed State

Chien-Jang Wu
Institute of Electro-Optical Science and Technology
National Taiwan Normal University, Taipei 116, Taiwan

Abstract— Microwave reflection and transmission properties for a superconducting bilayer in the mixed state have been theoretically investigated. The bilayer consists of a high-T_c superconducting system, $YBa_2Cu_3O_{7-x}$ (YBCO) and a nonlinear substrate, $SrTiO_3$ (STO) as well. Reflectance and transmittance are calculated based on the self-consistent treatment of vortex dynamics together with the matrix method in a stratified structure. Due to the presence of vortices in superconducting film and the strongly temperature-dependent permittivity of STO, simultaneous peaks in both reflectance and transmittance below T_c have been found. The simultaneous existence of peaks could be used to design a narrowband reflection-and-transmission filter at microwave. The simultaneous peaks are shown to strongly be influenced by the thickness of STO. The role played by this size effect is numerically elucidated and is discussed in details.

High Frequency Bridge Type Capacitance Tester Design

Jan-Dong Tseng[1], **Tatsuya Kashiwa**[2], **Kohzoh Ohshima**[3], **and Pei-Chi Wang**[1]

[1]Department of Electronic Engineering, National Chin Yi University of Technology
No. 35, Lane 215, Sec. 1 Chun Shan Road, Taiping City, Taichung County, Taiwan
[2]Department of Electrical and Electronic Engineering, Kitami Institute of Technology
Kitami 090, Japan
[3]Department of Electrical and Computer Engineering, Asahikawa National College of Technology
2-2-1-6, Syunkodai, Asahikawa, Hokkaido 071-8142, Japan

Abstract— A bridge type planar structure with four transmission line sections is introduced for capacitance determination in microwave frequency band. The tested capacitor is placed between two transmission lines and with one end connected to ground plane. The circuit analysis based on even- and odd-mode analysis results in scattering parameters in terms of physical parameters. The simulation results are obtained from Microwave Office v.2.66 and IE3D microwave simulators. From the results, we find a capacitance value dependent dip curve in frequency response below the setting frequency. This phenomenon shows a very good capacitance determination mechanism.

For performance testing, a proposed capacitance tester is fabricated in FR-4 substrate, the substrate height is 1.6 mm and relative dielectric is 4.3. Fig. 1 shows the layout of the proposed structure with dimensions 50 mm $(L) \times 30$ mm (H). The physical parameters are based on the maximum operating frequency, 1GHz, the setting frequency. The measurement are performed by vector network analyzer Anritsu 37269D. Fig. 2 shows the measured scattering parameters, S_{11} and S_{21}. The results show that S_{11} curves possess very sharp dips for different capacitor values below 1 GHz and at these points the testing signal can pass through the circuit very easily. By reading out the frequency of the dip, we can find the corresponding capacitance.

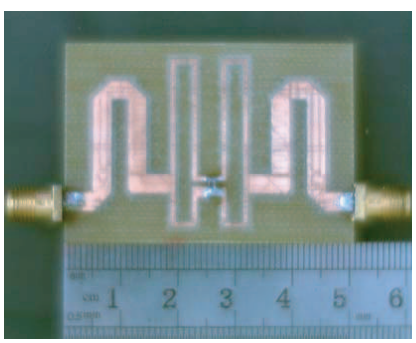

Figure 1: The layout of the capacitance tester.

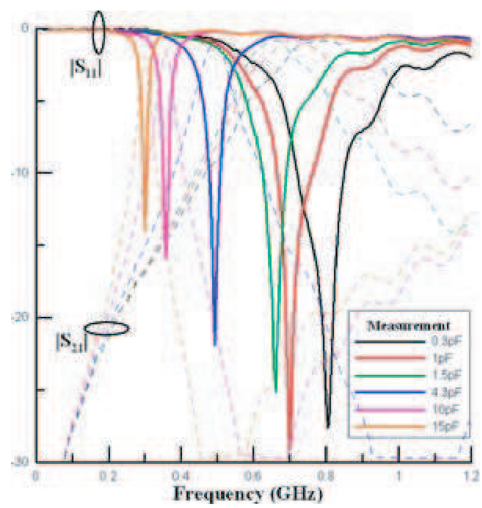

Figure 2: The measured results of different capacitors values.

Miniature Broadband Phase Shifter Based on 3 dB Directional Coupler

E. Yu. Zameshaeva, P. A. Turalchuk, and D. V. Kholodnyak
Department of Microelectronics & Radio Engineering, Saint-Petersburg Electrotechnical University
5, Prof. Popov st., 197376, St. Petersburg, Russia

Abstract— Digital and analog phase shifters are widely used in phased arrays and telecommunication systems.

A design of a 360° transmission type phase shifter for 2.5–3.5 GHz is presented. The device is designed as a cascade of two similar sections: the digital phase shifter providing 180° phase shift and the analog phase shifter providing any phase shift in the range of 0–180° phase shift. Every section (Fig. 1) consists of 3 dB directional coupler terminated with two identical reflection type phase shifters [1]. The reflection type phase shifter comprises a varactor diode and a LC-circuit. The flip-chip varactor diodes MV39003 by MDT are used as controlling components. The varactor diode exhibits a low insertion loss and a high commutation quality factor $K \geq 3 \cdot 10^4$ [2]. The transmission type phase shifter design is realized using Low Temperature Cofired Ceramics (LTCC) technology. Seven layers of DuPont Green Tape 951 with the thickness of 95 µm are used.

The results of electromagnetic simulation of the 360° transmission type phase shifter performance reveal the reflection coefficient better than 15 dB and the insertion loss less than 2.5 dB in the frequency range of 2.5–3.5 GHz. The phase error is not higher than 13.5° in all different states. The area of the phase shifter is $8 \times 6\,\mathrm{mm}^2$. The EM simulated characteristics of the 180° section of the phase shifter are presented in Fig. 2. The experimental investigation of the device is in progress.

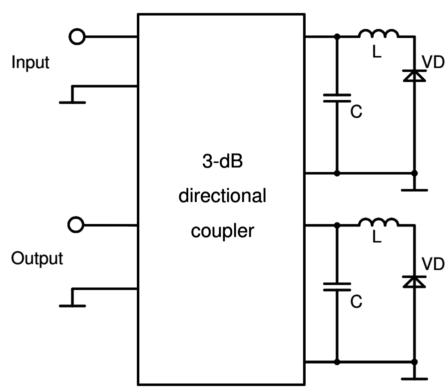

Figure 1: Phase shifter section.

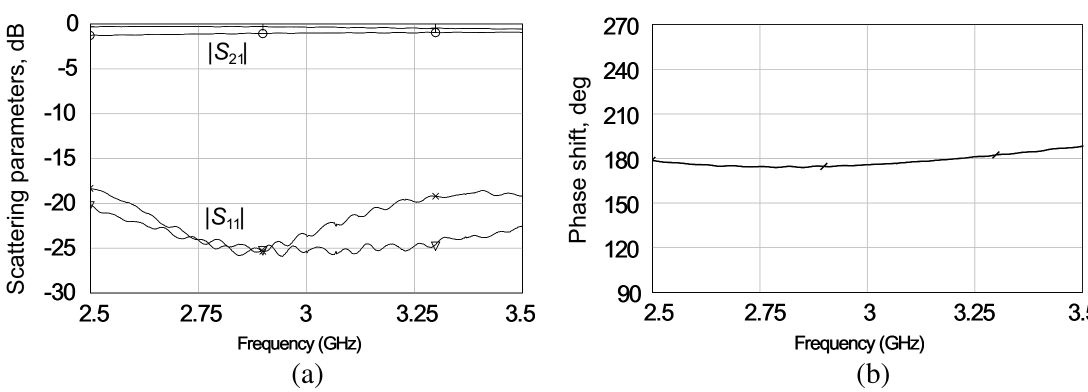

Figure 2: Characteristics of 180° phase shifter.

REFERENCES

1. Koul, S. K. and B. Bhat, *Microwave and Millimeter Wave Phase Shifters, V. 2. — Semiconductor and Delay Line Phase Shifters*, Artech House, Boston, MA, 1991.
2. Vendik, I., O. Vendik, and E. Kollberg, "Criterion for a switching device as a basis of microwave switchable and tunable components," *Proc. of 29th European Microwave Conf.*, Vol. 3, 187–190, 1999.

A Coupled-Mode Theory of Band-Pass Filters Composed of an Arbitrary Number of Resonators

Toyokatsu Miyashita
Department of Electronics and Informatics, Ryukoku University, Otsu 520-2194, Japan

Abstract— We have developed a simple and useful method of theoretical analyses of band-pass filter composed of a chain of coupled resonators. In various fields, various types of waveguide filters have been developed. Optical and microwave defect-mode waveguides have one of the most prominent features of photonic crystals [1, 2]. Sonic/phononic defect-mode waveguides have also attractive and efficient properties of band-pass filter in the acoustic region [3]. Classically coupled-mode theory was developed for coupling between electron beams and travelling waves [4].

Our theory deals with an arbitrary number of linearly coupled resonators, as shown in Fig. 1. This model includes microwave cavities, defects in a photonic or sonic crystal, or electrical resonators. Simply we assume an equal resonant frequency of f_0 for all resonators, linear mode-coupling between adjoining resonators and negligible small internal and external losses of each resonator. Under the constraint of energy conservation of the whole system, the forward and backward coupling coefficients have a simple relation, that is, C_n and $-C_n^*$. From a set of coupled-mode equations for an arbitrary number of such resonators, we have derived a recursive formula for eigen-value equations. Here we show a set of equations for eigen-frequencies f in the case of equal coupling coefficients $C_n (n = 1, 2, \ldots) = C$.

$$X = 0, \tag{1}$$
$$X - 1 = 0, \tag{2}$$
$$X(X - 2) = 0, \tag{3}$$
$$X^2 - 3X + 1 = 0, \tag{4}$$
$$X(X^2 - 4X + 3) = 0, \tag{5}$$
$$X^3 - 5X^2 + 6X - 1 = 0, \tag{6}$$
$$\ldots$$
$$X\left(X^7 - 14X^6 + 78X^5 - 220X^4 + 330X^3 - 252X^2 + 84X - 8\right) = 0, \tag{15}$$
$$\ldots$$

Here, $\sqrt{X} = 2\pi(f - f_0)/|C|$.

We have solved numerically Eqs. (1)–(15) to obtain eigen-frequencies for one to 15 resonators. In principle, those for infinite number of resonators can be solved. The spread of the obtained eigen- frequencies, that is, a difference between the highest and the lowest, increases monotonically with the number of resonators, and the frequency-spread Δf seems to converge approximately to a specific value of $3.87|C|/(2\pi)$, and does not increase no more, as shown in Fig. 2, where $\delta = |C|/(2\pi f_0)$.

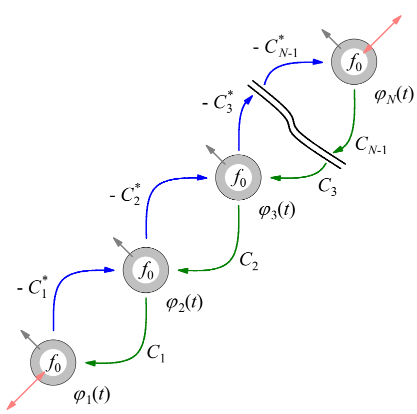

Figure 1: A model of a chain of resonators.

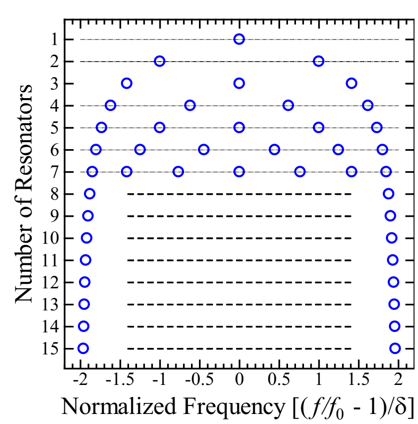

Figure 2: Eigen-frequencies.

Theoretical value of the frequency spread is a measure of pass-bandwidth of a chain of resonators, and its specific value is derived to be proportional to the coupling coefficient. Even if the coupling coefficients have different values, this model is valid, although the coupled-mode equations are not easily solved analytically, and numerical methods will be required. An attractive and complicated case is a defect-mode waveguide with stubs for the purpose of tuning additional inhibited frequency bands.

This theoretical method is further expected to be applicable to standard and complicated waveguide filters in various fields.

REFERENCES

1. Taylor, J. D., L. R. Chen, and X. Gu, "Simple reconfigurable photonic microwave filter using an arrayed waveguide grating and fiber Bragg gratings," *IEEE Photonics Technology Letters*, Vol. 19, No. 7, 510–512, 2007.
2. Joannopoulos, J. D., S. G. Johnson, J. N. Winn, and R. D. Meade, *Photonic Crystals, Molding the Flow of Light*, 2nd Edtion, Princeton University Press, Princeton and Oxford, 2008.
3. Miyashita, T., "Acoustic defect-mode waveguides fabricated in sonic crystal: Numerical analyses by elastic finite-difference time-domain method," *Jpn. J. Appl. Phys.*, Vol. 45, No. 5B, 4440–4447, 2006.
4. Louisell, W. H., *Coupled Mode and Parametric Electronics*, John Wiley & Sons, Inc., New York, 1960.

A Novel Compact Thru-silicon-via On-chip Passive MMW Bandpass Filter for 77GHz Applications

W. Woods[1], **G. Wang**[1], **J. Xu**[1], **H. Ding**[1], **Shurong Dong**[2], **Wei Wei Cheng**[2], **and A. Bavisi**[3]

[1]IBM Microelectronics, USA
[2]Zhejiang University, China
[3]Freescale Semiconductor, USA

Abstract— This paper presents a novel on-chip passive bandpass filter for millimeterwave (MMW) applications that utilizes a pair of electrically-coupled thru-silicon vias (TSV). The presented TSV bandpass filter can be used in MMW applications such as radar, medical imaging, and communication. The TSV bandpass filter uses two TSVs to extend two electrically-coupled conductors into the silicon substrate in the z-direction instead of horizontally in the x-y plane. There is a metal layer on the bottom side of the silicon substrate that shorts the ends of the two TSVs to ground. Using TSVs in the bandpass filter design reduces the silicon area required to implement the filter compared to the silicon area required for the equivalent conventional filter in the above-silicon metal-dielectric interconnect stack. The operating performance of the bandpass filter is controlled at the design stage by choosing the separation distance between the TSVs. In this work, the two TSVs were 145 μm in height (z-direction) and $3\,\mu\text{m} \times 50\,\mu\text{m}$ in the x-y plane. The long edges of the TSVs (50 μm long edges) faced each other to maximize capacitance coupling between the TSV pair. The TSVs were separated by a distance of 5 μm. Full-wave electromagnetic simulations of a TSV filter designed in an IBM SiGe technology that included TSVs show a minimum pass-band insertion loss of -3.9 dB at 77 GHz with a usable pass band from 75–85 GHz is possible. The simulated operating range of the TSV bandpass filter design presented in this paper show that it is well suited for automotive radar applications.

Bandstop Filter Using Slow-wave CPW Resonator with Defected Ground Structure

A. Görür[1], C. Karpuz[2], and Ö. Akgün[3]

[1]Department of Electrical and Electronics Engineering
Nigde University, Nigde 51245, Turkey
[2]Department of Electrical and Electronics Engineering
Pamukkale University, Denizli 20100, Turkey
[3]Department of Electrical and Electronics Engineering
Aksaray University, Aksaray 68100, Turkey

Abstract—

Introduction: Coplanar waveguides (CPWs) can be a solution to some problems encountered in microwave applications because they provide a single metal level for signal strip and ground plane. For planar circuit applications, slow-wave CPW structures can be realized by removing some conductor parts in the ground planes of CPW. The one of the important properties of such a structure with defected ground structure (DGS) is the slow-wave effect. Hence, circuit size can be reduced using this property. However, reduction in the size provided utilizing such a structure is insufficient for practical use in many microwave applications. Consequently, we have proposed a new slow-wave CPW resonator using DGS. The proposed type of DGS is realized by etching rectangular spacing on both ground planes of a conventional CPW without any dimensional changes. Its bandstop filter applications are designed, realized and measured.

The Proposed DGS: The DGS has been created in the ground planes of a conventional CPW for three substrate materials. DGS has two variable dimensions such as the length and the width. The length and width of DGS are denoted as L and W, respectively. The resonant frequency of the proposed slow-wave CPW resonator can be adjusted to desired values by changing the dimensions L and W. The structure has been simulated with the use of a full-wave Sonnet EM simulator. The simulation results have shown that the length L and width W of the DGS significantly affect the resonant characteristics of the proposed slow-wave CPW resonator.

In this study, it has been shown that a DGS length of $\lambda/4$ instead of the DGS length of $\lambda/2$ is sufficient to obtain minimum resonant frequency and hence, maximum miniaturization. The dimensions L and W of the DGS etched in ground planes affect directly and significantly the resonant frequency because these geometrical dimensions change the input impedance of the structure. By using of a suitable combination of the length L and width W of the proposed DGS, a size reduction of about 33% with respect to the conventional CPW structure can be obtained.

Bandstop Filter Application: It is possible to realize and design two bandstop filters using rectangular spacing shaped DGS. First, a bandstop filter with two spiral-shaped stubs is designed and simulated using a full-wave EM simulator. Two spiral-shaped stubs are inserted into the rectangular spacing shaped DGS etched on the ground planes of CPW resonator. The

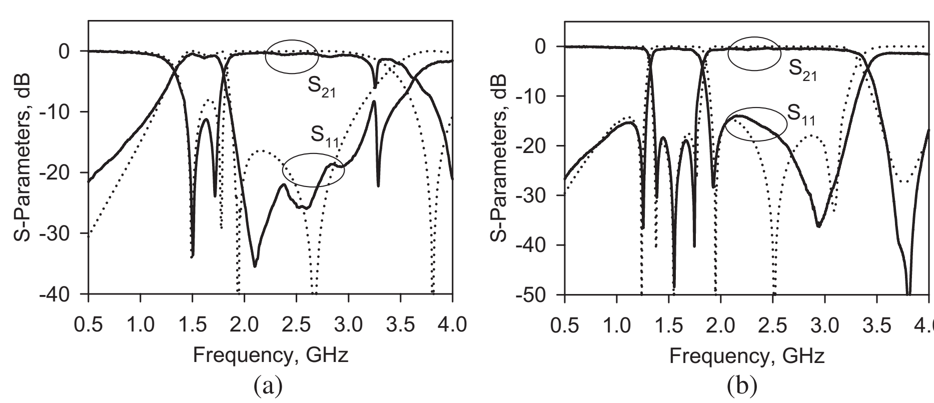

Figure 1: (a) Simulated (dotted line) and measured (solid line)responses of bandstop filter using two spiral-shaped stubs. (b)Simulated (dotted line) and measured (solid line) responses ofbandstop filter using four spiral-shaped stubs.

CPW bandstop filter was fabricated on an RT/Duroid substrate ($h = 1.27\,\text{mm}$ and $\varepsilon_r = 10.2$). Fig. 1(a) illustrates the measured and simulated results. The filter has a fractional 3-dB rejection bandwidth of about 30% at about 1.565 GHz and 10-dB rejection bandwidth of 21% at the same center frequency with insertion loss better than 10-dB. The maximum return loss in the stopband was measured as 0.45 dB. The measured responses present a good agreement with simulated responses.

A second bandstop filter is designed and realized utilizing four spiral-shaped resonators. The filter employs the same geometrical parameters as the filter realized using two spiral-shaped stubs. The total surface area of the bandstop filter is $20.5 \times 12.75\,\text{mm}^2$. Fig. 1(b) illustrates the measured and simulated results. The filter has a fractional 3-dB rejection bandwidth of 32% at 1.575 GHz and 20-dB rejection bandwidth of 25% at the same center frequency. The maximum return loss and minimum insertion loss in the stopband was measured as 0.38 dB and 18 dB, respectively. The maximum insertion losses in the lower passband and the upper passband were measured as 0.57 and 0.72 dB, respectively. The loss is due to circuit loss, including conductor and dielectric losses. The discrepancies between the measured and simulated results are due to simulation, fabrication, and measurement tolerances.

Artificial Dielectric Resonator with Anisotropy

Ikuo Awai[1], **Nobuyuki Hitoi**[1], **and Toshio Ishizaki**[2]

[1]Department of Electronics & Informatics, Ryukoku University, Japan
[2]R&D Advanced Devices Development Center, Panasonic Corporation, Japan

Abstract— Artificial dielectrics that are composed of metal particles are intrinsically anisotropic unless they are made of spherical balls. Reflecting the fact that current flows on a metal particle either by the magnetic or electric fields, both permittivity and permeability exhibit anisotropy. According to the dimension to each direction of the particle, the relative permittivity takes different values of more than 1, whereas the relative permeability less than 1 due to Lentz law. Figure 1 shows a typical example of the anisotropy.

In order to study the possibility of its application to the microwave technology, we have derived the analytical expressions for the electromagnetic field and the resonant frequency of a rectangular resonator TE modes in a waveguide, whereas TM modes are similarly analyzed. Its configuration is shown in Figure 2. Due to its good symmetry, the derivation has successfully been carried out. The fields and the resonance conditions are given by the following equations. The some significant advantages of the anisotropic resonator made of artificial dielectric include miniaturization and good spurious control, which will be presented at the venue.

TE mode

$$E_x = \frac{-A\beta_x j\omega\mu_x}{-\beta^2+\omega^2\varepsilon_y\mu_x}\sin\left(\frac{n\pi}{a}x\right)\cos\left(\frac{m\pi}{b}y\right) \quad E_y=\frac{A\beta_y\gamma}{-\beta^2+\omega^2\varepsilon_x\mu_y}\cos\left(\frac{n\pi}{a}x\right)\sin\left(\frac{m\pi}{b}y\right) \quad E_z=0$$

$$H_x = \frac{A\beta_x\gamma}{-\beta^2+\omega^2\varepsilon_y\mu_x}\sin\left(\frac{n\pi}{a}x\right)\cos\left(\frac{m\pi}{b}y\right) \quad H_y=\frac{A\beta_y\gamma}{-\beta^2+\omega^2\varepsilon_x\mu_y}\cos\left(\frac{n\pi}{a}x\right)\sin\left(\frac{m\pi}{b}y\right)$$

$$H_z = A\cos\left(\frac{n\pi}{a}x\right)\cos\left(\frac{m\pi}{b}y\right)$$

$$\tan\left[(\beta d - s\pi)/2\right] = -\beta/(\alpha\mu_{xr})$$

$$\beta^2 = \frac{-\left(\frac{\mu_x}{\mu_z}\left(\frac{n\pi}{a}\right)^2+\frac{\mu_y}{\mu_z}\left(\frac{m\pi}{b}\right)^2-\omega^2(\varepsilon_x\mu_y+\varepsilon_y\mu_x)\right) \pm\sqrt{\left(\frac{\mu_x}{\mu_z}\left(\frac{n\pi}{a}\right)^2+\frac{\mu_y}{\mu_z}\left(\frac{m\pi}{b}\right)^2\right)^2+\left(\omega^2(\varepsilon_x\mu_y-\varepsilon_y\mu_x)\right)^2+2\left(\omega^2(\varepsilon_x\mu_y-\varepsilon_y\mu_x)\right)\left(\frac{\mu_x}{\mu_z}\left(\frac{n\pi}{a}\right)^2-\frac{\mu_y}{\mu_z}\left(\frac{m\pi}{b}\right)^2\right)}}{2}$$

$$\alpha^2 = \left(\frac{n\pi}{a}\right)^2+\left(\frac{m\pi}{b}\right)^2-\omega^2\varepsilon_0\mu_0$$

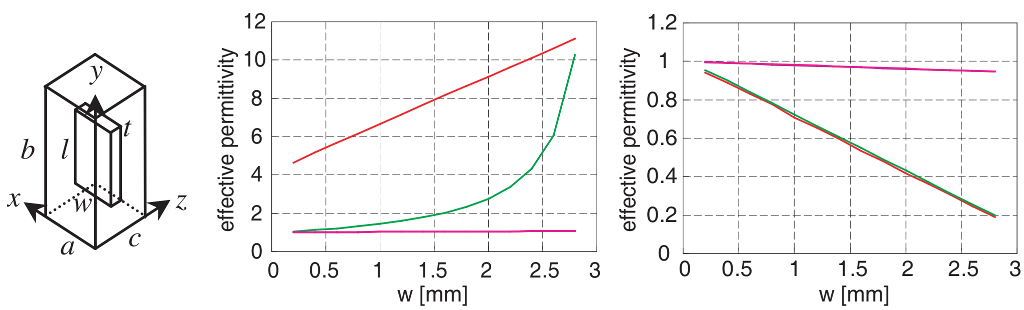

Figure 1: Anisotropy of artificial dielectrics made of rectangular metal strips ($a = 3.0,\ b = 9.0,\ c = 0.25,\ l = 8,\ t = 0018\,\text{mm}$).

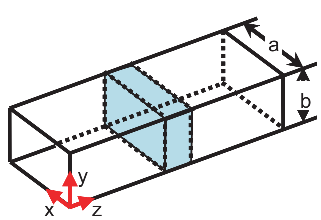

Figure 2: Artificial dielectric resonator inserted in rectangular waveguide.

An Analytical Method for Optimization of RF MEMS Wafer Level Packaging with CPW Detuning Consideration

Zheng Wang and Zewen Liu
Institute of Microelectronics, Tsinghua University, Beijing, China

Abstract— An analytic solution for detuning effect of CPW with cap wafer by applying the conformal mapping method is presented in the paper. A wafer level packaging structure for RF MEMS devices is designed with the developed analytic formula. The cavity depth of 40 μm is adequate to reduce the detuning of the MEMS circuit to an acceptable level for the 50 Ω CPW on the glass substrate for the glass cap wafer.

Introduction and Results: With the rapid development of MEMS technology, the prominent RF performance of RF MEMS devices such as varactors [1], switches [2], and resonators has been attained. Considering that the movable friable parts of RF MEMS devices must be protected and packaged in a clean and stable environment, high-performance wafer level packaging (WLP) is a good choice for RF MEMS packaging. However, the performance of MEMS devices and the coplanar waveguide (CPW) lines will detune due to the close proximity of the wafer-level package to the MEMS surface. While the detuning effect can be diminished by providing an etched cavity in the cap wafer as shown in Fig. 1, the quantitative method for detuning effect with different cap wafer materials and different lateral dimensions of CPW has not been demystified yet, which is very important for the efficient packaging structure optimization.

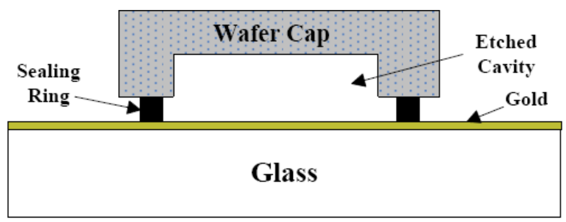

Figure 1: The wafer level packaging for RF MEMS.

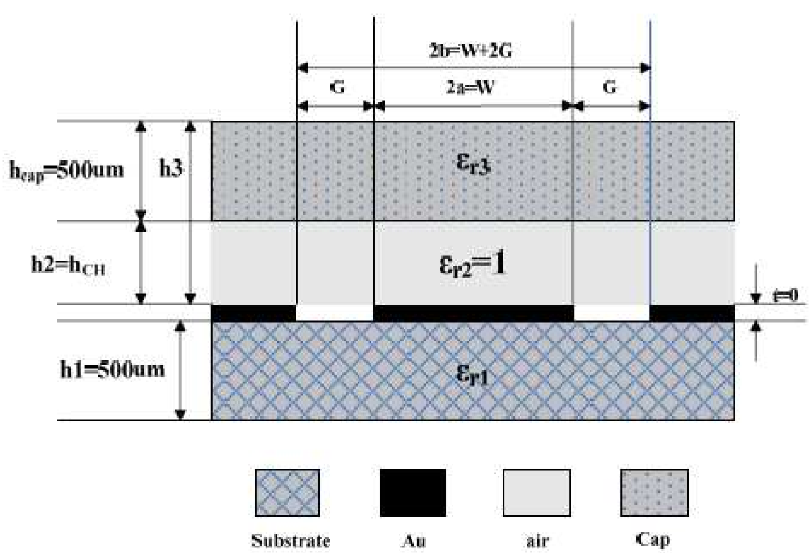

Figure 2: Cross section of the packaged CPW with cap wafer.

In this paper, we derive a closed-form analytic formula for detuning effect of CPW with a wafer cap. The conformal mapping method is applied to derive the analytical approximations, based on the extension of the partial capacitance technique [3] as shown in Fig. 2. The region above CPW line, constitutive of wafer cap and the air, is considered as the superposition of three parts with different relative permittivities, 1, $\varepsilon_{r3} - 1$ and $1 - \varepsilon_{r3}$ respectively as shown in Fig. 3. The effective permittivity can be expressed as

$$\varepsilon_{eff} = \frac{C_{CPW}}{C_{air}} = 1 + q_1(\varepsilon_{r1} - 1) + q_2(1 - \varepsilon_{r3}) + q_3(\varepsilon_{r3} - 1) \tag{1}$$

Then we can calculate the characteristic impedance:

$$Z_0 = \frac{1}{c\,C_{air}\sqrt{\varepsilon_{eff}}} = \frac{c\mu_0}{4\sqrt{\varepsilon_{eff}}}\frac{K(k_0')}{K(k_0)} \tag{2}$$

The impedance variation for a 50 Ω CPW line with glass cavity depth is computed as shown in Fig. 4. The results show close agreement with the fine element numerical simulation results.

It can be concluded that the developed analytical method works well, and a cavity depth in the order of 40 µm is adequate to reduce the detuning of the MEMS circuit to an acceptable level for glass cap.

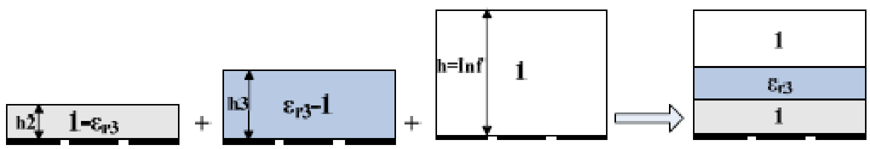

Figure 3: Configuration for partial capacitances for region above CPW.

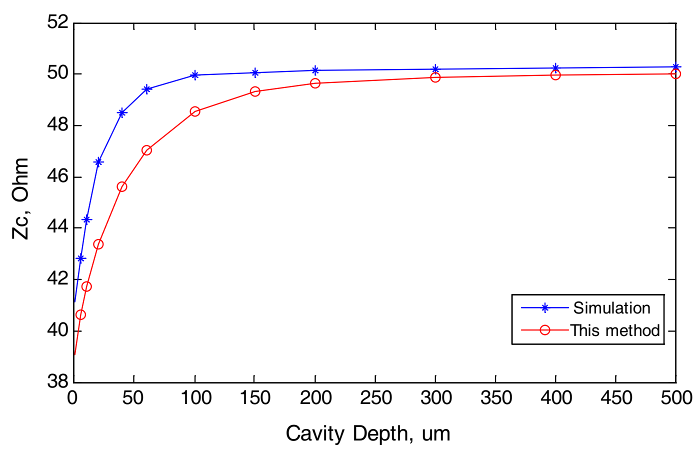

Figure 4: The comparison of analytic results with simulated results.

REFERENCES

1. Lakshminarayanan, B. and G. Rebeiz, "High-power high-reliability sub-microsecond RF MEMS switched capacitors," *IEEE MTT-S International Microwave Symposium Digest*, 1801–1804, 2007.
2. Hou, Z., Z. Liu, and Z. Li, "Al/Au composite membrane bridge DC-contact series RF MEMS switch," *Proceedings of the 2008 9th Conference on Solid-State and Integrated Circuit Technology*, 2488–2491, 2008.
3. Gevorgian, S., L. J. P. Linner, and E. L. Kollberg, "CAD models for shielded multilayered CPW," *IEEE Trans. Microwave Theory Tech.*, Vol. 43, No. 4, 772–779, 1995.

Compact UWB L and C-shaped Resonator of PCML Bandpass Filter

J. Marimuthu and M. Esa
Faculty of Electrical Engineering, Universiti Teknologi Malaysia, UTM Skudai, Johor 81310, Malaysia

Abstract— A novel ultra-wideband (UWB) bandpass filter with four resonant modes is proposed based on parallel coupled microstrip line (PCML) with L and C-shaped resonators. The coupling factor of PCML structure depends on impedance of feeding network. PCML coupling factor can be enhanced by using feeding network with smaller characteristics impedance. With an L-shaped feeding network and C-shaped middle microstrip line a non-uniform resonator is constructed with the first two resonant modes falling within the UWB. The other two resonant modes within UWB can be obtained by adjusting the width of both L and C-shaped resonators. Overall the designed filter exhibits good UWB passband behavior with insertion loss < -0.2 dB and group delay < 0.15 ns.

In recent years, significant research activities using ultra-wideband (3.1–10.6 GHz) related applications have been carried out. UWB is a radio communications technology that promises very high data rates over short distances. Although the concept has been around since the early 1970s, recent advances in semiconductor and radio communication technology have made UWB devices a reality. UWB bandpass filter is one of the key passive components in UWB radio communication system. Various type of UWB bandpass filter has been reported with 110% fractional bandwidth at the center frequency of 6.85 GHz.

In this paper, we proposed an improved and reduced size of UWB bandpass filter based on PCML structure with L and C-shaped resonator. Non-uniform transmission line resonator was designed with three different sections. The filter is composed of a pair of tight PCML structure, high impedance C-shaped resonator between the PCML structure as a middle resonator and two sides of low impedance L-shaped resonator as a feeding network. We found that, the PCML coupling factor not only depend on the strips and slots width but also to the finishing impedance of the network. PCML structure with strips of broader width and slots of narrower width can produce almost constant coupling factor over broader bandwidth. The respective coupling factor can be further enhanced by using a C-shaped resonator with low impedance. By selecting a proper tight PCML structure with L and C-shaped resonator a UWB bandpass filter with good passband response over wide band can be achieved. Details of the UWB filter design are presented and measured results are given to demonstrate the performance of the proposed filter.

Compact Dual Broadband Ladder PCML Filter with Rectangular Resonators

J. Marimuthu and M. Esa
Faculty of Electrical Engineering, Universiti Teknologi Malaysia, UTM Skudai, Johor 81310, Malaysia

Abstract— A simple configuration of dual broadband parallel coupled microstrip line (PCML) bandpass filter with rectangular resonators operating at 2.65 GHz and 7.85 GHz frequency bands with wide stopband design is presented. The proposed filter is composed of a pair of high coupling factor PCML structure, low impedance rectangular resonators as a middle resonator and a feeding network. Overall the simulated and measured results of insertion and return loss show good agreement with BW = 1.8 GHz (85%), $|S_{11}| < -12$ dB, $|S_{21}| > -0.3$ dB at 2.65 GHz and BW = 1.8 GHz (25%), $|S_{11}| < -10$ dB, $|S_{21}| > -0.5$ dB at 7.85 GHz with overall stopband of 5.2 GHz.

In recent years, dual-band bandpass filter has been receiving a great interest in the design of advanced wireless communication system. Various types of dual band bandpass filter have been proposed for narrow band applications.

In this paper, a simple dual broadband bandpass filter is proposed. The proposed filter is composed of a pair of high coupling factor PCML structure, low impedance rectangular resonators as a middle resonator and a feeding network. The middle resonator and feeding network width and length was adjusted accordingly to improve the insertion loss, return loss and harmonic suppression at both operating frequency in order to achieve dual band. The middle resonator and input output feeding network width was adjusted to improve the insertion loss and return loss performance of dual passband response. The length of the middle resonator was adjusted for harmonic cancellation by transmission zero frequency. Details of the dual broadband filter design are presented and measured results are given to demonstrate the performance of the proposed filter.

A simple PCML structure was designed to investigate the dual band performance with respect to feeding network width. The physical parameters of PCML as strip and slots widths $w_1 = 0.6$ mm, $s_1 = 0.2$ mm and the length $l_1 = 14$ mm ($\approx \lambda/4$ at 2.65 GHz). The PCML feeding network of fixed length $l_o = 4$ mm, width was adjusted accordingly to investigate the overall coupling factor at both band. The design was constructed on a substrate with the relative permitivity $\varepsilon_r = 6.15$ and the thickness $h = 1.27$ mm.

Session 3A10
Advanced Photonics-based Devices for Telecom Systems

TCAD and ECAD Modeling of Microwave and Millimeter Wave Photonic Devices

Mikhail E. Belkin
Moscow State Technical University of Radio-Engineering, Electronics and Automation
Moscow, Russian Federation

Abstract— At present time a computer-aided design (CAD) system usage for innovative high-tech production R&D acceleration is a common way [1]. This is especially important for microwave and millimeter wave semiconductor components with measurement equipment and experimental work's cost being considerably more expensive compare to that in lower frequency bands. As a feasible tool for the device structural, electrical DC and small-signal frequency characteristics analysis and optimization a technology CAD (TCAD) simulation is usually considered [2]. To our knowledge today there is no a special TCAD program for microwave photonic devices simulating but this is possible in some multipurpose TCAD programming environments, e.g., Synopsys Sentaurus TCAD. However, updating TCAD tools are unusable for a simulation of distributed-configuration nonlinear microwave electrical circuits that precede laser and follow photodetector chips in real transmitter or receiver module (e.g., LC package parasitics, matching networks, driver, front-end amplifier). Fortunately, a circuit designer could accurately account these circuits' effects with a modern microwave electronic CAD (ECAD) tool [1], e.g., AWR Microwave Office or Agilent ADS.

Therefore, based on the above methodology, one can realize end-to-end computer-aided design of a laser, photodiode, and optical transmitter, receiver or transceiver modules with microwave and millimeter wave bandwidths. Also the above approach is corrected and usefull for different microwave optoelectronic hybrid and monolithic integrated circuits design.

The paper describes the TCAD&ECAD design procedure and experimental verification results of laser modules with the 50-mW average power and direct modulation bandwidth of 10 and 15 GHz and pin-photodiode and optical receiver modules with bandwidth of 30 GHz for the promising Passive Optical Networks (PON) and Radio-over-Fiber (RoF) systems.

REFERENCES

1. Blakey, P. A., "Technology CAD," *RF and Microwave Circuits, Measurements, and Modeling*, 34-1–34-11, Editor-in-Chief M. Golio., CRC Press, 2008.
2. Minixhofer, R., "TCAD as an integral part of the semiconductor manufacturing environment," *2006 International Conference on Simulation of Semiconductor Processes and Devices, SISPAD*, 9–16, Sept. 2006.

Smooth Functional for Optimization of Peak to Average Ratio

D. A. Shapiro[1] **and A. I. Latkin**[2]

[1]Institute of Automation and Electrometry, Siberian Branch, Russian Academy of Sciences
1 Koptjug Ave, Novosibirsk 630090, Russia
[2]Novosibirsk State University, 2 Pirogov Str., Novosibirsk 630090, Russia

Abstract— The biquadratic functional is proposed for optimizing the sampling functional. Its minimum is compared with mini-max profiles calculated numerically.

Minimizing of the crest factor for multitone signals is an important problem known for a long time [1]. Optimization of optical comb filters based on fiber Bragg grating put in the forefront this problem [2].

The maximum absolute value of sampling functional

$$S(z;\varphi_1,\ldots,\varphi_N)=\sum_{l=1}^{N}\exp[i(l-1)x+i\varphi_l], \tag{1}$$

where $x=\Delta kz$ is the dimensionless coordinate z, Δk is the distance between the channels, N is the number of channels, should be minimized with respect to phases φ_l. Kolossovski et al. [3] suggested the functional approach. Functional $\langle|S|\rangle$ of phases is minimized, then its minimum is exploited for numerical calculation of the mini-max value.

In the present report we propose to refine the approach, changing the functional by

$$X(\varphi_1,\ldots,\varphi_N)=\frac{\langle|S|^4\rangle}{N^2}-1=\frac{2}{N^2}\sum_{l=1}^{N-1}|c_p|^2,\quad c_p=\sum_{l=1}^{N-p}\exp(i\varphi_{l+p}-i\varphi_l). \tag{2}$$

The absolute value of sampling functional and results of its further minimization obtained by Powell-Brent method are shown in Fig. 1. Plots demonstrate that the minimum of functional X is very close to min-max. At high number of channels the proposed functional is shown to be a good starting point for subsequent numerical procedure. The advantage of X is smooth φ-dependence even under small number N.

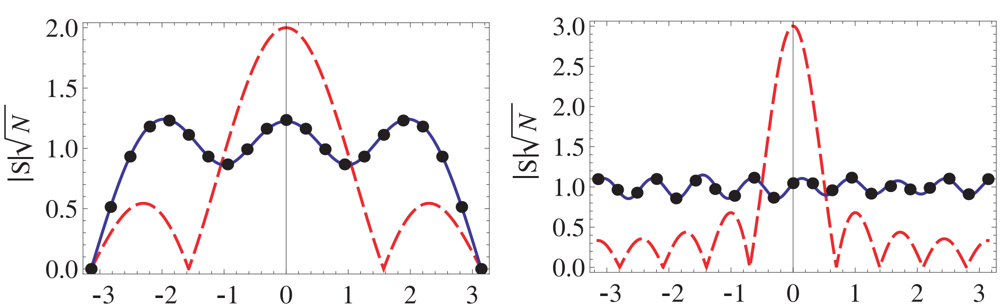

Figure 1: Left: Profiles $|S(x)|/\sqrt{N}$ at $N=4$ corresponding to the minimum X (solid), to the mini-max strategy (dots) and absence of dephasing (dashed). Right: The same for $N=9$ channels.

REFERENCES

1. Friese, M., "Multitone signals with low crest factor," *IEEE Trans. on Comm.*, Vol. 45, No. 10, 1338–1244, 1997.
2. Al-Marzoug, S. M. and R. J. W. Hodgson, "Luus-Jaakola optimization procedure for phase-only sampled-fiber Bragg gratings," *Appl. Opt.*, Vol. 47, No. 13, 2275–2280, 2008.
3. Kolossovski, K. Y., R. A. Sammut, A. V. Buryak, and D. Y. Stepanov, "Three-step design optimization for multi-channel fibre Bragg gratings," *Optics Express*, Vol. 11, No. 9, 1029–1038, 2003.

Femtosecond Laser Pulses Propagation in Silicon-based Planar Waveguide Structures

A. V. Chetvertukhin[1], **A. A. Grunin**[1], **E. V. Drynkina**[1], **M.-H. Hong**[2], **and A. A. Fedyanin**[1]

[1]Faculty of Physics, Lomonosov Moscow State University, Russia
[2]Department of Electrical and Computer Engineering
National University of Singapore, Singapore

Abstract— The study of femtosecond laser pulses propagation in photonic crystal waveguide structures is an important topic in modern nanophotonics since creating photonic devices is expected to be able controlling the light signal on silicon chip. Two-dimensional photonic crystals which represent themselves a 2D-array of nanoholes with subwavelength period allow the control a lateral propagation of light by effect of photonic band gap. Combination of 2D photonic crystal with single-mode planar waveguide leads to full three-dimensional control of light propagation. It is a very important to optimize photonic crystal parameters to obtain a lossless propagation and minimizing the reflection in nodes of waveguide structure as well as compensating the dispersion of different frequency components within femtosecond laser pulse. This paper is devoted to design, numerical optimization and fabrication of silicon-based planar waveguides microstructures. At the first step, parameters of photonic crystal waveguide structure are numerically optimized using FDTD simulation method. Optimal structures of photonic crystal waveguide, Y-connectors and Mach-Zehnder interferometer consisting of two Y-connectors are found for femtosecond laser pulses with central wavelength of 1.55 microns. Another important problem solved is optimization of coupling of femtosecond light signal to two-dimensional photonic crystal waveguide slab utilizing the silicon film with thickness of half of a wavelength as waveguide by using diffraction grating coupling method. Optimal configuration implies the use of diffraction maximum and guide mode of the slab. For this purpose diffraction gold grating couplers are designed and numerically optimized using eigenmodes expansion method. The samples of silicon-based planar waveguide structures are fabricated by e-beam-sputtering of silicon onto fused quartz substrate for creating the silicon waveguides optimized for 1.55 microns. Gold grating couplers are fabricated using UV-photolithography and characterized using optical, scanning electron and atomic force-microscopy.

Linear Dichroism and Birefringence in Anisotropic Plasmonic Metamaterials

M. R. Shcherbakov[1], P. P. Vabishchevich[1], M. I. Dobynde[1], A. S. Sigov[2], A. A. Zaitsev[2], and A. A. Fedyanin[1]

[1]Faculty of Physics, Lomonosov Moscow State University, Russia
[2]Moscow Institute for Radioengineering, Electronics and Automation, Moscow, Russia

Abstract— Plasmonics is a vastly growing area of optics and condensed matter physics which opens new ways of subwavelength information transmission and processing. Not being restricted by diffraction limit, plasmonic devices are able to couple, decouple and convert radiation at sub-micron scales. Plasmon-active structures usually represent nanostructured films of noble metals which gain optical properties not observable for bulk metallic medium due to their subwavelength patterning. These artificial composite materials are usually referred to as so-called metamaterials. It was shown recently that depending on their geometry metamaterials possess unique optical properties from extraordinary optical transmission [1] to negative refraction [2], optical cloaking [3] and superlens [4].

Along with previously reported plasmonic metamaterials anisotropic transmission and their ability to convert polarization and depolarize light [5] wavelength-dependent linear birefringence and dichroism of such media are reported. Two samples of plasmonic metamaterials are considered. The first one is a square 400 nm period array of rectangular holes with sides of 100 and 300 nm etched in a 150 nm thick silver film using focused ion beam lithography. The second one consists of golden stripes of 130 nm width and 30 nm height deposited onto quartz substrate via electron beam lithography and having 330 nm period. Visible and near-IR spectropolarimetry at normal incidence demonstrated strong dependence of birefringence and dichroism on the radiation wavelength reaching 2.5 ± 0.1 and 2.7 ± 0.1 respectively for golden sample. Crucial role of plasmonic resonance in the mechanism of polarization transformation in metamaterials is also emphasized on.

REFERENCES

1. Ebbesen, T. W., et al., *Nature*, Vol. 391, 667, London, 1998.
2. Shalaev, V. M., *Nature Photonics*, Vol. 1, 41, 2007.
3. Pendry, J. B., et al., *Science*, Vol. 312, 1780, 2006.
4. Pendry, J. B., *Phys. Rev. Lett.*, Vol. 85, 3966, 2000.
5. Gordon, R., et al., *Phys. Rev. Lett.*, Vol. 92, 037401, 2004.

Advanced Applications of Fiber Bragg Gratings for Telecom Systems

R. N. Nogueira, M. V. Drummond, C. Marques, R. Monteiro, A. Albuquerque, A. Teixeira, P. S. Andre, and J. F. Rocha
Instituto de Telecomunicações, Campus de Santiago, Aveiro 3810-193, Portugal

Abstract— The increasing information traffic, driven by the new technologies which have risen in the last decade, is accelerating the renewing process of the current fiber optic communication systems. In this way, it is important to have technologies that allow a smooth transition to higher capacity systems, with increased bit rate and better spectral efficiency. One of the challenges in this transition is related to the necessity of having low-cost components and new techniques for all-optical processing of optical signals. That would avoid the constrains associated with optical-electrical-optical conversions, especially at high bit rates ($> 10\,\mathrm{Gbit/s}$). Among the different technologies available today, fiber Bragg gratings (FBG) are a quite interesting passive device for performing all-optical signal processing. An FBG is a submicrometer perturbation of the refractive index of the core of an optical fiber and can be produced by irradiating a photosensitive fiber with an UV laser. The advantages of FBG include passive operation, reduced dimensions and the possibility to custom design the transfer function. The applications in telecom systems are vast and include optical filtering and dispersion compensation as the most common. However, in the recent years, newer applications have arise such as all-optical clock recovery, polarization mode dispersion (PMD) compensation, pulse shaping, gating or coding/decoding in optical code division multiplexing systems (OCDMA). In this paper, we will show new applications for telecom systems, based on special FBG, developed by our group. Two kind of grating were produced: FBG written in highly birefringent fibers for advanced polarization processing in applications such as wavelength conversion, OCDMA or PMD compensation and superstructured FBG for clock recovery at ultra high bit rates. The results show the feasibility of using these special FBGs in advanced applications for optical communication systems.

Microwave vs Optical Injection-locked Devices Comparison

Mikhail E. Belkin and Alexey Loparev
Moscow State Technical University of Radio-Engineering, Electronics and Automation
Moscow, Russian Federation

Abstract— The basic theoretical principles of injection locking to be concurrently corrected for microwave and optical active devices are discussed. Realistic analyzing techniques for injection-locked microwave transistor oscillators and semiconductor laser oscillators are investigated. Namely, in former the locking phenomena result in transformation of the nonlinear negative resistance therefore, wave approach and Kirchgoff rules are usually in practice. On the contrary under optical outer injection the optical gain rate and carrier and photon lifetimes of the locked laser are changed therefore the simulating techniques in the temporary realm using nonlinear differential equations system are more convenient.

During the current status of recent experimental works reviewing it is noted that the major goals of injection-locked microwave oscillators were in high-fidelity steady-state mode and frequency stability securing of high power devices so as the power and high-stability HEMT-based synthesized microwave oscillators become available needs in injection locking are substantially weaken. In spite of that optical injection locking is able to perfect a lot of keyed parameters of modern semiconductor laser to be suffer from such as direct-modulation bandwidth, RIN, nonlinearity, total link gain. This fact predetermines their updating impetuous development.

Switchable Nonlinear Metalloferroelectric Photonic Crystals

N. Ilyin[1], **N. Sherstyuk**[1], **E. Mishina**[1], **and V. Muhortov**[2]

[1]Moscow State Institute of Radioengineereing, Electronics and Automation (Technical University)
Prospect Vernadskogo 78, Moscow 119454, Russia
[2]South Center of Russian Academy of Science, Rostov-on-Don 344006, Russia

Abstract— Photonic crystals (PhCs) are essential ingredient for the miniaturization of photonic components and the development of monolithic photonic integrated circuits. Typical integrated systems will include passive and active two dimensional (2D) photonic elements: waveguides, switches, multiplexers, and demultiplexers. Active elements imply tunability or switchability. Tuning of 2D photonic crystals is possible through the temperature dependence of the refractive index or the electro-optical effect.

Although $LiNbO_3$ ultrafast electro-optical modulaters were proposed recently, the advantage of $BaSrTiO_3$ (BST) over $LiNbO_3$ was demonstrated. Contrary to $LiNbO_3$, BST is well compatible with planar technology and integration and possesses ultrafast low-voltage in-plane switching accompanied by very high nonlinear susceptibilities. This is why BST is very attractive to be used as a basis for switchable nonlinear photonic crystals.

Here we report the fabrication and demonstration of two types of nonlinear switchable photonic crystals based on thin BST ferroelectric films. These photonic crystals allow to control the direction of second harmonic generated (SHG) light propagation by applying low voltages to the system.

Two types of low-voltage electroswitchable nonlinear photonic crystals were fabricated providing spatial-frequency control of second harmonic generation radiation of visible light. A two-dimensional photonic crystal was fabricated by focused ion beam etching of a ferroelectric $BaSrTiO_3$ thin film and switched by an electric field applied by an interdigital electrode system, which simultaneously acted as a one-dimensional photonic crystal. The fabricated device operates at a second harmonic wavelength in the range of 350–500 nm in diffraction geometry which allows spatio-spectral electro-swhitching. The switching efficiency depends on the wavelength: the highest value was about 30.

Based on these results two types of electrooptical devices are suggested: spatio-spectral switch and electro-optical modulator.

Two-photon Autocorrelation in a MQW GaAs Laser at 1.55 μm

D. Duchesne[1], **L. Razzari**[1,2], **L. Halloran**[1], **M. Giguère**[1], **F. Légaré**[1],
R. Morandotti[1], **A. J. SpringThorpe**[3], **D. N. Christodoulides**[4], **and D. J. Moss**[1,5]

[1]INRS-EMT, Varennes, Qubec, Canada
[2]Dipartimento di Elettronica, Università di Pavia, Pavia, Italy
[3]Canadian Photonics Fabrication Centre (CPFC), National Research Council
Ottawa, Ontario, Canada
[4]College of Optics and Photonics, CREOL & FPCE, University of Central Florida
Orlando, USA
[5]IPOS/CUDOS, School of Physics, University of Sydney, Sydney, Australia

Abstract— Current all-optical techniques used to measure ultra-short optical pulse durations and profiles in the picosecond regime typically rely on temporal or frequency mapping methods employing nonlinear effects, such as FROG, SPIDER and most commonly simple cross and auto-correlations based on second harmonic generation. Unfortunately, these techniques are often bulky and difficult to implement in an integrated format. As an alternative, two-photon detectors were developed and experienced a great deal of interest in the 1990s as efficient measurement tools for sub-picosecond pulses. However, research in this area tapered off around 8 to 10 years ago, paradoxically just as interest in all-optical signal processing gained significant momentum. Today, information processing in the optical domain has the potentiality of greatly reducing the size, cost, energy consumption as well as increasing the speed of network components and routers for ultrahigh bandwidth telecommunications systems at 1550 nm [1]. Twophoton absorption (TPA) detectors have been shown to be ideal for optical time division multiplexing [1], optical performance monitoring [2], switching [3], and for optical thresholding devices in code division multiple access (CDMA) systems [4]. However, despite the volume of work on TPA detectors in the 1990s, as well as concurrent work on linear quantum well optoelectronic devices, comparatively little has been done on GaAs Multiple Quantum Well (MQW) waveguides in terms of their potential use as TPA detectors at 1.55 μm. While TPA photocurrent in a MQW AlGaAs waveguide has been explored, it was either in a limited context to assess the quality factor for alloptical switching [5], or for applications in the mid-infrared [6]. Given the surge in activity in all-optical signal processing in the last 6 to 8 years [1, 2] it is of significant interest to see whether the enhanced performance of the linear GaAs/AlGaAs MQW optoelectronic devices developed in the 1990s [7, 8] for operation at ∼775 nm also translate into improved performance for nonlinear operation at 1550 nm (near the half-bandgap). Here, we report two-photon photocurrent at 1550 nm in a (reverse biased) GaAs/AlGaAs quantum well laser [7–9], designed to achieve efficient multifunctional (laser, electroabsorption modulator, photodetector) performance at 850 nm, as well as new results demonstrating performance as an auto-correlator of sub-picosecond optical pulses. Our device displays several advantages as a nonlinear photodetector such as improved quantum efficiency, high speed operation, and negligible saturation effects at high intensities due to carrier pileup effects. Because these components operate efficiently both as reverse-biased electroabsorption modulators and two-photon detectors, they raise the prospect of being able to electrically modulate the TPA coefficient and hence the nonlinear figure of merit (FOM) at 1550 nm via the quantum confined Stark Effect, as well as possibly the ability to generate two-photon entangled pairs [10].

REFERENCES

1. Dorrer, C., "High-speed measurements for optical telecommunication systems," *IEEE J. Sel. Top. Quant. Elect.*, Vol. 12, 843, 2006.
2. Wielandy, S., M. Fishteyn, and B. Zhu, "Optical performance monitoring using nonlinear detection," *J. Lightw. Tech.*, Vol. 22, 784, 2004.
3. Tsang, H. K., R. S. Grant, R. V. Penty, I. H. White, J. B. D. Soole, E. Colas, H. P. Leblanc, N. C. Andreadakis, M. S. Kims, and W. Sibbett, "GaAs/GaAlAs multiquantum well waveguides for all-optical switching at 1.55 μm," *Electr. Lett.*, Vol. 27, 1993, 1991.
4. Zheng, Z., A. M. Weiner, J. H. Marsh, and M. M. Karkhanehchi, "Ultrafast optical thresholding based on two-photon absorption GaAs waveguide photodetectors," *IEEE Photon. Tech. Lett.*, Vol. 9, 493, 1997.
5. Laughton, F. R., J. H. Marsh, and A. H. Kean, "Very sensitive two-photon absorption GaAs/AlGaAs waveguide detector for an autocorrelator," *Electr. Lett.*, Vol. 28, 1663, 1992.

6. Schneider, H., T. Maier, H. C. Liu, and M. Walther, "Two-photon photocurrent autocorrelation using intersubband transitions at nearly-resonant excitation," *Optics Express*, Vol. 16, 1523, 2008.
7. Moss, D. J., D. Landheer, D. Halliday, S. Charbonneau, F. Chatenoud, and D. Conn, "High speed photodetection in a reverse biased GaAs/AlGaAs GRINSCH SQW laser structure," *Phot. Tech. Lett.*, Vol. 4, 609, 1992.
8. Moss, D. J., D. Landheer, A. Delage, F. Chatenoud, and M. Dion, "Laser compatible waveguide electroabsorption modulator with high contrast and low operating voltage in GaAs/AlGaAs," *IEEE Photon. Tech. Lett.*, Vol. 3, 645, 1991.
9. Duchesne, D., L. Razzari, L. Halloran, R. Morandotti, A. J. Springthorpe, D. N. Christodoulides, and D. J. Moss, "Two-photon photodetector in a MQW GaAs laser structure at 1.55 μm," *Optics Express*, Vol. 17, 5298, 2009.
10. Van Driel, H. M., "Semiconductor optics — On the path to entanglement," *Nature Photonics*, Vol. 2, 212, 2008.

Session 3P1
Synthetic Aperture Radar (SAR) Satellite Status and Evolution

CONAE's SAR Missions Overview

L. A. Frulla, G. Rodríguez Ortega, and J. A. Milovich
CONAE, Av. Paseo Colon 751, 1063 Buenos Aires, Argentina

Abstract— The National Commission on Space Activities of Argentina (CONAE, *Comisión Nacional de Actividades Espaciales*), as a specialized agency, has been explicitly enacted by the national legislation, in order to propose and execute a National Space Program for peaceful use of space science and technology. In this frame, and considering the Argentinean user needs obtained from national user consultations, CONAE took the drivers to conceive SAOCOM satellites series as end-to-end Earth Observation Systems dedicated to the remote sensing and data exploitation for enhancing socioeconomic activities and performing scientific studies.

The first constellation of the SAOCOM series is the SAOCOM 1 constellation which consists of SAOCOM 1A and SAOCOM 1B satellites. They are presently under development and it is foreseen to be launched during 2012, with an estimated lifetime of at minimum 5 years each. Each satellite will provide global coverage and a repeat cycle of 16 days, with 8 days for the whole constellation. SAOCOM 1A and SAOCOM 1B share the same technical and operative design requirements, and are being developed simultaneously, carrying each one, a polarimetric L-band SAR as a main payload.

The two SAOCOM satellites integrate the SIASGE constellation (Italo-Argentine Satellite System for Emergency Management) implemented jointly by CONAE and the Italian Space Agency (ASI, *Agenzia Spaziale Italiana*). This System consists of the Argentinean SAOCOM 1 constellation and the Italian COSMO-SkyMed constellation composed of four satellites carrying each one, an X-band SAR as a main payload.

As starting point and with the aim of learning in advance about the technological aspects and the use of this kind of information, CONAE has developed an L-band polarimetric instrument called SARAT (Airborne Synthetic Aperture Radar).

The present paper is particularly dedicated to SAOCOM 1 mission with the following general objectives:

- To provide all weather, day/night polarimetric L-Band SAR information, and
- to satisfy most of the applications considered in the Argentinean National Space Program, involving studies on agriculture, fishing, forestry, weather, hydrology, oceanography, emergencies, natural resources of land and sea, urban areas, cartography, geology, mining, soil exploitation, archeology and health. Emergencies, such as floods, droughts, desertification, landslides, oil slicks in land and ocean, fires, seismology, earthquake activity and volcanism, are mainly considered.

Finally, the SAOCOM Mission main drivers are:

- To develop soil moisture map products for giving support to agricultural, hydrological and health applications, and emergencies in general.
- To develop SAR interferometric techniques for collaborating with the development of the different applications above mentioned.

The presentation will provide the present status of the mission, a description of its capabilities, the potential applications and products that are expected to be derived, and the corresponding algorithm developments involved.

Achievements and Perspectives of the COSMO-SkyMed Mission

Giovanni Valentini, **Fabrizio Battazza**, **Alessandro Coletta**, **Fabio Covello**, **and Gemma Manoni**
ASI — Italian Space Agency, Viale Liegi 26, Rome I-00198, Italy

Abstract— In 2007 and 2008 ASI (Agenzia Spaziale Italiana/Italian Space Agency) launched three out of four X-band SAR satellites of the COSMO-SkyMed (COnstellation of small Satellites for Mediterranean basin Observation) Mission, making available to the users a unique SAR constellation dedicated to the Earth Observation.

The constellation will be completed with the launch of the forth satellites in the first half of 2010. COSMO-SkyMed is the largest Italian investment in Space Systems for Earth Observation, commissioned and funded by Italian Space Agency (ASI) and Italian Ministry of Defense (MoD). COSMO-SkyMed is a Dual-Use (Civilian and Defence) end-to-end Earth Observation System aimed to establish a global service supplying provision of data, products and services relevant to a wide range of applications, such as Risk Management, Scientific and Commercial Applications and Defence/Intelligence Applications.

The system consists of a constellation of four Low Earth Orbit mid-sized satellites, each equipped with a multi-mode high-resolution Synthetic Aperture Radar (SAR) operating at X-band. The system is completed by dedicated full featured Ground infrastructures for managing the constellation and granting ad-hoc services for collection, archiving and distribution of acquired remote sensing data.

The first and second COSMO-SkyMed satellites are in the operational phase while the third one is completing its commissioning phase.

The results coming from the utilisation of the two first satellites, after the first year of life, revealing an excellent performance of the X-band SAR and the importance of a fast response time in several application as risk and emergency management (i.e., China's earthquake, Myanmar and Haiti flood), ice monitoring (reduction of the glaciers, Wilkins Ice Shelf disintegration), multi-temporal acquisition for agriculture monitoring, ship detection, interferometry, landslides monitoring, maritime surveillance and security, rapid mapping.

A further step forward will be realised when COSMO-SkyMed 3 will be operative, since the third satellite is positioned in the so-called "one-day interferometry configuration", it will allow the constellation to detect interferometric acquisitions with a de-correlation time equal to one day.

The first COSMO-SkyMed Announcement of Opportunity for scientific data exploitation will give the chance to achieve innovative and valuable results using the COSMO-SkyMed data, products and services.

The Overview of the L-band SAR Onboard ALOS-2

Yukihiro Kankaku, **Yuji Osawa**, **Shinichi Suzuki**, and **Tomohiro Watanabe**
JAXA, Japan

Abstract— JAXA has been operating the Advanced Land Observing Satellite (ALOS) "Daichi" since January 2006. The PALSAR onboard ALOS is the L-band Synthetic Aperture Radar (SAR) to observe large area by electronic beam steering with active phased array antenna (APAA) technology, and has the full-polarimetric measurement capability first in the world. The L-band microwave can penetrate leaves and grasses to measure the ground directly. By this unique characteristic, PALSAR has been used for monitoring the world forest, the polar ice and the crustal movements and so on. Especially PALSAR has contributed to domestic and international disaster management activities by its interferometry capability (INSAR) with high coherence. ALOS has completed nominal three years mission life and continues to work. "ALOS-2" is the satellite carrying an L-band SAR succeeding to PALSAR.

The L-band SAR onboard ALOS-2 has higher resolution, better noise equivalent sigma zero (NESZ), and higher signal to ambiguity ratio (S/A) than PALSAR in order to meet the requirements for disaster monitoring. To realize these requirements. the new technologies have been adopted: the maximum bandwidth allocation for L-band SAR and the spotlight mode with APAA for high resolution, the development of high power and efficient device for high NESZ, and chirp modulation technique for high S/A. In addition, very accurate orbit control (orbital tube $< 500\,\mathrm{m}$) and short repeat-pass orbit (14 days) achieve the higher coherence of INSAR both between stripmap modes and between ScanSAR modes.

This paper introduces the overview of the L-band SAR onboard ALOS-2 as the post-ALOS mission.

The RADARSAT Constellation Concept

Guy Séguin and Jérôme Colinas
Canadian Space Agency, Space Technologies/Spacecraft Payloads
6767, route de l' Aeroport, Saint-Hubert (Quebec), J3Y 8Y9, Canada

Abstract— The Canadian Space Agency (CSA) is currently developing a C-band SAR satellite constellation referred to as RADARSAT Constellation Mission (RCM) as follow-on project to the RADARSAT-2 program.

The concept involves three satellites. This is to provide operationally SAR imagery for key maritime surveillance applications such as ship detection, oil spill monitoring, and sea ice mapping. Other applications focus on disaster management and SAR interferometry (InSAR) coherent change detection of land surfaces for geohazards, climate change, and environment monitoring.

The SAR satellites will operate in two principle modes: a wide-area ScanSAR and a high-resolution strip-map mode. The wide-area ScanSAR mode with a swath width of 350 km and a 4-look medium resolution of 50 m will be used specifically for maritime surveillance and sea ice monitoring. The high-resolution mode with a 1-look spatial resolution of 3 m is intended for specific on-demand imagery acquisitions.

The orbital configuration of the constellation is such that the satellites fly in the same orbital plane, following each other with a time separation of ~ 32 min. While the ground track of each satellite is slightly shifted due to the Earth rotation, it provides combined ground coverage of up to 1000 km using the medium resolution ScanSAR mode.

The preliminary configuration concept envisages a 12-day repeat orbit cycle for each satellite with the goal to maintain its orbit within an orbital tube on the order of 100–200 m in diameter with respect to other satellites in the constellation. Using data from these different satellites, this allows the formation of SAR interferometry scene pairs having 4-day time interval.

This configuration enables a frequent monitoring of areas affected by geohazards, climate change related processes, and man-made activities by using SAR interferometry techniques. The relative short time interval between SAR data acquisitions minimizes temporal decorrelation effects. Also, small interferometric baselines will support the measurement of ice velocities and small-scale surface deformation caused by tectonic processes, volcanic activities, landslides, and subsidence.

The constellation will use much smaller and lighter satellite than the previous RADARSAT mission with imaging capability distributed on the three satellites. The cost will be similar to the cost of the RADARSAT-1 program. The presentation will provide an overview of the overall concept of the RADARSAT Constellation satellites.

RADARSAT Constellation Antenna Design and Performance

J. Colinas, **P. Plourde**, and **M. Lapointe**
Canadian Space Agency, 6767 route de l'aéroport, Saint-Hubert, QC, J3Y 8Y9, Canada

Abstract— The RADARSAT Constellation Mission (RCM) will consist of a constellation of three satellites that will ensure C-band data continuity with RADARSAT-2. The phase A was completed successfully and the phase B is currently ongoing. The first satellite is scheduled to enter in operation toward the end of the RADARSAT-2 mission, for a gradual implementation of the constellation between 2014 and 2016. RCM is designed to improve significantly the availability of SAR data for main Canadian Government departments, the main applications areas being maritime surveillance, ecosystem monitoring and disaster management. An important constraint on the mission was to reduce significantly the overall mission cost (spacecraft fabrication cost and launching cost), while meeting requirements similar to RADARSAT-2. This paper presents the main mission requirements as well as a trade-off analysis by comparing different antenna sizes and their respective performances. The different antenna sizes and aspect-ratios lead to technical challenges, such as meeting the RF performances, decreasing the deployment complexity, the mass and fitting within the fairing envelope.

Requirements of C-Band data continuity imposed the central frequency of 5.405 GHz, a bandwidth of 100 MHz, a NESZ better than −22 dB and total ambiguity level below −16.5 dB. The coverage requirements for ice, ship and oil slick detection required that the payload can provide a compromise mode with a resolution of 50 m and four looks. An imaging swath of about 1000 km is required to cover Canada's maritime areas. A constellation of three satellites located at approximately 600 km and equally spaced along the orbiting plane, each having an imaging swath of 350 km was selected to fulfill this coverage requirement. Moreover, an access swath requirement of 500 km was set in order to obtain an average daily access over the globe. An additional access swath of 100 km was also defined but the ambiguity requirements are not enforced over that area. To ease up the selection of imaging areas, a requirement was made to provide four 350-km imaging swaths over the 600 km accessible area.

Various antenna sizes fitting within the fairing envelope while meeting the RF performances were studied in Phase A and revisited at the beginning of Phase B to improve the mass margin. Among the options that were studied, two antenna configurations were of special interests: option (1) a 4-panel antenna with an aperture of 6.9×1.4 m and option (2) a 2-panel antenna with an aperture of 9.2×1.0 m. The power and the antenna aperture area are kept equal in both options. So far, option (1) is compliant with the mission imaging requirements but the overall spacecraft envelope and mass makes it difficult to fit in a small low cost launcher such as DNEPR. On the other hand, the configuration of option (2) makes the payload performances incompliant with the 3 m stripmap mode resolution, which requires a NESZ of −17 dB and an integrated ambiguity ratio less than −16.5 dB, but would probably lead to a smaller and lighter folded antenna and is therefore more likely to fit within a small fairing. Option (2) incidentally has an aspect ratio closer to what has been selected for Sentinel-1. With the option (2) though, the requirement for a 3-meter mode can only be met using the spotlight mode, which by definition doesn't offer continuous images along track that were requested by the users. In order to eliminate this non-compliance on option (2), a new beam configuration is presented in this paper, which would offer a continuous image strip and yet comply with the 3-meter resolution stripmap mode requirements.

The standard approach to achieve a 3-meter azimuth resolution with a long and narrow antenna would be to spoil the beam to increase the Doppler bandwidth, which degrades the NESZ and forces the use of a higher PRF. To maintain the same range ambiguities with a higher PRF requires a wider antenna, but this would increase the area and mass. Instead, it is proposed to introduce a new beam consisting in two distinct sliding interleaved spotlight beams. The odd beam is pointing fore and the even beam is pointing aft (transmitter bursts are alternating from fore beam to aft beam and at the same time beam are swept in azimuth) and the PRF is doubled. Both fore and aft beam are swept in azimuth but never cross each other, indeed the separation angle between the fore and aft beam is kept constant along the spot sweeping process. Because fore and aft beams are interleaved and separated in azimuth by a certain angle, both range ambiguities (fore and aft beams are received at different time in range) and azimuth ambiguities are minimized and it is possible to configure the radar system such that total ambiguities and NESZ requirements for the stripmap mode are met. The paper describes the performance of the new beam mode and assesses its compliance to RCM requirements. The new beam mode is not part of RCM design but could be of interest to others systems that have a spotlight capability.

A Novel Approach for Ship Detection by High Resolution Synthetic Aperture Radars

Seong-In Hwang and Kazuo Ouchi
Department of Computer Science, School of Electrical and Computer Engineering
National Defense Academy, 1-10-20 Hashirimizu, Yokosuka, Kanagawa 239-8686, Japan

Abstract— The main purpose of ALOS (Advanced Land Observation Satellite) launched by JAXA (Japan Aerospace Exploration Agency) is land observation. However, it can also be used to monitor ocean surface, and the present article deals with ship detection by PALSAR for for monitoring maritime traffic, fishing control, surveillance of illegally operating boats, and those responsible for oil pollution.

In our previous experiments [1], we deployed 3 small fishing boats whose size are comparable to SAR range resolution in order to test the ship detection ability of PALSAR. Via these experiments, we found out that the MLCC (Multi-Look Cross-Correlation) [2] algorithm is very useful to detect small ships embedded in sea clutter. However, the algorithm has some problems such as low SNR (Signal to Noise Ratio) and high FAR (False Alarm Rate). In this paper, we propose a novel method to improve SNR and FAR in the MLCC method.

The approach is to combine CFAR (Constant False Alarm Rate) [3] and MLCC processing. For CFAR, we first estimated the PDF (Probability Density Function) which fits best to the coherence image after the MLCC by using AIC (Akaike Information Criterion) [4]. Five PDFs were considered, including Weibull distribution, Rayleigh distribution, K-distribution, log-normal distribution and Gamma distribution. The result showed that the coherence image obeys the Gamma distribution. This was re-confirmed by simulation. We then applied CFAR based on the Gamma distribution to the MLCC coherence image in order to improve the SNR.

From our present study, it was found this novel approach can improve the SNR by keeping CFAR at low levels, yielding a high detection probability in the presence of clutter background.

REFERENCES

1. Hwang, S.-I. and K. Ouchi, "Detection of small fishing vessels by ALOS-PALSAR — Comparison of PALSAR modes and algorithms," *IEICE Tech. Rep.*, Vol. 108, No. 76, 35–40, 2008.
2. Ouchi, K. et al., "Ship detection based on coherence images derived from cross-correlation of multilook SAR images," *IEEE Trans. Geosci. Remote Sens. Lett.*, Vol. 1, 184–187, 2004.
3. Sekine, M. and Y. Mao, *Weibull Radar Clutter*, Peter Peregrinus, London, 1990.
4. Akaike, H., "Information theory and an extension of the maximum likelihood principle, " *Proc. 2nd International Symposium on Information Theory*, 267–281, 1973.

Study of Ocean Wave Propagation Direction and Effects of Bottom Topography under Inclement Weather Condition by Multi-look Processed SAR Images Using Weighed Cross-correlation Function

Shunsuke Taniguchi and Kazuo Ouchi
Department of Computer Science, School of Electrical and Computer Engineering
National Defense Academy, 1-10-20 Hashirimizu, Yokosuka, Kanagawa 239-8686, Japan

Abstract— The purpose of this paper is to develop an algorithm to estimate the direction of ocean wave propagation under the inclement weather condition such as typhoons. The algorithm is based on the weighed cross-correlation function of multi-look processed images acquired by SAR (Synthetic Apparture Radar), utilizing the inter-look time difference, and the SAR data used for the study are those of C-band SAR on board of RADARSAT-2 and L-band PALSAR on board of ALOS (Advanced Land Observing Satellite). Although many studies of estimating ocean wave spectra by SAR were reported, a few studies are known on the ocean wave spectra under such inclement weather conditions as typhoons and cyclones. Generally, a standard Fourier transform is used to extract ocean wave spectra from retrieved SAR images. In order to reduce the noise in the wave spectrum, the look-sum method is used, where the wave spectrum is computed by taking a Fourier transform of averaged intensity sub-images; the spectral sum technique is also used, where the averaging is performed on the sub-spectra bases.

These methods enable to reduce speckle noise and improve the estimation of ocean wave spectra, but these techniques yield the wave spectrum with 180° directional ambiguity, and the propagation direction of the dominant wave can not be resolved.

In order to resolve this problem, a method based on the weighed cross-correlation function was proposed [1–3]. This method uses the center time difference between sub-apertures during which the wave field moves with the wave phase velocity. Thus, by applying a weighting function with the expected wave angular frequency to the inter-look cross spectrum, the directional wave spectrum can be derived. The accuracy of this technique is how correctly the weighting function is made. The experimental results, however, showed that the weighting function is robust and does not have to be precise.

By applying this method, we estimate the direction of ocean wave propagation under inclement weather from the RADARSAT-2 and ALOS-PALSAR data. From the estimated directional wave spectra, the effects of wave propagation direction on SAR images and the effects of sea bottom topography [4] are investigated.

REFERENCES

1. Engen, G. and H. Johnsen, "SAR-ocean wave inversion using image cross spectra," *IEEE Trans. Geosci. Remote Sens.*, Vol. 33, 1047–1056, 1995.
2. Ouchi, K., S. Maedoi, and H. Mitsuyasu, "Determination of ocean wave propagation direction by split-look processing using JERS-1 SAR data," *IEEE Trans. Geosci. Remote Sensing*, Vol. 37, 849–855, 1999.
3. Vachon, P. W. and J. C. West, "Spectral estimation techniques for multilook SAR images of ocean waves," *IEEE Trans. Geosci. Remote Sensing*, Vol. 30, 568–577, 1992.
4. Mitsuyasu, H., *Physics of Ocean Waves (in Japanese)*, Iwanami Press Publishing Co., 2002.

Application of PSInSAR for Monitoring Urban Subsidence in Beijing

Hong-Li Zhao[1,2], **Jian-Ping Chen**[1,2], **Xiao-Fang Guo**[3], **and Jing-Hui Fan**[3]

[1]School of the Geosciences and Resources, China University of Geosciences (Beijing)
Beijing 100083, China
[2]Beijing Land Resources Information Development Research Laboratory
Beijing 100083, China
[3]China Aero Geophysical Survey & Remote Sensing Centre for Land & Resources
Beijing 100083, China

Abstract— In many cities all over the world, overexploitation of groundwater, especially the concentrated well fields' pumping, has caused the constant drawdown of the regional groundwater level accompanied with the lacunaris media compact and the land subsidence. To satisfy the water needs of tens of millions of citizens, Beijing, an ever-enlarging, urbanizing city, has had to exploit underground water, which contributes to almost two thirds of the city's life-use water. As a result, subsidence has seriously affected Beijing's city planning and construction, and caused certain damage to city infrastructures, thus bringing harm to citizens' lives and properties. The subsidence monitoring system in Beijing is mainly made up of the monitoring stations, the bedrock bench marks, the layered bench marks, the groundwater level observation wells, the pore-water pressure observation wells, the exterior groundwater observation wells, the GPS monitoring sites and the special monitoring sites.

By the end of 2003, according to the ground monitoring results, five subsidence areas in the Beijing area had been determined, with the biggest one reaching 722 mm, affecting an area of nearly 5,000 km^2. Subsidence at the eastern suburb, such as Changping, Shunyi, Fengtai, Tongzhou and Daxing etc., appeared more serious than other parts in Beijing and was over 1800 km^2.

Although Beijing's subsidence monitoring system is necessary and reliable, its sparse data grid in the area is a limitation which makes it difficult for us to understand the whole deformation field. Spaceborne differential radar interferometry (DInSAR) has proven a remarkable potential for mapping ground deformation phenomena over tens-of-kilometers-wide areas with centimeter-scale accuracy on a more dense space grid and time series. But geometrical and temporal decorrelation factors are important hindrances that prevent DInSAR from being an operational tool for displacement monitoring. Moreover, atmospheric inhomogeneities produce an atmospheric phase screen (APS) on every SAR image, which can contaminate the results of the deformation monitoring.

By identifying temporarily stable natural reflectors or persistent scatterers (PS), Persistent Scatterers InSAR (PSInSAR) technique can overcomes the drawbacks and analyzes this subset of pixels in SAR images, even with long temporal and space baselines, and then detects displacements in urban areas with millimeter accuracy per year. Using ENVISAT ASAR images, we apply this method in the eastern suburb of Beijing to detect the deformation phenomena.

16 ENVISAT ASAR images covering the period from March 2003 to October 2006 have been selected to retrieve the subsidence phenomena in the research area. In the data stack, a master image, which optimizing the distribution of the baselines, is selected and 15 interferometric pairs are generated. The absolute values of perpendicular baselines are less than 1000 m, and the time baselines vary from -630 to 595 d.

During the course of computing the reference phase, i.e., "flat earth phase", the precise DELFT orbits are used. In the process of removing topographic component from the inerferometric images, SRTM DEM data are used. While the orbit data of ENVISAT have been referenced to the WGS84 ellipsoid, the EGM96 geoid has been chosen as the reference for the SRTM DEM height values. So the geoid height in the area has been compensated.

Before selecting the PS candidates (PSC) by analyzing the statistical characteristic of the pixels in the data stack, the 16 ASAR images are all calibrated. By computing the amplitude dispersion index and using a threshold, we can select a part of pixels. However, only using this method, some pixels in water area, whose amplitude values are relatively stable and whose backscattered signals are weak and incoherent, are not properly selected. Using coherence map associated with the interferograms, we set a correlation threshold. Then we pick out some pixels using both the

two thresholds. Because a PS's backscattered signal is relatively strong and may contaminate the phase of its surrounding pixels, we further select PSC with lowest amplitude dispersion index in a cluster of pixels and discard the surrounding pixels.

We triangulate the selected PSC to a grid and the distance of each couple of PSC is less than 1.5 km for retaining the atmosphere correlation. After calculating the phase difference between two neighboring pixels, we estimate the residual elevation difference from a reference pixel, and estimate the mean velocity difference between two neighboring pixels by the 2-d periodogram method. On the sides whose ensemble coherence value above a threshold, the weighted minimum cost flow algorithm is carried out, and the elevation error and the mean velocity of each PSC can be unwrapped with respect to the reference point.

After detrending the phases of the elevation error and the mean velocity from each PSC's differential phases, we estimate the APS superimposed on each image by high-pass filtering the residual phases in time then low-pass filtering in space. By removing all the APS, we identify more PSs and re-estimate the motion of these PSs to recognize the deformation phenomena with respect to the reference point in the research area.

Compared with previous knowledge shown in some published papers, the distribution of the subsidence cone exposed by this research is reliable. As far as the real deformation value is concerned, the deformation estimations derived from our work still need validation and correction by in-situ measurements observed in the research area.

Session 3P2
Light Scattering and Radiative Transfer: Theories and Applications 2

Equations for Electromagnetic Radiation Transfer in Dielectric Random Media with Effects of Near Fields and Opposite Wave Streams' Interference

Yu. N. Barabanenkov[1] **and M. Yu. Barabanenkov**[2]

[1]Institute of Radioengineering and Electronics, Russian Academy of Sciences
Mohovaya 11, 103907 Moscow, GSPC3, Russia
[2]Institute of Microelectronics Technology and High Purity Materials, Russian Academy of Sciences
142432 Chernogolovka, Moscow Region, Russia

Abstract— During the last several years a substantial progress was reached in theoretical study the near field effects in electromagnetic wave multiple scattering by inhomogeneous dielectric media. This progress, having been based on Sommerfeld-Weyl angular spectrum decomposition of wave amplitudes, included in itself the extended unitarity for 2×2 block S-scattering matrix [1, 2], effect of energy emission from evanescent wave at scattering by a dielectric structure [1, 2], and physical mechanism of this emission as consequence of interference between two opposite decaying evanescent wave streams [3]. To study the near field effects in the case of random dielectric media, the Dyson equation in the Bourret approach for the ensemble averaged angular spectrum amplitudes and the Bethe-Salpeter equation in the ladder approximation for the coherence matrix of angular spectrum amplitudes were written in [4, 5], respectively.

In this report we apply the above Dyson and Bethe-Salpeter equations to get a generalization for the phenomenological radiative transfer theory [6] on the case including near fields effects in wave multiple scattering. We derive the four equations' system for two autocoherences of waves propagating forward and backward with respect to embedding parameter into the medium slab and two cross-coherences of evanescent waves decaying in opposite directions. The derived system of equations satisfies to the energy conservation law, with taking into account the energy transformation between propagating and evanescent waves. Having been written in integral form, the derived system of equations satisfies to the given boundary conditions on the slab boundaries.

REFERENCES

1. Gulyaev, Y. V., Y. N. Barabanenkov, M. Y. Barabanenkov, and S. A. Nikitov, *Phys. Lett. A*, Vol. 335, 471–472, 2005.
2. Gulyaev, Y. V., Y. N. Barabanenkov, M. Y. Barabanenkov, and S. A. Nikitov, *Phys. Rev. E*, Vol. 72, 026602-1–026602-12, 2005.
3. Barabanenkov, M. Y., Y. N. Barabanenkov, Y. V. Gulyaev, and S. A. Nikitov, *Phys. Lett. A*, Vol. 364, 421–424, 2007.
4. Barabanenkov, Y. N. and M. Y. Barabanenkov, *Progress In Electromagnetic Research Symposium Abstracts*, 23, Cambridge, Massachusetts, USA, March 26–29, 2006.
5. Barabanenkov, Y. N., and M. Y. Barabanenkov, *Progress In Electromagnetic Research Symposium Abstracts*, 21, Cambridge, Massachusetts, USA, March 26–29, 2006.
6. Chandrasekhar, R., *Radiative Transfer*, Dover, New York, 1960.

Recent Progress in Simulating the Optical Properties of Nonspherical Ice Crystals and Dust Aerosols: Theories and Applications

Ping Yang[1] **and K. N. Liou**[2]

[1]Department of Atmospheric Sciences, Texas A & M University, College Station, TX 77843, USA
[2]Joint Institute for Regional Earth System Science and Engineering and
Department of Atmospheric and Oceanic Sciences
University California, Los Angeles, Los Angeles, CA 90095, USA

Abstract— Determination of the accurate single-scattering properties (extinction efficiency, single-scattering albedo, and phase matrix) of realistic nonspherical and inhomogeneous ice crystals and dust aerosols is fundamental to remote sensing of cirrus clouds and airborne dust, as well as to the study of the radiative and climate forcings of these two types of atmospheric particulates. In the past few years, substantial progress has been made in the study of the scattering and absorption properties of ice crystals and dust particles, including the definition of more realistic particle geometries in single-scattering computations and the improvement of computational accuracy based on the principle of geometric optics (IGOM) for moderate and large size parameters. For example, the edge effect has been included in IGOM to calculate the extinction and absorption efficiencies of nonspherical particles. Moreover, a new geometric ray-tracing algorithm has been developed to fully account for the inhomogeineity effect of refracted waves within an absorbing particle. In this talk, we will review the recent progress in simulating the single-scattering properties of ice crystals and dust particles and pertinent applications and assessment to satellite remote sensing and atmospheric radiative transfer.

Real and Apparent Changes in Aerosol Optical Properties near Cumulus Clouds: A Modeling Case Study and Implications for Passive and Active Remote Sensing

M. Ovchinnikov, E. Kassianov, and J. M. Comstock
Pacific Northwest National Laboratory, Richland, USA

Abstract— The observed increase in the aerosol optical depth (AOD) retrieved using passive remote sensing in the presence of clouds can be attributed to various aspects of the cloud-aerosol interaction. Dynamical and microphysical interactions are known to affect aerosol composition and size distributions. The radiative interaction, on the other hand, may only make areas near clouds appear brighter thereby introducing a bias in the retrieved AOD. Separating real and apparent changes in the aerosol optical properties is critical for many studies of aerosol indirect effect that rely on the AOD retrievals. In the presented study, a large eddy simulation model that explicitly predicts aerosol and cloud particle size distributions is used to separate contributions of various processes to the changes of aerosol properties in a field of cumulus clouds. The effect of clouds on AOD retrievals via radiative interaction is quantified by using a Monte-Carlo three-dimensional (3D) radiative transfer model to compute radiances which would be observed by satellite and suborbital sensors and to which the retrieval algorithms are subsequently applied. Based on our simulations of continental shallow convective clouds, it is found that swelling of aerosol due to higher relative humidity near clouds increases AOD by less than ten percent while the bias due to the 3D cloud radiative effect in retrievals based on independent pixel approximation is several times larger. An alternative to passive measurements is the active remote sensing. Aerosol optical properties can be retrieved from ground, airborne, or satellite lidar observations, which are not susceptible to the 3D cloud radiative effects. To investigate the potential of such observations in the vicinity of clouds, a lidar simulator is developed and applied to the modeled cloud and aerosol fields. The simulator computes attenuated backscatter, extinction, and depolarization ratio using scattering properties for aerosol and cloud particles from Mie calculations.

BDRF Models for Soil and Vegetation Terrestrial Surfaces from Multiple-viewing Angle Photopolarimetric Measurements

Pavel Litvinov[1], **Otto Hasekamp**[1], **Brian Cairns**[2], **and Michael Mishchenko**[2]

[1]SRON Netherlands Institute for Space Research, The Netherlands
[2]NASA Goddard Institute for Space Studies, USA

Abstract— The development of models for the bidirectional reflectance function (BDRF) of terrestrial surfaces in the spectral range from the blue to the shortwave infrared is very important for the retrieval of aerosol properties over land. We investigated the reflection properties of soil and vegetation types of terrestrial surfaces using multiple-viewing angle photopolarimetric airborne measurements of the Research Scanning Polarimeter (RSP) at low altitude over land (about 200–600 m) obtained during the ALIVE (Aerosol Lidar Validation Experiment) measurement campaign performed in Oklahoma (USA, Southern Great Plains) in September of 2005. After the correction of the RSP data for the atmosphere contribution it was found that the difference of the polarized reflectance values in the 'red' and 'infrared' channels is significant. Therefore, it may be important to account for spectral dependence of surface polarization in algorithms for the retrieval of aerosol properties over land.

The ratios of the total reflectances as well as the ratios of the polarized reflectances taken at two different wavelengths were obtained from the RSP measurements for different illumination and viewing geometries. They were compared with those ones obtained from the theoretical models based on the vector radiative transfer theory for discrete random medium and Kirchhoff approximation in the geometric optics limit for Gaussian rough surfaces. It was found from RSP measurements that in the backscattering region the angular dependences of the ratios of polarization values in the 'red' and 'infrared' bands differ from those ones obtained from the models with Fresnel's reflection from surface facets. The ratios of total reflectances taken at two different wavelengths were found to be almost independent on scattering angle and is the same for different illumination and scattering geometries for the same type of surfaces. On the basis of this analysis models of the BDRF for the surfaces have been developed and tested.

Discrete Ordinate Method to Modelling of Radiation Transfer in Atmosphere under Tabular Presentation of Phase Functions

L. P. Bass[1], **O. V. Nikolaeva**[1], **and V. S. Kuznetsov**[2]

[1]Keldysh Institute of Applied Mathematics, Russian Academy of Science, Moscow, Russia
[2]Research Scientific Center "Kurchatov Institute", Moscow, Russia

Abstract— Modelling of radiation transport in atmosphere via discrete ordinate methods is essentially hard due to complicated forms of cloudy and aerosol phase functions. They are usually peak-forward and often backward-forward and strongly oscillating in large scattering angles area. Decomposition of such phase functions into short Legendre series can lead to wrong solutions; using Legendre series of high order takes large computation times.

We developed the special algorithm to solving the transport equation via the discrete ordinate method under tabular presentations of phase functions. It is based on approximation of a collision integral by a scattering matrix, each element of which is defined by integration of a phase function over a small interval of transport directions. Such a technique is more time-consuming compared to well-spread methods based on short Legendre approximations and more economic than long Legendre polynomials algorithms. To reduce computation time parallel technique is applied.

Calculation results showing influence of phase functions presentations on reflected and transferred radiation intensity are presented.

ACKNOWLEDGMENT

This work was supported by Department of Mathematics of Russian Academy of Science via research program No. 3.

Matrix Form of VRTE Solution for Vertically Stratified Slab

A. I. Brill[1], **V. P. Budak**[2], **Ya. A. Ilyushin**[3], **S. V. Korkin**[2], **and S. L. Oshchepkov**[1]

[1]National Institute for Environmental Studies, Tsukuba, Japan
[2]Moscow Power Engineering Institute (TU), Moscow, Russia
[3]Moscow State University, Moscow, Russia

Abstract— This paper presents a mathematical model of the spatial-angular distribution for the reflected radiation polarization state. We have not assumed restrictions on the optical characteristics of scattering media such as those related to the artificial smoothness of the phase matrix elements. This model was developed for the purposes of validation study and precise processing of the satellite-borne data that would be available from the Greenhouse Gases Observing Satellite (GOSAT) [1] and from the Orbiting Carbon Observatory (OCO) [2]. We consider the scattering medium as a horizontally infinite and vertically inhomogeneous slab irradiated at an arbitrary angle by a plain unidirectional (PU) source of light. The bottom boundary (ground surface) is considered as a reflecting one with arbitrary BRDF.

The physical basis for the radiative transfer theory is the ray approximation that causes spatial singularities, described by Dirac δ-function, in the solution of the vectorial radiative transfer equation (VRTE). It is possible to formulate an equation upon the analysis of the spatial spectrum of the Stokes vector — the vectorial modification of the spherical harmonics method (VMSH). The VMSH is an approximate solution of the VRTE that includes the solution singularities together with the anisotropic part. The method proposed in this study provides a higher accuracy in radiative transfer modeling as compared with the small angle approximation [3]. The source function built upon the VMSH does not change the form of the VRTE boundary problem for the regular (smooth) part. The superposition of the VMSH (singular part) and a regular part gives the complete solution of the VRTE boundary problem [3].

The regular part of the boundary problem is solved using the Discrete Ordinates Method. The same method allows to obtain exact analytical solutions for the sampled VRTE in the matrix form and to describe the vertical heterogeneity of the slab through the division of the complete radiation flux upon the descending and ascending ones and thus to include the symmetry of the VRTE boundary problem for the case of PU source.

The extraction of the singularities together with the anisotropic part upon the VMSH from the complete VRTE solution reduces time consuming in the modeling of reflected light polarization and eliminates oscillation of the solution that would inherent to other methods. The results obtained form the basis for solving the problem of 3D polarized radiative transfer [3].

REFERENCES

1. Yokota, T., et al., "A nadir-looking 'SWIR' sensor to monitor CO_2 column density for Japanese 'GOSAT' project," *Proceedings of the Twenty-fourth International Symposium on Space Technology and Science*, 887, Japan Society for Aeronautical and Space Sciences and ISTS, Miyazaki, 2004.
2. Crisp, D., et al., "The Orbiting Carbon Observatory (OCO) mission," *Adv. Space Res.*, Vol. 34, 700, 2004.
3. Budak, V. P. and S. V. Korkin, "On the solution of vectorial radiative transfer equation in arbitrary three-dimensional turbid medium with anisotropic scattering," *JQSRT*, Vol. 109, 220, 2008.

Matrix Green's Functions Method in Statistical Optics

V. P. Budak[1] **and B. A. Veklenko**[2]

[1]Moscow Power-Engineering Institute (Technical University), Moscow, Russia
[2]Joint Institute for High Temperature, Russian Academy of Science, Moscow, Russia

Abstract— It is shown that the method of matrix Green's functions elaborated for the solution of quantum mechanic kinetic problems can be used successfully in classical optics. It occurs to be useful in the investigation of the light propagation in randomly perturbed media. The coupled evolution of the determinate and fluctuating component of the classical electromagnetic field can be adequately described in the terms of two-particle matrix Green's functions. This method allows avoiding the unwieldy formalism of the Bethe-Salpeter equation, and advancing for this reason the theory in general much further. In the case of random media there is an independent equation for the determined (coherent) component of radiation describing the interference phenomena. Second member of the integral equation for the fluctuating (non-coherent) component of radiation contains an interference figure formed by the coherent channel of scattering, which serves as a source forming the non-coherent channel. Thus the non-coherent channel of scattering depends on the coherent channel that is on the phase properties of radiation, the memory about which is erased with time. The density and inhomogeneity of media can be arbitrary. There are no restrictions on the speed of processes. The method covers such phenomena as the boson peak, flickering noise, backscattering processes, van Cittert-Zernicke theorem, radiative transfer equation, Fresnel formulas etc. The approach is completely taken into account the polarization phenomena. The only one restriction of this method is requirement of relative small fluctuations of optical characteristics in scattered media. The disregard of such restriction is technically complicate.

Optical Characterization of the Static and Dynamic Properties of Media Containing Nanoscale Non Uniformities

A. Brodsky and L. Burgess
University of Washington, Seattle, WA 98195, USA

Abstract— Many objects of physical, biological, and industrial interest include randomly distributed nanoscale non uniformities (e.g., nanoparticles). The characterization of such objects online in dynamic industrial processes and *in situ* in biological systems faces serious practical challenges, especially when the rapid formation and distribution of nanoparticles takes place. Optical methods are often considered as the best tools for nanoparticle monitoring as they are fast, noninvasive, and can in principle provide a broad range of information in real time, especially when using visible or near infrared light with wavelength on the order of the dimensions of the particles under observation.

The research presented in this talk centers around two optical sensing techniques developed in our laboratory in response to the problem of characterizing systems of nanoparticles. These techniques include optical low coherence reflectometry (OLCR) [1] and grating light reflection spectroscopy (GLRS) [2, 3]. OLCR and GLRS are complimentary techniques capable of providing, in real time, information about highly scattering dynamic systems with nanoscale non uniformities. OLCR is based on measuring time-resolved coherence loss and the destruction of backscattered optical wave packets in random media using a modified Michelson interferometer. GLRS consists of measuring light which interacts with a sample in contact with a transmission diffraction grating. The central element of GLRS analysis is the observation of square root singularities near the threshold of the transition of a traveling wave in a particular diffraction channel into an evanescent field. Near such singularities it is possible to combine all grating characteristics except the period into a small number of constant parameters which can then be excluded from the analysis, greatly simplifying the interpretation of the observed spectral data.

In this talk, we will present a theoretical description of our experiments with model nanoparticle systems and discuss future theoretical and experimental strategies. We will discuss possibilities for the application of the above-mentioned experimental techniques to the analysis of nanoscale dynamic phenomena, both in molecular biology and nanotechnology. Special attention will be devoted to the kinetics of phase transitions of the first and second kinds near the classical limits of stability, which despite long-standing interest and great theoretical and practical importance, are phenomena which are still poorly understood [4, 5].

REFERENCES

1. Brodsky, A. M., G. T. Mitchell, S. L. Ziegler, and L. W. Burgess, "Coherence loss in light backscattering by random media with nanoscale nonuniformities," *Phy. Rev. E*, Vol. 75, 046605 2007.
2. Anderson, B. B., A. M. Brodsky, and L. W. Burgess, "Threshold effects in light scattering from a binary diffraction grating," *Phy. Rev. E*, Vol. 54, No. 1, 912–923, 1996.
3. Anderson, B. B., A. M. Brodsky, and L. W. Burgess, "Grating light reflection spectroscopy for determination of bulk refractive index and absorbance," *Anal. Chem.*, Vol. 68, No. 7, 1081–1088, 1996.
4. Debenedetti, P. G., *Metastable Liquids*, Princeton University Press, Princeton, NJ, 1996.
5. Hernández-Rojas, J. and J. M. Gomez Llorente, "Microcanonical versus canonical analysis of protein folding," *Phys. Rev. Lett.*, Vol. 100, 258104, 2008.

Extension of Null-field Method for Anisotropic Crystals

V. A. Schmidt[1] and T. Wriedt[2]

[1]Universität Bremen, Germany
[2]Institute für Werkstofftechnik, Germany

Abstract— Simulation of the optical properties of anisotropic scatterers of arbitrary shape is important in different scientific and technology applications. Such particles can be found for example as white pigments in paper and color pigments in paints. Light scattering by such particles can be simulated by different approximate methods: the discrete dipole approximation (DDA), the method of moments (MoM) and the generalized multipole technique (GMT). All of them have own range of applicability due to approximation, e.g., the size of scatterer must be much smaller than the wavelength. The T-matrix method is an effective numerical tool for exactly solving the scattering problem proposed by Waterman [1] and extensively reviewed by Mishchenko et al. [2]. But it has been applied almost exclusively to isotropic scatterers. The solutions for anisotropic scatterers are obtained only for simple shapes or for axisymmetric particles.

In this work we extended the null-field method with discrete sources (NFM-DS) [3] to anisotropic scatterers considering homogeneous arbitrary shaped non-axisymmetric particles. A review of the capabilities of NFM-DS has been published by Wriedt [4]. Electromagnetic fields inside the scatterer are expressed by a system of the so-called quasi-spherical vector wave functions (qSVWF) which are derived by use of inverse Fourier transform. Using this expansion a solution of the light scattering problem in the framework of NFM-DS is obtained.

Our approach based on the work by Doicu [5], where the set of vector wave functions for uniaxial anisotropic medium was obtained and the scattering problem for corresponding particles was solved. A similar basis (except for a multiplicative constant) was obtained by Kiselev et al. [6] when the light scattering problem for radially and uniformly anisotropic spheres was solved.

For fast computation we developed a parallelized Fortran code using OpenMP technology. Numerical convergence of proposed approach and efficiency of developed program is considered. Additionally for validation we compare our simulation results with those obtained by other light scattering programs such as DDSCAT [7] and ADDA [8]. Numerical results, e.g., results of comparison with other programs, for some shapes are presented.

ACKNOWLEDGMENT

We would like to acknowledge support of this work by Deutsche Forschungsgemeinschaft (DFG).

REFERENCES

1. Waterman, P. C., "Symmetry, unitary and geometry in electromagnetic scattering," *Phys. Rev. D*, Vol. 3, 825–839, 1971.
2. Mishchenko, M. I., N. G. Khlebtsov, G. Videen, T. Wriedt, and N. T. Zakharova, "Comprehensive T-matrix reference database: A 2006-07 update," *JQRST*, Vol. 109, 1447–1460, 2008.
3. Doicu, A., T. Wriedt, and Y. A. Eremin, *Light Scattering by Systems of Particles*, Springer, Berlin, 2006.
4. Wriedt, T., "Review of the null-field method with discrete sources," *JQSRT*, Vol. 106, 535–545, 2007.
5. Doicu, A., "Null-field method to electromagnetic scattering from uniaxial anisotropic particles," *Optics Comm.*, Vol. 218, 11–17, 2003.
6. Kiselev, A. D., V. Y. Reshetnyak, and T. J. Sluckin, "Light scattering by optically anisotropic scatterers: T-matrix theory for radial and uniform anisotropies," *Phys. Rev. E*, Vol. 65, 056609, 2002.
7. Draine, B. and P. Flatau, "Discrete-dipole approximation for scattering calculations," *J. Opt. Soc. Am. A.*, Vol. 11, 1491–1499, 1994.
8. Yurkin, M. A. and A. G. Hoekstra, "The discrete dipole approximation: An overview and recent developments," *JQSRT*, Vol. 106, 558–589, 2007.

A Fast Method for Atmospheric Multiple-scattering Based on DISORT

Xiuhong Chen[1], **Heli Wei**[1], **and Ping Yang**[2]

[1]Key Laboratory of Atmospheric Composition and Optical Radiation
Chinese Academy of Sciences, P. O. Box 1125, Hefei 230031, China
[2]Department of Atmospheric Sciences, Texas A&M University
College Station, Texas 77843, USA

Abstract— The discrete ordinate radiative transfer (DISORT) is a powerful method to rigorously simulate the transfer of radiation in vertically inhomogeneous, nonisothermal, plane-parallel media. However, DISORT is not feasible for hyperspectral remote sensing applications because of its computational efficiency. We have developed a Combined Atmosphere Radiative Transfer Model (CARTM) to compute atmospheric transmittance and thermal infrared radiation with a spectral resolution of $1\,\mathrm{cm}^{-1}$ in the spectral region from 1 to $25000\,\mathrm{cm}^{-1}$. However, it is computationally costly to apply the CARTM in conjunction with DISORT to the transfer of radiation involving a scattering medium. In this study, a fast method based on the DISORT is developed and incorporated into CARTM.

In the model, the spectral range of interest is divided into several subsections. For each subsection, the pre-computed atmospheric optical depths using the pre-calculated moderately-spectral-resolution transmittance based on fitting to the line-by-line algorithm are sorted in an ascending order. Only several optical depths at of uniformly spaced spectral nodes are computed and input into the DISORT to obtain the scattered radiations. Radiances at any other wave numbers are interpolated according to the pre-computed optical depths and the surface albedo. The computational efficiency and accuracy are tested by comparing with DISORT. For the upward radiances at the top of the atmosphere with a spectral region from 1 to $25000\,\mathrm{cm}^{-1}$, this fast method requires only 5 minutes on the PC with 3.2G CPU, whereas the DISORT takes more than 15 hours. Thus, the fast model is approximately 200 times faster than DISORT. The maximum relative error between results computed from this fast model and DISORT is less than 10%.

Characterization of Lymphocytes Using the Scanning Flow Cytometry

M. A. Yurkin[1,2], **D. I. Strokotov**[1,2], **K. V. Gilev**[1,2], **D. R. van Bockstaele**[3], **A. G. Hoekstra**[4], **N. B. Rubtsov**[5], **and V. P. Maltsev**[1,2,6]

[1]Institute of Chemical Kinetics and Combustion, Institutskaya 3, Novosibirsk 630090, Russia
[2]Novosibirsk State University, Pirogova 2, 630090, Novosibirsk, Russia
[3]Esoterix, Clinical Trials Services, LabCorp, Gen. De Wittelaan L11-A2, B-2800 Mechelen, Belgium
[4]Faculty of Science, University of Amsterdam, Kruislaan 403, 1098 SJ, Amsterdam, The Netherlands
[5]Institute of Cytology and Genetics, Lavrentyeva 10, Novosibirsk 630090, Russia
[6]State Research Center of Virology and Biotechnology "VECTOR"
Koltsovo, Novosibirsk Region 630559, Russia

Abstract— A method to characterize individual mononuclear cells using light scattering patterns measured with a scanning flow cytometer has been developed. It is based on a coated sphere model and a global optimization algorithm DIRECT and provides not only parameter estimates but also rigorous estimates of its errors. The latter are obtained using Bayesian inference method taking into account correlation between residual errors. We applied this method to samples of T- and B-lymphocytes from several donors, determining cell diameter, ratio of nucleus to cell diameters, nucleus and cytoplasm refractive index for each cell. These parameters have potential diagnostic value, since they may be sensitive to certain disorders of the human immune system. The main difference in morphology of T- and B-lymphocytes was found to be the larger mean diameters of the latter. However, the difference is smaller than natural biological variability of a single cell type. We propose nucleus inhomogeneity as a possible reason for the deviation of real lymphocyte's light scattering patterns from that of a coated sphere model. This hypothesis is supported by several models simulated using the discrete dipole approximation.

ACKNOWLEDGMENT

This work was supported by the grants of the Russian Foundation for Basic Research, No. 07-04-00356-a, and No. 08-02-91954-NNIO-a, integration grants of the Siberian Branch of the Russian Academy of Science, No. 2009-37, and No. 2009-7, grant from the program of Presidium of the Russian Academy of Science, No. 2009-27b, and grant of the Novosibirsk city hall for young scientists.

Session 3P3
Plasmonics, Metamaterials, and Magneto-Optics 2

Active Control of Photonic Properties of Plasmonic Crystals: Electric and Magnetic Field Effects

Gregory A. Wurtz[1], **Wayne Dickson**[2], **and Anatoly V. Zayats**[2]

[1]Department of Chemistry and Physics, University of North Florida
Jacksonville FL 32224, USA
[2]Centre for Nanostructured Media, The Queen's University of Belfast
Belfast BT7 1NN, United Kingdom

Abstract— Optical properties of metallic nanostructures are in many cases determined by one or another type of plasmonic excitations such as surface plasmon polaritons, localized surface plasmons, particle plasmons, etc. Surface plasmon polaritons (SPPs) are the electromagnetic excitations coupled to collective motion of conduction electrons near a metal surface, existing on an interface between metal and dielectric media. Periodically structured metal surfaces or films acts as two-dimensional photonic crystals for surface plasmon polariton waves and are dubbed surface plasmon polaritonic crystals or plasmonic crystals in short. They allow to achieve precise control over the dispersion of SPP waves as well spatial distribution of the electromagnetic field. Optical properties of periodically structured metals such as transmission, reflection, absorption, are completely determined by the SPP Bloch modes [1].

Hybritization of plasmonic crystals with functional materials, such as ferroelectric, magneto-optical, nonlinear optical materials and molecular species, results in metamaterials or stand-alone nanostructures whose photonic response can be actively controlled by application of external stimuli [2–4]. Plasmonic dispersion and, thus, optical properties of such nanostructures and their response to applied control signal can be designed in a straightforward and controllable way by the appropriate structuring of the metallic host.

In this talk, we will discuss how optical properies of plasmonic crystals can be controlled with applied external electric or magnetic field. Such active plasmonic devices are important in nanophotonic applications for controlling light on the nanoscale as well as for development of tuneable and active optical metamaterials.

REFERENCES

1. Zayats, A. V., I. I. Smolyaninov, and A. A. Maradudin, "Nano-optics of surface plasmon polaritons," *Phys. Rep.*, Vol. 408, 131–314, 2005.
2. Wurtz, G. A. and A. V. Zayats, "Nonlinear surface plasmon polaritonic crystals," *Laser and Photon. Rev.*, Vol. 2, 125–135, 2008.
3. Dickson, W., G. A. Wurtz, P. R. Evans, R. J. Pollard, and A. V. Zayats, "Electronically-controlled surface plasmon dispersion and optical transmission through hole arrays in metal films with liquid crystal," *Nano Letters*, Vol. 8, 281–286, 2008.
4. Wurtz, G. A., W. Hendren, R. Pollard, R. Atkinson, L. Le Guyader, A. Kirilyuk, Th. Rasing, I. I. Smolyaninov, and A. V. Zayats, "Controlling optical transmission through magneto-plasmonic crystals with external magnetic field," *New J. Phys.*, Vol. 10, 105012, 2008.

Nanofocusing of Light Using Plasmonic Lenses Illuminated by Radially Polarized Light

Avner Yanai, **Gilad Lerman**, **and Uriel Levy**
Department of Applied Physics, Benin School of Engineering and Computer Science
Hebrew University of Jerusalem, Jerusalem, 91904, Israel

Abstract— Focusing of surface plasmon polaritons by plasmonic lenses is attracting much interest recently, with applications in microscopy, lithography and sensing to name a few. A variety of focusing schemes were introduced, including focusing by circularly shaped slits, in-plane focusing, and focusing by dielectric lenses. A major challenge related to SPP focusing is achieving of tight focusing with high energetic efficiency. To mitigate this goal we propose, analyze and experimentally demonstrate a plasmonic lens that is illuminated by a radially polarized light. In our devices, focusing is obtained by coupling of the incident light to SPPs that propagate through a subwavelength dielectric slit milled into a metallic layer, and interfere constructively along the other side of the metallic layer.

For a plasmonic lens having cylindrical symmetry, an incident radially polarized beam is TM polarized along the entire metal\dielectric interface. Therefore, radially polarized light is a natural choice for SPP excitation in such structures, allowing efficient coupling to SPP modes, and preventing radiation into free space of the azimuthal field components which cannot contribute to the focusing process as they are TE polarized with respect to every point of the metal\dielectric interface. Moreover, with radial polarization the E_Z (out of plane) components interfere constructively at the focal region, while the E_R (in plane) components interfere destructively. This is exactly opposed to the case where the structure is illuminated with linearly polarized light. Because the longitudinal (Z) field components are inherently stronger than the transverse components the spot size is significantly reduced.

We analyze the performance of the plasmonic lens theoretically and by numerical simulations. We exploit the use of gratings for enhancing the energy density in the focal region. Finally, we validate our predictions by experimentally demonstrating the functionality of the plasmonic lens using near field scanning optical microscopy.

Nanoimprinting and Contact Printing Lithography for Fabricating Micro/Nano-structures and Sub-wavelength Devices

Yung-Chun Lee
Department of Mechanical Engineering, National Cheng Kung University
Tainan 70101, Taiwan

Abstract— Nanoimprinting technology was first developed in 1995 and is now recognized as one of the most promising approaches for large-area and low-cost fabrication of nanostructures. In this presentation, three types of roller-based nanoimprinting and contact-printing methods developed in NCKU in recent years will be addressed. First of all, a Laser-Assisted Roller Imprinting (LARI) method which can directly transfer the pattern from a quartz mold to a silicon substrate is introduced. The advantage of LARI is that the pattern transformation is direct, fast, and without any chemical etching processes. Secondly, a Light-Assisted Metal Film Patterning (LAMP) method which transfers a patterned metal film directly from a silicon mold to a substrate is discussed. The pattern transformation relies on both mechanical contact pressure and optical heating at the interface. Metal patterns with 100 nm feature size can be easily transferred in laboratory using simple equipments and setups. Finally, a Contact-Transfer and Mask-Embedded Lithography (CMEL) is proposed which cleverly arranges pure mechanical forces and surface energy difference to achieve the patterning of nano-structures on various kinds of substrates. Applications of these developed methods are also demonstrated on the fabrication of sub-wavelength devices such as metal wire grid optical polarizers. Future developments and potential applications of these roller-based nanoimprinting and nano-patterning methods will be addressed.

Surface Plasmons in Metallic Films with Non-drude Dispersion

A. G. Schuchinsky
Institute of Electronics, Communications & Information Technology (ECIT)
School of Electronics Electrical Engineering & Computer Science
The Queens University of Belfast
Northern Ireland Science Park, Queen's Road, Queen's Island, Belfast, BT3 9DT, UK

Abstract— Surface plasmons (SP) in metallic films have recently attracted considerable attention in connection with their potential applications in all-optical circuits for information processing, computing, and photonic and opto-electronic devices.

Drude model is usually employed to describe the metal permittivity $\varepsilon_s(\omega)$ in THz and optical ranges

$$\varepsilon_s(\omega) = 1 - \omega_p^2/\omega(\omega - i\nu) \tag{1}$$

where ω is angular frequency and the time convention is assumed in the form $\exp(i\omega t)$; ω_p and ν are the plasma and collision frequencies.

While the Drude model (1) provides an adequate description of the metal permittivity at mm-wave and THz frequencies, its accuracy deteriorates in the optical range, where ω_p and ν become frequency dependent. The measured optical constants of metals available in the tabulated form can be used instead for modelling SP propagation in thin metallic films. However, the recent numerical studies have demonstrated significant deviations of SP characteristics in Ag and Au films from those predicted when using the frequency independent ω_p and ν.

In this work, the fundamental SP and complex modes in the metallic films on glass substrates are investigated in a broad frequency range on the basis of the rigorous solutions of the full-wave dispersion equation (DE). The effects of the dispersion of ω_p and ν on the characteristics of SP in metallic films with the optical permittivity $\varepsilon_m(\omega)$ given by table data are discussed and illustrated by the field and Poynting vector distributions of the SP modes to provide an insight in the mechanisms underlying the qualitative changes in the SP properties at optical frequencies.

To take advantage of the known asymptotic dispersion relations for the SP, the Drude model parameters ω_p and ν have been interrelated with the table data for the metal permittivity $\varepsilon_m(\omega) = \varepsilon'_m + i\varepsilon''_m$. Making use of the $\varepsilon_s(\omega)$ defined in (1), ω_p and ν can be expressed in terms of $\varepsilon_m(\omega)$ at each frequency ω

$$\nu(\omega) = \frac{\varepsilon''_m(\omega)}{1 - \varepsilon'_m(\omega)}; \quad \omega_p(\omega) = \sqrt{[1 - \varepsilon'_m(\omega)][\omega^2 + \nu^2(\omega)]}. \tag{2}$$

It is important to note that $\omega_p(\omega)$ and $\nu(\omega)$ are the frequency dependent parameters here because in a broad frequency range the actual dispersion of $\varepsilon_m(\omega)$ substantially deviates from that given by the Drude model (1) with the constant ω_p and ν. Since both $\omega_p(\omega)$ and $\nu(\omega)$ are relatively slow varying functions, they can be utilised in the numerical analysis of the canonical dispersion equations for SPs.

To discriminate the effects of the loss and $\varepsilon_m(\omega)$ dispersion, the SP characteristics have been evaluated at a few values of $\nu_n(\omega) = \nu(\omega)/\omega$, viz. the actual $\nu_n(\omega)$, retrieved from the table data, and $\nu_n(\omega)$ scaled by the factors 10^{-3}, 10^{-2}, 0.1, and 0.25. While the SP attenuation constant $\mathrm{Im}\gamma_n$ varied accordingly with the scaled ν_n, the respective changes of $\mathrm{Re}\gamma_n$ were surprisingly small. Moreover, instead of expected sharp rise of the $\mathrm{Re}\gamma_n(\omega)$ peak, attributed to the plasmonic resonance ω_{res}, the peak magnitude remained practically unchanged when the scaling factor decreased from 0.25 to 10^{-3}. This suggested that the peak of $\mathrm{Re}\gamma_n(\omega)$ do not represent the plasmonic resonance but has a different nature.

Thorough analysis of the dispersion equation has revealed that the weak dispersion of $\omega_p(\omega)$ and $\nu(\omega)$ but not the losses in the Ag and Au films destroy the resonance of SP at optical frequencies because the necessary condition $\omega = \omega_{res}(\omega)$ cannot be fulfilled for the measured permittivities $\varepsilon_m(\omega)$. This phenomenon will be further discussed in the presentation.

Experimental and Theoretical Study of Plasmonic Gratings with Subwavelength Grooves

V. I. Belotelov[1,2], **A. N. Kalish**[1,2],
A. K. Zvezdin[1,3], **and A. S. Vengurlekar**[4]

[1]A. M. Prokhorov General Physics Institute of RAS, Moscow 119991, Russia
[2]M. V. Lomonosov Moscow State University, Moscow 119992, Russia
[3]Fondacione ISI, Torino 10133, Italy
[4]Tata Institute of Fundamental Research, Mumbai 400005, India

Abstract— Optical properties of plasmonic heterostructures, i.e., metal-dielectric periodically nanostructured materials (e.g., metallic gratings, perforated films) which can sustain the propagation of the surface plasmon-polariton (SPP) waves, were shown to have some peculiarities leading to new optical effects like extraordinary optical transmission and magnetooptical Faraday effect [1, 2]. Recent transmission and reflection spectral measurements [3, 4] in the visible and infrared revealed some further interesting properties of a one-dimensional grating having a gold film deposited on deep rectangular subwavelength grooves etched in quartz. Both classical and conical diffraction geometries are studied. In this work, we compare the experiments with numerical modeling to obtain an insight into the observed peculiar spectral features. For this, we use an algorithm based on the RCWA (rigorous coupled-wave analysis). One of the highlights is the use of special factorization rules for improvement of the algorithm's convergence.

Reflection and transmission spectra as well as the electromagnetic field distribution are modeled for the experimental structures. Pronounced spectral features namely dips and peaks are found to be related to the Wood's anomalies: surface plasmon polaritons and Rayleigh anomalies. As the walls and bottoms of the grooves are covered with metal, cavity resonances related to Fabry-Perot modes also contribute to the optical properties providing some additional reflection dips. We further address the question of the reciprocity of the transmission and reflection spectra for light incident from the metal side and the substrate side. While the reciprocity is maintained for transmission as expected, the simulations are able to reproduce the contrasting behavior shown by reflection from the two sides. Finally, the conditions under which the transmission is negligible irrespective of light polarization and angle of incidence are found.

ACKNOWLEDGMENT

The work is supported by RFBR (07-02-01445, 08-02-00717, 07-02-92183), Leading Scientific Schools grant NSh. 671.2008.2.

REFERENCES

1. Ebbesen, T. W., H. J. Lezec, H. F. Ghaemi, T. Thio, and P. A. Wolff, *Nature*, Vol. 391, 667, 1998.
2. Belotelov, V. I., L. L. Doskolovich, and A. K. Zvezdin, *Phys. Rev. Lett.*, Vol. 98, 77401, 2007.
3. Vengurlekar, A. S., *Opt. Lett.*, Vol. 33, 1669, 2008.
4. Vengurlekar, A. S., *J. Appl. Phys.*, Vol. 104, 023109, 2008.

Surface Plasmon Polariton Analogues of Volume Electromagnetic Wave Effects

Alexei A. Maradudin and Tamara A. Leskova
Department of Physics and Astronomy and Institute for Surface and Interface Science
University of California, Irvine, CA 92697, USA

Abstract— In recent years effects originally associated with volume electromagnetic waves have begun to be studied in the context of surface plasmon polaritons. These include negative refraction [1], cloaking [2], the Talbot effect [3], and lasing [4]. The investigations of these effects are prompted on the one hand by a desire to uncover new properties of surface plasmon polaritons, and on the other hand by a growing interest in the use of these waves in novel nanoscale devices.

We consider surface plasmon polariton analogues of some of these effects for structures that differ from those assumed in [1, 4] and by approaches that differ from the ones used in these references. In addition, we discuss new effects that have not been studied until now.

When a metal film is deposited on an anisotropic dielectric substrate, the dispersion curve for the surface plasmon polaritons supported by this structure consists of two branches. The higher frequency branch possesses an isotropic negative group velocity in the nonradiative region of the frequency-wave vector plane [5]. We use this result to construct a planar surface structure that produces all-angle negative refraction of a surface plasmon polariton incident on it.

We study the transmission of a surface plasmon polariton through a periodicically corrugated interface between two different metals. The field of the surface plasmon polariton transmitted through this interface displays periodic self-images of the interface that are separated from it by multiples of a characteristic distance. This is the analogue of the Talbot effect for surface plasmon polaritons.

A surface plasmon polariton beam of frequency ω and $1/e$ half width w propagating in the x_1 direction on the surface $x_3 = 0$ of a semi-infinite metal is incident on a slit on this surface defined by $|x_1| < L/2,\ |x_2| < d$. The region $|x_1| < L/2,\ |x_2| > d$ on this surface is a medium defined by a dielectric constant ϵ_2. The field of the surface plasmon polariton emerging from the slit into the region $x_1 > L/2$ is calculated, and from it the transmissivity of the slit as a function of its frequency. It is found that as the frequency of the incident surface plasmon polariton is increased, the transmissivity increases in a step-wise fashion at each frequency at which an additional guided surface plasmon polariton is supported by an infinitely long slit.

Finally, we study the reflectivity of a surface plasmon polariton incident obliquely on a one-dimensional structure defined by a profile function that is the sum of a periodic function and one that increases linearly with the coordinate perpendicular to the generators of the surface. The reflectivity consists of a sequence of dips in a narrow range of the angle of incidence of the surface plasmon polariton. These are associated with a Wannier-Stark ladder of a surface plasmon polariton.

REFERENCES

1. Shin, H. and S. Fan, "All-angle negative refraction for surface plasmon waves using a metal-dielectric-metal structure," *Phys. Rev. Lett.*, Vol. 96, 073907, 1–4, 2006.
2. Smolyaninov, I. I., Y. J. Hung, and C. C. Davis, "Two-dimensional metamaterial structure exhibiting reduced visibility at 500 nm," *Opt. Lett.*, Vol. 33, 1342–1344, 2008.
3. Dennis, M. R., N. I. Zheludev, and F. J. García de Abajo, "The plasmon Talbot effect," *Opt. Express*, Vol. 15, 9692–9700, 2007.
4. Bergman, D. J. and M. I. Stockman, "Surface plasmon amplification by stimulated emission of radiation: Quantum generation of coherent surface plasmons in nanosystems," *Phys. Rev. Lett.*, Vol. 15, 027402, 1–4, 2003.
5. Mills, D. L. and A. A. Maradudin, "Properties of surface polaritons in layered structures," *Phys. Rev. Lett.*, Vol. 31, 372–375, 1973.

Mid-infrared Surface-plasmon-resonance Technique and Its Biological Applications

M. Golosovsky[1], **V. Yashunsky**[1], **V. Lirtsman**[1], **D. Davidov**[1], **and B. Aroeti**[2]

[1]The Racah Institute of Physics, The Hebrew University of Jerusalem, Israel
[2]The Alexander Silberman Institute of Life Sciences
The Hebrew University of Jerusalem, Jerusalem, Israel

Abstract— The surface plasmon penetration depth into biomedium is very low, in such a way that it propagates in a thin layer adjacent to the metal-coated sensor. The optical reflectivity in the surface plasmon resonance regime is extremely sensitive to changes in thickness and refractive index of this thin layer. Surface plasmon waves in the visible range are not optimal for studying living cells because the cells' size considerably exceeds the penetration depth of visible-range surface plasmon waves. Infrared (IR) surface plasmons, on the other hand, penetrate much deeper and are more appropriate for studying living cells.

We demonstrate here a mid-IR SPR technique that is based on a gold-coated ZnS prism and uses a Fourier-transform infrared (FTIR) spectrometer as a light source. This technique is sensitive enough to measure physiological concentrations of glucose in water and in human plasma. It allows real-time and label-free studies of lipid membranes and cells cultured on the gold-coated surface, particularly drug and protein penetration into cells. In addition, this SPR-FTIR technique enables detection of biomolecules based on their spectral fingerprints, thus bridging traditional plasmonics with mid-IR spectroscopy.

We consider surface plasmon propagation in a planar array of living cells, in particular, surface plasmon propagation length; we also discuss possibility of guided optical waves in a living cell culture.

REFERENCES

1. Golosovsky, M., V. Lirtsman, V. Yashunsky, D. Davidov, and B. Aroeti, *J. Appl. Phys.*, Vol. 105, 102036, 2009.
2. Golosovsky, M., D. Davidov, and B. Aroeti, *BioOptics World*, Vol. 1, 27, Sept./Oct. 2008.

Fractal Plasmonic Metamaterials for Subwavelength Imaging

Xueqin Huang[1], **Dexin Ye**[2], **Shiyi Xiao**[1], **Jiangtao Huangfu**[2], **Zhiyu Wang**[2], **Lixin Ran**[2], **and Lei Zhou**[1]

[1]Surface Physics Laboratory (State Key Laboratory) and Physics Department
Fudan University, Shanghai 200433, China
[2]The Electromagnetic Academy at Zhejiang University
Zhejiang University, Hangzhou 310027, China

Abstract— We show that a metallic plate with fractal-shaped slits supports surface plasmon polaritons mimicking a natural plasmonic metal (such as silver), but with plasmon frequency *tunable* in an ultra-wide frequency range dictated by the fractal geometry. As one application of this plasmonic metamaterial, we show by both experiments and finite-difference-time-domain (FDTD) simulations that it works as a *super* lens to focus light sources with subwavelength resolution and enhanced field strengths. Microwave experiments reveal the best achievable resolution is only $\lambda/15$ (see the figure below), and FDTD simulations demonstrate that similar effects can be realized at other frequencies with appropriate designs [1]. We analyze the imaging mechanism thoroughly and compare it with other available imaging mechanisms in details [2].

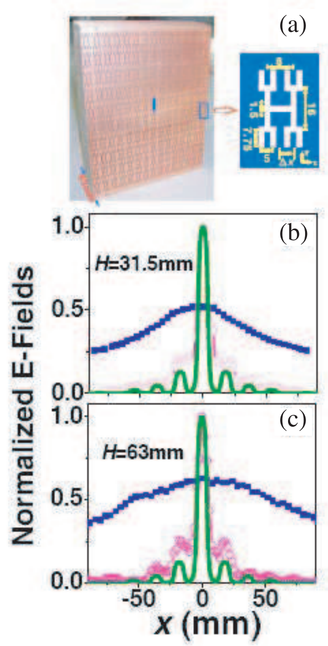

REFERENCES

1. Huang, X. Q., et al., *Phys. Rev. Lett.*, 2009 (submitted).
2. Xiao, S. Y., et al., unpublished.

Broadband Terahertz Metamaterial for Negative Refraction

C. Sabah and H. G. Roskos
Physikalisches Institute, Johann Wolfgang Goethe-University
D-60438, Frankfurt am Main, Germany

Abstract— Negative refraction metamaterials can be realized with structures containing elements with negative material parameters, electric permittivity ε and magnetic permeability μ. A well-known resonating structure that can be used to obtain negative permeability is a split-ring resonator (SRR), which creates nonlinear magnetic behavior due to the resonant interaction between the inductance of the rings and the capacitance across the gaps. In this work, it is shown that the frequency range of negative refraction index can be increased by introducing a periodic structure combining two different SRRs and wires in a unit cell. In our model, the magnetic effects of SRR are greatly improved by using two different SRRs and combining their effects to achieve a greater range of working frequencies for negative refraction at THz frequencies. The effective magnetic permeability of SRRs for a unit cell of N can be modeled by the summation expression for frequency dependence. Our unit cell is made of two SRRs that exhibit negative effective permeability functions around 3 THz. The two SRRs are designed with lattice parameter $a = 55\,\mu\text{m}$, stacked at a layer spacing of $l = 20\,\mu\text{m}$. Numerical results illustrate that the wider frequency range of magnetic response can be achieved by combining the SRRs. Then, a material with negative index of refraction can be constructed by combining proposed structure with an array of wires with $r = 2.5$ spaced at $l = 20\,\mu\text{m}$, incorporating one thin copper wire into each SRR layer. This produces a negative permittivity effect in a frequency region that overlaps with the negative permeability region of the SRRs. The negative root must be chosen for the index of refraction when the permittivity and permeability are simultaneously negative, thus the refractive index for this structure is negative at frequencies between 2.7 and 4.0 THz. It is shown that our structure offers more favorable frequency dispersion for material parameters than single SRRs. This model can be taken further to incorporate additional SRRs for an even more dispersive index of refraction.

The Radiators Based on Metamaterials Waveguides

Nikolay P. Balabukha, **Alexey A. Basharin**, **and Vladimir N. Semenenko**
Institute for Theoretical and Applied Electromagnetics, Russian Academy of Sciences
ITAE, Izhorskaya, 13, Moscow 125412, Russia

Abstract— The radiation of antennas based on metamaterials waveguides is investigated in the work. It is shown, that such antennas can radiate in forward, backward and simultaneously in both directions. Results of antennas measurements in anechoic chamber are presented. The experiment results prove the opportunity for such antennas to radiation in the backward direction. The research results for wideband waveguides antenna with the radiation pattern of the special form are also shown.

In particular, it is shown in theory for an antenna based on planar waveguide of metamaterial with negative values of relative permittivity and permeability (Fig. 1) that power flux in the metamaterial layer is of negative value; though it is positive in the ambient space. The total flux (the total of fluxes in the metamaterial layer and in the ambient space) may be positive, negative and equal to zero. The mode analysis reveals that the two wave types can propagated in such a waveguide at the same time.

Figure 1: The radiator based on a planar metamaterial waveguide.

Figure 2: The radiator based on a two-layer planar metamaterial waveguide.

Figure 3: The radiator based on a two-layer rectangular metamaterial waveguide.

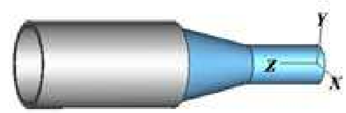

Figure 4: The radiator based on a two-layer circular metamaterial waveguide.

In the event of a positive total power flux the antenna based on such a waveguide radiates in the forward direction. If a power flux is negative it radiates in the backward direction. And in the case of a zero total flux the antenna radiates equally in the forward and backward directions. The radiation pattern in this case is an interference of radiation patterns in the forward and backward directions [1].

In a two-layer planar metamaterial waveguide, the case nearly approaching a single-layer waveguide, power fluxes in metamaterial layers, as opposed to fluxes in the internal layer and the ambient space, are negative. Therewith the total power flux may be positive, negative and equal to zero. The antenna on the basis of the two-layer planar waveguide, presented in Fig. 2, may radiate both in the forward and backward directions depending on a frequency.

The backward radiation capability of the antenna based on a twolayer rectangular metamaterial waveguide was shown by experiments [2] (Fig. 5). The antenna under investigation consisted of the coaxialwaveguide adapter loaded by a rectangular metamaterial tube (Fig. 3). The tube thickness varied from 0 to 30 mm, the tube length was 150 mm. The radiation pattern corresponds to 5 mm tube thickness and positive total power flux (Black curve). In the event of negative values for relative permittivity and permeability of the metamaterial and the tube thickness exceeding than 10 mm, the antenna radiates in the backward direction (Red curve). The total flux (in this case) is negative. If the tube thickness is 10 mm, the antenna radiates in the 0° and 180° directions. Simultaneously (in this case the total power flux is equal to zero) (Blue curve).

Thus the effect of backward radiation for antennas based on metamaterial waveguides has been predicted theoretically and experimentally.

Application of metamaterials makes possible to design wideband antennas. The horn antenna with 5 cm diameter circular mouth loaded by a circular metamaterial waveguide is shown in Fig. 4. The presence of frequency dispersion of the relative permittivity and permeability enables to form the radiation pattern for the specific antenna with the Π-shaped main lobe which varies slightly depending on a frequency in the angle sector. The antenna based on the horn with the metamaterial circular tube of 10 cm long and 4.4 mm thick enables to obtain radiation patterns within the frequency range from 8 GHz to 12 GHz for the Π-shaped main lobe vertex with a 1 dB irregularity. It may vary slightly depending on the frequency in the $\pm 20^\circ$ angle sector. Black curve is the experimental radiation pattern on frequency 8 GHz (Fig. 6), Red curve -10 GHz, Blue curve -12 GHz. The application of such an antenna, for example as a feed of Compact range, enables to widen a working zone and frequency band of the Compact range when compared to standard types of feeds [3].

Thus, unusual properties and application of antennas based on metamaterials waveguides are shown.

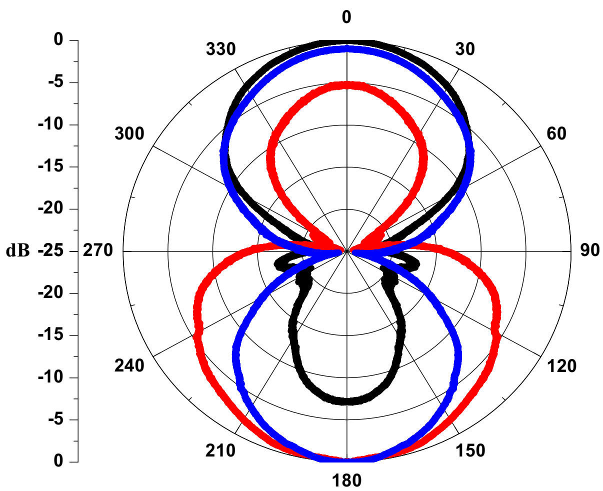

Figure 5.

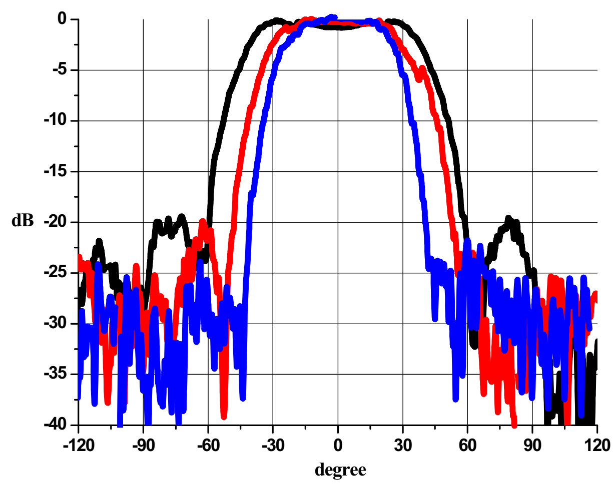

Figure 6.

REFERENCES

1. Balabukha, N. P., A. A. Basharin, and V. N. Semenenko, *Journal of Communications Technology and Electronics*, No. 7, 2009, In Print.
2. Lagarkov, A. N., V. N. Semenenko, A. A. Basharin, and N. P. Balabukha, "Abnormal radiation pattern of metamaterial waveguide," *PIERS Online*, Vol. 4, No. 6, 641–644, 2008.
3. Balabukha, N. P. and A. A. Basharin, *Rod Dielectric WideBand Feed, Antennas*, No. 12, 2008.

Session 3P4
Biomedical Electromagnetism Instruments, Electromagnetism Condensed Materials and Imaging 1

Electromagnetic Fields of Medical Devices as Risk Factor for Medical Personnel

N. B. Rubtsova, D. V. Markov, and S. Yu. Perov
RAMS Institute of Occupational Health, Moscow, Russian Federation

Abstract— Medical personnel are one of staff that is professionally exposed by electromagnetic field (EMF). Medical devices, introduced resent years are the sources of EMF of different frequency ranges and create new complexes of occupational factors on work places.

New medical appliances — Magnetic Resonance Imaging (MRI) Systems generate complex of electromagnetic factors. Static magnetic fields levels on work places of medical staff can be up to 500 mT, exceeding of shot-term threshold permissible values (TPV) of total and local (to extremities) exposure, (according to Russian hygienic regulations). Medical staff is exposed by pulsed radiofrequency EMF (at frequency range from 240 Hz to 10 MHz) too. Than is medical staff under carrying out of MRI diagnostics is exposed by repeated exposure of static magnetic field combined with radio frequency EMF with other additional occupational factors. Biological effects of this kind of exposure are not investigated now.

New kinds of surgery appliances can also be a source of potential electromagnetic hazard for medical staff during surgical procedures. For example, at surgeon work place EMF levels in frequency range from 340 to 450 kHz during operation can be up to 320 V/m, and under higher frequency modes these levels can exceed TLV.

New models of physiotherapy devices are also the sources of combined exposure of different frequency ranges EMF and pulse modulated. A number of appliances are the emitters of EMF modes without hygienic standards that prevents from evaluation those type exposure actual health risks.

Thus, methods and technologies improvement of EMF of different frequency ranges and modes of medical application with their advantages for diagnostics and treatment of various health disorders can be additional risk factor for medical personnel.

Temperature Reconstruction in Depth of Biological Object by Acoustical Radiometer

Yu. N. Barabanenkov[1], **A. A. Anosov**[1,2], **A. S. Kazanskij**[1], **A. D. Mansfel'd**[3], and **A. S. Sharakshane**[4]

[1]Institute of Radioengineering and Electronics of RAS, Russia
[2]Sechenov Moscow Medical Academy, Russia
[3]Institute of Applied Physics of RAS, Russia
[4]Institute of Biochemical Physics of RAS, Russia

Abstract— It is well known that the temperature in depth of a human body can be measured using the thermal electromagnetic radiation of the body. In 1983, Bowen [1] suggested to use for this purpose the thermal acoustic radiation in megahertz frequency interval. This radiation emitted by an object results from the thermal movement of atoms and molecules in it. The intensity of the thermal acoustic radiation is determined by the absolute temperature and absorption coefficient in the object. Both methods have the advantages and imperfections. The advantage of the acoustothermography over the radiothermography is the better spatial resolution for the temperature reconstruction because of the small wave lenght (about 1 mm). The advantage of the radiothermography is the smaller measurement error because of the bigger frequency bandpass. We suggest to use the acoustothermography for the temperature distribution reconstruction in depth of a human body.

Acoustothermometrical measurements were carried out for the model biological objects [2, 3]. As model objects we used the plasticine bodies placed in the water and the beef liver. In the experiment the model objects were being heated up and cooled down. The temporal dependences of their acoustobrightness temperatures were obtained and the reconstruction of the 2-D and 3-D temperature distribution was made. The position, size and temperature of the thermal source were detected. The reconstruction error was about 1–2 mm for the position and size and about 1 K for the temperature. These results were obtained when the measurement time was about 20 s. As well we carried out the acoustothermometrical control during the laser hyperthemia of the mammary gland. The medicine procedure was continued 10 min and the maximum gland acoustobrightness temperature was increased at about 5 K. These results allow us to advance to acoustothermography of biological objects.

ACKNOWLEDGMENT

This work has been supported by Russian Foundation for Basic Research (# 08-02-00240).

REFERENCES

1. Bowen, T., *Automedica (UK)*, Vol. 8, No. 4, 247–267, 1987.
2. Anosov, A. A., Y. N. Barabanenkov, K. M. Bograchev, R. V. Garskov, A. S. Kazanskij, and A. S. Sharakshane, *Acoustical Physics*, Vol. 54, 432–436, 2008.
3. Anosov, A. A., R. V. Bel'aev, V. A. Vilkov, A. S. Kazanskij, A. D. Mansfel'd, and A. S. Sharakshane, *Acoustical Physics*, Vol. 54, 464–468, 2008.

Inversion Algorithm for Microwave Breast Cancer Detection Using Level Sets

N. Irishina, **D. Álvarez**, **O. Dorn**, **P. Medina**, **and M. Moscoso**
University Carlos III de Madrid, Spain

Abstract— Microwave tomographic imaging is a promising direction for the early detection of breast cancer. Its physical basis is the high contrast between the dielectric properties of the healthy breast tissue and the malignant tumors at microwave frequencies. This advantage can be used to enhance the diagnosis at early stage of cancer.

We present a four stages reconstruction algorithm for breast cancer detection from microwave data. The main idea is to use submodels of increasing complexity at each new stage of the algorithm. At each new stage, the reconstructed breast model incorporates more features of the complete breast, so it is more refined than the reconstruction of the previous stages. Moreover, the result of each preceding stage is used as the starting guess for the next one in which more details of the breast interior are sought in a sequential way.

The inverse problem associated to the reconstruction of the breast interior is formulated as a shape reconstruction problem. This assumption reduces the dimensionality of the inverse problem and thereby stabilizes the reconstruction process. The shape-based approach offers several advantages compared to more traditional pixel-based approaches, as for example, well-defined boundaries and the incorporation of an intrinsic regularization regarding the types of tissues composing the breast, which in our case are: the skin, fibroglandular tissue fat, and tumorous tissue (each one having different dielectric properties). We use the level set technique for the implicit representation of the shapes of regions with each type of tissue. The implicit representation of shapes by level set functions easily handles the topological changes during the reconstruction.

Our reconstruction strategy is able to detect millimeter size tumors and simultaneously determine their locations, sizes, and permittivity values. Our numerical experiments show that the detection and characterization of small tumors are robust even when applied to realistic MRI derived breast models. Being able to recover the dielectric properties of a detected object in the breast could help to discriminate between benign and malignant tumors, and may lead to determine whether a normal tissue is in the process of becoming malignant.

We present numerical results in 2D which demonstrate the performance of our scheme in various simulated realistic situations. We show that using our four stages strategy, we are able to reconstruct successfully the distribution of the dielectric parameters of the breast interior even without the prior knowledge of neither the skin characteristics nor the average dielectric properties of the tissues that compose the breast.

SQUIDs for Magnetic Resonance Imaging at Ultra-low Magnetic Field

A. N. Matlashov, **V. S. Zotev**, **R. H. Kraus, Jr.**, **H. Sandin**,
A. V. Urbaitis, **P. L. Volegov**, **and M. A. Espy**
Los Alamos National Laboratory, Applied Modern Physics Group,
MS D454, Los Alamos, NM 87545, USA

Abstract— Nuclear magnetic resonance (NMR) methods are widely used in medicine, chemistry and industry. One NMR application is magnetic resonance imaging or MRI. MRI is among the most effective diagnostic tools in medicine. Conventional MRI instruments use strong magnetic fields for nuclear spin polarization and Faraday coil variants for signal detection. NMR signal strength and frequency is proportional to the strength of the polarizing field. In addition, the sensitivity of Faraday coil based receivers tends to increase with frequency. The common trend in NMR instrumentation is the pursuit of the highest possible field strength associated with the polarizing field. Commercial or nearly commercial efforts have field strengths approaching 7 Tesla. Recently it has become possible and practical to perform NMR and MRI at a small fraction of these enormous field strengths. The now so-called "Ultra-low Field" (ULF) regime requires field strengths only on the order of a few Gauss (1 Tesla = 10,000 Gauss). These ultra low field techniques exploit the properties of superconducting quantum interference devices or SQUIDs. SQUID magnetic sensing technology allows for ultra-sensitive detection while a class of strong pulsed pre-polarizing fields greatly enhance signal. SQUID sensing technology is a key component for Biomagnetism instrumentation such as magneto-encephalography (MEG). Modern MEG systems have a few hundred SQUID-based detectors working inside large magnetically shielded rooms. Such SQUID arrays could be used in conjunction with ultra-low field MRI techniques to record MEG signals as well as the anatomical data associated with conventional MRI. The first ever human brain ULF MRI and simultaneous MEG signals were recorded in LANL in 2008. SQUID arrays and the associated gradiometers as a key sensing component for ULF MRI instrumentation, require different approaches to design and construction than SQUIDs for MEG. In this paper we describe the world first SQUID-based instruments that are capable of performing simultaneous ULF MRI and MEG. Computer models and simulations have been used for further optimization of these designs. Present status and future design trends of this revolutionary new instrumentation will be also discussed.

Utilizing the Superconducting Bilayer As a Spintronic Sensor

J. G. Lin[1], **Daniel Hsu**[1], **Awadhesh Mani**[2], **and T. Geetha Kumary**[2]

[1]Center for Condensed Matter Sciences, National Taiwan University, Taipei 106, Taiwan
[2]Materials Science Division, Indira Gandhi Centre for Atomic Research, Kalpakkam 603102, India

Abstract— The experimental investigation on the physical properties of superconducting/magnetic S/F layer system started around 1980's, and continued with a longstanding importance due to the novelty of its underlying potential for the technological applications. Based on the physics of proximity and spin-injection, the magnet/superconductor bilayer can be utilized as a spintronic sensor. In this work, we demonstrate the magnetic and transport properties of various hybrid systems consisted of manganite/$YBa_2Cu_3O_7$ (YBCO) bilayer. It is clearly shown that the superconducting transition temperature is very sensitive to the degree of spinpolarization and the magnetic state of the manganite. In particular, the spin-canting state in $Nd_{0.35}Sr_{0.65}MnO_3$ (NSCO) effectively induces a finite resistance in the superconducting state of YBCO, which may be attributed to the interfacial vortex penertration induced by the internal field. As shown in the upper panel of Fig. 1, the temperature dependent resistivity of NSMO displays a dip around 46 K, which is marked as the spin-canting transition temperature T_{CAF}. In the lower panel of Fig. 1, the bilayer of NSMO (40 nm)/YBCO (70 nm), denoted as NY47, has zero-resistance below the transition temperature T_c. However, finite resistance appears between T_{CAF} and the re-entrance temperature of superconducting state T_{re}, owing to the vortex dissipation.

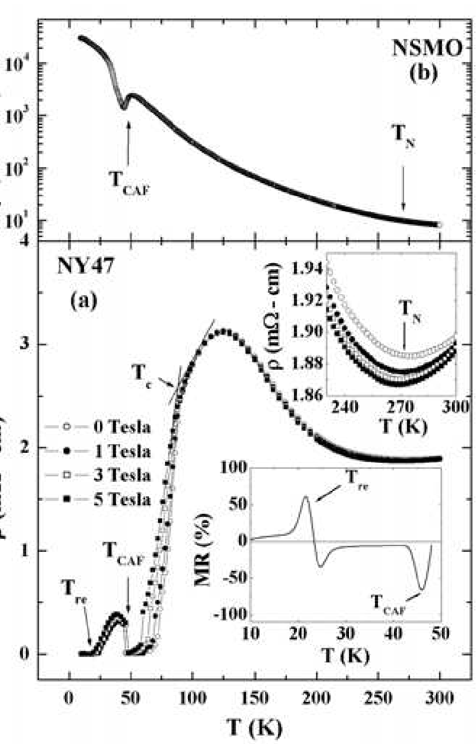

Figure 1: The resistivity vs. temperature for single layer of NSMO and the bilayer NY47.

Applications of Ultra-low Field Magnetic Resonance: From Brains to Bombs

Michelle Espy, **Andrei Matlashov**, **Yonathan Araya**, **Mark Flynn**, **John Gomez**, **Cristina Hanson**, **Robert Kraus**, **Per Magnelind**, **Karlene Maskaly**, **Pulak Nath**, **Shaun Newman**, **Tuba Owens**, **Mark Peters**, **Henrik Sandin**, **Igor Savukov**, **Larry Schultz**, **Al Urbaitis**, **Petr Volegov**, **and Vadim Zotev**
Los Alamos National Lab, P. O. Box 1663, MS D454, Los Alamos, NM, USA

Abstract— It has become possible and practical to perform magnetic resonance imaging (MRI) at magnetic fields from μT to mT, the so-called ultra-low field (ULF) regime, using SQUID sensors and a pulsed pre-polarizing field. The ULF approach affords scientific advantages such as unique relaxation contrast and the overlap of the Larmor frequency with interesting and unexplored areas of molecular dynamics and biological processes. The instrumentation allows for flexibility in signal acquisition sequences such as the ability to easily change the measurement field strength or orientation, and practical benefits such as the ability to image through conducting containers. The SQUID instrumentation enables simultaneous measures of brain anatomy via MRI, and function via magneto-encephalography (MEG). The technology may produce a new generation of light-weight and affordable MRI medical instrumentation for medical, security, and industrial applications. We describe the motivation, and advantages of the ULF MRI approach, several approaches to realizing ULF MR instrumentation, and present an overview of recent results for several applications of ULF MRI exploiting the unique abilities of the method. Included are novel ways to image both brain structure and function either by combination of MRI with MEG or direct observation of the interaction of neural currents with the spin population. We present recent data from computational models of the brain, and measurements of the interaction of weak ($\sim$10 μA) currents with a spin-population in a water phantom, as studied by ULF MRI with implications for neural current imaging. We also present progress on detection and determination of enrichment fraction in uranium hexafluoride, a significant issue for treaty verification and non-proliferation. Finally, we present the results from a ULF MR relaxometer developed and deployed to an airport for inspecting liquids in a check-point for the presence of hazardous materials.

X-rays Source Using Thermal Excitation of Pyroelectric Crystal for Medical Application

S. Fukao[1], Y. Nakanishi[1], Y. Guan[1], Y. Sato[1], Y. Ito[2], and S. Yoshikado[1]

[1]Department of Electronics, Doshisha University, Kyoto, Japan
[2]Institute for Chemical Research, Kyoto University, Kyoto, Japan

Abstract— The electromagnetic wave of which wavelength is between approximately 10 and 0.01 nm is called X-ray. Although this electromagnetic wave is currently generated by an X-ray tube and so on, Brownridge has reported that X-rays are radiated by changing the temperature of a polarized pyroelectric crystal [1]. Downsizing of the device is possible using this method because the mechanism is simple. This small sized X-ray radiation device can be applied to the medical purpose because this device can radiate X-rays direct to cancer cells and cavity-causing bacterium. However, the X-ray intensity radiated by pyroelectric crystal is weaker than that radiated by X-ray tube. In this study, an investigation of X-ray radiation was carried out by changing the pressure and types of cylindrical material using a $LiNbO_3$ single crystal to enhance X-ray intensity.

Z-cut single crystal of $LiNbO_3$ ($10 \times 10\,\mathrm{mm}^2$ area, 5 mm thickness) polarized along the c-axis (z-axis) direction was used. An oxygen-free copper foil of 10 μm thickness placed at a distance of approximately 27 mm from the negatively charged surface ($-z$-surface) of the crystal. The crystal with the Peltier device was placed at the center of a hollow cylinder of 26 mm inner diameter and 19 mm height. The ambient gas was N_2 and the pressure in the vacuum chamber was set in the range from 7×10^{-3} to 5 Pa. The temperature of the crystal was changed from 0 to 80°C by supplying a triangular-wave bias voltage to the Peltier device. This temperature cycle was repeated with the duration of each cycle being 1000 s.

In the low vacuum range from 1 to 5 Pa, the integrated X-ray intensity for one cycle in the energy range from 1 to 20 keV was the same when the cylindrical material was aluminum, oxygen-free copper, and nickel, and became maximum at a pressure of approximately 4.5 Pa. When the cylindrical material was nickel, the characteristic X-ray of nickel was not detected. This result indicates that X-ray was more radiated from the target rather than the inner wall of cylinder. The integrated X-ray intensity decreased with increasing pressure from high vacuum range and had local minimum at approximately 1 Pa. This phenomenon was independent of cylinder material. When the cylindrical material is oxygen-free copper and the pressure is 7×10^{-3} Pa, the integrated X-ray intensity was the same intensity which was obtained in the low pressure range. It was suggested from above result that the mechanism of the electron generation was different between low and high vacuum. In the low vacuum, the gas molecules become ionized by the electric field formed by the crystal, and electrons were generated. Meanwhile, it has been reported that electrons are emitted from the cylinder and target by field emission in the high vacuum [2]. If the temperature of crystal is increased, the electrons emitted by field emission collide with the $-z$-surface of the crystal and characteristic X-rays specific to the elements of the crystal is radiated. Then, the electrons are accumulated on $-z$-surface, because $-z$-surface is net positively charged and the crystal is insulator. When the temperature of crystal is decreased, $-z$-surface becomes neutrality and is net negatively charged. Thus, accumulated electrons are accelerated towards the target and cylinder. In the low vacuum, it is speculated that the gas molecules around the target become ionized by the electric field formed by the crystal, and electrons are generated. These electrons collide with the target, and X-rays are radiated. Meanwhile, in the high vacuum rage, X-rays are radiated due to the collision of accumulated electrons with the target and cylinder. This is because the number of electron which is generated during decreasing the temperature is little and the mean free path of an electron is larger than the distance between the crystal and target.

REFERENCES

1. Brownridge, J. D. and S. Raboy, *J. Appl. Phys.*, Vol. 86, 640, 1999.
2. Fukao, S., et al., *AIP Conference Proceedings*, Vol. 1099, 88, 2009 (in press).

Session 3P5
Novel Mathematical Methods in Electromagnetics 3

The Time-domain Waveguide Modes Unlike to the Classical Time-harmonic Waves

O. A. Tretyakov[1] **and Ö. Akgün**[1,2]

[1]Department of Electronics Engineering, Gebze Institute of Technology, Gebze, Kocaeli, Turkey
[2]Electrical and Electronics Engineering, Aksaray University, Aksaray, Turkey

Abstract— We consider an ideal medium-free waveguide having a cross-section domain S invariable along the waveguide axis Oz. It is supposed that the domain S is bounded by a closed singly connected contour L. The contour has an arbitrary but enough smooth shape. The latter implies that none of its possible *inner* angles (i.e., measured within S) exceeds π. It is supposed as well that the waveguide surface has the physical properties of the perfect electric conductor. Formulation of the problem involves the following statements: 1) the system of source-free Maxwell's equations with time derivative, 2) the boundary conditions over the waveguide surface, 3) the initial conditions for the modal fields at an initial instant of time ($t = 0$), and 4) the modal fields subjected to the causality principle (weak and strong causalities both). The electric and magnetic intensity vectors of the modal fields are presented as the sums of the two-component transverse (in regard to Oz) vectors and the one-component axial vectors. The cases of TE- and TM-waveguide modes are considered in parallel. Every field component is obtained as a product of a vector function of transverse coordinates and a scalar function depending on z and t. The latter has the physical sense of the modal amplitudes of appropriate modal field components. It is proved that the modal amplitudes are expressible via the linearly independent solutions to Klein-Gordon equation with variables z and t. Klein-Gordon equation has remarkable properties of symmetry in the sense of the group theory. Main subject of this presentation is a discussion on various applications of just these properties of symmetry in the waveguide theory. Many theorists are of opinion that using $\exp\left[i\left(\omega t \pm \gamma z\right)\right]$ is nearly one way available for presentation of the modal amplitudes (where $i = \sqrt{-1}$, ω is the given frequency parameter, γ is the wave number). However, the above mentioned properties of symmetry disclose that it is simply and solely one way among 11 possible others. One of them will be presented here in which the modal amplitudes are expressible via product of Airy functions with special arguments depending on z and t.

Reflection and Scattering of Electromagnetic Waves in Spatial Grids Consisting of Multiple Lossy Waveguides

Yasumitsu Miyazaki
Department of Media Informatics, Aichi University of Technology
50-2 Manori, Nishihasama-cho, Gamagori 443-0047, Japan

Abstract— Medical diagnosis technologies using X-ray and optical wave transmitted tomography have been rapidly developed with computer processing. X-ray and optical transmitted field characteristics in CT, that depend on biomedical absorption due to bio-molecules and atoms, yield biomedical information of human body tissues and cells. However, X-ray and optical transmitted field signals at receiving output of diagnosis CT sensors are disturbed by scattering waves in random bio-medical inhomogeneities around objects of body tissues and cells. Before signal processing of received signals by computer, hardware tools of spatial filtering of disturbing scattering fields for absorption characteristics in bio-medical tissues and cells are very useful system functions.

Spatial filtering of scattered fields by grid arrays consisting of transversely multiple lossy waveguides is one of excellent device function for spatial filtering in X-ray and optical diagnosis. Spatial filter of grid arrays consisting of multiple lossy waveguides is waveguide array consisting of waveguides with transparent cores and lossy clads. Each waveguide has core size of a, clad size of b and waveguide length of ℓ. Scattered fields in random bio-medical media are incident on input plane of spatial filter array, and coupled to lower modes of low losses for small scattering angles and higher modes of large losses for large scattering angles, in lossy waveguide array. Low angle scattered fields couple to lower modes and large angle scattered fields couple to lossy higher modes.

Scattered fields coupled to lossy higher modes are filtered in lossy grid arrays. Mode characteristics in lossy grid arrays excited by scattered field in random bio-medical media are discussed by mode expansion methods using boundary condition at input plane of lossy grid array, and filtered fields at output plane of lossy grid array are shown by integral equations using Green's dyadics. Mode characteristics and filtered fields are also investigated by the Wiener-Hopf method with spectral functions.

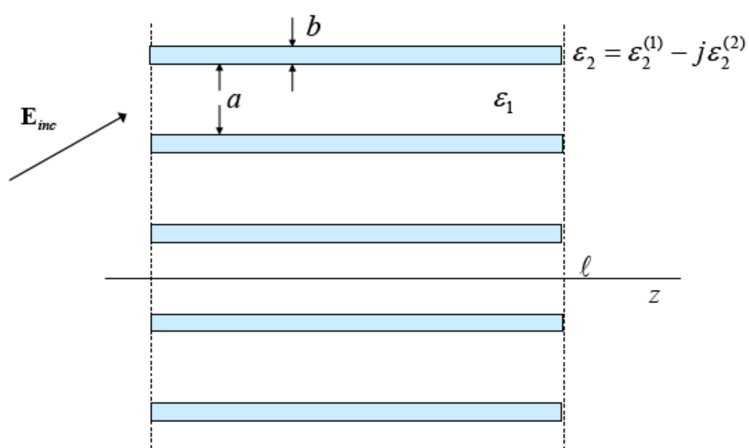

Figure 1: Filtered fields in lossy waveguide grid arrays.

REFERENCES

1. Miyazaki, Y., "Electromagnetic characteristics of grid structures for scattering fields of nanometer electromagnetic waves and X-rays," *Progress In Electromagnetics Research Symposium Proceedings*, 643–647, Tokyo, Japan, August 2006.
2. Miyazaki, Y., "Partially coherent optical waves in random gradient fibers," *Optical and Quantum Electronics*, Vol. 9, 153–165, 1977.

3. Miyazaki, Y., "Electromagnetic characteristics of waveguide-type grid filters for scattered nanometer waves in transmitted X-ray diagnostic images," *Proc. of EMTS 2007*, EMTS128, Ottawa, ON, Canada, Jul. 2007.
4. Miyazaki, Y., "Spatial filtering characteristics of scattered fields by inhomogeneous waveguide grids for X-ray image diagnosis," *Progress In Electromagnetics Research Symposium Proceedings*, 497–503, Cambridge, USA, July 2–6, 2008.

Electromagnetic Analysis of Propagation and Scattering Fields in Dielectric Elliptic Cylinder on Planar Ground

Yasumitsu Miyazaki[1], **Tadahiro Hashimoto**[2], **and Koichi Takahashi**[1]

[1]Department of Media Informatics, Aichi University of Technology
50-2 Manori, Nishihasama-cho, Gamagori, Aichi 443-0047, Japan
[2]Broadband Technology Department, Synclayer, Inc.
1-20 Himegaoka, Kani, Gifu 509-0249, Japan

Abstract— Radio wave technologies using electromagnetic waves of microwaves and ultra-high frequencies have been rapidly developed for high bit rate wireless communications and RFID application in out-door and in-door spaces. Signal detection evaluation is very important factor in these systems including several objects along propagation paths of urban streets and country suburb, and, in houses and building.

In order to estimate scattering and interference fields in many environments, typical useful models for scattering objects are dielectric elliptic cylinders on the planar ground. Field intensity distributions of electromagnetic waves in these circumstances are studied by Mathieu function expansion with addition theorems. Incident and scattering fields are expanded by Mathieu function series and coefficients of series are derived by electromagnetic field continuity equations of boundary conditions on the elliptic cylinder and planar surface.

Reflection and scattered fields by elliptic cylinders on planar ground are shown by these series coefficients, and also fields in shadow regions between dielectric elliptic cylinders and planar ground. Field intensities in the elliptic cylinder including resonance cases for particular frequencies are evaluated. Reflection and scatted fields are compared with computer simulation results derived by numerical calculation of the FDTD method. Based on these field calculations optimum system design of WiMAX wireless communications and RFID systems in out-door and in-door space regions. Positions and locations of radiating and receiving antenna for RF stations and RF readers may be decided from field results of this theory.

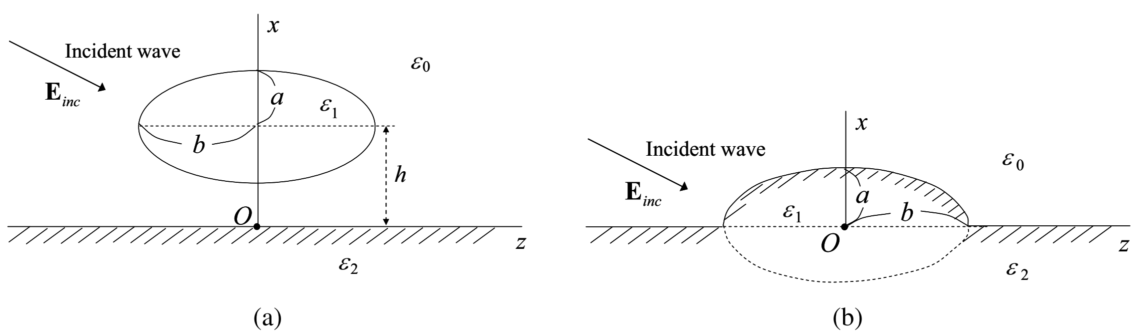

Figure 1: Dielectric elliptic cylinder on planar ground.

REFERENCES

1. Rodriguez, G., Y. Miyazaki, and N. Goto, "Matrix-based FDTD parallel algorithm for big areas and its applications to high-speed wireless communications," *IEEE Trans. Antennas and Propagation*, Vol. 54, No. 3, 785–796, 2006.
2. Masuda, T. and Y. Miyazaki, "Scattering characteristics of electromagnetic environment by construction on the ground," *Trans. IEE Japan*, Vol. 118-C, No. 1, 112–117, 1998.
3. Taki, K. and Y. Miyazaki, "Input impedances and current distributions for meander line antennas with planar coupled parasitic meander element," *Progress In Electromagnetics Research Symposium Proceedings*, 1700–1703, Beijing, China, March 26–30, 2007.
4. Masuda, T., Y. Miyazaki, and Y. Kashiwagi, "Analysis of electromagnetic wave propagation in out-door active RFID system using FD-TD method," *Progress In Electromagnetics Research Symposium Proceedings*, 1713–1715, Beijing, China, March 26–30, 2007.

Eigenvalue Analysis of Waveguides and Planar Transmission Lines Loaded with Full Tensor Anisotropic Materials

C. S. Lavranos, D. G. Drogoudis, and G. A. Kyriacou
Department of Electrical and Computer Engineering, Microwaves Lab.
Democritus University of Thrace, Xanthi, Greece

Abstract— The eigenvalue analysis, providing the propagation constants and the corresponding fields distributions, of waveguiding structures comprise a significant key tool in the design of several microwave devices, e.g., filters, dividers and couplers. Due to the interest of the subject, a variety of such techniques have been presented in the literature [1]. But, to the authors knowledge, none of them can handle curved geometries or planar curved waveguides. The latter can be found in a plethora of microwave circuits and systems, such as airborne platforms, modern phased arrays and Radar systems. Moreover, the recent adoption of "smart skin" ideas demands the whole RF front end to be conformal to the host objects surface. Thus, the accurate design of conformal systems demands the knowledge of curved waveguides and printed transmission lines characteristics.

Our research effort is based on a two-dimensional Finite Difference Frequency Domain (2-D FDFD) eigenvalue method formulated in orthogonal curvilinear coordinates. The theoretical basics and a variety of applications have been presented in our previous works, e.g., [2]. The finite difference discretization is applied by means of an orthogonal curvilinear grid, which leads to an eigenvalue problem formulated for the complex propagation constants and the corresponding fields distributions of curved structures. Following a 2-D scheme, this analysis is restricted to structures uniform along the propagation direction. Its direct implementation in orthogonal curvilinear coordinates leads to an accurate description of curved or bent geometries with a coarse enough grid but free of the well known stair case effect. The waveguiding structure can be curved in all directions (obeying some limitations with respect to the curvature along the propagation axis) and this constitutes its main advantage.

An inherent feature of the elaborated FDFD method is the well-known Finite Difference ability of handling anisotropic materials. In particular, its matrix-format implementation in conjuction with its formulation with complex mathematics enables the introduction of anisotropic materials, including their losses, through a simple modification of the corresponding permittivity or permeability matrices. However, until now our work mainly included isotropic or diagonally anisotropic materials. Thus, in this paper our method is extended in order to accurately handle arbitrarily shaped curved geometries full or partially loaded with full tensor anisotropic materials. These materials can be full tensor anisotropic media, ferroelectrics or magnetized ferrites, or even artificial metamaterials, provided that their complex tensors constitutive parameters are available. Numerous investigations are carried out involving all type of forward or backward propagating modes as well as complex ones. The most interesting structures, involving non-reciprocal or electrical tunable behavior, will be discussed during the presentation.

ACKNOWLEDGMENT

This work is implemented in the framework of Measure 8.3 through the O. P. Competitiveness 3rd Community Support Programme and is co-funded by: 75% of the Public Expenditure from the European Union — European Social Fund, 25% of the Public Expenditure from the Hellenic State — Ministry of Development — General Secretariat for Research and Technology, and Private Sector (INTRACOM SA).

REFERENCES

1. Hwang, J. -N., "A compact 2-D FDFD method for modeling microstrip structures with nonuniform grids and perfectly matched layer," *IEEE Transactions on Microwave Theory and Techniques*, Vol. 53, No. 2, 653–659, 2005.
2. Lavranos, C. S. and G. A. Kyriacou, "Eigenvalue analysis of curved waveguides employing an orthogonal curvilinear frequency domain finite difference method," *IEEE Transactions on Microwave Theory and Techniques*, Vol. 57, No. 3, 594–611, 2009.

Numerical Investigation of Sensitivity Matrix in Three-dimensional Microwave Tomography

D. G. Drogoudis[1], **G. A. Kyriacou**[1], **and J. N. Sahalos**[2]

[1]Department of Electrical & Computer Engineering, Democritus University of Thrace, Xanthi, Greece
[2]Department of Physics, Aristotle University of Thessaloniki, Thessaloniki, Greece

Abstract— Sensitivity analysis is widely used during optimization for the design of various microwave devices as well as in microwave tomography to evaluate their performance or to locate any critical parameters. Exploiting the field distributions over the structure, obtained through a number of electromagnetic simulations with appropriate sources, the sensitivities can be evaluated through closed form expressions. The latter can be extracted by combining the adjoint network theorem and the reciprocity theorem of electromagnetics [1, 2]. The present effort is focused on microwave tomography application. So the desired sensitivities are the derivatives of the electric field with respect to the object's complex permittivity.

$$\varepsilon^* = \varepsilon_0 \varepsilon_r (1 - j \tan \delta) = \varepsilon \left(1 - j \frac{\sigma}{\omega \varepsilon}\right) \tag{1}$$

First two sets of Maxwell equations are considered, one for the normal problem-normal fields and one for the adjoint problem — adjoint fields. Combining these two sets in a procedure similar to that used in the derivation of the reciprocity theorem and defining the adjoint sources we conclude to the final sensitivity equation. Now considering that the Finite Element method (FEM) is used for the solution of the forward problem the unknown sensitivity integrals can be calculated since their integrands are comprised of the FEM basis functions. So following this procedure the sensitivity matrix for a microwave tomography application can be effciently evaluated. A numerical investigation of this matrix will be given in terms of the antennas number, position, and frequency and in terms of the number of the problem unknowns. The numerical investigation will be based on a Singular Value Decomposition (SVD) of the Sensitivity Matrix [3] and the degree of ill-posedness will be calculated for each case. The resulting singular vectors constitute the numerical basis functions on which the reconstruction scheme is developed. The aim of the present analysis is to investigate how these singular vectors cover the whole domain to be imaged, as well as how each one of them can be realized through appropriate excitation. In turn, this knowledge will be exploited in the establishment of an appropriate data collection strategy. Namely define the appropriate antenna position, orientation and polarization for both transmit (illumination) and receive (sensing) functions.

ACKNOWLEDGMENT

This work is implemented in the framework of Measure 8.3 through the O.P. Competitiveness 3rd Community Support Program and is co-funded by: (75%) of the Public Expenditure from the European Union — European Social Fund, (25%) of the Public Expenditure from the Hellenic State — Ministry of Development — General Secretariat for Research and Technology, and Private Sector (INTRACOM SA).

REFERENCES

1. Nikolova, N. K., Z. Jiang, L. Dongving, M. H. Bakr, and J. W. Bandler, "Sensitivity analysis of network parameters with electromagnetic frequency-domain simulators," *IEEE Trans. on Microwave Theory and Techniques*, Vol. 54, No. 2, 2006.
2. Dyck, D. N., D. A. Lowther, and E. M. Freeman, "A method of computing the sensitivity of electromagnetic quantities to changes in materials and sources," *IEEE Trans. on Magnetics*, Vol. 30, No. 5, 1064–1076, 1994.
3. Fang, Q., P. M. Meany, and K. D. Paulsen, "Singular value decomposition of the jacobian matrix in microwave image reconstruction," *IEEE Trans. on Antennas and Propagation*, Vol. 54, No. 88, 2006.

Exact Explicit Solution for Electromagnetic Step Signals Propagating along Waveguides

O. A. Tretyakov[1, 2], **S. Aksoy**[1], **and E. Eroğlu**[1]

[1]Department of Electronics Engineering, Gebze Institute of Technology, Gebze, Kocaeli, Turkey
[2]Chair of Theoretical Radiophysics, Kharkiv National University, Kharkiv, Ukraine

Abstract— Complete set of the digital signals given within a finite time interval $[0, T]$ as the functions of time, where T is the base time, can be presented as appropriate linear combination of the Heaviside step functions. Eventually, in order to study the digital signal transferring along the waveguides, it is necessary to solve carefully the problem of waveguide propagation for a single Heaviside step *electromagnetic* signal. Some preliminary results on this topic were published recently in article [1]. In this presentation, we extend that analysis on a more wide set of the situations. The waveguide under study is geometrically regular along its axis, its cross section is bounded by a closed singly-connected domain. The waveguide surface has the properties of the perfect electric conductor. The problem is solved within the analytical framework of the evolutionary approach to electromagnetics. One can find rigorous description of this method and appropriate historical background in [1]. Complete sets of the *TM*- and *TE*-modes are obtained. Every field component is product of two factors. One of them is a vector function of *transverse* waveguide coordinates. They are specified via the well studied solutions to Dirichlet and Neumann boundary eigenvalue problems for transverse Laplacian as their potentials. Physically, these vector functions specify the distributions of the modal force lines in the waveguide cross section. The other factors, which are scalar functions, have physical sense of the modal amplitudes for the waveguide field components. They are obtained explicitly as the products of a simple algebraic function and the Bessel functions, the order (index) of which is a *free parameter*. Both of these factors, which specify the modal amplitudes, depend on the waveguide axial coordinate and time. Analytical and graphical results are presented for the cases when the orders of the Bessel functions are all possible integer and semi-integer numbers.

REFERENCES

1. Aksoy, S. and O. A. Tretyakov, "Evolution equations for analytical study of digital signals in waveguides," *Journal of Electromagnetic Waves and Applications*, Vol. 17, No. 12, 1665–1682, 2003.

Revised Optical Properties of Turbid Media on a Base of General Improved Two-flux Kubelka-Munk Approach

D. A. Rogatkin[1] **and V. V. Tchernyi**[2]

[1]Moscow Regional Research & Clinical Institute "MONIKI"
Shepkina Str., 61/2, Moscow 129110, RF, Russia
[2]Scientific Agency "SAIBR", Vavilova Str., 97, Fl. 14, Off. 35, Moscow 117335, RF, Russia

Abstract— Kubelka-Munk (KM) two-flux transport one-dimensional (1D) model is the most widely used Radiative Transport Theory (RTT) approach in a modern optics of turbid media because of its simplicity and existence of its clear and analytical solution. Moreover, the KM approach is the best approximation of the general Radiative Transport Equation (RTE) in the case of 1D theoretical problem. But it is well known from the literature that the KM model doesn't allow anyone to obtain an exact solution, especially in the case of highly-absorbing and weakly-scattering media. In the most of publications, it is assumed that the light must be diffuse on a surface as well as within the medium for a correct application of the KM equations. However, it was recently shown [1], contrary to the well-known literature data, that the classical KM model could give absolutely exact values for the boundary fluxes (transmitted and backscattered radiation) for any cases of scattering and absorbing media by means of small reformulation of initial differential equations and by means of more correct initial definition of transport optical properties of the media — absorption and scattering. It was estimated that in a general case, when absorption is presented, the first coefficient in the right side of the differential RTE and/or KM equations cannot be separated into two independent transport coefficients — absorption and scattering ("K" and "S" in the KM notations or "mu_a" and "mu_s" in the RTE notations). It must be considered as one, united attenuation coefficient "AC". The absorption transport property "K" (mu_a) is included into "AC" as well as into the second coefficient of equations ("S" or "mu_s"), but not additively. Without absorption K = 0 and AC = S, without scattering S = 0 and AC = K, like it exists in the classical RTT, but if both an absorption and scattering are presented, then the classical phenomenological assumption AC = K+S is wrong. It is the main source of errors in both classical theories if the boundary fluxes, for example, are calculated. Only if the absorption in a medium is small, much less than scattering, then the classical assumption can take place. Moreover, such modification of the KM equations showed anyone an equivalence between absorption coefficients in both theories, i.e., allowed us to estimate exactly that K = mu_a, what is contrary to the well-known literature data as well, but, in our opinion, is more reasonable than K = 2 * mu_a, what is widely used today in a lot of publications. Basing on this improvement of 1D theoretical approach it is easily to show that such optical properties of turbid medium like albedo (W_0) needs a reformulation as well. In the classical case of KM equations $W_0 = S/(K+S)$ what strongly means a relation between second and first coefficients of the initial differential equations. Modified coefficients of the differential equations will give a little bit another value of W_0 than it is in the classical case.

REFERENCES

1. *Biomed. Engin.*, Vol. 41, No. 2, 59–65, 2007.

Modeling of Infinite Periodic Arrays with Dielectric Volumes and Quasi-3D Oriented Conductors

V. Volski and G. A. E. Vandenbosch
ESAT-TELEMIC, Katholieke Universiteit Leuven, Belgium

Abstract— A further development of a new asymptotic extraction technique used to model periodic arrays within the MoM formulation is reported. This technique was consecutively applied to model periodic arrays only with horizontal conductors and then with the combination of vertical and horizontal conductors. In this paper dielectric volumes are included into consideration. The combination of vertical and horizontal conductors with dielectric volumes widens considerably the variety of modelling topologies. Several examples will be presented in the final paper.

A mixed potential integral equation approach in the MoM formulation requires the calculation of the Green's functions in the spatial domain for different source types (electric horizontal, vertical dipoles and volumes). The algorithm of their calculation is quite cumbersome and its implementation needs a lot of efforts. The chosen approach relies on a strong resemblance between the two algorithms to calculate Greens Functions (GFs) for a single dipole and a periodic array of dipoles. The original algorithm for a single dipole is slightly adjusted in such a way that the periodicity of the dipoles can be implemented easily. In practice this means that major steps like the calculation of GFs in the spectral domain can remain almost the same and only a few additional procedures are required. The main advantage of this approach is that it is a modular analysis technique, which allows to develop and to test new features in the global modelling scheme simultaneously for a single dipole and a periodic array of dipoles. This becomes possible because in both cases the GFs in the spatial domain are calculated via the Inverse Fourier Transform (IFT) from the same spectral GFs. Fundamentally, the only difference consists of how the IFT is expressed in terms of double infinite integrals (single dipole) or a double infinite series (periodic array). The main problem in the numerical evaluation of the IFT is the poor convergence of the spectral components. The extraction technique allows to solve this problem. By subtracting the asymptotes from the spectral GFs and adding them again but to the spatial GFs, the numerically calculated part of the transform becomes much easier to handle. The calculation of coupling matrix needed in the MoM formulation is based on the expansion of GFs in the Taylor series. This procedure remains similar in both cases, only for periodic arrays a 2D interpolation routine is used instead of a 1D interpolation routine for a single dipole.

The main idea of our asymptote extraction technique is to use the same asymptotes in both cases (for a single dipole and a periodic array). The application of this technique was shown at EUCAP 06 for horizontal conductors and at EUCAP07 for horizontal and vertical conductors. In this paper we report our progress in the implementation of dielectric volume.

Over Set Grid Generation Method for the Analysis of Electromagnetic Field While Considering the Lorentz Transformation

Hiroshi Iwamatsu and Michiko Kuroda
School of Computer Science, Tokyo University of Technology, Japan

Abstract— In this paper, a new approach, which is a combination of the FDTD method and the Over Set Grid Generation method while considering the Doppler Effect, is proposed for the analysis of the moving boundary problem for higher velocity values. By using the overset grid generation method with the interpolation technique, the FDTD method can be applied to solve the electromagnetic field around a complicated or moving object easily and accurately. We have already proposed this technique for the analysis of electromagnetic field with moving boundaries for lower velocity value. Here, for higher velocity value, Lorentz Transformation is applied to this technique to analyze the moving boundary problems. To calculate FDTD method, time that changed by Lorentz Transformation must be fixed.

In this technique, the position of the points on the moving boundary is defined relative to a static main grid. The values of the boundary of the overlapped region are obtained by interpolating the values on the static main grid. It is the advantage of this approach that the complex moving domains are dealt with more easily.

Here, the new scheme of the calculation parameter was proposed and as a bench mark, the received wave at the observation point is calculated when the observation point moves. It can be shown that the frequency and the amplitude of the received wave are shifted, according to the velocity. To verify these methods, some numerical results are compared with the theoretical results and good agreements are obtained. The numerical technique for the analysis of the electromagnetic field with moving boundaries for higher velocity values is shown.

REFERENCES

1. Iwamatsu, H., R. Fukumoto, M. Ishihara, and M. Kuroda, "Comparative study of over set grid generation method and body fitted grid generation method with moving boundaries," *IEEE APS 2008*, July 2009.
2. Iwamatsu, H., R. Fukumoto, and M. Kuroda, "Over set grid generation method for the analysis of the Doppler effect in the electromagnetic field," *ACES 2009*, March 2009.

Session 3P6
Microwave Treatment of Materials

Microwave Penetrating and Heating of Metallic Powders

A. P. Anzulevich[1], V. D. Buchelnikov[1],
I. V. Bychkov[1], and D. V. Louzguine-Luzgin[2]

[1]Chelyabinsk State University, Russia
[2]WPI Advanced Institute for Materials Research, Tohoku University, Japan

Abstract— Owing to so-called skin-effect bulk metals reflect microwaves (MWs) and can hardly be heated. They can undergo only surface heating due to limited penetration of the MW radiation. Whereas metallic powders can be penetrated into itself and absorb such radiation and efficiently heat. Recently MW heating has been successfully applied to powdered metals and fully sintered samples were obtained in 1999 in a multimode cavity. Later MW heating in separated electric (E-) field and magnetic (H-) field of a standing wave was performed. The MW sintering of various metals powders, steels and non-ferrous alloys helped to produce sintered samples within tens of minutes at sintering temperature ranges from 1370 K to 1570 K. Moreover, nanomaterials and some composite materials can also be produced by such a technique.

The reason of heating of metallic powders has not been clarified fully yet. Here for explanation of MW heating of metallic powders we propose the following model. We consider the metallic powder as some composite medium. This composite medium consists from the mixture of spherical metallic particles covered by thin oxide dielectric shell and gas (or vacuum) [1, 2].

Thus eddy currents can penetrate into metallic powders at a depth of the size of metallic particles due to sphericity of the skin-depth of these particles [3]. Whereas in bulk metals eddy currents can penetrate into a planar skin-depth only. But eddy currents in metallic powders can be generated on all surface of conductive particle if allowed a condition of quasistationarity. Condition of quasistationarity is requirement that a size of conductive domains less than wavelength of incident MWs.

So, in the present work, we theoretically studied using a model of conductive composite the MW penetrating mechanisms, the possible MW heating mechanisms of metallic powders and provide some theoretical explanation of the MW penetrating and MW heating behavior for iron powder (Fig. 1).

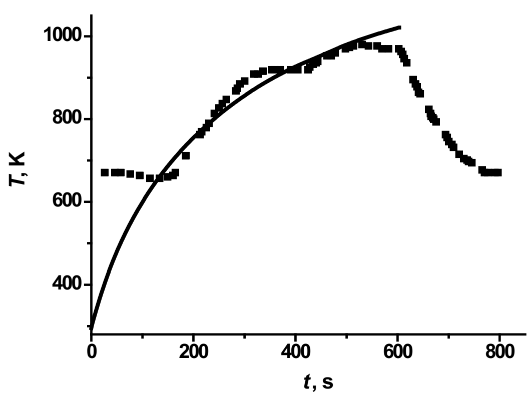

Figure 1: The time dependence of temperature for iron powder. The solid line is the modeling results; the dark square is the experimental ones.

REFERENCES

1. Buchelnikov, V. D., D. V. Louzguine-Luzgin, G. Xie, S. Li, N. Yoshikawa, A. P. Anzulevich, I. V. Bychkov, and A. Inoue, "Heating of metallic powders by microwaves: Experiment and theory," *J. Appl. Phys.*, Vol. 104, No. 9, 01, November 2008.
2. Anzulevich, A. P., V. D. Buchelnikov, I. V. Bychkov, D. V. Lousguine-Luzgin, N. Yoshikawa, M. Sato, and A. Inoue, "Penetration of microwave radiation into and through metallic powders," *Solid State Phenomena*, Vol. 152–153, 361–364, 2009.
3. Smythe, W. R., *Static and Dynamic Electricity*, 2nd Edition, New York, Toronto, London, 1950.

Effective Medium Approximation for Composite from Three-layered Spherical Particles

D. M. Dolgushin[1], **A. P. Anzulevich**[1], **V. D. Buchelnikov**[1], **I. V. Bychkov**[1], **and D. V. Louzguine-Luzgin**[2]

[1]Condensed Matter Physics Department, Chelyabinsk State University, Chelyabinsk 454021, Russia
[2]WPI Advanced Institute for Materials Research, Tohoku University, Sendai 980-8577, Japan

Abstract— Let us consider the three-layered spherical particles, which randomly distributed in gas (for example, in air) or vacuum. According to effective medium approximation (EMA) an average value of electric displacement of effective medium connects with an average value of electric field strength as

$$\langle \mathbf{D} \rangle = \varepsilon_{eff} \langle \mathbf{E} \rangle = \varepsilon_{eff} \mathbf{E}_0, \tag{1}$$

where ε_{eff} is the effective permittivity of composite, $\mathbf{E}_0$ is the external electric field, $\langle \mathbf{D} \rangle = (1/V) \int_V \mathbf{D} dV$, V is the volume of the whole composite.

In EMA, we deal with a mixture of two types of spherical particles, which are randomly distributed in the effective medium. The first type of particles is three-layered particles. As second type of particles we will consider spherical inclusions of gas (vacuum). It is considered that the permittivity of such a composite is equal to the permittivity of the effective medium.

After substitution of electrical fields in Eq. (1) and their integration we find the final equation for calculation of the effective permittivity of composite from three-layered spherical particles

$$\begin{aligned} &(\varepsilon_1 - \varepsilon_{eff}) K_1 p \frac{x_1}{x_2} + (\varepsilon_2 - \varepsilon_{eff}) K_2 p \frac{(1-x_1)}{x_2} + (\varepsilon_3 - \varepsilon_{eff}) K_3 p \left(1 - \frac{1}{x_2}\right) \\ &+ \; 3(1-p) \frac{(\varepsilon_g - \varepsilon_{eff})(2\varepsilon_{eff} A - \varepsilon_3 B)}{\varepsilon_g + 2\varepsilon_{eff}} = 0, \end{aligned} \tag{2}$$

where

$$\begin{aligned} K_1 &= 9\varepsilon_3 x_2 \beta_2 \left(1 + \frac{\alpha_1}{\beta_1}\right), \quad K_2 = 9\varepsilon_3 x_2 \frac{\alpha_1 \beta_2}{\beta_1}, \quad K_3 = 3x_2 (\alpha_1 \alpha_2 - 2x_1 \beta_1 \beta_2), \\ A &= x_1 \beta_1 (2\varepsilon_2 (1 - x_2) + \varepsilon_3 (1 + 2x_2)) - \alpha_1 (\varepsilon_2 (1 - x_2) - \varepsilon_3 (1 + 2x_2)), \\ B &= x_2 (2x_1 \beta_1 \beta_2 - \alpha_1 \alpha_2) - 2(\alpha_1 \beta_2 - x_1 \beta_1 \alpha_3), \\ x_1 &= \left(\frac{r_1}{r_2}\right)^3, \quad x_2 = \left(\frac{r_3}{r_2}\right)^3, \\ \alpha_1 &= \varepsilon_1 + 2\varepsilon_2, \quad \alpha_2 = \varepsilon_2 + 2\varepsilon_3, \quad \alpha_3 = \varepsilon_3 + 2\varepsilon_2, \\ \beta_1 &= \varepsilon_2 - \varepsilon_1, \quad \beta_2 = \varepsilon_2 - \varepsilon_3, \end{aligned}$$

ε_1, ε_2, ε_3, ε_g is permittivity of core, first shell, second shell and gas, p is the volume fraction of solid spherical particles in effective medium.

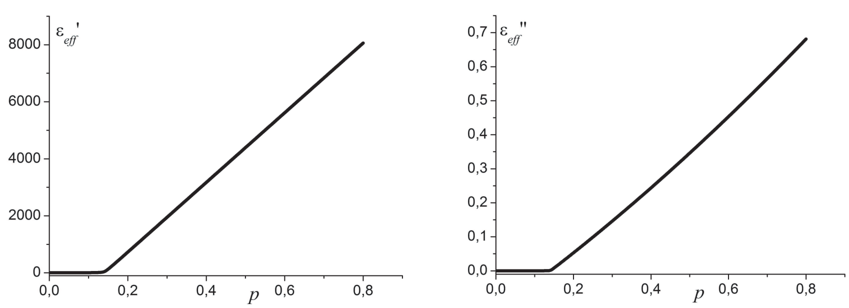

Figure 1: The dependences of real and imaginary parts of effective permittivity of composite from the volume fraction of solid spherical particles for one set of parameters.

Metallic Glassy and Composite Samples Produced by Using Microwave Radiation

D. V. Louzguine-Luzgin[1], **V. D. Buchelnikov**[2,3], **G. Xie**[2], **S. Li**[2], **A. Inoue**[1], **N. Yoshikawa**[4], **and M. Sato**[5]

[1]WPI Advanced Institute for Materials Research, Tohoku University, Sendai 980-8577, Japan
[2]Institute for Materials Research, Tohoku University, Sendai 980-8577, Japan
[3]Condensed Matter Department, Chelyabinsk State University, Chelyabinsk 454021, Russia
[4]Graduate School of Environmental Studies, Tohoku University, Sendai 980-8579, Japan
[5]National Institute for Fusion Science, 322-6 Oroshi, Toki, Gifu 509-5292, Japan

Abstract— Microwave heating is recognized for its various advantages, such as: time and energy saving, very high heating rates, considerably reduced processing cycle time and temperature, improved mechanical properties, better product performance, etc. In the present work, we study heating, phase transformations and sintering behavior of metallic glassy, crystalline and composite samples under microwave (MW) radiation. We developed new metallic glassy alloys and composites having a large supercooled liquid (SCL) region (temperature range between the glass-transition (T_g) and crystallization temperatures (T_x)) and significant flow-ability which can be used for MW treatment and sintering. We prepared powder glassy and nanocrystalline samples by gas atomization and mechanical milling techniques. We studied heating behavior of metallic powders by MW radiation and performed numerical fitting of the observed heating curves. We build a new custom-made MW radiation treatment machine (915 MHz), which allows electrical and magnetic field separation and pressing. We processed the metallic glassy and crystalline powders using a single mode MW applicator.

The metallic glassy alloy powders were produced by a high pressure argon gas atomization method using argon gas. The specimen powders were placed in a position of either E-field or H-field maximum area in the single-mode wave guide applicator and heated by energy absorption of MWs having 2.45 GHz or 915 MHz (for some samples) frequency. Among the studied alloys are $Fe_{73}Si_7B_{17}Nb_3$ and $Fe_{65}Co_{10}Ga_5P_{12}C_4B_4$, $Zr_{55}Cu_{30}Al_{10}Ni_5$ $Cu_{50}Zr_{45}Al_5$ and $Ni_{52.5}Zr_{15}Nb_{10}Ti_{15}Pt_{7.5}$ alloys sintered samples were obtained. Composite $Ni_{52.5}Zr_{15}Nb_{10}Ti_{15}Pt_{7.5}$/Sn and $Cu_{50}Zr_{45}Al_5$/Fe samples were also produced. Bulk metallic glasses (BMGs) exhibit high thermal stability, ultra-high strength and good corrosion resistance. The combination of superior properties and low material cost enhances BMGs to have promising applications as engineering and functional materials. However, the critical size of various BMGs obtained is much smaller compared to conventional crystalline alloys. Microwave heating of iron boride, Fe_3C powders, and mixtures of iron and iron boride powder was performed in the separated E- and H-fields. The heating mechanisms of metallic powder samples have also been studied and will be discussed in detail. The heating rate was found to depend upon various factors including electrical conductivity, thickness of the oxide layer, volume fraction of metallic part etc. which will also be discussed. We also studied phase transformations and heating behavior of iron based ceramic powders in a single mode microwave applicator.

Full Wave Analysis of Cylindrical Microwave Reactor

P. Pribetich[1], **C. Lohr**[2], **and D. Stuerga**[1,2]

[1]GERM/ICB, (Institut Carnot de Bourgogne), UMR 5209 CNRS, Université de Bourgogne
BP 47870, 21078 Dijon Cedex, France
[2]NAXAGORAS Technology, France

Abstract— Study of high power industrial applicators implies full wave analysis of loaded device as waveguides and especially cylindrical waveguides. Many interests have been shown in cylindrical geometry because of the extensive use of this geometry for fluids heating within a pipe. In case of lossy media, due to high level of dielectric losses, limits of classical perturbations approaches and modes established for lossless structures can be completely avoided.

Authors describe an original technique for making full wave analysis of an inhomogeneous cylindrical waveguide loaded by a lossy pipe. The mode spectrum of the studied structure can be obtained by use of analytical and numerical techniques. These matching conditions lead to the characteristic equation which is expressed by a matrix. The eigenvalue or complex propagation constant for each mode could be found within complex plane by a numerical procedure based on the residue theory. This procedure calculates the zeros of the characteristic equation within complex plane.

The results describe modes available in this kind of microwave applicators very close to industrial operating devices. TE and TM modes have been studied and all these modes obtained have been classified according to four classes: the propagative ($\beta > \alpha \approx 0$), the quasi-propagative ($\beta \approx \alpha$), the attenuated ($\alpha > \beta$), and the evanescent ($\alpha > \beta \approx 0$).

Thermal Tuning and Loop Modes within Cylindrical Applicator

D. Stuerga[1, 2], **C. Lohr**[2], **and P. Pribetich**[1]

[1]GERM/ICB, (Institut Carnot de Bourgogne), UMR 5209 CNRS, Université de Bourgogne
BP 47870, 21078 Dijon Cedex, France
[2]NAXAGORAS Technology, France

Abstract— The microwave applicator studied is constituted by two coaxial rods. The water pipe to be heated is described by the central lossy rod and the other medium is air (lossless dielectric). The cylindrical applicator has been shown because of the extensive use of this geometry for heating pipe. In conventional heating techniques or conduction techniques, high-power densities at the outer surface of the pipe lead to excessive heating of boundary layers, compared with higher flow rates along the pipe axis.

Full-wave analysis make by the authors have shown that it is possible to minimize electric field amplitude on the wall water pipe in order to reduce superheating. The advantage would be the highest value of electric field at specific regions where the loads are normally inserted. Moreover, the tuning due to thermal dependency of dielectric properties of water induces consequent change of the phase (β) and attenuation (α) constants of the propagation constant ($\gamma = \alpha + j$) within the temperature range 10°C–140°C.

The authors have obtained original modes which exhibit loop within (α, β) complex plane. Despite the strong tuning due to thermal dependency of dielectric properties of water, the mode guided wavelength has variation close to few millimetres within the temperature range 10°C until 140°C. According to these results; predictive control and design of optimized travelling wave applicators could be obtained. According to authors, a viable alternative to the trial and error methods currently used for designing microwave applicator for industrial heating applications has been set up.

Effects of Geometrical Parameters within Microwave Applicator Design

D. Stuerga[1,2], **C. Lohr**[2], **and P. Pribetich**[1]

[1]GERM/ICB, (Institut Carnot de Bourgogne), UMR 5209 CNRS, Université de Bourgogne
BP 47870, 21078 Dijon Cedex, France
[2]NAXAGORAS Technology, France

Abstract— The classical industrial design of microwave applicators and specifically the choice of the geometrical shape are based on a simple similarity principle between the wave propagation and spatial distribution within the empty and the loaded microwave applicator. The dielectric load is the object to be heated. Moreover, dielectric tuning due to thermal dependency of dielectric properties must be taken into account. Hence, this design method will be only valid if the dielectric perturbation induced by the reactor is negligible. In fact, the magnitude of the perturbation is proportional to reactor to applicator volume ratio. Hence, it is more efficient but also more complicated to be guided by a geometrical matching principle. According to this geometrical matching principle the microwave applicator designer want to ensure a good match between electric field spatial distribution and geometrical shape of the chemical vessel used. This geometrical matching principle is easier to apply for monomodes applicators because of the knowledge of the wave propagation directions and spatial distribution. The limit of this design method is that it requires the knowledge of the empty applicator modes, but also the of the loaded applicator modes.

The authors will show effect of geometrical parameters of a microwave applicator constituted by two coaxial rods. Effects of cylindrical waveguide and load diameters will be discussed in term of TE and TM modes propagation constants.

Measurement of Dielectric Properties and Finite Element Simulation of Microwave Pretreatment for Convective Drying of Grapes

S. R. S. Dev, Y. Gariépy, and G. S. V. Raghavan
Department of Bioresource Engineering, McGill University, QC, Canada

Abstract— In this study measurement and modelling of the dielectric properties of grapes was conducted on a matrix of frequencies (from 200 MHz to 10 GHz) and temperatures (5°C to 80°C). There are studies on the measurement and modelling of dielectric properties of grapes at 2.45 GHz for different temperatures. But there is no data available on the dielectric properties of grapes at different frequency. This gives a better understanding of the behaviour of the grapes on a broader electromagnetic spectrum and helps further simulation studies at other permitted frequencies like 915 MHz.

Mass production of dried raisins is often done by convective drying. The main problem in grape drying has been slow drying rate due to waxy layer at skin. Dipping in hot water or the use of chemicals such as sulphur, NaOH, and ethyl or methyl oleate emulsions are some of pretreatments widely used for grape drying to increase drying rate of raisins. While subjecting the grape berries to microwave heating, the moisture in the berry is heated to a saturation temperature, the temperature rises with pressure, resulting in volume expansion, causing the berry to rupture.

Research on the possible use of microwave as a pretreatment for the convective drying of grapes was conducted and found that if the rate of vaporization is controlled by the level of microwave energy applied, a puffed nature can be achieved by the rupture of different layers. In grapes, this rupturing is reported to start near the surface and propagate into the interior, giving the raisins a puffy texture, thus providing the necessary pathways for moisture migration from different layers of the berry. This enhances the drying rate in further drying process. But there is poor understanding of the mechanisms involved and actual energy distribution inside the grapes creating new channels for moisture migration.

In this study, a Finite Element Model (FEM) of the microwave pretreatment of the grapes was made and simulation studies were conducted for grapes subjected to 5 minutes pretreatment under 915 MHz and 2450 MHz and power densities of 0.5 W/g, 5 W/g and 50 W/g in order to visualize and investigate the energy distribution within the berries.

Multiphysics Simulations of Microwave Heating Phenomena in Domestic Ovens

Michal Soltysiak[1], **Malgorzata Celuch**[1], **and Ulrich Erle**[2]

[1]Institute of Radioelectronics, Faculty of Electronics and Information Technology
Warsaw University of Technology, Nowowiejska 15/19, 00-665 Warszawa, Poland
[2]Nestlé Product Technology Centre, Lebensmittelforschung GmbH Singen
Lange Str. 21, 78224 Singen, Germany

Abstract— This work presents a **multiphysics technique** for microwave heating simulations. Experimental validation for the case of food products in domestic microwave ovens is provided. Hence, the presented technique facilitates better understanding and more effective design of systems for microwave treatment of materials.

The multiphysics simulation technique combines **three building blocks**: a full-wave 3D electromagnetic solver, a set of thermal analysis modules, and temperature-dependent material data obtained via measurements. A commercial FDTD simulator, QuickWave-3D, constitutes the **electromagnetic** part of the system. It serves to calculate electromagnetic power converted into heat within the treated product. To this end, electromagnetic steady state with initial material parameters is first reached, and average values of power dissipated due to electric, magnetic, and metal losses are extracted. These are further applied as a 3D source function by a thermal module. Several **thermal modules** are available within the system, and an appropriate one is chosen depending on phenomena relevant to a particular scenario. In the simplest approach, the temperature pattern is updated from the initial state via a linear solution of the 3D heat diffusion equation. More typically, nonlinear problems are solved, where dielectric and/or thermal material parameters automatically varying as a function of local temperature or enthalpy density. These data are generated with the **in-house measurement** setups that will also be presented at the Symposium. The effects of load movement, including rotation in popular domestic ovens but also translation along user-defined trajectories, can also be taken into account. After each thermodynamic solution over a user-defined heating time step is completed, the electromagnetic analysis is resumed from the previous electromagnetic steady state, but with the modified material parameters.

Essentially, a nonlinear electromagnetic-thermodynamic problem is converted to a **multistep parametric** problem, with bilateral coupling between the two solvers. The user decides about the number of heating time steps to cover the total heating time.

The coupled electromagnetic — thermal simulations become **powerful tools** for microwave engineers. They allow one to produce and inspect the temperature patterns within the whole volume of the heated product. Different shapes, dimensions and initial positions of the sample inside the oven cavity can easily be considered from the viewpoint of their influence on the final temperature patterns. Additionally, high costs associated with physical experiments, such as production of samples, manufacturing of apparatus prototypes, and measurements, are reduced to the necessary minimum (being a priori investigation of thermal and dielectric properties of the sample as a function of temperature).

The results of multiphysics simulations are compared to temperature patterns actually measured in selected food products treated in a domestic microwave oven. The measurements are conducted with an **infrared camera** or **fibre optic** thermal probes. Good overall agreement between simulations and measurements is noted. Discrepancies are related to uncertainties in material characterisation, which therefore requires enhancements. Elements crucial for correct mapping between the laboratory and virtual scenarios are pointed out.

Efficiency Optimization for Microwave Thermal Processing of Materials with Temperature-Dependent Media Parameters

Ethan K. Murphy and Vadim V. Yakovlev
Department of Mathematical Sciences, Worcester Polytechnic Institute
Worcester, MA 01609, USA

Abstract— Microwave heating of materials is known to be the technology capable of substantial improvement in the efficiency and quality for a variety of applied thermal processes. However, corresponding industrial implementations are still quite limited because, as a physical phenomenon, microwave heating is hard to control. Several years ago, it was suggested that, with the remarkable progress in efficient numerical techniques allowing for quite accurate computer simulation of complex microwave systems, the problem of optimization of microwave thermal processing can be approached through modeling-based techniques [1]. One crucial aspect of this type of optimization, namely, optimization of microwave energy coupling interpreted as a numerical characteristic of system efficiency, has been discussed and conceptualized, for the first time, in [1]. Then in [2] an artificial neural network (ANN)-based finite-difference time-domain (FDTD)-backed algorithm has been introduced as an optimization procedure suitable for viable multi-parameter optimization of energy efficiency for microwave heating systems.

Recently, the critical upgrade of the algorithm proposed in [2] has been reported [3, 4]. The revised version of the optimization technique deals now with a new objective function and features a principal improvement of dynamic training of the RBF network by Constrained Optimization Response Surface (CORS) technique — global response surface type algorithm designed to minimize the number of function evaluations in the process of finding the global minimum. It has been shown [3, 4] that the new technique substantially outperforms its predecessor [2] by getting optimal solutions of better "quality" and substantially reducing the number of FDTD analyses (and thus dramatically cutting the optimization's computational cost) for such systems as a waveguide band-pass filter, a dielectric resonator antenna, and a loaded microwave oven.

In this contribution, we demonstrate how the CORS-RBF optimization procedure [3, 4] can be applied for efficiency optimization of the systems of microwave heating of materials whose media parameters (the dielectric constant ε' and the loss factor ε'') change in the course of heating. The considered scenario is concerned with a microwave oven (with the dimensions and feed location of *Sanyo EM-N105W*) containing a glass shelf and a cylindrical sample of processed material on it. The optimization problem is formulated as follows:

Given:

(1) the processed material with temperature characteristics $\varepsilon'(T)$ and $\varepsilon''(T)$ for the working temperature range, and
(2) the fixed dimensions of the cylinder (diameter D and height H);

Find:

(a) thickness of the glass shelf t,
(b) diameter of the shelf d,
(c) the position of the shelf above the bottom h, and
(d) the position of the cylinder on the shelf with respect to its center, d_x and d_y

such that the reflection coefficient of the entire system is guaranteed to be less than 0.3 (i.e., less than 9% of microwave energy is reflected back to the magnetron) in 75% of the frequency range from 2.4 to 2.5 GHz.

The 5-parameter optimization problem is solved for a particular pair of (ε', ε'') corresponding to a certain temperature; the optimization is then repeated, for the same space of design variables, for the values of the dielectric constant and the loss factor at a number of other temperatures. In the considered illustration, we work with experimentally determined values of ε' and ε'' of resin R498 at $T = 30$, 80, and 120°C [5]. The underlying FDTD model developed for the 3D conformal FDTD simulator QuickWave-3D [6] consists of 166,000 to 189,000 cells (16 to 18 MB RAM), so one analysis of the system involving 20,000 time-steps takes 2.2 to 2.5 min of CPU time on Xeon 3.2-GHz PC operating under Windows XP. It turns out that the CORS-RBF procedure requires as little as 177, 160, and 185 simulations (i.e., about 10 h total) for each of these temperatures, respectively, to find an optimal solution satisfying the 75% frequency band

constraint. (For comparison, the best solution found by the previous version of this optimization algorithm [2] corresponds to 52% bandwidth, and it needs 462 analyses to get this solution.) Finally, the optimal configuration for each temperature is tested for two other pairs of $(\varepsilon', ', \varepsilon'')$, and the one demonstrating best bandwidth is chosen as overall optimal.

Due to a fully parameterized underlying FDTD model, the optimization problem can be instantly formulated for any other set of parameters in accordance with the practical need of the system designer. Thanks to its computational effectiveness, the presented optimization tool may assist in fairly practical CAD projects in microwave power engineering easily dealing with several design variables and performing optimization of regular widely available PCs.

REFERENCES

1. Mechenova, V. A. and V. V. Yakovlev, "Efficiency optimization for systems and components in microwave power engineering," *J. Microwave Power & Electromag. Energy*, Vol. 39, No. 1, 15–29, 2004.
2. Murphy, E. K. and V. V. Yakovlev, "RBF network optimization of complex microwave systems represented by small FDTD modeling data sets," *IEEE Trans. Microwave Theory Tech.*, Vol. 54, No. 7, 3069–3083, 2006.
3. Murphy, E. K. and V. V. Yakovlev, "Reducing a number of full-wave analyses in RBF neural network optimization of complex microwave structures," *IEEE MTT-S Intern. Microwave Symp. Dig.*, Boston, MA, June 2009.
4. Murphy, E. K. and V. V. Yakovlev, "Optimization of complex microwave systems with the CORS RBF neural network backed by FDTD analysis data," *Progress In Electromagnetics Research Symposium*, Moscow, Russia, August 18–21, 2009.
5. Akhtar, M. J., L. E. Feher, and M. Thumm, "Nondestructive approach for measuring temperaturedependent dielectric properties of epoxy resins," *J. Microwave Power & Electromag. Energy*, Vol. 42, No. 3, 17–26, 2008.
6. QuickWave-3D, QWED Sp. z o. o., Warsaw, Poland, 1998–2009, http://www.qwed.com.pl/.

Coupled Electromagnetic-thermal 1-D Model of Combined Microwave-convective Heating with Pulsing Microwave Energy

Erin M. Kiley[1,2], **Suzanne L. Weekes**[2], **and Vadim V. Yakovlev**[2]

[1]Department of Mathematics, University of New Hampshire, Durham, NH 03824, USA
[2]Department of Mathematical Sciences, Worcester Polytechnic Institute, Worcester, MA 01609, USA

Abstract— As a result of the well-known tendency of microwave (MW) heating to develop hot and cold spots in practically unpredictable locations, special measures must be undertaken to simultaneously bound the maximum temperature (which occurs at the hot spots) while still sufficiently heating the rest of the object (in particular, the cold spots). This difficulty has been ameliorated with use of turntables [1], or mode stirrers [2], or multiple feeds [3], while an alternative approach used in industry, which has not been systematically studied yet, features a MW pulsing regime [4] in which periods of relaxation allow the effects of thermal diffusion, a naturally-occurring mechanism that operates on a vastly different time scale from MW heating, to make the temperature distribution more uniform.

This contribution presents an algorithm and modeling software allowing for 1D simulation of thermal processing of dielectrics by pulsed MW energy. The presented technique is a continuation of our earlier study [5], which first presented software to consider the pulsing regime as a technique to ensure heat diffusion through the load in the time intervals when the microwave is off, and thus to evaluate its efficacy as a controlling parameter in making the resulting temperature field more uniform. The algorithm is also capable, in accordance with industrial practices, of simulating combined MW-convective heating. Here we report an upgraded version of the algorithm and a new series of computational experiments which allow us to see the pulsing regime with different pulsing parameters on the materials with different electromagnetic and thermal properties and with the new option of adiabatic boundary conditions.

The software is implemented as a MATLAB code executing an analytical-numerical solution of a 1-D fully coupled electromagnetic-thermal problem, with temperature-dependent electromagnetic parameters (dielectric constant and the loss factor) and thermal parameters (heat conductivity, heat capacity, and density). We account for these dependencies in the solution of the coupled problem using a special numerical procedure implementing a finite-difference computational scheme. Similarly to [5], performance of the code was validated by the 3-D conformal FDTD simulator *QuickWave-3D* [6].

While a 1D solver cannot be applied to realistic MW heating systems and be considered as a tool for practical CAD, it is effective in the context of studying the functionality of a MW pulsing regime, and as it is fully parameterized, can be used to study pulsing in the context of a variety of scenarios actually used by industry.

A series of performed computational experiments shows that microwave pulsing in combination with convective heating at a temperature equal to or greater than the minimum temperature required for the load to be sufficiently heated is more effective than microwave pulsing alone, because during periods when the microwave is off, diffusion is conditioned by both thermal conductivity and additional heat introduced to the load. Naturally, when the boundaries are maintained at a temperature lower than the intended minimum threshold, then truly sufficient heating can never be achieved; yet, even this kind of convective heating is beneficial for uniformity in the first stages of heating. We also note the general trend that the greater the number of pulses over a given time interval, the more quickly uniformity is achieved. The developed model can therefore be conceptually and specifically instructive in designing practical applicators with pulsing MW energy.

REFERENCES

1. Kopyt, P. and M. Celuch, "FDTD modeling and experimental verification of electromagnetic power dissipated in domestic microwave oven," *J. Telecomm. & Information Techn.*, No. 1, 59–65, 2003.
2. Plaza-Gonzalez, P., J. Monzó-Cabrera, J. M. Catalá-Civera, and D. Sánchez-Hernández, "Effect of mode-stirrer configurations on dielectric heating performance in multimode microwave applicators," *IEEE Trans. Microwave Theory Tech.*, Vol. 53, No. 5, 1699–1706, 2005.

3. Pitarch, J., A. J. Canós, F. L. Peñaranda-Foix, J. M. Catalá-Civera, and J. V. Balbastre, "Synthesis of uniform electric field distributions in microwave multimode applicators by multifeed techniques," *Proc. 9th Conf. Microwave & High-frequency Heating*, 221–224, Loughborough, U.K., 2003.
4. Gunasekaran, S. and H.-W. Yang, "Effect of experimental parameters on temperature distribution during continuous and pulsed microwave heating," *J. Food Engineering*, Vol. 78, 1452–1456, 2007.
5. Feldman, D. A., E. M. Kiley, S. L. Weekes, and V. V. Yakovlev, "Modeling of temperature fields in 1D and 2D heating scenarios with pulsing microwave energy," *Proc. 41st Microwave Power Symp.*, 130–134, Vancouver, BC, Canada, 2007.
6. *QuickWave-3D*, QWED Sp. z o.o., Warsaw, Poland, 1998–2009. http//: www.qwed.com.pl/.

Regularities of Semiconductor Powders Dynamics in Chladni Effect

V. I. Kuzmin[1] **and D. L. Tytik**[2]

[1]Moscow State Institute of Radio Engineering, Electronics, and Automation
pr. Vernadskogo 78, Moscow 119454, Russia
[2]Frumkin Institute of Physical Chemistry and Electrochemistry
Leninskii pr. 31, Moscow 119991, Russia

Abstract— This article is a presentation of powder pattern dynamics (Chladni figures) on the plates in a variety of shapes and critical dimensions under acoustic and magnetic fields applied in the vicinity of bifurcation points. The study involved the use of powders with critical size of particles of diverse composition — semiconductor material B_4C and dielectric material SiO_2. The study detected the acoustic field frequencies at which powder figures (B_4C) rearrange themselves on the plane by escaping into the third dimension (forming a vortex above the plane at the point of bifurcation). Dielectric powders (SiO_2) at certain frequencies form stationary vortex above the plane due to the natural lumpiness effect, which is the cause of existence of dominant sizes of material structures in the nature, regardless of their phase state. They are consistent with dominant values of time intervals (frequencies) forming the rhythm quantization system. The natural lumpiness effect serves as technological basis for the transfer of electromagnetic signals in various media at specific frequencies (transparency windows).

Combined effect of the acoustic and magnetic fields defines the specifics of powder figures (B_4C) on the plane and brings forth the problem of electromagnetic impact on powder materials with various physical and chemical properties. These experiments demonstrate that the phase state of a substance can be controlled through application of alternating fields of diverse origin along with critical values of wavelengths (frequencies).

Session 3P7
Antenna Theory and Radiation 2

Double-folded Monopole Antenna with Coaxial Cable

Takehiko Tsukiji, **Masaaki Yamasaki**, **and Yasunori Kumon**
Department of Electronics and Computer Science, Faculty of Engineering, Fukuoka University
8-19-1, Nanakuma, Jounan-ku, Fukuoka 814-0180, Japan

Abstract— Previously, we proposed a small high-active-gain antenna called the double-folded monopole antenna with coaxial cable. This antenna consists of two 0.15-wavelength coaxial cables, each of which has one end that is short-circuited. The source is connected to the center conductor of one of the coaxial cables, and the center conductor of the other coaxial cable is grounded to the ground plane. Two coaxial cables are arranged in parallel and are perpendicular to the ground plane, thereby forming a parallel monopole antenna. Finally, the outer cylinders of each coaxial cable are connected by a short wire at the open end of the cables near the feed point. Although this antenna has a very small height, it has high active gain due to its high input impedance of approximately 50 ohm. This antenna has a relatively simple structure and a complicated electrical operational principle. The present paper is the first report of the coaxial cable loaded monopole antenna of reduced size. Using this antenna, we describe the construction of the double-folded monopole antenna with a coaxial cable. Finally, we discuss the operational principle of the coaxial cable loaded monopole antenna with respect to the relationship between the resonant length of this antenna and the input impedance. It is hoped that the present paper will clarify the theory of the double-folded monopole antenna with coaxial cable.

All-planar Penta-band Strip-loaded Slit Antenna for Laptop Applications

Ching-Wei Ling, Sy-Been Wang, and Shyh-Jong Chung
Department of Communication Engineering, National Chiao Tung University, Taiwan, R.O.C.

Abstract— Owing to the rapid growth in wireless communications, the antenna design for laptop computer is generally required to be capable of multiband operation. For the Wireless Wide Area Network (WWAN) penta-band application, the frequency bands cover the GSM850 (824–894 MHz), GSM900 (880–960 MHz), DCS (1710–1880 MHz), PCS (1850–1990 MHz), and UMTS (1920–2170 MHz). Besides, with the thin laptops getting readily available nowadays, the available antenna volume is reduced. Hence, the antenna design is a challenge for fitting the limited space inside the laptop computer and covering a wider bandwidth operation.

In this study, an all-planar penta-band antenna for laptop applications is presented. This antenna is placed parallel to the upper edge of the laptop panel ($300 \times 200\,\mathrm{mm}^2$) with a restricted available space ($120 \times 10 \times 0.4\,\mathrm{mm}^3$). The antenna is printed on two sides of a 0.4 mm thick FR4 substrate, which is mainly composed of two back-to-back slit antennas with different sizes and a T-shaped feeding network. Each slit antenna is loaded with a metal strip extended from the T-shaped feeding network for wideband performance. The metal strip is placed within the slit. Good impedance matching can be obtained by varying the position of the metal strip. Each strip-loaded slit antenna has two resonances, respectively provided by the strip metal and the slit. A wide operating band is achieved by changing the slit and the metal strip length. Here, the larger strip-loaded slit antenna is designed for lower operating band (GSM850/900) and the smaller is for the higher band (DCS/PCS/UMTS) operation.

The simulation results are obtained by using Ansoft HFSS and they agree well with the measurement. For the measured results, the lower band with 140 MHz bandwidth is provided by two resonant modes. The higher band also has two resonances and the bandwidth is about 460 MHz. The antenna radiation patterns are omnidirectional in the H-plane. Over the GSM850/900 and the GSM/1800/1900/UMTS bands, the average gains in this plane are about 2.06 dBi and 0.02 dBi, respectively. The antenna gain variations are less than 1 dB which shows the stable radiation characteristics across the WWAN band. Good antenna features and the planar configuration make the proposed antenna attractive for ultra-thin laptop applications.

Investigation of Radiation Efficiency and Bandwidth of Electrically Small MNG ZOR Metamaterial Antenna

Seung-Wook Lee, Jae-Hyun Park, and Jeong-Hae Lee
Department of Electronic Information and Communication Engineering, Hongik University
Seoul 121-791, Korea

Abstract— In this paper, the radiation efficiency and fractional bandwidth of an electrically small zeroth order resonance (ZOR) antenna based on mu-negative (MNG) metamaterials were theoretically investigated. To investigate the radiation efficiency and bandwidth of the electrically small antenna, various types of MNG ZOR antennas such as a meander line inductor and a spiral inductor with different current path have been designed. The equivalent circuits of MNG ZOR antennas are derived for theoretical analysis of an antenna. The parameters of antenna such as radiation resistance and dissipated loss have been obtained by the equivalent circuit of the MNG ZOR antennas. The dissipated loss and radiation resistance were affected by the current distribution of meander line and the direction of current path of the antenna. It is confirmed that both the radiation efficiency and bandwidth of the MNG ZOR antenna can be improved when the cancellation of current on the antenna is minimized if the losses are assumed to be the same.

Circularly Polarized Slotted Conductor-backed Coplanar Waveguide (CBCPW) Antenna Array with Sequentially Rotated Feeding Structure

Yow-Shyan Lin[1], **Lieh-Chuan Lin**[1], **Toshihide Kitazawa**[2], **and Yu-De Lin**[1]

[1]Department of Communication Engineering, National Chiao Tung University, Hsinchu, Taiwan
[2]Department of Electrical and Electronic Engineering, Ritsumeikan University, Kusatsu, Japan

Abstract— This paper presents a circularly polarized slotted conductor-backed coplanar waveguide (CBCPW) antenna array with sequentially rotated feeding structure. In CBCPW, the background substrate mode is the parallel-plate waveguide mode and its propagating constant is always larger than that of the CBCPW mode. Therefore, the CBCPW mode will always leak into the background parallel-plate mode. By appropriately arranging radiating slots along the leaky path of the parallel-plate mode, we can design a slotted array similar to the design of slotted waveguide antenna array. In our previous paper, we have designed a kite-shaped linearly polarized slotted CBCPW antenna array as shown in Fig. 1. The return loss of the slotted CBCPW antenna less than −10 dB is from 11.2 GHz to 12.54 GHz. The gain is 24.4 dBi at designed frequency 12 GHz. And the mainbeam is in the broadside direction. In this paper, we put together four kite-shaped slotted CBCPW arrays as shown in Fig. 2. By using a sequentially rotated feeding structure as that used in the design of microstrip patch arrays, we can implement a circularly polarized slotted CBCPW antenna by arranging the feeding phases in a 0°/90°/0°/90° or 0°/90°/180°/270° fashion. Simulation results show that the array has a left-hand circular polarization level 40 dB lower than that of the right-hand circular polarization wave in the broadside direction. The antenna gain is 25.90 dBi. The bandwidth of the axial ratio less than 3 dB is 250 MHz, from 11.85 GHz to 12.1 GHz.

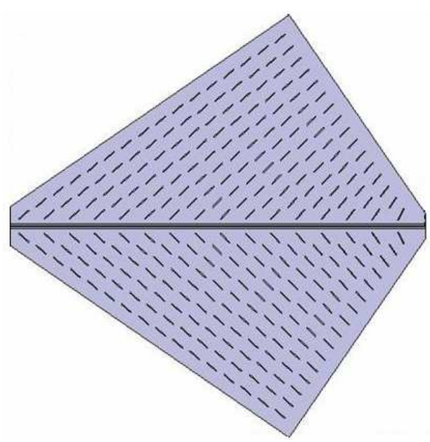

Figure 1: Top view of the kite-shaped linearly polarized slotted CBCPW antenna array.

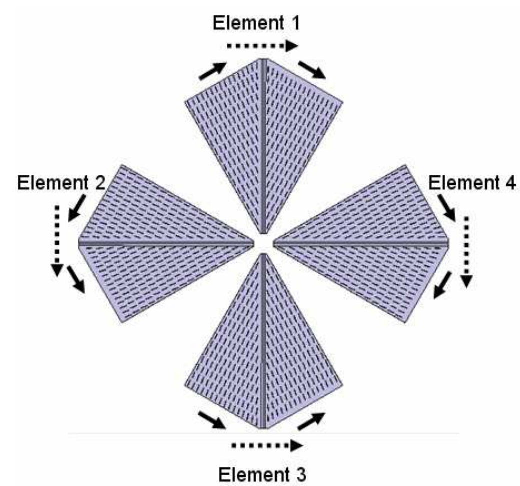

Figure 2: Circularly polarized slotted conductor-backed coplanar waveguide (CBCPW) antenna array with sequentially rotated feeding structure composed of four kite-shaped subarrays.

Microstrip Patch Antenna Designs with Reduced Surface Wave Excitation

S. F. Mahmoud[1] **and A. R. Al-Ajmi**[2]

[1]Electrical Engineering Department, Kuwait University, Kuwait
[2]Telecommunication and Navigation Institute
The Public Authority for Applied Education and Training, Kuwait

Abstract— One of the major operational disadvantages of microstrip antennas is their excitation of surface waves. These surface waves cause undesired mutual coupling between components printed on the same substrate, and disturb the radiation pattern due to diffraction at the edge of a finite ground plane. Besides, the presence of surface waves is usually associated with lateral waves, which cause low angle interfering signals such as the case in global positioning system GPS receiving antennas. Several designs have been proposed to reduce these undesired waves. A circular patch having a certain critical radius will not excite the TM_{11} surface wave [1] which is the only surface wave mode for electrically thin substrates. However, a circular patch having this critical radius will not in general be of resonant size. In order to make the patch resonant, a short-circuited inner boundary is embedded into the design where the radius of this boundary is chosen to place the antenna resonance at the desired frequency. The short circuit is implemented by inserting a very high number of via pins between the patch and the ground [2].

In this paper, we propose a reduced surface wave (RSW) patch design using a small number of shorting pins (8 pins). While the outer radius is maintained at the critical radius for RSW, the shorting pins tend to reduce the effective patch area which readjusts the resonance frequency as desired. In another design, we propose a RSW circular patch loaded with four shorting pins arranged at the vertices of a square inside the patch so as to achieve the required resonant frequency. The modal equation of this design has been derived and solved numerically.

A comparison between the above two proposed designs has shown that both have the capability of reducing the surface waves and lateral waves. However, the four pins loaded patch has a better gain and radiation efficiency. Moreover, by embedding a narrow slot at the center of the four pins loaded patch, a circular polarization has been achieved using a single, rather than dual probe feed. Simulation results using the IE3D software facility support the theory and verify the reduced surface wave and lateral wave capability.

REFERENCES

1. Jackson, et al., *IEEE, AP*, Aug. 1993.
2. Basilio, et al., *IEEE, AWPL*, 2005.

Circular Polarized Patch Antenna with a Small Ferrite Disk

M. Sigalov[1,2], R. Shavit[2], E. O. Kamenetskii[2], R. Joffe[1], D. Rahmilov[1], and S. Tapuchi[1]

[1]Electrical and Electronics Engineering Department, Sami Shamoon College of Engineering
Beer-Sheva 84100, Israel
[2]Electrical and Computer Engineering Department, Ben-Gurion University of the Negev
Beer-Sheva 84105, Israel

Abstract— The inherent anisotropy and nonreciprocal properties of the ferrite materials make them very attractive for using in different types of antenna structures. Recently, several applications for frequency tuning, pattern beam steering and radar cross section control using an integration of ferrite materials into printed microstrip antennas have been published in the literature [1–3].

A ferrite is a magnetic dielectric with low losses. This characteristic allows the electromagnetic waves to penetrate into the ferrite and results in an effective interaction between the electromagnetic waves and the ferrite magnetization. Such an interaction results into very interesting physical features like making the electromagnetic-field eigenfunctions of a microwave resonator complex, when a gyrotropic sample like a ferrite disk is enclosed. Consequently, the fields of the complex eigen oscillations are not equal to the fields of the standing waves in the resonator in spite of the fact that their corresponding eigen frequencies are real [4]. Recently, it has been shown that insertion of a piece of a magnetized ferrite into a microwave resonator imposes on the resonator to behave under odd-time-reversal symmetry. In this case a ferrite sample may act as a topological defect causing induced electromagnetic vortices of power flow into the resonator domain [5].

In this work we will show numerical and experimental results to support the claim that circularly polarized (CP) electromagnetic radiation can be obtained from a microstrip patch antenna with small ferrite disk inclusions. This CP radiation can be considered as being originated from the vortex topological states in the cavity region of the antenna. We will show that switching between the right hand (RH) and left hand (LH) circular polarizations of the antenna is possible. The scattering and radiation parameters of the antenna are investigated. The dependence of the axial ratio and the reflection coefficient of the antenna on the position and number of ferrite disks underneath the patch is analyzed and an optimization procedure is proposed.

REFERENCES

1. Pozar, D. M., "Radiation and scattering characteristics of microstrip antennas on normally biased ferrite substrates," *IEEE Trans. AP.*, Vol. 40, 1084, 1992.
2. Rainville, P. J. and F. J. Harackiewiz, "Magnetic tuning of a microstrip patch antenna fabricated on a ferrite film," *IEEE Microwave Guided Wave Lett.*, Vol. 2, 483, 1992.
3. Henderson, A. and J. R. James, "Magnetized microstrip antenna with pattern control," *Electron. Lett.*, Vol. 24, 45, 1988.
4. Gurevich, A. G. and G. A. Melkov, *Magnetic Oscillations and Waves*, CRC Press, New York, 1996.
5. Sigalov, M., E. O. Kamenetskii, and R. Shavit, "Chiral states of electromagnetic fields originated from ferrite-based electromagnetic vortices," *J. Appl, Phys.*, Vol. 104, 113921, 2008.

Anomalously High Propagation Velocity of Bound Electromagnetic Fields in Near Zone of Radiating Sources: Experimental Observation

A. L. Kholmetskii[1], **O. V. Missevitch**[2], **and R. Smirnov-Rueda**[3]

[1]Department of Physics, Belarus State University, Minsk 220030, Belarus
[2]Institute of Nuclear Problems, Minsk 220030, Belarus
[3]Faculty of Mathematics, Complutense University, Madrid 28040, Spain

Abstract— Modern classical electrodynamics makes clear distinction between velocity-dependent (bound) and acceleration-dependent (radiation) field components. It is well-known that the ratio of the radiation to bound electromagnetic (EM) field strength increases with a distance from EM emitting sources (antennas etc). The radiation is dominant in *far zone* whereas bound fields predominate close to a radiating source within the region less then one sixth of EM radiation wavelength (*near zone*).

Transmission of EM energy and propagation characteristics of EM fields within the near zone nowadays receive more attention due to proper needs of technological progress. Nevertheless, since Hertz's discovery of EM waves at the end of the 19th century no systematic study of EM field propagation within the near zone has been achieved. In spite of very intensive studies in the area of near-field antenna testing, all developments and progress mainly concern two aspects — distribution of currents in the antenna elements and prediction of the radiation spatial diagram in far-zone. As a consequence, there is no explicit and reliable information (fundamentally and technologically relevant) on propagation characteristics and transmission of energy related to properly bound EM fields that are dominant in the near zone of radiating EM sources.

As response to the above-mentioned uncertainty we proposed a general approach based on conventional solutions to Maxwell's equations and applied it to show how in the near zone of an emitting loop antenna the electromotive force produced in a receiving loop antenna is uniquely linked to the superposition of bound and radiation components. On the basis of this analysis, we implemented a direct experimental procedure for rigorous identification of retarded positions of bound EM fields on time scale as function on a distance between emitting and receiving antennas. Measurements [1, 2] were carried out in two different configurations at VHF 125 MHz (2.4 m EM radiation wave-length). Anomalous propagation rate of bound EM fields (highly exceeding the velocity of light) was observed within the near zone (up to 0.6 m), contrarily to what the conventional classical electrodynamics predicts implying equal propagation velocities for both component. However, in the far zone the anomaly disappears and the propagation rate is already equal to that of radiation EM field component (equal to the velocity of light within the near and the far zones).

REFERENCES

1. Kholmetskii, A. L., O. V. Missevitch, R. Smirnov-Rueda, R. Ivanov, and A. E. Chubykalo, *J. Appl. Phys.*, Vol. 101, 023532, 2007.
2. Kholmetskii, A. L., O. V. Missevitch, and R. Smirnov-Rueda, *J. Appl. Phys.*, Vol. 102, 013529, 2007.

Classification of Fractal Antenna Radiation Patterns by the Spectrum Enhancement Algorithm

Giovanni F. Crosta
Inverse Problems & Mathematical Morphology Unit
Department of Environmental Sciences, University of Milan-Bicocca
1, Piazza Della Scienza, Milan, IT 20126, Italy

Abstract—

Spectrum Enhancement: Let g denote a scalar function which is at least continuous on the surface $\mathcal{T}$ of a torus. Let $\mathbf{u} \equiv \{u_1, u_2\}$ denote the spatial frequency vector and $G[\mathbf{u}]$ the (distribution-valued) Fourier transform of g. The spectrum enhancement (SE) algorithm, which was introduced a few years ago [e.g., [1]] consists of suitable transformations of the function $H^{(p)}[\mathbf{u}] := |\mathbf{u}|^{2\beta} \frac{|G[\mathbf{u}]|^2}{|a_{0,0}|^2} + \delta[\mathbf{u}]$, where δ is the Dirac measure, $a_{0,0}$ is the Fourier amplitude at the origin such that $\mathcal{F}(g)[\mathbf{0}] = a_{0,0}\delta[\mathbf{u}]$, $\beta \in \mathbf{R}^+$ is the *enhancement order* and $\beta = 2p$. It has been recently shown that SE is related to Fourier transforms of derivatives of $g[.]$, which are of integer order whenever $\beta \in \mathbf{N}$ [2] and of fractional order otherwise ($\beta \notin \mathbf{N}$) [3]. Herewith, the role played by the enhancement order β in the fractal analysis of $g[.]$ will be described.

Fractal Radiation Patterns: Array antennas exhibiting fractal radiation patterns are synthesized by means of generalized Weierstraß functions [4]. For example, in one spatial dimension (x_1) one has

$$f[x_1] := \sum_{m=1}^{\infty} \eta^{(D-2)m} h[\eta^m x_1]$$

where $1 < D < 2$, $\eta > 1$ and $h[.]$ is a suitably chosen bounded, periodic function of one variable. It can be shown that the box-counting (B) fractal dimension ($\dim_B$) of the graph of $f[.]$ (graph$[f]$) satisfies $\dim_B[\text{graph}[f]] = D$. Two-dimensional fractal radiation patterns can be synthesized in a similar way e.g., by separation of variables.

Recognition of Fractal Radiation Patterns: Let simulated or measured radiation patterns be available on the whole surface of the unit sphere or part thereof. Let the pattern $\dim_B$ be unknown or assume the pattern has to be classified by fractal dimension. The SE algorithm can be used to extract features from said patterns and estimate their $\dim_B$. Moreover, patterns can be classified by a procedure which includes supervised training. Some preliminary classification and recognition results will be provided, based on numerically synthesized fractal radiation patterns.

REFERENCES

1. Crosta, G. F., C. Urani, L. Fumarola, *J. Biomed. Optics*, Vol. 11, No. 2, 024020.1–024020.18, 2006.
2. Crosta, G. F., "Feature extraction by differentiation of fractional order," *Progress In Electromagnetics Research Symposium Abstracts*, 425, Cambridge, USA, March 26–29, 2006.
3. Crosta, G. F., "Morphological characterization of two-dimensional random media and patterns by fractional differentiation," *Progress In Electromagnetics Research Symposium Abstracts*, 627, Cambridge, USA, July 2–6, 2008.
4. Werner, D. H. and P. L. Werner, *Radio Science*, Vol. 30, No. 1, 29–45, 1995.

A New Eigenvalue Based Radiation Efficiency Analysis for Multiple Antenna Systems

Jui-Ting Chuang and Fu-Chiarng Chen
Department of Communication Engineering
National Chiao Tung University, 1001 Tahsueh Rd., Hsinchu 300, Taiwan

Abstract— This paper presents a new analysis strategy for multiple antenna system using eigenvalue based reflection coefficient and eigenvalue based radiation efficiency. Multiple antennas systems play a crucial role in the wireless communication systems over multiple fading channels. When implementing multiple antenna elements on small personal communication devices, the resulting closely spaced antenna elements exhibit well-known mutual coupling, which alters the radiation pattern characteristics and obviously impacts the performance of the multiple antenna systems. The radiation efficiency is considered as an important factor to measure the performance of the multiple antenna systems including mutual coupling. In this work, we represent the embedded radiation efficiency as the combination of eigenvalues of antenna reflection power matrix utilizing eigenvalue decomposition (EVD) and further derive a new representation of the reflection coefficient and the radiation efficiency for multiple antenna systems. We redefine this reflection coefficient and radiation efficiency as eigenvalue based reflection coefficient (EVRC) and eigenvalue based radiation efficiency (EVRE). By utilizing the characteristics of this representation, we not only able to evaluate how the radiation efficiency may change when the antenna ports excite signals with different phases, but also estimate the maximum and minimum values of EVRC and EVRE quickly as the number of antenna increase, which benefits the performance evaluation of multiple antenna systems. Realizing multiple antenna systems in radio channels becomes challenging because of the unavoidable mutual coupling effect between multiple antennas in portable devices. Mutual coupling effect distorts the far-field patterns and therefore has great impact on how much power radiates without reflection resulting from impedances mismatch and absorption by adjacent antenna elements. Therefore, with this new strategy, we further investigate how antenna termination networks influence the EVRC and EVRE in the multiple antenna systems.

Fractal Electrodynamics: Analysis and Synthesis of Fractal Antenna Radiation Pattern

Aleksandr Nikolaevich Bogolyubov, **Artem Aleksandrovich Koblikov**, **and Natalia Evgenievna Shapkina**
Faculty of Physics, Lomonosov Moscow State University, Russia

Abstract— The problem of fractal antenna radiation pattern synthesis considered. The theory of electromagnetic wave interaction with fractal was developed recently and it is progressing rapidly. The term "fractal electrodynamics" is now embedded in literature.

Unlike traditional methods, when smooth antenna radiation pattern are synthesized, the theory of fractal synthesis is based on the principle of scale invariance i.e., radiation characteristics with replicated structure are scale-independent. Therefore, it makes possible to realize new modes in fractal electrodynamics and to find fundamentally new properties. For example, fractal elements disposition on the object body may essentially change indication. Fractal antennas may be used in telecommunication, nonlinear radiolocation, search systems, radar detection etc.

Fractal radiation patterns are synthesized with the help of the Weierstrass function

$$f(x) = \sum_{n=1}^{\infty} \eta^{(D-2)n} g(\eta^n x) \tag{1}$$

where $1 < D < 2$; $\eta > 1$; g is a bounded periodic function.

Here D is a modified fractal dimension

$$D = -\log(N)/\log(r), \tag{2}$$

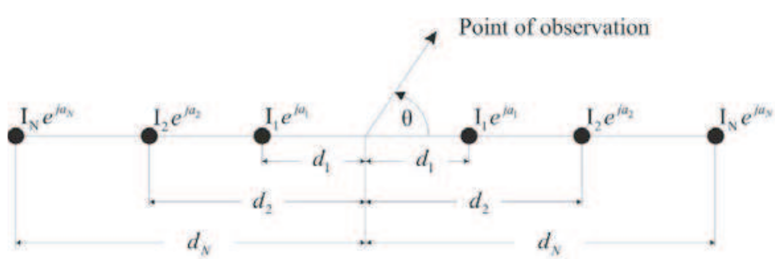

Figure 1: Symmetric antenna array of $2N$ elements with presented distribution of the excitation current distribution.

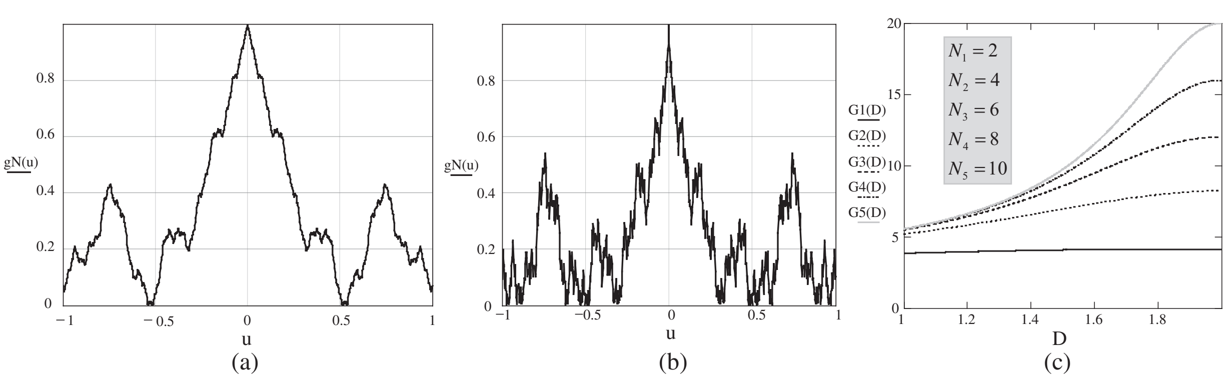

Figure 2: Normalized factor for Weierstrass array for different fractal dimensions D. ((a) $D = 1$; (b) $D = 1,5$). In (c) normalized current distributions i_N for radiation patterns with different fractal dimensions D are presented in dependence of N.

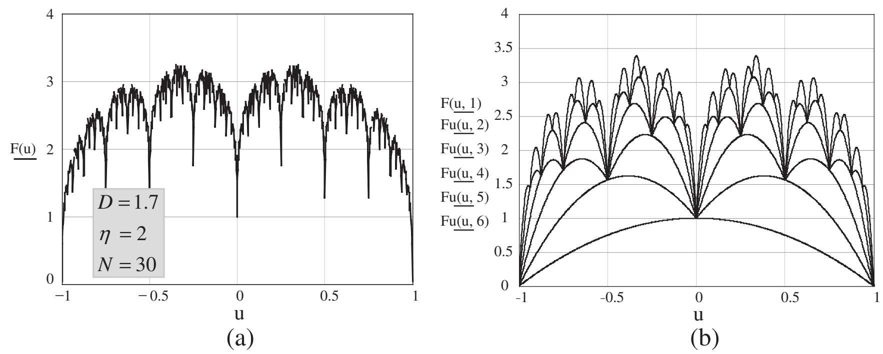

Figure 3: Synthesized radiation patterns. (b) The first 6 steps of fractal radiation pattern synthesis ($N = 1$–6).

where N is a number of elements in one subarray; $r = r_1/r_2$; r_1 is an average distance between subarray (generator) elements; r_2 is an average distance between elements of a random exciter.

With three variables (radiator volume distribution, amplitude and phase of array excitation current) it is possible to control antenna radiation pattern.

Let us consider the following symmetric antenna array.

Then the fractal dimension of the radiation pattern may be controlled by the array current distribution. As the D decreases, the radiation pattern main lobe widens and the corresponding values of antenna gain $G(u)$ become less.

Now let us analyze a long radiating system L with continuous current distribution $I(z)$. The procedure of the radiation linear source synthesis for the generator general function (a) $g(\theta) = 1 - |1 - \cos\theta|$, $0 \leq \theta \leq \pi$, (b) $g(\theta) = \sin^2\theta$, $0 \leq \theta \leq \pi$ is realized as in Fig. 3.

The investigation showed that fractal antennas application permits to develop new modes and find new properties improving operating characteristics of the objects thus making such antennas to be widely used. At present time the mathematical modeling is one of the main method for these structures' investigation as it allows to find optimal parameters a priory.

A 30 GHz Bow-tie Slot Antenna Fed by a Microstrip to CPW Transition

Angel Colin
Instituto de Física de Cantabria (CSIC-UC)
Av. Los Castros s/n, Santander 39005, Spain

Abstract— In this paper a modified bow-tie slot antenna fed by a microstrip to coplanar waveguide (CPW) transition is investigated for wideband operation. The design is suitable to be included in arrays for applications in radar, communications, radioastronomy or Cosmic Microwave Background (CMB) experiments. The antenna exhibits small size and symmetric geometry, suitable for the integration with monolithic microwave integrated circuits (MMIC), microstrip circuits and for the connection with active or passive elements. The antenna is designed to work on a thin alumina substrate (0.254 mm thickness) covered by 3 μm electroplated gold, relative permittivity of 10, and loss tangent of 0.001. The geometry and parameters of the antenna are shown in Fig. 1(a), where $a = 0.05$, $b = 0.25$, $c = 8$, $d = 5$, $e = 2.38$, $f = 0.12$, $g = 5.525$, $h = 0.05$, $i = 0.125$, $j = 0.05$, and $k = 7.6$. All dimensions are in mm. Bottom ground plane only covers the microstrip line section (c dimension). The widths of the microstrip line and gaps of the CPW were calculated to be approximately 50 Ohm.

All parametric variables in the simulation results were controlled under the environment of the HFSS-Ansoft software, considering two cases: I) using an open radiation type boundaries for the substrate's surroundings box, and II) introducing a brass reflector plane placed below the substrate at distances of $\lambda/4$, $\lambda/2$, and λ respectively. In both cases we used an excitation wave port of 50 Ohm.

Return loss for a single antenna without reflector plane is shown in Fig. 1(b). It shows a wide operation range that covers completely the Ka-band (27–40 GHz) thus giving a wideband of 43% with VSWR < 2. Fig. 1(c) shows the normalized (dB) directivity pattern at 30 GHz with beamwidths of approximately 120° for the E (thick line) and H (thin line) planes respectively.

Radiation characteristics will be presented in the final paper for a single element and for two aligned elements. The prototypes are being manufactured and will be tested in the antenna measurement facility at the UC. The measurements will be compared with their corresponding simulation results.

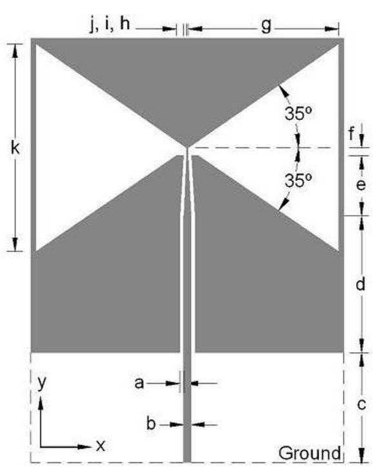

(a)

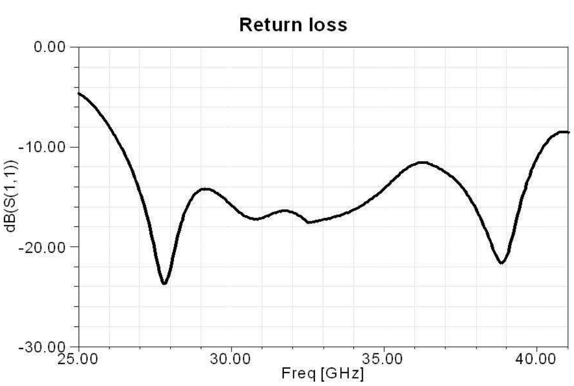

(b)

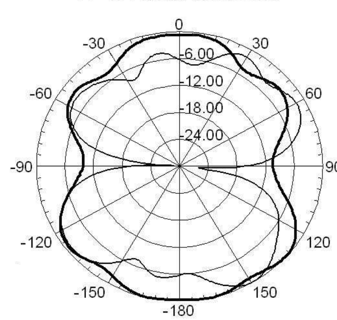

(c)

Design of Gathered Elements for Reconfigurable-beam Reflectarrays Based on Patches Aperture-coupled to Delay Lines

E. Carrasco, M. Barba, and J. A. Encinar
Universidad Politécnica de Madrid
ETSI-Telecomunicacin (B-403), Ciudad Universitaria S/N, Madrid 28040, Spain

Abstract— Reflectarray antennas based on patches aperture-coupled to delay lines are one of the most interesting technological solutions to achieve reconfigurable-beam antennas. An important advantage of this configurations is the available room for implementing phase control devices as PIN diodes [1] or MEMS [2] attached to microstrip line segments. However, for a large reflectarray with a reconfigurable beam, the cost and manufacturing complexity increases considerably because hundreds of control elements are required.

Combining two or four elements turning into a sub-array can reduce to a half or a quarter the number of switches required to achieve the beam configuration. This gathering can be performed combining several radiating elements by a common delay line, in a similar way to the microstrip beam forming networks used to feed classical arrays. This gathering also increases the available area for obtaining True-Time Delay (TTD) and compensate the effects of the differential spatial phase delay [3]. The sub-array implementation in a reflectarray requires the careful redefinition of the required phase-shift in the reflectarray elements to obtain the desired beam without distortion or reduction in gain.

In this contribution, different reflectarray elements based on sub-arrays with two and four elements, as those shown in Fig. 1 are proposed. The adequate adjustment of the geometrical parameters of the individual elements allows to obtain reflection curves with very linear phase response and low losses, which are very important in the design of reflectarrays. The results of phase-shift and losses will be presented for different configurations.

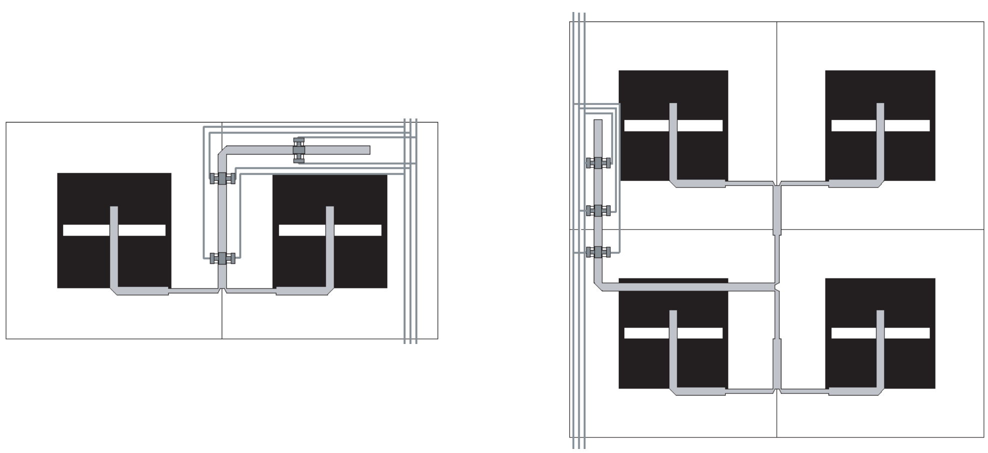

(a) (b)

Figure 1: Gathering of reflectarray elements for vertical polarization. (a) Two elements sub-array. (b) Four elements sub-array.

REFERENCES

1. Barba, M., E. Carrasco, J. E. Page, and J. A. Encinar, "Electronic controllable reflectarray elements in X band," *Journal of RF-Engineering and Telecommunications*, No. 9–10, 203–206, Frequenz, September/October 2007.
2. Mencagli, B., R. Vincenti, L. Marcaccioli, and R. Sorrentino, "Design of large mm-wave beam-scanning reflectarrays," *35th Europ. Microwave Conf.*, París, France, October 2005.
3. Carrasco, E., J. A. Encinar, and M. Barba, "Bandwidth improvement in large reflectarrays by using true-time delay," *IEEE Trans. on Antennas and Propagat.*, Vol. 56, 2496–2503, August 2008.

A Novel Design of Ultrawide-band Antenna

D. Bouchouicha[1], **M. Latrach**[2], **F. Dupont**[1],
A. Bremond[1], **and L. Ventura**[3]

[1]STMicroelectronics, Rue Pierre et Marie Curie, BP 7155, Tours 37071, France
[2]Groupe RF & Hyperfréquences, ESEO
4 Rue Merlet de la Boulaye, BP 30926, Angers 49009, France
[3]Laboratoire de Microélectronique de Puissance
16 Rue Pierre et Marie Curie, Tours 37071, France

Abstract— A CPW fed UWB non-concentric circular slot antenna with an inner circular cut-out is presented in this paper. Slots and CPW fed are etched on the same layer on a surface of $70 \times 75\,\mathrm{mm}^2$ by 1.6 mm thick on FR4 substrate with relative permittivity 4.4 (Fig. 1). r_1 and r_3 represent respectively the radius of the two slots and d_1 represent the distance between the centers of the slots. The CPW fed is a $50\,\Omega$ line where the width $W = 1.88\,\mathrm{mm}$ and the gap $s = 0.21\,\mathrm{mm}$.

Antenna impedance and bandwidth are studied as function of the radius and the centers positions of two circular slots. The obtained impedance bandwidth, assuming a limit of $-10\,\mathrm{dB}$ return loss, (Fig. 2) is from 2.3 GHz to 20 GHz (about 159% fractional bandwidth). The peak gain increases from 4 dBi to 8 dBi according to the use frequency (Fig. 3). A quasi-unidirectional radiation is obtained below 5 GHz (Fig. 4).

The proposed antenna is characterized by the simplicity in design and feeding, a very low cost and by a relatively stable radiation pattern over larger part of the bandwidth.

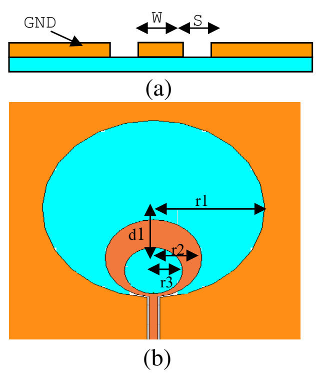

Figure 1: (a) Feed line (CPW), (b) antenna geometry.

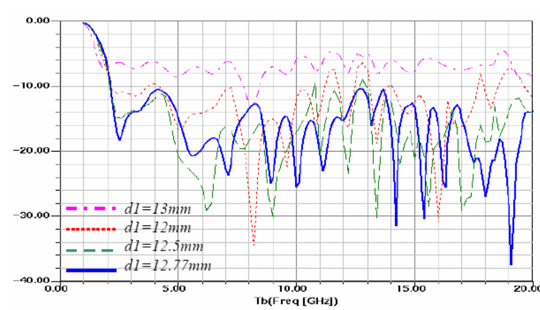

Figure 2: Antenna return loss.

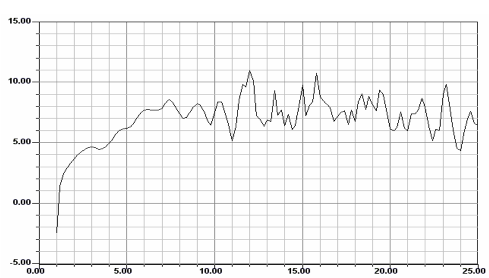

Figure 3: Maximum gain.

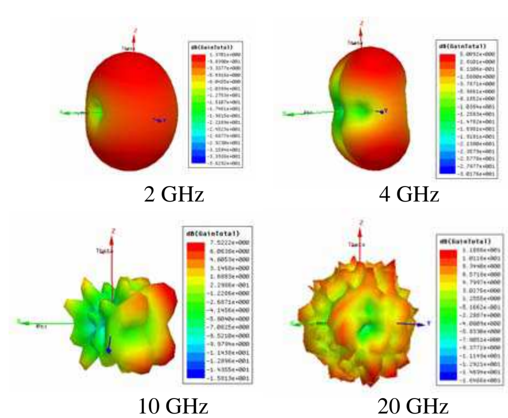

Figure 4: Antenna radiation.

Session 3P8
Electromagnetic Theory and Applications

Quantum ElectroDynamical Mechanisms of Resonant Effects Development inside Coherence Domains at Combined Magnetic Fields Action

Mikhail Zhadin
Institute of Cell Biophysics of RAS, Moscow Region 142290, Russia

Abstract— The Physical mechanism of resonant action of weak combined static and alternating magnetic fields at cyclotron frequency of the alternating magnetic fields was unintelligible for many years. For free ions it was impossible because of great dimensions of a required ion rotation radius measured by meters at room temperature and for bound ions the insuperable obstacle stayed the high viscosity of biological liquid media. However, inside coherence domain this obstacle disappears because inside coherence domains the water viscosity is about more than ten times lower and fluidity much lower than in incoherent water surrounding the domains. But firstly for this we should consider the domain walls not as a rectangular barrier for ions and molecules as one usually considered a coherence domain wall, but as an elastic barrier of finite thickness. Earlier (Zhadin, Barnes, 2005) we elaborated the physical model of ion rotating under the action of an elastic restoring force and under the influence of week combined static and alternating magnetic fields. Now we, without any problems, modified this model to the one considering an ion motion under the elastic force within the narrow limits of the centrally symmetric restoring force of domain border. In this case, it was a model of the ion motion along the elastic border of a coherence domain. In this model we received resonant peaks very similar to observed ones in our previous experiments with weak combined magnetic fields, if the theoretical parameters coincided with experimental ones appropriately. Especially close analogies one can see between biological ion resonance and physical accelerators when we see them among some modern plasma accelerators where the beam of particles with mixed different of positive and negative particles with different masses are accelerated togethr. The analogies of such sorts are quite surprising. We should point that within coherence domains there is not any need to accelerate ions till high energy. The increase of kinetic energy till twice is quite enough for escape of an ion from a domain for essential biological effect. Earlier we (Zhadin, Giuliani, 2006) have shown the important role of coherence domain in molecular processes in a living organism functioning.

Spectral Characterization of 2D Complex Beams and Its Relation to Gaussian Beams

Raul Mahillo-Isla, **Maria-Jesus González-Morales**, and **Carlos Dehesa-Martínez**
Universidad de Valladolid, Valladolid 47011, Spain

Abstract— 2D complex beam solutions to Helmholtz wave equation are obtained by displacing a point source from a real to a complex position [1]. These solutions have been extensively investigated in the real space [2], finding that Gaussian beams are a good approximation to complex beams under certain error criteria.

The starting point in this paper is the plane wave spectrum of 2D complex beams [3], which is closely related to the radiation pattern. Therefore, the main characteristics of complex beams radiation patterns, divergence angle and the ratio of the radiated power inside the divergence angle to the total radiated power, are parameterized.

Paraxial Gaussian beams and non-paraxial Gaussian beams will be distinguish. Paraxial Gaussian beams have no plane wave spectrum decomposition since they are solutions to the paraxial wave equation, and plane wave spectrum is defined only for solutions to the Helmholtz wave equation. A Gaussian beam is defined as a solution to the Helmholtz equation with a Gaussian field profile at the beam waist. For this beam, the plane wave spectrum can be obtained through the Fourier Transform of the sources.

The main contribution of this work will be a comparative numerical analysis of the three aforementioned solutions, concluding that both, complex beams and non-paraxial Gaussian beams, approach to paraxial Gaussian beams only for well-confined beams.

Finally, the paraxial condition which was analyzed in the spatial domain in [2] is analyzed in this paper in the spectral domain. Moreover, the spectral conditions that two solutions to the Helmholtz equation must fulfill in order to lead to the same paraxial approximated solution are set.

ACKNOWLEDGMENT

This work is supported by the Spanish C.I.C.Y.T. under grant TEC2006-12254-C02.

REFERENCES

1. Felsen, L. B., "Complex-source-point solutions of the field equations and their relations to the propagation and scattering of Gaussian beams," *Symposia Mathematica*, Vol. 18, Istituto Nazionale di Alta Mathematica, Bologna, 1976.
2. Gago-Ribas, E., M. J. Gonzalez-Morales, and C. Dehesa-Martínez, "Analytical parametrization of a 2D real propagation space in terms of complex electromagnetic beams," *IEICE Trans. on Electronics: Special Issue on Electromagnetic Theory — Scattering and Diffraction*, Vol. E80-C, No. 11, 1434–1439, Japan, November 1997.
3. Mahillo-Isla, R., M. J. González-Morales, and C. Dehesa-Martínez, "Spectral considerations about 2D paraxial and non-paraxial beam solutions," *Progress In Electromagnetics Research Symposium*, Japan, August 2006.

Mechanism of Dissipation Loss in Artificial Dielectrics

Ikuo Awai[1], **Makoto Furuta**[1], **and Toshio Ishizaki**[2]

[1]Department of Electronics & Informatics, Ryukoku University, Japan
[2]R&D Advanced Devices Development Center, Panasonic Corporation, Japan

Abstract— Artificial dielectrics react not only to the electric field, but also to the magnetic field, which results in high permittivity and low permeability, respectively. These two reactions induce two types of losses in artificial dielectrics, the electric and magnetic losses. We have discriminated these by assuming the magnetic or electric walls at the end of the transmission line where the thin artificial dielectric plate is located as shown in Fig. 1 (The thickness l is assumed very much smaller than λ).

We have calculated the magnetic and electric losses numerically by computing the input impedances for the structure in Fig. 1(a) with HFSS, comparing it with the analytical counterpart for (b), and found out the following features;

(1) The magnetic loss is generally far greater than the electric loss.
(2) The magnetic loss decreases with the signal frequency, whereas the electric loss increases.
(3) Bigger dimensions of a unit particle increase both losses to the corresponding directions anisotropically.
(4) Thinner strip for a unit particle has a special importance, because it may reduce the magnetic loss drastically when the thickness becomes smaller than the skin depth.
(5) When one packs unit particle denser, it will increase the electric loss proportionally, but the magnetic loss a little.
(6) For host materials with the relative permittivity ε_r, the permittivity and electric loss increase by ε_r.
(7) The increase of a unit particle decreases both losses in inversely proportional way, but its decrease affects both losses in a complex way, corresponding to the variation of skin depth.

We will physically explain these features based on a proposed current model, and also confirm the model experimentally.

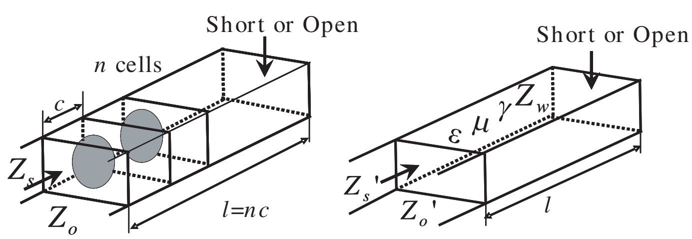

(a) artificial dielectric (b) equivalent continuous medium

Figure 1: Structure for discriminating magnetic and electric losses.

Influence of Field Potential on the Speed of Light

Zi-Hua Weng
School of Physics and Mechanical & Electrical Engineering, Xiamen University
Xiamen 361005, China

Abstract— The invariable speed of light has been doubted for two hundred years. And this question remains as puzzling as ever. However, the existing theories do not illuminate why the speed of light has to keep unchanged, and then do not offer reasonable explain for this empirical fact. The paper attempts to reason out why the speed of light keeps the same in most cases, even in the electromagnetic field.

The invariable speed of light has not been validated in fairly strong electromagnetic field, although the speed of light is variable in various optical waveguide materials. Some experiments for the variable speed of light have been performed. But all of these verifications are not dealt with the electromagnetic field potential, and have been validated in neither strong electromagnetic field nor gravitational field. So this puzzle of invariable speed of light remains unclear and has not satisfied results. The paper carries out the speed of light will be changed with the high potential of electromagnetic field.

The characteristics of electromagnetic field can be described with the algebra of quaternions. In the treatise on electromagnetic field theory, the quaternion was first used by J. C. Maxwell to demonstrate the electromagnetic field. In the quaternion space, the radius vector can be combined with the integral of field potential to become one compounding radius vector. And then we found one relation equation between the field potential and the speed of light.

The speed of light changes with the electromagnetic field potential, and has a tiny deviation from its theoretical value. The speed variation of light has a limited effect on the motion of light, because the speed variation is quite small. Therefore the invariable speed of light is believed to be correct in most cases. However, when there is a very high potential of electromagnetic field, the speed variation of light will become huge enough to impact the dispersion of light obviously.

ACKNOWLEDGMENT

The author is grateful for the financial support from the National Natural Science Foundation of China under grant number 60677039.

Mass Continuity Equation in the Electromagnetic Field

Ying Weng[1] and Zi-Hua Weng[2]

[1]College of Chemistry & Chemical Engineering
Xiamen University, Xiamen 361005, China
[2]School of Physics and Mechanical & Electrical Engineering
Xiamen University, Xiamen 361005, China

Abstract— The algebra of quaternion was first used by J. C. Maxwell to describe the property of electromagnetic field. Similarly, the quaternion can also be used to demonstrate the characteristics of gravitational field, although these two kinds of fields are quite different. By means of the scalar invariant of quaternions, we find that the mass continuity equation is an invariant in the gravitational field and electromagnetic field. With the characteristics of the quaternion, the field strengths of gravitational field and gravitational field have a few influences on the mass continuity equation.

The mass continuity equation was limited to the case of weak gravitational strength. In the quaternion spaces, the definition of mass continuity equation can be extended to the case for coexistence of electromagnetic field and gravitational field. With the characteristics of quaternions, we discuss some impact factors of the mass continuity equation in the electromagnetic field and gravitational field, including the velocity and field strength.

The results state that the gravitational strength and electromagnetic strength have tiny influence on the mass continuity equation, although the impact of electromagnetic strength and gravitational strength both are usually very tiny when the fields are weak. And then, the mass continuity equation is conserved in most cases. However, when the electromagnetic field and gravitational field are strong enough, their field strengths will affect the mass continuity equation obviously in the electrolysing solution.

It should be noted that the study for the mass continuity equation examined only one simple case of weak field strength. Despite its preliminary characteristics, this study can clearly indicate the mass continuity equation is an invariant and is only one simple inference due to the weak strength of the electromagnetic field. For the future studies, the investigation will concentrate on only some predictions about the mass continuity equation under the high speed and strong strength of electromagnetic field.

ACKNOWLEDGMENT

The author is grateful for the financial support from the National Natural Science Foundation of China under grant number 60677039.

Adjoint Charge in Electromagnetic Field

Zi-Hua Weng
School of Physics and Mechanical & Electrical Engineering, Xiamen University
Xiamen 361005, China

Abstract— The algebra of quaternions was first used by J. C. Maxwell to describe the electromagnetic field. While the algebra of octonions can be used to demonstrate the characteristics of electromagnetic field and gravitational field, including the conservation of mass etc. The related inferences are only dealt with quaternion operator but octonion operator. In the octonion space, the operator should be extended from the quaternion operator to the octonion operator.

Making use of the octonion operator, the electromagnetic field demonstrated by the octonion operator will generate an adjoint field. The source of adjoint field includes the adjoint charge and adjoint current. The adjoint charge and its movement can not be observed by usual experiments. However, when the adjoint charge is combined with the ordinary charge to become the charged particles, their movements will be accompanied by some mechanical or electric effects.

The electromagnetic field and its adjoint field both can be demonstrated by the quaternions also, although they are quite different from each other indeed. With the invariant property of octonions, we find that the adjoint charge has an influence on the conservation of mass in the electromagnetic field. The adjoint charge takes part in the gravitational interaction and impacts the mass distribution, and then can be considered as one kind of candidate for dark matter.

It should be noted that the study for the influence of adjoint field on the conservation of mass examined only one simple case with weak field strength in the electromagnetic field. Despite its preliminary character, this study can clearly indicate the adjoint field of electromagnetic field has a limited influence on the conservation of mass. For the future studies, the related investigation will concentrate on only the predictions about the variation of mass distribution in the strong adjoint field of electromagnetic field.

ACKNOWLEDGMENT

The author is grateful for the financial support from the National Natural Science Foundation of China under grant number 60677039.

Dispersion Equations for Multilayer Planar Dielectric Waveguides

M. D. Kovalev
BMSTU, Moscow

Abstract— We consider the propagation of monochromatic polarized electromagnetic waves trough a multilayer planar dielectric waveguide. An equation with roots equal to the eigenvalues of effective refractive index of the waveguide is called a dispersion equation for this waveguide. A new form of dispersion equation appeared in [1]. Later the author, who had guessed the form of this equation in the case of arbitrary number of layers, called it the multilayer equation.

Previously two kinds of dispersion equations were known for planar waveguides. The first one is traditional dispersion equation D1, obtained by the well known method of characteristic matrices of layers [2]. The second is equation D2, derived by equating to zero the determinant of the system of linear equations, expressing boundary conditions on the surfaces of layers.

In the case of great number of layers the multilayer equation has substantial advantages over traditional dispersion equations D1 and D2. It is compact and easily written. Its roots are easily found with the help of computer for the rather large number of the layers (< 30). Analyzing this equation the author derived formulas for the numbers of TE and TM-waves possible in an arbitrary planar bimaterial waveguide.

The author proved a sequence of theorems on the relations between the multilayer equation and equations D1 and D2 for the same structure. For example: the set of roots of equation D1 coincides with the set of eigenvalues of effective refractive index of the waveguide, while multilayer equation and equation D2 may have some extra roots (equal to refractive indices of layers) in addition to this eigenvalues [3]. Moreover, every refractive index of the inner layer of the waveguide is a root of equation D2.

REFERENCES

1. Maer, A. A. and M. D. Kovalev, "Dispersion equation for eigenvalues of the effective refractive index in a multilayered waveguide structure," *Doklady Physics*, Vol. 407, No. 6, 766–769, Doklady Akademii Nauk, 2006.
2. Born, M. and E. Wolf, *Principles of Optics*, Pergamon Press, 1964.
3. Kovalev, M. D., "Multilayer equation in optics and quantum physics. in Differential equations and topology. Abstracts," *International Conference Dedicated to Centennial Anniversary of L. S. Pontryagin*, 140–141, Moscow, June 17–22, 2008.

The Number of Energy Levels of a Quantum Particle in a Piecewise Constant Potential Field

M. D. Kovalev
BMSTU, Russia

Abstract— A formula for the number of energy levels of a quantum particle in an arbitrary one-dimensional piecewise constant potential field is derived. The only restriction is a finite number of segments of constant potential. We call such segments — the layers. Let us consider a structure consisting of $n \geq 3$ layers, let U_1, and U_n be the potentials in external layers of infinite width, and U_k — the minimal potential of the layers. The obvious condition of the existence of at least one stationary state (consequently, an energy level) of the particle in such a structure is the validity of the inequality $U_k < \min\{U_1, U_n\}$.

The formula obtained is effective. There are no obstacles to calculate quickly the number of energy levels for the structures with the large numbers of layers.

The deduction of the formula is based on the analysis of the recently obtained multilayer equation [1], allowing to calculate eigenvalues of energy E of a quantum particle in a piecewise constant potential field. The multilayer equation looks like $F_i(E) = 0$, where $F_i(E)$ is a rather complex function, built by a given multilayer structure and depending on the number i of an arbitrary chosen internal layer. Though an equation $F_i(E) = 0$ may have some extra roots besides the eigenvalues of the energy of the particle, the roots of the equation $F_k(E) = 0$ are distinctly coinciding with the eigenvalues of the energy. This circumstance allows to obtain our formula.

Besides the problem treated here, the multilayer equation is extremely important in the theory of optical waveguides [2]. It permits to calculate the eigenvalues of effective index of refraction for the planar multilayer dielectric waveguide. Using the method discussed here one can deduce formulas for the number of optical TE and TM-modes in an arbitrary planar dielectric waveguide.

REFERENCES

1. Maer, A. A. and M. D. Kovalev, "Dispersion equation for eigenvalues of the effective refractive index in a multilayered waveguide structure," *Doklady Physics*, Vol. 407, No. 6, 766–769, Doklady Akademii Nauk, 2006.
2. Kovalev, M. D., "The number of energy levels of a particle in a MWQ structure," *Computational Mathematics and Mathematical Physics*, Vol. 47, No. 9, 1496–1513, 2007.

Effect of Exciter Shape on Magnetic Field and Its Impedance in the Vicinity of a Multilayer Slab Conductor

Mohammad Fatehi Marji[1] **and Hossein Fatehi Marj**[2]

[1]Mine Exploitation Engineering Department, Faculty of Mining and Metallurgy
Yazd University, Yazd, Iran
[2]Electrical Engineering Department
Shahrbabak Islamic Azad University, Shahrbabak, Kerman, Iran

Abstract— If a coil is located in the vicinity of a slab conductor the distribution of magnetic field and the coil impedance will be changed due to conductor's electromagnetic induction. One of the main applications of changing in the electromagnetic field and coil impedance is in the non-destructive evaluation of conductors. In this study, effect of various coil shapes (i.e., elliptic and rhombic with different axes ratios) on the distribution of magnetic field was analyzed based on electromagnetic field distribution method which solves the Helmholtz equation in three dimensions semi-analytically. For solving an n-layer problem with several coil exciters, the boundary condition equations in between the two neighboring layers (and also the first and last layers opening to air) were arranged in a sparse matrix form. To solve this matrix, a suitable computer program was provided in MATLAB. Several example problems were solved showing the effects of elliptic and rhombic coil shapes on the magnetic field. The computed results were obtained considering several coil axes ratios. The effect of source frequency variations on the coil impedance was also analyzed and discussed. These computed results were given in suitable figures.

Effect of Variation of Slab Conductor Electromagnetic Parameters on the Electromagnetic Field Distribution

Hossein Fatehi Marj[1] **and Mohammad Fatehi Marji**[2]

[1]Electrical Engineering Department
Shahrbabak Islamic Azad University, Shahrbabak, Kerman, Iran
[2]Mine Exploitation Engineering Department, Faculty of Mining and Metallurgy
Yazd University, Yazd, Iran

Abstract— If a slab conductor is located near an arbitrary shape exciter, the electromagnetic field distribution near its surface will be changed. These changes are due to the electromagnetic parameters (permeability and conductivity) of the conductor. The conductor's permeability and conductivity may be changed due to corrosion, heat, impact, etc. In this study, the effect of changes in the electromagnetic parameters of slab conductor on the electromagnetic field distribution near the surface of that conductor was analyzed. A semi-analytical potential scalar method was used for the analysis of the electromagnetic field distribution using the Fast Fourier Transform (FFT). It is a three dimensional method which solves the problem analytically in the vertical direction and numerically in the horizontal surfaces of the conductor. In this method, a slab conductor with variable electromagnetic parameters is divided into n layers of constant electromagnetic parameters (n should be sufficiently large depending on the range of variations). A suitable computer program was provided in MATLAB and several example problems were solved. The computed results showed the effect of conductivity changes under a constant permeability and also the effect of both conductivity and permeability changes on the electromagnetic field distribution. Various problems were solved and the results were compared with each other and given in suitable figures.

Splitting of One and Conjunction of Two Coherent Beams of the Electromagnetic Radiation in Condition of the Broken Full Internal Reflection (BFIR)

Yu. A. Zyuryukin and D. R. Drevko
Saratov State Technical University, Russia

Abstract— In modern technical optics and electrodynamics there are problems both the splitting of an initial stream of electromagnetic radiation into two with their certain parity of intensities, and the connection of two similar streams for the purposes of the interference result obtaining. In particular these problems take place in Mach-Zehnder interferometers, used as for research of optical or electrodynamics properties of various mediums, and also for creation on their basis of modulators of electromagnetic radiation. The decision of these problems on the practical level can be carried out by the effect of the broken full internal reflection. The essence of this effect in case of stream splitting consists in falling at an angle more corner of full internal reflection of an electromagnetic wave with flat wave front on dielectric (are possible as air or vacuum) a plane-parallel gap and infiltration through it of an electromagnetic field that creates as a result together with reflection of an initial wave two split streams. In other case of conjunction of two initial streams falling on a similar gap with two opposite sides, there are in two directions of initial streams reflection two streams with changed intensities. More often incident angles are equal 45°, and these cases are responsible for creation splitting or the connecting optical or quasi-optical prisms finding today the applications. The theoretical description of both considered situations unfortunately in the scientific literature is absent. Therefore the purpose of the present work was liquidation of this lack. Authors on the basis of the writing of decisions of the Maxwell equations for the considered situations, due to the satisfactions of the boundary conditions for fields on interfaces and by the way the search of resultants of waves at set intensities initial waves have received analytical decisions of the formulated problems. As a result a number of the most important situations, and in particular cases when the splitting is carried out with equal shares, or when the connection of streams is realized at their equal intensities have been analyzed in details.

Session 3P9a
Electromagnetic Noise Exploitation: from Stochastic Resonance to Energy Harvesting

Stochastic Bifurcations and CR-like Effect in Bistable Self-sustained Noisy Oscillators

A. S. Zakharova[1], **T. E. Vadivasova**[2], **V. S. Anishchenko**[2], **and J. Kurths**[1]

[1]University of Potsdam, Germany
[2]Saratov State University, Russia

Abstract— We study stochastic bifurcations [1, 2] in bistable oscillators and analyze their connection to an effect similar to coherence resonance.

The classical model of the bistable Van der Pol — Duffing oscillator with additive noise is given by:

$$\ddot{x} - \left(\varepsilon + x^2 - x^4\right)\dot{x} + x + \beta x^3 = \sqrt{2D}n(t), \quad \beta \geq 0. \tag{1}$$

where $n(t)$ — normalized source of Gaussian white noise, D — noise intensity. The parameter β defines the anisochronism of oscillations. At $\beta = 0$ we have an isochronous oscillator. Without noise system (1) is characterized by bistable behavior — there are two coexisting attractors: a stable focus and a stable limit cycle. The bistability region is restricted by a saddle-node bifurcation of cycles at $\varepsilon = -\frac{1}{8}$ and a subcritical Andronov-Hopf bifurcation at $\varepsilon = 0$. By averaging one can obtain the stationary amplitude distribution: $p(a) = Na\exp[-a^2(a^4 - 3a^2 - 24\varepsilon)/48D]$ (N — normalization constant). As at the quasiharmonic approach the instantaneous amplitude does not depend on phase, its shape is for both isochronous and anisochronous oscillators the same. While varying parameters ε and D the number of extrema of the stationary amplitude distribution is changed, i.e., stochastic P-type bifurcations take place [2]. Having fixed the parameter ε at some interval we observe stochastic bifurcations by changing the noise intensity D (Fig. 1(a)).

It is important to note that behavior of the power spectra for changing the noise intensity is different for isochronous and anisochronous oscillators. For isochronous oscillator we observe an effect that is similar to coherence resonance. At a certain noise value (close to the center of the bimodal amplitude distribution) the spectral line width becomes minimal (Fig. 1(b)). This effect was firstly found experimentally in an optical bistable oscillator [3] and was called coherence resonance. This term is not correct because, as the investigations showed, its mechanism is principally different. Power spectrum of anisochronous oscillator behaves differently with the increasing of noise (Fig. 1(c)). For a small noise, the spectrum has the only one maximum at the frequency $\omega_0 = 1$. For increasing D, there appears the second maximum at the frequency ω_1. In some interval of D, there are two spectral maxima. Then the first one disappears and there remains only the maximum at the frequency ω_1. In this case, we can not speak about the effect of spectrum narrowing. All the peculiarities found for the anisochronous oscillator (1) were also observed for a self-sustained system represented by a mathematical model of synthetic gene oscillator [4]. In this case, anisochronism also destroyes the effect of spectral line narrowing.

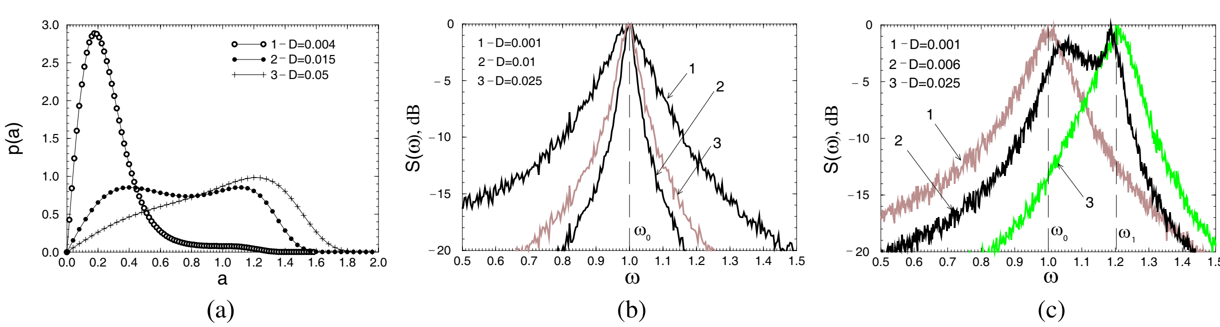

Figure 1: (a) Stationary amplitude distributions at $\varepsilon = -0.13$, (b) normalized power spectra of the isochronous oscillator at $\beta = 0$, $\varepsilon = -0.13$, (c) normalized power spectra of the anisochronous oscillator at $\beta = 0.5$, $\varepsilon = -0.13$.

ACKNOWLEDGMENT

This work was supported by the U.S. Civilian Research and Development Foundation (grant N BP4M06) and the Ministry of Education and Science of the Russian Federation, analytical departmental special-purpose program "Development of Scientific Potential of the Higher School (2009-2010)" 2009 (grant N 2.2.2.2/229).

REFERENCES

1. Horsthemke, V. and R. Lefever, *Noise-induced Transitions*, M., Mir, 1987.
2. Arnold, L., *Random Dynamical System*, Springer, Berlin, 2003.
3. Ushakov, O. V., H.-J. Wünsche, et al., "Coherence resonance near a Hopf bifurcation," *Phys. Rev. Lett.*, Vol. 95, 123903(4), 2005.
4. Hasty, J., M. Dolnik, V. Rottschäfer, and J. J. Collins, "Synthetic gene network for entraining and amplifying cellular oscillations," *Phys. Rev. Lett.*, Vol. 88, No. 14, 148101(1-4), 2002.

Nonlinear Energy Harvesting

Helios Vocca
INFN, Perugia, Italy

Abstract— Ambient energy harvesting has been in recent years the recurring object of a number of research efforts aimed at providing an autonomous solution to the powering of small-scale electronic mobile devices. Among the different solutions, vibration energy harvesting has played a major role due to the almost universal presence of mechanical vibrations. Here we propose a new method based on the exploitation of the dynamical features of stochastic nonlinear oscillators. Such a method is shown to outperform standard linear oscillators and to overcome some of the most severe limitations of present approaches. We demonstrate the superior performances of this method by applying it to piezoelectric energy harvesting from ambient vibration.

Noise Tolerant Reconfigurable Logic Gates with Resonant Tunneling Diodes

L. Worschech[1], **F. Hartmann**[1], **A. Forchel**[1], **J. Ahopelto**[2], **I. Neri**[3,4], **and L. Gammaitoni**[3,4]

[1]Technische Physik, Physikalisches Institut, Universität Würzburg
Am Hubland, Würzburg 97074, Germany
[2]VTT Micro and Nanoelectronics, P. O. Box 1000, FI-02044 VTT Espoo, Finland
[3]NiPS Laboratory, Dipartimento di Fisica, Università di Perugia, I-06123 Perugia, Italy
[4]Istituto Nazionale di Fisica Nucleare, Sezione di Perugia, I-06123 Perugia, Italy

Abstract— Submicron-sized mesas of resonant tunneling diodes (RTDs) with split drain contacts have been realized and the current-voltage characteristics have been studied in the bistable regime at room temperature. Dynamically-biased, the RTDs show noise-triggered firing of spike-like signals and can act as reconfigurable universal logic gates for small voltage changes of a few mV at the input branches. These observations are interpreted in terms of a stochastic nonlinear processes in the split RTD, which are found to be robust against noise. The split RTDs show also gain for the fired-signal bursts, can be easily integrated to arrays of multiple inputs and have thus the potential to mimic neuron nodes in nanoelectronic circuits.

Developments in Noise Temperature of Cryogenically Cooled InP HEMT Amplifiers Versus Physical Temperature

R. J. Davis and A. Wilkinson
Jodrell Bank Centre for Astrophysics, Alan Turing Building, University of Manchester, M13 9PL, UK

Abstract— Radiometer design is largely driven by the need to suppress $1/f$-type noise induced by gain and noise temperature fluctuations in the amplifiers which would be unacceptably high for a simple total power system. A differential pseudo-correlation radiometer is a scheme in which signals from the sky and from a black-body reference load are combined by a hybrid coupler, amplified in two independent amplifier chains, and separated out by a second hybrid.

Most HEMT amplifiers we have used seem to have a noise temperature that flattens out around 20 K physical temperature. In the case of the InP HEMT amplifiers used in Planck this is not the case and both noise temperature and gain vary with the physical temperature of the Front End Module (FEM), because the properties of the HEMT devices are still dependent on physical temperature at 20 K. In this paper measurements are shown which demonstrate this effect and an empirical behaviour is found which agrees with a theoretical model of M. Pospieszalski. If the temperatures are extrapolated to 4 K physical temperature, the noise temperature could be considerably improved.

Session 3P9b
Microwave Devices Using Composite Materials

Microwave Dispersion of Ferroelectric Capacitor Dielectric Properties at the Frequencies of Acoustic Resonances

A. Mikhailov, **A. Prudan**, **S. Ptashnik**, **and A. Kozyrev**
Saint-Petersburg State Electrotechnical University (LETI), Russia

Abstract— Multilayer structures, comprising thin films of barium-strontium titanate (BST) in the paraelectric (centrosymmetric) state are commonly used for frequency agile applications due to the dc bias dependent capacitance of the structure. However, if a dc bias is applied the abnormal frequency behavior both of capacitance and loss tangent is observed. The abnormal frequency behavior of dielectric properties is caused by resonance excitation of bulk acoustic waves by microwave signal. Although this phenomena can be useful for development of novel class of microwave devices like tunable thin-film bulk acoustic resonators, oscillators, filters, etc., it is negative in point of the conventional microwave application of such ferroelectric capacitance structures.

If a dc bias is applied to the multilayer structure with ferroelectric film, the central symmetry of the BST crystal structure is broken due to electrostriction and piezoelectricity is induced. The multilayer structure in microwave frequency range seems like high Q-factor acoustic resonator with hypersound source, because the BST film generates bulk acoustic waves with microwave electric field frequency. Existing to date analytical technique for this phenomena based on calculation of multilayer structure complex impedance. However, there are no data about spatial distribution pattern of eigen acoustic modes and its correlation with the microwave dispersion of dielectric properties.

In present paper, the variational-differential calculation of eigen acoustic modes of metal-dielectric-metal structure with thin ferroelectric film in paraelectric state is carried out. For estimation of excitation efficiency of bulk acoustic waves by ferroelectric film the system of electromechanical equations is solved and spatial distribution of deformation amplitudes along the multilayer structure is presented. Finally, the influence of spatial distribution pattern on the abnormal capacitance and dielectric loss dispersion is discussed. The analysis is carried out for thin ferroelectric films with composition $Ba_XSr_{1-X}TiO_3$ ($X = 0.3 - 0.5$), looking very promising for microwave applications at room temperature.

New NRD-waveguide Devices Using Metamaterials

António L. Topa, Carlos R. Paiva, and Afonso M. Barbosa
Department of Electrical and Computer Engineering and Instituto de Telecomunicações
Instituto Superior Técnico, Lisboa, Portugal

Abstract— The electromagnetic wave propagation along waveguiding structures containing metamaterials has been subject to intense investigation in the last years, due to their potential application to microwave and millimeter-wave devices. One of the most promising metamaterials is the double-negative (DNG) medium, where both the electric permittivity and the magnetic permeability can be negative in a given frequency band. Within this topic, a great variety of waveguides has been revisited.

The non-radiative dielectric (NRD) waveguide is a very popular technology in the millimetre-wave integrated circuit regime [1]. This paper addresses the issue of the electromagnetic characterization of NRD waveguiding structures where the common dielectric slab is replaced by a metamaterial slab. NRD waveguides involving DNG metamaterials have been already addressed in the literature [2–5], but the analysis has been mostly limited to its modal characterization.

The main goal of this work is to show new applications of this type of waveguides when DNG metamaterials are involved. In fact, new effects produced by the introduction of metamaterial may suggest potential applications. For example, the propagation of leaky modes is investigated [6] and its application is envisaged. On the other hand, it is shown that, in the presence of small losses, this type of waveguides may exhibit sharp narrow passbands, hence suggesting its application in the design of waveguiding filters [7]. The full-wave analysis of a DNG-NRD directional coupler is also presented. New propagation characteristics, such as contra-directional coupling [2], are review in detail. New unusual features may provide physical insight into other waveguide geometries, with potential applications in the design of new devices and components.

REFERENCES

1. Yoneyama, T. and S. Nishida, "Nonradiative dielectric waveguide for millimeter-wave integrated circuits," *IEEE Trans. Microwave Theory Tech.*, Vol. 29, 1188–1192, Nov. 1981.
2. Topa, A. L., "Contradirectional interaction in a NRD waveguide coupler with a metamaterial slab," *Dig. of XXVII URSI General Assembly*, No. 1878, Maastricht (The Netherlands), Aug. 2002.
3. Topa, A. L., C. R. Paiva, and A. M. Barbosa, "Novel propagation features of double negative H-guides and H-guide couplers," *Microwave Opt. Technol. Lett.*, Vol. 47, No. 2, 185–190, Oct. 2005.
4. Yang, P., D. Lee, and K. Wu, "Nonradiative dielectric waveguide embedded in metamaterial with negative permittivity or permeability," *Microwave Opt. Technol. Lett.*, Vol. 45, No. 3, 207–210, May 2005.
5. Baccarelli, P., P. Burghignoli, F. Frezza, A. Galli, P. Lampariello, and S. Paulotto, "Unimodal surface-wave propagation in metamaterial nonradiative dielectric waveguides," *Microwave Opt. Technol. Lett.*, Vol. 48, No. 12, 2557–2560, Dec. 2006.
6. Topa, A. L., C. R. Paiva, and A. M. Barbosa, "Dispersive leaky-mode propagation in metamaterial nonradiative dielectric waveguides," *Proc. of IEEE 2007 AP-S Int. Symp.*, Honolulu, Hawaii, Jul. 2007.
7. Topa, A. L., C. R. Paiva, and A. M. Barbosa, "Dispersion and losses in metamaterial DNG H-guides," *Chap. in Metamaterials and Plasmonics: Fundamentals, Modelling and Applications*, S. Zouhdi, A. Sihvola, and A. Vinogradov, Springer, Jan. 2009.

Design and Development of Low Cost and Light Weight Cavity and Microstrip Band Pass Filters for Communication Systems

Jagdish Shivhare[1] **and S. B. Jain**[2]

[1]Department of Electronics and Communication, Institute of Technology and Management
Sector-23 A, Gurgaon, Haryana, India
[2]Department of Electronics and Communication
Indira Gandhi Institute of Technology, Indraprashth University Campus, Delhi, India

Abstract— The main objective to introduce the ABS plastic in place of metal and other substrates for cavity and planar structure communication filters is to reduce the weight and cost. The specific gravity of ABS plastic is $1.05\,\mathrm{gm/cm^3}$ against 2.7, 8.5, $8.9\,\mathrm{gm/cm^3}$ for commercial Aluminum, Brass and Copper respectively. The cost of ABS plastic substrate may be substantially less than compared to the cost of RT-Duroid laminates. Some Cavity Band Pass Filters at centre-frequencies of (53.5 ± 1.5) MHz, (86.5 ± 4) MHz, (324 ± 4) MHz, (600 ± 9) MHz, (1200 ± 150) MHz, (1537.5 ± 7.5) MHz, (1636 ± 10) MHz, (4190 ± 20) MHz, (4590 ± 20) MHz, $(5.850 - 5930)$ GHz have been developed and tested. Two-hairpin line filters at 1537.5 ± 10 MHz and 1575.5 ± 10 MHz, also have been developed and tested [1].

Propagation Characteristics of Gyrotropic Medium

Abdullah Eroglu
Department of Engineering, Indiana University-Purdue University
Fort Wayne, IN 46805, USA

Abstract— Gyrotropic medium is extensively used in microwave and millimeter wave applications. The main reason of their common use is their natural nonreciprocal characteristics. This allows researchers and scientists to implement them in multilayered composite structures and have more control using material properties on the overall response. This can be achieved by adjusting the external applied magnetic field which changes the electrical properties of the material if it's electrically gyrotropic and magnetic properties of the material if it is magnetically gyrotropic.

Barlow and Koike [1] described a very weak effect of non-reciprocity in a waveguide loaded with thin polarized germanium plate in a transverse magnetic field over 40 years ago. Mok and Davis [2] analyzed the nonreciprocal wave propagation in three multilayer gyrotropic thin film semiconductor waveguides comprising S-I GaAs/AlAs/ n- GaAs/AlGaAs in a static magnetic field of 0.15 T over the frequency range of 0–200 GHz. The operation of the devices which are constructed using gyrotropic medium is best understood with the analysis of the wave propagation and dispersion characteristic in that a medium.

In this paper, general dispersion and constitutive relations for a gyrotropic medium are derived and used to analyze the wave propagation characteristics of electrically and magnetically gyrotropic media. A detailed analysis of wave propagation in a gyrotropic medium is given. The conditions for principle waves, cut offs, and resonances are presented. The benefit and use of the non-reciprocity property of the gyrotropic medium is illustrated. The results of this paper can be utilized in the design of microwave and millimeter wave devices where gyrotropic medium is used.

REFERENCES

1. Barlow, H. E. M. and R. Koike, "Microwave propagation in a waveguide containing a semiconductor," *Proc. IEE Microwaves, Optics and Antennas*, Pt. H, Vol. 110, 2177–2181, Dec. 1963.
2. Mok, V. H. and L. E. Davis, "Nonreciprocal wave propagation in multilayer semiconductor films at frequencies up to 200 GHz," *IEEE Trans. Microwave Theory Tech.*, Vol. 51, No. 12, 2453–2460, Dec. 2003.

CMA Diagram in the Design of Nonreciprocal Devices

Abdullah Eroglu[1] **and Jay Kyoon Lee**[2]

[1]Department of Engineering, Indiana University-Purdue University
Fort Wayne, IN 46805, USA
[2]Department of Electrical Engineering and Computer Science, Syracuse University
Syracuse, NY 13244, USA

Abstract— Microwave and millimeter wave devices have been widely used in industrial and military applications. As operational frequency increases, the requirements for the devices get more stringent and demanding. The requirements involve minimal loss, greater bandwidth and higher efficiency. The search is continuing relentlessly to find new types of materials and composites to meet all the needs of high frequency operation and have nonreciprocal effects. Nonreciprocal effects can be obtained using anisotropic or gyrotropic media which have natural gyrotropic-anisotropic crystals. Artificial composites, e.g., magnetically biased plasma or ferrite can be easily realized using anisotropic or gyrotropic media due to their natural non-reciprocity. This can lead to realization of microwave devices such as circulators, isolators, resonators, and optical devices such as modulators, switches, and phase shifters. The realization of these devices is only possible with the knowledge of high frequency characteristics of the materials used in their construction.

Materials that are anisotropic and exhibit nonreciprocal behavior can be combined with isotropic, reciprocal substrates in planar circuitry to obtain composite structures [1]. Magnetically gyrotropic or gyromagnetic materials such as ferrites can also be integrated with semiconductor substrates such as GaAs or Si to produce nonreciprocal antenna components which are merged with microwave integrated circuit (MIC) structures [2]. Ferrites also have been widely used as the key elements in microwave devices such as phase shifters, isolators, and circulators [3–5].

In this paper, we introduce Clemmow-Mullaly-Allis (CMA) diagram as a tool in the design of nonreciprocal devices. CMA diagram gives classification of wave propagation in a nonreciprocal medium such as electrically gyrotropic medium, i.e., cold plasma. The cut offs and resonances of principle waves in electrically gyrotropic medium have been investigated and used to establish the wave propagation regions. These regions are used to construct the CMA diagram. CMA diagram is then utilized as a tool to identify radiation characteristics of an unbounded electrically gyrotropic medium in the presence of Hertzian dipole. We show that key antenna parameters such as antenna gain, radiation pattern, and beamwidth in a nonreciprocal medium can be optimized for the selected operational frequency band with the use of CMA diagram.

REFERENCES

1. Hsia, I. Y., H. Y. Yang, and N. G. Alexopoulos, "Basic properties of microstrip circuit elements on nonreciprocal substrate-superstrate structures," *Journal of Electromagnetic Waves and Applications*, Vol. 5, No. 4/5, 465–476, 1991.
2. Hsia, I. Y., H. Y. Yang, and N. G. Alexopoulos, "Fundamental characteristics of microstrip antennas on ferrite semiconductor interfaces," *Proc. Int. Conf. Electromagn. in Aerosp. Appl.*, 169–171, Torino, Italy, Sept. 12–15, 1989.
3. Adam, J. D., L. E. Davis, G. F. Dionne, E. F. Schloemann, and S. N. Stitzer, "Ferrite devices and materials," *IEEE Trans. Microwave Theory Tech.*, Vol. 50, 721–737, Mar. 2002.
4. Meng, C. and R. Pietig, "Ferrite coupled-line circulator with reduced length," *IEEE Trans. Microwave Theory Tech.*, Vol. 53, No. 8, 2572–2579, Aug. 2005.
5. Erickson, N. R. and R. M. Grossien, "A low-loss 74–110-GHz faraday polarization rotator," *IEEE Trans. Microwave Theory Tech.*, Vol. 55, No. 12, 2495–2501, Dec. 2007.

Session 3P10
Electromagnetic Field Modeling, Inversion and Applications 1

Electromagnetic Phenomena in Resistance Spot Welding and Its Effects on Weld Nugget Formation

Yong Bing Li, **Zhong Qin Lin**, **Xin Min Lai**, **and Guan Long Chen**
Shanghai Key Lab of Digital Auto-body Engineering, Shanghai Jiao Tong University
Shanghai 200240, China

Abstract— Resistance Spot Welding (RSW) is a major sheet-metal joining process in automotive industry. The underlying principle of RSW is to join the sheet metals by melting the interfacial surfaces through Joule heating under the action of a current and an electrode force. The root mean square value of the alternating welding current flowing through the sheets and electrodes is generally about 10,000 Amperes for two 1.5 mm thick sheets. Therefore, a very large magnetic field is induced in the nugget area. At the same time, the current density field and magnetic field interact with each other to produce a strong electromagnetic force in the nugget area. Once molten metals appear in the nugget, the force will act and drive the metals to flow. In this research, an ANSYS-based hybrid finite element model, which consists of a two-dimensional electric model, a three-dimensional magnetic model, and a two-dimensional fluid dynamics model, is utilized to investigate the electric field, magnetic field, thermal field, and fluid flow field in the weld nugget. The interactions among the electromagnetic field, thermal field and fluid flow field are also researched. The ANSYS Parametric Design Language (APDL) is used to realize the coupling of different physical fields of different dimensionalities. Temperature-dependent physical properties, such as electric conductivity, thermal conductivity, specific heat and viscosity, are used to improve the accuracy of the model. Since the nugget area is not directly observable, the electric, magnetic, thermal and flow field cannot be measured with experimental means. As a result, the final nugget size from metallographic experiments is used to validate the proposed hybrid model. A good agreement is found between the experiments and numerical model.

Magnetic Field Solutions: A Sumudu Transform Treatment of Maxwell's Equations

Fethi Bin Belgacern
Arab Open University, Kuwait

Abstract— Sumudu Reciprocity property was advocated for the first time in the PIER Hussain-Belgacem 2007 paper to present direct time domain transient solutions of Maxwell's equations electric field. Here we give a parallel treatment for the magnetic field, using favorable attributes and newly established properties of the Sumudu Transform.

The GL EAI EM Modeling for Electromagnetic Propagation in the Earth-Air-Ionosphere

Ganquan Xie[1], **Jianhua Li**[1], **Lee Xie**[1], **Xianwei Zhou**[2], **C. S. Chen**[3], **and Michael Oristaglio**[4]

[1]GL Geophysical Laboratory, USA
[2]Department of Communication Engineering, School of Information Engineering
University of Science and Technology, Beijing, China
[3]Department of Earth Science and Graduate Institute of Geophysics
National Central University, Taiwan
[4]Schlumberger Doll Research, USA

Abstract— In this paper, we propose a Global and Local field (GL) electromagnetic (EM) modeling for simulations of the EM wave propagation in the Earth-Air-Ionosphere (EAI). The Earth, air and ionosphere have different electric conductivity and form large scale waveguide. A multiple layered EM Green's function in Cartesian, spherical and cylindrical mixed coordinate system is constructed. Unlike exist TEM type spherical and cylindrical Green function, there is no delta function and its derivative in our Green's function in mixed system. The EM integral equation with the multiple layered mixed Green's function is presented. Based on the mixed coordinate system Green's function, the Global and Local field EM modeling for Earth-Air-Ionosphere is proposed in this paper. There is no large matrix to be solved and has no artificial boundary in the GL method. The large scale GL EAI EM modeling has advantages over FEM and FD methods. We presented simulations of the low frequency electromagnetic wave scattering through Earth-Air-Ionosphere by the GL method. The GL EAI EM modeling has wide applications in the atmosphere, geophysics and Earth sciences and remote sciences and engineering.

The Method of Fundamental Solutions for Exterior Problems

Tzon-Tzer Lu[1] **and Zi-Cai Li**[2]

[1]Department of Applied Mathematics, National Sun Yat-sen University, Kaohsiung 80424, Taiwan
[2]Department of Applied Mathematics and Department of Computer Science and Engineering
National Sun Yat-sen University, Kaohsiung 80424, Taiwan

Abstract— In the electromagnetic field inversion to detect the object in the far way, the DC field modeling is reduced to the exterior problem of Laplace's equation with some boundary conditions. In this talk, we solicit the method of fundamental solutions (MFS) to seek numerical solutions. However, most of reports of the MFS deal with bounded simply-connected domains; only a few papers involve in exterior problems. For exterior problems of Laplace's equations, there exist two kinds of infinity conditions, (1) $|u| < C$ and (2) $u = O(\ln r)$, which must be complied with by the fundamental solutions chosen. For $u = O(\ln r)$, the traditional fundamental solutions can be used. However, for $|u| \leq C$, new fundamental solutions are explored, with a brief error analysis. Numerical experiments are carried out to verify the theoretical analysis made. The MFS and the method of particular solutions (MPS) are classified into the Trefftz method (TM) in 1926 using fundamental solutions and particular solutions (PS), respectively. The remarkable advantage of MFS over MPS is the uniform $\ln |PQ_i|$, to lead to simple algorithms and programming, thus to save a great deal of human power. Hence, the MFS may satisfy the engineering requirements by much less computational efforts and a little payment. Besides, the crack singularity in unbounded domains is also studied. A combination of both PS and FS is also employed, called combination of MFS. The numerical results of MPS and combination of MFS are coincident with each other. The study in this paper may greatly extend the application of MFS from bounded simply-connected domains to other more complicated domains.

Effective Condition Number and Applications to Numerical Solutions of Motz's Problem

Zi-Cai Li[1] **and Yimin Wei**[2,3]

[1]Department of Applied Mathematics and Department of Computer Science and Engineering
National Sun Yat-sen University, Kaohsiung 80424, Taiwan
[2]School of Mathematical Sciences, Fudan University
Shanghai 200433, China
[3]Key Laboratory of Mathematics for Nonlinear Sciences
(Fudan University) Ministry of Education, Shanghai 200433, China

Abstract— Consider the over-determined system $\mathbf{Fx} = \mathbf{b}$ where $\mathbf{F} \in R^{m\times n}$, $m \geq n$ and rank $(\mathbf{F}) = r \leq n$, the effective condition number is defied by Cond_eff $= \frac{\|\mathbf{b}\|}{\sigma_r\|\mathbf{x}\|}$, where the singular values of $\mathbf{F}$ are given as $\sigma_{\max} = \sigma_1 \geq \sigma_2 \geq \ldots \geq \sigma_r > 0$ and $\sigma_{r+1} = \ldots = \sigma_n = 0$. For the general perturbed system $(\mathbf{A}+\Delta\mathbf{A})(\mathbf{x}+\Delta\mathbf{x}) = \mathbf{b}+\Delta\mathbf{b}$ involving both $\Delta\mathbf{A}$ and $\Delta\mathbf{b}$, the new error bounds pertinent to Cond_eff are derived. Next, we apply the effective condition number to the solutions of Motz's problem by the collocation Trefftz methods (CTM). Motz's problem is the benchmark of singularity problems. We choose the general particular solutions $v_L = \sum_{k=0}^{L} d_k(\frac{r}{R_p})^{k+\frac{1}{2}}\cos(k+\frac{1}{2})\theta$ with a radius parameter R_p. The CTM is used to seek the coefficients D_i and d_i by satisfying the boundary conditions only. Based on the new effective condition number, the optimal parameter $R_p = 1$ is found. which is completely in accordance with the numerical results. However, if based on the traditional condition number Cond, the optimal choice of R_p is misleading. Under the optimal choice $R_p = 1$, the Cond grows exponentially as L increases, but Cond_eff is only linear. The smaller effective condition number explains well the very accurate solutions obtained. The error analysis in [1] and the stability analysis in this paper grant the CTM to become the most efficient and competent boundary method. The effective condition number can be applied for numerical partial differential equations (PDEs), e.g., the method of fundamental solutions for exterior problem [2], to show that Cond_eff is much smaller than Cond. The effective condition number may become a new trend of stability analysis of numerical PDEs.

REFERENCES

1. Li, Z. C., T. T. Lu, H. Y. Hu, and A. H.-D. Cheng, *Trefftz and Collocation Methods*, WIT Publisher, Southsampton, January 2008.
2. Lu, T. T. and Z. C. Li, "The method of fundamental solutions for exterior problems," Presentation at The PIERS 2009, Moscow, August 2009.

Fields and Waves: Acoustics, Electrodynamics, Elastodynamics

K. J. Langenberg
Dept. El. Eng., University of Kassel, 34121 Kassel, Germany

Abstract— The propagation of electromagnetic waves is governed by Maxwell's equations; in Heaviside's notation they involve first order time derivatives of vector field quantities — electric and magnetic flux densities — relating them to first order spatial derivatives of electric and magnetic vector field strengths, i.e., curl-operators; the fields are excited by electric and magnetic current densities. This system of equations bears a formal similarity to the (linear) governing equations of acoustic and elastic wave propagation. In acoustics, one of the equations involves a scalar field quantity —the pressure — and in elastodynamics second rank tensors — the strain and stress tensors — have to be dealt with. As can be readily derived, all field quantities must satisfy inhomogeneous transition conditions on surfaces representing a jump discontinuity of material properties; notice: At this point, no further specification of materials is needed. Yet, in order to combine the governing equations, constitutive relations specifying materials are needed in all cases; their simplest versions come with the keywords: linear, time-invariant, instantaneously reacting, locally reacting, homogeneous and isotropic. They introduce the permittivity and permeability in electrodynamics, the mass density and the compressibility in acoustics, again the mass density plus the two Lamé constants in elastodynamics. Now, second order partial differential wave equations are immediately obtained. Their homogeneous versions — zero sources — exhibit plane wave solutions, where the constitutive parameters enter the respective phase velocities. Due to the curl-free particle velocity, acoustic plane waves are longitudinally polarized, whereas the divergence-free electric field strength yields transversely polarized plane waves. In the elastodynamic case, the requirement for two Lamé constants leads to two different phase velocities for longitudinal pressure and transverse shear waves.

As soon as inhomogeneous wave equations are considered, the similarity between all these fields and waves goes even further: Green functions can be defined relating each particular source to each respective field quantity, where the required vector and tensor Green functions all relate to the well-known free-space scalar Green function. Therefore, the mathematical representation of source fields has striking similarities. The same is true for consecutive Huygens-type representations of scattered wave fields, that are intuitively obtained with the help of suitably specified transition conditions. In principle, these ideas can be found in a fundamental book [1], yet the indicial notation makes it rather difficult to read; therefore, we translate it with the help of Chen [2] into a coordinate-free notation that makes all the above facts much more obvious.

These mathematical similarities — as well as differences — of acoustic, electrodynamic and elastodynamic wave propagation are intuitively illustrated with wave movies for impulsive aperture radiation and scattering by a circular cylinder.

REFERENCES

1. De Hoop, A. T., *Handbook of Radiation and Scattering of Waves*, Academic Press, London, 1995.
2. Chen, H. C., *Theory of Electromagnetic Waves*, McGraw-Hill, New York, 1983.

Analysis of the Dielectric Loss as Applied to Uniform Transmission Line Load Response

Jianshu Luo, **Min Zhou**, **Wanjin Wang**, **and Ying Li**
College of Science, National University of Defense Technology, Changsha 410073, China

Abstract— Dielectric around the uniform transmission line is imperfect insulation with high frequency excited source, the current through the dielectric from the one wire to the other, which is leak conductance. And then the dielectric loss occurs, which affect the signal in the transmission line. This paper considers the effects of dielectric loss in the interaction between the source and the lines, with analysis of load response as applied to uniform transmission line. It gives the issue that the effects of the load response with dielectric loss is non-linear. And in the beginning signals attenuate quickly as to the good conductor. It is important to use the much more insulated conductor to design transmission line systems, for the signal interference is depressed.

New Solutions of Nonlinear Force-free Magnetic Field

Xu-Feng Zhang, **Jian-Shu Luo**, **and Ying Li**
Science College, National University of Defense Technology, Changsha 410073, China

Abstract— The force-free magnetic field equation looks very simple, but very few solutions have been obtained so far. For a special class of nonlinear force-free magnetic field equation in cylindrical coordinates, we found new analytic solutions. And a general approach to get some new solutions from known ones for this type of field is presented.

Frequency Dependence of Permittivity of Free and Bound Water in Soils for Different Textures

P. P. Bobrov[1,2], **V. L. Mironov**[2], **O. V. Kondratieva**[1], **and A. V. Repin**[1,2]

[1]Omsk State Pedagogical University, Russia
[2]Kirensky Institute of Physics SB RAS, Krasnoyarsk, Russia

Abstract— Dependence on the complex dielectric constant (CDC) of moist soil on the moisture and frequency is an important characteristic used in the microwave remote sensing of the land. The mayor contribution in the CDC of moist soil is made by the water which is present in moist soil into two states — free water and bound water. Measurements of soil CDC indicates that the dielectric properties of water in different soils depend on the contents of clay. Also the "free" soil water CDC was found to differ from that of free water out of soil and varies with the type of soil.

To study the CDC dependence for both the free and bound water in soil we measured moist soil CDC spectra for a set of manmade mixtures consisting of quartz particles with different granulometric content and bentonite clay. The measurements were made in the frequency range from 30 MHz to 4 GHz. Twelve different mixtures were studied in total.

The CDCs of bound and "free" water were found with the use of the refractive mixing dielectric model [1]. Our studies showed that the "free" water CDC depends on the size distribution of quartz particles, with the clay percentage being constant. There was also studied the dependence of the free soil water CDC on the percentage of clay, the size distribution of quartz particles being constant. The CDSs of both the free and bound soil water were noticed to substantially increase with decreasing frequency and the rate of CDC increase was seen to grown with the increasing percentage of clay.

REFERENCES

1. Mironov, V. L., M. C. Dobson, V. H. Kaupp, S. A. Komarov, and V. N. Kleshchenko, "Generalized refractive mixing dielectric model for moist soils," *IEEE Trans. Geosci. Remote Sensing*, Vol. 42, No. 4, 773–785, 2004.

Electromagnetic Scattering from an Infinite Dielectric Cone

Taha Mosayebi-Dorcheh, Laleh Seyyed Kalantary, Shahram Mohanna, and Saeed Tavakoli
Faculty of Electrical and Computer Engineering
The University of Sistan and Baluchestan, Zahedan, Iran

Abstract— Electromagnetic scattering plays an important role in target detection in radar systems. Conical surfaces are widely used in wide-band antennas, target detection, waveguide junctions, etc. There have been some works dealing with electromagnetic scattering of a cone, such as calculating the diffraction of conducting semi-infinite cone. There are different ways to calculate scattering of a cone such as asymptotic, numerical, and numerical-analytical methods. In this paper, scattering of a dielectric cone is analytically obtained. To solve the problem, the internal and scattering fields should be expanded with respect to the following equations (as the scattering region involve origin of coordinate, so just Bessel function should be used and spherical Neumann function is omitted):

$$\begin{aligned} Rg\bar{M}_{m\nu_{ml}}(kr,\theta,\varphi) &= \gamma_{m\nu_{ml}} j_{\nu_{ml}}(kr)\left[\hat{\theta}\frac{im}{\sin\theta}P^m_{\nu_{ml}}(\cos\theta)-\hat{\varphi}\frac{d}{d\theta}P^m_{\nu_{ml}}(\cos\theta)\right]e^{im\varphi} \\ Rg\bar{N}_{m\nu_{ml}}(kr,\theta,\varphi) &= \gamma_{m\nu_{ml}}\left\{\hat{r}\frac{\nu_{ml}(\nu_{ml}+1)j_{\nu_{ml}}(kr)}{kr}P^m_{\nu_{ml}}(\cos\theta)\right. \\ &\quad \left.+\left[\frac{j_{\nu_{ml}}(kr)}{kr}+\frac{dj_{\nu_{ml}}(kr)}{d(kr)}\right]\left[\hat{\theta}\frac{d}{d\theta}P^m_{\nu_{ml}}(\cos\theta)+\hat{\varphi}\frac{im}{\sin\theta}P^m_{\nu_{ml}}(\cos\theta)\right]\right\}e^{im\varphi} \end{aligned}$$

where r, θ and φ are in spherical coordinates, $j_{\nu_{ml}}(kr)$ is a spherical Bessel function, $P^m_{\nu_{nm}}(\cos\theta)$ is an associated Legendre function, $\gamma_{m\nu_{ml}}$ is equal to

$$\sqrt{(2\nu_{ml}+1)(\nu_{ml}-m)!/4\pi\nu_{ml}(\nu_{ml}+1)(\nu_{ml}+m)!},$$

k is the wavenumber of free space and ν_{ml} is the lth roots of the equation $\frac{d}{d\theta}P^m_{\nu_{ml}}(\cos\theta)\big|_{\theta=\pi-\beta}=0$. In this equation, β is the angle of the head of the cone (see Figure 1). This choice of ν_{ml} results in simply obtaining the expansion coefficients. For internal field, k should be replaced by k_p. k_p is the wavenumber of dielectric cone. If ν_{ml} is substituted by an integer, the expansion coefficients of the internal and external electric fields will become zero. To find the roots, derivation of the associated Legendre function should be expanded with respect to θ. Then Newton method is employed to find ν_{ml}. The boundary conditions are the continuity of tangential electric and magnetic fields. This leads to equations involving the expansion coefficients of the internal and external electric fields. To do this, it is necessary to expand $j_{\nu_{ml}}(kr)/kr$, $d(j_{\nu_{ml}}(kr))/d(kr)$, $j_{\nu_{ml}}(k_pr)/k_pr$ and $d(j_{\nu_{ml}}(k_pr))/d(k_pr)$ with respect to $j_s(kr)$ (s is an integer). Then, linear fixed-coefficient equations are obtained using orthogonality of $j_s(kr)$. As the number of equations are infinite, the values of m and l should be limited to M and L, respectively. M and L should be chosen in such a way that a good approximation of the electric fields is obtained. Finally, the expansion coefficients of the internal and external electric fields are calculated.

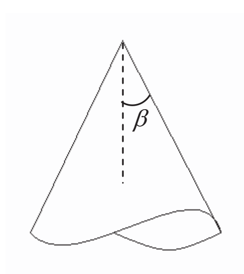

Figure 1: Geometry of the problem.

An Iterative Method for Inverse Medium Scattering for the Full Maxwell Equations

A. Lakhal
Faculty of Mathematics and Computer Sciences, Institute of Applied Mathematics
University of Saarland, Postfach 15 11 50, D-66041 Saarbrücken, Germany

Abstract— Inverse electromagnetic scattering arises as an imaging technique in many areas of application such as medical diagnosis, geophysical exploration, nondestructive testing, remote sensing etc. We consider here an inverse scattering problem for the full three-dimensional time-harmonic Maxwell's model, where we seek the reconstruction of the electromagnetic properties of an unknown inhomogeneous object laying in a known homogeneous background. Data are near-field measurements of scattered waves for multiple illuminations at a fixed frequency. Maxwell's model may be reformulated as system of integro-differential equations for the contrast functions between the object and its background. The inverse problem is of high mathematical complexity as all components of the electromagnetic fields are coupled. Besides, it is ill-posed and nonlinear. The ill-posedness is here twofold since the inverse problem is under-determined and ill conditioned. Although the integro-differential system is linear for a fixed contrast function, the dependence of the fields on the medium properties may be highly nonlinear. Hence, we should use an iterative method and apply a regularization to obtain a stable solution. We introduce the new concept of generalized induced source (GIS) to recast the intertwined vector equations in the full Maxwell's system into decoupled scalar scattering problems. This generalizes, see also [2], the decoupling procedure presented in [1] for the Maxwell equations. The GIS involves three terms, first the induced current source which corresponds also to scalar waves modelled as a Lippmann-Schwinger equation, a diffusive term and finally a term related to the coupling between the electric and magnetic fields. Hence, we may solve the inverse medium problem for the general Maxwell's equations iteratively, where we combine three steps. In the first step, the problem is scalar, linear and ill-posed, in the second step it is vector, linear and well-posed, in the last step it is nonlinear. To determine the contrast functions, we use Kaczmarz' algorithm, which is also known as ART-method and widelly used in computer tomography. We avoid solving the forward problem at each iteration through using an approximation due to Habashy and co-workers. For regularization, we use the method of the approximate inverse. It is an adjoint-field method which is stable and efficient. It consists in the computation of a reconstruction kernel for a given mollifier, independently from data. Thus, any new data can be rapidly inverted for the price of a matrix-vector multiplication. Furthermore, it is flexible as we can choose the mollifier adequately to the problem. Numerical experiments in 3D with noisy data show that our imaging method is efficient and stable.

REFERENCES

1. Lakhal, A. and A. K. Louis, "Locating radiating sources for Maxwell's equations using the approximate inverse," *Inverse Problems*, Vol. 24, 045020, 18, 2008.
2. Lakhal, A., "A decoupling method for the full Maxwell equations applied on inverse electromagnetic scattering," submitted to *Inverse Problems*, 2009.
3. Torres-Verdin, C. and T. M. Habashy, "Rapid 2.5-dimensional forward modeling and inversion via a new nonlinear scattering approximation," *Radio Sci.*, Vol. 29, 1051–79, 1994.

Session 3P11
New Applications of Ground Penetrating Radar for Non-destructive Testing 2

Depth Information from Holographic Radar Scans

C. G. Windsor[1], **A. Bulletti**[2], **L. Capineri**[2], **P. Falorni**[2], **S. Valenini**[2], **M. Inagaki**[3], **T. Bechtel**[4], **E. Bechtel**[4], **A. Zhuravlev**[5], **and S. Ivashov**[5]

[1]116, New Road, East Hagbourne, OX11 9LD, UK
[2]Dipartimento Elettronica e Telecomunicazioni, Università di Firenze, Firenze, Italy
[3]Walnut Ltd, 4-2-54 Sakaecho Tachikawa 190, Japan
[4]Enviroscan Inc, 1051 Columbia Avenue, Lancaster, PA 17603, USA
[5]Remote Sensing Laboratory, Bauman Moscow State Technical University, Russia

Abstract— Holographic radar has several potentially important advantages over conventional pulsed radar for buried object location and identification. In particular the sensor can be lightweight, of low cost and provide images of the object with good resolution. This work reports that it can give some depth information also. Two simple experiments using the Rascan system operating at 5 discrete frequencies between 1.5 and 2.0 GHz are described. The first "calibration" experiment used an aluminium plate buried in sand and inclined at a known angle to give a range of depths between 0 and 85 ± 5 mm over a length of 300 mm. The sensor was manually moved on a thin plate of glass placed over the sand above the plate. The scan down the plate showed characteristic bands in the backgound-corrected reflected intensity — the "zebra effect". The five frequencies are seen to vary differently in reflected intensity at each depth. These are interpreted qualitatively in terms of the simplified theory involving interference between the reflected wave and the incident wave at the sensor position. This theory did demonstrate the zebra effect and suggested that the amplitude variation with frequency was characteristic of depth. The cyclic nature of the zebra stripes meant that the more frequencies were available the better would be the depth discrimination. Quantitatively the true theory is complex, especially in the presence of the glass. However we suggest that the measurements can at least be used as calibration signals for a metal reflector at a given depth. The second "test" experiment involved nine US pennies buried in sand at known depths between 0 and 56 mm with a lateral separation of about 50 mm. A background-corrected total reflected intensity (the summed modulus of the reflected amplitude over all frequencies) revealed the outline of each penny quite distinctly. For each penny the set of reflected signal amplitudes at each frequency was determined where the signal was maximised over the scan area of the penny. This "best" response for each penny gave a response over the five frequencies which was distinctive and is indeed characteristic of the depth. A precise simulation theory is not available but the best frequency responses of each penny could be compared with the frequency response curves from the aluminium plate as a function of the known depth. A least squares fit was made between the best amplitudes of as a function of frequency for each penny, compared to the amplitude variation of each frequency as a function of known depth in the inclined aluminum plate experiment. With arbitrary amplitude scaling a good least squares residual minimum was always obtained for any one penny. There were some problems. The amplitude scaling varied for each penny, presumably as its surface quality and orientation altered the intensity reflected into the sensor. Also the signal quality deteriorated with depth and the frequency variation became less distinct at depths greater than 4 cm. However for the six pennies covering the depth range up to 3.4 cm the fitted depth agreed with the actual measured depth to within a standard deviation of 3 mm.

REFERENCES

1. Ivashov, S. I., V. V. Razevig, A. P. Sheyko, I. A. Vasilyev, and T. D. Bechtel, "Holographic radar as a tool for non-destructive evaluation of structural materials," *Proceedings of the 2005 SEM Annual Conference & Exposition on Experimental and Applied Mechanics*, Portland, Oregon, USA, Tuesday, June 7–Thursday, June 9, 2005.
2. Chapursky, V. V., S. I. Ivashov, V. V. Razevig, A. P. Sheyko, I. A. Vasilyev, V. V. Pomozov, N. P. Semeikin, and D. J. Desmond, "Subsurface radar examination of an airstrip," *Proceedings of the 2002 IEEE Conference on Ultra Wideband Systems and Technologies, UWBST'2002*, 181–186, Baltimore, Maryland USA, May 20–23, 2002.
3. Chapursky, V. V., S. I. Ivashov, V. V. Razevig, A. P. Sheyko, and I. A. Vasilyev, "Microwave hologram reconstruction for the RASCAN type subsurface radar," *Proceedings of the Ninth International Conference on Ground Penetrating Radar, GPR'2002*, 520–526, Santa Barbara, California USA, April 29–May 2, 2002.

Antipersonnel Landmines Detection by Holographic Radar Imaging: An Experimental Study of Soil Effects

T. Bechtel[1], **E. Bechtel**[1], **G. Borgioli**[2], **A. Bulletti**[2], **L. Capineri**[2], **P. Falorni**[2], **M. Inagaki**[5], **S. Ivashov**[3], **S. Valentini**[2], **C. G. Windsor**[4], **and A. Zhuravlev**[3]

[1]Enviroscan Inc, 1051 Columbia Avenue, Lancaster, PA 17603, USA
[2]Dipartimento Elettronica e Telecomunicazioni, Università di Firenze, Firenze 50139, Italy
[3]Remote Sensing Laboratory, Bauman Moscow State Technical University, Russia
[4]116, New Road, East Hagbourne, OX11 9LD, UK
[5]Walnut Ltd., 1-19-13, Saiwaicho, Tachikawa, Tokyo 190-0002, Japan

Abstract— Subsurface radar is a mature technology for use in dual-sensor (metal detector and radar) systems [1]. Such devices generally use ultrawideband impulse radar with a center frequency near 1 GHz in a bistatic array. The large bandwidth of these radars allows adequate penetration and depth resolution in some soils. However, the effects of soil properties on the radar response require investigation. The aim of this work is to study the effect of soil conditions on RASCAN type holographic radars. This unique type of subsurface radar produces grey scale images with plan view resolution of about $1/4\,\lambda$. This allows RASCAN to delineate the shape of buried objects at shallow depth ($< 2\lambda$) in low loss soils [2]. In order to investigate the radar's ability to detect dielectric targets with small dimensions ($\Phi = 7.5$ cm, $h = 1.9$ cm), a cylindrical plastic box filled with RTV epoxy was buried in a sand bed together with clutter objects. These targets were scanned with a RASCAN 4/4000 radar operating at five discrete frequencies close to 4 GHz, with two receiving antennae in parallel and cross polarizations relative to the transmitter. The radar head was in contact with the soil surface during scanning through a thin plastic mat. The images acquired in different soil conditions reveal some difficulty in the detection of such small dielectric targets in damp sand. With dry sand, the radar had no difficulties in delineating the shapes of all shallow objects. In another experiment, we compared the radar performance in sand versus a gravel test bed with metal and plastic targets at different depth and positions. In this case, we used RASCAN radars with discrete operating frequencies near 4 GHz and 2 GHz, with the latter providing increased penetration depth. Experiments with the same plastic mine simulants at different depths and orientations gave negative outcome due to a combination of unfortunate (but realistic) factors such as: high attenuation in damp sand, low dielectric contrast, target tilt, and irregularities in the dielectric properties of the gravel. The latter lead to false targets or noise which partially mask the target reflections. Finally, we evaluated RASCAN over uneven surfaces that more closely resemble an actual minefield. In these experiments, metal and plastic mine simulants were buried in sand and the surface was intentionally disturbed with ripples and deep footprints. The data acquired during this experiment reveal that an uneven surface and elevation of the radar head above the surface do not deteriorate the reflected signal significantly, and the buried targets were visible.

REFERENCES

1. Daniels, D. J., "A review of GPR for landmine detection," *Sensing and Imaging International Journal*, Vol. 7, No. 3, Sept. 2006. http://www.springerlink.com/content/b6356481x7340258/fulltext.pdf.
2. Capineri, L., S. Ivashov, T. Bechtel, A. Zhuravlev, P. Falorni, C. Windsor, G. Borgioli, I. Vasiliev, and A. Sheyko, "Comparison of GPR sensor types for landmine detection and classification," *12th International Conference on Ground Penetrating Radar*, Birmingham, UK, June 16–19, 2008. http://www.rslab.ru/downloads/capineri_et_al.pdf.

Noise Performances of Two Recently Reported Electromagnetic Target Classification Techniques in Resonance Region: A Comparative Study for the WD-PCA Based Classifier and the MUSIC Algorithm Based Classifier

E. Ergin[1, 2] and G. Turhan-Sayan[1]

[1]Department of Electrical and Electronics Engineering
Middle East Technical University (METU), Ankara, Turkey
[2]STM-Savunma Teknolojileri Muh. A.S., Ankara, Turkey

Abstract— Recognition of targets from their electromagnetic scattered signals is a complicated problem as such data are highly aspect and polarization dependent. Most of the target recognition techniques in resonance region make use of target system poles (also called as complex natural resonance frequencies) either directly or indirectly because the complete set of system poles constitutes an aspect and polarization independent descriptor of a given finite sized scattering object. Although target poles are perfect target features, accuracy of pole extraction from measured scattered data is very sensitive to the level of signal-to noise ratio (SNR). Therefore, alternative target feature extraction techniques (indirectly related to target poles) have been suggested in literature.

In a recently introduced electromagnetic target classification technique, natural resonance based target features were extracted from the late-time scattered signals by using the Wigner distribution (WD), a well-known time-frequency transformation, and then fused by a technique based on the principal component analysis (PCA). Another late-time resonance region target classification technique was reported very recently which was based on the use of multiple signal classification (MUSIC) algorithm for target feature extraction. Both techniques were demonstrated to be very successful in classifying conducting and dielectric objects of arbitrary shapes under noise-free design/test conditions. Furthermore, noise performances of the classifiers designed by both techniques were found quite satisfactory when tested against targets whose scattered natural response waveforms decay slowly in time. Low-Q targets (i.e., targets having natural resonances with low quality factors) such as a perfectly conducting sphere, on the other hand, have quickly decaying natural resonances leading to extremely low signal levels (and hence very small effective SNR values) over the late-time intervals. This situation makes the target classification problem highly challenging under noisy conditions.

In this paper, we designed various WD-PCA based and MUSIC algorithm based classifiers for a set of five perfectly conducting spheres (with radii of 8, 9, 10, 11 and 12 cm) and tested them against noisy test data. The results showed that a slightly noisy set of reference data (instead of noise-free reference data) must be used in the classifier design phase of both techniques to obtain acceptable noise performances in classifying low-Q targets such as perfectly conducting spheres.

Eddy-current NDE Using an AMR Magnetometer

D. F. He
Superconducting Materials Center, National Institute for Materials Science
1-2-1 Sengen Tsukuba, Ibaraki 305-0047, Japan

Abstract— Using a commercially available AMR (anisotropic magnetoresistance) sensor of HMC1001, we developed a sensitive magnetometer. The readout circuit operated in feedback mode and linearity was improved. The magnetic field resolutions of about $12\,\mathrm{pT}/\sqrt{\mathrm{Hz}}$ at 1 kHz and about $20\,\mathrm{pT}/\sqrt{\mathrm{Hz}}$ at 100 Hz were obtained. Using it as the magnetic field sensor, an eddy-current nondestructive evaluation (NDE) system was developed. A 50 turn 2 cm double-D coil wounded by 0.1 mm copper wire was used to produce the excitation field. Instead of moving the sample, we fixed the AMR sensor with an X-Y stage and moved the sensor with the X-Y stage. 2D scanning could be done. To reduce the influence of lift-off variation, dual-frequency excitation method was also used. For the high excitation frequency (5 kHz), due to its small penetration depth, only the information of the surface or the lift-off variation could be detected; for the low excitation frequency (175 Hz), both the surface information and the deep defect information were detected. By subtracting the locked outputs of two lock-in amplifiers for the low frequency and the high frequency, and choosing proper subtraction factor, the influence of the change of the lift off could be reduced and the artificial hole defects under 6 mm aluminum plate could be successfully detected. The experiments were done in unshielded environment.

Session 4AP
Poster Session 2

A Simple Method to Find the Number of Branch Points of Propagation Constants of a Lossless Closed Guide without Constructing the Dispersion Curve

K. Karayahsi[1] **and N. Yener**[2]

[1]Kırac Namık Kemal Mah, 510 Sk. Bankkent Sit. A5 Blok D:2
Esenyurt, Istanbul, Turkey
[2]Technical Education Faculty, Umuttepe Campus, Kocaeli University
Izmit 41380, Kocaeli, Turkey

Abstract— Making use of the fact that the characteristic equation that results from application of the moment method, is an algebraic equation for closed and lossless guides filled with inhomogeneous and/or gyrotropic media, we attempt to determine the degree of the discriminant of this equation, assuming we have no explicit expression for the coefficients of this equation in terms of frequency. This is achieved by successive numeric differentiation of the discriminant which we know is a polynomial, and the number of such differentiations to yield a constant value will be the degree of this polynomial. This information gives the number of branch points in the dispersion curve of a lossless closed waveguide, without having to draw the dispersion curve over the full frequency axis. Maxwell's partial differential equations can be transformed into a linear algebraic equation system whose coefficient matrix has squares of the propagation constant functions as eigenvalues. It is also discussed that the discriminant of the algebraic equation is a polynomial in the complex frequency $p = \sigma + j\omega$ and that the zeroes of this polynomial correspond to singular points (branch points) of the square of the propagation constant function and this function attains multiple values at these zeroes. In our problem, we assume that the coefficients of the characteristic equation are not known analytically. Considering for instance a 20TE + 20TM truncation of the coefficient matrix which has entries that are functions of p, it is pointed out in the literature also that, it is cumbersome to compute these coefficients analytically as functions of p. In our approach, we have chosen to use the numeric evaluation of these coefficients. Hence the aim of this work is to determine the degree of the discriminant polynomial of the characteristic equation when the coefficients of this equation are not known analytically. This degree will give us the total number of multiple roots of the characteristic equation without having to draw the dispersion curve along the full frequency axis. As an example, for a structure consisting in a lossless closed circular guide loaded with a coaxial dielectric rod, we compute derivatives of the discriminant with respect to p in the complex frequency plane numerically with a view to reach a constant value after successive differentiations. The number of such differentiations will give the sought after degree. This procedure is effected through obtaining contour-plots of the various differentiations over a region of the complex frequency plane in the neighborhood of the origin. Then the same procedure is repeated yet for another region of the complex frequency plane. The set of results in both regions confirm each other by yielding the same degree for the discriminant.

Peculiarities of Intelligence Optimization of a Microstrip Filter on Folded Dual-mode Resonators

I. A. Dovbysh and V. V. Tyurnev
Kirensky Institute of Physics of SB RAS, Krasnoyarsk, Russia

Abstract— It is known that an intelligence method of microwave filter optimization, based on usage of a priori knowledge of the device properties, differs from standard optimization methods in high efficiency [1, 2].

In this method, a distortion of the current frequency response in the passband is expanded in a series of complete basic distortions. The expansion coefficients are components of vector goal function to be used in optimization. All basic distortions subdivide into even and odd ones relative to passband center frequency.

In the case of single-mode resonators, there are conjugate correction operators, eliminating basic distortions. A correction operator, corresponding to an odd distortion, performs certain resonant frequency tunings of certain resonators. Whereas a correction operator, corresponding to an even distortion, performs certain tunings of certain resonator couplings [1, 2].

In the case of dual-mode resonators, intelligence method of microwave filter optimization needs in updating. Most complexity arises when resonators have not tetrad symmetry axis and two modes, forming the passband, are not degenerate. Just this case takes place in the filter under consideration, where every folded stepped-impedance microstrip resonator has one open end and one closed end [3].

This paper shows that the correction operators, built for single-mode resonator case, are valid for dual-mode one, if a pair of proper imagine coupled single-mode resonators be corresponded to every dual-mode resonator in the filter. The correction operators for a two-resonator four-pole filter are expressed in terms of structural parameters. In particular, increase of coupling between two imagine resonators require increasing the spacing S between parallel strips of folded dual-mode resonator, but not decreasing. Tuning of resonant frequencies difference for two imagine resonators require varying strip width product w_1w_2, but not ratio w_1/w_2. Presented intelligence optimization method, realized in the form of computer program, successfully passed an examination.

REFERENCES

1. Belyaev, B. A., M. I. Nikitina, and V. V. Tyurnev, "Effective method of microstrip filter optimization," *1997 IEEE-Russia Conference "High Power Microwave Electronics: Measurements, Identification, Applications" (MIA-ME'97)*, 104–109, Novosibirsk, Russia, September 23–25, 1997.
2. Belyaev, B. A. and V. V. Tyurnev, "The method for microstrip filters parametric synthesis," *16th Int. Crimean Conference "Microwave & Telecommunication Technology" (CriMiCo'2006)*, Vol. 2, 517–519, Sevastopol, Crimea, Ukraine, September 11–15, 2006.
3. Belyaev, B. A., L. T. Rachko, and A. M. Serzhantov, "Broad-band microstrip bandpass filter," Patent RU No. 2182738, Bulleten' Izobretenii. No. 14, 2002.

Numerical Investigation of Rectangular Dielectric Resonator Antennas (DRAs) Fed by Dielectric Image Line (DIL)

Hamide Dashti[1], **M. H. Neshati**[2], **and F. Mohanna**[1]

[1]Electrical Department, Sistan and Baluchestan University, Iran
[2]Electrical Department, Ferdowsi University of Mashhad, Iran

Abstract— In this paper Rectangular Dielectric Resonator Antennas (RDRA) fed by Dielectric Image Line (DIL) which is excited through a narrow slot on the ground plane is numerically investigated. The antenna structure is studied based on the Finite Element Method (FEM) using High Frequency Structure Simulation (HFSS) package. The effects of the slot size are considered on the radiation performance of the antenna. Results show that the optimum length and width of the slot, for 7 dB gain at 10 GHz, are 3.7 mm and 0.144 mm respectively. The return loss and radiation patterns of the antenna are also provided for a specific DRA.

UWB Antenna with Band-stop Filter

Seokjin Hong, **Dongho Kim**, **and Jaehoon Choi**
Department of Electronics Computer Engineering, Hanyang University
17 Haengdang-Dong, Seongdong-Gu, Seoul 133-791, Korea

Abstract— We propose a novel antenna with band-stop filter for UWB application. This antenna is composed of two spiral elements, 50 Ω microstrip line, ground plane with two circular slots, and two open stubs. To widen the antenna impedance bandwidth, two spiral elements are used. To achieve the band-stop filtering property at the WLAN band, two L-shaped stubs are attached to the microstrip line. The fabricated antenna has stop-band of 5.14 GHz to 5.96 GHz while maintaining the ultra-wideband characteristic from 3.17 GHz to more than 11 GHz for the −10 dB return loss requirement and near omni-directional radiation patterns except for the stop-band. The simulated and measured return loss characteristics, radiation patterns, and gain performance are present.

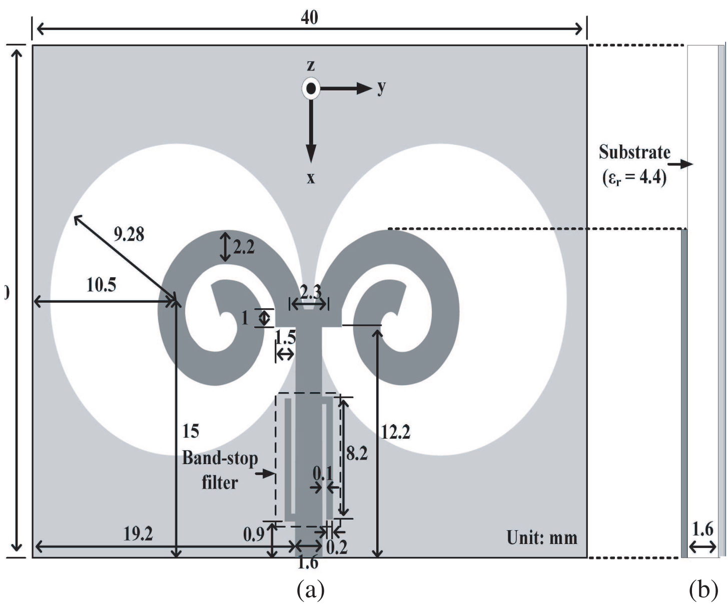

Figure 1: Geometry of the proposed antenna (a) top view, (b) side view.

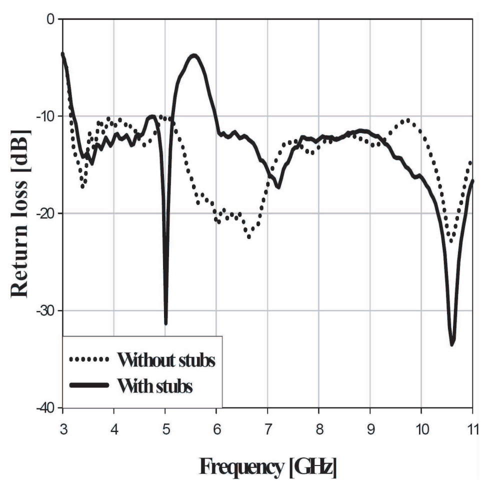

Figure 2: Measured results.

Design of an Orthomode Transducer for Use in Multi-band Antenna Feeds

Soon-Mi Hwang, **Sung-Soon Choi**, **Jea-Min Kim**, **and Bierng-Seok Song**
Korea Electronics Technology Institute (KETI), Republic of Korea

Abstract— In this paper, we present the design of an Orthomode Transducer (OMT) to be used in multi-band antenna feeds. The OMT is realized in the form of a tapered square waveguide, where two side ports of 18–20 GHz are placed in the taper region, while 30–45 GHz ports are placed in line with the waveguide axis. Each port is designed that the return coefficient is less than −20 dB and the isolation between ports is lower than 15 dB. Thin septum is inserted in side ports to reduce the effect of side ports on the return loss of the in-line port. The commercial software HFSS® is used to design the whole structure.

Wideband Microstrip Array Antenna Using Aperture Coupled Elements

N. Ghassemi and Sh. Mohanna
Electrical Engineering Department, University of Sistan & Baluchestan, Zahedan, Iran

Abstract— Microstrip antennas have a number of advantages consist of low cost and easy to fabricate, however, they have lower gain and narrower bandwidth in comparison to other antenna shapes. An ultra wideband aperture coupled microstrip antenna with non-symmetric U-shaped feed line for applications in S and C bands has been reported recently [1]. This structure has been employed here, as a basic element for designing two array antennas configurations including one 1×2 and one 1×4. The array structures comprise three dielectric layers, a feed network which made under the bottom layer and the patches which placed on top of the upper dielectric layer. Fig. 1 compares the gain and VSWR of the two proposed array antennas, with the single element microstrip antenna. It can be seen that, the impedance bandwidth (VSWR < 2) of the array antennas are more than 60% and the gain of the 1×2 array antenna is above 10 dB from 2.8–4.5 GHz and the 1×4 array has more than 12 dB gain from 2.8–4.6 GHz (48%). The results show that, the proposed array structures can be used to improve antennas specifications.

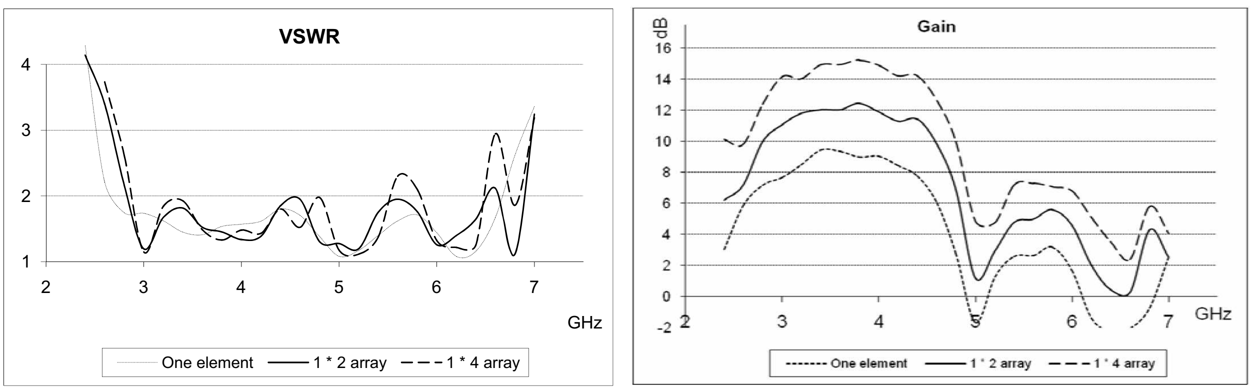

Figure 1: VSWR and Gain of one element, 1×2 and 1×4 array antennas.

REFERENCES

1. Ghassemi, N., S. Mohanna, J. Rashed-Mohassel, and M. H. Neshati, "A UWB aperture coupled microstrip antenna for S and C bands," *4th IEEE International Conference on Wireless Communication, Networking and Mobile Computing*, Dalian, China, October 12–14, 2008.

Design of a Miniaturized Broadband Tag Antenna for UHF RFID System

Xingyu Zhang and Anping Zhao
Advanced Systems Engineering, Nokia Research Center, Beijing 100176, China

Abstract— Radio frequency identification (RFID) has attracted considerable attention in recent years since it is an automatic identification method for the efficient tracking and managing of individual consumer goods, relying on the storing and remotely retrieving data in an RFID chip. Demands from the manufacturer or retailer for increasing reading range, reading speed, and anti-collision are pushing the systems toward higher operating frequencies (UHF band). The technology used to realize the antenna is perhaps the most important technology for improving the performance of the RFID system. Various kinds of RFID tag antennas have been reported in open literatures. However, many of them are neither miniaturized nor broadband, which limits the world-wide circulation and applications of the merchandise.

A novel miniaturized UHF RFID tag antenna with broadband characteristics is proposed in this paper. The proposed RFID tag antenna is inductively coupled and comprised of a long folded dipole and a modified double T-matching network. The antenna was constructed with a thin copper layer printed on a 0.24 mm thick PET substrate (with relative permittivity ε_r of 3.6 and loss tangent δ of 0.003) for low cost production. The reported antenna with a volume of $40 \times 50 \times 0.28\,\mathrm{mm}^3$ provides a fairly broad bandwidth for conjugate-matching with a commercial microchip (ALN-9338-R), which covers the entire UHF band of worldwide RFID systems. The main radiation direction of the proposed antenna tends to the orientation that is vertical to the antenna surface, which helps to the identification of objects for the antenna. Gain of the antenna ranges from 0.78 to 2.11 dBi in the band of 0.84–0.96 GHz. All these features make the antenna applicable in use for RFID tags.

Design and Demonstration of 1-bit and 2-bit Transmit-arrays at X-band Frequencies

H. Kaouach[1], **L. Dussopt**[1], **R. Sauleau**[2], and **Th. Koleck**[3]

[1]CEA, LETI, MINATEC, F38054 Grenoble, France
[2]IETR, UMR CNRS 6164, Université de Rennes 1, 35042 Rennes, France
[3]CNES, 18 avenue Edouard Belin, 31401 Toulouse, France

Abstract— This article presents the design and demonstration of planar transmit-arrays at 10 GHz with 1-bit and 2-bit phase quantization. The influence of the main design parameters are investigated theoretically. The simulated directivity/gain are 26/23 dB for the 1-bit design, and 23.7/14.3 dBi for the 2-bit design, respectively. Both designs are built on a two-layer printed board assembly and operate with linear polarization. Beamsteering performances are investigated by tilting the feed source and by changing the phase-shift distribution across the array for angles up to ±30°.

Introduction: At millimeter-wave frequencies, antenna arrays are generally implemented as lens-arrays or reflect-arrays with free-space feeding schemes to minimize the inherent loss and parasitic radiation of the feed network. Transmit-arrays (double-array discrete lenses) are low-profile and low-cost planar alternatives to dielectric lens antennas for millimeterwave applications like automotive radars, high data rate wireless communication systems, imaging systems, and quasioptical power combiners [1–5].

They typically consist of two planar arrays of printed antennas, whose elements are interconnected or coupled with a specific transmission phase in order to generate a uniform or linear phase distribution across the array (Fig. 1).

Transmit-arrays are based on similar concepts as for reflect-arrays except that they operate in a transmission mode rather than in reflection [6]. In contrast to reflect-arrays, such configurations offer several advantages, such as reduction of blockage effects due to the focal source, and easier integration and mounting onto various platforms. On the other hand, transmit-arrays are more complex to design and optimize.

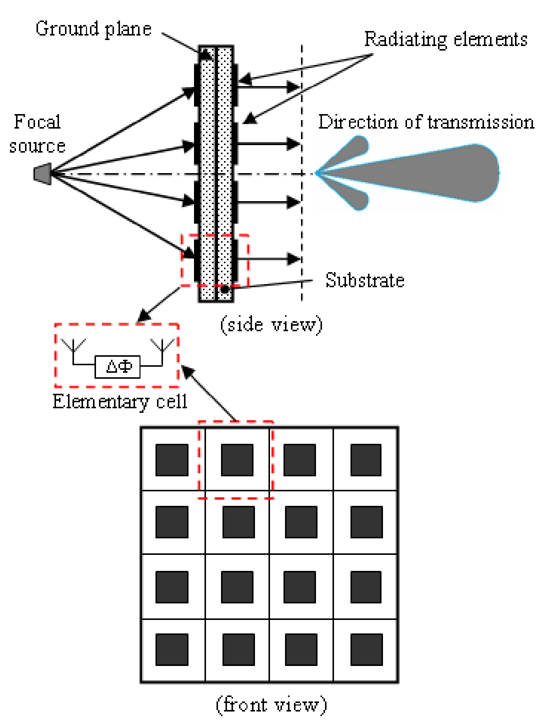

Figure 1: General description of a transmit-array.

Transmit-array Design: An in-house CAD tool has been developed to design and compute the performance of transmit-arrays, using the electromagnetic characteristics of the elementary cell and the focal source. The radiation pattern of the feed is first used to determine the electric field distribution illuminating the first antenna array. The radiation patterns and S-parameters of each elementary cell are then used to compute the radiation pattern, gain and directivity of the transmit-array.

A preliminary study has been performed in order to investigate the influence of the main design parameters as well as performances achievable. This study is based on a generic elementary cell with a gain of 5 dBi, which is a typical value for patch antennas. The total array area is fixed at 300×300 mm, which aperture corresponds to a maximum directivity of 31 dBi at 10 GHz. The feed is a 10 dBi horn antenna with 3-dB beamwidths of 52° and 49° in E- and H-planes, respectively. This feed is placed at 260 mm from the array and results in 1.82 dB of spill-over losses.

Conclusions: We will present in this paper theoretical and experimental results on the design of passive transmit-arrays operating at X-band. The theoretical study has shown the impact of cell spacing, phase quantization and focal length on the gain and directivity of the array. Two designs are presented with 1-bit and 2-bit phase quantization and different elementary cell configurations. The first design provides 23 dBi of gain, while the second demonstrated only 15 dBi due to larger element spacing. The beam-steering capabilities of both arrays have been investigated as well for $\pm 30°$ angles.

Amplification of Space Charge Waves of Millimeter Wave Range in Transversely Nonuniform n-GaN Films

V. Grimalsky, S. Koshevaya, M. Tecpoyotl-T., and J. Escobedo-A.
CIICAp, Autonomous University of Morelos (UAEM), Cuernavaca ZP 62209, Mor., Mexico

Abstract— Amplification of traveling space charge waves (SCW) of the microwave range in n-GaAs films has been under investigations for many years. When propagating in bias electric fields higher than the critical value for observing negative differential conductivity (NDC), SCW are subject to amplification. But the critical value of bias electric field in GaAs is $E_c = 3.5\,\mathrm{kV/cm}$ that limits the maximum values of the microwave electric field of amplified SCW. The frequency range of amplification of SCW in GaAs films is $f < 50\,\mathrm{GHz}$. At frequencies $f > 50\,\mathrm{GHz}$, it is better to use the materials possessing NDC at higher frequencies $f = 100 \ldots 500\,\mathrm{GHz}$, like gallium nitride GaN. The properties of GaN are: a high critical bias field $E_c \sim 100\,\mathrm{kV/cm}$; extended frequency range for observing NDC $f \leq 500\,\mathrm{GHz}$; high temperature stability and NDC at higher values of doping $\leq 10^{18}\,\mathrm{cm}^{-3}$.

In thin films of submicron thicknesses, an influence of surfaces on electron mobility can be essential, due to additional surface mechanism of scattering of carriers. Namely, the mobility near the surfaces is lower than in the center of the film, and NDC can be absent there. Therefore, the transverse nonuniformity of the film should be taken into account properly. In this report, the amplification of SCW of the millimeter wave range in nonuniform n-GaN films is analyzed.

Consider n-GaN film of a submicron thickness ($0 < x < 2l$) placed onto a semi-infinite dielectric substrate. Here GaN of cubic symmetry (zinc blende structure) is considered. The bias electric field is directed along z-axis, the SCW are excited by an input antenna and propagate in z-direction. The dynamics of SCW is described by the equations of motion of electrons jointly with the Poisson equation for the electric field. Because the frequency range $f \leq 200\,\mathrm{GHz}$ is considered, it is possible to use the hydrodynamic diffusion-drift equations for the electron fluid:

$$\begin{aligned} &\frac{\partial n}{\partial t} + \mathrm{div}(\vec{v}(E)n - D(x)\nabla n) = 0, \quad \vec{v} = \mu(|E|, x)\vec{E}; \\ &\mathrm{div}(\varepsilon_0 \varepsilon(x) \nabla \tilde{\varphi}) = -e(n - n_0(x)), \quad \vec{E} = -\nabla\tilde{\varphi} + \vec{e}_z E_0 + \vec{e}_x E_{x0} \end{aligned} \tag{1}$$

Here n is the electron concentration, $\tilde{\varphi}$ is the electric potential of the alternative field, v is the electron velocity, n_0 is the equilibrium electron concentration, D is the diffusion coefficient, $\mu(E)$ is electron mobility, E_0 is the bias electric field is z-direction; the transverse field $E_{x0}(x)$ is due to a possible nonuniform doping. The coordinate frame is aligned along the crystalline axes. The data for GaN are taken from the Internet site: http://www.ioffe.ru/SVA/NSM/Semicond/GaN/.

The boundary conditions for the density of the electric current j at the boundaries of the film are used:

$$j_x(x = 0) = 0, \quad j_x(x = 2l) = 0; \quad \vec{j} = e(\vec{v}(E)n - D\nabla n).$$

The following simple model of transverse nonuniformity is considered:

$$\mu(x) = \mu_0 - (\mu_0 - \mu_f)F(x), \;\; \mu_d(x) = \mu_{d0} - (\mu_{d0} - \mu_{df})F(x); \;\; F(x) = \exp\left(-\frac{x^2}{x_0^2}\right) + \exp\left(-\frac{(2l - x)^2}{x_0^2}\right).$$

It is assumed that in the center of the film $x = l$ the value of electron mobility is maximum: $\mu = \mu_0$ and the differential mobility μ_d is negative: $\mu_d = \mu_{d0} < 0$. At the surfaces the electron mobility takes a smaller value $\mu_f < \mu_0$ whereas the differential mobility is negative or positive there: $\mu_d = \mu_{df}$. The scale of the transverse nonuniformity is $x_0 < l$. Also the nonuniform doping of the film by donors is taken into account:

$$N_d(x) = N_{d0} \exp\left(-(x - l)^2 / x_d^2\right).$$

Here N_{d0} is the donor concentration in the center of the film, x_d is the scale of the nonuniform doping.

The calculations of spatial increments of instability of space charge waves in n-GaN films, possessing NDC, of submicron thicknesses have demonstrated a possibility of amplification of SCW up to the frequencies $f \leq 300\,\mathrm{GHz}$. When the decrease of electron mobility at the surfaces of the

film is taken into account, the spatial increments are smaller, compared with an uniform film. It is possible to compensate an influence of the surfaces by means of nonuniform doping by donors. Because the values of the bias electric fields, which are necessary for observations of NDC in n-GaN films, are one order higher than for n-GaAs ones, it is possible to obtain the values of electric fields in the millimeter wave range of about 10^4 V/cm. Direct numerical simulations of the nonlinear set of Eq. (1) added by boundary conditions confirm the results of calculations of spatial increments in the film of a finite thickness obtained in the linear approximation. Also it is demonstrated that nonlinear processes like frequency doubling and frequency mixing can be realized effectively in n-GaN nonuniform films, because of the presence of additional nonlinearity due to the transverse electric field.

The Treatment of Resonance Chart with Direct Non-resonance Power Leakage

Victor N. Egorov
East-Siberian Branch of FSUE "VNIIFTRI", Russia

Abstract— The resonance methods are wide applicable in microwave measurement technique. In many cases, the experimental resonance charts are distorted and resonance (Lorenz) function cannot be used for successful approximation of experimental data. The resonant frequency f_0 determined as frequency of maximum of device transmission coefficient is shifted for non-symmetrically distortion of resonance curve. The experimental loading quality factor Q and resonator coupling coefficients β_i have error also in this case. Most frequently the resonance chart distortion is caused by direct transmission of small part of input microwave power to resonator output without its transformation into resonance mode field. This phenomenon in open resonators is known as "non-resonance background" [1]. Cavity and dielectric resonators have often "non-resonance background" also, which is not zero for big frequency offset from f_0.

The power transmission coefficient of two-port resonator with direct non-resonance leakage will be expressed as

$$Kp\left(\xi_{\mathcal{H}}\right) = \left|S\left(\xi_{\mathcal{H}}\right)\right|^2 = (1+M)^{-2}\left\{\left|S_{21}\left(\xi_{\mathcal{H}}\right)\right|^2 + M^2 + 2\left|S_{21}\left(\xi_{\mathcal{H}}\right)\right| M\cos\left[\Psi\left(\xi_{\mathcal{H}}\right)+\psi\right]\right\}, \quad (1)$$

where $\left|S_{21}\left(\xi_{\mathcal{H}}\right)\right| = \frac{S_{21}(0)}{\sqrt{1+\xi_2}}$, $S_{21}(0) = \frac{2\sqrt{\beta_1\beta_2}}{1+\beta_1+\beta_2}$, $\Psi\left(\xi_{\mathcal{H}}\right) = -\operatorname{atan}\left(\xi_{\mathcal{H}}\right)$, $M = a_1'/a_1$-leakage coefficient, a_1, a_1'-amplitudes of incident resonance wave and direct non-resonance wave, $\xi_{\mathcal{H}} = 2Q\Delta f/f_0$-generalized loading offset, ψ-phase shift of direct non-resonance wave. The expression (1) allows to approximate the experimental resonance chart more exactly, than classic function $Kp\left(\xi_{\mathcal{H}}\right) = S_{21}^2(0)\left(1+\xi^2\right)^{-1}$. The results of least square approximation (line) of experimental data (o) in coordinates $x, vx = \xi_{\mathcal{H}}$ and $y(x), vy = Kp(x)/Kp(0)$ by classic and generalized function (1) are shown on Figs. 1(a), (b). The phase shift of direct non-resonance wave ψ was assumed as constant (not dependent on $\xi_{\mathcal{H}}$).

The unknown resonance frequency shift Δf_0, correction factor for Q, phase shift ψ and leakage coefficient M were determined as results of approximation by (1) for distorted resonance chart.

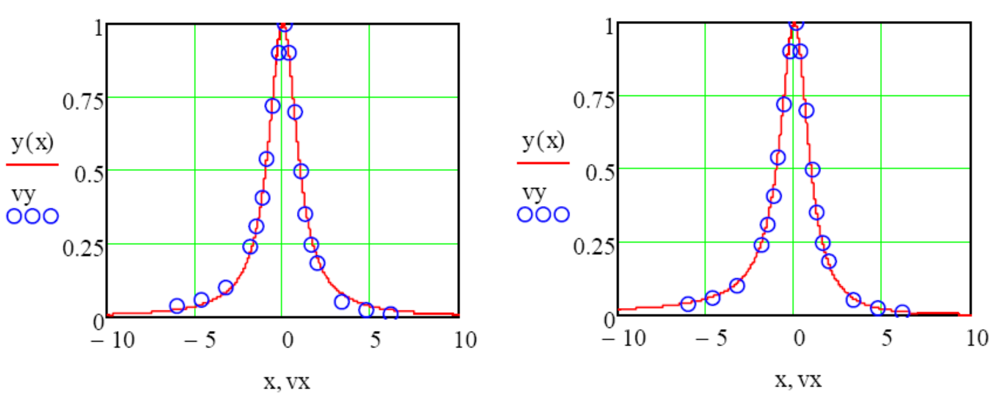

(a) (b)

Figure 1.

REFERENCES

1. Vynshtein, L. A., "Open resonators and open waveguides," *Sov. Radio*, Moscow, 1966 (in Russia).

Characterization of Ferroelectrics for Microwave Applications

A. Altynnikov, A. Gagarin, I. Kotel'nikov, A. Kozyrev, and A. Mikhailov
St. Petersburg Electrotechnical University (LETI)
197376, 5 Prof. Popov Str., St. Petersburg, Russia

Abstract— Paraelectric state ferroelectric films are the basis for development of a new class of controlling microwave devices which employ their nonlinear properties (tunable filters, phase shifters, delay lines, etc.). The analysis of general requirements on parameters of ferroelectric elements to provide their effective use on microwave is presented.

Procedures and results of small signal measurements of parameters of ferroelectric films and structures on their base in the frequency range (1–70) GHz are considered. The use of electrodeless measurements in parallel with measurements of FE film elements with metal electrodes (varactors, transmission lines) makes it possible to evaluate separately the dielectric and metal losses of elements.

Power handling capability is one of the main characteristic of microwave devices. Results of experimental investigations and simulation of the non-linear response of ferroelectric films to a high level of the microwave signal are presented. Two different techniques were used to estimate the non-linear response of ferroelectric films to microwave signal: i) measurements of the anharmonic response to pulsed microwave signal; ii) intermodulation distortion measurements (IMD). Mechanisms defining the power handling capability of ferroelectric microwave devices under microwave power were experimentally identified and theoretically described. Results obtained allow us to establish the power handling capability of ferroelectric devices and estimate the signal distortion corresponding to any operating level of microwave power.

The time required to tune microwave devices under controlling pulses is the important parameter for tunable microwave devices. Procedures and results of measurements of switching and relaxation time (down to 1 ns) for different types of ceramics and thin film ferroelectric elements are analysed and the possible mechanisms of nature of the "slow" relaxation and the ways of its suppression are considered. The possibility to create the fast acting microwave devices on the base of ferroelectric films is demonstrated.

Design of Dual-band Implantable Microstrip Antenna

Ho-Jun Lee, **Jin-Sup Kim**, **and Se-Hwan Choi**
System Packaging Research Center, Korea Electronics Technology Institute, R. O. Korea

Abstract— In this paper, we proposed a novel design of dual band microstirp antenna for implantable biometry in the Medical Implant Communication Services band (MICS band: 400 MHz, 2.4 GHz). The proposed antenna configuration is shown in Fig. 1. The proposed antenna has a simple structure. This antenna has a coplanar waveguide (CPW) fed that is optimized the 50 Ω impedance matching by positioning feed line and slot width. Antennas in this paper are simulated by using the Ansoft simulation software high-frequency structure simulator (HFSS) for achieving the broad bandwidth of 40 MHz (Low Band: 380 ∼ 420 MHz) and 300 MHz (High band: 2.2 ∼ 2.5 GHz) at return loss of 10 dB in the MICS band. Details of the proposed antenna designs are described, and typical experimental results are presented and discussed.

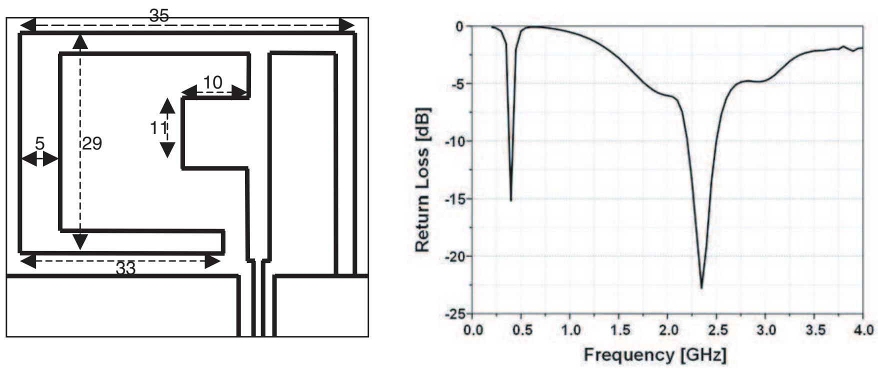

Figure 1: Proposed antenna and simulation result.

REFERENCES

1. Jaehoon, K. and Y. Rahmat-Samii, "Implanted antennas inside a human body: Simulations, designs, and characterizations," *IEEE Trans. Microw. Theory Tech.*, Vol. 52, No. 8, 1934–1943, 2004.
2. Soontornpipit, P., C. M. Furse, and C. C. You, "Design of implantable microstrip antenna for communication with medical implants," *IEEE Trans. Microw. Theory Tech.*, Vol. 52, No. 8, 1944–1951, 2004.

Simple Structure Circularly Polarized Microstrip Antenna

Ho-Jun Lee, **Jae-Young Lee**, **Kyu-Ho Park**, **and Kyu-Bok Lee**
System Packaging Research Center, Korea Electronics Technology Institute, R. O. Korea

Abstract— In this paper, we proposed a novel design broadband circularly polarized microstrip antenna. It has the advantage of improving the axial ratio bandwidth for single feed CP antennas by using a thick air substrate and corner truncated patch configuration. The impedance bandwidth (VSWR is less than 2) is 12.7%, 3-dB axial ratio bandwidth is 5%, and antenna gain is more than 8 dBi. Good agreement is obtained between simulation and measurement results.

A novel single-feed broadband circularly polarized patch antenna is proposed. The proposed antenna has a simple structure consisting of a two corner-truncated radiating patch. The substrate of the microstrip antenna is composed of a air-layer and an FR4 (relative permittivity = 4.4, loss tangent = 0.018) dielectric layer. The radiating element is a nearly square patch with two truncated corners, one is triangular corner and the other is rectangular corner. The probe at proper feed position can excite these two modes with 90phase difference and equal amplitude to produce CP radiation. Antennas in this paper are simulated by using CST Microwave Studio 2006.

REFERENCES

1. Finkenzeller, K., *RFID Handbook*, 2nd Edition, John Wiley & Sons, 2004.
2. Chen, H. M. and K. L. Wong, "Circular polarization design of annular-ring microstrip antenna," *IEEE Trans. Antennas Propagat.*, Vol. 47, 1289–1292, Aug. 1999.
3. Wong, K. L. and J. Y. Wu, "Single-feed small circularly polarized square microstrip antenna," *Electron. Lett.*, Vol. 33, 1833–1834, Oct. 23, 1997.
4. Lu, J. H., J. Y. Wu, and K. L. wong, "Circular polarization design of a single-feed equilateral-triangular microstrip antenna," *Electron. Lett.*, Vol. 34, 319–321, Feb. 19, 1998.

A Novel Microwave Absorbing Structure Using FSS Metamaterial

H. Y. Chen, X. Y. Hou, and L. J. Deng
State Key Laboratory of Electronic Thin Film Integrated Device
University of Electronic Science and Technology of China, Chengdu, China

Abstract— Artificially constructed electromagnetic metamaterials have attracted much interest recently. A novel absorbing structure in microwave range with metamaterial frequency selective surface (FSS) is presented in this paper. The absorber is a simple unit cell layer planar structure based upon two metamaterial resonators that couple separately electric and magnetic fields so as to absorb almost all incident fields. The resulting structure which consists of metallic elements has superior absorbance characteristics compared to conventional passive absorbers of corresponding thickness. Experimental results are presented and compared to obtained from a finite difference time domain (FDTD) approach, demonstrates a peak absorbance greater than 87% at 12.8 GHz.

Introduction: Artificially constructed electromagnetic metamaterials have attracted much interest recently due to the potential to produce exotic electromagnetic phenomena such as negative index of refraction [1, 2] or the possibility to fabricate an invisible device such as an electromagnetic cloak [3]. The realization of such properties lies in these materials which response to incident radiation have the opposite direction between the group velocity, which characterizes the flow of energy, and the phase velocity, which characterizes the movement of the wave fronts. The electromagnetic metamaterial structures which are very freedom in geometrically have been widely used in every technologically relevant frequency distribution range from radio to optical [4–8], due to their low loss, low cost and flexibility in adjusting the frequency. Recently these exotic characteristics which the electromagnetic metamaterial constructions have behaved demonstrate great presage for future application.

After the early work of Veselago [9], research enthusiasm about negative index materials has been in a recession, because no naturally occurring material meet simultaneously with $\mu < 0$ and $\varepsilon < 0$ in a frequency band [10]. The situation changed in 2000, however, when a composite structure based on split ring resonators (SSRs) was presented and demonstrated existing a frequency band over which μ and ε were both negative. As such, the primary focus has been on the characteristic impedance of the media for propagating electromagnetic wave defined as, where a metamaterial can be impedance-matched to free space by matching ε and μ, minimizing reflectivity. As we know, metamaterials can be regarded as effective media and characterized by a complex electric permittivity and complex magnetic permeability. The electric loss and magnetic loss of metamaterial can be respectively characterized by the ratio of the imaginary and real part of electric permittivity $\mathrm{tg}\delta_\varepsilon = \varepsilon_2/\varepsilon_1$, and the ratio of the imaginary and real part of magnetic permeability $\mathrm{tg}\delta_\mu = \mu_2/\mu_1$, the more its value, the higher the rate of absorption of the metamaterial. The loss componements of the media constant (ε_2 and μ_2) have much potential for the creation of exotic and useful materials as well. In this paper, a novel absorbing structure which shows a high absorbance and can be used in some devices such as bolometric wave detector.

24-GHz Front-end Monolithic Microwave Integrated Circuits Using 0.5-μm GaAs Enhancement/Depletion-mode (E/D-mode) PHEMT Technology for Automotive Radar Applications

Hong-Yeh Chang[1], **Yi-Shuo Wu**[1], **Shou-Hsien Weng**[1], **Yan-Liang Yeh**[1], **Chi-Hsein Lin**[1], **Sheng-Ming Luo**[1], **and Yu-Chi Wang**[2]

[1]Department of Electrical Engineering, National Central University
Chungli 32001, Taiwan, R.O.C.
[2]WIN Semiconductors Corp., Taoyuan 333, Taiwan, R.O.C.

Abstract— In this paper, 24-GHz front-end monolithic microwave integrated circuits (MMICs), including a voltage controlled oscillator (VCO), a power amplifier (PA), a low noise amplifier, and a single-balance mixer, using 0.5-μm GaAs enhancement/depletion-pseudomorphic high-electron mobility transistor (E/D-PHEMT) technology are presented for automotive radar applications. The dc supply voltage of the MMICs is only 2 V, and therefore they can be further applied to low voltage and low dc power automotive radar transceivers. In addition, an advantage for the E-mode PHEMT process is positive gate bias, and the bias circuit for the modulation would be less complicated. Moreover, the VCO demonstrates a phase noise of better than −109 dBc at 1 MHz offset frequency, a RF output power of higher than 5 dBm, and a tuning range of between 20 and 28 GHz. The small signal gains of the PA and LNA are 10 and 15 dB, respectively. The output 1-dB compression point ($P_{1\,\mathrm{dB}}$) of the PA and LNA are higher than 5 and 21 dBm, respectively. The noise figure of the LNA is lower than 7 dB between 20 and 26 GHz. With a local oscillator (LO) power of 0 dBm, the mixer demonstrates a maximum conversion loss of 13 dB from the 20 and 40 GHz, an IF bandwidth of wider than 3 GHz, and a LO-to-RF isolation of better than 45 dB. The chip sizes of the VCO, LNA, and mixer are all within $1 \times 1\,\mathrm{mm}^2$, and the PA is $2 \times 1\,\mathrm{mm}^2$. In our future works, the MMICs will be further packaged in a mechanical metal housing for the 24-GHz automotive radar applications.

MMIC Process: For the 24-GHz automotive radar transceiver design, a 0.5-μm GaInAs E/D-PHEMT process on 4-mil substrate provided by WIN Semiconductors Corp. is adopted. An E-mode PHEMT device typically exhibits a unity current gain frequency (f_T) of 35 GHz, and a maximum oscillation frequency ($f_{\max}$) of greater than 80 GHz [1]. In this MMIC process, D-mode PHEMT device, slot VIA hole, backside metal, thin film resistor, metal-insulator-metal (MIM) capacitor, and spiral inductor are also available.

ACKNOWLEDGMENT

The chip was fabricated by WIN Semiconductors Corporation, Taiwan, R.O.C.. This work was supported in part by the National Science Council of Taiwan, R.O.C., under Grants NSC 96-2221-E-008-117-MY3, NSC 96-2628-E-008-119-073-MY3, and the ALMA-T research project. The authors would like to acknowledge Pei-Lun Chang, Taiwan Agilent, Jhongli, Taiwan, R.O.C., for technical assistance in the MMW measurement, the Chip Implementation Center (CIC), Taiwan, for providing EDA design software.

REFERENCES

1. WIN Semiconductors, "0.5 μm InGaAs PHEMT enhancement/depletion-model device (E/D-mode) device model handbook," ver.1.0.1, May 2006.

Design of an Antenna System for UWB-MIMO Communications

Ali Imran Najam and Yvan Duroc
Grenoble Institute of Technology (Grenoble-INP), France

Abstract— Ultra-wideband (UWB) technology has gained a lot of popularity since its approval by FCC in 2002 for the band of 3.1–10.6 GHz as it is capable of providing very high data rates. However, the transmitted power for UWB systems is kept very low to make sure of its existence with other wireless standards without interfering them and it became the reason for not achieving high data rates over larger distances. In context to finding the solution, some research work has been demonstrated to use Multiple-Input Multiple-Output (MIMO) techniques along with UWB to improve the capacity of the system. Aiming at the implementation of MIMO with UWB, it is required to develop an antenna system that can operate in 3.1–10.6 GHz as well as can provide diversity performance. It is well known that diversity performance is related to the correlation which is also mainly dependent on mutual coupling between the antenna elements. It is therefore critical to have mutual coupling as low as possible for MIMO antennas. In this paper, four-element MIMO antenna is designed for UWB systems. The single element for the proposed antenna system i.e., circular disc monopole fed by 50 Ω microstrip line is already presented in [1] and its selection can be justified by its good performance for UWB communications. In the next step, four identical elements have been integrated on FR4 substrate with 0.8 mm thickness as shown in Fig. 1. The radii of the discs and the dimensions of ground planes are optimized to ensure the required impedance bandwidth. The distance 'd' is optimized to attain as low mutual coupling as possible. In addition to this, the isolation is being improved by exciting the elements in orthogonal polarization. The dimensions of the proposed antenna system are: radii of disc (R) = 10.7 mm, length of ground plane = 12.2 mm, width of ground plane = 40 mm, distance between adjacent elements = 37.8 mm, width of substrate = length of substrate = 80 mm. The simulations are performed in CST Microwave Studio. Due to symmetry, $S_{11} = S_{44}$ and $S_{22} = S_{33}$, only S_{11} and S_{22} are presented in Fig. 2. Also, the mutual coupling is shown in Fig. 3 for the element #1 is excited and others are terminated by 50 Ω. The mutual coupling between elements 1 and 4 is always less than −14 dB while S_{13} and S_{12} are efficiently very low. These low values of mutual coupling ensure low correlation resulting good diversity gain.

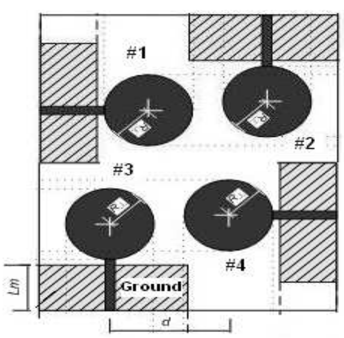

Figure 1: Layout.

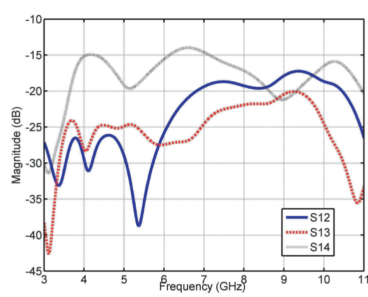

Figure 2: Reflection coefficients.

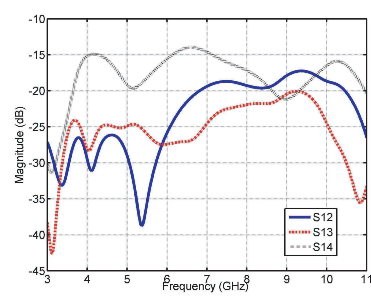

Figure 3: Mutual couplings when element # 1 is excited.

REFERENCES

1. Liang, J., C. C. Chiau, X. Chen, and C. G. Parini, "Study of a printed circular disc monopole antenna for UWB systems," *IEEE Transactions on Antennas and Propagation*, Vol. 53, No. 11, 3500–3503, Nov. 2005.

Measurement of Dielectric Anisotropy of Microwave Substrates by Two-resonator Method with Different Pairs of Resonators

Plamen I. Dankov, **Boyan N. Hadjistamov**, **Iliyana P. Arestova**, **and Valda P. Levcheva**
Faculty of Physics, University of Sofia, Sofia, Bulgaria

Abstract— The measurement of the dielectric material parameters is one of the most important things connected with the modern electronics, computer and communication hardware. The main reason is the new modern manner of design of the electronic devices, based on electromagnetic or schematic simulators, where the knowledge of the accurate values of the substrate dielectric constant and the loss tangent is very important.

We have developed a number of resonance methods for determination of the dielectric parameters of samples in different directions — parallel and normal to the substrate surface. In fact, these two-resonator methods have ability to determine the dielectric anisotropy of the substrates. The simplest method, based on two cylindrical resonators with different modes TE_{011} and TM_{010} and different diameters, is suitable for determination of the substrate anisotropy at a set of fixed frequencies. The determination of the substrate anisotropy is possible in a relatively big frequency interval, when we utilize pairs of tunable coaxial and re-entrant resonators, operating at relatively low frequencies. In this presentation we investigate a new pair of measurement resonance tools, based on dielectric cylindrical, ring or rectangular resonators inserted into cylindrical metal cavities (entire or splitted). First of all, we investigate numerically by electromagnetic simulators a number of configurations with different dielectric resonators DR's in different frequency ranges in order to obtain the best measurement condition and the optimal DR shape. Next, we introduce suitable 3D models of the chosen cavities ensuring best accuracy and computational efficiency. An error analysis has been done. Finally, we present measurement data for the dielectric properties of several known commercial substrates, and compare these results with data from our previous investigations. We use DR's based on high-quality sapphire and alumina with very high Q factors.

A Study on the Coupled Image Guide Structures

I. I. Arestova, P. I. Dankov, and V. P. Levcheva
Department of Radio Physics and Electronics, Faculty of Physics
University of Sofia "St. Kliment Ohridski", Bulgaria

Abstract— The objective of this investigation is to help understanding the processes of wave propagation in coupled image guide structures (CIGSs). CIGSs have been traditionally considered as perspective for design of components at millimeter wavelengths, in particular nonreciprocal components — isolators and circulators. The nonreciprocal behavior is obtained usually with magnetized ferrite materials.

There have been various configurations of nonreciprocal CIGSs proposed by investigators, containing ferrite image guide (IG) sections with different magnetization — longitudinal, transverse or mixed one. The difficulties in design and optimization of nonreciprocal devices on the base of CIGSs are due not only to the complexity of wave propagation in a magnetized ferrite IG and its coupling to the dielectric IG, but also to the processes at the existing open ends of the dielectric or ferrite IGs with finite length (reflection, radiation).

In attempt to clear up the operating mechanism of such CIGSs, first we have examined experimentally using electric probes the distribution of all three electric field components at several IG structures — single dielectric IG with two transitions to the rectangular metal waveguide, single open ended dielectric IG, two coupled dielectric IGs, coupled dielectric and ferrite IGs at different magnetizations. This labour and time consuming investigation has shown, that the electric probes no matter all their imperfections, can be used as a testing instrument in design procedure of such open structure devices. After that, we have used the finite element method (FEM) to simulate some of experimentally investigated structures. The results of both approaches — electric probe measurements and computer-aided design (CAD) are believed to ease the future design of nonreciprocal components for millimeter wavelengths.

Efficient Sidelobe Reduction Technique for Linear Antenna Arrays Using Step-function Feeding Systems

Fikret Tokan and Filiz Güneş
Department of Electronics and Communication Engineering, Yıldız Technical University
İstanbul, Turkey

Abstract— Smart antenna systems have been widely considered to provide interference reduction and improve the capacity, data rates, and performance of wireless mobile communication. Smart antenna arrays with adaptive beam forming capability are very effective in the suppression of interference and multipath signals. Many synthesis methods are concerned with suppressing the sidelobe level (SLL) while preserving the gain of the main beam. The evolutionary algorithms such as genetic algorithms (GA) [1], particle swarm optimization [2], a clonal selection algorithm [3] are still of great interest in synthesizing the antenna arrays. On the other hand, the recent works deals with the most accurate approach to the far field calculations taking into account the individual patterns in the real environment where mutual coupling between the antennas exist [4]. In this work, step-functions are used for excitation amplitudes of linear antenna arrays. The excitation amplitude of first antenna is 6 times the excitation amplitudes of last antenna in all examples. Dolph-Chebyshev arrays which have continuous values are usually used for sidelobe reduction. The increase of number of antennas causes higher ratio between first antenna excitation amplitude and last antenna excitation amplitude which means the raise of dynamic range ratio (DRR). In our technique, DRR is fixed to 6 and this value does not change with number of elements. The "Pattern Search (PSearch)" algorithm is introduced for the optimization of the antenna system, which is experienced as a fast algorithm for optimization. The interelement spacings between elements are taken 0.5λ in all examples and the excitation amplitudes are optimized. The geometry of the antenna array used in our examples is given in Fig. 1.

The excitation amplitude distribution of step-functions and Dolph-Cheb. functions are given in Fig. 2 and the values of excitation amplitudes are given in Table 1.

The comparative examples for suppression of whole sidelobe region while obtaining a fairly high gain using the Psearch Algorithm and Dolph-Chebyshev method for $N = 15$, $N = 20$ and $N = 25$ are given in Figs. 3(a), (b) and (c) respectively.

In conference, many typical examples for the linear array synthesis will be presented.

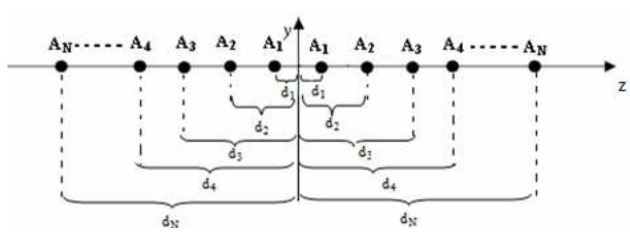

Figure 1: The linear antenna array geometry for the sum pattern.

Table 1: The excitation coefficients used to obtain Figs. 2(a), (b) and (c).

$N = 15$	Step-Function	[6 6 6 5 5 5 4 4 4 3 3 2 2 1 1]
	Dolph-Cheb.	[1 0.987 0.961 0.923 0.875 0.818 0.753 0.682 0.608 0.532 0.456 0.382 0.312 0.247 0.423]
$N = 20$	Step-Function	[6 6 6 5 5 5 5 5 4 4 4 3 3 3 2 2 2 1 1 1]
	Dolph-Cheb.	[1 0.992 0.978 0.957 0.929 0.895 0.856 0.812 0.764 0.712 0.658 0.603 0.546 0.489 0.433 0.379 0.326 0.277 0.230 0.526]
$N = 25$	Step-Function	[6 6 6 5 5 5 5 5 5 4 4 4 4 3 3 3 3 2 2 2 2 1 1 1 1]
	Dolph-Cheb.	[1 0.995 0.986 0.972 0.954 0.932 0.906 0.877 0.844 0.809 0.770 0.730 0.688 0.644 0.600 0.555 0.509 0.465 0.420 0.377 0.335 0.295 0.257 0.220 0.632]

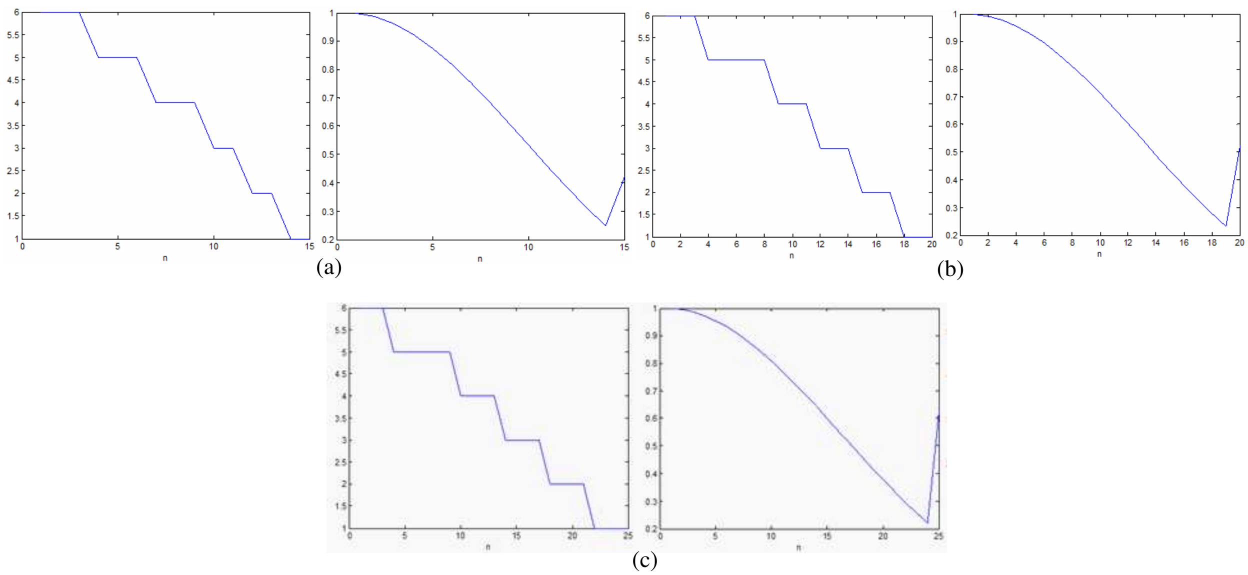

Figure 2: The excitation amplitude distribution of step-functions and Dolph-Cheb. functions. (a) $N = 15$, (b) $N = 20$, (c) $N = 25$.

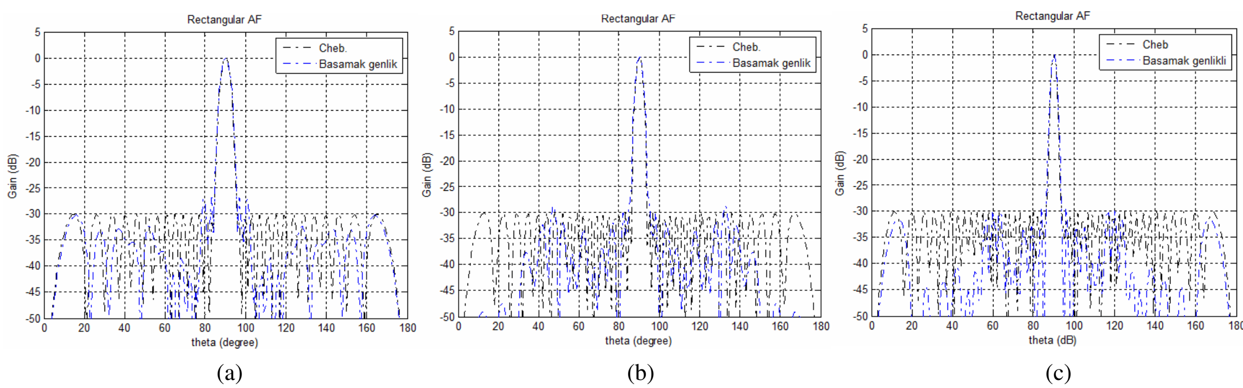

Figure 3: Comparative plot of Psearch versus Dolph-Cheb. for SLL suppression of whole sidelobe region (a) $N = 15$, (b) $N = 20$, (c) $N = 25$.

REFERENCES

1. Tonn, D. A. and R. Bansal, "Reduction of sidelobe levels in interrupted phased array antennas by means of a genetic algorithm," *International Journal of RF and Comp. Aided Engineering*, Vol. 17, No. 2, 134–141, March 2007.
2. Khodier, M. M. and C. G. Christodoulou, "Linear array geometry synthesis with minimum sidelobe level and null control using particle swarm optimization," *IEEE Trans. on Antennas and Propagation*, Vol. 53, No. 8, 2674–2679, August 2005.
3. Karaboğa, D., K. Güney, and A. Akdağlı, "Antenna array patern nulling by controlling both amplitude and phase by using modified touring ant colony optimization algorithm," *International Journal of Electronics*, Vol. 91, No. 4, 241–251, April 2004.
4. Mahmoud, K. R., M. I. Eladawy, R. Bansal, S. H. Zainud-Deen, and S. M. M. Ibrahem, "Analysis of uniform circular arrays for adaptive beamforming applications using particle swarm optimization algorithm," *International Journal of RF and Comp. Aided Engineering*, Vol. 18, No. 1, 42–52, 2007.

Design of Stacked Power Amplifiers Using GaAs Monolithic Microwave Integrated Circuit (MMIC) Technology

Chih-Chun Shen[1], **George D. Vendelin**[1], **Hong-Yeh Chang**[1], **and Yu-Chi Wang**[2]

[1]Department of Electrical Engineering, National Central University
Chungli 32001, Taiwan, R.O.C.
[2]WIN Semiconductors Corp., Taoyuan 333, Taiwan, R.O.C.

Abstract— Design of stacked power amplifiers (PAs) using monolithic microwave integrated circuit (MMIC) technology is presented in this paper. The stacked PA is an output power enhancement circuit based on voltage multiplication, and the higher output power can be obtained as the transistors are connected in series. For dual-stacked PA, it consists of a common-source (CS) and common-gate (CG) stages. For triple-stacked PA, an addition CG stage is cascaded in the output of the dual stacked PA to increase the output swing voltage, as well as the output power. The capacitance of the capacitor at the gate of the CG stage plays a key role for the output power of the PA, and therefore the capacitance should be properly designed. The design theory of the capacitance is also presented. Based on our proposed design procedure for the stacked PA, a dual-stacked and two triple-stacked PAs are successfully implemented using GaAs HBT and PHEMT processes. The measured 3-dB bandwidth of the PAs are all from 2.4 to 6 GHz, and the measured power gains of the dual-stacked and the triple-stacked PAs are higher than 12 and 15 dB, respectively. The measured saturation output power (Psat) of the PAs are all higher than 23 dBm with power added efficient (PAE) higher than 20%. Moreover, the chip areas of the PAs are very compact due to the MMIC technologies, and they have good potential to be further applied to the modern communication applications.

ACKNOWLEDGMENT

The chips were fabricated by WIN Semiconductors Corporation, Taiwan, R.O.C.. This work was supported in part by the National Science Council of Taiwan, R.O.C., under Grants NSC 96-2221-E-008-117-MY3, and NSC 96-2628-E-008-119-073-MY3. The authors would like to acknowledge Pei-Lun Chang, Taiwan Agilent, Jhongli, Taiwan, R.O.C., for technical assistance in the MMW measurement, the Chip Implementation Center (CIC), Taiwan, for providing EDA design software.

A Support Vector Regression Machine Model for a Coax-fed Circular Microstrip Antenna

G. Angiulli, D. De Carlo, P. Quattrone, and S. Tringali
DIMET, University Mediterranea, Reggio Calabria 89100, Italy

Abstract— A fast method for the design of coax-fed circular microstrip antennas, based on a support vector regression machine approach is presented. The obtained model transforms the dielectric constant ϵ_r, substrate thickness h, air gap h_g and dominant mode resonant frequency f_0 to patch radius a. Very good agreement between the SVRM computed resonant dimensions and Moment Method ones is found, revealing the effectiveness of the proposed approach. Furthermore, the SVRM reduces dramatically the design time. Accordingly, this approach can be very useful for the development of fast CAD models.

REFERENCES

1. Lee, K. F. and J. S. Dahele, "Mode characteristics of annular-ring and circular-disc microstrip antenna with and without air gaps," *IEEE Antennas Propagation Soc. Int. Symp. Dig.*, 55–58, 1983.
2. Dahele, J. S., S. Mem, and K. F. Lee, "Theory and experiment on microstrip antenna with an air gap," *Proc. Inst. Elect. Eng.*, Pt. H, Vol. 32, 455–460, 1985.
3. Angiulli, G., M. Cacciola, and M. Versaci, "Microwave devices and antennas modelling by support vector regression machines," *IEEE Trans. on Magnetics*, Vol. 43, No. 3, 1589–1593, 2007.
4. Angiulli, G., D. De Carlo, G. Amendola, E. Arnieri, and S. Costanzo, "Support vector regression machines to evaluate resonant frequency of elliptic substrate integrate waveguide resonators," *Progress In Electromagnetics Research*, PIER 83, 107–118, 2008.

Performance Investigation of Microstrip Exponential Tapered Line Impedance Transformer Using MathCAD

Mazlina Esa, **Nik Noordini Nik Abd Malik**,
Nadiyatulakmar Abdul Latif, **and Jayaseelan Marimuthu**
Faculty of Electrical Engineering, Universiti Teknologi Malaysia
81310 UTM Skudai, Johor, Malaysia

Abstract— Impedance transformer is an essential part of a system which allows two different loads to be perfectly connected without any loss due to reflections. This paper presents investigations performed on a microstrip exponential taper impedance, ETLI, transformer. Mathematical computations were performed using MathCAD software. The reflection coefficient and return loss responses are in good agreement with theory. Broadband characteristics have been observed. To further investigate the performance of the taper, the ETLI transformer is simulated. Four different load impedances have been considered and various lengths of ETLI were investigated. It was found that as the frequency increases, the number of optimum lengths has also increased with a smaller difference between the optimum lengths. The same pattern occurs with any load impedance, from 70 to 100 ohm. In addition, the behaviour of ETLI transformer with variation of loads at a particular frequency showed that 80 ohm load appeared to be the most matched. As the frequency increases, higher loads are matched with longer ETLI. Different loads are well-matched with longer ETLI transformers at higher frequencies from 6 GHz.

A Novel Bandpass Defected Microstrip Structure (DMS) Filter for Planar Circuits

M. Kazerooni[1], **A. Cheldavi**[1], **and M. Kamarei**[2]

[1]College of Electrical Engineering, Iran University of Science and Technology, Tehran, Iran
[2]Faculty of Electrical and Computer, University of Tehran, Tehran, Iran

Abstract— A new defected microstrip structure (DMS) unit lattice is proposed in order to perform a bandpass filter (BPF). The proposed DMS provides the good cutoff and passband characteristics. Also in this paper, we extract the model of BPF. In order to show the improved the parameters, several circuits were designed and simulated. The BPF has a bandwidth more than 39%.

U-shaped RFID Tag Antenna for Isotropic Radiation Pattern

Sangwoon Lee[1], **Hak-Joo Jung**[1], **Hosung Choo**[2],
Keekeun Lee[1], **and Ikmo Park**[1]

[1]Department of Electrical and Computer Engineering, Ajou University
5 Wonchon-dong, Youngtong-gu, Suwon 443-749, Korea
[2]School of Electronics and Electrical Engineering, Hongik University
72-1 Sangsu-dong, Mapo-gu, Seoul 121-791, Korea

Abstract— Recently, radio frequency identification (RFID) in the ultra high frequency (UHF) band has been gaining popularity in many applications. It offers a broad detectable range, fast read speed, and the ability to read multiple objects. To maximize system performance, RFID requires a tag antenna that can provide adequate readability with restricted system power. The antennas of dipole structure are widely used as a RFID tag antenna owing to their simple structure and adequate performance in recognizing objects. However, the antenna of dipole structure has a problem where a readable range of the reader system is remarkably reduced due to the null of doughnut-shaped radiation pattern. Therefore, the tag antenna design is needed to have equally recognizable zone in every direction to ensure reliability of the tag. This requires the tag to have a radiation pattern close to an isotropic pattern. In this paper, we proposed a simple U-shaped RFID tag antenna with an isotropic radiation characteristic for the stable operation of RFID system. The proposed antenna is composed of a U-shaped half-wavelength dipole and a rectangular-shaped feed as shown in Fig. 1. The rectangular-shaped feed is connected at the bottom of a U-shaped dipole for conjugate impedance matching with the commercial tag chip. On the condition of VSWR < 2, the tag antenna has the measured bandwidth in the range 900 to 919 MHz that satisfies the Korea UHF RFID specifications, and showed the efficiency of greater than 90% and the gain deviation of less than 1.62 dB in all directions within the bandwidth.

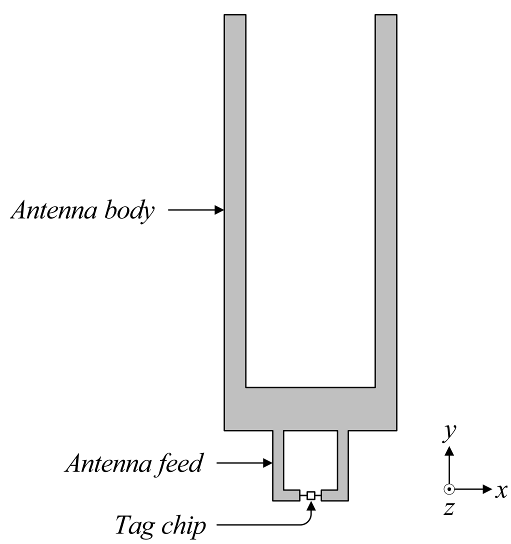

Figure 1: Structure of the U-shaped RFID tag antenna.

Cavity Backed Slot Antenna of Rectangular Waveguide

Ho-Jun Lee, **Jae-Young Lee**, **Kyu-Bok Lee**, **and Kyu-Ho Park**
System Packaging Research Center, Korea Electronics Technology Institute, R. O. Korea

Abstract— In this paper, we proposed a novel design of cavity backed 4×2 slot antenna arrays with lower side lobe levels and higher front-to-back ratio are designed to improve isolation between receiving and transmitting antennas, which can be suitable the limited installation space. The proposed cavity backed 4×2 slot antenna array has an impedance bandwidth of 700 MHz (VSWR < 2) and gain of 15.3 dBi. Side lobe levels in E-plane and H-plane are under -22.4 dB and -39.7 dB respectively. Half power beam width in E-plane and H-plane are 17.3 degree and 55 degree respectively. Details of the proposed antenna designs are described, and typical experimental results are presented and discussed.

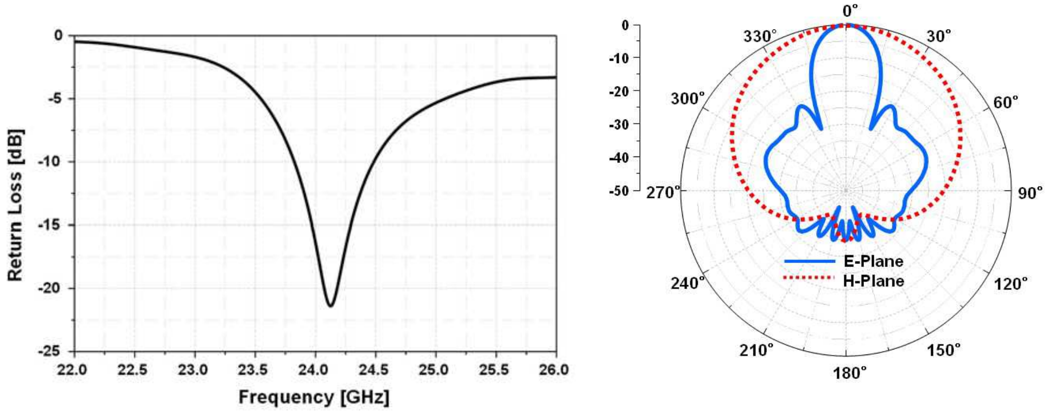

Figure 1: Proposed antenna and simulation result.

REFERENCES

1. Balanis, C. A., *Advanced Engineering Electromagnetics*, John Wiley & Sons, 1989.
2. Collin, R. E., *Foundations for Microwave Engineering*, 2nd Edition, McGraw-Hill, 1992.

Investigation of Static Phasing Distribution Characteristics of Passive Reflectarray Antenna Elements

M. Y. Ismail, **M. F. M. Shukri**, **Z. Zakaria**, **A. F. M. Zain**,
M. F. L. Abdullah, **and M. A. Ubin**
Wireless and Radio Science Center (WARAS), Faculty of Electrical & Electronics Engineering
University Tun Hussein Onn Malaysia, Malaysia

Abstract— There has been much interest recently in developing reflectarray antenna design due to significant advantages offered by the reflectarray antenna as compared to the conventional parabolic reflector and phased array antennas. In this paper, the characteristics of the static phase distribution of different resonant elements of reflectarray are demonstrated. Numerical analysis using CST computer model has been carried out in order to study the scattering behavior of the three elements of square patch, dipole and ring respectively. Waveguide simulator designed to operate at X-band region has been constructed to investigate the plane wave scattering from square patch, dipole and ring reflectarray cells constructed on TACONIC substrate of thickness 1.524 mm. The static phase range distribution, bandwidth and reflection loss performance are shown to be dependent on both the substrate thickness and the type of reflectarray elements printed on a grounded dielectric substrate. A static phase range greater than 220° is shown to be achieved for ring elements compared to the other elements of dipole and square patch. The static phase range is demonstrated to be traded-off with the bandwidth of the elements in which square patch elements are shown to give wider bandwidth of greater than 6.5% over the static phase range of 170°. S-shaped phase curves generated from the CST computer model demonstrate that ring elements which have greater static phase range contribute to the highest figure of merit of 1.4°/MHZ compared to dipoles and square patches. The reflection loss of 2 dB for ring elements is observed to be more lossy than square patches which give reflection loss of 0.55 dB.

Investigation of Broadbanding Techniques on a Novel Folded Meander Line Antenna (FMLA)

A. A. M. Ezanuddin, **P. J. Soh**, **M. F. Malek**, **and M. Z. A. Abdul Aziz**
School of Computer and Communication Engineering, University Malaysia Perlis (UniMAP)
No. 12 & 14, Jalan Satu, Tmn Seberang Ramai, Fasa 3, 02000 Kuala Perlis, Perlis, Malaysia

Abstract— In this work, Folded Meander Line Antennas (MLAs) have been designed to operate in WLAN b/g band. Two prototypes were tested: the first antenna is shaped like a fish-bone (Fish Bone MLA), while the second design has a structure of a folded meander line looped back to its starting position (Folded MLA). Both designs are either fabricated on FR-4 or RO3010 boards. Two broadbanding techniques are investigated in this work, by adding vias and implementing the proximity coupling technique, using CST software. Investigation is aimed to determine and compare the effectiveness between the two techniques on these new antenna structures. Investigations have found that prototype 2 fed using the proximity coupling technique has produced the widest bandwidth with a value of 939.5 MHz.

Microwave Corona Breakdown in rf Devices

J. Rasch[1], **D. Anderson**[1], **M. Lisak**[1],
V. E. Semenov[2], **and J. Puech**[3]

[1]Chalmers University of Technology, Göteborg, Sweden
[2]Institute of Applied Physics, Nizhny Novgorod, Russia
[3]Centre National d'Études Spatiales, Toulouse, France

Abstract— Corona breakdown is a potentially serious failure mechanism in many gas-filled microwave devices. The basic physics involved in the breakdown process — the avalanche-like growth of the free electron density in the microwave device under the ionizing action of high energy electrons created by the microwave field — is rather well understood for homogeneous microwave fields. However, many rf components involve inhomogeneous fields due to mode structure and/or to the presence of e.g., tuning screws or other details introduced for constructive purposes (e.g., impedance matching) or simply defects in the device. When the electric field in a gas-filled microwave device is inhomogeneous in space, the interplay between the concomitant inhomogeneous ionization, which tends to create free electrons, and the diffusion and attachment mechanisms, which tend to decrease the free electron density, becomes complicated and depends significantly on the geometry of the device and on the gas pressure. In cases with locally enhanced ionization, the breakdown threshold is determined as an interplay between diffusion and attachment where diffusion may transfer free electrons out of the localized region with high field into regions with weaker fields where attachment effectively may operate as a sink for the free electrons. For small pressures, diffusion is a strong electron redistributing effect and the influence of the high field region is small, but for large pressures, diffusion is weak and the breakdown threshold is set by attachment balancing the locally high ionization, which may significantly lower the breakdown threshold as compared to the corresponding homogeneous situation. Although corona breakdown in gas filled rf devices has been analyzed for a number of different designs and microwave mode structures, including situations involving field singularities e.g., sharp corners or edges where the electric field strength (and the ionization) becomes locally very high, no complete understanding of this problem has been reached. In the present work, we will analyze, both analytically and numerically, this coupling between diffusion, attachment, and the inhomogeneous ionization in determining the breakdown threshold, trying also to determine the pressure transition region between diffusion and attachment controlled limits and the importance of the enhanced ionization region for the breakdown threshold. A comparison with previously published experimental results shows good agreement.

Measurement of Differential Radar Cross Section of UHF RFID Tags

A. Pouzin[1, 2], T. P. Vuong[3], S. Tedjini[1], M. Pouyet[2], and J. Perdereau[2]

[1]Laboratoire de Conception et d'Intégration des Systμemes (LCIS), Grenoble INP, France
[2]Laboratoire National de Métrologie et d'Essais (LNE), France
[3]IMEP-LAHC, Grenoble INP, France

Abstract— This paper presents an analysis and a methodology for Differential Radar Cross Section ΔRCS measurement. To modulate the backscattered signal, the RFID chip switches its input impedance between two states, which can be seen as an amplitude modulation. In order to improve the reading range, the tag's antenna is generally matched to the impedance of the chip. The matching is performed in special conditions, i.e., at a given frequency and usually for tag placed in free space. However, we know that the impedance of the chip is a function of frequency and received power and the impedance of the antenna is highly dependent on the support on which the tag is placed [1]. There are numerous papers on the RCS [2] but only few works are related to the analysis of the ΔRCS and its importance on the determination of the tag performances [3]. The ΔRCS is an important parameter in the tag performance determination when the distance of communication is dependent on the quality of backscattered signal by the tag. This is the case of semipassive tags and in some conditions when a passive tag is no longer in the expected configuration of use, for example when it is mounted on a disruptive, or it is physically deformed, or the reader operates at a frequency other than the tag's resonance.

For the ΔRCS measurement, we reform the "transmitter-tag-receiver" link (Fig. 1). The Agilent MXG-N5182A vector signal generator sends a query command. The tag response is received on the Tektronix RSA3408A real-time spectrum analyzer in the form of I/Q baseband signals.

Calibration of the measurement system is necessary in order to remove systematic errors due to the input port mismatch and internal reflections inside the anechoic chamber. To calculate backscattered signal by the tag, we subtract the reference measurement for empty anechoic chamber without tag from the measured value in the presence of the tag.

And the ΔRCS can be determined from the difference between the low and high levels of the backscattered power as

$$\Delta SER = \frac{\Delta P_R}{P_T}\frac{(4\pi)^3 R^4}{G_{ref}^2 \lambda^2} \tag{1}$$

Figure 2 shows the ΔRCS of a commercialized tag as a function of the reader output power for a frequency set at 868 MHz. As specified in the ISO 18000-3 standard, the ΔRCS is greater than 50 cm^2 when output power is equal to 1.2 times the threshold power. Furthermore, it decreases when the power increases, in this manner the depth of modulation seen by the reader remains constant.

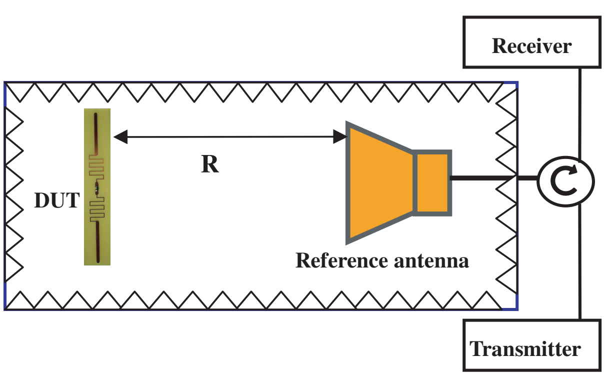

Figure 1: Experimental setup to measure the ΔRCS of the tag in the mono-static configuration.

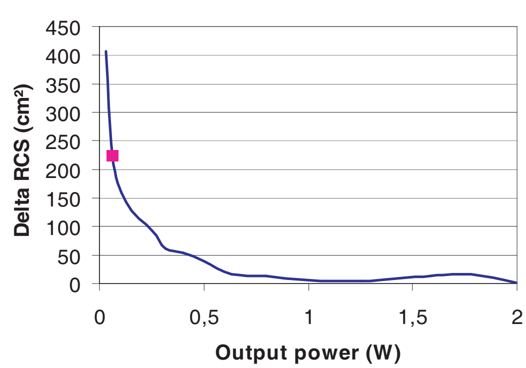

Figure 2: Measurement result of the ΔRCS of a tag as a function of the transmitter output power at a frequency of 868 MHz.

REFERENCES

1. Pillai, V., "Impedance matching in RFID tags: to which impedance to match?" *IEEE Antennas and Propagation International Symposium*, 3505–3508, June 2006.
2. Penttilä, K., et al., "Radar cross-section analysis for passive RFID systems," *IEE Proceeding — Microwaves Antennas and Propagation*, Vol. 153, No. 1, 103–109, February 2006.
3. Nikitin, P. V., K. V. S. Rao, and R. D. Martinez, "Differential RCS of RFID tag," *Electronics Letters*, Vol. 43, No. 8, 2007.

Shunt-series Shunt-shunt Dual-deedback CMOS Wideband Amplifier

J.-S. Syu, T.-H. Wu, and C. C. Meng
Department of Communication Engineering, National Chiao Tung University
Hsinchu 300, Taiwan, R.O.C.

Abstract— Two wideband amplifiers with the dual feedback technique are demonstrated in this paper using 0.35-μm CMOS technology. Both wideband amplifiers have a local shunt-shunt feedback path and a global shunt-series feedback path. To widen the operating bandwidth, the Darlington configuration and the capacitive gain peaking technique are applied to the second stage of both wideband amplifiers. Furthermore, the shunt-type feedback can reduce the input/output resistance and achieves the 50-ohm port matching. The first design uses a traditional resistive shunt-shunt feedback at the second stage of the wideband amplifier while a common-drain (CD) configuration is applied to the feedback path of the other design. This CD transistor does not affect the feedback mechanism because of its unity gain behavior and therefore the similar operating bandwidth is achieved. However, the use of this CD transistor blocks the gate-to-drain feedforward mechanism in the second stage from the resistive feedback path and thus results in a higher gain performance but a relatively poor output port matching (S_{22}).

As a result, the wideband amplifier with/without CD configuration has the power gain of 15/18 dB and the noise figure of 9.5/10 dB, respectively. The input and output matching of the traditional dual-feedback wideband amplifier are both better than 10 dB within the operating frequency of 1 GHz while the input and output return loss of the wideband amplifier with CD configuration are both about 5 dB worse those of the traditional one. The current consumptions are 31 and 32 mA for the wideband amplifiers with/without CD configuration, respectively, when the supply voltage is 3.3 V.

Optimising of Node Coordination in Wireless Sensor Network

Nik Noordini Nik Abd Malik, **Mazlina Esa**,
Sharifah Kamilah Syed Yusof, **and Jayaseelan Marimuthu**
Faculty of Electrical Engineering, Universiti Teknologi Malaysia
81310 UTM Skudai, Johor, Malaysia

Abstract— Beamforming has been introduced in Wireless Sensor Networks (WSNs) in order to increase the transmission range of individual sensor nodes. One approach of optimizing node coordination is by implementing the theory of linear array for beamforming method. The approach is presented in this paper. The linear sensor node array (LSNA) is constructed within random sensor node deployment. The LSNA is optimized as a conventional uniform linear array (ULA) to minimize the position errors which will improve the beamforming performance in terms of gain, transmission range and characteristics. A simulation model is implemented to study the adaptive LSNA. Several scenarios were evaluated by comparing with the theoretical results of conventional ULA. The performance of the constructed adaptive LSNA demonstrated an excellent agreement compared to the conventional ULA.

The Influence of Fog on the Propagation of the Electromagnetic Waves under Lithuanian Climate Conditions

S. Tamosiunas[1,2], **M. Tamosiunaite**[1,2], **M. Zilinskas**[1,3], **and M. Tamosiuniene**[4]

[1]Faculty of Physics, Vilnius University, Sauletekio 9, LT-10222 Vilnius, Lithuania
[2]Institute of Materials Science and Applied Research, Vilnius University
Sauletekio 9, LT-10222 Vilnius, Lithuania
[3]Department of Radio Communication
Communications Regulatory Authority of the Republic of Lithuania
Algirdo 27, LT-03219 Vilnius, Lithuania
[4]Semiconductor Physics Institute, A. Gostauto 11, LT-01108 Vilnius, Lithuania

Abstract— Fog may be one of the factors that influence the attenuation of electromagnetic waves that are propagating in the atmosphere. Cooling, moistening, and vertical mixing of air parcels with unequal temperatures and humidity lead to the formation of the fog. All processes mentioned above can occur simultaneously. However, in most cases one of these meteorological mechanisms becomes dominant. As a result, it leads to the different types of fog.

Moist fog frequently occurs over the localities of Lithuania. The foggiest month since 1875 was July 1977. There were 20 foggy days in that month. In light of the fact that in 15–17 October 1991 the visibility in Lithuania was only 100 meters, it is necessary to take into account the influence of fog on the attenuation of the electromagnetic waves. The calculation of this influence becomes very important in planning of new electromagnetic wave systems in Lithuania. As far as we know, the influence of fog on the propagation properties of the electromagnetic waves under the Lithuanian climatic conditions has not yet been examined.

The types of the fog and the existing methods of calculation of the electromagnetic waves attenuation due to fog are reviewed. The meteorological data, which was measured in Lithuanian Weather Stations, have been analyzed. According to this data, the specific attenuation due to fog, which is a function of liquid water content, temperature and frequency, has been computed under the Lithuanian climatic conditions. The models that have been used in these calculations of fog attenuation are based on the liquid water content and optical visibility.

Bandwidth Efficient Inter-carrier Interference Cancellation Technique for OFDM Digital Communication Systems

Akhil Kamboj[1], **Abhinav Keshari**[1], **Vivek K. Dwivedi**[1], **and G. Singh**[2]

[1]Department of Electronics and Communication Engineering
Jaypee Institute of Information Technology University, Noida-201 307, India
[2]Department of Electronics and Communication Engineering
Jaypee University of Information Technology, Solan-173 215, India

Abstract— Orthogonal Frequency Division Multiplexing (OFDM) is a promising technique for the broadband wireless multimedia communication systems. This system is very sensitive to the carrier frequency offset that destroys the orthogonal properties of OFDM subcarriers and introduces inter-carrier interference (ICI) which degrades the bit error rate (BER) performance. To mitigate the ICI problem, various schemes have been proposed [1–4]. However, these schemes are bandwidth inefficient. In this paper, we have proposed a novel bandwidth efficient ICI cancellation technique which have bit error rate comparable to that of conjugate cancellation method [1] as shown in Fig. 1. We also discussed carrier-to-interference ratio (CIR) and compared with the other reported literature.

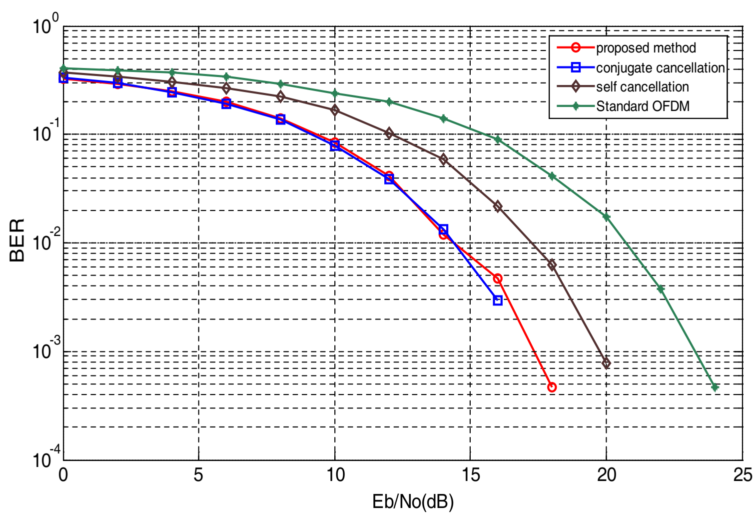

Figure 1: BER comparison of BPSK OFDM system with different cancellation techniques (for $N = 64$).

REFERENCES

1. Dwivedi, V. K. and G. Singh, "An efficient BER analysis of OFDM systems with ICI conjugates cancellation method," *PIERS Proceedings*, 166–171, Cambridge, USA, July 2–6, 2008.
2. Zhao, Y. and S.-G. Haggman, "Inter-carrier interference self-cancellation scheme for OFDM mobile communication systems," *IEEE Trans. Commun.*, Vol. 49, No. 7, 1185–1191, Jul. 2001.
3. Armstrong, J., "Analysis of new and existing methods of reducing inter-carrier interference due to carrier frequency offset in OFDM," *IEEE Trans. Commun.*, Vol. 47, 365–369, Mar. 1999.
4. Yeh, H.-G., Y.-K. Chang, and B. Hassibi, "A scheme for canceling inter-carrier interference using conjugate transmission in multicarrier communication systems," *IEEE Trans. Wireless Commun.*, Vol. 6, No. 1, 3–7, Jan. 2007.

Performance Analysis of Coded OFDM System Using Various Coding Schemes

Vivek K. Dwivedi[1], **Abhinav Gupta**[1], **Richansh Kumar**[1], **and G. Singh**[2]

[1]Department of Electronics and Communication Engineering
Jaypee Institute of Information Technology University, Noida, India
[2]Department of Electronics and Communication Engineering
Jaypee University of Information Technology, Solan-173 215, India

Abstract— Wired and wireless communication systems have to support continuously increasing data rates with a desired quality of service. In order to increase the throughput and ensure high spectral efficiency, a multi-tone transmission in the form of the orthogonal frequency division multiplexing (OFDM) is employed. OFDM uses a number of sub-carriers, which are orthogonal to each other and the data is placed on each of the sub-carriers. It can be recovered at the receiver by exploiting the orthogonality among the sub-carriers. Presently, the OFDM is used in several applications such as xDSL, DVB, DAB and WLAN standards [1]. It is also considered for future 4G solutions. The immunity to the inter-symbol-interference (ISI) and high spectral efficiency are the most important advantages of the OFDM modulation. The proposed scheme compares various forward error correction coding techniques such as trellis coding, space time trellis coding (STTC) [2], turbo coding [3], and concatenated coding and compares the bit error rate for a 128 sub-carrier OFDM system at different frequency offsets.

The result of OFDM using a large number of narrowband sub carriers is that each sub-carrier suffers from flat fading. Because the sub carriers are subject to flat fading, COFDM (coded OFDM) is used. The type of error correction coding that is used in COFDM is convolutional coding. The error correction decoder used in COFDM is the Viterbi algorithm. It is shown that space-time coding can be used to achieve high data rates at low signal-to-noise ratios (SNRs) over different channels with different multi-path delay profiles. Space-time trellis coding (STTC) technique has been proposed to achieve both the diversity and coding gains in multi input multi-output (MIMO) fading channels. Also turbo codes are compared. The high error correction power of turbo coders originates from random like coding achieved by random interleaving in conjunction with concatenated coding and iterative decoding using uncorrelated extrinsic information.

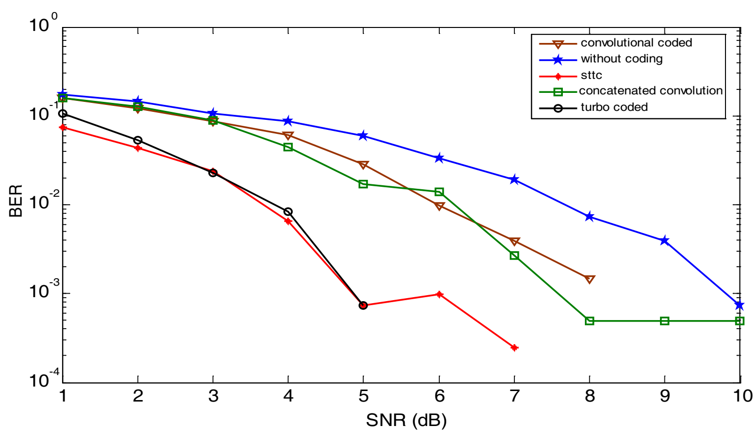

Figure 1: BER versus SNR plot for diff. OFDM systems at frequency offset 0.01 for $N = 128$.

REFERENCES

1. Van Nee, R. and R. Prasad, *OFDM for Wireless Multimedia Communications*, Artech House Publishers, Boston, USA, 2000.
2. Hong, Y. and Z. Y. Dong, "Performance analysis of space time trellis coded OFDM system," *Int. J. Applied Mathematics and Computer Sciences*, Vol. 2, 59–65, 2006.
3. Burr, A., "Turbo-codes: The ultimate error control codes?," *Electronics and Communication Engineering Journal*, Vol. 13, 155–165, August 2001.

Electromagnetic Field Analysis of Axial Flux High Temperature Superconducting Synchronous Motor

L. Y. Li, **B. Q. Kou**, **and J. W. Cao**
School of Electrical Engineering, Harbin Institute of Technology, China

Abstract— we are developing a 15 kW–250 rpm synchronous motor with a superconducting winding as the armature winding. The excitation superconducting winding is located in the cover in cake-type, and rotor doesn't have any excitation winding. The stator has iron metrical and the HTS (High Temperature Superconducting) coils locate in the stator slot. This structure can ensure the HTS coils can afford larger current because the magnetic field around the HTS coil is smaller in the same temperature. So we plan to use the liquid nitrogen to cool the HTS coils. In this paper, we analyses the electromagnetic field characteristic of the novel structure HTS motor.

Introduce: HTS motors have great advantages in weigh, power density and efficiency in comparison to conventional motors. Recently, we are developing the large power HTS motor system. The novel HTS motor's structure is different from the conventional synchronous motor and superconducting motor. Compared with the conventional synchronous motor, the novel HTS motor's rotor doesn't have any excitation winding and the rotor's structure only has attract and allot the flux which is produced by the cover's HTS coils. Compared with conventional HTS motor and LTS motor, the HTS motor's excitation magnetic field is produced by cover's HTS coils, and the excitation magnetic field through the rotor into the air gap; the armature winding are also used by HTS coils, and located in the stator iron slot. We analyze the novel HTS motor's electromagnetic field characteristics and design a 15 kW–250 rpm HTS motor with copper coils.

Electromagnetic Field Analysis: The HTS motor the paper presents is composed of the covers, HTS excitation coils, the magnetic out claws, the magnetic inner claws, rotor, shaft, stator, the armature HTS coils, as shown in the Fig. 1.

Because we cancel structure that the excitation coils in the rotor, using the cover's HTS coils produces the magnetic field. So during the HTS motor's design, the electromagnetic field of the novel structure HTS motor is needed to analyze detail. The path of the flux produced by the cover HTS coils is as shown in Fig. 2.

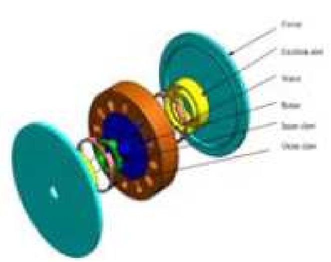

Figure 1: HTS synchronous motor structure.

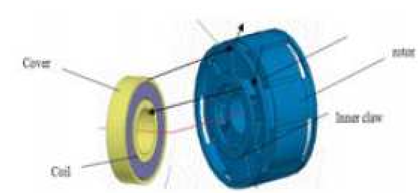

Figure 2: The path of the cover flux.

Electromagnetic Field around the HTS Coils: The value of electromagnetic field around the HTS coils can decide the critical current of the HTS coils, so the electromagnetic field in the stator slot and the terminal of the coils is needed to analyze.

Conclusion: This paper analyzes the electromagnetic field characteristic, and the electromagnetic field distribution around the HTS coils.

Novel Compact Three-layer Wideband Phase Shifter in SIW Technology

Ahmed Ali[1,2], **Hervé Aubert**[1,2] **Nelson Fonseca**[3], **and Fabio Coccetti**[1]

[1]LAAS, CNRS, 7 avenue du colonel Roche, F-31077 Toulouse, France
[2]UPS, INSA, INP, ISAE, LAAS, Université de Toulouse, F-31077 Toulouse, France
[3]CNES, 18 avenue Edouard Belin, 31401 Toulouse, France

Abstract— Substrate integrated waveguide (SIW) combines the advantages of rectangular waveguides while being compatible with low-cost standard PCB and LTCC technologies, giving rise to the design of microwave and millimeter wave components with high Q factor, low loss and ease of integration with planar circuits. This paper addresses the design of a novel compact wideband phase shifter in SIW technology. The structure consists of a three-layer folded waveguide employing the recently developed low-loss two-level SIW transition [1] according to the layout structure of Fig. 1(a). The phase difference is achieved by varying the propagation constant β between two similar structures of different widths achieving a normalized phase difference given by:

$$\frac{\phi_1 - \phi_2}{\ell} = \beta_1 - \beta_2; \quad \ell = 2\left(L_1 + 2L_2\right) \tag{1}$$

where ℓ denotes the propagation path length of the waveguide and ϕ_i is the transmission phase for the structure having the SIW width a_i.

According to (1), the larger the required phase difference is, the longer ℓ will be leading to relatively large sizes for single-layer phase shifters [2]. The proposed structure has the advantage that its physical length ($2L_1$) is different than its propagation path length achieving up to 66% size reduction (for $L_1 = L_2$) compared to the latter phase shifters. Moreover, the developed structure allows the introduction of slight length variations for different structures to compensate the slopes of the associated propagation factor curves, adding therefore one more design parameter to achieve well-controlled arbitrary wideband phase shifts while maintaining the same physical length (the length variations are realized within the path L_2).

The developed structure has been designed and optimized on a Neltec NY9208 substrate with $\varepsilon_r = 2.08$, thickness $h = 0.762$ mm, the via-hole diameter $d = 0.5$ mm while the pitch size $s = 0.95$ mm. The length L_1 governing the physical length of the structure has been kept constant at 8.8 mm while both a and L_2 have been modified to obtain the transmission phase curves shown

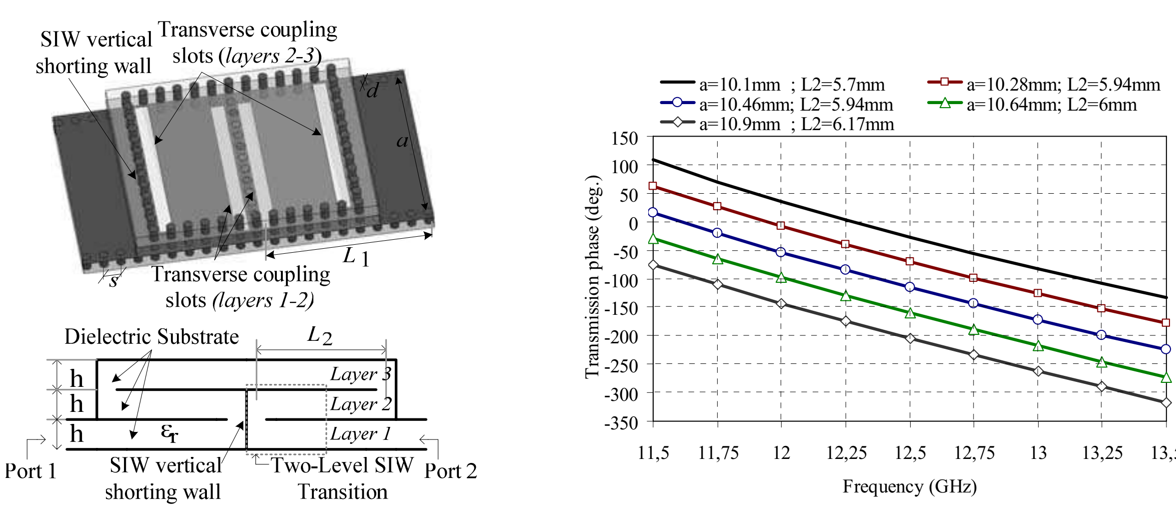

(a) (b)

Figure 1: (a) Structure layout of the developed three-layer SIW phase shifter, perspective and longitudinal elevation views. (b) HFSS simulated transmission phase ($\arg(S_{21})$ curves for different widths a and different lengths L_2, slot length $= a - 2\delta$, $\delta = 0.125$ mm, slot width $= 0.75$ mm.

in Fig. 1(b) ensuring therefore phase shifts — with respect to the narrowest structure — of $-45°$, $-90°$, $-135°$ and $-180°$ over 2 GHz bandwidth centered at 12.5 GHz.

The proposed phase shifter is expected to be used with the components of [1] to design compact, multi-layer beam forming matrices in SIW technology.

REFERENCES

1. Ali, A., N. Fonseca, F. Coccetti, and H. Aubert, "Novel multi-layer SIW broadband coupler for Nolen matrix design in Ku-band," *IEEE Int. Symp. on Antennas and Propagat.*, July 2008.
2. Cheng, Y., W. Hong, and K. Wu, "Novel substrate integrated waveguide phase shifter for 180-degree directional coupler," *IEEE MTT-S Int. Microw. Symp.*, June 2007.

A New Perspective and Applications of Amorphous Microwires on Electromagnetic Shielding

O. Baltag
Faculty of Medical Bioengineering
"Gr. T. Popa" University of Medicine and Pharmacy, Iasi, Romania

Abstract— The paper presents the results of a research regarding new applicatiopns of amorphous microwire in realisation of somme new composite textile material and the possibility to use it in electromagnetic shielding and protection equipment manufacturing. The textile material and the technical problems raised by its manufacturing techology are described, and its shielding, reflection and polarization properties are evaluated. A biocompatibility study was carried out to highlight certain of its possible allergic effects. The composite textile materials represent a group of multi-functional materials with special properties confered by imbedding structures with electromagnetic properties within the textile material.

The goal of this research is:

- to evaluate of the amorphous materials capability of absorbing the e.m. radiation in UHF range.
- to evaluate the implement possibilities of new materials, composite structure (texture type), utilizing amorphous magnetic materials.
- to achieve a protective composite material (textile type) with absorbing properties, in order to protect human body and residential areas.

The composite textile materials represent a group of multi-functional materials with special properties confered by imbedding structures with electromagnetic properties within the textile material. These structures can be of various types and compositions — metallic or metal coated wires, metallic particles — but the properties of these materials also depend of the manner in which the metallic particles and wires were incorporated, namely by weaving or thin layer deposition.

The material was subjected to sanitation action by washing with liquid solution of water and domestic detergents. After this, it apparently preserved its mechanical characteristics, suffered no distortion through manual squeezing, registered no shrinking (no size diminution). The measurement of the attenuation coefficient before and after washing was carried out with the same installation within the frequency range of 900 MHz–1800 MHz. No modifications were found out after washing.

A protective equipment was experimented, made of a coupon of material sized 500×500 mm and lined with a material neutral from the electromagnetic point of view. The equipment was previously evaluated from the standpoint of its electromagnetic shielding capacities, and it was found out that the values measured under laboratory conditions had not changed. The equipment was used daily, two hours a day, for two weeks, under various conditions of temperature and humidity, both indoor and outdoor, and in environments with different degrees of electromagnetic pollution. The equipment was used such that to ensure mechanical protection, to perform the shielding function in electromagnetically polluted environments.

Novel Principle of Transformer Protection Based on Variable Window Parameter Estimation

Heng-Xu Ha[1], **Zhi-Qiang Zhang**[1], **Yu-Zhen Tan**[1], **Bo Chen**[2], **and Z. Q. Bo**[3]

[1]Shandong University of Technology, Zibo 255049, China
[2]Dispatching Center, Shaanxi Electric Power Company, 710045, China
[3]AREVA T&D UK Limited, UK

Abstract— Transformer plays an important role in electric power system, so that the transformer protection is one of the most important elements in power system protective relaying areas as well. The differential protective relay based on the Kirchhoff's Law is widely used in transformer protection, which is however suffered the disadvantage of mal-operation caused by unbalanced currents due to the different characteristic of both sides and the saturation characteristic of current transformer etc. Particularly, the magnetizing inrush current which is induced by the saturation of ferromagnetic cores of the transformers could cause the mal-operation of transformer differential protection. Additionally, the identification of the inrush current and internal fault current is also difficult to solve.

A novel principle of transformer protection based on variable window parameter estimation, which is not influenced by the magnetizing inrush current, is proposed in this paper. According to the flux linkage equations of the primary and secondary windings, the saturation fluxes are eliminated by the two equations, based on which the internal fault and external fault discriminative expressions are established. However, the coefficients of equivalent resistance and leakage inductance should be precisely estimated instantaneously.

The least square method can accurately realize the parameter estimation, at the same time the errors of estimated parameters are dependant on the width of data window. Because there are 4 unknown variables for a two-winding transformer, at least 4 sampling points are needed, so that the time window should be more than 4 sampling points. With the increasing of data window constantly, the error of estimation is decreased first and then increases because the errors are accumulated and increases rapidly, which can lead to the overreach of the protective discrimination. Moreover it can lead to large amount of calculations, hence, a novel variable window least square estimation method is proposed in the paper as well, which can self-adaptively select the optimal data window width. Not only the error of the estimation is minimized, but also the calculation quantities are also decreased.

The ATP and Mat lab simulations associated with single-phase transformers and three-phase transformers showed that the principle is correct and quite efficient. The protective relay responses correct which can discriminate the internal faults and external faults accurately. It can not be influenced by the excited magnetic inrush currents as well as not sensitive to the fault types and fault inception angles.

The Susceptibility of Microcontroller Device with Coupling Caused by UWB-HPEM

Sun-Mook Hwang[1], **Joo-Il Hong**[1], **Seung-Moon Han**[1], **Chang-Su Huh**[1], **Uk-Youl Huh**[1], **and Jin-Soo Choi**[2]

[1]Department of Electrical Engineering, INHA University, Incheon, Korea
[2]Agency for Defense Development, Daejeon, Korea

Abstract— Modern electronic circuits are of importance for the function of communication, traffic systems and security systems. An intentional threat to these systems could be of big casualties and economic disasters. This paper examined damage effect of microcontroller device with coupling caused by UWB-HPEM (Ultra Wideband-High Power Electromagnetic). The UWB measurements were done at an Anechoic Chamber using a RADAN UWB voltage source, which can generate a transient impulse of about 180 kV. The susceptibility level for microcontroller has been assessed by field strength. The failure modes were observed in microcontroller. The A type of malfunction returned original level of functioning by external rest at lower field strengths (9.1 kV/m). The B type of malfunction was recovered to original level of functioning by power supply on/off when the amplitude of the electromagnetic pulse increases by about 4 times. Further increase of the amplitude leads to destruction. Based on the results, susceptibility of microcontroller can be applied to database to elucidate the effects of microwaves on electronic equipment.

Characterisation and Testing Shielding Fabrics

Zoltán Szabó and Pavel Fiala
BUT Brno, UTEE, Kolejní 2906/4, Brno 612 00, Czech Republic

Abstract— In connection with rapidly increasing progress in the radio communication services and other technical branches, which influence electromagnetic environment, the problems coupled with electromagnetic compatibility occur. Because of the electromagnetic interference minimization, it is necessary to ensure the shielding of sensitive device, buildings and not least persons. The suitable alternative to the classical shielding materials can be special shielding-fabrics. The main advantages of these fabrics are the low weight, flexibility and its easy processability. Shielding is a very popular method of ensuring electromagnetic compatibility and of protecting electronic and electrical equipment and human beings against radiated electromagnetic energy. The knowledge of shielding effects of different types of material represents a basic prerequisite for further development and implementation of shielding devices. This paper presents an analysis of the measuring methods and a comparison of different materials in terms of their specific shielding effects. The absorption properties of the various submitted samples were measured using both a Crawford chamber and the Insertion loss method. In the samples, the capacity to absorb electromagnetic waves was determined with the help of a spectral analyzer.

REFERENCES

1. Koprowska, J., M. Pietranik, and W. Stawski, "New type of textiles with shielding properties," *Fibres & Textiles in Easten Europe*, July/October 2004.
2. Agilent CSA Measurement Guide and Programming Examples, USA, 2006.
3. Pocai, M. R. and E. Bottari, "Electromagnetic characterization of protective clothing," *International Symposium on Electromagnetic Compatibility*, Tokyo, May 17–21, 1999.
4. Wilson, P. F. and M. T. Ma, "Techniques for measuring the electromagnetic shielding effectiveness of materials: Part 11-near-field source simulation," *IEEE Transactions on Electromagnetic Compatibility*, Vol. 30, No. 3, Part 2, 251–259, Aug. 1988.
5. Wilson, P. F. and M. T. Ma, "Techniques for measuring the electromagnetic shielding effectiveness of materials. I. Far-field source simulation," *IEEE Transactions on Electromagnetic Compatibility*, Vol. 30, No. 3, Part 2, 239–250, Aug. 1988.

Susceptibility of TTL Logic Devices to Narrow-band High Power Electromagnetic Threats

Joo-Il Hong[1], **Sun-Mook Hwang**[1], **Kwang-Yong Kim**[1], **Chang-Su Huh**[1], **Uk-Youl Huh**[1], **and Jin-Soo Choi**[2]

[1]Department of Electrical Engineering, INHA University, Incheon, Korea
[2]Agency for Defense Development, Daejeon, Korea

Abstract— The aim of this paper is to investigate the damage effects of TTL AND and NAND logic devices manufactured using five different technologies (schottky, low power schottky, advanced schottky, advanced low power schottky, and Fairchild advanced schottky) under narrow-band high power electromagnetic (NB-HPEM) waves by magnetron. The output of the magnetron was controlled from 0 to 1 kW and the operating frequency was narrow-band at 2460 ± 50 MHz. NB-HPEM waves were propagated into a closed-ended standard rectangular waveguide (WR-340) for 1 s. NB-HPEM waves were coupled with a directional coupler probe and the device under tests (DUTs) were placed under the probe. DUTs for the malfunction and destruction test setup were used for a light-emitting diode (LED) circuit and LEDs were used as loads to observe the operating states of the device. The electrical characteristics before and after NB-HPEM waves expose such as input and output voltage of the gates respectively, and supply current were measured. The TTL logic devices showed two types of damage i) malfunction, which means that no physical damage occurred in the device and after a self-reset or power-reset, the device returned to normal function, and ii) destruction, which means that the device incurred physical damage, and operation could not be recovered without replace by a new device. When the devices were damaged, the logic output of the TTL gate was connected to ground voltage (pulled down). The surfaces of the destroyed TTL logic devices were removed and the chip conditions were investigated with a microscope. The microscopic analysis of the damaged devices showed component, onchipwire and bondwire destruction such as breakthroughs and melting due to thermal effects.

Research on the Interference Effect of Wireless LAN by Analogdigital Interference Signal Using GTEM Cell

Sangbong Jeon[1], **Suk-Tai Kwun**[1], **Youngho Kim**[2], **Yeon-Choon Chung**[3], **and Sangho Choi**[1]

[1]Korea Radio Promotion Association, Korea
[2]Electronics and Telecommunications Research Institute, Korea
[3]Seokyeong Univiversity, Korea

Abstract— Electromagnetic wave environment is becoming complex due to the expansion of various radio communications. Especially in 2.4 GHz band, radio communication service such as Bluetooth and WLAN is widely used. This frequency band is assigned by ISM (Industrial, Scientific, and Medical) band and a lot of industry apparatus are used. For example, the apparatus such as microwave oven causes the electromagnetic wave noise in 2.4 GHz, so radio communication services ceases due to electromagnetic interference. Therefore the research to evaluate the interference of communication is actively being done. Also the signals for digital and analog signal exist in the electromagnetic wave environment. Therefore we need to evaluate the immunity characteristics of WLANs against digital and analog signal especially modulation signal. This research evaluated the interference effect of IEEE802.11b using three kinds of undesired wave. First is the analog Amplitude Modulation (AM) signal assigned in IEC61000-4-3 (1 kHz and modulation depth 80%), second is Amplitude Shift Keying (ASK), digital modulation signal, and third is the multi typed signal (ASK + AM). In case multi typed undesirable wave is used as the interference signal, it is embodied using coupler as shown in Figure 1. The undesired wave is measured by electric field made within GTEM Cell using standard dipole. Also the setup of the effect of the electromagnetic interference is done using GTEM Cell unaffected by the interference from the other noise of the environment to ensure the reliability. GTEM Cell is the equipment that makes the frequency range of TEM Cell to GHz and this makes the EUT immunity test in electromagnetic field possible. EMC measurement using TEM waveguide is done according to the method of IEC61000-4-20 [1]. In this paper, we evaluated EMI characteristics of WLAN using GTEM Cell.

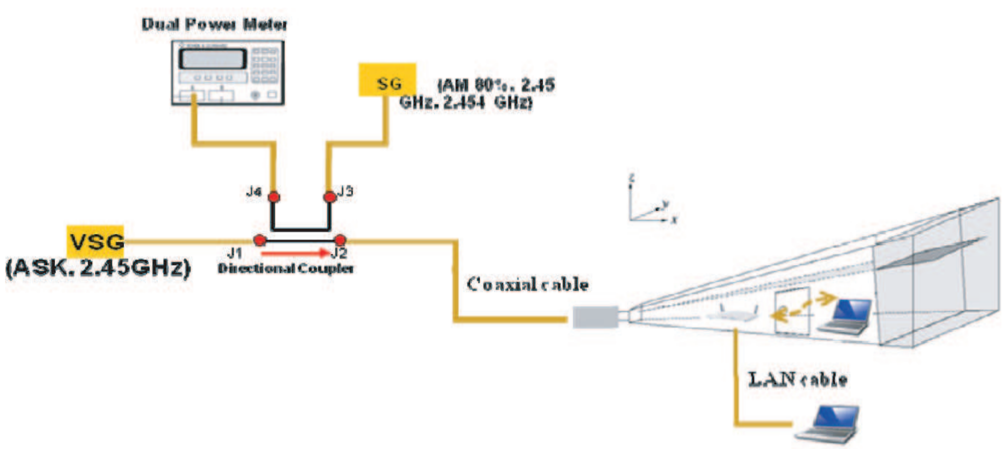

Figure 1: Setup for interference measurement.

ACKNOWLEDGMENT

"This work was supported by IT R&D program of MKE/IITA. [2008-F-014-01, Study on Electromagnetic Compatibility for Protecting Electromagnetic Environment in Ubiquitous Society]".

REFERENCES

1. IEC 61000-4-3, *Electromagnetic Compatibility, Part 4: Testing and Measurement Techniques, Section 3: Radiated Radio Frequency, Electromagnetic Field Immunity Test*, Edition 2.1, 2002.

Evaluation of Interference between Microwave Oven Noise and IEEE802.11b Using a GTEM Cell

Sangbong Jeon[1], **Yeon-Choon Chung**[2], **Chang-Han Jun**[1], **Suk-Tai Kwun**[1], **Jae Hoon Yun**[3], **and Sangho Choi**[1]

[1]Korea Radio Promotion Association, Korea
[2]Seokyeong University, Korea
[3]Electronics and Telecommunications Research Institute, Korea

Abstract— In this paper, to analyze the mutual effect of the noise of the microwave oven and the IEEE 802.11b, the microwave noise is realized by combining the amplitude and the frequency modulation [1]. Also a GTEM Cell was used to embody the environment for the character assessment and to generate the uniform electric field within GTEM Cell in time and frequency domains, the assessment for the uniform electric field in the frequency range and the effect of the pulse input in the time range is conducted through the correction. Figure 1 shows the embodied environment. Using this throughput is monitored by the analyze for the noise effect of the microwave oven for each channel of the IEEE 802.11b and this is verified by LAN channel using the APD (Amplitude Probability Distribution). Figure 1 shows the waveform of microwave oven noise by channel in time domain. As result of the measurement for the interference to IEEE802.11b using the noise source of Figure 2, in case of ch1, ch2 and ch3 that have on the sharing bandwidth, the APD that throughput over 5.5 Mbps is presented is over 90%. But for the other channel, the more the noise bandwidth of the microwave oven and the bandwidth of LAN channel are overlapped, the higher the probability the throughput is presented is low. But when comparing the ch8 and ch9 with ch7, ch10 and ch11, the sharing bandwidth is wide but the throughput is high over 1 Mbps. This is due to the share of the tine range the noise of the microwave oven has. It is judged that the noise bandwidth in time range is more affected to LAN throughput than the bandwidth in the frequency range.

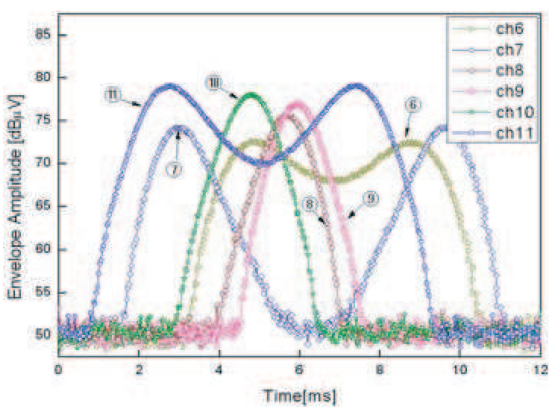

Figure 1: The waveform of microwave oven noise in time domain.

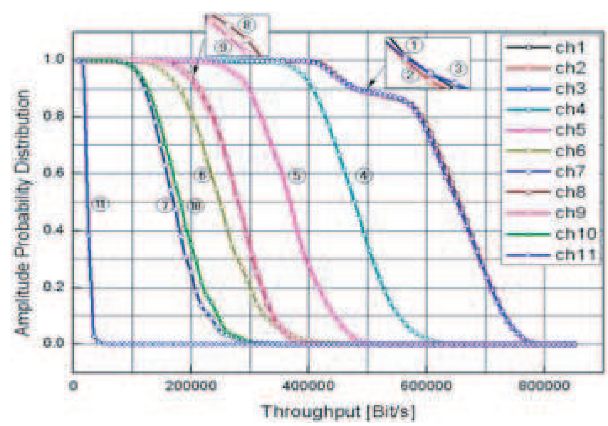

Figure 2: The APD of the measured interference between microwave oven noise and wireless LAN.

ACKNOWLEDGMENT

This work was supported by IT R&D program of MKE/IITA. [2008-F-014-01, Study on Electromagnetic Compatibility for Protecting Electromagnetic Environment in Ubiquitous Society].

REFERENCES

1. Matsumoto, Y., M. Takeuchi, K. Fujii, A. Sugiura, and Y. Yamanaka, "A time domain microwave oven noise model for the 2.4 GHz band," *IEEE Trans. EMC*, Vol. 45, No. 3, 561–566, Aug. 2003.

Investigation of an Agricultural Waste as an Alternative Material for Microwave Absorbers

H. Nornikman, **P. J. Soh**, **A. A. H. Azremi**, **F. H. Wee**, **and M. F. Malek**
School of Computer and Communication, University Malaysia Perlis, Perlis, Malaysia

Abstract— Agricultural waste bears huge potential to be applied as an alternative and beneficial invention for various applications. One such identified purpose is as an effective microwave signal absorbers for anechoic chambers. In this work, a type of agricultural waste — the rice husk, which is a by-product of paddy, is used in the design of a pyramidal microwave absorbers. It will be able to operate effectively in the microwave frequencies, from 1 GHz to 20 GHz. In order to test its feasibility, the best type of bonding resin must first be identified. Two types of resin, Urea Formaldehyde (UF) and Phenol Formaldehyde (PF) are mixed with the rice husk in order to investigate the dielectric property resulting from this blending process. Both materials are compared using three different percentage of binder content, which are 10%, 20% and 30%. Free Space Measurement Method (FSMM) was chosen to measure the dielectric constant of the different blends of rice husk. These microwave absorbers were also simulated in CST Microwave Studio using the values that were obtained from FSMM. This is done in order to determine and compare the reflectivity performance in terms of S_{11} result. Observation of the results showed that different blends produced a variation of relative dielectric constant, and as a result, a different microwave absorber reflectivities. It also proved that with an increasing binder percentage, reflectivity of the pyramidal microwave absorber has also improved. Thus, an alternative material, which used to be a less useful agricultural waste, was proven to be potentially suitable for application as microwave absorbers.

Thermal Stability of the Microwave Permeability of Nanocrystallized Glass Coated Microwires up to 350°C

Anne-Lise Adenot-Engelvin, Jean-Hugues Le Gallou, and Olivier Acher
CEA/Le Ripault, B. P. 16, Monts 37260, France

Abstract— Ferromagnetic glass coated microwires have been studied for long as soft magnetic materials suitable for a variety of applications ranging from Giant Magneto Impedance to smart microwave materials and metamaterials [1]. The composition of the ferromagnetic nucleus was generally an amorphous CoFeSiB alloy. However, more and more attention is now paid to a new family in the last few years: the nanocrystalline alloys epitomized by the "Finemet" trademark. The main feature of this new class is the nanocrystalline state obtained after a thermal devitrification stage of the amorphous precursor. In addition to their very good magnetic properties, they possess a very good thermal stability because of a stabilized atomic structure and a higher Curie temperature than their amorphous counterparts (600°C versus 350°C for the common alloys of CoFeSiB family).

Our purpose is then to assess the good thermal stability of the microwave permeability of microwires of such alloys.

A Finemet composition with a slightly negative magnetostriction coefficient was prepared in a cold crucible furnace. Glass coated microwires with metallic diameter ranging from 5 to 10 μm and total diameter ranging from 10 to 16 μm were drawn. They were nanocrystallized by annealing at 580°C during 1 hour. Samples for APC7 coaxial line measurements were then elaborated by winding the microwire into a torus of inner diameter 3 mm and outer diameter 7 mm with a mineral binding. Microwave permeability measurements were then performed at various temperatures using a dedicated set-up [2].

The thermal stability of the Finemet based microwires is good, with a decrease of the permeability of less than 40% up to 350°C.

REFERENCES

1. Vazquez, M. and A. L. Adenot-Engelvin, *J. Magn. Magn. Meter.*, http://dx.doi.org/10.1016/j.jmmm.2008.10.040.
2. Le Gallou, J.-H., M. Ledieu, and O. Acher, "High temperature coaxial line measurement cell using room temperature calibration," *CPEM*, W2d5, 2004.

Magnetooptical Kerr Effect in Ferromagnetic Nanostructured Media

V. I. Belotelov[1,2], **A. N. Kalish**[1,2], **A. G. Zhdanov**[1], **A. A. Grunin**[1], **E. A. Ganshina**[1], **A. A. Fedyanin**[1], **and A. K. Zvezdin**[2,3]

[1]M. V. Lomonosov Moscow State University, Russia
[2]A. M. Prokhorov General Physics Institute, Russia
[3]Fondacione ISI, Torino 10133, Italy

Abstract— It was demonstrated recently that new materials, usually referred as plasmonic materials with specially tailored structure and topology are of prime importance from the fundamental and applications point of view. At the same time, magnetooptical properties of such systems are also expected to demonstrate some interesting peculiarities and effects.

In this work, we investigate one-dimensional nickel magnetoplasmonic crystals formed by periodical nickel grooves made on the nickel surface. The period of the grating is 320 nm and the depth of the grooves is about 50 nm. Due to phase matching conditions between wave-vector of incident light surface plasmon polariton (SPP) wave-vector and vector of reciprocal lattice the SPP can be excited on such periodically patterned metal surface. Such excitation is experimentally observed as a dip in reflection spectra for p-polarized light, corresponding to energy flux redistribution between reflected light and the SPP. At the same time no dips in spectra are observed for s-polarization of incident light which vividly indicates on plasmonic interpretation of observed phenomenon due to restriction rule for excitation of s-polarized SPP.

Azimuthal dependences of reflection spectra are also measured. The shift of the dip position corresponding to the SPP excitation is shown to be the same as the one predicted by the calculations. Magnetooptical Kerr effect measurements in transversal geometry at 68 degrees of incidence angle demonstrate that the SPP excitation leads to the magnetooptical transverse Kerr effect (MOKE) enhancement resulting as a sharp peak in the MOKE spectrum.

Theoretical analysis of the problem reveals that in the presence of the transverse magnetization of the dielectric remains p-polarized wave localized. Nevertheless, it influences on the SPP wave number. Indeed, in the first order of magnitude on Ni gyration g, i.e., for $g \ll 1$, a dispersion law of the SPP is linear with g and the SPP in this case can be called magnetoplasmon.

Our modeling is based on the rigorous coupled wave analysis (RCWA) extended to the case of magnetized gratings. Numerical simulations demonstrated good agreement with experiment data and confirm the plasmonic nature of the found resonances of the MOKE.

ACKNOWLEDGMENT

The work is supported by RFBR (07-02-01445, 08-02-00717, 07-02-92183), Leading Scientific Schools grant NSh.671.2008.2.

Gradient Magnetostriction and Field Induced Deformation of a Magnetostrictive Cantilever

B. Narsu[1] **and Guohong Yun**[1, 2]

[1]Key Laboratory of Physics and Chemistry of Functional Materials
College of Physics and Electronic Information, Inner Mongolia Normal University
Hohhot 010022, China
[2]Institute of Science and Technology, Inner Mongolia University
Hohhot 010021, Inner Mongolia, China

Abstract— The electromagnetic solid state mechanics is one of the most popular, but still open issues in the study on material science due to the multifield coupling. In the magnetostrictive thin films the magnetic field strongly couples with the mechanical deformations and modulates the material properties, and vice versa. Multilayered thin film structures usually exhibit unbalanced residual stress due to surface and interface effects in both the fabrication process and post fabrication process [1], which affects the magnetostriction of the films and may induce a magnetostriction gradient. In this work we report a method to characterize the residual stress modulated magnetostriction of the thin film cantilever system.

We have developed a self consistent theory for the cantilever actuated by magnetostrictive films with initial strain gradient based on the four-parameter model [2]. The magnetostriction strain with gradient was modeled as an n order polynomial. The exact solution of the bending state was obtained, and furthermore, an effective experimental method for measuring the magnetostriction strain and its gradient on the basis of curvature measuring technique of the bent cantilever is proposed. By modulating the thickness of the substrate in the cantilever system), one can measure the magnetostrictive biaxial strainand its gradient definitely. The numerical work shows that relatively thick and soft substrate is favorable for this method. In addition, the advantage of the proposed method over the in situ measurement of the film stress in the growing process is that the inhomogenety and the surface effect can be avoided.

Analysis and Improvement for Thrust Fluctuation of Flat Type Voice Coil Motor

Liyi Li, **Donghua Pan**, and **Baoquan Kou**
School of Electrical Engineering, Harbin Institute of Technology, Harbin, China

Abstract— In the some special situation, the thrust of motor is required harshly for locating precisely, for instance, the linear motors hardly have thrust fluctuation in the lithography system. Voice coil motor has small thrust fluctuation, but it is necessary to improve thrust fluctuation of the voice coil motor for more precisely locating. In this paper, the thrust fluctuation of the voice coil motor is improved by optimizing pole-arc coefficient, Halbach array magnet, and adding two end coils. The function of elimination is proved by finite element method and the experimentation.

Introduction: The structure of voice coil motor is simple, and the coils are operated under DC, so it has little thrust fluctuation and often is used to accurately locating servo system [1].

Analysis and Improvement for Thrust Fluctuation: For increasing thrust of plat type voice coil motor, the serial magnet structure which can add the area of the flux is used by the voice coil motor. The serial magnet structure decreases the volume and mass of the mover yoke, and increases the density of the voice coil motor thrust. The rational pole-arc coefficient can improve the thrust, so the best pole-arc coefficient is calculated out by finite element optimized method.

The Halbach array magnet structure can improve the wave of air gap flux density to minish the thrust fluctuation, and increases the air-gap flux density to increase the thrust density of the voice coil motor. Though the mass of magnet is added, the mass of mover is decreased because the mass of move yoke is decreased by the Halbach array structure.

The magnetic flux leakage exists at two ends of the mover in the moving direction, and this magnetic flux leakage is changing with the mover is moving, that is to say, the magnetic flux leakage is different when the mover is at different position. The force F is proportional to product of air-gap magnetic flux density B and coil current I, so F is fluctuating as different magnetic flux leakage of the end mover at different position if coil current I keeps constant. The Figure 1 shows the force F at different position. When the mover is at the intermediate position, the force F is maximal, and F is monotone decreasing when the mover is moving from intermediate position to left or right. For decreasing the thrust fluctuation, add two compensating coils at two ends of the stator. The current of the compensating coil is controlled individually for restraining thrust fluctuation, and the current of main coil is unchanged for reducing response time of the voice coil motor. Figure 2 shows the prototype of the voice coil motor [2, 3].

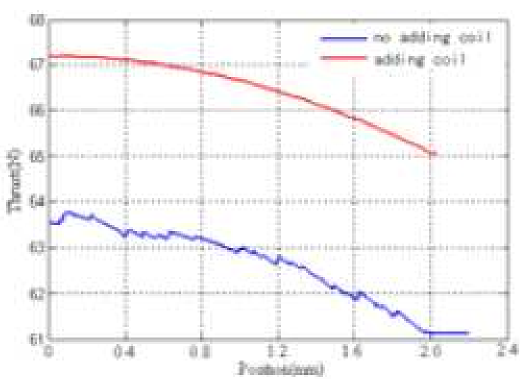

Figure 1: The force $\boldsymbol{F}$ at different position.

Figure 2: The prototype of the voice coil motor.

Conclusion: Optimizing pole-arc coefficient, Halbach array magnet, and adding two end coils could improve the thrust fluctuation of the flat type voice coil motor. The thrust fluctuation is restrained could be proved by finite element method and the experimentation.

REFERENCES

1. Lee, D. J., K. N. Lee, N. C. Park, and Y. P. Park, "Development of 3-axis nano stage for precision positioning in lithography," *International Conference on Mechatronks and Automation Niagara Falls*, 1598–1603, Canada, Jul. 2005.
2. Cui, J. and C. Wang, "Design characteristic and force analysis of PM linear motor for fast response servo system," *Power Electronics and Motion Control Conference*, Vol. 2, 1001–1004, Aug. 14–16, 2004.
3. Luo, H., J. Wu, and W. Chang, "Minimizing thrust fluctuation in moving-magnet permanent-magnet brushless linear DC motors," *IEEE Transactions on Magnetics*, Vol. 43, No. 5, 1968–1972, May 2007.

Angular Dependence of the Exchange Bias with the Uniaxial Anisotropy Perpendicular to the Unidirectional Anisotropy

Yuhao Bai[1], **Guohong Yun**[1,2], **and B. Narsu**[2]

[1]College of Physical Science and Technology, Inner Mongolia University, Hohhot 010021, China
[2]Inner Mongolia Key Laboratory of Physics and Chemistry of Functional Materials
College of Physics and Electronic Information, Inner Mongolia Normal University, Hohhot 010022, China

Abstract— The angular dependence of exchange bias is of crucial importance in unraveling the nature of exchange coupling in the ferromagnetic/antiferromagnetic bilayers [1], which has found important technological application in magnetoelectroinc devices [2]. Recently, the jump phenomenon in angular dependence of the exchange bias has been discovered [3, 4], however, the mechanism of this phenomenon is still point in issue. In this work, the angular dependence along with the jump phenomenon of the exchange bias has been investigated.

When the applied field is absent, according to the relation between energy of the system and the orientation of ferromagnetic magnetization, the locations of the intrinsic easy axes and intrinsic hard axes of the system have been obtained. It is found that the system will be in monostable state or bistable state, which is controlled by the competition between uniaxial anisotropy and the exchange anisotropy. When the field is applied parallel to the intrinsic easy axes, the exchange bias field and the coercivity will appear a jump. Both the exchange bias field and coercivity have greater values at the point of jump.

Our study demonstrates that monostable state or bistable state of the system determine the angular dependence of exchange bias immediately. The jump phenomenon of the exchange bias is an intrinsic property of the bilayers, it is determined by the magnitude of the exchange anisotropy, the uniaxial anisotropy and the thickness of the ferromagnetic layer.

REFERENCES

1. Ambrose, T., R. L. Sommer, and C. L. Chien, "Angular dependence of exchange Coupling in ferromagnet/antiferromagnet bilayers," *Phys. Rev. B*, Vol. 56, No. 1, 83–86, 1997.
2. Dieny, B., V. S. Speriosu, S. S. P. Parkin, B. A. Gurney, D. R. Wilhoit, and D. Mauri, "Giant magnetoresistive in soft ferromagnetic multilayers," *Phys. Rev. B*, Vol. 43, No. 1, 1297–1300, 1991.
3. Kim, D. Y., C. Kim, C. O. Kim, M. Tsunoda, and M. Takahashi, "Angular dependence of exchange bias and coercivity in polycrystalline CoFe/MnIr bilayers," *J. Magn. Magn. Mater.*, Vol. 304, No. 1, e56–e58, 2006.
4. Spenato, D., V. Castel, S. P. Pogossian, D. T. Dekadjevi, and J. Ben Youssef, "Asymmetric magnetization reversal behavior in exchange-biased NiFe/MnPt bilayers in two different anisotropy regimes: Close and far from critical thickness," *Appl. Phys. Lett.*, Vol. 91, No. 6, 062515-1-3, 2007.

Module of the Ionospheric Support

V. M. Smirnov and E. V. Smirnova
Fryazino Branch of the Institution of Russian Academy of Sciences
Kotel'nikov Institute of Radio Engineering and Electronics of RAS
Fryazino, Russia

Abstract— The ionosphere state forecasting is one of the major making systems of decametric radiowaves communications. Despite of a number of the lacks inherent in a radio communication of this range of wave lengths, its role and a place in the common communication system remain significant enough. It speaks that the short-wave radio communication allows establishing operatively a direct communication on big distances, including remote water and mountain areas. The organization of constantly operating points of communication in such regions is practically impossible because of absence in them of any infrastructure.

Work of a radio communication facility of a short-wave range in many respects depends from refraction properties of an ionosphere on a trajectory of radio signal propagation. The ionosphere state as electrically charged environment depends on many factors both natural, and anthropogenic character. Influence of these factors can result as in blackout of quality of a radio communication in this range, and to its full disappearance on the chosen carrying frequency.

The account of an actual ionosphere state at the analysis and forecasting of work of communication facilities now is complicated because of small amount of stations of vertical sounding or their full absence along the chosen direction of communication. To liquidate this blank it is possible at presence of global system of monitoring an ionosphere and software realization of a decision method of the radio translucence return task.

ACKNOWLEDGMENT

The work is executed at financial support of the Russian Academy of Science program "Environment in conditions of a changing climate: The extreme natural phenomena and accidents".

The Diagnostics of Ionosphere and Earth Ground Surface by Backscatter Sounding Data

S. N. Ponomarchuk, V. I. Kurkin, and A. V. Oinats
Institute of Solar-Terrestrial Physics SB RAS, Irkutsk, Russia

Abstract— In spite of intensive development of satellite systems for diagnostics of upper atmosphere and ground surface, the overland monitoring techniques remain actual. One of such techniques that possess the most potential possibilities in decameter wavelength range is the technique of backscatter sounding (BS). By using this technique, we can diagnose medium in large spatial regions within several thousands kilometers. The registration of backscatter ionograms allows us to control ionosphere conditions and investigate diffusing properties of ground surface.

Our report deals with modeling results of chirp signals characteristics under ionosphere backscatter sounding in the framework of waveguide approach. We use approximation in which the scattered field is expressed by characteristics of falling field (falling angle, amplitude) and local scatter diagram or scatter coefficient. The modeling results are used for analysis and interpretation of backscatter ionograms that were obtained under sounding in various directions by chirp ionosonde of Institute of Solar-Terrestrial Physics SB RAS. The analysis is carried out on long series of experimental data that were obtained for period of last solar cycle and stored in ionosphere radio sounding database. The accumulated data array allows us to investigate the regularity of ionosphere conditions changes in various gelio and geophysical conditions. We also develop the techniques of radio channel current diagnostics in sounding sector for real-time ionosphere parameters correction and backscatter ionogram reconstruction under conditions of strong absorption. On the base of operative algorithms for BS signals characteristics calculation by upper front and secondary processing of experimental ionograms we carry out the identification of registered signals and tracks. The interpretation results are input data for maximal usable frequencies determination for backscatter propagation modes under given distance in sounding direction.

ACKNOWLEDGMENT

The work is done under support of Russian fund of basic research (grant No. 08-05-00658).

Experimental Studies of the Ionosphere During Stratospheric Warming Events

V. I. Kurkin, A. V. Podlesny, and Y. S. Mikhailov
Institute of Solar-Terrestrial Physics, Siberian Branch of Russian Academy of Sciences, Irkutsk, Russia

Abstract— We carried out long-duration continuous ionospheric sounding with high temporal resolution (1 min) in January–February of 2008 and 2009 during stratospheric warming events. In 2008, the ionosonde measurements were made over a slightly oblique Usolie-Tory path (the length is ∼126 km). Transmitter operated in 2–12 MHz frequency range with sweep rate of 200 kHz/s. In 2009, we performed the measurements over three paths: Usolie-Tory (126 km length, 1.5–12 MHz frequency range, 200 kHz/s sweep rate); Magadan-Tory (3034 km length, 4–28 MHz frequency range, 500 kHz/s sweep rate) and Norilsk-Tory (2088 km length, 4–28 MHz frequency range, 500 kHz/s sweep rate).

The digital record of signals was made with two receivers: the analog-digital device on the base of "Katran" receiver and two-channel "Strela" receiver.

We performed modeling of slightly oblique ionograms using International Reference Ionosphere (IRI-2001), wave-like model of traveling ionospheric disturbances (TID) and ray tracing technique. Using different TID parameters we reproduced the main features of the observed ionograms. During stratospheric warming events the "loops" on observed ionograms may be caused by wave-like TIDs with wavelength of ∼100 km and elevation angle of ~ -60 degrees (downward propagation).

The SAR Ocean Image Correlation Model and Its Validation by MultiBand SAR Ocean Images

Xiaoqing Wang[1], **Yongqiang Chen**[1], **Minhui Zhu**[1], **Yunxiang You**[2], **and Tianqun Hu**[2]

[1]National Key Lab of Microwave Imaging Technology, Institute of Electronics
Chinese Academy of Sciences, China
[2]School of Naval Architecture and Ocean Engineering, Shanghai Jiaotong University, China

Abstract— The correlation characteristic plays an important role in the SAR ocean image mechanism. The radiometric resolution of high correlation SAR images is lower than that of the SAR images with lower correlation. The correlation length of SAR ocean images is usually assumed simply to be the same as the size of the resolution cell in the past studies. However, the SAR ocean images of different bands and platforms show quite different speckle patterns. The speckle noise of some SAR images looks quite larger while it looks very small in some other SAR images, and the large size of speckle noise means long correlation lengths. So the correlation length of SAR images cannot be supposed simply to be the same as the resolution size, it depend on the frequency band and platform. In this paper, a new correlation function model of SAR ocean images is present. The model shows that the correlation length in range direction is approximated to be range resolution, but the correlation length along the azimuth is rather complex, it depends on azimuth resolution, ocean scattering coherent time and platform velocity. Some airborne multiband (L, X, and Ku band) and spaceborne SAR ocean images data are used to validate this model and support its conclusion. According to this model, the azimuth correlation length can be significant shorter than SAR azimuth resolution if the coherent time is short enough and the platform velocity is low. So the speckle noise in airborne high frequency band (such as X or Ku band) SAR ocean images looks very small because that the scattering coherent time of high band is shorter and the velocity of airborne platform is relatively low. So the airborne high band SAR system can obtain higher radiometric resolution ocean images than lower band or spaceborne SAR systems with the same multilook number.

Experimental Researches of Dielectric Properties of Ore Minerals in the Frequencies Range 10–150 GHz

O. N. Polyakova[1], **V. V. Tikhonov**[2], **D. A. Boyarskii**[2], **and G. N. Gol'tsman**[1]

[1]Department of Physics, Moscow State Pedagogical University
M. Pirogovskaya, 29, Moscow, GSP-2, 119992, Russia
[2]Earth's Exploration from Space Department, Space Research Institute
Russian Academy of Sciences, Profsojuznaya, 84/32, Moscow 117997, Russia

Abstract— Development of methods of multifrequency remote sensing enables quantitative definition of parameters of the researched natural environment. One of objects of research by methods of the remote sensing including radiometry, a radar-location, dielectric spectroscopy are soils, rocks and ground. Dielectric characteristics of minerals making them are insufficiently investigated. It creates a problem for practical application of methods of remote sensing of these natural environments. Research of dielectric properties of ore minerals in a microwave range is technically difficult. The data on values of dielectric permeability of such minerals in the literature practically are absent.

In the report methods of definition of complex dielectric permeability of ore minerals are considered: chalcopyrite, pyrite and a nonmetallic mineral labrador in frequencies range 10–40 GHz and 77–150 GHz. During work measurements of frequency dependences reflective $R(f)$ and transmission $T(f)$ abilities of minerals in two ranges were carried out: in a range of frequencies 10–40 GHz a standard technique on a panoramic measuring instrument of voltage standing-wave and attenuation; in a range of frequencies 77–150 GHz on installation of a millimetric carcinotron-spectrometer.

For definition of the real and imaginary part of complex dielectric permeability of minerals from received experimental values $R(f)$ and $T(f)$ samples of minerals, the problem{task} about transmission and reflection of electromagnetic radiation through multilayered structure with alternation of layers of high-absorption substances — an ore mineral and low-absorption substances a nonmetallic mineral has been considered.

In the report results of frequency dependences of the real and imaginary part of dielectric permeability of minerals are submitted: chalcopyrite, pyrite, labrador in ranges of frequencies 10–40 GHz and 77–150 GHz.

Ground Penetrating Radar Exploration for Ground Water and Contamination

Ziaqiang Zhu, **Xianqi He**, **Guangyin Lu**, **Qunyi Liu**, **and Jianhui Li**
Geomatics and Info-physics School, Central South University, Changsha, China

Abstract— GPR is a non-destructive technique that uses electromagnetic (EM) waves to "look" into a material. GPR systems operate in a similar manner to sonar — i.e., by emitting a series of brief pulses and estimating distance to objects from the time it takes to detect reflections. The strength of the reflection depends on the electrical contrast between materials.

The portion of the profile between the ground surface and the ground water table, the vadose zone, can be divided into a number of regions. In the upper part of the vadose zone, the water is held at a minimum, residual saturation. In the lower part of the vadose zone, known as the transition (funicular) zone, the water saturation rises above residual levels, increasing with depth until the groundwater surface is reached. The capillary fringe is located below the funicular zone where saturation approaches 100%. The capillary fringe above the water table is almost saturated with water, but the pressure head in this region is still slightly less than atmospheric. The water table is simply known as an interface between the unsaturated and saturated zones. It is best described as the depth where the pore water pressure is equal to the atmospheric pressure. The thickness of the capillary fringe and transition zone depends largely on the grain size distribution. The distinguishable reflections of main concern occurred at the top of the water saturated zone which is located at the top of the capillary fringe above the water table. The GPR response from the top of the capillary fringe was assumed to be the location of the water table. Annan et al. show that the radar reflection from the water saturated zone becomes more dispersed as the thickness of the transition zone above capillary fringe increases.

GPR can also be used to estimate hydraulic conductivity.

The GPR technique successfully yielded quantitative information about water table change, and the hydraulic properties could be estimated by combining GPR data and hydrogeologic data.

GPR profiles show consistency by locating the antenna position accurately. The groundwater table change could be quantitatively estimated by comparing the two sets of GPR data acquired under different conditions. Quantitative information extracted from the GPR data indicates that GPR is a good tool for estimating the hydraulic properties of the aquifer. Quantitative information extracted from the GPR data with hydrogeological data, the estimation of hydraulic properties showed encouraging results. The study show that the physical and attenuation enhances characteristics of the contaminated areas and reveals that the most significant attenuation is related to smeared zone surrounding the seasonally changing water table interface.

Spatial Polarization Signal Processing in Circular Polarization Antenna

D. D. Gabriel'yan, **M. Yu. Zvezdina**, **E. D. Bezuglov**,
Yu. A. Zvezdina, **and S. A. Sil'nitsky**
Rostov Academy of Service of South Russian State University of Economy and Service, Russia

Abstract— The usage of adaptive antenna systems is determined by the need to provide stable radio communications under the conditions of wide usage of communications electronics. The main device that allows forming the "null" of directivity pattern in the noise direction is noise covariance matrix forming module. With the occurrence of the components resulting from both signal and its correlation to the noise signals in the elements of the noise covariance matrix leads to a sudden decrease of a signal noise ratio that is considered to be the main efficiency measure of adaptive array functioning. To increase the signal noise ratio we propose to insert an additional device of prior signal processing that allows excluding signal components when forming the noise covariance matrix and taking into an account the differences of signal polarization properties by separate management of cruciform dipole arms. In terms of practical realization it leads to redoubling the antenna array dimensions, but it allows forming the "null" of directivity pattern not in the both components of vector directivity pattern but only in those corresponding to the noise signal polarization.

The device of prior signal processing is constructed by combining antenna radiating elements into subarrays. In such a case selection of the weighting coefficients in subarray elements is carried out in a way that would form "null" of directivity pattern in the signal direction in the combined radiating element pattern. Then, the modified signals enter the noise covariance matrix forming module. The insertion of device of prior signal processing leads to a case where signal noise ratio would guarantee quasioptimal processing of the received signals, because the control vector would deliver not a global, but local extremum after linear transformations.

Fractal Analysis of Chaff and Sea Mixed Clutter on Ka Band

Guangfu Tang, **Jianxiong Zhou**, **Hongzhong Zhao**, **and Qiang Fu**
ATR Lab., National University of Defense Technology, Changsha 410073, China

Abstract— The traditional fractal Brown model (FBM) is only valid for the clutter containing only one fractal process, and it is no longer valid to describe the mixed clutter's fractal characteristics. A combined fractal Brown model (CFBM) is proposed to describe the mixed clutter, and an iterative estimation procedure is designed to extract the fractal parameters of the CFBM. The mixed fractal process widely exists in many applications, such as radar echoes contaminated by different clutters, etc.

When chaff cloud above the sea surface is measured by a radar system, its echo will be mixed with the sea clutter, as shown in Fig. 1. Many literatures have studied the fractal characteristics of sea clutter, and came to a conclusion that sea clutter is a fractal process. Although there are no literatures studying the fractal characteristics of chaff clouds, we can make an analysis on principle as follows: cloud is made up of numerous small water droplets and ice crystals, while chaff cloud is made up of numerous dipoles, cloud and chaff cloud are formed exactly in the same way, although the elements are different. Since cloud is fractal, there are reasons to assume that chaff cloud is also fractal. So the mixed clutter consists of two different fractal processes.

In the experiments using the outfield measured data, for those range bins consist of pure sea clutter, the traditional FBM can be used to extract the pure sea clutter's fractal parameters, while for those range bins consist of both chaff and sea clutter, the CFBM can be used to extract the mixed clutter's fractal parameters. It is proper to assume that the sea clutter's fractal parameters of different range bins remain the same under one experimental scene, so the chaff clutter's fractal parameters can been determined by comparing the mixed clutter's fractal parameters with that of the pure sea clutter.

The experimental results not only verify the validity of the CFBM, but also achieve the chaff clutter's fractal parameters for the first time. The fractal characteristics of chaff clutter may help us to build a more accurate mathematical model to describe it, and also enlighten novel approaches to counter the chaff jamming.

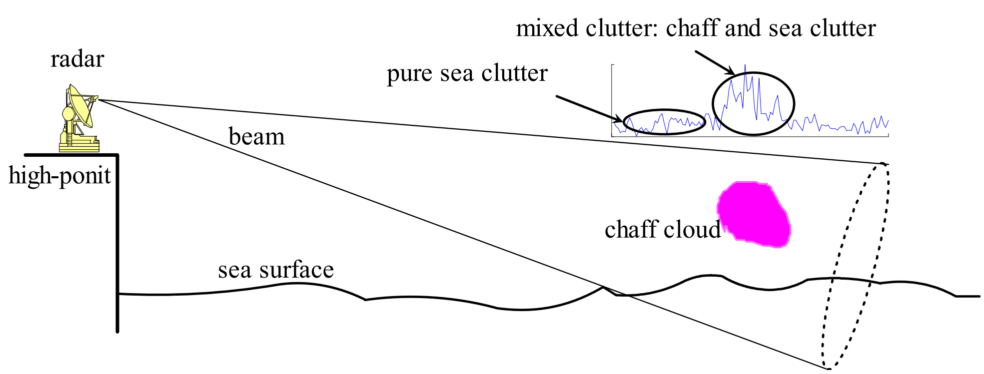

Figure 1: The sketch of experimental scene.

A Rigorous Analysis of VHF-UHF Bistatic Scattering Mechanisms in Forested Areas

S. Bellez, C. Dahon, and H. Roussel
Laboratoire des Signaux et Systèmes (L2S), Université Pierre et Marie Curie-Paris 6, France

Abstract— A scattering model based on the volumetric integral representation of the electric field to determine the scattered field from a forest has been developed [1]. This model is well adopted to the analysis at low frequencies (VHF-UHF Bands) for both monstatique and bistatique radar configurations. It is improved to extract the contribution of tree trunks, branches, and ground as well as the contribution of the various scattering mechanisms. In the frequency range under consideration, the effects of leaves, needles, the roughness of the soil, and the foliage attenuation are ignored and the trees are modeled by dielectric vertical and tilted parallelepipeds, representing respectively trunks and branches. They are placed over a horizontal interface separating two semi-infinite homogeneous media, the air and the forest ground.

The electric field integral equation is solved using a method of moment. The scattered field is obtained by summing up coherently the contributions of each scattering mechanism involved in the interaction of an electromagnetic plane wave of arbitrary polarization with the forest. Several mechanisms are involved, the single-bounce scattering mechanism, the double-bounce scattering mechanism, and the triple-bounce scattering mechanism [2]. Concerning the double-bounce scattering mechanism, two different contributions are considered, the scatterer-soil contribution and the soil-scatterer contribution. Here, the scatterers are the tree trunks and the branches. In our treatment, we have to calculate the incident and the reflected field from the ground at the position of the trees. Then, we compute the internal field inside the trees by tacking into account of the mutual interactions between the trees and those with ground to obtain the scattered fields related to the three scattering mechanisms. Finally, the total scattered field appears as a sum of those scattering mechanisms. That way, it is possible to analyze the relative contribution of each mechanism to the scattered field for various scattering angles as in [3]. The relative contribution of the tree trunks and the branches to the total scattering from the forest can be also studied.

For forests having a weak or moderate tree density, the total scattered field can be approximated by the sum of the scattered fields from each scatterer of the forest. In this case, the mutual interactions are neglected [4]. We also study the effects of the mutual interactions (electromagnetic coupling) for bistatic configuration by comparing both cases (with and without electromagnetic coupling between the scatterers and between the scatterers and the ground).

REFERENCES

1. Nguyen, H., H. Roussel, and W. Tabbara, "A coherent model of forest scattering and SAR imaging in the VHF and UHF band," *IEEE Trans. Geosci. Remote Sens.*, Vol. 44, 838–848, April 2006.
2. Thirion, L., E. Colin, and C. Dahon, "Capabilities of a forest coherent scattering model applied to radiometry, interferometry, and polarimetry at P- and L-band," *IEEE Trans. Geosci. Remote Sens.*, Vol. 44, No. 4, 849–862, April 2006.
3. Liang, P., L. E. Pierce, and M. Moghaddam, "Radiative transfer model for microwave bistatic scattering from forest canopies," *IEEE Trans. Geosci. Remote Sens.*, Vol. 43, 2470–2483, November 2005.
4. Thirion, L., et al., "Modelling of the bistatic scattering of a forested area at P-band," *EUSAR 2006*, Germany, May 16–18, 2006.

Reflectivity of Monolayer of Nanoparticles

A. A. Tishchenko, **A. N. Kalenyuk**, **and M. N. Strikhanov**
Moscow Engineering Physics Institute (State University), Moscow, Russia

Abstract— To change optical properties of the surfaces is very actual problem. One of the most promising ways here is to make very thin layers on the surface. Modern methods of nanotechnologies allow cover surfaces with monolayers of nanoparticles with dimensions of 30–100 nm. So, it would be of interest to consider the optical properties of monolayers [1] both as properties of independent system and as the first step to the exploring the more complicated systems, which consist of monolayer on the surface of semi-infinite media.

In this paper, the electrodynamics of two-dimensional systems, which was proposed in Ref. [1], is applied to the describing the reflection by a monolayer. The monolayer is taken to consist of single particles with the same polarizability and is characterized by the structure, i.e., by the average distance between molecules in the monolayer.

It is known that the spectrum of radiation of such a monolayer can increase sharply at some frequencies [2, 3]. Here we consider the oblique incidence of the plane electromagnetic wave onto the monolayer. On the basis of the local field theory, the exact microscopic field in all the space is founded analytically. The spectrum of transmitted and reflected waves is analyzed and is proved to be very sensitive to microscopic properties of the monolayer. The case of layer consisting of metal nanoparticles is investigated. The conditions for considerable amplification of reflectivity or decrease of transmission coefficient have been obtained and discussed.

REFERENCES

1. Gadomskii, O. N. and A. S. Shalin, *JETP*, Vol. 105, 761, 2007. [*ZhETF*, Vol. 132, 870, 2007].
2. Ryazanov, M. I. and A. A. Tishchenko, *JETP*, Vol. 103, 539, 2006. [*ZhETF*, Vol. 130, 621, 2006].
3. Ryazanov, M. I. and A. A. Tishchenko, *Laser Physics*, Vol. 12, 1442, 2002.
4. Ryazanov, M. I., M. N. Strikhanov, and A. A. Tishchenko, *Nucl. Instr. and Meth. B*, Vol. 266, 3811, 2008.

Electromagnetic Orbital Angular Momentum in Remote Sensing

Y. S. Jiang, **Y. T. He**, **and F. Li**
School of Electronic and Information Engineering
Beijing University of Aeronautics and Astronautics
37# Xueyuan Rd., Haidian District, Beijing 100191, China

Abstract— Phenomena of electromagnetic wave carrying orbital angular momentum (OAM) was first proposed by J. H. Poynting theoretically in 1909 [1], and was proved experimentally by R. A. Beth and A. H. S. Holbourn in optical waveband (wavelength = 1.2 μm) during 1935–1936 [2–4]. Electromagnetic waves with angular momentum in centimeter wavelength was confirmed by N. Carrara in 1949 [5]. It was not until 1992, that generations and torque effects of orbital angular momentum carried by a laser beam had been studied detailed by L. Allen et al. [6]. Great attentions has been concentrated on the studies of orbital angular momentum of electromagnetic waves. The researchers have studied not only the common themes, such as orbital angular momentum of the continuous and pulse electromagnetic wave, law of the angular momentum conversation, the generation, propagation, transformation and measurement of the angular momentum [7–14], but also the specific themes, such as the scattering and absorption of the specific object, the torque of orbital angular momentum of application and so on [6, 15]. For example, G. F. Brand studied the generation, transformation and measurement of the orbital angular momentum of millimeter-wave [16]. J. Wu applied parametric encoding on the orbital angular momentum of the electromagnetic wave (optical wave) beam to free-space communication [17]. Recently, B. Thide performs further research on the generation and measurement of the orbital angular momentum of the electromagnetic wave whose wavelength is shorter than decimeter waveband by using of soft simulation and numerical computation [18]. In summary, the generation, propagation and interaction with object for orbital angular momentum of electromagnetic wave in various wave-band are more and more subject to attentions by scientific workers in different fields, for instance, material scientists applying orbital angular momentum of the electromagnetic wave to research characters and constructions of molecule and atom, biologists and medical scientists manipulating atom, molecule or cell by the torque effect of the orbital angular momentum, communication technicians studying quantum encoding on the orbital angular momentum of the electromagnetic wave in free-space security communication, and so on. But, the researches on applying orbital angular momentum to remote sensing has little been proceeded. In this paper, we propose a novel concept to remotely acquire information of objects based on the orbital angular momentum of electromagnetic waves.

Here we show how measurements of orbital angular momentum of photons and feasibility of a number of remote sensing applications. In Section 2 of this paper, we provided a short introduction to OAM of electromagnetic waves and multipole radiation fields which could be used in active and passive remote sensing respectively, followed in Section 3, by a description of the remote sensing instrumentation required to detect OAM of millimeter-wave and photon. Section 4 a number of phenomena and results are cited to elucidate feasibility of applying to remote sensing. Section 5 briefly summarizes the findings.

Accuracy Evaluation of the Huygens Subgridding Method

G. Gradoni, V. Mariani Primiani, and F. Moglie
Dipartimento di Ingegneria Biomedica, Elettronica e Telecomunicazioni
Università Politecnica delle Marche, Via Brecce Bianche 12, Ancona 60131, Italy

Abstract— In the last decades, subgridding techniques have been widely investigated as an extension of the finite-difference time-domain (FDTD) lattice. They become particularly useful to simulate actual heterogeneous structures, like a filled waveguide. In this kind of electromagnetic (EM) problems, a spatial step contraction is required to include the material in the main grid. There, electrical parameters to be used in the algorithm are usually calculated averaging over medium and air: this could result in a (non-negligible) lack of predicted fields accuracy. A different way to realize the subgridding is grounded to the concept of domain decomposition: the EM problem is modeled by multiple FDTD grids coupled through physical principles. Basically, the (lossy) medium is removed from the principal lower-resolution (LR) domain and inserted into a separate higher-resolution (HR) domain [1]. In so doing, an iterate application of the Huygens principle leads to the Huygens Subgridding (HSG) method [2]. In this work, an application of this recent method to study lossy materials with the FDTD scheme is presented and a related error analysis is discussed. The simulated physical structure, a standard WR-340 waveguide inside which a thin slab of lossy material is placed, has been modeled by three *separate* Yee lattices providing proper rescaling rules and an algorithm implementing the physical coupling mechanism. Thus, the thin and lossy sample is embedded into a separate higher resolution lattice, where a spatial contraction is required only along the longitudinal direction as the material conductivity is high. However, higher conductivities result in increasingly values of decimation factors (N_s) causing intrinsic inaccuracy phenomena. Hence, the comparison with two single-lattice reference waveguides (full HR and full LR) has been used to evaluate the goodness of the method. Furthermore, increasing N_s effect has been investigated to quantify the subgridding accuracy through a relative error inspection, revealing HSG reliability in EM modeling. Achieved results show a good agreement with the full higher-resolution reference guide for different electrical parameter values, indicating a negligible numerical dispersion on the transverse section. Findings are of interest in the numerical prediction of planar screens shielding effectiveness, material parameters retrieval and microwave spectroscopy. Finally, work is in progress for the introduction of a random field excitation, appealing for reverberation chamber (RC) applications.

REFERENCES

1. Gradoni, G., F. Moglie, A. P. Pastore, and V. Mariani Primiani, "FDTD analysis of the field penetration through lossy materials in a reverberation chamber," *Proceedings of the 18th International Zurich Symposium on Electromagnetic Compatibility*, 24–28, September 2007.
2. Berenger, J. P., "A huygens subgridding for the FDTD method," *IEEE Transactions on Antennas and Propagation*, 3797–3804, December 2006.

Electromagnetic Exploration Based on System Identification for Seafloor Hydrocarbon Reservoir and Gas Hydrate

Weibin Luo and Qingchun Li
Department of Geology Engineering and Geomatics, Chang'an University, China

Abstract— A novel marine controlled-source electromagnetic method based on system identification using Invert-Repeated m-pseudo-random binary Sequence (IRmPRBS) is introduced. The IRmPRBS signal has the similar auto-correlation with white noise and the spectrum distributed at same interval discrete frequency within its wide bandwidth. Derived from Wiener-Hopf equation, the earth impulse response and frequency characteristic correlation identification using IRmPRBS signal are analyzed. So the seafloor thin resistor can be detected both in time domain and frequency domain. In time domain, the first transient impulse peak time can be an indicator for seafloor conductivity. And in frequency domain we define the percent frequency effect (PFE) and relative phase with multi frequency electric field response. The differentiation of percent frequency effect with offset and differentiation of relative phase with offset are sensitive to the seafloor thin resistor. So the seafloor hydrocarbon reservoir and gas hydrate can be identified by multi parameters. The numerical result implies that when exciting source is a wide band signal such as inverted-repeat m binary sequence, and simultaneous observation with multi offsets inline dipole-dipole configuration, the differentiation of percent frequency effect with offset and differentiation of relative phase with offset can indicate whether or not a high or a low resistor with induced polarization effect thin abnormality is present. The low frequency grounded dipole can generate galvanic current which is effective for detecting the deeply buried thin resistor with IP effect. Simultaneous observation with multi offsets inline dipole-dipole configuration is a geometry sounding method. If a high resistor with induced polarization (IP) formation is present, the differentiation of percent frequency effect with offset or the differentiation of relative phase with offset will have a peak value at appropriate offset, this offset can be used to estimate the buried depth of the resistor IP formation, it is empirically about 2.2 to 3.5 times of the buried depth.

Canopy Spectral Invariants for Remote Sensing of Vegetation Structure

Yuri Knyazikhin[1], **Ranga Myneni**[1], **Mitchel Schull**[1], **Liang Xu**[1], **Arindam Samanta**[1], **and Pedro Latorre**[2]

[1]Department of Geography and Environment, Boston University
675 Commonwealth Avenue, Boston, MA 02215-1401, USA
[2]Complex System Departmento de Lenguajes y Sistemas Informáticos
Universitat Jaume I, Castellón de la Plana, Spain

Abstract— The extinction coefficient in vegetation canopies is wavelength independent, considering the size of scattering elements (leaves, branches, etc.) relative to the wavelength of solar radiation. Although the scattering and absorption process are different at different wavelengths, the optical distance between two arbitrary points within the vegetation canopy does not depend on wavelength. This property underlies the concept of canopy spectral invariants which expresses the observation that simple algebraic combinations of leaf and canopy spectral reflectances become wavelength independent and determine two canopy structure specific variables — the recollision and escape probabilities. These variables specify an accurate relationship between the spectral response of a vegetation canopy to incident solar radiation at the leaf and the canopy scale. They are sensitive to important structural features of the canopy such as forest cover, tree density, leaf area index, crown geometry, forest type and stand age. We will discuss theoretical basis of the concept and show how the spectral invariants are related to maximum eigenvalue of the radiative transfer equation.

Figure 1 demonstrates the spectral invariant phenomenon. By plotting values of the ratio between the surface reflectance (=*solution of the transport equation at the upper "canopy boundary"*) and leaf albedo (=*single scattering albedo*) versus reflectance values for a vegetated pixel, a linear relationship is obtained, where the slope and intercept give the recollision and directional escape probabilities, respectively [2, 5].

The wavelength independent recollision probability is the probability that a photon scattered from a phytoelement will interact within the canopy again [6] and is equal to the maximum *eigenvalue* of the radiative transfer equation [3]. This parameter accounts for a cumulative effect of the canopy structure over a wide range of scales [2, 4]. For example, if a vegetation canopy

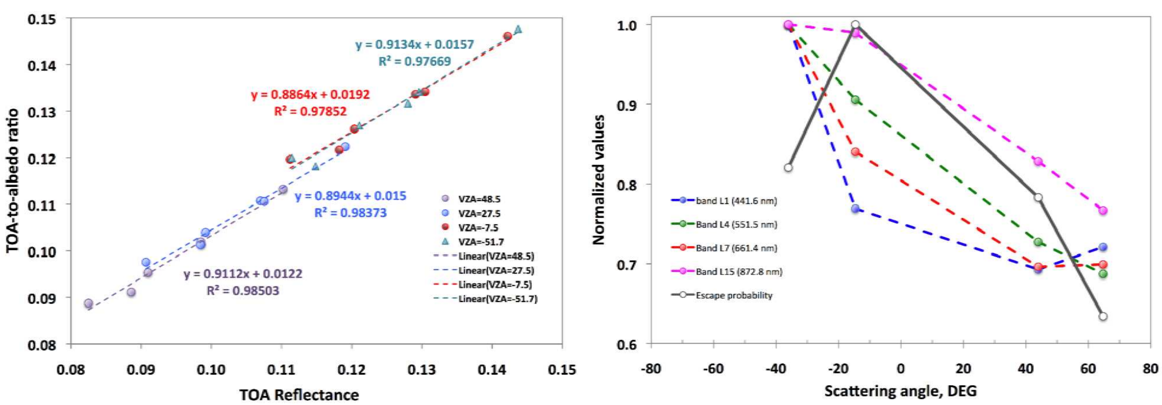

Figure 1: *Left Panel*: By plotting values of the surface reflectance to leaf albedo ratio versus reflectance values for a vegetated pixel, a linear relationship is obtained, where the slope and intercept give the recollision and directional escape probabilities, respectively. PROBA/CHRIS data acquired over Harvard Forest, Massachusetts, are used in this example. The CHRIS sensor on ESA's PROBA platform provides multi-angular imagery for up to 62 spectral bands in the range 415–1050 nm with a spectral resolution of 5–12 nm at 5 nominal angles (55, 36, 0, −36, −55), at a spatial resolution of 20 m. Right Panel: The directional escape probability as a function of the scattering angle. Surface reflectances at blue (band L1), green (band L4), red (band L7) and ner-infrared (band L15) are added for comparison. The angular signatures are normalized by corresponding maximum values.

is treated as a big leaf (=*horizontal surface is the scattering center*), i.e., no structure, Leaf Area Index (LAI) is 1 (=*optical depth is* 1), the recollision probability is zero because a photon reflected or transmitted by one "big" leaf will not encounter another leaf. If one cuts the leaf into "small pieces" and uniformly distributes the pieces in a canopy layer (the structure has changed with LAI unaltered), the recollision probability changes its value from zero to about 0.3 [5]. At a given LAI, the recollision probability increases with the number of hierarchical levels present in the landscape (e.g., the clumping of needles into shoots, shoots and leaves into crowns, etc.). This property can be used to discriminate between broadleaf and coniferous canopies as illustrated in Fig. 2.

The wavelength independent directional escape probability (Fig. 1, Right Panel) is the probability that a scattered photon will escape the vegetation in a given direction. Its angular variation is

THE RECOLLISION PROBABILITY COMBINED WITH THE LAI HAS THE POTENTIAL TO DISCRIMINATE BETWEEN BROADLEAF AND CONIFEROUS CANOPIES

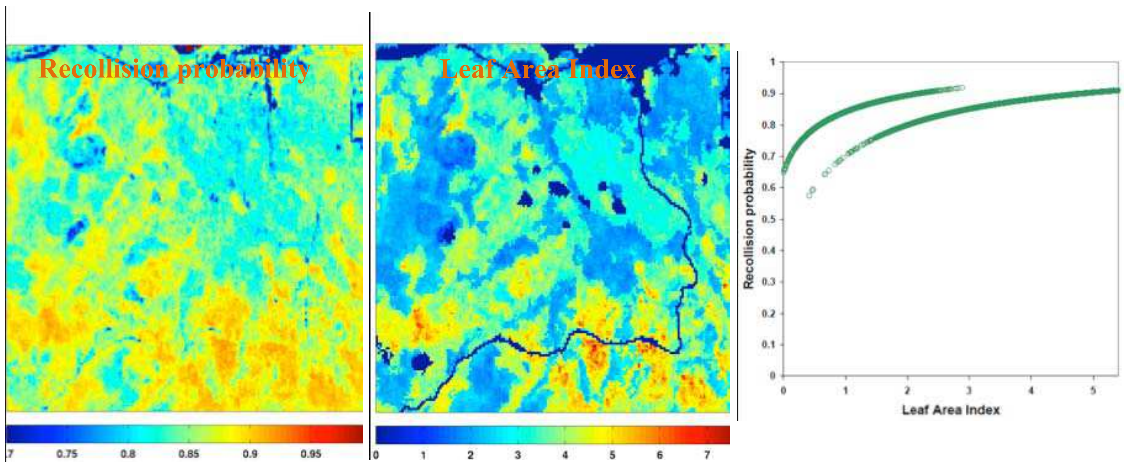

Figure 2: *Left and Middle Panels*: Recollision probability and LAI at the Bartlett Experimental Forest derived from Airborne Visible/Infrared Imaging Spectrometer data acquired over Bartlett Experimental Forest, New Hampshire.The AVIRIS sensor provides calibrated images of the up-welling spectral radiance in 224 contiguous spectral channels with wavelengths from 400 to 2500 nanometers at a spatial resolution of 3.3 m. *Right Panel*: By plotting the recollision probability versus LAI, two curves are obtained. The upper and lower curves corresponds to needleleaf and broadleaf pixels, respectively.

FOREST TYPE DISTRIBUTION

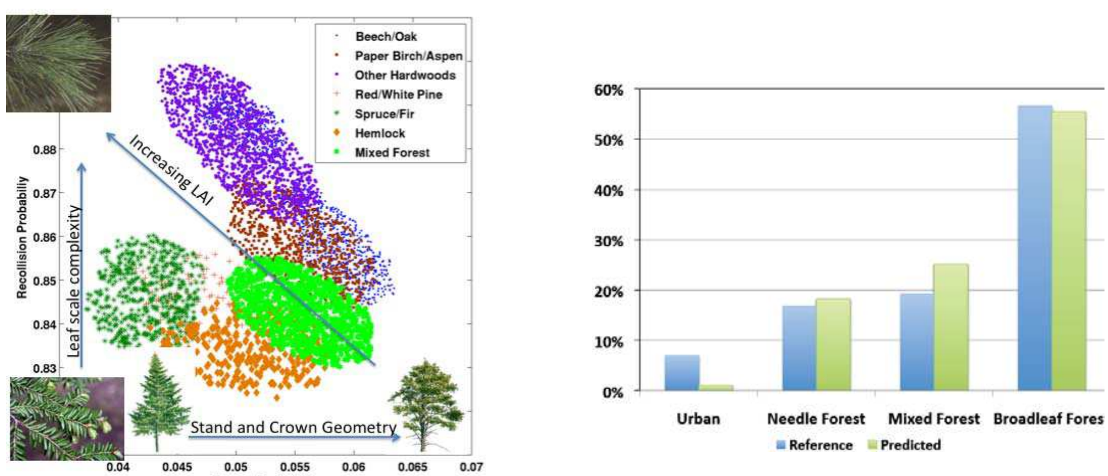

Figure 3: *Left Panel*: Recollision versus escape probability in the nadir direction for different forest types. The probabilities were derived from AVIRIS data acquired over Bartlett Experimental Forest. *Right Panel*: Distribution of forest types at the Bartlett Experimental Forest site derived from *spectral invariants* by applying a threshold approach (right bars). Left bars represent the ground truth data.

related to forest cover, plant LAI (=*optical depth of a tree crown*) and crown shape (the aspect ratio). Disney et al. [1] documented the sensitivity of the escape and recollision probabilities to the stand age.

Figure 3 (Left panel) illustrates the separation of forest classes in the *spectral invariant space*. The location of a point on the recollision versus escape probability plane depends on properties of the canopy structure at both microscale (e.g., leaf vs. shoot) and macroscale (e.g., dimensions of trees and their spatial distribution). In this example, the Spruce/Fir and Hemlock classes have approximately the same LAI. Because Hemlock shoots are "flatter" and therefore less complex compared to their Spruce/Fir counterparts, the Hemlock recollision probability is smaller than that of the Spruce/Fir class at a given LAI. This results in a lower location of the Hemlock pixels on the plane with respect to the Spruce/Fir class. The horizontal shift is determined by stand (e.g., tree density) and crown (e.g., aspect ratio) geometries. The mixed forest class occupies a space between needle leaf and broadleaf forests. In this example the broadleaf class has a higher LAI and a "simpler" microscale structure (flat leaf) compared to its needle leaf counterpart (low LAI and shoot-like leaf scale complexity). The LAI and stand geometry is a dominant factor determining the location of the broadleaf class in the spectral invariant space.

A simple threshold approach has been applied to maps of the recollision and escape probabilities. Results shown in Fig. 3 (Right Panel) suggest that the canopy spectral invariants convey information needed to discriminate between forest types.

REFERENCES

1. Disney, M., P. Lewis, T. Quaife, and C. Nichol, "A spectral invariant approach to modeling canopy leaf scattering," *Proc. The 9th ISPMSRS*, Part 1, 318–320, 2005.
2. Huang, D., Y. Knyazikhin, R. E. Dickinson, M. Rautiainen, P. Stenberg, M. Disney, P. Lewis, A. Cescatti, Y. Tian, W. Verhoef, J. V. Martonchik, and R. B. Myneni, "Canopy spectral invariants for remote sensing and model applications," *Remote Sensing Environment*, Vol. 106, 106–122, 2007.
3. Knyazikhin, Y., J. V., Martonchik, R. B. Myneni, D.J. Diner, and S. W. Running, "Synergistic algorithm for estimating vegetation canopy leaf area index and fraction of absorbed photosynthetically active radiation from MODIS and MISR data," *J. Geophys. Res.*, 32257–32276, 1998.
4. Lewis, P. and M. Disney, "Spectral invariants and scattering across multiple scales from within-leaf to canopy," *Remote Sensing of Environment*, Vol. 109, 196–206, 2007.
5. Schull, M. A., S. Ganguly, A. Samanta, D. Huang, N. V. Shabanov, J. Jenkins, J. C. Chiu, A. Marshak, J. B. Blair, R. B. Myneni, and Y. Knyazikhin, "Physical interpretation of the correlation between multi-angle spectral data and canopy height," *Geophys. Res. Lett.*, Vol. 34, 2007. doi:10.1029/2007GL031143
6. Smolander, S. and P. Stenberg, "Simple parameterizations of the radiation budget of uniform broadleaved and conifersous canopies," *Remote Sensing of Environment*, Vol. 94, 355–363, 2005.

High-frequency Magneto-impedance in Ultra-thin Magnetically Soft Glass-coated Amorphous Microwires

M. Ipatov[1], A. Zhukov[1,2], J. Gonzalez[1], and V. Zhukova[1]

[1]Dpto. de Física de Materiales, Fac. Químicas
Universidad del Pais Vasco, San Sebastián 20009, Spain
[2]TAMAG, San Sebastin 20009, Spain

Abstract— Thin amorphous magnetically soft microwires attract recently growing attention because of their excellent soft magnetic properties and giant magneto-impedance (GMI) effect, extremely thin dimensions and possibility for applications in magnetic micro-sensors and tuneable composite materials. Magnetically soft properties and consequently GMI effect can be optimized in according to concrete applications by using appropriate heat treatments and manipulating fabrication parameters and/or chemical composition of metallic nucleus [1, 2]. GMI attracted great attention in then field of applied magnetism owing to the large sensitivity (up to 600%) to the DC magnetic field, H, when the high-frequency current flows along the magnetic conductor [3]. Additionally recently new class of tuneable composite materials based on thin ferromagnetic wires with the effective microwave permittivity depending on an external stimuli, such as DC magnetic field, tensile stress and/or temperature have been introduced [4].

Here we report novel results on high frequency GMI effect (diagonal and off-diagonal components, between 10 MHz and 7 GHz) and its correlation with soft magnetic behaviour in thin amorphous microwires (Co-Fe-rich with nearly-zero magnetostriction constant) with metallic diameter between 3 and 10 μm. Choosing adequate samples composition and geometry we able to tailor their magnetoelastic anisotropy and respectively magnetic softness and GMI. Frequency dependence of GMI effect (microwire impedance Z) has been measured and analyzed. Hysteresis on Z(H) curves has been observed at low H.

From point of view of applications excellent magnetic softness and high GMI effect have been obtained in thin Co-rich microwires.

REFERENCES

1. Zhukov, A. and J. González, *Advanced Magnetic Materials*, (Eds. David J. Sellmyer, Yi Liu, and Daisuke Shindo), Vol. 3, Ch. 26, Kluwer Academic Publishers, Norwell, 2005.
2. Zhukova, V., A. Chizhik, A. Zhukov, A. Torcunov, V. Larin, and J. Gonzalez, *IEEE Trans. Magn.*, Vol. 38, 3090, 2002.
3. Panina, L. V. and K. Mohri, *Appl. Phys. Lett.*, Vol. 65, 1189, 1994.
4. Panina, L. V., S. I. Sandacci, and D. P. Makhnovskiy, *J. Appl. Phys.*, Vol. 97, 13701, 2005.

Method of Definition of Parameters Layered Ground on Measurements of Radiowave Reflection Coefficient

N. A. Armand, O. V. Yushkova, and V. M. Smirnov
Fryazino Branch of the Institution of Russian Academy of Sciences
Kotel'nikov Institute of Radio Engineering and Electronics of RAS
Fryazino, Russia

Abstract— Mathematical modeling and interpretation of received results is one of the basic stages of planning of the radar experiments connected with definition of electro physical parameters of a ground of space objects, detection in it a natural no uniformities and an estimation of borders depth of geological structures.

In spite of the fact that for definition of ground parameters frequency dependence of radio wave reflection coefficient is used, as a basis of the decision of a return task the solution of a direct task serve. Such approach allows revealing of parameter change mechanism of a complex spectrum of a signal, propagated in the non-uniform environment. Modeling of this process allows to allocate and estimate that it is essential and that it is minor at the decision of a return task and to simplify statement of last.

In work the analytical decision of a determination task of layer parameters, laying on dielectrically-homogeneous half-space is offered. Complex dielectric permeability of a layer and half-space and layer thickness are restored on frequency dependence of a square of the reflection coefficient module known on the limited interval of frequencies. The task has the unique decision in the field of restored values. Requirements to length of the frequency range necessary for the decision of a task are formulated.

The work is executed at financial support of the Russian Academy of Science program "Plasma process in solar system".

Subsurface Sounding Phobos Ground in "Fobos-Grunt" Project

N. A. Armand[1], **V. N. Marchuk**[1], **V. M. Smirnov**[1], **O. V. Yushkova**[1], **V. V. Abramov**[2], **A. S. Bajanov**[2], **and B. S. Lifanzev**[2]

[1]Fryazino Branch of the Institution of Russian Academy of Sciences
Kotel'nikov Institute of Radio Engineering and Electronics of RAS, Russia
[2]Special Design Bureau of Kotel'nikov IRE RAS, Russia

Abstract— Research of electrophysical characteristics of the Phobos ground, revealing of deep structure and density determination of breeds composing it, research of a relief and roughness of Martian satellite surface will allow understand better the nature of relic substance from which, probably, the Phobos consists. With a greater share of reliability, it is possible to search for answers on these questions using data of radar-tracking sounding of the Phobos ground. The long-wave planetary radar LWPR which is a part of a complex of the scientific equipment of the project "Phobos-Grunt" is intended for remote sounding a surface and subsurface structures of the Phobos ground by a method of pulse radiosounding along a flight line of a spacecraft "Fobos-Grunt".

The long-wave planetary radar represents the radar-tracking complex intended for sounding a ground of the Martian satellite on frequencies of 125–175 MHz. The chosen range of frequencies will allow carry out deep sounding of the Phobos ground at the accepted model of structure of a surface and subsurface up to depths from units up to hundreds meters. LWPR differs from the existing radar necessity to work both from varying spacecraft orbit and from the Phobos surface. Parameters and types of radiated signals are determined by statement of a task on sounding structure of a ground and technical opportunities of a spacecraft.

Remote Crust's Sub Cells Satellite Analysis Central Asia, Caspian Basin and Med

Karl Federico Kaspareck
CTE, Rome, Italy

Abstract— Analysis of satellite images of Central Asia and the Caspian basin is performed with reference to main surface features co relatable to sub surface. Images shown consist of two visible light centred on the Caspian, Med, North Africa and Caucasus taken from Flash Earth and one gravitational taken from GRACE.

The last image shows a local mass synthesis around Central Italy following a mid earthquake. Interpretation started from eastern images and was carried out independently in different years moving westward by observing the original geometrical relations derived on the Caspian basin. The delineation and correlation of visible patterns in relation to gravitational lows in the Med provides a quantifiable insight into large energy releases occurred in 2009 in central Italy.

The interpretation of main features east was performed in 2007 and it indicates a large EW crust fracture intersecting the well known SWNE earth break. The EW fracture aligns at the base of several low gravity anomalies. These two main lineaments induced subsequent deep fracture patterns, which in turn act as basins structural constraints, also delimiting sour areas (H_2S rich).

Red traverse line is identified as Med-Pakistan lineament (crust's fracture), coinciding with Caucasus EW, intersecting at 90 degrees the other large lineament NESW, clearly visible NE to N Siberia and SW to the Atlantic Ocean. The red traverse line is tangent to south margin of gravitational low centred on Caspian depression (-20, -30 mGal). In blue crust's induced fractures. Smaller lineaments in red, predominantly NS, were derived according to main lineaments distribution, a first approach casual derivation.

Plus and minuses indicate sub cell rotation direction, minus anticlockwise. Anticlockwise rotation appears to coincide with negative sign of surface tangent gravitational gradient (10 mGal accuracy). Clockwise rotation is in the direction of increased surface gravitational values (positive surface tangent gradient).

The respective changes in rotational sign could be explained as compensation between subsurface differential mass movements, of opposite sign either side of main crust fracture lines. Anisotropy

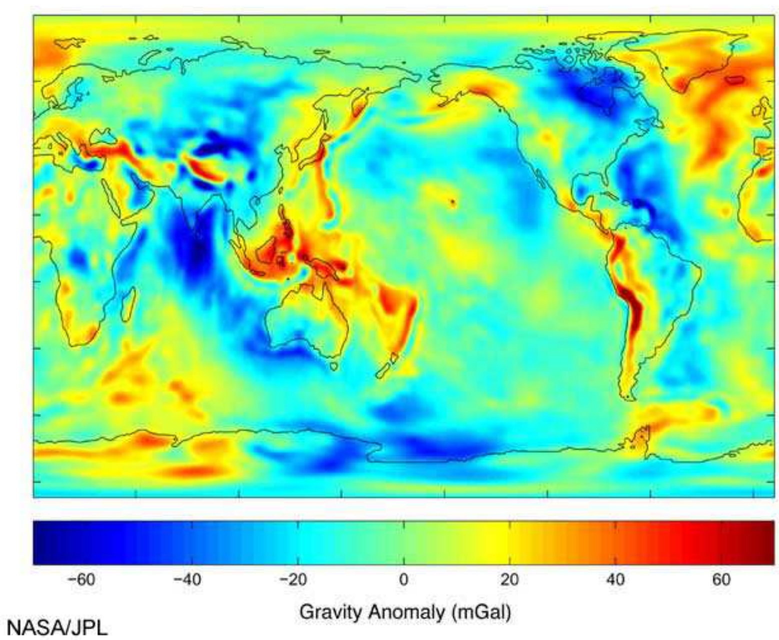

Figure 1.

at smaller scale generates different azimuths, seen as random without a deeper knowledge of rock physical parameters.

Clockwise sub cells material could be sinking in low gravity patches according to Eotvos principle, effectively lowering gravity further, whereas sub cells with opposite momentum could contribute to the formation of a funnel acting as a conveyor towards surface. The resultant funnel would be the interaction of the two opposite sub cells angular forces simplified in the form $F = -2m\omega \sin \alpha$, controlled by the difference of the two masses, the funnel between eddies acting as a conveyor towards surface. Similar spins interaction form quasi linear tangent drags.

A triple point junction is noticeable either side of south Caucasus. H_2S rich area is east. Two main hydrocarbon sources can be hypothesised: 1) Armenia 2) Turkmen-Iran border, SEE SWW Caspian. A triple point can be identified further west. Potential deeper migration accumulation traps are highlighted only around the Caspian area. These appear to be better spread and developed in anticlockwise rotational sub basins. Preferential H_2S presence can be linked to H_2 supply related to electric potential differences between sub cells. All deep sources are close to triple junctions.

All main faults or fractures cross near prolific oilfields or are connected to oilfields by subsidiary

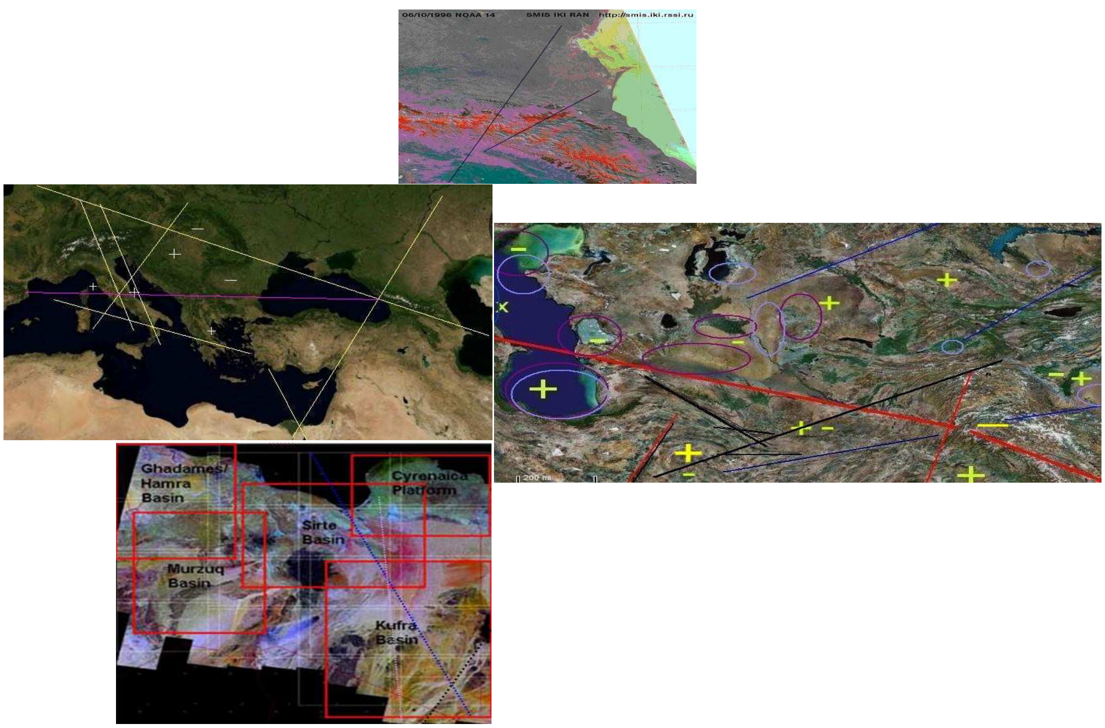

Figure 2.

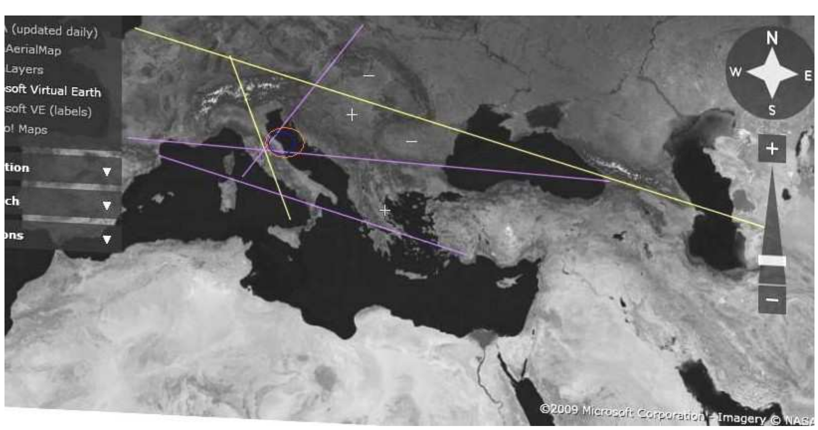

Figure 3.

paths. Main structural lines may act as pipelines. Sour fields and sour gas bubbles are critically linked to vicinity of deep sources. The overall migration path is consistent throughout approximately SN. Moving SW, tangent to south Mediterranean through N Africa, the relative rotational sign distribution is consistent.

Another deep source is noticeable near the Gulf and one further South, indicating that there are at least two major junctions over less than 120 degrees latitude near gravitational lows and antithetic to the main EW line. The N Africa image is also characterised by a relatively shallow Mohr and a strong electromagnetic anomaly.

Main fractures EW and NS could be gravitational pull orbital inertial change/rotation induced, could be assimilated to sudden cooling, they are independent from most pre-existing structure and appear to span a maximum of 180 degrees. Mean cell thickness, rigidity and relative system(s) anisotropy(ies) are other controlling factors.

The following values were derived in first approximation during a 5.5 mid peak earthquake in Italy in 2009. The mass results are shown in the third image, also computed independently. Based upon the fracture geometry a first approximation was carried out on the seismic momentum. The result in dynes as first try was $M0 = (30000\,\mathrm{Gp} \times 250\,\mathrm{sqkm} \times 0.01\,\mathrm{m}) = 7.5 \times 10^{24}$. The resulting value on the seismic momentum scale $2/3 \log M0$ was 24.8. The resulting Richter magnitude for this value is 5.8, very close to what recorded. Mass correlation with NE Italy (several times moved mass) gives a first try magnitude of 6.5 that is well in line with past major seismological event magnitude. Eastward block deformation along latitude relates to NE rotational stress induced by main lineaments.

To assess the findings and theory exposed, it may be necessary to derive the roots of Riemann surface through angular momentum or Riemann drags and to integrate results with flow modelling for deep migration definition. Main and subsidiary fracture patterns geometry may be assessed through spheroid-hyperboloid surface deformation related to system(s) speeds and cross-orbital trajectory assuming that over 180 degrees the curvature is closely related to the conjugated radius of the spheroid and the stretch related to resultant earth angular eccentricity = arccosine traverse radius/approximate curvature.

Of interest would be the correlation with high frequency sun planetary variations as per climatic envelope on record, in the next figure, and ocean stationary currents period variations. Highest envelope variations fall in SHF range. The existing climatic trend, influenced by GHG, green house agents such as CO_2, CH_4 — highly compressible fluids and effective low pass filters, correlates with a function, the product of a greenhouse hyperbola linearly scaled by radiation intensity. Local climatic anomalies and their displacement are thus relatable to differentials in re-radiating wave fronts and thermal wave fronts backscatter. To this end, earth thermal gradients and baseline changes may be significant undetected contributors.

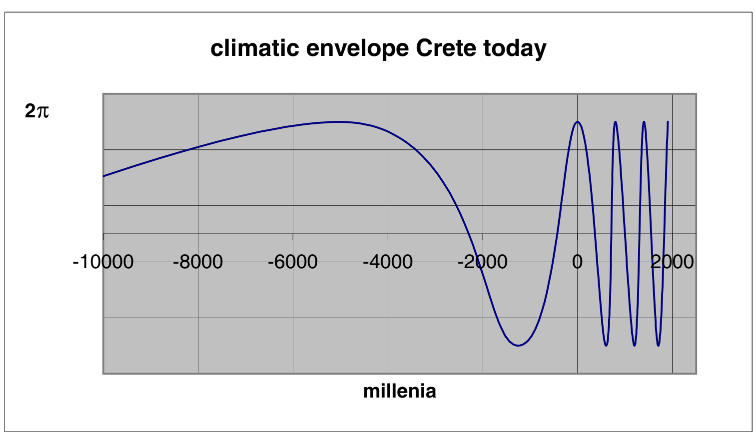

Figure 4.

A Way of Modeling Radiation-Matter Interaction

S. L. Vesely[1] **and A. A. Vesely**[2]

[1]I.T.B.-C.N.R., Italy
[2]Via L. Anelli 13, Milano 20122, Italy

Abstract— Quantum mechanics interprets the interactions between radiation and matter energetically, taking recourse to spectral data. As an alternative, this paper suggests that the reactions induced in the matter by light or electromagnetic waves, when they can be controlled by means of a feedback loop, admit a different interpretation. In that case, the same model that allows for controlling the reaction can be taken as an *explanation* of the phenomenon itself. It is beyond the scope of this paper to further investigate the relationship between controlling and comprehending. Network theory also avails itself of feedback loops for describing information exchanges in complex systems. However, it is dubitable whether that body of achievements can be extended as-is to the study of signals between natural objects and experimenters.

In this paper, we distinguish between radiation-matter interactions that only result in images, and those that besides altering the radiation also tend to alter the matter. In telecommunications, those two classes of interactions are separately considered as reception and transduction. That is mostly an abstract distinction; for example, it doesn't necessarily imply that distinct hardware components are associated with processes of one or the other class. However, reception and transduction of a signal bear distinct conceptual characteristics: linear the former, non-linear the latter. Criteria to extract information from encoded signals exist in the framework of the linear response theory, while transduction phenomena depend on multiple not easily identifiable factors. Applying that distinction to a piece of matter under test, we wonder if, given a signal received in the receiver's normal functioning range, we can indeed distinguish between 1) a linear response, and 2) a response also related with a permanent or transient alteration of the irradiated matter. The question of whether it is possible to detect matter alterations *by only analyzing the received signal* is ambiguous, because the meaning of the response of the matter has to be ascertained by crosschecking some more factors. Conversely, if it is not possible to verify the response of the matter by some other means, one cannot know what hypothetical alteration, if any, would correspond to the signal received. It is worth mentioning that quantum mechanics makes no distinction between linear response and transduction: It uses the radiation-matter interaction for linearly "decoding" each element's spectral response. A possible limit of crosschecking the resulting atomic model with the periodic table is that Mendeleev made it by determining each element's valence according to its role as a reagent in specific chemical reactions, neglecting *photochemical reactions.* Photochemical reactions imply transduction.

To illustrate by example, in this paper, we consider the Einstein-de Haas experiment as a transduction process at resonance conditions at low frequency, and describe what was the signal they looked at and how they controlled the electromagnetically induced torque oscillations. Next, we show that the other emblematic experiment for determining the charge/mass ratio, namely the Zeeman experiment, consists in observing a purely electromagnetic signal at much higher frequencies. Both experiments are carried out at resonance conditions. We wonder if the Zeeman effect could be "amplified" so as to obtain some kind of (non-mechanical) transduction associated with its electromagnetic response.

We conclude that feedback loops might be used to model the radiation-matter interactions, in the cases where the net effects are not limited to the resulting images.

Scattering Characteristics and Star-shaped Cylinder Parameters Correlation

D. D. Gabriel'yan, **M. Yu. Zvezdina**, **E. D. Bezuglov**,
S. N. Zabelkin, **and M. M. Mednaya**
Rostov Academy of Service of South Russian State University of Economy and Service, Russia

Abstract— To increase the quality of functioning of multipurpose radioelectronics it is possible to use lifting surface scattering characteristics to control both radiation and scattering characteristics of antenna system. In most of the cases magnetodielectic coating is used to change scattering properties. But it is difficult to control the parameters of this kind of coatings. Moreover, the coatings have fair weight and require special selection of both material and structural parameters. Another way of changing the scattering properties is to change the shape of ideally conducting lifting surface. In particular, shaping the lifting surface with gutters of various outline allows changing scattering properties considerably. In such a case rather simple technical solutions guaranteeing gutter outline parameter change are possible.

Paper objective is to investigate the scattering characteristics and shaping gutters parameters correlation for cylinder lifting surfaces.

The development of a method allowing to find the required correlation is based upon accounting 2π periodicity of currents and fields that are excited and scattered by cylinder constriction. Field and current distribution presentation as Fourier series and usage of orthogonal properties of terms of these series allows obtaining the correlations in the closed form that are convenient for scattering characteristics and shaping gutters parameters correlation analysis. These correlations can be interpreted as surface impedance tensor spectral components evaluation. It allows more common approach both to the investigation of scattering properties of various surface types and to ascertainment of the most important principles. The proposed method adequacy as well as the reliability of results obtained using the method is verified by considering the subcases of circular and elliptic ideally conducting cylinders.

The obtained correlations and the results of numerical investigations are given in the paper. A case of circular cylinder with cosinusoidal shape gutters forming the star-shaped cross-section is observed closely. Physical interpretation of the obtained results is given.

Analytic Conversions in Diffraction Problems on Metal Cylinders with Multilayer Magnetodielectric Coating

D. D. Gabriel'yan, **M. Yu. Zvezdina**, **E. D. Bezuglov**, **S. N. Zabelkin**, **and M. M. Mednaya**
Rostov Academy of Service of South Russian State University of Economy and Service, Russia

Abstract— The solution of electromagnetic wave diffraction problem on multilayer magnetodielectic coating is used in many practical applications. It is determined by the wide usage of this kind of radio absorbing coatings. It's necessary to know the electromagnetic field structure both inside the coating and in its outer region. Usually the problem is solved by joining the fields on layer boundaries using the numerical methods. But this kind of solution has a number of disadvantages. Firstly, computational costs are rather huge. Secondly, using simple numerical methods makes it impossible to take account of effects of multilayer structure residue and attached waves excitation. Thirdly, it is necessary to create a model for each coating structure.

We suggest using a convolution algorithm developed for an arbitrary source type and positioning inside the coating layer to get rid of the disadvantages listed above. The algorithm is an extension of the results in works of L. M. Brehovskih and J. R. Wait and allows reducing the analysis of initial multilayer coating field to the analysis of the field of equivalent coating of the same thickness but consisting of less layers. Decreasing the layers quantity makes it possible to hold the computational costs down while preserving the field structure within the layers provided by transmission matrix in the first place. Secondly, it allows obtaining the dispersion equation solution in a closed form by not complicated analytic transformations. Thirdly, it allows obtaining in a closed form the correlations that describe tangential components of electromagnetic field on the outer border of the coating and, thus, to link the surface impedance tensor element values to the multilayer coating parameters.

In the paper, the expressions obtained for multilayer magnetodielectric coating situated on a circular metal cylinder are given.

Our analytical results are compared with the existing ones which were obtained using different techniques. Agreement is observed on all of them.

Study of Relationship between Multiple Scatter and Backscatter Enhancement from Rough Surfaces

Chin-Yuan Hsieh[1] **and Ling-Hsuan Hsieh**[2]

[1]IT Dept., Kao Yuan University, Kaohsiung, Taiwan
[2]ECE, University of Waterloo, Canada

Abstract— The backscattering enhancement from rough surfaces is predicted due to the constructive interference of multiple surfaces scattering. For specialized surfaces involving roughness large compared with the incident wavelength, the multiple scatter and backscattering enhancement takes place. The phenomenon of backscatter enhancement becomes evident for both larger normalized surface height and surface rms slope. In this paper we take further study to predict the backscattering enhancement mainly comes from upward multiple scattering. On the contrary the downward multiple scattering has no contributions to the scatter strength of backscattering enhancement. The existing integral equations model is modified to be able to predict the phenomena of multiple scattering and backscattering enhancement. The total multiple scattering strength is the summation of upward and downward multiple scattering strength. The depolarized multiple scattering makes much contribution to the strength of backscatter enhancement in the backward direction along the plane of incidence from random rough surfaces, but depolarized single scattering makes little. In comparison of model prediction of total multiple scattering strength with measured data along the specular plane, excellent agreement is obtained.

Introduction: The experimental study of backscattering enhancement from characterized random surfaces was studied by L. Ailes-Sengers in 1995. The comparisons of Monte Carlo numerical studies and experimental measurement of backscattering enhancement from 2-D perfectly conducting random rough surfaces was made by Joel T. Johnson in 1996. Up to date a theoretical model for studying the backscattering enhancement and the relationship among the backscattering enhancement and the multiple scattering is still lacking. Further the study of upward or downward multiple scattering making major contributions to backscattering enhancement is also lacking.

In this paper we develop the scattering model to predict the multiple scattering and backscattering enhancement and the relationship between them. Due that the phase terms of Green's function and its derivative in the integral equation pairs is a possible candidate for the multiple scatter and backscattering enhancement from very rough surfaces, the model developed in this paper is based upon the integral equation pairs with tangential electric and magnetic surface fields.

Model Description: The modified integral equations for tangential surface fields on a dielectric interface are applied to predict the contributions of multiple scattering from rough surfaces. In the model development the estimates of the tangential surface electrical and magnetic fields in the dielectric medium are more general than Kirchhoff, perturbation surface fields and the existing integral equation model [Fung, 1994].

The spectral representation for the Green's function is stated below

$$G=\left(-\frac{1}{2\pi}\right)\int\frac{j}{q}\exp\left[ju(x-x')+jv(y-y')-jq|z-z'|\right]dudv \tag{1}$$

The absolute value term in the Green's function represents the downward and upward scattering pattern and strength. When the phase term of the Green's function with an absolute value sign is included, the major impact is on the evaluation of the ensemble averages for finding the ensemble average scattered power.

The bistatic scattering coefficients related to the ensemble average scatter power can be obtained with the given Kirchhoff and complementary scattered field by

$$\sigma^0_{qp}=(4\pi R^2P_{qp})/(E_0^2A_0) \tag{2}$$

The scatter strength of multiple scattering with the correction of shadowing function is therefore expressed as

$$\begin{aligned}\sigma^s_{qp} \;&=\; s(\theta_{in})\cdot s(\theta_s)\cdot\frac{(kL)^2}{4}e^{-(k\sigma)^2(\cos\theta_s^2+\cos\theta^2)}\\ &\cdot\sum_{n=1}^{\infty}(k\sigma)^{2n}|I_{qp}|^2\,\frac{\exp\left\{-\frac{(kL)^2}{4n}\cdot\left[(\sin\theta_s\cos\phi_s-\sin\theta\cos\phi)^2+(\sin\theta_s\sin\phi_s-\sin\theta\sin\phi)^2\right]\right\}}{n\cdot n!}\end{aligned} \tag{3}$$

Model Prediction and Comparisons: To evaluate the validity of model prediction for the depolarized multiple scattering for rough surfaces we compare the level and trend of depolarized scattering coefficient of model prediction with the measured data. The measurements were made by Hauck et al. [1]. Due to the scatter energy transmitting into the second medium, the specular peak and the backscatter peak decreases with smaller surface dielectric constant. The normalized surface correlation length is 13.2 and surface standard deviation is 4.4. The incident angle is chosen to be 20 degrees. For further evaluating the model developed in this paper, we show the comparisons of model prediction with the measured data from rough surface [Hauck, 1998]. The excellent prediction is shown in Figure 1. The difference is less than a dB.

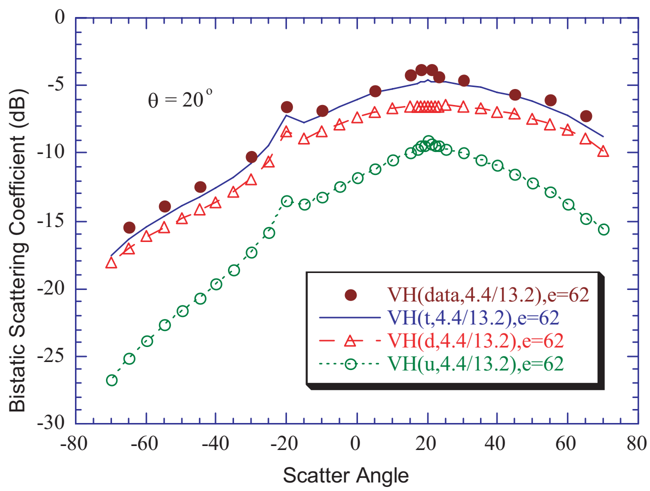

Figure 1: Comparisond of prediction with measurement (d = downward multiple, u = upward multiple, t = total multiple).

REFERENCES

1. Hauck, B., F. Ulaby, and R. DeRoo, "Polarimetric bistatic measurement facility for point and distributed targets," *IEEE Transactions on Antenna and Propagation Magazine*, 40, February 1998.

The Study on RCS of 2-dimensional Dielectric Wedge Loaded with Conduct Grid

Xiaolei Feng[1] **and Qiang Zhang**[2]

[1]Nanjing Research Institute of Electronics Technology, Nanjing, China
[2]China National Key Lab. of Antenna and Microwave Technology, China

Abstract— In this paper, the RCS characteristic of 2-dimensional dielectric wedge loaded with conduct grid is present. The RCS of 2-dimensional dielectric wedge is calculated, then the RCS of 2-dimensional dielectric wedge loaded with conduct grid as well as mesh. It has shown that the difference of RCS characteristic is significant and interesting.

Let's consider a 2-dimensional dielectric wedge whose corner angle is 120 degree (i.e., $\alpha = 120$ degree) and $w = 4\lambda$, $d = 3\lambda$. As is shown in Fig. 1.

It is assumed that a plane wave incident upon the wedge with different polarization, i.e., parallel and perpendicular polarization relative to the z axis. In Fig. 2, it is found that the RCS of wedge loaded with grid or mesh decreased apparently about 10 dB, compared with that without grid or mesh for parallel polarized plane wave excitation. In Fig. 3, by comparision between RCS of wedge loaded with grid and with mesh for parallel polarized plane wave excitation the difference is observed.

The results are given in Fig. 2 and Fig. 3. The incidence angle is 30 degree (i.e., $\theta = 30$ degree).

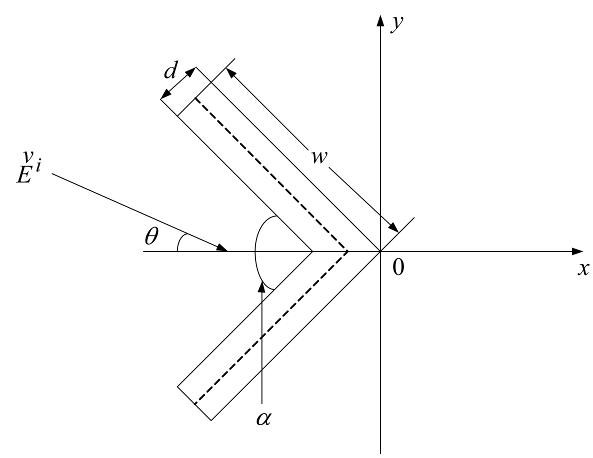

Figure 1: Scattering of 2-dimensional dielectric wedge loaded with conduct grid/mesh.

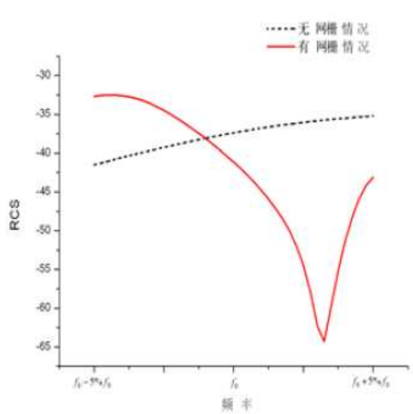

Figure 2: RCS of wedge with/without grid.

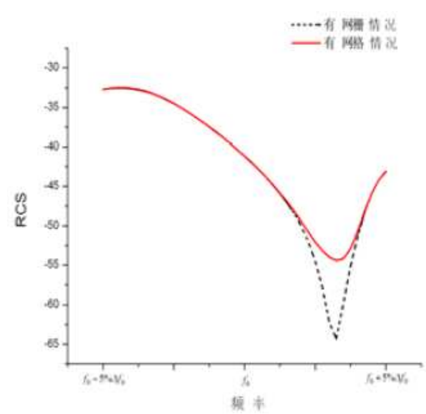

Figure 3: RCS of wedge with grid/mesh.

Topological Properties of a Chain of Vortices

Karen Volke-Sepulveda
Universidad Nacional Autonoma de Mexico, Mexico

Abstract— A wave vortex is a screw type dislocation of the wavefront [1]. The amplitude of the wave vanishes in the vortex core and its phase changes by an integer multiple of 2π (known as the topological charge) along a closed loop around this point. In this work we present a theoretical analysis of a wave field constituted by an axial array of vortices consecutively inverting the topological charge over distances of quarter a wavelength. This chain of vortices exhibits a periodic gradient of the angular momentum density along a single axis, although it is generated by means of a co-lineal superposition of counter-propagating modes possessing no angular momentum themselves, with an arbitrary phase difference between them. The main topological characteristics of the wave field are identified and discussed, and results on its experimental generation are also presented. Our analysis is not restricted to light waves, but can be applied to other kinds of wave fields, including sound and matter waves, for instance, which may lead to a number of potential applications that are also discussed.

REFERENCES

1. Nye, J. F. and M. V. Berry, *Proc. R. Soc. Lond. A*, Vol. 336, 165–190, 1974.

2D Magnetophotonic Crystals Fabricated Atop Patterned Substrates

Seung Min Baek, **Alexander V. Baryshev**, **Kazuo Yayoi**, **JooYoung Kim**,
Hironaga Uchida, **and Mitsuteru Inoue**
Toyohashi University of Technology, Toyohashi, Aichi, Japan

Abstract— Artificial structures composed of alternating dielectric materials with different refractive indices, known as photonic crystals (PCs), have been shown to manipulate the flow of light. For magnetophotonic crystals (MPCs) [1] — PCs with magnetic constituents, characteristics of light beams can be influenced by the external magnetic field. Enhancements of magneto-optical (MO) responses of magnetic materials introduced into different one-dimensional MPCs are experimentally observed. However, experimental performances of two-dimensional (2D) MPCs were not demonstrated until now. In this work we have demonstrated new approaches for fabrication of two-dimensional MPCs made of yttrium iron garnet (YIG) or bismuth-substituted yttrium iron garnet (Bi:YIG). Optical and MO responses of these MPCs were studied.

We prepared three different patterned substrates. First of them was a 2D array of platinum dots created onto a gallium gadolinium garnet substrate. This was made using e-beam lithography and ion beam milling. Also, thin opal films fabricated by vertical deposition were used as 2D patterned substrates. The third type was a 1D periodic array of bars of photoresist fabricated by e-beam lithography onto a glass substrate. These patterned substrates were used for depositing magnetic materials or multilayers with following structures: GGG substrate/2D array of Pt dots/YIG film (sample 1), glass substrate/opal thin film/Bi:YIG film (sample 2), and glass substrate/1D array of photoresist bars/$(\mathrm{Bi{:}YIG}/\mathrm{SiO_2})^7$ multilayer (sample 3). We found that 2D (and 1D) structure of substrates transposes into structure of magnetic materials. SEM observations showed that sample 3 had a quasi-2D structure. Optical spectra of the fabricated samples were governed by diffraction from 2D gratings. MO spectra of samples 2 and 3 demonstrated significant enhancement of Faraday (and Kerr) rotation in comparison with their conventional counterparts (fabricated atop of flat substrates). Also, the sign of rotation of the polarization plane was found to change in narrow spectral ranges corresponding to transmission/reflection resonances.

REFERENCES

1. Inoue, M., R. Fujikawa, A. Baryshev, A. Khanikaev, P. B. Lim, H. Uchida, O. Aktsipetrov, A. Fedyanin, T. Murzina, and A. Granovsky, *J. Phys. D: Appl. Phys.*, Vol. 39, R151, 2006.

Session 4A1a
Satellite Thermal Monitoring of the Ocean Surface and the Earth Surface

Error and Domain of Applicability Studies for the Schmugge's Dielectric Model of Moist Soils

V. L. Mironov[1], **J.-P. Wigneron**[2], **F. Demontoux**[3], **S. V. Fomin**[1], **and L. G. Kosolapova**[1]

[1]Kirensky Institute of Physics SB RAS, Krasnoyarsk, Russia
[2]EPHYSE INRA Centre Bordeaux Aquitaine, France
[3]Bordeaux University, IMS Laboratory, France

Abstract— An adequate dielectric model is an essential element of all the data processing algorithms used in the radar and radio thermal remote sensing of the land. The well known Schmugge dielectric model for moist soils [1] is used in the algorithms of radio brightness data processing [2]. This model is based on the dielectric data measured only at three frequencies 1.4, 1.412 and 5.0 GHz, moistures varying from 0 to the field capacity values, and soil clay contents from 0 to 62 percent. The diel predictions by this model are accurate for all the diel data used for its development in [1]. The main reason for good accuracy achieved is that it takes into account the property of the initially adsorbed molecules of the bound water in soil. At the same time, a domain of applicability and error of the Schmugge model have not been studied yet, regarding other frequencies and soils. This problem is analyzed by the authors on the bases of the comprehensive dielectric data set available in [3]. The data base taken from [3] covers the frequency range from 0.3 to 24.5 GHz, clay contents from 0 to 76 percent and the moistures up to field capacity ones.

To consider the error and domain of applicability for Schmugge model there was analyzed the correlation between the dielectric constant (DC) and loss factor (LF) predicted with the Schmugge model and independently measured data available in [3]. As far as it concerns the dielectric constant, the Schmugge model provides for the predictions on the same order of error for all frequencies, soils and moistures independently measured in [3] as it does for the soils, frequencies and moistures measured in [1]. As a result the Schmugge model was shown to be applicable to the soils beyond the ensemble of soils with dielectric data of which it was developed and not only for the frequencies of 1.4, 1.412 and 5.0 GHz, but in the whole range from 0.3 to 24.5 GHz. At the same time in the case of loss factor, the Schmugge model was found to provide for accurate dielectric predictions only over the frequency range from 5.0 GHz and higher, concerning ensemble of soils independently measured in [3].

We applied the recently published mineralogy based soil dielectric model (MBSDM) [4], which exploits generic dielectric spectra for bound water, to understand this conclusion. Indeed, the ratio of a bound water DC spectrum to that of free water was found to deviate as a function of frequency from a mean value only on the order of $\pm 15\%$ in the whole range of clay contents. This estimate justifies the eristic assumption about bound water DC spectra accepted by Schmugge in his model. On the contrary, the ratio of a bound water LF spectrum to that of free water appeared to substantially deviate from the mean value up to $\pm 40\%$. This may explain why the Schmugge model failed to predict LFs through the whole range of frequencies measured in [3]. It is worth to mention that, with generic bound water dielectric spectra being used in the MBSDM it proved to provide for accurate predictions for the DC as well as, the LF in the whole range of frequencies and clay contents met in both [1, 3].

REFERENCES

1. Wang, J. R. and T. J. Schmugge, "An empirical model for the complex dielectric permittivity of soils as a function of water content," *IEEE Trans. Geosci. Remote Sens.*, Vol. 18, No. 4, 288–295, 1980.
2. Wigneron, J.-P., et al., "L-band Microwave Emission of the Biosphere (L-MEB) model: Description and calibration against experimental data sets over crop fields," *Remote Sens. Env.*, Vol. 107, 639–655, 2007.
3. Curtis, J. O., C. A. Weiss, Jr., and J. B. Everett, "Effect of soil composition on dielectric properties," Technical Report EL-95-34, December 1995.
4. Mironov, V. L., L. G. Kosolapova, and S. V. Fomin, "Soil dielectric model accounting for contribution of bound water spectra through clay content," *PIERS Online*, Vol. 4, No. 1, 31–35, 2008.

Effect of Antireflective Surface at the Radiobrightness Observations for the Topsoil Covered with Coniferous Litter

V. L. Mironov[1], **P. P. Bobrov**[1, 2], **A. S. Yashchenko**[1, 2], **I. V. Savin**[1], **and A. V. Repin**[1, 2]

[1]Kirensky Institute of Physics, SB RAS, Krasnoyarsk, Russia
[2]Omsk State Pedagogical University, Omsk, Russia

Abstract— Given the radiothermal remote sensing of the land, a spot on the earth surface generating the signal received by the microwave radiometer antenna can be partially or completely covered by forest. A layer of a deciduous litter was shown [1] to exert a great impact on the radiobrighness of the topsoil. To continue this research, we conducted the radiobrighness observations for the forest moist soil covered with a coniferous litter. In the summer time continuously during a week, there were conducted radiobrighness around-the-clock measurements at the frequencies of 1.4 and 6.9 GHz, for horizontal and vertical polarizations, and at the observation angle of 45° relative to the nadir. The maximum radiobrightness through diurnal cycles appeared to be registered before dawn when the thermodynamical temperature at the soil surface was minimum. This phenomenon must be attributed only to the antireflective layer effect induced by the litter.

We developed a theoretical model to calculate radiobrightness of the layered topsoil. Using this model, we derived the dielectric constants pertaining to the separate layers of topsoil. For this purpose, we applied the least squares method for fitting the calculated diurnal radiobrightness dependences to those measured. The forest soil covered with coniferous litter was modeled by a three steps dielectric profile, the interfaces between the separate layers being smooth. The theoretical modeling conducted confirmed that, at the moments of maximal radiobrightness, an antireflective layer was formed on the topsoil surface, most probably due to nonisothermal upward moving of soil moisture. At that, the theoretically calculated dielectric constant of the litter antireflecting layer was found to be on the same order as the value measured at the laboratory environment.

REFERENCES

1. Wigneron, J.-P., Y. Kerr, P. Waldteufel, K. Saleh, M.-J. Escorihuela, P. Richaume, P. Ferrazzoli, P. de Rosnay, R. Gurney, J.-C. Calvet, J. P. Grant, M. Guglielmetti, B. Hornbuckle, C. Mätzler, T. Pellarin, and M. Schwank, "L-band Microwave Emission of the Biosphere (L-MEB) model: Description and calibration against experimental data sets over crop fields," *Remote Sens. Env.*, Vol. 107, 639–655, 2007.

Monitoring of Satellite Thermal Pattern of an Ocean Front as a Hydrodynamic Convergence

Shigehisa Nakamura
Kyoto University, Kyoto, Japan

Abstract— This is an over view of an ocean front as a hydrodynamic convergence. The author has noted the ocean front formed by two waters, i.e., a coastal and ocean waters to be found as a line on the sea surface. This ocean front can be well monitored by using a satellite. This technique has helped the author's finding of the specific properties of an ocean front on the sea surface. By this time, it was discussed mainly about several specific patterns of an ocean front, for example, in the northwestern Pacific. Similar pattern can be found in the Atlantic (around the Gulf Stream) or in the South Pacific (as the western boundary flow off the eastern boundary of Australia). After the author's monitoring of satellite thermal pattern of the ocean front in the northwestern Pacific, it is clarified that the front has a close relation to the western boundary current named as "Kuroshio". The front pattern is significantly governed by the coastal configuration and varies its spacial pattern with the time elapse. The author has first introduced several cases that including some specific pattern of the ocean front at a shot reduced from the signals directly received by a system of an antenna and a software for the data processing. Successively, several case of timely change process of the ocean surface front has been obtained during a continuous satellite monitoring of the sea surface in the foot print covering the interested ocean front. This monitoring has given a key to the author for helping to develop a model of ocean front evolution on the sea surface referring to his understanding of hydrodynamics. Adding to the above, it was found that a satellite thermal plateau and a satellite thermal pinnacle can be understood as the specific cases a physical processes after an application of Stefan-Boltamann's radiation theory. A satellite thermal pinnacle could be a set of concave facets as a part of the sea surface waves concentrating at the related pixels in the monitoring. A satellite thermal plateau could be formed by an ensemble of the set considered above for the pinnacle. The author has to take it necessary to relate these processes to the meteorological processes on the sea surface. Several cases of the interested processes were well related to an effect of a set of wind induced waves radiated out of a distant storm (more than one thousand kilometer far from the interested area) even in the satellite's foot print covering. Following the author's satellite monitoring of the ocean front evolution, it is clarified that the front is an example of a line where the waters converge to maintain the ocean front. Now, the knowledge of hydrodynamics lead us to see where the divergent area is existing to support the convergent line as the ocean front on the sea surface. One of the idea to this problem might be to consider a global circulation of the ocean waters. There are many works reported as a new contributions or "geophysics". That is to say, one of the most recent reviews on the global ocean circulation is noted a pattern of surface ocean circulation combined to a deep ocean circulation. It is now understood as that a significant convergent is seen in the area between Green land and New Found Land on the sea surface at the north arctic zone in the Atlantic. This convergence might be governed by the transport of the tropical water by Gulf Stream and by the effect of latitudinal cooling of the water at meeting the Arctic water. This could be understood as that of a specific example of the ocean front formed by two waters of the Arctic water and of the tropical waters. This convergence is connected to a water sinking down to form a deep water circulation. An estimated age of the ocean water tells us that the oldest deep water is mid in the North Pacific. This suggests us the ocean surface in the North Pacific must be the area of divergence. The author now is facing to solve a local problem in relation to a global process of the ocean circulation.

Monitoring of Satellite Thermal Pattern of Ocean Front in Relation to a Double Diffusion Process

S. Nakamura
Kyoto University, Japan

Abstract— After monitoring of satellite thermal pattern of an ocean front evolution, the author has had a step to see a double diffusion process on an interface in relation to ocean front evolution.

As has been well understood by this time, the ocean water contents in the ocean controls the density of the water. Several ions of the inorganic elements, the dissolved materials and the suspended materials are the contents of the ocean water. The ocean scientists have had taken conveniently that any ocean water sample could be specified by the two main factors, that is to say, the salinity and the water temperature. This means that they had been taken as that the motion of the ocean water could be taken a densirnetric motion in the gravity field of the Earth. With this, each of the salinity and the water temperature has a diffusive property respectively. It is understood that the diffusivities of the two factors, i.e., salinity and water temperature are never same to each other. Essentially, this difference of the two factors raises a problem of double diffusion in a scope of fluid mechanics. In these years, ocean front evolution has been studied as a simple process of the water density. In ocean, density of the water in the ocean is easily defined by the two factors at formulating water motion in the ocean under the earth's gravity field. An ocean front is evolving at any time and at any location. The author has introduced a model for an ocean front evolution for a purpose of his realizing what thermal pattern found on the sea surface monitored by using his simple system for directly receiving a satellite signal at a time just passing above his station settled on the coast facing the ocean. Boldly, a thermal factor is the most effective for finding the ocean front evolution which is found between the coastal water and ocean water. A case of the monitored thermal patterns monitored in an area of the NW Pacific in practice, could be seen by a simple model with an understanding of classic hydrodynamics, though to the details it must be referred to geophysical hydrodynamics. Another specific example is an eddy and a front monitored in the area of the NE Atlantic. Formulation of the water motion may be simple in form when one factor may be enough to consideration. In some specific cases, salinity is more important for analyzing salt finger or salt lens in relation to the Mediterranean outflow. Nevertheless, the author has to note here no one of the existing satellites is hard to detect any structure of the water motion under the ocean surface even around an interface as the extension of the ocean front on the ocean surface. What is noted above is left to be discussed in future in relation to any process found in the global ocean circulation in order to obtain a key to global waking control system.

Monitoring of Satellite Thermal Pattern of a Drifting Ocean Front

S. Nakamura
Kyoto University, Japan

Abstract— This work concerns about a problem of drifting ocean front. The author has been studied on satellite thermal pattern of a ocean front evolution. For this purpose, the author has had received directly the satellite signal just at the satellite passing time above his station. This make the author to be possible to refer to the satellite data for his monitoring of satellite thermal pattern of a drifting ocean front. An ocean front distorts after an shearing effect to the ocean front formed between the two water masses. The ocean front has been taken as one of the related indices for understanding the ocean currents just around the front. The ocean current is taken to be geostrophic. Geostrophic ocean current in the gravity field is governed by the gradient of water density, which is mainly determined by the two factors of salinity and water temperature. The interested ocean current should be understood in a scope of geophysical hydrodynamics, though this current could be formulated in a simple form. Generally, the ocean front is evolving time to time so that its pattern is not simple as the author's model. Nevertheless, what is essential for realizing can be seen after a model. The ocean current and ocean front is evolving time to time and location to location in the interested sea area. Some specific thermal pattern along a section crossing the front might be well demonstrated by a model. Even though, the author uses to trust a satellite thermal pattern on the sea surface to be true if the data in-situ at or in any part or point is well identified. Now, the author raise a problem of ocean surface thermal pattern in-situ obtained by the research ships. Any ship positioning in the ocean along a survey line shows where the ship is at the time of interested watch, though the satellite thermal pattern is covered in the foot print in a short time. The author has to notice that it is necessary to see the data in-situ obtained by the ship even along a single survey line. It is reminded that a long time should be spent for obtaining the sea surface thermal pattern along a survey line on the sea surface. The ship positioning must be adjusted though it is hard to escape from any drifting after the ocean current affecting to shift the ship position.

The author here note that the satellite thermal pattern should be compared to the data on the sea surface. What the author wish to notice is an "instrumentation effect". po his effect might control the accuracy of the data obtained on the sea surface. An actual pattern might be obtained under a survey condtion for a correct pattern. Occasionally, the pattern might be not in the expected one but in a degenerated or intruding pattern. The author has to notice that it is conditional what pattern could be founded in the descriptions of the survey data on the sea surface. Adding to the above, the author notice the ocean structure under the sea surface can not be well monitored by the satellite and electromagnetic waves.

Session 4A1b
Scattering, Emission and Remote Sensing of the Atmosphere

Characteristics of Spread-F in the Storm Time in the Ionosphere

Jiankui Shi[1], **Zhixian Luo**[1,2], **Taichang Gao**[2], **and Guojun Wang**[1]

[1]State Key Laboratory of Space Weather, CSSAR, Chinese Academy of Sciences
Beijing 100190, China
[2]Institute of Meteorology, PLA University of Science and Technology, China

Abstract— Ionospheric spread-F has serious influence on wave propagation. In this research, the characteristics of the Ionospheric spread-F in the storm time in low latitude region are studied by statistical analysis with the data from the DPS-4 digisonde in Hainan region during February 2002 to December 2007. We divide the spread-F into 4 types whose are Frequency Spread-F (FSF), Range Spread-F (RSF), Mixed Spread-F (MSF) and Strong Range spread-F (SSF). The main results are as below: the occurrence of spread-F is suppressed by magnetic storm as a whole. During storm time, FSF is motivated in 2002 and 2003, while it is suppressed during 2004–2007; RSF is suppressed during 2002–2005 and becomes more weaker, while it is weakly motivated in 2006 and 2007; MSF is suppressed in 2002, while it is motivated in 2003 and 2004, from 2005, it is suppressed again and becomes more stronger; SSF is suppressed during 2002–2004, while it is motivated in 2005 and 2006, in 2007, it is weakly suppressed. During the storm and nonstorm time, among four types of spread F, the most active ones are SSF and MSF, and then FSF, RSF seldom take place. These are new outcome from the statistical analysis of ionospheric observation in Hainan region. In order to understand the physics mechanism of the different spread-F, the relationship between the occurrence of ionospheric spread F and the disturbed electric fields during the storm time are also discussed.

Application of Microwave Radiometry for Urban Heat Island Study

E. N. Kadygrov[1], **E. A. Vorobeva**[1], **I. N. Kuznetsova**[2],
V. V. Folomeev[1], **and E. A. Miller**[1]

[1] Central Aerological Observatory, Russian Federation
[2] Hydrometeorological Centre of Russia, Russian Federation

Abstract— One of the phenomena of urban climate meteorology is a heat island above the big city when temperature in the city center more high then temperature in suburb. The numbers of researches dedicated to the urban heat island (UHI) study were considerably increased in recent years. These investigations show anthropogenic interactions in the form of the powerful sources of pollution and water vapor and supplemental heat sources can exert a substantial influence on the intensity and form of the environmental in the large industrial cities and megalopolises. These factors lead to special climate formation in a megalopolis. For study of UHI ordinary were used near-surface data from meteorological stations at the city and in suburb. Our new technology based on consuming of microwave temperature profilers gave possibility to provide more detail investigation of heat island parameters including three dimension distributions of the temperature data. During 2000–2009, three microwave temperature profilers (MTP-5H) were used simultaneously in the Moscow region for continuous measurements of the atmospheric boundary layer (ABL) temperature profile. One MTP-5H was installed in the center of Moscow city, the second in the north part of Moscow (Dolgoprudny), and the third about 50 km west ward from the Moscow city center (Zvenogorod). The simultaneous measurement had two objectives. The first was to determine a Megacity impact to the ABL parameters which led to creation of UHI. The second objective was investigate the ABL stability and its influence a radiation balance near the ground surface. Quantitative parameters of Moscow UHI will be presented in the report.

REFERENCES

1. Kadygrov, E. N., G. S. Golitsin, and I. N. Kuznetsova, "Study of urban heat island on the basis of microwave remote sensing data," *Reports of Russian Academy of Science*, Vol. 385, No. 4, 541–548, 2002.
2. Khaikine, M. N., I. N. Kuznetsova, E. N. Kadygrov, and E. A. Miller, "Investigation of thermal-spatial parameters of an urban heat island on the basis of passive microwave remote sensing," *Theoretical Applied Climatology*, Vol. 84, No. 1–3, 161–169, 2006.

Missile Radar Cross Section Calculation and Its Use in 3-D Anti-missile Defense System

Laleh Seyyed Kalantary, **Taha Mosayebi-Dorcheh**, **Shahram Mohanna**, **and Saeed Tavakoli**
Faculty of Electrical and Computer Engineering
The University of Sistan and Baluchestan, Zahedan, Iran

Abstract— The use of multistatic radars in homeland security is of interest to many researchers. In this paper, the semiexact radar cross section (RCS) of a missile is analytically calculated. As shown in Figure 1, the missile composes of two finite-length cylinders, two finite cones and four wings. To find the scattering matrix of the missile, the scattering matrix of all the components should be added to each other, considering the phase of each component. As the thickness of a wing is too small in comparison with its length and width, it is assumed that the internal electric fields of the wings are equal to the internal electric field of an infinite disk with the same thickness. Considering this internal electric field, the scattering electric field of each wing is obtained. The semiexact scattering matrix of the finite-length cylinder is already calculated in [1]. In the microwave region where the length of the finite cone is much larger than the wavelength, the effect of the longitudinal traveling waves on a finite cone can be ignored. Therefore, having the same head angle of the cone, the internal electric fields of a finite cone may be approximated by those of an infinite cone. To find the internal electric field of an infinite cone, this electric field is expanded with respect to spherical Bessel function ($j_{\nu_{ml}}(kr)$), associated Legendre function ($P^m_{\nu_{ml}}(\cos\theta)$) and exponential function ($e^{im\varphi}$). ν_{ml} is the lth root of the equation $\frac{d}{d\theta}P^m_{\nu_{ml}}(\cos\theta)\big|_{\theta=\pi-\beta}=0$. In this equation, β is the head angle of the cone. This choice for ν_{ml} satisfies the boundary conditions. In the far field approximation, the relationship between internal electric field and scattering electric field is as follow

$$\bar{E}_s=-\frac{k^2e^{ikr}}{4\pi\varepsilon r}\hat{k}_s\times\left[\hat{k}_s\times\iiint dx'dy'dz'\left(\varepsilon_p\left(\bar{r'}\right)-\varepsilon\right)\bar{E}_{\text{int}}\left(\bar{r'}\right)e^{-ik\hat{k}_s\cdot\bar{r'}}\right]$$

where integrating is over the volume of the scatterer, $\bar{E}_s$ the scattering electric field, k is the wavenumber, $\hat{k}_s$ is the direction of the scattering wave, ε_p is the permittivity of the cone, ε is the permittivity of the free space and $\bar{E}_{\text{int}}$ the internal electric field of the scatterer.

Using multistatic radars, the defense system calculates the location and velocity of an object in three-dimension (3-D) coordinate. Then, applying Frii's formula, the RCS can be found with measuring the received power of each receiver. If this RCS is approximately equal to the calculated RCS, the anti-missile defense system identifies the object as a missile. When a missile is detected for the first time, the simulating software can estimate its launching and targeted places as well as its approximate path in a 3-D coordinate system.

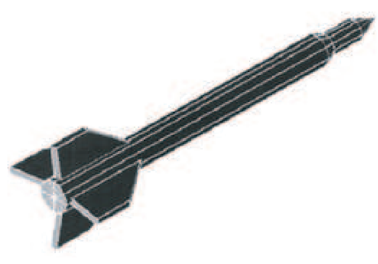

Figure 1: Geometry of the missile.

REFERENCES

1. Tsang, L., J. A. Kong, and K-H. Ding, *Scattering of Electromagnetic Waves: Theories and Applications*, John Wiley & Sons, Inc., 2000.

Session 4A2a
Light Scattering and Radiative Transfer: Theories and Applications 3

Training and Validation of a Wide-angle Optical Scattering (TAOS) Pattern Classifier

Giovanni Franco Crosta[1], **Yong-Le Pan**[2], **and Gustavo Eddino Fernandes**[2]

[1]Dipartimento di Scienze dell'Ambiente & Territorio, University of Milan-Bicocca, Milan, Italy
[2]Department of Applied Physics, Yale University, New Haven, CT 06520, USA

Abstract— *TAOS* (two-angle optical scattering) is a well-known experimental technique which records the intensity patterns of laser light scattered by single aerosol particles over an extended range of the scattering angles $\{\theta, \phi\}$ [1]. In the absence of a method which solves the inverse obstacle problem from intensity data, patterns have to be classified by artificial intelligence techniques. The classifier described herewith extracts features from *TAOS* patterns by the spectrum enhancement algorithm [2], which is controlled by a few parameters (the n-tuple ψ), not described herewith. Training corresponds to finding a ψ which maximizes a suitable figure of merit (F). The newly developed training-validation scheme is illustrated by the following example. **1)** Out of 100 *TAOS* patterns produced by clusters of polystyrene spheres of controlled size (material $a6$, **class 1**) and 100 patterns from single spores of *Bacillus globigii* (material bg, **class 2**), form e.g., 10 training (T) sets of 50 patterns from each class, which differ by at least $5 + 5$ patterns from one another. Two sample patterns are shown by Figures 1 and 2 below.

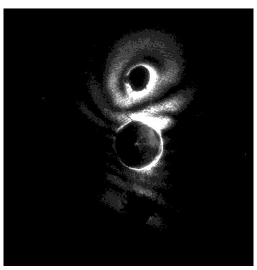

Figure 1: Scattering pattern of a polystyrene (PS) sphere aggregate (**class 1**).

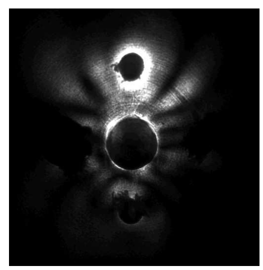

Figure 2: Scattering pattern of Bacillus globigii (Bg) spores. (**class 2**).

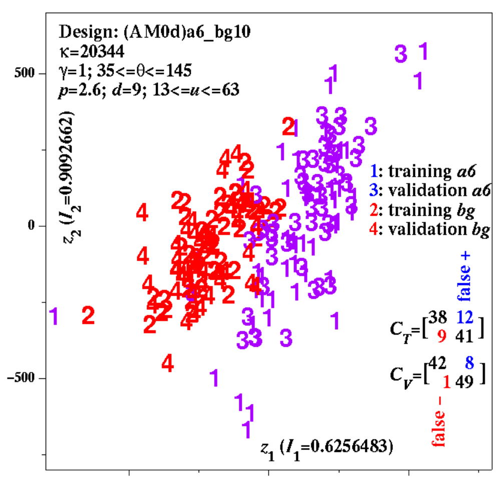

Figure 3: Classifier output: representation of *TAOS* patterns on the plane of the first two principal components z_1, z_2. To each pattern there corresponds a point on $\{z_1, z_2\}$. Patterns are labeled after their class of belonging and role in either T- or V-mode. The parameters γ, p, d and the endvalues of both θ and u form the n-tuple ψ; u is the spatial wavenumber on which enhanced spectra depend. I_1, I_2 are the fractions of sample variance explained by z_1 alone and by z_1 and z_2 together. C_T and C_V are the T- and V-mode confusion matrices. A "false-" (false negative) is a misclassified bg pattern.

2) Evaluate $F[\psi]$ for all available ψ and all T-sets, keep those ψ such that $F[\psi] > \tau$, a threshold value. **3)** Select a ψ which minimizes $H[\psi] := -\Sigma_\psi \ln[f[\psi]]F[\psi]$, where $f[\psi]$ is the relative frequency by which $F[\psi]$ occurs. **4)** Use the leftover patterns for classifier validation (V).

Figure 3 displays the classification result which corresponds to $F = 0.824$ in training (T) and $F = 0.883$ in validation (V) mode. The eventual goal is to implement a realtime TAOS pattern classifier.

REFERENCES

1. Fernandes, G. E., Y.-L. Pan, R. K. Chang, K. Aptowicz, and R. G. Pinnick, "Simultaneous forward- and backward-hemisphere elastic-light-scattering patterns of respirable-size aerosols," *Opt. Lett.*, Vol. 31, 3034–3036, 2006.
2. Crosta, G. F., C. Urani, and L. Fumarola, "Classifying structural alterations of the cytoskeleton by spectrum enhancement & descriptor fusion," *J. Biomed. Optics*, Vol. 11, No. 2, 024020:1–18, 2006.

Radiative Transfer and the Eigenfunction Approach in Different Geometries

Juris Freimanis[1, 2]

[1]Ventspils International Radio Astronomy Center, Ventspils University College, Latvia
[2]Institute of Astronomy, University of Latvia, Latvia

Abstract— Currently most of radiative transfer calculations are numerical solutions of the matrix transfer equation for Stokes vector, within framework of realistic, complicated three-dimensional geometric models, with inhomogeneous, anisotropic and probably gyrotropic scattering medium, with redistribution of radiation over frequencies etc. Nevertheless analytic results for the simplest models are benchmarks for numerical calculations at least because they provide the general behaviour and singularities of the solution. Correct reproduction of the singularities is essential for the numerical solution to be stable and to converge to exact solution.

Generalized eigenfunctions of plane-parallel radiative transfer equation have proved to be a powerful tool which allows to obtain analytic results in classical radiative transfer theory for both unpolarized and polarized radiation. Up to now, the simplest nonplanar geometries are partially included. Green's function for monochromatic stationary polarized radiative transfer equation inside homogeneous isotropic infinite medium in case of spherical and cylindrical symmetry of the primary sources and radiation field is an example of it.

Plane-parallel eigenfunctions generally have Cauchy type singularities leading to well-known and powerful apparatus of singular integral equations with Cauchy type kernels. The early results for nonplanar (spherical) geometry were based on use of the so-called spherical eigenfunctions of homogeneous transfer equation which really exist only partially and are insufficient for the solution of transfer problems. If one formally solves the eigenvalue equation in spherical geometry it appears that the eigenvalue spectrum is the same as for plane-parallel geometry, but one part of eigenfunctions are very well convergent series without Cauchy type or similar singularities, and the another part are formal, very strongly divergent series which really do not exist.

The appearance of correct formulae for spherical geometry seemingly resemble "spherical eigenfunctions", but the correct order of mathematical operations (summation of series over spherical harmonics and Stieltjes integration over eigenvalues using plane-parallel functions) must be observed in order to obtain valid expressions. Just this order of operations ensures that spherical eigenfunctions do not appear in the results. It seems very plausible that the situation for cylindrical symmetry is the same.

Discrete Sources Method: Light Scattering by Real Erythrocyte Shapes and Results Validation

Elena Eremina[1] **and Konstantin Gilev**[2]

[1]University of Bremen, Badgasteiner Str. 3, Bremen 28359, Germany
[2]Institute of Chemical Kinetics and Combustion, Institutskaya 3, Novosibirsk 630090, Russia

Abstract— An improved algorithm of the Discrete Sources Method (DSM) is applied to simulation of lights scattering by realistically shaped human erythrocyte. Numerical results obtained with DSM are compared to those obtained by the Discrete Dipole Approximation (DDA) and show good agreement.

In the last years, light scattering by erythrocyte has been intensively studied by different scientific groups worldwide. In particular, studying light scattering by erythrocytes is a suitable method for the detection of certain blood diseases. Correct interpretation of the measuring data is of interest for different biological and clinical applications. In reality the shape of human erythrocyte varies in form from nearly spherical through biconcave to toroidal ones. Together with the relative big size of an erythrocyte of 6–10 μm, its realistic shape with deep concavities makes modeling complicated.

Previously different simplified analytic approximation for the shapes, similar to spheres, spheroids and oblate discs have been used for erythrocyte modeling, but it has been shown that such approximations can lead to non adequate results [1]. Recently, more realistic analytical erythrocyte shape models have been suggested to reproduce a real biconcave shape of an erythrocyte calculation from the condition of minima of the membrane potential energy.

In the last years, different simulation methods have been applied to model a light scattering by erythrocyte. The DSM [2] proved itself as rigorous, precise and fast method. The DSM allows making use of the axial symmetry of the particle and the polarization of an incident excitation, which sufficiently reduces the time of calculations. Also the DSM allows calculation of all the incident angles and polarizations at once [1]. Additionally, the DSM gives the opportunity to control the accuracy of obtained results by surface residual evaluating.

In this work, the DSM is applied to simulate light scattering by realistically shaped human erythrocyte with its deep concavities. An improved numerical scheme allows the calculation of scattering characteristics with high precision, especially in side-scattering direction. The results obtained by the DSM are compared to the results obtained by the DDA and show good agreement. The basics of the improved DSM algorithm together with numerical results will be presented at the conference.

ACKNOWLEDGMENT

Authors would like to acknowledge financial support of this work by Deutsche Forschungsgemeinschaft (DFG) and Russian Foundation of Basic Research (RFBR).

REFERENCES

1. Eremina, E., Y. Eremin, and T. Wriedt, "Analysis of light scattering by different shape models of erythrocyte based on Discrete Sources Method," *Opt. Comm.*, Vol. 244, 15–23, 2005.
2. Eremin, Yu. A., "The method of discrete sources in electromagnetic scattering by axially symmetric structures," *J. Comm. Technology and Electronics*, Vol. 45, No. 2, 269–280, 2000.

Modelling of Ultrashort Laser Pulse Propagation in Biotissue in Application to Problems of Non-invasive Biomedical Diagnostics

L. P. Bass[1], **O. V. Nikolaeva**[1], **V. S. Kuznetsov**[2], **A. V. Bykov**[3,4], **and A. V. Priezzhev**[3]

[1]Keldysh Institute of Applied Mathematics, Russian Academy of Science, Moscow, Russia
[2]Research Scientific Center "Kurchatov Institute", Moscow, Russia
[3]Lomonosov Moscow State University, Moscow, Russia
[4]University of Oulu, Oulu, Finland

Abstract— In optical diffusion tomography of biotissues, an important role is assigned to numerical simulation of probing light propagation and formation of the signal from a pulsed laser. The comparison of the measured and calculated magnitudes underlies the solution of the inverse problem of the optical diagnostics.

The main difficulties arising in the simulation of laser beam propagation in biotissue are due to:

- complicated spatial structure of biotissues,
- high anisotropy of biotissues (mean scattering angle cosine is higher than 0.7 and can even exceed 0.95),
- small aperture of point source (laser),
- short duration of the pulse (in case of femtosecond laser) and comparatively long registration time (picosecond scale).

The Monte-Carlo method (MCM) of statistical testing accurately accounting for both the medium properties and the source — detector geometry, is time consuming. Besides, it produces solution results with high statistical noise under large times of signal propagation and source-detector separations.

Hence an alternative discrete ordinate method (DOM) for solving the radiative transfer equation was developed. This method is based on grid approximations to the source — detector geometry, anisotropy, solutions and therefore requires a special technique for simulating the nonscattered and single-scattered photons intensities (singular components of a solution) and wave front surface interpolation. As a result the computer realization of the DOM is more complicated compared to MCM, but the obtained solutions are not distorted by statistical noise inherent to MCM.

Calculation results of temporal distribution of diffuse scattered light pulses at probing the biotissue phantoms with laser beams of different apertures obtained by MCM and DOM are presented and compared. Example of implementing the two approaches to the problem of noninvasive sensing of glucose in a biotissue phantom is presented.

All calculations were run on a supercomputer with parallel architecture. Calculation times for both methods are compared.

ACKNOWLEDGMENT

This work was supported by Presidium of Russian Academy of Science via research program N2.

The 3D Radiative Effects of Clouds in Aerosol Retrieval: Can We Remove Them?

Evgueni Kassianov, **Mikhail Ovchinnikov**, **Larry K. Berg**,
Sally A. McFarlane, **and Connor Flynn**
Pacific Northwest National Laboratory, Richland, WA 99352, USA

Abstract— Cloud properties have strong spatial gradients, thus the radiative transfer in a cloudy atmosphere is a three-dimensional (3D) problem. It is known that the 3D radiative effects of clouds can increase substantially the clear-sky reflectance. Currently, different modifications of the independent pixel approximation (IPA), which are based on 1D radiative transfer model, remain a stalwart of the operational aerosol optical depth (AOD) retrievals for two main reasons: (1) this model is computationally inexpensive and (2) information about 3D cloud structure is not commonly available. Since the IPA ignores the 3D cloud effects, the IPA-based retrievals can substantially overestimate AOD for clear-sky pixels. Here we introduce a novel method for AOD retrieval that exploits ratios of reflectances in the visible spectral range and provides an effective way to reduce substantially the 3D cloud effects. To illustrate the potential of the ratio method, we use both the sensitivity study and comparison of retrieved AOD values with independent data collected during the Cloud and Land Surface Interaction Campaign (CLASIC). In particular, the sensitivity studies demonstrate the following. Similar to the traditional IPA-based retrievals, the ratio method has a low computational cost for retrieving AOD. In contrast to the IPA-based retrievals, the ratio method provides much more accurate estimations of the AOD values under broken cloud conditions.

Session 4A2b
Optical Solitons 1

All-optical Soliton-based Processing of Noisy Signals

Sergei K. Turitsyn
Photonics Research Group, Aston University, Aston Triangle, Birmingham, B4 7ET, UK

Abstract— Separation of signal from noise is one of general fundamental research problems that occur in a broad range of scientific and technological applications. Use of nonlinear techniques in this field offers unique opportunities that cannot be realized in linear systems. For instance, nonlinear optical processing might enable a distinction in the optical domain to be drawn between the signal and the noise accumulated in the signal bandwidth — somewhat that is not possible using linear techniques. Optical fiber nonlinearity is of particular interest, because resulting nonlinear systems in some range of parameters are described by well studied soliton models and powerful mathematical techniques can be applied to a variety of physical and technical problems. Note that optical soliton techniques are widely known in context of signal transmission, but their high potential in signal processing is not yet fully exploited. All-optical signal processing holds one of the keys to further progress in high-speed optical communication. The ability to control, manipulate and detect optical phase (even if differential) is of critical importance for development of new approaches and devices in high-speed communication. Stable optical structures with controllable phase such as, e.g., solitons might play a crutial role in design and development of new generation of optical processing devices using signal phase. Recent experimental demonstration of quasi-lossless fiber span that can be used as building blocks of true optical soliton devices has re-created interest to soliton-based signal processing. Practical implementation of ultra-long fibre lasers has opened a way to new applications based on unique properties of such non-traditional optical devices. There is an interesting connection between optical fibre communications and mathematical concept of the nonlinear integrable systems. Compensation of fibre loss continuously with ultra-high precision along the fibre span opens a way to implement integrable soliton systems in a fibre waveguide. I will introduce a concept of noncoherent optical pulse discrimination from a coherent (or partially coherent) signal of the same energy using soliton generation.

Widely Wavelength-tunable Soliton Generation and Few-cycle Pulse Compression with the Use of Dispersion-decreasing Fiber

Alexey Andrianov[1], **Sergey Muraviev**[1], **Arkady Kim**[1], **and Aleksei Sysoliatin**[2]

[1]Institute of Applied Physics, Russian Academy of Sciences
46 Ulyanov st., Nizhny Novgorod 603950, Russia
[2]Fiber Optics Research Center, Russian Academy of Sciences
53 Vavilov st., Moscow 119333, Russia

Abstract— We have demonstrated all-fiber source of both widely wavelength tunable femtosecond solitons and few-cycle pulses as well. The latter is obtained by using the tunable supercontinuum generation and subsequent pulse compression of the femtosecond soliton pulses. It is done in the following three-stage scheme. A silica fiber with slowly decreasing dispersion (DDF) is used for super-broadband wavelength tuning, preliminary pulse compression and pulse shape refinement due to solitonic effects at the first stage. At the second stage, the highly nonlinear dispersion-shifted fiber with a small normal dispersion is spliced to the DDF for supercontinuum generation, which is then compressed to the few-cycle pulse in the fiber compressor. The high efficiency of the pulse transformation in DDFs can be achieved by the joint action of two nonlinear effects: the adiabatic compression of the soliton pulse, occurring due to the fact that the zero-dispersion point in the DDF approaches to the carrier frequency of the pulse, and the soliton Raman self-frequency shift [1]. Stable soliton pulse propagation along the fiber was also observed in numerical simulations where the carrier frequency is permanently detuned from the zero dispersion point which monotonically shifts along the DDF. A simplified theoretical model for the self-frequency shift and pulse duration of the fundamental soliton, which propagates almost parallel to the zero-dispersion line in the spectral domain, reveals existence of a one-parameter set of quasi soliton pulses for which frequency shift and pulse duration depend on its energy only. Energy losses accompanying soliton propagation, as well as disregarded factors leading to a decrease of the pulse intensity, can be compensated by the adiabatic compression of the pulse through the appropriate smooth decrease of the anomalous dispersion coefficient along the fiber. Thus, DDFs can provide efficient conversion of the input pulse regardless of its shape into widely wavelength tunable high quality solitonic pulses, which can be further compressed down to few-cycle durations by using spectral broadening via self-phase modulation in the highly-nonlinear fiber and subsequent recompression in the standard telecom fiber.

The all-fiber experimental setup consists of Er:fiber passively modelocked master oscillator, erbium fiber amplifier, silica DDF and highly-nonlinear normal dispersion fiber with directly spliced short standard single mode fiber used as dispersive compressor. Clear sech-shaped 50-fs solitons with the wavelength tunable in the range of 1.6–2.1 μm were obtained at the output of the DDF. The solitons were used as a pump for the generation of smooth and tunable supercontinuum, which was then recompressed downt to duration of 24 fs corresponding to 4 optical cycles at the central wavelength 1.8–1.9 μm. This design, which we believe to be the first of its kind, can produce widely tunable few-cycle pulses in the range of 1.6–2.1 μm and in near infrared with the use of second harmonic generation.

REFERENCES

1. Andrianov, A. V., A. V. Kim, S. V. Muraviev, and A. A. Sysoliatin, "DDF-based all-fiber optical source of femtosecond pulses smoothly tuned in the telecommunication range," *Laser Physics*, Vol. 11, 1296, 2007.

Gap Soliton Propagation in Extended Oppositely-directed Coupler

A. I. Maimistov[1], **S. S. Ozhenko**[1], **and E. V. Kazantseva**[2]

[1]Moscow State Engineering Physics Institute, Moscow 115409, Russia
[2]Laboratoire de Math'ematiques, INSA de Rouen
B. P. 8, Mont-Saint-Aignan cedex 76131, France

Abstract— A system of two coupled waveguides with opposite signs of the refractive index is known to support the propagation of linear waves with a gap in their spectrum. As result this coupler acts as a mirror: the radiation entering one waveguide leaves the coupler through the other waveguide at the same end but in the opposite direction. For this reason, this device can be called the oppositely-directed coupler. The group velocities of the wave packets propagating in separate waveguides are oppositely directed, while the phase velocities have the same value and direction. If the carrier frequency of a wave is localized inside the gap, then some part of the incident radiation is reflected, while another part of the radiation penetrates and decays inside the waveguide structure. An increase in the electromagnetic wave intensity, for which the nonlinear properties of the medium become noticeable, leads to the formation of coupled wave packets (gap solitons) that simultaneously travel through both waveguides. The analytical expression for gap soliton is found. The interaction between these solitons was investigated by numerical simulations.

Relativistic Phenomena in Interaction of Optical Pulses and Solitons with Radiation in Nonlinear Media

Nikolay N. Rosanov
Institute of Laser Physics, Vavilov State Optical Institute
Saint-Petersburg 199034, Russia

Abstract— When propagating in nonlinear media, high-power pulses and solitons induce in the media inhomogeneities of their characteristics, e.g., refractive index, moving with relativistic speed. Next, even weak probe radiation can reflect on these "relativistic mirrors" which results in essential transformations of the radiation characteristics. The goal of this report is to analyze such the phenomena on the basis of solution of Maxwell's equations [1, 2].

In the approximation of fixed pump, high-power pulses or solitons can be considered as given moving structures unperturbed by the weak probe radiation. In this case the medium inhomogeneities are also fixed, and the problem is reduced to the solution of linear Maxwell's equations for probe radiation propagating in dispersive medium with inhomogeneities moving with light speed. In the talk, first is consider the problem of reflection and transmission of a monochromatic plane wave incident normally on the inhomogeneity of dielectric and magnetic permittivities moving with a fixed speed V in the regime of homogeneous waves (with real wavevectors). The approach is beyond the framework of the traditional for nonlinear optics approximation of slowly varying envelope or profile. Demonstrated is that both the Doppler shift of the frequency of reflected radiation and reflection coefficient tend to infinity when the speed V approaches the phase velocity at the frequency of reflected wave. It corresponds to the threshold of the Vavilov-Cherenkov effect produced by the high-power pulse in the nonlinear medium. Additionally, the problem of the reflected wave frequency ambiguity is discussed (the so called complex Doppler effect). Second, the regime of inhomogeneous waves is considered; it is shown that in this case, the reflected wave has a complex frequency. Third, for regimes of weak radiation oblique incidence, calculated is the dependence of reflection angle and the frequency of reflected radiation on the angle of incidence. Finally, possibilities of effective radiation frequency up-conversion on the basis of such the phenomena are discussed.

REFERENCES

1. Rosanov, N. N., *JETP Lett.*, Vol. 88, 501, 2008.
2. Rosanov, N. N., *JETP*, Vol. 108, 141, 2009.

Soliton Resonances in Dispersion Oscillating Optical Fibers

Andrey Konyukhov[1], **Leonid Melnikov**[1], **Vladimir Khopin**[2], **Vladimir Stasuyk**[3], **and Alexej Sysoliatin**[4]

[1]Saratov State University, Saratov, Russia
[2]Institute of High Purity Substances, N. Novgorod, Russia
[3]Pritel, Naperville IL, USA
[4]Fiber Optics Research Center, Moscow, Russia

Abstract— The single mode fibers with chromatic dispersion varying along the length are attracting a considerable attention due to their value for optical soliton processing and applications in stable and ultrafast fiber lasers. For instance, dispersion decreasing fibers (DDF) have been recognized to be useful for high-quality soliton pulse compression and stable against pump noise continuum generation. Undoped fibers with varying normal dispersion are an efficient medium for similariton and coherent continuum generation. In this work we propose a novel method to generate and control the ps and subps optical pulses by its amplitude and width in dispersion oscillating fiber. We present both the numerical simulation and experimental results. The dispersion variation $D(z)$ of the fiber along its length is described by sine-wave function:

$$D(z) = D_0(1 + d_m \sin(2\pi z/z_m + \varphi_m)), \tag{1}$$

where D_0 is initial dispersion value, d_m is the modulation depth, z_m is the modulation period, φ_m is the modulation phase.

Dispersion oscillation provide splitting of high-order solitons. In experiments the splitting of second-order soliton was obtained. Each of the input pulse splits into a pair of pulses which carrier frequencies are shifted. This result in generation of a train of picosecond pulses with alternate carrier frequencies. In particular, second-order soliton splits into two pulses which carrier frequencies are located symmetrically with respect to the initial pulse frequency. The separation between carrier frequencies of output pulses depends on the phase of periodical oscillation of the fiber dispersion. The dispersion oscillating fibers (DOF) have been fabricated from standard optical preforms. It is possible to produce fibers with a prearranged length dependence on the outer diameter and dispersion with necessary accuracy. During the drawing process information about the current diameter is processed by digital control unit and compared with a value of the set. The dispersion deviation from the prearranged value is less than 0.1 ps/nm/km.

Experimental observations are agree with numerical simulations. The model includes the Raman self-frequency shift, third-order dispersion, and nonlinear dispersion as well as modulation of fiber parameters. The fibers with oscillating along length dispersion can have the different applications in optical signal processing (like LC-contour in microwave).

Session 4A3
Nanophotonics: Materials and Device Applications 1

Engineering Photons in Nanostructures: Energy Conversion and Nonlinear Dynamics

Chee Wei Wong
Optical Nanostructures Laboratory, Center for Integrated Science and Engineering
Solid-State Science and Engineering, and Mechanical Engineering, Columbia University
New York, NY 10027, USA

Abstract— Recent important advances in subwavelength optical nanostructures offer extraordinary control over the properties of light. We can now manipulate the generation, conversion, and dynamics of photons in engineered nanostructures directly from geometry, as well as practically prescribe its light-matter interaction based on first principles.

Photonic crystals, in particular, offer the arbitrary control of dispersion and strong localization of light in subwavelength modal volumes. First, we will present our observations of negative-refraction sub-diffraction imaging and zero-index band gaps in photonic crystal superlattices. Second, we will describe our measurements of high quality factors at 1,000,000 or more in these optical cavities. These long photon lifetimes, together with the high-field intensities per photon, permit studies of nonlinear optics at low threshold powers, involving for example our observations of Raman scattering and femto-joule optical bistability. Enhanced spontaneous Raman scattering was also recently observed by our group in slow-light photonic crystal waveguides, where a double slowlight region was achieved, characterized in our measurements with good matching with our theoretical and numerical models.

Furthermore, we will present our recent studies in nonclassical optics in chipscale nanostructures, involving interactions of near-infrared quantum dots with our optical cavities. We present our observations of enhanced spontaneous emission at cryogenic and room-temperatures. We advance the cavity quantum electrodynamical interactions as possible efficient sources of single photons, and proposed schemes for controlled quantum logic gates for quantum information processing. In this section, we will also describe dynamical Forster energy transfer between quantum dots observed during our time-resolved and spectrally-resolved experiments. Surprisingly high quantum efficiencies can be achieved with temperature tuning. These studies have implications for exciton generation in quantum dot thin-film solar photovoltaics.

Light Localization and Light-matter Interaction in Photonic Crystal Microcavity

Tomoyuki Yoshie and Lingling Tang
Duke University, USA

Abstract— Among available microcavity designs, a photonic crystal is a major focus of localizing light in sub-wavelength-dimensions. The most popular photonic crystal system has been a two-dimensional (2D) photonic crystal slab cavity, thanks to the development of simple, high quality (Q) factor resonator designs since the demonstration of photonic crystal laser in 1999. Vacuum Rabi splitting was demonstrated on a single quantum dot coupled to a single-mode 2D photonic crystal microresonator. The observed interaction rate g, which is proportional to a square root of volume, was as high as 20.6 GHz for $Q \sim 10,000$ and $V \sim 8\ (\lambda/2n)^3$, where V, λ and n are the mode volume, the wavelength of light in vacuum and the refractive index in a maximum field position. However, due to the imperfect optical confinement resulting from an escaping light cone, the Q factor is limited even for a structure with an infinite number of layers. The maximum Q factor is dependent upon the mode volume. Thus, it is still a challenge to build ultra-high-Q (UHQ) resonators as the mode volume approaches $(\lambda/2n)^3$. One promising solution is to use a complete photonic band gap (PBG) provided by 3D photonic crystal. Due to its property of omnidirectional confinement of light, the Q factor can increase as an increase in the passive photonic crystal size unless other physical mechanism limits it. The authors will discuss their recent advance in improving the quantum coherence in photonic crystal nanocavities coupled with a single quantum dot and efforts in developing low-loss 3D photonic crystal nanocavities.

Germanium Photonic Devices on Silicon for Optical Modulators

Yu-Hsuan Kuo[1,2], **Yin-Shun Li**[2], **and Tsang-Long Chen**[2]

[1]Department of Electrical Engineering, National Taiwan University, Taipei 10617, Taiwan
[2]Graduate Institute of Electronics Engineering, National Taiwan University, Taipei 10617, Taiwan

Abstract— The optical interconnects with silicon-compatible photonic devices can enable high-speed interconnects for silicon chips. One challenge is to develop optical modulators in the transmitter end for encoding the laser signal at high data ate. Germanium is a silicon-process-compatible material and possesses III-V-like direct-gap transition characteristics with high absorption coefficient. In this report, we present recent studies in the excitonic absorption behaviors of the Ge quantum well system and in the novel Ge thermo-optic modulator, both of which are critical to enable high-performance modulators integrated with the silicon platform.

The Ge quantum-confined Stark effect (QCSE) utilizes the strong electric-field-dependence of excitonic absorption in the Ge quantum well. The variational method is used here to evaluate the exciton behavior and optical oscillator strength for various well thicknesses and electric fields simultaneously. The relative contrast ratio between the direct-gap absorption and indirect-gap background absorption is compared, indicating a relatively wide quantum-well thickness design range for the Ge QCSE modulators. Ge also has one-order-higher thermo-optic coefficient than silicon at 1550 nm, owing to its strong absorption edge at 0.8 eV. We have fabricated a vertical Fabry-Perot thermo-optic modulator based on Ge-on-insulator-on-silicon with a buried metal reflector, which exhibits strong resonance and high contrast ratio (> 8 dB) in the C-band with low operation voltage swing.

ACKNOWLEDGMENT

This research was supported by National Science Council (NSC-96-2221-E-002-267-MY3 and NSC-96-2221-E-002-272-MY2).

Nanoscale Plasmonic Probes for Advanced Microscopy

G. Zoriniants[1], **W. L. Barnes**[1], **C. W. See**[2], **C. Chin-Jung**[2], **S. Liu**[2], **and M. Somekh**[2]

[1]School of Physics, University of Exeter, Stocker Road, Exeter EX4 4QL, UK
[2]School of EEE, University of Nottingham, University Park, Nottingham, NG7 2RD, UK

Abstract— Gold nanostructures support localized surface plasmon resonances that can be used in advanced near-field optical spectroscopy. We manufactured and tested dimers of nanorods that have tuneable hybrid plasmonic modes and switchable arrays of nanorods to achieve superresolution via structured illumination.

Nanoparticles of noble metals exhibit localised surface plasmon resonances (LSPR) at optical frequencies. The electric field in the vicinity of a nanoparticle is strongly localized and enhanced. Nanoparticles have been widely used as probes to enhance the signal and resolution in fluorescence microscopy, Raman spectroscopy, and magneto-optical near-field microscopy. Recently, it became clear that simple objects like spheres or cylinders offer limited possibilities to tune their plasmonic properties. We report on manufacturing and testing of more complicated nanostructures that have unique plasmonic properties, including field distribution and strength.

For near-field fluorescence microscopy and spectroscopy, it is essential to have strongly localized fields. Also, the LSPR resonance has to match the absorption or/and emission of the chosen dye. Using electron-beam lithography (EBL), we manufactured nanostructures that consist of dimers of gold nanorods with an extremely small gap between them (typically 50–20 nm, down to 2 nm, and overlapping particles), see Figure 1(a). We showed that, in agreement with previous theoretical and experimental studies, the LSP resonance of the dimers shifts with the change of the gap size, and this depends on the relative orientation of the rods and the electric field. We demonstrated a clear correlation of the enhanced fluorescence intensity with the scattering efficiency at the frequency which was used to excite the fluorescence. This indicates that the dominant mechanism of the fluorescence enhancement in the system studied is the coupling of the incident excitation light to the plasmonic mode of the dimer [1].

Traditional scanning probe techniques, such as SNOM, suffer from slow imaging rate and low data throughput as a single nanometre-sized tip has to probe all points of the sample. We propose to use an array of identical gold nanoantennae to image microscopically large areas in a parallel way.

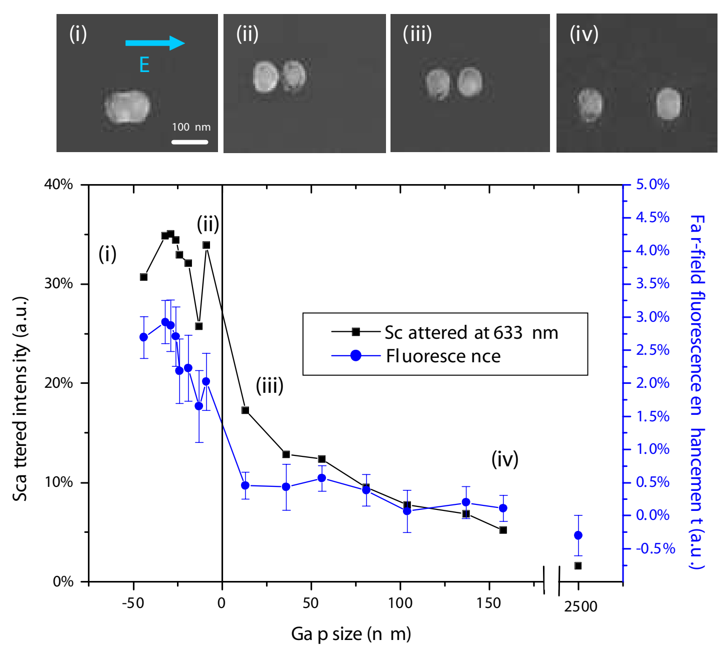

Figure 1.

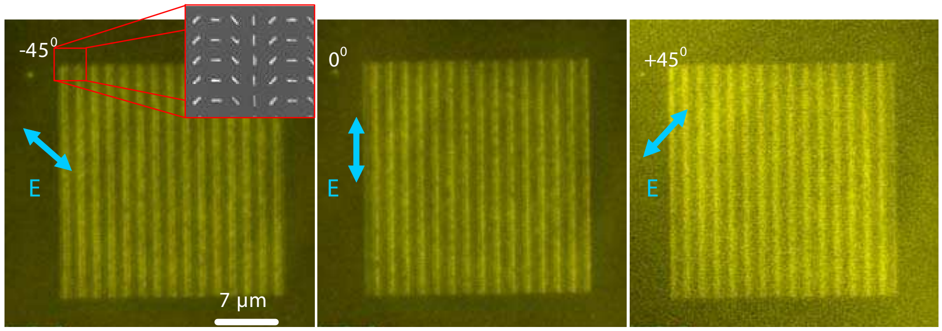

Figure 2.

It is known that the resolution of far-field optical microscopy can be improved by using structured illumination and subsequent digital recovery of higher spatial harmonics of the object from the moir pattern. However, the classical structural illumination is done by interference of plane waves, so the maximum improvement of the resolution in linear optical processes is limited by a factor of 2 [2]. We propose to use an array of lithographically produced nanoparticles to create the structured illumination pattern in the near-field. The spatial frequency of the array is limited only by EBL, so the resolution enhancement can be much higher than a factor of 2. However, for recovery of the ultra-resolved image it is essential to take a few shots with different spatial phase of the structured illumination: this is easy in the case of standing waves, but problematic in the case of lithographic arrays, where the particles are rigidly attached to the substrate. We propose a way to overcome this problem by introducing switchable arrays of nanorods.

To realise this concept, we manufactured arrays of gold nanorods where the orientation of the rods was gradually changing (see inset in Figure 2). LSPR of each rod is closely related to its symmetry: there are two distinct modes associated with the long and the short axes of the rod. We used linear polarized light with a frequency that corresponds to the long-axis resonance. Thus, only the rods that have a field component parallel to their long axis are excited. Varying the polarization of the incident light, we can shift the maximum of the near field intensity in the plane of the sample. This effect was visualised by placing a thin layer of dye-labelled polymer in the near-field created by the nanoparticle array (see Figure 2). We will show how we have used this technique to image a test object thereby demonstrating the feasibility of this approach.

REFERENCES

1. Zoriniants, G. and W. L. Barnes, *New Journal of Physics*, Vol. 10, 105002, 2008.
2. Gustafsson, M. G. L., *PNAS*, Vol. 102, 13081, 2005.

Metal Nanoantennas and Dielectric Microresonators for Solid-state Quantum Optics

R. Bratschitsch
Department of Physics and Center for Applied Photonics (CAP)
University of Konstanz, Germany

Abstract— The efficient coupling of light from the far field into nanometer sized objects is one of the fundamental challenges in current nanooptics. We present two ideas to reach this goal. On the one hand, we place the nanoobject (in our case a colloidal semiconductor quantum dot) into an optical micropillar resonator [1]. Three-dimensional light confinement is observed. Calculations of the cavity modes by modeling the pillar microcavity as a waveguide with an effective refractive index are in excellent agreement with the measurements. The concept is extended into the ultraviolet region of the electromagnetic spectrum and the first dielectric pillar microcavity with colloidal ZnO quantum dots is demonstrated [2]. On the other hand, we fabricate metal optical nanoantennas by various techniques (electron-beam lithography, focused ion beam milling, and colloidal masks). In particular, we present a tunable bowtie optical nanoantenna which consists of two gold nanotriangles [3]. The feedgap can be continuously varied by manipulation of an antenna arm with nanometer precision via an atomic force microscope. At the same time the optical response of the nanoantenna is determined via darkfield scattering spectroscopy. Exciting with ultrafast laser pulses, we investigate the nonlinear optical properties of single metal nanoantennas.

Both concepts are suitable not only for semiconductor quantum dots but also for other nanoemitters of light, such as defect centers in diamond nanocrystals [4], carbon nanotubes, or organic dye molecules. This route may lead to a new class of ultrafast optical quantum devices based on single nanoobjects.

REFERENCES

1. Kahl, M., T. Thomay, V. Kohnle, K. Beha, J. Merlein, M. Hagner, A. Halm, J. Ziegler, T. Nann, Y. Fedutik, U. Woggon, M. Artemyev, F. Pérez-Willard, A. Leitenstorfer, and R. Bratschitsch, "Colloidal quantum dots in all-dielectric high-Q pillar microcavities," *Nano Lett.*, Vol. 7, 2897, 2007.
2. Thomay, T., T. Hanke, M. Tomas, F. Sotier, K. Beha, V. Knittel, M. Kahl, K. M. Whitaker, D. R. Gamelin, A. Leitenstorfer, and R. Bratschitsch, "Colloidal ZnO quantum dots in ultraviolet pillar microcavities," *Opt. Express*, Vol. 16, 9791, 2008.
3. Merlein, J., M. Kahl, A. Zuschlag, A. Sell, A. Halm, J. Boneberg, P. Leiderer, A. Leitenstorfer, and R. Bratschitsch, "Nanomechanical control of an optical antenna," *Nature Photonics*, Vol. 2, 230, 2008.
4. Balasubramanian, G., I. Y. Chan, R. Kolesov, M. Al-Hmoud, J. Tisler, C. Shin, C. Kim, A. Wojcik, P. R. Hemmer, A. Krüger, T. Hanke, A. Leitenstorfer, R. Bratschitsch, F. Jelezko, and J. Wrachtrup, "Nanoscale imaging magnetometry with diamond spins under ambient conditions," *Nature*, Vol. 455, 648, 2008.

Enhanced Raman Light Scattering by a Dipole Placed between Two Metallic Nanoparticles

P. I. Geshev
Institute of Thermophysics, Lavrentyev Ave. 1, Novosibirsk 630090, Russia

Abstract— Opened twelve years ago, in colloidal solutions of silver nanoparticles (NPs) the Single Molecule Surface Enhanced Raman Scattering (SM-SERS) can reach enhancement factors $EF = 10^{14}$ (Kneipp et al., Nie, Emory, Xu et al. [1-3]). It allows detect a Raman signal from an individual molecule adsorbed in the gap between the NPs. In our report, the scattering problem is considered for axially symmetrical Bessel beam (BB) and for a dipole placed between two metallic NPs (Fig. 1(a)) or between Scanning Tunnel Microscope (STM) tip and a thin metallic film covering a dielectric substrate (Fig. 1(b)). The last scattering configuration is used in Tip Enhanced Raman Scattering (TERS, Pettinger, [4]). Calculations were performed by the boundary element method based on Green's function of Helmholtz equation for layered medium, [5, 6]. The metallic NP closely placed at the film surface acts as nanoantenna. Plasmons excited in the particle and film convert the incident propagating EM field into non-propagating evanescent near-field. For small gaps the field is strongly enhanced and confined in the particle/film gap [6]. Our purpose is: to evaluate the maximal enhancement for SM-SERS and SM-TERS. We also represent new analytical formulae for resonant plasmon frequencies in the two sphere scattering system (Fig. 1(a)) obtained in non-retardation approach.

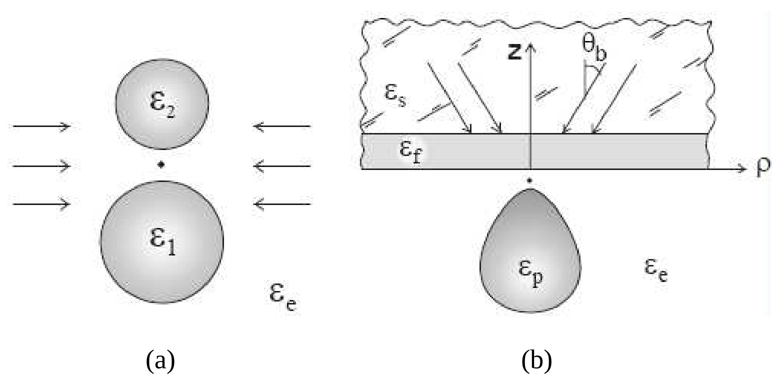

Figure 1: Scheme of light scattering systems.

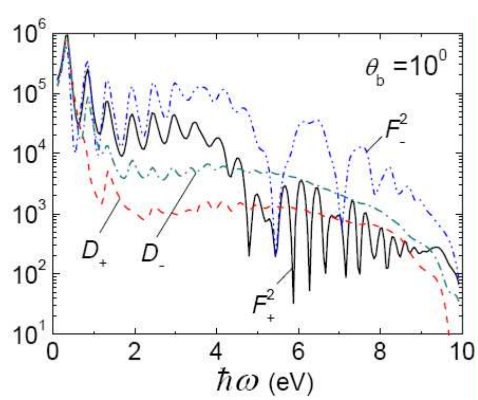

Figure 2: Spectra of relative enhancement factors F^2 and D vs. photon's energy for long Al nanorod (diameter 100, length 1000 nm, ended by semi-spherical caps); the BB illumination angle is 10^0. Signs +, − designate upper and lower semi-space in Fig. 1(b), respectively, from that one the illumination comes (F^2), or to that one the dipole radiation goes (D).

An enhanced field at the dipole position and a dipole radiation into the upper and lower semi-spaces (Fig. 1(b)) are considered. By dividing the calculated field intensity and dipole radiation flux on the same values obtained without NP, the relative enhancement factors F^2 and D, respectively, are introduced in [7], as natural measures for enhancement caused by NP. The total enhancement factor is represented as $EF = F^2D$. Special attention is devoted to large and long NP (nanorod) made of aluminium (Al) as a good plasmonic material. Our results for F^2 and D (see Fig. 2) show that the calculated total enhancement factor EF for TERS can reach huge values $\sim 10^{10} \div 10^{12}$ for gaps $g \sim 1$ nm.

In this report, the angular distribution of dipole radiation $f(\theta)$ and its correspondence to the known Optical Reciprocity Theorem (ORT) is studied. By direct calculation of the distribution function $f(\theta)$ the validity of ORT was demonstrated. It is strong confirmation of quality of our calculations and also the direct indication on the validity of the "4-power law" often simply assumed in SERS and TERS: $EF \sim E^4$, where E is the electric field at the dipole's position.

REFERENCES

1. Kneipp, K., et al., *Phys. Rev. Lett.*, Vol. 78, 1667, 1997.
2. Nie, S. and S. R. Emory, *Science*, Vol. 275, 1102, 1997.
3. Xu, H., et al., *Phys. Rev. Lett.*, Vol. 83, 4357, 1999.
4. Pettinger, B., et al., *Single Molecules*, Vol. 3, 285, 2002.
5. Geshev, P. I., et al., *Phys. Rev. B*, Vol. 70, 075402, 2004.
6. Geshev, P. I. and K. Dickmann, *J. Opt. A: Pure Appl. Opt.*, Vol. 8, S161–S173, 2006.
7. Geshev, P. I., et al., *Optics Express*, Vol. 15, 13796, 2007.

Enhancement of Magneto-optical Effects of Au Particles and Bi : YIG Composite Films

H. Uchida, Y. Mizutani, Y. Masuda, A. V. Baryshev, and M. Inoue
Toyohashi University of Technology, Tempaku, Toyohashi, Aichi 441-8580, Japan

Abstract— Localized surface plasmon resonance (LSPR) is excited by coupling between light and electron wave in noble metal particles. So far, magneto-optical effects affected by plasmon were reported in metallic magnetic layer1, nano-onion2 and Au particles/YIG granular film3. In our study, enhancement of Faraday rotation assisted by the LSPR was observed in Au particles and magnetic B : YIG composite films4. In the article, we describe fabrication method of a composite film to obtain large enhancement of the Faraday rotation. A repeated particle formation was used to control size and number density of Au particles, which are strongly related to wavelength and strength of the LSPR.

Au particles were prepared by using the repeated particle formation using 5 nm Au thin films on fused quartz substrates. An Au film was heated at a temperature of 1000°C in an electric furnace in air for 10 min. We obtained diameter distributions of fabricated Au particles by using SEM. When the repetition number was one (total Au thickness of 5 nm), a curve of diameter distribution for the Au particles was narrow with a full width at half maximum (FWHM) of 25 nm and a mean diameter of 48 nm. With increasing the repetition number, diameter distribution of the Au particles separated to two groups with small and large diameters. In the transmittance spectra, attenuations around wavelength of 520 nm were observed, which correspond to absorption of light by excitation of the LSPR.

On the Au particles formed on the substrates, $Bi_{0.5}Y_{2.5}Fe_5O_X$ films with thicknesses of 60 nm were deposited by using a RF magnetron sputtering system, and then the samples were heated at 750°C for one hour to crystallize the garnet films. In the fabricated composite films with Au particles and Bi : YIG, the magneto optical effects were enhanced around the wavelength of LSPR. With increasing the repetitive number, the Faraday rotation angle increased. Especially, large enhancement of Faraday rotation of $-0.94°$ was obtained for the composite film formed by the five times repetitive formation, which was 15.6 times larger than one of the single Bi : YIG film.

REFERENCES

1. Feil, H. and C. Haas, *Phys. Rev. Lett.*, Vol. 58, 65, 1987.
2. Abe, M. and T. Suwa, *Phys. Rev. B*, Vol. 70, No. 23, 235103-1-15, 2004.
3. Tomita, S., T. Kato, S. Tsunashima, S. Iwata, M. Fujii, and S. Hayashi, *Phys. Rev. Lett.*, Vol. 96, 167402, 2006.
4. Uchida, H., Y. Masuda, R. Fujikawa, A. V. Baryshev, and M. Inoue, *J. Mag. Mag. Mat.*, in press.

Enhanced Surface Plasmon Effects Excitation from Several Pair Arrays of Nanoshell Structurers

Yuan-Fong Chau[1], **Din Ping Tsai**[2], **and Tzong-Jer Yang**[3]

[1]Department of Electronic Engineering, Ching Yun University, Jung-Li 320, Taiwan, R.O.C.
[2]Department of Physics, National Taiwan University, Taipei 10617, Taiwan, R.O.C.
[3]Department of Electrical Engineering, Chung Hua University, Hsinchu, Taiwan, R.O.C.

Abstract— We studied numerically the performance of surface plasmon effects by employing several pair arrays of silver-shell nanocylinders. The optical properties of the proposed structures are discussed in detailed with respect to the field enhancement in the gap between the nanoparticle pairs. Effects from different number of pair arrays, interparticle distance, interpair distance, and the thickness of nanoshell are studied by using the finite element method. Compared to the pair arrays of solid silver nanocylinders, the near-field optical response of the nanoshell structures exhibits electric field enhancements and red-shift which are found to be strongly influenced by tuning the radius of the air-hole in the nanocylinders. This is attributed to the large field enhancement within metallic nanoshell structures, as well as to far-field effects, which play an important role in field enhancement along the pair arrays of nanoshell structurers.

Electrodynamics of Plasma Oscillations in Nanotransistor Arrays

V. V. Popov
Kotelnikov Institute of Radio Engineering and Electronics
Saratov Branch, Saratov 410019, Russia

Abstract— Terahertz (THz) response of field-effect nanotransistors (FENTs) with two-dimensional (2D) electron channels is strongly affected by plasma oscillations exited in the channel under the gate electrode. This phenomenon in its various manifestations can be used for the detection and generation of THz radiation.

Two different types of 2D plasma oscillations exist in a FENT structure. They are plasma oscillations excited in gated or ungated regions of the electron channel which are termed as gated and ungated plasmons, respectively. The gated plasmons have linear (acoustic) dispersion while the frequency of ungated plasmons is proportional to the square root of their wavevector. The gated plasmons were considered to be more attractive for electronic applications because their frequencies can be effectively tuned by varying the gate voltage. However, simple estimations show that the frequency of the fundamental plasmon mode ($n = 1$) may exceed 5 THz only in a FENT with the gate shorter than 100 nm, which sets a limitation for designing the single-gate FENT plasmon devices in the high-frequency THz range. Another problem to be solved is how to effectively couple the gated plasmons to THz radiation. Unfortunately, the gated plasmons in a single-gate FENT are weakly coupled to THz radiation because they have a vanishingly small net lateral dipole moment due to their acoustic nature (in this mode, electrons oscillate out-of-phase in the gate contact and in the channel under the gate). Higher-order gated-plasmon modes ($n > 1$) have greater frequencies but even a smaller net dipole moment as compared to the fundamental plasmon mode. Hence, the higher-order gated plasmon modes in a single-gate FENT can hardly be used for increasing the operation frequency of a single-gate THz plasmonic nanotransistor.

In this paper, we show that the coupling between 2D plasmons and THz radiation in the FENTs arrays may be strongly enhanced due to synchronizing the plasma oscillations in all FENT units and formation a cooperative plasmon mode over the entire FENT array. Due to the strong coupling between plasmons and THz radiation, intensive higher-order plasmon resonances (up to the tenth order) can be effectively excited in high-frequency terahertz range (up to 15 THz) in the array of FENTs [1–3]. We consider in this paper two different types of FENT arrays: the FENT array with a common channel and a large-area grating gate and the array of FENT units having separate channels and combined intrinsic source and drain contacts. These results open a gateway to designing the FENT plasmonic devices in the high-frequency THz range up to 15 THz and even higher.

REFERENCES

1. Popov, V. V., et al., "Absorption of terahertz radiation by plasmon modes in a grid-gated double-quantum-well field-effect transistor," *J. Appl. Phys.*, Vol. 94, No. 5, 3556–3562, 2003.
2. Popov, V. V., G. M. Tsymbalov, D. V. Fateev, and M. S. Shur, "Cooperative absorption of terahertz radiation by plasmon modes in an array of field-effect transistors with two-dimensional electron channel," *Appl. Phys. Lett.*, Vol. 89, No. 12, Art. No. 123504, 2006.
3. Popov, V. V., G. M. Tsymbalov, D. V. Fateev, and M. S. Shur. "Higher-order plasmon resonances in GaN-based field-effect-transistor arrays," *Int. J. High Speed Electronics and Systems*, Vol. 17, No. 3, 557–566, 2007.

Toward a New NanoLIFT Transfer Process

L. Hallo[1], **C. Mezel**[1], **A. Bourgeade**[2], **and J. Breil**[1]

[1]CELIA, France
[2]CEA, France

Abstract— Electron generation and heating in dielectrics such as silica is a well known phenomena. The control of the deposited energy in the material allows to predict, thanks to models, its behaviour when submitted to a femtosecond, ultra-intense laser shot.

A self-consistent model is developed that describes ionization process in dielectrics with ultraviolet to infrared laser beams. The energy deposition is described by a full set of Maxwell's equations in the three-dimensional geometry and it accounts for non-linear propagation phenomena in the femtosecond time scale. Ionization is described first with multiphoton ionization, then electrons are heated by Joule effect and perform collisional ionization provided they get enough energy. Then, the calculated energy deposition is transferred to an hydrodynamic code that describes the shock and compression waves formation and expansion in the material.

In untrammeled backgrounds, sub-micron cavities are formed. Comparison to experiments carried out in silica and sapphir have permitted a good understanding of this process, and parameters of laser energy release and cavity formation are now well known in silica.

The above method is now applied to a confined background, where cavity expansion leads to a jet formation at the interface. The dielectric used is water, as applications in biomedecine are under consideration. The aim is to understand the process of transfer of cells and biomolecules via LIFT (Laser-Induced Forward Transfer) technique. In this technique, the biomaterial to be transfered is deposited on a target submitted to a laser shot, and the ejecta are collected at the backsurface on a substrate.

Currently performed with nanosecond lasers, this technique would be useful in tissue engineering and provides the main advantage of controlling the amount of material transferred. Thanks to an hydrodynamic code, simulations have been carried out with a nanosecond ultraviolet laser and the jet diameter (10 microns) and velocity (tens of meter/second) are comparable to that obtained in experiments. A correlation between the cavity diameter and the jet diameter has been established, both being of the same ordre of magnitude.

The objective is to transfer the smallest possible amount of biomaterial (molecules for instance), that means the smallest possible jet diameter. Using the LIFT technique with femtosecond lasers would be of great interest since the cavities obtained are much smaller than those obtained with nanosecond lasers. Jet formation in the nanosecond regime is first presented from a modeling point of view and compared with experiments. Improvement of the technique using femtosecond laser pulse is then investigated and leads to the formation of jet of diameter hundred of nanometers. This new regime is called nanoLIFT technique. Finally, influence of parameters such as laser energy, pulse duration, beam waist and released energy zone on the process of jet formation is analysed in order to predict futur experimental results.

Session 4A4
Biomedical Electromagnetism Instruments, Electromagnetism Condensed Materials and Imaging 2

Waveguide System for Whole-body Exposure of Unrestrained Small Animals

Lukáš Víšek and Jan Vrba
Department of Electromagnetic Field, Czech Technical University
Technická 2, Prague 166 27, Czech Republic

Abstract— The rapidly increasing use of sophisticated devices emitting microwave electromagnetic field, mobile phones in particular, has raised public concern about possible harmful health impacts.

The main aim of this work is the design, optimization, realization and verification of the whole-body exposure setup for unrestrained small animals to radiofrequency electromagnetic field.

The setup operating at 900 MHz was designed with respect to induced uniform field, external radiation elimination, accurate absorbed power determination, sufficient space for mice, even mice exposure and costs. Previously mentioned conditions assure an accurate Specific absorption rate (SAR) determination together with the elimination of stress induced in mice.

The setup consists of circular waveguide chamber terminated by matched loads. The electrical resistance of the matched load should grow linearly in a direction of the wave's propagation. Therefore the shapes of matched loads are conical and are made of plastics filled up with salted water. The loads serve for preventing from possible unwanted resonances between mouse and waveguide's bottoms. The circular polarized wave is excited in the waveguide. This wave is comprised by two monopoles which are mutually orthogonal oriented. Circular polarized wave provides relatively constant coupling of the field to each mouse regardless of its position, posture or movement. There are two other monopoles serving for scatter parameters measurement. There is a ventilation hole through which electric fan-forced ventilation air is introduced and exhausted through second hole in order to reduce the mouse's stress and maintain constant temperature inside the waveguide.

The setup basic properties such as electromagnetic field distribution and impedance matching were optimized and verified by 3D simulator of EM field based on the finite-difference-timedomain method (FDTD). The dosimetry results were obtained in conjunction with homogenous mouse model and experimental validation was based on analysis of measured scatter parameters.

ACKNOWLEDGMENT

This research is supported by Grant Agency of the Czech Republic, project: "Non-standard application of physical fields — Analogy, modeling, verification and simulation" (102/08/H081) and by Internal Grant of the CTU in Prague.

Application of Bioradiolocation for Estimation of the Laboratory Animals' Movement Activity

L. N. Anishchenko[1], **A. S. Bugaev**[2], **S. I. Ivashov**[1], **and I. A. Vasiliev**[1]

[1]Remote Sensing Laboratory, Bauman Moscow State Technical University, Russia
[2]Moscow Institute of Physics and Technology, Russia

Abstract— Radiolocation of biological objects named as bioradiolocation is an intensively developing area in radio engineering. There are some medical engineering problems which could be solved by means of radiolocation, among them are disaster medicine (searching of survivals under debris and rubbles of buildings), monitoring of breath and heart beating parameters for burned patients (it would cut down the number of used contact censors and thus decrease the risk of infection inoculation into burning wounds), sleep apnea diagnostics, monitoring of breath and heart beating parameters for sick persons, which are the carriers of extra-hazardous infections (it would decrease the risk of medical staff infection), and etc [1, 2].

Besides the over listed fields of application there is an interest in usage of bioradiolocation for remote diagnostics of rats and other laboratory animals by estimation of their moving activity in time of zoo-psychological experiments.

At present, invasive methods of physiological parameters determination are used during testing of some medicine and poisonous substances on laboratory animals. Their moving activity used to be estimated visually by researcher. Another method is currently in use for animals' behavior reaction analysis. Specially designed video tracking system such as Ethovision [3] can be applied to decrease a workload of the researcher and create automatic approach to estimation of moving activity. The main disadvantage of this type of systems is necessity to use sophisticated software and some restriction on long time recording with duration more than several hours because of data storage capacity limitations. So, that is why in most cases estimation of rats' moving activity is carried out by researcher visually [4], which might cause in the quality of obtained information.

Doppler radar has advantage of direct measurements of animal's moving parameters. It can be used for creation of a fully automatic moving activity integral estimation procedure. In this case the size of data is so small comparing to the video file that it would allow to record data continuously during several days or more. Moreover in condition of creation special recognition algorithms of radar signals that were reflected from animal, it would be possible to discriminate different types of its movements (horizontal and vertical activities, grooming, steady state). In that case bioradiolocation can be also applied to data analysis of the open field experiments.

REFERENCES

1. Staderini, E. M., "UWB radars in medicine," *IEEE Aerospace and Electronic Systems Magazine*, 13–18, January 2002.
2. Ivashov, S. I., V. V. Razevig, A. P. Sheyko, and I. A. Vasilyev, "Detection of human breathing and heartbeat by remote radar," *Progress In Electromagnetics Research Symposium*, 663–666, Pisa, Italy, March 28–31, 2004.
3. Site of the firm Noldus, Ethovision 3.1. http://www.noldus.com/animal-behavior-research/products/ethovision-31.
4. Cieślar, G., J. Fiolka, J. Mrowiec, et al., "Influence of long-term exposure to static, high voltage electric field antioxidant activity in rats," *XXVIIIth General Assembly of the International Union of Radio Science 2005*, New Delhi, India, 2005. http://rp.iszf.irk.ru/hawk/URSI2005/pdf/K06.1(0462).pdf.

Extension of Whole-Heart Model by Coupling with Human Ventricular Cell Model

E. Ryzhii[1], **M. Ryzhii**[2], **and D. Wei**[1]

[1]Biomedical Information Technology Laboratory, University of Aizu, Japan
[2]Computational Nanoelectronics Laboratory, University of Aizu, Japan

Abstract— The experimental possibilities for studying cardiac arrhythmias in human ventricular myocardium are very limited. Thus, the utilization of computer simulation is an important alternative method.

In this work, we extend the 3D Wei-Harumi whole-heart model by coupling with ion channel human ventricular cell model developed by ten Tusscher et al.. We adopted the model of the action potential of human ventricular cells to simulate sex differences in accordance to experimental data for male and female hearts of different species. Using the extended model the surface 12-lead Electro-cardiogram (ECG) waveforms were simulated. The obtained results conform adequately to the available clinical reports.

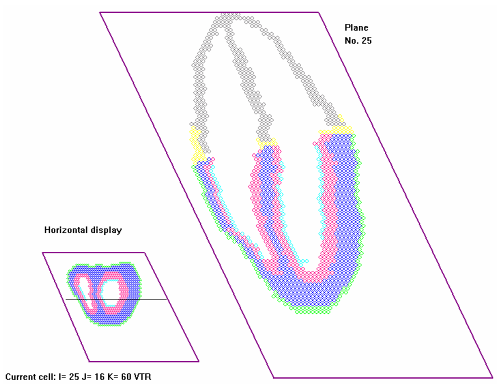

Figure 1: Frontal and horizontal cross sections of the whole-heart model.

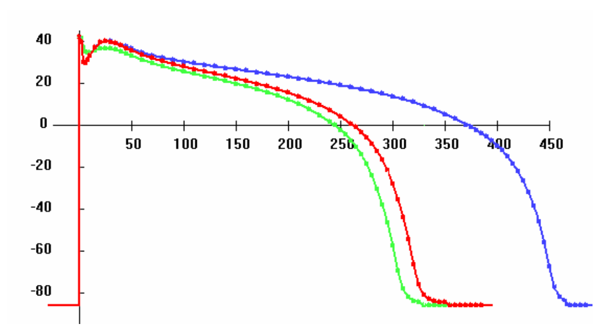

Figure 2: Normal action potentials for female case.

The developed extended model can reproduce a variety of electrophysiological behaviors and provides a good basis for understanding the genesis of ECG under normal and abnormal conditions.

Changes in Morphology and Function of Intact and Damaged Articular Cartilage: Evaluation Using Polarization Sensitive Optical Coherence Tomography

Wen-Chuan Kuo[1], **Che-Hung Chan**[1], **Jeou-Jong Shyu**[2], **and Huei-Wen Chen**[1]

[1]Institute of Electro-optical Science and Technology, National Taiwan Normal University
88, Sec. 4, Ting-Chou Road, Taipei 116, Taiwan
[2]Department of Veterinary Medicine, National Taiwan University, Taipei 106, Taiwan

Abstract— This study presents a diagnosing method on articular cartilage using polarization-sensitive optical coherence tomography (PS-OCT). Subsurface structure changes including fine fibrillations and isolated gaps, which are the early signs of cartilage degeneration, were detected by PS-OCT and were confirmed with histology. Through signal analysis, the optical characteristics of the intact and different types of mild lesions within cartilages can also be quantified using measures including scattering coefficient (μ_s), effective anisotropy factor (g_{eff}), and birefringence coefficient (Δn). The μ_s can be though of as the reciprocal of the average distance a photon travels between scattering events. The g_{eff} factor describes how isotropic or anisotropic the scattering is, that is related to the particle size in the specimen. The Δn value characterizes the differential speed of propagation between two orthogonal polarized states of light in specimen; it may change with derangement and mechanical failure of the collagen network in cartilage. Our preliminary investigation of porcine articular indicated that PS-OCT in combination with extracted optical properties support efforts to develop a quantitative diagnosing method in arthritis research, which could be a convenient complement to facilitate qualitative image-based articular cartilage diagnosing methods. In the future, an analysis from a much larger set of specimens will be obtained.

Numerical Simulation of Specific Absorption Rate and Induced Currents in a Rat's Pixel Brain due to Radiofrequency Fields

R. Rojas, S. E. Solis, and A. O. Rodríguez
Centro de Investigacion en Instrumentacion e Imagenologia Medica
Universidad Autonoma Metropolitana
Iztapalapa, Av. San Rafael Atlixco 186, Mexico DF 09340, Mexico

Abstract—

Introduction: The Specific Absorption Rate (SAR) has been adopted as the metric for RF power safety for performing MRI procedures. When the magnetic field is greater than 3 T, the performance of the RF coil is strongly dependent of the interaction with organic tissues, then the rat head/body size becomes comparable to the RF wavelength and the interactions between the tissue and the coil become important, because the eddy currents production are increasing. Mathematical expressions based on the Maxwell equations, can be derived for the simplest cases, but is very difficult derive expressions for more complex geometries. A numerical method based on Finite Element Method (FEM) to compute the electric field and the induced currents in a pixeled rat brain model, and a methodology for SAR calculations is presented here.

Theoretical Background: The SAR is a measure of power dissipated in biological sample and can be defined by:

$$SAR = \textit{Total RF energy dissipated in sample/Exposure time sample weight.} \tag{1}$$

Power losses in the form of Joule heating within the specimen will derive from eddy currents induced by the alternating magnetic field, it is given by:

$$P = 0.5\sigma|E|^2, \tag{2}$$

where σ is the effective conductivity, and $|E|$ is the amplitude of the electric field produced by the sample. Using (2), considering that the loss power is absorbed by tissue, and using there mass density ρ_m (Kg/m^3), the SAR can be determined by:

$$SAR = P/\rho_m = \sigma|E|^2/(2\rho_m). \tag{3}$$

Rojas and Rodriguez proposed a matrix scheme based on FEM to compute the electric and magnetic fields using a commercial software tool.

Method: An anatomical 3D pixel model of the rat brain head was designed, and a single loop coil figure was developed and placed over the rat head model as shown in Figure 1. The electric and magnetic fields were computed with FEM using the tissue electromagnetic properties at 10, 50, 100 and 300 MHz. The coil produce a magnetic field over the pixeled rat brain (Figure 2 shows a 3D coronal cut of the magnetic field over the sample) then the electric current density induced in the head model by the coil was estimated. The electric field were used to assess the SAR with MATLAB.

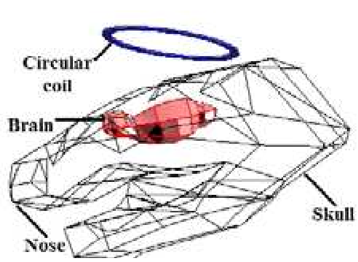

Figure 1: Brain and skull pixel head model, with RF single loop coil.

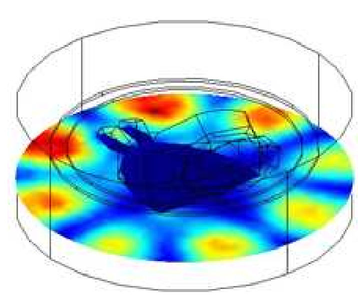

Figure 2: Magnetic field produced over the sample. Coronal cut of pixel head model at 50 MHz.

Results and Discussion: Figure 3 shows the induced currents displaced from the meddle to the surface of the brain, and the intensity are proportional with the frequency. A single surface coil was chosen for simplicity, however it can also be extended to more complex coil configurations such as the birdcage or coil arrays. Other pixel anatomical models for human organs can be constructed and numerically simulated with this method. This numerical method can offer a graphical tool to illustrate the behaviour of the SAR and the eddy currents. Like a validation method, we obtain a MRI of a rat brain using a single surface coil designed and developed in our laboratory, with a GEMS sequence in a 7 T Varian system. Figure 4 shows the single circular coil (left up), coil collocation under the rat head (left down), and the MRI rat's brain (right), in that last we can see the high light intensity on brains border.

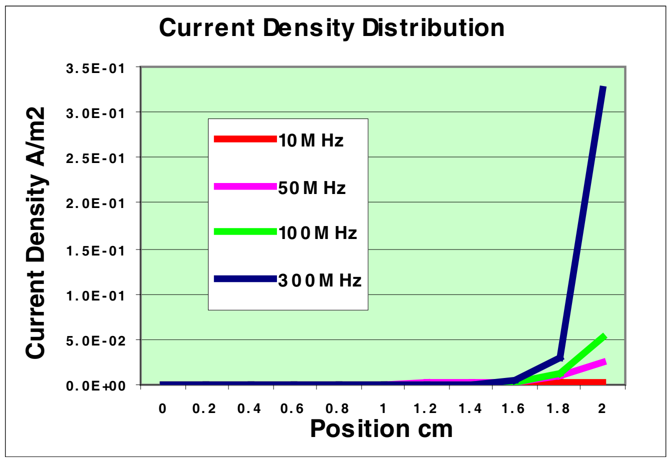

Figure 3: Graphic: distance from meddle to the surface of the pixel rat's brain vs. current density.

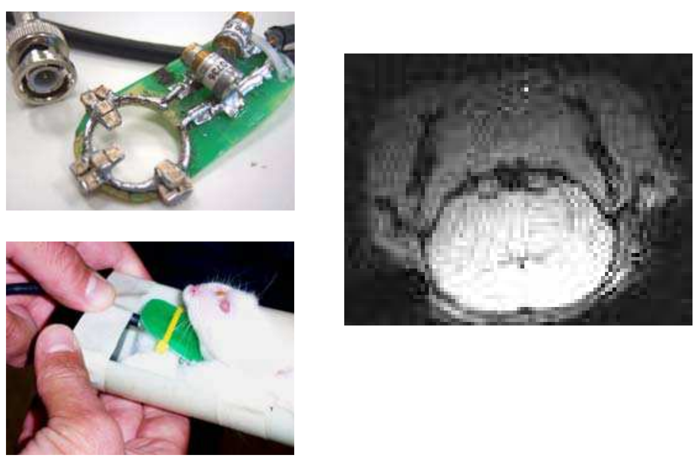

Figure 4: Single circular coil (left up). Rat head collocation (left down). Brain's MRI (right).

Computation of SNR and SAR Based on Simple Electromagnetic Simulations

R. Rojas and A. O. Rodriguez
Centro de Investigacion en Instrumentacion e Imagenologia Medica, Universidad Autonoma Metropolitana
Iztapalapa, Av. San Rafael Atlixco 186, México DF 09340, México

Abstract—

Introduction: The signal-to-noise ratio (SNR) is an accepted to measure RF coil performance. The specific absorption rate (SAR) is the only quantifiable safety measure for RF coils. Analytical expressions based on the Maxwell equations, can be derived for the simplest cases of surface coils, but is very difficult derive expressions for more complex geometries due to the complicated mathematical framework involved in it. The numerical study of the electromagnetic behaviour for MRI coils and biological tissues is a good alternative. A numerical method based on the Finite Element Method (FEM) to compute the electromagnetic fields of single surface coil is presented here. These numerical simulations are the base to finally calculate the SNR and SAR for a circular-shaped coil and, the induced currents generated by it.

Method: An anatomical pixel model of the human head (brain and skin) was designed. This model was imported to the software tool, then a single loop coil figure was developed and placed over the head model as shown in Figure 1(a). The electric and magnetic fields were computed with FEM using the tissue electromagnetic properties at 128 MHz. In the first run, the coil was operated in transmission mode and the electric current density induced in the head model by the coil was estimated. In the second run, the induced currents were used to numerically compute the electric field produced by the head. The magnetic field of the coil operating in the transmission-only mode and the electric field generated by the sample were used to assess the SNR and the SAR with MATLAB (MathWorks, USA) programs developed for all matrix calculations. Figure 1(b) shows a three-dimensional illustration of the electric field of the sample in the sagittal orientation.

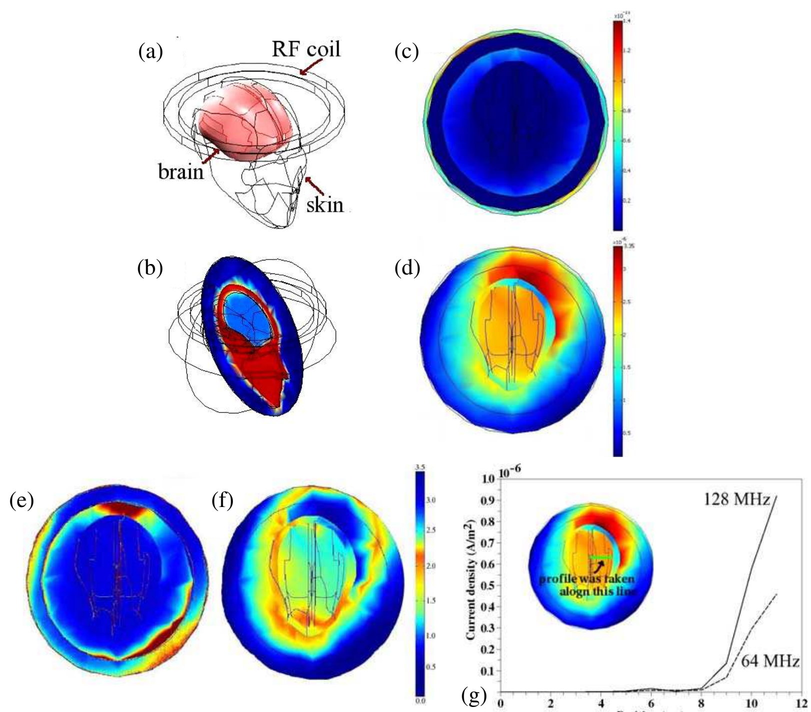

Figure 1: (a) Brain-skin-head model and RF single loop coil, (b) pixeled-brain electric field in the sagittal orientation, (c) coil magnetic field simulation, (d) pixeled-brain electric field simulation, (e) SNR numerical simulation, (f) SAR numerical simulation, (g) profiles of current density along the green line for two frequencies.

Results and Discussion: Figure 1(c) gives an image of the coil magnetic field in the transmission-mode operation. Figure 1(d) shows the electric field generated by the sample after excitation by the RF coil. Figure 1(e) shows the SNR and Figure 1(f) shows the SAR for the simulation setup of Figure 1(a). A surface coil was chosen for simplicity, however it can also be extended to more complex coil configurations such as the birdcage or coil arrays. Figure 1(g) shows two profiles of current density as a function of position for two different frequencies. This is another important result, since due to the electric properties of the brain, an increase in the induced currents is observed at the surface of the brain, as was expected an increase in frequency led to a higher current density. Other pixel anatomical models of human organs can be constructed and numerically simulated with this method at higher resonant frequencies too. This numerical method can offer a graphical tool to illustrate the behaviour of the SNR and SAR. It can be particularly useful for those students and researchers starting to familiarise with the development of RF coil for MRI, since the simulation method is easy to implement. Additionally, induced currents were also computed from the numerically computed electromagnetic fields and showed an expected pattern. The induced current intensity increases as a function of the frequency. These results may serve as guidelines to study safety issues involving RF coils. A simple numerical method to assess the SNR and SAR is presented using the FEM and this can be extended to other coil configurations and regions of interest.

Methodology for Local and Average SAR Evaluation at Millimeter Waves

Maxim Zhadobov[1], **Ronan Sauleau**[1], **Daniel Thouroude**[1], **Christophe Nicolas Nicolaz**[1,2], **Catherine Le Quement**[2], **and Yves Le Dréan**[2]

[1]Institute of Electronics and Telecommunications of Rennes (IETR)
University of Rennes 1, UMR CNRS 6164, Rennes, France
[2]Cellular and Molecular Interactions Group, University of Rennes 1
UMR CNRS 6026, Rennes, France

Abstract— Nowadays, the number of exposure sources to electromagnetic fields increases exponentially in parallel with the decrease of the life time of wireless technologies. The saturation of the lower part of the microwave spectrum and the need for higher data rate transmissions impose using broadband signals for communication purposes and increasing of the operating frequencies up to millimeter and sub-millimeter frequency bands. Recently, the frequency range around 60 GHz has been clearly identified by standardization committees (IEEE 802.15, TG 3c) and world-leading telecommunication companies as extremely promising for short-range high-data-rate secure communications particularly in indoor environment (WiHD, wireless USB, wireless video, streaming data, etc.). Simultaneously, public concerns about potential biological effects and related health impacts have raised. From the scientific point of view, two facts confirm that millimeter waves around 60 GHz could interact with biological systems. First, these radiations were originally absent in our natural environmental electromagnetic spectrum because they are totally absorbed by molecular oxygen in the atmosphere. Second, these radiations have been used in Eastern European countries for therapeutic purposes, providing as scientific evidence for such applications Fröhlich theory and results of some scientific studies.

In this context, a number of research groups in Europe, United States, and Asia started to investigate different biological aspects of possible interactions, including *in vitro* studies at sub-cellular and cellular levels. One of the major challenges of these studies is providing well-controlled and reproducible experimental protocols and dosimetry to ensure precise experimental replication. Performing accurate dosimetry studies at millimeter waves is a complicated scientific task because of the two following reasons. First, limitations for numerical dosimetry approaches are determined by the inhomogeneity of biological media and the presence of small sub-structures in biological samples, as well as by the large computational resources required at millimeter waves. Second, local experimental electromagnetic micro-dosimetry in this frequency band is an extremely challenging task as the skin depth of millimeter waves in biological tissues and media is limited to several tenths of a millimeter. Possible solutions of these problems imply the use and adaptation of advanced numerical techniques or development of indirect experimental approaches.

The main purpose of this study is to develop methodological approaches for numerical and experimental dosimetry at millimeter-waves for *in vitro* bioelectromagnetic investigations. Several numerical models were developed and compared to experimental results obtained using high-resolution infrared thermometry. To validate the implemented approaches, power density, as well as local and average specific absorption rate distributions were determined for commonly used typical biological samples.

Near-field Microwave Temperature Tomography with Scanning Diffraction Grating

Yu. N. Barabanenkov and M. Yu. Barabanenkov
Russian Academy of Sciences, Russia

Abstract— In 1953, Rytov [1] has predicted theoretically the near-field (quasistationary) component in a form of evanescent waves in thermal radiation of heated absorbing dielectric media. Gaikovich et al. [2] have shown experimentally that under definite choosing the size of the receiver antenna and its height above a heated body surface the main contribution into received microwave thermal radiation gives the near-field component. In this case, the authors retrieved also a depth profile of the temperature distribution inside a near-surface body layer, with depth being less the skin-layer depth. A restriction of method [2] consisted in supposition about one-dimension temperature distribution of body in depth, without accounting the temperature variation along parallel to the body surface elementary layers.

We discuss an approach to retrieval a three dimensional temperature distribution inside a heated body, for example a biological medium, with applying for the microwave thermal body radiation receiving a diffraction grating that is shifted along the body surface inside the near-field zone. Actually, we consider a semi-infinite heated absorbing dielectric media with three-and two-dimensional temperature distribution, using the fluctuation-dissipation theory and Green function method [3], and the transfer relations for electromagnetic wave scattering by dielectric diffraction gratings [4, 5]. An inverse problem under study is resolved with the aid of derived basic functional equation between a space Fourier — harmonics of thermal radiation energy flux through an elementary cell of the grating as function of grating shift and corresponding space Fourier — harmonics of the temperature distribution along an elementary inside body layer parallel the body surface. The grating period is chosen being small compared with empty space wavelength and being close in value to wavelength inside body medium, which may have a big dielectric permittivity for microwave frequencies. Such choice gives possibility to get maximum (resonant) thermal radiation from a space Fourier — harmonics of the temperature distribution along an elementary inside body layer parallel the body surface that simplifies resolution of the inverse problem under study.

ACKNOWLEDGMENT

This work has been supported in part by Russian Foundation for Basic Research-09-02-00920-a and Russian Academy of Sciences projects "Passive multichannel radio-and acoustothermotomograpy of human body in near zone".

REFERENCES

1. Rytov, S. M., *Theory of Electrical Fluctuations and Heat Emission*, Akademii Nauk SSSR, Moscow, 1953.
2. Gaikovich, K. P., A. N. Reznik, V. L. Vaks, and N. V. Yurasova, *Phys. Rev. Lett.*, Vol. 88, 104302, 2002.
3. Tsang, L., J. A. Kong, and R. T. Shin, *Theory of Microwave Remote Sensing*, J. Wiley, New York, 1985.
4. Gulyaev, Y. V., Y. N. Barabanenkov, M. Y. Barabanenkov, and S. A. Nikitov, *Phys. Rev. E*, Vol. 72, 026602-1–026602-12, 2005.

Biological Measurement in Healthcare Refrigerator

Bo-Rim Ryu[1] **and Heung-Gyoon Ryu**[2]

[1]Seoul Women's University, Korea
[2]Chungbuk National University, Korea

Abstract— In this paper, we like to investigate the biological measurement in the healthcare refrigerator, which can be implemented by body data measuring sensors and internet access. Some desired body data can be measured by the handle sensor and foot mat sensor in front of the refrigerator without extra health sensor on the body. Especially, the refrigerator can provide healthcare functions: 1) basic body diagnosis and monitoring, 2) healthcare and report 3) provision of well-being menu or healthy menu and 4) search and recommendation of restaurant information, etc. The refrigerator furnished in all home could play important roles including both healthcare and personal nutritionist. Health or well-being meals after checking health state can be recommended to help improvement of dietary or health life. Also, we will show the function realization in the above proposed structure.

AGILD EM and ME Coupled Modeling to Simulate Piezoelectric Materials

Jianhua Li[1, 2], **Chien-Chang Lin**[1], **and Ganquan Xie**[2]

[1]Department of Mechanical and Automation Engineering, Da Yeh University, Taiwan
[2]GL Geophysical Laboratory, USA

Abstract— In this paper, we present the AGILD Electromagnetic (EM) and Mechanical (ME) Coupled modeling to simulate a special piezoelectric material. The effect from Electric to mechanic or from mechanic to electric or mixed process are all simulated. Many simulations show that EM and ME translate effect is an mixed coupled macro And micro transport effect. They show that the AGILD EM ME coupled modeling is Accurate and suitable to simulate piezoelectric materials The internal EM and ME micro structure of the InGaN/GaN is a main reason of their EM and ME coupled effect. The simulation imaging will be presented in the PIERS 2009 in Moscow.

Session 4A5
Computational Techniques

Scale-changing Technique for the Numerical Modeling of Large Finite Non-uniform Array Structures

Aamir Rashid[1, 2], **Hervé Aubert**[1, 2], **and Hervé Legay**[3]

[1]CNRS; LAAS; 7 avenue du colonel Roche, F-31077 Toulouse, France
[2]University of Toulouse; UPS, INSA, INP, ISAE; LAAS; F-31077 Toulouse, France
[3]Thales Alenia Space, 105 Av. Gen Eisenhower, Toulouse 31100, France

Abstract— The design and analysis of electrically large structures e.g., phased antenna arrays or reflectarrays are complicated due to huge processing and memory requirements of their numerical simulations. Classical techniques based on infinite array approach are not only approximate but also not applicable in the case of arrays composed of dissimilar cell geometries. Numerical techniques allowing the electromagnetic simulation of the complete structure on the other hand require impractical processing resources. Scale-Changing Technique (SCT) has been found to be a very efficient tool for the electromagnetic simulation of complex planar structures [1]. The technique is applied by partitioning the planar array geometry into multiple scales. Electromagnetic coupling between two successive scale-levels is modeled by a multipole called Scale-Changing Network (SCN) [2]. At a given scale level s the modes that participate to the electromagnetic coupling with the lower scale-level $s-1$ are called active modes and are symbolized by ports of the SCN multipole; the rest are named passive modes and are used to describe the fine-scale variations of the electromagnetic field at that scale. SCN multipoles are calculated independently and they are cascaded only in the final step to obtain the complete solution. The mutually independent nature of SCN mutipoles allows their parallel execution on separate machines thus drastically reducing the execution time of the simulation. Moreover the modification in geometry of the structure at one scalelevel only requires the calculation of two SCN multipoles and not the recalculation of the complete structure. In case of finite arrays this concept has been validated by successfully simulating a 1-D finite array of non-uniform metallic strips in a parallel waveguide (Figs. 1 and 2). SCT has been found to be highly efficient as compared to an FEM based technique for large sized arrays. The work on the simulation of 2-D finite arrays is currently in progress and the results will be presented at the conference.

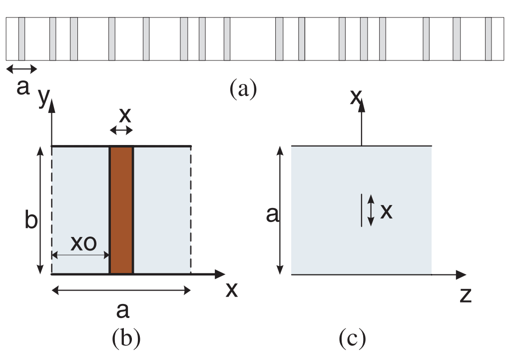

Figure 1: (a) A finite non-uniform array of metallic strips. (b), (c) Transverse and longitudinal views of a unit-cell.

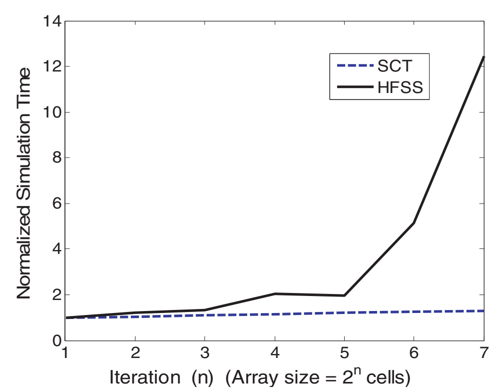

Figure 2: Increase in simulation times of SCT and HFSS with respect to the simulated array size.

REFERENCES

1. Voyer, D., H. Aubert, and J. David, “Scale changing technique for the electromagnetic modeling of planar self-similar structures,” *IEEE Transactions on Antennas and Propagation*, Vol. 54, No. 10, 2783–2789, October 2006.
2. Aubert, H., “Monolithic electromagnetic modeling of multi-scale structures based on scalechanging networks,” *IEEE Antenna Propagation Symposium*, San-Diego, USA, 2008.

Light Propagation in a Disordered Waveguide System: Average Amplitude

Akira Komiyama
Osaka Electro-Communication University, Hatsu-cho Neyagawa-shi 572-8530, Japan

Abstract— Mode waves in a disordered waveguide system composed of randomly different cores in size are localized. The density of localized modes can be accurately calculated by the coherent potential approximation. When one of cores of the waveguide system is illuminated several localized modes are excited and propagate through the system. In this paper, the average amplitude of light in a disordered waveguide system is analytically derived by using a perturbation series.

In the Laplace transform domain the amplitude of light is expressed as

$$\tilde{a} = \tilde{G}_0 a(0) - j\tilde{G}_0 \Delta\beta \tilde{a}.$$

Here $\tilde{a}$ is an amplitude vector, $a(0)$ an initial value vector and $\Delta\beta = (\delta\beta_n \delta_{nm})$ where $\delta\beta_n$ is the fluctuation of the propagation constant of the mode in the core n. $\tilde{G}_0 = (\tilde{G}_0(n, m, s))$ is the function describing the light propagation in an ordered system composed of identical cores, which can be analytically obtained. By iterating on $\tilde{a}$ we have

$$\tilde{a} = \tilde{G}_0 a(0) - j\sum_l \tilde{T}_l \tilde{G}_0 a(0)$$

where $\tilde{T}_l$ is the scattering matrix,

$$\tilde{T}_l = \tilde{t}_l - j\sum_{p\neq l} \tilde{t}_p \tilde{t}_l - \sum_{p\neq l}\sum_{q\neq p} \tilde{t}_q \tilde{t}_p \tilde{t}_l + \dots$$

$\tilde{t}_l$ is the scattering matrix for the core l. The average scattering matrix is approximated as

$$\langle \tilde{T}_l \rangle = \langle \tilde{t}_l \rangle - j\sum_{p\neq l} \langle \tilde{t}_p \rangle \langle \tilde{t}_l \rangle - \sum_{p\neq l}\sum_{q\neq p,l} \langle \tilde{t}_q \rangle \langle \tilde{t}_p \rangle \langle \tilde{t}_l \rangle + \dots$$

The sum of the series can be analytically calculated and the average amplitude of light is expressed as

$$\langle \tilde{a} \rangle = \langle \tilde{G}_0 \rangle a(0)$$

where

$$\begin{aligned} \left(\langle \tilde{G}_0 \rangle\right)_{nm} &= \tilde{G}_0\left(n, m, s + M(s)\right) \\ M(s) &= \frac{M_0(s)}{1 - M_0(s)(\tilde{G}_0)_{ll}}, \quad M_0(s) = \left\langle \frac{j\delta\beta_l}{1 + j\delta\beta_l \left(\tilde{G}_0\right)_{ll}} \right\rangle \end{aligned}$$

$M(s)$ in $\tilde{G}_0$ can be approximated by $M(0)$. Then the expression for $\langle \tilde{G}_0 \rangle$ shows that the average amplitude decreases exponentially with increasing distance and $M(0)$ is the damping factor for amplitude. The result is in good agreement with the result obtained by applying the coherent potential approximation to the coupled mode equation in the Laplace transform domain.

Scattering of Electromagnetic Waves by Dielectric Gratings with Dielectric Rectangular Cylinders Sandwiched between Two Multilayers

Ryosuke Ozaki, **Tsuneki Yamasaki**, **and Takashi Hinata**
Department of Electrical Engineering, College of Science and Technology
Nihon University, 1-8-14, Surugadai Kanda Chiyoda-ku, Tokyo 101-8308, Japan

Abstract— Scattering of electromagnetic waves by dielectric gratings is of both theoretical and practical interest for integrated optics, optical filters, and holography. Due to recent advances, the refractive index can easily be controlled in the manufacture of periodic structures to serve as fiber gratings, frequency-selective or polarization-selective devices, and photonic crystals. Thus, many analytical and numerical methods have been proposed that are applicable to dielectric gratings having arbitrary structures. In the multilayer method (see Fig. 1(b)), as the inhomogeneous region is divided into an assembly of stratified thin layers with modulated indices, the order of the matrix depends on the number of layers. In our approach, the order of characteristic matrix equation depends on the modal truncation number, but it does not depend on the number of layers. Therefore the range of applicability to periodic structures is much wider than that of the other method. Our method also can be applied easily to the scattering problems as well as guiding problems, such as surface relief gratings, planar slanted gratings, and columnar dielectric gratings. On the other hand, to deal with multilayered dielectric gratings such as photonic crystals, it is necessary to analyze multilayered circular cylinder arrays.

In this paper, we proposed a new technique to examine the scattering of both TM and TE waves by dielectric gratings with dielectric rectangular cylinders sandwiched between two multilayers, by combining an improved Fourier series expansion method and multilayer method.

Numerical results are given for the power transmission coefficients in terms of the parameter $\varepsilon_3/\varepsilon_0$ of rectangular cylinders in the middle layer, yielding the basic characteristics of the power transmission and reflection coefficients of switching of frequency selective devices for both TM and TE waves. The influence of the incident angle and frequency characteristics of the transmitted power are discussed.

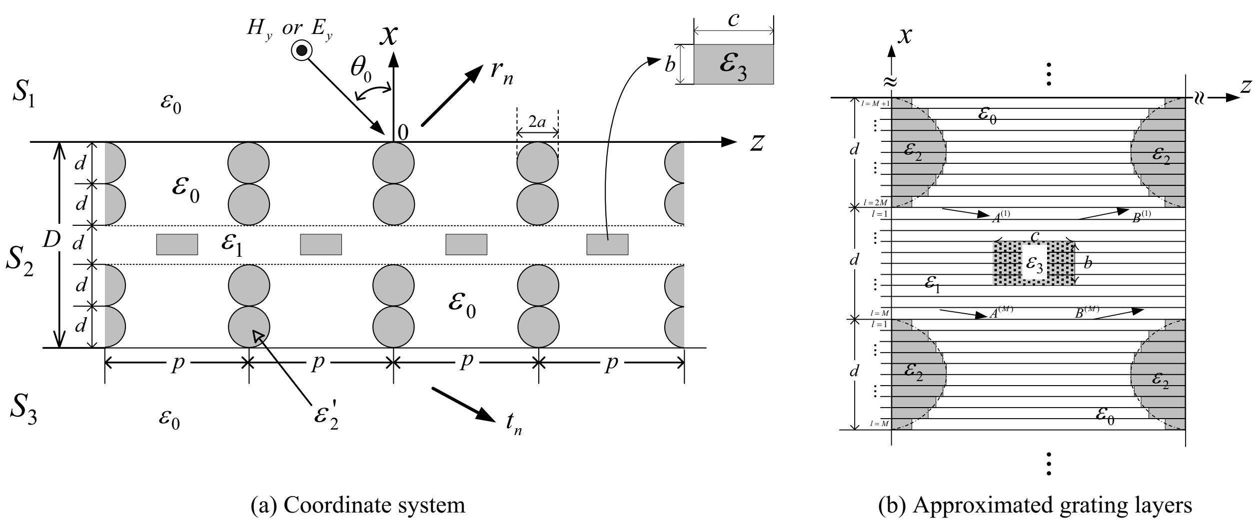

Figure 1: Structure of dielectric gratings with rectangular cylinders sandwiched between two multilayers.

Diffraction by an Impedance Strip: A New Presentation Based on Physical Optics Approach

M. V. Ivakhnychenko[1], **E. I. Veliev**[1], **and T. M. Ahmedov**[2]

[1]IRE NAS of Ukraine, 12 Proskury, Kharkov 61085, Ukraine
[2]Institute of Mathematics NAS of Azerbaijan, 9 F. Agaeva, AZ 1141, Baku, Azerbaijan

Abstract— Diffraction of plane electromagnetic waves by an infinitely long strip having the same impedance on both faces is investigated. The solution for impedance surface with arbitrary value of the surface impedance is constructed as a linear combination of known solutions for perfectly electric conducting (PEC) and perfect magnetic conducting (PMC) surfaces. Solutions for PEC and PMC strip of the same width are found numerically. The coefficients in the presentation for the radiation pattern for the impedance strip take into account losses which depend on the surface impedance. These coefficients are evaluated analytically in physical optics approximation when all solutions (PEC, PMC and impedance strip) can be obtained analytically. For other values of the wave length the resulting fields are examined numerically. It is necessary to solve once the diffraction problem by PEC and PMC strips numerically for a given strip width, after that the solution for an impedance strip is obtained as a simple superposition of both solutions for any value of the impedance. The method of solving considering diffraction problems is based on presenting the diffracted field in terms of the induced electric and magnetic current densities. The problem is formulated as simultaneous integral equations. Obtained integral equations allow to derive the high frequency asymptotic expressions of the far field radiation pattern. Utilizing the Fourier transform to the integral equations the unknown current density functions can be expanded into the infinite series containing the Chebyshev polynomials. Finally, the problem is reduced to infinite systems of linear algebraic equations satisfied by the expansion coefficients. Radiation pattern, radar cross section are plotted for different values of the impedance, the wave length and the incidence angle showing the comparison of the constructed solution and exact solution for impedance strip. It is showed that presented expression allows to obtain the solution for impedance strip with good accuracy for wide range of values of impedance and wave length.

Total-field/Scattered-field Boundary for Multi-dimensional CIP Method

Yoshiaki Ando, **Satoi Murakoshi**, **and Masashi Hayakawa**
The University of Electro-Communications
1-5-1 Chofugaoka, Chofu, Tokyo 182-8585, Japan

Abstract—

Introduction: The constrained interpolation profile (CIP) method is the numerical method using field values and their spatial derivatives, and is originally developed in the area of fluid dynamics. Recently, the application of the CIP method to electromagnetic dynamics acquires many attention, and related papers have been published [1, 2]. In this paper, we consider the CIP solution of total-field/scattered-field boundary for electromagnetic waves.

Formulation: Here we present formulation of the TF/SF boundary for the two-dimensional TM_z case as an example. The type-M CIP scheme used in this paper is summarized in [1], in which we use the scaled electromagnetic fields: $e_z = \sqrt{\epsilon_0}E_z$, $h_x = \sqrt{\mu_0}H_x$, and $h_y = \sqrt{\mu_0}H_y$. From the linearity of Maxwell's equations, the total electromagnetic fields ($e_{t,\,z}$, $h_{t,\,x}$, and $h_{t,\,y}$) are separated into the incident fields ($\hat{e}_z$, $\hat{h}_x$, and $\hat{h}_y$) and the scattered ones ($e_{s,\,z}$, $h_{s,\,x}$, and $h_{s,\,y}$), i.e., $e_{t,\,z} = \hat{e}_z + e_{s,\,z}$, and so on. The advection field components for CIP method are then defined as [1]

$$f^{\pm}_{t,\,x}=e_{t,\,z} \mp h_{t,\,y},\ g^{\pm}_{t,\,x}=\partial_x f^{\pm}_{t,\,x},\ \eta^{\pm}_{t,\,x}=\partial_y f_{t,\,x},\ f^{\pm}_{t,\,y}=h_{t,\,x} \pm e_{t,\,z},\ g^{\pm}_{t,\,y}=\partial_y f^{\pm}_{t,\,y},\ \eta^{\pm}_{t,\,y}=\partial_x f_{t,\,y}, \tag{1}$$

where ∂_α stands for the partial derivative operator with respect to α. Using the spatial and the temporal discretization, Δx, Δy, and Δt, the field components at the position $(i\Delta x,\, j\Delta y)$ and at the time $n\Delta t$ are expressed as $f^{\pm,\,n}_{t,\,x}(i,\,j) \equiv f^{\pm}_{t,\,x}(i\Delta x,\, j\Delta y,\, n\Delta t)$. The computational region is separated into the TF region $T = \{(i,\,j)|i_1 \leqq i \leqq i_2 \cap j_1 \leqq j \leqq j_2\}$ and the SF region $S = \bar{T}$. We store the total and the scattered fields into the memory in the TF and the SF regions, respectively. In the TF and the SF regions, the update equations for the total and the scattered fields are the same as the conventional ones. At the TF/SF boundary, the update equations need to be modified in order to satisfy the advection equation for either the total or the scattered field. The detail is described in [2]. For example,

$$\begin{aligned} f^{+,\,*}_{t,\,x}(i_1,\,j) \;=\; & A^{+}_{x1} f^{+,\,n}_{t,\,x}(i_1,\,j) + A^{+}_{x2}\{f^{+,\,n}_{s,\,x}(i_1-1,\,j) + \hat{f}^{+,\,n}_{x}(i_1-1,\,j)\} \\ & + A^{+}_{x3} g^{+,\,n}_{t,\,x}(i_1,\,j) + A^{+}_{x4}\{g^{+,\,n}_{s,\,x}(i_1-1,\,j) + \hat{g}^{+,\,n}_{x}(i_1-1,\,j)\}, \end{aligned} \tag{2}$$

where $j_1 \leqq j \leqq j_2$. $\hat{f}^{\pm,\,n}_{x}(i,\,j)$, $\hat{g}^{\pm,\,n}_{x}(i,\,j)$, and $\hat{\eta}^{\pm,\,n}_{x}(i,\,j)$ are the prescribed incident fields of $f^{\pm}_{x}$, $g^{\pm}_{x}$, and $\eta^{\pm}_{x}$, respectively, and they are given by

$$\begin{aligned} \hat{f}^{\pm,\,n}_{x}(i,\,j) &= \hat{e}^{n}_{z}(i,\,j) \mp \hat{h}^{n}_{y}(i,\,j), \\ \hat{g}^{\pm,\,n}_{x}(i,\,j) &= \partial_x \hat{e}^{n}_{z}(i,\,j) \mp \partial_x \hat{h}^{n}_{y}(i,\,j), \\ \hat{\eta}^{\pm,\,n}_{x}(i,\,j) &= \partial_y \hat{e}^{n}_{z}(i,\,j) \mp \partial_y \hat{h}^{n}_{y}(i,\,j). \end{aligned} \tag{3}$$

The update equations for the advection in $-x$-direction to calculate the scattered fields at $(i_1 - 1,\,j)$, i.e., $f^{-,\,*}_{s,\,x}(i_1-1,\,j)$, $g^{-,\,*}_{s,\,x}(i_1-1,\,j)$, and $\eta^{-,\,*}_{s,\,x}(i_1-1,\,j)$, and the ones at another TF/SF boundary to do $f^{+,\,*}_{s,\,x}(i_2+1,\,j)$, $g^{+,\,*}_{s,\,x}(i_2+1,\,j)$, $\eta^{+,\,*}_{s,\,x}(i_2+1,\,j)$, $f^{-,\,*}_{t,\,x}(i_2,\,j)$, $g^{-,\,*}_{t,\,x}(i_2,\,j)$, and $\eta^{-,\,*}_{t,\,x}(i_2,\,j)$, are modified similarly [2].

After the advection in x-direction, we proceed the advection in y-direction. In this phase also, we need to add or subtract the incident fields at the TF/SF boundary. Although CIP fields in the y-advection are given by $f^{\pm}_{y} = h_x \pm e_z$, the incident CIP fields $\hat{f}^{\pm}_{y}$ are not given by $\hat{h}_x \pm \hat{e}_z$ because in this phase $\hat{e}_z$ must be experienced in the x-advection.

We define $\hat{e}^{*}_{z}$ is $\hat{e}_z$ after the x-advection, and $\hat{e}^{*}_{z}$ is given by $\hat{e}^{*}_{z}(i,\,j) = \frac{1}{2}\{\hat{f}^{+,\,*}_{x}(i,\,j) + \hat{f}^{-,\,*}_{x}(i,\,j)\}$, where $\hat{f}^{\pm,\,*}_{x}$ are the incident waves after the advection in x-direction, and are given by

$$\hat{f}^{\pm,\,*}_{x}(i,\,j) = A^{\pm}_{x1}\hat{f}^{\pm,\,n}_{x}(i,\,j) + A^{\pm}_{x2}\hat{f}^{\pm,\,n}_{x}(i \mp 1,\,j) + A^{\pm}_{x3}\hat{g}^{\pm,\,n}_{x}(i,\,j) + A^{\pm}_{x4}\hat{g}^{\pm,\,n}_{x}(i \mp 1,\,j). \tag{4}$$

We then get the incident fields for y-advection:

$$\hat{f}_y^{\pm,*}(i,j)=\hat{h}_x^n(i,j)\pm\hat{e}_z^*(i,j),\ \hat{g}_y^{\pm,*}(i,j)=\partial_y\hat{h}_x^n(i,j)\pm\partial_y\hat{e}_z^*(i,j),\ \hat{\eta}_y^{\pm,*}(i,j)=\partial_x\hat{h}_x^n(i,j)\pm\partial_x\hat{e}_z^*(i,j), \quad (5)$$

$$\partial_y\hat{e}_z^*(i,\,j)=\frac{1}{2}\{\hat{\eta}_x^{+,*}(i,\,j)+\hat{\eta}_x^{-,*}(i,\,j)\},\ \partial_x\hat{e}_z^*(i,\,j)=\frac{1}{2}\{\hat{g}_x^{+,*}(i,\,j)+\hat{g}_x^{-,*}(i,\,j)\}, \quad (6)$$

$$\hat{g}_x^{\pm,*}(i,\,j)=B_{x1}^{\pm}\hat{g}_x^{\pm,n}(i,\,j)+B_{x2}^{\pm}\hat{g}_x^{\pm,n}(i\mp 1,\,j)+B_{x3}^{\pm}\hat{f}_x^{\pm,n}(i,\,j)+B_{x4}^{\pm}\hat{f}_x^{\pm,n}(i\mp 1,\,j), \quad (7)$$

$$\hat{\eta}_y^{\pm,*}(i,\,j)=C_{x1}^{\pm}\hat{\eta}_x^{\pm,n}(i,\,j)+C_{x2}^{\pm}\hat{\eta}_x^{\pm,n}(i\mp 1,\,j). \quad (8)$$

The TF/SF boundary for y-advection is given, in $i_1 \leqq i \leqq i_2$, by

$$\begin{aligned}
f_{t,\,y}^{+,\,n+1}(i,\,j_1) &= A_{y1}^{+}f_{t,\,y}^{+,*}(i,\,j_1)+A_{y2}^{+}\{f_{s,\,y}^{+,*}(i,\,j_1-1)+\hat{f}_y^{+,*}(i,\,j_1-1)\}\\
&\quad +A_{y3}^{+}g_{t,\,y}^{+,*}(i,\,j_1)+A_{y4}^{+}\{g_{s,\,y}^{+,*}(i,\,j_1-1)+\hat{g}_y^{+,*}(i,\,j_1-1)\}, && (9)\\
g_{t,\,y}^{+,\,n+1}(i,\,j_1) &= B_{y1}^{+}g_{t,\,y}^{+,*}(i,\,j_1)+B_{y2}^{+}\{g_{s,\,y}^{+,*}(i,\,j_1-1)+\hat{g}_y^{+,*}(i,\,j_1-1)\}\\
&\quad +B_{y3}^{+}f_{t,\,y}^{+,*}(i,\,j_1)+B_{y4}^{+}\{f_{s,\,y}^{+,*}(i,\,j_1-1)+\hat{f}_y^{+,*}(i,\,j_1-1)\}, && (10)\\
\eta_{t,\,y}^{+,\,n+1}(i,\,j_1) &= C_{y1}^{+}\eta_{t,\,y}^{+,*}(i,\,j_1)+C_{y2}^{+}\{\eta_{s,\,y}^{+,*}(i,\,j_1-1)+\hat{\eta}_y^{+,*}(i,\,j_1-1)\} && (11)
\end{aligned}$$

ACKNOWLEDGMENT

This work is partially supported by KAKENHI (18760212), and a part of "R&D promotion scheme funding international joint research" promoted by NICT (National Institute of Information and Communications Technology).

REFERENCES

1. Ando, Y. and M. Hayakawa, "Implementation of the perfect matched layer for the CIP method," *IEICE Trans. Electron.*, Vol. E89-C, No. 5, 645–648, May 2006.
2. Ando, Y., H. Saito, and M. Hayakawa, "A nearly perfect total-field/scattered-field boundary for the onedimensional CIP method," *IEICE Trans. Electron.*, Vol. E91-C, No. 10, 1677–1683, October 2008.

Computerized Calculation of Complex Object RCS Using Physical Theory of Diffraction

A. M. Lebedev, A. I. Fedorenko, and V. N. Kisel
Institute for Theoretical Applied Electromagnetics, Russian Academy of Sciences, Russia

Abstract— Various aspects of Ufimtsev's physical theory of diffraction (PTD) application to computer-aided backscattering RCS calculation for complex metal objects are discussed in this work. In [1, 2], it was suggested to approximate the contribution into the scattered field produced by near-the-edge inhomogeneous part of the current (which is the difference between actual current and its homogeneous physical optics (PO) part) by the superposition of elementary edge waves (EEW). EEW is the field generated by inhomogeneous currents on the pair of semi-infinite strips of small width. The strips are directed along the diffracted rays on the sides of the (tangent) wedge which locally duplicates the edge.

Smooth variation of backscattered EEW in azimuth-elevation coordinates related to the local piece of the edge, the absence of field magnitude singularities and phase jumps are favorable features of EEW. By contrast, the fields generated by PO current and, consequently, the actual current do have magnitude singularities and phase jumps. That is why the EEW must be carefully calculated in the vicinity of PO field singularity. The EEW expressions in [1, 2] also contain some other not physical, but removable singularities of "zero divided by zero" type.

In course of computer-aided simulation, complex object is fully depicted in geometrical CAD. Then the meshed model is created either in the same CAD, or with some attendant program. The appropriate location and configuration of Ufimtsev's tangent wedges is also specified within the 3D model. Further the RCS diagram is calculated as a sum of PO currents backscattering and Ufimtsev's EEW contributions.

Comparisons with the method of moments calculations for plates, cones and cylinders demonstrate applicability and high accuracy of PTD approximation.

If one or both forming the edge surfaces end abruptly in close proximity to the edge, then PTD approximation can not provide literally exact results of calculation. However, PTD-based calculation is worthwhile if RCS is averaged in angular and/or frequency range. Finally, some numerical correction of EEW is possible for certain deviations of edge cross section from canonical form. The latest two points substantially widen the scope of PTD approximation application.

REFERENCES

1. Butorin, D. I., D. A. Martinov, and P. Y. Ufimtsev, "Asymptotic expressions of elementary edge wave," *Radiotechnics and Electronics*, 1818–1829, 1987 (in Russian).
2. Ufimtsev, P. Y., "Improved physical theory of diffraction: Removal of the grazing singularity," *IEEE TAP*, Vol. 54, No. 10, 2698–2702, 2006.

Trend Analysis of Insertion Loss Data Associated on a Naval Vessel with Large, Significantly Loaded Compartments

Cynthia Ropiak[1], **Matthew McQuage**[2], **and Wilfredo Padilla-Vargas**[2]

[1]SAQ Consulting, Ltd., 109 Gander Way, Suite B, Chestertown, MD 21620-2885, USA
[2]Directed Energy Technology Office, Naval Surface Warfare Center, Dahlgren Division
Code Q22 BLDG 1470, 18444 Frontage Road, Dahlgren, VA 22448-5161, USA

Abstract— Unforeseen electromagnetic interference (EMI) onboard Naval vessels is an important area of concern for the United States Navy. A significant amount of time and resources are devoted to investigating and mitigating this phenomenon. A central piece of these investigations relates to quantifying the potential build up of electromagnetic energy in ship compartments. Due to their metallic structure, it is not unreasonable to presume that the compartments of a Naval vessel are appreciably reverberant when injected with an electromagnetic signal of reasonable wavelength. This assumption was put to the test when a series of measurements of the insertion loss were made in twelve ship compartments onboard a United States Naval vessel. The measurement technique assumes a reverberant environment (an assumption that was experimentally verified) and the test frequency range spans 200 MHz through 10 GHz. In References [2] and [7] the data is analyzed in order to assess the validity of the reverberant assumption and a summary of these finding is reported herein. Historically, for a reverberant environment the insertion loss is expected to behave linearly with the logarithm of the frequency [1]. However, the ship compartment data is found to substantially deviate from the historical linear dependence for the lower frequencies (below 1.5 GHz). This paper details a trend analysis of the frequency dependence of the insertion loss data and offers a new functional form for the frequency dependence of the insertion loss results, which mimics historical dependencies in the high frequency regime, yet captures observed deviations from this traditional form in the lower frequency regime.

REFERENCES

1. Hatfield, M., W. Pluim, and W. Price, "Investigation of In-SITU shielding effectiveness testing of transport aircraft," *IEEE EMC*, 2003.
2. Ropiak, C., W. Vergas, and F. Peterkin, "Insertion loss measurements onboard a united states naval vessel," *Proceedings of the North American Radio Science Meeting*, Ottawa, Canada, June 2007.

Variational Effective Index Method for 3D Vectorial Scattering Problems in Photonics: TE Polarization

O. V. Ivanova[1], **R. Stoffer**[2], **L. Kauppinen**[1], **and M. Hammer**[1]

[1]MESA+ Institute for Nanotechnology, University of Twente, Enschede, The Netherlands
[2]Phoenix Software, Enschede, The Netherlands

Abstract— Fully vectorial 3D simulations of photonic components are often almost prohibitively CPU-time and memory-intensive, so one would opt for reduced models that capture the essence of the full 3D structure, while being computationally much more efficient. Traditionally, integrated optics designers use a technique called the Effective Index Method (EIM) to reduce a simulation of a 3D structure to two spatial dimensions. However, frequently, as is the case for the photonic crystal slabs (Figure 1), the effective parameters for the 2D simulation are only rather ambiguously defined, i.e., rely more or less on guesswork. Here we have developed a mathematical formulation that allows to a priori derive these parameters when going from 3D to 2D based on a sound variational reasoning (Variational EIM, VEIM). This is achieved by approximating the total 3D vectorial electromagnetic field along one spatial dimension by a suitable 1D TE mode profile. Then, by means of a variational procedure, the field distribution in the other two dimensions is found, such that the product of these two fields represents as well as possible the true 3D vectorial solution. On the boundaries of the computational domain we use combined Transparent Influx Boundary Conditions with Perfectly Matched Layers in order to allow influx into the domain to be prescribed and radiation to freely pass through the computational window boundaries. Results for a photonic crystal slab waveguide show that this approach predicts the location of the bandgap and other spectral features much more precisely than any guesses using a 'standard' EIM. A similar procedure has also been developed for TM polarization. Currently, work is in progress to extend the method to deal with the third dimension even more accurately.

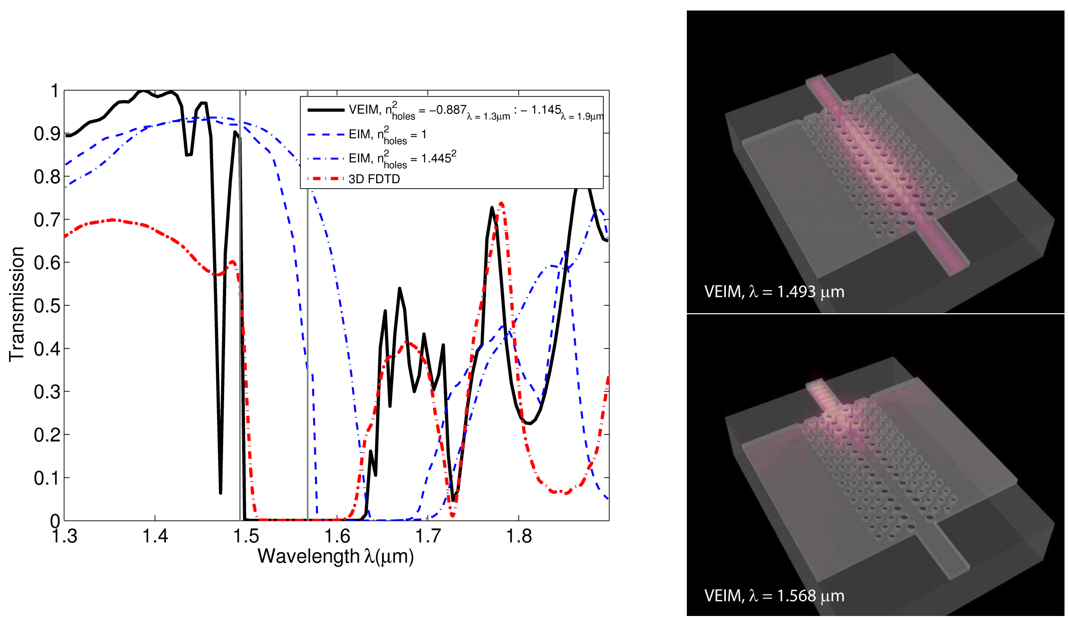

Figure 1: Left: Transmission spectrum of the photonic crystal waveguide. The VEIM predictions of the location of the stopband and the general spectral features are reasonably close to the 3D FDTD reference results, while the 'conventional' EIM data, using either the cladding (1.0) or substrate refractive indices (1.445) as effective values for the hole regions, are much further off. Right: Light propagation through the photonic crystal slab waveguide, absolute value of the principal magnetic component of the optical field; almost full transmission at a vacuum wavelength of 1.493 μm and hardly any transmission at 1.568 μm.

Scattering of Electromagnetic Waves by Inhomogeneous Dielectric Gratings with Perfectly Conducting Strips

Tsuneki Yamasaki, Ryosuke Ozaki, and Takashi Hinata
Department of Electrical Engineering, College of Science and Technology, Nihon University, Japan

Abstract— In Integrated optics, the inhomogeneous dielectric gratings are useful in optical fiber gratings, photonic bandgap crystals, frequency selective devices, and other applications by the development of manufacturing technology of optical devices. However, the theoretical and numerical studies have considered the periodic structures in which the material forming grating was either metallic or dielectric.

In this paper, we proposed a new method for the scattering of electromagnetic waves by inhomogeneous dielectric gratings loaded with three adjacent perfectly conducting strips slanted angle γ using the combination of improved Fourier series expansion method and point matching method for TE waves.

In the inhomogeneous dielectric grating $S_2\,(0 < x < D)$, the permittivity profile $\varepsilon_2(x, z)$ is generally not separable with respect to the x and z variables. So main process of our methods are as follows: (1) The inhomogeneous layer is approximated by a transformation of coordinates system of modulated index profile with period $p' = p\cos(\gamma)$. (2) Taking new coordinate system, the electromagnetic fields are expanded appropriately by a finite Fourier series. (3) In the perfectly conducting strip and gap regions at $C_1\,(or\,\bar{C}_1)$, $C_2\,(or\,\bar{C}_2)$ and $C_3\,(or\,\bar{C}_3)$, boundary, the electromagnetic fields are matched using an orthogonality relation which makes the matrix relation on both sides using point matching method. (4) Finally, all layers include the metallic regions are matched using appropriate boundary conditions to get the slanted dielectric gratings loaded with two adjacent perfectly conducting strips.

Numerical results are given for the transmitted scattered characteristics for the case of incident angle and frequency with $\delta[\gamma = \tan^{-1}(\delta/D)]$ for TE waves.

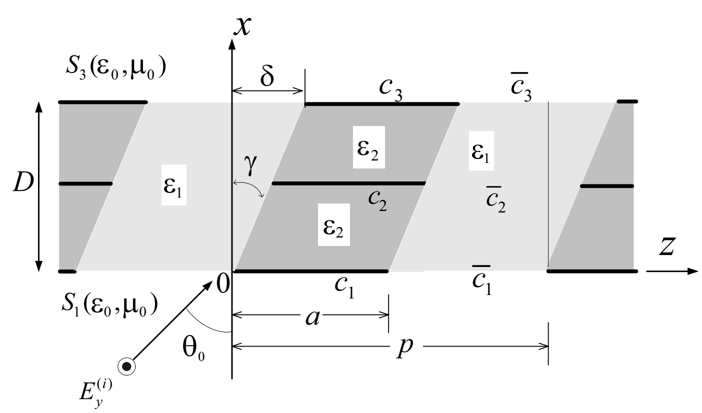

Figure 1: Structure of inhomogeneous dielectric gratings with perfectly conducting strips.

Session 4A6
Advanced High Frequency Electromagnetic Simulation Tools 1

The A, B, C Numbers and Their Application in the Theory of Waveguides

Mariana Nikolova Georgieva-Grosse[1] **and Georgi Nikolov Georgiev**[2]

[1]Meterstrasse 4, D-70839 Gerlingen, Germany
[2]Faculty of Mathematics and Informatics, University of Veliko Tirnovo "St. St. Cyril and Methodius"
BG-5000 Veliko Tirnovo, Bulgaria

Abstract— The circular waveguides with azimuthally magnetized ferrite have been explored to develop nonreciprocal phase shifters for electronically scanned antenna arrays, operating in the normal TE_{01} mode [1–5]. Entirely filled with ferrite circular [1] and coaxial [2] configurations, as well as ones, containing coaxially positioned ferrite and dielectric layers [3–5] have been treated. Finding the differential phase shift produced, being the main aim of the study, turned out to be a very complicated task [1, 5]. An original approach to its solution in case of circular geometry is the introduction of the A, B, C numbers [1], allowing to construct simple formulae for computation of this important quantity [1].

A new definition of the numbers mentioned is given here, holding both for the circular and coaxial structures. It is set that: $A = A_- - A_+$, $B = B_- - B_+$ and $C = C_- - C_+$ where $A_\pm = \sigma_{1\pm}/\sigma_{2\pm}$ or $A_\pm = \sigma_{2\pm}/\sigma_{1\pm}$, $B_\pm = \sigma_{1\pm}\bar{r}_0$ or $B_\pm = \sigma_{2\pm}\bar{r}_0$ and $C_\pm = (\sigma_{1\pm}/\sigma_{2\pm})\bar{r}_0$ or $C_\pm = (\sigma_{2\pm}/\sigma_{1\pm})\bar{r}_0$, depending on the relations between $\sigma_{1\pm}$ and $\sigma_{2\pm}$. The quantities $\sigma^2_{1\pm,2\pm} = 0.5[(1-\bar{\beta}^2_{2\pm}) \pm \sqrt{(1-\bar{\beta}^2_{2\pm})^2 - 4\times 4\bar{\beta}^2_{2\pm}k^2_\pm}]$ in that $1-\bar{\beta}^2_{2\pm} \geq 4\bar{\beta}_{2\pm}|k_\pm|$, $(1 > \sigma_{1\pm} \geq \sigma_{2\pm} \geq 0)$ are the roots of the biquadratic equation $\sigma^4_\pm - (1-\bar{\beta}^2_{2\pm})\sigma^2_\pm + 4\bar{\beta}^2_{2\pm}k^2_\pm = 0$, equivalent to two identical ones for $\bar{\beta}_\pm$ and $|\alpha_\pm|$, resp., ($\bar{\beta} = \beta/(\beta_0\sqrt{\varepsilon_r})$, $\bar{\beta}_2 = \beta_2/(\beta_0\sqrt{\varepsilon_r})$ and $\bar{r}_0 = \beta_0 r_0\sqrt{\varepsilon_r}$ — normalized phase constant, radial wavenumber and guide radius, resp., $\beta_0 = \omega\sqrt{\varepsilon_0\mu_0}$, $k = \alpha\bar{\beta}/(2\bar{\beta}_2)$, $\bar{\beta}_2 = (1-\alpha^2-\bar{\beta}^2)^{1/2}$, α — off-diagonal tensor element, ε_r — relative permittivity of the ferrite). The term $\bar{\beta}_{2\pm} = \chi^{(c)}_{k\pm,n}(\rho)/(2\bar{r}_0)$ yields the eigenvalue spectrum of configurations for the normal TE_{0n} modes, $\chi^{(c)}_{k\pm,n}(\rho)$ — roots of the corresponding characteristic equations, written by complex confluent hypergeometric functions [1, 2, 6], ($c = 3$, $n = 1, 2, 3, \ldots$, $\rho = \bar{r_1}/\bar{r_0}$, $\bar{r_1} = \beta_0 r_1\sqrt{\varepsilon_r}$ — normalized axial conductor radius). (The subscripts "+" and "−" relate to positive ($\alpha_+ > 0$, $k_+ > 0$) and negative ($\alpha_- < 0$, $k_- < 0$) magnetization, resp.) The quantities A_{cr}, B_{cr}, C_{cr} (a partial case of A, B, C, relevant to the cutoff state) are figured for the normal TE_{01} mode ($n = 1$), by iterative techniques. The effect of structures parameters on them is examined. Using these numbers, an approximate method for differential phase shift computation is suggested, valid for both geometries which brings in a negligible error.

REFERENCES

1. Georgiev, G. N. and M. N. Georgieva-Grosse, "Formulae for differential phase shift computation in an azimuthally magnetized circular ferrite waveguide," in *Proc. Millenn. Conf. Antennas Propagat. AP-2000*, 1002, in CDROM, Davos, Switzerland, April 9–14, 2000.
2. Georgiev, G. N. and M. N. Georgieva-Grosse, "A property of the $L(c, \rho, n)$ numbers and its application to waveguide propagation," in *Proc. XXIX URSI General Assembly*, in CDROM, Chicago, IL, USA, August 7–16, 2008, BK. 6 (120).
3. Georgiev, G. N. and M. N. Georgieva-Grosse, "Propagation in an azimuthally magnetized circular ferrite-dielectric waveguide," in *Proc. 3rd Europ. Conf. Antennas Propagat. EuCAP 2009*, 345–349, in CDROM, Berlin, Germany, March 23–27, 2009.
4. Georgiev, G. N. and M. N. Georgieva-Grosse, "Phase behaviour of a two-layered circular ferrite-dielectric waveguide with azimuthal magnetization," *in Proc. 26th Progr. In Electromagn. Res. Symp.*, Moscow, Russia, August 18–21, 2009 (in print).
5. Georgiev, G. N. and M. N. Georgieva-Grosse, "An application of the complex Tricomi function," in *Proc. Eleventh Int. Conf. Electromagn. Adv. Applicat. ICEAA'09*, Turin, Italy, September 14–18, 2009 (in print).
6. Tricomi, F. G., *Funzioni Ipergeometriche Confluenti*, Edizioni Cremonese, Rome, Italy, 1954.

Ray Tracing Scattering Simulations for Cavities Filled with Dielectric Material

F. Weinmann
Research Institute for High Frequency Physics and Radar Techniques
FGAN e.V., Neuenahrer Str. 20, Wachtberg 53343, Germany

Abstract— This contribution presents a very efficient Shooting-and-Bouncing-Rays (SBR) algorithm, which has been combined with Physical Optics (PO) and the Physical Theory of Diffraction (PTD). According to previous studies, this algorithm has been proved to provide very accurate results when calculating mono- or bistatic RCS of arbitrary large metallic objects. To enhance the accuracy of the simulations, diffracted rays according to the well-known Uniform Theory of Diffraction (UTD) have been implemented. Also dielectric objects, such as radomes, have been modeled. However, there is a lack of validation possibilities because numerically exact methods generally require much more computational resources for dielectric objects.

Recent advances of the presented ray tracing algorithm include the modeling of objects composed of metallic as well as dielectric parts. A special class of such objects are cavities with a dielectric filling, which can easily be studied in terms of RCS measurements in a standard anechoic chamber and thus serve as ideal objects for validation purposes. Furthermore, the simulations allow the fast generation of data over a certain frequency band, which can be used for calculating a two-dimensional image of the object. Such images can also be used for visualization of the main scattering phenomena. In the case of the empty cavity, virtual scattering centers can clearly be assigned to specific directions of incidence and multiple reflections inside the cavity. These directions also coincide with RCS maxima in the azimuth plane. If the cavity is filled with a PVC cube or slab, propagation mechanisms become much more complex due to multiple reflections inside the dielectric material and enclosed air space, respectively. This leads to a much more complex shape of scattering centers.

Overall, the ray tracing simulations show an excellent agreement with measurement results for both empty cavities and cavities filled with dielectric material. Thus, this ray tracing algorithm is well-suited not only for metallic objects but also for the modeling of objects composed of different materials, e.g., interiors of vehicles, antennas covered by radomes, etc.

REFERENCES

1. Weinmann, F., "Ray tracing with PO/PTD for RCS modeling of large complex objects," *IEEE Trans. Antennas Propagat.*, Vol. 54, 1797–1806, Jun. 2006.
2. Weinmann, F., "PO/PTD ray tracing for arbitrary metallic and dielectric objects," *Proceedings of the EuCAP 2006 — European Conference on Antennas & Propagation*, Nice, France, Nov. 6–10, 2006.

Millimeter Wavelength Limiters Analysis Using RFS-3 Radio Frequency Simulator

Andrey D. Grigoryev
Saint-Petersburg Electrotechnical University "LETI", Russia

Abstract— Designers of *p-i-n* diode microwave limiters and switches encountered serious problems in their drive for better device parameters. These problems are especially hard to solve in millimeter wave band, where parasitic parameters of active and passive elements becomes crucial. So thorough computer simulation and optimization of the limiter have to be performed in order to find optimal design.

This paper presents results of the analysis of a 8-millimeter wave band *p-i-n* diode limiter by means of RFS-3 computer code, implementing vector finite element method (VFEM). The limiter consists of a silicon plate (substrate) *1* (see Fig. 1) placed in the cross section of a rectangular waveguide *2*. Grooves and stubs were made on the one side of the plate by means of anisotropic etching. After that grooves were plated by gold to make power traces *3*. The silicon stubs were implanted by *p*-type dope from one side and *n*-type dope from the other to form *p-i-n* diodes *4*. All diodes are connected in parallel for d. c. and form several columns. In each column diodes are in series connection for RF current and all columns are parallel connected for RF. Such structure provides high limiter attenuation in "closed" state and high level of dissipated power. Total number of diodes changed from 16 (as shown on Fig. 1) to 196 (14 columns each containing 14 diodes) depending on working frequency and maximum input power.

At the first step of simulation parameters of single diode were extracted from its physical model by means of SILVACO ATLAS$^{\text{TM}}$ code. The results showed good agreement with measurement data. Then a model of limiter was created by RFS-3 code (Fig. 1). The diodes were incorporated into VFEM model as surface lumped elements [1] defined by their resistance and capacitance. Fig. 2 shows limiter attenuation versus frequency for two values of diode resistance R and diode capacity C. Attenuation in the "open" state for $C = 0.01\,\text{pF}$ on the central frequency 35 GHz is about 0.2 dB, and in the "closed" state 18 dB. While for $C = 0.01\,\text{pF}$ curve is rather smooth, for $C = 0.03\,\text{dB}$ there exists a number of resonances, caused by distributed slot inductance and diodes capacitance. So it is very important to minimize diode capacitance.

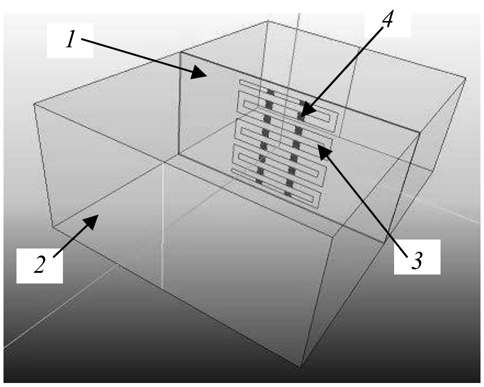

Figure 1.

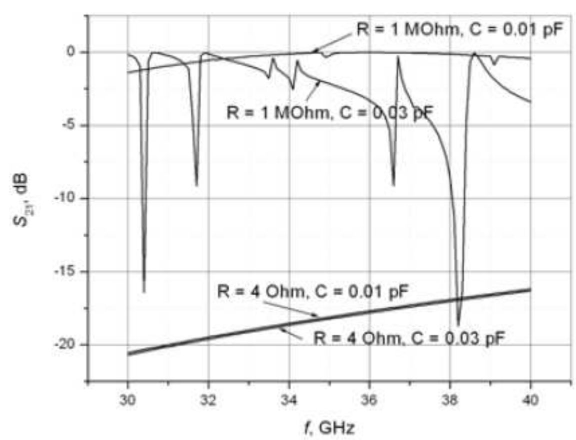

Figure 2.

REFERENCES

1. Grigoryev, A. D., R. V. Salimov, and R. I. Tikhonov, "Multiple-cell lumped element and port models for the vector finite element method," *Electromagnetics*, Vol. 28, No. 1, 18–26, January 2008.

Electromagnetic Simulations of Periodic Structures with FDTD Tools

Bartlomiej Salski, Malgorzata Celuch, and Wojciech K. Gwarek
Institute of Radioelectronics, Nowowiejska 15/19, 00-665, Poland

Abstract— This work discusses formulations of the finite-difference time-domain (FDTD) method for space-periodic problems. Recently, engineering of artificial materials and devices that exploit unique properties of regular periodic structures has become very popular in optics. It also finds recognition in millimeter-wave applications. This includes photonic crystals, metamaterials, microstructured telecommunication fibers, superlensing devices, scatterometry overlay (SCOL) technologies for integrated circuits and many others that take the advantage of specific behaviour of electromagnetic wave in periodic like structures.

This paper presents a brief review of FDTD application to the modelling of these kinds of devices and shows the authors' experience in this field. We will concentrate on two modelling approaches:

The first approach is an eigenvalue analysis of infinite periodic structures that demonstrates their filtering properties and helps in finding photonic band gaps (PBG) to be further exploited in real devices. Of several periodic FDTD algorithms reported in the literature, Complex Looped FDTD (CL-FDTD) with periodic boundary conditions (PBC) is chosen for further developments and use, due to its combined advantages of stability within the whole Courant region and direct Maxwellian form of its internal variables.

The other approach focuses on application of periodic structures in real devices like planar optical waveguides, microstructured fibers with well-controlled dispersion characteristic or SCOL targets. Models of incident plane wave excitation and near-to-far field transformation procedures are customized to the periodic FDTD requirements.

While the whole scope of applications surely exceeds the volume of this contribution, the authors believe that it gives a good grasp of how FDTD method can support electromagnetic modelling of periodic problems. Specific attention will also be given to the physical insight into the nature of solutions produced by periodic FDTD algorithms.

Ultra-wideband Co-planar Boat Microstrip Patch Antenna with Modified Ground Plane by Using Electromagnetic Band Gap Structure (EBG) for Wireless Communication

Dalia Nashaat[1], **Hala A. Elsadek**[2], **Esamt Abdallah**[2], **Hadia Elhenawy**[3], **and Magdy Iskander**[1]

[1]Hawaii Center for Advanced Communication, Hawaii, Honolulu, USA
[2]Electronics Research Institute, Giza, Egypt
[3]Faculty of Engineering, Ain Shams University, Cairo, Egypt

Abstract— Although, the remarkable characteristics of the microstrip patch antennas including low profile structure, light weight, and low cost in fabrication extensive researches have been done over the past years to overcome their major drawback of such antennas which is the narrow bandwidth. There were various efforts from researchers toward achieving broader bandwidth. Ultra-wideband (UWB) is an emerging radio technology that has received much attention recently. Ultra-wideband (UWB) communication systems can be broadly classified as any communication system whose instantaneous bandwidth is many times greater than the minimum required to deliver particular information. A new antenna structure using triangular microstrip patch antenna alongside a small trapezoidal shape ground plane with proximity fed by a microstrip line is proposed in this paper. This printed antenna structure resembles as a boat hence it is called boat microstrip patch antenna. The boat MPA is used for ultra-wide bandwidth intelligent antenna systems applications. This antenna was numerically designed using HFSS simulation software package that is based on finite element method. The final proposed antenna design provides an impedance bandwidth ($S_{11} < -10\,\mathrm{dB}$) over the range from 2 GHz to up 35 GHz with a lot of bandwidth discontinuities. Etching 2D electromagnetic band-gap structure (2D-EBG) as dumb-bell shaped shape in line feed results in improving the bandwidth more three times compared with the original bandwidth and reduces the antenna size as well as enhances the antenna gain. Details of the antenna design, simulations and measured results based on the reflection coefficient are presented in this paper. Simulations and measurements were carried out, and there are very good agreement between the simulated and measured results. The gain of antenna is also studied and the radiation pattern in both E and H-plane of the proposed antenna are presented.

Optimization of Complex Microwave Systems with CORS RBF Network Backed by FDTD Analysis Data

Ethan K. Murphy and Vadim V. Yakovlev
Department of Mathematical Sciences, Worcester Polytechnic Institute, Worcester, MA 01609, USA

Abstract— With computer-aided design (CAD) and optimization of microwave (MW) systems being the subjects of considerable interest due to their potential of direct practical use, computational tools available for efficient optimal design still remain relatively limited. They are effectively restricted to certain classes of MW systems for which suitable physical or empirical models exist (and thus make space-mapping (SM) technologies [1] applicable) and to those structures whose electromagnetic (EM) analysis takes reasonably low CPU time. Optimization techniques based on the EM-simulated responses seem to be attractive for a very large group of MW systems whose complex physics is accessible for 3-D full-wave numerical analysis. However, direct optimal CAD of such devices may require a large number of design variables (and thus substantial amount of EM analyses) to be involved and hence be impractical.

This explains the motivation for the current trend of further cultivation of the SM-based optimization techniques, but also indicates that new avenues enhancing efficiency of methodologies backed by full-wave EM simulation are definitely worth further exploring. In our previous study [2], we have explicitly addressed, for the first time, the problem of reduction of the number of necessary simulations in FDTD-backed optimization: the introduced artificial neural network (ANN) algorithm featuring special mechanisms (e.g., the decomposed radial basis function (RBF) network, its dynamic training with adding a local minimum from each iteration to the database, etc.) has been shown to be capable of finding good local optimal solutions in specified domains with the use of relatively small data sets.

In this contribution, we outline two crucial revisions of the RBF network optimization algorithm [2] that result in dramatic improvement of its performance. Dealing with frequency responses of S-parameters of MW structures, we introduce a new objective function (OF) that measures the bandwidth of the respective characteristic over specified "optimality zones". Second, we principally advance the technique of dynamic training: when selecting additional sample points, we use, for the first time in electromagnetic optimization, constrained optimization response surfaces (CORS) technique [3] — a global optimization response surface type algorithm designed to minimize the number of function evaluations in the process of finding the global minimum. As earlier in [2], analysis data for this optimization algorithm are generated by the 3-D conformal FDTD simulator QuickWave-3D [4].

We compare the resulting technique with its predecessor [2] by monitoring the effects of the new OF and the CORS sampling. The CORS-RBF technique operating with the new OF appears to be responsible for getting optimal solutions of better "quality" (when the solution satisfying all the applied constraints does not exist in the specified domain) and a spectacular reduction of the number of EM analyses in comparison with the technique [2]. Performance of the CORS-RBF algorithm is illustrated by optimizing $|S_{11}|$ frequency responses of an inductively coupled waveguide band-pass filter, a microwave oven with a cylindrical load, and a dielectric resonator antenna. Their optimal designs are found from 5-parameter optimizations requiring only 167, 177, and 99 analyses, respectively, whereas the RBF technique [2] with both old (norm-based) and new (bandwidth-based) OFs and the CORS-RBF algorithm with the old OF are merely unable to find those optima with as many as 1000 analyses. These examples show that the reported algorithm substantially outperforms its predecessor [2].

It is important to note that the CORS-RBF technique and the new OF are independent of the source of data. That is, even though in the presented version the algorithm works with data of FDTD analyses, it will be fully operational working with data generated by other numerical techniques (MoM, FEM, etc.). Overall, the results of this paper clearly show a feasibility of further development of full-wave modeling-backed techniques and a great potential of the CORS-RBF algorithm as a practical CAD tool applicable to a wide array of complex MW systems.

REFERENCES

1. Koziel, S., J. W. Bandler, and K. Madsen, "A space mapping framework for engineering optimization: Theory and implementation," *IEEE Trans. Microwave Theory Tech.*, Vol. 54, No. 10, 3721–3730, 2007.

2. Murphy, E. K. and V. V. Yakovlev, "RBF network optimization of complex microwave systems represented by small FDTD modeling data sets," *IEEE Trans. Microwave Theory Tech.*, Vol. 54, No. 7, 3069–3083, 2006.
3. Regis, R. G. and C. A. Shoemaker, "Constrained global optimization of expensive black box functions using radial basis functions," *J. Global Optim.*, Vol. 31, No. 1, 153–171, 2005.
4. QuickWave-3D, QWED Sp. z o.o., Warsaw, Poland, 1998–2009. http//:www.qwed.com.pl/.

Microwave Imaging in Closed Cavities — Locating Spatial Inhomogeneities of Dielectric Objects

Alexander V. Brovko[1], **Ethan K. Murphy**[2], **Matthias Rother**[3], **Heike P. Schuchmann**[3], **and Vadim V. Yakovlev**[2]

[1]Department of Applied Information Technologies, Saratov State Technical University
Saratov 410070, Russia
[2]Department of Mathematical Sciences, Worcester Polytechnic Institute
Worcester, MA 01609, USA
[3]Institute of Life Sciences, University of Karlsruhe (TH), Karlsruhe 76131, Germany

Abstract— Detection of inhomogeneities in dielectric materials is required in many practical applications; these include reconstruction of voids inside concrete structures or bricks, detection of defects in wood slabs and in composite panels, detection of porosity in ceramics and molded rubber, monitoring of inhomogeneities in food products, etc. One of possible techniques for its solution is microwave (MW) imaging [1]. The recent advances in the theory and solution techniques for inverse problems in free space (see, e.g., [2]) has inspired substantial progress of MW imaging in open space despite the fact that corresponding experimental implementations of practical techniques of non-destructive evaluation and testing (NDE/NDT) are typically quite complicated. In terms of measurements, MW imaging in closed systems may be simpler and provide high accuracy of measurements [3], however, the techniques of NDE/NDT of materials by the waveguide/resonator fields have not received an in-depth consideration so far — in part, likely due to substantial complexity of theoretical aspects of the related inverse problem.

In this contribution, we present an extension of our original technique [4] for the detection of a position and a size of an object in a dielectric sample placed in a waveguide. The technique relies on an artificial neural network used for the numerical inversion of the problem and reconstruction of geometrical parameters of the tested object. It requires only elementary measurements of complex reflection and transmission coefficients. A direct scattering problem is solved with the use of full-wave 3D FDTD analysis; corresponding numerical data are employed for network training and testing. Here we explore the applicability of this technique introduced in [4] for spherical inclusions to diverse combinations of materials (low and high contracts) and alternative shapes. Required numerical data are obtained with the 3-D conformal FDTD simulator *QuickWave-3D* [5].

We present the numerical results for detection of an inhomogeneity in an object for:

(1) a glass sphere in a rectangular Teflon block,
(2) an air sphere in a rectangular Teflon block,
(3) a sphere of unfrozen raw beef in a rectangular block of frozen raw beef, and
(4) a sphere of frozen raw beef in a rectangular block of unfrozen raw beef.

Our computational experiments with the WR975 (248×124 mm) waveguide show that, at 915 MHz, the sizes and position of the glass and air spheres of more then 15 mm diameter are detected with the average error of 0.9–2.2%. The cases involving raw beef are more complex due to the significantly larger loss factor of the unfrozen beef. However, our technique allows for reconstructing, with an acceptable accuracy and for a reasonable computational cost, the unfrozen spheres of more then 12 mm diameter and the frozen spheres of more then 40 mm diameter. Finally, it is shown that the method can also be straightforwardly adjusted to the scenarios of reconstruction of inclusions of other (e.g., cylindrical, ellipsoidal, etc.) shapes.

REFERENCES

1. Zoughi, R., *Microwave Testing and Evaluation*, Kluwer, Amsterdam, 2000.
2. Colton, D. and R. Kress, *Inverse Acoustic and Electromagnetic Scattering Theory*, Springer, Berlin, 1998.
3. Meyer, T., A. Jostingmeier, and A. S. Omar, "Microwave imaging using a novel regularization scheme," *Proc. IEEE AP-S Intern. Symp.*, Vol. 3, 175–178, Jun. 2003.
4. Brovko, A. V., E. K. Murphy, M. Rother, H. P. Schuchmann, and V. V. Yakovlev, "Waveguide microwave imaging: Spherical inclusion in a dielectric sample," *IEEE Microwave and Wireless Comp. Lett.*, Vol. 18, No. 9, 647–649, 2008.
5. *QuickWave-3D*, QWED Sp. z o.o., Warsaw, Poland, 1998–2009 http://www.qwed.com.pl/.

Cell Bathing Medium as a Target for Non-thermal Effect of MMW on Heart Muscle Contractility

G. S. Ayrapetyan, **E. H. Dadasyan**, **E. R. Mikayelyan**, **S. V. Barseghyan**, **and Sinerik Ayrapetyan**
UNESCO Chair-Life Sciences International Postgraduate Educational Center, Armenia

Abstract— In may presentation I will present data on the comparative study of the effects of weak intensity specific absorption rate (SAR = 2 mW/g) of 60 GHz millimeter wave (MMW) and near Infrared (IR) irradiation on thermodynamic properties, specific electrical conductivity (SEC) and hydrogen peroxide (H_2O_2) content of distilled water (DW) and physiological solution (PS), as well as on MMW-treated PS on heart muscle contractility, neuronal membrane functional activity and on the number of cellular mechanisms regulating the muscle contractility and neuromembrane activity. The thermal effect of MMW and IR on DW and PS has different kinetics: MMW heating inhibits in the first minute of exposure, while the IR-induced heating starts sharply from the first minute of irradiation. The heat fusion of MMW-pretreated DW and PS after freezing by liquid nitrogen (N_2), is significantly less than the heat fusion of sham and IR-treated DW and PS. MMW irradiation has time-dependent elevation effect on water SEC and SAR, which is accompanied by the increase of H_2O_2 formation in it. We suggest that the MMW-induced vibration of water dipole molecules causes the non-thermal changes of physicochemical properties of DW and PS as a result of the increase of water molecules dissociation bringing to the formation of H_2O_2 in it.

The direct exposure of MMW (SAR = 2 mW/g), MMW-pretreated PS and H_2O_2-containing PS has a similar stimulation effect on heart muscle contractility, modulation effect on agonist-induced and potential-dependent membrane currents, which was accompanied by the increase of intracellular cAMP and Ca concentration, muscle dehydration and the decrease of the number of functionally active ouabain receptors in membrane.

The Na^+/K^+ pump inhibition elevates the effect of MMW, MMW-treated and peroxide containing PS on heart muscle and neurons.

Thus, the obtained data allow us to consider the water dissociation as a main target through which the non-thermal effect of MMW on physicochemical properties of water is realized, while the MMW-induced formation of H_2O_2 in cell bathing medium serves as a messenger through which the modulation of intracellular metabolism takes place.

Computer Simulation of *p-i-n* Diodes for Integrated Millimeter Wavelength Limiters

Vladimir V. Popov
Svetlana JSC, Saint-Petersburg, Russia

Abstract— Microwave limiters and switches are an integral part of each radar station. Parameters of these devices, especially in millimeter wave-band are mainly determined by the quality of *p-i-n* diodes, used in the equipment. This paper presents results of computer simulation of millimeter wavelength *p-i-n* diodes which were used for developing an electromagnetic model of the limiter. In order to enlarge input power and attenuation of the parasite signal the diodes were arranged in a matrix formed on the surface of the semi-insulating silicon substrate by means of anisotropic etching. The matrix contains from 8 to 196 diodes and is placed in the cross-section of a standard waveguide. A view of a diode matrix with metal power traces, placed into the waveguide is shown on Fig. 1.

Diode simulation was performed by the computer code TCAD$^{\mathrm{TM}}$ SILVACO. Diode structure used in simulation is shown on Fig. 2. The silicon substrate *1* with specific resistance 6 kOhm·cm (acceptor doping $N_a = 2.2 \cdot 10^{12}$) was etched to form grooves *4* and ledges. Each ledge having height 10 µm and, 20 µm and length 70 µm formed *p-i-n* diode base. Vertical edges of the ledges were doped to form p^+ and n^+ contact regions *3* 0.8 µm wide. Grooves were covered with metal to form power traces. Upper surface of the structure was protected by silicon dioxide film *5*.

The described model was analyzed using 2D and 3D TCAD simulators. Differential resistance and capacitance of the diode under various conditions (life time of the carriers, structure temperature, bias voltage) were extracted. It was shown that fringe fields and currents play a significant role and dramatically change diode parameters. For example, diode capacitance enlarges by factor 3 when in 3D simulation compared to 1D result.

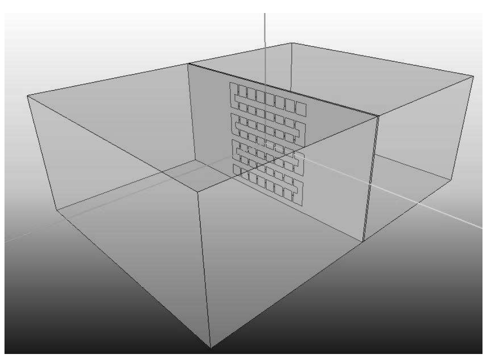

Figure 1.

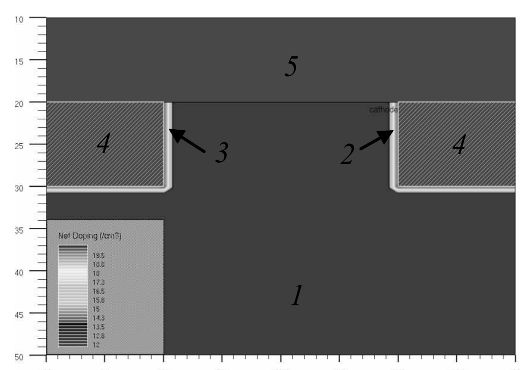

Figure 2.

Calculation of Optimal Volume Ratio at Parallel Using of Ray and FDTD Method

Robert Dady, **Andrea Farkasvolgyi**, **and Lajos Nagy**
Department of Broadband Infocommunications and Electromagnetic Theory
Budapest University of Technology and Economics (BME)
H-1111 Budapest, Goldmann György tér 3, Hungary

Abstract— In this paper we would like to present our results of combining the ray methods and FDTD for office environment. For the optimal combination we have determined several parameters accordingly by minimal calculation electrical field level can be calculated in a good resolution around the receiver.

In our earlier publication we demonstrated the algorithmic complexity for ray method and FDTD. Our simulation environment has been developed for solving a new problem. In this problem we encountered that we have to give the ratio of the size of the space around the receiver and th whole environment size. In the space around the receiver we used the FDTD method while in the other space the ray method was used.

In this article we confirm that the combined using of ray and FDTD methods is more effective than the other calculation procedures.

REFERENCES

1. Wang, Y., S. Safavi-Naeini, and S. K. Chaudhuri, "A hybrid technique based on combining ray tracing and FDTD methods for site-specific modeling of indoor radio wave propagation," *IEEE Transactions on Antennas and Propagation*, Vol. 48, No. 5, 743–754, May 2000.

Session 4A7
Antenna Theory and Radiation 3

Reducing Measurement Uncertainty of Radiated Emission in Fully Anechoic Chamber

András Fehér
Radio Frequency Test Laboratory, Széchenyi István University, H-9026 Győr, Egyetem tér 1, Hungary

Abstract— During the interpretation of the measured results for EMC testing of equipments, the measurement uncertainty values for each of the probable parameters shall be recorded. The value of the measurement uncertainty shall be for each measurement lower than or equal to the data given in the applied standards, e.g., for radiated emissions 6 dB.

The most precise requirements are given for antenna testing, especially at measuring antenna gain. Therefore, usually an outdoor test site is used for antenna measurement and antenna calibration. This fact affects and restricts the antenna measurement possibilities due to the outer climatic conditions.

In case of indoor testing, the value of measurement uncertainty for radiated emission primarily depends on the quality of fully anechoic chamber (FAC), which is usually proportional to the price of the FAC. The biggest component of the measurement uncertainty for radiated emission is the range of normalized site attenuation (NSA), which depends on the reflection of the electromagnetic waves in the FAC. During EMC testing the effect of reflection can be eliminated by changing the height of the measuring antenna. But during antenna testing this method is not an efficient way because of the affect of the transmission characteristic of the antenna under test, the lobes, and the antenna pattern to the measured values.

In the forthcoming paper, we examine the effect of moving of the elements of the measuring system in the FAC to the measurement uncertainty. The distribution of the radiated electromagnetic waves is studied and the effect of the displacement of the measuring and/or measured antenna is mapped. By this method an optimal solution can be found for reducing the measurement uncertainty in the FAC for radiated emission measurements, which can make a smaller chamber be applicable for antenna measurements too.

Effect of Antenna Space on MIMO Channel Capacity in Practicable Antenna Structures

Andrea Farkasvolgyi, **Robert Dady**, **and Lajos Nagy**
Department of Broadband Infocommunications and Electromagnetic Theory
Budapest University of Technology and Economics
H-1111 Budapest, Goldmann Sq. 3, Hungary

Abstract— This article presents our simulation results of 3×3 MIMO (Multiple Input Multiple Output) antenna systems for channel capacity maximization by correlation coefficient between antennas.

We have analysed the effect of different antenna structures for channel capacity values. Several different optimal-structures were found which effect approximately maximal channel capacity. Several structures had to be investigated. The applicability and practicability of structures are the most significant problem and regrettably the realization of some of the constellation is very difficult or impossible.

In the course of this project we have inquired the variation of the correlation coefficient between antennas versus antenna space. In a specific structure the highest channel capacity can be realised if the antenna distances are chosen for optimal. In view of the fact that correlation coefficient is a perfect parameter for characterization of channel capacity. Mention must be made that low correlation issue in high cannel capacity.

It contrasts with our early simulation, in this project the antenna space was changed by different MIMO structures. In this paper, the primary purpose is that we confirm that the maximal channel capacity parallel with minimal antenna correlation coefficient can be realized by selecting of perfect antenna space in a given MIMO antenna structure.

REFERENCES

1. Wallace, J. W. and M. A. Jensen, "Mutual coupling in MIMO wireless system: A rigorous network theory analysis," *IEEE Trans. Wirel. Commun.*, Vol. 3, No. 4, 1317–1325, 2004.
2. Jakes, W. C., *Microwave Mobile Communications*, IEEE Press, 1993.

Investigation for Maximal MIMO Channel Capacity by Genetic Algorithm

Andrea Farkasvolgyi, **Robert Dady**, **and Lajos Nagy**
Department of Broadband Infocommunications and Electromagnetic Theory
Budapest University of Technology and Economics
H-1111 Budapest, Goldmann Sqr. 3, Hungary

Abstract— In this article, we would like to present our results on channel capacity maximization by indoor environment. In this simulation we investigated a 3×3 indoor MIMO (Multiple-Input Multiple-Output) antenna system. By the used indoor model we could perfectly describe the office environment.

In an indoor scenario the standard propagation is NLOS (Non-Line of Sight) thus there are several jamming objects between the transmitter and the receiver devices. The jamming objects around the antennas change phase and level of the transmitted signal. The model statistically describes the material, surface and place of these objects which result in phase and amplitude error in the course of propagation. By this method we could describe the continuously varying indoor environment.

In the actual model the antennas are also inside of the theoretical ball and the scatterer points are on a spherical surface. It contrasts with our earlier simulation, the structure of antennas is not fixed at present, but the antennas can take free position within the ball.

We looked for the perfect antenna structure and position for maximal channel capacity by applying genetic algorithm. In this paper, we would like to present the results of this simulation. In our each simulation we calculated with mutual coupling effect because generally the antennas are not separated neither on transmitter nor on receiver side.

REFERENCES

1. Getu, B. N. and R. Janaswamy, "The effect of mutual coupling on the capacity of the MIMO cube," *IEEE Wireless Propagation Letters*, Vol. 4, 240–244, 2005.
2. http://www.mathworks.com/matlabcentral/fileexchange.

Low Profile Circular Yagi-Uda Array and Planar Collinear Monopole Antenna Comparison

Lajos Nagy, **Andrea Farkasvölgyi**, **and Róbert Dady**
Department of Broadband Infocommunications and Electromagnetic Theory
Budapest University of Technology and Economics
H-1111 Budapest, Goldmann György tér 3, Hungary

Abstract— The paper presents an overview on the development of Circular Yagi-Uda Array and collinear type of antenna. The genetic algorithm is used to optimize the two antenna architecture. The main goal of the article is a comparison of directivity and bandwidth of the two omnidirectional types of antennas. In our analysis, the method of moments (MoM) is used to compute the current distribution and directivity of the yagi antenna. Micro-strip technology is used for planar collinear monopole antenna and simulation with ground plane has been performed using Ansoft HFSS-3D simulator. Prototypes have been realized and measured.

Growing interest in 802.11b, 802.11g and 802.11a has precipitated the need for omnidirectional antennas at 2.4–2.5 GHz, 5.15–5.35 GHz and for special applications in the C band. A number of approaches for gained omnidirectional antennas researches have taken in the past. One of these most promising designs is the collinear dipole arrays which are built up from half wavelength radiators.

A geometry for a planar micro-strip omnidirectional antenna introduced by Bancroft and Bateman is presented [1]. Additionally the circular Yagi-Uda antenna geometry is started from the linear element antenna and by rotating of the elements we have a low profile omnidirectional antenna. The antenna is optimized by varying the lengths and spacing of the circular elements. As comparison the radiation pattern, gain, input reflection and bandwidth are compared for the two antennas.

REFERENCES

1. Bancroft, R. and B. Bateman, "An omnidirectional planar micro-strip antenna," *IEEE Transactions on Antennas and Propagation*, Vol. 52, Nov. 2004.

A Method for Formation of Both Deep and Wide Nulls in the Radiation Pattern of a Phased Array Antenna That Is Resistant to the Presence of Random Distortions of the Amplitude-phase Distribution

A. O. Manichev, **V. A. Balagurovskii**, **and A. S. Kondratiev**
JSC "Altair", Russia

Abstract— Today, control of the radiation pattern of an antenna array operating in a noisy environment that provides the minimum level of the interfering signals is of great practical interest. Here, it is desirable to form nulls by varying only phases of the array elements, because the possibility of phase control is inherent in any phased array and does not require any extra hardware. This procedure is often referred to as phase-only synthesis.

Phase-only synthesis is a complex mathematical problem, which generally allows only an approximate numerical solution. There are many numerical phase-only synthesis procedures. However, most of these procedures imply that the amplitude-phase distribution (APD) over the array elements is exactly known.

At the same time, in practice the APD is realized with certain random errors (distortions). These distortions result in filling the nulls of the array pattern averaged over the ensemble of random realizations of APD distortions. In the case of stationary independent distortions, the minimum level of the average array pattern is determined by the number of the array elements and their amplitudes, as well as the parameters of the APD distortions. This level is further referred to as the background level.

Recently, a method for the phase-only formation of deep nulls in the pattern of a phased array with APD distortions was proposed. This method uses measured complex values of the array pattern. However, this method does not control the width of the formed nulls. This means that, generally, the angular width of these nulls can be unacceptably small, while, in practice, formation of wide nulls is often required (for example, in order to suppress interferences with extended frequency spectrum or interferences moving in space).

If the array APD is exactly known, wide nulls can be formed via the phase-only synthesis of a group of closely spaced nulls in prescribed directions. Unfortunately, the presence of random distortions usually leads to substantial difference between perfect and real array APDs, and, hence, to filling of the pattern nulls.

In order to form both deep and wide nulls in the pattern of an array with random APD distortions, the following method is proposed.

(i) The complex values of the voltage array pattern in the directions of interferences (basic directions) are measured.

(ii) In order to widen the formed nulls, several additional directions in the neighborhood of the respective basic directions are chosen.

(iii) Nulls are formed by the univariate search technique in both basic and additional directions, the initial complex values of the array pattern being determined as follows:

(a) in the basic directions, the measured values $\dot{f}_{Meas}$ are used;
(b) in each of the additional direction, the following linear approximation is used

$$\dot{f}_{Add} = \dot{a}\dot{f}_{Meas} + \dot{b},$$

where $\dot{f}_{Add}$ is the approximated value and $\dot{a}$ and $\dot{b}$ are the complex constants whose values are determined so that synthesized average power pattern in the given direction of the additional null is no greater than the background level.

The efficiency of the proposed method was tested experimentally via formation of one null in the radiation pattern of an unequally spaced phased array with 384 uniformly excited elements. The null was formed sequentially in ten different directions in the nearest side lobes through the use of the following three phase-only synthesis methods:

(i) using theoretical error-free APD;

(ii) using the measured complex pattern value in the basic direction;

(iii) using the proposed method.

The average array patterns in the neighborhood of the formed null are presented in Fig. 1. Curves 1–3 correspond to the methods (i)–(iii), respectively. The obtained results confirm the efficiency of the proposed method and its applicability to solution of a wide class of interference suppression problems.

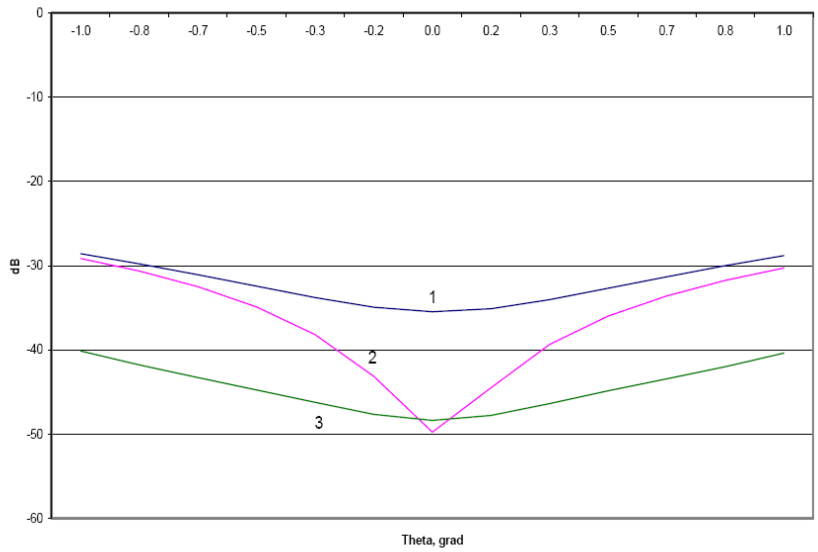

Figure 1: Average array patterns in the neighborhood of the null formed by methods (i)–(iii) (curves 1–3, respectively).

Testing and Optimizing of 16-element Antenna Array

A. Jeziorski[1], **W. Kolosowski**[1], **P.Gajewski**[1], **E. Sedek**[2], **and Z. Bielecki**[1]

[1]Military University of Technology, Poland
[2]Telecomunication Research Institute, Poland

Abstract— The objective of this study is to test and optimize the design of a 16-element antenna array made up of radiating elements in the form of Tapered Slots Antenna (TSA). Optimization of array construction and results of measurement of radiating characteristic of antenna is presented in the paper. The results from the needs to develop broadband antenna elements suitable for a variety of application in the UWB systems.

TSA elements represent now one of the antenna technology areas that develop at the highest rate. This results from the needs to develop broadband antenna elements suitable for a variety of applications on the one hand, and on the other hand from the TSA elements' capacity to meet numerous requirements that are specific to the needs. The aforementioned applications include dynamically developing UWB (Ultra Wide Band) systems and georadars, but also traditional radiolocation and telecommunication systems, a broadening of the antenna bandwidth of which may result in increased data throughput rate and significant improvement of radar system performance. A TSA antenna design should feature a low wave standing coefficient over as wide frequency band as possible, with a symmetrical radiation characteristic retained at minimum side-lobes. A significant requirement was also suitability to transmission operation, i.e., with a high microwave power. Also important were antennas' design simplicity and low manufacturing cost.

A traditional tapered slot antenna (initially called the Vivaldi antenna) was developed on a laminate with appropriately etched fields and power supply paths. Authors of this study have developed a number of such antenna's varieties. It was maintained in the published at that time literature that an antenna developed on a dielectric base (a laminate) may not be used as a transmitting antenna meant to radiate large powers. Therefore a concept was devised of a "metal" antenna made up of two slots cut in two parallel metal walls and an activation loop set perpendicular to the slots. Analysis of measurement results has shown that the TSA elements are the most promising, so it was decided to choose it for multi-element aerial arrays.

The main factors of antenna performance include the slot's shape, as well as the supply loop's design, size, and position. Therefore the designers focused on solving just this problem. For this purpose a computer analysis was completed using WIPL-D software.

Based on the performance of the already developed TSA antenna and the algorithm of programming in the WIPL-D environment a design, development, and computer simulation should be possible of a new TSA antenna and an aerial array made up of eight radiating elements. This should result in better radiation characteristics and broader bandwidth than those of the TSA antenna model hereby presented.

REFERENCES

1. Prasad, S. N. and S.Mahapatra, "A new MIC slot-line aerial," *IEEE Transactions on Antennas and Propagation*, Vol. 31, No. 3, May 1983.
2. Janaswamy, R. and D. H. Schaubert, "Analysis of the tapered slot antenna," *IEEE Transactions on Antennas and Propagation*, Vol. 35, No. 9, Sept. 1987.
3. Kołosowski, W., H. Gruchała, M. Wnuk, and A. Jeziorski, "Antena z rozszerzająca się szczeliną zasilana z linii komplanarnej," *KKRRiT*, Wrocław, 2003.
4. Kołosowski, W., M. Wnuk, and A. Jeziorski, "New construction of tapered slot antennas," *ICAP'2003*, Exeter, 2003.
5. Kołosowski, W., P. Gajewski, A. Jeziorski, and A. Sedek, "The dielectric-free tapered slot antennas array," *EuMW*, Manchester, 2006.
6. Kolundzija, B. M., J. S. Ognjanovic, and T. K. Sakar, *WIPL-D: Electromagnetic Modeling of Composite Metallic and Dielectric Structures: Software User's Manual*, Artech House, Boston, London, 2000.

Miniaturized and Multiband Operations of Inset Feed Microstrip Patch Antenna by Using Novel Shape of Defect Ground Structure (DGS) in Wireless Applications

Dalia Nashaat[1], **Hala A. Elsadek**[2], **Esamt Abdallah**[2], **Hadia Elhenawy**[3], **and Magdy Iskander**[1]

[1]Hawaii Center for Advanced Communication, Hawaii, Honolulu, USA
[2]Electronics Research Institute, Giza, Egypt
[3]Faculty of Engineering, Ain Shams University, Cairo, Egypt

Abstract— Microstrip patch antenna (MPA) with inset feed has been studied extensively over the past two decades because of its advantages. However length of MPA is comparable to half wavelength with single resonant frequency with bandwidth around 2%. Electromagnetic bandgap (EBG) structure as defected ground structure (DGS) is proposed in this paper so that significant improvement in antenna size reduction and multi-band resonant frequencies operation are achieved. Two novel shapes of DGS are investigated. First DGS is comparable to the first iteration of a fractal carpet concept. Second one is composed of four arms of a spiral shape. More than 45% reduction in size is achieved in the first shape. While second shape is two cells of spiral-shaped with four arms are used in the design. Simulation results show that more than 50% reduction in size was achieved as well as fives resonant frequencies resulted from the new design. One resonance resulted from the fundamental patch antenna while the other four resulted from each spiral arms. Acceptable E-plane and H-plane radiation patterns and an antenna gain of about 4 dB are achieved. The band-gap characteristics of the DGS are explained by using high frequency structure simulator HFSS®.

Qualitative Analysis of Dipole Antennas Impulse Radiation

V. A. Permyakov, D. V. Sorokovik, and A. N. Korykin
Moscow Power Engineering Institute (Technical University)
Krasnokazarmennaya St., H. 14, Moscow 111250, Russia

Abstract— Practical applications of ultrashort impulse signals in an radar and radio communications stimulated theoretical studying of non-stationary antenna radiation processes [1]. We had posed a problem of studying the non-stationary field structure for simple antennas (such as the electric dipole, the system of dipoles) with the aid of qualitative theory methods for ordinary differential equations (ODE).

The general approach to the analysis of electromagnetic fields in a pulse radiation mode.

Harmonic fields, as it is known, are defined by its amplitude, phase and polarization. In case of arbitrary dependence of a field intensity vs. coordinates and time curves, the phase concept loses its sense. Instead of the phase concept such field needs to characterize by its components zeros locations in a space-time domain. From this it follows, that as the important parameters of field vector structure in a space-time domain we can consider zeros of this field representing space-time points, in which $\mathbf{E}(\boldsymbol{r}, t) = 0$, $\mathbf{H}(\boldsymbol{r}, t) = 0$. Thus, we arrive at necessity of zeros evolution studying for vector field in a space-time domain. This is a typical problem of the qualitative theory of the differential equations.

In a free space the antenna field is determined in any space point outside of the antenna with the method of retarded potentials for the given exterior charge (a current) impulse of antenna in a space-time. For obvious representation of vector fields we use the concept of force lines. Force lines ODEs can be written with respect to the orthogonal coordinates system, for example, Cartesian. At this one can be limited by the analysis of fields structure in three-dimensional space, but considering the time as a parameter. In general we shall find out the system of three ODEs for force lines in space. The situation becomes simpler in the case of antennas systems with the axial symmetry and for the axial excitation. At thus the problem is reduced to the analysis of the one nonlinear ODE of force lines on a plane.

Analysis results: With the help of ODE qualitative solution methods the impulse fields of electric dipole and the dipoles system, including turnstile and unidirectional antennas are studied . The radiation analysis for antennas being examined was executed by the uniform method both in harmonic, and in impulse radiation modes. At spatial-time method of the analysis both generality and distinctions of radiation processes in these modes have been revealed. In all cases the local qualitative analysis of singular points of fields **E**, **H** and Poynting vector **S** was fulfilled in the beginning. In results, singular points types, their bifurcation conditions and singular points trajectories in space-time domain were determined. The global analysis (construction of force lines as a whole) was performed by numerical methods.

Numerical calculations of force lines **E**, **H**, **S** in a space-time domain for some functions of current impulses upon dipoles are fulfilled. Our qualitative analysis of electromagnetic energy flux for Hertzian dipole matched the numerical results obtained in [1]. It is shown that in a system of N parallel electrical dipoles one can form from 1 to $N - 1$ of fixed zeroes of an electric field near dipoles.

The qualitative analysis of impulse antennas fields represents both methodical, and practical interest. Numerical research meets the certain difficulties in vicinities of singular points of vector field, and qualitative methods are effective exactly in these cases. Therefore, the combination of qualitative and numerical methods is the most expedient and effective way of the analysis of impulse electromagnetic fields.

REFERENCES

1. Hans, S., *The Art and Science of Ultrawideband Antennas*, Artech House, 2005.

Annular Ring Microstrip Patch Antenna on a Double Dielectric Anisotropic Substrate

C. F. L. Vasconcelos[1], **S. G. Silva**[1], **M. R. M. L. Albuquerque**[1], **J. R. S. Oliveira**[2], **and A. G. d'Assunção**[1]

[1]Universidade Federal do Rio Grande do Norte (UFRN), 59078-970 Natal, RN, Brazil
[2]Centro Federal de Educação Tecnológica do Rio Grande do Norte (CEFET-RN)
59015-000 Natal, RN, Brazil

Abstract— There are many commercial applications such as mobile radio and wireless communications that use patch antennas. The interest in designing such microstrip antennas has increased because of light weight, easier to fabrication, conformability, and so forth. In this class of antennas, the annular-ring microstrip antennas exhibit interesting features associated with the annular ring patch. For a given frequency, these antennas, when operating in the fundamental mode, have smaller size as compared to the rectangular or circular patch antennas. This characteristic allows the antenna elements in array designs to be more compacted, favoring the flexibility and the miniaturization of the antenna arrays. The small size is an important requirement for portable communication equipment, such as global positioning satellite (GPS) receivers. Moreover, when compared to the circular patch antenna, the annular ring microstrip antenna has less stored energy and, in this way, a smaller quality factor, resulting in a larger bandwidth [1–3].

Much of the previous work on annular-ring microstrip antenna has been devoted to antennas on isotropic substrates. However, many materials used in microstrip structures have some degree of natural anisotropy, or unintended anisotropy may be present due to material processing. The use of these materials provides flexibility and accuracy in integrated circuit designs because of their intrinsic properties. Also, the anisotropy can be used to overcome patch antennas limitations imposed by the dielectric substrates.

It is the aim of this work to perform an accurate and efficient analysis of annular-ring microstrip antennas on double uniaxial anisotropic substrates, as well as to perform the analyses for annular ring microstrip antennas on a single layer substrate and on a suspended substrate, as particular cases. The analysis uses the full-wave formulation by means of the Hertz vector potentials method in the Hankel transform domain. The dyadic Green function and Galerkin's method are used to determine the resonant frequencies and radiation patterns.

The analysis for suspended annular ring microstrip antenna shows that the various parameters of the annular ring patch antenna are found to depend on the thickness of the air gap between

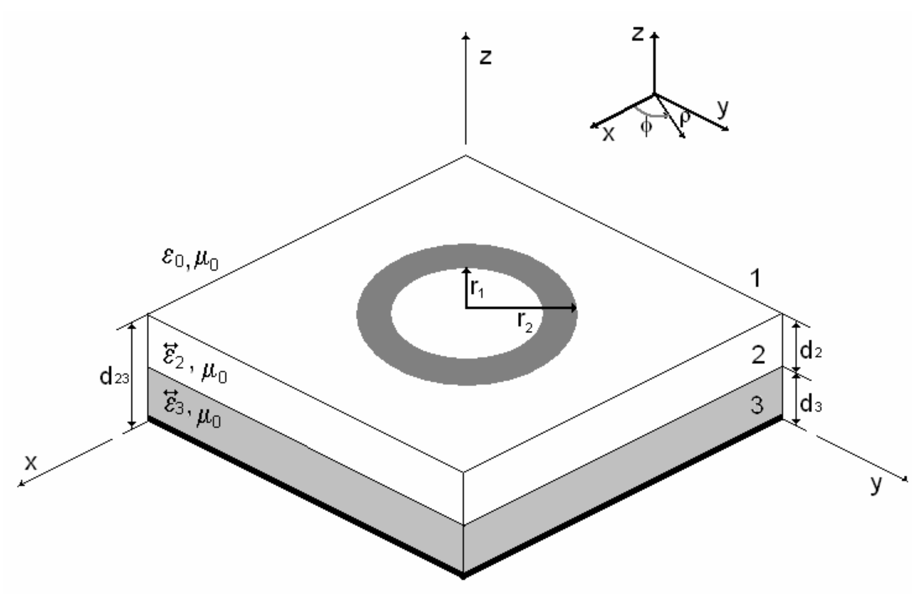

Figure 1: Annular ring microstrip patch antenna on a double dielectric anisotropic substrate.

the anisotropic substrate and the ground plane. Instead of controlling the resonance frequency by changing the radii of annular ring microstrip antenna, it is also possible to adjust the antenna resonant frequency by varying the height of the air layer thickness.

Furthermore, it is shown that anisotropy plays an important role in the designing of microstrip antennas and can not be neglected. It is also found that the resonant frequency of the suspended annular ring microstrip patch antenna can be tuned by controlling the air gap thickness variation.

ACKNOWLEDGMENT

The authors want to acknowledge the Brazilian Research Agencies CNPq and CAPES.

REFERENCES

1. Kanaujia, B. K. and B. R. Vishvakarma, "Some investigations on annular ring microstrip antenna," *Proceedings of the IEEE Antennas and Propagation Society International Symposium*, Vol. 3, 466–469, San Antonio, Tex, USA, 2002.
2. Vasconcelos, C. F. L., S. G. Silva, M. R. M. L. Albuquerque, J. R. S. Oliveira, and A. G. d'Assunção, "Annular ring microstrip antennas for millimeter wave applications," *Int. Journal of Infrared Millimeter Waves*, Vol. 28, 821–829, 2007.
3. Chew, W., "A broad-band annular-ring microstrip antenna," *IEEE Transactions on Antennas and Propagation*, Vol. 30, 918–922, 1982.

Benefits of Material Loading of Electrically Small Resonant Antennas

A. O. Karilainen[1], **P. M. T. Ikonen**[2], **C. R. Simovski**[1], **and S. A. Tretyakov**[1]

[1]Department of Radio Science and Engineering/SMARAD, TKK Helsinki University of Technology
P. O. Box 3000, FI-02015 TKK, Finland
[2]Nokia Research Center, Itämerenkatu 11-13, Helsinki 00180, Finland

Abstract— In this presentation, we study the most advantageous strategies of improving performance characteristics of small resonant antennas using material loading. In the known literature, it is usually assumed that the nature of the equivalent circuits that describe the antenna impedance behaviour near the resonance defines the best loading strategy. In particular, if the antenna resonates as a parallel circuit, its quality factor reads $Q = R/(\omega_0 L)$, where R is the total loss resistance, ω_0 is the resonant frequency, and L is the equivalent antenna inductance. A typical example is a patch antenna. Apparently, such antennas should benefit from magnetic loading, which increases inductance and helps to maintain the same bandwidth with a smaller antenna size. Similarly, antennas which resonate as a series RLC circuit are expected to benefit from dielectric loading. However, we have found that this criterion is not enough general and can bring misleading recommendations. In this presentation, we will discuss the role of the feeding elements and, most importantly, the role of the radiation mechanism of antennas in what concerns the useful effect of material loading. The study is based on comparing the properties of a loaded antenna with a reference antenna which has the same volume and the same resonant frequency as the loaded antenna. This study leads us to rather general conclusions and recommendations on the choice of the type of loading material and on the proper position of the loading material sample in the antenna volume. In particular, we will show that in the majority of situations partial loading is preferable to filling the whole antenna volume with a material.

Session 4A8
Extended/Unconventional Electromagnetic Theory, EHD/EMHD, and Electro-biology

Effect of Exposure to Static, High Voltage Electric Field Generated Nearby HVDC Transmission Lines on Antioxidant Activity of Hepatocytes in Rats

G. Cieslar[1], J. Fiolka[2], J. Mrowiec[1], P. Sowa[3], S. Kasperczyk[2], E. Birkner[2], and A. Sieron[1]

[1]Department and Clinic of Internal Diseases, Angiology and Physical Medicine
Silesian Medical University, Poland
[2]Department of Biochemistry, Silesian Medical University, Poland
[3]Institute of Power System and Control, Silesian University of Technology, Poland

Abstract— In this study the effect of long-term, whole-body exposure to strong, static electric field generated usually nearby high voltage direct current (HVDC) transmission lines on activity of some antioxidant enzymes in liver homogenats of rats was investigated. Experimental material consisted of 64 male Wistar albino rats aged 8 weeks, weighting 180–200 g. During the whole experiment all animals were placed in identical environmental conditions under a 12 h light-dark cycle with free access to standard laboratory pellet food and tap water. All animals were randomly divided into 2 groups (32 animals each). The rats from experimental group were exposed for 56 consecutive days (8 hours daily) to static electric field with electric field intensity values of 25 kV/m (usually measured nearby actually existing HVDC transmission lines), in a specially designed experimental system. The control animals were subjected to a sham-exposure in the same experimental system, during which no electric field was generated between electrodes. At 14th, 28th and 56th day of exposure cycle and then in 28th day after the end of exposure cycle a part of animals from all groups (8 rats at a same time) was exsanguinated in Morbital narcosis. Then in homogenats prepared from obtained liver samples the activity of some antioxidant enzymes as catalase, glutathione S-transferase, glutathione peroxidase, glutathione reductase and superoxide dismutase was determined with use of spectrophotometric methods as well as the concentration of malone dialdehyde (marker of intensity of oxidative processes in tissues) was estimated. As a result of repeated exposures in experimental electric field-exposed group of rats a significant increase in activity of glutathione peroxidase and glutathione reductase at 56th day of exposure cycle, a significant decrease in superoxide dysmutase activity at 14th day of exposure cycle as well as no statistically significant changes in activity of catalase and glutathione S-transferase both during and after the end of exposure cycle were observed. Moreover in experimental group of rats a significant decrease in malone dialdehyde concentration in homogenats of liver tissue at 28th day after the end of exposure cycle as compared to control rats was observed. On the basis of obtained results it was concluded that strong static electric fields with parameters generated usually nearby high voltage direct current transmission lines does not cause any persistent unfavorable effect on antioxidant reactions in the liver of rodents. These data indicate that proper construction of high voltage direct current transmission lines enables to avoid serious health hazards for human population related to disturbances of antioxidant processes in living organisms.

Effect of Exposure to Static, High Voltage Electric Field Generated Nearby HVDC Transmission Lines on Behavior of Rats

G. Cieslar[1], **J. Mrowiec**[1], **P. Sowa**[2], **S. Kasperczyk**[3], **and A. Sieron**[1]

[1]Department and Clinic of Internal Diseases, Angiology and Physical Medicine
Silesian Medical University, Poland
[2]Institute of Power System and Control, Silesian University of Technology, Poland
[3]Department of Biochemistry, Silesian Medical University, Poland

Abstract— In this study, the influence of long-term, whole-body exposure to strong static electric field generated usually near high voltage direct current (HVDC) transmission lines on such behavioral reactions as locomotor activity, exploratory activity, space memory and irritability in rats was estimated. Experimental material consisted of 16 male Wistar albino rats aged 8 weeks, weighting 180–200 g. During the whole experiment, all animals were placed in identical environmental conditions, under a 12 h light-dark cycle with free access to standard laboratory pellet food and tap water. All animals were randomly divided into 2 groups (8 animals each). The rats from experimental group were exposed for 56 consecutive days (8 hours daily) to static electric field with electric field intensity values of 25 kV/m (usually measured nearby actually existing HVDC transmission lines), in a specially designed experimental system. The control animals were subjected to a sham-exposure in the same experimental system, during which no electric field was generated between electrodes. Rats from control group were sham-exposed in the same experimental system, with no electric field generated between electrodes during exposure. The evaluation of behavior was made at 24 hours before first exposure, at 24 hours after first exposure, at 7th, 14th, 21st, 28th, 42nd and 56th day of exposure cycle and at 28th day after the end of a cycle of exposures. A locomotor activity was determined in the "open field" test by recording a number of episodes of crossings, peepings, rearings, washing and defecation per 3 minutes of observation. An exploratory activity was examined in the "hole" test by recording a number of head dips into a board hole per 3 minutes. Space memory was determined by means of water maze test on the basis of measurement of time required for crossing of a specially constructed water maze. An irritability was investigated by means of Nakamura and Thoenen's score test. As a result of repeated exposures in experimental group of electric field-exposed rats a significant decrease in the number of episodes of crossings (at 7th day of exposure cycle), peepings (at 7th and 14th day of exposure cycle) and defecations (at 28th day of exposure cycle) in the "open field" test was observed as compared to control animals. On the other hand, in experimental group of electric field-exposed rats no significant changes in the water maze crossing time, in the number of episodes of rearings and washing in the "open field" test as well as in the number of head dips in the "hole" test and in irritability score were observed comparing with control animals. On the basis of obtained results, one can conclude that long-term, whole-body exposure of rats to strong, static electric field with parameters generated nearby high voltage direct current transmission lines causes only a transient, significant reduction of locomotor activity in the initial phase of exposure cycle, without any persistent changes in the behavior.

Gradient Decay Measurement in NMR Tomography

R. Kubásek[1], **E. Gescheidtová**[1], **and K. Bartušek**[2]

[1]Department of Theoretical and Experimental Electrical Engineering
Brno University of Technology, Kolejní 2906/4, Brno 612 00, Czech Republic
[2]Institute of Scientific Instruments, Academy of Sciences of the Czech Republic
Královopolská 147, Brno 612 64, Czech Republic

Abstract— The magnetic resonance (MR) imaging techniques of tomography and spectroscopy are exploited in many applications. For the MR instruments to function properly, it is necessary to maintain a high quality of homogeneity of the fundamental and gradient magnetic field. The method described leads us to measure gradient decay [1] and determine the quality of generated gradient field [2]. Also, pre-emphasis compensation of the generated gradient can be set correctly and precisely.

The principle of measuring the waveform of gradient pulse consists in determining the changes in the instantaneous frequency [3] of an MR signal produced by the resonance of nuclei excited in two thin layers positioned symmetrically about the gradient field centre. The layer ($30 \times 30 \times 0.6$ mm) of ^{1}H nuclei being measured is staked out using a special fixture. The average inductions of magnetic field $B(r_n, t)$ are measured in the excited layer in the $+r_n$ and $B(r_n, t)$ positions in the $-r_n$ layer; r is one of the (x, y, z) directions. From the differences of the two inductions measured the magnitude of gradient can be calculated according to the relation.

$$G_r(t) = \frac{1}{2r_n}\left[B(r_n, t) - B(-r_n, t)\right]$$

The classical pre-emphasis adjustment sequence (Fig. 1) was used. This sequence outputs a gradient pulse followed by an RF pulse and then acquires data. This series of events can be repeated up to 10 times with varying delays between the gradient pulse and the RF pulse with flip angle α. The delay between the end of the gradient pulses and the FIDs is 0.1 ms. The gradient pulse duration is 30 ms.

The experiments were carried out on an MR tomograph system 4.7 T/120 mm (i.e., 200 MHz for ^{1}H nuclei). Actively shielded gradient coils yield a maximum gradient field magnitude of 180 mT/m. The data measured were processed in the MAREVISI and MATLAB programs.

The novel idea is in mechanically defined measured layer and measured instantaneous frequency of MR signal. This enables long-time measurement with great accuracy, as can be seen from the pulse sequence in Fig. 1.

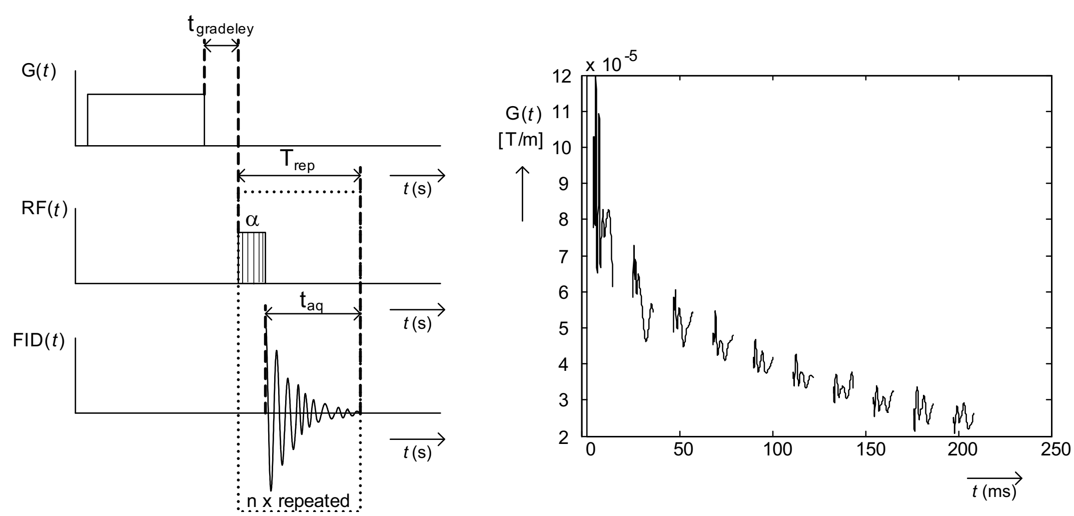

Figure 1: The pulse sequence for gradient decay measurement and measured gradient.

ACKNOWLEDGMENT

This work was supported within the framework of research plan MSM 0021630513 and project of the Grant Agency of the Czech Republic No. 102/07/0389.

REFERENCES

1. Kubásek, R., E. Gescheidtová, and K. Bartušek, "Measurements of time characteristics of the gradient magnetic field," *27th Annual International Conference Medicine and Biology Society*, 1–4, Shanghai, 2005.
2. Bartusek, K. and E. Gescheidtova, "Testing the quality of magnetic gradient fields for studying self-diffusion processes by magnetic resonance methods," *Measurement Science and Technology*, Vol. 17, 2256–2262, 2006.
3. Bartusek, K. and E. Gescheidtova, "MR measurement technique of rapidly switched gradient magnetic fields in MR tomography," *Applied Magnetic Resonance*, Vol. 29, No. 12, 675–686, 2006.

On Compatibility of Classical Electromagnetism with Elements of Non-locality

A. L. Kholmetskii[1], **O. V. Missevitch**[2], **and R. Smirnov-Rueda**[3]

[1]Department of Physics, Belarus State University, Minsk 220030, Belarus
[2]Institute of Nuclear Problems, Minsk 220030, Belarus
[3]Faculty of Mathematics, Complutense University, Madrid 28040, Spain

Abstract— The absence of analogy of quantum mechanical non-locality unavailable in the framework of classical relativistic field theories makes them incompatible with quantum mechanics hindering any foreseeable prospects of success for constructing a consistent physically meaningful description for the transition from quantum to classical phenomena. Moreover, the continuous failure to unlock the problem becomes disappointing and annoying since the majority of physicists consider relativistic field theories and quantum mechanics as being correct in their own domain. Perhaps, the task of reconciling them might be a question of introducing modifications into one of the theories in order to bring it in line with the other.

As response to this fundamental challenge, in this work, we attend some possible aspects of non-locality within the framework of classical electromagnetism from the perspective newly opened by experimental results [1, 2] on manifest non-locality of classical bound electromagnetic (EM) fields in the near zone of a radiating source. The important consequence of having new empirical data is that relativistic locality might have clear limits of applicability resulting in a certain rearrangement in the structure of relativistic field theories leaving vacancy to be filled by non-locality.

To be more specific, we propose to analyze some shortcomings in the conventional procedure for the derivation of symmetric EM energy-momentum tensor which is actually compatible only with homogeneous Maxwell's equations. The trace of such symmetric tensor is always equal to zero that makes it incompatible with any mass tensor. As an alternative to this well-known difficulty, we offer a generalized approach compatible already with inhomogeneous Maxwell's equations [3, 4]. A modified EM energy-momentum tensor turns out to be consistent with non-zero trace requirements for any mass tensor but logically brings to non-locality within the near zone.

REFERENCES

1. Kholmetskii, A. L., O. V. Missevitch, R. Smirnov-Rueda, R. Ivanov, and A. E. Chubykalo, *J. Appl. Phys.*, Vol. 101, 023532, 2007.
2. Kholmetskii, A. L., O. V. Missevitch, and R. Smirnov-Rueda, *J. Appl. Phys.*, Vol. 102, 013529, 2007.
3. Kholmetskii, A. L., *Found. Phys.*, Vol. 36, 715, 2006.
4. Kholmetskii, A. L., *Found. Phys. Lett.*, Vol. 19, 695, 2006.

Fiber Optic Current Sensing in Pulsed Power Application

Radek Kubasek, **Pavel Fiala**, **and Petr Drexler**
FEEC, BUT, UTEE, Kolejni 2906/4, Brno 612 00, Czech Republic

Abstract— In order to optical fiber linear birefringence compensation a promising method was chosen for pulsed current sensor design. The method employs orthogonal polarization conjugation by the back direction propagation of the light wave in the fiber. The Jones calculus analysis presents its propriety. Presented result is a new approach to the Jones calculus treatment in birefringent media. This approach simplifies the analysis. An experimental fiber optic current sensor has been designed and realized. The advantage of the proposed method was proved considering to the sensitivity improvement. The sensitivity has improved by a factor $A_S = 174$ in to compare to the basic sensor setup. The detailed description of the experimental setup is described. For measurement of the sensor bandwith a pulsed current source with very fast rise time is required. The description of the fast rise time current source is presented also.

REFERENCES

1. Rose, A., Z. F. Ren, and G. W. Day, "Twisting and annealing optical fiber for current sensors," *Journal of Lightwave Technology*, Vol. 14, No. 11, 2492–2498, 1996.
2. Tang, D., A. H. Rose, G. W. Day, and S. M. Etzel, "Annealing of linear birefringence in single-mode fiber coils: Applications to optical fiber current sensors," *Journal of Lightwave Technology*, Vol. 9, No. 8, 1031–1037, 1991.
3. Pavlu, M., "The suppression of mechanical stress impacts in fiber optic transmission systems," Bachelor's Thesis, FEEC, Brno University of Technology, Brno, 2008.
4. Drexler, P. and P. Fiala, "Methods for high-power EM pulse measurement," *IEEE Sensors Journal*, Vol. 7, No. 7, 1006–1011, 2007.

Air Ions Concentration Influence on Bacterial Colony Count in the Dwelling Spaces

Z. Szabó[1] **and K. Bartušek**[2]

[1]Department of Theoretical and Experimental Engineering
Faculty of Electrical Engineering and Communication, Brno University of Technology
Kolejní 2906/4, Brno 612 00, Czech Republic
[2]Institute of Scientific Instruments, Academy of Sciences of the Czech Republic, v.v.i.
Královopolská 147, Brno 612 64, Czech Republic

Abstract— The influence of air ion concentration on the bacterial colony count in the living spaces was examined by means of guardian condenser and aeroscopic method. Experiment was realized at the Department of Theoretical and Experimental Electrical Engineering (DTEEE) in the Faraday cage room and in the common laboratory. The methodology and the technique of our measurement are described in this article. Some of our measurement results are presented. The relation between the measured bacterial colony count and the air ion concentration was evaluated. The conclusion is made on the basis of the relations which were found out.

REFERENCES

1. Alpin, K. L., "Instrumentation for atmospheric ion measurements," PhD Thesis, University of Reading, August 2000.
2. Steinbauer, M., P. Fiala, K. Bartušek, and Z. Szabó, "Experiments of accuracy air ion field measurement," *PIERS Online*, Vol. 3, No. 8, 1330–1333, 2007.
3. Bartušek, K., "Měření spektrálních charakteristik iontových polí," 2001. http://www.elektrorevue.cz/clanky/01038/index.html.
4. Bartušek, K., "Měření s aspiračním kondenzátorem," http://www.elektrorevue.cz/.

A Simple Economical Building FDNR Blocks with Modern Operational Amplifiers

Jiří Sedláček and Zoltán Szabó
BUT Brno, UTEE, Kolejní 2906/4, Brno 612 00, Czech Republic

Abstract— Active RC filters designed using non-cascade filter synthesis method exhibit some advantages — namely low sensitivities. However these parameters are paid on the other hand due to the necessity to use more complicated building blocks which should be able to realize a circuit simulation of required ideal RLC ladder prototype elements (e.g., ideal inductors). That fact unfortunately brings higher filter sensitivities to real parasitic properties of active function blocks. Usage of new modern active elements (operational amplifiers with high GBW) and possibilities of goal — directed lossy RLC ladder prototypes enables to design optimized ARC filter realizations with simple and economic active building blocks. These simple grounded active selective blocks working only with one active element enable in present time to design active filters with optimized parameters and minimized influence of real active elements for frequency range up to 1 MHz. In paper here are some parameters of simple and economic building selective blocks with modern active elements at higher frequencies discussed and briefly new possibilities of ARC lowpass filter optimization in some practical examples presented. The active filter research was requested for preprocessing analog signals before digitalization in the NMR signal processing area.

REFERENCES

1. Hájek, K. and J. Sedláček, "Kmitočtové filtry," *Vydavatelství BEN Praha*, 2002.
2. Hájek, K. and J. Sedláček, "Lossy LC ladder prototypes and their use for arc filter optimization," *Wseas Transactions on Electronics*, Vol. 2, No. 3, 94–99, July 2005.
3. Martinek, P. and T. Daša, "Evolutionary algoritmes by ARC filter synthesis," *ECCTD 05*, 155–159, Cork, 2005.
4. Hájek, K., V. Michal, J. Sedláček, and M. Steinbauer, "A simple method of goal-directed lossy synthesis and network optimization," *Advances in Electrical and Electronic Engineering*, 249–253, Žilina, 2006.
5. Hájek, K., V. Michal, and J. Sedláček, "Modern operational amplifiers and their degeneracy effects on active filter performance," *IC-SPETO 2006*, 505–507, Gliwice-Ustroň, 2006.

Noise Spectroscopy in Micro-wave Material Structute Examination

R. Kubásek[1], P. Drexler[1], P. Fiala[1], and K. Bartušek[2]

[1]Dept. of Theoretical and Experimental Electrical Engineering
Brno University of Technology, Kolejní 2906/4, Brno 612 00, Czech Republic
[2]Institute of Scientific Instruments, Academy of Sciences of the Czech Republic
Královopolská 147, Brno 612 64, Czech Republic

Abstract— In the complicated material structure for the micro-wave application (tensor and composite character) is its material properties study by classical single frequency methods connected with a difficulty [1]. In boundary changes with the size close to wave-length can occurs fake information about the examined objects [2]. One possible way to suppress the negative sources of signals is use of wide-band signals, as white noise, and study absorption in the examined material.

The article describe base study of wide-band noise signal use for material study [3]. The aim is find the metrology method for metamaterial study in the frequency range about 100 MHz to 10 GHz.

ACKNOWLEDGMENT

This work was supported within the project of the Grant Agency of the Czech Republic No. 102/09-/0314.

REFERENCES

1. Maslovski, S., S. Tretyakov, and P. Alitalo, "Near-field enhancement and imaging in double planar polariton-resonant structures," *J. Appl. Phys.*, Vol. 96, 1293, 2004.
2. Freire, M. and R. Marques, "Near-field imaging in the megahertz range by strongly coupled magnetoinductive surfaces: Experiment and ab initio analysis," *J. Appl. Phys.*, Vol. 100, 063105, 2006.
3. Machac, J., P. Protiva, and J. Zehentner, "Isotropic epsilon-negative particles," *2007 IEEE MTT-S Int. Microwave Symp. Dig.*, TH4D-03, Honolulu, USA, June 2007.

Session 4A9
Theory and Modeling of Multimode Transmission Lines: Waveguides, Microstrip Lines, Dielectric Waveguides 1

Integral Equation Method in the Theory of Dielectric Waveguides

E. M. Karchevskiy
Kazan State University, Russia

Abstract— The eigenvalue problems for generalized natural modes of dielectric waveguides are formulated as problems for the set of time-harmonic Maxwell equations with partial radiation conditions (Sveshnikov radiation conditions) at infinity in the cross-sectional plane. All of the known natural-mode solutions (i.e., guided modes, leaky modes, and complex modes) satisfy the partial radiation conditions at infinity. The generalized eigenvalues of these problems are the complex propagation constants β on a logarithmic Reimann surface. The partial radiation conditions in these problems are connected with the fact that wavenumbers may be complex. For real wavenumbrs on the principal ("proper") sheet of this Reimann surface, one can reduce the partial radiation conditions to either the Sommerfeld radiation condition or to the condition of exponential decay. The partial radiation conditions may be considered as a generalization of the Sommerfeld radiation condition and can be applied for complex wavenumbers. These conditions may also be considered as the continuation of the Sommerfeld radiation condition from a part of the real axis of the complex parameter to the appropriate logarithmic Reimann surface.

The generalized natural modes of an inhomogeneous dielectric waveguide without a sharp boundary and a step-index dielectric waveguide with smooth boundary of cross-section are considered. The original problems by integral equation method are reduced to nonlinear spectral problems with Fredholm integral operators. Theorems on spectrum localization are proved, and then it is proved that the sets of all eigenvalues of the original problems can only be some sets of isolated points on the Reimann surface, ant it also proved that each eigenvalue β depends continuously on the frequency and refraction index and can appear and disappear only at the boundary of the Reimann surface. The Galerkin methods for numerical calculations of the generalized natural modes are proposed, and the convergence of the methods is proved. Some results of numerical experiments are discussed.

Exact Nonlocal Boundary Conditions in the Theory of Dielectric Waveguides

R. Z. Dautov and E. M. Karchevskiy
Kazan State University, Russia

Abstract— Optical waveguides are dielectric cylindrical structures that can conduct electromagnetic energy in the visible and infrared parts of the spectrum. The waveguides used in optical communication are flexible fibers made of transparent dielectrics. The cross section of a waveguide usually consists of three regions: the central region (core) is surrounded by a cladding which, in turn, is surrounded by a protective coating. The refractive index of the core can be constant or can vary over the cross section; the refractive index of the cladding is usually constant. The coating is optically isolated from the core; for this reason, it is usually neglected in mathematical models, and it is assumed that the cladding is unbounded from the outside. We use the classical model, in which the waveguide is assumed to be unbounded and linearly isotropic.

The original problem is formulated for the entire cross-sectional plane and (except for a point spectrum) has a continuous fragment of the spectrum. Although the location of this fragment is known exactly, a numerical solution requires that false approximate solutions be detected and discarded. The original problem using exact nonlinear boundary conditions is reduced to a linear parametric eigenvalue problem in a circle, which is convenient for numerical solution. This problem has no continuous spectrum. Moreover, its spectrum is identical to the point part of the spectrum of the original problem. The examination of solvability of the obtained problem is based on the spectral theory of compact self-adjoint operators. The existence of surface waves is proved, and properties of the dispersion curves are investigated. An algorithm for the numerical solution of the problem based on the discretization of the equations using the finite element method is proposed. The convergence of the numerical method is proved. Numerical results are discussed.

The Over-determined Boundary Value Problem Method in the Electromagnetic Waves Propagation and Diffraction Theory

N. B. Pleshchinskii[1], **I. E. Pleshchinskaya**[2], **and E. M. Karchevskiy**[1]

[1]Kazan State University, Russia
[2]Kazan State Technological University, Russia

Abstract— The over-determined boundary value problems in the partial domains are proposed to be used as the auxiliary problems to investigate the wave processes in the complex structures. It is necessary to have more boundary conditions on the common part of boundary of the partial domains than it is necessary to obtain the unique solution. Both the tangential components of the electric vector and of the magnetic vector are to be given by connecting of the electromagnetic fields. The necessary and sufficient conditions of solvability of the over-determined problem are the dependences between the boundary functions. These dependences can be obtained in terms of the Fourier transforms or Fourier coefficients of the boundary functions. The linear sets of equations appear by connecting of the domains by homogeneous surfaces or lines. All boundary functions can be found by these linear equations. In the case when we have the inhomogeneity (thin screen) on the media interface such sets of the equations transform into integral or summatorial equations. By this the solvability conditions for the over-determined problems essentially are used to regularize the equations. The diffraction problems for the electromagnetic waves on the conducting screens in the space and in the waveguides with metallic walls are considered as the examples.

The solvability conditions for the over-determined boundary value problem for Maxwell's set of equations are obtained in the form of the connection between Fourier transforms of the boundary functions. The conditions at the infinity are formulated by the analogous way. The integral equations of different forms equivalent to the diffraction problem of electromagnetic wave on the conducting thin screen are obtained. The diffraction problems for electromagnetic wave in the closed waveguides of arbitrary section on the coordinate and non-coordinate inhomogeneities are considered.

Eigenmodes of a Screened Slot Line

A. S. Il'inskiy and E. V. Chernokozhin
Moscow State University, Faculty of Computational Mathematics and Cybernetics, Russia

Abstract— The problem of eigenmodes of a screened slot line is considered. The line consists of two rectangular waveguides coupled through a slot in the common horizontal wall and is characterized by the total width c, heights of the waveguides b_1 and b_2, and permittivities of the waveguide fillings ε_1 and ε_2. The aim is to find solutions to the system of the homogeneous Maxwell equations that correspond to traveling waves.

This problem is reduced to a boundary value problem for the system of the Helmholtz equations

$$\begin{aligned} \Delta E_z^i + \tilde{k}_i^2 E_z^i = 0 \\ \Delta H_z^i + \tilde{k}_i^2 H_z^i = 0 \end{aligned} \tag{1}$$

with respect to the longitudinal field components E_z^i and H_z^i in the upper and lower waveguides ($i = 1$ and 2, respectively), where $\tilde{k}_i^2 = k_i^2 - \gamma^2$, $k_i^2 = \omega^2 \varepsilon_i \mu_0$.

Using the Green's functions G_1^2, G_2^2, G_1^1, and G_2^1 of the first and second boundary value problems for the Helmholtz equation in the upper and lower rectangles, the boundary value problem for system (1) is reduced to the uniform matrix integral equation

$$\begin{pmatrix} K_{11}(\gamma) & K_{12}(\gamma) \\ K_{21}(\gamma) & K_{22}(\gamma) \end{pmatrix} \begin{pmatrix} \varphi \\ \psi \end{pmatrix} = \begin{pmatrix} 0 \\ 0 \end{pmatrix} \tag{2}$$

with respect to the unknowns $\varphi = \frac{1}{\tilde{k}_2^2} \frac{\partial H_z^2}{\partial y}\Big|_{y=0}$ and $\psi = \omega \frac{\partial E_z^2}{\partial x_0}\Big|_{y=0}$.

The half-slotwidth l is treated as a small parameter. The study of the spectrum of the operator-valued function $K(\gamma)$ of system (2) is based on the possibility to represent $K(\gamma)$ by the sum

$$K(\gamma) = X(\gamma) + C(\gamma) + s(\gamma), \tag{3}$$

where operator $X(\gamma)$ is an explicitly invertible operator, $C(\gamma)$ is a one-dimensional operator, and $s(\gamma)$ is a small operator, which means that $\|s(\gamma)\| \to 0$ as $l \to 0$. Representation (3) depends on the point γ.

It is shown that, for sufficiently small l, the points of spectrum can be situated only in the vicinity of the poles of Green's functions G_1^2, G_2^2, G_1^1, and G_2^1 and the roots of equation

$$k_1^2 + k_2^2 - 2\gamma^2 = 0.$$

Therefore, the dispersion curves can only pass near the line

$$(\gamma/k_1)^2 = (1+\varepsilon)/2. \tag{4}$$

and the curves

$$\frac{\gamma}{k_j} = \sqrt{1 - \pi^2 \left(\frac{n^2}{c^2} + \frac{m^2}{b_j^2} \right)}, \quad j = 1,\, 2; \quad n, m = 0,\, 1,\, 2, \ldots \tag{5}$$

The dispersion curves can be classified according the proximity to one or another limiting curves (4) or (5). Thus, pole curves (5) are the limiting curves for dispersion curves corresponding to the quasi-TE- and quasi-TM-modes of the slot line. Line (4) is the limiting curve for the dispersion curve corresponding to the slot mode. Since some of the limiting curves intersect with each other, mutual transformation of different types of modes with changing frequency take place.

Representation (3) makes possible an approximate inversion of the operator valued function $K(\gamma)$ and obtain the dispersion equations, which also can be solved approximately in the explicit form and allow the analysis of the mutual transformation of modes.

The Radiotransparent Windows Formed of Waveguides with Complex Cross Sections

A. S. Ilinskiy[1] **and Yu. Ya. Kharlanov**[2]

[1]Moscow State University, Russia
[2]16th Central Research Institute, Russia

Abstract— The use of radiotransparent waveguide windows (frequency-selective surfaces) is a promising line in the development of highly durable and vibrostable centimeter- and millimeter-wave antennas. One of the main requirements of radiotransparent waveguide windows is good matching of their aperture surfaces with free space. Reflections from a window are determined to a considerable extent by reflections from the apertures of its waveguide elements. Available structures of waveguide windows contain square, circular, and rectangular waveguides whose open ends are poorly matched with free space. In addition, windows based on square and circular waveguides cannot be applied in a wide frequency band when frequency-coverage coefficient K_f equal to the ratio of the upper and lower frequencies of a waveguide window exceeds ~ 1.2–1.3.

The use of waveguides with a complex shape of the cross section can improve the characteristics of radiotransparent windows. A change in the parameters of sections can govern the internal and external characteristics of radiators and radiotransparent windows based on such waveguides.

When the operating frequency band is relatively narrow ($K_f < 1.3$–1.4), square, hexahedral, cross-shaped, and square four-ridge waveguides are of the most practical interest for designing waveguide windows ensuring operation with the rotating field polarization. Such waveguides form dense cellular packages without parasitic zones in the aperture that are not related with the waveguide channels of the window.

Wideband waveguides with a complex shape of the cross section, e.g., H-shaped, modified cocoon-shaped, etc., waveguides, that efficiently operate within the necessary frequency band in the single-mode regime should be applied when radiotransparent windows are employed in a continuous frequency range.

When neighboring frequency bands are considerably spaced, the use of combined structures each of which operates in one of the frequency bands is more efficient. Variants of double-band combined radiating apertures based on cross-shaped and four-ridge (circular and square) waveguides are considered.

Combination of radiating elements of different bands in one aperture may lead to noticeable interaction between these elements due to diffraction effects on their surface. The interaction of subarrays of a combined double-band aperture can be eliminated by using open ends of diaphragmatic waveguides as radiators of a low-frequency subarray. In the high-frequency range, these waveguides should have stopbands for all of the supported modes. This possibility is considered in our study.

We have simulated the aperture efficiency for radiotransparent windows with plane surfaces that are periodic structures based on double-polarization and wideband waveguides of a complex section with minimal intercenter distances between waveguides. The results of simulation are presented in this report.

In our investigations, we used the mathematical model of an infinite antenna array of waveguides with an arbitrary section. The model involves solution of the exterior problem by means of the solution-joining projection method and solution of the interior problem by means of the finite element method.

The Investigation of Properties of Periodic System of X-ray Waveguides

A. M. Lerer, **M. I. Mazuritsky**, **P. V. Makhno**,
V. V. Makhno, **and G. P. Synavsky**
Southern Federal University, Rostov-on-Don, Russia

Abstract— The performance of X-ray waveguides is based on the phenomenon of total external reflection (TER), which is due to the fact, that dielectric constant of almost all materials for X-ray is less than 1 ($n \approx 1-\delta$). Because $0 < \delta \ll 1$, the vacuum in this frequency range is optically more dense medium than any material matter.

The investigation of peculiarities of X-ray transmission through microcapillary structures in order to develop new focusing devices in longwave X-ray range is one of the priority problems of modern physics, and it's solving could lead to creation of essential methods, instruments and effective technologies for physics, material science, biology, medicine.

It's well-known that at high angles of incidence of electromagnetic waves on the boundary of two mediums with quite close values of coefficients of refraction, the coefficients of reflection of two orthogonal polarizations are also quite close. This allows to calculate dielectric waveguides (DW), which have close coefficients of refraction of waveguiding region and surrounding media, in scalar approximation. The examples of such DW are optical fibers, especially single-mode fibers, and X-ray waveguides.

Let's consider in scalar approximation the propagation of eigenwaves in $2d$-periodic system of dielectric waveguides. DW are infinite in z-direction. The indices of refraction of DW and surrounding media are equal n_1 and n_2, correspondingly, periods of grating in x and y axes are $d_{x,y}$. Lets write down the Helmholtz equation for y-component of electric field intensity:

$$\left[\frac{\partial^2}{\partial x^2}+\frac{\partial^2}{\partial y^2}-\gamma^2+(kn_2)^2+k^2\delta(x,y)\right]E(x,y)=0, \tag{1}$$

where γ — wave's propagation constant along z-axis, k — wave number in the vacuum,

$$\delta(x,y)=n_1^2(x,y)-n_2^2.$$

Let's take double Taylor of Equation (1) and function $\delta(x,y)$

$$E(x,y) = \frac{1}{d_x d_y}\sum_{m=-\infty}^{\infty}\sum_{n=-\infty}^{\infty}E_{m,n}\exp\left[i\left(\alpha_m x+\beta_n y\right)\right], \tag{2}$$

$$\delta(x,y) = \frac{1}{d_x d_y}\sum_{m=-\infty}^{\infty}\sum_{n=-\infty}^{\infty}\delta_{m,n}\exp\left[-i\left(\alpha_m x+\beta_n y\right)\right], \tag{3}$$

where $\alpha_m=\frac{2m\pi}{d_x}$, $\beta_n=\frac{2n\pi}{d_y}$.

Substituting (2), (3) into (1) and setting equal terms with identical numbers of spatial harmonics. In assumption of continuity of intensities of electric and magnetic fields, we shall obtain the system of linear algebraic equations (SLAE) in variables $E_{m,n}$.

$$\left[-\alpha_m^2-\beta_n^2-\gamma^2+(kn_2)^2\right]E_{m,n}+k^2\frac{1}{d_x d_y}\sum_{p=-\infty}^{\infty}\sum_{q=-\infty}^{\infty}E_{p,q}\delta_{p-m,q-n}=0, \tag{4}$$

$$m=0,\ \pm1,\ \pm2,\ \ldots,\quad n=0,\ \pm1,\ \pm2,\ \ldots.$$

The equality to zero of SLAE (4) determinant is the dispersion equation in γ.

Obtained solution was applied to investigation of propagation of electromagnetic waves in X-ray waveguides and bi-dimensional photonic crystals.

Obtain approximate solution of scalar Helmholtz equation allows to solve quite wide range of boundary problems of applied electrodynamics, including problems of X-ray waves' propagation in waveguides. It was shown, that in practically used microcapillary structures (in $2d$-periodic X-ray waveguides) propagation constants of periodic and single DW are quite close. The problem of electromagnetic waves propagation in photonic crystals ($2d$ periodic system of cylinders) was solves, the influence of cylinder parameters on the location and sizes of opacity window of crystal was investigated.

Mathematical Modeling of Waveguiding Systems Based on Photonic Crystals

A. N. Bogolyubov, I. A. Butkarev, and Yu. S. Dementieva
Faculty of Physics, M. V. Lomonosov Moscow State University, Russia

Abstract—

Introduction: In this paper, we present mathematical model and numerical algorithm allowing to investigate two-dimensional and three-dimensional photonic crystals and waveguiding systems based on photonic crystals. We demonstrate spectral characteristic of photonic crystals and systems based on them.

Photonic crystals have been considered as composite structures made up of two lossless isotropic media with different refractive indices n_1 and n_2. In photonic crystals, the propagation of electromagnetic waves is forbidden for a certain frequency range. This property provides a promising tool to control the flow of light in integrated optical devices. In the last several years, there is a great deal of interest in developing photonic crystal based components such as waveguides, lasers, splitters, fibers, optical circuits, and ultrafast optical switches.

Numerical Algorithm: We construct numerical algorithm allowing to calculate propagation of electromagnetic waves across systems based on photonic crystals. Using this algorithm we calculated spectral characteristics of photonic crystals and waveguiding systems based on them. The algorithm consists of finite-difference time-domain method (FDTD), perfectly matched layer technique (PML) and total-field/scattered-field formulation (TF/SF).

The FDTD method gives the easy way to construct numerical algorithms for calculation of electromagnetic wave propagation in different waveguiding systems. Main disadvantage of this method is high computational cost, it can be overcome by using computer clusters.

The total-field/scattered-field (TF/SF) formulation has been used to model infinite plane wave excitation in two-dimensional (2-D) and three-dimensional (3-D) finite-difference time-domain (FDTD) grids.

The perfectly matched layer is a technique of free-space simulation developed for solving unbounded electromagnetic problems with the finite-difference time-domain method. Referred to as PML, this technique is based on the use of a layer especially designed to absorb the electromagnetic waves without reflection from the vacuum-layer interfaces.

Results: Using this algorithm, we calculated spectral characteristics of two-dimensional and three-dimensional photonic crystals and waveguiding systems based on them. We obtain spectral characteristic of various configurations of photonic crystals, for example, straight waveguides, bends, T-waveguides.

Also we considered bistable photonic crystal configuration consisting of a waveguide sided coupled to a single-mode cavity with Kerr nonlinearity. The results showed the characteristic change of the transmission spectrum resulting in the strong saturation of the response.

Calculation results show that photonic crystals allow to decrease size of optical devices and they are a promising tool to control the flow of light in integrated optical devices.

Our recent investigations concern modeling various waveguiding systems using three-dimensional algorithm.

Improvement on the Stop-band Caracteristics of the LPF Using Coupled Lines and a Chip Capacitor

T. Yasuzumi[1], **O. Hashimoto**[1], **and T. Uwano**[2]

[1]Aoyama Gakuin University, Japan
[2]Office-Uwano, Japan

Abstract— Microwave low-pass filters (LPFs) are well known as a key building block to suppress the unwanted harmonics in various wireless communication systems. Recent years, various types LPFs have been investigated for improving stop-band characteristics using attenuation poles. If the attenuation pole is formed near the passband, sharp skirt characteristics will be obtained. To achieve the requirements above, we focused on a coupled-line hairpin filter.

In this paper, a microstrip LPF with sharp attenuation and broad stopband by using hair-pin structural coupled lines and chip-capacitor is proposed. Figure 1 shows a schematic circuit model of a LPF using coupled lines and a chip-capacitor, and the resonance characteristics of the filter are shown in Figure 2. As shown in Figure 2, the attenuation poles are increased and one pole is realized at near the passband by using 1 pF value capacitor. Moreover, Figures 3 and 4 show the PCB pattern of the LPF and the measured results of the filter shown in Figure 1. As a result, the fabricated LPF has a low insertion loss, the sharp attenuation slope at cutoff frequency and wide-band rejection characteristics.

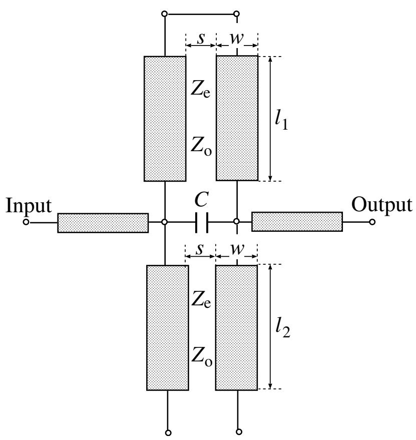

Figure 1: Circuit model of the LPF using coupled lines.

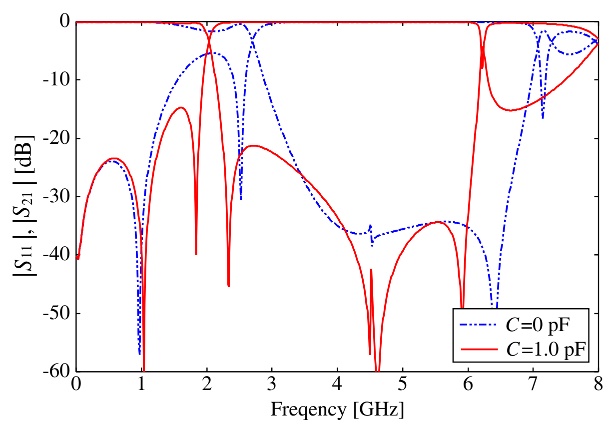

Figure 2: Calculated characteristics of the LPF shown if Figure 1.

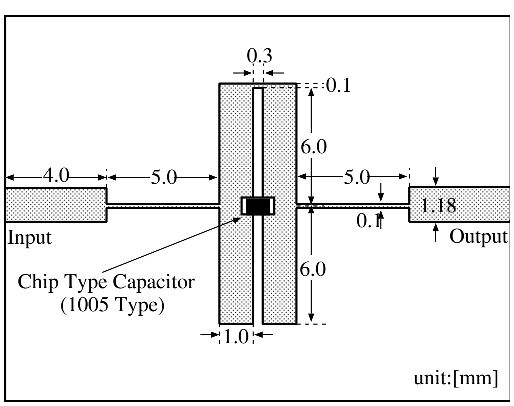

Figure 3: PCB pattern of the LPF shown in Figure 1.

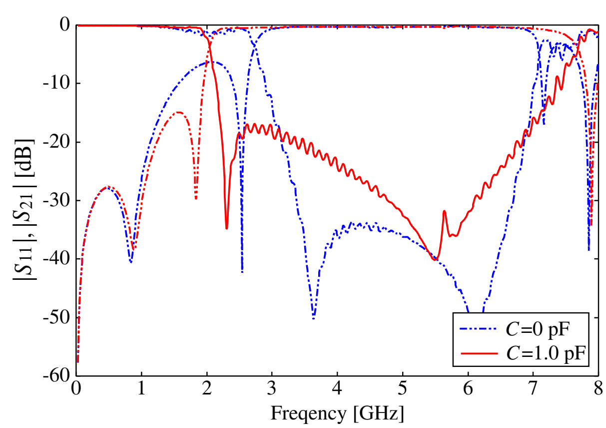

Figure 4: Measured results of the fabricated filter shown in Figure 3.

A Study on the Center Frequency Tunable BPF Using Resonators Loaded by Varactor Diodes

T. Yasuzumi[1], **R. Monzen**[2], **T. Uwano**[1], **and O. Hashimoto**[1]

[1]Aoyama Gakuin University, Japan
[2]Office-Uwano, Japan

Abstract— Recently, tunable BPF's have become an interesting subject. The tunable filters with constant bandwidth, however, not common as topics. In this study, a filter with a tunable bandwidth is proposed.

This paper shows the design of the center frequency tunable BPF with a constant bandwidth using varactor diodes. First, capacitances of a varactor diode is measured with the vias voltages. Fig. 1 shows the measured results. Next, the tunable BPF loaded by varactor diodes is designed based on results in Fig. 1. The circuit model of BPF is shown in Fig. 2. The BPF takes the microstrip line structure with the capacitances connected at the line ends. The circuit pattern of the BPF is shown in Fig. 3. The transmission and return performances of the BPF in Fig. 3 are measured. The results are shown in Fig. 4. From Fig. 4, the tunable characteristics of the center frequency are realized with a constant bandwidth, although the center frequency shift to be lower sides due to the losses caused by the resistance components of the diodes.

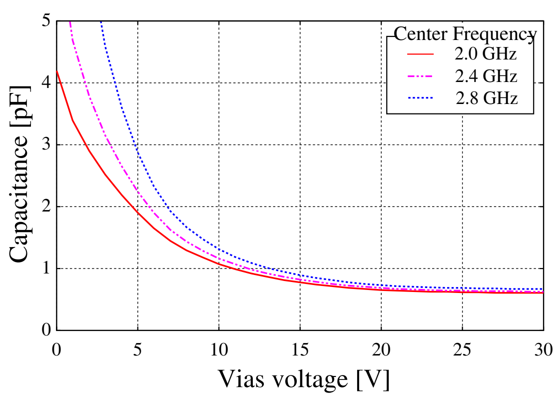

Figure 1: Capacitance variations by frequency.

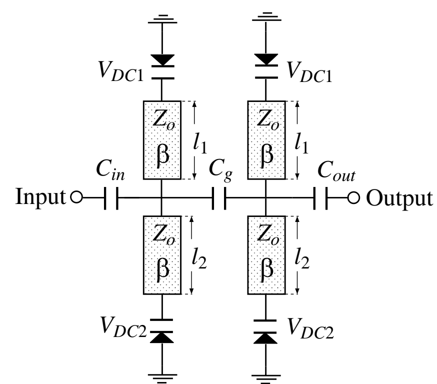

Figure 2: The circuit model of the BPF.

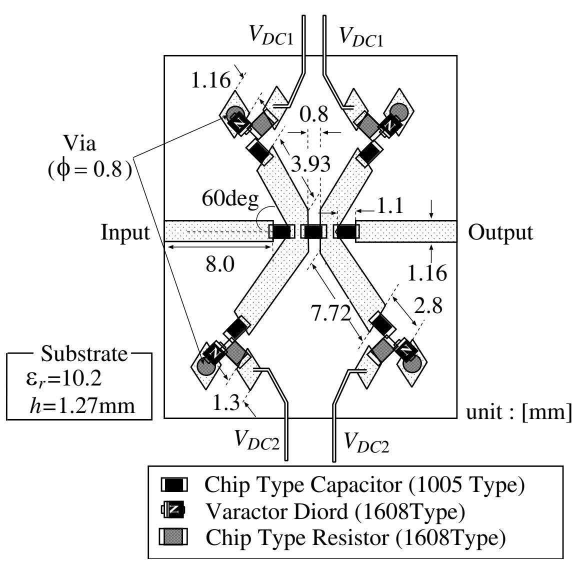

Figure 3: The PCB pattern of the BPF shown in Fig. 2.

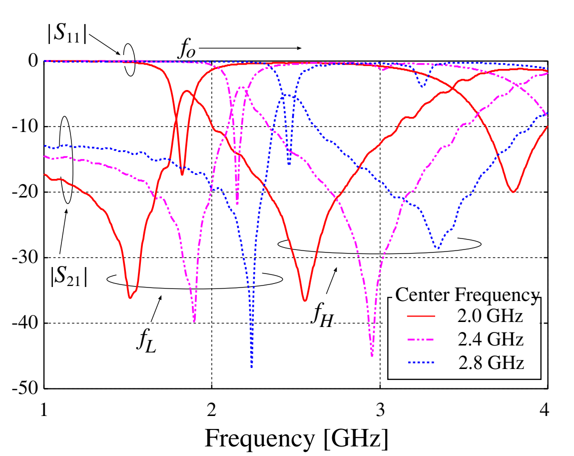

Figure 4: Measured results of the PCB pattern shown in Fig. 3.

Session 4A10
Electromagnetic Field Modeling, Inversion and Applications 2

Fast Evaluation Techniques to Demonstrate Compliance in the Near Field of Active and Passive Transmitters

Niels Kuster[1], **Sven Kühn**[1], **Sergey Perov**[2], **and Quirino Balzano**[1,3]

[1]Foundation for Research on Information Technologies in Society, ETH Zurich, Switzerland
[2]RAMS Research Institute of Occupational Health, Moscow, Russia
[3]Department of Electrical and Computer Engineering, University of Maryland, Maryland, USA

Abstract— Dosimetric compliance tests in the vicinity of active and passive transmitters are extremely time-consuming because the current standards require measurements in 3-D on an exposure-pattern adaptive grid inside a phantom filled with a tissue simulating medium. Since compliance has to be demonstrated for all configurations with every accessory, tests of a single device can take several days. Faster and simpler evaluation techniques are desirable, especially as near field data provide further valuable product design information such as: 1) output power under loaded conditions, and 2) changes of the internal radio frequency pathways, e.g., because of poor contacts.

Several techniques for fast dosimetric evaluations have been proposed in the past including E-field sensor arrays implanted inside a medium [1] [www.speag.com] or free-space H-field based evaluations [2]. The latter exploits the dominant coupling mechanism of radiofrequency energy in materials placed in the close near field of transmitters [3], that is the local SAR is approximately proportional to the square of the magnetic field incident at the surface of a dissipative body. We have evaluated various phones with the standard technique as well as fast evaluation techniques. We will discuss the advantages, disadvantages and the uncertainties of these techniques, and whether the free-space H-field technique is suitable for merging the compliance requirements of ICNIRP [4] with those of the Russian Federation [5].

REFERENCES

1. Kühn, S. and N. Kuster, "Experimental EMF exposure assessment," *Bioengineering and Physical Aspects of Electromagnetic Fields*, 381–410, 3rd Edition, F. S. Barnes and B. Greenebaum, Editors, CRC Press, 2007.
2. Ogawa, K., A. Ozaki, S. Kajiwara, A. Yamamoto, Y. Koyanagi, and Y. Saito, "High-speed SAR prediction for mass production stages in a factory by H-field measurements," *IEEE Antennas and Propagation Society Symposium*, Vol. 2, 1843–1846, June 2004.
3. Kuster, N. and Q. Balzano, "Experimental and numerical dosimetry," *Mobile Communications Safety*, 13–64, N. Kuster, Q. Balzano, and J. C. Lin, Edtors, Chapman & Hall, London, 1996.
4. ICNIRP Guidelines, "Guidelines for limiting exposure to time-varying electric, magnetic and electromagnetic fields (up to 300 GHz)," *Health Physics*, Vol. 74, No. 4, 494–522, 1998.
5. SanPiN 2.2.4.1191-03 Sanitary norms and rules "Electromagnetic fields in occupational conditions," Moscow, 2003 (in Russian).

Temperature Dependable Microwave Dielectric Model for Frozen Soils

V. L. Mironov and Yu. I. Lukin
The Kirensky Institute of Physics of SB, RAS, Russia

Abstract— Data processing in the radar and radiothermal remote sensing of the land requires the knowledge about the impact of the geophysical parameters such as, temperature, soil moisture, and mineralogy, on the soil complex permittivity (CP). Therefore, it is significant to develop adequate dielectric model which takes into account these geophysical parameters. There is the generalized refractive mixing dielectric model (GRMDM) for moist soils suggested in [1]. This model allows to predict the CP frequency spectra of moist soil as a function of parameters dependable on the soil texture and temperature. In the case of thawed soils, the GRMDM has been advanced to establish a physical dependence of spectroscopic parameters on the temperature [2]. Meanwhile, the physical dependence of the GRMDM spectroscopic parameters on the temperature in the case of frozen soils has not being studied yet.

To solve this problem we conducted measurement of the CP of loam soil in the range of temperatures from 25 °C to −25 °C and frequencies from 0.5 GHz to 15 GHz and the temperature dependable GRMDM for this soil was developed, including the frozen soil conditions. The measurements were conducted in the process of both freezing and thawing. While processing the dielectric data measured, we dealt with such types of soil water as liquid and icy unbound water, as well as bound water, having different dielectric properties. The relevant GRMDM spectroscopic parameters were separately determined for all the types of soil water as a function of the temperature. Finally, an assemblage of physical parameters consisting of volumetric expansion coefficients, starting low frequency dielectric constants, activation energies, entropies of activation, starting conductivities, and conductivity incriminations were derived to turn the GRMDM into a parameterized temperature dependable dielectric model pertaining to a given soil texture, the frozen soil condition being included. These physical parameters, in conjunction with dry soil CP and maximum bound water fraction value, were shown to be an all-sufficient set of parameters to make possible predictions of the moist soil CP as a function of frequency, volumetric moisture, and temperature.

The study conducted revealed that bound water did not freeze sharply, and its phase transition was found to be "smeared" over a wide temperature range. Whereas an unbound water had a pronounced phase transition corresponding to crystallization of water and formation of ice. The methodology applied can be used for any type of soil, since it exploits physical parameterization, unlike empirical fitting.

REFERENCES

1. Mironov, V. L., M. C. Dobson, V. H. Kaupp, S. A. Komarov, and V. N. Kleshchenko, "Generalized refractive mixing dielectric model for moist soils," *IEEE Trans. Geosci. Remote Sensing*, Vol. 42, No. 4, 773–785, 204.
2. Mironov, V. L. and S. V. Fomin, "Dependable microwave dielectric model for moist soils," *Progress In Electromagnetics Research Symposium*, Beijing, March 23–27, 2009, to be published.

Mobile Location Method of Radio Wave Emission Sources

P. Gajewski, C. Ziółkowski, and J. M. Kelner
Military University of Technology, Poland

Abstract— Over last decade, the emerging location service of electromagnetic waves sources has found numerous applications in the commercial as well as the military radio systems. The rapid technological advances have made it to implement radio navigation, radio communication nets and military radio electronic recognition. In this paper, we concentrate on location of a radio wave sources in radio communication nets.

This paper deals with the new location method of radio wave sources, based on the Doppler effect. This unique approach was worked out on the ground of analytical solutions, that describe the Doppler frequency in free-space propagation. In this method, the position of radio signal source is calculated on the basis of momentary frequency measurements taken by mobile receiver. Theoretical and simulation analysis of the presented methodology was made before empirical verification process was introduced. This analysis enabled to evaluate technical capabilities and precision of this new location method. Following problems are discussed in this presentation: general outline of the method on the basis of the Doppler effect and preliminary empirical verification results.

Dependence of received signal frequency $f(\mathbf{x}, t)$ in function of movement measuring receiver trajectory was obtained on basis of the analytic description of Doppler effect [1]. Founding, that receiver moves with constant velocity $\mathbf{v} = (\mathrm{v}, 0, 0)$, the Doppler frequency is expressed by following dependence:

$$f_D(\mathbf{x}, t) = f(\mathbf{x}, t) - f_0 = \frac{f_0 k}{1-k^2}\left[k + \frac{x - \mathrm{v}t}{\sqrt{(x-\mathrm{v}t)^2 + (1-k^2)(y^2+z^2)}}\right]$$

where: $\mathbf{x} = (x, y, z)$ — co-ordinates of located radio emission sources, $k = \mathrm{v/c}$, v — measuring receiver velocit, c — speed of light, f_0 — transmitted signal frequency, $f(\mathbf{x}, t)$ — received signal frequency.

The Doppler frequency $f_D(\mathbf{x}, t)$ value depends not only on signal source velocity and carrier frequency but also on mutual space location of a signal source and a receiver. Notice the $f_D(\mathbf{x}, t)$ linear dependence on the frequency carrier, whereas the dependence on velocity and space coordinate has a more complex character. Location calculation are made on the basis of the above formula and the described value of the Doppler frequency shifts as a function of movement and coordinates of signal source parameters. The temporal frequency value $f_{(\mathbf{x}, t)} = f_0 + f_D(\mathbf{x}, t)$ measurement over mobile station is the basis of the new method of the signal source location. The diverse courses of the Doppler curves are characteristic for every location of the electromagnetic wave emission source. It determinates methodology of the frequency offset value using to three-dimensional location.

Basing on above formula individual x, y, z co-ordinates relative to initial mobile station location can be obtained. In case of the mobile station is moving at fixed altitude ($y = \text{const.}$), then it should mark only two x and z co-ordinates. After elementary transformation of the analysis expression for two moments t_1 and t_2 the formulas described x and z co-ordinates are following:

$$\begin{cases} x = \mathrm{v}\dfrac{t_1 A(t_1) - t_2 A(t_2)}{A(t_1) - A(t_2)}, \\ z = \pm\sqrt{\dfrac{\left[\dfrac{\mathrm{v}(t_1 - t_2)A(t_1)A(t_2)}{A(t_1) - A(t_2)}\right]^2}{1-k^2} - y^2}, \end{cases}$$

where $A(t) = \dfrac{\sqrt{1 - F^2(t)}}{F(t)}$, $F(t) = \dfrac{f_D(t)}{f_0}\dfrac{1-k^2}{k} - k$.

The empirical investigation was performed. In experiment, source (target) was situated in position $(x_0, y_0, z_0) = (50.0, 13.4, 21.4)$ m relative the begin of the right-handed cartesian co-ordinate system. Vehicle with receiver moves with constant velocity 36 km/h (in this interval were made momentary frequency measurements) and on finish section vehicle stopped. The vehicle average velocity on measurement route was calculated on the basis of the riding time measurements.

Curves of the Doppler frequency in function of the time or covered path were obtained out of momentary frequency measurements using the Universal Frequency Counter Agilent 53132A. Average values of the source co-ordinates were calculated on the basis of the Doppler frequency curves. In order to precision valuation of this location methodology following new quality measure Δr, further called location error, was introduced:

$$\Delta r = \sqrt{(\Delta x)^2 + (\Delta z)^2} = \sqrt{(x - x_0)^2 + (z - z_0)^2}$$

where: x_0 and z_0 — real position co-ordinates of the radio emission source (in experiment these values were determined on the basis of laser radar measure), x and z — source co-ordinates calculated from above formulas (on the basis of momentary frequency measure).

The experiment results give possibility to do initial opinion of location method precision. Possibility of these results comparison with different location methods [2–4] is basis of this opinion. This comparison permits to infer about large effectiveness of the new method. Errors estimation of individual co-ordinates Δx, Δz and location errors Δr in presented method amounted below 1 m.

It is needed to emphasize, that this method is dedicated first of all to location in open area, where it occurs so-called: down-to-earth space propagation or free space propagation. The measuring route in this experiment could be classified as suburban terrain. On this stage of the empirical verification, the test route was choice by possibilities of test realization. The measuring route was chosen to conditions which were reminding down-to-earth space propagation (direct visibility of antennas on whole measuring route). This empirical test is initial usefulness verification of this new location method. Many tests in different space conditions should be conducted, to get the full information of method effectiveness.

REFERENCES

1. Rafa, J. and C. Ziółkowski, "Influence of transmitter motion on received signal parameters — analysis of the doppler effect," *Wave Motion*, Vol. 45, No. 3, 178–190, Elsevier, January 2007.
2. *An Introduction to Mobile Positioning*, Mobile Lifestreams Limited, 1999.
3. Zhao, Y., "Standardization of mobile phone positioning for 3G systems," *IEEE Communications Magazine*, Vol. 40, No. 7, 108–116, July 2002.
4. Vossiek, M., L. Wiebking, P. Gulden, J. Weighardt, and C. Hoffmann, "Wireless local positioning — concepts, solutions, applications," *Proceedings of IEEE Radio and Wireless Conference, RAWCON'03,* Vol. 10–13, 219-224, Boston, USA, August 2003. *IEEE Microwave Magazine*, Vol. 5, No. 4, 77–86, December 2003.

Temperature and Mineralogy Dependable Model for Microwave Dielectric Spectra of Moist Soils

V. L. Mironov and S. V. Fomin
Kirensky Institute of Physics, SB RAS, Krasnoyarsk, Russia

Abstract— Dielectric models of the soil is an essential part in the algorithms used for data processing with regard to the problems of radar and radiothermal remote sensing [1]. Recently, a mineralogy based spectroscopic dielectric model (MBSDM) [2] has been developed and validated over a large dielectric data set [3] to ensure microwave dielectric spectra predictions as a function of moisture and soil clay content at the fixed temperature of 20°C. According to [2], this model proved to give a substantially less error of predictions as compared the ones ensured by the semiempirical dielectric model (SDM) of [1] with regard to the dielectric data of [3], though the SDM is at present considered as a routine tool for predicting complex dielectric constant (CDC) spectra of moist soils in the microwave band. Meanwhile, a joint impact of the clay content and temperature on the dielectric spectra of moist soils has not been analyzed yet.

In this paper, such a task was formulated and accomplished using the soil dielectric data for a set of 15 soils acquired in [3] at the temperatures of 10, 20, 30 and 40°C, over the frequency ranges from 45 MHz to 26.5 GHz, with the moistures spanning from the nearly dry samples to the ones close to field moisture capacity. Using the methodology of the temperature dependable refractive mixing dielectric model (TD GRMDM) [4] and the data set of [3], there was derived the assemblage of the TD GRMDM physical parameters, consisting of volumetric expansion coefficients, starting low frequency dielectric constants, activation energies, entropies of activation, starting conductivities, and conductivity incriminations pertaining to the bound and unbound types of soil water. Further, the TD GRMDM parameters obtained were fitted as a function of clay percentage with second order polynomial functions. Derived by this way coefficients of the polynomial fits, in conjunction with dry soil CDC and maximum bound water fraction value, can be considered as input parameters for a new temperature and mineralogy dependable spectral dielectric model (TMD SDM) presented in this paper.

Given these input parameters are known, the CDC predictions of moist soils can be calculated with the use of the TMD SDM as a function of frequency, soil moisture, soil clay content, and temperature through a sequence of the following steps. Firstly, with the clay percentage of the soil assigned, the TD GRMDM input parameters are determined. Secondly, for a given temperature, using the TD GRMDM of [4] the dielectric spectroscopic parameters are calculated, as stated in the generalized refractive mixing dielectric model (GRMDM) earlier developed in [5]. To make assessments for the error of the TMD SDM predictions, the latter were calculated according to the methodology of [5] and then correlated with the respective values measured in [3]. The error of the predictions obtained with the TMD SDM proved to be on the same order as that of the MBSDM predictions estimated in [2].

REFERENCES

1. Dobson, M. C., F. T. Ulaby, M. T. Hallikainen, and M. A. El-Rayes, "Microwave dielectric behavior of wet soil — Part II: Dielectric mixing models," *IEEE Trans. Geosci. Remote Sensing*, Vol. 23, No. 1, 35–46, 1985.
2. Mironov, V. L., L. G. Kosolapova, and S. V. Fomin, "Soil dielectric model accounting for contribution of bound water spectra through clay content," *PIERS Online*, Vol. 4, No. 1, 31–35, 2008.
3. Curtis, J. O., C. A. Weiss, Jr., and J. B. Everett, "Effect of soil composition on dielectric properties," Technical Report EL-95-34, December 1995.
4. Mironov, V. L. and S. V. Fomin, "Temperature dependable microwave dielectric model for moist soils," *PIERS Online*, Beijing, 2009 (to be published).
5. Mironov, V. L., M. C. Dobson, V. H. Kaupp, S. A. Komarov, and V. N. Kleshchenko, "Generalized refractive mixing dielectric model for moist soils," *IEEE Trans. Geosci. Remote Sensing*, Vol. 42, No. 4, 773–785, 2004.

Cable Transmission Lines Magnetic Field Compensation

M. Sh. Misrikhanov[1], **N. B. Rubtsova**[2], **and A. Yu. Tokarskij**[1]

[1]JSC Federal Network Company Branch "Main Power Networks of the Center", Russian Federation
[2]RAMS Institute of Occupational Health, Moscow, Russian Federation

Abstract— The typical dual transforming station (TS) 10/0.4 kV built in residential building with an arrangement of 0.4 kV cable transmission lines (CL) under ceiling in asbestos-cement pipes is examined. Under typical arrangement of each phase cable and zero wire bundle in separate pipe on floor surface, located above TS on 965 mm distance from CL, CL currents ($I_{\mathrm{CL}} = 1800\,\mathrm{A}$) at maximal symmetric load induce magnetic field (MF) value up to $H = 100\,\mathrm{A/m}$, that in 25 times exceeds general public hygienic norms in the Russian Federation (maximum permissible level it is equal 4 A/m). The method of phases and zero wire virtual cables axes rapproachement is developed. With this purpose heteronymic phases and zero wire in each cable bundle are represented n cables placed around of the center of cable bundle. In any point D located outside of cable bundle phase cable or zero wire currents induce MF with resulting strength vector equal to $\dot{\vec{H}}_{n\Sigma}$. If from the beginning of vector $\dot{\vec{H}}_{n\Sigma}$ draw perpendicular directed to the center of cable bundle, the axis of virtual cable with current $n\dot{I}_n$ is possible to place on distance $r_n = \frac{nI_n}{2\pi H_{n\Sigma}}$ as result induce in point D the same vector. The arrangement of cables of phases and zero wire in cable bundle can be chosen for minimization of distance between axes of their virtual cables. Such CL design allows decreasing of MF intensity of MT on surface of living room up to 5×10^{-3} A/m.

Cavity Imaging System Dependence on Sampling Rate

J. Blas[1], **R. M. Lorenzo**[1], **A. Bahillo**[2], **S. Mazuelas**[2], **P. Fernández**[1], **D. Bullido**[2], **and E. J. Abril**[1]

[1]Department of Signal Theory and Computer Engineering, University of Valladolid, Spain
[2]Centre for the Development of Telecommunications of Castilla y León, Spain

Abstract— Interference patterns inside a calibrated cavity which is being illuminated by external sources through asymmetric apertures can be processed in order to obtain an image of these external sources. In fact, a single snapshot of the interference pattern can reveal several sources which are spaced apart in azimuth range, even if they have different intensity levels. The imaging algorithm combines a recently published propagation model based on sub-apertures and a metric that achieves enough exibility to avoid the need of an exact prediction of the deterministic spatial distributions. The statistical characterization of the field pattern, namely the experimental cumulative distribution function, constitutes the signature analyzed in order to test whether an external point source can be responsible or not, at least in part, of the overall interference pattern. In particular, this contribution is focused on the effect of decimation in the system capability to identify the external sources. This decimation is applied to the spatial sampling rate employed to capture the cavity interference pattern. A progressive degradation of the image resolution has been found. However, for a low decimation factor the system preserves its major features. This consistent behavior provides additional evidence about the system performance. In addition, we analyze the minimum extension of the interference pattern that must be sampled in order to achieve accurate results. A comparative analysis is performed with the decimation experiment. As a conclusion, the reduction of the number of samples is worse for performance when it corresponds to a reduction in the overall sampling area in spite of keeping the spatial sampling rate.

The Calibration Technique for Moist Soils Complex Permittivity Measurements in the Microwave Band

V. L. Mironov and Yu. I. Lukin
The Kirensky Institute of Physics of SB, RAS, Russia

Abstract— The study of complex permittivity (CP) of soil and vegetation is an essential part for developing the algorithms used for data processing with regard to the problems of radar and radiothermal remote sensing. From this viewpoint, developing laboratory methods of CP measurements for moist soils adjusted to a given domain of temperatures, frequencies, and moistures is an actual problem. There are some calibration methods to take into account features of a waveguide circuit installation containing a measuring cell [1–5]. Meanwhile, it is very difficult to apply them to soil dielectric measurements because some liquid samples are needed to perform such calibration. This requires to use a somewhat universal sample holder, which is suitable for both liquid and soil samples.

In the present work, a calibration method for measurements of complex permittivity spectrum of moist soils in microwave frequency range is proposed, with coaxial sample holder being applied as a measuring cell. The calibration procedure proposed is based on measurements of S-scattering matrix for two empty sample holders of different lengths. This approach allows to use the same sample holders for both the calibration and soil dielectric measurements. The error analysis of the CPs retrieved was carried out. As an example, the results for the measurement error is analyzed in the case of CPs spectra pertaining to a loam soil measured in both thawed and frozen conditions. There was found a serious of frequencies ranges in which the measurement error increased to a large extend due to a resonance effects existing in a measuring cell. Beyond these ranges the method proposed provided quiet reasonable error of the CP measurements relating to both the thawed and frozen soils, with the relative error estimates not exceeding the values of ($\frac{\Delta\mathrm{Re}(\epsilon)}{\mathrm{Re}(\epsilon)} = 4\%$, $\frac{\Delta\mathrm{Im}(\epsilon)}{\mathrm{Im}(\epsilon)} = 20\%$) and ($\frac{\Delta\mathrm{Re}(\epsilon)}{\mathrm{Re}(\epsilon)} = 3\%$, $\frac{\Delta\mathrm{Im}(\epsilon)}{\mathrm{Im}(\epsilon)} = 10\%$), respectively. In the method proposed, the resonance frequency ranges can be avoided with the use of sample holders of varying lengths.

REFERENCES

1. Bois, K. J., F. Handjojo, A. D. Benally, K. Mubarak, and R. Zoughi, "Dielectric plug-loaded two-port transmission line measurement technique for dielectric property characterization of granular and liquid materials," *IEEE Trans. Instrum. Meas.*, Vol. 48, No. 6, 1141–1148, Dec. 1999.
2. Zheng, H. and C. E. Smith, "Permittivity measurements using a short open-ended coaxial line probe," *IEEE Microwave and Guided Wave Letter*, Vol. 1, No. 11, 337–339, Nov. 1991.
3. Folgero, K., "A broad-band and high-sensitivity dielectric spectroscopy measurement system for quality determination of low-permittivity fluids," *Meas. Sci. Technol*, Vol. 6, 995–1008, 1995.
4. Folgero, K., "Bilinear calibration of coaxial transmission/reflection cells for permittivity measurement of low-loss liquids," *Meas. Sci. Technol*, Vol. 7, 1260–1269, 1996.
5. Baker-Jarvis, J., E. J. Vanzura, and W. A. Kissick, "Improved technique for determining complex permittivity with the transmission/reflection method," *IEEE Trans. Microwave Theory Tech.*, Vol. 38, No. 8, 1096–1103, 1990.

Estimating the Ore Volume in AC Smelting Furnaces Using Finite-Element Analysis of Surface Current Density

A. Jeremic and A. Atalla
McMaster University, Hamilton, Canada

Abstract—

Introduction: One of the primary reasons for large power fluctuations in smelting furnaces is loss of contact between the electrode and ore. Therefore one of important aspects of controlling power fluctuations is a predictive algorithm for the positioning of the electrode. Most of the existing solutions are non-model based algorithms that focus on blind prediction of load resistance. In this paper we propose a model-based approach that estimates the volume ratio of solid and liquid phases of the ore. The resulting estimates can then be used in predictive algorithms for vertical positioning of the electrode since the height of the ore is directly related to the volumes of solid and liquid phases.

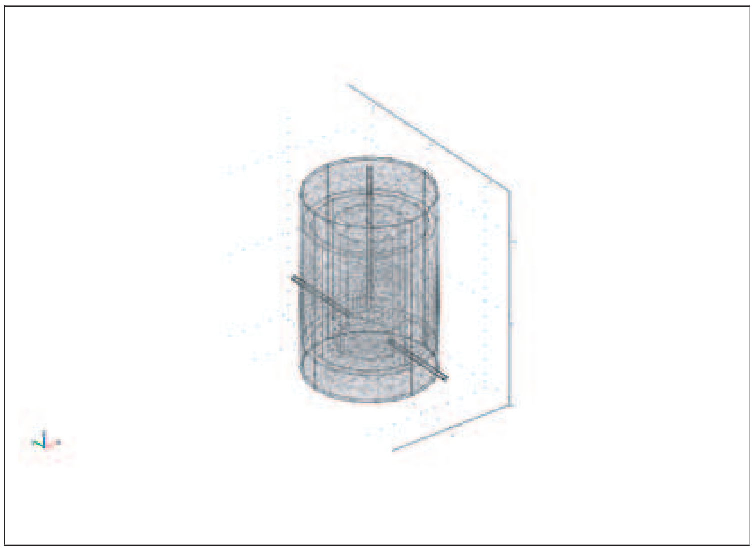

Figure 1: COMSOL Mesh of AC Smelting Furnace.

To this purpose we develop a finite-element model of AC smelting furnace using COMSOL Multiphysics software. We build coupled thermo-electromagnetic model and model the conductivity of the ore as temperature dependent. We assume that furnace is nickel smelting furnace and use somewhat simplified design (two layer temperature insulation) with electromagnetic shielding. According to information provided by Hatch McDonald, Inc., we assume there are ten (10) grounding points on the furnace shell and develop finite-element model for calculation of electric and induction currents in the electromagnetic shielding.

Furthermore we assume that the melted ore consists of multiple phases (pieces) and that shape of these pieces can be approximated with a prolate spheroid. We consider two cases: deterministic, in which the spheroid parameters (axes) are unknown, and Bayesian (probabilistic) in which spheroid parameters follow the Gaussian distribution. We then derive the measurement model in which the grounding currents are expressed as a nonlinear function of solid ore parameters and estimate these parameters using least-squares optimization.

In Figures 2 and 3, we illustrate the mean square error in estimating the volume ratio (solid vs. liquid phase) averaged over 1000 simulations. The results presented in Figure 2 illustrate the error when the shape of ore is perfectly known. In Figure 3, we illustrate the same results but assuming that the shape and location of ore are unknown. As expected the estimation error is significantly larger but can still provide important insight into the internal state of smelting furnaces.

Considering the current state of industrial need for raw materials and price of energy the proposed approach provides potential of providing an insight into the state of melting ore in AC furnaces.

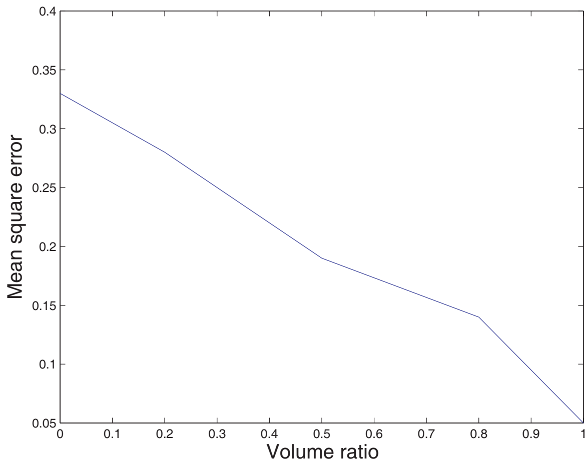

Figure 2: Single phase — Known shape.

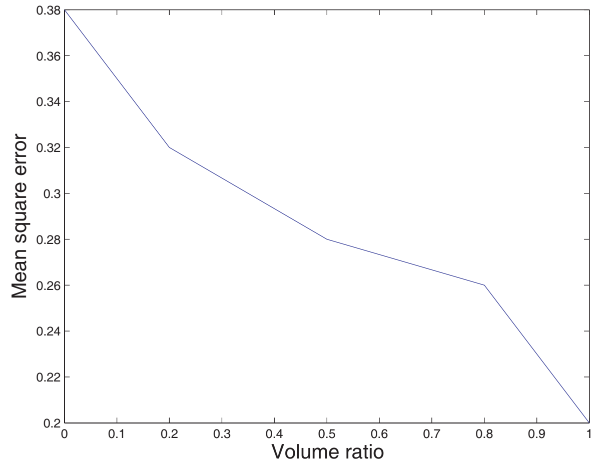

Figure 3: Two phase — Unknown shape.

To the best of our knowledge such information is currently unavailable. In addition being able to predict the volumes (or equivalently the height/shape) of the ore can improve currently existing blind algorithms and thus minimize the power fluctuations (i.e., losses). Furthermore we expect that significant improvement can be achieved if the volume of the liquid phase is modeled as a function of the total power delivered to the furnace and this topic is left for future research.

3D AGILD Mechanical Modeling for Simulations of New Materials

Jianhua Li[1,2], **Feng Xie**[2], **Ganquan Xie**[2], **Chien-Chang Lin**[1], **and Michael Oristagli**[3]

[1]Department of Mechanical and Automation Engineering, Da-Yeh University, Taiwan
[2]Department of Modeling and Inversion, GL Geophysical Laboratory, USA
[3]Schlumberger-Doll Research Center, Cambridge, MA, USA

Abstract— The Advanced Global Integral and Local Differential (AGILD) modeling is a development and improvement of GILD modeling. AGILD preserves the all merits of GILD method and is simpler than GILD. In this paper, a new 3D mechanical differential integral strip equation is derived. The new mechanical equation on strip boundary and LAME differential equation in the internal domain are coupled to construct AGILD mechanical (AGILDME) modeling. AGILDME can be applied in developing of new materials such as nanometer materials and left hand materials; it can be used in the areas of stirring, geophysics, GPR, nondestructive testing etc. sciences and engineering.

Exterior Electromagnetic Field Boundary Scattering

Ganquan Xie[1,2], **Tzon-Tzer Lu**[1], **Xianwei Zhou**[3], **V. G. Veselago**[4,5], **and Clement Kostov**[6]

[1]Applied Mathematical Department, National Sun Yat-sen University, Taiwan
[2]GL Geophysical Laboratory, USA
[3]Department of Communication Engineering, School of Information Engineering
University of Science and Technology, Beijing
[4]A. M. Prokhorov General Physics Institute, Moscow 119991, Russia
[5]Moscow Institute of Physics and Technology, Dolgoprudny 141700, Russia
[6]Schlumberger Moscow Research Center, USA

Abstract— In this paper, we propose a method to solve the exterior electromagnetic field boundary scattering. The EM exterior problem is different from the acoustic and Laplace exterior problem. Suppose that the boundary is a 2D closed curve surface, on which the tangential electromagnetic scattering field is measured, we want calculate the exterior electromagnetic field outside the curve surface. Using the background Green's function, we build a thin strip domain integral equation. In the thin strip domain around boundary, the discrete collocation equation is solved with small matrix equation solving cost. Then, using the boundary strip integral equation, we can calculate the electromagnetic scattering everywhere in the exterior domain. The method is developed from the improved GILD.

Session 4P1
Rough Surface Scattering and Related Phenomena

Nonstandard Refraction of Light from 1-D Quasi-periodic Surfaces

Zu-Han Gu[1] **and Anting Wang**[2]

[1]Surface Optics Corporation, 11555 Rancho Bernardo Road, San Diego, CA 92127, USA
[2]Department of Physics, University of Science & Technology of China, Hefei, Anhui 230026, China

Abstract— The negative index materials (NIM) have shown some unusual properties, such as an inverse Snell's law, which can be applied to the construction of a perfect lens for sub-wavelength imaging, a perfect corner cube, and many other applications. Not only do meta-materials have the properties of negative refraction, the planar designer surfaces have shown some of these properties as well [1].

Recently, we have undertaken an experimental study of nonstandard refraction of light from one-dimensional dielectric quasi-periodic surfaces. The mechanism behind this is that the large local slope of the quasi-periodic surface causes the nonstandard refraction.

REFERENCES

1. Leskova, T. A., A. A. Maradudin, and I. Simonsen, "The design of random surfaces that produces nonstandard refraction of light," *SPIE*, 7065–06, 2008.

Multiple Scatter of Vector Electromagnetic Waves from Random Surfaces with Infinite Slopes Using the Kirchhoff Approximation

N. C. Bruce
Centro de Ciencias Aplicadas y Desarrollo Tecnológico
Universidad Nacional Autónoma de México, México

Abstract— One of the most popular and useful methods for calculating the scattering of light from rough surfaces is the Kirchhoff approximation. This method has been developed to include shadowing and multiple scatter effects. A recent modification of the Kirchhoff approximation allows calculation of the scattering of electromagnetic radiation from rough surfaces with very high, or even infinite, slopes in the 1D surface roughness case [1]. This type of surface structure occurs frequently in, for example, printed circuits or remote sensing applications. The modification involves a simple change in the way the surface normal is described which allows the diffraction integral to be written as the sum of two contributions, one for the contribution along the surface and the other for the contribution due to the changes in height. This paper presents the generalization of the modified Kirchhoff approximation to vector electromagnetic scattering from 2D rough surfaces with infinite slope [2]. The Stratton-Chu equation [3] is used to calculate the distribution of the scattered light. The results presented are for a perfectly conducting surface although future work will generalize the method to any material. The single and double scatter contributions to the total scattered intensity have been calculated numerically with this new formulation including geometrical shadowing explicitly by using ray tracing directly on the surface. The theoretical basis and preliminary numerical results of the application of this method to vector electromagnetic scattering from simple rough surfaces (plane surfaces with single grooves or with a small number of identical grooves) with infinitely sloped structure will be presented.

ACKNOWLEDGMENT

This research was supported by CONACYT, México through project 79814 and DGAPA, UNAM through project PAPIIT IN115209-3.

REFERENCES

1. Bruce, N. C., "Control of the backscattered intensity in random rectangular-groove surfaces with variations in the groove depth," *Applied Optics*, Vol. 44, 78–791, 2005.
2. Bruce, N. C., "Single-scatter vector-wave scattering from surfaces with infinite slope using the Kirchhoff approximation," *J. Opt. Soc. Am. A*, Vol. 25, 2011–2017, 2008.
3. Ogilvy, J. A., *Theory of Wave Scattering from Random Rough Surfaces*, IOP Publishing, Bristol, 1991.

The Scattering of Electromagnetic Waves from Two-dimensional Randomly Rough Surfaces

Alexei A. Maradudin[1], **Tamara A. Leskova**[1], **and Ingve Simonsen**[2]

[1]Department of Physics and Astronomy and Institute for Surface and Interface Science
University of California, Irvine, CA 92697, USA
[2]Department of Physics, Norwegian University of Science and Technology
NO-7491, Trondheim, Norway

Abstract— By a computer simulation approach we study the scattering of p- or s-polarized light from very rough two-dimensional metallic or dielectric surfaces. The use of the Stratton-Chu formulas yields a set of six coupled two-dimensional inhomogeneous integral equations from which the source functions in terms of which the scattered field is expressed with the use of the Franz formulas can be determined. This set of six equations is reduced to a set of four coupled integral equations by the use of the relations between the divergences of the surface current densities and surface charge densities. Finally, the use of an impedance boundary condition for a two-dimensional metallic or dielectric rough surface reduces the number of coupled integral equations for the source functions to two. The occurrence of hypersingular kernels in our integral equations is avoided by numerical differentiation of the unknown functions that appear in some of the integrands. The pair of coupled integral equations is converted into a pair of coupled matrix equations by the method of moments, and this pair of equations is solved by an iterative Krylov method, the biconjugate gradient stabilized method. The solutions are obtained for two forms for the incident field, namely a plane wave because of its simplicity, and a Gaussian beam, to minimize edge effects. The results are used to calculate the mean differential re ection coefficients for in-plane co- and cross-polarized scattering, and for out-of-plane co- and cross-polarized scattering.

The Scattering of a Surface Plasmon Polariton by a One-dimensional Defect on an Otherwise Planar Surface of a Lossy Metal

Alexei A. Maradudin[1], **Tamara A. Leskova**[1], **Enrique Efren Garcá-Guerrero**[2], **and Eugenio R. Méndez**[3]

[1]Department of Physics and Astronomy and Institute for Surface and Interface Science
University of California, Irvine, CA 92697, USA
[2]Facultad de Ingenería, Universidad Autónoma de Baja California, Ensenada, B. C. 22870, México
[3]División de Física Aplicada, Centro de Investigación Científica y de Educación Superior de Ensenada
Ensenada, B. C. 22860, México

Abstract— When a surface plasmon polariton interacts with a one-dimensional defect in its propagation path on an otherwise planar metal surface, it is partly re ected as a surface plasmon polariton, it is partly transmitted as a surface plasmon polariton, and it is partly converted into volume electromagnetic waves propagating away from the surface in the vacuum above it. In virtually all existing calculations of these interaction processes the metal on which the surface wave propagates has been assumed to be lossless. This appears to be due to the fact that while the dissipation in the metal attenuates the amplitude of the surface plasmon polariton in the direction of its propagation, it gives rise to an exponential increase of that amplitude in the opposite direction. This gives rise to conceptual problems in defining the field of the incident surface plasmon polariton, and to divergences of some integrals arising in the theory.

In this presentation, we present a rigorous approach to the problem of the interaction of a surface plasmon polariton with a one-dimensional defect on a lossy metal surface defined by $x_3 = 0$. It is based on Green's second integral identity in the plane. The surface profile function of the defect is assumed to be nonzero only in the interval $-L < x_1 < L$ of the x_1 axis. The incident surface plasmon polariton is excited by a planar source far from the leading edge of the defect at $x_1 = -L_0$, with $L_0 \gg L$. The strength of this source decreases exponentially with increasing distance into the vacuum $x_3 > 0$ and into the metal $x_3 < 0$. It excites a surface plasmon polariton that decays exponentially in amplitude due to dissipation in the positive x_1 direction and in the negative x_1 direction. An integral equation for the scattering amplitude is derived, and it is solved numerically by transforming it into a matrix equation by the use of the extended midpoint numerical integration algorithm. Results for the transmissivity and re ectivity of the surface plasmon polariton are obtained for a single defect or a row of defects each of the form of a Gaussian ridge or groove, as well as for the conversion of the surface wave into volume electromagnetic waves in the vacuum.

Optical Spectrum and Electromagnetic-Field Distribution at Double-Groove Metallic Surface Gratings

L. David Wellems[1], **D. H. Huang**[1], **T. A. Leskova**[2], **and A. A. Maradudin**[2]

[1]Air Force Research Laboratory, Space Vehicles Directorate
Kirtland Air Force Base, NM 87117, USA
[2]Department of Physics and Astronomy and Institute for Surface Science
University of California, Irvine, CA 92697, USA

Abstract— The previous Greens function model [1] for etched single-groove gratings on both sides of a thin silver film was extended to study the case of double-groove gratings. A splitting of surface-plasmon-polariton (SPP) modes was found due to electromagnetic (EM) coupling between the two grooves in the complex unit-cell of the grating. The spectral features corresponding to the split SPP branches (a new peak in the transmissivity) as well as the minigap (a new peak in the reflectivity) between them were found in this system. In addition, the calculated full spatial distributions of the total EM field were used to provide intuitive explanations for these observations by indicating the high-surface-field regions, the coupling between two grooves in the same complex unit-cell, and the coupling between two nearby grooves located at the upper and lower surfaces of the metal film. The effects of the depth ratio of and the separation between two grooves in the complex unit-cell, as well as the effect of the lattice constant, on the transmissivity and reflectivity were also shown.

REFERENCES

1. Baumeier, B., T. A. Leskova, and A. A. Maradudin, *J. Opt. A: Pure Appl. Opt.*, Vol. 8, S191, 2006.

Direct Numerical Simulations and Analysis of Wide-band Low-grazing HF Backscatter from Evolving Ocean-like Surfaces

Jakov V. Toporkov and Mark A. Sletten
Naval Research Laboratory, Code 7264, Washington DC, 20375-5320, USA

Abstract— Vertically polarized sea surface backscatter in the High-Frequency (HF) band (3–30 MHz) is used in a number of maritime remote sensing applications, such as measuring and mapping oceanic currents. With the HF wavelengths ranging from 100 to 10 m, a simple Bragg scattering concept is often adequate to describe the observed effects, making data analysis and surface feature retrieval appealingly simple. Another attractive aspect of HF radiowaves is strong backscatter level at vertical polarization even for large distances, which allows gathering information about surface regions tens of kilometers away. Lately, there has been interest in wide-band (WB) HF applications, with mapping the instantaneous wave height being one of the goals. While implementation of such wide-band systems today can still present certain technological challenges, direct numerical simulations can be used to gauge the expected performance, assess the data information content and check the adequacy of analytical scattering models intended to describe the received data and guide the system development.

Surface backscatter at a particular electromagnetic frequency is calculated using the Method of Ordered Multiple Interactions (MOMI) — a first-principles technique that solves a discretized boundary integral equation for the surface electric current. Dielectric properties of sea water are accounted for using the impedance boundary condition. A surface profile is generated as a realization of a Gaussian random process with the Pierson-Moskowitz spectrum. Its time evolution is achieved by varying the phases of surface harmonics according to the free-wave dispersion relation. Calculations are repeated for closely spaced frequencies covering the entire HF band allowing synthesizing the surface response to a short pulse. While limited to the 2-D space for computational reasons, these simulations yield valuable exact solution that captures, for example, all shadowing and multiple scattering effects.

Simulations were performed for two time-evolving 40-km long surface realizations corresponding to wind speeds of 5 and 20 m/s respectively. It is noted that the numerical scattering solution yields backscatter levels consistent with scattering theories that account for the presence of the Norton surface wave (something not observed at L- or X-band frequencies where the numerical technique of this type has been used extensively). Analysis of the range-time plots of the backscatter power reveals the presence of wave-like pattern (especially visible for the higher wind speed case) that is not predicted by the first-order small-perturbation method (SPM-1) applied to the same surface profile. The difference with the SPM-1 predictions is even more evident when Fourier transform in both range and "slow" time is applied to the evolving signal power. In this "K-omega" domain the results obtained from direct numerical simulations display a signature consistent with the dispersion curve of the surface waves — something completely lacking in the backscatter calculated with the SPM-1. We investigate if the next, second order of SPM can reproduce this phenomenon. The feasibility of using this spectral signature to reconstruct surface wave profile (containing important energy-bearing wave lengths that are often longer than those engaged in Bragg interaction) is also considered.

Maximums of Backscattering from the Surface Edge above Mirror

A. M. Lebedev and A. I. Fedorenko
Institute for Theoretical and Applied Electromagnetics, Russian Academy of Sciences, Russia

Abstract— The backscattering (BS) of extended complex object can tentatively be divided into contributions cased by 1) shape and 2) local inhomogeneities on its surface. In turn, the edges often generate most of shape's BS contribution. For example, when the normals to the surfaces are redirected outside the meaningful angular range (the object is stealthy shaped). Hence the analysis of BS from the edges above the mirror is of major importance for prediction of radar signature of objects above the underlying surface.

Here the RCS angular dependence of metal triangular above the mirror $\sigma(\varphi, \alpha)$ is considered, φ and α are azimuth and elevation. The triangular was intentionally chosen as the simplest type of surface.

The geometry is shown in Fig. 1, calculations were conducted for wavelength $\lambda_o = 3\,\text{cm}$. Thus, the horizontal base of triangle is updrawn $10 \cdot \lambda_o$, the base length is $15 \cdot \lambda_o$, normal to the triangle is oriented at $\varphi = 0°$, $\alpha = 10°$.

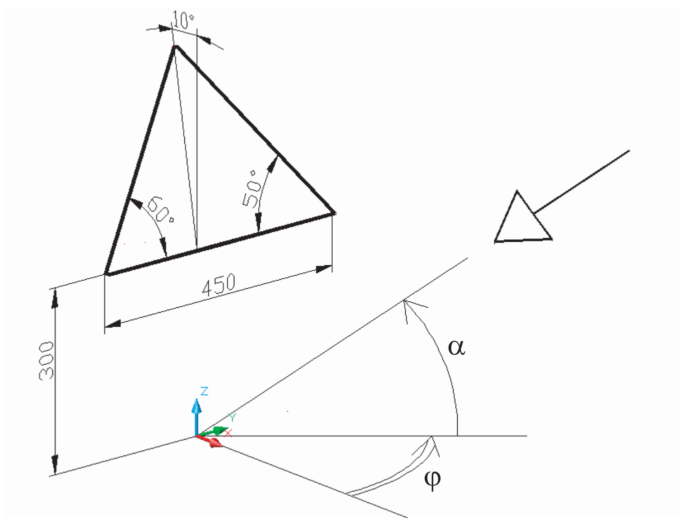

Figure 1.

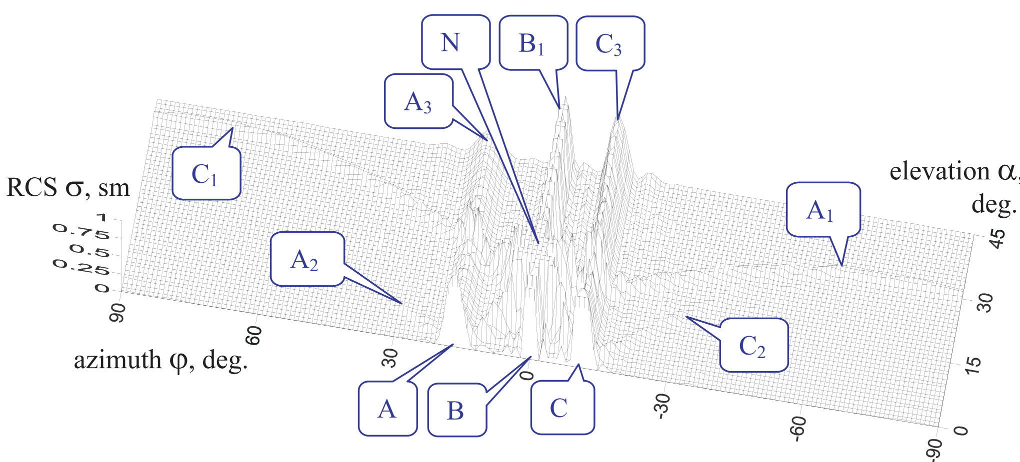

Figure 2.

BS maximums, caused by the edge, occur in plane, perpendicular to the edge. Indeed, the BS observer can only get on the diffracted ray cone in this plane. The RCS distribution $\sigma(\varphi, \alpha)$ for the vertically polarized incident plane wave is presented in Fig. 2. Here the ridges AA_1, BB_1, CC_1 correspond to BS of the incident wave from the real triangular edges. The ridges intersect at point N, corresponding to the BS at normal direction. The ridges AA_2 and CC_2 correspond to BS from the inclined edges of mirrored triangular. The reason for ridges AA_3 and CC_3 is the occurrence of BS ray on the diffracted ray cone, which results from the mirrored incidence upon the inclined edge.

So the interesting phenomenon of backscattering from the inclined edge above the mirror is found out. The azimuthal RCS diagram for nonzero elevation has three maximums per inclined edge.

Characterization of Surface Roughness Parameters of Low Reflectance Dielectrics Using Terahertz Fourier Transform Infrared Spectroscopy

A. Jagannathan, **A. J. Gatesman**, and **R. H. Giles**
Submillimeter-Wave Technology Laboratory, University of Massachusetts Lowell
Lowell, MA 01854, USA

Abstract— Understanding the scattering behavior of terahertz waves from rough dielectric surfaces is of great significance to the development of terahertz imaging and remote sensing applications. In this paper, the impact of surface roughness on the terahertz reflection spectra of low reflectance dielectrics was investigated using Fourier Transform Infrared Spectroscopy (FTIR). Roughness present on a surface is primarily characterized by the root mean square roughness (rms) parameter. Rough dielectric surfaces with rms roughness of 5 μm–50 μm were prepared and measured using a surface profilometer. The reflectance of a rough surface in the specular direction is given by the Kirchhoff diffraction approximation. The Kirchhoff approximation predicts a Gaussian roll-off to the reflectance of a rough surface as a function of frequency, rms roughness, and angle of incidence. Reflectance data were acquired using a Fourier Transform Infrared Spectrometer at a fixed angle of incidence of 11° in the frequency range of 0.3 THz to 3 THz. All measurements were taken under vacuum conditions. A 4.2 K helium cooled silicon bolometer was used as the detector. By comparing the spectroscopic data to the Kirchhoff approximation, the rms roughness of the dielectric surface was determined. The rms roughness data determined using FTIR techniques were compared to surface profilometer data to test the agreement between theory and experiment. The experimental results presented in this paper will help determine the feasibility of using a terahertz non-destructive evaluation system to determine the surface roughness present in low reflectance dielectrics.

The Second-order SPM Solution for Scattering from Multi-layer Dielectric Media with Slightly Rough Surface

Z. W. Lin[1,2], **X. J. Zhang**[1], **and G. Y. Fang**[1]

[1] Institute of Electronics, Chinese Academy of Sciences, China
[2] Graduate University of Chinese Academy of Sciences, China

Abstract— A munber of natural targets encountered in microwave remote sensing can be modeled as multi-layer dielectric media with slightly rough surface, such as snow, sea ice, bare soil, etc. The same model also can be used in the non-destructive detection of MMIC and optical instruments. Several researches have investigated the bistatic scattering from multi-layer subsurface structure with rough surface based on the first order small-perturbation method (SPM). However, the first-order SPM solution is unable to characterize the cross-polarized property in backscattering case, which is essential in polarimetric measurements of microwave remote sensing. An analytical approach is presented to obtain the scattering field of multi-layer subsurface structure with rough surface up to second-order SPM solution which exhibits primary cross-polarized component in backscattering case. The electric and magnetic fields in each region are expanded in spectral domain. The amplitudes of electric and magnetic fields in spectral domain are expanded into perturbation series, while the exponential term of the surface height is expanded into Taylor series. By applying the boundary conditions, the amplitudes of electric and magnetic fields in each region can be solved from zeroth- to high-order. The scattering fields in the far-field zone are approximated by using the stationary phase method. The bistatic scattering coefficients for different linear polarizations of the scattering fields of a two-layer subsurface structure with a slightly rough surface are derived under the assumsion that odd moments of the surface profile are zero. Sample results show the contribution that the second-order terms make to the cross-polarized backscattering of the layered structure. The results are validated against known solutions for simple case of single rough surface.

Session 4P2
Optical Solitons 2

Propagation of Partially Coherent Light in Nonlinear Media

T. Hansson, D. Anderson, and M. Lisak
Department of Radio and Space Science, Chalmers University of Technology, Gothenburg, Sweden

Abstract— Propagation of partially coherent light in nonlinear media is an exiting field that has attracted strong interest during the last ten years. Many of the classical phenomena associated with nonlinear coherent wave propagation, e.g., solitons, self-focusing, and modulational instability have been found to be present also for partially coherent light, although with new features that depend on the coherence properties of the light. Several different formalisms have been developed for theoretical investigations of the propagation of partially coherent light. Three of the most commonly used ones are based on the coherent density function, the mutual coherent function, and the Wigner function, respectively. Although the characteristic propagation equations appearing in these formalisms are very different in form, they provide equivalent descriptions of the propagation properties and depending on the problem under study, one or a combination of these methods may prove the most convenient. Due to the mathematical complexity of the propagation equations in all used methods of analysis (in some approaches being nonlinear integro-differential equations), very few explicit exact solutions have been found. A notable exception is media where the nonlinearity can be modelled in terms of a logarithmic nonlinearity, i.e., media where the nonlinear change in the refractive index is given by $\Delta n \propto \ln I$ with I denoting the wave intensity.

In the present work, we make a comparative discussion of the connection between these methods by analyzing partially coherent wave solutions in the case of the saturable logarithmic nonlinearity. In particular, we discuss the properties of exact self-similar dynamic solutions which also incorporate stationary soliton solutions of varying degree of coherence as a special case. The discussion illustrates the different character of the approaches, e.g., whereas the mutual coherence and the Wigner functions are stationary functions for the soliton solutions, the coherent density function is not, but exhibits significant oscillatory motion, in spite of the fact that the averaged light intensity profile remains constant during propagation. Finally we also analyze the interaction of these solitons by means of a variational approach and discuss the effects of partial coherence on the mutual interaction.

Chirped Self-similar Spatial Solitary Waves

K. Senthilnathan[1], **Abdosllam M. Abobaker**[2], **and K. Nakkeeran**[3]

[1]Department of Physics, National Institute of Technology, Rourkela 769008, Orissa, India
[2]The Higher Institute of Electronics, Department of Computer Engineering
P. O. Box: 38645, Bani-Waild, Libya, Africa
[3]School of Engineering, Fraser Noble Building, King's College, University of Aberdeen
Aberdeen AB24 3UE, Scotland, UK

Abstract— We consider the evolution of nonlinear optical pulses in graded-index amplifiers exhibiting self-focusing or self-defocusing non-Kerr nonlinearities. The pulse propagation in such nonlinear media is governed by the generalized cubic-quintic nonlinear Schrödinger equation. Using the self-similar analysis, we analytically find the chirped bright soliton solutions in the anomalous and normal dispersion regimes. From the Vakhitov-Kolokolov criterion, we show that the soliton in the anomalous dispersion regime is stable whereas the soliton in the normal dispersion regime is unstable. These chirped spatial solitary waves may find applications in future all optical networks.

Theoretical model and chirped spatial bright solitary wave solution:

The propagation of optical beam inside a planar, graded-index nonlinear waveguide amplifier under the influence of quintic nonlinearity is governed by following generalized cubic-quintic nonlinear Schrödinger (CQNLS) equation:

$$i\frac{\partial E}{\partial Z} + \frac{1}{2}\frac{\partial^2 E}{\partial X^2} - \frac{iG}{2}E + \frac{1}{2}X^2E + \gamma|E|^2E + \alpha|E|^4E = 0$$

Here all the physical parameters are in normalized form. The parameter E is the envelope of the wave and G is the gain. γ and α represent the cubic and quintic nonlinearities, respectively.

For the above CQNLS equation, we get the following chirped spatial bright solitary wave under the influence of cubic-quintic nonlinearities

$$E = \frac{1}{W(z)}\left[\frac{\gamma}{4\beta} + \left[\frac{\alpha(Z)}{3\beta} + \frac{\gamma^2}{16\beta^2}\right]^{\frac{1}{2}}\cosh\left[\sqrt{8\beta}T\right]\right]^{-\frac{1}{2}}\exp[i\Phi],$$

where $T = \left[\frac{X - X_c(z)}{W(Z)}\right]$ and $\Phi(X, Z) = -\frac{1}{2}X^2 + B_0e^ZX + \frac{\left(2\beta - B_0^2W_0^2\right)}{4W_0^2}e^{2Z}$.

Polarization Domain Wall Solitons in Elliptically Birefringent Optical Fibers

S. Wabnitz
Dipartimento di Elettronica per l'Automazione, Università degli Studi di Brescia
Via Branze 38, Brescia 25123, Italy

Abstract— We present analytical and numerical studies of the dynamics of polarization domains and domain wall solitons in optical fibers with elliptical birefringence. Applications to loss-free nonlinear polarizers and to cross-polarization modulation between signals in wavelength division multiplexed transmissions are discussed.

Optical Solitons of the Discrete Reduced Maxwell-Bloch System in a Ring Cavity

J. M. Arnold
University of Glasgow, UK

Abstract— The mathematical system of discrete reduced Maxwell-Bloch type, consisting of lumped atomic slices separated by free space, is shown to be exactly integrable by virtue of an infinite number of conserved invariants that are polynomial functions of the field. The physical realisation of this system in a ring cavity, with an atomic or semiconductor medium for the active layer, is shown to be feasible. If the ring cavity contains an output coupler of small transmission coefficient, and the atomic medium is pumped to provide small but sufficient gain to overcome the cavity loss of the ouput coupler, the lowest-order breather soliton of the discrete RMB system forms a self-sustaining recirculating optical pulse in the cavity and the resulting device is a mode-locked laser in which the sole pulse formation mechanism consists of soliton formation in the discrete active layer. This mode-locked laser requires no saturable absorber, and the saturated gain is not required to recover on the same time-scale as the pulse duration. A short-cavity ($\sim 100\,\mu\mathrm{m}$) with low output coupling (~ 0.01) should produce femtosecond optical pulses with terahertz repetition frequencies at practically useful levels of average output power.

The discrete RMB system, in normalised form, is approximated for small changes in field $|\psi_{k+1} - \psi_k| \ll \psi_k$ by

$$\psi_{k+1} - \psi_k = \alpha \mathrm{Tr}[\Gamma_k \sigma_1], \quad \mathrm{i}\hbar\partial_\tau \Gamma_k = [H_k, \Gamma_k], \quad H_k = \frac{1}{2}\hbar(\Omega_0\sigma_3 + (\psi_{k+1} + \psi_k)\sigma_2) \tag{1}$$

where σ_j are standard Pauli matrices, $\psi_k(\tau)$ is the optical field in the k-th region of free space, $\tau = t - c^{-1}z$ is the shifted time variable, $z = z_k$ is the location of the k-th slice of atomic medium, and Ω_0 is the resonant frequency of the atoms. For a single atomic layer at $z = z_1$ placed in a cavity of total length L, the periodic boundary conditions $\psi_2(\tau) = \psi_1(\tau + \delta)$, $\psi_1(\tau) = \psi_1(\tau + T)$ define the stationary state of recirculating solitons with temporal period T and time shift δ propagating through the medium [1]. The solitons of this system can be determined by a commuting ladder of Darboux transformations on the differential equation $\partial_\tau v_k = -\mathrm{i}(\zeta\sigma_3 + \psi_k\sigma_2)v_k$ for the 2×2 complex vector v_k with a parameter ζ, starting with the vacuum state $\psi_k = 0$.

The discrete version of the RMB system differs from earlier variants that are continuous in space in that the nonlinear behaviour is lumped into spatially discrete sections, with free linear propagation between the sections. The nonlinear behaviour is essentially coherent self-induced transparency at or near optical resonance with the atomic transition. The discrete system differs mathematically from the continuous version in that the evolution part of the Lax pair is a full operator, not just differential, but the Darboux transformations generating solitons are essentially the same as in the continuous case. The conserved quantities serve also to constrain the stability of the steady states such as the recirculating breather.

REFERENCES

1. Arnold, J. M., "Dynamical systems in nonlinear optics: Maxwell-Bloch models," *Optical and Quantum Electronics*, to be published, 2009.

L-band Tunable High Repetition Rate Synchronized Fiber Laser

A. A. Sysoliatin[1], **M. Y. Salganskii**[1], **A. I. Konyukhov**[2], **L. A. Melnikov**[2], **and V. A. Stasyuk**[3]

[1]Fiber Optics Research Center, Russia
[2]Saratov State University, Russia
[3]Pritel, Inc., USA

Abstract— We experimentally demonstrate the possibility to build up the L-band tunable GHz repetition rate fiber laser via a dispersion flattened dispersion decreasing fiber. Our experimental setup includes an UOC (ultrafast optical clock, fiber laser operating at $5\ldots40$ GHz) as a source of 2.6 ps pulses with central wavelength $\lambda_0 = 1552$ nm, high gain fiber amplifier, dispersion flattened dispersion decreasing fiber (DFDDF), bandpass filter at 1610 nm after DFDDF. The DFDDF fiber has convex dispersion function vs wavelength and linear dispersion function vs fiber length. In experiments 42 m-length fiber was used. Outher diameter of the fiber decreases from 148 µm to 125 µm. That correspond to the change of group velocity dispersion from $10\,\mathrm{ps(nm\,km)}^{-1}$ to $-1.17\,\mathrm{ps(nm\,km)}^{-1}$. The propagation of a pulse in a waveguide with a length varying chromatic dispersion is formally equivalent to the propagation of the pulse in a fiber amplifier with a certain gain. This effect is physically based on the fact that nonlinear effects increase as compared to the dispersion effects in the process of propagation through the waveguide.

We performed numerical simulations of picosecond pulse propagation in DFDDF. The initial stage of the pulse propagation corresponds to solitonic regime. Due to the Raman scattering high-intensity pulse appears after the propagation 0.1 km of the fiber. The central frequency of this pulse is red-shifted. As result the output spectrum become broadened. Using bandpass filter the picosecond pilses at 1610 nm can be obtained. It is essential that the pump current should not exceed some critical value to obtain at 1610 nm the high quality pulses fully synchronized with clock source.

To the best of ur knowledge this is the first demonstration of the generation of high quality 1.0 ps pulses at 1610 nm, fully synchronized with basic clock at GHz repetition rate.

Dissipative Solitary Waves in Negative Index Materials with Added Gain

Ildar Gabitov[1], **Andrei Maimistov**[2], **and Bridget Kennedy**[1]

[1]Department of Mathematics, University of Arizona, 617 N. Santa Rita, Tucson, AZ 85721, USA
[2]Department of Solid State Physics and Nanosystems, Moscow Engineering Physics Institute, 31 Kashirskoe Shosse, Moscow 115409, Russia

Abstract— Negative index materials offer new perspectives for light manipulation which are important for both basic science and for applications. Currently design of these materials is based on use of plasmonic resonances in metallic structures embedded within a dielectric and therefore they are very lossy. We consider a model describing optical pulse dynamics in a metamaterial with loss compensation due to doping with active atoms. In the framework of this model we have demonstrated existence of dissipative solitary wave solutions and calculated their parameters in terms of metamaterial and gain properties. These analytic results are verified against numerical simulations.

Self-propelled Cavity Solitons in VCSEL with Frequency Selective External Feedback

P. V. Paulau[1,2], **D. Gomila**[2], **P. Colet**[2],
M. A. Matías[2], **N. A. Loiko**[1], **and W. J. Firth**[3]

[1]Institute of Physics, NASB, Scaryna Prospekt 70, Minsk 220072, Belarus
[2]IFISC (CSIC-UIB), E-07122 Palma de Mallorca, Spain
[3]Department of Physics, University of Strathclyde, 107 Rottenrow East, Glasgow G4 0NG, UK

Abstract— The existence of self-propelled cavity solitons (CS) in broad-area semiconductor lasers was recently shown theoretically in [1]. Their properties are quite distinct from those of CS in driven systems, for which induced motion was recently demonstrated [2]. We investigate here the appearance of self-propelled CS and analyze their bifurcation diagram and dynamics. For high input currents, stable self-propelled CS bifurcate from the branch of resting CS, in a similar way to the case studied in [3]. Using continuation techniques we build the complete branch of self-propelled states and find that this branch connects the above mentioned bifurcation with the modulational instability (MI) point of the trivial solution, where traveling waves with the critical wavenumber are born — see Figure 1. Interestingly enough, both self-propelled CS and traveling wave appear super-critically. We suppose that this is a quite general feature which can be related to many other systems, because we found that the SLS are envelope solitons of the traveling wave, and move with its group velocity.

We previously showed semiquantitative agreement with experimental data for the case of resting solitons [1, 4], therefore our theoretical results should facilitate experimental observation of self-propelled states. Experimental systems usually have transverse inhomogeneities of the system parameters [2]. Hence it can be important to distinguish whether a stationary CS is really in the resting state or is actually a self-propelled soliton trapped by a material defect. We will report studies of the dynamics in traps, and in parameter gradients, of self-propelled CS. Recent work proposes induced CS motion is for use in optical delay lines [5]. Self-propelled SLS in lasers could prove to be simpler and more versatile for such applications.

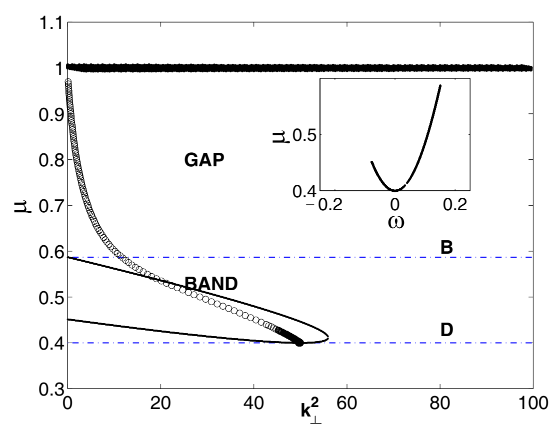

Figure 1: The thin solid curve denotes marginal stability against transverse waves of the nonlasing state in the VCSEL with external feedback. The inset shows the frequencies of the corresponding modes, which lie in the "band" between lines D and B in the main figure. The black bold line corresponds to the excitation of modes with frequencies close to those of solitary laser. Self-propelled CS are asymmetric and hence their far field is off-axis. Circles show their far field maximum as a function of current.

REFERENCES

1. Paulau, P. V., D. Gomila, T. Ackemann, N. A. Loiko, and W. J. Firth, *Phys. Rev. E*, Vol. 78, 016212, 2008.
2. Pedaci, F., et al., *Appl. Phys. Lett.*, Vol. 93, 111104, 2008.
3. Scroggie, A. J., J. M. McSloy, and W. J. Firth, *Phys. Rev. E*, Vol. 66, 036607, 2002.
4. Tanguy, Y., et al., *Phys. Rev. Lett.*, Vol. 100, 013907, 2008.
5. Pedaci, F., et al., *Appl. Phys. Lett.*, Vol. 92, 011101-1, 2008.

Cavity Polariton Solitons

F. Lederer[1], **D. V. Skryabin**[2], **O. Egorov**[1], **and A. V. Yulin**[2]

[1]Institute of Condensed Matter Theory and Solid State Optics
Friedrich-Schiller-Universität Jena, Germany
[2]Centre for Photonics and Photonic Materials, Department of Physics
University of Bath, United Kingdom

Abstract— We report the existence of bright and dark cavity polariton solitons. The lower branch of the dispersion relation of exciton polaritons in semiconductor microcavities, operating in the strong-coupling regime, contains sections of both positive and negative curvature. Thus, in one configuration both bright and dark solitons can be observed. We study their stability and symmetry breaking. These half-light half-matter solitons are potential candidates for applications in all-optical signal processing. Their excitation time and required pump powers are a few orders of magnitude less than those of their weakly coupled light-only counterparts.

Polaritons are mixed states of photons and material excitations and are well-known to exist in many condensed matter, atomic and optical systems. We are dealing with a semiconductor microcavity, where polaritons exist due to mixing of quantum well excitons and resonant microcavity photons. In the strong coupling regime photons excite the medium and are re-emitted in a cascaded manner, which gives rise to so-called Rabi oscillations. The measured spectral width of the peaks corresponds to the picosecond polariton life time. This is in contrast with the more usual weak-coupling regime (typical for operation of vertical cavity surface emitting lasers (VCSELs), where the slow (nanosecond) carrier dynamics does not catch up with the fast (picosecond) photon decay. Thereby most of the photons leave the cavity as soon as they are emitted. In this regime the response to a pulse, resonating with a cavity mode, results in a single spectral peak. Thus any potential application of microcavity polaritons in optical information processing leads to a 2–3 orders of magnitude response time reduction relative to the VCSEL-like operating regimes.

Weak and strong coupling regime differ mainly in that in the latter case the dispersion curve exhibits two branches signalling mixing of light and matter excitations. Namely, additionally to the upper parabolic branch, which is largely a photonic one, the lower polariton branch appears. In our context the most relevant feature is that this lower branch exhibits an inflection point where the second order dispersion changes sign [Fig. 1(a)]. It is worth noting that this effect is merely evoked by the strong photon-exciton coupling, hence it appears even in a homogeneous cavity and does not require any modulation as in the weak coupling regime. Whereas the existence of dark solitons can be anticipated for the repulsive (defocusing) exciton-exciton interaction [1] we demonstrate that the peculiar dispersion curve can be exploited for the formation of stable *bright* cavity polariton solitons [2] without requiring any periodic modulation in the cavity for dispersion control.

The widely accepted dimensionless mean-field model for excitons strongly coupled to the circularly polarized cavity photons is

$$\begin{aligned} \partial_t E - i(\partial_x^2 + \partial_y^2)E + (\gamma_c - i\Delta)E &= E_p + i\Psi, \\ \partial_t \Psi + (\gamma_0 - i\Delta + i|\Psi|^2)\Psi &= iE. \end{aligned} \quad (1)$$

Here E and Ψ are the averages of the photon and exciton creation or annihilation operators. Normalization is such that $(\Omega_R/g)|E|^2$ and $(\Omega_R/g)|\Psi|^2$ are the photon and exciton numbers per unit area. Here, Ω_R is the Rabi frequency and g is the exciton-exciton interaction constant. $\Delta = (\omega - \omega_r)/\Omega_R$ describes detuning of the pump frequency ω from the identical resonance frequencies of excitons and cavity, ω_r. Time t is measured in units of $1/\Omega_R$. γ_c and γ_0 are the cavity and exciton damping constants normalized to Ω_R. Transverse coordinates x, y are normalized to the value $x_0 = \sqrt{c/2kn\Omega_R}$ where c is the vacuum light velocity, n is the refractive index and $k = n\omega/c$ is the wavenumber. The normalized amplitude of the external pump E_p is related to the physical incident intensity I_{inc} as $|E_p|^2 = g\gamma_c I_{inc}/\hbar\omega_0{\Omega_R}^2$.

The key of understanding for soliton formation is the linear dispersion relation of cavity polaritons, which follows from the linear version of Eq. (1).

We show the formation of spatially localized polariton-solitons in the strong coupling regime. The microcavity polariton solitons reported here exhibit a picosecond excitation time and can

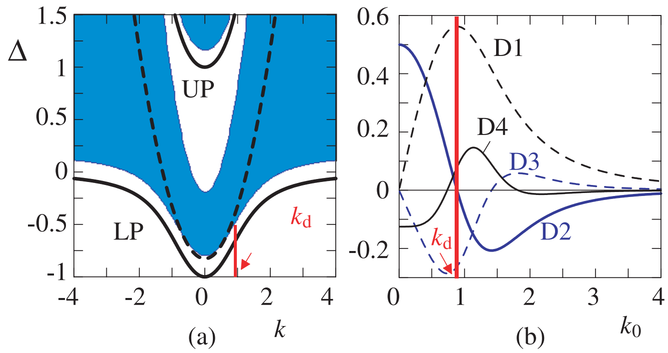

Figure 1: (a) Polariton dispersion: lower (LP) and upper(UP) branch in the strong coupling regime. The lower branch allows for the existence of dark (near the center) and moving bright solitons (beyond the inflection point). (b) Dispersion coefficients vs. inclination of the holding beam k_0.

be observed at pump powers a few orders of magnitude lower than those required in the weak coupling regime of semiconductor microcavities. Various stable and unstable dark solitons may be excited near the center of the lower branch of the dispersion relation whereas all bright solitons appear unstable there.

But, stable moving 1D cavity polariton solitons can form provided that the lower polariton dispersion is used beyond the inflection point. We also demonstrate the continuous transformation between cavity soliton polaritons shaped by the different dispersion orders, including the regimes where the influence of the usual second order dispersion is negligible.

Soliton existence and guiding mechanisms established here form the basis for future studies of soliton-polariton logic and processing schemes.

REFERENCES

1. Yulin, A., et al., "Dark polariton-solitons in semiconductor microcavities," *Phys. Rev. A*, Vol. 78, 061801, 2008.
2. Egorov, O., et al. "Bright cavity polariton solitons," *Phys. Rev. Lett.* (submitted).

Towards Linear and Nonlinear Integrated MagnetoOptics

R. Morandotti[1], **Y. Linzon**[1], **M. Ferrera**[1], **C. S. Manda**[1], **M. Zaezjev**[1], **L. Razzari**[1], **J.-Y. Hwang**[1], **K. A. Rutkowska**[1], **A. Pignolet**[1], **and B. A. Malomed**[2]

[1]INRS-Énergie et Matériaux, Univérsite du Québec, Varennes (Québec), J3X 1S2, Canada
[2]Department of Physical Electronics, School of Electrical Engineering
Faculty of Engineering, Tel Aviv University, Tel Aviv 69978, Israel

Abstract— New technologies, based on materials whose ferrimagnetic transition can be controlled by light, have oriented research towards the study of the magneto-optical properties of garnet thin films. Epitaxial garnets have a low optical absorption in the near infrared, adequately high refractive indeces, and a significant magneto-optical response, which make this class of materials particularly promising for magneto optical applications. All together, the previously listed properties have been concretized in a myriad of applications such as the realization of temperature-independent optical isolators (for eliminating undesired back-reflection in active laser systems), and recently of magneto-optic visualizers in which the use of Bi substituted iron garnet epitaxial films has been exploited. Yet, the versatility of these materials can lead to even more (and often unexpected) applications. In the first part of the paper, we will review our ongoing activities in (integrated) magneto-optics. We will start by reporting on fully substituted iron garnet epitaxial thin films, where a strong magneto-optic (MO) enhancement has been induced by the co-modification of Ce and Bi ions in iron garnet films, leading to the highest Faraday rotation ever obtained in magneto-optical garnet thin films (0.55 degrees/μm, @1550 nm). In the second part of the paper, we will focus our attention on the possible use of the same class of nonreciprocal materials to control the propagation of a high intensity light beams.

In particular, nonlinear light propagation in multidimensional self-focusing media is generally influenced by instabilities that, if the input power exceeds a certain threshold value, can lead to catastrophic collapse after a finite propagation distance. In the past decade, the problem of the collapse of (2+1)-dimensional [(2+1)D] optical beams in Kerr-type media has become the subject of intensive studies. In such cases, which typically take place when light propagates through amorphous media and crystals without any specific symmetry, the nonlinear Schrödinger equation (NLSE) can be applied to theoretically investigative the nonlinear behavior associated to light propagation. The possibility of wave collapse control (in particular to prevent its negative effects leading to material damage) has recently drawn much attention. Such control can be achieved via the use of optical birefringence, which in turn allows for the control of energy and phase transfer between the beam polarization components. Here, we will demonstrate that the optical birefringence can act as a powerful tool for (2+1)D beam collapse management. Our numerical studies, as well as the results of a series of experiments we have performed show that the combined effects of linear and circular birefringences can affect the dynamics of beam collapse in bulk self-focusing media. We find that the acceleration, the deceleration, or even the suppression of light collapse can be obtained for certain values of birefringence. We also show experimentally that the linear and circular birefringences required for the collapse management can be easily induced in transparent magneto-optical (MO) Yttrium Iron Garnet (YIG) crystals by applying an external dc magnetic field.

Moving Solitons in a Cavity Soliton Laser

K. Mahmoud Aghdami[1], **F. Prati**[2], **G. Tissoni**[2], **M. Brambilla**[3], **and L. A. Lugiato**[2]

[1]Physics Department, Payame Noor University, Mini City, Tehran 19569, Iran
[2]INFM-CNR and CNISM, Dipartimento di Fisica e Matematica, Università dell'Insubria, Como, Italy
[3]INFM-CNR and CNISM, Dipartimento di Fisica Interateneo, Politecnico di Bari, Italy

Abstract— Cavity solitons (CSs) are bright intensity peaks over a dark homogeneous background. They arise in the coherent field transmitted by nonlinear optical resonators, and are generated through diffraction-mediated lightCmatter interaction which leads to field self-localization within the cavity [1]. CSs have been experimentally demonstrated in broad area, driven vertical cavity surface emitting laser (VCSELs) below and above threshold. In a laser with a saturable absorber (LSA) it is possible to achieve the optimal condition where CSs coexist with a dark state of pure spontaneous emission corresponding to a laser below threshold. Under this condition the contrast between the CSs and the homogeneous background is maximum. On the other hand, since such a device is able to generate CSs without an external holding beam, it is the realization of a Cavity Soliton Laser (CSL).

A theoretical prediction of dissipative optical localized structures (autosolitons) in a laser with a saturable absorber was first proposed by Rosanov and co-workers [2]. Here, we considered a VCSEL with an absorbing medium integrated in the cavity, taking into account the finite relaxation rates of the material, the saturable dispersion associated to the linewidth enhancement factors [3], and the radiative recombination processes typical of semiconductors [4].

In particular, we investigate the mechanism giving rise to a dynamical instability, leading to the spontaneous motion of cavity solitons [5]. A key role is played by the ratio between the lifetimes in the amplifier and in the absorber (parameter $r = \tau_{amp}/\tau_{abs}$) (see figure). In conditions of perfect homogeneity, when the threshold is crossed, a stable fixed cavity soliton starts to move along a straight line, whose direction is arbitrary, that is, determined by the noise of the system. Nevertheless, it is possible to address this motion by injecting an additional driving pulse in the vicinity of the CS, which is very important for application purposes.

Another important aspect is the interactions of the travelling CS with the boundaries of the device, or of the pumped region. A travelling CS can be confined inside the active region, bouncing against the boundaries and displaying a trajectory that strongly depends on the geometry of the borders.

Finally, the interactions between two travelling CS will be investigated. The picture is very complicated, because of the rapidly varying phase of the travelling CS, and their extended phase profile, which originates long rangeinteractions.

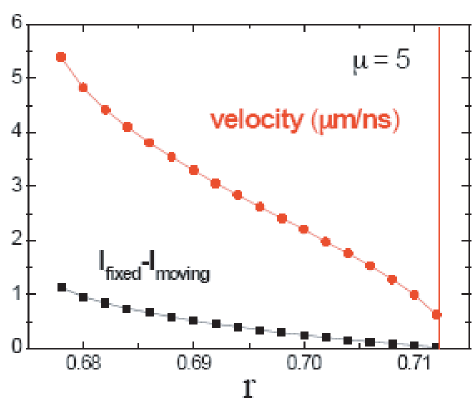

Figure 1: Velocity and peak intensity of the travelling cavity soliton, as a function of the bifurcation parameter r.

REFERENCES

1. Lugiato, L. A., *IEEE J. Quantum Electron.*, Vol. 39, 193, 2003.
2. Rozanov, N. N. and S. V. Fedorov, *Opt. Spectrosc.*, Vol. 72, 1394, 1992.
3. Bache, M., et al., *Applied Physics B: Lasers and Optics*, Vol. 81, 913, 2005.
4. Prati, F., et al., *Applied Physics B: Lasers and Optics*, Vol. 88, 405, 2007.
5. Fedorov, S. V., N. N. Rozanov, and A. N. Shatsev, *Opt. Spectrosc.*, Vol. 102, 449, 2007.

Session 4P3
Nanophotonics: Materials and Device Applications 2

Novel Silicon Nanophotonic Structures Lab-on-a-chip Sensing

Ali Adibi
School of Electrical and Computer Engineering, Georgia Institute of Technology
Atlanta, GA 30332-0250, USA

Abstract— The development of ultra-compact and sensitive sensing structures with minimal sample requirement for accurate sensing have been of great recent interest for multiple applications including bio and environmental sensing, chemical agent detection, and bio- threat detection. With recent advancement in the development of design and fabrication tools for photonic nanostructures, integrated photonic platforms are a strong candidate for the development of such sensing structures.

In this talk, I will first present the requirements for the development of photonic lab-on-a-chip sensing structures. I will then explain how these requirements are met by two recent developments in our group in the area of silicon photonics, i.e., ultra-high Q micro-resonators, and ultra-compact photonic crystal on-chip spectrometers with orders of magnitude smaller size compared to the other implementations with the same performance. These spectrometers are enabled by dispersion engineering in photonic crystal to simultaneously achieve the superprism effect, negative diffraction, and negative refraction. Details of the design of such structures along with their experimental demonstrations will be presented.

Progress in Metal-insulator-metal Waveguide Lasers at Near-infrared Wavelengths

Milan J. H. Marell and Martin T. Hill
COBRA Research Institute, Technische Universiteit Eindhoven
Postbus 513, 5600 MB Eindhoven, The Netherlands

Abstract— Strong light confinement can be achieved in metallic cavities which can confine light to volumes with dimensions considerably smaller than the wavelength of light. It was commonly believed, however, that the high losses in metals are prohibitive for laser operation in metallic nano-cavities. Recently we have reported lasing in a metallic nano-cavity filled with an electrically pumped semiconductor. Importantly, the manufacturing approach employed for these devices permits even greater miniaturization of semiconductor lasers. Furthermore, the approach allows for complex device shapes and the guiding of light between devices. Of particular interest are the metal-insulator-metal (MIM) waveguides. These MIM waveguides can propagate a transverse magnetic (TM0) mode which permits true deep sub-wavelength guiding of light in two dimensions. The manufacturing process is adapted to produce a variant of MIM waveguides. The presentation will look at the modeling, fabrication and operation of these devices. An overview will also be given of latest results from devices.

Previously reported devices observed light that leaked out of the metallic nano cavity through the device base. This is not optimal as the lasing light travels transversally between the metal sidewalls of the pillar structure. Ideally, the transverse propagating mode needs to be coupled directly out to either a conventional dielectric waveguide or free space. We will discuss our progress in making metallic cavity nano lasers with coupling of the transverse propagating mode directly to free space, and present results from our latest attempts.

Finally future development directions, challenges and prospects for such lasers will be discussed. In particular, it is interesting to examine ways that such devices can be made significantly smaller, where the dimensions of the guided mode in the laser approaches approximately one hundredth of the free space wavelength of light.

Nano-plasmonic Devices: From Nano-confinement to Stopped Light

Pavel Ginzburg, **Alex Hayat**, **Nikolai Berkovitch**, **Gilad Rosenblat**, **and Meir Orenstein**
EE Dept. Technion, Haifa 32000, Israel

Abstract— Surface Plasmon Polaritons (SPPs) are electromagnetic waves propagating along the interface between materials with positive/negative electric permittivity — commonly dielectric/metal interfaces. This intense negative polarization reflects the collective oscillations of the metal conduction electron coupled to the electromagnetic wave. The field of SPP exhibits its maximal value at the interface and exponentially decays into both adjacent media, thus localized in the immediate vicinity of the interface. Supported and guided by interfaces, the width of SPP consists of the "skin depth" into both media, thus not limited to be above half the wavelength in the material and consequently not subject to the "diffraction limit". This surface wave sustained only for TM mode, enabled by the coupling of plasma oscillations to the electric field component normal to the surface.

We demonstrate both theoretically and experimentally the possibility of nanoscale plasmonic waveguiding. We investigate trench [1], slot and strip waveguide geometries [2] and waveguides exhibiting plasmonic mode hybridization from various edges and wedge constituents [3]. Furthermore, we study the in depth the so called "plasmonic gap" structures, where dielectric medium is sandwiched between two metal plates. We show interesting dispersion characteristics of the gap structures, which support modes that are not limited by the diffraction limit and look at the circular power flow in the gap structures — leading to slow waves, slow light, stopped light and negative index characteristics at optical frequencies. Specifically, we demonstrate that a tapered structure [4] and even simpler transmission-line like quarter wave plasmon transformer [5] are capable to confine and even stop the light propagation. As a further step towards 3D nano-confinement we proposed different gap-based cavities, capable to beat diffraction limit [6]. In this context the fundamental question arise: "How small the modal volume could be?" is related to the inherent large plasmonic field gradients, resulting in nonlocal nonlinearity. We'll report on the plasmonic modes propagation under such gradients — where the metal becomes nonlinear medium due to collective ponderomotive force — resulting in charge carriers repelled from the high field intensity region, locally reducing the plasma frequency, and thus making the dielectric constant intensity-dependent. We develop a theoretical model for this ponderomotive nonlinearity in SPP propagation calculations, and study the nonlinear propagation behavior of an SPP, which exhibits strong self-focusing and "slow light" properties before its cutoff point [7].

REFERENCES

1. Satuby, Y. and M. Orenstein, "Surface-Plasmon-Polariton modes in deep metallic trenches-measurement and analysis," *Opt. Express*, Vol. 15, 4247–4252, 2007.
2. Satuby, Y. and M. Orenstein, "Surface plasmon polariton waveguiding: From multimode stripe to a slot geometry," *Appl. Phys. Lett.*, Vol. 90, 251104, 2007.
3. Arbel, D. and M. Orenstein, "Plasmonic modes in W-shaped metal-coated silicon grooves," *Opt. Express*, Vol. 16, 3114–3119, 2008.
4. Ginzburg, P., D. Arbel, and M. Orenstein, "Gap plasmon polariton structure for very efficient microscale-to-nanoscale interfacing," *Opt. Lett.*, Vol. 31, 3288–3290, 2006.
5. Ginzburg, P. and M. Orenstein, "Plasmonic transmission lines: From micro to nano scale with $\lambda/4$ impedance matching," *Opt. Express*, Vol. 15, 6762–6767, 2007.
6. Feigenbaum, E. and M. Orenstein, "Optical 3D cavity modes below the diffraction-limit using slow-wave surface-plasmon-polaritons," *Opt. Express*, Vol. 15, 2607–2612, 2007. "Ultrasmall volume plasmons, yet with complete retardation effects," *Phys. Rev. Lett.*, Vol. 101, 163902, 2008.
7. Ginzburg, P., A. Hayat, N. Berkovitch, and M. Orenstein, arXiv:0708.3959v1.

Charged Type-II Quantum Dots and Quantum Dot Dendrimers

Sungjee Kim
Department of Chemistry, Pohang University of Science and Technology
San 31, Hyojadong, Pohang 790-784, Korea

Abstract— We report photoluminescence (PL) spectral switching of quantum dots (QDs) by chemically controlling transfers of electrons in and out of the type-II heterostructures. When electron charged, CdTe/CdSe (core/shell) QDs show huge PL blue shifts (up to $\sim 100\,\mathrm{nm}$) whereas PL of CdSe/CdTe (core/shell) QDs red-shifts. We demonstrate reversible spectral switching of type-II QDs by repeated charging and neutralization processes. The PL spectral shifts are due to the interactions between injected spectrator electrons and type-II character excitons. Electron charged CdTe/CdSe QDs show PL blue shifts because of the strong repulsions between the shell-localized excitonic electrons and injected spectrator electrons. It is opposite for CdSe/CdTe QDs, where injected electrons in surface states attract the holes in the shells. We investigate the interactions of spectrator electrons and excitons as varying the dimensions of type-II QDs. We also compare the type-II QDs with type-I QDs such as CdSe, CdTe, and CdTeSe alloyed QDs. We showcase unique optical properties of charged type-II QDs, which have many potential applications such as electro-optic modulators. Quantum dot dendrimers are introduced that consist of a few hundred CdSe or CdTe quantum dots. Surfactant limited condition is used to induce attachments between quantum dots to comprise the dendrimers. Size of the dendrimers can be flexibly tuned from 40 to 200 nm with the distribution less than 5%. The dendrimers show great analogy to quantum dots in growth and assembly. Growth of the dendrimers is monitored using a flow reactor. Polyhedrally-shaped dendrimers are found in early stage, which may be equivalent to 'magic size' quantum dots. 'size-focusing' and 'size-defocusing' behaviors are also observed for multiple precursor injections. The self-organization of the dendrimers into three dimensional superlattices is demonstrated. We fabricate quantum dot or quantum dot dendrimer — conducting polymer composite photovoltaic devices with the identical inorganic weight percentage. The dendrimers show an order of magnitude higher energy conversion efficiency over individual quantum dots.

Slow-light Enhanced Nonlinear Optics in Silicon Photonic Crystal Waveguides

D. J. Moss[1], B. Corcoran[1], C. Monat[1], C. Grillet[1], T. P. White[2], L. O'Faolain[2], T. F. Krauss[2], and B. J. Eggleton[1]

[1]IPOS, CUDOS, School of Physics, University of Sydney, New South Wales 2006, Australia
[2]School of Physics and Astronomy, University of St Andrews, St Andrews, Fife, KY16 9SS, UK

Abstract— There has been growing interest in slow light due to its potential application for optical delay lines and nonlinear optical signal processing [1]. The increase of the optical energy density due to spatial pulse compression in the slow light regime is regarded as a means for enhancing nonlinear phenomena such as Raman scattering, 2nd and 3rd harmonic generation or frequency conversion. However, apart from theoretical predictions this enhancement process has not been systematically demonstrated to date, partly due to the high dispersion that typically accompanies slow light, causing pulse distortion that compromises its benefit. Planar photonic crystals (PhCs) represent an attractive platform for integrating many optical functions onto a single compact chip. In addition, PhC waveguides can be engineered so that both the dispersion and group velocity can be fully controlled, thereby producing slow light modes with limited dispersion over a substantial bandwidth. Here, we demonstrate slow light enhancement of nonlinear processes in engineered silicon PhC waveguides, including third harmonic generation (THG), self phase modulation, and nonlinear absorption. Both the strong optical confinement within the waveguide and the slow light (c/40) mode supported by the PhC structure have enabled us to observe visible green light (at 520 nm) at low (∼several watts) peak pump powers at 1560 nm [2]. This is 5–6 orders of magnitude lower than previous free-space coupling experiments in porous silicon PhC geometries, and is a result of the increased optical energy density in our slow light PhC waveguide. As another example of a slow light enhanced nonlinear effect, we also report the experimental observation of slow light enhanced SPM exhibited by picosecond-pulses propagating through silicon PhC waveguides as short as 80 μm [3]. This was made possible due to engineering the PhC geometry to provide a series of waveguides with (i) a controlled low group velocity ranging between c/20 and c/50 and (ii) a limited group velocity dispersion associated to the slow light regime over at least 5 nm bandwidth for all of the guides. The experimental results are supported by Split-Step-Fourier-Method (SSFM) modeling, including Two Photon Absorption (TPA) and free carrier (FC) effects in silicon, which gives further insight into the various contributions of these effects to both the output pulse signature and the power transfer function. In particular, both experiment and simulation highlight the reinforcement of TPA and FC effects in the slow light regime. In conclusion, we demonstrate slow-light enhancement of nonlinear effects undergone by picosecond-pulses propagating through 80 μm long silicon PhC waveguides with group velocities ranging between c/20 and c/50. The comparison of the respective output spectral signatures through fast and slow waveguides reveals significant enhancement in both SPM induced spectral broadening and optical third harmonic generation (THG) due to slow light.

REFERENCES

1. Krauss, T. F., "Why do we need slow light?," *Nature Photonics*, Vol. 2, 448, 2008.
2. Corcoran, B., C. Monat, C. Grillet, D. J. Moss, B. J. Eggleton, T. White, and T. Krauss, "Slow light enhanced visible optical third harmonic generation in 2D silicon photonic crystal waveguides," to be published, *Nature Photonics*, Vol. 3, No. 4, April 2009.
3. Monat, C., B. Corcoran, M. Ebnali-Heidari, C. Grillet, B. J. Eggleton, T. P. White, L. O'Faolain, and T. F. Krauss, "Slow light enhancement of nonlinear effects in silicon engineered photonic crystal waveguide," *Optics Express*, Vol. 17, No. 4, 2944, 2009.

NIR, MWIR and LWIR Quantum Well Infrared Photodetector Design Using Transfer Matrix Method

R. A. T. Santos[1], **F. D. P. Alves**[1], **J. de Amorim**[1], **C. G. R. Taranti**[1], **and G. Karunasiri**[2]

[1]Instituto Tecnologico de Aeronautica, Pca Mal Eduardo Gomes, 50
Sao Jose dos Campos, SP 12228-900, Brazil
[2]Department of Physics, Naval Postgraduate School, Monterey, CA 93943, USA

Abstract— The advances in material sciences and semiconductor growth technology have allowed the use of bandgap engineering to design quantum well infrared photodetectors (QWIPs) with high sensitivity, high selectivity, controlled multispectral capability [1–3]. This paper demonstrates the use of the Transfer Matrix Method (TMM) [4] to estimate the confined energy levels and their respective wavefunction of complex heterostructures in both valence and conduction band. The potential profile of the structure is sliced and made constant within each layer. By solving the Schrodinger equation for a constant potential in each slice and using the continuity of the wavefunction at the interfaces it is possible to handle virtually any potential profile. Comparison between numerical results and analytical solutions of potentials such as Modified Posch-Teller Hole [5] shows errors smaller than 0.1%. To solve structures with heavily doped layers, a self consistent approach is employed to include the charge distribution influence in the overall potential. In addition, strain effects are taken into account for structures with significant differences in lattice constant. The method is employed to estimate the luminescence peaks in GaAs/AlGaAs/InGaAs symmetric and asymmetric quantum wells. Comparison between measurements and TMM numerical results shows errors averaged in 1%. Finally, the method is used to estimate the responsivity wavelength peak of a QWIPs that use interband and intersubband transitions to detect near-, mid- and long infrared (NWIR, MWIR, LWIR) [6]. The TMM predictions are in good agreement with the average error within 3%. The errors are most likely due to uncertainties in semiconductor parameters such as bandgap and junction band offsets. Those results indicate that the adapted TMM, despite its simplicity, is a suitable method to be used in QWIP design.

REFERENCES

1. Levine, B. F., *Journal of Applied Physics*, Vol. 74, R1, 1993.
2. Rogalski, A., *Infrared Physics and Technology*, Vol. 38, 295, 1997.
3. Olsen, R. C., *Remote Sensing from Air and Space*, 157–178, SPIE Press, Bellingham, WA, 2007.
4. Pérez-Alvarez, R. and F. García-Molina, *Transfer Matrix, Green Functions and Related Techniques*, Publicacions de la Universitat Jaume I, Castello de la Plana, 2004.
5. Harrison, P., *Quantum Wells, Wires and Dots: Theoretical and Computational Physics*, 23–30, John Wiley & Sons Inc., New York, 2001.
6. Alves, F. D. P., et al., *Journal of Applied Physics*, Vol. 103, 114515, 2008.

830–940 nm Tunable Quantum Well Infrared Photodetector Using Interband Transitions

F. D. P. Alves[1], **R. A. T. Santos**[1], **and G. Karunasiri**[2]

[1]Instituto Tecnologico de Aeronautica, Pca Mal Eduardo Gomes, 50
Sao Jose dos Campos, SP 12228-900, Brazil
[2]Department of Physics, Naval Postgraduate School, Monterey, CA 93943, USA

Abstract— Earth observation, remote sensing and military applications have demanded infrared photodetectors with high sensitivity, high selectivity, controlled multispectral capability [1–3]. The advances in material sciences and semiconductor growth technology have allowed the use of bandgap engineering to design quantum well infrared photodetectors (QWIPs) with those characteristics. This paper presents the design and characterization of a QWIP capable of detecting wavelengths within the near-infrared (NIR) band with a bias adjustable spectral response. The detection was achieved using interband electron transitions between quantized energy levels for holes (light and heavy) in the valence band and quantized energy levels for electrons in the conduction band. The quantum wells were made asymmetric (step wells) to allow transitions between energy levels with different parity quantum numbers [4]. The structure was modeled by solving self-consistently the Schrödinger and Poisson equations using the shooting method [5]. The fabricated photodetector consists of 64 semiconductor layers grown by molecular beam epitaxy (MBE) on a GaAs substrate as follows: a $2 \times 10^{18}\,\mathrm{cm}^{-3}$ Si doped GaAs (0.7 µm) buffer layer, followed by 20 periods of undoped GaAs (300 Å)/$In_{0.10}Ga_{0.90}As$ (43 Å)/$In_{0.25}Ga_{0.75}As$ (40 Å)/GaAs (300 Å) step quantum wells, ended by a $2 \times 10^{18}\,\mathrm{cm}^{-3}$ Si doped GaAs (0.5 µm) contact layer. Responsivity measurements were performed and the observed response lies in the 825–950 nm wavelength range. By varying the bias on the device it was possible to modify the spectral response. With lower bias the detector response presents a narrow peak around 840 nm due to transitions from heavy hole first excited state (HH2) to electrons first exited state (E2). With higher bias the responsivity presents a narrow peak around 930 nm due to transitions from heavy hole ground state (HH1) to electrons ground state (E1). A quasi-flat response along the detection range was also achieved, showing that the device responsivity shape can be manipulated by the applied bias. The results demonstrate the possibility to achieve tunable detection in the NIR band with great versatility using QWIPs. Furthermore, by varying the dimensions and composition of the device materials it is possible to cover virtually the entire band to fit the application requirements.

REFERENCES

1. Levine, B. F., *Journal of Applied Physics*, Vol. 74, R1, 1993.
2. Rogalski, A., *Infrared Physics and Technology*, Vol. 38, 295, 1997.
3. Olsen, R. C., *Remote Sensing from Air and Space*, 157–178, SPIE Press, Bellingham, WA, 2007.
4. Alves, F. D. P., et al., *Journal of Applied Phisics*, Vol. 103, 114515, 2008.
5. Harrison, P., *Quantum Wells, Wires and Dots: Theoretical and Computational Physics*, 23–30, John Wiley & Sons Inc., New York, 2001.

Session 4P4a
Superconductive Active and Passive Devices and Circuits: Models and Techniques of Simulation

Electro-thermal and Optical Modeling of Superconducting Nanowire Single-photon Detectors

Alexei D. Semenov
Institute of Planetary Research, Germany

Abstract— Single photon detectors from ultra-thin NbN nanowires offer moderate broadband quantum efficiency and photon-energy resolution in the visible and near infrared spectral range along with the counting rates up to hundred of millions per second. Demonstrated detector parameters favor applications in several fields like secure communications, quantum optics or fluorescence correlation spectroscopy. Operation of an NbN single-photon detector at lower temperatures in the range from 6 K to 1.2 K results in the gradual increase of the quantum efficiency and energy resolution while substitution of SQUID readout for microwaves amplifier additionally improves energy resolution in near infrared down to 0.5 eV. Typical broadband quantum efficiency of a few percent can be resonantly enhanced to reach almost one half. The rate of dark counts also reduces at low temperatures giving rise to the detector sensitivity. The ultimate values set by optical properties of the detector structure, transport parameters of NbN films and physics of fluctuations and photon counting will be discussed. The underlying electro-thermal mechanism of the detector response will be described with an emphasis on the requirements to the readout electronics. Finally, absorbance of nanowire metal gratings on dielectric substrates will be considered as well as its impact on the polarization sensitivity of single-photon detectors.

Focal Plane Array of Cold-Electron Bolometers

Leonid Kuzmin
Chalmers University of Technology, S-41296 Gothenburg, Sweden

Abstract— Novel concepts of the parallel and series array of Cold-Electron Bolometers (CEB) with Superconductor-Insulator-Normal (SIN) Tunnel Junctions have been proposed and simulated for a distributed focal plane antenna. The arrays are developed for a pixel design based on arrays of CEBs coupled to a distributed slot antenna or dipole antenna [1].

Two variants of the CEB arrays have been considered for both types of antenna on bulk substrate.

The series connection of CEBs with SIN tunnel junctions in current-biased mode [2] is optimal for dipole antennas. Estimations of the CEB noise with JFET readout have shown an opportunity to realize NEP less than photon noise for typical power load.

The parallel connection of CEBs with SIN tunnel junctions in voltage-biased mode [3] is optimal for a slot antenna. Some improvement of responsivity and noise properties can be achieved by using the optimal configuration of CEB with SIN junction and Andreev contact. Remarkable progress in performance is expected from implementation of a new technology for fabrication of the CEB and SQUID on the same chip in one vacuum circle [4]. Estimations of the CEB noise with SQUID readout have shown an opportunity to realize background-limited performance for typical power load of 5 pW proposed for BOOMERanG.

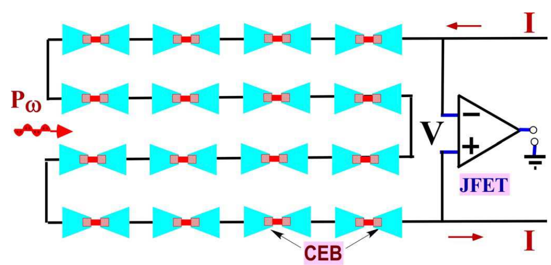

Figure 1: A distributed single polarization dipole antenna with a series array of CEBs and a JFET readout. This dipole antenna will be sensitive only to horizontal component of RF signal.

REFERENCES

1. Day, P. K., et al., "Far-infrared imager-polarometer using distributeted antenna-coupled transition-edge sensors," *SPIE*, Vol. 5498, 856–875, 2004.
2. Kuzmin, L., "Array of Cold-Electron Bolometers with SIN tunnel junctions for cosmology experiments," *Journal of Physics: Conference Series (JPCS)*, Vol. 97, 012310, 2008.
3. Kuzmin, L., "Ultimate Cold-Electron Bolometer with SIN tunnel junction and andreev contact," *Proceedings of the 17th Int. Symp. on Space Terahertz Technol.*, *ISSTT-2006*, 183–186, Paris, 2006.
4. Kuzmin, L., "Hybrid on-chip technology of Cold-Electron Bolometer and SQUID readout," US Patent, to be filed, 2009.

Low Loss Nb and NbTiN Circuit Design for the THz SIS Mixer

A. Karpov[1], **D. Miller**[1], **J. A. Stern**[2],
B. Bumble[2], **H. G. LeDuc**[2], **and J. Zmuidzinas**[1]

[1]California Institute of Technology, Pasadena, CA 91125, USA
[2]Jet Propulsion Laboratory, Pasadena, CA 91109, USA

Abstract— We present the development of the low loss superconductive circuits for an application in SIS mixers at the Terahertz frequencies.

One of the motivations for the development of the Terahertz receivers lay in the need of an efficient detector for radio astronomy. The astronomer's interest in the Terahertz detection is related to the fact that the biggest number of the photons traveling in space belongs to the Terahertz frequency band. The last years the main focus of the receiver development was on the heterodyne receiver technology using a low-noise frequency mixer to down-convert the signals. The fundamental limitation of the heterodyne receiver sensitivity is the quantum noise limit resulting from the Heisenberg uncertainty principle. In terms of the receiver equivalent noise temperature the quantum noise limit is $T_Q = h\nu/k$ where, h and k are the Planck and Boltzmann constants. The SIS mixer is a photo-mixer, and in theory may approach closely the quantum limit of the receiver noise.

We developed the Nb and NbTiN circuits suitable for the SIS mixer matching circuits. In the SIS mixer, we used the Nb/Al-AlN/NbTiN SIS junctions with the critical current density of 30–50 kA/cm^2. At the frequency close to 1 THz we demonstrated a sensitive SIS mixer with the noise equivalent temperature close to 4–5 $h\nu/k$. We will discuss the frequency and sensitivity limitations and the possible improvements of SIS frequency mixers at the Terahertz frequencies.

Electrodynamic Modeling and Measurement of Non-uniform Arrays of Josephson Junctions

F. Boussaha[1], **L. Loukitch**[2], **M. Salez**[1], **A. Féret**[1], **C. Chaumont**[2], **and J. G. Caputo**[2]

[1]LERMA, Observatoire de Paris, 77 avenue Denfert-Rochereau, Paris 75014, France
[2]Laboratoire de Mathématiques, INSA de Rouen, B. P. 8, 76131 Mont-Saint-Aignan Cedex, France
[3]GEPI, Observatoire de Paris, 77 avenue Denfert-Rochereau, Paris 75014, France

Abstract— We investigate non-uniform arrays of N small Josephson junctions of Nb/Al-AlO_x/Nb embedded in a Nb/SiO/Nb superconductive stripline. From the theorical point of view, for an array of small junctions in a passive region, the model can be reduced to a 1D linear partial differential equation with Dirac distribution sine nonlinearities. We present a detailed comparison of measurements and numerical simulations of model devices where we varied the number, sizes and positions of the junctions in the arrays. These show that such circuits can be tailored for different specific applications in magnetometery, quasiparticle microwave sensors, Josephson oscillators, and superconducting electronics.

Design of a Wideband Slot Bow-tie Antenna Excited by a Microstrip to CPW Transition for Applications in the Millimeter Wave Band

A. Colin[1] **and P. Febvre**[2]

[1]Instituto de Física de Cantabria (CSIC-UC), Av. Los Castros s/n, Santander 39005, Spain
[2]IMEP-LAHC, UMR 5130 CNRS, Campus Scientifique, University of Savoie
Le Bourget du Lac 73376, France

Abstract— We propose a design of a slot bow-tie antenna excited by a microstrip to coplanar waveguide (CPW) transition, operating at the central frequency of 45 GHz in the millimeter wave range from 26 to 64 GHz. The antenna is suitable to be included in arrays, series-fed arrays, for applications in radar, communications, radioastronomy or Cosmic Microwave Background (CMB) experiments. The small size and symmetric geometry of the antenna facilitates the integration with monolithic microwave integrated circuits (MMIC), microstrip circuits and for the connection with active or passive elements. Simulation results, computed under the environment of the HFSS-Ansoft software have shown a wideband for this antenna of 85% with VSWR < 2. Since such antennas are designed to be part of arrays ultimately fabricated with thin film microelectronics techniques, normal metal conductors will lead to increased losses caused by the skin depth of the order of magnitude of the film thickness. To avoid this issue, and since these arrays need to be cooled with the detectors, it is advisable to use superconducting materials. Consequently the feed lines have been simulated and optimized as well with superconducting materials in order to keep the good microwave matching properties to the antenna.

Antenna Design: The antenna is designed on Alumina substrate; 3 μm electroplated gold, 0.254 mm thickness, relative permittivity of 10, and loss tangent of 0.001. The geometry and parameters of the antenna are shown in Fig. 1, where $a = 0.05$, $b = 0.1$, $c = 0.25$, $d = 7.5$, $e = 0.5$, $f = 10$, $g = 5.65$, $h = 0.1$, and $i = 7.3$. All dimensions are in mm. Bottom ground plane only covers the microstrip lines section (d and e dimensions). The widths of the microstrip line and gaps of the CPW were calculated to be approximately 50 Ohm, whose transition between them is made by means a smaller and thinner strip line ($b \times e$ dimensions) of about 73 Ohm.

Computation Results: All parametric variables were controlled in the HFSS design environment considering two cases: a) using an open radiation type boundaries for the substrate's surroundings box, and b), introducing a brass reflector plane placed below the substrate and varying its height for each run. In both cases, we used an excitation wave port of 50 Ohm. Return loss for a single antenna with and without reflector plane is shown in Fig. 2. It shows a wide operation range (26–64 GHz) with a central frequency at 45 GHz thus giving a wideband of approximately 85%. Fig. 3 shows the normalized directivity pattern at 40 GHz for the E-plane ($\varphi = 0°$) and H-plane ($\varphi = 90°$) using reflector plane. The characteristic input impedance throughout the feed

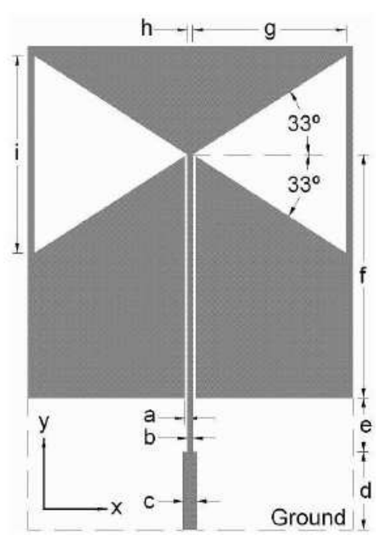

Figure 1: Antenna geometry (not to scale) and parameters.

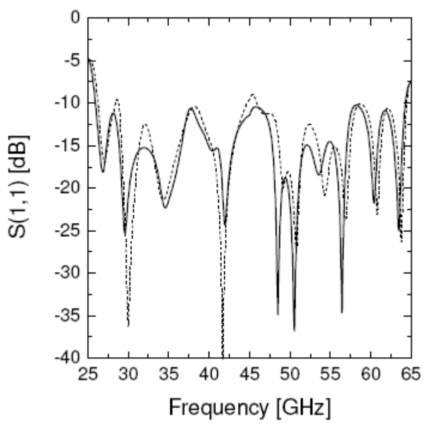

Figure 2: Return loss using a reflector plane placed at $\lambda_0/4$ below the substrate (dashed line), and without reflector plane (solid line).

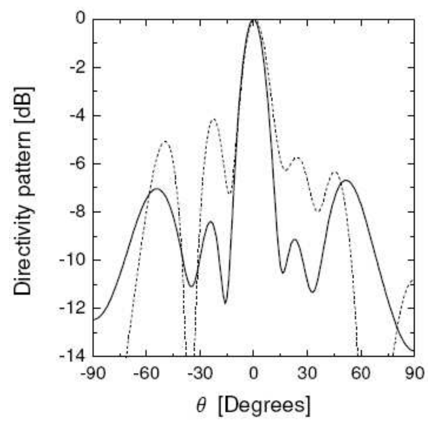

Figure 3: Normalized directivity pattern of the bow-tie slot antenna at 40 GHz for the E-plane (solid line) and H-plane (dashed line), using a reflector plane placed at $\lambda_0/4$ below the substrate.

line is one of the deciding factors which is directly associated to the bandwidth, therefore the length and width of the transition strip line turns to be crucial for this study. The above results provide good expectation to be confirmed with the measurements of the prototypes.

Modelling and Simulation Techniques to Calculate Passive Component Characteristics in Superconductive Integrated Circuits

C. J. Fourie, A. Young, and D. B. Davidson
Stellenbosch University, South Africa

Abstract— Reliable design of superconductive integrated circuits (ICs) requires accurate modelling and extraction of passive component characteristics. This is becoming especially important as superconductive electronic systems mature from all-digital Rapid Single-Flux Quantum (RSFQ) circuits to mixed-signal electronics with logic gates, antennas, detectors, mixers and other microwave or millimetre-wave components integrated on a chip.

For all-digital superconductive circuits, accurate inductance extraction is a primary concern. Analytical solutions for simplified structures and two-dimensional inductance matrix solvers have sufficed until recently, but as process dimensions shrink and layer counts increase, the accuracy of any technique that does not involve three-dimensional modelling of circuit structures becomes severely limited.

We discuss three-dimensional circuit structure modelling and segmentation for magneto-quasistatic (MQS) inductance calculation algorithms that use the method of moments (MoM) technique, and show how mutual inductance calculations and even finite ground planes with moats can be accommodated. Simulation results for real structures are compared to to practical inductance measurements, and software calibration and limitations are discussed.

As digital circuit complexity and speed increase, and analogue circuits are added to IC designs, more than just inductance needs to be extracted from simulation models. Calculating propagation constants, S-parameters and dispersion curves requires the use of full-wave computational electromagnetic (CEM) algorithms. However, CEM algorithms have different properties, and not all are suitable for application to IC simulations where the dimensions of substrates are in the order of millimetres, line widths in the order of micrometres, and isolation and conduction layer thicknesses in the order of hundreds of nanometres. We show how the popular CEM techniques, namely FDTD, MoM and FEM weigh up when applied to typical superconductive IC structures, and discuss the use of frequency and time domain analysis to calculate a range of passive component characteristics.

Comparison of Typical Superconducting Structures with Analytical and 3D Modelling Methods

P. Febvre[1], **D. Bouis**[1], **and A. Colin**[2]

[1]IMEP-LAHC, UMR 5130 CNRS, Campus Scientifique, University of Savoie
73376 Le Bourget du Lac, France
[2]Instituto de Física de Cantabria (CSIC-UC), Av. Los Castros s/n, Santander 39005, Spain

Abstract— Superconducting structures are widely used in different systems, ranging from passive microwave filters to superconducting digital electronics or sensors for astronomy. As long as the circuits stay simple enough, analytical formulas can be used for the most basic devices: transmission lines, corners, tees or stubs as a few examples. With these basic blocks, complex circuits can be built. Technologies with microstrip elements are widely used because they are usually well adapted and better mastered in circuits used with superconducting sensors, like Superconductor-Insulator-Superconductor mixers, or Hot Electron Bolometers. Coplanar elements are also used, especially when the 50-ohm characteristic impedance is required at the input/ouput of the circuits. Some analytical formulas have been used in the past to calculate the scattering parameters of the simplest circuits. Nevertheless, at very high frequencies and cryogenic temperatures, it is uneasy to perform measurements to validate the approach. On the other hand, several 2D, 2.5D and 3D simulation tools can be used to perform simulations of superconducting structures that are potentially more accurate.

In this work, we present the results of several simulations of typical superconducting structures with different set of parameters. Analytical techniques and 3D simulation tools are used separately and the results are compared in order to assess the limits of the analytical techniques. The objective is to be able to perform fast calculations of the most commonly used structures, by ad apting the analytical formulas for defined ranges of geometrical and material parameters. From these results, we expect to build some simple tools for future design of superconducting circuits.

Session 4P4b
Inverse and Forward Problems in Radiative Transport

Numerical Reconstruction of the Refractive Index from the Reflection Data

O. V. Belai, L. L. Frumin, E. V. Podivilov, and D. A. Shapiro
Institute of Automation and Electrometry, Siberian Branch, Russian Academy of Sciences
1 Koptjug Ave, Novosibirsk 630090, Russia

Abstract— A new method of numerical reconstruction of the refractive index from the complex reflection coefficient is tested using the Rayleigh layer and the hyperbolic secant layer. The method demonstrates its high efficiency and accuracy.

The inverse scattering problem (ISP) for one dimensional Helmholtz wave equation is of interest in optics, radiophysics, acoustics, geophysics. It is reduced to the reconstruction of the refractive index n as a function of coordinate x from the complex reflection coefficient. As a rule, only numerical solution is possible. The direct solution of ISP requires N^5 operations [1], where N is the number of discrete intervals. The layer peeling method requires N^2 operations [2], but it provides the first order approximation $O(h)$, where $h \sim 1/N$ is the step of discretization. Aiming at the accuracy ε we see the layer peeling requires ε^{-2} operations. "Inner-bordering" method was proposed recently [3] ensuring h^2 approximation and N^2 operations, see also [4]. It requires only ε^{-1} operations. The new method was tested at Bragg gratings with deep refractive index modulation. The direct scattering problem for these gratings was solved numerically. To study its own accuracy excluding that of the input data it is necessary to test it at exactly solvable cases.

In the present paper we test the inner-bordering method at the Rayleigh layer [5] and at the hyperbolic secant layer. After the Bremmer transformation [6] and choice of the optical path $\xi = \int n(x)\, dx$ as a new coordinate the Helmholtz equation reduces to a pair of equations analogous to the coupled mode equations. For hyperbolic secant coupling coefficient

$$q(\xi) = \frac{d \ln \sqrt{n}}{d\xi} = Q \operatorname{sech}(x/L), \tag{1}$$

where Q, L are parameters, the equations can be solved analytically. At $N = 2^{12}$ the accuracy of numerical reconstruction occurs to be 4×10^{-7}. The accuracy for Rayleigh layer is 2×10^{-2}, since it corresponds to square coupling coefficient providing wide spectrum, which is hard to treat numerically.

Thus the inner bordering method demonstrates its high accuracy and efficiency. It could be helpful for ISP in different fields.

REFERENCES

1. Chen, Y. and V. Rokhlin, "On the inverse scattering problem for the Helmholtz equation in one dimension," *Inverse Probl.*, Vol. 8, No. 3, 365–391, 1992.
2. Belai, O. V., L. L. Frumin, E. V. Podivilov, and D. A. Shapiro, "Inverse scattering for the one-dimensional Helmholtz equation: Fast numerical method," *Opt. Lett.*, Vol. 33, No. 18, 2101–2103, 2008.
3. Belai, O. V., L. L. Frumin, E. V. Podivilov, and D. A. Shapiro, "Efficient numerical method of the fiber Bragg grating synthesis," *J. Opt. Soc. Am. B*, Vol. 24, No. 7, 1451–1457, 2007.
4. Rayleigh, L., "On the propagation of waves through a stratified medium, with special reference to the question of reflection," *Royal Society of London Proceedings Series A*, Vol. 86, 207–226, Feb. 1912.
5. Bremmer, H., "The propagation of electromagnetic waves through a stratified medium and its W.K.B. approximation for oblique incidence," *Physica*, Vol. 15, No. 7, 593–608, 1949.

The Exact Solution for Inverse Problem in Transmission Optical Tomography for a Proportional Scattering Medium

Sergey A. Tereshchenko
Moscow Institute of Electronic Technology (MIET), Russia

Abstract— The tomographical reconstruction of the internal structure of biological (high scattering) objects is an actual problem of modern physics. The radiation transport equation (RTE) is the most general way for a description of an interaction between a radiation and a medium. The most important characteristics of scattering medium included in radiation transport equation are a radiation absorption coefficient $\mu_a(\vec{r})$ and an angle differential radiation scattering coefficient $\mu_s(\vec{r},\vec{\Omega}' \to \vec{\Omega})$, where $\vec{r}$ is a point of the medium, $\vec{\Omega}'$ and $\vec{\Omega}$ are directions of the photon before and after scattering respectively. Thus in most general problem formulation there is needed to reconstruct two independent functions of three variables ($\mu_a(\vec{r})$) and seven variables ($\mu_s(\vec{r},\vec{\Omega}' \to \vec{\Omega})$). In this formulation, the problem becomes too difficult for solution, therefore the main objective of presented work is the mathematical solution of this problem under additional conditions.

For a description of the optical radiation propagation through the non-homogeneous turbid medium is used the "Scattering-Straight-Back" (SSB) approximation for RTE in which $\mu_s(\vec{r},\vec{\Omega}' \to \vec{\Omega}) = m_s(\vec{r})\delta_2(-\vec{\Omega}'\vec{\Omega})$ [1], where $m_s(\vec{r})$ is the radiation scattering coefficient and $\delta_2(\vec{\Omega}'\vec{\Omega})$ is the surface delta-function, that is 2-D delta-function on a unit sphere. For a reconstruction of both medium characteristics there is not enough the initial information in the traditional measurement scheme as in the X-ray CT. One way for further simplification is the postulation of the proportionality of the radiation scattering coefficient $m_s(\vec{r})$ to the extinction coefficient $m(\vec{r}) = \mu_a(\vec{r}) + m_s(\vec{r})$. It is just the proportional scattering medium (PSM). It reduces two unknown functions $\mu_a(\vec{r})$ and $m_s(\vec{r})$ to one unknown function $m(\vec{r})$. In this case, the RTE has the exact analytical solution [2]. Let it $m_s(x,y) = \beta m(x,y)$, then the projections $p(\xi,\theta) = \int\limits_{-\infty}^{+\infty} m(\xi,\zeta)d\zeta = -\ln(\dfrac{I(1+\sqrt{1-\beta^2})}{\sqrt{1-\beta^2}+\sqrt{1-\beta^2+\beta^2 I^2}})$, where I is the ratio of passed and initial radiation, θ is the angle of the turning of the rotating co-ordinate system (ξ,ζ) relative to the absolute co-ordinate system (x,y). Applying inverse Radon transformation $\mathfrak{R}^{-1}\{\cdot\}$ to projections $p(\xi,\theta)$ it can be obtained the reconstructed image of the unknown function $m(x,y) : m(x,y) = \frac{1}{\sqrt{1-\beta^2}}\mathfrak{R}^{-1}\{p(\xi,\theta)\}$.

Thus with no additional assumptions the inverse problem of transmission optical tomography has been solved in the special case of the proportional scattering medium, in which $\mu_s(\vec{r},\vec{\Omega}' \to \vec{\Omega}) = \beta m(\vec{r})\delta_2(-\vec{\Omega}'\vec{\Omega})$, that is absolutely analogous to the case of the pure absorbing medium for the X-ray CT, in which $\mu_s(\vec{r},\vec{\Omega}' \to \vec{\Omega}) = 0$.

REFERENCES

1. Tereshchenko, S. A., *Methods of Computed Tomography*, Fizmatlit, Moscow, 2004 (in Russian).
2. Tereshchenko, S. A., "Transmission tomography of proportional scattering media," *Zhurnal Tekhnicheskoi Fiziki*, Vol. 78, No. 7, 69–75, 2008 (in Russian).

Three-dimensional Förster Resonance Energy Transfer Imaging in Turbid Media by Using Time-gated Data Acquisition

Vadim Y. Soloviev[1], **James McGinty**[2], **Alessandro Sardini**[3], **Daniel W. Stuckey**[3], **Khadija B. Tahir**[2], **Romain Laine**[2], **Joseph V. Hajnal**[3], **Paul M. W. French**[2], **and Simon R. Arridge**[1]

[1]Department of Computer Science, University College London
Gower Street, London WC1E 6BT, UK
[2]Blackett Laboratory, Imperial College Photonics
Prince Consort Road, London SW7 2BW, UK
[3]MRC Clinical Sciences Centre, Imperial College Faculty of Medicine
Hammersmith Hospital Campus
Du Cane Road, London W12 0NN, UK

Abstract— Fluorescence lifetime imaging is well-established as a useful tool to provide molecular contrast in microscopy, offering many advantages over conventional intensity-based fluorescence imaging in terms of quantitation and the available functional information. Increasingly fluorescence is being exploited for tomographic imaging *in vivo* studies in small animals to study, for example, the localization of diseased tissue and of therapeutic agents using appropriate fluorescent labels. The measurement of fluorescence lifetime can provide further information, e.g., concerning the local fluorophore environment in biological tissue. Many protein interactions and conformational changes can be reported using Förster resonance energy transfer (FRET) and fluorescence lifetime provides a robust read-out for FRET studies. FRET is a mechanism describing energy transfer between two fluorophores when a donor fluorophore, initially in its electronic excited state, may transfer energy to an acceptor fluorophore in close proximity typically less than 10 nm, through non-radiative dipole-dipole coupling. We report an approach of FRET localization in turbid media based on the lifetime contrast. The algorithm was applied to a large time-gated experimental data set acquired by imaging a highly scattering cylindrical phantom concealing two fuorescent wells. Both wells contained cytosolic preparations of HEK293 cells tranfected with the plasmid TN-L15. TN-L15 codes for a FRET sensor constituting a fragment of the calcium binding protein Troponin-C flanked by two fluorophores: cyan fluorescent protein as donor and citrine as acceptor. One of the wells contained 10 mM calcium which, upon binding to Troponin-C, induces a protein conformation change accompanied by FRET from CFP to citrine. Our goal at this stage was to localize and discriminate these two wells from boundary tomographic measurements. Our approach employs the Fourier domain reconstruction of time gated imaging data. The diffusion approximation to the radiative transfer equation is assumed. The algorithm is designed as an iterative solution of a system of differential equations of the Helmholtz type, which is obtained by minimizing an appropriate cost functional.

Inverse Problem for the Radiative Transport Equation with the Method of Rotated Reference Frames

Manabu M. Machida, George Y. Panasyuk, John C. Schotland, and Vadim A. Markel
Departments of Radiology and Bioengineering, University of Pennsylvania, USA

Abstract— The method of rotated reference frames (MRRF) [1, 2] for solving the radiative transport equation (RTE) was developed with the inverse problem in mind. In particular, the MRRF has allowed us to obtain the plane-wave decomposition of the RTE Green's function. This mathematical construction is essential for solving the inverse problem in the slab geometry by the methods which were previously developed by us for the diffusion equation [3, 4].

Although the MRRF was formulated with the account of planar boundaries [2], numerical implementation of the boundary conditions posed a major challenge. This problem, however, has now been solved. We have implemented the forward solution to the RTE in the slab geometry and proceeded to apply the methods outlined in [4] to solve the inverse problem of the RTE. An absorptive tomographic image of a bar target is shown in the figure. Here the imaging is performed in a slab of the width $L = 6\ell^*$ where ℓ^* is the photon mean free path. The width is sufficiently large for the scattering to form a fundamental obstruction to imaging yet not large enough for the diffusion regime approximation to the RTE to be very accurate. This is illustrated in the figure: the reconstruction which is based on the diffusion approximation and on inverting the diffusion equation does not resolve the bars of the target while the RTE-based reconstruction does.

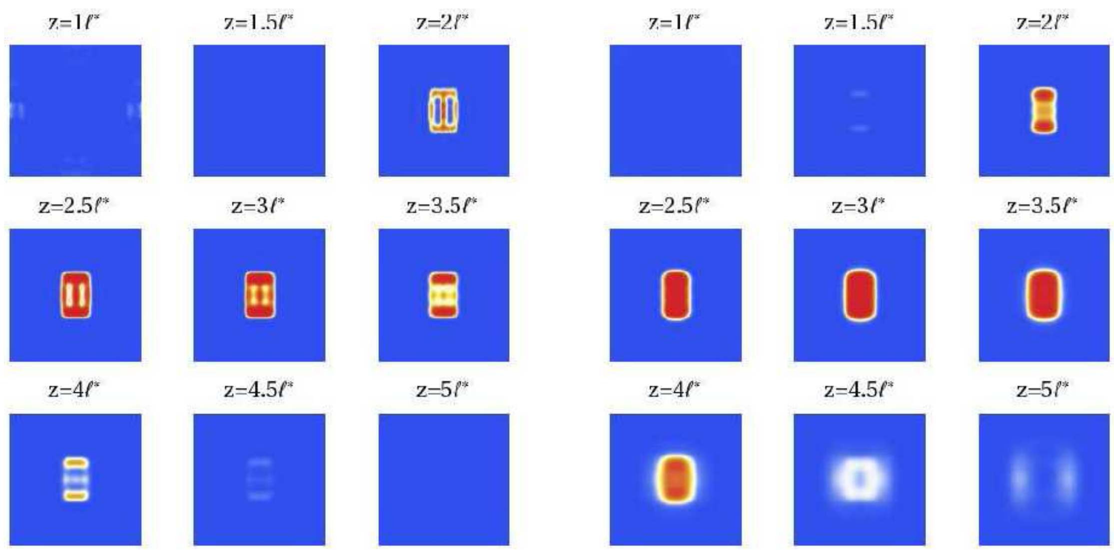

Figure 1: Reconstruction of the absorption coecient of a bar target of the bar target which is located at the depth of $z_0 3\ell^*$ in the center of a scatting slab of the width $L = 6\ell^*$, where ℓ^* is the photon mean free path. Slices drawn through the slab parallel to its surface at different depth z are shown. The left panel shows the reconstructions obtained by inverting the RTE and using the MRRF. The right panes shows reconstructions based on the diffusion approximation to the RTE.

REFERENCES

1. Markel, V. A., *Waves in Random Media*, Vol. 14, L13, 2004.
2. Pansyuk, G., J. C. Schotland, and V. A. Markel, *J. Phys. A*, Vol. 39, 115, 2006.
3. Markel, V. A. and J. C. Schotland, *Phys. Rev. E*, Vol. 70, 056616, 2004.
4. Schotland, J. C. and V. A. Markel, *Inverse Problems and Imaging*, Vol. 1, 181, 2007.

Session 4P5a
Computational Electromagnetics 1

Classical Theorems of Discrete Electrodynamics on Simplicial Complexes

J. M. Arnold
University of Glasgow, UK

Abstract— Maxwell's laws of classical electrodynamics have exact counterparts on a purely discrete space, reformulated as discrete Stokes' Theorems on simplicial complexes [1, 2]. The question naturally arises as to what other classical laws may be admitted by the discrete electrodynamical fields. We show the existence, under certain time-discretisations, of exact discrete versions of Poynting's Theorem, Green's Theorem, Kirchoff-Huyghens Theorems, plane wave superposition theorems, extinction theorems and other topological field theorems. These topological theorems constrain the numerical solutions of com- putational algorithms of discrete electrodynamics, particularly the FDTD method, on both structured and unstructured spatial meshes forming the simplicial complexes. Judicious application of constraint theorems potentially leads to significant reductions in the number of degrees of freedom necessary to compute in order that the algorithms produce topologically complete solutions.

The case of Poynting's Theorem for electrodynamics on a simplicial complex is considered. A discrete local quantity corresponding to total electric and magnetic field energy densities for the simplicial complex (a discrete 3-form W) is shown to lead to conserved global total energy $\sum W$ in continuous time, but energy is not conserved in discrete time with simple Euler explicit time-stepping (the explicit FDTD method); this behaviour is well-known for explicit methods [3]. To obtain a conserved total energy, implicit time-stepping is required. To obtain a Poynting Theorem there is also required in addition to W a discrete 2-form S such that $\partial_t W = \mathrm{d}S$ in continuous time, and $W^{m+1} - W^m = \mathrm{d}S^m$ in discrete time, where m indicates the time-stepping variable and d is the discrete exterior derivative on r-forms on the simplicial complex. It is not obvious how to construct the compatible local energy density W and Poynting flux 2-form S, along with a suitable time discretisation. When dynamical sources drive the discrete fields, in the form of discrete charges on vertices and discrete current 2-forms, it is also necessary to have consistent energy transfers between the sources and the fields when the sources themselves may have internal dynamics, as considered for example in FDTD coupled to model quantum systems [4].

These aspects of energy density and energy flux for discrete electrodynamics on simplicial complexes are studied and presented in detail.

REFERENCES

1. Desbrun, M., E. Kanso, and Y. Tong, "Discrete differential forms for computational modelling," *Discrete Differential Geometry*, ed. A. I. Bobenko, et al., Vol. 38, 287–323, Oberwolfach Seminars, Birkhauser Verlag, 2008.
2. Bossavit, A., *Computational Electromagnetism*, Academic Press, Boston, 1998.
3. Haiter, E., C. Lubich, and G. Wanner, *Geometric Numerical Integration, Springer Series in Computational Mathematics*, 31, 2006.
4. Slavcheva, G., J. M. Arnold, and R. W. Ziolkowski, "Coupled Maxwell-pseudospin equations for investigation of self-induced transparency effects in a degenerate three-level quantum system in two dimensions: Finite-difference time-domain study," *Phys. Rev. A*, Vol. 66, 063418, 2002.

Maintenance of Current Limited Reactor Electromagnetic Compatibility and Safety

M. Sh. Misrikhanov[1], **N. B. Rubtsova**[2], **and A. Yu. Tokarskij**[1]

[1]Open JSC Federal Network Company Branch "Main Power Networks of the Center", Russia Federation
[2]RAMS Institute of Occupational Health, Moscow, Russian Federation

Abstract— By means of computer program "Reactor MF" magnetic field (MF) levels created by four three-phase current limited reactors RTOS-10-3150-0.25-UZ in 220 kV substation management control panel building are calculated. It is shown, that in halls of 10 kV closed switch-gear (CSG-10 kV) where cases with automatics containing microprocessor devices are placed, MF intensity of MT considerably above than maximum permissible value (MPV) on noise immunity, and in located near reactor MF levels are more than occupational exposure hygienic norms. Combined electromagnetic screens (CEMS) application for decreasing of MF induced by current limited reactors levels efficiency is shown. CEMS allow reducing MF levels up to lower than corresponding norms both on noise immunity, and occupational exposure.

CEMS consists of four turns of voltage source 0.8 m in radius and two (top and bottom) two-layer, containing on two turns in layer, shielding turns (ST) with internal coils radius: $R_0 = 0.95\,\mathrm{m}$. Installation CEMS on reactor under coordinated-parallel electrical connection of voltage source turns and ST allows to decrease of MF levels in zone of microprocessor units arrangement in 10 kV closed switch-gear hall from 75 A/m up to 1 A/m, and on the surface of staircase wall — from 2000 A/m up to 800 A/m. CEMS installation reduces inductive resistance of reactor from 0.269 Ohm up to 0.184 Ohm.

A Parametric Analysis of Perfect Matched Layer Model of Finite Difference Time Domain Method

J. Sosa-Pedroza, **M. Benavides-Cruz**, **M. Nieto-Rodríguez**,
M. Galaz-Larios, **and M. Enciso-Aguilar**
Departamento de Telecomunicaciones, ESIME-SEPI, Instituto Politécnico Nacional
UPALM Edif. Z-4, 3er. piso, 07738, México, D.F.

Abstract— A basic consideration for the Finite Difference Time Domain method (FDTD) is to limit the computational space domain, to do so the Absorbing Boundary Conditions (ABC) should be defined to simulate an infinite domain. Special attention has devoted to this issue since the beginning of the method, from the theory of scattered-wave annihilating differential operators of Bayliss and Turkel to the actual Perfect Matched Layer (PML) of Jean-Pierre Berenger. Theory of Berenger ABC's, define a new computational space after the one of interest, which characteristics reduce the incoming computational wave almost to zero, avoiding any reflection get back to the main computational space.

We present in this paper an analysis of the parameters involved in the variable conductance of matched layer which follows the rule: $\sigma_m(\rho/\delta)^n$, where σ represents the variable conductivity, σ_m the maximum conductivity, ρ the distance of each element after the layer interface, δ the PML wide and n a parameter to be defined to reduce reflections. The paper presents results for different values of $\mathbf{n}$, σ_m and δ, comparing for each case the reflection coefficient.

Method of Optimum Simple Iteration for the Solution of Large Complex Systems of the Linear Algebraic Equations Arising in Scattering Problems

Sergey P. Kulikov
Moscow State Institute of Radio Engineering, Electronics and Automation
78, Vernadsky av., Moscow 117454, Russia

Abstract— Questions of optimum convergence of the modified method of simple iteration (MMSI) for the solution of the linear continuous operator equation of the second kind and, in particular, the integral scattering equation, and also following from it at numerical solution a large system of the linear algebraic equations (SLAE) with complex non-hermith matrix are considered. The complex optimum parameter κ which allows to achieve convergence MMSI and minimizes spectral radius of a transition operator (matrix), essentially depends on a configuration of spectrum area of this operator (matrix). Thus complex value of optimum parameter is the center of some circle which contains a convex envelope of a spectrum and is "visible" from a point of transition operator (matrix) singularity — the point 1 of a complex plane — under the minimal corner $\alpha < \pi$. Algorithms of definition of optimum parameter in cases when the convex envelope of a spectrum of transition operator (matrix) is in the form of figure of the simple form, such as a circle, a piece, a triangle, a convex polygon and such convex envelope does not contain a point of singularity are developed and proved. The denominator of convergence $q < 1$ of a method of optimum simple iteration (MOSI) in the considered cases is certain. MOSI is applied to the solution of integral equation arising in scattering problems of electromagnetic waves on locally non-uniform transparent dielectric. The integral operator of this equation is transition operator in usual method of simple iteration. Then MOSI is applied to the solution of large SLAE arising at digitization of integral equation and application of a method of the final sums. As an example of applicability MOSI it is considered scalar 2D case of E-polarization of a primary field. In this case the integral transition operator of a problem is compact and has only a discrete spectrum with a unique point of accumulation of a spectrum — origin of the complex plane. In case of Rayleigh (low frequency) scattering, area of a spectrum is the small area near this point and optimum parameter κ of convergence has value $\kappa = \varepsilon_1/2$, where ε_1 — is maximal on the module and isolated own number, which can be effectively found by means of an iterative degree method. Similarly optimum parameter is, if the area of scattering has the Rayleigh size only on one coordinate. In case of resonant scattering (length of a wave is of the order of the size of area) the spectrum of transition matrix and an optimum circle can approach rather close to a point of singularity, that worsens convergence MOSI. Value thus is defined by means of algorithms for a triangle or a polygon which tops are a point 0, the points of a spectrum nearest to a point of singularity and greatest on the module own number. It is important, that a spectral picture together with optimum parameter are established with sufficient accuracy at even weak physical accuracy of approximation of a problem in 2–3 units of a settlement grid for wavelength in the environment and do not change any more for the best approximation in 8–12 and more units. Thus, in considered scattering problems the optimum parameter is defined for a rare grid and small transition matrixes, and then is used for large systems with good physical accuracy of a problem approximation. In last case the definition of a spectral picture would demand an unreal computer resources.

Numerical Solution of 2D and 3D Scattering Problems on a Dielectric Body by a Method of Optimum Simple Iteration

Sergey P. Kulikov
Moscow Institute of Radio Engineering, Electronics and Automation
78, Vernadsky av., Moscow 117454, Russia

Abstract— Problems of the numerical solution two-dimensional (2D) and three-dimensional (3D) scattering and absorption of stationary electromagnetic waves Rayleigh and resonant ranges on locally-non-uniform non-magnetic dielectrics are considered. The integral operator which influences a vector of amplitude of an electric field is Fredholm compact operator in 2D case of E-polarization, but the singular operator in 2D case of H-polarization and in the general 3D case. The method of the final sums and digitization of the integral equation leads in these cases to system of the linear algebraic equations (SLAE) from N, $2N$ and $3N$ complex unknown values of an electric field in units of a settlement grid. Value N can be rather great for problems of resonant area of wavelengths. Therefore the numerical solution received SLAE can be based on iterative methods. In the given work the method of optimum simple iteration (MOSI) which essentially uses the information on a spectrum of the integral operator is applied. Numerically and also analytically laws of a spectrum of integral transition operator and corresponding matrix of a problem are established. This spectrum consists of two parts in considered vector cases — a continuous part, which has the established dependence on values of permittivity of a body, and a discrete part, which depends only from geometry and scattering region size. The points of accumulation of discrete spectrum are on a continuous component. In a Rayleigh range of wavelengths the discrete component is in rather small area near with a continuous one and at definition of optimum parameter it can be neglected. For a homogeneous body, for example, a continuous spectrum of the transition operator is a piecewise from a point 0 up to points $1-\varepsilon$, where ε is the relative value permittivity of a body and in this case optimum parameter is $\kappa = \frac{1-\varepsilon}{2}$. For the non-uniform body without losses the formula is the same, where ε is the maximal value in the body. In a resonant case, there is a discrete spectrum which for a body without losses fills some significant area in a low half of a complex plane and which forms an imaginary value component of optimum parameter. In cases of an extensive discrete spectrum the optimum parameter is defined by special algorithms for a spectrum of a triangle or a polygon with one straight line on a continuous real spectrum and with the remote tops near to a point of singularity and in low half of a complex plane. As the body has the losses the spectral area extends due to the of a continuous part as well on upper half of plane and contains also piecewises from 0 up to $1-\varepsilon$, when value of ε has negative imagine part. It has been shown that the use of approximation based on the first member of the optimal number of iterations allows to expand the effective use of the Born approximation. The principle of an invariance of a spectral picture and optimum parameter is used at transition from a rare settlement grid to a grid with good approximation of a problem. Numerical solutions of some 2D and 3D scattering and absorption problems in Rayleigh and a resonant range on non-uniform dielectric structures are presented.

Session 4P5b
Magnetoelectric Composites: Physics and Applications

Design and Optimization of Wideband Multi Section Coupled-line Phase Shifters with Impedance Matching

Homayon Oraizi and Alireza Shamsafar
Department of Electrical Engineering
Iran University of Science and Technology, Tehran 1684613114, Iran

Abstract— Consider the schematic diagram and equivalent circuit of a passive microstrip coupled-line phase shifter as shown on Figs. 1 and 2, respectively. The input and output ports are designated by 1 and 2, respectively. The reference and isolated ports are 4 and 3, respectively. The output phase shift is measured as the phase difference between S_{12} (phase of transmission coefficient from port 1 to port 2) and S_{14} (phase of transmission coefficient from port 1 to port 4) [1, 2].

$$\Delta\varphi = \angle S_{12} - \angle S_{14} \tag{1}$$

The even- and odd-mode analysis is used to determine the impedance matrix of the coupled-line phase shifter [3].

$$\begin{bmatrix} Z_{11} & Z_{12} \\ Z_{21} & Z_{22} \end{bmatrix} = \begin{bmatrix} \dfrac{(Z_{0e}\cot g\theta_e + Z_{0o}\cot g\theta_o)}{2} & \dfrac{(Z_{0e}\csc g\theta_e - Z_{0o}\csc g\theta_o)}{2} \\ \dfrac{(Z_{0e}\csc g\theta_e - Z_{0o}\csc g\theta_o)}{2} & \dfrac{(Z_{0e}\cot g\theta_e + Z_{0o}\cot g\theta_o)}{2} \end{bmatrix} \tag{2}$$

Then the $ABCD$ and scattering matrices are obtained [4, 5].

$$\begin{bmatrix} A & B \\ C & D \end{bmatrix} = \begin{bmatrix} \dfrac{Z_{11}}{Z_{21}} & \dfrac{Z_{11}Z_{22} - Z_{21}Z_{12}}{Z_{21}} \\ \dfrac{1}{Z_{21}} & \dfrac{Z_{22}}{Z_{21}} \end{bmatrix} \tag{3}$$

$$\begin{bmatrix} S_{11} & S_{12} \\ S_{21} & S_{22} \end{bmatrix} = \begin{bmatrix} \dfrac{AZ_L + B + CZ_LZ_S{}^* - DZ_S{}^*}{AZ_L + B + CZ_LZ_S + DZ_S} & \dfrac{2\sqrt{R_SR_L}}{AZ_L + B + CZ_LZ_S + DZ_S} \\ \dfrac{2\sqrt{R_SR_L}}{AZ_L + B + CZ_LZ_S + DZ_S} & \dfrac{AZ_L + B + CZ_LZ_S{}^* - DZ_S{}^*}{AZ_L + B + CZ_LZ_S + DZ_S} \end{bmatrix} \tag{4}$$

where Z_S and Z_L are the source and load impedances, respectively. The over all $ABCD$ matrix of the multi-section coupled-line phase shifter is obtained by the product of $ABCD$ matrices of each coupled-line section.

The phase shift is given by (1) and the reflection coefficient or the return loss is given by S_{11}.

Now, we construct an error function for the realization of specified phase shift ($\Delta\varphi$) and minimization of the reflection coefficient.

$$error = W_1 \sum_{f_k = 4\,\text{GHz}}^{10\,\text{GHz}} |\Delta\varphi_{f_k} - 70|^2 + W_2 \sum_{f_k = 4\,\text{GHz}}^{10\,\text{GHz}} |S_{11f_k}|^2 \tag{5}$$

where W_1 and W_2 are the weighting functions and the frequency bandwidth is divided into K discrete frequencies. The error is a function of lengths (l_i) and widths (w_i) of microstrips and gaps (g_i) between them. The dispersion relations due to Jansen and Kersching for the coupled-line are also used [4].

The minimization of error function is performed by the combination of genetic algorithm (GA) and conjugate gradient (CG) method. Consequently, the lengths, widths, and gaps of microstrip lines are determined.

For example, we design a three section coupled-line phase shifter for a phase difference of $\Delta\varphi = 70°$ over the frequency bandwidth 4–10 GHz. The substrate Roger Ro3210 is used, for which the dielectric constant of the substrate is $\varepsilon_r = 10.2$ and its thickness is $h = 0.4$ (mm).

The source and load impedances are selected as $R_s = 50\,\Omega$ and $R_L = 50\,\Omega$. The initial values of l_i, w_i and g_i are selected by the random generation in MATLAB under constraints. The

constraints for w_i and g_i were specified as 0.1 h and 10 h, and the upper limit for the length of line sections was set at the wavelength of center frequency (λ).

The phase shift of the coupled-line phase shifter is drawn versus frequency in Fig. 3. The scattering parameters S_{11}, S_{12}, S_{13} and S_{14} are drawn in Fig. 4. The results of the MLS algorithm are verified by the HFSS and CST full-wave software. The dimensions of the optimized phase shifter configuration is given in Table 1.

REFERENCES

1. Free, C. E. and C. S. Aitchison, "Improved analysis and design of coupled-line phase shifters," *IEEE Trans. Microwave Theory Tech.*, 2126–2131, Sept. 1995.
2. Leong, Y. C. and S. Weinreb, "Novel technique of phase velocity equalization for microstrip coupled-line phase shifters," *IEEE MTT-S Intl. Microwave Symp. Digest*, 1453–1456, Boston, MA, 2000.
3. Pozar, D. M., *Microwave Engineering*, 2nd Edition, Wiley, New York, 1992.
4. Edwards, T. C., *Foundations for Microstrip Circuit Design*, 2nd Edition, Wiley, New York,1992.
5. Frickey, D. A., "Conversions between S, Z, Y, h, $ABCD$, and T parameters which are valid for complex source and load impedances," *IEEE Trans. Microwave Theory Tech.*, Vol. 42, No. 2, Feb. 1994.
6. Ramos Quirarte, J. L. and J. P. Starski, "Novel schiffman phase shifters," *IEEE Trans. Microwave Theory Tech.*, Vol. 41, No. 1, Jan. 1993.

Thick Film Lead Zirconate Titanate — Nickel Zinc Ferrite Heterostructures: Fabrication by Screen Printing Tecknology and Magnetoelectric Properties

A. Bush, V. Shkuratov, and Y. Fetisov
Moscow Institute of Radio Engineering, Electronics and Automation
Pr. Vernadskogo 78, Moscow 119454, Russia

Abstract— The paper describes screen printing technology which allows fabrication of heterostructures consisting of thick ceramic films of piezoelectric lead zirconate titanate (PZT) and magnetostrictive nickel zinc ferrite (NZF). The PZT and NZF powders of submicron size, mixed with a plasticizer and a binder, have been used [1]. The structures were fabricated on alumina substrates with a thin conducting layer preliminary formed on their surfaces. The samples containing single PZT film, single NZF film, a PZT-NZF bilayer, and a PZT-NZF-PZT trilayer with a film thickness of 40–70 μm have been synthesized. After fabrication the structures were sintered at 1100°C, covered with thin upper electrodes, and then poled by applying a permanent electrical field. The X-ray analysis has shown that structures contained only initial phases; no any additional phases appeared after the thermal treatment.

The measurements showed that fabricated structures possessed both electrical and magnetic properties which were determined by characteristics of the PZT and NZF layers. The piezoelectric and pyroelectric effects in the structures containing PZT film were of the same order of magnitude as for bulk samples. Dependences of effective dielectric permeability ε_{eff} and dielectric loss coefficient tgδ_{eff} on the temperature (300–900 K) and frequency (25–10^6 Hz) were formed as result of combination of PZT and NZF films properties. Saturation magnetization of the structures was equal to ∼290 emu/cm^3 and coercitive field did not exceed 10 Oe, in accordance with data for NZF ceramics.

For the PZT-NZF-PZT structures with layer thickness of 40–70 μm, we observed the magnetoelectric (ME) effect at room temperature in the bias magnetic field of 100–500 Oe. The ME coefficient was equal to $\alpha \sim 57$ mV/(Oe·cm) in the whole frequency band of 0–200 kHz and it increased up to ∼2 V/(Oe·cm) at selected frequencies of acoustical resonances of the structures. These values of ME coefficients are comparable to the best values for bulk composite bilayers made of the same materials [2].

The results obtained show that screen printing technology may be used to fabricate thick film PZT-NZF heterostructures. Thus made layered structures demonstrate rather high ME interaction efficiency at room temperature in relatively low bias magnetic fields. These structures are suitable to design high sensitive magnetic field sensors, voltage transformers, generators, and the others electronic devices.

ACKNOWLEDGMENT

The work was supported by Ministry of Education and Science of Russia and Russian Foundation for Basic Research.

REFERENCES

1. Srinivasan, G., E. T. Rasmussen, J. Gallegos, et al., *Phys. Rev. B*, Vol. 64, 214408, 2001.
2. Nan, C.-W., M. I. Bichurin, S. Dong, et al., *J. Appl. Phys.*, Vol. 103, 031101, 2008.

Magnetoelectric Interaction in a Cylindrical Piezoelectric-metal Structure

Y. K. Fetisov and D. V. Chashin
Moscow State Institute of Radio Engineering, Electronics and Automation
Pr. Vernadskogo 78, Moscow 119454, Russia

Abstract— Magnetoelectric (ME) interaction in a piezoelectric cylinder with metal electrodes arises due to combination of piezoelectricity and electromagnetic induction. The interaction takes place for the cylinder electrically poled in radial direction and magnetized with dc magnetic field H in axial direction. A voltage u is generated between the electrodes when ac magnetic field h is applied to the structure or field h is created inside the cylinder when ac voltage U is applied to the electrodes.

The ME voltage with magnitude of 300 mV was measured on ceramic lead zirconium titanate cylinder (18.5 mm in diameter) for applied fields $H = 1$ kOe and $h = 2$ Oe at acoustical resonance frequency $f = 58$ kHz. The cylinder generated ac field with magnitude $h \sim 0.1$ mOe when H=1 kOe and ac voltage $U = 10$ V of the same frequency was applied to electrodes. A theory describing ME interaction in piezoelectric-metal structure was developed. The effect is promising for application in magnetic field sensors and magnetic field modulation systems. The research was supported by the Ministry of Education and Science of Russia (project 2.1.1/6650) and Russian Fund for Basic Research (grant 08-02-12151).

Magnetoelectric Interaction in Amorphous Magnetic-piezoelectric Structures

Leonid Fetisov[1], **Nikolai Perov**[1], **and Yuri Fetisov**[2]

[1]Physics Department, Moscow State University, Russia
[2]Moscow State Institute of Radio Engineering, Electronics and Automation, Russia

Abstract— Magnetoelectric (ME) interaction in hybrid structures consisting of amorphous magnetic film and piezoelectric plate has been investigated. The structures of rectangular ($4 \times 10\,\mathrm{mm}^2$) and disk (15 mm in diameter) shapes contained a 30 μm thick $Fe_{90.3}Ni_{1.5}Si_{5.2}B_3$ film and a 200 μm thick $Pb_{0.52}Zr_{0.48}TiO_3$ plate. The layers were coupled to each other with epoxy glue. The ME interaction efficiency was measured in dc bias fields up to 2 kOe and ac magnetic field frequency band of 1–200 kHz for different fields orientations. Magnetic ac field to electrical voltage conversion efficiency as high as 9.2 V/Oe cm was achieved at frequency of 8.7 kHz and as high as 17 V/Oe cm at frequency of 160 kHz. These frequencies correspond to bending and radial acoustical resonances of the disk structure. Due to low saturation field of amorphous film the maximum efficiency was observed at low dc field of ~ 40 Oe. The structures investigated can be used to design high sensitive magnetic field sensors.

ACKNOWLEDGMENT

The work was supported by the RFBR, grants 05-02-19643 and 08-02-12151.

Session 4P6a
Modern Hybrid Methods in the Problems of Computational Electromagnetics

The Theory of R-functions and Wavelets in the Boundary Value Problems of Electrodynamics

V. F. Kravchenko[1] **and A. V. Yurin**[2]

[1]Kotel'nikov Institute of Radio Engineering and Electronics of RAS, Moscow, Russia
[2]Bauman Moscow State Technical University, Moscow, Russia

Abstract— The new approach of solving boundary value problems for differential equations of the elliptic type partial derivatives is represented. It is based on Galerkin classic variation diagram which is converted with the help of R-functions structural method [1] and wavelet-basis properties. The main point of such approach is the construction of the computational algorithm concerning the wavelet approximation of the analytic and geometric components of the boundary value problem. To convert the geometric information into analytic one as well as to satisfy the boundary conditions of the problem using the structures of solution helps the R-functions body of mathematics. The basic elements of the obtained functional is the wavelet-basis [2], the expansion coefficients of the domain function, the function of the right part of the equation and the function of boundary conditions of the wavelet-basis. As a result while matrix system compiling we obtain some calculating advantages: matrixes of the system are discharged, the calculation of matrix elements does not demand the integration and is carried out with the help of finite number of elementary mathematical operations over the coupling coefficients of the corresponding wavelet system. New fast computational algorithms based on fundamental wavelet properties for coupling coefficients are also introduced and founded in this work.

REFERENCES

1. Kravchenko, V. F. and V. L. Rvachov, *Boolean Algebra, Atomic Functions and Wavelets in Physical Applications*, Fizmatlit, Moscow, 2006.
2. Resnikoff, H. L. and R. O. Wells, *Wavelet Analysis: The Scalable Structure of Information*, Springer, New York, 1998.

Full Wave Hybrid Technique for CAD of Passive Waveguide Components with Complex Cross Section

M. B. Manuilov[1], **K. V. Kobrin**[1], **G. P. Sinyavsky**[1], **and O. S. Labunko**[2]

[1]Southern Federal University, Russia
[2]FGUP "Radiochastotny Centr YUFO", Russia

Abstract— Passive components based on waveguides with complex cross section are widely used in many microwave and millimeter-wave applications. For example, waffle-iron filters are employed in both high-power and low-power applications as low-pass filters. The main advantages of waffle-iron filters are both extended stop-band and pass-band and low insertion loss over a pass-band. Besides, waffle-iron filters attenuate all propagating waveguide modes whose frequency lies in the stop-band of filter. From this viewpoint, the waffle-iron filters are very appropriate candidates for some satellite communications applications. For example, in reflector antennas of earth stations operating in S, C, X, Ku frequency bands multi-band feeders are used. Typically, diplexers included into multi-band waveguide feeder are implemented on the base of low-pass waffle-iron filters. Ridged and all-metal finned waveguide structures find extensive applications in microwave and millimeter-wave filters, diplexers/multiplexers, transformers, polarizers etc.

A fast and accurate EM analysis of waffle-iron filters and ridged waveguide filters is based on Galerkin Method/Mode Matching Technique/Generalized Scattering Matrix Method. It is assumed that a waveguide structure under consideration consists of an arbitrary number of multi-ridged waveguide sections and stepped transitions connecting the filter with input and output waveguides. The solution is subdivided into the following steps: (i) decomposition of waveguide structure into elementary basic blocks, (ii) solving eigenvalue problem for multi-ridged waveguide sections, (iii) solving key scattering problems for basic discontinuities, (iv) direct combination of all **S**-matrices and evaluation of total **S**-matrix of filter.

The eigenvalue problems for both H- and E-modes are reduced to the system of integral equations of the first kind for unknown electric field components on the common interfaces of regular regions. For the solution of the integral equation system the Galerkin's method is utilized. A key point of this approach is a special choice of basis functions. The unknown tangential electric field components on the common interfaces are expanded into series of Gegenbauer or Chebyshev polynomials with weight factor taking into account field asymptotic at the edges. Such a choice of basic functions dramatically accelerates the convergence of the method. We used Mode Matching Technique for analysis of junction between rectangular and multi-ridged waveguide and both Mode Matching Technique and Galerkin method for analysis of step waveguide junction and waveguide bifurcation. Eigenfunctions of multi-ridged waveguide were written in accordance with transverse resonance method.

Thus, a hybrid full wave method for analysis and design of a wide class of ridged and finned waveguide components and waffle-iron filters is presented. The solution is based on Galerkin's Method/Mode Matching Technique/Generalized Scattering Matrix Method. By implementation of Galerkin's method to solving eigenvalue problems and key scattering problems the weighted Gegenbauer and Chebyshev polynomials were used as basis functions taking into account the field asymptotic at the edges. It leads to dramatically fast convergence and high accuracy of the solution. The obtained results are in good correspondece with available experimental and theoretical data of references.

A number of waffle-iron filters for multi-band feeders of reflector antennas operating in S, C, X, Ku bands has been designed. The potential of the new quasi-planar waveguide filter configuration has been studied. This filter configuration has improved pass-band selectivity and extended stop-band in comparison with the conventional ridge waveguide filters. Some modified quasi-planar pass-band filters with improved performance has been designed for Ka-band.

On the Number of TE and TM-modes in a Multilayer Planar Dielectric Waveguide with the Layers of Two Types

M. D. Kovalev
BMSTU, Moscow, Russia

Abstract— Convenient in applications formulas for calculating the numbers of optical TE and TM-modes in a planar dielectric waveguide including arbitrary number of layers are obtained. The only two restrictions on the waveguides are the following: the number of the layers is finite and the indices of refraction may admit only two different values. Evidently the bounding layers are of infinite width, and have the smaller one refractive index.

The derivation of the formulae is based on a new form of the dispersion equation for a planar waveguide. Dispersion equations give the eigenvalues of the effective refractive index of a waveguide. This new form of the dispersion equation in the general case was first developed by the author in joint work with A. A. Maer [1], and called by the author the multilayer equation. Earlier the author obtained by his method a similar formula for the number of energy levels of a quantum particle in a multiwell quantum potential structure [2].

The multilayer equation has significant advantages over traditional dispersion equation, obtained by the well known method of characteristic matrices [3, 4]. When the number of the layers is large the traditional equation contains too many members and becomes practically boundless. But the multilayer equation remains rather compact, its structure is simple and therefore it turns out to be analyzable. Lets note that the form of the multilayer equation was guessed by the author and later the connections of this equation with traditional dispersion equations were analyzed.

REFERENCES

1. Maer, A. A. and M. D. Kovalev, "Dispersion equation for eigenvalues of the effective refractive index in a multilayered waveguide structure," *Doklady Physics (Doklady Akademii Nauk)*, Vol. 407, No. 6, 766–769, 2006.
2. Kovalev, M. D., "On energy levels of a particle in a comblike structure," *Doklady Physics*, Vol. 53, No. 4, 201–205, 2008.
3. Born, M. and E. Wolf, *Principles of Optics*, Pergamon Press, 1964.
4. Yariv, A. and P. Yeh, *Optical Waves in Crystals*, Wiley, New York, 1984.

3D-EMHD-FDTD Simulation of Plasma Propulsion

D. S. V. Alves and A. J. F. Orlando
Departamento de Microondas e Optoeletrônica, Instituto Tecnológico de Aeronáutica
São José dos Campos, SP 12, 228-900, Brasil

Abstract— The method of finite differences in time domain, FDTD, is used for simulation of constricted electric discharge generated in the high atmosphere for UAV propulsion. At each time step and in each cell are computed the parameters of the discharge channel, flow of charges and energy through the equations of the electro-magneto-hydro-dynamic coupling, EMHD, in the three-dimensional space. The radiated fields are computed in the environment around the electric discharge by FDTD.

Introduction: Plasma propulsion is always boarded through the conception of the plasma torch, that is, the gas passes through a heat source, is ionized and then sped up. The models vary with the choice of the heat source, the process of ionization and acceleration of ions. The proposal of this article for electromagnetic propulsion is based on an efficient transformation of the electromagnetic energy in kinetic energy of molecules of air.

Electric discharges can be simulated by modelling air disruption and avalanche formation. A simple discretization of Maxwell equations, transport and conservation of mass, charge and energy results in a complicated system of equations and high computing cost, especially in three-dimensions. Electric discharges are constricted waves. The use of constrictions limits the computation of discharge channel evolution to the cells where the constrictions occur. In the other cells around the channel are computed the electromagnetic fields radiated from the discharge, reducing computing time and memory.

The use of constrictions means the use of boundary conditions for the cells in the discharge channel, where occurs the EMHD. The discharge channel region possesses high temperature, falling off in the radial direction, which defines thermal constriction. Resonant absorption and emission of photons occur in the head of the discharge, generating ions and free electrons. The channel shines from thermal emission and recombination, which defines optical constriction. The heat of the channel increases its electric conductivity and ionic and electronic current, which defines electric constriction. The axial electric current generates transversal magnetic fields, that pinch the electric current and its thermal effect, which defines magnetic constriction.

This work is an application of EMHD modelling for local plasma behaviour and FDTD modelling for global plasma behaviour in the numerical simulation of electric discharge in the atmosphere.

The application of EMHD coupling results a new load and mass distribution. The currents are computed in accordance with the scheme shown in the Figure 1(a). The new electromagnetic fields distribution is computed through FDTD on the Yee cell presented in the Figure 1(b).

The result gotten for 10,000 time steps is presented in Figure 2 for Gray levels of íon density.

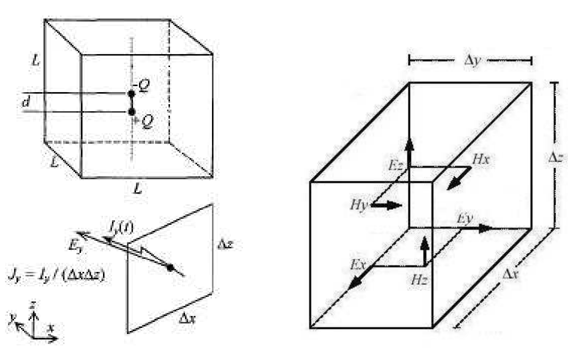

(a) (b)

Figure 1: (a) Computation of currents. (b) FDTD Yee cell.

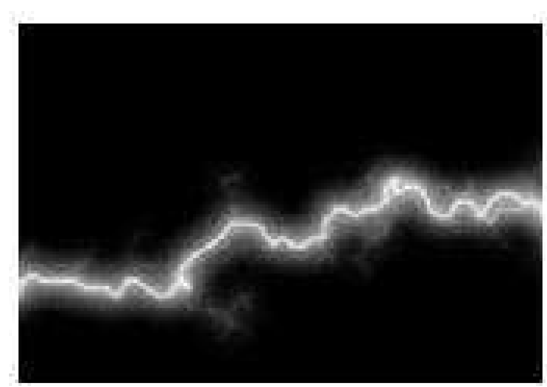

Figure 2: Ion density for 10,000 time steps.

Diffraction of the Electromagnetic Pulses on Apertures in the Screen

E. V. Golovacheva, **A. M. Lerer**, **V. A. Lerer**,
P. V. Makhno, **and O. S. Labunko**
Southern Federal University, Rostov-on-Don, Russia

Abstract— Diffraction of the H- and E-polarized electromagnetic pulses (EMP) on infinitely long slit in perfectly conducting screen located on a boundary between two dielectric layers.

This problem is of great importance because the diffraction on the slit is the classical problem in the theory of diffraction; and methods, applied to solve this problem, were also applied in the present work to solve the more complicated problem — diffraction of electro-magnetic pulse on the system of square apertures. Space-time integral equations (IEs) were obtained; methods of solving them, which consider the singularity at the edge and the logarithmic singularity of IE's kernel, were developed; the expression of the far field was obtained.

The space-time integro-differential equation with logarithmic singularity of distribution of the magnetic field on the system of N narrow square holes in the screen was obtained and solved.

The regularization of the equation was performed by isolation of analytically transformed static singular part. Transformed IEs we solved: by space coordinate using the collocation method, by time coordinate — using the method of step-by-step marching with spline-approximated time dependence.

Taking into account the singularity at the edge, isolation and analytical transformation of singular part of the kernel allowed to obtain quick internal convergence. The order of the system of linear algebraic equations (SLAE) N depends on the accuracy of solving and the length of the EMP. Let's introduce the parameter $\chi = \frac{cT}{l}$, which equals to distance $c2T$, passed by the EMP in time of it's length $2T$, divided by the width of the slit $2l$. If $\chi \gg 1$, then such EMP is long, if $\chi \approx 1$ — then short, $\chi \ll 1$ — ultrashort. To have inaccuracy of internal convergence less than 1% it's enough to set $N = 5 - 10$ at $\chi \geq 1$ and $N = 10 - 30$ at $\chi \ll 1$. For E-polarized EMP the order of the SLAE is of 30%–50% higher. Time to calculate a curve is less than a second on any modern computer.

Some results of calculation of pulse characteristics of the far field for the problems of non-stationary diffraction for isolated slits, and for the system of apertures are shown. The dependence of amount of interference of elements in the system on their relative position and orientation of exciting field, the influence of dielectric substrate on pulse characteristics were investigated.

Mathematical Model of the Phased Open Ended Waveguides Array Antenna with Multilayered Grids from Cylindrical Conductors before the Aperture

Andrey A. Prilutskiy
Scientific Research Institute of Long Distance Radio Communication, Russia

Abstract— The decision of an electrodynamics problem of radiation of waves from infinite periodic array antenna, generated of the open ends of flat wave guides in case of TE-waves with multilayer grids from cylindrical conductors before the aperture is offered. The problem is reduced to system of the integral equations which dares concerning unknown fields in the aperture of wave guides and currents on conductors. In a wideband of frequencies, the numerical analysis of influence of multilayer grids parameters on electrodynamics characteristics of phased array antenna carried out at scanning.

It is known, that owing to a mutual coupling between elements of array antenna from the open ends of waveguides at a beam there is a mismatch of entrance resistance of the aperture to a power supply circuit that at the scan angles of a deviation can lead to considerable falling of strengthening of array antenna. To weaken this effect, it is possible introduction of elements which provide indemnification of change of entrance resistance of the aperture at scanning. The simple jack is sub array from the passive cylindrical wires, established before aperture. In the given work, the electrodynamics analysis of radiation of the TM-waves from an infinite periodic array of flat wave guides is resulted, before aperture which the multilayered grid of cylindrical wires in parallel the E-plane of waveguides is established. The step sub array from wires coincides with period waveguides array antenna. Multilayered grids of wires can structurally settle down in dielectric layers, forming the artificial medium.

Session 4P6b
Advanced High Frequency Electromagnetic Simulation Tools 2

Phase Behaviour of a Two-Layered Circular Ferrite-Dielectric Waveguide with Azimuthal Magnetization

Georgi Nikolov Georgiev[1] **and Mariana Nikolova Georgieva-Grosse**[2]

[1]Faculty of Mathematics and Informatics, University of Veliko Tirnovo
"St. St. Cyril and Methodius", BG-5000 Veliko Tirnovo, Bulgaria
[2]Meterstrasse 4, D-70839 Gerlingen, Germany

Abstract— The circular waveguides, containing ferrite, magnetized in azimuthal direction, are appropriate for the design of nonreciprocal phase shifters, working in the normal TE_{01} mode [1–5]. Of special interest are the multilayered ferrite-dielectric geometries which could provide an increased value of the differential phase shift produced [1, 5]. Their phase performance, however, still is not known in sufficient extent.

The emphasis in this paper is placed on the computation and analysis of the phase curves of a two-layered waveguide, loaded with a coaxially positioned dielectric rod, surrounded by an azimuthally magnetized ferrite toroid in contact with the structure wall that sustains normal TE_{0n} modes. The boundary-value problem approach is employed. The real Bessel and the complex Kummer and Tricomi confluent hypergeometric functions [6] are accepted as wave functions for propagation in the dielectric and in the ferrite medium, resp. A procedure is developed, using the numerically found purely imaginary roots of characteristic equation of the configuration which yields the curves mentioned for both signs of ferrite magnetization in normalized form. To simplify the study, the ferrite and dielectric relative permittivities are considered equal. A set of phase portraits of the geometry for normal TE_{01} mode is compiled as a function of the dielectric rod to guide radius ratio ρ. The phase behaviour of the structure explored is much more complex than that of the circular and coaxial ferrite waveguides [2–4]. In particular, for both signs of off-diagonal ferrite tensor element α envelope curves exist at which the phase characteristics end. Thus, unlike the simpler ferrite geometries [2–4], the propagation may take place in restricted frequency bands both for $\alpha < 0$ and $\alpha > 0$. This is due to the appearance of the $L_\pm$ numbers, linked with the roots of characteristic equation [5]. In case of small ρ, e.g., $\rho = 0.1$, the characteristics for negative lie above those for positive magnetization. For the relevant normalized phase constants $\bar{\beta}_-$ and $\bar{\beta}_+$, corresponding to specific normalized guide radius $\bar{r}_0$ and $|\alpha|$ ($|\alpha| < 1$), it holds $\bar{\beta}_- > \bar{\beta}_+$ and the structure provides positive differential phase shift $\Delta\bar{\beta} = \bar{\beta}_- - \bar{\beta}_+$. There are values of $\bar{r}_0$ and $|\alpha|$, however, for which no $\Delta\bar{\beta}$ is obtained or it changes sign. To the left of cutoff there is a backward-wave region where $\bar{\beta}_-$ is a double-valued function of $\bar{r}_0$. If ρ grows, e.g., $\rho = 0.4$, the phase performance alters. Now the curves for positive are situated above the ones for negative magnetization (i.e., $\bar{\beta}_- < \bar{\beta}_+$ and $\Delta\bar{\beta} < 0$). This holds for $|\alpha| < 0.885895$. If $|\alpha|$ gets larger, e.g., $|\alpha| = 0.9$, the curves for $\alpha > 0$ lie entirely to the left of cutoff, i.e., a vast backward-wave region is observed. Here $\bar{\beta}_+$ could be one or double-valued function of $\bar{r}_0$. Moreover, for all ρ values of $|\alpha|$ may be found, for which a magnetically controlled cutoff exists.

REFERENCES

1. Clarricoats, P. J. B. and A. D. Olver, "Propagation in anisotropic radially stratified circular waveguides," *Electron. Lett.*, Vol. 2, 37–38, January 1966.
2. Georgiev, G. N. and M. N. Georgieva-Grosse, "A new property of the complex Kummer function and its application to waveguide propagation," *IEEE Antennas Wireless Propagat. Lett.*, Vol. 2, 306–309, December 2003.
3. Georgiev, G. N. and M. N. Georgieva-Grosse, "An approximate method for analysis of azimuthally magnetized circular ferrite waveguide phase shifter," in *Proc. 1st Europ. Conf. Antennas Propagat. EuCAP 2006*, in CDROM, Nice, France, November 6–10, 2006.
4. Georgiev, G. N. and M. N. Georgieva-Grosse, "A theorem for the properties of some classes of numbers, connected with the zeros of complex Kummer function and its application in the theory of circular ferrite waveguides with azimuthal magnetization," in *Proc. XXIX URSI General Assembly*, in CDROM, Chicago, IL, USA, August 7–16, 2008, D05.4(182).
5. Georgiev, G. N. and M. N. Georgieva-Grosse, "Propagation in an azimuthally magnetized circular ferrite-dielectric waveguide," in *Proc. 3rd Europ. Conf. Antennas Propagat. EuCAP 2009*, 345–349, in CDROM, Berlin, Germany, March 23–27, 2009.
6. Tricomi, F. G., *Funzioni Ipergeometriche Confluenti*, Edizioni Cremonese, Rome, Italy, 1954.

Theorem for the L (c, ρ, n) Numbers

Georgi Nikolov Georgiev[1] **and Mariana Nikolova Georgieva-Grosse**[2]

[1]Faculty of Mathematics and Informatics, University of Veliko Tirnovo
"St. St. Cyril and Methodius", BG-5000 Veliko Tirnovo, Bulgaria
[2]Meterstrasse 4, D-70839 Gerlingen, Germany

Abstract— The L numbers appeared in the theory of azimuthally magnetized circular ferrite waveguides, propagating normal (slow) TE_{0n} modes, built in terms of complex (real) confluent hypergeometric functions (CHFs) [1–4]. They have been defined as the common limits of certain infinite sequences of positive real numbers, connected with the positive purely imaginary (real) zeros of definite special (generating) functions which involve one or several complex (real) CHFs [5] of expressly picked out parameters and possibly also a few cylindrical functions [1–4]. The structures considered have been analyzed to design nonreciprocal digital phase shifters for electronically scanned antenna arrays, employing the normal TE_{01} mode [1–4].

In this work the theorem for existence and for the basic properties of one representative of the class mentioned — the $L(c, \rho, n)$ numbers, is formulated and proved numerically. Its statement is accepted as a general definition of the latter. The theorem is composed of three lemmas. Lemma 1 demonstrates the existence of numbers and specifies them for $c \neq l$, $l = 0, -1, -2, \ldots, n = 1, 2, 3, \ldots$ and $0 < \rho < 1$. For the purpose, the new function $F(a, c; x, \rho) = \Phi(a, c; x)\Psi(a, c; \rho x) - \Phi(a, c; \rho x)\Psi(a, c; x)$ is advanced in which $\Phi(a, c; x)$ and $\Psi(a, c; x)$ are the Kummer and Tricomi CHFs, resp. [5] with c — any real number, except $c = l$, $a = c/2 - jk$, k — real, $-\infty < k < +\infty$, $x = jz$, z and ρ — real, positive, $0 < \rho < 1$. The positive purely imaginary zeros $\chi^{(c)}_{k,n}(\rho)$ of $F(a, c; x, \rho)$ in x (in z) for $c = 3$ coincide with the roots of characteristic equation of the coaxial ferrite waveguide that sustains normal TE_{0n} modes [3]. It is proved numerically that if $k \to -\infty$, the numbers $K(c, \rho, n, k) = |k|\chi^{(c)}_{k,n}(\rho)$ and $M(c, \rho, n, k) = |a|\chi^{(c)}_{k,n}(\rho)$ tend to the same finite positive real limit, called $L(c, \rho, n)$ number. Lemma 2 defines the quantities for $c = l$ (when the Kummer function has no sense) through the relation $L(c, \rho, n) = L(2 - l, \rho, n)$. Lemma 3 states that for any allowable c, ρ, and n it is true: $L(c, \rho, n) = L(2 - l, \rho, n)$ and $L(1 + h, \rho, n) = L(1 - h, \rho, n)$, $(h = \pm(1 - c))$.

The L numbers for a certain choice of their parameters determine special envelope curves in the phase diagrams of the aforesaid geometries at which the characteristics for negative or both for negative and positive magnetization end [1, 3, 4]. The notion characteristic parameter of the coaxial structure referred to $\lambda = \Delta\bar{\beta}\bar{r}_0/|\alpha|$ where $\lambda = \lambda(c, n, \rho, |\alpha|, \bar{r}_0)$ is introduced ($\Delta\bar{\beta}$ and $\bar{r}_0$ — normalized differential phase shift and guide radius, resp., α — off-diagonal ferrite permeability tensor element, ρ — inner to outer conductor radius ratio, $c = 3$ and $n = 1$ for normal TE_{01} mode). Neglecting its slight dependence on $|\alpha|$ and $\bar{r}_0$, established numerically, a simple approximate methods is developed, using the envelopes, resp. the $L(c, \rho, n)$ numbers that yields the values of λ, resp. the ones of the differential phase shift $\Delta\bar{\beta} = \lambda|\alpha|/\bar{r}_0$ produced by the configuration pointed out in normalized form. The error of the approach is insignificant.

REFERENCES

1. Georgiev, G. N. and M. N. Georgieva-Grosse, "A new property of the complex Kummer function and its application to waveguide propagation," *IEEE Antennas Wireless Propagat. Lett.*, Vol. 2, 306–309, December 2003.
2. Georgiev, G. N. and M. N. Georgieva-Grosse, "The $L(c, n)$ numbers and their application in the theory of waveguides," in *Proc. Int. Conf. Days Diffr. DD'08*, St. Petersburg, Russia, June 3–6, 2008, 44–56.
3. Georgiev, G. N. and M. N. Georgieva-Grosse, "A property of the $L(c, \rho, n)$ numbers and its application to waveguide propagation," in *Proc. XXIX URSI General Assembly*, in CDROM, Chicago, IL, USA, August 7–16, 2008, BK.6 (120).
4. Georgiev, G. N. and M. N. Georgieva-Grosse, "Propagation in an azimuthally magnetized circular ferrite-dielectric waveguide," in *Proc. 3rd Europ. Conf. Antennas Propagat. EuCAP 2009*, in CDROM, Berlin, Germany, March 23–27, 2009, 345–349.
5. Tricomi, F. G., *Funzioni Ipergeometriche Confluenti*, Edizioni Cremonese, Rome, Italy, 1954.

Comparative Analysis of Approaches for High Frequency Electromagnetic Simulation

D. S. Butyugin, **V. P. Il'in**, **and A. V. Petukhov**
Institute of Computational Mathematics and Mathematical Geophysics, SBRAS
Novosibirsk, Russia

Abstract— The efficiency of various numerical approaches are compared for solution of 3D electromagnetic problems in frequency domain. The differential and variational statements in terms of electric field as well as in terms of vector and scalar potentials, with different types of boundary conditions (electrical and magnetic walls, absorption conditions, wave ports) are approximated at the non-structured grids by finite volume method (FVM) or finite element methods (FEM) respectively. FVM is applied for barycentric Voronoi cells, with computing the local balance matrices and assembling the global matrix of the system of linear algebraic equations (SLAE). In FVM, the first and second types of vector basis function are implemented at the tetrahedral elements.

The solution of obtained non-symmetric SLAES is made by different preconditioned iterative processes in Krylov subspaces. The Eisenstat modification of incomplete factorization and various preconditioning matrices are combined with semi-conjugate residual, BiCGStab and other Krylov algorithms.

The results of computational experiments for the representative set of the model problems are presented and demonstrate the performance of the proposed algorithms. Numerical investigations include parallelization and using the computational tools of Mathematical Kernel Library of Intel.

Session 4P7
Ultra Wide Band and Chaotic Communications

Experimental Characterisation of Radiowave Signal Propagation for Indoor UWB Wireless Communications

T. H. Loh and L. R. Arnaut
National Physical Laboratory, United Kingdom

Abstract— The methodology for experimental characterisation of signal propagation in an indoor electromagnetic environment for wireless communication networks is of interest in this research work. In recent years, there has been extensive research activities in the application of multiple-input-multiple-output (MIMO) channels for wireless systems due to their rich scattering nature that provides improved spectral efficiencies and increased network capacity. However, the presence of uncontrollable multiple scattering, fading and diffraction can potentially decrease indoor channel capacity. Hence a full characterisation of indoor propagation is needed to take into account all electromagnetic aspects on a firm physical basis, using precision measurement methods, and be rooted in accurate yet sufficiently simple models to be of practical use. To achieve the capacity increase envisaged for future mobile radio systems, it is necessary to exploit the entire spatial-temporal characteristics of the propagation channel. Accurate characterisation of the indoor environment model for the propagation channel relies on extensive measurement data collection.

We report on time-harmonic S-parameters measurement of radio wave propagation and scattering inside a typical indoor office environment between 500 MHz and 3 GHz. Single-input-single-output (SISO) and multiple-input-single-output (MISO) channels measurements were methodically carried out to simplify the propagation channels considered. The measurements were performed across a scanned sampled volume. To study the multipath effects, the fields that are reflected, scattered, or diffracted by the walls and artefacts are extracted experimentally, by subtracting corresponding measured values for the same antenna configuration replicated inside a fully-anechoic chamber. It was observed that there is a significant spatial dependence on the quality of a channel link. The multipath effects for SISO and MISO channel propagation are compared.

Performance of Wireless Communication System with Ultrawideband Chaotic Signals in the Multipath Channel

L. V. Kuzmin[1], **S. O. Starkov**[2], **and A. V. Kletzov**[3]

[1]Institute of Radio Engineering and Electronics of the RAS, Russia
[2]Obninsk State Technical University for Nuclear Power Engineering, Russia
[3]Moscow Institute of Physics and Technology (State University), Russia

Abstract— Performance of wireless ultrawideband (UWB) direct chaotic communication system (DCCS) in multipath fading channel is considered. The result of multipath propagation of UWB signals as well as signals of other type imposed restrictions on possible bitrates and determines the realistic link margin of UWB channel.

Statistical multipath channel models proposed by IEEE 802.15 working group is considered as a "fast" channel model (IEEE 802.15.3a channel model, bitrates up to 500 Mb/s, distances up to 10 m) and as a "slow" one (IEEE 802.15.4a channel model, bitrates up to 10 Mb/s, distances up to 30 m). These channel models specify path loss exponents for indoor environments of different types and provide statistical methods for simulation of multipath propagation of UWB signals occupying bandwidth no less than 500 MHz in the frequency band 3.1–10.6 GHz and having permitted power spectral density no more than $\sim 0.1\,\mu$W/MHz (-41.3 dBm/MHz).

First properties of chaotic radio pulse undergoing multipath propagation are considered and algorithms of reception of such pulses is proposed and analyzed. Analysis was carried out from the point of view of bitrates and link margin can be achieved with the use of proposed reception algorithms.

Fraction of channel realizations of ensemble of UWB wireless channels of a given class of indoor channel models is evaluated from the point of view of achievable bitrates for a prescribed value of Bit-Error-Ratio in the DCCS, when the bitrate is limited by the multipath interference. Evaluation was obtained in approximation of dominant multipath interference and it give reference for analysis of the influence of other types of additive interference (thermal noise, external disturbances) under restrictions on allowable power spectral density of emitted UWB signal. It also allow to predict throughput bitrates of the wireless UWB network based on DCCS.

The propagation experiment allowing to calculate the path loss exponent for UWB chaotic pulses by means of direct measurements of the chaotic pulses envelope at the output of the receiver is described.

Performance obtained for DCCS is compared with performance for UWB communication systems of other types.

Multipath Amplification in UWB Chaotic Communications

Yuri V. Andreyev, Alexander S. Dmitriev, and Andrey V. Kletsov
Kotelnikov Institute of Radio Engineering and Electronics of RAS
Mokhovaya 11-7, Moscow 125009, Russia

Abstract— Recently, direct chaotic communication systems with chaotic carrier were adopted by international community in 802.15.4a standard [1–3]. Chaotic signals have a number of features that make them perspective for communications, including naturally wide and ultrawide spectrum, simple transceiver layout, immunity to multipath propagation, etc.

Chaotic signals prove to be especially effective in multipath environment. Autocorrelation time of chaotic signals is inversely proportional to bandwidth, so for UWB signals with bandwidths 1–2 GHz, autocorrelation time is as small as 0.5–1 nsec. Consequently, in multipath environment chaotic radio pulses from different paths appear uncorrelated at the receiver input. Therefore, they exhibit no fading, and the more paths come to the receiver, the more energy is gathered and the stronger is the received signal. We call this effect "multipath amplification" of chaotic radio pulses.

In this report, the nature of this effect is investigated, and multipath gain is estimated for various sets of communication parameters. Multipath gain is evaluated as the ratio of the signal energy received in multipath channel with respect to the case of single-path channel. UWB multipath channel models of IEEE 802.15.4a channel modeling subgroup are used in simulations [4]. These UWB models cover the whole variety of short-range environments (office, residence, industrial, outdoor).

As is shown, with these channel models the effect begins in systems with pulses longer than approx. 20 nsec. Estimates of multipath gain as functions of data rate are presented. Multipath gain varies from 4 (outdoor, office NLOS) to 13–14 dB (residence, industrial NLOS). Also the effect of the signal bandwidth on multipath gain is investigated.

As is shown in the report, multipath amplification effect can substantially enhance the performance of chaotic communications.

REFERENCES

1. Dmitriev, A. S., A. I. Panas, and S. O. Starkov, "Direct chaotic communication in microwave band," *Electronic NonLinear Science Preprint*, nlin.CD/0110047, 2001.
2. Dmitriev, A. S., B. Ye. Kyarginsky, A. I. Panas, and S. O. Starkov, "Experiments on ultra wideband direct chaotic information transmission in microwave band," *Int. J. Bifurcation & Chaos*, Vol. 13, No. 6, 1495–1507, 2003.
3. IEEE 802.15 WPAN Low Rate Alternative PHY Task Group 4a (TG4a), IEEE Std 802.15.4a3-2007 (Amendment to IEEE Std 802.15.43-2006), August 31, 2007.
4. Molisch, A. F., "IEEE 802.15.4a channel modeling sub-committee report final," IEEE P802.15 Working Group for Wireless Personal Area Networks (WPANs), December 2004.

Experimental Generation of Chaotic Oscillations in Microwave Band by Phase-locked Loop

A. S. Dmitriev, **A. V. Kletsov**, **and L. V. Kuzmin**
Institute of Radio Engineering and Electronics of the RAS, Russia

Abstract— At present ultrawideband (UWB) signals attract significant attention as a carrier for wireless communication systems. One of promised UWB signal type is chaotic signal produced by dynamical systems. For example such signals are exploited as a carrier in a direct chaotic communication scheme (DCCS) proposed in IRE RAS, where chaotic radio pulse stream is used for wireless data transmission. DCCS is adopted for international standard (IEEE 802.15.4a) as an optional solution for physical level of UWB wireless local area networks. As a chaotic source in DCCS a transistor-based chaotic oscillators with low degrees of freedom is used. This generation technique allows to build small-size UWB transceivers and can be implemented in integrated circuits.

Transistor-based chaotic sources generate oscillations ("amplitude" chaos) with irregular envelope. However for some applications it is preferably to use chaotic pulses generated by a source of "phase" chaos, i.e., chaotic oscillations with constant envelope and chaotically changing phase.

In order to generate phase chaos at least two approaches can be considered and implemented. First one is the use of phase (frequency) modulator controlled by the source of amplitude chaos. Such modulator is usually implemented on the base of voltage-controlled oscillator (VCO). According to the second approach phase chaos is generated by a phase-locked loop (PLL) operating in chaotic mode.

This work is devoted to the theoretical and experimental investigations of wideband phase-chaotic signal generation in microwave band by PLL.

It was carried out mathematical simulation of third order PLL with taking into account realistic properties of phase comparator, frequency dividers in the feedback loop of PLL and VCO. It allows to determine parameters of elements consisting of PLL test-bed operating in chaotic mode. Traditionally dynamical modes of PLL are analyzed by means of VCO oscillation phase. Meanwhile from the point of view of wireless data transmission it is interesting to consider properties of oscillations at the VCO output. So our efforts were focused on the analysis of oscillations at the VCO output.

Finally the PLL test-bed generating UWB phase chaotic oscillations with a flat power spectrum density in the frequency band 700–1300 MHz was designed and experimentally tested.

Ultrawideband Direct Chaotic Transceiver for Multimedia Applications

Lev Kuzmin[1], **Andrey Kletsov**[2], **and Vadim Lazarev**[2]

[1]Institute of Radio Engineering and Electronics of the RAS
Mokhovaya St., 11/7, Moscow 125009, Russia
[2]Moscow Institute of Physics and Technology (State University)
Mokhovaya St., 11/7, Moscow 125009, Russia

Abstract— For today special attention of developers and manufacturers of communication systems is concentrated on development of ultrawideband (UWB) communication systems. One of perspective directions of UWB communication development is radio communication based on UWB chaotic radio impulses. At present some kinds of low-rate devices are being designed, ex for, in sensor networks. An interesting area is transmition of video information, high-quality sound, etc. However, the given applications can serve demand high speed of data transmission.

In the report design of UWB direct chaotic transceiver with a transfer rate up to 25 Mbps is considered which is necessary for implementation of multimedia applications. The transceiver structure is described. Its difference from before developed devices with lower rates consists in the following: increase in speed of modulation, reduction of duration of received chaotic radio impulses, support of shorter impulse processing by the digital block.

The transceiver must contain a digital part, a transmitter, a receiver and an antenna. Low-rate UWB direct chaotic transceiver PPS-40 was taken for this design, because its modulator provides 20 to 100-nsec pulses and its 50-MHz receiver filter allows reception of necessary signals. One of the main problems is recognition of received bits with a low-frequency quartz generator. In PPS-40 for decision it was necessary to take 4 samples on pulse (bit). With 10 times greater data rate the number of samples is reduced by 10 and that is not enough for correct recognition of bits. This problem was solved at the expense of creating delays in CPLD (complex programmable logic device) for the pulses arriving from quartz generator. Part of functions, which in PPS-40 was run by microcontroller, was transferred to CPLD. The algorithm developed for CPLD is intended for reception of data, verification of the address, version, control sum, synchronisation of inner clock with received data, forming a package of the data sent to modulator.

Thus, in this report, ultrawideband direct chaotic transceiver for multimedia applications with rates up to 25 Mbps was proposed, developed, realized and experimentally tested.

Multi-band Chaotic Oscillator with Phase-locked Loop

K. G. Mishagin[1,3], **V. V. Matrosov**[1], **L. V. Kuzmin**[2], **and A. V. Kletsov**[2]

[1]University of Nizhny Novgorod, Russia
[2]Institute of Radioengineering and Electronics of RAS, Russia
[3]JSC "Vremya-Ch", Nizhny Novgorod, Russia

Abstract— At the present research activity in the field of communications using chaotic signals switches from theoretical studies to the area of real engineering developments, which have perspectives of commercial application. The majority of developed chaotic oscillator schemes produce chaotic signals with amplitude, varying irregularly in time. However, for simple receiving systems it is preferable to use wideband signals with fixed amplitude and chaotic phase. In a number of theoretical and experimental works the possibility of applying phase locked loops to produce oscillations with chaotic phase was shown. The results presented in these works tell us that voltage controlled oscillator with phase locked loop can produce wideband and ultra-wideband oscillations with homogeneous spectrum in different frequency ranges, including UHF range. The use of phase locked loops gives the opportunity to develop wideband oscillator with manipulated spectrum (electronic switching between non-overlapping frequency bands, electronic control of spectrum width). This report contains results on numerical study of mathematical model of phase locked loop and results of modeling with the use of specialized electronic design software. Considered models take into account peculiarities of modern components of phase locked loops (pulse phase discriminators, frequency dividers). We present results of detailed analysis of chaotic behavior of the system, including maps of dynamic regimes, areas of parameters with chaos, analysis of spectral properties of different chaotic modes. Possibility of control of spectrum width and possibility of electronic shifting of spectrum of chaotic phase-modulated signals in wide frequency range is shown. Shift of the frequency range is obtained by changing coefficients of frequency dividers in phase locked loop. Additional control of the loop gain allows keeping the same dynamic properties of chaotic frequency modulation during spectrum shifting. Accurate modeling of voltage controlled oscillator has been carried out to estimate maximal rate of frequency modulation in phase locked loop. As an example we have modeled generator of phase chaos with spectrum width about 500 MHz and ability of spectrum steering in the range 3–5 GHz.

UWB Microwave Chaotic SiGe Generator

E. V. Efremova
Kotel'nikov Institute of Radio Engineering and Electronics of RAS, Russia

Abstract— Chaotic signals are perspective information carriers for ultra-wideband wireless communication systems. This is quite a new area, its possible applications are WLANs and wireless sensor networks.

Key element of communication system based on chaotic signals is chaotic generator.

However, potential use of chaotic transceivers in consumer electronics and sensor networks applies some restrictions on the characteristics of generator. Chaotic generators for such applications must provide generation of ultra-wideband chaotic signal in prescribed frequency band with rather smooth power spectrum envelope and prescribed power spectral density. At the same moment they must be compact and have low power consumption, repeatable characteristics by mass production and be implementable as a microchip.

Possibility to create microwave chaotic oscillators on microchip can open wide prospects for application of these oscillators and devices based on them in home and industrial electronic systems.

This work is devoted to development and investigation of SiGe ultra-wideband microwave chaotic generator. Electric scheme of single-transistor generator is proposed. Integrated circuit model is simulated both with ideal active and passive circuit elements and with models of the elements from 0.25 μm SiGe technology library. Simulation is made in Cadence IC software. The obtained model is used as a prototype for integrated circuit topology. Based on the of proposed topology, experimental samples of microchip microwave chaotic generator are produced.

Results of experimental investigation of generator microchip are presented in the report. Ultra-wideband microwave chaotic oscillations in 3–8 GHz range are verified in the experiment.

An Ultra Wideband Spatio-temporal Channel Sounder Using an OFDM Signal

H. Iizuka, M. Takahashi, N. Iwakiri, and T. Kobayashi
Tokyo Denki University, Japan

Abstract— Ultra wideband (UWB) spatio-temporal propagation measurements have been carried out mostly using virtual array antennas and a vector network analyzer (VNA). The VNAs transmit only sinusoidal signals at discrete frequencies, and thus a number of snapshots is limited to unity. To remedy this drawback, we propose a UWB channel sounder using an orthogonal frequency division multiplexing (OFDM) signal, which exhibits a nearly flat frequency spectrum occupying a wide bandwidth. A prototype has been developed, comprising a transmitter, a receiver, transmitting and receiving virtual array antennas, and a controlling and data processing computer, as shown in Fig. 1. In the transmitter, the baseband OFDM signal is generated with a 2.5-Gsample/s arbitrary waveform generator (AWG); next, a 3.5-GHz carrier frequency is modulated with the OFDM signal by using an orthogonal modulator; then the resulting radiofrequency UWB signal is amplified to feed the transmitting antenna (an omnidirectional UWB monopole antennas mounted on a three-axis positioning scanner). In the receiver, the received signal is amplified with a low noise amplifier, demodulated with an orthogonal demodulator, and analog-to-digital converted with a 2.5-Gsample/s digital storage oscilloscope. The digitized data are processed to compute a cross correlation between the transmitting baseband OFDM and the receiving signals. Angles of arrival are computed by estimating phase differences between the signals received at the array elements.

Performance of the prototype was evaluated, by comparing with a VNA-based channel sounder and a pseudo-noise-based one. An artificial multipath generator (a microwave hybrid and a coaxial cable with the end shortened, shown in Fig. 2(a)) was directly connected to the channel sounders. Measured delay profiles are shown in Fig. 2(b), which yields well-agreed results to validate the proposed design. Spatio-temporal channel sounding was also carried out in a radio anechoic chamber (1-, 2-, and 3-path environments with and without using planar reflectors). Consistent results were also obtained with ray tracing calculation. Further detailed results will be described in the final paper.

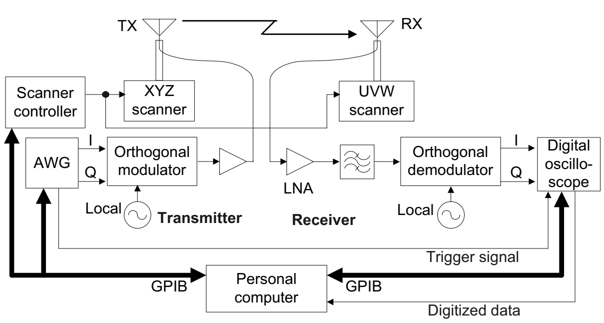

Figure 1: Block diagram of the proposed OFDM-based UWB channel sounder.

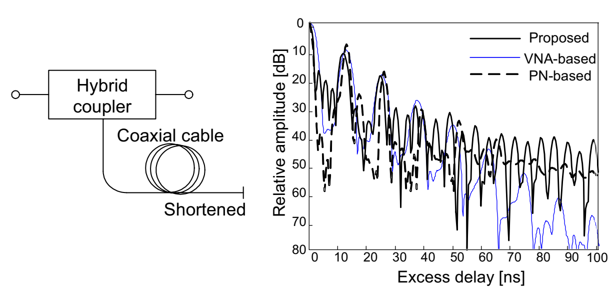

Figure 2: Comparison of delay profiles measured with the prototype and the other sounders: (a) artificial multipath generator and (b) measured delay profiles.

The Peculiarities of Spatial Combined Effects of UWB Chaotic Signals

Lev Kuzmin[1] **and Sergei Starkov**[2]

[1]Institute of Radio Engineering and Electronics of RAS, Russia
[2]Obninsk State Technical University for Nuclear Power Engineering, Russia

Abstract— The problem of electromagnetic compatibility is of great importance for various ultra wideband networks, including sensor networks and wireless local and personal area networks (WLAN and WPAN). One of possible kind of information carrier for UWB system is chaotic radio pulses, formed with chaotic dynamical radio systems directly in microwave frequency region. Up to day there are known number of practical radio systems using such UWB carrier. The mutual effects of such unusual signals, their combined impact on various radio systems needs additional investigations.

The peculiarities of the spatial forming of ultra wideband chaotic signals are considered in this paper.

The analysis of statistical properties of the electromagnetic signal, produced by a spatial combination of chaotic pulse oscillators, is provided. The model of chaotic pulse interaction is proposed. We describe the technique for computer modeling and discuss a set of parameters, taking into account in our simulations. The results of modeling are presented for different multipath propagation (IEEE 802.15.4a channel models), wide rang of bitrates, set of distances (1–100 m) and number of chaotic oscillations ($N = 2 \div 100$). One more parameter was the bandwidth of UWB signals. The analysis showed that in spite of the complex envelope distribution function of total chaotic signal the degradation of probability estimates was negligible in the wide changes in model parameters. In particular, we can substitute the large number of chaotic sources by 2–5 in order to get practically the same impact effects.

3–5 GHz Ultra-wideband Omnidirectional Printed Circuit Antenna

Ant. V. Uvarov[1], **N. P. Chybinskiy**[1], **and Andr. V. Uvarov**[1,2]

[1]Moscow Institute of Physics and Technology (State University), Moscow, Russia
[2]Kotel'nikov Institute of Radio Engineering and Electronics of Russian Academy of Sciences, Russia

Abstract— Evolution of miniature ultra-wideband transceivers for wireless communication networks has led to the integration of antennas on the same substrate with a transceiver microwave module. The standard approach means separate developing of both microwave printed circuit board (PCB) topology and antenna topology, e.g., die mounting on the PCB surface. Integration of printed circuit antenna on the same substrate with the microwave electronics module lets achieve new levels of compactness, get rid of unnecessary processes (surface assembling nonstandard size antenna installation) and investigate further interaction between antenna and electronics. The article describes developed ultra-wideband omnidirectional printed circuit antenna with small dimensions and simple (well-reproduced in standard manufacturing processes of two-layer printed circuit board technology) topology. The initial analysis has examined the various electrodynamics configurations of antennas, such as either dipole antenna or monopole polygon antenna with different forms of the radiating surface. Finally, we chose the monopole antenna with a radiating surface in the form of a ring segment. Substrate properties analysis and their influence on antenna characteristics have been made. Based on analysis, several types of antennas at 3–5 GHz frequency range were developed and optimized.

Designed monopole microstrip antenna with the shape of the radiating area in the shape of an annular sector provides VSWR better than 2 : 1 in 3–5 GHz frequency range. After antenna configuration had been optimized, achieved geometric size of the antenna to wavelength ratio became less than 0.12, that is 2 times less than for the quarter wavelength bow-tie dipole antenna. FR-4 and Rogers RT-5870 materials were used as a substrate, with an approximately two times different permittivity and four times — thickness. Antenna tuning for each of the substrates properties was achieved by choosing appropriate length and width of matching strip, with constant form a radiating surface that makes the antenna a universal for different technology processes. Due to a sharp steepness of the VSWR frequency dependence the lower limit of the range of the antenna can act as a high-pass filter that can suppress the industrial noise and the signals at frequencies below 2.5 GHz.

Session 4P8
Asymptotic High Frequency Methods

Asymptotic Currents on a Strongly Elongated Body Illuminated by a Plane Wave in the Paraxial Direction

Ivan Andronov[1], **Daniel Bouche**[2], **Frédéric Molinet**[3], **and Hervé Stève**[4]

[1]Institute on Physics, St. Petersburg University, Ulianovskaja 1, St. Petersburg 198904, Russia
[2]CEA/DIF/DPTA, BP 12, Bruyères le Chatel 91680, France
[3]MOTHESIM, 9, Villa Pierre Loti, L'Hay-les-Roses 94240, France
[4]Dassault Aviation, 78, Quai Marcel Dassault, Cedex 300, Saint Cloud Cedex 92552, France

Abstract— When the radius of curvature ρ_τ of the curves orthogonal to the geodesics is small compared to the radius of curvature ρ of the geodesics, $\frac{\rho_\tau}{\rho} \sim (k\rho)$.

with $k\rho \gg 1$, the body is considered to be strongly elongated. By extending the boundary layer method to this case, it has been shown by Andronov and Bouche [1] that under these conditions the asymptotics of the creeping waves are modified in the principal order and that the Fourier transform of their amplitude no longer satisfies an Airy equation, but a biconfluent Heun equation.

Whereas the theory of creeping waves on strongly elongated bodies is now well established, some difficulties remain in controlling the accuracy of the formulas obtained which, as shown by Andronov [2], predict an enhancement of the magnetic creeping wave. One of the difficulties is that no analytical solution of the Heun equation expressed in terms of tabulated functions is available. Another problem is the difficulty to derive a closed form expression of the incident field in the semi-geodesic co-ordinate system used in the boundary layer theory.

In this paper, we will present several approaches to overcome both difficulties and test their accuracy on an elongated prolate ellipsoid by comparing the asymptotic currents to the currents obtained by numerical methods (MoM or FE).

In the first approach, the Heun equation is solved numerically by the method of Runge-Kutta and a closed form expression for the incident field is obtained separately by solving the eikonal equation expressed in the semi-geodesic co-ordinate system.

The second approach is founded on the fact that the incident field verifies the Heun equation and on the behavior of the Wronskian of the incident and the diffracted field, at large distance from the surface.

The third approach uses a direct geometrical method for expressing the incident field on the semi-geodesic co-ordinates.

Numerical results will be presented showing the accuracy of each of these approaches.

REFERENCES

1. Andronov, I. and D. Bouche, "Asymptotics of creeping waves on a strongly prolate body," *Annales des Télécommunications*, Vol. 49, Nos. 3–4, 205–210, 1994.
2. Andronov, I., "Weakly attenuated waves on elongated bodies," *Days on Diffraction*, 96, St. Petersburg, June 1996.

High Frequency Asymptotics of Electromagnetic Field on a Strongly Elongated Spheroid

I. V. Andronov
University of St. Petersburg, Russia

Abstract— The process of high frequency diffraction on a strongly elongated body has its specifics being in the necessity to take into account the three dimensional character of the problem. The large transverse curvature ρ_t may cause significant decrease of creeping waves attenuation. Though many results for creeping waves on strongly elongated bodies are known (see e.g., [1]) there is still no satisfactory agreement between numerical results and asymptotic theory. In particular this may be caused by variation of transverse curvature along the geodesics which was not properly taken into account in the previous analysis.

In this paper, we consider the problem of plane electromagnetic wave diffraction by an elongated spheroid. In the process of high frequency asymptotics construction we introduce another large parameter that characterizes the elongation and assume that ($\rho/\rho_t = O((k\rho)^{2/3})$, here ρ and ρ_t are the radii of curvature along the geodesics and in perpendicular cross-section, k is the wave number. We introduce spheroidal coordinates, by the boundary layer method reduce Maxwell equations to a system of coupled parabolic equations which due to the above assumption allow variables separation. The solution is represented in the form of inverse Mellin transform involving Whittaker functions. Matching with the incident field allows the amplitudes to be found. These amplitudes have the denominator

$$\Delta(\mu) = W_{\mu\,0}(-iz)W_{\mu+1\,1}(-iz) + W_{\mu\,1}(-iz)W_{\mu+1\,0}(-iz) + 2\left(\mu + \frac{iz}{2}\right)W_{\mu\,0}(-iz)W_{\mu\,1}(-iz),$$

where $W_{\alpha\,\beta}(z)$ are Whittaker functions, μ is the variable of integration and $z = (k\rho)(\rho_t/\rho)^{3/2}$ characterizes the elongation (ρ and ρ_t are the values of the corresponding radii on the light-shadow boundary). Solutions of the dispersion equation $\Delta(\mu) = 0$ define the attenuation

$$\exp\left(-\frac{2\mathrm{Re}(\mu)}{\rho\rho_t}s\right)$$

of creeping waves along the arc-length s. Comparison of this formula with the usual creeping waves attenuation shows that when z is large, that is the body is not too elongated, the attenuation is the same as in the usual case. When z decreases the attenuation of one of the creeping waves decreases and reaches its minimum at $z \approx 2$. At lower values of z the effect of large torsion prevails the effect of large transverse curvature which causes the attenuation to increase again.

Other results of analytical and numerical analysis of the asymptotics are to be presented.

REFERENCES

1. Molinet, F., I. Andronov, and D. Bouche, *Asymptotic and Hybrid Methods in Electromagnetics*, IEE Electromagnetic Waves Series 51, The IEE, London, 2005.

Radiation of a Dipole on a Strongly Elongated Body of Revolution Truncated by a Plane Perpendicular to Its Axis

Frédéric Molinet
MOTHESIM, 9, Villa Pierre Loti, 94240 L'Hay-les-Roses, France

Abstract— In this article the radiation problem of an infinitesimal tangential magnetic dipole or normal electric dipole excitation on a perfectly conducting strongly elongated body of revolution truncated by a plane perpendicular to its axis is considered. The field radiated by the dipole at an observation point away from the body in the region directly illuminated by the source comprises two main contributions : the direct field and the edge diffracted creeping wave field. Since the magnetic creeping wave on a strongly elongated perfectly conducting body is enhanced, one expects a stronger diffraction process when this wave strikes a sharp edge. In a previous publication [1] new formulas for the diffraction problem involving a combination of surface and edge diffraction on a strongly elongated object have been presented for the case of plane wave illumination.

The technique used for establishing these formulas is an extension of Michaeli's procedure developed for the classical creeping wave asymptotics. The same procedure is here extended to the radiation of a source located on the surface on a strongly elongated object. In this case, instead of generalized Fock functions, the field incident on the edge involves generalized Nicholson's functions. In order to establish the hybrid diffraction coefficient for the edge diffracted creeping wave excited by the source, the Heun functions appearing in the generalized Nicholson's functions are expended in the boundary layer in Taylor series in the parameter $v = \frac{kn}{m}$ (k = wave number, n = height of a point M in the boundary layer, m = Fock parameter), which is supposed small. Then by using Heun's equation, the field in the boundary layer can be written in the form of a spectral representation of inhomogeneous incident and reflected plane waves. The rest of the procedure is similar to that developed by Michaeli for the classical asymptotics, but now the reflection coefficient R depends on the elongation parameter $\kappa = \frac{k\rho_\tau}{m}$ where ρ_τ is the radius of curvature of the wave front. It is shown that R is identical to the reflection coefficient of an impedance surface with equivalent impedance $Z =?\frac{i}{2m\kappa}$. As a consequence, the hybrid diffraction coefficient involves the diffraction coefficient of a plane wave by an impedance wedge.

It will be shown that the strongly elongated body behavior exists only in the neighborhood of the paraxial direction where the creeping wave path is perpendicular or quasi-perpendicular to the edge. Malyuzhinets diffraction coefficient can therefore be used. It tends smoothly to Keller's diffraction coefficient when the elongation parameter κ becomes large.

REFERENCES

1. Molinet, F., "Diffraction of a creeping wave on an elongated object by an edge," *Progress In Electromagnetic Research Symposium*, Beijing, March 23–27, 2009.

Electromagnetic Creeping Waves and Their Degeneration

I. V. Andronov[1] **and D. Bouche**[2]

[1]University of St. Petersburg, Russia
[2]CEA-DAM-DIF, F 91297 Arpajon, France

Abstract— In the general case a high frequency electromagnetic field on a smooth convex surface is composed of infinite series of creeping waves having two different polarizations (TE and TM in isotropic case). However, there are many cases of degeneration which invalidate the usual asymptotics. Some of these degenerations appear due to geometrical characteristics of the surface (caustics and focal points on the surface).

On the envelope, or caustic C of creeping rays, the term $h^{-1/2}$ in the regular asymptotic for creeping wave amplitude diverges. In the vicinity of C, we use coordinate (s, t, n), where s is the curvilinear abscissa along C, t the geodesic distance from C, n the distance from the surface. The caustic of creeping ray problem decouples into the usual creeping wave problem, which determines the normal dependency $w_1(\xi - \nu)$, $\nu = 2^{1/3}k^{2/3}\rho_n^{-1/3}n$ and a 2D caustic problem which determines the binormal dependency $v(-\mu), \mu = 2^{1/3}k^{2/3}\rho_g^{-1/3}t$.

For on axis illumination of an axisymmetric object, a focal point of creeping rays appears. We use polar geodesic coordinate system: l geodesic distance from focal point, φ polar angle, and stretched coordinate kl. Near the focus, we show that the binormal component H_b of H is given by $H_b \approx e^{-i\pi/4}\sqrt{2\pi}A(J_1'(kl) + \frac{\xi}{2^{1/3}(k\rho)^{2/3}}J_1''(kl))w_1(\xi - \nu)$.

Other types of degeneration may be caused by the impedance that characterizes the surface. The case when the attenuation parameters of two creeping waves of one polarization coincide is studied in [1]. A special resonant solution is derived in a boundary layer of length $k^{-2/9}$ where the field of two creeping waves can not be distinguished. This solution is matched to the usual creeping waves asymptotics which allows to describe the effect of creeping wave passing through the line of degeneration. The effects appear somewhat similar to the case of a caustic. However the amplification is of order $O(k^{1/18})$.

Another case when all the creeping waves of one type coincide with the corresponding creeping waves of the other type was partly studied in [2]. The zone of degeneration in this case is of the length of order $O(k^{-1/6})$. In that zone the effect of torsion appears more significant than in the usual nondegenerated case. The creeping waves do not differ by their polarization, such difference appears only in the next order correction.

In this paper, we give a comparative analysis of the effects of degeneration being in field amplification, coupling of modes, more pronounced influence of torsion and other parameters of the surface.

REFERENCES

1. Andronov, I. V. and D. P. Bouche, "Degeneration of electromagnetic creeping waves in a vicinity of critical values of anisotropic impedance," *IEEE Transactions on Antennas and Propagation*, Vol. 56, No. 7, 1984–1992, 2008.
2. Andronov, I. V. and D. P. Bouche, "Asymptotics of creeping waves in a degenerated case of matrix impedance," *Progress In Electromagnetics Research*, PIER 59, 215–230, 2006.

The Interaction of Creeping Waves on a Smooth Anisotropic Impedance Surface

D. Yu. Zaika[1], **M. V. Perel**[1,2], **and I. V. Andronov**[1]

[1]St. Petersburg University, Russia
[2]Ioffe Institute, Russia

Abstract— Creeping waves describe high frequency electromagnetic field on a shadowed side of a smooth convex surface. The important characteristics of a creeping wave is its attenuation parameter ξ defined form the dispersion equation

$$\dot{w}_1(\xi) = iZ_{1,2}w_1(\xi),$$

where w_1 is the Airy function in Fock notations and $Z_{1,2}$ are the equivalent stretched impedances of the surface for the creeping waves of two types (TM and TE for isotropic surface) (see e.g., [1–3]). Though the principal order approximation of the creeping waves field do not feel the coincidence of Z_1 and Z_2, the first order correction gets a diverging term at the line where $Z_1 = Z_2$ which invalidates the asymptotics.

In this paper, we consider the effects of creeping wave propagation through the zone near the line of such degeneration. We use the technique developed in [4–6]. We find that the length of the resonant zone is of order $O(k^{1/6})$, where k is the wave number, and construct resonant solution in the form of asymptotic series by $k^{1/6}$. By matching this solution to the asymptotics of the incident creeping wave we define the amplitude of the resonant solution. After the zone of degeneration the resonant solution is matched to two outgoing creeping waves. Thus the effect of mixed polarized creeping wave excitation is discovered and studied.

REFERENCES

1. Molinet, F., I. Andronov, and D. Bouche, *Asymptotic and Hybrid Methods in Electromagnetics*, The IEE, London, 2005.
2. Andronov, I. V. and D. Bouche, "Asymptotics of creeping waves ia a degenerated case of matrix impedance," *Progress In Electromagnetics Research*, PIER 59, 215–230, 2006.
3. Andronov, I. V. and D. Bouche, "On the degeneration of creeping waves in a vicinity of critical values of the impedance," *Wave Motion*, Vol. 45, 400–411, 2008.
4. Perel, M. V., J. D. Kaplunov, and G. A. Rogerson, "An asymptotic theory for internal reflection in weakly inhomogeneous elastic waveguides," *Wave Motion*, Vol. 41, 95–108, 2005.
5. Perel, M. V., I. V. Fialkovsky, and A. P. Kiselev, "Resonance interacrion of bending and shear modes in a nonuniform Timoshenko beam," *Journal of Mathematical Sciences*, Vol. 111, 3775–3790, 2002.
6. Perel, M. V., "Reexcitation of modes in an anisotropic earth ionosphere wave-guide along transequatorial paths, provided 2 close points of degeneracy," *Izvestiya Vysshikh Uchebnykh Zavedenii Radiofizika*, Vol. 33, No. 11, 1208–1216, 1990.

Gaussian Beams Summation to Simulate Hight Frequencies RCS

Thierry George[1] and Phillipe Pouliguen[2]

[1]Celum, 6 rue 8 mai 1945 78220 Viroflay, France
[2]CELAR, 35174 Bruz-cedex, France

Abstract— Geometrical Optics fails in the vicinities of caustics. For RCS computations, the caustics are generated by the zero curvature of the reflection surface. Plane facets produce degenerated caustics: in the reflection direction, all rays have the same phase. The simplest way to use Geometrical Optics in RCS simulations is to integrate Geometrical Optics results on a diffraction surface like in Physical Optics but this solution fails if caustic lays on the diffraction surface. For these reasons, Geometrical Optics is difficult to employ in RCS modeling.

At finite distance, Gaussian Beams Summation is used to overcome caustic problems and to provide continuous solution near the transition zones of Geometrical Theory.

For 2D problems, two approaches are discerned.

The first approach uses the saddle point method to match a formal decomposition in Gaussian Beams to Geometrical Optics solution at the receiver, in asymptotic geometrical regular domain.

The second approach decomposes the field in an aperture or in the vicinity of the source then the Gaussian beams are launched over the receivers. This is an initial value problem.

Of course, it is possible to use these two approaches in 3D spatial domain.

The spatial ray coordinates used at finite distance change into their conjugate coordinates, the slowness $\underline{p}$ at infinite distance.

Our RCS Gaussian Beams solution has the following properties, they are:

- Equivalent to Geometrical Optics in regular domain of reflection field, by normalization with high frequencies saddle point method.
- Continuous in the vicinity of non-degenerate caustics and transition zones of the Geometrical Diffraction Theory (shadow frontiers, ...).
- Equivalent to degenerate caustic field, by normalization with Physical Optics.

In homogeneous medium, we consider a Gaussian beam from the point $\underline{B}_0$ toward the slowness direction $\underline{p}_0$. The point $\underline{B}_0$ lies on the central ray and on the beam axis. Electric field is $\underline{E}_0 = E_0 \times \hat{e}$ where $\hat{e}$ is the normalized polarization.

If $|\underline{\delta_p}| << \underline{p}_0$, we write the radiation of a Gaussian beam in the slowness perturbed direction $\underline{p}_0 + \underline{\delta_p}$ as:

$$\underline{R}(\underline{p}_0 + \underline{\delta p}, \omega, \underline{O})_{GB} = \frac{4\pi \times E_0}{\sqrt{|\det(\underline{\underline{M}}_0)|}} \times \hat{e}(\underline{\delta p}) \times e^{-j\times\omega\times\left[\tau_0 - \frac{1}{2}\times\underline{\delta p}^t\times\underline{\underline{M}}_0^{-1}\times\underline{\delta p}\right]} \times e^{+j\times\omega\times\underline{p}_0\cdot\underline{OB}_0}$$

where the subscript 0 means quantities are measured at the point $\underline{B}_0$, $\underline{O}$ is the phase center, $\underline{\underline{M}}_0$ is the complex curvature matrix of the wave front and τ_0 is the travel time.

The polarization term $\hat{e}(\underline{\delta p})$ is a perturbation from the central beam polarization $\hat{e} = \hat{e}(\underline{\delta p} = \underline{0})$.

We consider monostactic RCS case in the $\underline{p}_0$ slowness direction.

Rays are launched on the target from a reference incident plane wave, outside the target. They are parametrized by two Cartesian coordinates $\underline{\gamma}$ in the reference plane wave.

The slowness ray direction of the last central ray interaction with the object is $\underline{p}(\underline{\gamma}) = \underline{p}_0 + \underline{\delta p}(\underline{\gamma})$ at the $s_{\underline{\gamma}}$ curvilinear abscissa. The point $\underline{B}$ is the last point interaction $\underline{B} = \underline{B}(s_{\underline{\gamma}})$.

The formal summation is written:

$$\underline{R}(\underline{p}_0, \omega) = \iint \Psi(\underline{\gamma}, \omega) \times \hat{e}(\underline{\gamma}, \underline{\delta p}) \times e^{-j\times\omega\times\{\tau(s_{\underline{\gamma}}) - \frac{1}{2}\times\underline{\delta p}^t\times\underline{\underline{M}}(s_{\underline{\gamma}})^{-1}\times\underline{\delta p} - \underline{p}(\underline{\gamma})\cdot\underline{OB}(s_{\underline{\gamma}})\}} \times d\Delta_{\underline{\gamma}}$$

where $d\Delta_{\underline{\gamma}}$ is the differential surface element on the incident plane wave and Ψ is a normalization term.

In the proposed Fourier convention, the imaginary part of matrix $\underline{\underline{M}}^{-1}$ is negative definite to assure evanescent contribution from $\underline{p}_0$ slowness direction.

This approach simulates the reflections, the transmissions and the vicinities of shadow boundaries.

A few "canonical" RCS examples are shown under this text.

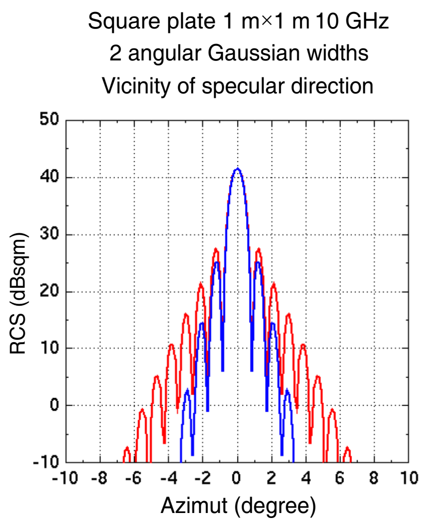

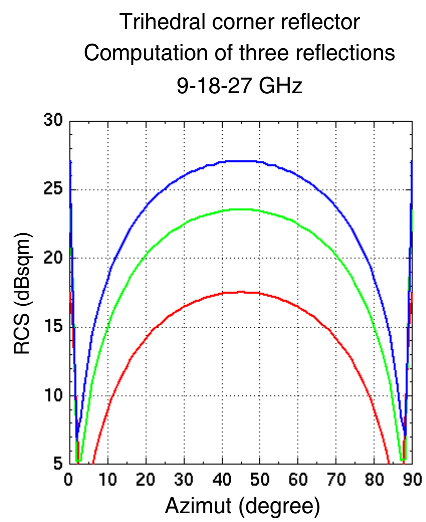

"Complex Source": Singularities in Real Space

A. M. Tagirdzhanov[1], **A. S. Blagovestchenskii**[1], **and A. P. Kiselev**[2]

[1]Physical Faculty, St. Petersburg State University, Russia
[2]St. Petersburg Department, Steklov Mathematical Institute, Russia

Abstract— The complexified Green function for 3D Helmholtz operator

$$\Delta + k^2 = \partial^2/\partial x^2 + \partial^2/\partial y^2 + \partial^2/\partial z^2 + k^2$$

in free space is

$$G_* = \exp(ikR_*)/R_*,$$

where

$$R_* = \sqrt{x^2 + y^2 + (z - i\varepsilon)^2}$$

with $\varepsilon > 0$ a free positive constant, is widely considered in literature. It is termed "complex source function". This function G_* is interesting as an exact solution of the Helmholtz equation showing a Gaussian beam behavior near z-axis and is often referred to as Gaussian beam beyond paraxial approximation. However, authors mainly fail to notice that the equation $(\Delta + k^2)G_* = 0$ is never satisfied in the full 3D space (G. Kaiser recently discussed the right-hand side of the equation

$$(\Delta + k^2)G_* = F$$

in *complex* space). We perform accurate and simple calculation showing that the correct equation in real space has the same form with F a generalized function essentially dependent on the exact definition of the square root. The matter is that the root has jumps at branch cuts. We discuss several choices of branch cuts and describe corresponding generalized functions F.

High Frequency Electromagnetic Wave Diffraction by a Curved Wedge Illuminated with a Complex Source Point Beam

Prabhakar H. Pathak, Youngchel Kim, and Robert J. Burkholder
Electro Science Lab., The Ohio State University, 1320 Kinnear Rd., Columbus, Ohio 43212, USA

Abstract— In the case of an electromagnetic (EM) current source in real space which produces a spherical wave, the high frequency diffraction of such a wave by an arbitrary three dimensional (3-D) curved wedge with perfect electrically conducting (PEC) faces can be predicted via uniform asymptotic ray theories of diffraction, such as the UTD developed by Kouyoumjian and Pathak [1], or the UAT of Lee and Deschamps [2], as well as that developed by Borovikov and Kinber [3]. In this paper, the asymptotic analysis which is available for the case of illumination of curved wedges by a real source point (RSP) is analytically continued into complex space to now allow for the illumination of curved wedges by a complex source point (CSP). It is well known that a CSP generates a beam type illumination (which reduces to a Gaussian beam within the paraxial approximation) as demonstrated by Keller and Striefer [4], and also by Deschamps [5]. Felsen and Heyman have exploited this CSP concept extensively to treat a variety of problems involving beam propagation in complex environments, for example, beam transmission through radomes [6], and through inhomogeneous and anisotropic media [7], etc. Also, Popov [8] has developed Gaussian beam methods to deal with EM and seismic wave propagation problems. In this paper, the problem of diffraction of a CSP beam by a fully 3-D PEC curved wedge in an isotropic homogeneous medium is studied specifically within the framework of the UTD. From the uniform asymptotic evaluation of an appropriate integral representation for the fields present in the 3-D canonical problem of CSP beam diffraction by a straight PEC wedge with planar faces, it is seen, analytically, that the UTD solution is, by itself, strictly not able to provide a continuous total field across the CSP beam optical shadow boundaries, but that an additional small correction term, which is present in the uniform asymptotic reduction of the field integral, serves to correctly enforce this continuity. The resulting canonical asymptotic solution leads to a modified UTD (or MUTD) solution for a wedge excited by a CSP beam. Here, $\mathrm{MUTD} = \mathrm{UTD} + \Delta$ where Δ is the field correction term to the conventional UTD (which is now analytically continued into complex space). However, it is important to note that, in practice, numerical results show that the field discontinuity at a CSP beam optical shadow boundary is generally always negligible (or that Δ is ignorable); the reason for Δ being generally negligible will be explained from analytical considerations. Finally, the generalization of MUTD to treat 3D curved wedges will be described for the case of CSP beam illumination. Also, numerical results will be presented to demonstrate the high speed and accuracy of this MUTD when it is applied to treat large 3-D reflector antennas illuminated by CSP beams. In contrast, conventional methods based on numerical evaluation of a physical optics (PO) radiation integral are seen to be highly inefficient for analyzing large reflector antenna systems. Future extensions of the MUTD for CSP excitation to treat multi-reflector system will be briefly discussed.

REFERENCES

1. Kouyoumjian, R. and P. Pathak, *Proc. IEEE,* Vol. 62, 1448–1461, Nov. 1974.
2. Lee, S. W. and G. A. Deschamps, *IEEE Trans. Antennas and Propagation*, Vol. 24, No. 1, 25–34, Jan. 1976.
3. Borovikov, V. A. and B. Ye. Kinber, *IEEE Proceeding*, Vol. 62, 1416–1437, Nov. 1974.
4. Keller, J. B. and W. Streifer, *J. Opt. Soc. Amer.*, Vol. 61, 40–43, 1971.
5. Deschamps, G. A., *Electron. Lett.*, Vol. 7, 684–685, 1971.
6. Gao, X. J. and L. B. Felsen, *IEEE Trans. Antennas and Propagation*, Vol. 33, No. 9, Sept. 1985.
7. Heyman, E., *IEEE Trans. Antennas and Propagation*, Vol. 42, No. 3, 311–319, Mar. 1994.
8. Popov, M. M., *Ray Theory and Gaussian Beam Method for Geophysicists*, Editora da Universidade Federal da Bahia, 2002.

Radon Transform Interpretation of Physical Optics Integral for Scalar Waves: The Near-Near Field Case

H. Arda Ülkü and A. Arif Ergin
Electronics Engineering Department, Gebze Institute of Technology
Çayırova, Gebze, Kocaeli 41400, Turkey

Abstract— The physical optics (PO) method is a useful asymptotic technique to analyze the radiation and scattering problems at high frequencies. PO involves a surface integral over the scatterer surface that can be called as the PO integral. It has been recently shown that the conventional PO integral for the electromagnetic (vector) waves can be interpreted as a Radon transform (RT) and this interpretation allows evaluating the PO integral exactly by means of geometric quantities in the time domain [1]. In [1], the exact formulae for the scattered fields observed in the far-field when the scatterer is illuminated by an incident plane wave are derived. In other words, both the source and observer are in the far-field (as in the definition of the radar cross section), i.e., the Far-Far case. Specifically, it is shown that once the analytical formula for a triangular scatterer is derived, the scattered field can be evaluated via the superposition of the effects of the triangles that model the scatterer after discretization. In [1], it is shown that plane wave scattering can be regarded as the intersection of a specific plane (defined by the incidence and scattering directions) with the triangles that model the scatterer via the planar RT. Also the approach is extended to NURBS surfaces for Far-Far case problems [2].

Beyond the Far-Far case problem, the RT interpretation is a general approximation and it is presented in [3], in a similar manner, that the analytical formulae when the observer and the source are at near or far field can be derived in terms of geometric quantities via the RT interpretation.

In the present work, the case when both the observer and the source are in the near field region (Near-Near case) is investigated in detail. It is shown that, instead of the planar RT that appears in the Far-Far case, an ellipsoidal RT emerges. Closed-form expressions for scalar scattered waves that are excited by a point source, scattered via a triangular surface, and observed at near field are derived. The exact formulae for the scattered field can be determined by the intersection of a triangular surface with an ellipsoidal surface whose foci are located at the observation point and the point source. The validity of the closed-form expressions obtained in the time domain is demonstrated through comparison with the frequency domain counterpart of the problem evaluated by using numerical quadrature.

REFERENCES

1. Bolukbas, D. and A. A. Ergin, "A radon transformation interpretation of the physical optics integral," *Microw. Opt. Technol. Lett.*, Vol. 44, 284, Feb. 2005.
2. Serim, H. A. and A. A. Ergin, "Computation of the physical optics integral on NURBS surfaces using a radon transform interpretation," *IEEE Antennas and Wireless Propagation Letters*, Vol. 7, 70–73, 2008.
3. Serim, H. A., H. A. Ülkü, S. Karaca, H. Öztürk, and A. A. Ergin, "Geometric evaluation of physical optics integrals using a time-domain approach," *IEEE International Symposium on Antennas and Propagation and USNC/URSI National Radio Science Meeting*, San Diego, California, USA, Jul. 5–12, 2008.

Progress on the Hybridization of Simulation Codes Based on Numerical High and Low Frequency Techniques for the Efficient Array Antenna Design in the Presence of Electrically Large Structure

Hsi-Tseng Chou, **Fang-Yao Kuo**, **and Heng-Tung Hsu**
Department of Communications Eng., and Communications Research Center
Yuan Ze University, Chung-Li, Taiwan, R.O.C.

Abstract— The booming of wireless communications spurs the need of using array antennas under electrically large structures such as in the applications of smart antennas installed on the structures of cars, aircrafts and buildings. An optimum design of such array antenna requires simultaneously the prior knowledge of mutual coupling between antenna elements and scattering resulted from environmental structures to interfere their radiation patterns. Currently available commercial codes do not seem to fulfill this need effectively. It is thus motivated to perform a hybridization to integrate numerical high frequency (HF) and low frequency (LF) techniques in a proper way such that the array antenna design can be performed to account for the environmental effects at the stage of design. The main issue involved in such problems lies in how to characterize the electromagnetic couplings between the radiating elements and the platforms accurately and efficiently. Based on the principle of equivalence, the hybridization approach has shown its superiority in terms of its computing efficiency. In such approach, discrete samplings of continuous electric or magnetic field components resulted from LF sub-domain are required to be converted to the excitation current sources for the HF sub-domain. Thus, the overall accuracy of the calculation results will strongly depend on the similarities between the sampled and original filed distributions with both the magnitude and phase involved. Tradeoff between the accuracy and efficiency is often necessary to balance the computation effort and the correctness of the design results. In this paper, the progress on the hybridization works will be presented. Especially the effective schemes for a fast array synthesis, as well as their convergence analysis of electric and magnetic current sampling, is developed to assure their uses in HF techniques for propagation consideration. Impact of the different sampling profiles on the overall accuracy and computation effort is also investigated through numerical examples.

A New UTD Based Relation between Modified Pauli-Clemmow and Van Der Waerden Methods for Asymptotic Evaluation of Wedge Diffraction Integrals

Giuliano Manara[1], **Prabhakar H. Pathak**[2], **and Paolo Nepa**[1]

[1]Department of Information Engineering, University of Pisa
Via G. Caruso, 16, I-56122 Pisa, Italy
[2]ElectroScience Lab, The Ohio State University
1320 Kinnear Rd, Columbus Ohio 43212, USA

Abstract— Two methods have been extensively used in the past for the asymptotic evaluation of wedge diffraction integrals, namely the Modified Pauli-Clemmow (MPC) method and the Van der Waerden (VdW) method. In particular, the MPC method has been used in the derivation of the Uniform Geometrical Theory of Diffraction (UTD) by Kouyoumjian and Pathak [1], while the solution via the VdW method can be expressed in terms of the Uniform Asymptotic Theory (UAT) of diffraction by Lee and Deschamps [2]. The main purpose of this paper is to show that by retaining all terms of order $K^{-1/2}$ (where K is the asymptotic large parameter) in the complete asymptotic expansion of the MPC method [3], the leading term of the VdW series is recovered. Moreover, it is shown that the VdW solution can be conveniently rewritten as a summation of the classical leading term of the MPC expansion, plus a new term providing a UTD slope like diffraction contribution; this special rearrangement of the VdW solution provides a transparent relationship between MPC and VdW not previously reported. The final diffraction coefficients obtained are expressed in a UTD format, which provide the proper discontinuities for the compensation of those exhibited by the Geometrical Optics (GO) field, in a bounded fashion. The extra term introduced in the UTD formula based on a rearrangement of the VdW solution renders the complete diffraction coefficients very accurate, even when the observation point is located in the close vicinity of the edge. As a byproduct, a new relation is also obtained between the UAT and UTD.

It is important to note that the new UTD expressions which serve to rigorously tie the ordinary UTD and the slope like UTD contributions together, rather than through a disjoint or separate development for each, can also be conveniently applied to analyze the scattering of evanescent waves by perfectly conducting and impedance wedges. In this latter case, a new compensation mechanism takes place namely that the discontinuities in the diffraction contribution are here provided by the UTD transition function, rather than by the non uniform diffraction coefficients which multiply the transition functions in the UTD format; however, the argument of the transition function is now extended to complex values as in [3].

Work is in progress to show that the new slope like UTD extra terms indeed provide the standard UTD slope diffraction contribution [4]. In particular, the reciprocity principle will be used in the derivation. Samples of numerical results will be presented at the conference, to demonstrate the accuracy and effectiveness of the new formulas by comparisons with reference data.

REFERENCES

1. Kouyoumjian, R. G. and P. H. Pathak, *Proc. IEEE*, Vol. 62, 1448–1461, Nov. 1974.
2. Lee, S. W. and G. A. Deschamps, *IEEE Trans. Antennas and Propagation*, Vol. 24, No. 1, 25–34, Jan. 1976.
3. Kouyoumjian, R. G., G. Manara, P. Nepa, and B. J. E. Taute, *Radio Sci.*, No. 6, 1387–1397, Nov.–Dec. 1996.
4. Pathak, P. H., "Techniques for high-frequency problems," *Antenna Handbook — Theory, Applications, and Design*, Y. T. Lo and S. W. Lee, Eds., Ch. 4, Van Nostrand Reinhold, New York, 1988.

Session 4P9a
Theory and Modeling of Multimode Transmission Lines: Waveguides, Microstrip Lines, Dielectric Waveguides 2

Developing Sample Holders for Measuring Shielding Effectiveness of Thin Layers on Compound Semiconductor Substrates

A. Fehér[1], Sz. Nagy[1], and I. Mojzes[2]

[1]Department of Telecommunications, Széchenyi István University
H-9026 Győr, Egyetem tér 1, Hungary
[2]Department of Electronics Technology, Budapest University of Technology and Economics
H-1111, Budapest, Goldmann Gy. tér 3., Hungary

Abstract— Ohmic contacts can be formed, if thin metallic layers grown on compound semiconductor substrates are heat treated. The type of the arising contact depends on the composition of the materials and the growing and thermal treating circumstances. If the layers of are thin enough, fractal-like topology of the metallic clusters can also occur. The systems can be studied by scanning electron microscopy or atomic force microscopy and the images can be analyzed by various topology determining algorithms. These values can characterize the metal-semiconductor contact. Also, resistance and other electromagnetic properties are needed for a proper description.

In the present work sample holders and measuring setups for determining the shielding effectiveness or the reflectivity of such small scale, thin, planar samples are tested. The measured data are compared to finite element model results using a commercial program package for electromagnetic calculations materials with well known electromagnetic properties. The irregular shape, the small size and the mechanical rigidity of the samples makes the measurements complicated. In the models high cylindrical symmetry is used with surprisingly good accordance. The frequency range is rather large, 9 kHz to 8 GHz, which is not covered by the current standards of shielding effectiveness measurements. The sample holders originate from those of the standards with much smaller size and specially modified flanges and fixing.

The measured data is shape and size independent up to a certain level. In the model finite element calculations various sample sizes are applied with similar results. Since the sample holders are filled with Teflon for the mechanical stability, the effect of possible air holes is also determined. Two-layer samples are modeled with relatively thin cover layer in order to derive the shielding effectiveness and the dielectric properties of the fractal samples.

Analysis, Simulation and Equivalent Circuit of Defected Microstrip Structures (DMS) and Their Applications in Microwave Filter Design

Z. Kordiboroujeni, **M. Kazerooni**, **and A. Cheldavi**
Iran University of Science and Technology, Iran

Abstract— This paper presents a new method to analyze and design a desired frequency band gap in microstrip transmission line with defected signal strip. These structures are named Defected Microstrip Structures (DMS). No etching is introduced in the ground plane of these structures. Instead, a DMS is made by etching specific patterns on the signal line (upper conductor) of a microstrip line. These defects cause a band gap in the frequency response of the circuit, just as in the Defected Ground Structures (DGS).

Defected Microstrip Structures have features which are useful in microwave circuits design and millimeter wave fields. Applications of DMS are similar to those of DGS such as planar resonators, high characteristic impedance transmission lines, filters, couplers, divider/combiners, power amplifiers and etc, but since the ground plane is left intact in this structure, it doesn't have as much cross talk and Electromagnetic Interference (EMI) as DGS. Another advantage of DMS is smaller circuit size compared to that of a non defected one, because of slow wave characteristic.

In this paper, we study different patterns of defects including rectangular, slotted rectangular, triangular, slotted triangular and also an array of these patterns on the signal line. Analytical results are provided and are followed by a proposed model and equivalent circuit for each structure. Effect of each parameter in these structures such as dimension and position of defect and slot on the frequency response of circuit is studied thoroughly. Also we design different band reject microstrip filters by these structures and compare different patterns by each other. The results from the models are compared with full wave simulation results (full-wave simulator is Ansoft HFSS 10) to verify the correctness of the model. It is shown that the model properly describes circuit's behavior and is in very good agreement with simulation results. Experimental results are also provided to confirm the simulation and proposed model results.

On Explicit Solutions to the Problem of Plane Wave Diffraction by a Kerr-type Nonlinear Dielectric Layer

Yury Shestopalov
Karlstad University, Karlstad, Sweden

Abstract— The analytical and numerical techniques for the solution to the problem of diffraction of a plane wave by a transversely inhomogeneous isotropic nonmagnetic linearly polarized dielectric layer filled with a Kerr-type nonlinear medium have been developed by many authors; we refer here only to papers [1–3] and also [4], where the author employs the fundamental technique set forth in [5], and address the reader to the bibliography therein. In this work we show that, looking for certain families of particular solutions to the Maxwell equation system, one can reduce, as in [6], the problem in question to a singular boundary value problem (BVP) on an interval for a semilinear second-order ordinary differential equation with a cubic nonlinearity (if the layer is situated in the homogeneous free space). The BVP is solved in terms of the analysis of an associated cubic-nonlinear integral equation (IE). Considering the latter as a nonlinear operator equation of the second kind in appropriate function spaces, one can can show that this IE can be solved using iterations; sufficient conditions of the unique solvability can be obtained similarly to [2, 3, 6] using the contraction principle.

In [3], it was shown that when the layer permittivity is modelled by a function having the form of a trigonometric polynomial, then one can obtain explicitly every iteration using the linearization. A similar approach developed in [7] leads to obtaining explicit particular soliton-type solutions to the cubic-nonlinear Helmholtz equation. We extend the technique by verifying that both linear and nonlinear operator terms in the considered nonlinear IE of the second kind (where the factor involving the layer permittivity is treated as a weight function) are invariant with respect to (preserve) trigonometric polynomials so that the image of a trigonometric polynomial is also a trigonometric polynomial that can be determined explicitly. Finally we construct the solution to the BVP in the form of the Neumann series in which every iteration can be calculated explicitly. The next step is to obtain the solution to the problem of the plane wave diffraction by a Kerr-type nonlinear dielectric layer by expanding the permittivity function in a Fourier series.

REFERENCES

1. Schürmann, H. W., V. Serov, and Y. Shestopalov, "Reflection and transmission of a TE-plane wave at a lossless nonlinear dielectric film," *Physica D*, Vol. 158, 197–215, 2001.
2. Serov, V., H. W. Schürmann, and E. Svetogorova, "Integral equation approach to reflection and transmission of a plane TE-wave at a (linear/nonlinear) dielectric film with spatially varying permittivities," *J. Phys. A: Math. Gen.*, Vol. 37, 3489–3500, 2004.
3. Schürmann, H. W., V. Serov, and Y. Shestopalov, "Waves in three-layer structures with Kerr-type nonlinearity and variable permittivity: Linearized solutions," *Proc. Int. Conf. on Mathematical Modelling of Wave Phenomena*, Växjö, Sweden, November 3–8, 2002, Växjö University Press, 217–226, 2004.
4. Yatsyk, V., "Eigenmodes of a nonlinear dielectric layer and algorithm of the solution to nonlinear spectral problems," *Dop. Nat. Acad. Nauk Ukrainy*, Vol. 11, 96–103, 2000.
5. Shestopalov, V. and Y. Sirenko, *Dynamical Theory of Gratings*, Kiev, Naukova Dumka, 1989.
6. Smirnov, Y., H. W. Schürmann, and Y. Shestopalov, "Integral equation approach for the propagation of TE-waves in a nonlinear dielectric cylindrical waveguide," *J. Nonlin. Math. Phys.*, Vol. 11, 256–268, 2004.
7. Shestopalov, Y., "Solitary waves in unbounded cubic-nonlinear media," *PIERS Online*, Vol. 1, No. 4, 483–486, 2005.

Cross-linked Transmission Line Based Planar TLM-net with Effective Dispersion of 4th Order

S. A. Ivanov[1], **B. V. Sestroretsky**[2], **and A. N. Bogolyubov**[1]

[1]Moscow State University, Moscow, Russia
[2]Lavochkin Association, Moscow, Russia

Abstract— Hereby the technique of optimization of dispersion of classical planar TLM net [1, 2] is suggested. This technique is based on partial elimination of spatial anisotropy and frequency dispersion which is expressed in the dependence of phase velocity and intrinsic impedance of plane net wave from frequency and direction of propagation.

The idea of this procedure is composed of integrating of two classical TLM nets turned against each other by 45° into one whole net and its further optimization. The optimization of the resulting net consists of two steps. The first step is the optimization of the spatial dispersion. For this purpose parameters of the integrated net are selected in such a way that amplitude-phase dispersion not to be dependant on the direction of propagation at the 2nd order of accuracy. The second step is the optimization of frequency dispersion of the resulting net. This optimization is based on the procedures of correction of phase velocity and intrinsic impedance of plane net wave. The procedure of phase velocity correction is based on the following considerations. Let's propose that we need to research stationary processes in TLM net at some frequency ω_0. Then if we excite the net on some easily determined effective frequency ω_{eff} the phase velocity of plane net wave will be equal to light velocity with the 2nd order of accuracy. Thus the using of effective frequency ω_{eff} let us decrease the phase dispersion up to the 4th order of accuracy. The procedure of intrinsic impedance correction resolves to the correction of internal impedance of exciting circuits.

As a result of this optimization the planar TLM net with amplitude-phase dispersion independent of the direction of propagation at 2nd order of accuracy (i.e., still describing transient processes in the net at the 2nd order of accuracy) and simultaneously with amplitude-phase dispersion of the 4th order of accuracy at some shifted frequency (i.e., describing stationary processes in the net at the 4th order of accuracy) was constructed.

The advantages of the constructed net are the large time step (larger than original net has) and high efficiency computational algorithm which need to store two parameters for one node and take 8–10 operations for one node per one time step.

The numerical tests have shown the high accuracy of the constructed net.

REFERENCES

1. Johns, P. B. and R. L. Beurle, "Numerical solution of 2-dimensional scattering problems using a transmission-line matrix," *Proc. Inst. Elec. Eng.*, Vol. 118, 1203–1208, Sept. 1971.
2. Sestroretsky, B. V., "Opportunities of direct numerical solving of boundary value problems based on the method of impedance analogue of electromagnetic space (IAES)," *Problems of Radioelectronics, Ser. "General problems of radioelectronics"*, Vol. 2, 113–128, 1976.

Session 4P9b
Microwave and Milllimeter-wave Devices and Circuits with CAD 1

Novel Compact Defected Ground Structure Based Bandpass Filters on Coplanar Waveguide

Heba B. El-Shaarawy[1,2], **Fabio Coccetti**[1,2], **Robert Plana**[1,2], **Mostafa El-Said**[3], **and Essam A. Hashish**[3]

[1]CNRS, LAAS, 7 avenue du colonel Roche, Toulouse F-31077, France
[2]Université de Toulouse, UPS, INSA, INP, ISAE, LAAS, Toulouse F-31077, France
[3]Electronics and Communications Department, Cairo University, Cairo, Egypt

Abstract— In this paper, we present three different defected ground structure (DGS) based bandpass filters on CPW. Each filter is composed of two parts, the first is the inductively coupled resonator, and the second is the DGS cell.

The conventional inductively coupled BPF consists of a $\lambda_g/2$ resonator terminated by short circuited shunt stubs producing the inductively coupled scheme. The inductor value is obtained by $L = 2l\{ln(2\pi l/w) - 1 + w/\pi l\}(nH)$ where l and w are the stub length and width in cm. A filter is designed on 0.635 mm thick Teflon substrate of $\varepsilon_r = 9.5$, $\tan(\delta) = 0.0035$ and CPW dimensions $G/W/G = 0.45/1.4/0.45$ mm corresponding to 50 Ω with 0.72 nH coupling inductance. The structure resonates at 5 GHz, with insertion loss −0.66 dB, return loss −22 dB and 3-dB fractional bandwidth 5.09%.

To reduce the filter length, a DGS cell is implemented between the two stubs of the resonator, Fig. 1(a). The filter is designed using the same substrate. Its insertion loss is 0.759 dB, return loss is −23.5 dB, and 3-dB fractional bandwidth is 5.28%, which makes the results comparable with those of the conventional BPF, Fig. 1(b). In addition, the length of the resonator is reduced from 12.9 mm to 5.55 mm due to the slow wave effect introduced by the DGS.

To increase the filter selectivity, a second order filter is implemented using the previously explained technique. The filter is designed using the immittance inverter method. The filter length is 13.22 mm, insertion loss at 5 GHz is −1.35 dB, return loss is −16.3 dB, and 3-dB fractional bandwidth is 4.26%, as shown in Fig. 1(b).

Finally, a reconfigurable DGS BPF is implemented. The DGS presented here consists of two rectangular resonators of different sizes, Fig. 2(a). A MEMS capacitive switch is used to connect and disconnect the second resonator from the structure allowing the reconfigurability of the resonant frequency. The MEMS switch is assumed to be an ideal switch, i.e., it is modeled as an open circuit in the OFF state and capacitive short circuit in the ON state. Therefore, two structures have been fabricated representing the ON and OFF states of the switch. Fig. 2(b) shows the simulated and measured responses in two cases. In the first case, the MEMS switch is ON, which means that the virtual capacitive short circuit introduced impedes the signal transfer to the second resonator. Hence only one single resonator is involved in the transfer function of the filter. This corresponds to one resonance frequency, at 5 GHz with insertion loss −1.24 dB, return loss −18.43 dB, and 3-dB fractional bandwidth 4.26%. The second case is when the MEMS switch is OFF, that means that the second resonator is connected along with the first one, yielding two

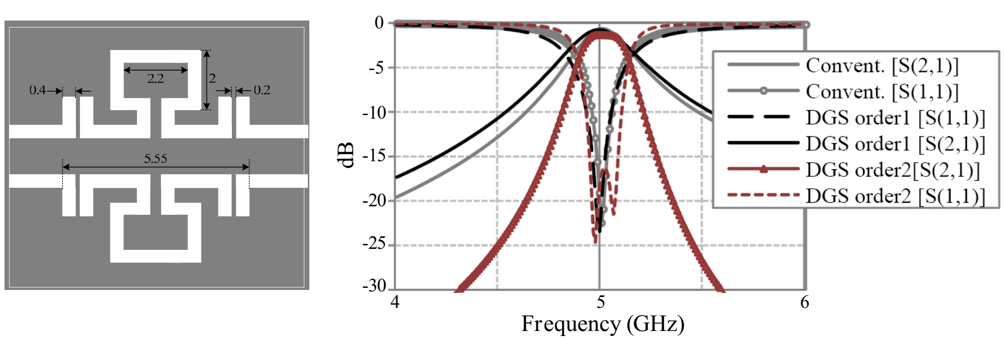

Figure 1: (a) Layout of the proposed DGS CPW filter of order one. (b) Simulated responses of the conventional BPF, proposed DGS CPW filters of orders one and two.

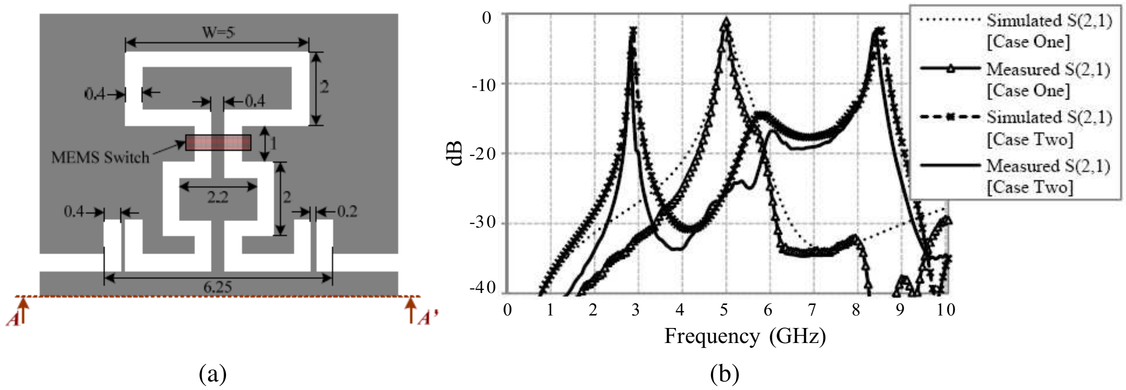

Figure 2: (a) Layout of the proposed reconfigurable inductively coupled BPF with DGS (Dimensions in mm). (b) Its simulated and measured responses.

resonant frequencies at 2.8 GHz and 8.46 GHz. At 2.8 GHz, the insertion loss is −2.36 dB and return loss is −9.5 dB and at 8.46 GHz, the insertion loss is −2.2 dB and return loss is −10.9 dB.

Design and Development of Helical Band Pass Filters for Satellite Receivers

Jagdish Shivhare[1] **and S. B. Jain**[2]

[1]Department of Electronics and Communication, Institute of Technology and Management
Sector-23 A, Gurgaon, Haryana, India
[2]Department of Electronics and Communication
Indira Gandhi Institute of Technology, Indraprashth University Campus, Delhi, India

Abstract— This paper describe the design, development and performance of helical band pass filters for ground and space applications. The performance of filters have been verified at different environmental conditions. The centre frequency and pass bands are 70/20 MHz, 230/10 MHz, 325/6 MHz and 600/18 MHz. The test results of silver plated ABS (Achrolonitrile Butadiene Styrene) plastic body helical filters are also reported in this paper.

A Low Phase-noise Low-power PLL in 0.13-μm CMOS for Low Voltage Application

Q. Guo, **H. F. Zhou**, **W. W. Cheng**, **Y. Han**, **X. X. Han**, **and X. Liang**
Department of Information Science and Electronic Engineering
Zhejiang University, Hangzhou, Zhejiang 310027, China

Abstract— A low voltage, low power phase-locked loop (PLL) using a standard 0.13-μm CMOS 1P8M process is presented. Due to the use of the wideband nulling of flicker noise up conversion technique, the voltage-controlled oscillator (VCO) can operate from a 0.5 V supply while the phase-frequency detector (PFD), charge pump (CP) and the divider use 0.8 V supply. The dc power consumption of the PLL is only 2.5 mW.

Figure 1 shows the block diagram of the proposed PLL. In the PLL design, one of the most challenging tasks is to realize a high performance VCO with a reduced supply voltage and power consumption. In order to operate at an ultra-low supply voltage, a differential NMOS-only topology is adopted for VCO because it reduces the voltage headroom and provides higher output swing for low supply voltage. We realize the elimination of flicker noise through the construction shown in Fig. 2 [1]. Removing the tail current source and using two tail inductors instead of the tail current source can raise the tail impedance at the oscillation frequency and its harmonics at the output node and also lower the voltage headroom. An inductor and varactors in series with passive metal-isolator-metal capacitors are used to make a clean control voltage as shown in Fig. 2. It only suppresses the high frequency signal and has no effect on dc voltage [2].

The PFD is implemented by modified precharge [3] topology since it can operate from a 0.8 V supply (Fig. 3). The proposed charge pump is shown in Fig. 4. With the reduced supply voltage, stacking transistor stages should be prevented. Thus, the switches at the gate terminals of M2 and M3 are utilized to control the functionality of charging or discharging the loop filter. The controlled voltage is connected to the gate terminals of M5 and M6 establishing a negative feedback to suppress the mismatch [4]. For the desirable output characteristics, a third-order loop filter is employed.

A divided-by 128/129 dual-modulus perscaler circuitry using the traditional transmission gate flip-flop (TGFF), was shown in Fig. 5. The speed is limited by divide-by 4/5 prescaler circuit. E-TSPC proposed a high speed divided-by 4/5 prescaler [5, 6] circuit using “E-TSPC flip-flop”.

The simulation results presented are for a standard 0.13-μm CMOS 1P8M technology. Fig. 6 shows the current variations against the output voltage variations of the charge pump circuit. For the proposed charge pump, the sourcing/sinking current matching is nearly perfect. By a combining discrete and continuous tuning [7], a family of overlapping tuning curves which guarantee continuous frequency coverage over the tuning range, as shown in Fig. 7. This VCO is tunable over 170 MHz with a sensitivity of about 25 MHz/V. The Fig. 8 shows the phase noise at 1 MHz offset along the whole frequency tuning range. With a reference frequency of 18.75 MHz, the output frequency of the loop locked at 2.4 GHz is shown in Fig. 9 and the settling time of the proposed PLL is less than 30 μs. The power consumption is 1.3 mW for the VCO, 1.2 mW for the other blocks of the PLL. The performance of the proposed PLL is summarized in Table 1.

REFERENCES

1. Ismail, A. and A. A. Abidi, “CMOS differential LC oscillator with suppressed up converted flicker noise,” *Proc. of Int. Solid-Stage Circuits Conference, ISSCC*, 98–99, San Francisco, USA, Feb. 2003.
2. Zhou, H. F., Y. Han, S. R. Dong, et al., “An ultra-low-voltage high-performance VCO in 0.13 μm CMOS,” *Journal of Electromagnetic Waves and Applications*, Vol. 22, No. 17/18, 2417–2426, 2008.
3. Lee, G. B., P. K. Chan, and L. Siek, “A CMOS phase frequency detector for charge pump phase-locked loop,” *42nd Midwest Symposium on Circuits and Systems*, Vol. 2, 601–604, Aug. 1999.
4. Hsieh, H. H., C. T. Lu, and L. H. Lu, “A 0.5-V 1.9-GHz low-power phase-locked loop in 0.18-μm CMOS,” *20th Symposium on VLSI Circuits*, 164–165, Kyoto, Japan, Jun. 2007.
5. Jau, T. S., W. B. Yang, and Y. L. Lo, “A new dynamic floating input D flip-flop (DFIDFF) for high speed and ultra low voltage divided-by 4/5 prescaler,” *13th IEEE International Conference on Electronics, Circuits and Systems*, 902–905, Nice, France, Dec. 2006.

6. Navarro, J. and W. V. Noije, "A 1.6-GHz dual modulus prescaler using the extended true-single-phase-clock CMOS circuit technique (E-TSPC)," *IEEE J. Solid-State Circuits*, Vol. 34, 97–102, 1999.
7. Hegazi, E. and A. A. Abidi, "A 17-mW transmitter and frequency synthesizer for 900 MHz GSM fully integrated in 0.35-μm CMOS," *IEEE Journal of Solid-State Circuits*, Vol. 38, No. 5, 782–792, 2003.

A Concurrent Triple-band CMOS LNA Design for 4G Applications

Yohan Jang, Nackgyun Seong, and Jaehoon Choi
Division of Electrical and Computer Engineering, Hanyang University
17 Haengdang-dong, Seongdong-gu, Seoul 133-791, Korea

Abstract— In this paper, a concurrent triple-band low noise amplifier (LNA), which operates at 698 MHz–800 MHz and 1920 MHz–2170 MHz, 2300 MHz–2400 MHz, is designed for Long Term Evolution (LTE) and WCDMA/HSDPA, WiBro applications. The circuit is designed with TSMC 0.18 µm RF CMOS process. As shown in Figure 1, a triple-band CMOS LNA with an input LC-tank circuit is designed by using source degeneration inductance. In order to obtain the necessary triple-band gain at the frequency of interest, a series LC circuit is added in parallel with the parallel LC tank of a single-band LNA. The output buffer (composed of M3, M4) is added for output matching. As shown in Figure 2, the proposed LNA has voltage gains of 17.79 dB and 18.58 dB, and noise figures of 3.7 dB and 3.9 dB at 749 MHz and 2160 MHz, respectively while dissipating 7 mA with 1.8 V supply. The proposed concurrent triple-band CMOS LNA could be a good candidate for 4G mobile systems.

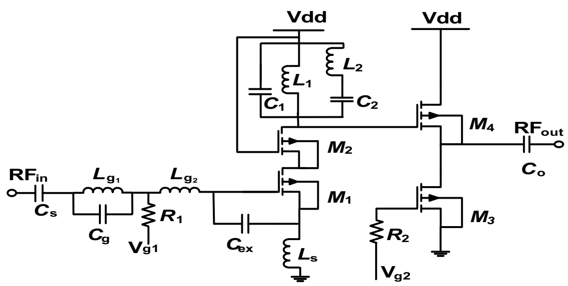

Figure 1: The proposed concurrent dual-band CMOS LNA.

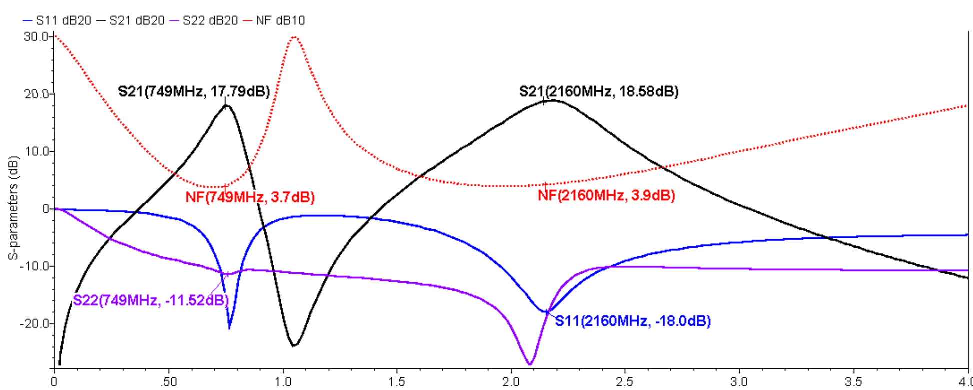

Figure 2: Simulated S-parameter characteristics (S_{11}, S_{22}, S_{21} and NF).

Particle Swarm Optimization Applied to Determination of the Equivalent Circuit Subject to Noise Parameters of the FETs

Ufuk Özkaya and Filiz Güneş
Department of Electronics and Communication Engineering
Yildiz Technical University, Istanbul, Turkey

Abstract— In this work, determination of small-signal equivalent circuit for a microwave field effect transistor (FET) is presented within the operation band subject to the noise behavior of FETs employing particle swarm optimization (PSO). As it is well known, gain and noise performance of an active device is expressed in terms of its small-signal equivalent circuit elements. Thus, accurate determination of the small-signal equivalent circuit elements is not only important in designing of the active devices and their circuits, but also characterizing the fabrication process of the device.

Many analytical and computer-aided design (CAD) techniques have been utilized to obtain the small-signal equivalent circuit elements from measured scattering parameters. However, analytical methods such as direct extraction methods cannot model the frequency dependences of the intrinsic elements in sufficient accuracy that results in errors between the predicted and measured scattering parameters. In CAD approaches such as optimization algorithms, optimum values are highly dependent upon starting values and suitability of cost function.

In order to overcome these stringent drawbacks and to determine both intrinsic and extrinsic elements of the small-signal equivalent circuit of the device, a new method is developed. This method aims to extract the optimum circuit elements from measured noise parameters $\{F_{\min}(\text{dB}), |\Gamma_{\text{opt}}|, \varphi_{\text{opt}}, R_N\}$ by particle swarm optimization method because, particle swarm optimization is a powerful global optimum searcher method. For the optimization procedure, cost function to be minimized is developed upon the relation between measured and predicted noise parameters. The PSO results are compared with the measured s-parameters and noise parameters and with the ones obtained from direct extraction method. Excellent agreement are resulted, intrinsic and extrinsic elements are obtained with high accuracy, thus we present an efficient method to be used during the determination of small-signal equivalent circuit for noise modeling of the active devices.

Design of Metallic Cylindrical Waveguide Bandpass Filters Using Genetic Algorithm Optimization

R. Thabet and M. L. Riabi
Laboratory of Electromagnetism and Telecommunications, University of Constantine, Algeria

Abstract— The analysis of uniaxial discontinuities in waveguides is at the basis of the design of a great number of microwave components. In this paper, we propose to use the mode matching analysis for the study of such discontinuities. This method, combined with the generalized scattering matrix technique, has been applied for the design of coupled cavity band-pass filters in metallic cylindrical waveguides. The characterization of the whole structure is carried out by computing the generalized scattering matrix of each discontinuity, then, cascading the different matrix taking in consideration the length between them.

Waveguide filters are considered in satellite communication systems, antennas, airborne radar system and other applications. Therefore, size and weight of components represent critical parameters. The objective will be to determine the optimal set of geometrical parameters required to yield better performances in pass-band and satisfy specifications. The problem is reformulated as a problem of optimization and the genetic algorithm synthesis procedure is introduced.

Genetic algorithms are classified in the category of global optimization techniques. They present the advantage to be more robust towards problems with several local optima and in presence of constraints on discontinuities and derivability. They are based on the concepts of natural selection and reproduction. The combination of these two mechanisms ensures the evolution of a population of individuals (potential solutions). This population will contain increasingly better individuals and will eventually converge to an optimal population that consists of the optimal solutions.

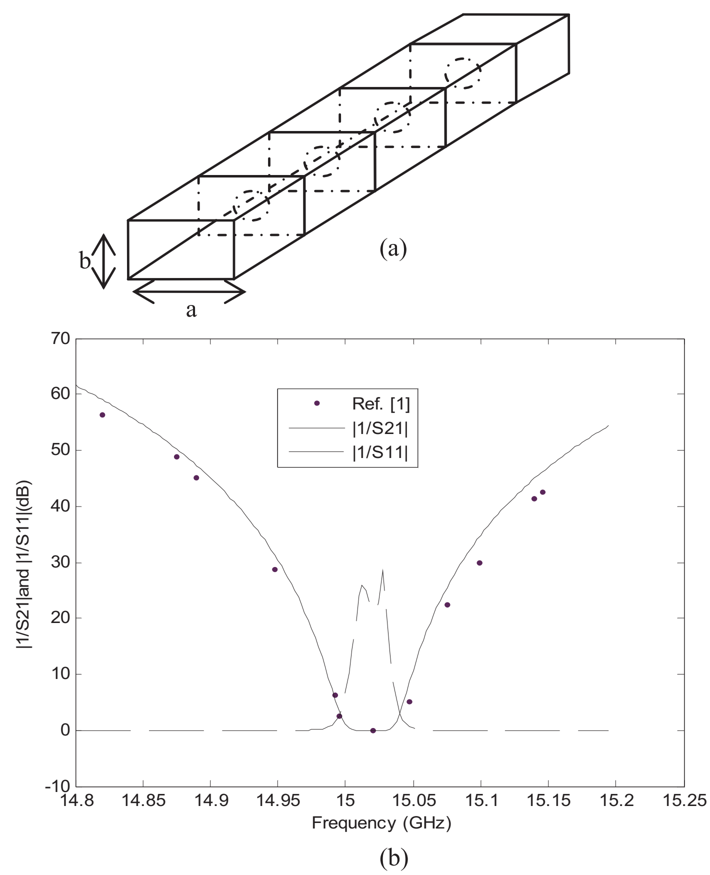

Figure 1: (a) Three-resonator rectangular waveguide narrow-band filter coupled by circular irises. (b) Frequency response of the filter.

In this work, we present the study of rectangular and circular waveguide filters coupled by circular irises where irises thickness is taken into account. Our aim is to define filters with better selectivity and lower insertion losses together with minimizing structures size and weight.

A three-resonator rectangular waveguide narrow-band filter coupled by circular irises is presented (Fig. 1(a)). Starting with a design specification, the geometrical dimensions of the filter have been computed by the Cohn's synthesis method together with Levy's large-aperture design formulas extended to the design of circular waveguide irises in coupled-resonator waveguide filters. This approximate treatment results in a designed pass-band filter which needs to be improved to satisfy design specifications.

Figure 1(b) represents the improved characteristic of the filter (WR62 housing: 15.8 mm×7.9 mm) working in Ku band. The thickness of the irises is 0.218 mm. The excitation at the input waveguide is realized by the TE_{10} fundamental mode. The plotted curve is the frequency response of the TE_{10} fundamental mode in pass-band. Our results are compared to those of Ref. [1]. A rigorous study on the convergence of the results obtained is made for the optimization of computational time. The number of modes taken into account for the field theory modeling is for TE_{mn} and $TM_{m'n'}$ up to $m = 24$, $n = 12$, $m' = 8$ and $n' = 6$ in the resonator sections and $m = 5$, $n = 12$, $m' = 5$ and $n' = 5$ in the circular iris sections (Fig. 2).

The optimized filter performances show improved pass-band performance, improved selectivity and better rejection quality in the stop-band. The return losses are larger than 21.23 dB in the pass band.

The use of GA adapts to the numerical answers provided by the mode-matching method and does not require any assumption a priori on the structure to be studied.

Table 1: Dimensions (in mm) of the optimized three-resonator filter.

		Ref. [1]	Optimized by GA
Radius of the irises (in mm)	R_1	2.577	2.5598
	R_2	1.142	1.1454
	R_3	1.125	1.1456
	R_4	2.592	2.5848
Lengths of the resonators (in mm)	L_1	12.499	12.4916
	L_2	12.819	12.8334
	L_3	12.461	12.4807

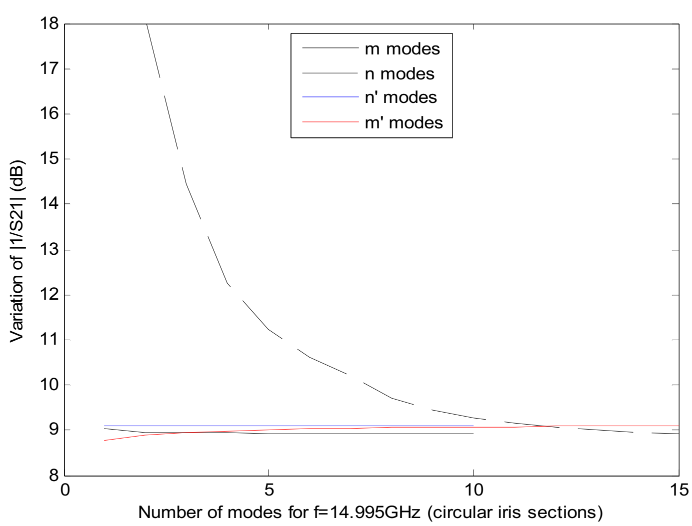

Figure 2: Variation of $|S_{21}|$ versus number of modes (in circular iris sections).

REFERENCES

1. Papziner, U. and F. Arndt, "Field theoretical computer-aided design of rectangular and circular iris coupled rectangular or circular waveguide cavity filters," *IEEE Trans. Microwave Theory Tech.*, Vol. 41, No. 3, 462–471, March 1993.

General Design of Compact T-shaped Line Filter with Ultra-wide Stopband

Y. Z. Zhu[1,2], **X. J. Zhang**[1], **and G. Y. Fang**[1]

[1]Institute of Electronics, Chinese Academy of Sciences, China
[2]Graduate University of Chinese Academy of Sciences, China

Abstract— Filters are one of the necessary components in microwave circuits. In the system of broad-band communications, conventional filters always suffer from the interference of its spurious bands, which are normally at its second or third harmonic resonant frequencies. Later, by replacing the series quarter-wavelength connecting lines of conventional filters with the equivalent open-stub T-shaped lines, we could have compact open-stub bandpass or lowpass filters with good second harmonic suppression. However, the lengths of used open-stub are fixed at quarter-wavelength, which restrain the second harmonic band. In this paper, generalization of this compact open-stub T-shaped transmission structure is presented. By substituting the generalized T-shaped transmission lines for the series transmission line of conventional filters, we could get a bandpass or lowpass filter with ultra stopband as well as a smooth passband and a steep transition band. The design equations for generating the parameters of the equivalent open-stub T-shaped lines are derived by building transmission-line model. Based on this model, the equivalent T-shaped lines show good passband characteristics in the fundamental resonant band and sharp band-rejection characteristics in the harmonic frequency band. Furthermore, this open-stub T-shaped transmission structure can also reduce the size of conventional filter. A hairpin bandpass filter with center frequency at 2.5 GHz and 400 MHz bandwidth is designed with the proposed structure. The simulation and measurement show good agreements. The insertion loss is less than 1.4 dB and the VSWR is less than 1.5 in the passband. The 40 dB stopband reaches 8 GHz and 35 dB stopband reaches 10.6 GHz. Its size is 23.4% less than the conventional hairpin bandpass filter.

The results show that the strong restriction band can be as high as the fourth order harmonic frequency with compact structure and good passband.

Session 5AP
Poster Session 3

Experimental Study on Super-resolution Techniques for High-speed UWB Radar Imaging of Human Bodies

T. Sakamoto, **H. Taki**, **and T. Sato**
Graduate School of Informatics, Kyoto University
Yoshida-Honmachi, Sakyo-ku, Kyoto 606-8501, Japan

Abstract— UWB (Ultra Wide-Band) radar systems are used in a variety of applications including security surveillance systems. The fast UWB radar imaging algorithm SEABED [1, 2], is, however, the only method that can be used in applications demanding real-time operation, such as surveillance. The SEABED algorithm is based on a reversible transform IBST (Inverse BST) between the target shape and a time delay observed at multiple locations. Because the IBST is incredibly sensitive to the resolution of the time delay, it is imperative that high-resolution data is obtained to estimate various parts of the human-body. Although the resolution of radar is basically restricted by its bandwidth, super-resolution techniques have been applied to GPR (Ground Penetrating Radar) to enhance the conventional resolution limit [3]. In this paper, we investigate experimentally super-resolution techniques for UWB radar data using a pig's anterior abdominal wall as a model of the human body. The results show that the super-resolution techniques are indeed capable of improving the performance of the SEABED algorithm.

Figure 1 shows the experimental UWB radar site in an anechoic chamber. The system includes a short pulse generator, a pair of omni-directional wideband planar patch antennas, and a wideband oscilloscope. The transmitted pulse has a center frequency of 3.7 GHz and bandwidth of 3.0 GHz, of which the classical range resolution is about 50 mm. As seen in the figure, the pair of antennas are positioned above the pig's anterior abdominal wall. The two antennas are scanned in a straight line and the received signal is recorded every 5 mm.

The MUSIC algorithm is applied in the frequency domain to enhance the resolution as in [3]. First, we select $2M - 1$ frequency-domain data samples with S/N larger than -20 dB, where the maximum power density is 0 dB, and $M = 70$ is empirically chosen. Next, a frequency smoothing technique is applied to resolve correlated interferences, where $M \times M$ covariance matrices are averaged M times. Then, an eigenvalue decomposition is applied and a MUSIC spectrum produced for each antenna location assuming a 2-dimensional signal subspace. Figure 2 shows the estimated image, in which a clear target boundary is visible with a high resolution of about 10 mm. This is 5 times higher than the classical resolution of 50 mm. This super-resolution technique can be employed in conjunction with the SEABED algorithm to obtain a detailed structure of the human body.

Figure 1: Experimental site for UWB radar with an anterior abdominal wall.

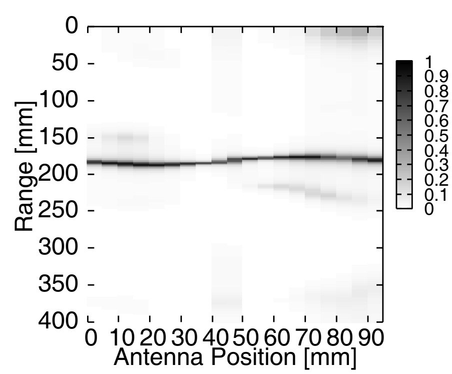

Figure 2: Super-resolution image of the surface of an abdominal wall.

REFERENCES

1. Sakamoto, T. and T. Sato, *IEICE Trans. on Commun.*, Vol. E87-B, No. 5, 1357–1365, 2004.
2. Sakamoto, T., *IEICE Trans. on Commun.*, Vol. E90-B, No. 3, 636–644, Mar. 2007.
3. Le Bastard, C., V. Baltazart, Y. Wang, and J. Saillard, *IEEE Trans. on Geosc. & Remote Sensing*, Vol. 45, No. 8, 2511–2519, 2007.

Novel Mathematical Model for the Analysis of Flat Substrate Imperfections

A. Baryshev
Moscow Lomonosov State University, Moscow, Russia

Abstract— Substrate imperfections analysis based on light scattering measurements associated with the presence of shallow pit or bump on the substrate surface have been a subject of interest in last decades. Especially in the field of semiconductor manufacturing where the detection and identification of imperfections arising at different stages of the manufacturing process seems to be one of the most important problem now. Direct analysis methods often fail for several reasons. For instance, the defects analysis based on the Discrete Sources Method (DSM) [1] fails because of the difficulties associated with the disposition of the discrete sources which are multipoles of high order inside very shallow pit or bump under consideration. In this presentation, we would like to suggest a novel mathematical model for the analysis of flat substrate imperfections. According to that model we can consider shallow pit or bump as a part of more extensional obstacle.

Let the upper half-space be a free space and the lower half-space be a substrate. Then we can consider a bump on the substrate as a particle merged into the substrate, where the wave number of the particle slightly differs from the wave number ambient substrate. A pit can be considered as a merged particle with the wave number that slightly differs from the wave number of the free space. We will consider scattering of a plane wave by a penetrable particle in R^3 which is partly merged into a substrate. The model used here is based on the DSM [1]. This technique constructs the scattered field everywhere outside a local obstacle as a finite linear combination of the fields resulting from sources distributed over an auxiliary surface located inside the obstacle. The Green Tensor of a half-space is incorporated to fit the transmission conditions enforced at the substrate surface. Then the scattered field analytically satisfies transmission conditions at the substrate surface, thus accounting for all interactions between the particle and the substrate automatically. Internal field is represented on the basis of regular functions, which fit Helmholtz equations [2]. Sources representing internal field are also distributed over an auxiliary surface located inside the obstacle. So the DSM solution constructed satisfies Helmholtz equations everywhere outside the obstacle, required infinity conditions and transmission conditions at the substrate surface. Then the unknown DS sources amplitudes are to be determined from boundary conditions enforced at the surface of the local obstacle only.

The convergence of the approximate solution to the exact one has been proved in [3] on the basis of the system of surface integral equations. The Fredholm property of the obtained system and its unique solvability has also been established.

In the presentation scattering of a plane wave by a shallow pit and bump will be considered. Computer simulating results including far-field pattern associated with an influence of the presence of a pit and a bump on the substrate surface will be presented.

REFERENCES

1. Eremin, Yu. A. and A. G. Sveshnikov, "Computer technology for analysis of scattering problems based on discrete sources method," *Comput. Maths. Math. Phys.*, Vol. 40, No. 12, 1769–1783, 2000.
2. Eremin, Yu. A., "Complete system of functions for the study of boundary value problems in mathematical physics," *Sov. Phys. Dokl.*, Vol. 32, No. 8, 635–637, 1987.
3. Baryshev, A. V. and Yu. A. Eremin, "Justification of an integro-functional method for diffraction problems in the presence of a half-space," *Differential Equations*, Vol. 44, No. 9, 1281–1288, 2008.

Solution of Electromagnetic Wave Scattering Problems from Inhomogeneously Layered Bodies

Alexander G. Kyurkchan and Dmitrii B. Demin
Moscow Technical University of Communication and Informatics
Aviamotornaya Street 8A, Moscow 111024, Russia

Abstract— In this abstract the problem of electromagnetic wave scattering by three-dimensional (3D) inhomogeneously layered scatterers is considered. The pattern equation method (PEM) has been used to solve this problem. Earlier, this method has been applied for solving to a number of diffraction, scattering, and wave propagation problems for such as the wave scattering by a single impedance and dielectric bodies, the conducting bodies coated with dielectric materials as well as the groups of impedance and dielectric bodies.

The PEM is based on a reduction of the initial boundary-value problem for the Maxwell equations to an infinite system of linear algebraic equations with respect to the coefficients of expansion of the scattering pattern (spectral function of a wave field) in terms of vector angular spherical harmonics. Under certain restrictions on the geometry of the problem, which can be strictly determined, the aforementioned infinite linear system of algebraic equations can be solved by the method of reduction, i.e., truncation. In this case, the expansion of the scattering pattern in terms of the vector angular spherical harmonics contains a finite number of addends, this number being determined by the maximal harmonic index.

In the PEM the required characteristic is the scattering pattern function that determines the diffracted field for the far zone. Various quantities such as the integral, bistatic and monostatic radar cross sections, etc., can be obtained by using the scattering pattern.

The PEM differs from other numerical methods for solving the problems of diffraction that one directly seeks the scattering pattern. For instance, in the integral equation method the required unknown function is either the volume current density or the surface one. For scatterers of arbitrary shapes, it will lead to cumbersome calculations since the distribution of current density is very sensitive to a various sort of the local disturbances, such as the breaks of a surface of scatterers and so forth. The scattering pattern, being the integrated characteristic, is considerably independent against such disturbances.

The PEM is one of the most effective methods for solving the problem under study. Earlier, it was found that, when this method is used for solving the scattering problems with impedance and dielectric scatterers, the rate of the algorithm convergence is mainly governed by the scatterer size and weakly depends on its surface breaks.

Under the developed numerical algorithm of the PEM, we carried out researches of accuracy of numerical calculations for dielectric bodies coated with several dielectric layers. In particular such bodies as a sphere, a spheroid, a finite circular cylinder, a superellipsoid and the Chebyshev's particles were examined. The complete agreement between our results with the results obtained by the other numerical methods has been established.

A Scheme to Analyze Scattering from an Iris on an Infinite Waveguide Structure Using the Conjugate Gradient Method

H. Belhadj and T. Aguili
Sys'Com Lab, National Engineering School of Tunis, Tunisia

Abstract— The conjugate gradient method has been applied to various electromagnetic field problems, and it has been efficient to solve electromagnetic scattering problem when combined with a fast Fourier transform technique [1]. It guarantees convergence of any problem to a specified degree of accuracy and with a less number of operations compared to other numerical method such as the method of moment [2].

On this paper, the conjugate gradient method is developed, to solve an operator equation representing electromagnetic scattering problem, from a structure of an irregular iris on an infinite rectangular waveguide. First, we are modeling our problem using the method of generalized equivalent circuit MGEC [3]. We have then deduct the equation to solve: $\hat{Z}J = -E_0$, where E_0 is the TE_{10}-mode propagating in a rectangular waveguide and denotes the excitation field, J is the unknown current density vector and $\hat{Z}$ is the impedance operator.

The impedance operator is described on the mode basis, it is a discrete operator applied on the spectral domain. We have a one dimensional problem, then when applying the impedance operator to J we have: $\hat{Z}J(x) = \sum_n |f_n\rangle z_n \langle f_n, J(x)\rangle$, where n denotes the mode number, f_n define the base functions and z_n is the mode impedance.

The CG algorithm is then implemented for a one dimensional problem since there are no variations with y-axis. Convergence is obtained when the error criterion $\boldsymbol{r_k}/\boldsymbol{r}_0$ ($\boldsymbol{r_k}$ is the residue at the kth iteration) is lower than one fixed small value. Also we stop to vary the mode number when there's no change in the current values. We draws the current distribution at convergence for $n = 5000$ and $N = 64$.

Results obtained are conformed to theory with respect to the boundary conditions. In fact the tangential current component is null on the dielectric and is maximum on the magnetic wall and minimum on the electric one. Convergence is obtained after only 4 iterations with a computational CPU time at about one minute for an error less than 10^{-2}. Also results obtained are conformed to those finding by the moment method, with a significant computational time gain.

We have also plotted the total electric field obtained and we have determinate the scattering electric field. Results are compared to those finding by the moment method when using new software TMWLAB designed to supports the MGEC method, and provides results obtained using the Moment method [4]. The input impedance have been also computed and compared to the one finding by Markuwitz [5].

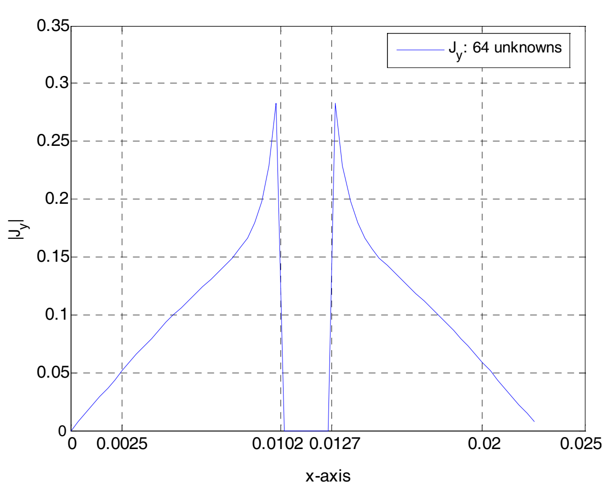

Figure 1: Numerical convergence of the current distribution for an irregular iris evaluated by the CG method.

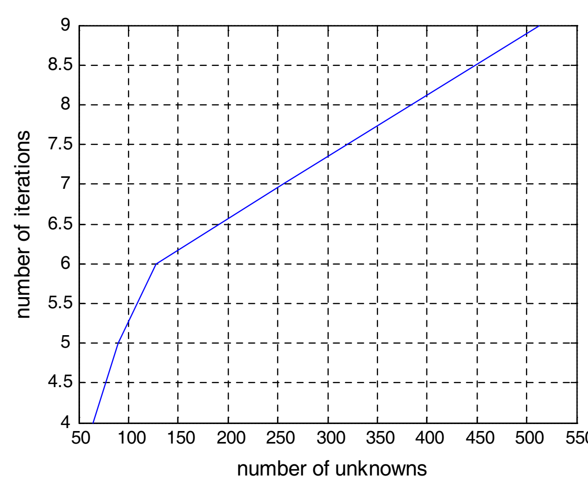

Figure 2: Number of iterations to compute the current distribution using the CG method.

On other hand, we are thinking of using subdomain basis functions as extension to the conjugate gradient method, in order to improve convergence behavior, especially for problem with large scales and with a large numbers of unknowns.

REFERENCES

1. Sarkar, T., "The conjugate gradient method as applied to electromagnetic field problem," *IEEE Antennas and Propagation Society*, Newsletter, August 1986.
2. Harrington, R. F., "Field computation by moment methods," *IEEE Press Series on Electromagnetic Waves*, Syracuse University, 1993.
3. Aguili, T., "Modélisation des composantes SFH planaires par la methode des circuits equivalents généralisée," Thesis manuscript, ENIT, Tunisia, 2000.
4. Ben Salah, T. and T. Aguili, "Software implementation of a new multi-scale method for fractal shaped structure's diffraction analysis," *Progress In Electromagnetics Research Symposium*, Cambridge, 2008.
5. Markuwitz, N., *Waveguide Handbook*, The Institution of Electrical Engineering, 1986.

Interaction of Infrared Electromagnetic Pulses in Resonant Layered Structures with n-GaAs Semiconductor Film

V. Grimalsky, S. Koshevaya, J. Escobedo-A., and M. Tecpoyotl-T.
CIICAp, Autonomous University of State Morelos (UAEM)
Cuernavaca, ZP 62209, Mor., Mexico

Abstract— Multilayer structures, both periodic and nonperiodic, are widely investigated in optics. Various nonlinear phenomena, both resonant and nonresonant, were observed. The layered structures with semiconductor layers are of a great interest because they give a possibility to control effective refraction indices due to changing the electron concentration. The semiconductors with multi-valley structure of conduction band, like n-GaAs, possess electron nonlinearity in millimeter, terahertz wave ranges, and in the infrared range. In this report, a case of the infrared range is considered. A fabrication of multilayer structures is difficult, and, moreover, the dissipation of infrared waves is high. Therefore, to investigate an interaction of infrared waves in layered structures with semiconductor films, it is rather better to use simpler structures that include only a few layers.

A simple resonant structure is formed by three layers with relative dielectric permittivities ε_1, ε_2, ε_1. The surrounding medium has a dielectric permittivity ε_4. It is assumed that the following inequalities are satisfied: $\varepsilon_1 < \varepsilon_4 < \varepsilon_2$. In the case of the oblique incidence of an infrared wave, when the total internal reflection at interfaces occurs, such a structure behaves as a double barrier for an incident electromagnetic wave and a phenomenon of resonant transmission at a set of frequencies can be observed. This phenomenon is similar to the resonant tunneling of electrons through a two-barrier system in quantum mechanics.

The present report is devoted to theoretical investigations of the linear and nonlinear interaction of infrared pulses in double barrier structures with n-GaAs films. If the central layer is n-GaAs, then there is a possibility to change the effective dielectric permittivity in the infrared range by means of redistribution of electrons between the valleys, because of an essential difference of effective masses and collision frequencies of electrons in lower (Γ) and upper (L, X) valleys [1, 2]. Consider the simplest two-valley model of the conduction band of GaAs, where the lowest (Γ) and upper (L) valleys are taken into account. The balance equations for electron concentrations $n_{1,2}$, velocities $V_{1,2}$, and average energies $W_{1,2}$ for electrons in each valley, added by the Poisson equation, are used [1]. Generally, the effective dielectric permittivity of n-GaAs possesses both real and image parts. The redistribution of electrons can be produced either by applying a bias electric field to the semiconductor layer or by the electron heating in the field of the strong infrared electromagnetic wave. In the first case, an amplitude modulation of reflected (and transmitted) wave occurs. In the second case, various nonlinear phenomena could take place, like the nonlinear switching, the bistability, and the modulation instability.

We have investigated a modulation of a continuous EM wave in the infrared range by applying the bias electric field to n-GaAs layer. To obtain 50% transfer of electrons into the upper valleys, it is necessary to apply the bias electric field $\sim$5 kV/cm. A bias electric field leads to a redistribution of electrons between the valleys, so there is $n_2 \sim n_1$ within the n-GaAs film [2]. The incident wave amplitudes are assumed as small there.

More interesting results have been obtained when the pulses of high input amplitudes interact with the structure without a bias electric field. In this case, various dynamic nonlinear phenomena take place. A possibility of the auto switching of the short pulses and the modulation instability of long pulses has been investigated. When the amplitude of the input pulse increases gradually, the shape of the transmitted pulse changes drastically. Namely, at low input amplitudes, the reflection of the pulse is weak there. At higher amplitudes, the reflection increases and the shape of transmitted pulse changes, when compared with the linear case. The opposite situation, namely a transition from reflection to transmission, also can take place.

The interesting phenomenon is an occurrence of the modulation instability of long input pulses. The modulation instability takes place in the vicinity of the higher resonant transmission frequencies, where the peaks of transparency are narrow. To produce the modulation instability, the amplitude of the incident pulse should be higher than some threshold value (the intensity is of about $5\,\mathrm{mW/cm^2}$).

REFERENCES

1. Tomizawa, K., *Numerical Simulation of Submicron Semiconductor Devices*, 340, Artech House, London, 1993.
2. Web Site, New Semiconductor Materials. Characteristics and Properties, http://www.ioffe.ru/SVA/NSM/.

Photo-induced Modification of Refractive Index in Compounds As_xS_{1-x}

A. Popescu, **D. Savastru**, **and S. Micloş**
National Institute of R&D for Optoelectronics INOE-2000
409 Atomiştilor Str., Magurele, Ilfov 077125, Romania

Abstract— Non-crystalline chalcogenide compounds have a large domain of glass formation, good optical transparency including middle IR, consistent large value of refractive index (2.4–3.3). The films of As_xS_{1-x} with thickness of 0.5–3.0 μm and different composition were obtained by vacuum thermal evaporation. The refractive index for thin films was calculated from transmission spectra $T(\lambda)$ of films measured in spectral range of 300–2000 nm and the transmission spectra of pure oxide glass substrate. The transmission spectra of films modified by argon laser irradiance were measured and the modification of refractive index was calculated. The permanent modification value of Δn is 0.05.

The dynamic nonlinear coefficient n_2 defined by relation $n(I) = n_0 + n_2 I$ for the wave length 1.064 μm was measured experimentally by determining the threshold of autofocalisation for irradiance of Q-switched Nd : YAG laser. The bulk materials of the composition As_2Se_3 had been used. The Kerr type nonlinear coefficient is about 100 times larger then the same in silica. We have to mention that for As_2S_3 materials the measuring of Kerr nonlinearity for this wavelength was not been possible because of biphotonic absorption.

The obtained results proof that materials are promising for use in photonics.

Oxidation-reduction Cycle of Water — The Primary Source of Energy for Biophoton Emission

Vladimir Voeikov
Faculty of Biology, Lomonosov Moscow State University, Moscow, Russia

Abstract— Living matter the matter should reside in an excited state for biophoton emission from it to take place. The major source of energy for living matter excitation is respiration. Respiration is generally defined as oxidation of organic food by oxygen resulting in the production of water, CO_2, and energy in the form of ATP.

However, it is known that animals and even human beings may gain enough energy without food consumption for extended periods of time. Biology gives examples that normal aerobic respiration may take place at very low ambient oxygen concentrations. If to consider respiration as reduction of oxygen to water with electrons (hydrogen) abstracted from available electron donors, one of the candidates for the role of electron donor besides organic substrates may be water, representing 99+% of all the molecules of any living matter. Water may also serve the source of oxygen.

Until recently such a role of water in respiration was neglected since very high energy quanta are needed to split water molecules into hydrogen and oxygen. Now more and more evidence accumulates that "real" liquid water is a heterogeneous system. Basically two different phases are present in water — water domains with quazi-liquid crystal structure and "gas" — like water. Water molecules reside in organized domains in an excited state. Much less energy of activation is needed to split it into constituent parts. Water splitting results in oxygen and hydrogen appearance, and oxygen may accumulate in less organized phase of water system. When oxygen concentration exceeds a threshold value it may start to abstract electrons from organized water capable to donate electrons. Full reduction of one oxygen molecule is accompanied with release of big quanta of energy. This process represents combustion of water. Peculiarity of this reaction is that from chemical point of view reagents and the reaction products are the same molecules ($O_2 + 2H_2O \rightarrow 2H_2O + O_2$) However the reaction of water oxidation as any other oxidation is the source of energy. It is energy of non-equilibrium (excited) state of liquid crystalline water phase is released when two water molecules belonging to it (left side of the equation) convert into the ground state water molecules (right side of the equation). The process described above proceed permanently and with high efficiency in "real" water containing dissolved substances, in particular, carbon dioxide, bicarbonates, nitrogen, and also interfaces with gas nanobubbles and solid particles covered with organized water.

Reactions of combustion usually proceed in an oscillatory matter. Thus energy in the course of water combustion may be released in discrete portions, in a more or less organized manner. Energy released in the course of water "burning" may be used in complex aqueous systems as energy of excitation for the driving chemical processes including synthetic reactions that increase the system complexity. This energy may be pooled as the energy of excitation of the whole aqueous system. Excess of this energy may be released in the form of photon emission. Adequate external stimuli of even very low intensity may induce more or less intense flashes of photon emission from the such excited aqueous systems ("Light Amplification by Stimulated Emission of Radiation", LASER-like effect). Such phenomena may be observed even in the most "simple" aqueous systems such as bicarbonate water solutions (see the accompanying report of Voeikov et al.).

A significant part of water in living matter is present at the interphases with macromolecules and supramolecular complexes and has the properties of a liquid crystalline phase. According to the concept presented here the suggested oxidation-reduction cycle of water realizing self-pumping of aqueous systems in which it takes place is very likely to be a fundamental source of energy for living systems and the basis of their highly excited state.

Phase Transition Determination Using Continuous and Pulsed Laser

F. M. Sánchez-Arévalo[1], **C. Aldama-Reyna**[2], **T. García-Fernández**[3],
G. A. Lara-Rodríguez[4], **and M. Villagran-Muniz**[1]

[1]CCADET, Universidad Nacional Autónoma de México (UNAM)
A. P. 70-186, México D. F., C. P. 04510, México
[2]Departamento Académico de Física, Universidad Nacional de Trujillo, Trujillo, Perú
[3]Universidad Autónoma de la Ciudad de México (UACM)
Prolongación San Isidro 151, Col. San Lorenzo Tezonco, México D. F., C. P. 09790, México
[4]IIM, Universidad Nacional Autónoma de México (UNAM)
Apdo. Postal 70-186, Cd. Universitaria, México, D. F., C. P. 04510, México

Abstract— Solid phase transition of materials can be present locally, superficially or in bulk. In this work, two different methods to evaluate this phase transition, using continuous and pulse electromagnetic radiation, are presented. Applying the dynamic speckle technique the surface changes of the samples can be detected. On the other hand the photoacustic technique allows determining the material phase transition in bulk.

For the dynamic speckle and photoacoustic techniques a continuous 10 mW–632 nm HeNe and a nanosecond 10 mJ/cm^2–532 nm Nd-YAG laser were used; respectively.

Here we present the analysis results of CuAlNi shape memory alloy using both previously mentioned techniques as a function of temperature. In both cases the correlation analysis of the obtained data allows to determine the phase transition temperature. This result agree with the one obtained by differential screw calorimetry (DSC).

The Figure 1(a) shows the time history speckle pattern and the correlation coefficient function obtained by dynamic speckle technique. The solid phase transition provokes a surface change that was detected by this technique allowing the determination of the transition temperature of this material. Figure 1(b) shows the correlation coefficient function obtained by the photoacoustic method, which is in agreement with the former one and the results obtained by DSC.

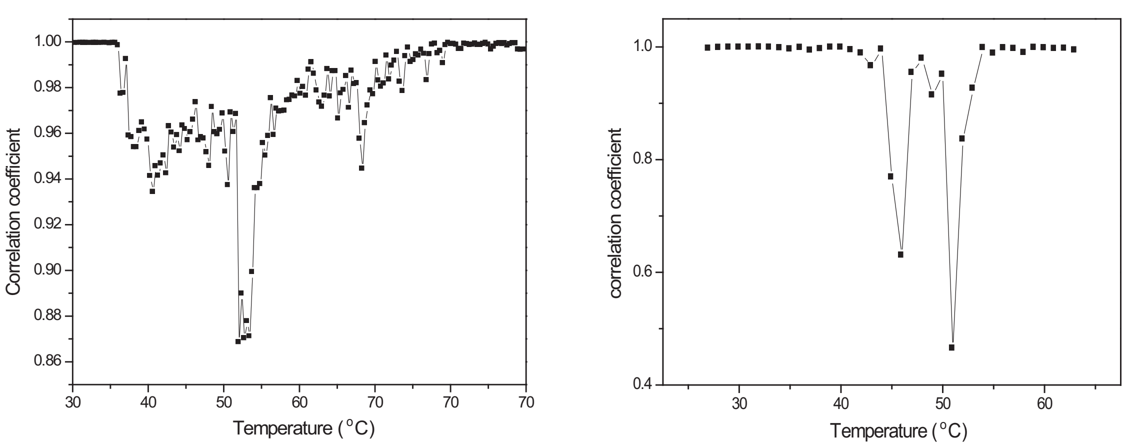

(a) (b)

Figure 1.

Nonreciprocal Effects in the Magnetoplasmonic Crystals

V. I. Belotelov[1,2], **D. A. Bykov**[3], **L. L. Doskolovich**[3], **A. N. Kalish**[1,2], **M. Vanwolleghem**[4], **and A. K. Zvezdin**[1,5]

[1]A. M. Prokhorov General Physics Institute of RAS, Moscow 119991, Russia
[2]M. V. Lomonosov Moscow State University, Moscow 119992, Russia
[3]Image Processing Systems Institute RAS, 151, Molodog. St., Samara 443001, Russia
[4]Institute d'Electronique Fondamentale (IEF UMR 8622), Université Paris-Sud, Orsay 91405, France
[5]Fondacione ISI, Torino 10133, Italy

Abstract— When the magnetization lies in the film plane and is perpendicular to the plane of light incidence the transversal Kerr effect (TKE) is observed. The TKE is odd in magnetization and is measure by the relative change of the reflected light intensity $R(\mathbf{M})$ when the medium's magnetization $\mathbf{M}$ is switched:

$$\delta = (R(\mathbf{M}) - R(-\mathbf{M}))/R(0). \tag{1}$$

Nowadays, the enhancement of the TKE is an important issue. In this work, we consider a sample of a smooth ferromagnetic dielectric film covered with a thin noble metal layer periodically pierced by subwavelength slits.

Reflection and the TKE spectrum for the perforated metal film of period $d = 480\,\text{nm}$ are shown in Fig. 1. The TKE spectrum has two pronounced features at around $\lambda = 1049\,\text{nm}$ and $\lambda = 1188\,\text{nm}$, corresponding to two surface magnetoplasmon polariton (SMPP) excitations at the metal-dielectric interface. Comparison of the reflection coefficients for the oppositely magnetized dielectric $R(\mathbf{M})$ and $R(-\mathbf{M})$ reveals that the intensity effect arises from the magnetization induced shift of the reflection spectra (see bottom insert in Fig. 1). The values of the wavelength shift are 1.6 and 1.2 nm, respectively. The condition for the SMPPs emergence includes the multiple of the reciprocal lattice vector $G = 2\pi/d : \kappa = k_x^{(i)} + mG$. The magnetic field assisted SMPP's wavelength shift is measured by:

$$\frac{\Delta\lambda}{\lambda_0} = \frac{\kappa_0 \alpha}{mG} g. \tag{2}$$

It explains the growth of the shift with the frequency increase. The sign of the shift depends on the SMPPs order, so the profiles of the TKE positive and negative peaks are inverted with respect to each other, as they are assisted by SMPPs of the plus and minus first orders. Furthermore, the magnetization induced shift is linear in the gyration g.

It is shown that the reason for the difference in the $R(\mathbf{M})$ and $R(-\mathbf{M})$ is related to the non-reciprocity of the magnetoplasmons excited at the grating.

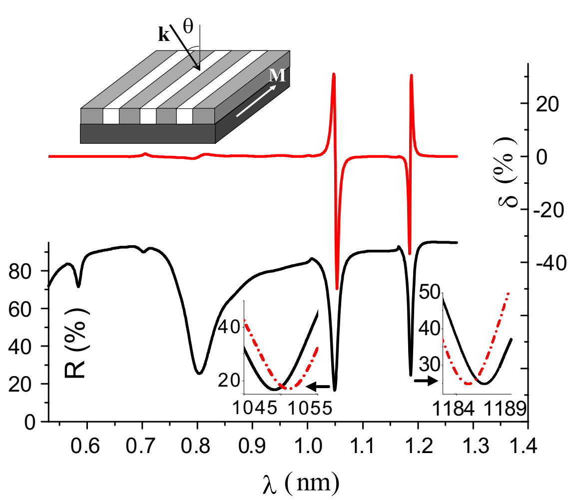

Figure 1.

To conclude, we have shown that if a smooth magnetic dielectric film is covered with a thin noble metal layer perforated with subwavelength slit arrays, the slits being parallel to the magnetization the transverse Kerr effect gets increased substantially. The giant values of the Kerr effect are caused by the magnetization induced change of the phase velocity of the SMPPs. The giant Kerr effect can be used as an efficient tool for the surface plasmons detection. Similar effect can be observed in transmitted light, which is of prime interest for possible applications.

ACKNOWLEDGMENT

The work is supported by RFBR (07-02-01445, 08-02-00717, 07-02-92183), Leading Scientific Schools grant NSh. 671.2008.2.

Temperature Dependence of Piezoelectric Potential Phonon Scattering Properties of ZnO Of the Quantum — Qusi Two Dimensional System under Two Directional Circularly Polarized Oscillating Fields

Su-Ho Lee[2], **Joung-Young Sug**[1], **Jun-Yong Choi**[1], **Ji Ho Park**[1], **Gi-Dong Oh**[3], **and Geon Sa-Gong**[2]

[1]Electronic and Electrical Engineering School, Kyungpook National University
Daegu 702-701, Korea
[2]Department of the Electrical Engineering, Dong-A University
Pusan 604-714, South Korea
[3]Research Institute of Myoung-Bo Electronic Company
Pusan 604-714, South Korea

Abstract— We investigated theoretically the quantum optical transition properties of ZnO, in qusi 2-Dinensinal Landau splitting system, based on quantum transport theory. We apply the Quantum Transport theory (QTR) to the system in the confinement of electrons by square well confinement potential. We consider two systems — one is subject to right circularly oscillating external fields and the other is subject to left circularly oscillatory external fields. The main purpose of this work is to compare QTLSs, which indicate absorption power, in the two oscillating external fields. Our results indicate that the QTLSs of right circularly oscillating external fields is larger than the QTLSs of left circularly oscillating external fields, while the opposite result is obtained for the QTLWs. We use the projected Liouville equation method with Equilibrium Average Projection Scheme (EAPS). In order to analyze the quantum transition, we compare the temperature field dependencies of the QTLW and the QTLS on two transition processes, namely, the phonon emission transition process and the phonon absorption transition process.

Magnetic Field Dependence of Electron Phonon Scattering Properties of ZnS of the Quantum — Qusi Two Dimensional System

Joung-Young Sug[1], **Su-Ho Lee**[2], **Jun-Yong Choi**[1], **Ji Ho Park**[1], **Cheol-Hwan Kim**[3], **and Geon Sa-Gong**[2]

[1]Electronic and Electrical Engineering School, Kyungpook National University
Daegu 702-701, Korea
[2]Department of the Electrical Engineering, Dong-A University
Pusan 604-714, South Korea
[3]Research Institute of Myoung-Bo Electronic Company
Pusan 604-714, South Korea

Abstract— It is well known that ZnS is the piezoelectric potential phonon interaction scattering effect active. The reason why we are mostly interested in these materials The wide band-gap semiconductors, including ZnS, AlN, InN, and their ternary compounds, have great potential for applications in high-power and optoelectronic devices in the blue and the ultraviolet regions. Than, the investigation of quantum optical transition properties of this materials is very important, So, in this research, we investigated the quantum optical transition properties of ZnS, in qusi 2-Dinensinal Landaue sppliting system, based on quantum transport theory.

There are many theories regarding the quantum transport problems in various methodologies, such as the Boltzmann transport theory, the Green's function approach, the force-balance approach, Feynman's path-integral approach and the projection operator approach. Alternatively, in similar methodologies by Zwanzig, by directly using a projection operator on the Liouville equation, Kenkre's group suggested a response function which contains Kubo's theory as the lowest-order approximation. The study of the quantum transport theories based on the projected Liouville equation method provides a useful tool for investigating the scattering mechanism of solids. Using the projected Liouville equation method with the Equilibrium Average Projection Scheme (EAPS), we have suggested a new quantum transport theory of linear-nonlinear form. The merit of using EAPS is that the quantum response function and the scattering factor formular can be obtained in a one step process by expanding the quantum transport (QTR) theory.

In this work, we investigate the optical Quantum Transition Line Shapes(QTLSs) of ZnS which show the absorption power and the Quantum Transition Line Widths(QTLWs) of ZnS, which show the scattering effect in the electron-piezoelectric potential phonon interacting system under circularly polarized oscillatory external fields. The analysis of the temperature and the magnetic field dependence of the QTLW is very difficult in alternative theories or experiment, because the absorption power in the various external field wavelengths is required to be calculated or observed. The QTR theory of EAPS is advantageous in this respect as it allows the QTLW to be directly obtained, through EAPS, in the various external field wavelengths. In short the calculation of the absorption power is not required to obtain the QTLW.

With the numerical calculation, we analyzed the temperature and the magnetic-field dependences of the QTLW and QTLS in various cases. In order to analyze the quantum transition, we compare the magnetic field dependencies of the QTLW and the QTLS on four transition processes, namely, the intra-leval transition process, the the inter-leval transition process, the phonon emission transition process and the phonon absorption transition process.

Effect of the Hand-hold Position on the EM Interaction of Clamshell-type Handsets and a Human

S. I. Al-Mously[1] **and M. M. Abousetta**[2]

[1]Department of Electrical and Electronic Engineering, School of Applied Sciences and Engineering
Academy of Graduate Studies, Tripoli, Libya
[2]Department of Electrical and Electronic Engineering, Faculty of Engineering
Al-Fateh University, Tripoli, Libya

Abstract— A thorough investigation into the effect of the hand-hold positions on the electromagnetic (EM) interaction of a clamshell-type cellular handset and a human is presented in this paper. A FDTDbased platform, *SEMCAD-X*, is used to achieve the simulations, where two semi-realistic handset models of different external-antenna attachment positions (left and right-side) are designed with the most parts configuration and operating at different GSM-frequency standards (GSM-900, GSM-1800/DCS, and UMTS/IMT-2000). Moreover, homogeneous and heterogeneous CAD models are used to simulate the user's head, whereas, a semi-realistic model with three different tissues is designed to simulate the user's hand-hold. The antenna performance, as well as, the specific absorption rate (SAR) in tissues are both examined for different (42) possible cases, where several antenna/hand positions are considered in simulation.

The simulation results show a significant decrease in the handset total efficiency due to the impact of holding the handset in close proximity to head, where a maximum reduction in the total efficiency is obtained at GSM-1800 frequency, about 94.2%. The maximum difference due to hand position change is obtained at UMTS/IMT-2000 frequency, about 32.1%. Moreover, the results demonstrate a considerable deviation in both values of SAR and power absorption in head-tissues owing to the hand presence at different positions, where the maximum percent difference in the $\mathrm{SAR}_{1\mathrm{g}}$ is obtained at UMTS/IMT-2000 frequency, about -61%.

Even though a user's hand has a negative impact on the antenna performance of a handset in close proximity to head, changing its position may reduce the amount of the induced SAR and power absorption in head-tissues. This reduction in the induced SAR and power absorption in head-tissues is also affected by the antenna position, as well as, the operating frequency, as the results show.

Impact of Human Head with Different Originations on the Anticipated SAR in Tissue

S. I. Al-Mously[1] **and M. M. Abousetta**[2]

[1]Department of Electrical and Electronic Engineering, School of Applied Sciences and Engineering
Academy of Graduate Studies, Tripoli, Libya
[2]Department of Electrical and Electronics Engineering, Al-Fateh University, Faculty of Engineering
Tripoli, Libya

Abstract— The impact of RF emissions of cellular handsets on the exposed human head with different originations is intensively investigated in this paper. Different realistic handset CAD models, i.e., candy-bar with external antenna and candy-bar with internal antenna, are hereby simulated with configuration of the most parts in order to achieve the commercially available handset model design. These handset models are simulated to operate in the GSM900 and GSM1800.

Four homogeneous head CAD models with non-pressed ears are involved in simulations, i.e., head models of thirty years old African female, thirty years old European male, thirty years old Latin American male and sixty years old European male.

A handset in close proximity to head at check position in compliance with the IEEE-Standard 1528–2003 is considered in calculations. To simulate a real non-pressed ear, every adopted homogeneous head model is considered as a single-tissue model having the similar dielectric properties of the Specific Anthropomorphic Mannequin (SAM)-Liquid.

A Finite-Difference Time-Domain (FDTD)-based platform, SEMCAD X, is used to compute the specific absorption rate (SAR) in human head models, in compliance with the ICNIRP Guidelines, associated with exposure to the handset RF emissions at 900 MHz and 1800 MHz with antenna radiated power of 250 mW and 125 mW, respectively.

For the same conditions, the difference in head model size, mass, ear thickness and ear level with respect to mouth due to different originations, show, first, different values of SAR in head tissue exposed to the handset RF emissions at the adopted frequencies, second, different impact on the handset antenna performance, i.e., input return loss, mismatch efficiency, radiation efficiency and the total isotropic sensitivity (TIS).

Application of New Algorithms of Electrical Impedance Tomography in Biomedicine

T. Kříž, J. Dědková, and E. Gescheidtová
Department of Theoretical and Experimental Electrical Engineering, Brno University of Technology
Kolejní 2906/4, Brno 612 00, Czech Republic

Abstract— This paper describes an usage of new techniques to solve electrical impedance tomography (EIT) inverse problem in the biomedical engineering. Usually, a set of voltage measurements is acquired from the boundaries of an investigated volume, whilst this is subjected to a sequence of low-frequency current patterns. In principle, measuring both the amplitude and the phase angle of the voltage can result in images of the electric conductivity and permittivity in the interior of a body. It is well known that while the forward problem is wellposed, the inverse problem is nonlinear and highly ill-posed. The recently described methods are based on deterministic or stochastic approach to solve mainly 2D problems. The aim of this paper is to introduce new techniques of reconstruction of EIT images for their using in a biomedicine. New techniques, which make use of combination of well known methods for reconstruction EIT images (Total Variation Method and Tikhonov Regularization Method) and method used for image segmentation. This way enable exactly specify boundaries of an area with a known conductivity. In this paper are used new techniques for a specification of a human tissue, based on the tissue conductivity. Numerical results of the reconstruction based on new methods are presented and compared.

REFERENCES

1. Cheney, M., D. Isaacson, and J. C. Newell, "Electrical impedance tomography," *SIAM Rev.*, Vol. 41, No. 1, 85–101, 1999.
2. Olmi, R., M. Bini, and S. Priori, "A genetic algorithm approach to image reconstruction in electrical impedance tomography," *IEEE Trans. Evol. Comp.*, Vol. 4, 83–88, 2000.
3. Borsic, A., "Regularization methods for imaging from electrical measurement," PhD. Thesis, Oxford Brookes University, 2002.
4. Burger, M., "A level set method for inverse problems," *Inverse Problems*, Vol. 17, 1327–1356, 2001.

Using Electromagnetic Microwave Field in Treatment of Lumbar Pain

L. Rabenok[1], **Noe Oroza Hernandez**[1], **and Jesús Escobedo Alatorre**[2]

[1]IMSS, Plan de Ayala, Cuernavaca, Morelos, Mexico
[2]CIICAp, Autonomous University of Morelos State (UAEM), Cuernavaca, 62209, Mor., Mexico

Abstract— The authors analyzed the results of a treatment of 28 patients with a lumbar pain. The patients with a lumbar pain underwent a method of treatment using electromagnetic microwaves field (EM). We used a portable apparatus that operates in the millimeter (mm) wave range in 4 regimes. The intensity of EM radiation was 2–10 mW/cm^2. A peculiarity of the method was an absence of any pharmaceutical medicine. The exposure of the radiation was 10 min. The total course included 7–10 procedures. An application of low intensity EM radiation was started to the biological active points of acupuncture (VG3, VG4, VB30) in the sedative regime (the repetition rate 9–10 Hz) during 10 min. Clinical symptomatology, radiographic findings were analyzed as well. The results were acknowledged to be satisfactory, there were no complications. A pain disappear, movements in vertebral column have improved. We consider the use of low intensity electromagnetic radiation to be effective in the treatment of patients with a lumbar pain.

Real-time Measurement of Air Ion Spectrum Using Gerdien Tube with Segmented Inner Electrode

Z. Roubal, M. Steinbauer, Z. Szabó, and R. Kubásek
Department of Theoretical and Experimental Electrical Engineering
University of Technology Brno Kolejni, 4, 612 00 Brno, Czech Republic

Abstract— The gerdien tube measurement method is useful to measure spectrum of air ions. In a standard type of the gerdien tube with non-segmented electrode we must change voltage in the time. The disadvantage of this method is impossibility of real time measurement because the measurement is very time-consuming. Using the segmented inner electrode, it is possible to measure the air ions spectrum without necessity of the time variant voltage between the electrodes. This paper deals with a mathematic analyze and numerical modeling of ions trajectories in the gerdien tube with the segmented inner electrode. The method of computing of the distribution of air ions mobility from currents measured on each of electrodes will be shown.

REFERENCES

1. Charry, J. M. and R. Kavet, *Air Ions: Physical and Biological Aspects*, CRC Press, Inc., Boca Raton, Florida, 1987.
2. Bartušek, K., "Merení spektrálních charakteristik iontových polí," http://www.elektrorevue.cz/clanky/01038/index.htm.
3. Vojtek, T., T. Skoupil, P. Fiala, and K. Bartusek, "Accuracy of air ion field measurement," *PIERS Online*, Vol. 2, No. 4, 412–415, 2006.

Interaction between a Triple Band Handset Antenna and Human Head by Applying Various Head Models

D. Davoodi, P. Saghatoleslami, and M. A. Ebrahimi-Ganjeh
Sadjad Instate of Higher Education, Mashhad, Iran

Abstract— The interaction between human head tissues and handset antennas is a crucial concept in mobile communications. This paper presents a comprehensive study on the performance of a triple band PIFA antenna designed for operating in DCS, PCS and UMTS frequency bands, next to various human head models. Radiation patterns and VSWR of this antenna are computed in free space as well as in the presence of head models. Three different models are investigated: a spherical six layer model, a glass sphere model and a flat phantom. for six layer model and the glass phantom a 82 percent scaled model is also used in order to examine the interactions in presence of a child's head (seven years old). All the simulations are done for three different distances between the antenna and the model (5 mm, 15 mm, 25 mm). The specific absorption rate (SAR) is calculated in the glass sphere model. In addition, radiation efficiencies of the handset antenna is computed in the presence of head. All numerical simulations are performed using the Ansoft HFSS software. For validation of the numerical simulations, the simulated peak 1 g-SAR in the glass sphere model is compared to measured 1 g-SAR.

Use of Magnetic Resonance to Determine Radial Slices of Plants

K. Bartusek[1], **E. Gescheidtova**[2], **and Z. Dokoupil**[1]

[1]Institute of Scientific Instruments, Academy of Sciences of the Czech Republic
Kralovopolska 147, Brno 612 00, Czech Republic
[2]Faculty of Electrical Engineering and Communication, Brno University of Technology
Kolejni 2906/4, Brno 612 00, Czech Republic

Abstract— Magnetic resonance (MR) enables studying the motion of liquids in the stalks of plants via radial slices of plants. MR is a non-destructive examination method but its drawback is lower resolution (100 μm) and higher image noise. Its advantage is the possibility of obtaining images weighted by relaxation times and diffusion. Making use of subsequent image processing, new information can be obtained on the plant structure and motion of liquids through the plant.

Radial MR images were obtained using the classical SE sequence with the following parameters: spin echo time $T_{\mathrm{E}} = 11\,\mathrm{ms}$, repetition time $T_{\mathrm{R}} = 1.5\,\mathrm{s}$, matrix dimension 256×256 pixels (26×26 mm with a resolution of 100 μm/pixel), layer thickness $d = 3$ mm, and without averaging operation. There is a connection between the signal-to-noise ratio and the size of the image being measured. The repetition time is equal to the spin-lattice relaxation time and the measurement time equals $256\,T_{\mathrm{R}}$. To reduce noise in the image, wavelet filtering with optimally chosen functions is used.

The samples of scanned vegetables were prepared at Mendel University of Agriculture and Forestry in Brno. The experiments were carried out on an 4.7 T/120 mm MR tomograph system (i.e., 200 MHz for ^{1}H nuclei) with actively shielded gradient coils ($G_{\max} = 180\,\mathrm{mT/m}$). The data measured were processed in the MAREVISI and MATLAB programs.

Post-acquisition processing of images enhances vascular bundles and various image contrasts. Relaxation time T_2 is calculated for the images $M_1(x, y)$ and $M_2(x, y)$ measured for different echo times T_{E1} and T_{E2} from the relation $T_2 = (T_{\mathrm{E1}} - T_{\mathrm{E2}})/\{\ln[M_1(x, y)] - \ln[M_2(x, y)]\}$. For the chosen parameters of the pulse sequence the diffusion contrast in the image is given by the relation $D = \ln(\frac{M_{G_{\mathrm{D}}} M_{-G_{\mathrm{D}}}}{M_0 M_0})/(-6\gamma^2\delta^2(\Delta - \frac{\delta}{3})G_{\mathrm{D}}^2)$.

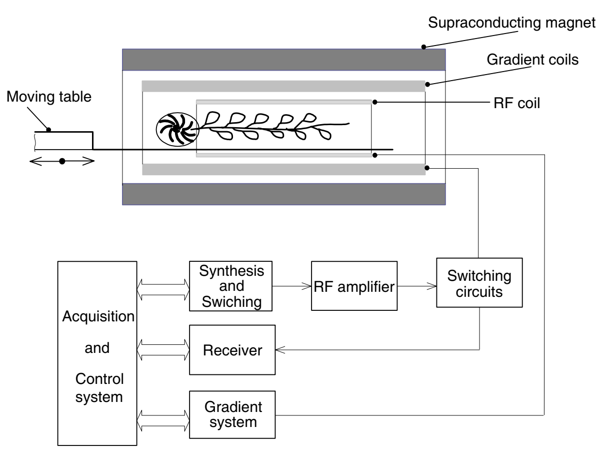

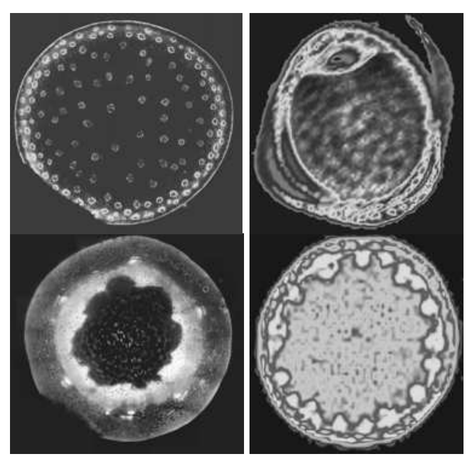

Figure 1: Schematic of MR measurement lay-out. Examples of slices through maize stalk: top left — image obtained by classical method, top right — MR image. Bottom left — classical image of slice through sunflower stalk, bottom right — MR image.

ACKNOWLEDGMENT

This work was supported within the framework of the research plan MSM 0021630513 and project of the Grant Agency of the Czech Republic No. 102/07/0389.

REFERENCES

1. Scheenen, T., et al., “Functional imaging of plants: A NMR study of a cucumber plant,” *Biophysical Journal*, Vol. 82, 481–492, 2002.

Distribution and Influence of Magnetic Field Applied in Magnetotherapy. Analysis of Selected Issues

Antoni Cieśla, **Wojciech Kraszewski**, **and Przemysław Syrek**
Department of Electrical and Power System Engineering
AGH University of Science and Technology, Al. Mickiewicza 30, Cracow 30-059, Poland

Abstract— Clinical investigations on advantages of magnetotherapy are run since many years. Small coil applicators may be also helpful in process of rehabilitation conducted home. Magnetotherapy in overwhelming majority of cases, is very helpful and advisable, but there are yet some situations in which it may pose a threat. In the paper, few aspects and cases are presented and also relationship of distance between fracture and cured areas is evaluated.

There is an interaction between condition of living organisms and magnetic field affecting them. Strong magnetic field may be harmful. People exposed to magnetic field, working in surroundings of electric machines a few hours a day or living next to high-voltage lines, are subject to the risk of many ailments, e.g., headache, distortion of heart rhythm; in extreme case, magnetic field can induce serious diseases like tumour.

Magnetotherapy brings opposite effects. Magnetic field with correctly selected parameters (intensity, time of exposition, frequency) stimulates cured parts of organism.

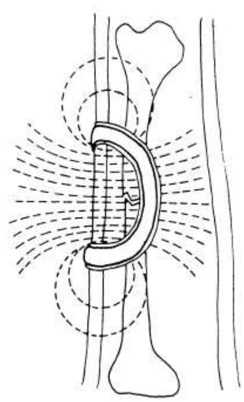

Figure 1: Line forces of magnetic field induced through small coil applicator.

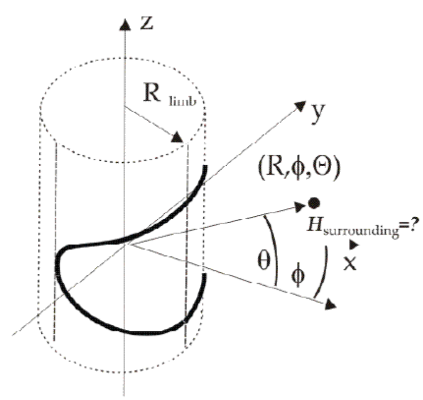

Figure 2: Geometric description of field in two coordinate systems.

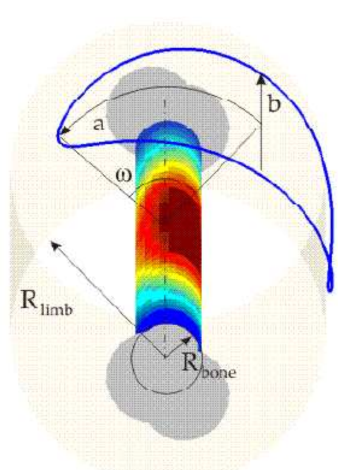

Figure 3: Magnetic field distribution on the limb surface.

Description of analyzing space is presented on Fig. 1. In case of field on bone's surface cylindrical coordinates are very convenient. Field around the coil is characterized by spherical coordinates (center is put on z-axis in point meaning center of broken bone).

Cured persons have the opportunity to put applicators on broken limbs and use them at home single-handedly in every of three-dimensional orientation (it refers especially to fractures of upper limbs). Coil may be oriented in way, that maximum of magnitude (in analyzed surface) influences on banned areas. That's why during estimating the influence of distance between coil and banned areas it is so important to take into consideration a maximum magnitude of field that can appeared.

Field distribution (and its affecting) on surface of broken limbs are presented on Fig. 2. Small coil applicators (of selected shapes) are put on broken limb in suitable point. It secures correct distribution of field inner the limb.

Consideration of influence of magnetic field in surrounding of applicator (depended on distance), is held with additional parameter — average value of magnetic field in segment of broken bone:

$$H_{AVG} = \frac{1}{V} \iiint\limits_V H(x, y, z) dV$$

Way of evaluating the influence of magnetic field around of applicator, is initial method of estimating values used in magnetotherapy of fractures combined with other ailments or pregnancy. Every event needs to be considered separately and with respect of specific situation.

Finite Size Effect on the Resonant Microwave Absorption of Er^{3+} Doped Ag Nanoparticles

J. M. Vargas[1], **W. Iwamoto**[1], **L. M. Holanda, Jr.**[1], **P. G. Pagliuso**[1], **C. Rettori**[1], **and S. B. Oseroff**[2]

[1]Instituto de Física "Gleb Wataghin", UNICAMP, Campinas-SP, 13083-970, Brazil
[2]San Diego State University, San Diego, California 92182, USA

Abstract— The study of surface and finite size effects in nanoparticles (NPs) is a subject of growing interest today in nanoscience from both, academic and technological point of view. Despite the large number of investigations, still there are many open questions about the surface and size influence on the microwave absorption in metallic NPs.

In particular metallic Ag and Au systems in the nanoscale regime show striking features that are not observed in the bulk counterparts, for example, ferromagnetic properties are reported in Au NPs coating by protective agents, such as dodecane thiol [1].

Electron spin resonance (ESR) is a powerful technique because it may provide information about CF effects, RE ground state, site symmetry, valence of the paramagnetic ions, g-value, fine and hyperfine interaction, in a wide variety of doped magnetic compounds. Moreover, the ESR spectra of the magnetic doped ions allow not only to learn about the doped ion, but also about the properties of the host lattice.

In this work we show that by ESR experiments between 4.2 K and 15 K it is possible to observe the microwave resonant absorption of Er^{3+} impurities doped in Ag host NPs with size down to 20 nm. These results are compared with the ESR data of Er^{3+} impurities doped in Ag metallic bulk. Metallic Ag NPs of 25 nm to 200 nm, doped with $\sim 4\%$ of magnetic Er impurities, were prepared by chemical route via co-thermolysis of Silver nitrate and $Er(CF_3COO)_3$ precursor in Oleylamine/Oleic acid surfactant and phenylehter solvent [2].

The main features revealed by the microwave resonant absorption in the Ag:Er NPs were: i) the g-value of 6.8 and the hyperfine constant are about the same as those in the bulk material: ii) the lineshape of the microwave resonant absorption goes from dysonian shape (microwave skin depth $\ll$ particles size) to lorentzian shape (microwave skin depth $\gg$ particles size) as the size of the particle decreases; iii) the thermal broadening of the microwave resonant absorption linewidth, $\Delta H/\Delta T$, decreases from ~ 7 Oe/K to ~ 0 Oe/K as the size of the particles decreases. The analysis of these results allowed us to conclude that the Kramers doublet Γ_7 ground state of the Er^{3+} crystal field splitted $J = 15/2$-multiplet remains the same in the NPs as in the bulk material [3]. Therefore, no change in the local crystal and hyperfine fields at the Er^{3+} site was observed. However, the striking result was that the usual Er^{3+} spin-lattice relaxation, via an exchange interaction with the conduction electrons (Korringa mechanism) [3], monotonically decreases with the size of the particles. This property make the Ag:Er NPs suitable for potential applications in Ag:Er NPs doped quartz fibers and optical devises. A discussion about the influence of the conduction electrons spin-flip scattering at the particles surface on the Korringa relaxation mechanism will be given.

REFERENCES

1. Hori, H., Y. Yamamoto, T. Ywamoto, T. Miura, T. Teranishi, and M. Miyake, *Phys. Rev. B*, Vol. 69, 174411, 2004.
2. Tang, Y. and M. Ouyang, *Nature Materials*, Vol. 6, 754, 2007.
3. Davidov, D., C. Rettori, A. Dixon, K. Baberschke, E. P. Chock, and R. Orbach, *Phys. Rev. B*, Vol. 8, 3563, 1973.

Damaging Effect of Electromagnetic Field on Tumour Cell Membrane by Scanning Electronic Microscopy and Scanning Tunneling Microscopy

Run-Guang Sun, **Hao Qi**, **and Jing Zhang**
Laboratory of Biophysics and biomedical Engineering
College of physics and Information Technology, Shaanxi Normal University
P. O. Box 18-3-12, Xi'an 710062, China

Abstract— The effect of electromagnetic field on tumour cell membrane has been studied by scanning electronic microscopy (SEM), scanning tunneling microscopy (STM) and MTT analysis. The experiments show that the surface of tumour cell membrane is smooth in the photograph of scanning electronic microscope. There are a lot of openings and holds on the surface of tumour cell membrane under the effect of electromagnetic field. More and holds were observed with increase of the intensity of electromagnetic field. It is not well distributed that the holds, big or small, are dispersed over the surface of tumour cell membrane, which are caused by the electromagnetic field. They may relate to the big or small shape of proteins that are dispersed over the surface of tumour cell membrane. High damaged rate was also detected with increase of the intensity of magnetic field. Lower survival rate and high damaged effect was found when it was prolonged that tumour cells were exposed to the electromagnetic field. The magnetoporation relate to the intensity of electromagnetic field and the time that tumour cells were exposed to the magnetic field.The motion of peripheral orextrinsic proteins is caused by the effect of electromagnetic field so that the peripheral or extrinsic proteins are lost away. Some hold and damage tracks are observed on the surface of tumour cell membrane.

Diagnostic Volume Phenomenon in Noninvasive Medical Spectrophotometry and a Simple Theoretical Definition of That

D. A. Rogatkin, L. G. Lapaeva, and E. N. Petritskaya
Moscow Regional Research & Clinical Institute "MONIKI", RF, Russia

Abstract— In recent 10–15 years a general medical practice has been successfully enriched with different new methods of noninvasive optical diagnostics such as a Laser-Doppler Flowmetry, Laser Fluorescent Diagnostics, Tissues Reflectance Oximetry, etc., which all in totality we now call a *Noninvasive Medical Spectrophotometry* (NMS). All these methods allow a doctor to evaluate *in vivo* and more exactly a clinical condition of soft tissues, especially to study finenesses of respiratory and blood microcirculation processes in a skin or mucosa. NMS technique is based on the dependence of photometric properties of biological tissues and liquids (spectral coefficients of absorption, scattering, fluorescence, etc.) on the anatomical and morphological structure of the tissue as well as on the content of various biochemical components (hemoglobin, collagen, fat, water, natural porphyrins, etc.) in it. Regarding a quantitative evaluation of volume concentration of different biochemical substances in tissues by NMS methods, while conducting comparative (relative) measurements in the pathological area and in a chosen intact point on patient's body, it is necessary for the depth of penetration of radiation in the object being researched to be the same every time. At least, during each diagnostic measurement, the doctor needs to have an opportunity to evaluate the effective volume of biological tissue, from which the main useful signal arrives into the registration system. Thus, it is necessary to have an opportunity to evaluate the so called "sampling volume" or "*diagnostic volume*" (DV) of the object being studied during the experiment. In a case of any functional or physiological changes caused by the sickness in biological tissues, their DV will change as a result of change of optical properties of blood, changes of the blood fraction in the volume of examination, changes of optical properties of the skin, etc. That is why the evaluation and determination of DV are extremely important in the practice of NMS.

Nowadays the notion of DV has not yet been strictly determined and widely accepted in biomedical optics. This is the reason why in our research it has been specifically introduced and defined. We have defined the notion of DV as "*an effective volume of biological tissue (the medium of propagation of radiation) in the area being tested, which brings in the registered optical signal at least $P_{\min}$ of power, where $P_{\min}$ is estimated at a 75–95% level of the total power of radiation being registered from the biological tissue (signal evaluation by the level of 0.75 (P 0.75), the level of 0.95 (P 0.95) etc.)*". This definition potentially allows anyone to evaluate DV which is reached in the experiment in the strict terms of physics-mathematical models of the Radiative Transport Theory. For a purpose of creation of the first simplified theoretical model, describing DV in NMS, the theoretical problem of one-dimensional distribution of optical radiation in a macro-homogeneous turbid medium with multiple scattering has been considered with the use of modified Kubelka-Munk approach (KM). The formulation of the task: to find such an effective depth H of scattering medium with predefined transport optical properties K and S (absorption and scattering in the terms of KM model) from which the backscattered radiation $P_{\min}(H)$, being registered by the NMS device, constitutes a part of $\gamma = 0.9$–0.95 of the total backscattered radiation P_{bs} from a semi-infinite medium (the medium of the geometrical depth significantly exceeding H). In the most simple and explicit case $K = 0$. So, in a case of unit stream of outer radiation, the effective H values for typical biological tissues will range 0.16–19 cm. It is necessary to note, that for every separate wavelength λ the DV will differ because of the dependence of $S(K)$ on λ. Analogous assessments in the general case of light-scattering medium with absorption $K \neq 0$ we have made as well. As the results of calculation have shown, the presence of absorption in a medium significantly decreases the effective DV. If transport optical properties of a biological tissue are not known *a priory*, the only way out while defining DV is to evaluate DV directly from the results of the experiment.

The Use the Strong Magnetic Field to Biostymulation Pre-sowing Seed

Antoni Cieśla and Mikołaj Skowron
Department of Electrical and Power System Engineering
AGH University of Science and Technology, Al. Mickiewicza 30, Cracow 30-059, Poland

Abstract— The influence of magnetic field on alive organisms as well as on germination of seeds and growth of plants was already known in the XIX century. The fast increase of the interest in influence and utilization of the magnetic field to biostimulations developed in second half of the XX century.

The authors of the article propose to add mathematical description of the grain of wheat co-ordinate oblate spheroids. The description of shape grain in this arrangement of co-ordinates will be the answer for the real best shape. The calculations of the distribution of the magnetic field are led in grain and around him in the received arrangement of co-ordinates.

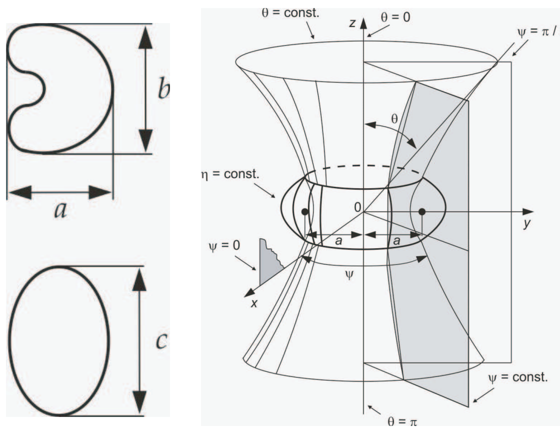

(a) (b)

Figure 1: (a) Projections and basic dimensions grain: a — thickness, b — width, c — the length, (b) co-ordinate oblate spheroids.

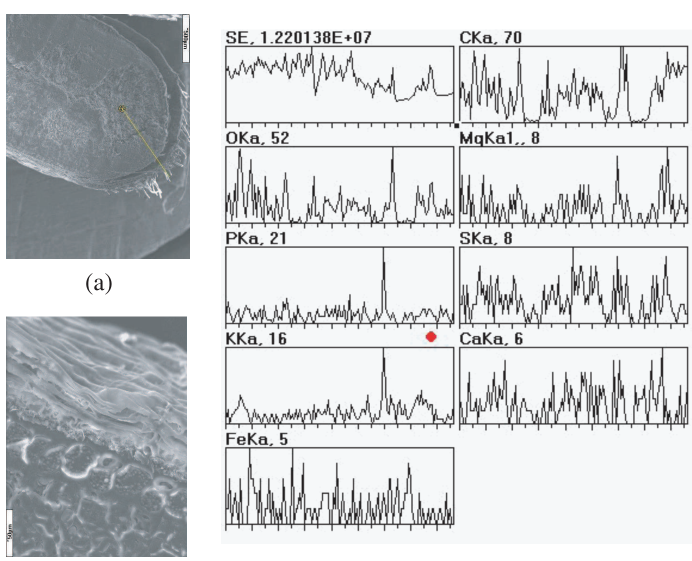

(a) (b) (c)

Figure 2: Foto grain wheat made with using of a skaning microscope (a) magnified 50 times, (b) magnified 500 times, (c) chemical elements inside it.

The real shape grain was introduced on Fig. 1(a).

The dimensions of seeds differ from each other in dependence from weather conditions at the given year, soil conditions, the species of the cereal. They contain in range: thickness 2.26–3.09 mm, width 2.59–3.65 mm, length 5.72–6.60 mm. The considered grain has the form to oblate, paramagnetic spheroid. It consists of the core and two surrounding layers, as: layer endosperm aleuron and seed fruit cover.

We should mark inside and outside the distribution of the magnetic field in the received arrangement of co-ordinates and in the geometry of the arrangement grain.

$$\nabla^2\phi = \frac{1}{a^2(\cosh^2\eta - \sin^2\theta)}\left(\frac{\partial^2\phi}{\partial\eta^2} + \mathrm{tgh}\eta\frac{\partial\phi}{\partial\eta} + \frac{\partial^2\phi}{\partial\theta^2} + \mathrm{ctg}\theta\frac{\partial\phi}{\partial\eta}\right) + \frac{1}{a^2\cosh^2\eta\sin^2\theta}\frac{\partial^2\phi}{\partial\Psi^2} = 0$$

We use the Laplace equation for that purpose. In co-ordinate of oblate spheroid the Laplace equation has the following form (1). Co-ordinate oblate spheroids introduced on Fig. 1(b).

The authors made some research on grain wheat using a skaning microscope. The aim of this research was to observe the structure of the grain and of the chemical elements inside it. The result can be seen on the Fig. 2.

This research let to create a model of the observed grain and to place it in a magnetic field.

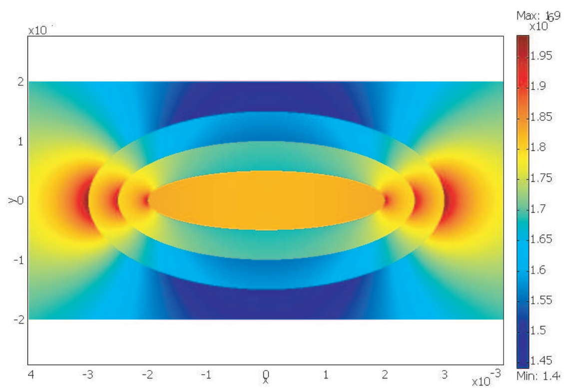

Figure 3: The distribution of the energy of the magnetic field for whole grain.

The Effect of Weak Low-frequency Magnetic Field in Combination with Collinear Constant Geomagnetic Field on the Activity of Peroxidase in Water Solutions

E. V. Yablokova, **G. V. Novikov**, **V. V. Kuvichkin**, **V. V. Novikov**, **and E. E. Fesenko**
Institute of Cell Biophysics, Russian Academy of Sciences, Russia

Abstract— Recently a series of convincing experimental and theoretical studies demonstrating involvement of reactive oxygen species (ROS) in realization of biological effects of weak magnetic fields (Novikov, Fesenko, 2001; Ponomarev, Novikov, 2009) have been reported. In this line studying the effect of weak magnetic fields (MF) on enzymatic systems of generation and degradation of ROS seems especially of current importance.

Exposure of combined action of weak permanent (42 μT, geomagnetic range) and alternating (80–250 nT, frequencies in a range of 4.4 and 16.5 Hz) magnetic fields is shown to have an influence on reaction rate in course of oxidation of o-phenylendiamine by hydrogen peroxide where a catalyst is the enzyme of horseradish peroxidase. In comparison with control samples, the activity of horseradish peroxidase changes significantly in a reaction if enzyme solutions are exposed to magnetic fields. The observed effect depends on a number of physico-chemical parameters during reaction. Salt composition of water solution, temperature and pH have effect on change of enzyme (peroxidase) activity after exposure to magnetic field. How the reaction depends on components concentration has been investigated. It should be pointed out that maximum changes of enzyme activity exposed to MF are registered when high purity water is used as medium. In buffer solution in the presence of salts changes of horseradish peroxidase activity become considerably weaker after exposure to magnetic field but in a number of cases no activity is found at all. It has been demonstrated that action of magnetic field has no effect on reaction process if components of reaction mixture, such as hydrogen peroxide and solution of some salts have been exposed. Most probably that a decrease of horseradish peroxidase activity exposed to MF is related to conformational alterations of a structure of this protein since spectra of its fluorescence (intrinsic and in the presence of fluorescent probes) differ.

Thus, this study describes changes of structural and functional properties of peroxidase water solutions as a result of exposure of extremely weak magnetic fields. This may provide a basis for investigation of properties of another enzymes involved in regulation of ROS concentrations.

Look at the Spark Cross Size Development in a Sliding Submicrosecond Discharge from the Theory of Ionization Wave Front Propagation

K. K. Trusov
P. N. Lebedev Physical Institute of RAS
Leninsky prospect 53, Moscow 119991, Russia

Abstract— The work is aimed at studying the initiation, development and scaling of multichannel and quasi-homogeneous pulse high-current sliding discharges in gases, and assumes the analysis of both the separate channel formation and their structure in the discharge gap. In this report the results from experimental measurement of the spark channel widths in sliding multichannel discharge of opposite polarities in Ne, Ar and Xe are presented and discussed. The experiments were performed at submicrosecond discharge pulse duration ($50 \div 200$ ns) and gas pressures of 30 and 100 kPa, with alumina ceramics as the dielectric substrate. The data showed the optical width of the channels at negative voltage supply polarity to be $1.27 \div 1.6$ times greater than that at positive polarity, depending on the gas type and its pressure. The earlier theoretical study by U. Ebert, W. van Saarloos and C. Caroly on the propagation of opposite polarity ionization wave fronts in gases was applied to the experimental results analysis. The registered difference between the widths of opposite polarity channels and the estimations prove our earlier viewpoint of a negligible effect of electron diffusion process (as compared to the electron drift) on the channel cross expansion within the pulse duration studied. From two approaches of the above pointed theory only the "nonlocalized initial conditions" one can reasonably explain: a) the interrelation between the channel optical width and the electron mobility that was revealed in our previous experiments; b) experimental ratios of the widths of negative-to-positive channels; c) comparatively short (≤ 0.5 ns) and approximately equal time intervals of channel cross expansion for the gases and their pressures studied; d) expansion of the negative polarity channels with a velocity not less (but actually exceeding) than the electron drift velocity in the transverse electric field round the spark channel. Numerical solutions of the channel expansion equation specified that the channel expansion velocity is set by both the drift electrons and free electrons generated by a short-range source in a narrow layer ahead of the channel expansion wave front. The depth of the latter layer was estimated to be comparable to the wave front depth and, thus, much less than the channel radius. The most probable source of free electrons round the channel is gas photoionization by the radiation from the channel.

Modeling of Two-component Plasma Dynamics in Near-wall Region of Charged Probe with Coulomb Collisions

I. A. Kudryavtseva and A. V. Panteleyev
The Moscow Aviation Institute (State Technical University), Russia

Abstract— One of low-temperature plasma diagnostics methods is the probe diagnostics [1, 2]. Edge plasma dynamics in disturbed area near the probe on the stipulation that the ratio of free length of particles to probe curvature radius (Knudsen number) is equal to 1 is researched in the article. In this case consideration to collisions between charged particles and neutral atoms and Coulomb collisions must be given. Models with collisions between charged particles and neutral atoms are viewed in detail [2]. In this paper, the model considering ion collisions and ion-electron collisions influence on measured plasma parameters is developed.

The charged probe is immersed into undisturbed plasma consisting of electrons and single charged ions. Suppose, on the probe surface the condition of ideal absorption is obeyed. Temperatures and concentrations of particles in undisturbed plasma are defined. Initial distribution functions are Maxwellian. In the paper, three geometric shapes of probe are observed. These are plane, cylinder and sphere.

The mathematical model of the problem including the Fokker-Planck equation and Poisson equation. The Fokker-Planck equation describes particles transport processes and charged particles collision processes. The Poisson equation is used for describing external electric field influence on plasma particles.

The solution method of the problem for different probe shapes described above is based on the Monte-Carlo Method [3]. The Fokker-Planck equation should be replaced by the stochastic differential equation (Ito equation). The stochastic Euler method is used for solution of Ito equation. The solution of Poisson equation for the flat probe is found by using of finite-difference approximation. In the case of cylindrical and spherical probes the variable separation method (the Furrier method) is applied. The algorithm based on described solution method is constructed. The program consisting of three modules for plane, cylinder and sphere-shaped probe is built. In computational experiments dynamics of particles current density, self-consistent electric field intensity, concentrations of particles are obtained, and graphics of current-voltage characteristics of probes are illustrated.

REFERENCES

1. Bernstein, I. B. and I. N. Rabinowitz, "Theory of electrostatic probes in low-density plasma," *Phys. Fluids*, Vol. 2, No. 2, 112–121, 1959.
2. Alekseev, B. V. and V. A. Kotel'nikov, *The Probe Method of Plasma Diagnostics*, Energoatomizdat, Moscow, 1988 (in Russian).
3. Kudryavtseva, I. A. and A. V. Panteleyev, "The applying of the Monte-Carlo Method for analysis of two-component plasma behavior with charged particles collisions," *The Collection of MIREA*, 122–128, 2008 (in Russian).

Metamaterials with Tunable Negative Refractive Index Fabricated from Amorphous Ferromagnetic Microwires: Magnetostatic Interaction between Microwires

A. V. Ivanov[1], **A. N. Shalygin**[1,2], **V. Yu. Galkin**[2], **A. V. Vedyayev**[1], **and K. N. Rozanov**[3]

[1]M. V. Lomonosov Moscow State University, Moscow, Russia
[2]R & P Vichel (High-frequency Systems), Moscow, Russia
[3]Institute for Theoretical and Applied Electromagnetics of the RAS, Moscow, Russia

Abstract— For a few recent years, new developments in artificially structured materials giving rise to negative refractive index $n = \sqrt{\varepsilon(\omega) \cdot \mu(\omega)} < 0$ with simultaneously negative real parts of frequency dependent permittivity $\varepsilon(\omega)$ and permeability $\mu(\omega)$ in some frequency ranges have been attracting much attention. They are named left-handed materials [1–3], negative-index mediums, negative phase-velocity mediums (NPVM), backward wave mediums or even double negative media. Recently developed *homogeneous NPVM* have been paid much attention in journals and press. For NPVM anomalous effects such as negative refraction, Doppler shift, Cherenkov-Vavilov radiation, light pressure, invisibility effect have been discovered in different frequency ranges. For them the gyrotropic phenomena are possible as well [4–6]. But other electromagnetic effects such as optical Magnus effects are given by a circular polarization of propagating waves and ∇n. In the presentation, the optical circular polarized effects are calculated for inhomogeneous mediums. It is shown that these are anomalous in NPVM with respect to right-handed materials. The proposed metamaterials fabricated from glass coated amorphous ferromagnetic Co-Fe-Cr-B-Si microwires [7] are shown theoretically [8] and experimentally [9] to exhibit a negative refractive index for electromagnetic waves over scale of GHz frequencies. The magnetostatic interaction between microwires has been taking into account by calculating of magnetic field excited by each other microwires. Optical properties of such metamaterials are tunable by an external magnetic field, magnetic field from neighbourhood microwires and mechanical stress. The work is supported by RFBR Project 08-02-00830-a.

REFERENCES

1. Veselago, V. G., *Soviet Physics — Uspekhi*, Vol. 10, 509, 1968.
2. Veselago, V. G., *Uspekhi Fizicheskih Nauk*, Vol. 92, 517, 1967 (in Russian).
3. Veselago, V. G., *ZHETF*, Vol. 52, 1025, 1966.
4. Lindell, I. V., S. A. Tretyakov, K. I. Nikoskinen, et al., *Microwave and Opt. Tech. Lett.*, Vol. 31, 129, 2001.
5. Mackay, T. G. and A. Lakhtakia, *Phys. Rev. E*, Vol. 69, 026602, 2004.
6. Ivanov, A. V., O. A. Kotel'nikova, A. V. Vedyayev, et al., *JMMM*, Vol. 300, 67, 2006.
7. Molokanov, V. V., P. P. Umnov, N. V. Kurakova, et al., *Perspektivnye Materialy (in Russian), (Journal of Advanced Materials)*, No. 2, 5, 2006.
8. Ivanov, A. V., A. N. Shalygin, A. V. Vedyayev, et al., *JETP Lett.*, Vol. 85, 565, 2007.
9. Ivanov, A. V., V. Yu. Galkin, V. A. Ivanov, et al., *Solid State Phenomena*, Vol. 152–153, 333, 2009.

Optical Response of a Multilayer System with Strongly Anisotropic Thin Films as Nonmagnetic Negative Phase Velocity Materials

X. I. Saldaña and Gregorio H. Cocoletzi
Instituto de Física, Universidad Autónoma de Puebla, Apartado Postal J-48, Puebla 72570, México

Abstract— The predictions made by V. Veselago [1] in 1968 of novel properties for materials having dielectric permittivity and magnetic permeability simultaneously negative, have been the focus of attention in the past decades. In these materials the propagation wave vector points in an opposite direction to the Poynting vector. In a resent work [2] it has been demonstrated the possibility of inducing a negative phase velocity propagation of light in a strongly anisotropic film considering that the incident light comes from a medium with a refractive index $n_1 > 1$ at an incident angle which depends on the dielectric constant characterizing the anisotropic film. In this work we study the possibility of obtaining a negative phase velocity propagation of the electromagnetic radiation in a periodic multilayer medium whose unit cell consists of two dielectrics; one isotropic and the other a strongly anisotropic one. For this purpose, we calculate the optical properties of the multilayer system using the transfer matrix method.

REFERENCES

1. Veselago, V. G., *Usp. Fiz. Nauk*, Vol. 92, 517, 1967; [*Sov. Phys. Usp.*, Vol. 10, 509, 1968].
2. Hernández, P. H., G. Martínez, G. H. Cocoletzi, H. Azucena-Coyotecatl, and J. Díaz-Hernández, *J. Appl. Phys.*, Vol. 101, 093103, 2007.

Ventilation Efficiency and Carbon Dioxide (CO_2) Concentration

M. N. Halgamuge[1], **T. K. Chan**[2], **and P. Mendis**[1]

[1]Department of Civil & Environmental Engineering, The University of Melbourne
Parkville, VIC 3010, Australia
[2]Faculty of Architecture, Building & Planning, The University of Melbourne
Parkville, VIC 3010, Australia

Abstract— This study will analyze the ventilation efficiency of student lecture halls. Analytical and experiments will be performed to investigate health effect such as pollutant distribution, shortness of breath, unconsciousness, muscular pain due to high carbon dioxide concentration.

Introduction: The most periodic found gases on the earth is carbon dioxide (CO_2) [1]. This produces from natural metabolism of living organisms and combustion processes. We inhale oxygen (O_2) and exhale carbon dioxide. As in [1], indoor CO_2 levels in general vary between 400 and 2000 ppm (parts per million) while outdoor CO_2 levels are 350–450 ppm and also heavily industrialized or contaminated areas may occasionally have a CO_2 concentration of up to 800 ppm. Moreover with very heavy traffic area the levels of outdoor CO_2 are higher.

Expected Results & Discussion: Our aim here is to study analyze the ventilation efficiency to investigate health effect student lecture halls. We have developed a sensor network in indoor or outdoor setting. The recorded out door CO_2 level at out side office room for 24 hours is shown in Figure 1. From our pilot project, it was observed that the CO_2 level is above the air quality standards as indicated in [1]. Figure 1 shows the CO_2 level between 9.00 AM and 3.00 PM on February 15 is higher than 500 ppm which is bit higher.

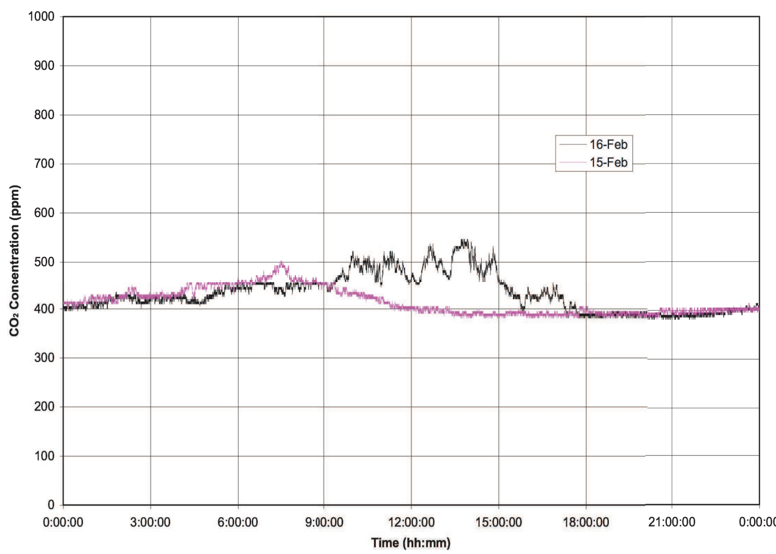

Figure 1: The recorded out door CO_2 level at out side office room for 24 hours. This higher CO_2 level is due to forest fires in Melbourne, Victoria recently.

REFERENCES

1. Egeland, A. and H. Martin, "Research & development, production of gas sensors with IR-technique," *Sense Air AB*, No. 10, 1–7, 1993.

Consensual Modeling for Synthesis of the Microwave Transmission Lines

Nurhan Türker Tokan[1], **Filiz Güneş**[1], **and Fikret Gürgen**[2]

[1]Department of Electronics and Communication Engineering, Yıldız Technical University
Beşiktaş, Istanbul 34349, Turkey
[2]Department of Computer Engineering, Bogazici University
Bebek, Istanbul 80815, Turkey

Abstract— The drive in the electronics industry for manufacturability driven design and time to market, coupled with ever-increasing circuit complexities and operating frequencies, demands powerful computer-aided design (CAD) methodologies. Modeling still remains a major bottleneck for efficient RF/microwave CAD. Basic objective in modeling process is to generate models with the highest possible accuracy using the fewest accurate data. Analysis of a given microwave transmission line with the highest possible accuracy generally necessitates electromagnetic analysis subject to the structure using an electromagnetic simulator. Accurate data generation in this way is expensive as it involves both CPU time (for detailed model computations) and human time (for repetitive calls for changes in the input parameter-domain), and can slow down very much the model development. The other important issue is the selection of data to represent all the features of device in modeling without under/over fitting.

In this work, novel expert systems are employed to build synthesis models for the microwave transmission lines with the highest possible reliability and accuracy using fewest data. Firstly, we utilized preprocessing to obtain a sub-set of the whole data to represent the features of the device in modeling without under/over fitting. For this purpose, the ε — insensitive tube selection approach [1] is employed that results in the support vectors as a small sub-set representing the whole data to be used in the synthesis process. Accuracy of data can also be increased applying the coarse support vectors to the fine data generators which are generally electromagnetic simulators. In the second stage is to train the expert system ensemble by these fine synthesis support vectors. Our expert system ensemble consists of Artificial Neural Network (ANN), Support Vector Regression Machine (SVRM), k-nearest neighbor and least squares algorithms which perform generalization independently from each other. Thus a competition is arranged among the generalization abilities of the members of the expert system ensemble that results in an improved generalization outputting the consensual modeling with the highest possible reliability and accuracy. Typical worked examples on the consensual modeling of synthesis of the microwave transmission lines will be presented in the symposium.

REFERENCES

1. Vapnik, V., *The Nature of Statistical Learning Theory*, Springer-Verlag, New York, 1995.

A Knowledge-based Support Vector Synthesis of the Transmission Lines for Use in Microwave Integrated Circuits

Filiz Güneş[1], Nurhan Türker Tokan[1], and Fikret Gürgen[2]

[1]Department of Electronics and Communication Engineering, Yıldız Technical University
Beşiktaş, Istanbul 34349, Turkey
[2]Department of Computer Engineering, Bogazici University
Bebek, Istanbul 80815, Turkey

Abstract— In this paper, we proposed an efficient knowledge-based Support Vector Regression Machine (SVRM) method to build synthesis models of the transmission lines for the microwave integrated circuits, with the highest possible accuracy using the fewest accurate data. This method is based comprehensively on the powerful generalization capability of Support Vector Machine (SVM) over other classical optimization techniques; especially its working principle based on the small sample statistical learning theory is utilized in lessening the need for the accurate training and validation data together with the human time. Thus, synthesis models as fast as the coarse models and at the same time as accurate as the fine models are obtained for the RF/Microwave planar transmission lines. Since the method employs the reverse relations between the analysis and synthesis processes, therefore firstly general definitions of analysis and synthesis processes are made for the RF/Microwave planar transmission lines. Then the synthesis data are obtained by reversing the analysis data according to these definitions, where analysis process may be based on either the analytical formulation or empirical (coarse) formulas. Thereafter, generation process of the fine Support Vector (SV) expansion for synthesis from the coarse SVs is put forward in the form of block diagrammes, depending on type of the analysis processes. Finally, the proposed knowledge-based Support Vector method are demonstrated by the two typical worked examples, representing the typical analysis processes which belong to the commonly used transmission lines, conductor backed coplanar waveguides with upper shielding and microstrip lines. Besides, Artificial Neural Network (ANN)s are employed also in modeling as a competent regressor and it is also verified that only SVs would be sufficient to be used in training ANN models. Success of the method and performances of the resulted synthesis models are presented as compared to each other and the conventional ones.

Design and Produce an E-plane Filter in Ka-band

A. Mirtaheri and Z. Mehdipour
K. N. Toosi University, Iran

Abstract— Mode Matching Technique (MMT) is presented as a practical solution for solving Maxwell equation in waveguide structures. This method will be demonstrated by a bifurcated waveguide structure as a preliminary element of E-plane filters. The E-plane filter design procedure has been illustrated based on the results of MMT that includes both higher order mode interaction and thickness of the inserts. Validity of this method was confirmed by HFSS software and experimental measurements of the filter designed by it. All responses showed excellent agreement but the MMT method has the advantage of time saving. This method drastically reduces the CPU time for analysis. E-plane filters are introduced as a practical, inexpensive and easy to make among waveguide filters. An example of the design and produce of an E-plane filter in 22.432 GHz–23.030 GHz band with 5 resonators is presented. It comprises of two halves that were manufactured by a CNC machine and inserted plane that was made by laser-cut methods. This filter was tuned by Network Analyzer with three screws. The insertion loss in the middle of band width is 0.83 dB. Usually the Aluminum alloy with the industrial name 7075 for waveguide and the Copper for inserted plane are used.

Broad Omnidirectional Band of Reflection from Fibonacci One-dimensional Photonic Crystals

N. V. Grushina, **P. V. Korolenko**, **A. Y. Mishin**, **and A. M. Zotov**
Faculty of Physics, M. V. Lomonosov Moscow State University, Moscow 119992, Russia

Abstract— Now in optics of photon crystals the great attention is devoted to studying of Fibonacci 1D photon crystals (F1DPC). Their structure represents quasi-periodic stacking alternating layers of two materials according to the Fibonacci generation scheme. F1DPC are successfully applied in selective waveguide systems, in systems of impulse compression, in converters of frequency and amplifiers of optical radiation. In some cases in their use it is required to provide omnidirectional reflection of light waves in the certain spectral range, free of dissipative losses.

In this paper simulation of omnidirectional strong reflection from F1DPC with dielectric layers in preassigned frequency interval has been executed. It was supposed that refractive indices of layer materials can vary in area from 1.3 to 3.3. Calculations have been carried out for s- and p-polarisations of radiation. They have shown that for quarter-wave stack and at certain contrast of refractive indices of layers there is a possibility of total reflection in some frequency interval without introducing any changes in geometry of system. So, for 15-layer F1DPC at the ratio of high and low refractive indices of layer materials $n_h/n_l \approx 2.5$ the wave band with high value of reflection coefficients for s-polarisation, approximately, corresponds to area $0.64 < \varpi < 0.88$ ($\varpi = \omega/\omega_0$, ω — radiation frequency, ω_0 — frequency at which phase incursions in layers at normal incidence are equal $\pi/4$). At $n_h/n_l < 1.5$ conditions for formation of spectral region with total reflection at all angles disappear.

To expand spectral region of strong reflection and to reduce dependence on contrast of refractive indices of layer materials there is a possibility to modify the structure of multilayer system. During research different variants were considered. Among them: regular alternation of blocks F1DPC with certain sequence of layers, and also entering of the fixed or random mismatch into an optical thickness of layers with different refractive indices. All these ways along with advantages possess also lacks. Numerical simulation has shown that the most universal and simple way to broaden omnidirectional reflection band (from the viewpoint of practical realization) is based on linear increase in optical thickness of layer. Selecting the optimum factor of linear increase in optical thickness with the growth of a layer number, it is possible to expand several times frequency range with omnidirectional reflection. The given recommendation can find application in the different ranges of electromagnetic waves.

Charge Distribution in Lightning Leader Channels

Robert L. Gardner
6152 Manchester Park Circle Alexandria, VA 22310-4957, USA

Abstract— Much of the high-frequency RF emission from the lightning return stroke is emitted from the point where the return stroke propagates into the leader channel. Analytical and numerical models exist for this process [1] but such models require an understanding of the charge distribution remaining in the leader channel, i.e., the initial conditions of the return-stroke formation. The return stroke gathers that charge into a narrow highly-conducting channel that carries large, varying currents. The effects of that charge are often represented by uniform capacitance per unit length along the transmission line representing the return stroke. Since there is no outer conductor, this representation is not necessarily a good approximation.

Substantial charge is deposited in the leader channel before it is discharged: of the order of 0.01 C/m. Although there are other types of return stroke, we will assume the deposit of electrons in the channel to be discharged to the ground. These are electrons are rapidly bound to O_2 molecules forming O_2 minus charge carriers. These charged molecules respond several competing forces. First, there is the repulsive force from the like charges. Then there is the binding force of the current in the central channel. Even for the leader channel, there is a small (~ 200 A) current that continues flowing. After the return stroke begins the current becomes larger and the forces become larger. Finally, there is the electrostatic force from the potential of the central line. This last resembles the capacitive charge storage typically modeled in the return stroke.

Finally, the charges do not instantly respond to these forces, but are slowed by collisions with the background (neutral) atmosphere. While these collisions do not play as important a role as later in the return stroke, they do provide a background resistivity as well provide storage mechanisms for the heat energy in the channel.

All of these processes are included in a model similar to the one-dimensional model of the Physics of Fluids article referenced above and allowed to approach steady state. Deriving the various time-constants is also important.

REFERENCES

1. Gardner, R. L., et al., *Phys. Fl.*, Vol. 27, 2694, 1984.

Application of Graphical Processors in Signal Processing of MTI Systems

M. A. Ershadi and E. K. Keshmarzi
Department of Electrical Engineering, Sharif University of Technology, Tehran, Iran

Abstract—

Introduction: Moving target indicator (MTI) radars are developed and used extensively to detect and follow some specific moving targets and delete the constant background substances and also some undesired moving substances like clouds and rain which are called clutter.

Processing system in these radars is so massive and complex as it is supposed to perform a great amount of processing in very short time. These processing include pulse compression, filtering, calculation of threshold values and applying them to the data, ...

Generally these processing are performed on digital signal processors, however these cards are so expensive and in some applications they seem to be ineffective. In this paper a cost effective approach is introduced that is based on parallel processors of computer graphic cards.

In recent years, application of graphical processors in non-graphical processing has been increased, this is mainly due to their high capability of parallel processing which is used basically to process the 3D environments. Therefore the main space of these cards is dedicated to data and program operation control.

In our project the whole works related to signal processing is done using graphical card processors, simulation has been performed using graphical library of open GL in Visual C++ environment, which the results are given in the paper.

Innovation, Advantages and Applications: As it had been mentioned before, great amount of processing in limited time in MTI radars require powerful DSPs that cost much and in some applications, this cost reduces efficiency of the system. In contrast graphical cards are available with relatively lower cost and the same performance. So they can be applied to low cost projects or in the case that DSPs are not available. To get an overview of the processing volume, a numerical example is given.

Digital to analog converters create more than 10 Mega Sample per channel. This gives rise to 20 Mega sample per second that must be processed and more than 2 Giga flop operations per second that must be done aggregately. Although these extra operations can be done on the main processors of the computer, However due to the high jumping accesses and taking samples from analog to digital converters, operation on these processors in a specified time can be done only on less than half of the data, Whilst graphical card processors are able to process 2 times more data in the same time.

Other advantages of graphical cards include their ability to display data. In digital signal processors, the produced data should be synchronized with display system using some peripheral equipment. But in graphical cards, the output data can be displayed using only a few lines of code. Easier implementation and software debugging, ability to increase the number of processors instead of enhancement of the whole system and simplicity in generation of advanced MTI radar system are other advantages of using graphical card processors in these application.

Electromagnetic Interaction with Long Range Electron Transfer: A Key to Nonthermal Biological Effects?

Zvi Kirson
Research Laboratory of Water Quality, Ministry of Health, Tel Aviv 61080, Israel

Abstract— It is suggested that harmful biological effects may be related to non ionizing radiation through enhancing a damage already done, possibly by ionizing radiation or other damaging agent, when the range of charge migration in protein is increased under the influence of oscillating electric field. Calculations of time dependent electronic wave function at donor-bridge-acceptor system in presence of static and oscillatory electric field in a wide range of frequencies, oversimplified by ignoring all effects of intervening medium, support that assumption. Main conclusion is that the strength of field counts at the location of interaction with the biological material and not the energy absorbed. Non thermal biological effects are thus rendered possible.

Long range electron transfer (LRET) is related in the literature to health damage. LRET of unpaired electron may extend the target size for radiation-induced damage of sub cellular structures [1]. DNA damage produced, e.g., by direct effect of ionizing radiation or chemical oxidation involve transfer of electron away from the DNA [2]. Migration of charge over long molecular distances should be considered with respect to DNA damage [3]. The conjecture of Szent-Gyorgyi [4, 10], on the contrary, is that hindering the electron flow is hazardous for the cell. Typically the electron transits from donor D to empty acceptor A by tunneling through intermediate high lying empty electronic states ("bridge" B) [5, 9].

Effects of static and oscillating electric field on electron tunneling is demonstrated for varying barrier height and length. The electron is treated quantum mechanically. Time dependent electric field is treated as a classical variable

Results and Conclusions: Radiation in wide range of frequencies from ELF up to THz may, depending on characteristic of the barrier between donor and distant acceptor, may either extend the range of electron migration thereby mediating free radical damage initiated by ionizing radiation or oxygen assault, or decrease electron flow and thereby, according to Szent-Gyorgyi [10], change the self regulation of a cell into direction of cancerous state. Such effects are obviously non thermal though may be followed by an energy deposition. Adopting lorentz model for estimation of local field in biological matter under the influence of external field leads to the longed sleeked conclusion that low intensity ELF indeed may have damaging effects unrelated to thermal effects whatsoever. An option for therapeutic effect [11] have been also raised.

It is found that Donor-Bridge-Acceptor structure exhibits finite response time which imparts a lowpass response; that is, the system exhibits decreasing sensitivity to fields at higher frequencies if the barrier to tunneling is high. If the barrier is absent there is extreme "resonant" sensitivity to specific frequencies.

The model may be tested experimentally in vitro through measuring rate of electron transfer accompanying intramolecular radical redox reactions in solution of peptides such as H-Trp-$(Pro)_n$-Tyr_Met or H-Trp-$(Pro)_n$-Tyr_OH through fluorescence quenching, both in presence of field and its absence, given the measured permittivity of the solute.

Improving upon Lorentz local field [5, 6] based on modern advanced attitudes [7, 8] are imperative in regard of the obtained results.

REFERENCES

1. Bobrowski, K., *Int. J. Radiat. Biol.*, Vol. 62, 507–516, 1992.
2. Milligan, J. R., *Biochemistry*, Vol. 43, No. 17, 5102–5108, 2004.
3. Hall, D. B., et al., *Nature*, Vol. 382, 731–735, Aug. 1996.
4. Ladik, J., *Int. J. Quant. Chem.*, Vol. 64, No. 3, 379–385, 1997.
5. Steinbrecher, T., et al., *J. Phys. Chem. B*, Vol. 112, 16935–16944, 2008.
6. Sidorenko, V. M., *Biophysics*, Vol. 46, No. 1, 476–480, 2001 (translated from *Biofizika* (in Russian), Vol. 46, 500–504, 2001).
7. Lagendijk, A., et al., *Phys. Rev. Lett.*, Vol. 79, No. 4, 657–660, 1997.
8. Lagendijk, A., et al., *Phys. Rep.*, Vol. 270, 143–215, 1996. See in particular 176–177.
9. Nitzan, A., et al., *J. Phys. Chem. B*, Vol. 104, No. 24, 5661–5665, 2000.
10. Szent-Györgyi, A., *Electronic Biology and Cancer*, Marcel Dekker, New York, 1976.
11. Atkin, M. R., et al., *Science*, Vol. 273, 475–480, 1996.

Can We Build an Adaptive Fractal Radio System?

A. A. Potapov
Institute of Radio Engineering and Electronics of Russian Academy of Sciences
Building 11, Mokhovaya Street, Moscow 125009, Russia

Abstract— Main results of theoretical and experimental investigations since eighties of XX that led to formation and developing of new fundamental science discipline: "Fractal Radio Physics and Fractal Radio Electronics: Fractal Radio Systems Designing" are briefly classified in the paper. For a long time stationary behaviors and periodical motions were assumed to be the only possible conditions. However the discoveries of the latter part of XX century principally changed our idea of dynamic processes behavior. Now we realize that our world is not only non-linear but also is fractal. At present, the lack of conventional physical models is obviously felt. In other words, the full description of signals and fields up-to-date processing is impossible via classical mathematics formulas. It is absolutely evident for the author that the application of scale invariance ("scaling") conceptions and of modern functional analysis, which are related with set theory, theory of fractional dimension, general topology, geometrical measure theory and dynamic systems theory, to modern informational technologies reveals great potential opportunities and new prospects in multidimensional signals processing and in the related scientific and technical areas. Aim of the work — sufficiently thorough and at the same time compact presentation of "fractal computing technique" and "fractal language" for a quantity of modern physical and applied problems.

ACKNOWLEDGMENT

This work was financially supported by Russian Foundation for Basic Research (projects No. 05-07-90349-B, No. 07-07-07005-g, No. 07-07-12054 and No. 07-08-00637-a).

Eddy Current Modeling in Composite Materials

M. Cacciola, **S. Calcagno**, **G. Megali**,
D. Pellicanó, **M. Versaci**, **and F. C. Morabito**
University "Mediterranea" of Reggio Calabria, DIMET
Via Graziella Feo di Vito, Reggio Calabria I-89100, Italy

Abstract— Production of carbon fiber reinforced polymers, which are widely used both in civil and military applications, is an elaborate process un-free from faults and problems. Errors during the manufacturing such as, for instance, plies' overlapping, can cause flaws in the resulting material, this way compromising its integrity. Compared with metallic materials, carbon epoxy composites show a number of advantages, such as higher tensile strength, lower density and coefficient of thermal expansion, absence of fatigue state related phenomena, possible manufacturing of large layered structures. Within this framework, this work aims to propose a design of ferrite core probe for eddy current non destructive evaluation, in order to investigate the presence of defects in carbon fiber epoxy composite materials. The effect of the ferrite core is analyzed in order to focus magnetic flux density on the investigated specimen. In this framework, eddy currents generated by high speed ferrite core probe movement were investigated by using numerical simulation. Particularly, a Finite Element Approach will be exploited in order to characterize the transducer to specially emphasize the presence of defects in a multi-layer carbon fiber epoxy structure. Being eddy current-likes very sensitive and noisy signals, a Soft Computing approach able to recognize and classify the defects, starting from the measured eddy current signals, could be very useful. The ill-posedness of the so-defined process needs a regularization method. In this paper, an heuristic approach is proposed in order to solve the inverse problem for the characterization of the size of the defect. In particular, the adopted approaches will be tested, and the robustness to noise will be evaluated.

Effect of Surface Roughness on Determination of Tissue Optical Properties and Light Distribution in Intralipid

Chun-Ping Zhang[1], **Meixiu Sun**[1], **Jian-Guo Tian**[1], **Gui-Ying Chen**[2], **Shengwen Qi**[3], **Qing Ye**[1], **and Jin Wang**[1]

[1]Institute of Physics, Nankai University, Tianjin 300071, China
[2]Key Laboratory of Tropical Marine Environmental Dynamics
South China Sea Institute of Oceanology, Chinese Academy of Sciences
Guangzhou 510301, China
[3]Department of Physics, Dezhou University, Dezhou, Shandong 253023, China

Abstract— The optical properties of biological tissue are modeled by absorption coefficient (μ_a), scattering coefficient (μ_s), reduced scattering coefficient (μ_s'), and anisotropy of scattering (g). Spatially resolved steady-state reflection technique has been used for the determination of the reduced scattering coefficient, it major advantage is *in situ* measurement of the absorbed coefficient and the reduced scattering coefficient. The diffusion model fitting of the measured reflectance-distance curves is based on the assumption of smooth surface even though the surface is rough. Various authors have used the techniques to determine the tissue optical parameters and no one has considered the effects of surface roughness on the determination of the optical properties of the tissue. Xiaoyan Ma et al. studied the effect of surface roughness on determination of bulk tissue optical parameters by inverse Monte Carlo method and suggested that the surface roughness should be taken into account for determination of bulk tissue optical parameters. We used a nylon bar with different surface roughness as a simulation sample to determine its reduced scattering coefficients and absorption coefficient by a spatially resolved steady-state diffuse reflectance technique and the nylon bar and nylon film have strong scattering property like the intralipid suspension and their surface roughness is easy to be changed and to form different roughness. The results indicate the surface roughness has some effect on the determination of the reduced scattering coefficient of the nylon bar. The determined reduced scattering coefficient decreases with the decrease of the surface roughness of the nylon bar and goes to a constant for the lower surface roughness. So the reduced scattering coefficient obtained by spatially resolved steady-state reflection technique should be modified. The goniophotometric measurement technique was used for the measurement of the scattering phase function and determination of the anisotropy factor g of nylon film and the measured results show that the determined anisotropy factor g of the nylon film with different surface roughness decreases with the increase of the surface roughness. Light distribution in the biological tissue phantom Intralipid-20% suspension with different surface roughness was measured for quantitative understanding of the interface roughness effect on measurement of light distribution, the results indicate that the effect of the surface roughness on the light distribution in the intralipid suspension around the positions of the peaks is more than that besides the positions of the peaks.

In general, biological tissue surfaces possess a certain degree of roughness, so the reduced scattering coefficient obtained by using diffuse equation for reflectance to fit measured data of diffuse reflectance is not the real reduced scattering coefficient of the tissue, it should be modified and the modified coefficient depends on the surface roughness of the tissue. The determined anisotropy factor g of of the tissue with roughness surface should be modified. The surface roughness effects also the light distribution in the tissue.

Scattering of Dirac Particle at the Coulomb Scalar Potential and Vector Field in 3+1 Dimensions

H. Goudarzi and H. Sedghi
Department of Physics, Faculty of Science, Urmia University
Urmia, P. O. Box 165, Iran

Abstract— We consider the scattering of Dirac particle by the vector plus scalar coulomb potential in 3+1 dimensions. The phase shift and wave functions are obtained exactly. We calculate the scattering amplitude in a quasi-classical approximation as a partial wave series. By means of figures obtained for the cross section $\sigma(\theta)$ in general and special cases, such as $a \neq b$ and $a = b$, we find that $\sigma(\theta)$ is not exactly symmetric about $\theta = \pi$.

Introduction: One of the important physical effects is the scattering of fermions in the presence of external electromagnetic fields. In addition to interaction of fermions with an external vector field, one can consider interaction of Dirac fermions with external scalar field $U(r)$, which it models, for example the self-consistent field of quark system, or in some cases, an actual part of gravitational interaction in systems with massive fermions. Studying system of fermions in the presencs of a strong vector field of point-charge and a scalar coulomb field leads to this result that, the range of the value of external field parameters a and b, at which corresponding Hamiltonian operator becomes hermitian, essentially wider than in the absence of scalar field.

The scattering of particles by a coulomb field is discussed in some special cases in two, three and higher dimensions in several papers [1–6]. Also, the exact solutions of the relativistic Aharonov-Bohm effect [7] in the presence of two dimensional coulomb potential is studied in [8, 9]. It should be noted that, the study of the scattering of particles by a vector field and a coulomb scalar potential plays an important role in relativistic quantum mechanics, because it models the interaction between the Dirac filed and heavy atoms, i.e., quarkonium.

Recently, the Dirac equation with position-dependent mass in the coulomb field has been studied [10]. The exact solutions of the Dirac equation with the vector plus scalar coulomb potential in two dimensions [11, 12], three dimensions [13] and higher dimensions [14] have been carried out. The pair production process in the vector fields is studied in (1+1) and (2+1) dimensions [15] as well as in 3+1 dimensions [16–18].

The main purpose of this paper is to obtain the scattering amplitude of Dirac particles in the presence of combined vector field plus coulomb scalar potential as a partial wave series.

REFERENCES

1. Dong, S. H. and M. Lozada-Cassou, *Phys. Lett. A*, Vol. 330, 168, 2004.
2. Lin, Q. G., *Am. J. Phys.*, Vol. 68, 1056, 2000.
3. Lin, Q. G., *Phys. Lett. A*, Vol. 260, 17, 1999.
4. Khalilov, V. R. and C.-L. Ho, *Mod. Phys. Lett. A*, Vol. 13, 615, 1998.
5. Yafaev, D., *J. Phys. A Math. Gen.*, Vol. 30, 6981, 1997.
6. Lin, Q. G., *J. Phys. A*, Vol. 34, 1911, 2001.
7. Aharonov, Y. and D. Bohm, *Phys. Rev.*, Vol. 115, 485, 1959.
8. Lin, Q. G., *J. Phys. A*, Vol. 33, 5049, 2000.
9. Khalilov, V. R., *Theo. Math. Phys.*, Vol. 149, No. 3, 176, 2006.
10. Alhaidari, A. D., *Phys. Lett. A*, Vol. 322, 72, 2004.
11. Dong, S. H., X. Y. Gu, Z. Q. Ma, and S. S. Dong, *Int. J. Mod. Phys. E*, Vol. 11, 483, 2002.
12. Greiner, W., *Quantum Mechanics, An Introduction*, Springer-Verleg, Berlin, 1989.
13. Ikhadir, S. I., Q. Mustafa, and R. Sever, *J. Hadronic*, Vol. 16, 57, 1993.
14. Dong, S. H., G. H. Sun, and D. Popov, *J. Phys.*, Vol. 44, 4467, 2003.
15. Khalilov, V. R., *Theo. Math. Phys.*, Vol. 122, No. 3, 372, 2000.
16. Reinhardt, J. and W. Greiner, *Rep. Prog. Phys.*, Vol. 40, 219, 1977.
17. Soffel, M., B. Muller, and W. Greiner, *Phys. Rep. C*, Vol. 83, 51, 1982.
18. Khalilov, V. R., *Electrons in Strong Electromagnetic Fields: An Advanced Classical and Quantum Treatment*, Gordon and Breach Sci. Pub., Amsterdam, 1996.

The Use of Thin Layer Conditions for the Reconstruction of Objects Buried in a Layered Medium

Ö. Özdemir[1], **H. Haddar**[2], **and A. Yaka**[1]

[1]Istanbul Technical University, Turkey
[2]INRIA Saclay Ile de France & CMAP, France

Abstract— Equivalent boundary conditions are widely used for mathematical modeling in the solution of scattering problems [1]. Here the main idea is to replace the complex scattering problem with simple one having new boundary conditions which can be solved in a more easier way than the original one. In electromagnetics, equivalent boundary conditions are especially used to model geometrical and physical properties of the actual structure in scattering, propagation and antenna problems. Equivalent Boundary conditions are called as Thin Layer Conditions when they are used to model thin layers [2]. These conditions are very important for practical application in which layered medium is involved, such as geophysics, underground imaging, etc. On the other hand, reconstruction of objects buried in layered medium has been very popular subject in many areas and constitutes an inverse scattering problem. They have very important practical applications such as mine detection, tumor cells recognition, etc. Most of the methods in the literature which are used to detect buried objects need to know Green function of the background medium which is not always possible to obtain for complex structures.

The aim of this paper is to derive higher order thin layer conditions for three layered media and apply this conditions for the imaging of objects located in such a medium. The middle layer is modeled in terms of a thin layer boundary condition under the assumption that the thickness of the layer is sufficiently small through the Taylor expansion of the total field. The resulting boundary conditions connects the field values at the boundaries of the middle layer, which allows one to obtain the field values at the lower boundary from the measured on the upper boundary. Then Reciprocity Gap-Linear Sampling Method (RG-LSM) is applied to image buried objects [3]. Numerical simulations show that thin layer conditions gives quite satisfactory results to determine the field values on the lower boundary of the layer therefore RG-LSM can be applied to image objects by using this approximate values where we use only second order thin layer conditions. However, when the thickness is getting larger or the permittivity is higher, second order conditions are not enough for modeling therefore higher order terms are needed.

REFERENCES

1. Senior, T. B. A. and J. L. Volakis, "Approximate boundary conditions in electromagnetics," *IEE Electromagnetic Waves Series*, 1995.
2. Engquist, B. and J. C. Nedelec, "Effective boundary conditions for acoustic and electromagnetic scattering in thin layers," *Ecole Polytechnique-CMAP (France)*, 278, 1993.
3. Colton, D., H. Haddar, and M. Piana, "An application of the reciprocity gap functional to inverse scattering theory," *Inverse Problems*, Vol. 21, 2005.

Fractal Characteristics of Radio Thermal Radiation of a Different Layer of Atmosphere in a Range of Millimeter Waves

V. A. German, **A. A. Potapov**, **and E. V. Sukhonin**
Institute of Radio Engineering and Electronics of Russian Academy of Sciences, RAS
Mokhovaya Street, 11, Building 7, Moscow 125009, Russia

Abstract— In the report new results of measurement of characteristics of radio of thermal radiation of troposphere in a range of millimeter waves (8 mm) are presented. Measurements are spent in natural conditions at various weather conditions: - overcast; - rains of various intensity. On a basis, developed by authors fractal methods of researches of radio physical processes are investigated: - dynamics of fractal dimensions of thermal radiation of a layer of atmosphere, Herst exponent, characterizing non gauss physical processes; - the problem of restoration of phase portraits of attractors characterising dynamics of formation of process of own radiation of troposphere in different meteo-conditions is solved. The given researches are spent fist. The researches have allowed to make conclusions on conformity of estimations fractal characteristics of own radiation to meteo-conditions in which measurements were made. On the contrary, as shown, statistical characteristics of own radiation have no obvious dependence from meteo-conditions. For an estimation fractal parameters the original software developed by authors has been used. Use of this software has allowed to increase accuracy and to reduce time of calculations.

The Effects of Self Steepening and Intrapulse Raman Scattering on Frequency Spectrum of Dark Soliton Switching

F. Kargar[1], **M. Hatami**[2], **and P. Elahi**[3]

[1]Physics Department, Pyam-Noor University, Shiraz, Iran
[2]Atomic and Molecular Group, Faculty of Physics, Yazd University, Yazd, Iran
[3]Department of Physics, Faculty of Science, Shiraz University of Technology
P.O. Box 71555-313, Shiraz, Iran

Abstract— In this paper the nonlinear Schrödinger equation (NLS) is developed for nonlinear directional coupler switches (NLDS) by taking into account the self steepening and intrapulse Raman scattering effects. The nonlinear equation that governing the pulse propagation thought the (NLDC) by developing the nonlinear Schrödinger to consider the self steepening and intrapulse Raman effect is:

$$\begin{aligned}\frac{\partial U_1}{\partial Z} &= -\frac{i}{2}\frac{\partial^2 U_1}{\partial \tau^2} + i\left|U_1\right|^2 U_1 - s\frac{\partial}{\partial \tau}\left(\left|U_1\right|^2 U_1\right) - i\tau_R U_1 \frac{\partial \left|U_1\right|^2}{\partial \tau} - i\frac{\pi}{2}\kappa U_2 \\ \frac{\partial U_2}{\partial Z} &= -\frac{i}{2}\frac{\partial^2 U_2}{\partial \tau^2} + i\left|U_2\right|^2 U_2 - s\frac{\partial}{\partial \tau}\left(\left|U_2\right|^2 U_2\right) - i\tau_R U_2 \frac{\partial \left|U_2\right|}{\partial \tau} - i\frac{\pi}{2}\kappa U_1\end{aligned}$$

By numeric simulation of propagation of dark soliton in the nonlinear directional coupler switch we study of those effects. The result of simulation shows in high power input intensity the spectrum of pulse is a little change with respect to bright soliton switching. This result prove the stability of dark soliton for optical switching as we expected.

REFERENCES

1. Zakeri, A. and M. Hatami, "Nonlinear optical properties of pulsed laser-deposited GeAsSe films and simulation of a nonlinear directional coupler switch," *J. of Opt. Society of Am. B*, Vol. 22, 591, 2005.
2. Kivshar, Y. S. and G. P. Agrawal, *Optical Solitons*, Academic Press, 2003.
3. Hatami, M., H. Ghafouri-Shiraz, and A. Zakery, "Analysis of gained nonlinear directional coupler pulse switch," *Optical and Quantum Electronics*, Vol. 38, 1259–1268, 2007.
4. Zakeri, A. and M. Hatami, "Design of an ultra-fast all optical dark soliton switch in a nonlinear directional coupler (NLDC) made in chalcogenide glasses," *Applied Physicd D*, Vol. 12, 591, 2006.

Simulation of Soliton Propagation in Photovoltaic Photorefractive Two-photon Materials and Study the Switching Behavior

Alireza Keshavarz[1], **Leila Sadralsadati**[2], **and Mohsen Hatami**[2]

[1]Department of Physics, Faculty of Science, Shiraz University of Technology
P.O. Box 71555-313, Shiraz, Iran
[2]Atomic and Molecular Group, Faculty of Physics, University of Yazd, Yazd, Iran

Abstract— Photorefractive spatial solitons (PRSS) are useful for application in telecommunication system and the operating wavelenght is (1.5 µm). The nonlinearity of this material makes them as a good condidate for all optical switching and routing.

By assuming the two mutually incoheren beam with the same frequency that are polarized along x-direction in optical c axis of $LiNbO_3$ crystal it can be written the coupled nonlinear equations.

If the optical field of these pulses are expressed in the form $\overrightarrow{E}_1 = \widehat{x}\Phi(x,z)\exp(ikz)$ and $\overrightarrow{E}_2 = \widehat{x}\Psi(x,z)\exp(ikz)$ where $k = (2\pi/\lambda_0)\,n_e$ and Φ, Ψ are slowly varying envelopes then it can be shown that:

$$i\frac{\partial\Phi}{\partial z} + \frac{1}{2k}\frac{\partial^2\Phi}{\partial x^2} - \frac{k_0 n_e^3 r_{33} E_{sc}}{2}\Phi(x,z) = 0 \tag{1}$$

$$i\frac{\partial\Psi}{\partial z} + \frac{1}{2k}\frac{\partial^2\Psi}{\partial x^2} - \frac{k_0 n_e^3 r_{33} E_{sc}}{2}\Psi(x,z) = 0 \tag{2}$$

where r_{33} is electro-optic coefficient and E_{sc} [1] is the space charge field in the (PR) material. The nonlinearity originates due to induced space charge field, which perturbs the refractive index through the Pockel's effect [2]. Substituting expression for E_{sc} into Eqs. (1) and (2), we derive the following dimensionless dynamical equation for the incident pulses:

$$i\frac{\partial U}{\partial \zeta} + \frac{1}{2}\frac{\partial^2 U}{\partial s^2} + \frac{\alpha\eta\left(1+\sigma+|U|^2+|V|^2\right)\left(|U|^2+|V|^2\right)U}{\left(1+|U|^2+|V|^2\right)} = 0 \tag{3}$$

$$i\frac{\partial V}{\partial \zeta} + \frac{1}{2}\frac{\partial^2 V}{\partial s^2} + \frac{\alpha\eta\left(1+\sigma+|U|^2+|V|^2\right)\left(|U|^2+|V|^2\right)V}{\left(1+|U|^2+|V|^2\right)} = 0 \tag{4}$$

Eqs. (3) and (4) are coupled modified nonlinear Schrödinger equations, which are nonintegrable in nature. These may be solved by various approximation methods. An alternative approach is to solve these equations numerically that we will do it by modified the Crank-Nicolson method.

We have designed an all optical switch by simulation of propagation of two pulses along the z-direction in a (PR) material. The result show there is some critical input peak power that make it as an all optical self-routing switching that can be used in comunication system.

REFERENCES

1. Hou, C., Y. Zhang, Y. Jiang, and Y. Pei, "Photovoltaic soliton in two-photon photorefractive materials under open-circuit conditions," *Opt. Commun.*, Vol. 273, No. 2, 544–8, 2007.
2. Srivastava, S. and S. Koar, "Two-component coupled photovoltaic soliton pair in two photon photorefractive materials under open circuit conditions," *Optics and Laser Technology*, Vol. 41, No. 4, 419–423, June 2009.

Design of an All Optical Routing Self Switch by Using the Collision of the Spatial Solitons in a Non-Kerr Nonlinearity

Mohsen Hatami[1], **Alireza Keshavars**[2], **Najmeh Dehkordi Balali**[3], **and Fatemch Kargar**[3]

[1]Atomic and Molecular Group, Faculty of Physics, Yazd University, Yazd, Iran
[2]Department of Physics, Shiraz University of Technology, Shiraz, Iran
[3]Physics Department, Payam-Noor University, Shiraz, Iran

Abstract— In nonlinear optics, solitons are classified as being either temporal or spatial, depending on whether the confinement of light occurs in time or space during wave propagation. The intensity dependence of the refractive index leads to spatial self-focusing (or self-defocusing) and temporal self-phase modulation (SPM), the two effects that are responsible for the formation of optical solitons. Thus, two transversely moving spatial solitons can collide with each other. Collision between two spatial solitons of equal amplitude in non-Kerr nonlinear media depends on their relative phase φ. Two solitons attract each other when they are in phase ($\varphi = 0$), and fuse together when the collision angle is below a certain critical value. Two out-of-phase solitons ($\varphi = \pi$) repel each other and in phase ($\varphi = \pi/2$), solitons interaction is accompanied by a strong energy exchange. We have developed the equation related to collision of spatial solitons in non-Kerr nonlinear media by taking in to account the two-photon absorption coefficient. If we take α and β are two-order and four-order two-photon absorption coefficient we have:.

$$i\partial u/\partial z + 1/2(\partial^2 u/\partial x^2) + |u|^2 u = i\alpha|u|^2 u + i\beta|u|^4 u$$

In this paper we have simulated the evaluation of sech type of soliton and study the spatial collision and ffects of two-photon absorption, by using Fourier series analysis technique (FSAT). Two spatial solitons attract each other before considering the effect of two-photon absorption and output wave amplitude increase and its width decrease. The results show that effects of two-photon absorption has an important effect on pulse propagation, more detail analysis with different absorption parameters and input pulse amplitude, shows by interaction of two solitons it can be design an all optical routing self switch with operate in two different input intensity.

REFERENCES

1. Agrawar, G. P., *Optical Solitons*, Academic Press, San Diego, Academic Press, 2003.
2. Zakeri, A. and M. Hatami, "Nonlinear optical properties of pulsed laser-deposited GeAsSe films and simulation of a nonlinear directional coupler switch," *J. of Opt. Society of Am. B*, Vol. 22, 591, 2005.
3. Hatami, M., H. Ghafouri-Shiraz, and A. Zakery, "Analysis of gained nonlinear directional coupler pulse switch," *Optical and Quantum Electronics*, Vol. 38, 1259–1268, 2007.

DFB Laser Injection Locking on Brillouin Radiation in Optical Fiber

Vasily V. Spirin and Marcial Castro
Division de Fisica Aplicada, CICESE, AP2732, CP 22860, Ensenada, B.C., México

Abstract— Injection locking techniques have drawn attention for optical communication application as a means of achieving a single-frequency and chirp-free modulation of semiconductor laser diodes. As well as this technique opens new possibilities to generate signals for distributed optical sensing [1–3]. In so-called self-injection techniques the laser cavity receives some optical feedback — usually spectrally or/and polarization filtered that provides a stable single-frequency, single-polarization operation of the laser.

In this paper we report two novel optical injection-locking configurations which can be utilized in distributed fiber optical Brillouin sensor. The first one based on injection locking of DFB laser on ring Brillouin laser radiation and the second one on self-injection locking on Brillouin amplified radiation. Both configurations provide significant improvement in frequency- and intensity-stability of Stokes radiation and operate without a high-frequency modulator and generator. However, the second technique demonstrates significantly low relative intensity noise (RIN) level.

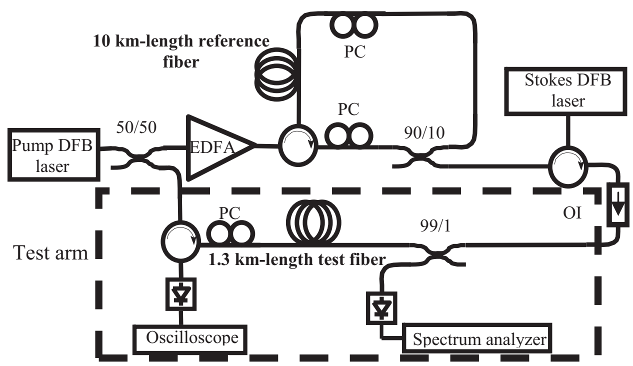

Figure 1: Experimental setup for injection locking of DFB laser on output radiation of Brillouin ring laser. EDFA-Er-doped fiber optical amplifier, OI-optical isolator, PC-polarization controller.

Figure 1 shows the experimental setup for study self-injection locking on Brillouin-amplified radiation in long optical fiber feedback. In this configuration the Stokes DFB laser is placed inside the Brillouin fiber optical ring laser cavity. The radiation of the Stokes DFB laser is Brillouin-amplified in the reference fiber and returned back to its cavity through optical circulators that definitely attributed to self-injection locking phenomena. However, as we found experimentally, the pump DFB laser can efficiently drive the self-locked Stokes DFB laser frequency inside an interval that significantly exceeds the width of Brillouin gain in optical fiber. Therefore, the proposed structure exhibits properties inherent in two phenomena, self-injection locking and injection-locking of two lasers in master-slave configuration at the same time.

Configuration based on self-injection locking demonstrates more than on 20 dB stronger beat signal for the same Stokes and pump powers in the test fiber. These results have important consequences for distributed temperature and strain Brillouin sensors, which utilized Stokes seed signals.

In conclusion, spectral and intensity property of injection locked and self-injection locked Stokes DFB laser was investigated. It was shown that self-locked Stokes laser is also locked through the Brillouin amplification on pump laser which can efficiently drive the Stokes laser frequency. Generally, the "double-locked" Stokes DFB laser demonstrates significantly low RIN level than the laser which directly locked on radiation of the ring Brillouin laser.

REFERENCES

1. Thévenaz, L., S. Le Floch, and J. Troger, "Novel schemes for optical signal generation using laser injection locking with application to Brillouin sensing," *Measuring Science Technology*, Vol. 15, 1519–1524, 2004.
2. Spirin, V. V., J. Kellerman, P. L. Swart, and A. A. Fotiadi, "Intensity noise in SBS with injection locking generation of Stokes seed signal," *Optics Express*, Vol. 14, 8328–8335, 2006.

3. Castro, M. and V. V. Spirin, "Self-injection locking of DFB laser diode with Brillouin amplification in optical fibre feedback," *Electronics Letters*, Vol. 43, No. 15, 802–803, 2007.

Effective Permittivity of a Regular Structure of Conductive Films

E. V. Ivanova[1], **M. Y. Koledintseva**[2], **and K. N. Rozanov**[1]

[1]Institute for Theoretical and Applied Electromagnetics, Russian Academy of Sciences, Moscow, Russia
[2]Missouri University of Science and Technology, Rolla, MO, USA

Abstract— The study is aimed at effective material parameters of regular composite structures made of thin conducting inclusions. The inclusions under study are thin squares distributed in a periodical matter perpendicularly to the wave vector of incident electromagnetic wave. Such structures have been thoroughly investigated in a resonance wave band in relation to the technical applications of these as frequency-selective surfaces [1] and circuit-analogue radar absorbing materials [2], but characterization of the effective material parameters in the low-frequency range is not found in the literature. From the standpoint of theory of composites, such materials are good model system for studying of such problems as the mixing rule for composite filled with elongated inclusions [3], electrodynamical boundary layer in composites [4, 5], etc.

The effective permittivity of the one or several planar periodic lattice of thin conducting squares has been obtained from numerical simulation of the reflectivity of the structure as a function of the square size to period ratio of the structure and the number of planar layers, with the wavelength being large compared to the period of the structure. It is shown that the numerical results are in a good agreement with the small perturbation approach and do not agree with the Maxwell Garnett approximation, which is conventionally considered to be an adequate mixing rule for periodic metal-dielectric structures. When several planar lattices are under treatment, the permittivity of the whole structure is reciprocal to its thickness, which is an evidence to the large contribution of the boundary layers to the effective material parameters of the structure.

REFERENCES

1. Munk, B. A., *Frequency Selective Surfaces*, Wiley, New York, 2000.
2. Vinoy, K. J. and K. M. Jha, *Radar Absorbing Materials*, Kluwer, Dodrecht, 1996.
3. Lagarkov, A. N., S. M. Matytsin, K. N. Rozanov, and A. K. Sarychev, "Dielectric properties of fiber-filled composites," *J. Appl. Phys.*, Vol. 84, 3806, 1998.
4. Acher, O., A. L. Adenot, and F. Duverger, "Fresnel coefficients at an interface with a lamellar composite material," *Phys. Rev. B*, Vol. 62, 13748, 2000.
5. Vinogradov, A. P., D. P. Makhnovskii, and K. N. Rozanov, "Effective boundary layer in composite materials," *J. Communic. Technol. Electron.*, Vol. 44, 317, 1999.

Performance Enhancement of Circularly Polarized Microstrip Antenna Using Electromagnetic Band Gap Structures

Muhammad Mahfuzul Alam, **Md. Mustafizur Rahman Sonchoy**, **and Md. Osman Goni**
Department of Electronics and Communication Engineering
Khulna University of Engineering and Technology, Bangladesh

Abstract— In this paper, simulation of two circularly polarized microstrip antennas and there performance improvements using Electromagnetic band gap structure are given. Square shape EBGs are used in a planar structure for this cases. Sharpe resonances are found with no harmonics for both of these antennas. The effectiveness of the use of EBG structure is also discussed. These antennas are operated in two different frequencies, one is 2.45 GHz and other is 2.50 GHz. To make theses antennas ideally circularly polarized, branch line coupler and power divider are used to feed the element at two adjacent edges. Performance improvement is achieved using EBGs with these antennas. For 2.45 GHz, antenna square EBGs with planar configuration are designed and the antenna is inserted between these EBGs. Distance between antenna edge and the EBG edge is maintained, at one side is 5.3 mm and in other side 9.1 mm to get improved return loss. Without EBG, we get a return loss of -17.11 dB and some shifting in operating frequency, but using EBGs, we found a return loss of -40.68 dB without any operating frequency shift. So there is a -23.57 dB improvement in return loss, as well as no frequency shift. Total dimension of the structure is $143 \times 136\,\text{mm}^2$. Considering vias radius that is more practical consideration, we obtain return loss -31.25 dB and this time total dimension of the antenna is $167 \times 166\,\text{mm}^2$. After using EBG, we also found axial ratio improvement. Similarly for 2.5 GHz antenna, we use same EBG structure. This time the antenna is feed by a branch-line coupler. The distance between antenna vertex and EBG edge is maintained 2–2.75 mm for better return loss. Without EBG, the return loss is -18.75 dB with little frequency shift, but when EBG structure is used, the return loss is -41.75 dB with a sharp resonance. For this antenna, total dimension is $137 \times 159\,\text{mm}^2$. Also considering vias radius for this antenna, we found improvement in return loss and axial ratio. At this time, the dimension of the antenna is $166 \times 175\,\text{mm}^2$. At last, we found that considering vias radius gives us more practical result, but the return loss value is relatively lower than without consideration of vias radius. These antennas are quite easy to fabricate and can be used in 2.4 GHz band WLAN and Satellite radio services such as GlobalStar (2.5 GHz).

Design and Performance Analysis of Microstrip Array Antenna

Muhammad Mahfuzul Alam, **Md. Mustafizur Rahman Sonchoy**, **and Md. Osman Goni**
Department of Electronics and Communication Engineering
Khulna University of Engineering and Technology, Bangladesh

Abstract— This paper describes the design of different microstrip array antennas. Series-feed, corporate-feed and their combination that makes series-corporate feed and full-corporate feed antennas are analyzed and simulated. These antennas are designed on a thin substrate for the application of conformal microstrip array antenna. In all cases, we get return losses less than −15 dB at resonance frequencies. Sidelobe label is always lower 11.0 dB or more than main lobe for these antennas. The gain of these antennas are simulated and found an adequate result. One of these simulated antennas is implemented for performance tests. Operating frequency of these antennas are 2.45 GHz and 1.88 GHz. Substrate with different dielectric constants are used for simulation, these are 2.2 (RT/duroid 5880), 4.4 (FR4) and 10.2 (R03010). High dielectric constant is used to design large array antenna for size reductions. Dielectric constant has a huge impact in antenna performance by using different dielectric constants we want to show the appropriate use of dielectric constant value in different application areas. Substrate height is always considered 1.58 mm in the design of these antennas. Element spacing is a prime factor for array design not only for size reduction but also to minimize the grating lobe. For the reduction of the grating lobes element spacing is a little bit more than half a wavelength in free space. Different types of bends, transmission lines, power combiner and quarter wave length transformers are also discussed. Inset-feed techniques are used in the design of corporate feed antennas for good impedance matching. In the deign process we always concern about the size reduction possibilities and how to make the antenna compact. The gains of these array antennas are found 8.67563 dBi, 11.3139 dBi, 15.1505 dBi and 16.4071 dBi. At last Comparison of these antennas and how to design optimum array antennas are included. These antennas can be used in 2.4 GHz band WLAN system,sub-array for radar system or wireless communication system.

A Special Use of Wavelet Transform for Detecting the Live after Earthquake with Radar Waves

N. Uzunoglu[1] **and S. J. Javadi**[2]

[1]School of Electrical and Computer Engineering, National Technical University of Athens, Greece
[2]Department of Electrical Engineering, University of Zabol, Iran

Abstract— In this paper, New algorithm for Detecting the Live after Earthquake is presented. Here the application of the Radar waves with frequency 2.45 GHz in a portable system for detecting the live below a mass of concrete or trash is introduced. The characters of radar hardware are shown too. The software which is used for computer process is Lab-View, that some part of it is presented. Output of the Radar system which is analog convert to digital signal and enters into PC then for using of continues filtering by a section of the program digital signal is converted to an analog signal again. Now a software band-pass filter with variable pass band is applied, which change the quantity of the system. For the mathematic analyze a special wavelet transform (in-place kind) is applied that its algorithm and its mathematic debate are existed.

Effects of the Air-Hole Positions on Transmission Spectrum of a Silicon Micro-Cavity Photonic Crystal Filter

F. Emami, **A. R. Kashavarz**, **and H. Sarikhani-Khorami**
Optoelectronic Research Centre, Shiraz University of Technology, Shiraz, Iran

Abstract— In this paper the two-dimensional finite difference time domain (2D FDTD) method [1–3] is used to verify the transmittance calculations of an air hole waveguide microcavity photonic crystal (PC) filter made on a ridge-waveguide structure. When we excite the waveguide, a uniaxial perfectly matched layer (UPML) [4] around the guide is considered for our computer simulations (Fig. 1). For a uniform guide there is a stop band (or mirror-like behavior) in the transmittance spectrum (Fig. 2). Inserting some defects between the holes can cause wave transmission [3] (or filter-like behavior) through this stop band [5], (Fig. 3). We changed the radius of the air hole and found that it is possible to alter the peak frequency of pass band and the filter full widths at half maximum (FWHM) (Figs. 4, 5) so decreasing the air hole radii can cause a frequency shift toward the lower frequencies (or higher wavelengths) and for smaller hole radii the transmission peak and bandwidth would be increased [6, 10].

Raising the FWHM for such filters is seen and simulated using a nonuniform hole radius structure for the cavities such as proposed in Fig. 5. For a uniform and nonuniform (or tapered) hole radius the results is plotted in Fig. 6. As shown, there is a transmission peak at $\approx 0.98\,\mu\text{m}$; which is not appropriate for optical communication. To overcome this, we impose an engineering designation on the defect width, b, and tapering structure simultaneously so the peak frequency shifts to almost $1.55\,\mu\text{m}$, the desired frequency. The results are drawn in Figs. 7 and 8.

Session 5A1a
Electromagnetic Waves and Media

Simulation of Transmission Characteristics in Columnar of Different Radius Using Magnetic/Metal Materials

Keiko Masuda and Masatoshi Sano
Department of Electrical Engineering, Faculty of Engineering, Tokyo University of Science
1–3 Kagurazaka Shinjyuku-ku, Tokyo 162-8601, Japan

Abstract— The density growth, the downsizing of the circuits and the higher frequency of the operating frequency are advanced. The circuits composed of various elements cannot be simply treated at the high frequency.

The socket pin was simplified to a columnar element. Various materials and structures were analyzed propagation characteristic, because the skin effect on the transmission line is undertaken at the high frequency. Magnetic materials and metals were used in this study. The reduction of columnar radius was treated in connected part.

In this simulation, the pin length was $l = 6$ mm in columnar elements and the analytical frequency range was from 10 GHz to 40 GHz. When the analyzing radius was changed from 150 μm to 5 μm (Type1), the bandwidth narrowed from 11.2 GHz to 8 GHz. The frequency of attenuation pole was approximately 24.5 GHz irrespective of radius size. The obtain results indicate that elements were composed using columnar of different r. When columnar element was analyzed as $l_1 = 6 \sim 3$ mm ($r_1 = 100$ μm) and $l_2 = 0 \sim 3$mm ($r_2 = 10$ μm) at $l = l_1 + l_2$, the bandwidth has changed between from 10 GHz to 7.8 GHz. The frequency of attenuation pole has changed between from 21.8 GHz to 24.6 GHz (Type2). Type3 line was structure to exchange the magnetic material into the metal in part of small radius of Type2. The frequency of attenuation pole was approximately 9 GHz irrespective of the length size. When the length of the line of the small radius was changed from 0 mm to 3 mm, the attenuation pole has changed between from 20.2 GHz to 24.6 GHz (Type3).

A New Method for Deriving the Time-dependent Dyadic Green's Functions in Conductive Anisotropic Media

V. G. Yakhno
Electrical and Electronics Engineering Department, Dokuz Eylul University, Turkey

Abstract— The fundamental models of electromagnetic waves in anisotropic materials used in science and engineering are based on the Maxwell's equations [1]. A homogeneous anisotropic conductor, characterized by a positive constant permeability μ_0 and a symmetric positive definite conductivity tensor $\bar{\bar{\sigma}} = (\sigma_{ik})_{3\times 3}$, is considered in the paper. The governing equations for the distribution of the electric and magnetic fields $\mathbf{E}$ and $\mathbf{H}$ throughout the anisotropic conductor are described by the time-dependent Maxwell's equations in quasi-static approximation (see, for example, [2]):

$$curl_x \mathbf{H} = \bar{\bar{\sigma}}\mathbf{E} + \mathbf{J}_p, \quad curl_x \mathbf{E} = -\mu_0 \frac{\partial \mathbf{H}}{\partial t}, \quad \mathrm{div}_x(\mathbf{H}) = 0,$$

where $x = (x_1, x_2, x_3)$ is a space variable from R^3, t is a time variable from R, $\mathbf{E} = (E_1, E_2, E_3)$, $\mathbf{H} = (H_1, H_2, H_3)$, $E_k = E_k(x, t)$, $H_k = H_k(x, t)$, $k = 1, 2, 3$; $\mathbf{J}_p = (j_1, j_2, j_3)$ is the density of source currents responsible for the generation of eddy currents throughout the anisotropic conductor.

The main object of the paper is the electric and magnetic dyadic Green's functions. They are defined as electric and magnetic fields arising from impulsive current dipoles and satisfying the time-dependent Maxwell's equations in quasi-static approximation.

A new method of deriving these dyadic Green's functions is suggested in the paper. This method consists of several steps: equations for electric and magnetic dyadic Green's functions are written in the terms of the Fourier images; explicit formulae for the Fourier images of dyadic Green's functions are derived using the matrix transformations and solving some ordinary differential equations depending on the Fourier parameters; the inverse Fourier transform is applied to obtained formulae to find explicit formulae for dyadic Green's functions. Using these formulae images of electric and magnetic dyadic Green's function components are obtained in such conductive anisotropic medium as the white matter of the human head. We note that the similar approach for constructing Green's functions in homogeneous anisotropic dielectrics has been successively applied in the works [3, 4].

REFERENCES

1. Kong, K. J., *Electromagnetic Wave Theory*, John Wiley and Sons, New York, 1986.
2. Vagner, D., B. I. Lembrikov, and P. Wyder, *Electrodynamics of Magnetoactive Media*, Springer, New York, 2004.
3. Yakhno, V. G., "Constructing Green's function for time-depending Maxwell system in anisotropic dielectrics," *Journal of Physics A: Mathematical and General*, Vol. 38, 2277–2287, 2005.
4. Yakhno, V. G., "Computing and simulation of time-dependent electromagnetic fields in homogeneous anisotropic materials," *International Journal of Engineering Science*, Vol. 46, 411–426, 2008.

Session 5A1b
Advances in Communication and Imaging in Complex Environment

Performance Analysis of HF-wave Propagating through Simplified Ionospheric Model

R. Talhi[1], **A. Lebrere**[1], **and C. Blanchard**[2]
[1]University of Tours & CNRS-UMR 6115, Orleans 45071, France
[2]Department of Applied Physics, University of Granada, Granada 18071, Spain

Abstract— Earth's ionospheric effects on radio-wave propagation have captured, for many years, the interest of scientists and satellite communications/navigation and Radar specialists. The main reason of this interest is the high ionization variability in space (low, middle, high latitudes) and time (time of day, season, year) of the ionosphere (ionized layers at latitudes ranging from approximately 90 to 500 km), also called Space Weather, that is driven by solar and geomagnetic disturbances. Space weather phenomena like solar flares or coronal mass ejections, eject energetic radiations (UV radiation, X-rays and particles) towards the Earth and may lead, for example at high latitudes, to various effects such as Polar Cap Absorption which can totally "blackout" the whole HF band for many days, Auroral absorption, signal Doppler spread, or signal rapid and deep fading (scintillation effects) [1, 2]. Some other significant effects are also of importance to mention particularly to satellites operators, like energetic charged particles which can cause risks to onboard electronics (surface charging and electrostatic discharge), thermal expansion of Earth's atmosphere increases drag on objects in low Earth orbit, which can lead to shortening the working lifetime of operational satellites, or GPS signals which may be affected, leading to signal timing and position errors [3]. In many applications including HF-communications, a reliable performance requires statistically accurate ionospheric predictions under all kind of geophysical conditions at all times. In practice, empirical methods are widely used, and there is no really efficient method to predict space weather effects such as ionospheric storm onset and evolution and its magnitude and duration, and to analyze the physical process that govern this effect.

This paper discusses the analysis of the statistical characteristics of electromagnetic waves propagating through three-dimensional turbulent magnetized ionospheric plasma. The conditions of a weakly or moderately disturbed mid-latitude ionosphere, and geomagnetic field-aligned ionospheric irregularities, are assumed. Using typical ionospheric parameters, turbulence spectrum, and electron density values, numerical examples are shown. The angular power distribution and rate of polarization of EM waves multiply scattered are formulated in terms of the frequency (HF range) and oblique incidence, for given electron density and turbulence strength. Effect of fluctuations of electron density and turbulence strength on the shape of the angular power spectrum and the rate of polarization of scattered radiation have also been investigated in small-angle scattering approximation. Some other related ewamples will be discussed, as well as the validity of our results [4, 5]. Besides the difficult phenomenon of the turbulence in plasma physics [6], HF waves attenuation and absorption in the ionosphere are the critical outstanding questions of this challenging problem. The knowledge of their physical processes will provide further understanding of the behaviour of the ionosphere and its impact on space-Earth communication links.

REFERENCES

1. Jodalen, V., "HF radio-wave propagation at high latitudes," *The 4th Radio Reconnaissance Symposium*, September 10, 2003.
2. Wyant, A., et al., "Investigation of high latitude D-region effects on RF propagation," *Ionospheric Effects Symposium*, City of Alexandria, USA, May 13–15, 2008.
3. Metlay, S., et al., "Space weather and international civil space situational awareness," *Space Weather Workshop*, Boulder, Colorado, USA, April 28–May 1, 2009.
4. Danilkin, N. P., et al, "Electron collision frequency and HF waves attenuation in the ionosphere," *International Journal of Geomagnetism and Aeronomy*, Vol. 5, GI3009, doi: 10.1029/2004GI000081, 2005.
5. Gavrilenko, V. G., et al, "Some properties of the angular power distribution of EM waves multiply scatterd in a collisional magnetized turbulent plasma," *Plasma Physics Reports*, Vol. 31, No. 7, 604–615, 2005 (translated from Russian).
6. Stanislavsky, A., "Subdiffusion of beams through interplanetary and interstellar media," *Astronomical and Astrophysical Transactions*, Vol. 26, No. 6, 655–658, December 2007.

Reservation Based Call Admission Control in Wireless Communication

Malay Ranjan Tripathy[1], **Ashish Sharma**[2], **and Rachid Talhi**[3]

[1]Department of Electronics and Communication Engineering
Jind Institute of Engineering and Technology
Panipat Road, Jind 126102, India
[2]Department of Information Technology, Maharaja Agrasen Institute of Technology
Rohini Sector 22, Delhi 110086, India
[3]University of Tours and CNRS-UMR 6115, Orleans 45071, France

Abstract— The recent developments in wireless network technology [1–3] has increased the need for better admission control strategies and efficient utilization of resources such as channel or band width to provide a better Quality of Service (QoS). Future networks will impose challenging QoS problems due to requirement of not only simple mobile voice and data services but also access to mobile internet-based services with varying bandwidth and QoS requirements. Call admission control [4, 5] is a key element in the provision of guaranteed QoS in wireless networks. It is a technique to provide QoS in a network by restricting the access to network resources. Simply stated, it is a mechanism that accepts a new call request provided there are adequate free resources to meet the QoS requirements of the new call request without violating the committed QoS of already accepted calls. Dropping a call in progress is more annoying than blocking a new call request. Hence handoff calls are typically given higher priority.

This work presents different reservation based call admission control algorithms. It compares different QoS factors and limitations involved with them. Guard Channel Schemes [6] is one of them. It falls under the categories of the call admission control strategies for 2G Systems. This basic Guard Channel Allocation algorithm is bound to have certain limitations. The other Approximation Method Guard Channel Scheme [7] provides an edge over the basic algorithm. However, 3G cellular networks are highly influenced by common channel interference in the air interface. Interference Based Channel Assignment Schemes [8, 9] deal with this to increase the system capacity.

REFERENCES

1. Murray, K. and D. Pesch, "Call admission and handover in heterogeneous wireless networks," *IEEE Internet Computing*, Vol. 11, No. 2, 16–24, March 2007.
2. Ghaderi M. and R. Boutaba, "Call admission control in mobile cellular Networks: A comprehensive survey," *Wireless Communications* & *Mobile Computing*, Vol. 6, No. 1, 69–93, 2006.
3. Karthikeyan, N. K. and P. Narayanasamy, "A novel mobility based bandwidth reduction algorithm in cellular mobile networks," *IJCSNS International Journal of Computer Science and Network Security*, Vol. 8, No. 5, 62–69, May 2008.
4. Jeon, W. S. and D. G. Jeong, "Call admission control for CDMA mobile communication systems supporting multimedia services," *IEEE Trans. on Wireless Communications*, Vol. 1, No. 4, 649–659, October 2002.
5. Falowo, O. E. and H. A. Chan, "Joint call admission control algorithms: Requirements, approaches, and design considerations," *Computer Communications*, Vol. 31, No. 6, 1200–1217, April 2008.
6. Luong, D. D., A. P. M. Tran, and T. V. Do, "Guard channel CAC algorithm for high altitude platform networks," *The fourth international working conference on performance modeling and evaluation of heterogeneous networks (HET-NETs-2006)*, Yorkshire, UK, 22/1–22/10, 2006.
7. Zhang, Y., B. H. Soong, and M. Ma, "Approximation approach on performance evaluation for guard channel scheme," *Electronics Letters*, Vol. 39, No. 5, 465–467, March 2003.
8. Shin, S. M., C. H. Cho, and D. K. Sung, "Interference based channel assignment for DS-CDMA cellular systems," *IEEE Trans. on Vehicular Technology*, Vol. 48, No. 1, 233–239, January 1999.
9. Chen, H., S. Kumar, and C. C. Jay Kuo, "QoS aware radio resource management scheme for CDMA cellular networks based on dynamic interference guard margin (IGM)," *Computer Networks*, Vol. 46, No. 6, 867–879, 2004.

3D Discrete Wavelet Transform VLSI Architecture for Image Processing

Malay Ranjan Tripathy[1], **Kapil Sachdeva**[1], **and Rachid Talhi**[2]

[1]Department of Electronics and Communication Engineering
Jind Institute of Engineering and Technology, Jind, Haryana, India
[2]University of Tours and CNRS-UMR 6115, Orleans 45071, France

Abstract— Many evolving multimedia applications require transmission of high quality images over the network. One obvious way to accommodate this demand is to increase the bandwidth available to all users. Of course, this "solution" is not possible without technological and economical difficulties. The other way of improving the performance of transmission is to reduce the volume of the data that must be transmitted. There has been a tremendous amount of progress in the field of image compression during the past 15 years. In order to make further progress in image coding, many research groups have begun to use wavelet transforms [1].

Wavelet Transform has been successfully applied in different fields, ranging from pure mathematics to applied science. Numerous studies, carried out on wavelet Transform, have proven its advantages in image processing and data compression and have made it a basic encoding technique in recent data compression standards as well as for multi-resolution decomposition of signal and image processing applications. Pure software implementations of the Discrete Wavelet Transform, however, appear to be the performance bottleneck in real-time systems in terms of performance. Therefore, hardware acceleration of the DWT has become a topic of recent research.

In this paper, we propose an improved version of lifting based 3D Discrete Wavelet Transform (DWT) VLSI architecture which uses bi-orthogonal 9/7 filter processing [2, 3]. This is implemented in FPGA by using VHDL codes. The lifting based DWT architecture has the advantage of lower computational complexities transforming signals with extension and regular data flow. This is suitable for VLSI implementation. It uses a cascade combination of three 1-D wavelet transform along with a set of in-chip memory buffers between the stages. These units are simulated, synthesized and optimized for Spartan-II FPGA chips using Active-HDL Version 7.2 design tools [4, 5]. The timing analysis tools of this (Active-HDL), reports the frequency above 100 MHz and ensures 100% hardware utilization.

REFERENCES

1. Daubechies, I., "Ten lectures on wavelets," *SIAM*, Philadelphia, 1992.
2. Jiang, R. M. and D. Crookes, "FPGA implementation of 3D discrete wavelet transform for real-time medical imaging," *ECCTD*, 519–522, August 2007.
3. Ferretti, M. and D. Rizzo, "A parallel architecture for the 2-D discrete for 2-D discrete wavelet transform with integer lifting scheme," *Journal of VLSI Signal Processing*, Vol. 28, 165–115, 2001.
4. "Spartan-II 2.5 V FPGA family: Complete data sheet," http://direct.xilinx.com/bvdocs/publications/ds001.pdf, Aug. 2, 2004.
5. Brown, S. and Z. Vranesic, *Fundamentals of Digital Logic with VHDL Design*, Tata McGraw Hill Publications, 2005.

Design of Novel Tunable Phase Shifter

Sharif Iqbal Mitu Sheikh, M. Basorrah, G. Alhulwah, K. Alanizi, and M. Alfarsi
Electrical Engineering Department, King Fahd University of Petroleum & Minerals (KFUPM)
Dhahran 31261, Saudi Arabia

Abstract— Phase shifters are widely used in wireless communication devices to electronically steer the antenna beams or nulls in the desired direction without physically re-positioning the antenna. With rapid growth in microwave integrated circuit technology, microstrip phase shifters received renewed interest due to its lightweight and compact size. But digital switched line phase shifter often involves complicated control circuits and considerable insertion loss. On the other hand, analogue ferrite phase shifters requires bulky external magnets. In this paper, an externally tunable microstrip phase shifter is designed, where control circuits are minimized by implementing the phase tuning using both digital and analogue techniques.

The designed axially magnetized ferrite phase shifter is shown in Figure 1(a). It uses switchable diodes to convert a microstrip line section into a rectangular waveguide and in turn achieve different phase shift due to changed propagation constant of the path. So, when the diodes are off, the device behaves as a all microstrip line (u-u-u) phase shifter. But when the diodes are on, the device will behave like microstrip-waveguide-microstrip (u-g-u) phase shifter. At a frequency of 5.5 GHz, the simulated differential phase shift for both cases are plotted in Figure 1(b). Note that due to digital switching, the phase response can be changed between the 'u-u-u' and 'u-w-u' curves. Also by changing the external biasing (H_0) from 69 kA/m to 79 kA/m, the phase response can be varied up to 250° in an analogue manner. The device exhibits acceptable insertion loss for all cases ($|S_{21}| < -0.05$ dB/mm). A multi-bit phase shifter of this class can be used to excite an array antenna for controlled beam scanning application, like WLAN.

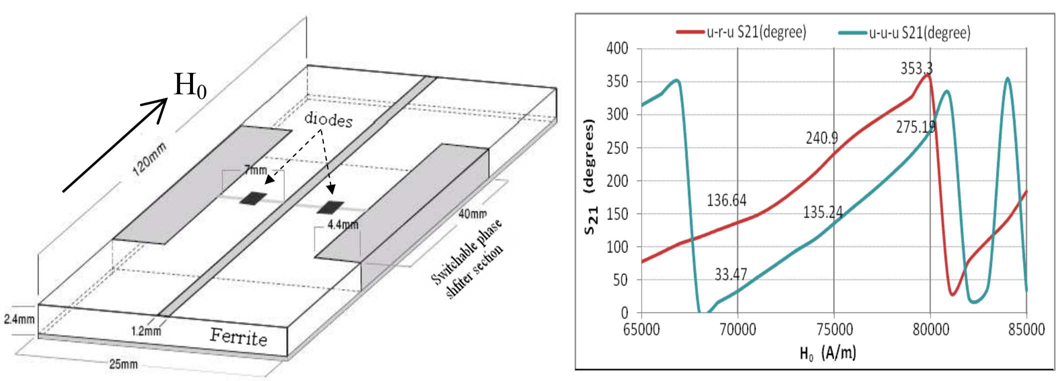

(a) (b)

Figure 1: (a) Schematic diagram of the designed phase shifter. (b) Simulated transmission phase response (S_{21}) at $f = 5.5$ GHz, which shows digital and analogue phase tuning.

ACKNOWLEDGMENT

The authors are thankful for the support of King Fahd University of Petroleum & Minerals (KFUPM), Dhahran, Saudi Arabia.

REFERENCES

1. Batchelor, J. C., et al., "Scanned microstrip arrays using simple integrated ferrite phase shifters," *IEE Proc. Microwave Antennas Propagation*, Vol. 147, No. 3, 237–241, 2000.
2. Jin, Z., et al., "Design and performance of a new digital phase shifter at x-band," *IEEE MWCL*, Vol. 14, No. 9, 428–430, 2004.

Intelligent Wireless Communication Enabled Sensor Network for Event Detection

Malay Ranjan Tripathy and O. P. Yadav
Department of Electronics and Communication Engineering
Jind Institute of Engineering and Technology (JIET), Jind, Haryana, India

Abstract— Wireless Sensor Networks (WSN) [1] present a new generation of real-time embedded systems with limited computation, energy and memory resources that are being used in a wide variety of applications where traditional networking infrastructure is practically infeasible. Recent advances in intelligent control mechanisms like fuzzy logic control systems [2] make these WSN applications more efficient and versatile. In WSN, a large number of low cost sensor nodes [3] are densely deployed to monitor the environment of interest. Due to its numerous applications WSN is a topic of prime interest to many researchers.

Sensor nodes in general powered by small batteries that are hard to replace or recharge. Therefore energy constraint is a major challenge for wide and remote applications [4, 5]. For an example deployment of large number of sensor nodes [3, 6] across a vast area of forest to detect, monitor or track of fire [7] is a difficult task to realize with these power hungry sensors for reliable and long duration operations. In a typical wireless enabled sensor system energy consumption occurs in three domains: Sensing, data processing and communication. During sensing the least possible of energy is consumed by the sensing circuits. In this paper we propose to use fuzzy logic control mechanism to activate rest of the sensing circuits (i.e., data processing and communication) only when the event of fire in the environment is available. So that WSN when empowered by Fuzzy logic control mechanism will work as an intelligent and power efficient fire detecting sensor network.

To address these issues we have used fuzzy logic approach for efficient detection. We have applied WSN to temperature sensor networks to trace fire in remote forest. In fact, fuzzy logic is reminiscent of human thinking processes and natural language enabling decisions to be made based on vague information [2]. The fire condition is described using linguistic variables. Fuzzy subsets and the corresponding membership functions describe temperature conditions of the fire. A knowledge base, comprising rule and data bases, is built to support the fuzzy inference. The fire condition is detected using a compositional rule of fuzzy inference.

REFERENCES

1. Akyildiz, I. F., W. Su, Y. Sankarasubramaniam, and E. Cayirci, "Wireless sensor networks: A survey," *Computer Networks*, Vol. 38, No. 4, 393–422, March 2002.
2. Mendel, J. M., "Fuzzy logic systems for engineering: A tutorial," *Proceedings of IEEE*, Vol. 83, No. 3, 345–377, March 1995.
3. Jain, E. and Q. Liang, "Sensor placement and lifetime of wireless sensor networks: Theory and performance analysis," *Sensor Network Operations*, S. Phoha, T. F. LaPorta, and C. Griffin, Eds. Wiley, New York, 2005.
4. Shu, H., Q. Liang, and J. Gao, "Wireless sensor network lifetime analysis using interval type-2 fuzzy logic systems," *IEEE Transaction on Fuzzy Systems*, Vol. 16, No. 2, 416–427, April 2008.
5. Estrin, D. and R. Govindan, "Next century challenges: Scalable coordination in sensor networks," *Mobicon'99*, Seattle WA, 263–270, August 1999.
6. Romer, K. and F. Mattern, "The design space of wireless sensor networks," *IEEE Wireless Communications*, Vol. 11, No. 6, 54–61, 2004.
7. Yu, L., N. Wang, and X. Meng, "Real-time forest fire detection with wireless sensor networks," *IEEE Conference on Wireless Communications, Networking and Mobile Computing*, Vol. 2, 1214–1217, Sep. 23–26, 2005.

Modeling of Dispersive Cloaks with the TLM Method

Cédric Blanchard[1], **Jorge Andrés Portí**[1], **Juan Antonio Morente**[1], **Alfonso Salinas**[1], **and Rachid Talhi**[2]

[1]Department of Applied Physics, University of Granada, Granada 18071, Spain
[2]CNRS, UMR 6115 and University of Tours, 3A Avue de la recherche scientifique, Orléans 45071, France

Abstract— The Transmission Line Modeling (TLM) [1–3] method can be considered as a modeling procedure rather than a direct numerical solution of Maxwell's equations. Indeed, the problem is rendered discrete in space by filling the region to be simulated with interconnected transmission lines that are capable of modeling the electromagnetic properties of the space. The interesting point in the TLM approach is that the transmission line mesh can be regarded as the numerical representation of a real structure. As a consequence, the mesh is expected to disperse with frequency, no artificial dispersion has to be added as it is the case for other time domain methods. On the other hand, the constitutive parameters of a cloaking shell [4] must also disperse so that no physical law is violated [5]. In this work, we will show how to simulate dispersive cloaks with TLM, and some of their interesting properties will be emphasized. Furthermore, we will previously show that highly accurate simulations of the cloaking effect can be achieved thanks to the versatility of TLM [6].

ACKNOWLEDGMENT

This work has been supported in part by the "Ministerio de Educación y Ciencia" of Spain under research projects No. FIS2004-03273 and FIS2007-63293, cofinanced with FEDER funds of the European Union.

REFERENCES

1. Johns, P. B. and R. L. Beurle, "Numerical solution of 2-dimensional scattering problems using a transmission-line matrix," *Proc. Inst. Elec. Eng.*, Vol. 118, 1203–1208, 1971.
2. Johns, P. B., "A symmetrical condensed node for the TLM method," *IEEE Trans. Microw. Theory Tech.*, Vol. 35, 370–377, 1987.
3. Portí, J. A., J. A. Morente, A. Salinas, M. Rodriguez-Sola, and C. Blanchard, "On the circuit description of TLM nodes," *Int. J. Electron.*, Vol. 93, 479–491, 2006.
4. Pendry, J. B., D. Schurig, and D. R. Smith, "Controlling electromagnetic fields," *Science*, Vol. 312, 1780–1782, 2006.
5. Yao, P., Z. Liang, and X. Jiang, "Limitation of the electromagnetic cloak with dispersive material," *Appl. Phys. Lett.*, Vol. 92, 031111, 2008.
6. Blanchard, C., J. Portí, B.-I. Wu, J. A. Morente, A. Salinas, and J. A. Kong, "Time domain simulation of electromagnetic cloaking structures with TLM method," *Opt. Express*, Vol. 16, 6461–6470, 2008.

Session 5A2
THz, Photonic Crystals, Nanophotonics and Plasmonics

Fringing Field Impact on Resonant Frequency in THz Plasma Wave Devices

I. Khmyrova
University of Aizu, Japan

Abstract— The growing interest to terahertz (THz) region of electromagnetic spectrum is pulled by a variety of its possible applications for sensing and imaging in biomedicine, radio astronomy, defense, etc. Despite strong demand in compact solid-state devices capable to operate as emitters, receivers, mixers of the THz radiation their development is still a challenging problem. Excitation of plasma oscillations in the two-dimensional electron gas (2DEG) channel of high-electron mobility transistor-like structures has been proposed as a promising approach for the realization of emission, detection, mixing and frequency multiplication of THz radiation [1]. If the length of the gate to the 2DEG channel is in submicrometer range, the latter can serve as a resonant cavity for plasma waves with the resonant frequency in the THz range. Such plasma oscillations in the HEMT-like structures have been observed experimentally [2, 3], however, measured frequencies of THz resonances occurred to be lower than theoretically predicted. Resonant frequency of plasma oscillations in 2DEG channel depends on its electron concentration which can be tuned by the gate bias voltage and is reciprocal to the gate length. Thus, to achieve higher resonant frequencies scaling down of the gate length below 100 nm has been performed. However, relevant reduction in the thickness of the layer separating the gate metal contact and 2DEG surface has technological restrictions. As a result, fringing of the electric field due to the gate bias voltage becomes an important issue.

Because of fringing gate bias voltage controls the electron concentration not only in the 2DEG channel beneath the gate but also in its ungated fringed parts. This effect can be interpreted as an effective gate extension. In this paper we develop the model in which the concept of gate extension is proposed to describe the fringing field. The distributions of the electric field and sheet electron density at 2DEG surface are calculated. The dependence of the resonant plasma frequency on the fringing field is obtained. To perform IsSpice simulation we develop an equivalent circuit model in which gated and fringed ungated 2DEG channel regions are represented by cascaded transmission line (TL) model. RLC-components of TL model are related to physical and geometrical parameters of the HEMT-like structure under consideration [4]. The results of analytical calculations and IsSpice simulation demonstrate that fringing field can cause the reduction of THz plasma resonances and should be taken into account. The results obtained in the paper are in rather good agreement with experimental data.

REFERENCES

1. Dyakonov, M. and M. S. Shur, *IEEE Trans. Electron Devices*, Vol. 43, 1640, 1996.
2. Otsuji, T., M. Hanabe, and O. Ogawara, *Appl. Phys. Lett.*, Vol. 85, 2119, 2004.
3. Teppe, F., W. Knap, D. Veksler, M. S. Shur, A. P. Dmitriev, V. Y. Kacharovskii, and S. Rumyantsev, *Appl. Phys. Lett.*, Vol. 87, 052107, 2005.
4. Khmyrova, I. and Y. Seijyou, *Appl. Phys. Lett.*, Vol. 91, 143515, 2007.

Single-photon Detectors for the Visible and Infrared Parts of the Spectrum Based on NbN Nanostructures

K. V. Smirnov[1,2], **Yu. B. Vakhtomin**[1,2], **A. V. Divochiy**[1,2], **R. V. Ozhegov**[1,2], **I. V. Pentin**[1], **E. V. Slivinskaya**[2], **M. A. Tarkhov**[1,2], **and G. N. Gol'tsman**[1]

[1]Moscow State Pedagogical University, 29 Malaya Pirogovskaya St., Moscow 119992, Russia
[2]SCONTEL, 5/22 Rossolimo St., Moscow 119021, Russia

Abstract— The research by the group of Moscow State Pedagogical University into the hot-electron phenomena in thin superconducting films has led to the development of new types of detectors [1, 2] and their use both in fundamental and applied studies [3–6]. In this paper, we present the results of the development and fabrication of receiving systems for the visible and infrared parts of the spectrum optimised for use in telecommunication systems and quantum cryptography.

At the heart of a receiving system is a superconducting detector [7, 8] fabricated from NbN films 3–4 nm thick. Depending on the application, a system has either one or two identical channels (two channels are needed for correlation measurements).

A single-photon detector is a long and narrow (~100 nm) superconducting strip patterned such as to cover the largest possible area with a maximum filling factor for the effective coupling with radiation. For example, when the standard single-mode fibre is used with a diameter of 9 μm the strip is patterned as a meander covering an area of 10 μm × 10 μm; the total length of the strip in that case is 0.5 mm.

For the precise coupling of a detector with a single-mode fibre we use the alignment machine Fineplacer-96 Lamda by Finetech (Germany).

The measurements performed at three wavelengths −0.94 μm, 1.3 μm and 1.55 μm — have shown that the quantum efficiency as high as 30% can be obtained at a level of dark counts of less than 10 counts per second (Fig. 1).

Other characteristics are as follows:

- output pulse duration: ≤ 5 ns;
- jitter: ≤ 40 ps;
- output pulse height: > 0.2 V;
- maximum counting rate: > 70 MHz.

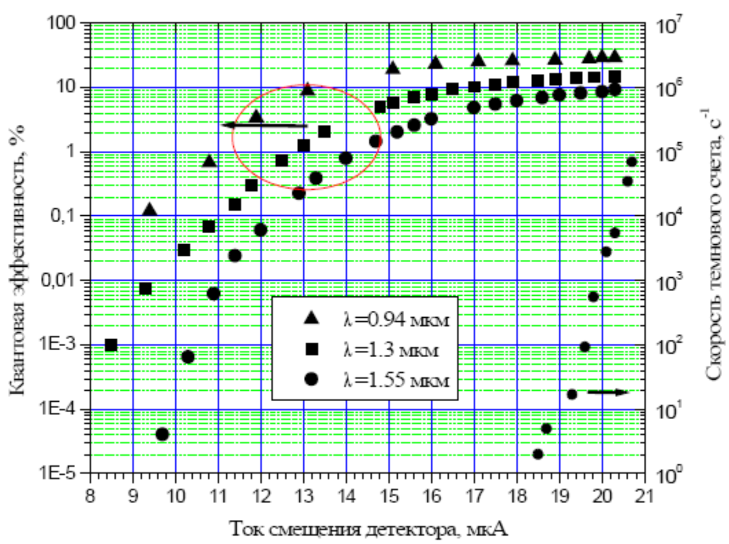

Figure 1: The dark counts rate and quantum efficiency as a function of the detector current at the wavelengths 0.94 μm, 1.3 μm and 1.55 μm. The operating temperature is 1.8 K.

The receiving systems are fabricated as dipsticks to be inserted into He transport tanks; He enters the dipstick volume, thermally insulated from the tank volume, through a capillary. An operating temperature of $\sim$1.8 K is achieved by pumping He vapour out of the dipstick volume.

REFERENCES

1. Divochiy, A., F. Marsili, D. Bitauld, et al., *Nature Photonics*, Vol. 2, 302–306, 2008.
2. ? T. 48, No. 10–11, CTP. 964, 2005.
3. Hostein, R., A. Michon, G. Beaudoin, et al., *Appl. Phys. Lett.*, Vol. 93, 073106, 2008.
4. Takesue, H., S. Nam, Q. Zhang, et al., *Nature Photonics*, Vol. 1, 343–348, 2007.
5. Planken, P., *Nature*, Vol. 456, 454–455, 2008.
6. Huber, A. J., F. Keilmann, J. Wittborn, et al., *Nano Lett.*, Vol. 8, No. 11, 3766–3770, 2008.
7. Gol'tsman, G., O. Okunev, G. Chulkova, et al., *Applied Physics Letters*, Vol. 79, 705–707, 2001.
8. Gol'tsman, G. N., K. Smirnov, P. Kouminov, et al., *IEEE Trans. Appl. Supercon.*, Vol. 13, No. 2, 192–195, 2003.

Absolute Power Measurement of Single THz Pulses Generated by Ultrashort Laser Pulses on Top of Gold Layered Nano Gratings

G. Zieger[1], **F. Garwe**[1], **T. May**[1], **U. Hübner**[1], **E. Kessler**[1], **M. Zeissberger**[1], **K. Wynne**[2], **W. Paa**[1], **and H.-G. Meyer**[1]

[1]Institute of Photonic Technology, Albert Einstein Straße 9, Jena 07745, Germany
[2]Department of Physics, University of Strathclyde, SUPA, Glasgow G4 0NG, UK

Abstract— Terahertz (THz) technology has been investigated extensively concerning its potential for numerous applications including spectroscopy, medical imaging, packing control, security, and many others. The major building blocks of a THz system are the source of THz radiation and the detector. THz sources can be sorted by the generation process of radiation. At first, direct incoherent sources like heat radiation provide weak intensity and broadband incoherent emission only. Direct coherent sources such as free electron lasers or gas lasers are still complex and expensive. Quantum cascade lasers and p-germanium lasers are compact and cost effective but both concepts require cryogenic cooling adding complexity and cost. The second class includes concepts with frequency multiplication, which however have poor tunability. The third class of sources is responsible for the fast development of THz technology in the last decade. It relies on THz generation from optical sources via either parametric generation, optical rectification, difference frequency generation, or photomixing. Another often-used alternative is electrooptic conversion in photoconductive switches. Newest photomixing technologies use cost effective diode lasers for generation of continuous wave THz radiation but the THz emission power is only about 100 pW and thus by far too low for applications. For the detection of THz radiation the most common concepts are bolometers, golay cells, and heterodyne or homodyne detection concepts.

In this work, we use another new method for producing THz radiation based on the excitation of surface plasmons (SP) on top of a gold layered nano grating (period 500 nm) by ultrashort laser pulses (wavelength 785 nm) with repetition rates of 1 kHz [1]. SP can facilitate multiphoton excitation of electrons in metals by 150 femtosecond laser pulses resulting in the emission of photoelectrons under vacuum conditions. Under the right conditions, an electric field associated with the surface plasmons is created causing a ponderomotive force pushing photoelectrons out of and away from the surface. These accelerated photoelectrons are the reason for the THz radiation with pulse durations increase proportional to the envelope of the laser pulse. To measure the absolute power of such short THz pulses we used a calorimeter principle. Before the detector, we used a filter passing THz radiation in the range from 0.30 THz to 0.38 THz. The detector was a homemade voltage biased transition edge sensor (TES) [2]. To date they offer the best combination of high sensitivity, speed, and operability. A TES transforms incident radiation power into an electric signal that can be measured. For that purpose, an absorber is connected

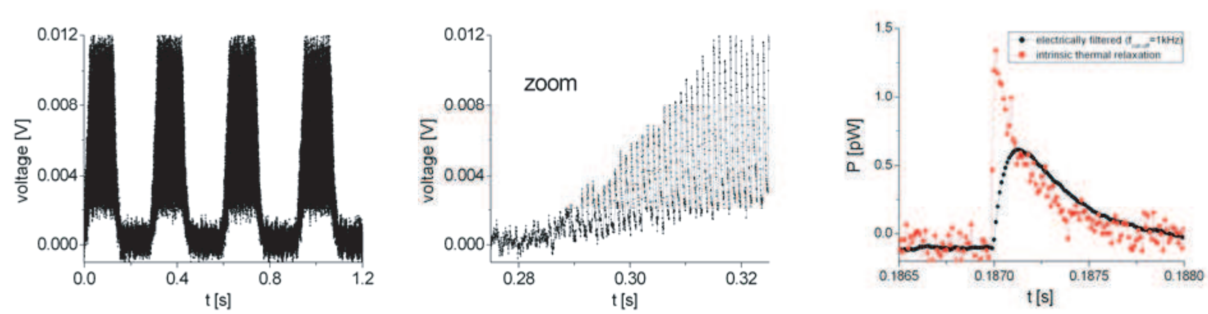

(a) (b) (c)

Figure 1: Left: With 3 Hz laser shutter modulated signals detected from THz pulses with repetition rates of 1 kHz. Middle: Zoom into the smooth transition between no signal to maximal THz signal, induced by the shutter controlled slow increasing of the laser radiated area of the gold grating. Right: Zoom into a single THz pulse signal. The black curve is the electric filtered detector signal. The red curve is the intrinsic thermal relaxation of the detector, the area under this curve is the energy of the pulse and from [1] we know the true THz pulse length (2 ps). Therefore, we estimate the pulse power some 100 μW.

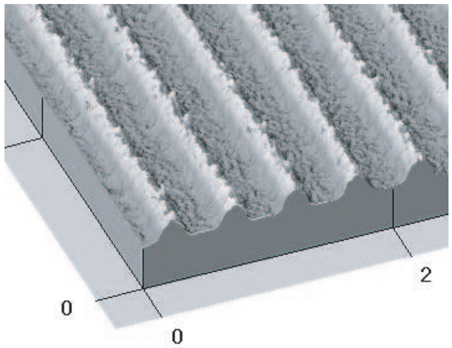

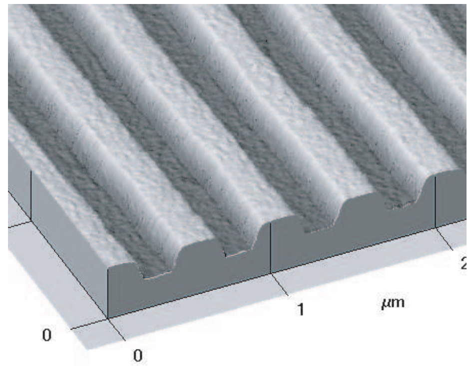

Figure 2: Shows AFM pictures of several gold layered nano gratings in glass slides. The thickness of the gold layer was 40 nm (not shown here). (left) Sinusoidal grating shows no detectable THz pulse by radiation with 150 fs laser pulses (right) grating with sharp edges shows a very strong THz pulse by radiation with fs laser pulses with the same laser parameters.

to a thermal bath at constant temperature T_0 (300 mK) by a weak thermal link with thermal conductivity. The superconducting thermometer is held at a working temperature $T > T_0$ in the transition range by electric heating. Incident electromagnetic power heats up the absorber and the thermometer. This leads to decreased heating because of the strong electrothermal feedback (ETF) [3], and the temperature falls back to the working point T. Therefore, the ETF mechanism reduces the thermal time constant and makes this type of bolometer typically by two orders of magnitude faster than the intrinsic thermal time constant would allow. The actually measured variable is the heating current which is proportional to the incident radiation power. This is realized using highly sensitive superconducting quantum interference device (SQUID) ampere meters.

The absorption coefficient of our detectors at the observed THz frequencies is better than 75%. We estimate the THz pulse power in the frequency range 0.34 THz +/− 40 MHz which impacts the detector area to some 100 μW (see Fig. 1(c)). These results were observed only by gold gratings with sharp edges. In our studies we have investigated samples with different methods such as photoelectron emission microscopy (PEEM) [4] and by doing FEM simulations in order to understand the true THz emission mechanism and to optimize the THz pulse power generated by ultra short laser pulses interacting with gold nano gratings. So we can use in future normal bolometer or thermopile [5] without cooling for detection.

REFERENCES

1. Welsh, G. H., N. T. Hunt, and K. Wynne, *Phys. Rev. Lett.*, Vol. 98, 026803, 2007.
2. May, T., V. Zakosarenko, R. Boucher, E. Kreysa, and H.-G. Meyer, *Supercond. Sci. Technol.*, Vol. 16, 1, 2003.
3. Lee, A. T., P. L. Richards, S. W. Nam, B. Cabrera, and K. D. Irwin, *Appl. Phys. Lett.*, Vol. 69, 1801, 1996.
4. Meyer zu Heringdorf, F., L. I. Chelaru, S. Möllenbeck, D. Thien, and M. Horn von Hoegen, *Surface Science*, Vol. 601, 4700, 2007.
5. Dillner, U., E. Kessler, V. Baier, A. Berger, T. Eick, D. Behrendt, and H. Urban, *Proceedings of IRS*^{2}, 2006.

Ultrafast Superconducting Bolometer Receivers for Terahertz Applications

R. V. Ozhegov[1,2], **A. V. Smirnov**[1], **Yu. B. Vakhtomin**[1,2], **K. V. Smirnov**[1,2], **A. V. Divochiy**[1,2], **and G. N. Goltsman**[1]

[1]Moscow State Pedagogical University, 29 Malaya Pirogovskaya St., Moscow 119992, Russia
[2]SCONTEL, 5/22 Rossolimo St., Moscow 119021, Russia

Abstract— The research by the group of Moscow State Pedagogical University into the hot-electron phenomena in thin superconducting films has led to the development of new types of detectors [1, 2] and their use both in fundamental and applied studies [3–6]. In this paper, we present the results of testing the terahertz HEB receiver systems based on ultrathin (~ 4 nm) NbN and MoRe detectors with a response time of 50 ps and 1 ns, respectively. We have developed three types of devices which differ in the way a terahertz signal is coupled to the detector and cover the following ranges: 0.3–3 THz, 0.1–30 THz and 25–70 THz. The main characteristics of the receiver systems are presented in Table 1.

Table 1.

Type of detector	1/1a	2/2a	3/3a
Frequency range, THz	0.3–3	25–70	0.1–30
NEP, $\mathrm{W \cdot Hz^{-0.5}}$	$5\text{–}7 \cdot 10^{-14}/3\text{–}5 \cdot 10^{-13}$	$1\text{–}2 \cdot 10^{-12}/4\text{–}5 \cdot 10^{-12}$	$4\text{–}6 \cdot 10^{-11}/1\text{–}2 \cdot 10^{-10}$
Response time, ns	1/0.05	1/0.05	1/0.05
Dynamic range, μW	1	50	10^5

In the case of the receiving system optimized for 0.3–3 THz, the sensitive element (a strip of a superconductor with planar dimensions of 0.2 μm (length) by 1.7 μm (width)) was integrated with a planar broadband log-spiral antenna (detector type 1/1a in Table 1). For additional focusing of the incident radiation a silicon hyperhemispherical lens was used. For the 0.1–30 THz receiving system (detector type 3/3a in Table 1), the sensitive element was patterned as parallel strips (2 μm wide each) filling an area of $500 \times 500\,\mu\mathrm{m}^2$ with a filling factor of 0.5. In the receiving system of this type we used direct coupling of the incident radiation to the sensitive element. In the 25–70 THz range (detector type 2/2a in Table 1) we used a square-shaped superconducting detector with planar dimensions of $10 \times 10\,\mu\mathrm{m}^2$. Incident radiation was coupled to the detector with the use of a germanium hyperhemispherical lens.

The response time of the above receiving systems is determined by the cooling rate of the hot electrons in the film. That depends on the electron-phonon interaction time, which is less for ultrathin NbN than in MoRe.

REFERENCES

1. Divochiy, A., F. Marsili, D. Bitauld, et al., *Nature Photonics*, Vol. 2, 302–306, 2008.
2. Finkel, M. I., S. N. Maslennikov, and G. N. Gol'tsman, "Terahertz heterodyne receivers based on superconductive hot-electron bolometer mixers," *Radiophysics and Quantum Electronics*, Vol. 48, No. 10–11, 859–864, 2005.
3. Hostein, R., A. Michon, G. Beaudoin, et al., *Appl. Phys. Lett.*, Vol. 93, 073106, 2008.
4. Takesue, H., S. Nam, Q. Zhang, et al., *Nature Photonics*, Vol. 1, 343–348, 2007.
5. Planken, P., *Nature*, Vol. 456, 454–455, 2008.
6. Huber, A. J., F. Keilmann, J. Wittborn, et al., *Nano Lett.*, Vol. 8, No. 11, 3766–3770, 2008.

Effective Refractive Index Approximation and Surface Plasmon Resonance Modes of Metal Nanoparticle Chains and Arrays

Ergun Simsek
Department of Electrical and Electronics Engineering, Bahcesehir University, Istanbul, Turkey

Abstract— Surface Plasmons (SPs), which are simply electromagnetic waves that propagate along a conductor-dielectric interface, are quite attractive to a wide spectrum of engineers and scientists due to their potential in developing new types of optical antennas, photonic devices and sensors. Their importance comes from the fact that the periodically located metal nanoparticles (MNPs) can lead to giant electromagnetic field enhancement and sub-wavelength lateral mode confinement. Some of the current SP applications are optical waveguides and antennas, surface or tip enhanced Raman scattering, and nonlinear frequency generation. In all of these SP applications, researchers tune up the properties of SPs and their interaction with light for their problem of interest by changing the shape, size, and material composition of the NPs.

It has been shown that optical waveguides with sub-wavelength lateral mode confinement can be build using periodically located MNP chains in which dispersion relation becomes a crucial parameter of the design. In this direction, many researchers have studied dispersion relation of SPR modes of MNP chains experimentally in the last decade. In the mean time novel theoretical models have been developed to analyze such systems. One very commonly used theoretical model is the discrete dipole approximation (DDA). DDA is a simple yet effective method but requires a homogeneous background that is not the case most of the time for real MNP applications, e.g., MNPs fabricated on top of ITO coated-glass slides creating a three-layer media. In such structures, background can be assumed to be a multilayered environment and DDA can be still helpful given it is implemented via layered-media Green's functions (LMGFs). However, the evaluation of these computationally expensive LMGFs is a bottleneck for many researchers due to their mathematical complexity. Some researchers have tried to overcome this problem by the help of image theory (IT). Experimental results support the validity of the theoretical model but it is still unclear how IT can be implemented for structures with more than two layers, especially for the case where the width of the layer (on which NPs are aligned) is less than the half of the height of the NPs.

To resolve the complexity of these problems, a simple effective refractive index (ERI) approximation is adopted to obtain the SPR modes of metal NP chains and arrays in multilayered structures. In this approximation if we deal with a half-space problem, we simply take the average of refractive indices of two neighboring layers. If the number of layer is more than two, ERI depends on the ratio of the width of the mid-layers to the wavelength. Here, this approximation is first applied to one dimensional (1D) periodically located NP chains. Numerical results show that ERI provides very close results to ones obtained experimentally. Then, this approximation is applied onto two dimensional (2D) periodically located NP arrays by extending the theory developed by Weber and Ford for the 1D case. In this method, we search for SPR wavelengths (frequencies) on the complex frequency (ω) domain, hence not only the resonant wavelengths can be revealed but also the propagation lengths. This fully retarded theoretical model includes the effects of retardation, radiative damping, and dynamic depolarization due to the finite size of the NPs based on the Modified Long Wavelength Approximation. In addition, the use of different polarizability coefficients along the semi-axes of ellipsoidal NPs reveals the existence of one longitudinal and two transverse modes.

An All Optical Switch Based on Nonlinear Photonic Crystal Microcavities

N. Nozhat, **A. Taher Rahmati**, and **N. Granpayeh**
Faculty of Electrical Engineering, K. N. Toosi University of Technology, Tehran, Iran

Abstract— In this paper, the performance of a 1×1 switch based on two dimensional (2-D) nonlinear photonic crystal (PC) microcavities has been presented. The proposed structure, as shown in Fig. 1, consisted of one waveguide and one resonant microcavity adjacent to it. We have used an effective numerical method based on the finite-difference time-domain (FDTD) method. The structure composed of a 15×15 square lattice of $AlGaAs$ rods with linear refractive index of $n_0 = 3.4$ and nonlinear-index coefficient of $n_2 = 1.5 \times 10^{-17}\,\mathrm{m}^2/\mathrm{W}$ at 1550 nm wavelength. The rods are located in air with radii of $r = 0.2a$, where a is the lattice constant. The structure has a large bandgap for transverse magnetic (TM) fields between normalized frequencies of $0.29(c/a)$ and $0.42(c/a)$, where c in the velocity of light in vacuum.

We have shown that by increasing the input signal power the refractive indices of the rods besides the waveguide are changed, due to the nonlinear Kerr effect. Therefore, the resonant frequency of the cavity shifts to a lower value than its linear resonant frequency. In the linear state, when the frequency of the input signal is the same as the resonant frequency of the cavity, the input lightwave couples to the cavity and there is no output power at port 2, as demonstrated in Fig. 2(a). By increasing the power of the input signal, the refractive indices of the rods and the resonant frequency of the cavity change, because of the nonlinearity of the rods. So, the input lightwave transmits through the waveguide, without coupling to the cavity, and there is an output power at port 2, as shown in Fig. 2(b).

In this paper, the performance of a 1×1 switch in linear and nonlinear states for various radii of the microcavity and different distances from the waveguide have been simulated and analyzed. The distributions of the electromagnetic fields have been shown. The nonlinear resonant frequency of the cavity and the refractive index variations of the rods due to the Kerr nonlinearity have been calculated.

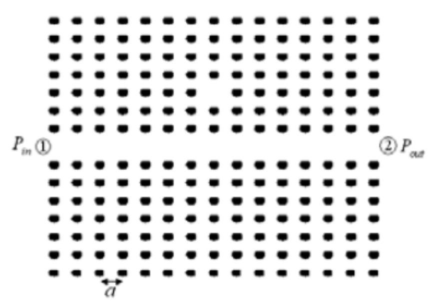

Figure 1: Schematic of proposed nonlinear photonic crystal switch with one waveguide and one cavity besides it.

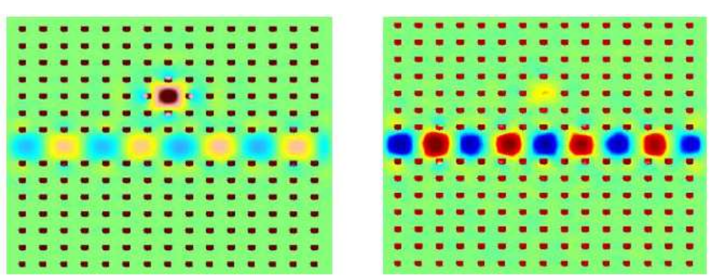

(a) (b)

Figure 2: Electric field distribution of the photonic crystal switch at normalized resonant frequency $f_c = 0.3816$ in (a) linear and (b) nonlinear states.

Homogenization of Dissipative Photonic Crystals

Lyudmila Gumen[1], **Jesús Arriaga**[2], **and Arkadii Krokhin**[3]

[1]Universidad Popular Autónoma del Estado de Puebla, Mexico
[2]Instituto de Física, Universidad Autónoma de Puebla, Mexico
[3]University of North Texas, USA

Abstract— We consider photonic crystal of parallel rods imbedded in a dielectric matrix in the low-frequency limit. We assume dissipative material for the rods and for the matrix with dielectric permittivities $\varepsilon_a(\omega) = \varepsilon'_a + i\varepsilon''_a$ and $\varepsilon_b(\omega) = \varepsilon'_b + i\varepsilon''_b$. In the limit of low frequencies, $\omega \to 0$, and low dissipation, $\varepsilon''_{a,b} \ll \varepsilon'_{a,b}$, we apply the Fourier expansion method and develop an effective medium theory for two-dimensional (2D) periodic composites. We give a rigorous proof that, in this limit, a periodic medium behaves like a dissipative homogeneous one and we derive analytical formulas for the imaginary part of the effective dielectric constants, $\varepsilon''_{\mathit{eff}}$, for the H- and E-polarization of the propagating wave. The real part of the effective dielectric constant, $\varepsilon'_{\mathit{eff}}$, has been calculated in our previous study [1, 2]. The obtained formulas are very general, namely the Bravais lattice, the cross-sectional form of the cylinders, their filling fractions and the dielectric constants are all arbitrary. The effective dielectric constants are expressed through the Fourier components of the dielectric function of the photonic crystal $\varepsilon(\mathbf{r})$.

We consider a special case when the dissipative constituent of the photonic crystal is metallic cylinders with $\varepsilon_a(\omega) = 1 - \omega_p^2/\omega(\omega + i\nu)$. Calculating the real and imaginary parts of the effective dielectric constant, we demonstrate that for the E-mode the medium exhibits strong dissipation and therefore the E-mode does not propagate in the low-frequency limit $\omega \ll \nu$. However, for the H-polarized mode the effective medium turns out to be a dielectric with weak absorption, $\varepsilon''_{\mathit{eff}} \ll \varepsilon'_{\mathit{eff}}$. In the latter case the dissipative part of the dielectric function grows linearly with ω, like in any weakly-absorbing medium.

Numerical calculations are presented for a uniaxial (biaxial) photonic crystal with square (rectangular) lattice and circular cylinders. Our results may find useful applications in tailoring metamaterials with perfect absorbing properties [3] and modified thermal emission [4].

ACKNOWLEDGMENT

Supported by the US Department of Energy, grant # DE-FG02-06ER46312.

REFERENCES

1. Halevi, P., A. A. Krokhin, and J. Arriaga, "Photonic crystal optics and homogenization of 2D periodic composites," *Phys. Rev. Lett.*, Vol. 82, 719, 1999.
2. Krokhin, A. A., P. Halevi, and J. Arriaga, "Long-wavelength limit (homogenization) for two-dimensional photonic crystals," *Phys. Rev. B*, Vol. 65, 115208, 2002.
3. Landy, N. I., S. Sajuyigbe, J. J. Mock, D. R. Smith, and W. J. Padilla, "Perfect metamaterial absorber," *Phys. Rev. Lett.*, Vol. 100, 207402, 2008.
4. Han, S. E., A. Stein, and D. J. Norris, "Tailoring self-assembled metallic photonic crystals for modified thermal emission," *Phys. Rev. Lett.*, Vol. 99, 053906, 2007.

Invariant Embedding Method in the Problem of 3D Photonic Crystal Modeling

V. L. Kuznetsov and A. S. Rudkovskiy
Moscow State Technical University of Civil Aviation, Russia

Abstract— In our work rather new approach in modeling effects of interaction electromagnetic field and photonic crystal (PC) is being developed. This approach is based on application of the invariant embedding method. The main advantage of this approach is that instead of solving Helmholtz equation for electromagnetic field in complex periodical structure, Cauchy's problem is calculating for individual embedding equations, which were created for reflection and transition operators of truncated periodical structure (PC layer) with variable thickness h, that appear to be an evolutional parameter (embedding parameter).

In this work, embedding non-linear matrix equations are presented. These equations describe 3D PC of Lin & Fleming architecture, which correspond to a stack of dielectric cylinders.

Under such geometry PC in space spectrum of reflected and transitioned fields there are plane waves with propagation vector $\vec{k}_n^p = (k_z, [\vec{q}_0 + \vec{\kappa}_x \cdot n + \vec{\kappa}_y \cdot p])$, $n, p \in Z$. Here $\vec{\kappa}_x, \vec{\kappa}_y$ — basis vectors of PC reciprocal lattice; $\vec{q}_0$ — projection of initial electromagnetic field propagation vector $\vec{k}_0$ on upper side of PC; $k_z = \pm\sqrt{k_0^2 - (q_{0x} + n \cdot \kappa_x)^2 - (q_{0y} + p \cdot \kappa_y)^2}$.

Embedding equations were developed subject to vector character of electromagnetic field. In this case reflection $\hat{R}(h)$ and transition $\hat{T}(h)$ operators — are six-index matrixes with elements of the following type $\alpha, \beta R_{n,m}^{p,s}$. Here (n, p, α) describes propagation vector and polarization of reflected components and (m, s, β) describes appropriate characteristics of initial field. To describe such elements, block matrixes were used in our work. Some simplification in description of electromagnetic field polarization structure was achieved by changing polarization basis to "vertical — horizontal polarization" for each space component of the field.

During numerical calculations we made truncation of embedding equations matrixes taking into account hypothesis about finiteness of cross modes interactions "radius". I.e., in calculations besides homogeneous modes some inhomogeneous modes were taken into account and their impact on homogeneous modes considered material.

We used the Pointing theorem as a test to check the results.

In our work we show dependencies of reflection and transition matrix coefficients as a function of PC layer height.

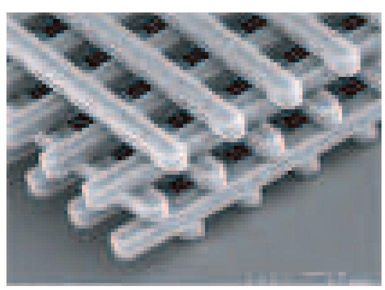

Switching Control of Spontaneous Emission by Polarized Atoms in Two-dimensional Photonic Crystals

Xue-Hua Wang
School of Physics and Engineering, Sun Yat-Sen (Zhongshan) University, China

Abstract— We calculate the lifetime distribution function of an assembly of polarized atoms in two-dimensional (2D) photonic crystals (PCs) at different polarization orientations of atomic dipole moments. We reveal a switching effect of atomic spontaneous emission (SE) and find a significant change of atomic lifetime, up to a factor of 33, by tuning the polarized orientation of the atoms. These observations suggest that the tuning of the polarized orientation of atoms provides a new way for the effective control of atomic SE processes in 2D PCs.

Session 5A3
Photonics — Theory and Applications

Simulation of an Ultrashort 2D Photonic Crystal Switch Based on Nonlinear Directional Coupler

A. Taher Rahmati and N. Granpayeh
Faculty of Electrical Engineering, K. N. Toosi University of Technology, Tehran, Iran

Abstract— In this paper, we have analyzed a nonlinear photonic crystal directional coupler by finite difference time domain method (FDTD). We have tried to increase the coupling efficiency and also reduce the coupling length in linear and nonlinear states in this device. In this coupler, refractive index of the rods of the central row is tuned by input signal power due to nonlinear Kerr effect, therefore, input signal beam can be controlled to be exchanged between two output ports. The coupling length, efficiency and performance of the switch in linear (low input power) and nonlinear (high input power) for different radii of rods of the central row in hexagonal lattice have been analyzed and simulated.

Description: Photonic crystal Directional couplers, as shown in Fig. 1, can be obtained by removing two rows, next to each other from a triangular lattice. It is composed of input, coupling and output regions.

The coupling length is the distance over which the phase difference between two modes is 180°, and depends on the difference between propagation constants of the odd and even modes,

$$L_c = \frac{\pi}{|\beta_{odd} - \beta_{even}|}. \tag{1}$$

Variations of radius (r_c) and refractive index of the central row rods cause shifting in even mode propagation constant in dispersion diagram and thus changing the coupling length.

In our proposed switched design, as shown in Fig. 1, the radius of the rods are $r = 0.2a$, where a is the lattice constant. The rods are made of $AlGaAs$ with dielectric constant of $\varepsilon = 11.56$ and nonlinear refractive index of $n_2 = 1.5 \times 10^{-17}\,\mathrm{m^2/W}$ at wavelength of 1.55 µm. The band gap of this structure is calculated by plane wave expansion (PWE) method. A TM band gap of the structure is in the range of $0.3034 \leq a/\lambda \leq 0.4833$, where λ denotes the optical wavelength in free space.

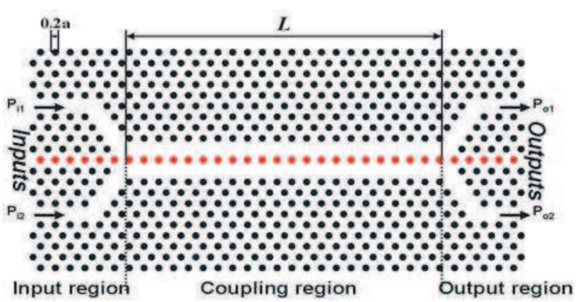

Figure 1: Schematic view of proposed directional coupler switch. It consists of three regions of input, coupling and output. Total length of the coupling region is L.

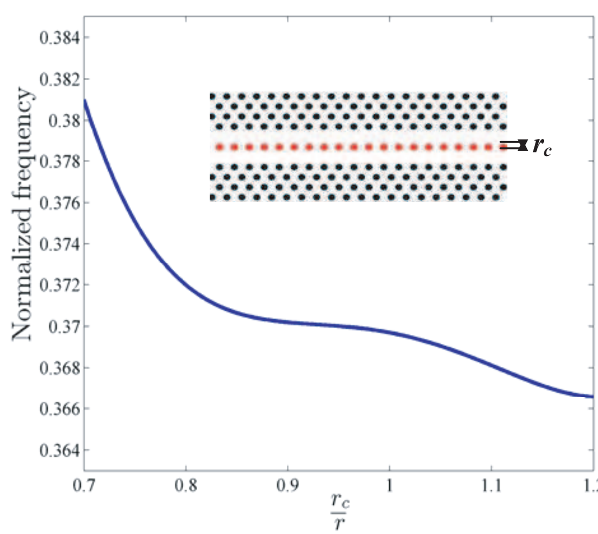

Figure 2: Normalized frequency of switching as a function of r_c/r. Normalized frequency range is from 0.3666 to 0.3810. The frequencies are selected in the range of TM bandgap in which a single mode from upper input is coupled to the upper output.

As shown in Fig. 2, by changing r_c, the switching frequency is also shifted and approximately in a constant coupling length, increasing r_c causing to decrease the frequency.

In linear regime with low input power and nonlinear regime with high input power, the ratio of the output power for different r_c were derived by FDTD, the result of which are shown in Fig. 3. In nonlinear state, when $r_c = r$, power required for switching is 1.55 W and it is 18% lower than status in which $r_c = 0.7r$. In Fig. 4, the field distributions for the case in which $r_c = r$, in linear and nonlinear regimes are demonstrated.

The refractive indexes of the coupler central row rods have been changed in the range of 0–0.192, and it shows when the refractive index variation (δn) is about 0.132 switch works in the cross state.

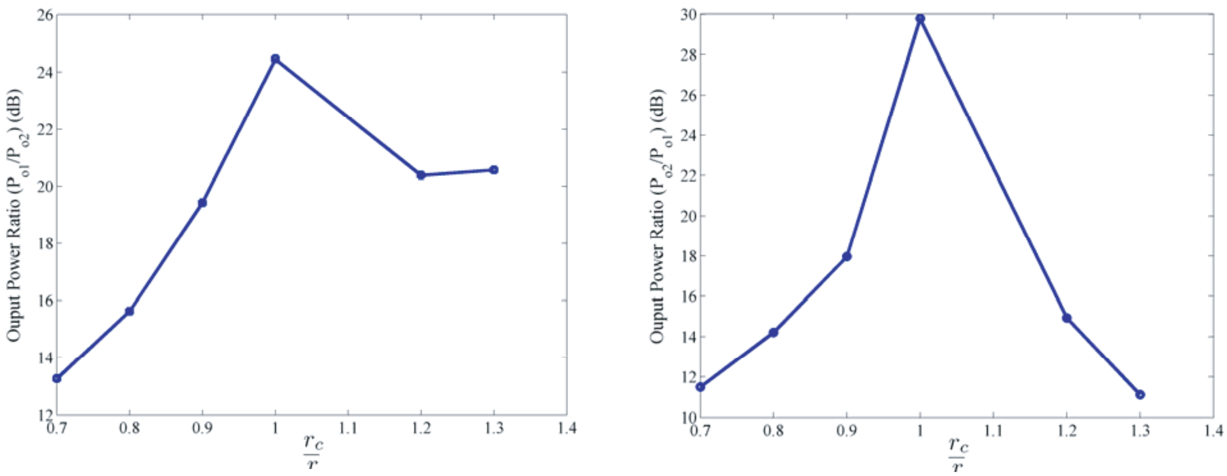

Figure 3: Output power ratio in (a) linear (b) nonlinear states.

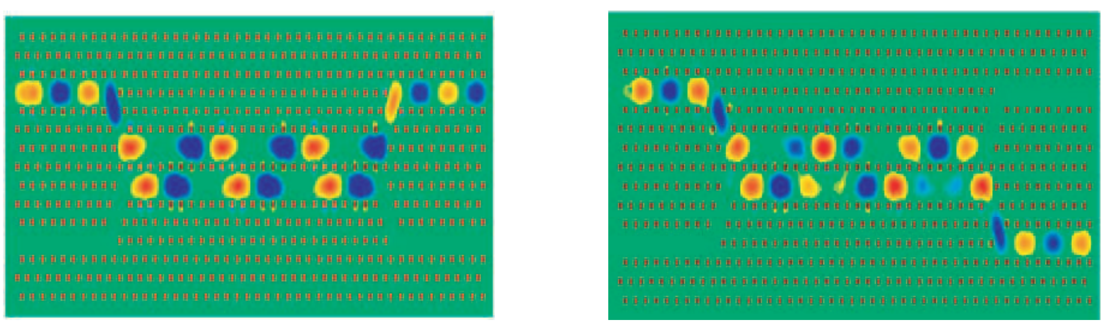

Figure 4: Electric field distribution of the coupler for $r_c = r$ in (a) linear and (b) nonlinear states.

XPM-based 2R-wavelenght Conversion with UL-SOA and Abrupt-band Optical Filtering

Cristiano M. Gallep[1,2], **Napoleão S. Ribeiro**[2], **and Evandro Conforti**[2]

[1]Applied Photonics Lab — LaFA, DTT/CESET, State University of Campinas
Limeira/Campinas, SP, Brazil
[2]Optical Communications and Microwave Research Laboratory, DMO/FEEC
State University of Campinas, Limeira/Campinas, SP, Brazil

Abstract— Optical carrier's filtering after SOA-induced XPM is used to promote wavelength conversion with re-shape capabilities. Successful experimental results were obtained for RZ signal at 7 Gbps, pointing to optimal performance at about 25 Gbps.

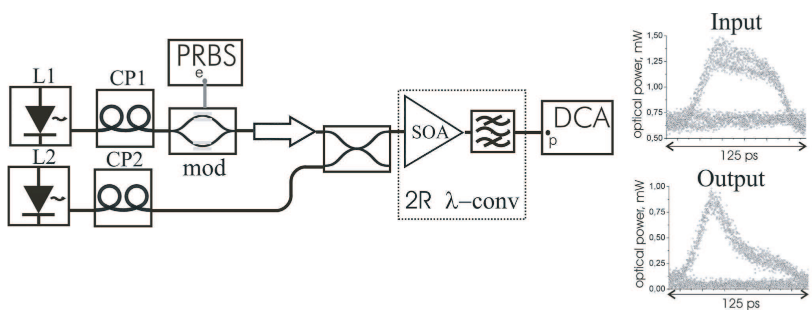

(a) (b)

Figure 1: (a) Experimental set-up for 2R conversion: modulated ($L1$) and CW ($L2$) carriers co-propagating in UL-SOA, with optimized optical polarization ($CP1$, $CP2$) for best gain; (b) eye-diagrams for the dirty input and reformatted output (7 Gbps-RZ).

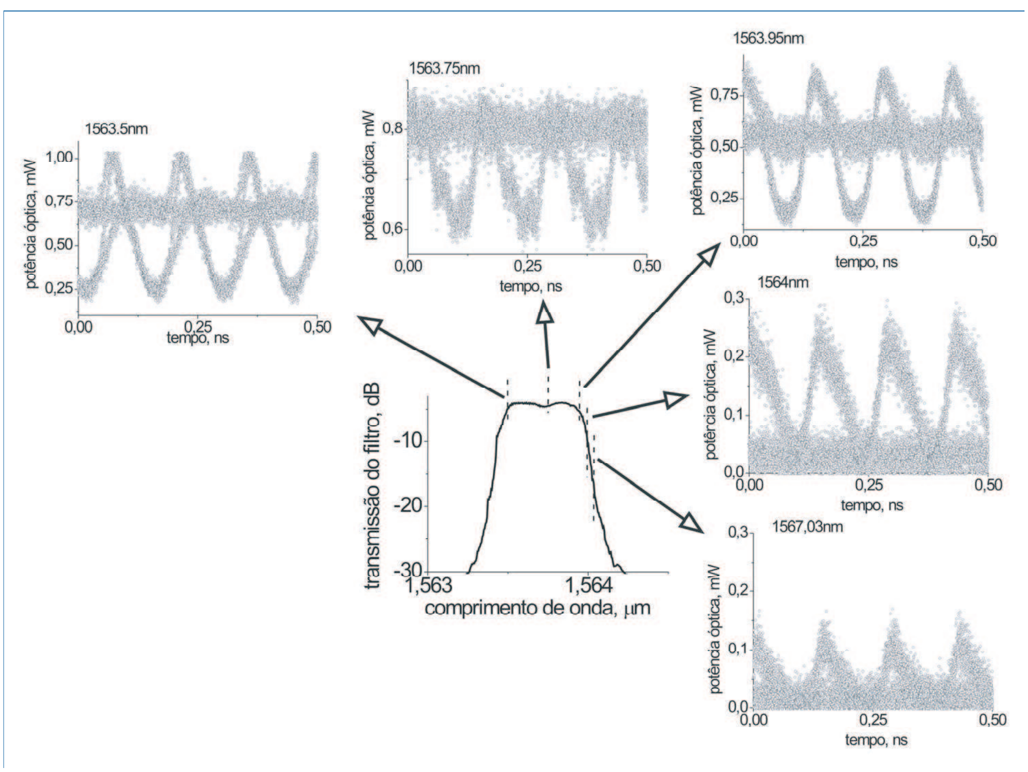

Figure 2: Output eyes related to the carrier position in the optical filter window.

Introduction: SOA-based sub-systems can be very useful for lambda-conversion and simultaneous pulse reshape, by using nonlinear amplification schemes to employ conveniently the XGM, XPM and FWM effects, within some intrinsic or extrinsic 'S'-like tranfer functions. These last two can easily work in tens of Gbps, but FWM needs very stable polarization control and XPM urge to convert frequency to amplitude modulation, usually in interferometers or the like. But this FM-AM conversions can also be obtained also by carrier filtering at the edge of a sharp optical filter, if the spectral chirp is high enough, what can be done using ultra-long SOAs [1]. Here are presented some experimental results obtained using an 8 mm-long SOA (*HHI*), with four current gates (cavity divided in 1-3-3-1 mm), and a simple WDM filter (50 GHz, *JDSU*), for pseudo-random bit-streams at 7 Gbps RZ.

Experimental Results and Discussion: Fig. 1(a) presents the basic set-up used, where the XPM, induced mainly at the pulse's front-edge, is turned to AM by properly tuning the CW laser ($L2$) at the optical filter's sharp edge, after co-propagating with the modulated channel ($L1$) in the SOA. The best regeneration performance where achieved for deteriorated inputs, obtaining relatively better outputs likewise that ones at Fig. 1(b), where the best achieved results are shown. The best response were optimized in relation to SOA's ASE noise by reducing the current of the first and last cavity sections near the threshold (~ 20 mA), and so acting as a non-linear absorber and enabling the reduction of the low-level (bit '0') power variance. A 3 dB penalty occurred for channel detuning $\Delta\lambda \sim 6$ nm, with quite no penalty up to $\Delta\lambda = 3$ nm. The time profile in the output eye suggest optimal performance for rates around 25 Gbps.

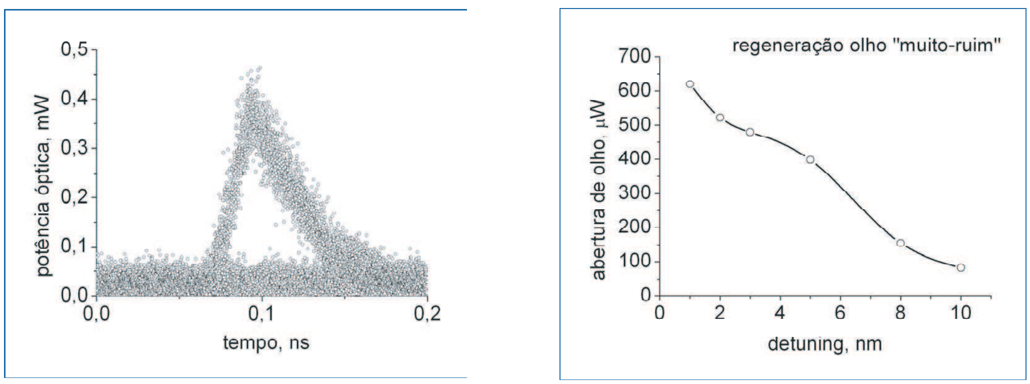

(a) (b)

Figure 3: (a) System response (~ 50 ps) to a 622 Mbps NRZ stream; (b) eye-opening decay with carrier detuning.

ACKNOWLEDGMENT

Acknowledge to CEPOF/FAPESP, CNPq and GIGA/FINEP support.

REFERENCES

1. Gallep, C. M. and E. Conforti, "Wavelength conversion with 2R-regeneration by UL-SOA induced chirp filtering," *Lecture Notes in Computer Science*, Vol. 3124, 304–311, 2004.

Electromagnetic Properties of Complex Metamaterials: from Near Field Imaging with Super Resolution to Mimicking Celestial Phenomenon in the Lab

Dentcho A. Genov
The LONI Institute, Louisiana Tech. University, Ruston, LA 92720, USA

Abstract— This talk will first review the physical principles behind the possibility to implement metamaterials for imaging with unsurpassed optical resolution. A novel type of media is proposed that allows the guidance of deep sub-wavelength beams of light over large distances under minimal transmission losses. This optical transformer can operate in any spatial dimensions and could be used for near field lithography or far field optical imaging with resolution up to $\lambda/30$. In the second part of this paper we demonstrate that the transformable optics could be used to mimic with photons celestial phenomenon such as orbital motion, light trapping and formation of chaos. Specifically, realistic designs will be presented that provide laboratory environments for studies of light in close proximity to massive objects including black holes. Revisiting of the Bertrand theorem of orbital motion for photons will be presented with important ramifications for development of highly stable photonic traps and optical cavities.

Estimation of PMD Impairment in Optical Networks with Weakly Inhomogenous Single Mode Fibers

Abhijit S. Chitambar, **K. Sivaprasad**, **and Charles H. Bianchi**
Department of Electrical & Computer Engineering, University of New Hampshire
Durham 03824, USA

Abstract— In our previous work [1] we had discussed the limitations in existing models used to characterize Polarization Mode Dispersion (PMD) impairment in single mode optical fibers. These limitations arise from the approximation of the discrete Differential Group Delay (DGD) distribution as a continuous envelope. Mean value of such an approximation does not adequately characterize the DGD that results from PMD because PMD produces an ensemble of discrete delayed components. We proposed a new approach for a statistical model which is able to retain the true discrete nature of the DGD distribution across spans of optical fibers and thus characterize the PMD impairment adequately. Subsequently we showed its numerical implementation [2] to generate the DGD distribution in single mode fibers. Results from this implementation showed very good agreement for the value of beat lengths obtained from physical measurements and from our simulation results. The unique capability of our model to be able to vary individual delays of beat length segments allows us to calculate the overall change in the resultant DGD distributions of the fiber spans.

In this paper, we integrate our DGD distribution model in an optical network system model to evaluate the impact of PMD impairment on optical link performance. We use the DGD distribution generated by our model to simulate eye closures and measure the impact of this signal degradation in terms of Q penalty since this directly correlates with transmission metrics like bit error rate (BER) and Optical Signal to Noise Ratio (OSNR). We show comparisons of Q penalties thus calculated using our model with published trends. The model can also be used to generate DGD distributions for different types of homogenous fibers and for homogenous fiber with waveguide defects (PMD artifacts).

REFERENCES

1. Chitambar, A., K. Sivaprasad, and C. Bianchi, "A new model for the computation of differential group delay from polarization distortion in single mode fibers," *Progress In Electromagnetics Research Symposium*, Hangzhou, China, August 22–26, 2005.
2. Chitambar, A., K. Sivaprasad, and C. Bianchi, "An implementation of novel numerical method for generating differential group delay distribution in single mode fibers," *Progress In Electromagnetics Research Symposium*, Beijing, China, March 26–30, 2007.
3. Corsi, F., A. Galtarossa, and L. Palmieri, "Beat length characterization based on backscattering analysis in randomly perturbed single-mode fibers," *J. Lightwave Tech.*, Vol. 17, No. 7, 1172–1178, 1999.
4. Pool, C. D. and R. E. Wagner, "Phenomenological approach to polarization mode dispersion in long haul fibers," *Electronic Letters*, Vol. 22, 1029–1030, 1986.
5. Gisin, N., R. Passy, J. C. Bishoff, and B. Perny, "Experimental investigations of the statistical properties of polarization mode dispersion in single mode fibers," *IEEE Photonics Technology Letter*, Vol. 5, No. 7, July 1993.

Processing Time of Photon Generation

Tibor Berceli
Budapest University of Technology and Economics, Hungary

Abstract— The paper presents a simple, new approach providing results on the processing time and, energy density of photon generation. The main goal is to establish some basic relationships.

Introduction: Processing time is an important characteristic of every process in physics. The main goal of the investigation is to establish some basic relationships for the process of photon generation. Its properties can be described more easily if we consider the generation of photons in a semiconductor material.

Photon Generation: The question arises: can the transition time be an immediate energy change without taking any time, or does it take some time although a very short time? We can get the answer to this question by considering that the generated photon has a specific frequency, f_{ph} [1]:

$$f_{ph} = \frac{E_b}{h} \tag{1}$$

where E_b is the band gap energy, and h is the Planck constant.

When we try to estimate the processing time of photon generation we can use Eq. (1) as a basis. This equation tells us that the photon has a specific frequency and this frequency is dependent only on the band gap energy.

Processing Time: However, the question is still arising: is the photon generation an immediate process in time or does it need some time? A photon can be represented by an extremely short electromagnetic wave with a frequency given by Eq. (1). Therefore, we suggest an assumption taking the half period of the photon frequency as its generation time. Consequently:

$$\tau_{ph} = \frac{h}{2E_b} \tag{2}$$

Here τ_{ph} is the processing time of photon generation. If the band gap energy is higher the generation time is shorter, or by other words the radiated pulse or burst is shorter.

Uncertainty Principle: We use the Heisenberg uncertainty relation [2] to check the former assumption. Based on the uncertainty principle we get:

$$\tau_{ph} = \frac{h}{2E_b} \geq \frac{h}{4\pi E_b} \tag{3}$$

Consequently, the estimation for the processing time of photon generation — see Eq. (2) — is in a proper conformity with the Heisenberg uncertainty principle [2, 3].

Relationship between Processing Time and Energy: As the processing time of photon generation is inversely proportional to its frequency and its frequency is directly proportional to the band gap energy — see Eq. (2) — we can state: the generation time is inversely proportional to the band gap energy.

Furthermore, it can be stated for a general case: the processing time is inversely proportional to the energy utilized for performing a specific process. Here it is assumed that the other parameters of the process, e.g. electric charge, mass, temperature, material composition, etc. are unchanged.

Energy Density: Based on Eq. (1) the energy of the photon is proportional to the band gap energy. Therefore, a higher frequency photon carries higher energy [3]. The energy density of a process can be defined as the ratio of the energy involved in the process and the processing time. In case of photon generation the energy density is:

$$\rho_{ph} = \frac{E_b}{\tau_{ph}} = \frac{2E_b^2}{h} \tag{4}$$

The energy density of photon generation is proportional to the square of the band gap energy.

REFERENCES

1. Einstein, A., "Zur quantentheorie der strahlung (On the quantum theory of radiation)," *Physikalische Zeitschrift*, Vol. 18, 121–128, 1917.
2. Heisenberg, W., *The Physical Principles of Quantum Theory*, 1930.
3. Burkhardt, C. E. and J. J. Leventhal, *Topics in Atomic Physics*, Springer, 2006.

Bit Error Rates for Focused General-type Beams

Serap Altay Arpali and Yahya Baykal
Electronic and Communication Engineering Department, Çankaya University, Öğretmenler Cad. No. 14, Yüzüncüyıl 06530, Balgat, Ankara, Turkey

Abstract— Using the scintillation index of general beam formulation, bit error rate (BER) is investigated for focused Gaussian, cos-Gaussian, cosh-Gaussian and annular beams in weak atmospheric turbulence. We have employed our previously derived formulation of the scintillation index of these beams by Rytov method. Rytov method scintillation theory is known to yield accurate results for focused beams on horizontal paths under certain regions. Therefore we find the scintillation indices of the mentioned beams for the valid region. Using the log-normal distributed intensity, BER values versus signal-to-noise ratio (SNR) are calculated for Gaussian, cos-Gaussian, cosh-Gaussian and annular beams. In our study, the focal lengths (radius of curvature) of all the mentioned focused beams are equal to the propagation distance. The improvement of BER is observed for variations of propagation length, source size and wavelength of operation. Based on these parameters, BER values of Gaussian, cos-Gaussian, cosh-Gaussian and annular beams are compared. BER values we found for the focused Gaussian, cos-Gaussian, cosh-Gaussian and annular beams decrease with increasing source sizes. Likewise, BER values of focused Gaussian, cos-Gaussian, cosh-Gaussian and annular beams decrease with increasing wavelength. The focused annular beam attains the lowest BER value for small source sizes and long propagation distances. Moreover, BER for focused beams is compared with their collimated counterparts. We observe that focused beams have lower BER values than the collimated beams on horizontal paths. Our formulation can easily be extended to cover corresponding higher order beams however in this paper we concentrate mainly on the zero order beams.

Analytic Estimate for the Mass of the Photon

A. H. J. Fleming
Biophotonics Research Institute, Melbourne, Australia

Abstract— Regardless of considerable speculation that a non-zero photon mass might not allow gauge invariance or would break the symmetry of the Lagrangian formulations of the various quantum field theories, an analytic expression has been derived for the mass of the photon. Self-field theory was recently used to investigate the role of the photon as the binding energy inside the hydrogen atom where it yielded deterministic eigensolutions to the Maxwell-Lorentz equations. This is a mathematically distinct method to the Lagrangian-based quantum field theories such as quantum electrodynamics. Fundamentally self-field theory obtains an expression for Planck's constant $\hbar = \frac{q^2}{4\pi\varepsilon_0 v_e}$ as the energy per cycle of the principal eigenstate thus providing the analytic origins of the various quantum theories. Based on a composite photon, an analytic expression for photon mass is also obtained $m_\gamma c^2 = \frac{\hbar\omega_\gamma v_e}{4c}$, where ω_γ is an integer photon transition frequency within each cycle that can be estimated via the experimentally and theoretically determined g-Landé factor for the electron, that is found to be compatible with the fine-structure constant $\alpha = \frac{v_e}{c} = \frac{4m_\gamma c^2}{\hbar\omega_\gamma}$, where $\omega_\gamma = 54$ and $m_\gamma = 0.396 \times 10^{-55}$ kg (0.221×10^{-19} eV). This value of the mass of the photon is commensurate with current estimates for the photon's upper limit. Thus the photon can be viewed both as a composite particle and a wave resolving its long-standing enigmatic dual nature. Also, the relativistic nature of the photon is understood via the two electromagnetic spinors describing its self fields where its internal motions are involved in the Lorentz transformations. In regards gauge and symmetry, it is noted there are two photons of conjugate spin involved. The photon's composite structure leads to the concept of photon chemistry where various bosons can be understood as compounds of sub-photonic particles, similar to atomic compounds. The various gluons can be understood as composites of three sub-photonic particles.

REFERENCES

1. Fleming, A. H. J., "Electromagnetic self-field theory and its application to the hydrogen atom," *Physics Essays*, Vol. 18, No. 3, 265–285, 2005.
2. Fleming, A. H. J., "Self-field theory, analytic spectroscopy of the ordinary photon," *Proc. 2nd EHE Intl. Conf.*, 18–23, Wroclaw, Poland, 2007.
3. Fleming, A. H. J. and E. B. Colorio (nee Bauer), "The spectroscopy of the EM field-a predicted photon chemistry," *3rd Intl. WKSP on Biol. Effects of EM Fields*, Kos, Greece, October 2005.

Resonances with the Vanishing Width and Non-linear Effects in Photonic Structures

Remy F. Ndangali and Sergei V. Shabanov
Department of Mathematics, University of Florida, Gainesville, FL 32611, USA

Abstract— By means of the Breit-Wigner resonant scattering theory it is proved that in Maxwell's theory there exist resonances with the vanishing width (bound states of electromagnetic waves in the radiation continuum), which are neither metal cavity nor photonic crystal defect standing modes. A similar phenomenon was predicted in quantum mechanics in 1929 by von Neumann and Wigner and discovered experimentally only in late 60's (by observing unusually stable two-electronic states in atomic systems). Analytical and numerical studies of simple nanophotonic devices are presented to demonstrate that resonances with the vanishing width can be observed for electromagnetic fields. Important applications of this new phenomenon include:

1. Controlled amplification of electromagnetic fields in designated domains of nanophotic devices.
2. New, more efficient, devices for generation of higher harmonics of light and applications to non-linear photonic devices.
3. New filtering and wave guides for photonic devices.
4. Detection of impurities and large (biological) molecules.

A brief overview of some results in the above studies is provided and illustrated with simple numerical and analytical examples.

REFERENCES

1. Shabanov, S. V., "Resonant phenomena in nanophotonic layered periodic structures: Theoretical and numerical methods," *Rev. Mod. Phys.*, 2009 (submitted), a commissioned contribution.
2. Marinica, D. C., A. G. Borisov, and S. V. Shabanov, "Bound states in the continuum in photonics," *Phys. Rev. Lett.*, Vol. 100, 183902, 2008.

Fundamental Modes of Electro-Magnetic Field in Free Space

Changjun Liao and Changqi He
Laboratory of Photonic Information Technology
School for Information and Opto-electronic Science and Engineering
South China Normal University, Guangzhou 510631, China

Abstract— Modes are usually studied in areas with definite boundary conditions such as cavities, wave guides and fibers, as well as in periodic structure, or assumed central force rule, while the modes in free space where the boundary seems extending to infinite were thought to have a number of mode extremely large that deserve the ergodic hypotheses. It deserves statistical study.

However, for very weak field such as in quantum optics where exists single photons and entangled photonsthe photons have discrete states which are clearly discriminated. And at very strong field the patterns that due to interference of the coherent light will evolve via nonlinear modulation instability into discrete modes such as some kinds of solitons, some of which are seeded with Gauss profile.

Start from the generalized quantization rule proposed by Einstein [1]

$$\oint_{C_i} \mathbf{p} \cdot d\mathbf{q} = n_i h \tag{1}$$

where C_i is the dimension independent closed loops, and n_i is the quantum numbers associated with the energy levels of the system. This quantization rule of coordinate-independent formulation holds for bound motion of a dynamic system with conserved angular momentum. This quantum condition does the same thing as the wave equation for quantum mechanics as indicated by Schrödinger [2]. It is not necessary to suppose a central force rule or a reflection of a boundary to form a cavity. The quantum condition is now used to deal with electro-magnetic field in free space when the angular momentums are nonzero to find two fundamental modes that corresponding to $n \pm 1$. Those are vortexes.

Suppose a thin sheet of optical field with wave vector varying in x-y plane and phase changing continuously only along one direction clockwise or anticlockwise, those fundamental modes will appear if the loop closed with phase difference of $\pm 2\pi$. The TM mode and TE mode have different mode patterns.

A Gaussian beam focused by a lens has a spherical wavefront with phase delayed at center, then the phase increases in both directions clockwise and anticlockwise, that including two different fundamental modes so that the combination of Gaussian beams meet troubles.

With photons belong to a single fundamental mode the energy will be easy focused then the laser fusion be realized.

REFERENCES

1. A translation of the papers in *The Collected Papers of Albert Einstein*, Vol. 6, 434, Engel Trans., Princeton U Press., Princeton, NJ, 1997.
2. Schrödinger, E., *Ann Phys.*, Vol. 489, 79, Leipzig, 1926.

Session 5A4
Electromagnetic Theory of Plasmas, Nonlinear and Chiral Media

Optical Absorption Enhancement by Metal Nanoparticles

Greg Sun[1] **and Jacob B. Khurgin**[2]

[1]Department of Physics, University of Massachusetts Boston
100 Morrissey Boulevard, Boston, Massachusetts 02125, USA
[2]Department of Electrical and Computer Engineering, Johns Hopkins University
3400 N. Charles Street, Baltimore, Maryland 21218, USA

Abstract— Recent years have witnessed an increased interest in "nano-plasmonics" relevant to sensor applications. In this talk, we discuss such applications and focus upon the increased optical absorption that results when absorbing molecules are placed near metal nanoparticles. This enhancement is part of the general study of field modification obtained in the vicinity of nano-structured metallic objects [1, 2] whose characteristic features are much smaller than the optical wavelength. Building upon our earlier developed model [3, 4] for evaluating the plasmonic enhancement of optical emissions by considering the most basic phenomena of radiative decay in the vicinity of metal nanoparticles, we are now taking a consistent analytical approach to investigate the reverse problem, i.e., enhancement of the absorption by molecules placed in the vicinity of metal nanoparticles. This issue is important for two reasons — first of all it had been proposed to use metal nanoparticles to enhance the efficiency of photo-detectors [5, 6] and solar panels [7, 8], and second, absorption is the first step in the photo-luminescence emission of PL sensors and thus enhanced absorption means improved sensitivity. Our rigorous yet simple analytic calculation takes into account all the radiative and nonradiative losses and, most essential, provides the optimization routine for a given absorber characterized by its original absorption strength. We will show that the degree of enhancement strongly depends on the metal particle dimension, thereby providing a straightforward route to optimizing the absorption enhancement. The main conclusion is that metal nanoparticles can dramatically improve the performance of optical sensors in which the active molecules are few and their original absorption is low. At the same time, when the original absorption is already significant, as is the case of most optical detectors and photovoltaic devices, the enhancement is weak or nonexistent due to metal loss.

REFERENCES

1. Barnes, W. L., A. Dereux, and T. W. Ebbesen, *Nature*, Vol. 424, 824, 2003.
2. Murray, W. A. and W. L. Barnes, *Adv. Mater.*, Vol. 19, 3771, Weinheim, Germany, 2007.
3. Khurgin, J. B., G. Sun, and R. A. Soref, *Appl. Phys. Lett.*, Vol. 93, 021120, 2008.
4. Sun, G., J. B. Khurgin, and R. A. Soref, *J. Opt. Soc. Am. B*, Vol. 25, 1748, 2008.
5. Westphalen, M., U. Kreibig, J. Rostalski, H. Luth, and D. Meissner, *Sol. Energy Mat. Sol. Cells*, Vol. 61, 97, 2000.
6. Rand, B. P., P. Peumans, and S. R. Forrest, *J. Appl. Phys.*, Vol. 96, 7519, 2004.
7. Tang, L., S. E Kocabas, S. Latif, A. K. Okyay, D.-S. Ly-Gagnon, K. C. Saraswat, and D. A. B. Miller, *Nature Photonics*, Vol. 2, 226, 2008.
8. Schaadt, D. M., B. Feng, and E. T. Yu, *Appl. Phys. Lett.*, Vol. 86, 063106, 2005.

Field-aligned Currents in Io's Plasma Wake

Chuxin Chen
School of Earth and Space Sciences, University of Science and Technology of China, China

Abstract— Four decades ago, the decametric radio emissions on the Jovian ionosphere were discovered to be controlled by Io. More recently, auroral emission associated with Io's footprint and its trailing emission were observed. Such auroral arc may extend longitudinally westward for more than 100 degrees. This trail of aurora is brightest near Io's footprint and dims with increasing downstream distance. There is no clear theoretical understanding of the physics that generates this downstream aurora. However it is generally believed that Io's plasma wake is associated with this phenomenon and field-aligned currents lead to downstream emissions. There are two theoretical frameworks in which these downstream emissions can be interpreted. The first one is corotational lag. When an Io-perturbed (mass loading and/or Io's conductivity) magnetic flux tube moves slowly relative to Jovian magnetosphere, an electric field would be induced at the equatorial plane of the flux tube, which in turn causes a current perpendicular to the field lines that is connected by field-aligned currents. The Lorentz force due to the perpendicular current would play the role of bring the lagged plasma up to corotation. The second is Alfvén wave, in which the Io-perturbed Alfvén wave is reflected between the Jovian ionosphere and the Io plasma torus edge, driving particles into loss cone. To tackle this problem, we provide an approach "theory of thin filament motion". We assume Io's plasma wake can be regarded as a tail of thin magnetic flux tubes perturbed by Io successively. In this assumption, a flux tube is considered as thin if the pressure variations across the flux tube are negligible compared to the total external pressure (gas plus magnetic pressure) representing the effects of the enveloping magnetized plasma (Jovian magnetosphere). Furthermore we assume that in Io's reference frame the variations of the physical quantities along the downstream distance do not change with time. After converting to the Jovian corotating frame, the study of Io's plasma wake can be simplified to investigate the evolution of a magnetic flux tube in Io's wake with appropriate initial conditions. Our simulations suggest that the mechanism for producing wake aurora could not be explained by either Alfvén wave or electric circuit alone, rather, the underlying physics possesses the characteristics typical for both Alfvén wave and corotational lag models. An upstream-coming flux tube must be in contact with Io for approximately 500 seconds, until a tilt angle of about 4 degrees has been developed, before it is released downstream. A magnetic field depression forms downstream as a result of the continual departure of the flux tubes from Io, which in turn has significant influence on the motion of a flux tube. A perturbed flux tube would undergo a subcorotational motion in Io's plasma wake. This motion is inevitably modulated by Alfvén wave bouncing back and forth inside the Io plasma torus. The scale of the subcorotation region is in the order of 1 Jovian radius. The distribution of the simulated field-aligned currents downstream is consistent with the observed wake aurora brightness profile; in particular, the periodic structure in the current distribution is in agreement with recent infrared and FUV observations showing the presence of secondary spots in the auroral emissions.

Ionization-induced Dynamics of Laser-matter Interaction in a Tightly Focused Laser Pulse

E. S. Efimenko and A. V. Kim
Institute of Applied Physics, Russian Academy of Sciences, Nizhny Novgorod, Russia

Abstract— The physics of laser-matter interaction where optical-field ionized plasmas are generated is of great interest owing to the unique properties of such plasmas and the fact that they suit many important applications, in x-ray lasers, attosecond and terahertz pulse generation. Recently, growing attention was also given to the field referred to as "extreme light" where extreme light parameters for laser-matter interactions, such as very high intensities and/or very short pulse durations, can be realized. For example, tight focusing optics is used in up-to-date experiments to make refractive index modifications in a small volume for waveguide writing in dielectric media and for relativistic laser-plasma interactions in a small, as compared to the wavelength, focal region. Additional stimulus nowadays comes also from the expected extremely high intensities approaching to the Schwinger limit when direct field-induced ionization of vacuum through pair production can occur.

In the present work we have found a new and unanticipated regime of laser-plasma interaction with a tightly focused wave beam when small-scaled plasma structures can be generated and strongly influence field distribution, energy deposition and scattering characteristics. We have shown that plasma-field dynamics significantly depends on focusing angle of the laser beam. Moreover, there is the critical angle which divides two qualitatively different regimes of laser-matter interaction. In the first one, for comparatively small focusing angles corresponding to the traditional quasioptical approach, smooth (on the laser wavelength scale) plasma structures are observed. In the second one, for angles exceeding the critical one, plasma density distribution is microstructured and these small-scaled plasma structures play a key role in the laser-matter interaction [1]. It should be noted that plasma density values in these structures can greatly exceed the critical density. We have also found that the critical angle and electron density-field dynamics depend significantly on the pulse spectrum; while the critical angle decreases for pulses with broad spectrum in comparison with pulses with narrow spectrum, regular ionization-induced dynamics may be even triggered into chaotic behavior.

REFERENCES

1. Efimenko, E. S., A. V. Kim, and M. Quiroga-Teixeiro, *Phys. Rev. Lett.*, Vol. 102, 015002, 2009.

Excitation and Propagation of Whistler Waves in a Magnetoplasma Containing Density and Magnetic-field Nonuniformities

P. V. Bakharev[1], **A. V. Kudrin**[1], **and T. M. Zaboronkova**[2]

[1]University of Nizhny Novgorod, Russia
[2]Technical University of Nizhny Novgorod, Russia

Abstract— Whistler-mode waves guided by cylindrical density enhancements have received much careful study and there are many accounts of them (see, e.g., [1] and references therein). However, there exists very little theory of the phenomena related to the source-excited whistler waves in the guiding structures located in an unbounded background magnetoplasma and formed by density depletions or nonuniformities of an external static magnetic field. Earlier studies of the whistler wave guidance by such plasma structures employed various approximate approaches such as the geometrical optics or the WKB approximation [2, 3]. In the present work, the full-wave approach is used to analyze the features of excitation and propagation of whistler waves in a magnetoplasma containing the above-mentioned cylindrical structures in the case where their radii are comparable to or less than typical wavelengths of guided modes.

We consider a cold unbounded magnetoplasma containing a magnetic-field-aligned cylindrical nonuniformity (duct) in which the plasma density or the external magnetic field is a function of radial distance from the duct axis. It is shown that at the frequencies belonging to the whistler range, a density depletion duct is capable of guiding surface-type eigenmodes bound to the duct wall and volume eigenmodes trapped in the inner region of the duct. Similar properties are found for eigenmodes supported by a nonuniformity in which the external magnetic field is enhanced compared to the ambient value. In contrast to this, the dispersion properties and field structures of modes guided by a magnetic-field depression turn out to be analogous to those of the well-studied modes of density enhancements.

Then radiation from spatially bounded electromagnetic sources located inside the above-described structures is considered. A rigorous solution for the total field comprising both the discrete and continuous parts of the spatial spectrum of the excited waves is found. Using the obtained field representation, an expression for the impedance of a source in the form of a loop antenna is derived and the contributions of eigenmodes (i.e., discrete-spectrum waves) and unguided continuous-spectrum waves of the duct to the antenna impedance are determined. Conditions have been revealed under which the real part of the antenna impedance (radiation resistance) is dominated by the contribution of either discrete- or continuous-spectrum waves.

The results obtained are useful for explanations of the data of some recent laboratory experiments on the excitation and ducting of whistler-mode waves in a magnetoplasma containing density and magnetic-field irregularities.

ACKNOWLEDGMENT

This work was supported by the RFBR (project Nos. 07–02–00436-a and 09–02–00164-a).

REFERENCES

1. Kondrat'ev, I. G., A. V. Kudrin, and T. M. Zaboronkova, *Electrodynamics of Density Ducts in Magnetized Plasmas*, Gordon and Breach, Amsterdam, 1999.
2. Karpman, V. I. and R. N. Kaufman, "Whistler wave propagation in density ducts," *J. Plasma Phys.*, Vol. 27, No. 2, 225–238, 1982.
3. Kaufman, R. N., "Whistler propagation in magnetic tubes," *Radiophys. Quantum Electron.*, Vol. 29, No. 7, 579–585, 1986.

Resonant Transmission through Dense Plasmas via Amplification of Evanescent Mode

N. Sternberg[1] **and A. I. Smolyakov**[2]

[1]Department of Mathematics and Computer Science, Clark University, Worcester, MA, USA
[2]Department of Physics and Engineering Physics, University of Saskatchewan, Saskatoon, Canada

Abstract— An analysis of electromagnetic wave propagation through a layer of opaque material with dense plasmas is presented. For high plasma electron density such that the wave frequency is below the electron plasma frequency, the transmitted electromagnetic waves are exponentially attenuated. Under certain conditions, however, the dense plasma may become transparent due to surface-mode resonance. Two asymmetric configurations are considered. In the first configuration, the layer of the dense plasma is combined with a transition layer of a thin plasma, and the whole two-layer structure is placed into air. In the second configuration, the layer of the dense plasma is preceded by a diffraction grating placed into air. Analytical models are studied and resonant conditions are derived.

Introduction: The recent years were sparked by a new wave of interest in the behavior of surface modes. Surface modes are (exponentially) localized eigen-modes which exist at the interfaces of two regions with opposite signs of the dielectric constants. A closely related field is the study of propagation of the electromagnetic radiation in metamaterials, which are materials with negative dielectric permittivity ϵ and negative permeability μ. The increased interest in those research areas has been driven by the tremendous potential to guide and manipulate electromagnetic radiation at the subwavelength scales below the diffraction limit, $L \ll \lambda$, in composite devices involving metallic nanostructures. The electromagnetic waves in these devices take the form of surface waves (Surface Plasmons) supported by free electrons in the metal and localized at the metal-dielectric interfaces.

In the present paper, we study resonant properties of surface modes and the resulting transparency of dense plasma layers. We study penetration of a plane electromagnetic wave incident from vacuum into structures of two basic configurations: 1) the composite two-layer structure consisting of a layer of dense plasma ($\epsilon < 0$) and a transition layer of a thin plasma ($0 < \epsilon < 1$) [1]; 2) a layer of dense plasma with $\epsilon < 0$ preceded by a diffraction grating in the air.

Energy Transport by Evanescent Waves: Inside the dense region electromagnetic wave energy is carried by evanescent modes. The general solution inside the negative ϵ medium is a sum of two exponential functions, one that decays with the distance $\sim e^{-z}$ (x points in the propagation direction) and the other grows $\sim e^{z}$. For the superposition of decaying and growing modes, $E, B \sim A_1 \exp[-ikz] + A_2 \exp[ikz]$ (z is the purely imaginary decay constant), the z component of the time averaged Poynting vector S_z is

$$S_z = -\frac{1}{2}\mathrm{Re}[E_y B_x^*] \sim 2\mathrm{Im}[A_1 A_2^*], \tag{1}$$

and may become finite when the combination $A_1 A_2^*$ has a finite imaginary part, which requires a finite phase shift between A_1 and A_2. Therefore, a finite energy flux occurs as a result of the superposition of two evanescent modes with a finite phase shift. The condition of the absolute transparency is equivalent to the resonant condition for the excitation of the surface plasma mode. At the resonance, the Poynting flux inside the slab becomes equal to that of the incident radiation and the opaque plasma slab becomes absolutely transparent [2].

Wave Transmission through a Two-layer Structure: The two-layer structure consists of a layer of thin plasma with $0 < \varepsilon_1 < 1$ of width a_1 and a layer of dense plasma with $\varepsilon_2 < 0$ of width a_2 [2]. The electromagnetic wave is incident at an angle θ, where $\sin\theta = k_y/k$, k_y is the wave vector along the interface, $k = (k_y^2 + k_z^2)^{1/2}$ is the total wave vector, and k_z is the wave vector normal to the interface in the direction of propagation. In particular, $k = \omega/c$ is the wave vector in vacuum to the left of the two-layer structure. Calculating the transmission coefficient for the wave penetrating into the vacuum region from the right of the structure, we find that there are two conditions that have to be satisfied simultaneously, to achieve the absolute 100% transmission. The first condition is exactly the surface wave dispersion relation $\kappa_1/\varepsilon_1 + \kappa_2/\varepsilon_2 = 0$, where $\kappa_1 = \sqrt{k_y^2 - \omega^2\varepsilon_1/c^2}$, and $\kappa_2 = \sqrt{k_y^2 - \omega^2\varepsilon_2/c^2}$. Note that $\kappa_{1,2}$ are the exponents of the fundamental evanescent wave solutions in the first and the second layers, respectively. The second required condition is $\kappa_1 a_1 = \kappa_2 a_2$. The latter condition is a matched amplification condition for evanescent waves, c.f. with the standard interference condition for propagating waves $k_1 a_1 = k_2 a_2$. It is interesting to note that these two conditions actually mean that the effective dielectric constant of the total structure is zero $\bar{\varepsilon} \equiv \varepsilon_1 a_1 + \varepsilon_2 a_2 = 0$. [2]

Resonant Transmission Induced by a Diffraction Grating: In this configuration, we consider the dense plasma layer of width d with $\varepsilon < 0$ nested between two vacuum regions, each of width a. In this case, the dispersion relation for the surface modes at the plasma-vacuum interface is $k_y^2 = (\omega^2/c^2)\varepsilon/(\varepsilon+1)$. For $\varepsilon < 0$, this means that $k_y^2 > (\omega^2/c^2)$, and therefore such a wave cannot match the propagating wave in vacuum. However, the resonance condition can be achieved, using a diffraction grating to shift the wave vector k_y of the incident wave. The diffraction grating (at $z = 0$) of thickness h_g, with a wave vector q and modulation parameter α is represented by the equation

$$\frac{d^2}{dz^2} H_x - k_y^2 H_x + \frac{\omega^2}{c^2} \varepsilon H_x + \frac{\omega^2}{c^2} \varepsilon_g h_g (\mu + \alpha \cos(qy)) \delta(z) H_x = 0, \tag{2}$$

The diffraction grating excites two sidebands so that the general solution has the form $H = (H(z)e^{ik_y y} + H_+(z)e^{i(k_y+q)y} + H_-(z)e^{i(k_y-q)y})$, and resonance occurs if the following holds for the impedance of the corresponding waves:

$$2\kappa_v^+ k_p^+ + {k_v^+}^2 L_p^+ + {k_p^+}^2 L_p^+ \ = \ 0, \tag{3}$$

$$\kappa_v^2 L_p^2 + \kappa_p^2 L^2 L_p^2 - 2iLL_p \kappa_p \kappa_v \ = \ 0. \tag{4}$$

where $L \equiv \tan(ka)$, $L_p \equiv \tanh(kd\sqrt{-\varepsilon})$, $L_p^+ \equiv \tanh(d\sqrt{q^2 - \varepsilon k^2})$, $k = \omega/c$. Note that for a large width of the plasma layer $L_p^+ \approx 1$ and $\kappa_v^+ + k_p^+ \approx 0$.

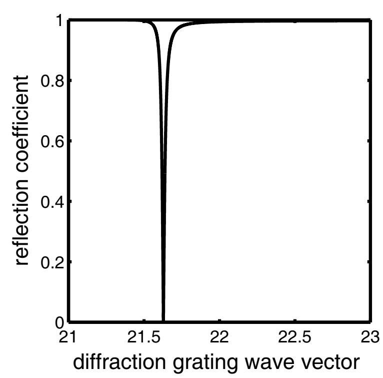

Figure 1: Reflection coefficient as a function of the diffraction grating wave vector.

Conclusion: Anomalously high transmission of electromagnetic radiation through dense plasmas has been observed in experiments and numerical simulations. We presented analytical results that clearly show that resonant transmission in the considered configurations is a result of resonant amplification of the surface modes. The role of the transition layer in the first configuration or of the diffraction grating in the second configuration, is to excite the surface wave and to create conditions for coupling of the surface mode with the electromagnetic wave propagating in vacuum. Contrary to the results of [1, 3], we have shown that resonant conditions for evanescent wave amplification and the resulting absolute transparency can be achieved in asymmetric configurations with a single transition layer or a single diffraction grating.

ACKNOWLEDGMENT

This work was supported in part by AFOSR Award #FA9550-07-1-0415.

REFERENCES

1. Dragilia, R., et al., "High transparency of classical opaque metallic films," *Phys. Rev. Lett.*, Vol. 55, 1117–1120, 1985.
2. Fourkal, E. A., et al., "Resonant transparancy of materials with negative permittivity," *Phys. Letters A*, Vol. 361, 277–282, 2007.
3. Bliokh, Y. P., "Plasmon mechanism of light transmission through a metal film or a plasma layer," *Optics Communic.*, Vol. 259, 436–444, 2006.

Analysis and Design of the Antenna Cover on the Electromagnetic Wave Logging Sonde

Li Hao[1], **Yuan Zhao**[1], **Yueqin Dun**[1], **Jiansheng Yuan**[1], **and Wei Zong**[2]

[1]Department of Electrical Engineering, Tsinghua University, Beijing 100084, China
[2]Department of Electrical and Electronic Engineering
North China Electric Power University, Beijing 102206, China

Abstract— To protect the well-logging sonde (mainly the transmitting coil or antenna and the receiving coil), a metal cover is installed outside the coils. The eddy current is induced in the metal cover by the magnetic field with a frequency of around 1 MHz, and the induced eddy current will generate another opposite magnetic field to weaken the original. To reduce the influence, the metal cover is slotted as shown in Fig. 1, so that the flow path of the eddy current in circumferential direction is cut off and the eddy current is weeken.

Actually, when the metal cover is full, i.e., it is not slotted, because of the symmetry of the cover structure, there is only circumferential eddy current and no axial eddy current. After slotting the cover, the circumferential eddy current is really weaken, but the eddy current in axial direction in each piece of conductor appears as shown in Fig. 2. The total eddy current are still offset the original magnetic field. Therefore, the number and the length of slots must be designed to meet the requirement of the restricted electromagnetic influence and the mechanical structure.

In this paper, the distribution of the electromagnetic field and the value of the induced electromotive force on the receiving coils, concerning with different structure and dimension as well as different materials of metal cover, are simulated by the finite element software. According to the simulation results, the number, the length and the width of the slots were suggested.

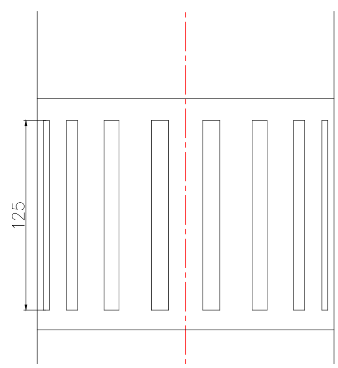

Figure 1: Slotted metal cover of the logging sonde.

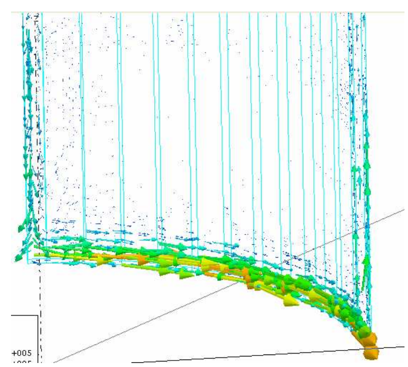

Figure 2: Eddy current in a piece of cover.

Nonreflection Interactions of Electromagnetic Wave with Inhomogeneous Chiral Plasma Layers

N. S. Erokhin, **G. V. Gakh**, and **A. B. Shvartsburg**
Space Research Institute of RAS, Moscow, Russia

Abstract— It has been studied analytically the linear nonreflection interaction of electromagnetic waves with the chiral plasma layer containing the small-scale inhomogeneties. On the basis of exactly solvable solution it is shown the possibility of plasma layer transillumination and the spatial profile of plasma inhomogeneity may includes some arbitrary function. Nevertheless the model considered allows to satisfy the nonreflection boundary conditions at both plasma-vacuum surfaces. The effect studied is of the great interest for a number of applications including the electromagnetic waves generation by charged particle beams, the plasma heating by electromagnetic waves, the wave barriers transillumination, the new mechanism of electromagnetic waves passage from astrophysical objects with plasma density above its critical value and so on. It was shown also that in some plasma sublayers the effective phase velocity of wave packes may be less than the speed of light. So it becomes possible to realize the cherenkov resonance of electromagnetic wave with relativistic charged particles in the external magnetic field absence. The effect considered may be observed also when the cubic plasma nonlinearity is taken into account.

Comparison of Uniform and Discontinuity Dielectric Profile in THz Radiation Field

P. Zobdeh[1], **S. Mahmoodi**[1], **and D. Sardari**[2]

[1]Department of Physics, Qom Branch, Islamic Azad University, Qom, Iran
[2]Science and Research Campus, Islamic Azad University, Tehran, Iran

Abstract— THz radiation is interested over the last decade. Various schemes are presented to generate THz radiation such as optical rectification, photoconductive antenna, Quantum cascade intersubband Varactor Frequency doublers. Using the femtosecond laser pulses with electro-optic crystals and semiconductors through optical rectification is a direct way to make THz by [1, 2]. Recently THz emission is generated by electron bunches bending in a magnetic field, traversing a discontinuous refractive index [3]. In high intense femtosecond laser interaction with plasma, THz emission was observed. A well collimated, ultra short MeV electron bunch is obtained due to the transverse wave breaking [4–6]. The plasma-vacuum boundary already acts as the emitting dielectric discontinuity. In this work we have presented the effect of linear plasma dielectric discontinuity in terahertz emission.

The dielectric function in plasma can be approximated by $\varepsilon(\omega) = 1 - \frac{\omega_p^2}{\omega^2}$ that ω is the angular frequency, *and* ω_p *is* the plasma frequency. It can be seen that the plasma-vacuum interface has indeed a strong dielectric discontinuity for laser frequencies $\omega \leq \omega_p$, in laser plasma interaction. This produces the coherent terahertz emission. In this work, we have considered the laser interaction with under dense plasma. We have modeled linear plasma density profile and obtained longitudinal and transverse fields numerically. Figure 1 shows the Emission spectra of terahertz radiation for both homogeneous and discontinuity *dielectric*. *Results* show the emission amplitude increases transversely for *discontinuity dielectric*.

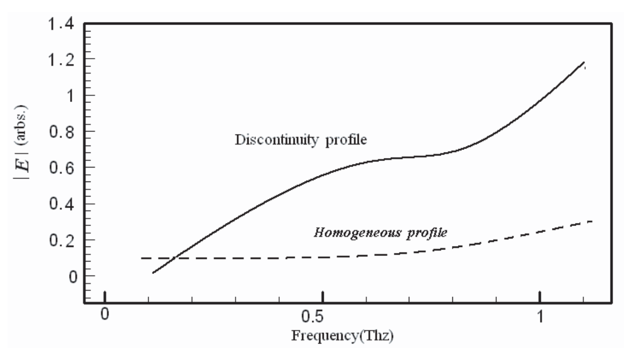

Figure 1: THz Emission spectra for uniform and discontinuity profile.

The electrons accelerated by high intense laser-plasma interaction are over millions electrons at femtosecond duration. The emitted THz radiation by propagation of electrons through a discontinuity dielectric can be more intensified than conventional laser-based THz source. This could be used for design and optimize powered THZ source instead of optical rectification or the photoconductive antenna sources.

REFERENCES

1. Melo, A. M., J. L. S. Lima, R. S. Oliveira, and A. S. B. Sombra, "Photonic time division multiplexing using ultrashort picoseconds pulses in terahertz optical asymmetric demultiplexer," *Optical Communications*, Vol. 205, 299–312, 2002.
2. Saeedikia, D. and R. R. Mansour, "A submiliwatt terahertz high-temperature superconductive photomixer array source: Analysis and design," *IEEE T. Appl. Supercon.*, Vol. 15, No. 3, 3868–3873, 2005.
3. Leemans, W. P., J. van Tilborg, J. Faure, C. G. R. Geddes, C. T'oth, C. B. Schroeder, E. Esarey, G. Fubiani, and G. Dugan, "Terahertz radiation from laser accelerated electron bunches," *Phys. Plasmas*, Vol. 11, No. 5, 2899, 2004.

4. Zobdeh, P., Sadighi-Bonabi, H. Afarideh, E. Yazdani, and R. Rezaei Nasirabad, "Using the steepened plasma profile and wave breaking threshold in laser-plasma interaction," *Contrib. Plasma Phys.*, Vol. 48, No. 8, 555–560, 2008.
5. Zobdeh, P., Sadighi-Bonabi, and H. Afarideh, "New ellipsoid cavity model in the high intense laser-plasma interaction," *Plasma Devices and Operations*, Vol. 16, No. 2, 105–114, 2008.
6. Sadighi-Bonabi, R., H. A. Navid, and P. Zobdeh, *Laser* & *Particle Beam*, Vol. 27, No. 2, 2009 (in print).

Using the High Intense Laser Interaction with Plasma for Generation of Clean Electron Beam

P. Zobdeh[1] **and R. Sadighi-Bonabi**[2]

[1]Department of Physics, Qom Branch, Islamic Azad University, Qom, Iran
[2]Department of Physics, Sharif University of Technology, 11365-9567, Tehran, Iran

Abstract— The intensity of laser beam could be increased up to $I = 10^{22}\,\mathrm{W/cm^2}$ by chirped pulse amplification technique in the new generation of table-top lasers. A high gradient electric field more than $10^{14}\,\mathrm{V/m}$ is generated by the interaction of this high intense laser beam with plasma gas [1]. In these high gradient fields electrons can be accelerated. Under proper conditions, a very efficient "bubble" regime can be realized. Recent investigation of the bubble regime has demonstrated the generation of high-quality electron bunches with energies as high as 1 GeV, with relatively small energy spread, and emittance approaching that of a conventional accelerator [2–5].

In this work, we have presented a clean electron beam generation in theory and experimental parts. Theoretical part describes a new ellipsoid model and develops bubble accelerator. Required conditions for producing of this cavity are obtained in this section and the electron trajectory is analyzed. We have shown the quality of the electron beam is improved in contrast to other methods such as that using periodic plasma wake field, spherical cavity regime and plasma channel guided acceleration. The trajectory of the electron motion can be described as hyperbola, parabola or ellipsoid path. It is influenced by the position and energy of the electrons and the electrostatic potential of the cavity.

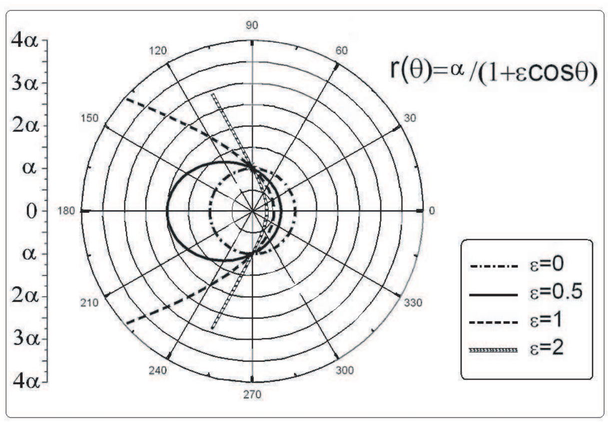

Figure 1: The trajectory of the electron motion in ellipsoid model.

A 20 TW power and 30 fs laser pulse was focused on a pulsed He gas jet in the experimental part of this work. The best matched laser focusing point above the nozzle gas is found to obtain a stable ellipsoid bubble. Method of finding the optimum points will be described in analytical details.

We have shown with an analytical calculation for our new ellipsoid model (instead of the previous cavity models such as the spherical model, Pukhov et al. 2004) a dense bunch of relativistic electrons with monoenergrtic spectrum is self-generated, and the fields depend linearly on the coordinates. Our results show the maximum electron energy is not affected by the cavity elongation for the laser propagated direction, so the quality of the electron is improved. Finally, based on our experiments and calculations we conclude only defined points can produce mono-energetic electron beam, and observation the bigger bubbles in order to trapping of more electrons, could be possible with higher laser powers. Larger focal spots will be obtained with intensities more than the critical relativistic intensities.

REFERENCES

1. Umstadter, D., "Relativistic laser-plasma interactions," *J. Phys. D: Appl. Phys.*, Vol. 36, R151–R165, 2003.

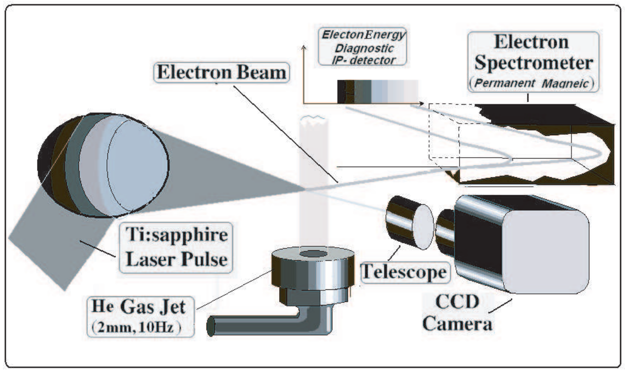

Figure 2: Clean electron beam generation, observation of quasi-monoenergetic electron beam.

2. Pukhov, A. and J. Meyer-ter-Vehn, "Laser wake field acceleration: The highly non-linear broken-wave regime," *Appl. Phys. B-Laser Opt.*, Vol. 74, 355–361, 2002.
3. Zobdeh, P., R. Sadighi-Bonabi, H. Afarideh, E. Yazdani, and R. Rezaei Nasirabad, "Using the steepened plasma profile and wave breaking threshold in laser-plasma interaction," *Contrib. Plasma Phys.*, Vol. 48, No. 8, 555–560, 2008.
4. Zobdeh, P., R. Sadighi-Bonabi, and H. Afarideh, "New ellipsoid cavity model in the high intense laser-plasma interaction," *Plasma Devices and Operations*, Vol. 16, No. 2, 105–114, 2008.
5. Sadighi-Bonabi, R., H. A. Navid, and P. Zobdeh, *Laser* & *Particle Beam*, Vol. 27, No. 2, in print, 2009.

Session 5A5
Computational Electromagnetics 2

Scattering by an Infinite Elliptic Metallic Cylinder Coated by a Circular Dielectric One

G. P. Zouros and J. A. Roumeliotis
School of Electrical and Computer Engineering
National Technical University of Athens, Greece

Abstract— In the present work the scattering of an electromagnetic plane wave by an infinite circular dielectric cylinder containing a coaxial elliptic metallic cylinder is treated. The geometry of the scatterer is shown in Fig. 1. The interfocal distance of the elliptic cylinder is $2c$, while $2a$ and $2a'$ are the lengths of its major and minor axes, respectively. The radius of the circular dielectric cylinder is b. The present geometry is a perturbation of the coaxial circular one with radii a and b. All the materials are lossless. Both polarizations are considered for normal incidence.

Using expansion formulas between elliptical and circular cylindrical wave functions and satisfying the boundary conditions we conclude, after some manipulation, to two infinite sets of linear nonhomogeneous equations for the electromagnetic field in region II.

For general values of $h = c/a$ these sets can be solved only numerically, by truncation, but for $h \ll 1$ an analytical solution is possible. After lengthy, but straightforward calculations, analytical expressions of the form $S(h) = S(0)[1 + g^{(2)}h^2 + g^{(4)}h^4 + O(h^6)]$ are obtained for the scattered field and the scattering cross-sections. The expansion coefficients $g^{(2)}$ and $g^{(4)}$ are given by exact, closed-form expressions, independently of h, while $S(0)$ corresponds to the coaxial circular problem ($h = 0$). The main advantage of this expression is that it is valid for each small value of h, "free" of Mathieu functions, while all numerical techniques should repeat the calculation, from the beginning, for each different h small or large. So, once $g^{(2)}$ and $g^{(4)}$ are known, $S(h)$ is immediately evaluated by quick "back-of-the-envelope" calculations, for each small h. Certainly, this is the result of a great analytical effort which, made once, reduces dramatically the otherwise necessary computer time for the numerical evaluation of the many Mathieu functions, in the case of small h.

The terms omitted in out solution are of the order of h^6 and higher. So the restriction $h \ll 1$ is not so severe as it may appear at first. Independent numerical solution of this same problem shows that the errors in the approximate analytical results of this paper remain low enough, even for values of h up to 0.7 or higher (maximum possible $h = 1.0$ corresponding to a metallic strip).

Apart from the mathematical interest of its solution, the circular-elliptical combination of the present problem may increase or decrease the scattering cross sections, as compared to the ones of the concentric circular geometry.

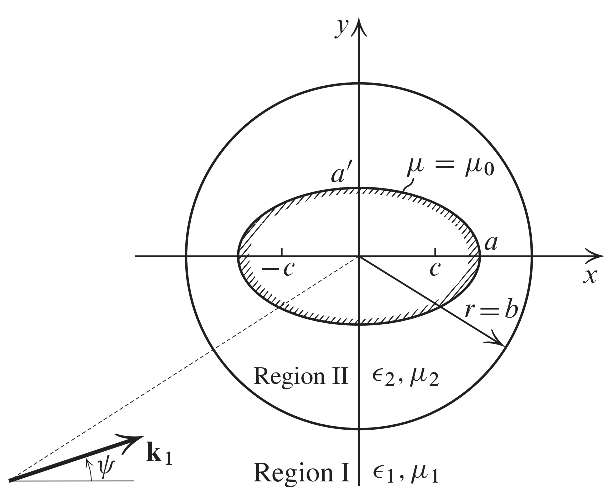

Figure 1: The geometry of the scatterer.

High Performance Angular Resolution Algorithm for Radar Systems

B. A. Lagovsky
Moscow State Institute of Radio Engineering and Automation, Technical University, Russia

Abstract— This paper describes how the angular resolution of radar and sonar systems can be improved in the problems of the target image identification. Rather simple algorithms, necessary for it, of an information reprocessing are proposed for practical embodiment. A comparison of the developed methods is carried out. The outcomes of numerical experiments are introduced. The boundaries of maximum possible angular resolution of observed objects are defined as functions of the noise level.

It is well known that to improve the quality of the target image identification we need to improve the angular resolution. In particular it is required to work out the intensity distribution of the echo signal over a surface or volume of the target.

For the targets located in a far zone, the angular resolution based on Rayleigh criterion is usually represented as

$$\delta\theta \cong \lambda/d, \tag{1}$$

where d is a size of antenna, λ-wave-length.

The estimation of beamwidth as in (1) has fundamental character. It follows from the uncertainty relation. The magnitude of the angular resolution (1) is introduced artificially, on the basis of the possibility of separate observation of two close located objects. It gives a principal opportunity to increase the angular resolution for processing results of measurements.

In this paper we consider the methods allowed to receive additional information on the angular intensity distribution $I(\alpha)$ inside the (1), that is equivalent, to increase an effective angular resolution of the system. Such improvement of the angular resolution is a result of the use of several measurements of scanning and their combined processing.

At scanning on an angle α we shall receive the signal $U(\alpha)$. The problem is to reconstruct an angular intensity distribution $I(\alpha)$ of the reflected signal on the basis of the analysis of an output signal $U(\alpha)$ and the known directional pattern $f(\alpha)$.

The considered problem relates to inverse ill-posed problems. The numerical solutions became unstable when we try to obtain the angular resolution better then (1).

The basic reason of the origin of instabilities is noise component of a received signal. At the angular resolution as (1) their influence is possible to neglect, but it sharply increases at attempts to receive the greater resolution. The increase in the resolution from above (1) is possible, but up to the certain limit determined, basically, by signal-to-noise ratio.

To improve the solution stability the various procedures of regularization are used. There efficiency depends on forms of the function $f(\alpha)$ and unknown function $I(\alpha)$. Therefore these procedures are not universal and are not always effective. Besides they are rather complicated for fast restoration of the image in a real time mode.

For this reason the offered algebraic methods of the analysis based on a representation of a signal and desired intensity distribution in a discrete form seem to be encouraging.

Numerical characteristics of increase of the angular resolution and its limits were investigated on mathematical model. The improving of the resolution was estimated in comparison with beamwidth (1).

As a whole, these algebraic methods allow to increase the effective angular resolution 2–4 times when using simple algorithms and by 5–10 when using composite specialized algorithms. It is shown, that the quality of restoration of images of the targets first of all depends on condition numbers of the relevant matrices. At close values of condition numbers the quality of the images is determined by a successful choice of system of orthogonal functions for the searched target. Systems of orthogonal functions which should be used for restoration of various types of targets are described. The limitations of increase of the angular resolution are found depending on the signal-to-noise ratio.

Algorithm for the Determination of Targets Coordinates in Structure of the Multiple Target with the Increased Effective Resolution

B. A. Lagovsky
Moscow State Institute of Radio Engineering and Automation (Technical University), Russia

Abstract— The approximate numerical solutions of some problems of electrodynamics allow to increase angular resolution of radar-tracking systems, systems of remote sensing.

The locked-on signal is connected with angular distribution of amplitude of the reflected signal by Fredholm integral equation of the first order. A kernel of the integrated equation is the directional pattern of antenna system.

It is required to restore angular distribution of amplitude of the signal reflected from the target on the basis of numerical processing the locked-on signal and the known directional pattern with the greatest possible angular resolution. The problem concerns to a class of inverse problems. Efficiency of known methods and algorithms of regularization of inverse problems depends first of all on a signal/noise ratio in the locked-on signal. These methods not always allow to increase the angular resolution noticeably. Besides they are not universal. They allow to increase the effective resolution in comparison with Rayleigh criterion at the signal/noise ratio above 25–30 dB. In the report it is shown, that the satisfactory approximation can be received at essential lower signal/noise ratio if more full to use a priory information on characteristics of the targets.

In many problems of radio navigation and a radiolocation, the angular sizes of the investigated targets there is less than width of the directional pattern. It is used as the a priory information at the solution. The problem consists in determination with possible greater accuracy the angular positions of the targets α_m and amplitudes of the reflected signal from each of targets A_m on the basis of the analysis of the locked-on signal.

The offered method consists in determination of values α_m and A_m, providing minimum of functional, describing mean square deviation of a synthesized signal from the accepted signal. The solution is based on the basis of iterative process. For the point targets the new method allows to increase; effective angular resolution in 2–5 times at a signal/noise ratio 10–25 dB, i.e., at essentially smaller values, than known methods.

Simulation of Scattered Fields from Rotating Cylinder in 2D: Under Illumination of TE and TM Gaussian Pulses

Mingtsu Ho
Department of Electronic Engineering, WuFeng Institute of Technology, Taiwan

Abstract— The computational results of the scattered EM fields from a rotating circular cylinder of infinite length were demonstrated in this paper. Maxwell's equations were numerically solved through the application of the method of characteristics (MOC) combined with a newly developed numerical technique, passing-center-swing-back-grids (PCSBG's). PCSBG is proposed as a treatment for the difficulty of grid deformation when objects of interest undergo rotational motion and originated from the fact that by MOC all field quantities are defined at the cell centroid. The explanation of the PCSBG technique is included as well. There are two types of excitations, transverse magnetic (TM) and transverse electric (TE) Gaussian EM pulses. Since a rotating circular cylinder, even with a relativistic angular velocity does not cause any relativistic effects, and in order to display the cylinder is rotating and scattering EM fields at the same time, the circular cylinder was equally split into an even number of slices which are one perfect reflector and one non-reflector by turns. The vortex structure observed in the field distribution over the domain is the evidence supporting the feasibility of the combination of MOC and PCSBG on solving the EM scattering problem by rotating circular cylinder.

An Efficient and Accurate MoM-based Method for the Analysis of Two Dimensional Dielectric Structures

E. P. Karabulut and M. I. Aksun
Koc University, Istanbul, Turkey

Abstract— The accurate and fast analysis of dielectric structures with the combination of metallic components is crucial to understand physical mechanisms involved in and design of many devices; such as antennas, microstrip lines, photonic band gap materials, left handed materials or other coupled geometries operating in different ranges of frequencies. In this paper, an efficient and general purpose approach, based on the application of Method of Moments (MoM) to the solution of Electric Field Integral Equation (EFIE), is proposed to analyze two-dimensional (2D) dielectric structures of arbitrary cross- sections. Although the method is first developed for two-dimensional dielectric structures, it can easily be extended to incorporate 2D metallic structures as well.

As it is well-known, when a dielectric structure is exposed to electromagnetic waves, it becomes polarized and, in turn, induces scattering waves. As a result, the total field in the structure can be written as the sum of incident field and the scattered field, which is represented as the superposition integral of the polarization current and Green's function of the structure, resulting in EFIE. Hence, the application of MoM for the solution of EFIE for the polarization current begins with expanding the unknown polarization current in terms of known basis functions with unknown coefficients, and it is followed by the testing procedure to convert the integral equation into a set of algebraic equations. Since each entry of the equations requires numerical integration of oscillatory and slow convergent functions over infinite domain, because of the superposition integral, the computational cost of the method is mainly defined by the evaluation of these entries, at least for small to moderate size structures compared to the wavelength of operation. In the proposed approach, a part of a typical integrand of the entries, say (m, n)-th entry, is approximated by complex exponentials with explicit functions of m and n, so that the resulting integrand can be evaluated analytically, using an integral identity of Hankel function, and that the (m, n)-th entry can be written in closed form in terms of functions with explicit m and n indices. Therefore, once this approach is implemented for a single entry of the set of algebraic equations, the rest of the entries can simply be obtained by evaluating the closed-form expression for the complete set of m and n, making the approach very efficient in getting the entries of the equations.

In this study, the proposed method is applied to 2D dielectric structures with arbitrary cross-sections and finite photonic crystals under the excitation of plane waves. The scattered and total fields are obtained and compared with the results obtained by EM based numerical simulation tool, *Comsol Multiphysics* by Comsol Inc.

Fast Algorithms for Solving the Volume Integral Equations

Alexander B. Samokhin
Moscow Institute of Radio Engineering, Electronics and Automatics
78 Vernadsky Av., Moscow 117454, Russia

Abstract— We consider the volume integral equations. Many important classes of the wave scattering problems can be described by equations of this form; for example, this is the case for problems of electromagnetic and acoustic scattering on 3D transparent bodies. The corresponding integral operator is compact in acoustic problems and singular in electromagnetic problems.

To solve the integral equation numerically, one reduces it to a system of linear algebraic equations (SLAE). The solution of that system must approximate the solution of the original problem with a prescribed accuracy. Let h be a typical length on which the solution varies only slightly. The specific values of h are determined by the desired accuracy of the solution. As a rule, *a priory* estimates of h necessary for obtaining the desired accuracy of the solution are known in specific problems. Then the dimension N of SLAE can be estimated as $N \approx (mesQ/h^3)$. It turns out that N is very large. Then it is virtually impossible to use direct methods since this would require performing $T \sim N^3$ arithmetic operations and storing N^2 entries of the matrix of the SLAE in computer memory.

It is clear that we must apply an iteration method. Number T of arithmetic operations that guarantees the required accuracy of solution and memory volume required for the implementation of the algorithm are the main efficiency criteria for any numerical algorithm. Multiplication of matrix SLAE by vector is the most laborious operation of the iteration method. Therefore, the number of multiplications for the implementation of a particular algorithm will be called the number of iterations. The value of T is estimated by the formula $T \approx LT_A$. Here, L is the number of iterations, T_A is the number of arithmetic operations required for multiplication of a matrix by a vector. Our main purpose is the minimization of the values T_A and L.

First, we consider minimal residual iteration method and formulate sufficient conditions for the convergence of the iterations. Based on the integral inequalities we show that this iteration method can be used for the integral equations.

Then, we deal with the discretization method applied to the integral equations, that is, the procedure reducing it to a SLAE. The kernel of the integral operator depends only on the difference of Cartesian coordinates of x and y. Therefore, in the discretization, it is desirable to take account of this fact so as to obtain a matrix of the SLAE with the corresponding symmetry properties. For that we consider Galerkin and collocation methods. Using discrete fast Fourier transform techniques we construct a fast algorithm for the multiplication of the SLAE matrix and the vector.

Let dimension N be represented as multiplication of prime numbers, i.e., $N = N_1^{l_1} N_2^{l_2} \dots N_m^{l_m}$

Denote

$$LOG(N) = \sum_{k=1}^{m} l_k N_k.$$

Then, the number of arithmetic operations for the fast multiplication of the matrix and the vector is estimated as $T_A \sim NLOG(N)$.

Then applying iterative methods we can build the effective methods and algorithms for the numerical solution of the initial problems based on the integral equations.

An Application of Multi-region FDTD with Plane-wave Time-domain Techniques

Jiun-Hwa Lin and Shih-Gia Chiu
Department of Electrical Engineering, National Taiwan Ocean University, Keelung 202, Taiwan

Abstract— The objective of this project is to apply a newly-developed algorithm, MR-FDTD-PWTD (Multi-Region Finite-Difference Time-Domain with Plane Wave Time-Domain method) in the field simulation for elongated-type objects. This new algorithm bas better computational efficiency compared to the traditional single-area FDTD, is capable of accommodating different grid densities in regions, and moreover different grid orientation [1].

An elongated object such as in Fig. 1, if by applying FDTD to field simulation, is enclosed in a single large region, the major part of which is empty, but field value storage and updating in this so-called "white space" cannot be spared. Aiming to alleviate this computing waste, MR-FDTD-PWTD is characteristic of the whole simulation region divided into several sub-regions as in Fig. 2, each of which is arranged to conform to the object outline so that the updating computation in the empty area can be avoided. The interaction among the sub-regions is accounted for by the Kirchhoff integral formula (KIF) evaluation, but direct KIF calculation imposes a computing cost $O(N^2)$, where N is the grid number on the sub-region surface and makes the MR-FDTD less efficient. PWTD method is introduced to accelerate the KIF calculation; like its counterpart in the frequency domain, FMM (Fast Multipole Method) to speed up the matrix-vector multiply, PWTD features the plane wave expansion of the Green's kernel, and instead of the point-to-point interaction implied in the KIF, the group-to-group fashion is incorporated in the PWTD to make the most of its characteristics and achieves better efficiency. We will demonstrate the applicability of this method applied to these cases.

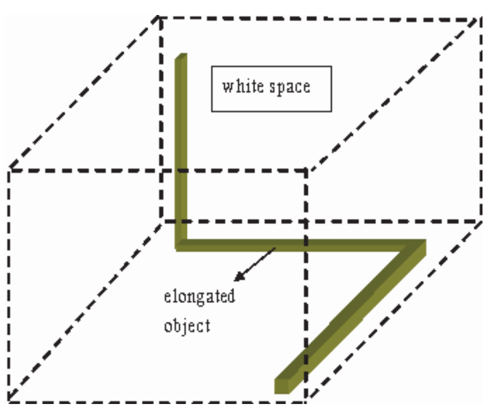

Figure 1: An elongated object in single-area FDTD.

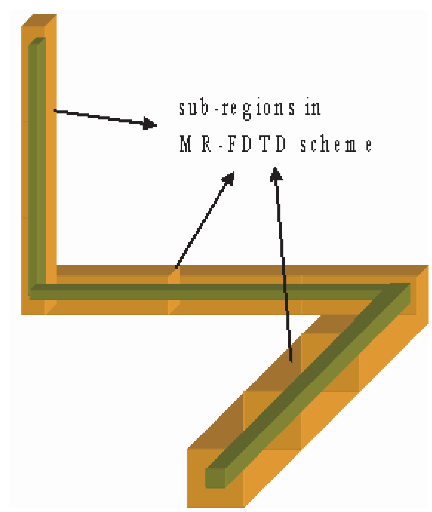

Figure 2: An elongated object in MR-FDTD.

REFERENCES

1. Lin, et al., *Asia Pacific Symposium on EMC*, 195–200, 2005.

Electric Current Behavior near Sharp Edges and Corners of Metallic Structures Analyzed with the EFIE and MFIE Comparison with Analytical Well Established Results

Thierry Gilles[1], **Marc Piette**[1], **and Christophe Craeye**[2]

[1]Ecole Royale Militaire, Laboratoire d'Electromagnétisme Appliqué (LEMA)
Avenue de la Renaissance 30, 1000 Bruxelles, Belgium
[2]Université Catholique de Louvain, Laboratoire TELE
Place du Levant 2, 1348 Louvain-la-Neuve, Belgium

Abstract— It is well known that electric currents flowing all around the surface of metallic structures excited by a source field may become infinite where sharp edges and corners are present. As most scattering or radiating structures show such edges and corners, it is essential to have both a good knowledge of the influence of these discontinuities and a reliable numerical tool to analyze them. We first summarize all the main well known results concerning the singular behavior of edge and corner currents, and relate these to the so called edge condition. Then we seek for an accurate numerical solution extremely close to edges and corners with the Method of Moments. Therefore, we introduce a multilevel meshing scheme allowing to closely approach these singular currents, both with an EFIE and a MFIE formulation. We will finally discuss the interests and limitations of such a refined modellisation of edge and corner currents.

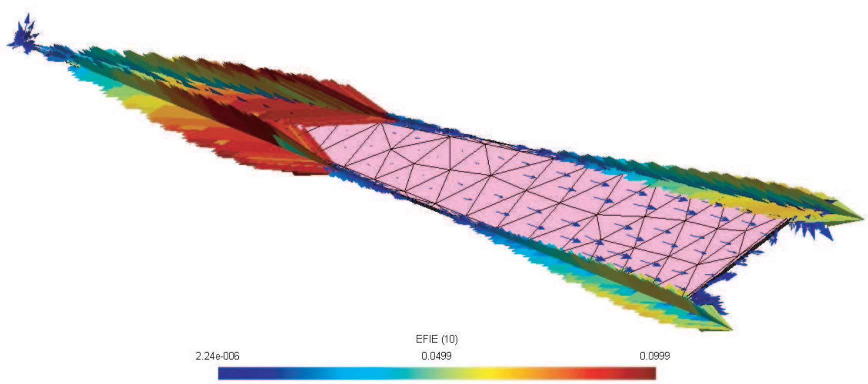

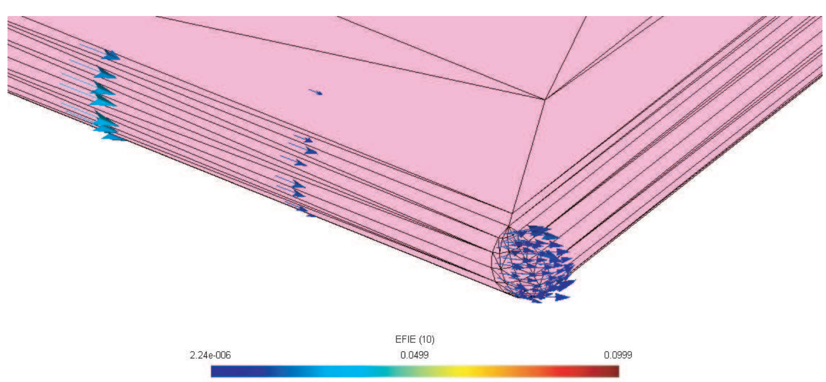

Analysis of Current Propagation on Single Conductor Line Using Point Charges and Propagating Line Currents

T. Sokooshi, **T. Hisakado**, **U. Paoletti**, **and O. Wada**
Department of Electrical Engineering, Kyoto University, Japan

Abstract— The common mode radiation is an important cause of EMI problem. In the case of two conductor transmission lines, the common mode has no explicit return path, whereas the differential mode has the return path. The purpose of this paper is to clarify the mechanism of common mode propagation which has no explicit return path. In order to simplify the problem, we consider a single conductor line, which also has no explicit return path. A. Sommerfeld originally studied the modes on the single conductor lines using Hankel function [1], and G. Goubau analyzed the surface waves in detail [2]. Recently, the single conductor line has attracted considerable attention also for power line communication and terahertz transmission. However, it is difficult to analyze the current propagation on the single conductor line with the existing circuit theories, because the voltage cannot be defined explicitly. We propose a simple model for analyzing the current propagation on the single conductor line.

First, we define point charges and propagating line currents as fundamental elements of the proposed model. The propagating line currents are composed of both forward and backward waves which propagate with the velocity of light on the finite length line elements. The point charges are accumulated at connected points of the line elements under the law of conservation of charge. Using the elements, we analytically derive the electric field. If we put together some elements, the proposed model can represent conductors of complex shape.

Second, we analyze the current propagation on a single cylindrical perfect conductor line which is bending at a right angle and confirm the reflection and transmission phenomena. Considering the boundary condition on the surface of the perfect conductor line, we derive the time domain current and charge waveforms using the numerical Laplace and inversion of Laplace transform. The mechanism of these phenomena is revealed by the current and charge distribution shown in Figs. 1, 2.

Finally, we consider the validation of the proposed model. A kind of transmission line model that could represent the current propagation on a single conductor line with few elements is highly desirable. We ascertain that this model can represent the current propagation with a small number of elements. It indicates that the proposed method is a valid model for the current propagation on a single conductor line.

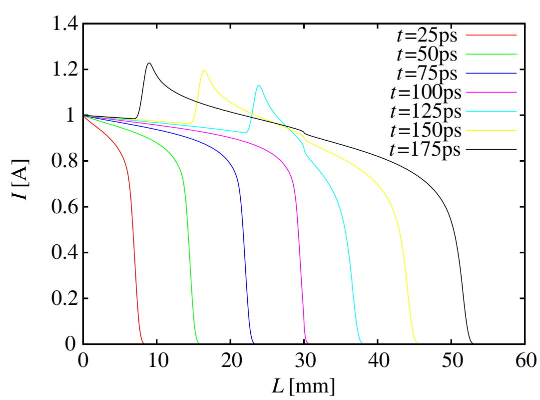

Figure 1: Current waveform.

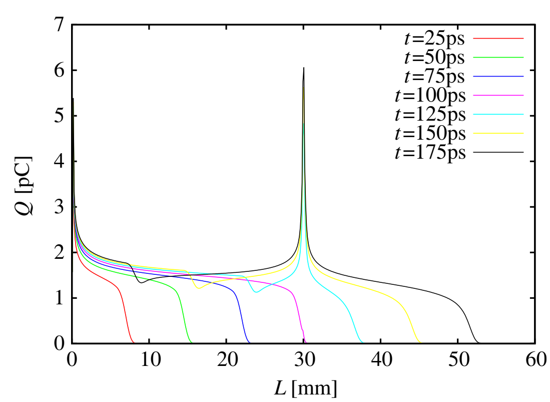

Figure 2: Charge waveform.

REFERENCES

1. Sommerfeld, A., *Electrodynamics*, Academic Press, New York, 1964.
2. Goubau, G., "Surface waves and their application to transmission lines," *Journal of Applied Physics*, Vol. 21, 1119–1128, 1950.

Nonlinear Optics of Metal Nanoclusters in Dielectric Matrices

D. F. Zaretsky
Kurchatov Institute, Moscow 123182, Russia

Abstract— It is well known that many media have the nonlinear polarizability and the wave frequency transformation is possible in these media. This effect is connected with nonlinear polarizability of atoms and molecules of these media. But during the last years the new mechanism of wave transformation was discovered both theoretically and by experiment. This mechanism is connected with nanodimentions of metal clusters irradiated by coherent laser wave. The experiment was performed with single cluster in a glass. In the experiment the intensity of third harmonic was discovered to have R4 dependence, but not R6 [R is cluster radius]. This difference is arized due to the nonlinear corrections in the interaction of electron cloud with ions core. These corrections are arized due to the nanodimentions and disappear with cluster radius increasing. In the talk the theory is formulated for the y mancase of many clusters in the dielectric volume. The coherency of nanoemitters is taken into account. The effectiveness of wave transformation for third harmonic is estimated for real parameters of clusters and laser wave. The short review of existed applications in biology and medicine will be given.

Session 5A6
Magnetic Microwave Smart Materials

Nanostructured Magnetic Microwires for Field-tunable Composites

H.-X. Peng[1], **N. Pankratov**[1], **F. Qin**[1], **L. V. Panina**[2], **and A. P. Zhukov**[3]

[1]Advanced Composite Centre for Innovation and Science, Department of Aerospace Engineering
University of Bristol, University Walk, Bristol, BS8 1TR, UK
[2]School of Computing, Communication and Electronics, University of Plymouth
Drake Circus, Plymouth, Devon PL4 8AA, UK
[3]Dpto. de Fisica de Materiales, Fac. Quimicas, Universidad del Pais Vasco
San Sebastian 20009, Spain

Abstract— Recent invention of metallic glasses produced in the form of amorphous microwires ($1\sim30\,\mu$m diameter) using rapid quenching techniques offers exciting new opportunities in the development of new magnetic sensing devices owning mainly to their excellent magnetic properties such as the giant magnetoimpedance (GMI) effect. Most recently, the microwires have been used for fabricating multifunctional composite materials with electromagnetic functionalities. It has been shown that the magnetic behaviour of the microwires especially its GMI property strongly depends on their dimensions and compositions [1].

The aim of this paper is (i) to evaluate mechanical properties and GMI effect of microwires through the analysis of internal stress; and (ii) to present tunable microwave response in glass fibre composites containing these magnetic microwires.

Glass coated microwires with different geometries were produced by a modified Taylor-Ulitovski process (MFT Ltd, Moldova). The amorphous structure of the wire was confirmed by X-ray Diffraction (XRD). The heat-treatment was conducted at a temperature range of 300–600°C. Magnetisation test in the magnetic field parallel to the axis of wire was carried out by LakeShore VSM in the magnetic field up to 5 kOe. Four layers of glass fibre 913 prepreg were used for the manufacture of composite samples containing long-wires or short-wires with different wires spacing. Scanning electron microscope (SEM JEOL JSM-6500) and optical microscope (VHF-500) were used for examining both wire and composite samples. The diameter of metal core and overall microwires diameter were determined from SEM analysis. Saturation magnetisation and coercive force were calculated from magnetisation hysteresis loop. The Young's modulus was obtained from the tensile test on the glass-removed wires. The study of tunable microwave response from wire-composites was conducted by modelling the effective permittivity and free-space measurement of the transmission/reflection spectra in the presence of external magnetic field. Both types of composites are characterized by the resonance type of the effective permittivity.

The results indicate that there is a correlation between the mechanical properties and the wire geometry. The relationship between the GMI properties and geometry factors of wires is established in the context of the internal stress condition. There exist a strong field dependence of the effective permittivity of the composites containing short wires and long continuous wires. It is shown that the magnetic properties strongly affect the dielectric response of the composite. A model is presented to account for these observations. The microwave dielectric function is found to depend on the microwave impedance of the microwires. All these indicate that these composites are promising candidate materials for a range of self-sensing applications.

ACKNOWLEDGMENT

The work is supported by the Engineering and Physical Science Research Council (EPSRC) UK under the Grant No. EP/FO3850X.

REFERENCES

1. Phan, M. H. and H. X. Peng, *Prog. Mater. Sci.*, Vol. 53, 2008.

Experimental Study of a Planar Inverted-F Antenna with a Magnetic Substrate

A. O. Karilainen[1], **P. Ikonen**[2], **C. R. Simovski**[1], **S. A. Tretyakov**[1], **A. N. Lagarkov**[3], **S. A. Maklakov**[3], **K. N. Rozanov**[3], **and S. N. Starostenko**[3]

[1]Department of Radio Science and Engineering/SMARAD
TKK Helsinki University of Technology, P. O. Box 3000, FI-02015 TKK, Finland
[2]Nokia Devices R&D, Nokia Group, P. O. Box 407, FI-00045, Finland
[3]Institute for Theoretical and Applied Electromagnetics, Russian Academy of Sciences
13 Izhorskaya ul., Moscow 125412, Russia

Abstract— It is well known that a magnetic substrate may reduce the size of a patch antenna without a significant effect on the operating frequency and antenna bandwidth. The presentation describes an experimental study of the performance of a meandered planar inverted-F antenna (PIFA) with magneto-dielectric and dielectric substrates and is aimed at the experimental demonstration of possibilities offered by the current manufacturing technologies for magnetic materials to improve the bandwidth to size ratio of the antenna.

The magnetic substrate employed is a bulk laminate of thin ferromagnetic films that has low specific weight and high microwave permeability. Several samples of $30\,\mathrm{mm} \times 20\,\mathrm{mm} \times 0.5\,\mathrm{mm}$ in size have been manufactured, each consisting of 28 multi-layer films glued to each other. Each film includes five Fe — N layers of 0.07-mcm in thickness deposited on both sides of a 12-mcm thick mylar substrate, with the total of ten layers. The concentration of the magnetic constituent in the sample is 3.5%. The measured permeability of the samples is about 5 at frequencies below 1 GHz; the magnetic loss tangent is below 0.1 at 500 MHz.

The performance of the meandered PIFA with partial magneto-dielectric and dielectric substrate filling was both simulated and measured. In most practical situations, partial magnetic filling is better than the complete one since the last scenario leads to excessive losses: Using the magneto-dielectric material in places where the magnetic field is not strong usually leads to worse obtained bandwidth and to the reduction of the radiation efficiency.

The best improvement in terms of the radiation quality factor was 4% with the measured antenna resonating at 556 MHz. Below this frequency, the improvement should be greater with the used antenna type since material losses of the magneto-dielectric material decrease with the frequency.

The choice of the "optimal" size and position of the sample is inevitably a result of a compromise between optimizing various parameters, and it is finally determined by what parameter of the antenna (size, efficiency, bandwidth) is more critical in a particular application.

Pico-Tesla Sensitivity Amorphous Wire Magneto-Impedance Sensor and Its Application for Bio-magnetic Measurement

Tsuyoshi Uchiyama[1] and Shinsuke Nakayama[2]

[1]Department of Electrical Engineering and Computer Science, Graduate School of Engineering
Nagoya University, Nagoya 464-8603, Japan
[2]Department of Cell Physiology, Graduate School of Medicine, Nagoya University
Nagoya, 466-8550, Japan

Abstract— Recently, micro magnetic sensors which use the Magneto-Impedance effect have been developed by Mohri et al. [1]. MI sensors have such features as high sensitivity, high stability, high spatial resolution, small size, light weight and low power consumption. Integrated MI sensors are being used commercially in today's mobile phones. Optimal sensitivity of MI sensors at around 100 pT has been reported [1].

In this paper, we report the performance of off-diagonal magneto impedance sensor [2], which consists of an amorphous wire and a pickup coil, with operating bandwidth from 0.3 Hz to 1 kHz. We describe improvements of pulse current excitation conditions of an amorphous wire. The relation between time interval T of pulse train current and magnetic noises was investigated in case of the pulse width of 10 ns. The magnetic noise is decreased clearly when T is smaller than 1.5 µsec. The rms noise was estimated as approximately $3\,\mathrm{pT/Hz^{1/2}}$ at 40 Hz$\sim$500 Hz, while a high resolution imaging SQUID microscope has rms noise of $0.1\,\mathrm{pT/Hz^{1/2}}$ at 1 Hz$\sim$1 kHz [3].

Here we demonstrate that this sensitivity is enough to clearly detect magnetic cardiogram signals. We also measured the biomagnetic field around a smooth muscle tissue sample isolated from a guinea-pig. We discovered that the magnetic field waveform of a small tissue sample had highly temperature dependences. The correlation between ion channel current and biomagnetic field was confirmed by means of simultaneous measurement using both electrode and the MI sensor. The results suggest that the localized biomagnetic field generated by smooth muscle cells can be detected by an MI sensor.

REFERENCES

1. Mohri, K. and Y. Honkura, "Amorphous wire and CMOS IC based mangeto-impedance sensors-origin, topics, and future," *Sensor Letters*, Vol. 5, 267–270, 2007.
2. Sanacci, S., D. Makhnovskiy, L. Pannina, and K. Mohri, "Off-diagonal impedance in amorphous wires and its application to linear mangnetic sensor," *IEEE Tanas. Magn.*, Vol. 40, 3505–5510, 2004.
3. Baudenbacher, F., N. T. Peters, and J. P. Wikswo, Jr., "High resolution low-temperature superconductivity superconducting quantum interference device microscope for imaging magnetic fields of samples at room temperatures," *Review of Scientific Instruments*, Vol. 73, No. 3, 1247–1249, 2002.

Ferromagnetic Microwires Composite Metamaterials with Tuneable Microwave Electromagnetic Parameters

M. Ipatov[1], **V. Zhukova**[1], **L. V. Panina**[2], **and A. Zhukov**[1]

[1]Dpto. de Física de Materiales, Fac. Químicas, Universidad del Pais Vasco
San Sebastián 20009, Spain
[2]School of Computing, Communications and Electronics, University of Plymouth
Plymouth, PL4 8AA, United Kingdom

Abstract— A possibility to control or monitor the electromagnetic parameters (and therefore scattering and absorption) of composite metamaterials is of great interest for different application such as remote non-destructive testing, remote stress and temperature monitoring, microwave tuneable coatings and absorbers. The composites with embedded arrays of metallic wires may demonstrate a strong dispersion of the effective permittivity ε_{ef} in the microwave range. The use of ferromagnetic wires in composites makes it possible to strongly change the dispersion of ε_{ef} by modifying the wire magnetic state with external stimulus such as a magnetic field, stress or temperature. The effect of wire magnetism on composite microwave scattering properties was experimentally demonstrated in [1] for composite with cut wires and ε_{ef} of a resonance type.

Here we report novel results on the dependence of the effective permittivity in arrays of parallel Co-based amorphous wires on the external magnetic field applied along the wires. Such composites have a plasmonic type dispersion of ε_{ef} with negative values of its real part below the plasma frequency which is in the GHz range for wire spacing of about 1 cm and wire diameter of few microns [2]. Scattering parameters were measured in free-space in the frequency range of 0.9–17 GHz from which the effective permittivity was deduced. Both the real and imaginary parts of ε_{ef} show strong variations with increasing the field owing to the field dependence of the wire impedance which controls the losses in the dielectric response. Above the plasma frequency, the sample becomes practically transparent for microwave radiation as the value of ε_{ef} tends to be unity and is independent of wire magnetic properties. The same composites were used to prepare cut wire ordered arrays. It was confirmed that their effective permittivity had resonance type dispersion due to the dipole resonance in wires at half wavelength condition. The application of the field strongly broadens the resonance. We can conclude that both types of wire composites possess a strong dependence of the effective permittivity on the external magnetic field and are suitable for large scale applications as tuneable microwave materials.

REFERENCES

1. Makhnovskiy, D. P., L. V. Panina, C. Garcia, A. P. Zhukov, and J. Gonzalez, *Phys. Rev. B*, Vol. 74, 064205, 2006.
2. Pendry, J. B., A. J. Holden, W. J. Stewart, and I. Youngs, *Phys. Rev. Lett.*, Vol. 76, 4773–4776, 1996.

Measurement of Tunable Permeability and Permittivity of Microwires Composites at Microwave Frequency

L. Liu, S. Matitsine, C. B. Tang, and L. B. Kong
Temasek Laboratories, National University of Singapore, 117508, Singapore

Abstract— Casting (Taylor-Ulitovsky) method was used to fabricate glass-coated microwires with different components and structures of metallic nucleus [1]. Microwires consist of an inner metallic nucleus covered by a Pyrex-like coating. The composition of alloy and process parameters (includes casting rate and cooling rate) determine the microstructure and geometrical characteristics, as well as static and dynamic magnetic behaviour. Composites filled with glass-coated ferromagnetic microwires attract great interesting recently due to high magnetic permeability and loss from MHz to GHz frequency, as well as negative permeability due to the ferromagnetic resonance and skin effect [2]. Since the conductive microwires are coated with a layer of glass which blocks the current flow from contacting microwires, composites with microwire inclusions are expected to have lower effective permittivity value than these with bare conductive wires. Field dependent permittivity of composite materials containing ferromagnetic wires was measured with free space method. Tunable transmission and reflection coefficient could be obtained when the bias magnetic field was only a few Oe [3].

In this study, Composites with randomly or regular distributed magnetic microwires were fabricated with molding method. Coaxial line method and free space method were employed to investigate the tunable permeability and permittivity, as well as tunable transmission and reflection coefficient of the composite sheet with thickness of 1 mm from 100 MHz to 18 GHz. It was found that both effective permeability and effective permittivity can be tuned significantly by the bias magnetic field up to 200 Gauss. Such features make glass-coated ferromagnetic microwires a promising candidate for many applications, such as smart absorbing materials, smart shielding materials, sensor or broadband Meta-materials, etc.

REFERENCES

1. Larin, V. S., A. V. Torcunov, A. Zhukov, J. Gonzalez, M. Vazquez, and L. Panina, "Preparation and properties of glass-coated microwires," *JMMM*, Vol. 249, 39, 2002.
2. Liu, L., L. B. Kong, G. Q. Lin, S. Matitsine, and C. R. Deng, "Microwave permeability of ferromagnetic microwires composites/metamaterials and potential applications," *IEEE Trans. on Mag.*, Vol. 44, 11, 2008.
3. Makhnovskiy, D. P. and L. V. Panina, "Field dependent permittivity of composite materials containing ferromagnetic wires," *J. of Appl. Phys.*, Vol. 30, 7, 2003.

Microwave Attenuators Based on Microwires Composites

A. Hernando[1], **A. Gorriti**[1], **P. Marín**[1], **and D. Cortina**[2]

[1]Instituto de Magnetismo Aplicado, ADIF-CSIC- Universidad Complutense
Las Rozas, P. O. Box 155, Madrid 28230, Spain
[2]Micromag 2000, S.L, Las Rozas, Madrid, Spain

Abstract— A detailed model for the physics of shielding microwaves by using composites of paint and non-magnetic and magnetic metallic microwires is presented here. The model successfully reproduces the experimental data.

The effective permittivity of the composite, ε_e, has been appoximated by simple expresions that reflect the influence of microwires volumen fraction and aspect ratio, a_r, geometrical apects as distance to the metallic sheet and width of the composite slab and the permitivity of the host.

In the limit of small ar, the case analysed here, ε_e is independent of the metallic inclusions permittivity, as has been experimentally corroborated, and only depends on the concentration and a_r of the microwires and the permitivity of the hosting material. In the opposite case, or high a_r limit, ε_e mainly converges to the permitivity of the inclusions times its volume fraction.

Composites with Ferromagnetic Wires for Remote Temperature Monitoring

L. V. Panina[1], **A. Zhukov**[2], **M. Ipatov**[2], **and V. Zhukova**[2]

[1]School of Computing, Communications and Electronics, University of Plymouth
Drake Circus, Plymouth, Devon PL4 8AA, United Kingdom
[2]Dpto. de Física de Materiales, Fac. Químicas, Universidad del Pais Vasco
San Sebastián 20009, Spain

Abstract— Recently it has been demonstrated that composites with ferromagnetic wires showing large magnetoimpedance (MI) effect may have a unique electromagnetic functionality such as a tuneable frequency selective microwave response. This can be achieved by sensitively changing the wire impedance with magnetic and mechanical stimuli, which controls the dispersion of the effective permittivity and scattering parameters. In this paper, we propose to utilise temperature dependent magnetic effects in amorphous and nanocrystalline wires to realise composites with thermally tuneable microwave response. They can find applications in remote temperate monitoring by microwave free-space methods, e.g., for composite curing control.

In amorphous and nanocrystalline materials the magnetic structure and MI can be made highly temperature dependent for moderate temperature regions (50–200°C) due to existence of the compensation point where the magnetostriction changes its sign and also by developing alloys with a reduced Curie temperature. Thus, in $Fe_{73}Cu_1Nb_3Si_{16}B_6$ nanocrystalline alloy the compensation point existing due to high volume fraction of bcc-FeSi is about 170°C [1]. The magnetisation of wires produced from such alloy will change from axial to circumferential direction when the temperature is increased beyond the compensation point resulting in decrease in the high frequency impedance. In the other approach, Co/Fe amorphous alloy systems with additions of Ni and Cr and possessing relatively low Curie temperature between 50–200°C can be used for designing temperature-sensitive composites. Proper alloys are $Co_{60.51}Fe_{3.99}Cr_{12.13}B_{13.53}Si_{9.84}$ and $Co_{23.67}Fe_{7.14}Ni_{43.08}B_{13.85}Si_{12.26}$ having a Curie temperature T_c between 75 and 90°C and also well defined axial magnetoelastic anisotropy. At approaching T_c, the magnetisation m scales with $(1|\frac{T}{T_c})^\gamma$ and the magnetostriction scales as m^3. It will result in increase in the initial rotational permeability but will deteriorate high frequency properties. Then, the high frequency impedance will decrease. In both cases, this decrease in the wire impedance as the temperature is increased produces substantial changes in the frequency dispersion of the effective permittivity and scattering parameters from such composites. For example, in the case of cut wire composites, the resonance type dispersion of the permittivity and band gap propagation regimes becomes more pronounce with increasing temperature.

REFERENCES

1. Duong, V. H., et al., *IEEE Trans. Mag.*, Vol. 32, 4821, 1996
2. Zhukova, V., et al., *J. Magn. Magn. Mat.*, Vol. 300, No. 16, 23, 2006.

Electromagnetic Wave Diffraction on Array of Complex-shaped Metal Elements Placed on Ferromagnetic Substrate

S. L. Prosvirnin[1] and V. A. Dmitriev[2]

[1]Institute of Radio Astronomy, Ukraine
[2]Federal University of Para, Brasil

Abstract— Periodic arrays of planar complex-shaped metal elements placed on a dielectric substrate are used as frequency selective surfaces (FSS), polarizers, absorbing layers, etc. It is well known, that ferrite materials in a magnetic biasing field are described by a permeability tensor. Combining resonance responses of metal arrays and ferromagnetic characteristics of the ferrite substrate, one can expect to find new functional features of such structures.

An important peculiarity of the metal array-ferrite structures is the possibility of controlling their properties by a dc magnetic field. Significant change of transmission, reflection and absorption characteristics can be obtained as a result of such control.

It was shown in paper [1], that the frequency shift of resonance response of FSS with metal crosses on a ferrite substrate depends significantly on the biasing magnetic field. But the presented in this paper results are concerned only to transmitted power, and the ferrite material of the substrate was considered to be lossless. Besides, the investigated frequency range was rather far from the ferromagnetic resonance where the possibilities of controlling are not very large. Thus, the electromagnetic properties of a metal array of complex-shaped elements placed on a ferrite substrate were not yet analyzed in detail.

The effects of interaction of electromagnetic waves with the suggested planar metamaterial structure can be described conveniently in terms of scattering matrix. Symmetry of the problem which depends on the symmetry of the ferrite substrate, of the metallic elements and of a dc magnetic field and its orientation, stipulates some restrictions on the operators entering the scattering matrix. Using the theory of magnetic groups we define these restrictions for some possible symmetries of the problem.

The fields, intensities, and polarization characteristics of the electromagnetic waves diffracted by these arrays were calculated by the full wave method described briefly in [2]. Earlier, the method of [2] was applied to structures with dielectric isotropic substrates. This approach is based on the method of moments for solution of vector integral equation for surface currents induced by the electromagnetic field on the array elements. The equation was derived with boundary conditions that assume a zero value for the tangential component of the electric field on metal strips. In our calculations, we used the Fourier transformations of fields and surface current distributions. The main original part of our work is the derived analytical expression for the transfer matrix of normally magnetized ferromagnetic layer for the case of *arbitrary* orientation of wave vector. This simplifies greatly the following numerical calculations.

In our paper, we present some results of numerical study of electromagnetic wave reflection from and transmitted through arrays of infinitely thin, perfect conducting, planar strip complex-shaped elements (cross-shaped, C-shaped, rosette-shaped elements) placed on a magnetized ferrite substrate. The width of metal elements is assumed to be narrow as compared with their stretched length and with the wavelength. The sizes of the array elements were chosen in such a way that their first low-frequency resonances to be near to the frequency of ferromagnetic resonance.

Our results show, in particular, that the absorbtion level and the frequency band of the discussed structure, when the ferromagnetic resonance and a metal element resonance coincide, are larger than the corresponding parameters of the ferrite substrate without metal elements. We also observed a significant enhancement of the Faraday rotation in the vicinity of the metal element resonances.

REFERENCES

1. Li, G. Y., Y. C. Chan, T. S. Mok, and J. C. Vardaxoglou, "Analysis of frequency-selective surfaces on a biased ferrite substrate," *Int. J. Electronics*, Vol. 78, No. 6, 1159–1175, 1995.
2. Prosvirnin, S. L., "Transformation of polarization when waves are reflected by a microstrip array made of complex-shaped elements," *J. of Communications Technology and Electronics*, Vol. 44, No. 6, 635–640, 1999.

Microwave Screen with Magnetically Controlled Attenuation

Sergey N. Starostenko and Konstantin N. Rozanov
Institute for Theoretical and Applied Electromagnetics RAS, Russia

Abstract— The effect of magnetic bias on dielectric spectra of composite sheets filled with Fe or Co-based microwires is studied experimentally and via simulation. The permittivity is measured using a free-space technique within the frequency band from 6 to 12 GHz. The bias is applied either parallel or perpendicular to the microwave electric field, the bias strength varies from 0 to 2.5 kOe. The composites with Fe-based wires reveal a single region of bias dependent permittivity under bias about 800–1000 Oe. The composites with Co-based wires reveal two such regions: the high-field region is near to that of composites with Fe wires, and the low-field region corresponds to the coercive field of Co wires (2–3 Oe). The high-field effect is related to the dependence of FMR parameters on bias, the low-field effect is related to the rearrangement of the domain structure of Co-based wires. The interference of magnetoimpedance and dipole resonance is analyzed, revealing the effects off wire length, diameter, parameters of magnetic resonance and composite structure. The results are considered in view of application to the problem of controlled microwave attenuation. Simulation shows that the narrower is the FMR spectrum and the higher is the admissible loss of a sheet in a transparent state, the wider is the dynamic range of attenuation control. The attenuation range of a lattice of continuous wires is smaller than that of a screen with identical wire sections, where the magnetoimpedance effect is amplified resonantly. At 15 GHz frequency the strength of the bias switching opaque sheet with Fe-based wires to the transparent state is about 2000 Oe. For 3 dB admissible loss, the range of attenuation control about 10 dB is feasible in a composite with aligned wire sections. If the aligned sections are distributed regularly, the loss in a transparent state is about 1 dB lower.

Session 5A7
Nonlinear and Tunable Metamaterials

Tunable Tunnelling in Epsilon-Near-Zero Channels

David A. Powell[1], **Andrea Alù**[2,3], **Brian Edwards**[2],
Ashkan Vakil[2], **Yuri Kivshar**[1], **and Nader Engheta**[2]

[1]Nonlinear Physics Center, Australian National University, Canberra ACT 0200, Australia
[2]Department of Electrical and Systems Engineering, University of Pennsylvania
Philadelphia, PA 19104, USA
[3]Department of Electrical and Computer Engineering, University of Texas at Austin
Austin, TX 78712, USA

Abstract— Epsilon Near Zero (ENZ) materials are those where the electric permittivity $\varepsilon\varepsilon$ is very close to zero over some frequency range. This regime of material parameters has potential applications in nanophotonic circuitry and controlling the radiation pattern of an embedded source. These special properties are due to the wavelength becoming extremely large within such structures. Another phenomenon which was predicted in such structures is the complete transmission of energy through a narrow channel coupled between two larger channels, despite a strong geometric mismatch [1].

This phenomenon has been demonstrated experimentally in a narrow waveguide channel at its cut-off frequency [2], where the guided wavelength becomes very large and the system is a very close analogue of a material with ε near zero. A previous study showed that the same effect could be achieved by patterning the surface of the waveguide with resonant elements [3].

Being almost independent of the structure length, this transmission is due to a tunneling phenomenon, which produces large enhancement of the local electric field in the ultranarrow channel. This opens up the possibility that by the insertion of appropriate materials or elements within the channel, the tunneling frequency may be tuned. In addition, the strong field enhancement and confinement within the channel and the near zero wavenumber of the structure make it highly interesting to study its power-dependent (or nonlinear) properties.

Using a section of rectangular waveguide at cut-off frequency acting as the ENZ channel, fed by external rectangular waveguides with PTFE infilling, we introduce a varactor diode as a nonlinear and tunable element. The transmission response as a function of the tuning voltage can be seen in Figure 1, showing a clear variation of the resonant frequency. Over a moderate tuning range we still observe very high transmission, although losses of the varactor do cause some attenuation. It was found that these transmission peaks corresponded to measured group index values of up to

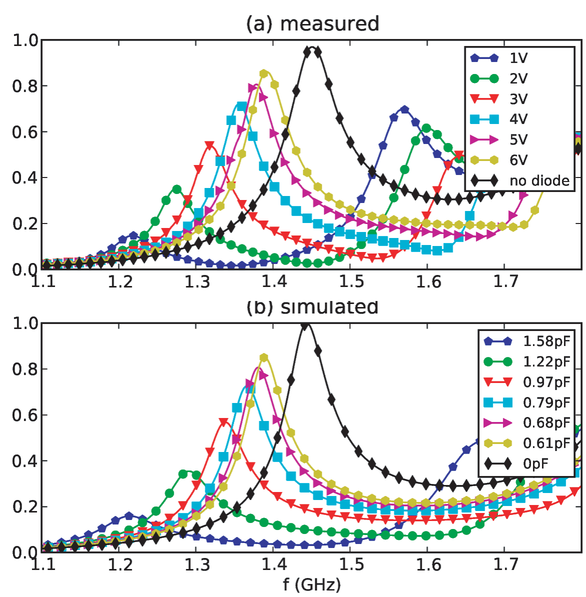

Figure 1: Transmission response through a narrow cutoff waveguide (as an ENZ channel), measured experimentally and simulated numerically.

25. The tuning of transmission and the group delay are in agreement with an equivalent circuit model which we developed.

By varying the input power, we are also able to demonstrate a nonlinear shift in the frequency of transmission resonance. This self-tuning effect is expected to form the basis of further interesting nonlinear phenomena.

REFERENCES

1. Silveirinha, M. G. and N. Engheta, *Phys. Rev. B*, Vol. 76, No. 24, 245109, 2007.
2. Edwards, B., A. Alu, M. E. Young, M. Silveirinha, and N. Engheta, *Phys. Rev. Lett.*, Vol. 100, No. 3, 033903, 2008.
3. Liu, R., Q. Cheng, T. Hand, J. J. Mock, T. J. Cui, S. A. Cummer, and D. R. Smith, *Phys. Rev. Lett.*, Vol. 100, No. 2, 023903, 2008.

Magnetic Antiresonance and Resonance of Ferrite-spinel Nanoparticles Embedded in Opal Matrix Package and Their Application in Microwave Devices

A. B. Rinkevich[1], **D. V. Perov**[1], **V. V. Ustinov**[1],
M. I. Samoilovich[2], **and S. M. Kleshcheva**[2]

[1]Institute of Metal Physics Ural Division of Russian Academy of Sciences, Ekaterinburg, Russia
[2]Central Research Technological Institute "TECHNOMASH", Moscow, Russia

Abstract— Investigation and application of extraordinary electromagnetic properties of metamaterials and nanocomposites becomes one of the most promising topics in last years. Resonance phenomena in 3D nanocomposites are studied here through frequency and magnetic field dependences of the transmission and reflection coefficients of millimeter waveband. First observation of magnetic antiresonance phenomenon is reported in 3D-nanocomposite based on opal packages with embedded ferrite particles. Antiresonance is seen at microwave frequencies of millimeter waveband and it results above all in sharp maximum of the reflection coefficient of electromagnetic wave. Measurements are carried out in frequency range of 26 to 38 GHz with two compositions of embedded particles, namely, $Co_{0.5}Zn_{0.5}Fe_2O_4$ and $Ni_{0.5}Zn_{0.5}Fe_2O_4$ ferrite-spinels. The reasons of physical nature of antiresonance are discussed. If the frequency exceeds 28 GHz, in magnetic fields lower than resonance field, the reflection coefficient at first increased and then decreased after maximum. This maximum is expressed especially clear for the 3D-nanocomposite with $Ni_{0.5}Zn_{0.5}Fe_2O_4$ particles. At frequency of 37 GHz the magnitude of maximum surpasses 150%. Microwave data are compared to structural and magnetic characterization data. The results obtained and giant variations of microwave parameters create suppositions for developing of magnetic field driven microwave devices based on magnetic resonance or antiresonance. In principle, the 3D-nanocomposites under study could be applicable for magnetic field driven attenuators and filters of millimeter waveband.

Electromagnetic Wave Propagation in Waveguide with Thin Superconducting Film and Metamaterial Slab

M. V. Golovkina
Povolzhskiy State University of Telecommunication and Informatics
23 Lva Tolstogo, Samara 443010, Russia

Abstract— Metamaterials are artificial composite materials that possess electromagnetic properties that are not found in natural environments. Of particular interest are those metamaterials that are characterized by a negative refractive index. One of the very interesting phenomena is the amplification of the evanescent components of electromagnetic waves in negative refractive index metamaterial (NIM). The presence of amplified evanescent waves in NIM has been demonstrated theoretically and experimentally. The observance of the growth of an evanescent wave through a NIM has been explained as a coupling surface plasmons that are excited at the edges of the metamaterial slab. Recently it was shown that the generation of growing evanescent waves is possible in the below cutoff waveguide that consist of NIM [1] or shunt capacitive post [2]. In this paper, we have investigated the amplification of the electromagnetic waves in cutoff waveguide with thin superconducting film and NIM slab. The reason of amplification is energy of moving Abrikosov vortex lattice in the superconducting film.

We have considered the wave propagation in two-layered waveguide divided by a thin superconducting film. On layer of thickness d_1 is a negative index material ($\varepsilon_1 < 0$, $\mu_1 < 0$) and the other one of thickness d_2 is an usual dielectric ($\varepsilon_2 > 0$, $\mu_2 > 0$) (Fig. 1). The thin film of type-II superconductor with thickness t is placed in the plane $y0z$. The thickness of superconductor $t \ll \lambda$, where λ is magnetic field penetration depth. A static magnetic field B is applied parallel the x axis, perpendicular to the plane of the film. The value of magnetic field does not exceed the second critical field for a superconductor. Under the impact of transport current directed along the $0y$ axis, the flux-line lattice in the superconductor film moves along the $0z$ axis. Recently the possibility of amplification the electromagnetic waves in layered superconductor-dielectric structure as a result of coupling of electromagnetic wave to the flux-line-lattice in superconductor layer was shown [3]. In this paper, we have demonstrated that the growing of electromagnetic waves can be observed in waveguide structure. We have considered the TE_{0n} modes which effective interact with flux-line lattice in superconductor. The electric and magnetic fields depend on time and the longitudinal coordinate as $\exp i(\omega t - \beta z)$. We have received the dispersion relation for the TE_{0n} modes in the following form

$$\frac{k_{x1}}{\mu_1} ctg k_{x1} d_1 + \frac{k_{x2}}{\mu_2} ctg k_{x2} d_2 = -\frac{i\mu_0 \eta t}{B_{x0}\Phi_0}\left(\frac{j_{y0}\Phi_0\beta}{\eta} - \omega\right), \tag{1}$$

where j_{y0} is the transport current density, η is the vortex viscosity, Φ_0 is magnetic flux quantum, β is the propagation constant, ω is angular frequency. One important difference from the two-layered waveguide without superconducting film is a presence of imaginary part of the propagation constant β. Numerical calculation has shown the following. When the condition of equality of group velocity and vortex velocity is fulfilled, the imaginary part of propagation constant becomes positive. The positive value of β indicates the presence of amplification. The amplification depends on frequency, parameters of superconducting film and magnetic field magnitude. We have found that the significant amplification is observed below a cutoff frequency of the two-layered waveguide. In this frequency domain, the growing evanescent waves increase additionally because of coupling to the moving vortex in superconductor.

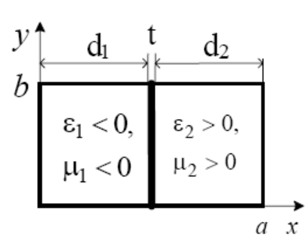

Figure 1.

Thus in our paper the dispersion properties of two-layered rectangular waveguide divided by a thin superconducting film have been studied. It has been revealed that the electromagnetic waves can propagate below cutoff frequency of the two-layered waveguide. It has been shown that the amplification of electromagnetic waves in considered waveguide is possible. The observed effects are explained via interaction between electromagnetic waves and moving flux-line-lattice in superconducting film. The dependency of amplification on magnetic field magnitude provides the possibility to create new devices and filters with parameters controlled by magnetic field.

REFERENCES

1. Hibbins, A. P., M. J. Lockyear, I. R. Hooper, and J. R. Sambles, "Waveguide arrays as plasmonic metamaterials: Transmission below cutoff," *Phys. Rev. Lett.*, Vol. 96, 073904, 2006.
2. Stickel, M. and G. V. Eleftheriades, "Growing evanescent waves in a cutoff rectangular waveguide loaded with an inductive iris and a capacitive post," *Journ. Appl. Phys.*, Vol. 97, 124910, 2005.
3. Glushchenko, A. G. and M. V. Golovkina, "Reflection of an electromagnetic wave by a layered superconductor-dielectric structure," *Technical Physics Letters*, Vol. 24, 4, 1998.

Directly Tunable Metamaterials for Microwave Applications

M. Lapine[1], **I. Shadrivov**[2], **D. Powell**[2], **M. Gorkunov**[3], **R. Marqués**[1], **and Y. Kivshar**[2]

[1]Dept. of Electronics and Electromagnetics, University of Seville, Spain
[2]Nonlinear Physics Center, Australian National University, Canberra, Australia
[3]Institute of Crystallography, RAS, Moscow, Russia

Abstract— We report theoretical analysis and experimental observations of direct tunability of metamaterial based on split-ring resonator (SRR) varieties, provided through the mechanical adjustment of the metamaterial lattice structure. The general principle of the proposed tunability scheme lyes in the essential dependence of the effective properties of metamaterials on the lattice structure [1], easily observable [2] provided that the density of structural elements is sufficiently high.

To demonstrate the arising tuning capabilities, we refer to anisotropic magnetic metamaterial, build of resonant conductive elements such as conventional SRRs or broadside-coupled SRRs, exhibiting a negative permeability band for appropriate microwave polarization. By varying one of lattice constant, namely, interlayer distance, it is possible to alter the value of the resonance frequency by a factor of 2, which provides an efficient switching between transparent, absorbing and reflecting states of a metamaterial slab. A drawback of this method is that the overall size of metamaterial sample have to be also changed remarkably.

We further propose another efficient tuning mechanism, which is easier to be realized in practice and which provides excellent transmission/reflection tuning. This is achieved through lateral displacement of the layers of resonators in parallel planes and requires just a subtle modification of the sample geometry. This enables remarkable tuning of the reflection/transmission already with small lattice shifts (Fig. 1(a)) applicable in a reasonably broad frequency range (Fig. 1(b)).

The reported tuning mechanism is highly useful for tunable superlenses, tunable microwave filters, reflectors, absorbers and similar devices.

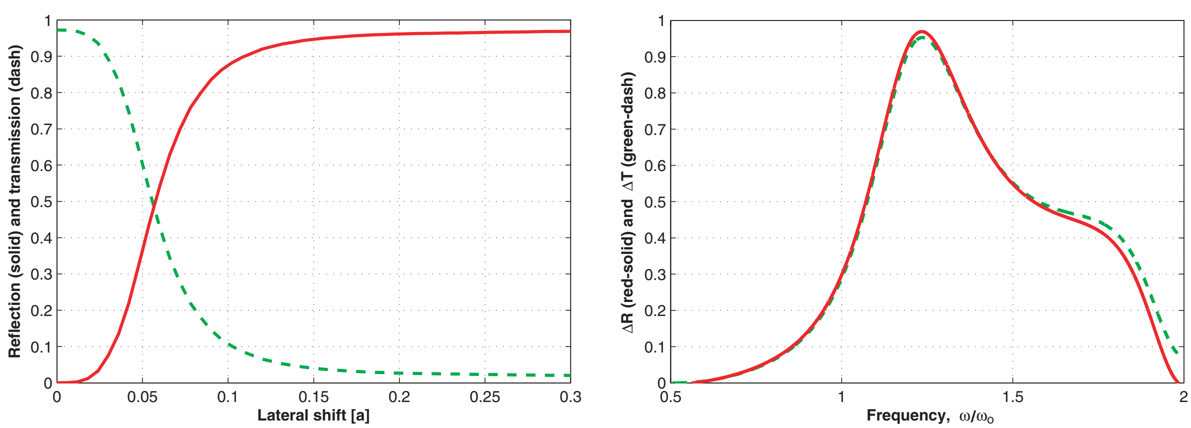

Figure 1: Reflection (solid red) and transmission (dash green) for a thin metamaterial slab at frequency $1.24\omega_o$, depending on the relative lateral shift in the lattice (left); difference in reflection and transmission characteristics for a non-tuned slab state and a state with layers shifted by 0.3 lattice constants, depending on frequency (right); (ω_o is the resonance frequency of a single element).

REFERENCES

1. Gorkunov, M., M. Lapine, E. Shamonina, and K. H. Ringhofer, "Effective magnetic properties of a composite material with circular conductive elements," *Eur. Phys. J. B*, Vol. 28, 263–269, 2002.
2. Shadrivov, I. V., D. A. Powell, S. K. Morrison, Y. S. Kivshar, G. N. Milford, "Scattering of electromagnetic waves in metamaterial superlattices," *Appl. Phys. Lett.*, Vol. 90, 201919, 2007.

Achieving Tunability by Combining Metamaterials with Liquid Crystals

M. V. Gorkunov[1] **and M. A. Osipov**[2]

[1]Institute of Crystallography, Russian Academy of Sciences, Moscow 119333, Russia
[2]University of Strathclyde, Glasgow G1 1XH, United Kingdom

Abstract— Subwavelength metallic structures (metamaterials, metal-dielectric arrays and gratings, etc.) have attracted much attention in recent years due to a variety of surprisingly unusual electromagnetic phenomena discovered and predicted. Their properties can be effectively controlled at the production stage by adjusting the assembly process. After the final arrangement, however, the structures are robust and their response typically cannot be altered by external physical factors (e.g., electric or magnetic fields).

We discuss a natural way of attaining the tunability by combining the advantages of metallic structures with the flexibility of liquid crystal (LC) media. We demonstrate the huge potential of novel hybrid metal-LC materials by using the examples of especially interesting tunable arrangements: 3D metamaterials filled with nematic LC and 1D subwavelength gratings with LC-filled cavities (see Fig. 1).

In particular, we show that the zero-frequency of the permittivity of LC-filled wire grid can be shifted by up to 20% by applying moderate voltage $\sim$8 V across the wires [1]. The transmittance of a LC-filled metal grating experiences drastic variation upon reorienting the LC inside the slits. The latter results in a substantial shift and even disappearing of the peaks of extraordinary light transmission.

We believe that the possibility to tune, spatially modulate or even switch on/off the unusual optical properties of metamaterial structures is extremely beneficial and review the potential applications in photonics, near-field microscopy, and imaging.

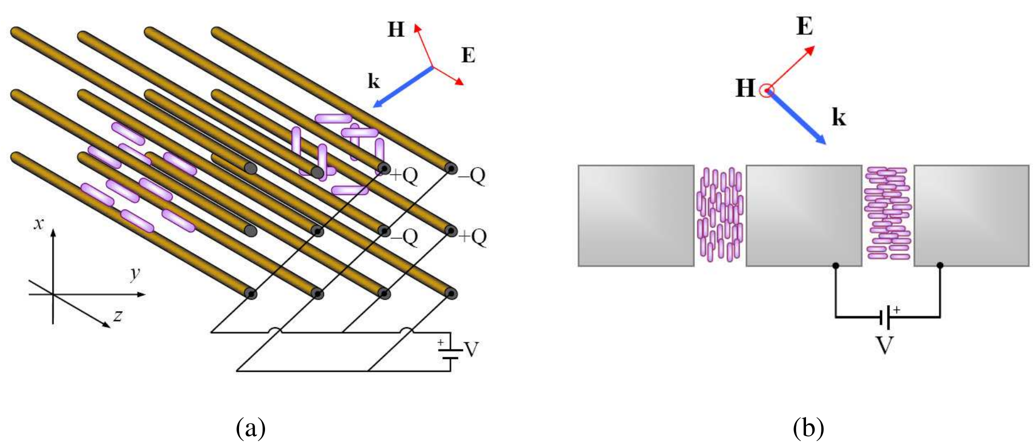

Figure 1: Electrically tunable LC-filled metamaterial systems: (a) Wire-grid metamaterial tuned by switching the LC environment, LC molecules arrange along the wires (left) or perpendicular to them (right) when the voltage is applied; (b) Tunable light transmitting metal grating, LC molecules align along the grating stripes (left) or perpendicular to them (right) when the voltage is applied. Polarizations of the affected light are shown. Note: the size of LC molecules is extremely exaggerated.

REFERENCES

1. Gorkunov, M. V. and M. A. Osipov, *J. Appl. Phys.*, Vol. 103, 036101, 2008.

Controllable Light Transmission through Perforated Metal Films of Periodic and Quasi-periodic Geometries

A. Minovich[1], **D. Liu**[2], **H. Hattori**[2,3], **I. McKerracher**[2], **H. H. Tan**[2], **D. N. Neshev**[1], **C. Jagadish**[2], **and Y. S. Kivshar**[1]

[1]Nonlinear Physics Centre, RSPE, ANU, Canberra, Australia
[2]Electronic Materials Engineering, RSPE, ANU, Canberra, Australia
[3]ADFA School of ITEE, UNSW, ADFA, Canberra, Australia

Abstract— In this work we study, both theoretically and experimentally, the nonlinear control of transmission of light through opaque gold films perforated with subwavelength apertures and slits in different arrangements. In our first step, we study the possibilities for obtaining an optimal geometry of the nanopaterns that features sharp transmission resonances. In the next step we explore the control of transmission through the optimised structures using nonlinear response of the surrounding dielectric medium. This nonlinear response results in changes of the refractive index of the dielectric and leads to shift in the spectral position of the transmission peaks.

For fabrication of our samples we use a focused ion beam (FIB) milling system to drill nanoholes and nanoslits in a 200 nm and 400 nm thick gold films. Five different sample geometries are fabricated and tested. The first two represent square-hole homogeneous lattices of 40×40 holes with spacing of 2 μm between them and a holes size of 800 and 300 nm, respectively. The other two samples represent somewhat the more complex geometries of Thue-Morse sequence of holes and chirped-size hole lattice, respectively. The last sample is a set of 100 nm width nanoslits located with period of 700 nm.

In our experiments with square lattices of 800 nm holes and period of 2 μm, we have measured transmission around 1% and a flat spectrum in the region 0.6–1.7 μm. In contrast, in the experiments with the square lattices of 300 nm holes and the same period, we have observed a number of resonant transmission peaks in the wavelength ranges of 0.6–1.0 μm and 1.4–1.7 μm. Our experimental results are in good qualitative agreement with the performed numerical FDTD calculations. Our simulations show that the periodic arrangement of nanoholes leads to more than sixfold transmission enhancement in comparison to a single hole.

In the experiments with nanoslits, we have designed our sample to exhibit strong and sharp transmission resonance at telecommunication wavelengths. Our spectral measurements demonstrated a stiff slope were the transmission changes from 2% to 28% over a wavelength range of 35 nm. Further measurements were performed when the sample was covered with different nonlinear liquids, including ethanol, castor oil, and solution of gold nanoparticales. With this arrangement we study the change of the transmission versus incident laser power.

In summary, we have analysed the spectral transmission of light through perforated metal films of various geometries and have found a nanopatern geometry that exhibits a rapid transmission change over a narrow spectral range. With this optimised geometry we have studied the possibilities for nonlinear control of the transmission through the metal film using the nonlinear response of covering liquids.

Nonlinear Coupling of Contra-propagating Electromagnetic Waves in Left-handed Nanocomposites

A. K. Popov[1], **S. A. Myslivets**[2], **and V. M. Shalaev**[3]

[1]University of Wisconsin-Stevens Point, Stevens Point, WI 54481, USA
[2]Siberian Federal University and Institute of Physics of Russian Academy of Sciences
Krasnoyarsk 660036, Russian Federation
[3]Birk Nanotechnology Center and School of Electrical and Computer Engineering
Purdue University, West Lafayette, IN 47907, USA

Abstract— Left-handed (negative-index) metamaterials (NIMs) form a novel class of electromagnetic media that promises revolutionary breakthroughs in photonics [1]. A significant progress has been achieved recently in the design of bulk multilayer negative-index plasmonic structures. The majority of NIMs realized to date consist of metaldielectric nanostructures that have highly controllable magnetic and dielectric responses. The problem, however, is that these structures have losses that are difficult to avoid, especially in the visible range of frequencies. Irrespective of their origin, losses constitute a major hurdle to the practical realization of the unique optical applications of these structures. Therefore, developing efficient loss-compensating techniques is of paramount importance. Herein, we explore the feasibility of the developing of such techniques making use the nonlinear-optical (NLO) response of the NIMs. Nonlinear optics in the LHMs remains so far a less-developed branch of optics. On a fundamental level, the NLO response of nanostructured metamaterials is not completely understood or characterized, and cannot be predicted effectively to date. Nevertheless, the fact of the local-field enhanced nonlinearities attributed to the plasmonic nanostructures is well established and some rough estimates of their magnitude can be done. The feasibility of crafting NIMs with strong NLO responses have been demonstrated in [2]. Unlike natural positive-index materials, the energy flow and the phase velocity are counter-directed in LHMs, which determines their extraordinary linear and NLO propagation properties. Counterintuitive features of nonlinear propagation processes in NIMs, such as three-wave mixing (TWM) optical parametric amplification (OPA), second harmonic generation and changes in the optical bistability which are in a stark contrast with their counterparts in natural materials, have been revealed to date.

Herein, we report the possibility to produce the transparency and amplification for LH signal controlled by another positive-index strong laser beam(s) and their extraordinary properties based on the coherent energy transfer from the control field to the signal through a TWM OPA of the signal. The option of independent engineering of resonantly enhanced frequency-nondegenerate four-wave mixing nonlinearity through the embedded four-level centers is also discussed and compared. The transparency is shown to exhibit unusual resonance behavior as a function of intensity of the control field and the NIM slab thickness. Basically, such resonances are narrow and the sample remains opaque anywhere beyond the resonance field's and the sample's parameters. Phase-matching of the contrapropagating waves also presents a technical challenge. We show the feasibility to remove such limitations, so that the transparency and the amplification of the NIMs slab at the signal frequency can be made robust and achievable through a wide range of the control field intensity and the NIM slab thickness. The possibility to eliminate the negative role of the phase-mismatch on the tailored transparency of the slab is also shown. The possibility of creation of microscopic mirrorless backward-wave optical parametric oscillator generating contradirected beams of entangled right- and left-handed photons is proposed and supported by numerical simulations. Some preliminary results of this work are reported in [3].

ACKNOWLEDGMENT

This work was supported by the U. S. Army Research Laboratory and by the U. S. Army Research Office under grants number W911NF-0710261 and 50342-PH-MUR.

REFERENCES

1. Shalaev, V. M., "Optical negative-index metamaterials," *Nat. Photonics*, Vol. 1, 41–48, 2007.
2. Klein, M. W., M. Wegener, N. Feth, and S. Linden, "Experiments on second- and third-harmonic generation from magnetic metamaterials," *Opt. Express*, Vol. 15, 5238–5247, 2007; erratum, Vol. 16, 8055, 2008.
3. Popov, A. K. and S. A. Myslivets, "Transformable broad-band transparency and amplification in negative-index films," *Appl. Phys. Lett.*, Vol. 93, 191117(3), 2008.

Metamaterial-based Tunable Phase Modulator

Iftekhar O. Mirza, Shouyuan Shi, and Dennis W. Prather
Department of Electrical and Computer Engineering, University of Delaware
Newark, DE 19716, USA

Abstract— In this paper we present numerical simulation data on phase only modulation using dual split ring resonators (DSRRs). The designed structure is a stack of single split rings packed very closely with the adjacent rings' split gaps alternated in orientation. The DSRRs are configured to be perpendicular to the incident wave along with the electric field (E) parallel to the gap of the rings to excite the structure. Such a configuration leads to a loop current within a ring which then couples to a magnetic resonance leading to a large effective index at an off-resonance frequency — a key feature of this configuration that helps to circumvent the inherent loss of resonant structures. Tunability is achieved by switching between the open and the closed state of the rings where the difference in the value of the effective index for the two different states is used to calculate the phase change. In particular, we demonstrate that for only a 2.28 mm thick structure on a Duroid substrate ($\varepsilon_r = 2.2$), a phase variation of 82 degrees can be obtained while sustaining a transmission loss of only 0.07 dB. We adopted a unit cell approach to study the DSRRs by employing Ansoft's HFSS software to extract the transmission and reflection parameters. We also calculated the change in phase using the volumetric field data obtained inside the computational region. Furthermore, we carry out a comparative study on the phase and amplitude variation for using substrate materials with different dielectric constants for the designed structure and the effect of transmission loss for such cases. The numerical results obtained by simulation matched well with the theoretical prediction. These tunable metamaterial-based phase modulators could possibly simplify future phased array antenna design and Digital Micromirror Devices (DMD) by controlling each element of the array or pixel electronically.

Session 5A8
Microwave and Milllimeter-wave Devices and Circuits with CAD 2

Broadband Integration and Packaging for W-band Operations

Rownak Shireen, **Shouyuan Shi**, **Peng Yao**, **and Dennis W. Prather**
University of Delaware, USA

Abstract— Millimeter-wave imaging arrays are becoming popular for their potential applications in remote sensing, airport security, and biomedical engineering. Two primary bands, centered at 35 GHz and 95 GHz, are of particular interests due to their relatively high atmospheric transmission. To date, most systems have been implemented in the 35 GHz band mainly because of easier detector fabrication and packaging. Recently, our group has demonstrated a novel detection scheme for the atmospheric window centered at 95 GHz. The idea is to capture millimeter-wave radiation by an antenna and use an electro-optic modulator to upconvert the received signal into sidebands of an optical carrier. Two of the key components of this system are the lithium niobate modulator and the antenna. The sensitivity of this detection system critically depends on the energy coupling efficiency from the antenna to the modulator.

The paper presents a broadband planar integration and packaging of the antenna coupled modulator based on the coplanar waveguide (CPW) transitions and integrated waveguide at W-band. Ribbon bonding is used for the transition of coplanar waveguides on two different substrates, lithium niobate and alumina. Alumina is chosen for chip integration since vias can be drilled easily using standard laser technology. The shape of the ribbon and the dimensions of the CPWs are numerically optimized for obtaining broadband impedance matching. The simulation result of the ribbon interconnects exhibits 30% bandwidth centered at 95 GHz for return loss more than 10 dB and insertion loss about 1 dB. Next, vias are employed to connect the CPW grounds at the top surface to the ground of microstrip line at the backside. The performance of CPW to microstrip transition mainly depends on the spacing between ground vias on either side of the signal line. Lastly, a novel wideband microstrip line-to-waveguide transition is designed for the planar integration of the rectangular waveguide device and the simulated insertion loss is found to be less than 0.15 dB from 75 to 110 GHz. The advantage of this design is that the microstrip substrate can be 2 mm wide while most of the conventional waveguide transitions use 550 μm wide substrates. Linear arrays of metalized vias are placed on both sides of the microstrip to confine the mode in a specific region.

Passive Microwave Mobile System for Atmospheric Boundary Layer Temperature Profilers and Total Water Vapour Content

E. N. Kadygrov[1], **V. V. Folomeyev**[1], **E. A. Miller**[1]
A. V. Troicky[2], **and E. A. Vorobeva**[2]

[1]Central Aerological Observatory, Russian Federation
[2]Radiophysical Research Institute, Russian Federation

Abstract— Remote sensing of low-altitude temperature profiles is important for a variety of studies, including air-sea interactions, studying the energy balance near surface, short-term meteorological forecasting, forecasting of dissipation of fog and stratus, air pollution and forecasting of radio waves propagation. New mobile microwave system for investigating a spatial variability of atmospheric boundary layer (ABL) temperature stratification has been developed in 2008 at the Central Aerological Observatory, Russia. The main parts of the system are scanning 5 mm radiometer for ABL temperature profile measurements, dual channel microwave radiometer for total water vapour content measurements, GPS receiver, meteostation and data collection system. Microwave temperature profiler is an angular scanning radiometer operated at a center frequency near 60 GHz and can to measure temperature profiles each 120 sec with an accuracy of 0.5°C up to the altitude 1000 m. Dual channel microwave radiometer with the frequencies 22.2 GHz and 25 GHz can measure total water vapour content at the atmosphere with accuracy 0.2 g/cm^2. Mobil system was successfully tested in September 2008 in the field expedition at mountains region.

REFERENCES

1. Kadygrov, E. N. and D. R. Pick, "The potential for temperature retrieval from an angular-scanning single-channel microwave radiometer and some comparisons with in situ observations," *Meteorological Applications*, Vol. 5, No. 4, 393–404, 1998.
2. Westwater, E. R., Y. Han, V. G. Irisov, V. Lenskiy, E. N. Kadygrov, and A. S. Viazankin, "Remote sensing of boundary layer temperature profiles by a scanning 5-mm microwave radiometer and RASS: Comparison experiments," *Journal of Atmosp., and Ocean. Techn.*, Vol. 16, 805–818, July 1999.
3. Kadygrov, E. N., G. N. Shur, and A. S. Viazankin, "Investigation of atmospheric boundary layer temperature, turbulence, and wind parameters on the basis of passive microwave remote sensing," *Radio Science*, Vol. 38, No. 3, Mar 13-1÷13-12, 2003.

Distance Measurement by Means of a Groove Guide Oscillator

Thomas F. Bechteler[1] **and A. Sevinç Aydınlık Bechteler**[2]

[1]İzmir University, Turkey
[2]İzmir Institute of Technology, Turkey

Abstract— In this work, a system for measuring the distance between two metallic plates is presented. A groove guide resonator operating in the X-band with an incorporated Gunn element serves as the distance sensor. Since the groove guide structure is made of two non-connected plates, contact-free distance measurements can be performed, for instance, on unbalanced rotating machines. According to the distance between the two metallic plates, the resonant frequencies of the groove guide oscillator change. Focus is on the fundamental resonant frequency of the TE_{111}-mode.

In a first step, the fundamental resonant frequency of the groove guide oscillator at various distances is computed by means of the FDTD method. The plate distances were 13.0 mm, 14.0 mm and 15.0 mm which corresponds to resonant frequencies of 8.978 GHz, 8.731 GHz and 8.484 GHz, respectively. In a second step, the resonant frequencies of the realized groove guide oscillator were measured. Measurements were taken once without biased Gunn element, i.e., in passive mode, and once with biased Gunn element, i.e., active mode. The frequency deviation of about 120 MHz between the simulated and measured results is due to the discretization error in the FDTD calculations and due to a fabrication accuracy of ± 0.05 mm of the realized resonator. The frequency deviation of about 30 MHz between the results of the oscillator in passive mode and in active mode is due to the capacitive respectively inductive behavior of the biased Gunn element.

Despite of the signal's wavelength of about 30 mm, the resolution of the measurement is in the submillimeter level, i.e., about 0.1 mm. Furthermore, in case of distance variations, even within a short time, the system is able to track distance variations nearly instantaneously.

The resonant frequency information is processed using a heterodyne system. After down conversion, the intermediate frequency is directly measured by a frequency counter which is connected to a computer. Using calibration data, the distance is displayed according to the oscillator's resonant frequency.

Microwave and Millimeter Wave EBG Waveguide Circuits

S. E. Bankov
Institute of Radio Engineering and Electronics of Russian Academy of Science, Russian Federation

Abstract— Novel waveguide circuits for microwave and millimeter wave applications based on electromagnetic bandgap (EBG) structures are presented. The following aspects of the problem are discussed: fundamentals of compensating sources technique (CST) for EBG circuits CAD, numerical analysis of regular waveguides inside EBG arrays, analysis of EBG waveguide components, experimental investigation of EBG components and devices.

Choice of EBG structures for microwave and millimeter wave circuits design. In this chapter several types of regular EBG structures which have sufficient advantages for design of microwave and millimeter wave devices will be selected. All these structures are based on the parallel plate waveguide inside which a two-dimensional array of cylinders is located. The following types of circular cylinders are considered: metal, dielectric, metal with lumped element, metal coaxial cylinders, ferrite cylinders.

Fundamentals of CST. In this chapter the main definitions of CST will be introduced. The CST is a new approach for electromagnetic field presentation inside periodical array with defects. This new field presentation allows one to formulate boundary problem for such array in a very effective way that produces a system of linear algebraic equation (SLAE) with order much lower than in cases of other known methods. A sufficient advantage of CST is a possibility to analyze infinite waveguides and to study their eigen modes. In its turn it gives one an opportunity to introduce in a correct way **S**-matrix of EBG multi-port junction. Some special techniques that are required for analysis of multi-port junctions with half-infinite waveguide are also discussed.

Regular waveguides. Regular waveguide is a fundamental for microwave devices element. Their technical characteristics strongly depend on waveguide parameters. Waveguides in arrays of metal cylinders are studied in details. Numerical results for their propagation and attenuation constants, cutoff frequencies, operating frequency range are presented. They are compared with data for waveguides in array of dielectric cylinders and standard rectangular waveguide. Regular waveguides for mechanically and electronically controlled circuits are studied. These waveguides are formed in arrays of coaxial cylinders and cylinders with lumped diodes respectively. Perspectives of such waveguides application in "intellectual" devices are discussed.

Waveguide components. A wide range of waveguide components is presented. Among them are waveguide discontinuities (shorted waveguide, waveguide with lumped discontinuity, waveguide stub, waveguide bend etc.), waveguide resonators, coupled waveguides and directional couplers, infinite system of coupled waveguides, waveguide dividers. More complicated components: transition from EBG waveguide to rectangular waveguide, EBG waveguide to coaxial and strip line transition, multi-layer transitions are also presented. Results of experimental investigation of waveguide components are presented. These results are compared with CST simulations.

Multi-channel dividers, antenna arrays and beam-forming networks. Several EBG circuits for microwave antennas and beam-forming networks design are presented and discussed. Among them are multi-channel parallel type divider, series type multi-channel divider, system of coupled EBG waveguides.

Phased-array Antenna Ferroelectric Phase Shifter for a Higher Microwave Power Level

O. G. Vendik[1], **A. N. Vasiliev**[1], **M. D. Parnes**[2], **A. E. Nikitenko**[2], and **R. G. Shifman**[3]

[1]St. Petersburg Electrotechnical University, Russia
[2]Resonance Ltd., St. Petersburg, Russia
[3]Svetlana-EP, St. Petersburg, Russia

Abstract— Development of the phased-array antenna technique raises new requirements with respect to the phase shifters, which provide the desired phase distribution along the array. The mass production of the phased-array antenna needs in the phase shifters with the following substantial characteristics: 1) Small power in the biasing networks, 2) Relatively high microwave power: about 20 Watt per a single phase shifter, 3) Low production cost: much less than the production cost of ferrite or *p-i-n* diode phase shifter.

This problem can be solved by using thin film ferroelectric tunable capacitors [1–3]. The basic components of the transmission type phase shifter are reflection type phase shifters in a combination with a branch line hybrid junction. The reflection type phase shifter is formed as a parallel junction of two ferroelectric tunable capacitors and an inductive component in form of a short circuited microstrip stub. Two ferroelectric tunable capacitors are connected in parallel with respect to the microwave voltage and in series with respect to the *dc* biasing voltage. Such a scheme provides sufficient decreasing of a modulation of the total capacitance of two capacitors by the microwave voltage and eliminating the cross modulation of the signals. Analysis shows that, if the maximum biasing voltage is 200 V, the amplitude of the microwave voltage across the tunable capacitors can reach 50 V without essential cross modulation. That provides 10 W in pulse for each reflection type phase shifter or 20 W in pulse for the transmission phase shifter.

The ferroelectric phase shifters are driven in an analogous (not digital) regime. The duration of the phase distribution rearrangement is estimated as nanosecond time interval. Thereafter, a small capacitance of the tunable capacitors provides a small recharge current. The leakage current of the ferroelectric capacitors is not higher than 10^{-9} A.

The methods of modeling and design of the ferroelectric components and systems have been developed [4, 5]. The information about industrial production of microwave ferroelectric devices of low cost is now available. The continuously variable phase shifters have been designed for phased-array antennas, smart antennas, and other communications and radar applications [6].

The original design of the phased-array antenna ferroelectric phase shifter for a higher microwave power level is in a progress. Results of the simulation and experimental investigation of the phase shifter based on $(Ba,Sr)TiO_3$ films at the frequency 5 GHz will be discussed.

ACKNOWLEDGMENT

The work was partly supported by the 6 FP of EC (Project NANOSTAR, No. 016340).

REFERENCES

1. Sherman, V., K. Astafiev, N. Setter, A. Tagantsev, O. Vendik, I. Vendik, S. Hoffmann-Eifert, and R. Waser, "Digital reflection-type phase shifter based on a ferroelectric planar capacitor," *IEEE Microwave and Wireless Components Letters*, Vol. 11, No. 10, 407–409, Oct. 2001.
2. Vendik, O. G., "Insertion loss in reflection-type microwave phase shifter based on ferroelectric tunable capacitor," *IEEE Trans. MTT*, Vol. 55, No. 2, 425–429, Feb. 2007.
3. Tagantsev, A. K., V. O. Sherman, K. F. Astafiev, J. Venkatesh, and N. Setter, "Ferroelectric materials for microwave tunable applications," *Journal of Electroceramics*, Vol. 11, 5–63, 2003.
4. Vendik, O. G. and S. P. Zubko, "Modeling microwave dielectric characteristics of thin ferroelectric films for tunable planar structures," *Integrated Ferroelecrics*, Vol. 34, No. 1–4, Pt. 5, 215–226, 2001.
5. Vendik, O. G. and M. Parnes, "A phase shifter with one tunable component for a reflectarray antenna," *IEEE Antennas and Propagation Magazine*, Vol. 50, No. 4, 53–65, Aug. 2008.
6. nGimat, C., "A low cost analog phase shifter product family for military, commercial and public safety applications," *Microwave Journal*, Vol. 49, No. 3, 152, Mar. 2006.

Wideband Waveguide Iris Filter Design with a Novel Synthesis Procedure

Qingfeng Zhang and Yilong Lu
School of Electrical and Electronics Engineering
Nanyang Technological University, Singapore

Abstract— This paper presents a novel dimensional synthesis procedure for wide-band waveguide iris filter design without global optimization. With the new mapping method, the distributed-element bandpass filters network is transformed directly from the lumped-element lowpass prototype filters network and both the center frequency and edge frequency information are considered in the design. Applications of this mapping method to lumped-element bandpass filters, distributed-element bandpass filters with ideal inverters, and distributed-element bandpass filters with frequency-dependent inverters are discussed. The exponent-weighted turns ratio is also proposed to incorporate the frequency dependence of immittance inverters in designing bandpass filters. Using the proposed technique, some waveguide filter design can be improved significantly in accuracy, time, and complexity. And the excessive use of optimization can be avoided especially in complicated structures with numerous dimensions to be optimized. A design example of four-pole H-plane waveguide iris filters is presented here. The examples are for WR90 waveguide with a center frequency of 10 GHz and use an iris thickness of 1.5 mm. The scattering parameters of the waveguide iris filters are calculated by finite integration techniques using the state of the art commercial software CST Microwave Studio and Ansoft HFSS. Fig. 1 shows the simulated and measured scattering parameters for the design example. One may note from the figure that the scattering parameters calculated using the two simulations agree well with the measured results and the equiripple performance is very good during the 17.6% fractional bandwidth (9.25–11.01 GHz). The proposed dimensional synthesis procedure is expected to find more applications in wide-band waveguide filters design.

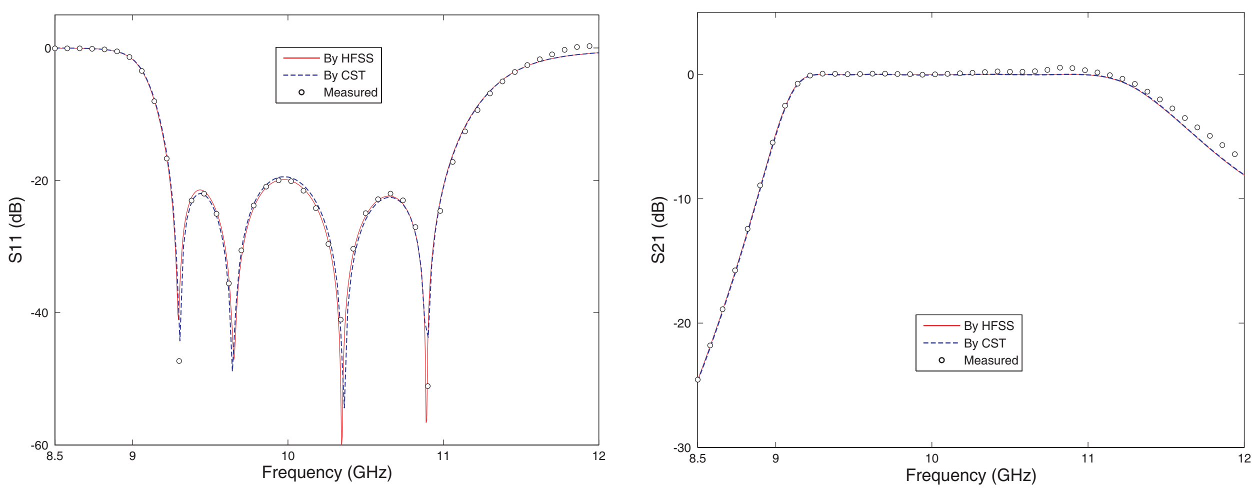

(a) (b)

Figure 1: Simulated and Measure (a) S_{11} and (b) S_{21} parameters.

Optimum Design of Low Pass Filters for General LC Network Configurations by the Method of Least Squares

H. Oraizi and M. S. Esfahlan
Department of Electrical Engineering, Iran University of Science and Technology
Tehran 1684613114, Iran

Abstract— There are several classic methods for the design of low pass, high pass, band pass and band stop filters, such as Butterworth, Chebyshev, elliptic, k-constant, m-derived and insertion loss methods [1, 2]. We present here a design procedure based on the method of least squares using the insertion loss, which also incorporates the impedance matching of the load to source impedances in the desired frequency bands.

REFERENCES

1. Hong, J. S. and M. J. Lancaster, *Microstrip Filter for RF/Microwave Applications*, Wiley, New York, 2001.
2. Pozar, D. M., *Microwave Engineering*, Third Edition, Wiley, New York, 2004.

An Analytical Treatment of High-frequency Impedance Extraction for Interconnects and Inductors in the Presence of a Multi-layer Substrate

Roberto Suaya[1], **Navin Srivastava**[2], **and Kaustav Banerjee**[2]

[1]Mentor Graphics Corp., 38334 St., Ismier, France
[2]Department of Electrical and Computer Engineering
University of California, Santa Barbara, CA 93106, USA

Abstract— Signals propagating on VLSI interconnects contain a broad frequency spectrum from nearly DC up to a significant frequency determined by the switching speed of the driving transistors. As technology scales beyond the 45 nm node, the significant frequency for digital circuits exceeds 50 GHz. For frequencies beyond a few 10 s of GHz, electromagnetically induced eddy currents in the Silicon substrate have a significant and measurable impact on the interconnect impedance, particularly in the presence of low resistivity substrate layers. As shown in this paper, at the maximum frequency of interest for CMOS-based circuits (about 100 GHz), these eddy currents alone can cause as much as 30% variation in the inductance of three-dimensional interconnect structures such as onchip inductors. We discuss the corrections to the impedance matrix of interconnects due to eddy currents in the substrate for a general multi-layer substrate configuration. We present a wire impedance extraction methodology that incorporates substrate eddy currents, to be able to compute its influence with a desired accuracy of better than 97% and computational efficiency suitable for system-level extraction of large integrated circuits.

We study this problem in two-dimensions (due to the simplicity of the 2D formalism) for interconnect structures that are much longer than the transverse dimensions, as well as in three-dimensions for general interconnects including inductors. We use a layered medium Green's function approach to compute the magnetic vector potential, where the sources and destinations (interconnects) are above the substrate, and we are interested in examining the near-field behavior for evaluating impedance in on-chip applications. For these problems, it is permissible to use the quasi-static approximation for the vector potential above the substrate, and neglect dielectric losses on the interconnect, while keeping a full-wave representation for the behavior of the vector potential at the interfaces between different regions, incorporating the substrate layer electromagnetic properties via boundary conditions.

In order to address computational efficiency, we use a modified form [1] of the Discrete Complex Images Method (DCIM) [2, 3], using complex exponential fits to obtain analytical solutions for the vector potential Green's function. We generate an approximate representation of the Green's function above the substrate in terms of dipoles that are images of the source and are located at a complex vertical distance below the substrate interface. Unlike existing implementations of the DCIM, our exploration strategy for the complex exponential fits involves non-uniform sampling of the spectrum [4], combined with an ansatz for the initial guesses [5]. The resulting analytical expressions are shown to be valid for the range of substrate and interconnect configurations relevant to CMOS technologies.

We apply this technique to evaluate the impedance matrix of interconnects as a function of frequency and compare our results to field solvers like HFSS and FastHenry. We discuss, in two and three dimensions, the performance gains of applying this methodology to VLSI extraction problems. A lower bound of an order of magnitude improvement in computation time with respect to PEEC is guaranteed, while maintaining better than 97% accuracy, permitting us to use this technology in a system-level computer-aided design environment.

REFERENCES

1. Srivastava, N., R. Suaya, and K. Banerjee, *Design, Automation and Test in Europe (DATE)*, 426–431, 2008.
2. Yang, J., Y. Chow, and D. Fang, *IEE Proceedings H: Microwaves, Antennas and Propagation*, Vol. 138, No. 4, 319–326, 1991.
3. Dural, G. and M. Aksun, *IEEE Transactions on Microwave Theory and Techniques*, Vol. 43, No. 7, 1545–1552, 1995.
4. Golub, G. and V. Pereyra, *SIAM Journal on Numerical Analysis*, Vol. 10, No. 2, 413–432, 1973.

5. Srivastava, N., R. Suaya, and K. Banerjee, *IEEE Transactions on Computer-Aided Design of Integrated Circuits and Systems*, 2009 (to appear).

Carbon Nanomaterials for Next-generation Interconnects and Passives: Physics, Status and Prospects

Kaustav Banerjee, Hong Li, Navin Srivastava, and Chuan Xu
Department of Electrical and Computer Engineering, University of California
Santa Barbara, CA 93106, USA

Abstract— The semiconductor industry is confronting an acute problem in the interconnect area due to the limited current carrying capability of copper wires, which are presently used to connect billions of transistors in every integrated circuit including microprocessors that are vital for information transmission, processing and storage. As IC feature sizes continue to be scaled below 45 nanometer, copper wires exhibit significant "size effects" resulting in a sharp rise in their resistivity, which, in turn, has adverse impact both on their performance as well as reliability — in the form of current carrying capacity. This limitation of copper interconnects has been recently highlighted by various leading semiconductor companies around the world as well as in the International Technology Roadmap for Semiconductors (ITRS), and threatens to slow down or even stall the traditional growth of the semiconductor and related industries. Hence, it is critical to identify and develop new interconnect solutions.

Carbon nanotubes and nano-ribbons, tiny nanostructures 80,000 times narrower than a human hair, are known to have amazing electrical, thermal and mechanical properties, and can potentially address the challenges faced by copper and thereby extend the lifetime of "electrical interconnects". Most of these outstanding properties arise from their ultra-strong SP^2 hybridized bonds and "low-dimensionality" — they are essentially 1-dimensional structures. This talk will provide a brief overview of the fundamentals of carbon nanomaterials such as carbon nanotubes and graphene nano-ribbons. It will discuss their prospects as interconnects and passives and how they can be efficiently integrated into microprocessors and other circuitry to address the dire need for faster and more reliable on-chip wiring and also open new opportunities in mixed-signal, analog and RF applications. It will also highlight the possible applications of these nanomaterials in off-chip wiring and packaging and in emerging 3-dimensional integrated circuits.

REFERENCES

1. Li, H., C. Xu, N. Srivastava, and K. Banerjee, *IEEE Transactions on Electron Devices*, in Press, 2009.
2. Srivastava, N., H. Li, F. Kreupl, and K. Banerjee, *IEEE Transactions on Nanotechnology*, in Press, 2009.
3. Xu, C., H. Li, and K. Banerjee, *IEEE International Electron Devices Meeting (IEDM)*, 201–204, 2008.
4. Li, H. and K. Banerjee, *IEEE International Electron Devices Meeting (IEDM)*, 525–528, 2008.
5. Li, H., et al., *IEEE Transactions on Electron Devices*, Vol. 55, No. 6, 1328–1337, 2008.
6. Li, H., et al., *IEEE International Electron Devices Meeting (IEDM)*, 207–210, 2007.

Session 5P1
Scattering and Rough Surface Scattering

3-dimensional Microwave Scattering Measurements on a Complex Aggregate with Fully Known Properties

O. Merchiers[1], **J. M. Geffrin**[2],
R. Vaillon[1], **P. Sabouroux**[2], and **B. Lacroix**[1]

[1]Université de Lyon, CNRS, INSA-Lyon, UCBL, CETHIL, UMR5008, France
[2]Institut Fresnel, Aix-Marseille Universités, Ecole Centrale Marseille, CNRS, France

Microwave analogy principles have been applied since the fifties in order to analyze optical scattering properties of non-spherical particles and systems [1]. The method is based on the Scale Invariance Rule (SIR) [2]. This property allows one to increase both object size (effective radius r) and incident wavelength (λ), keeping their size parameter $x = 2\pi r/\lambda$ and complex refractive index constant, such that the scattering behaviour of the analog object is identical to the original one.

The experiments of which we present here the results, were carried out by members of the Institut Fresnel in the anechoic chamber of the "Centre Commun de Ressources Microondes" (CCRM). Further details concerning the precise description of this system may be found in [3]. The main specificity of this equipment is the semi-circular vertical arch which allows to measure fields almost all around the target under test, especially outside of the target receiver plane (called here the azimuthal plane). The system performs field measurements from a few GHz up to 20 GHz with a good accuracy in both magnitude and phase. The target presented here is the smallest that we have ever measured with this equipment.

The choice of the aggregate was originally guided by the analogy with soot particles. These can generally be modeled as fractal aggregates. We generated numerically a set of 74 coordinates corresponding with the centers of the constituent spheres. Those coordinates were chosen such that the aggregate would satisfy the equation [4]

$$N = k_0 (R_g/a)^{D_f}, \tag{1}$$

where N is the number of monomers, k_0 is the prefactor, R_g the gyration radius, a is the monomer's radius and D_f is the fractal dimension. For those quantities we chose $N = 74$, $k_0 = 2$, $a = 2.5\,\mathrm{mm}$ and $D_f = 1.8$.

We will present comparisons of the experimental data for the four complex elements of the scattering matrix with simulated results obtained by Mackowski's T-matrix multi-sphere cluster code and Draine's ddscat7.0 [5, 6].

We plan to build and analyze other types of aggregates. Of special interest are the ones for which the constitutive material shows absorption in the microwave region. This kind of material offers a better approximation to realistic soot optical properties. Interpenetration of the neigbouring spherules is another subject of interest, since real soot particles show always some amount of it. Using a stereolithographic method, this kind of system is quite straightforward to build.

ACKNOWLEDGMENT

The authors would like to thank the ANR (Agence Nationale de la Recherche, France) for its financial support to the project "SOOT" ♯ANR-06-BLAN-0349-03 and also Prof. M. P. Mengüç (University of Kentucky, Lexington, USA) and his team for the many fruitful discussions.

REFERENCES

1. Gustafson, B. Å. S., *Light Scattering by Nonspherical Particles: Theory, Measurements, and Applications*, chapter Microwave Analog to Light-Scattering Measurements, 367–390, Academic Press, 2000.
2. Mishchenko, M. I., *Journ. Quant. Spectrosc. Radiat. Transf.*, Vol. 101, No. 3, 411–415, 2006.
3. Eyraud, C., et al., *Radio Science*, Vol. 43, 4018, August 2008.
4. Mackowski, D. W., *Appl. Opt.*, Vol. 34, No. 18, 3535–3545, 1995.
5. Draine, B. T. and P. J. Flatau, *J. Opt. Soc. Am. A*, Vol. 11, No. 4, 1491–1499, 1994.
6. Draine, B. T. and P. J. Flatau, *User Guide for the Discrete Dipole Approximation Code DDSCAT 7.0*, September 2008.

Detection of Three Dimensional Objects Buried in a Half-space by the Use of Surface Impedance

Egemen Bilgin and Ali Yapar
Electrical and Electronics Eng. Faculty, Istanbul Technical University, Istanbul, Turkey

Abstract— The objective of this study is to detect three dimensional objects buried in a lossy half space medium using equivalent surface impedance function. The method applied in this work is an extension of the one presented in [1] to the three dimensional case which is based on the reconstruction of the equivalent surface impedance of the planar interface via the remote field measurements of scattered field. The surface impedance requires the tangential components of the total electric and magnetic fields on the planar interface separating the two half-spaces. For this purpose, the half space is illuminated by a plane wave and resulting scattered field is assumed to be measured on a surface above the interface. The measured scattered field data is then analytically continued to the planar boundary by two dimensional Fourier transform technique. This spectral representation immediately allows us to write the required field values on the surface. It is shown that it is possible to detect the locations of the buried objects by observing the variatin of the surface impedance which will be a two dimensional function in the case of 3-D burials. Numerical simulations show that illumination by a plane wave with single frequency and incident angle results in enough information to detect dielectric and\or conducting objects of different size and depth. It is also observed that unless the objects are very close to each other, the surface impedance is highly effective in locating buried physical objects and also carries information about relative depth, size or material properties of the objects.

Two numerical examples are presented to show the validity of the method. In both situation, the scattered field is measured on a surface with an area of $4\,\text{m} \times 4\,\text{m}$, 1 m above the interface. The plane wave has the frequency of 300 MHz and it is normally incident from upper space. In the first example, two identical dielectric cubes of $0.2\,\text{m}^3$ are buried in a depth of 0.2 m under surface. In Figure 1, the normalized surface impedance clearly shows the location of both objects. In the second example, one of the cube is buried 0.1 m under surface therefore its contribution to the surface impedance is higher than the one that buried in deeper depth, i.e., 0.2 m. The amplitude of normalized surface impedance is shown in Figure 2. Similar simulations with multiple dielectric or conducting objects demonstrate that surface impedance can be used effectively to locate buried objects and also carries information about their positions and sizes.

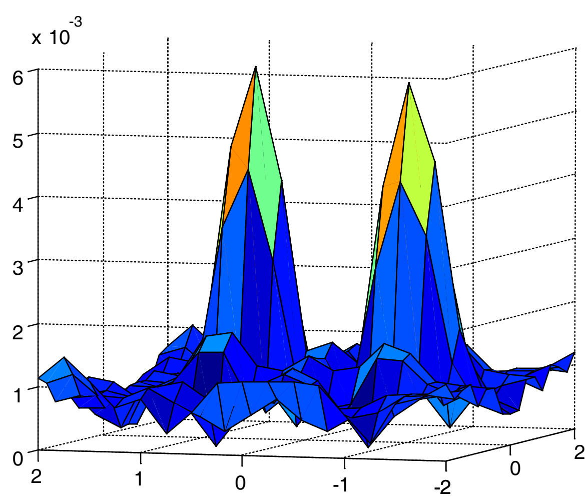

Figure 1: Two identical dielectric cube.

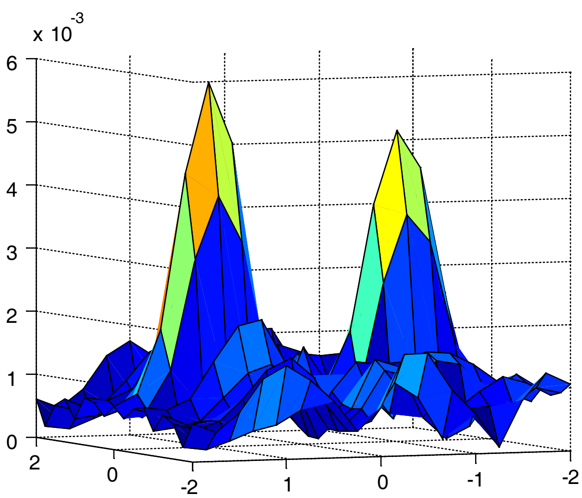

Figure 2: Two dielectric cube in different depth.

REFERENCES

1. Altuncu, Y., I. Akduman, and A. Yapar, "Detecting and locating dielectric objects buried under a rough interface," *IEEE Geoscience and Remote Sensing Letters*, Vol. 4, No. 2, 251–255, 2007.

Polarization Coupling in the PO and PTD Approximations

Pyotr Ya. Ufimtsev
EM Consulting, USA

Abstract— The Physical Optics (PO) and the Physical Theory of Diffraction (PTD) have been extensively used in antenna design and RCS calculations for a long time. The specific feature of these approximations is the so-called *polarization coupling* that has been known since 1975. However, the physics behind the polarization coupling has been established only recently [1]. The purpose of the present communication is to clarify this phenomenon.

There are two different, but equivalent, forms of the field representation in Electromagnetics. One of them involves only the vector potential. The other form contains both the scalar and vector potentials. It turns out, that this form is more physically meaningful: The scalar potential operates with electric charges and allows one to investigate their field in detail.

The present communication demonstrates that the polarization coupling is caused by the wave of electric charges traveling along the edge. These electric charges are accumulated at the edge of a scattering structure due to the discontinuity of the PO current component, which is normal to the edge. Though this phenomenon is investigated here only for a perfectly conducting structure, it also relates to the scattering structures, which can support both electric and magnetic currents.

REFERENCES

1. Ufimtsev, P. Ya., *IEEE Trans. AP*, Vol. 56, No. 12, 2008.

New Form of the Classical Physical Optics Approximation

Pyotr Ya. Ufimtsev
EM Consulting, USA

Abstract— Classical Physical Optics (PO) approximation was introduced by Mackdonald in 1912. Since then it has been widely used in analysis of antennas and scattering problems for electromagnetic and acoustic waves. The present communication suggests a new form of PO and explains its physical nature.

It is shown that the scattered field calculated in the PO approximation can be exactly separated into two parts:

- the *REFLECTED FIELD* containing all reflected rays and beams, and
- the *SHADOW RADIATION* responsible for the Grimaldi-Fresnel diffraction and the forward scattering.

This observation elucidates the physics behind the fundamental diffraction law about the total power scattered by large reflecting objects. It also establishes the diffraction limit for reduction of scattering by absorbing materials.

The concepts of the PO field and Shadow Radiation have existed independently for decades. A tight connection between them has been established only recently [1]. The purpose of the present communication is to clarify this connection.

REFERENCES

1. Ufimtsev, P. Ya., *IEEE AP Magazine*, Vol. 50, No. 3, 11–20; No. 4, 65, 2008.

Evaluation of Reduced Single and Coupled Integral Equations for Scattering by Layered Media

I. R. Ciric

The University of Manitoba, Canada

Abstract— Reduced single surface integral equations were formulated for the electromagnetic scattering from twodimensional layered dielectric structures [1, 2] and, recently, for three-dimensional fields [3, 4]. Using a single unknown function over each interface and a reduction procedure to relate recursively these functions from one interface to the next, a reduced integral equation can be obtained, which involves one interface only and the unknown function over it. The reduced single surface integral equations are much more efficient for the field analysis in the presence of multilayered media than the classical coupled integral equations, constructed in terms of two unknown functions associated with each interface.

A reduction/elimination procedure is also presented in this communication for the system of coupled integral equations describing the electromagnetic scattering from three-dimensional multilayered bodies, which yields two equations relative to only one interface, but with two unknown functions over it. It is shown that the method of reduced single integral equations is much more efficient even than the method of reduced coupled surface integral equations. Namely, for the schemes used for comparison and assuming the same number of surface elements for discretizing each interface, with one unknown and two unknowns for the single equation and for the coupled equations, respectively, the amount of computation is at least 2.56 times smaller in the single integral equation approach, when only counting the number of matrix-matrix multiplications and of matrix inversions. Moreover, computational experiments show that, for the same accuracy, the surface discretization grid should be more dense in the coupled integral equations approach than that in the single integral equation method, which further increases the efficiency of the latter.

REFERENCES

1. Maystre, D., "A new general integral theory for dielectric coated gratings," *J. Opt. Soc. Am.*, Vol. 68, 490–495, 1978.
2. Swatek, D. R. and I. R. Ciric, "Single integral equation for wave scattering by a layered dielectric cylinder," *IEEE Trans. Magn.*, Vol. 34, 2724–2727, 1998.
3. Ciric, I. R., "Reduced surface integral equations for Laplacian fields in the presence of layered bodies," *Can. J. Phys.*, Vol. 84, 1049–1061, 2006.
4. Ciric, I. R., "Formulation of reduced surface integral equations for the electromagnetic wave scattering from three-dimensional layered dielectric bodies," *Radio Science*, Vol. 43, RS4S05, 2008.

Scattering of TM Plane Waves from a Binary Periodic Random Surface

Kazuhiro Hattori[1], **Junichi Nakayama**[2], **and Yasuhiko Tamura**[2]

[1]Mayekawa MFG. Co., Ltd., Japan
[2]Kyoto Institute of Technology, Japan

Abstract— This paper deals with a TM wave scattering from a binary periodic random surface making use of the concept of periodic stationary process. We assume that the surface shown in Figure 1 is obtained by displacing the local surface profile by every integer multiple of the period and modulating their amplitudes by a stochastic binary sequence $\{b_m\}$ taking only ± 1 with equal probability.

For analysis, we employ the stochastic functional approach. Since the binary periodic random surface becomes a periodic stationary process and has shift invariance property in the probabilistic sense, the scattered wave has the stochastic Floquet form, which is a product of an exponential phase factor and an unknown periodic stationary process. Then, such an unknown periodic stationary process is expressed by a harmonic series representation given by mutually correlated stationary processes. These stationary processes are represented by a sum of orthogonal binary functional series with band-limited binary kernels. Hierarchical equations to determine such band-limited binary kernels are derived from the Neumann boundary condition without approximation.

When the periodic random surface is zero on average, effects of multiple scattering should be taken into account to obtain a physically meaningful solution. Thus, this paper employs the multiply renormalizing approximation to determine the band-limited binary kernels. Several statistical properties of the diffraction and scattering are numerically calculated in terms of such binary kernels [1].

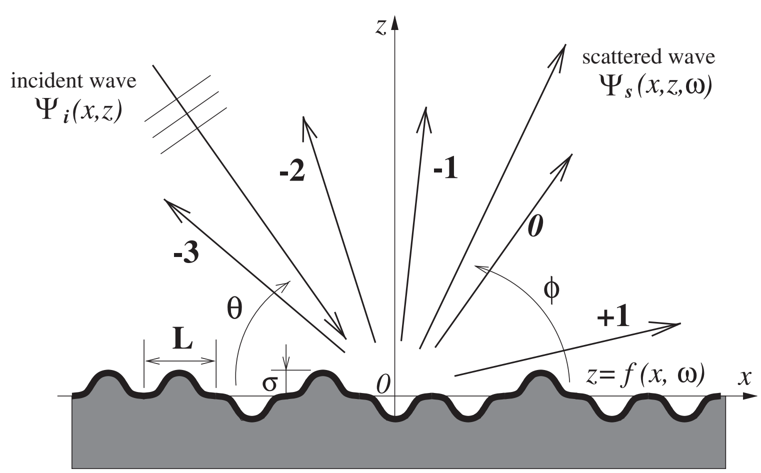

REFERENCES

1. Hattori, K., J. Nakayama, and Y. Tamura, “Diffraction and scattering of TM plane waves from a binary periodic random surface,” *Waves in Random and Complex Media*, Vol. 18, 585–613, 2008.

Design of High Symmetry Microwave Frequency Selective Surfaces with Trapped-mode Resonance

M. N. Kawakatsu[1], **V. A. Dmitriev**[1], **and S. L. Prosvirnin**[2]

[1]Federal University of Para, Brasil
[2]Institute of Radio Astronomy, Ukraine

Abstract— Achieving resonances with high quality factors is essential for various applications of planar frequency selective surfaces (FSS). Generally speaking, the high quality factor and small thickness of a dielectric layer are conflicting requirements. Actually, a thin open structure cannot have inner resonating volumes and on the other hand, resonating inclusions usually are strongly coupled with free space and this reduces the quality factor. Nevertheless, there are ways to produce very thin structures possessing high quality factor frequency resonances using a resonance regime with the so-called *trapped modes* [1].

A characteristic feature of the previously suggested FSS with excitation of trapped modes is their polarization sensitivity. For some applications however, it is necessary to use FSS which operate with any polarization of incident waves. In paper [2], an attempt was made to realize such a structure with the elements having a 4-fold symmetry. However, the quality factor of resonances for the suggested FSS is not so large as was observed in polarization sensitive structures.

The main objective of our work is to find some ways to enlarge quality factor of the discussed FSS by development of new geometries of arrays. An example of the application of this type of arrays can be found in reference [3].

In this paper, we present results of our study of resonance frequency dependencies of transmission and reflection by arrays of new complex-shaped particles, namely corrugated rings combined with ideal rings, as illustrated in Fig. 1.

The combined metal particles possess the *n-fold* symmetry. To vary the shape of the inner particle we consider the different number of periods in the sinusoidal strip n.

Basing on numerical analysis of such kind of arrays, we develop a method of design of this type of arrays for the trapped mode regime. It is known that the trapped mode is excited when there are two resonant elements of approximately equal resonant frequencies. Therefore, we studied firstly the resonant properties of each particles separately, i.e., the outer ring and the corrugated inner ring.

Several techniques were used for optimization of these structures. Optimization parameters are geometrical dimensions of the particles, dimensions of the cell and the number n which defines symmetry of the particles.

In microwave region, the analyzed structures can serve for example as filters.

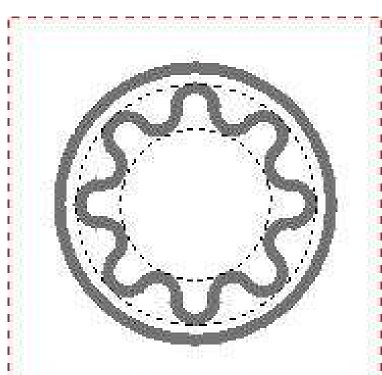

Figure 1: The unit cell of the planar array supported by a dielectric layer.

REFERENCES

1. Prosvirnin, S. L. and S. Zouhdi, "Resonances of closed modes in thin arrays of complex particles," *Advances in Electromagnetics of Complex Media and Metamaterials*, S. Zouhdi, et al., (eds.), 281–290, Kluwer Academic Publishers, 2003.
2. Prosvirnin, S., N. Papasimakis, V. Fedotov, S. Zouhdi, and N. Zheludev, "Trapped-mode resonances in planar metamaterials with high structural symmetry," *Metamaterials and Plasmonics: Fundamentals, Modelling, Applications*, S. Zouhdi, et al., (eds.), 201–208, Springer, 2008.
3. Zheludev, N. I., S. L. Prosvirnin, N. Papasimakis, and V. A. Fedotov, "Lasing spaser," *Nature Photonics*, Vol. 2, No. 6, 351–354, 2008.

A New Hybrid Numerical Method for the Scattering by a Plate above a Rough Surface

G. Kubické, C. Bourlier, and J. Saillard
IREENA, Fédération CNRS Atlanstic, Université de Nantes
La Chantrerie, Rue C. Pauc, BP 50609, 44306 Nantes Cedex 03, France

Abstract— The study of scattering by an object located above a one-dimensional randomly rough surface is a subject of great interest [1]. Since homogeneous media are considered, a rigorous formalism is used, based on the integral equations and discretized by the method of moments (MoM), which leads to a linear system. Since the surface has to be large enough for the scattered field to vanish at the surface extremities (to avoid edge effect), fast numerical methods are necessary to treat a large problem. In this paper a new hybrid method is proposed to solve such a complex problem.

The Extended-PILE method was developed recently [2] in order to compute the scattering from two scatterers. The main advantage of this rigorous approach is that the resolution of the linear system (obtained from the Method of Moments) is broken up into different steps. Two steps are dedicated to solving for the coupling interactions, and two other ones are dedicated to solving for the local interactions, which can be done from efficient methods valid for a single interface. In [2], the E-PILE method was combined with the Forward-Backward Spectral Acceleration (FB-SA) of Chou et al. [3] of complexity $\mathcal{O}(N)$, in which N is the number of samples on the surface. Results showed that if the number of unknowns on the surface is much greater than that on the object, the complexity of the method is then $\mathcal{O}(N)$. But for a scene which involves a very large plate (high-frequencies), the direct LU inversion for the computation of the local interactions on the plate could not be applied. The solution proposed here is to use Physical Optics approximation instead of the direct LU inversion. The consequences in the E-PILE algorithm is that the inversion of the impedance matrix of the plate is done analytically and the coupling matrices are modified to take into account shadowing effects.

During the presentation, this new hybrid method (E-PILE method combined with FB-SA and PO) will be detailed. Results will be given for the case of a Perfectly Conducting (PC) plate located above a rough surface. Radar Cross Sections and currents (on the plate and on the rough surface) will be compared with the results obtained with the MoM (with direct LU inversion).

REFERENCES

1. Johnson, J. T., "A numerical study of scattering from an object above a rough surface," *IEEE Trans. Antennas Propag.*, Vol. 50, No. 10, 1361–1367, 2002.
2. Kubické, G., C. Bourlier, and J. Saillard, "Scattering by an object above a randomly rough surface from a fast numerical method: Extended PILE method combined with FB-SA," *Waves in Random and Complex Media*, Vol. 18, 495–519, Aug. 2008.
3. Chou, H. T. and J. T. Johnson, "A novel acceleration algorithm for the computation of scattering from rough surfaces with the forward-backward method," *Radio Sci.*, Vol. 33, 1277–1287, 1998.

Scattering by an Object above a Dielectric Rough Surface with the Extended-PILE Method Combined with BMIA/CAG

G. Kubické, C. Bourlier, and J. Saillard
IREENA, Fédération CNRS Atlanstic, Université de Nantes
La Chantrerie, Rue C. Pauc, BP 50609, 44306 Nantes Cedex 03, France

Abstract— The study of scattering by an object located above a one-dimensional randomly rough surface is a subject of great interest. To solve such a difficult problem, some asymptotic models and exact numerical methods have been investigated [1, 2]. But, in the numerical simulations, the length of the surface plays an important role: it has to be large enough for the scattered field to vanish at the surface extremities, that is to avoid edge effect. Thus, it is interesting to investigate exact fast numerical methods to treat a large problem.

The Extended-PILE method was recently developed [3] in order to compute the scattering from two scatterers. The main advantage of this rigorous approach is that the resolution of the linear system, obtained from the MoM (Method of Moments), is broken up into different steps. Two steps dedicated to solving for the coupling interactions, and two other ones dedicated to solving for the local interactions, which can be done from efficient methods valid for a single rough interface. In [3], the E-PILE method was combined with the Forward-Backward Spectral Acceleration (FB-SA) of Chou et al. [4] of complexity $\mathcal{O}(N)$, in which N is the number of samples on the surface. The results showed that E-PILE+FB-SA can be considered as a benchmark method for an object above a perfectly conducting or highly conducting rough surface. But in the case of an object above a dielectric rough surface, E-PILE+FB-SA does not converge to the MoM since the deformation of the integration contour was evaluated only for a PC rough surface. In order to obtain a fast rigorous method, E-PILE is combined with the BMIA-CAG of Tsang et al. [5] of complexity $\mathcal{O}(N \log N)$.

During the presentation, the extended PILE method combined with BMIA/CAG will be detailed. Results will be given for the case of a perfectly conducting cylinder located above a dielectric rough surface. Comparisons with the results obtained with E-PILE+FB-SA will be presented in terms of convergence and computing time.

REFERENCES

1. Johnson, J. T., "A numerical study of scattering from an object above a rough surface," *IEEE Trans. Antennas Propag.*, Vol. 50, No. 10, 1361–1367, 2002.
2. Ye, H. and Y.-Q. Jin, "A hybrid analytic-numerical algorithm of scattering from an object above a rough surface," *IEEE Trans. Antennas Propag.*, Vol. 45, No. 5, 1174–1180, 2007.
3. Kubické, G., C. Bourlier, and J. Saillard, "Scattering by an object above a randomly rough surface from a fast numerical method: Extended PILE method combined with FB-SA," *Waves in Random and Complex Media*, Vol. 18, 495–519, Aug. 2008.
4. Chou, H. T. and J. T. Johnson, "A novel acceleration algorithm for the computation of scattering from rough surfaces with the forward-backward method," *Radio Sci.*, Vol. 33, 1277–1287, 1998.
5. Tsang, L., C. H. Chang, H. Sangani, A. Ishimaru, and P. Phu, "A banded matrix iterative approach to Monte Carlo simulations of large scale random rough surface scattering: TE case," *Journal of Electromagnetic Waves and Applications*, Vol. 29, 1185–1200, 1993.

A Research Overview on Numerical Simulation of Composite Scattering from the Object and Randomly Rough Surface in Fudan WSRSI

Ya-Qiu Jin
Key Laboratory of Wave Scattering and Remote Sensing Information (WSRSI)
Fudan University, Shanghai 200433, China

Abstract—

Introduction: Research progress of numerical simulation for electromagnetic (EM) composite scattering from the volumetric object and randomly rough surface in WSRSI, Fudan University is briefly reported in this paper, which are mostly based on the author's recent publications.

(1) Generalized Forward/Backward Method with Spectrum Accelerate Approach (GFBM/SAA)
GFBM/SAA is applied to numerically solve EM scattering from an ship-like object over a randomly rough oceanic surface. The FBM splits the surface current at each point into two components: forward and backward contributions. Scattering from the object area is calculated by MoM, and interactions between the object and rough surface is obtained by convergent iterations. SAA is applied to speed up the calculations.

(2) A Hybrid Method with Analytic Kirchhoff Approximation and Numerical Method of Moment (KA-MoM)
A hybrid KA-MoM is developed to numerically calculate the difference scattering fields due to the object presence above a randomly rough surface. The KA is first applied to the rough surface scattering. The integral equation of EM excitation on the object, which contains the difference scattering of rough surface, is updated to calculate new object currents with the conjugate gradient procedure.

(3) Finite Element Method with conformal perfectly matched layer (FEM/CMPL)
The FEM can accommodate differential equation of multiple scattering when an object above a rough surface. The CPML is employed as the truncation boundary of FEM to reduce the reflection error caused by conventional PML. It also includes the approaches such as the domain decomposition method (DDM) for large scale problem, and two level quasi-stationary algorithm (TLQSA) for a flying target above rough surface for Doppler calculation.

(4) Finite Difference Time Domain Method (FDTD)
The FDTD approach is developed for near and far fields computations for the model of a 3D-target above a randomly rough surface.

(5) Bidirectional Ray Method (BART)
Ray tracing is carried out both along the incident direction and converse direction of scattering recording different orders of ray's illumination on each facet or edge of the object and surface. Rough surface is modeled with 'rough facets' including coherent scattering and diffused incoherent scattering. The complexity due to the object electrical size is significantly reduced. Higher orders of scattering and, in particular, interactions between the 3D electrical large object and underlying rough surface are taken into account.

A Research Overview on Polarimetric Scattering and Information Retrieval from SAR Imagery in Fudan WSRSI

Ya-Qiu Jin
Key Laboratory of Wave Scattering and Remote Sensing Information (WSRSI)
Fudan University, Shanghai 200433, China

Abstract—

Introduction: Research progress on polarimetric scattering and information retrieval from SAR imagery in WASRSI, Fudan University is briefly reported in this paper, which are mostly based on the author's recent publications.

(1) The Mueller Matrix Solution of Polarimetric Scattering for the Model of Vegetation Canopy
The Mueller matrix solution and numerical approach for the scattering model of a layer of vegetation canopy with non-spherical scatterers above a randomly rough land surface are developed. It provides a parameterized modeling to simulate the scattering data of the terrain surface as numerical tool for SAR image analysis.

(2) Deorientation Theory and Surface Classification Using a Set of New Parameters
Making deorientation rotation to reduce the influence of fluctuating orientation of random scatterers, the generic characteristics of co-polarized scattering prominence of random scatterers are presented. A set of new parameters of the scattering vector is newly defined, and a new unsupervised classification of total 19 surface groups is developed.

(3) Automatic Detection of Terrain Surfaces from Multi-Temporal SAR Images
A two-threshold expectation maximum with Markov random field method (2EM-MRF) is developed for automatic change detection. It is applied to detection and classification of the urban area under multi-temporal change, and the terrain surface variance before and after serious earth quake.

(4) DEM Inversion from One-Flight Polarimetric SAR Image
A DEM (digital elevation mapping) inversion from one-flight fully polarimetric SAR image is developed using the third Stokes parameter and morphologic image processing.

(5) SAR Image Simulation Using the MPA (Mapping and Projection Algorithm)
A novel MPA computerized simulation of SAR imaging over a comprehensive terrain scene with heterogeneous terrain objects, which takes account of scattering, attenuation, shadowing and multiple scattering of spatially distributed volumetric and surface scatterers, is developed.

(6) Reconstruction of 3D Buildings from Multi-Aspect SAR Images
Based on the edge detection of CFAR, Hough transform technique, and a set of probability density functions using the maximum-likelihood estimation, an automatic reconstruction algorithm is developed to match object-images of different aspects and reconstruct the building objects from multi-aspect SAR images.

(7) Simulation and Analysis of Polarimetric Bistatic SAR Imagery
Extending the MPA to BISAR configuration, polarimetric BISAR image of a comprehensive scene is simulated. It is found that conventional classification parameters cannot work for bistatic configuration. A new concept of unified bistatic polar bases is proposed: both polar bases of incident and scattered waves are consistently defined paralleling in the coordinates determined by bistatic configuration. BISAR image simulation is applied to BISAR measurement analysis and image information retrieval.

(8) SAR Image simulation of Undulated Lunar Surface
Based on the statistics of the lunar cratered terrain, the terrain feature of cratered lunar surface is numerically generated. According to inhomogeneous distribution of the lunar surface slope, the triangulated irregular network is employed to make the digital elevation of lunar surface model. The Kirchhoff approximation is then applied to simulation of lunar surface scattering. The SAR image for comprehensive cratered lunar surface is numerically generated using back projection algorithm of SAR imaging.

Session 5P2
Optics and Photonics

Design of Very High Birefringence and Flat Near-zero Dispersion Photonic Crystal Fibers

D. H. Spadoti, B.-H. V. Borges, and M. A. Romero
Electrical Engineering Department, University of Sao Paulo, Sao Carlos, Brazil

Abstract— Photonic crystal fibers (PCFs) have attracted a great deal of attention in recent years because of the large number of possibilities offered in terms of design and applications. It becomes possible to tailor distinct optical properties, such as dispersion and birefringence characteristics, separately or simultaneously. Dispersion management can be achieved by changing the fiber cross-section or air-filling factor [1] while birefringence enhancing, by its turn, is mostly due to geometric anisotropy or to stress-induced during the handling process [2], but can also be intentionally induced [3]. Several non-linear photonics applications, including supercontinuum generation, would benefit from the availability of high birefrigence optical fibers with near-zero dispersion coefficients over a given wavelength range. These conditions allow phase-matching and favors a wide variety of non-linear phenomena [4].

In the present communication, we further explore our previously proposed D-shaped PCF geometry [5] in order to design a photonic crystal fiber with flat near-zero dispersion and high-birefringence. All PCFs considered in this communication have been numerically simulated with our H-field finite difference based full-vectorial successive over relaxation method (FD-SOR) [6]. In order to achieve the desired characteristics, the D-PCFs were numerically investigated for several distinct geometrical arrangements. Also, in order to attain an additional degree of freedom, the refractive index of the air-holes were varied to simulate the air-hole filling by a varied range of materials. The best result was achieved for a geometry with pitch of 3.0 μm, air hole diameter over pitch ratio around 0.8, and filling material refractive index of 1.38, yielding a birefringence around 10^{-4} and a flat near-zero $[2.5 \pm 2.5\,\mathrm{ps/(nm{\cdot}km)}]$ dispersion over the 1100–1700 nm wavelength range. Further details will be given at the conference presentation.

REFERENCES

1. Digweed-Lyytikainen, K., C. A. de Francisco, D. Spadoti, A. A. Juriollo, J. B. Rosolem, J. B. M. A. Neto, B. V. Borges, J. Canning, and M. A. Romero, "Photonic crystal optical fibers for dispersion compensation and Raman amplification: Design and experiment," *Microw. and Opt. Tech. Lett.*, Vol. 49, No. 4, 872–874, Apr. 2007.
2. Zhu, Z. and T. G. Brown, "Stress-induced birefringence in microstructured optical fibers," *Opt. Lett.*, Vol. 28, No. 23, 2306–2308, Dec. 2003.
3. Ortigosa-Blanch, A., J. C. Knight, W. J. Wadsworth, J. Arriaga, B. J. Mangan, T. A. Birks, and P. St. J. Russell, "Highly birefringent photonic crystal fibers," *Opt. Lett.*, Vol. 25, No. 18, 1325–1327, Sept. 2000.
4. Agrawal, G. P., *Non-Linear Fiber Optics*, 3rd Edition, Academic Press, 2001.
5. Martins, E. R., D. H. Spadoti, M. A. Romero, and B.-H. V. Borges, "Theoretical analysis of supercontinuum generation in a highly birefringent D-shaped microstructured optical fiber," *Opt. Express*, Vol. 15, No. 22, 14335–14347, Oct. 2007.
6. De Francisco, C. A., B. V. Borges, and M. A. Romero, "A semivectorial method for the modeling of photonic crystal fibers," *Microw. and Opt. Tech. Lett.*, Vol. 38, No. 5, 418–421, Sept. 2003.

Electric Field Measurement from Tremendously Low Frequency to DC Based on Electro-optic Integrated Sensors

Huan Li, **Rong Zeng**, **and Bo Wang**
High Voltage Lab, the Department of Electrical Engineering, Tsinghua University, China

Abstract— In this paper, a novel method of electric field measurement from tremendously low frequency to DC based on electro-optic integrated sensors is proposed and proves to be potentially much better than the previous ones.

Firstly, the previous efforts on the measurement of DC electric field are classified into two categories and concisely summarized. Into one category fall the conventional electrical methods, which inevitably involve the probability of severely distorting the measured electric field; while into the other category fall the methods utilizing electro-optic devices without integrated optical techniques, which inevitably involve sophisticated apparatus.

Secondly, the whole sensing system, including the electro-optic integrated electric field sensor and other peripheral devices, is briefly introduced. Then it is regarded as a linear time-invariant system under certain theoretical assumptions. Its frequency response from tremendously low frequency to DC is investigated experimentally and an equivalent RC network model is proposed particularly for the type of sensors used in this paper to analyze the frequency response. A vector fitting with three poles and three zeros is performed. The numbers of the poles and zeros are determined by the RC network model stated above. With the sensor frequency response, the electric field waveform being measured, i.e., the excitation signal of the sensing system is deduced from the response signal of the sensing system. Measurements at such low frequency band could not be carried out directly because the excitation and response signal waveforms of the sensing system are not identical in time domain.

Finally, the experiments have preliminarily verified the feasibility of this method. One of the possible applications of this method is measuring the electric field distribution along the High Voltage DC insulator strings.

Ultraviolet (UV) and X-ray Free-electron Lasers — Tutorial Review

Toshiyuki Shiozawa
Department of Electronics and Information Engineering, Chubu University, Japan

Abstract— The free-electron laser is expected to play an important role for the radiation source in the region of ultraviolet (UV) and X-ray wavelengths. In this range of the spectrum, the conventional quantum laser comes to work only poorly. This is because radiation absorption in the lasing medium increases rapidly as the region of UV and X-ray wavelengths is approached. Starting from the discussion of synchrotron radiation, the present paper briefly reviews the basic principles of free-electron lasers, from the viewpoint of classical electrodynamics [1–3]. The operation principle of the free-electron laser can be explained purely classically, as opposed to the conventional laser which resorts to the quantum-mechanical treatment. In particular, special attention is paid to research efforts for the UV and X-ray free-electron lasers.

The free-electron laser covers a broad continuous spectrum extending from the far infrared (FIR) through the visible to the UV and X-ray wavelengths. In the UV and X-ray wavelength region, in particular, free-electron lasers can generate coherent radiation with much higher brightness than that for synchrotron radiation. In recent years, research efforts to realize the X-ray free-electron laser have been made in major research facilities in the world such as SLAC [4] (the United States), DESY [5] (Germany), and Spring-8 [6] (Japan). With its short and coherent pulses carrying enormous peak power, the X-ray free-electron laser will open a whole new field of scientific research, such as new medical and life sciences, solid-state physics, and fabrication of nano-scale structures.

REFERENCES

1. Saldin, E. L., E. A. Schneidmiller, and M. V. Yurkov, *The Physics of Free Electron Lasers*, Springer, Berlin, 2000.
2. Shiozawa, T., *Classical Relativistic Electrodynamics — Theory of Light Emission and Application to Free-electron Lasers*, Springer, Berlin, 2004.
3. Schmuser, P., M. Dohlus, and J. Rossbach, *Ultraviolet and Soft X-ray Free-electron Lasers*, Springer, Berlin, 2008.
4. www.slac.stanford.edu.
5. www.desy.de.
6. www.spring8.or.jp.

Bistability of Nonlinear Photonic Crystal Microring Resonators

T. Ahmadi Tameh, B. Memarzadeh Isfahani, N. Granpayeh, and A. R. Maleki Javan
Faculty of Electrical Engineering, K. N. Toosi University of Technology
Tehran, Iran

Abstract— In this paper, two different structures of nonlinear photonic crystal microring resonators have been analyzed by finite-difference time-domain method and their optical bistabilities have been demonstrated. The optimized structure from the aspect of low threshold optical bistability has been introduced.

Description: The microring resonator is situated between two waveguides, as shown in Fig. 1. In the proposed structure, the waveguides are single moded in the whole PC band gap range and there is a proper coupling between waveguides and microring.

The transmission spectrum of these structures is derived for the linear case by obtaining the ratio between the Fourier transforms of the transmitted and input lightwave pulses. The structure is excited by a wide band Gaussian pulse from port A that contains the whole frequency range of the structure band gap. The transmision spectrum of this structure is illustrated in Fig. 2. As shown in Fig. 3, the structure resonant frequency in the linear case is $f_r = 0.4129\,c/a$, where c is the speed of light in vacuum and a is the lattice constant. In the frequency, the input energy couples to the ring and completely decouples to port D.

To obtain the optical bistabilities of the structure, the input lightwave to the structure of Fig. 2 os a triangular amplitude modulated plane wave propagated through the 2D-Nonlinear Photonic Crystal (NPC), given by:

$$E_z(t) = E_0\Lambda(t)\exp(j\omega_{in}t) \quad \text{where } \Lambda(t) \text{ is given by,} \quad \Lambda(t) = \begin{cases} 1 - \left|\frac{2t}{\tau_0} - 1\right| & 0 \le t \le \tau_0 \\ 0 & \text{otherwise} \end{cases}$$

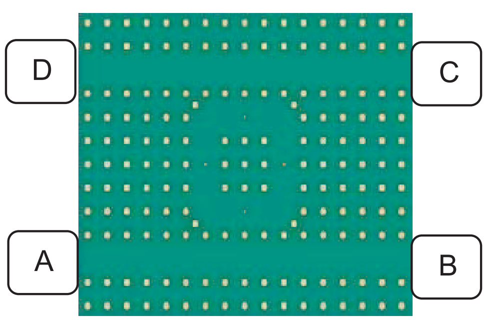

Figure 1: The structure of photonic crystal microring resonator with four additional rods.

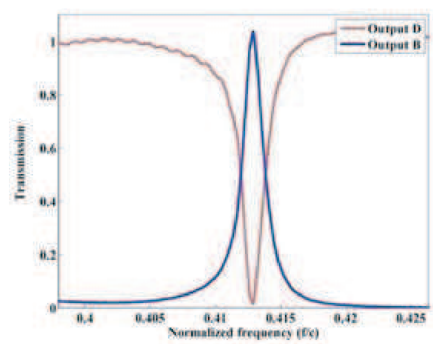

Figure 2: The transmission spectra of the photonic crystal microring resonator with four additional rods.

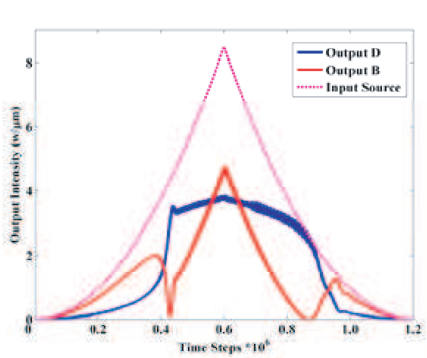

Figure 3: The input and output intensities of ports B and D of photonic crystal microring resonator with four additional rods vs. time steps.

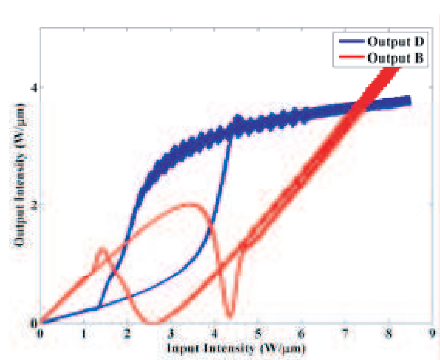

Figure 4: Bistable loop of the transmitted intensities vs. input intensity from ports B and D.

where E_0 is the maximum amplitude, τ_0 is teh pulse width of triangular source, and ω_{in} is the input lightwave angular frequency, which is selected between resonant frequencies of the states of low and high intensity inputs.

Figure 3 illustrates the output signals of ports B and D, and Fig. 4 shows the bistable loop of the transmitted output intensities vs. input intensity.

In modified proposed structure, the nonlinear effects are enhanced, becacuse of the existing nonlinear rods and vertical stretched structure. In Fig. 5, the structure is illustrated. In the novel structre dondition of two degenarete mode at resonant frequency and single mode of waveguide is still nessesary and considered. In this structure, the resonant frequency is derived to be $f_r = 0.3854\, c/a$, as shown in Fig. 6.

Figures 7 and 8 demonstrate the output field intensities of ports B and D of modified Photonic Crystal MicroRing Resonator (PC-MRR) and their bistable loops of transmitted intensities vs. input intensity.

By comparison of Figs. 4 and 8, it is obvious that the switching threshold of PC-MRR of the modified structure is lower than that of the first one. It is about one third of the first structure.

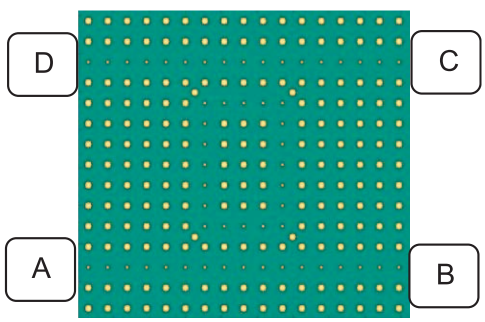

Figure 5: PC-MRR made of increased-index waveguide rods and stretched ring structure.

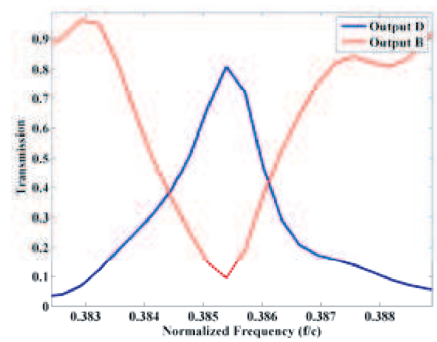

Figure 6: The transmission spectra of the photonic crystal microring resonator with increased- index waveguide rods and stretched structure.

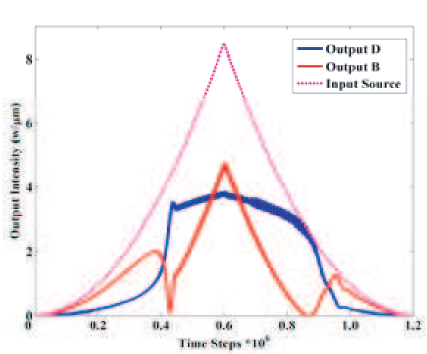

Figure 7: The input and output intensities of ports B and D of photonic crystal microring resonator with four additional rods vs. time steps.

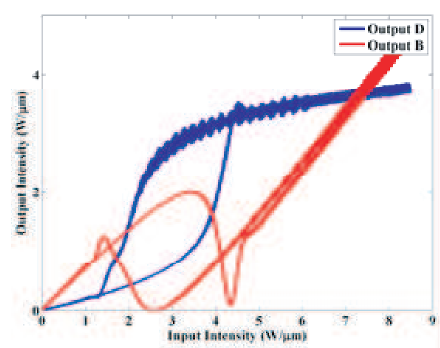

Figure 8: Bistable loop of the transmitted intensities vs. input intensity from ports B and D.

Time-domain Experimental Investigation of One-dimension Photonic Crystal Based on Microstrip

Shougang Liu, Ziying Li, and Yewen Zhang
Pohl Institute of Solid State Physics, Tongji University, 1239 Siping Road, Shanghai 200092, China

Abstract— In recent years, photonic crystal (PC) has aroused the attention of people as a new type of material that can be used to control electromagnetic waves. However, there are some uncertainties about the dispersion of photonic crystal passbands, especially in the second passband of photonic crystal. The time-domain method is used to study the normal dispersion in the second photonic crystal passband. The one-dimension photonic crystal is made of two kinds of microstrip lines with different widths. Tektronix arbitrary waveform generator (AWG710) is used to generate the envelop of signal and Agilent vector signal generator (E8267D) is used to generate the carrier frequency. The modulated signal is then inputted into the PC transmission line. In Fig. 1, the AWG710 gives a 10 MHz reference clock signal to the E8267D and a trigger signal to the oscilloscope. As a consequence, the three instruments are synchronized. The probe, which is Tektronix P7260 with an input impendence of 20 kΩ and bandwidth of 6 GHz, detects the waveform at different positions along the PC transmission line. The wave forms propagating along a PC TL have been measured in the time domain. The experimental results clearly demonstrate

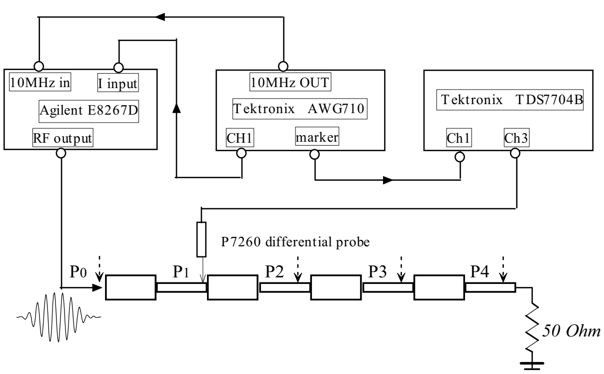

Figure 1: Experimental setup used to measure the PC TL in the time domain.

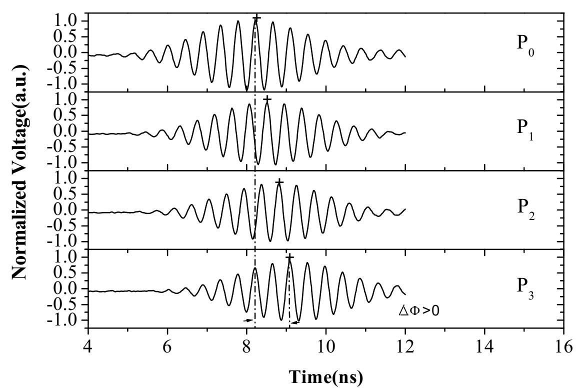

Figure 2: Time-domain experimental results at 2.3 GHz. P_0, P_1, P_2, and P_3 mean wave forms at the input port, the first unit, the second unit, and the third unit. The cross marks show the positive phase propagation, and the envelope shows the positive group delay.

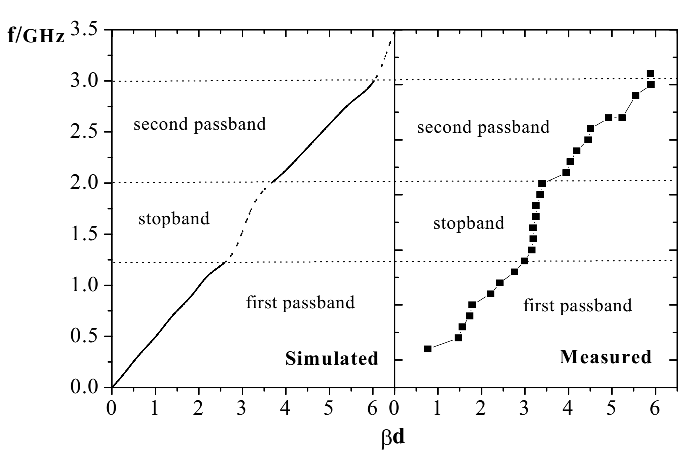

Figure 3: The ADS simulated and the time-domain measured dispersion diagrams of the individual PC TL.

that phase velocity and group velocity are positive and parallel at 0.8 GHz, 1.0 GHz, 2.3 GHz and 2.5 GHz in the frequency region of the first and second passbands of PC TL (see Fig. 2). The dispersion diagram is shown in Fig. 3. Dispersion diagrams for both experiment and simulation in the time domain are given. It is showed the dispersion in the second photonic crystal passband is normal. Phase velocities and group velocities obtained from the time-domain experiment are in good agreement with the results from the dispersion relation and theoretical values.

And we use the time-domain method to research the vortex-like interface mode exists at the interface of a PC-CRLH coupler. It clear shows that the average group delay of the PC-CRLH coupler is approximately ten times longer than that of the microstrip coupler, which indicates that vortex mode leads to slow propagation. It resembles the time-domain experiment results of the RH-CRLH coupler, which agrees well with the simulation and theoretical results. This is another way to prove that PC TL is such as RH TL, whose dispersion is normal.

ACKNOWLEDGMENT

Project supported by the 973 Project (Grant No. 2006CB0L0901), by the National Natural Science Foundation of China (Grant 1063405, and by by Shanghai Committee of Science and Technology (contract No. 07DZ22302).

Development of Modified Optical Fiber Cable with Long Excess-length of Fiber

Yiqiang Wang and Suming Li
Heng Tong Group, Wujiang, Jiangsu, China

Abstract— This article reports the progress in the T&D of a novel optical fiber cable structure featured by using an extra (or secondary) tube, in addition to an SS (stainless-steel) tube commonly used in a conventional optical cable. The predicted longer *excess-length* is confirmed in our pilot production of the optical cable. The measured change of the transmission characteristics with the temperature change is sufficiently small to ensure accurate and stable transmission of the lightwave signal. The increased loss due to evanescent wave scattering associated with micro bending is remarkably reduced as a result of the achieved longer *excess-length* of the fiber in cable.

With the aid of an SS tube, conventional optical cable is favored for its tensile strength, sealing capability and crush resistance, and has found various important applications in the art of communication. One major problem of the conventional optical cable involving an SS tube, especially when the cable is long, concerns micro bending of the fiber in cable, with the result of increase in transmission loss and deterioration of the light-wave signal. In order to minimize the increased transmission loss and signal deterioration, it is of primary importance to secure a sufficiently long *excess-length* of the fiber in cable. This is why we proposed the use of a secondary plastic tube in optical cable design, and investigated the fabrication method for its realization.

In our novel design, the secondary plastic tube is a liner-layer inside the SS tube and is so shaped that its geometry in the axial or transmission direction is an eccentric spiral (alternatively right-handed and left-handed) with variable pitch. An analytic design framework is structured with the prediction that the inclusion of a secondary plastic tube is capable of effectively increasing the *excess-length* of the fiber in cable.

Excess-length of fiber	$\geq 1.2\%$
Non-uniformity of a section of the *Excess-length*	$\leq 0.1\%$
Transmission loss	$\leq 0.34\,\mathrm{dB/km}$
Change of fiber loss due to temperature change ranging from $-40°\mathrm{C}$ to $+100°\mathrm{C}$	$\leq 0.03\,\mathrm{dB/km}$

The above table succinctly summarized the experimental data of the figures of merit of our fabricated optical cable including both an SS tube and a secondary plastic tube.

Modeling Quantum Cascade Lasers with Metal Gratings

M. Carras[1], **G. Maisons**[1], **B. Simozrag**[1], **M. Garcia**[1], **A. De Rossi**[2], **and X. Marcadet**[1]

[1]Alcatel Thales III-V Lab, France
[2]Thales Research and Technology, Rd. 128, Palaiseau, France

Abstract— We present electromagnetic modeling of quantum cascade laser (QCLs). We focus on the case of metal grating on top of the dielectric waveguide. We show that a Hamiltonian approach of the problem with a three wave model can account for most of the problems and compare it to exact calculations [1].

We apply our approach to the understanding of two important problems: realization of distributed feedback lasers [2] (DFBs) and surface emitting lasers. We show experimental result validating the calculations for both applications: first time continuous wave room temperature DFB QCLs with metal grating and first time room temperature surface emission of QCLs.

A laser waveguide can be seen as a cavity with a sufficient quality factor. In the case of quantum cascade lasers the overlap between the mode and the gain region should be high in order to compensate high losses at these wavelengths (3–12 µm). A consequence is that in on direction the waveguide is a superposition of strong index contract layers and in the other direction the waveguide is deeply etched and the problem becomes separable (in terms of Maxwell Equations) as opposed to classical shallow etched semiconductor waveguides and can be treated with two dimensional calculations.

An other specific point in the case of quantum cascade lasers is that the polarization of light is perpendicular to the layers of the active region. This point makes it possible to use the surface waves of metal deposit on top of the waveguide for example. In our case, we show that the surface waves can be used to obtain DFB effect or surface emission. Use of metal is also permitted by the interesting index of metal which reduces the overlap of the metal of the electromagnetic field. The interest of metal gratings lies in the fabrication easiness with the possibility of low cost and versatile realization of lasers with stringent specifications.

We present at first the properties of surface waves at such wavelengths supported by a metal grating. The possibility of tailoring the properties of the waves is shown as well as the physical origin of it. We introduce the surface wave dispersion in our Hamiltonian model together with the dielectric waveguide modes. The resulting system offers extremely interesting properties in terms of robustness, low losses, and versatility.

We deduce classical parameters of DFB like coupling coefficient and losses. Then, we introduce the radiation on our model to deal with surface emission. All models are compared with exact calculations using rigorous coupled wave theory adapted to the case of metals.

REFERENCES

1. Carras, M. and A. De Rossi, *Phys. Rev. B*, Vol. 74, 235120, 2006.
2. Carras, M., M. Garcia, X. Marcadet, O. Parillaud, A. De Rossi, and S. Bansropun, *Appl. Phys. Lett.*, Vol. 93, 011109, 2008.

Effect of FWM Output Power Induced by Phase Modulation in Optical Fiber Communication

Li Wang, **Wenzheng Ban**, **Yang Song**, **Jiangbo Chen**, **and Xinping Zhang**
College of Applied Sciences, Beijing University of Technology, Beijing 100124, China

Abstract— The Four wave mixing (FWM) power with pump light parameters in standard single-mode fiber, dispersion-shifted fiber, non-zero dispersion fiber and two kinds of dispersion compensating fibers have been compared through numerical simulated calculations. The effect of pump wavelength deduced to the phase-mismatching factor, pump wavelength, pump power and propagation distance to parametric gain and power of FWM have been analyzed in self-phase modulation and cross-phase modulation. The effect of the pump power, propagation distance and fiber effective core area to FWM have been obtained. It is useful to select the category of fiber and pump wave, signal wave in communication system devices.

Direct and Inverse Borrmann Effect in 1D Photonic Crystals

Alexander V. Dorofeenko[1], **Alexey P. Vinogradov**[1], **Alexander M. Merzlikin**[1], **Alexander A. Lisyansky**[2], **Alexander B. Granovsky**[3], **and Yuriy E. Lozovik**[4]

[1]Institute for Theoretical and Applied Electromagnetics of the Russian Academy of Sciences Moscow, Russia
[2]Department of Physics, Queens College, The City University of New York, USA
[3]Faculty of Physics, Moscow State University, Russia
[4]Institute of Spectroscopy of the Russian Academy of Sciences Moscow Region, Troitsk, Russia

Abstract— Many applications of photonic crystals (PCs) are connected with dispersion properties of Bloch waves. However, along with such microscopic description it is necessary to take into account field distribution inside an elementary cell of PC, which allows decrease losses or enhance magnetooptical [1] or other effects. Microscopic distribution of energy is responsible for the Borrmann effect, consisting in difference in absorption of X-rays by crystal at different angles of incidence.

It is common knowledge that at the bottom and top frequency edges of the first band gap of PC electric energy is concentrated in regions with higher and lower permittivity, respectively. Detailed analysis of fields' distribution has shown that mentioned rule also holds, with rear exclusion, for higher band gaps of nearly homogeneous PCs, when inhomogeneity is considered as a perturbation. The exclusion is following. At some relations between the layer thicknesses in PC, band gap closes [2]. In the vicinity of the closing point, the linear perturbation theory does not work and the Borrmann effect can be inverted, that is, the electric energy in higher permittivity layers is larger at the top band edge than at the lower one.

In the opposite extreme case of manifold difference in layers' permittivities the bands are formed by Fabry-Perot resonances in single layers. In the resonant layers concentration of energy appears. In this case, the Borrmann effect is often inverted.

Thus, the Borrmann effect in the two described extreme cases is caused by different mechanisms. In the intermediate case one obtains rather complicated interplay of these mechanisms.

As an illustration, enhancement of the Faraday effect in PC was calculated. The magnetooptical layers had higher permittivity, and the enhancement was observed in the vicinity of the lower edge of the band gap, when the direct Borrmann effect was the case. When the inverse Bormann effect was predicted, the enhancement of the Faraday effect appeared in the vicinity of the top edge of band gap.

REFERENCES

1. Erokhin, S., A. Vinogradov, A. Granovsky, and M. Inoue, *Phys. of the Solid State*, Vol. 49, 497–499, 2007.
2. Nusinsky, I. and A. A. Hardy, *Phys. Rev. B*, Vol. 73, 125104, 2006.

The Features of the Wideband Anisotropic Acousto-optic Interaction with Longitudinal Ultrasound in Lithium Niobate Crystal

Yuri A. Zyuryukin, Sergey V. Zavarin, and Alexander N. Yulaev
Saratov State Technical University, Russia

Abstract— There are numerous works reporting some results of the light anisotropic diffraction research by the acoustic signal possessing the wide range of frequencies. The main idea of the wideband diffraction consists in the special geometry of the interacting optical waves by the acoustic beam. The wideband acousto-optic interaction is realized if the ultrasonic wave vector is tangentially directed to the wave surface of the diffracted light beam. The other reason for the successful wideband anisotropic diffraction is the high level of the photo-elastic sensitivity coefficient for the given directions of the light and acoustic propagations. It is important to emphasize the lithium niobate crystal as the acousto-optic medium with the high level of the photo-elastic properties and capability of work at superhigh frequency of ultrasound. The previous works have reported results on the investigation of the wideband anisotropic diffraction by shear modes of the ultrasonic waves in lithium niobate crystal only.

This work is devoted to the investigation of the wideband anisotropic light diffraction by longitudinal elastic waves in the lithium niobate crystal. On the base of Bragg's conditions, the regimes corresponding to the wideband acousto-optic interaction have been researched. The two regimes of the geometry of the wideband diffraction for the optimal values of the photoelastic crystal properties have been calculated. For the one of them, the magnitudes of the electric fields of the incident and diffracted light beams under conditions of the given direction of the initial light and acoustic waves have been estimated. The width of the frequency band of the driven signal at the half-power level of the diffracted optical beam has been equal to the value of 430 MHz at the wavelength of 632 nm. The diffraction efficiency is equal to the 3.3% at the optimal acoustic frequency of 5.28 GHz.

Session 5P3
Magnetism, Magnetic Structures and Devices

Waveguide with Multilayer Nanostructure

A. B. Rinkevich[1], **L. N. Romashev**[1], **V. V. Ustinov**[1], **and E. A. Kuznetsov**[2]

[1]Institute of Metal Physics Ural Division of Russian Academy of Sciences, Ekaterinburg, Russia
[2]Nizniy Tagil State Socially-Pedagogical Academy, Nizhniy Tagil, Russia

Abstract— Interaction of traveling electromagnetic waves with multilayer Fe/Cr nanostructures obtained by molecular-beam-epitaxy method has been studied both experimentally and theoretically. The measurements are carried out in frequency range from 5.7 to 12.5 and from 26 to 38 GHz in magnetic fields up to 32 kOe. Variation in magnetic field of the wave constant of the H_{10} mode in rectangular waveguide is studied. The nanostructure sample is placed into the waveguide. It has been found that giant magnetoresistive effect in metallic multilayer defines the magnetic field dependency of microwave transmission coefficient. Interaction between traveling electromagnetic waves of centimeter and millimeter wavebands with $(Fe/Cr)_n$ superlattices was studied in detail. It was proved that microwave currents flow mostly perpendicularly to the plane of multilayered nanostructure that is perpendicularly to the individual layers planes. Microwave variations can by several times exceed the DC giant magnetoresistive effect. The model of interaction has been worked out. The expressions were obtained for the complex transmission and reflection coefficients. Field dependencies of the transmission and reflection coefficients are analyzed. It has been shown that the field dependence of the coefficients is similar to that for giant magnetoresistive effect. Two ways of disposition of the sample in the waveguide are studied both. The wave number changes by the value that is proportional to variation of electrical resistance of the nanostructure as a result of interaction. The model calculation is carried out of the structure of electromagnetic fields.

Based on the results obtained the stage for developing of magnetic field-driven microwave devices has already been set. The devices of this sort are expected to be rather simple and effective because of giant magnetoresistive effect is additionally increased due to a resonance electromagnetic system.

The Resonant Phenomena in Electromagnetic Wave Penetration through Thin Magnetic Films

D. V. Perov[1], **A. B. Rinkevich**[1], **and V. O. Vaskovsky**[2]

[1]Institute of Metal Physics Ural Division of Russian Academy of Sciences, Ekaterinburg, Russia
[2]Ural State University, Ekaterinburg, Russia

Abstract— The method has been worked up that allows to calculate the transmission and reflection coefficients for electromagnetic wave which interacts with a thin metal film. The computation has been fulfilled with taking into consideration the exchange effects, surface spin pinning conditions and finite conductivity of the film. To agree with the experimental compliance, it is supposed that the metal film is sputtered on a dielectric substrate. Taking into consideration all possible wave types, the equations set has been obtained from which the transmission and reflection coefficients can be found numerically. The numerical computations have been carried out as applied to the parameters of permalloy films and conditions of the experiment with the use of microwaves. The value areas of parameters have been determined in which the different types of resonance can exist. If the exchange factor is relatively small and surface spin pinning is weak, then the ferromagnetic resonance can only realize in the film. When the exchange factor is about 10^{-7} erg/cm, besides the ferromagnetic resonance, there are the spin wave resonance peaks in the wave penetration; their amplitudes increase on conditions that the surface spin pinning becomes stronger. Within the same value area of the exchange factor, the spin wave resonance is possible in the form of oscillations of the transmission coefficient.

The resonant phenomena experiments in electromagnetic wave penetration through thin permalloy films have been carried out. In the films of different thickness, we watched experimentally the minimum of transmission coefficient corresponding to the ferromagnetic resonance and the oscillatory changes of transmission coefficient because of the spin wave resonance. Furthermore the spin wave resonance was observed with the resonance line which was badly resolved of quite unresolved from the ferromagnetic resonance line. It has been established that the spectra of ferromagnetic resonance line are almost the same for all investigated specimens despite the presence of other types of resonant phenomena in addition to the ferromagnetic resonance. The experimentally obtained DC magnetic field dependences of the transmission coefficient modulus have been compared with the numerically computed ones.

Magnetic Particles (Magnetons) — Structural Components of Atoms and Substance, Immediate Sources of Magnetic Fields

Robert Sizov
Individual researcher, Moscow, Russia

Abstract— Theory and experiments as a result of more than 30 years of experimental and theoretical investigations, the author discovered and presented to the attention of scientific community (in 2001, in his first book [19]) the magnetic fundamental particle (magnetic charge, pole), which the author referred to as *magneton.* Magneton, which is a structural element of atoms and substance, was not discovered before, because the conditions of its bond with substance or the conditions of its confinement are other than those of electron. One has to recognize as another important reason, which served a barrier in the path toward detection and legalization of magnetons for 135 years, the fallacious Maxwell "virus" referred to in this book, i.e., the erroneous concept, according to which moving or rotating electric charges, for example, electrons, were taken to be immediate sources of all magnetic fields and magnetic manifestations. The basic physical parameters of magneton are as follows.

1. **Charge**. Magneton has a magnetic charge g, whose value is equal to that of electron charge ($g = e$).
2. **Sign of charge**. Like electron, magneton is negatively charged (g^-).
3. **Mass**. Similar to electron, magneton is a massless material particle exhibiting the property of inertia. The measure of inertia of magneton (designated as m_g^i) is equal to that of electron (condition: $m_g^i = m_e^i$).
4. **Class of elementary particles** — lepton.
5. **Statistical properties** — fermion.

Following are several possible terms involving the suggested name of magnetic particle:

- magneton current — the current of magnetic charges in a conductor;
- conduction magnetons — magnetic charges which define magnetic conduction.

In a number of cases, terms may be used which involve only the root of the name of magnetic particle:

- magnetostatic voltage — magnetic analog of electrostatic voltage;
- magnetic conduction — conductivity of magnetic charges.

It is to be reminded that the word *magneton* in the effective physical terminology defines the unit magnetic moment of electron. However, as was repeatedly mentioned above, electron does not have a magnetic moment (and never had), i.e., the electron is absolutely "bare" from the magnetic standpoint. It was dressed in magnetic "clothes" thanks to Maxwell; in 135 years that have passed, the magnetic "equipment" of electron was perfected in any possible way.

Of course, the electrons, which move in a conductor and "spin up" eddies of magnetic charges, turn out to be indirectly involved in the generation of magnetic field rot $\mathbf{H}^\circ$ but this is an entirely different "story". Note that electrons bear no relation, even indirectly, to the generation of, for example, magnetostatic field by a fixed magnetic pole. Therefore, the name of magneton must, in essence and by right, belong only to the true source of magnetic field, namely, to the magnetic fundamental particle suggested by the author.

Magnetons (magnetic poles) are natural and only sources of almost all universally known magnetic fields and manifestations, including magnetic components of EM fields and emissions. In order to explain magnetic manifestations in atoms, the so-called magnetic moment was ascribed to electrons in the existing physical theories; since the real magnetic charges were ignored, this magnetic moment bore their unquestionable pole "load".

The results of investigations of the present author and of other researchers enable one to state with assurance that atomic shells are electromagnetic rather than electronic, as is now customary to assume. In the case of EM shell made up of electrons and magnetons, the use of the concept of magnetic moment of electron ceases to make any sense and becomes useless, similar to a prosthesis which becomes useless after it has served its function.

REFERENCES

1. Sizov, R. A., *Electric, and Magnetic Spinor Particle — Structure-forming Component Mass and Electromagnetic Source of Gravitation*, Moscow, 2008.

Electrodynamic Analysis of Nonlinear Propagation of Electromagnetic Waves in Gyromagnetic Nanostructured Media at Microwave Frequencies

G. S. Makeeva[1], **M. Pardavi-Horvath**[2], **and O. A. Golovanov**[1]

[1]Penza State University, Russia
[2]The George Washington University, USA

Abstract— A rigorous mathematical model of the nonlinear propagation of electromagnetic waves (EMWs) in 3D periodic arrays of arbitrary shaped magnetic nanoelements for microwave and magnetophotonic applications is developed by solving the full nonlinear Maxwell's equations with electrodynamic boundary conditions, complemented by the Landau-Lifshitz equation of motion of the magnetization vector, taking into account the exchange interaction [1].

Using the decompositional approach on the autonomous blocks with Floquet channels, partially filled by the nonlinear gyromagnetic media (MFABs) [2], we consider MFAB as a model of the elementary cell of the 3D periodic nanoarray of nonlinear magnetic nanoelements. Using Floquet's theorem we obtain the scattering matrix of linearized MFAB and the characteristic equation to determine the propagation constants of the fundamental and higher-order spatial harmonics in 3D periodic nanoarrays [2]. For calculating the MFAB scattering matrices at the combination frequencies the computational algorithm to solve the nonlinear 3D diffraction boundary problem was developed, taking into account electrodynamical boundary conditions, the geometry of the array, and the shape of nonlinear magnetic nanoelements.

From the characteristic equation, using the developed algorithm, the propagation constants of fundamental modes of clockwise and counterclockwise polarized EMWs, and the ordinary and extraordinary EMWs, propagating in 3D periodic array of ferromagnetic nanoparticles in a dielectric matrix for longitudinal and transverse orientations of the bias magnetic field were calculated, depending on the ratio r/a of the radius r of the ferromagnetic (iron) nanospheres to the periodicity a of the array at a frequency $f = 30\,\mathrm{GHz}$.

As follows from the results of mathematical modeling the propagation constants change significantly with decreasing separation r/a on the interval $0.1 < r/a < 0.35$, due to the change of the character of propagation of EMWs. The propagation constants of counterclockwise polarized and extraordinary modes become imaginary for $r/a > 0.25$ and, consequently, they are not spreading. Upon reducing the separation of nanospheres $r/a > 0.25$ (transition to the range of exchange length), the exchange interaction in the system of strongly coupled magnetic nanoparticles plays a dominant role [3] and magnetic nanoarray starts to behave like a quasi-bulk continuum. As for the case of ferromagnetic metals, from the 4 normal modes [4] there are two, counterclockwise polarized and ordinary, modes with real propagation constants, having a large phase velocity, propagating in the gyromagnetic nanostructured media as the separation r/a of magnetic nanoparticles $0.25 < r/a < 0.35$ approaches the exchange length.

ACKNOWLEDGMENT

The work of G. S. Makeeva and O. A. Golovanov was supported by The Russian Foundation for Basic Research, Grant 05-08-33503a.

REFERENCES

1. Gurevich, G. and G. A. Melkov, *Magnetization Oscillations and Waves*, CRC Press, 1996.
2. Makeeva, G. S. and O. A. Golovanov, *Izvestiya vysshikh uchebnykh zavedenii, Physico-mathematisheskye nauki*, No. 4, 72–85, (In Russian), Transaction of the Volga region universities, 2008.
3. Pardavi-Horvath, M., G. S. Makeeva, and O. A. Golovanov, *IEEE Trans. Magnetics*, Vol. 44, 3067–3070, 2008.
4. Patton, C. E., *Czech. J. Phys.*, Vol. B26, No. 8, 925, 1976.

Size and Shape Effects in the Diffraction of Electromagnetic Waves on Magnetic Nanowire Arrays at Photonic Frequencies

G. S. Makeeva[1], **M. Pardavi-Horvath**[2], **and O. A. Golovanov**[1]

[1]Penza State University, Russia
[2]The George Washington University, USA

Abstract— Rigorous mathematical modeling of diffraction of electromagnetic waves (EMWs) on magnetic nanoarrays is based on the solution of the 3D diffraction boundary problem for full Maxwell's equations with electrodynamic boundary conditions, complemented by the Landau-Lifshitz equation of motion of the magnetization vector with the exchange term [1], taking into account constrained geometries.

The scattering parameters of the multimode, multi-channel **S** matrix of arrays of 2D periodic array of metallic magnetic nanowires, embedded in a dielectric matrix, were calculated by the numerical method of the autonomous blocks with Floquet channels, partially filled by gyromagnetic media (MFABs) [2].

The results of computing the modulus of the transmission $|R_{21}|$ and reflection coefficient $|R_{11}|$ of a ferromagnetic (iron) nanowire arrays, depending on the bias magnetic field, for various nanowires diameter and array periodicity, were obtained at $f = 30\,\mathrm{THz}$. A bias magnetic field is applied normal to the direction of EMWs propagation, along the axis of nanowires.

It follows from the results of mathematical modeling that the scattering parameters of magnetic nanowire arrays strongly depend on the value of the bias magnetic field for the actual geometry of the array, and for different wire diameter/periodicity ratios. For increasing wire diameter and array periodicity the maximum of the transmission coefficient is moving to lower fields and the transmission at the maximum is decreasing.

It is shown that the maxima of the transmission coefficients $|R_{21}|$ are located in the antiresonance points, because the increase of the skin-depth of penetration of electromagnetic field in a ferromagnetic metal near the antiresonance point results in the increase of the transmitted EMW through the magnetic nanoarray.

When the separation of the magnetic nanowires is large, then the model of the layer of non-interacting nanowires is a thin long cylinder in a longitudinal external magnetic field. Upon further reducing the diameter and the separation of nanowires (i.e., transition to the exchange length range), in the strongly coupled system the exchange interaction plays the dominant role and the magnetic nanoarray behaves as an effective quasi-continuum i.e., a thin magnetic film.

REFERENCES

1. Gurevich, G. and G. A. Melkov, *Magnetization Oscillations and Waves*, CRC Press, 1996.
2. Makeeva, G. S. and O. A. Golovanov, *Izvestiya vysshikh uchebnykh zavedenii, Physico-mathematisheskye nauki*, No. 4, 72–85, (In Russian), Transaction of the Volga region universities, 2008.

Investigation of the Nonlinearity Thresholds of Magnetic Nanostructures by Computing the Bifurcation Points at Microwave Frequencies

G. S. Makeeva[1], **M. Pardavi-Horvath**[2], **and O. A. Golovanov**[1]

[1]Penza State University, Krasnaya, 40, Penza 440026, Russia
[2]Department of Electrical and Computer Engineering, The George Washington University
Washington, D.C. 20052, USA

Abstract— For the analysis of the threshold for collective behavior, due to the instability of magnetostatic waves (MSW) and dipole-exchange spin-waves (SW) in the magnetic nanoparticle systems, the numerical method of bifurcation analysis of instabilities is developed. The technique involves the numerical calculation of bifurcation points of the nonlinear Maxwell operator, (the nonlinear Maxwell equations with electrodynamic boundary conditions complemented by the Landau-Lifshitz equation including the exchange term). The method was applied to magnetic nanocomposites of nanometer size magnetic particles or wires, embedded in a non-magnetic, insulating matrix. The original computational algorithm [1] is improved by combining it with a qualitative method of analysis, based on Lyapunov stability theory [2].

The threshold magnitudes of the pumping electromagnetic waves, where the nonlinear processes and the parametric instability excitation of MSW and SW occur in the ferromagnetic nanosphere and nanowire arrays, are determined by computing the bifurcation points. The instability regions for the parametric excitation of MSW and SW are obtained at microwave and photonic frequencies for different nm size nanoparticles and nanowires, and for various separations, taking into account constrained geometries.

The threshold magnitudes of parametric instability in the arrays of ferromagnetic nanospheres and nanowires depend on the MSW and SW spectrum of the collective modes in the magnetic particle array, and it is influenced by the frequency, the bias magnetic field, the magnetization, the shape of particles, and the geometry of the array. Computing the bifurcation points of the nonlinear Maxwell's operator permits to analyze and optimize the geometry of magnetic bandgap structures and the parameters of magnetic nanostructures at microwave and photonic frequencies.

REFERENCES

1. Makeeva, G. S., O. A. Golovanov, and M. Pardavi-Horvath, *IEEE Trans. Mag.*, Vol. 42, No. 10, 3550–3552, 2006,
2. Lyapunov, A. M., *Stability of Motion*, Academic Press, New York, 1966.

Progress in Thermal Near Field Detected Microwave Spectroscopy on Nano Structured 3d-metals

R. Meckenstock, **S. Stienen**, **I. Barsukov**,
C. Hassel, **N. Reckers**, **J. Lindner**, **and M. Farle**
Experimental Physics, AG-Farle, University Duisburg-Essen, Germany

Abstract— The continuous reduction in size of electronic and magnetic devices results in an increasing need for characterization methods with micron and submicron spatial resolution.

Microwave spectroscopy has proven to be an extremely sensitive and expressive method, to investigate the magnetism, spin dynamics, and the electronic structure of magnetic and semi-conducting heterostructures. However, the conventional microwave measurement techniques suffer from the lack of local resolution.

Scanning thermal microscope-detected ferromagnetic resonance (SThM-FMR) combines a thermal near-field microscope with a FMR spectrometer and detects the thermal response due to resonant microwave absorption by measuring the resistivity change in the thermal nanoprobe. This thermal detection provides a strict separation of photon excitation and phonon detection but exhibits an exact correlation of the SThM-FMR image and the simultaneously taken AFM-topography.

The technique provides imaging capabilities at fixed resonance conditions as well as local microwave spectroscopy at the nanoscale. With the SThM-FMR setup a temperature resolution of 1 mK and a local resolution of 30 nm are actually achieved, yielding a detection limit as low as 10^6 spins [1].

To demonstrate the potential of SThM-FMR, single 3d metal nano dot and stripe structures of Co and Permalloy are characterized yielding: local magnetic properties like magnetization and anisotropies, magnetization dynamics and inhomogeneous FMR excitations due to finite size effects. The experimental results are compared to micro magnetic FMR simulations by OOMMF [2].

ACKNOWLEDGMENT

This work is supported by the SFB491: magnetic heterostructures: spin structure und spin transport.

REFERENCES

1. *Rev. Sci. Instrum.*, Vol. 79, 041101, 2008.
2. Object oriented micro magnetic framework, http://www.math.nist.gov/oommf.

RF Emissions and Oscillation Modes in MgO Based Nanopillars

Gino Hrkac[1], **Alexander Goncharov**[1], **Julian Dean**[1], **Simon Bance**[1], **and Thomas Schrefl**[1,2]

[1]Department of Engineering Materials, University of Sheffield
Mappin Street, Sir Robert Hadfield Building, Sheffield S1 3JD, United Kingdom
[2]St. Pölten, University of Applied Science
Matthias Corvinus Straβe 15, St. Pölten A-3100, Austria

Abstract— It is known that a sufficiently large spin polarized current can impose a torque on a nanoscale ferromagnet either inverting the magnetization (switching) or exciting a stable oscillation of the [1]. Although the spin polarized current necessary to switch the magnetization in MTJ is similar to that of spin valves, there is maximum value for the current which can be applied before the breakdown of the tunnel barrier occurs. Taking these considerations into account, experiments have shown that MgO tunnel barriers in CoFe/MgO/CoFe pillars give the best performance so far, presented by a high TMR ratio of 200% and spin polarization ration of nearly 60%. In this paper we study the different excited magnetic modes in magnetic tunnel junctions (MTJs) with an extended micromagnetic model (LLG and Slonczewski term) where we compute the local current from tunnelling conductance which is based on the phenomenological Brinkman model. The stacks simulated are junctions of nominal composition PtMn 20 nm/CoFe30 2 nm/Ru 0.8 nm / CoFe20B20 2 nm/Mg 2 nm/CoFe20B20 3 nm, with the following dimensions $70 \times 140\text{nm}^2$ rectangles, with a TMR ratio of 13%. It is shown that once the applied current approaches the threshold current the magnetic modes become more uniform and uniform rotational precession can be observed. By increasing the current further, the magnetization behaviour becomes more non-uniform again and the peak disperses and the signal can't be distinguished from the background noise anymore. To quantify these effects we study the line width as function of current and the RF frequency as function of current and applied field for Tunamos MTJs produced by Singulus. We calculate the frequency as function of power for different currents for an applied field of 75 mT. The results show that once a current of −5 mA is applied a peak can be found at 9.64 GHz with a FWHM of 308 MHz. By decreasing the current to −4.5 mA the peak blue shifts to 9.75 GHz with a very narrow line width of 14 MHz, indicating that −4.5 mA is the threshold current of the system. By further decreasing the current to −4 mA, the frequency red shifts to 9.49 GHz with a slightly worse line width of 17.9 MHz. A further reduction of the current to −3.5 mA a frequency of 9.5 GHz can be observed with a line width of 43.6 MHz. For lower currents no RF oscillation are observed. The same current sweep was performed for applied fields of 0, 25, 50, 100, 125 mT. For the fields below 50 mT no RF oscillations are observed for any kind of current. For the 50 mT regime, RF oscillations can be observed only in a very narrow current regime, between −5 mA and −5.5 mA. For higher fields, above 75 mT RF oscillations are observed but with a bad signal to noise ratio. Secondly we perform a Lorentzian fit on the Fourier transformed signal of the magnetization and extract the full width at half maximum. As the simulations were performed at zero temperature the FWHM analysis is a comparable study to quantify the dispersion of the signal as it approaches the threshold current and thereafter. The simulations show that the line width quality increases as it approaches the threshold current, which is −4.5 mA. To understand the narrow line width around −4.5 mA, we studied the magnetic modes of our sample in the time domain. Simulations were performed over a time period of 100 ns. It is shown that the amplitude for the threshold current of −4.5 mA is stable and shows only small changes in magnitude. The results for −5 mA on the other hand indicate not only a huge change in the magnitude of the amplitude but also an overlap of different modes and a destructive interference. In summary, we have performed a numerical study on oscillation modes in MTJs fabricated by the Tunamos consortium. We investigated the frequency and FWHM as function of applied field and applied current. The study shows the following results: The line width reaches a minimum as the system approaches the threshold current, and gets worse as the current is increased beyond the threshold current. The improvement of the line width is due to a more uniform precession. Edge modes that oscillate out of phase contribute to the broadening if the full width at half maximum. Stable oscillations in the free layer are found only for fields of 50 mT and above.

REFERENCES

1. Slonczewski, J., *J. Magn. Magn. Mater.*, 159, L1, 1996.

Controllable Dynamic Switching of the Chirality of a Spin Vortex in a Cylindrical Magnetic Nanodisk

Roman Antos[1] **and Yoshichika Otani**[2,3]

[1]Institute of Physics, Faculty of Mathematics and Physics, Charles University, Czech Republic
[2]ISSP, University of Tokyo, Japan
[3]Advanced Science Institute, RIKEN, Japan

Abstract— Vortex states, occurring in submicron ferromagnetic disks, are promising for high-density data storage, signal sensing and manipulation, etc. [1]. One of the major issues is controlling their binary states (chirality and polarity), both of which suggest independent bits of data storage. The switching of the polarity has recently been demonstrated by field pulses and electrical currents, yielding considerable advantages over the traditional manipulation. On the other hand, it has been frequently claimed that the switching of the chirality requires a geometric asymmetry; it has thus been performed by a spin transfer torque and by a field pulse whose symmetry was broken by a mask. In this presentation we demonstrate that the chirality switching of a perfectly symmetric disk can be achieved by a uniform in-plane field pulse, while the only asymmetry required is the chirality itself. We use a fast and precise method of simulation of dynamics of a general 2D distribution of magnetization confined inside patterned soft magnetic thin-film elements, which is based on the time-integration of the Landau-Lifshitz equation. The approach is based on splitting the sample area into rectangular cells with lateral sizes smaller than the exchange length and with magnetization assumed constant inside each cell. Then the effective magnetic field acting on the sample is calculated as the sum of external field and the field derived from the exchange and magnetic-dipolar interactions of cell pairs. Besides the chirality switching (which is of the highest interest for experiments involving magnetic vortices with defined states), we also show interesting phenomena which strongly depend on the initial magnetization distribution and on the size and duration of the excitation field pulse, e.g., anomalous trajectories of vortex cores for particular dimensions of nanodisks, which might be utilized to study some fundamental physical phenomena in ferromagnetic nanodisks.

REFERENCES

1. Antos, R., et al., *J. Phys. Soc. Jpn.*, Vol. 77, No. 3, 031004, 2008.

The Microwave Study of Structure-dependent Properties of Thin Magnetic Films by Field-domain Resonance Technique

Sergey N. Starostenko and Konstantin N. Rozanov
Institute for Theoretical and Applied Electromagnetics RAS, Russia

Abstract— The technique is developed to study the structure-dependent properties of thin magnetic films, namely the effects of the morphology of substrate surface, of the thickness of metal film, of the heat treatment and of the mechanical tension affecting that affect the microwave permeability of laminated composites. In case of a saturated homogeneous film the permeability spectrum $\mu(f)$ consists of a single resonance line. Parameters of ferromagnetic resonance can be approximated with the Lorentzian formulae (1):

$$\mu(f) - 1 = (\mu_0 - 1) / \left(1 - \frac{f^2}{F^2} + i\Gamma \frac{f}{F}\right) \tag{1}$$

where F is the resonance frequency, Γ is the damping factor, μ_0 is the static permeability. These parameters depend on both the composition of permeable substance and on the structure of the sputtered film. The interpretation of results of frequency-domain $\mu(f)$ measurements is difficult because of effects of disordered domain structure of an unsaturated sample. The frequency-domain measurements under constant bias $H_{bias} = const$ are limited in case of a stripe-line technique by the operating frequency and by the setup sensitivity [1].

The dependence of complex permeability at frequency f on external bias H_{bias} is defined by Landau-Lifshits relation rewritten below for a thin film (2):

$$\mu(f, H_{bias}) - 1 = \frac{4\pi M / H_{eff}}{1 - 2(\pi f)^2 / (\gamma^2 4\pi M H_{eff}) + i\Gamma \times 2\pi f / \left(\gamma \sqrt{4\pi M H_{eff}}\right)} \tag{2}$$

where γ is the gyromagnetic factor, M is the saturation magnetization, H_{eff} is the effective field (the sum of the internal anisotropy field and of the external bias) that defines the resonance frequency. By comparing relations (2) and (1) it is easy to see that $4\pi M/H_{eff}$ corresponds to static permeability $\mu_0 - 1$, $\gamma\pi\sqrt{\pi M H_{eff}}$ corresponds to resonance frequency F, and the damping factor Γ is related to Gilbert's dissipation factor α as: $\Gamma = \alpha\sqrt{H_{eff}/(4\pi M)}$.

Relation (2) shows that the bias increase causes an increase of resonance frequency F and a decrease of permeance factor $(\mu - 1)S$ thus limiting the frequency-domain measurements under high bias.

The bias-domain technique [2] is free from the drawbacks inherent to frequency-domain measurements: the domain structure is uniform, while the measured reflectivity response is independent on the unaccounted for inhomogeneity of the measurement cell and on the frequency dependent noises. Therefore it is possible to study with the same hardware the samples with lower permeance factors and at the higher frequency than by the frequency-domain technique [1].

The treatment of FMR spectra measured at several frequencies allows one to calculate the saturation magnetization without applying the data on the amount of permeable substance. The extrapolation of $\Gamma(H_{bias})$ and $\mu_0(H_{bias})$ functions for $H_{bias} = 0$ reveals the effect of nonuniform domain structure on the damping factor and on the static permeability.

Permeability spectra of metal films are often distorted by the effect of eddy currents [4]. It is impossible to point out the distortion in sweep-frequency measurements of a single sample, while the value of $\mu_0 = 4\pi M/H_{eff}$ in sweep-bias measurements is frequency-dependent if the film thickness is close to or exceeds the skin-depth. As a result the dependence of effective Asher's constant [3] $K_{Acher} = \mu_0(H_{bias}) \times F^2$ on bias strength reveals the contribution of eddy currents and points out the frequency and film thickness where this contribution in negligible.

REFERENCES

1. Starostenko, S. N., K. N. Rozanov, and A. V. Osipov, *J. Appl. Phys.*, Vol. 103, 07E914, 2008.
2. Neudecker, I., G. Woltersdorf, B. Heinrich, T. Okuno, G. Gubbiotti, and C. H. Back, *JMMM*, Vol. 307, 148, 2006.
3. Acher, O. and A. L. Adenot, *Phys. Rev. B*, Vol. 62, 11324, 2000.

4. Lagarkov, A. N., A. V. Osipov, K. N. Rozanov, and S. N. Starostenko, "Microwave composites filled with thin ferromagnetic films. Part 1. Theory. Proc. of symposium R: Electromagnetic materials," *3rd Int. Conf. on Materials for Advanced Technologies ICMAT 2005*, Vol. 308, 74–77, Singapore, July 2005.

Session 5P4
Integral Equations Method in Large Electromagnetic Problems

Method of Volume Singular Integral Equation for Determination of Permittivity of Dielectric Body in a Waveguide

Yury G. Smirnov
Department of Mathematics and Mathematical Modelling, Penza State University
Penza, Russia

Abstract— The problem of diffraction of an electromagnetic field by a locally nonhomogeneous body in a perfectly conducting rectangular waveguide is considered. The boundary value problem for the system of Maxwell's equations is formulated in unbounded domain and with partial radiation conditions at infinity. This problem is reduced to solving a volume singular integral equation. The integral equation is solved only inside the body (in the nonhomogeneity region). The method of solution employ integral equation constructed using tensor Green's function of the domain occupied by a regular guide. The examination of this equation is based on the analysis of the corresponding boundary value problem for the system of Maxwell's equations and the equivalence of this boundary value problem and volume singular integral equation. In this method, the resulting volume singular integral equation operator is elliptic. The existence and uniqueness for volume singular integral equation in the space of square-integrable functions are proved. A numerical collocation method for the solution of volume singular integral equation is proposed and its convergence is proved.

Inverse boundary value problem for determination of effective permittivity of dielectric body in a waveguide is reduced to the nonlinear volume singular integral equation. We analyze the nonlinear integral equation on the basis of contraction theorem. This enables us to prove the existence and uniqueness theorem for the solution of nonlinear volume singular integral equation in the space of square-integrable functions and obtain some results concerning the solutions of inverse boundary value problem. A numerical iteration method for solving the nonlinear volume singular integral equation (and inverse boundary value problem) is proposed and its convergence is proved.

Parallel algorithms and computational techniques are developed for solving the nonlinear volume singular integral equation. Computations are fulfilled using supercomputers. Various numerical results are presented and discussed.

Collocation Method of Solving Volume Singular Integral Equation for Diffraction by Dielectric Body in Rectangular Waveguide

Yury G. Smirnov, **Mikhail Medvedik**, **and Ekaterina Derevyanchyk**
Department of Mathematics and Mathematical Modelling
Penza State University, Penza, Russia

Abstract— We consider the diffraction of an electromagnetic field by a locally inhomogeneous dielectric body in a perfectly conducting waveguide of rectangular cross section. The analysis of diffraction by dielectric bodies in resonators and waveguides is important for modeling the processes that take place in microwave ovens and when the scattering of electromagnetic fields by biological objects is considered. Such problems can be solved numerically by the finite element method. However, the direct use of this method is connected with certain difficulties. First, the corresponding boundary value problem (BVP) for Maxwell's equations is not an elliptic one; therefore, the standard schemes for the proof of the convergence of projection methods cannot be applied. Second, in order to ensure an acceptable accuracy of the calculation of the field in a body, a fine grid within the inhomogeneity region must be used, which requires that the grid outside the obstacle must be also fine. Since the problem is three-dimensional, the matrices that appear in the finite element method after discretization of the problem are sparse and have a very high order.

We develop the method of volume singular integral equations (VSIE) which is to a big extent free of those drawbacks. In this method, the resulting VSIE operator is elliptic and the integral equation is solved only inside the body (in the inhomogeneity region). We analyze the VSIE on the basis of the corresponding BVP using the equivalence of this BVP and the integral equation. This enables us to prove the existence and uniqueness theorem for the solution of VSIE in the space of square-integrable functions and obtain some results concerning the solutions of BVP. A numerical collocation method for the VSIE solution is proposed and its convergence is proved.

Parallel algorithms and computational techniques are developed for solving the volume singular integral equation. Computations are fulfilled using supercomputers. Various numerical results are presented and discussed.

Generalization of the Barnes-Hut Algorithm for the Helmholtz Equation in Three Dimensions

J. Aronsson, **I. Jeffrey**, **and V. Okhmatovski**
Department of Electrical and Computer Engineering, University of Manitoba
Winnipeg, Canada

Abstract— The Barnes-Hut algorithm originally developed for $O(N \log N)$ solution of N-body problem with the Laplace kernel is generalized to the case of the scalar Helmholtz kernel in three dimensions. Analogous to the center-of-charge concept used in the static algorithm, a center-of-radiation is associated with each box of the hierarchically partitioned space enclosing the sources of interest. The algorithm is applicable to the acceleration of electromagnetic interactions between sources confined to electrically small volumes. The method may be used in conjunction with the high-frequency Fast Multipole Method to eliminate its low-frequency breakdown.

Introduction: Today's wireless systems tightly integrate the antenna's radiating elements, feeding networks, and RF circuitry. Electromagnetic simulations used to validate system designs present various challenges. The most formidable of these challenges is the large size of the pertinent discrete models and multi-scale features of the designs. Among the limited computational techniques capable of conducting such simulations is the boundary-element method-of-moments [1] accelerated with broadband fast algorithms which allow for simultaneous $O(N \log N)$ evaluation of full-wave and quasi-static interactions [2].

In this work we propose a simple alternative to the low-frequency Fast Multipole Method (FMM) [2], applicable when two digits of precision in the evaluation of the pertinent matrix-vector product is sufficient for a given discretization scheme [1]. The proposed method is based on a generalization of the Barnes-Hut (BH) algorithm [3] for rapid evaluation of electromagnetic interactions from a large group of sources enclosed in an electrically small volume. Similar to the static BH algorithm that introduces centers-of-charge in association with each box of a hierarchically partitioned volume enclosing all static sources, the proposed full-wave version of the method introduces centers-of-radiation (CoR) in association with each box containing time-harmonic sources. The position and magnitude of the center-of-radiation in each box is determined by matching the zeroth and first order spectral moments of the true field produced by sources contained in that box to the field of a single point source acting as the CoR in the vicinity the stationary phase point [4]. Since the stationary phase point in k-space is a function of observation angle, so is the CoR. The CoR sources can be shown to allow for recursive clustering necessary for the development of an $O(N \log N)$ solution of the time-harmonic N-body problem. The error of the proposed method has been compared against that low- and high-frequency FMM [2] and validates the above statements.

REFERENCES

1. Andriulli, F. P., et al., "A multiplicative calderon preconditioner for the electric field integral equation," *IEEE Trans. Antennas Propag.*, Vol. 56, No. 6, 2398–2412, Aug. 2008.
2. Cheng, H., et al., "A wideband FMM for the Helmholtz equation in three dimensions," *J. Comp. Phys.*, Vol. 216, No. 1, 300–325, July 2006.
3. Barnes, J. and P. Hut, "A Hierarchical $O(n \log n)$ force calculation algorithm," *Nature*, Vol. 324, Dec. 1986.
4. Chew, W. C., *Waves and Fields in Inhomogeneous Media*, IEEE Press, Piscataway, NJ, 1995.

Tensor and Toeplitz Structures Applied to Direct and Inverse 3D Electromagnetic Problems

S. A. Goreinov, **D. V. Savostyanov**, **and E. E. Tyrtyshnikov**
Institute of Numerical Mathematics, Russian Academy of Sciences, Gubkina 8, Moscow 119333, Russia

Abstract— We discuss the matrices of special structure: multilevel matrices with Toeplitz and Hankel structure on different levels and tensor product matrices. These matrices appear as discretisations of volume integral equations in a cube. Generally, solving such an equation, we have to deal with n^3-size vectors and n^6-size dense matrix (n is the number grid elements along each side). This puts severe restrictions on the value of n, even if we use a multiprocessor system. Using the structure of data we can reduce the computational costs to a value of n^3 or even to n^2.

As a practical example, consider the electromagnetic problem in the heterogeneous 3D half-space bounded by a perfectly conducting plane. Using a local heterogeneity model, we reduce this problem to a volume integral equation. Applying the Galerkin discretisation on uniform Cartesian grids with special basis functions, we obtain a linear system with a three-level block matrix, with levels of Toeplitz or Hankel structure. This allows us to perform a multiplication with $n^3 \log(n)$ operations, where n^3 is a number of unknowns. We propose a parallel algorithm for the solution of the problem under consideration. The employment of this algorithm makes it possible to perform a numerical simulation of measurements with an accuracy sufficient for the solution of the inverse problem, i.e., for the study of heterogeneity structure. The results of solving the inverse problem with the use of Born approximation show a high accuracy of the method proposed.

On nonuniform (but still Cartesian) grids, the multiplication cost and the memory requirements for the matrix grow as n^6, that limits us to a very small values of n. To remove this restrictions, we approximate the matrix by a sum of tensor products. This reduce the storage requirements to about n^2, and allows us to construct super-fast multiplication algorithms. To construct the tensor aproximation, we propose the 3D-Cross algoritm, that use only a small number of matrix elements, and so also have complexity of about $n^2 \log(n)$. The application of the tensor product approximations allows us to store the 256 TB matrix (for $n = 256$) to a personal workstation memory.

ACKNOWLEDGMENT

This work was partially supported by RFBR grant 08-01-00115 and Priority Research Grant of Department of Mathematical Sciences of the Russian Academy of Sciences.

Fast Computation of Electromagnetic Fields in Structured 2.5D and 3D Problems

S. Goreinov, S. Stavtsev, and E. Tyrtyshnikov
Institute of Numerical Mathematics, Russian Academy of Sciences, Russia

Abstract— Accurate evaluation of electromagnetic fields from localized sources is crucial in the modelling of electromagnetic tools of oil industry.

The case of boreholes in a heterogeneous isotropic formation uniform in one particular direction (let it be z-axis) is a specific but still computationally difficult problem, especially in the case of highly varying conductivities and when the source is close to the boundaries. Such problems are simpler than general 3D but far more complicated than 2D ones, because of the source.

As we have found, this particular application is one where the method of integral equations can be much faster (1000 times and more, in some cases) and a lot more accurate than solution procedures based directly on the partial differential formulation.

The essentials of the efficiency are the following:

- fast approximation method (based on the Fourier polynomials) [1];

- fast algebraic solver (based on the block circulant preconditioners) [3];

- fast method of computation of the Fourier integrals (a new modification of the Chebyshev-Laguerre approach [2]);

- analytic computations of the collocation matrix in case of concentric discs (cylinders).

REFERENCES

1. Savostianov, D. V. and E. E. Tyrtyshnikov, "On the algebraic equivalence case of the collocation and Galerkin methods," *J. Comput. Math. and Math. Phys.*, Vol. 44, No. 4, 686–695, 2004.
2. Tyrtyshnikov, E. E., "Modification of the Chebyshev-Laguerre and Gauss-Legendre methods for computation of integrals," *J. Comput. Math. and Math. Phys.*, Vol. 44, No. 7, 1187–1105, 2004.
3. Tyrtyshnikov, E., "Structured preconditioners for operator equations," *Numer. Linear Algebra Appl.*, Vol. 12, 251–259, 2005.
4. Tyrtyshnikov, E., "Fast computation of Toeplitz forms and some multidimensional integrals," *Rus. J. Numer. Math. and Math. Modelling*, Vol. 20, No. 4, 383–390, 2005.
5. Olshevsky, V., I. Oseledets, and E. Tyrtyshnikov, "Tensor properties of multilevel Toeplitz and related matrices," *Linear Algebra Appl.*, Vol. 412, 1–21, 2006.
6. Oseledets, I., D. Savostianov, and E. Tyrtyshnikov, "Tucker dimensionality reduction of three-dimensional arrays in linear time," accepted by *SIMAX*.

Application of Mosaic-Skeleton Approximations for Solving EFIE

S. L. Stavtsev and E. E. Tyrtyshnikov
INM RAS, Russian Federation

Abstract— To solve EFIE on the surfaces of arbitrary shape, RWG functions are traditionally used. In spite of their effectiveness when solving diffraction problems on complex surfaces, on multiple objects as well as the problems with high frequencies, the necessity arises to calculate dense matrices of high dimensionality ($n > 10^4$) and also to solve correspondent linear systems.

We suggest using nonlinear matrix approximations to work with large matrices. We can calculate $O(n \log(n))$ elements of matrix (instead of $O(n^2)$), where n is a number of variables in system of linear equations. The multiplication of matrix and vector we can execute also for $O(n \log(n))$ operations. The nonlinear matrix approximations allow to operate with matrixes n 10^5–10^6. System of linear equation with matrixes of such order is solved by iterative method (GMRES). To reduce of number of iterations we are used precondition which is based on mosaic-skeleton approximations. Test calculations of diffraction of electromagnetic fields on area and a number of numerical experiments for objects of the any form are carried out on the personal and multiprocessor computers.

Subhierarchical Algorithm for Solving the Problem of Electromagnetic Diffraction by a Dielectric Body in Several Domains

A. Tsupak
Penza State University, Russia

Abstract— The three-dimensional time-harmonic problems of diffraction of electromagnetic field by an anisotropic dielectric body Q in 3D-domains P are examined. The following types of domains are considered: free space, half space ($x_3 > 0$), infinite layer ($x_3 \in (0, a)$), infinite or half-bounded rectangular waveguide and rectangular resonator. The boundaries of the domains in all cases except the 1st one are considered to be perfectly conducting. The surface of body Q is piece-wise smooth.

The body Q has constant magnetic permeability μ_0 and positive 3-by-3 matrix (tensor) permittivity $\hat{\varepsilon}(x)$. The components of $\hat{\varepsilon}(x)$ and $\hat{\varepsilon}^{-1}$ are bounded functions in $\bar{Q}$. The outside media $P\backslash\bar{Q}$ is characterized by constant permittivity permeability $\varepsilon_0(> 0)$, $\mu_0(> 0)$.

The diffraction problem is stated in terms of generalized boundary-value problem for the system of Maxwell's equations. The field $\vec{E}$, $\vec{H}$ is found in space $L_2(Q)$. Maxwell's equations as well as boundary conditions on perfectly conducting surfaces are considered in distributional sense.

The BVP is derived to integro-differential equation regarding the polarization current J. Galerkin method is used for numerical solution of this equation.

To find the numerical solution to the diffraction problems the subhierarchical algorithm is proposed.

Firstly, according to this algorithm it is necessary to find the solution to the problem of diffraction by a elementary rectangular body Q, which should be large enough. For that purpose we consider rectangular grid and finite elements of low order with rectangular support as basis and test functions in Galerkin method. The basis functions are numerated in a sufficient order. Then we form the matrix A of the system of linear algebraic equations according to Galerkin method. It is necessary to form a sufficiently dense grid and to calculate matrix elements as accurate as possible.

To solve the problem of scattering by an arbitrary body Q' it is 'cut' out of Q. More precisely, those cells of the grid are considered that are covered completely by Q'. Than the basis functions are re-enumerated and the new SLAE for Galerkin method is formed. It is important to emphasize that matrix elements shouldn't be recomputed — they are just selected from previously formed matrix A.

Galerkin Method and Parallel Computational Algorithm for Solving Problems of Diffraction by Dielectric Bodies in Free Space

D. Mironov and A. Tsupak
Penza State University, Russia

Abstract— The three-dimensional time-harmonic problems of diffraction of electromagnetic field by an anisotropic dielectric body Q in free space are examined.

The surface of body Q is piece-wise smooth, i.e., conical and corner points are available. The body Q has constant magnetic permeability μ_0 and positive 3-by-3 matrix (tensor) permittivity $\hat{\varepsilon}(x)$. The components of $\hat{\varepsilon}(x)$ are bounded functions in $\bar{Q}$: $\hat{\varepsilon} \in L_\infty(Q)$, and also $\hat{\varepsilon}^{-1} \in L_\infty(Q)$. The outside media $R^3 \backslash \bar{Q}$ is characterized by constant permittivity permeability $\varepsilon_0 (> 0)$, $\mu_0 (> 0)$.

The diffraction problem is stated in terms of boundary-value problem for the system of Maxwell's equations. The field $\vec{E}$, $\vec{H}$ is found in space $L_2(Q)$. Maxwell's equations as well as boundary conditions on perfectly conducting surfaces are considered in distributional sense.

The method of volume integral singular equations is applied to solve the problem.

The following integral equation is acquired:

$$\vec{E}(x) + \frac{1}{3}\left[\frac{\hat{\varepsilon}(x)}{\varepsilon_0} - \hat{I}\right]\vec{E}(x) - v.p.\int\limits_Q \hat{\Gamma}_1(x,y)\left[\frac{\hat{\varepsilon}(y)}{\varepsilon_0} - \hat{I}\right]\vec{E}(y)dy = \vec{E}^0(x)$$

Tensor $\hat{\Gamma}_1$ has the following singularity

$$\frac{1}{|x-y|^3}.$$

The equivalence of differential and integral problems is proved. The existence and uniqueness of solutions of the diffraction problem in free space is proved.

Galerkin method is used for numerical solution of integral equation. Finite elements of low order are applied as basis and test functions in Galerkin method. The explicit expressions for augmented matrix are written. The convergence of Galerkin method is proved for a wide class of dielectric bodies.

An approach involving parallel computations is proposed. At the first stage we propose "per line" filling of augmented matrix: each of the processors in cluster fills several matrix lines. After that the matrix is collected on one of the processors. Finally, the system of linear algebraic equations is solved on this single processor.

Subhierarchical method is also used to find the solution to problems of diffraction.

The results of computation for dielectric bodies are presented.

Parallel Computational Algorithm for Solving Problems of Diffraction by Plane Screen

M. Medvedik and A. Tsupak
Penza State University, Russia

Abstract— The problem of diffraction of electromagnetic wave by a bounded thin plane perfectly conducting screen Ω is considered.

The boundary-value problem for Maxwell's equations is reduced to the following integro-differential equation

$$Lu := Grad_\tau A(Divu) + k^2 A_\tau u = f, \quad x \in \Omega,$$

where operator A is specified as

$$A_\tau u = \int\limits_\Omega \frac{\exp(ik|x-y|)}{|x-y|} u(y) ds.$$

To find the approximate solution to this equation in Sobolev spaces we propose Galerkin method with basis functions according to Rao-Wilton-Glisson method. The convergence of Galerkin method is proved due to the ellipticity of operator L on subspaces.

The developed method is applied to calculation of surface currents on a plane perfectly conducting infinitely thin screen of an arbitrary shape.

Following the algorithm of Galerkin method we form a grid and construct basis functions φ_i which are enumerated in a special way. Then we form the matrix of system of linear algebraic equations $\left(I \middle| \vec{f}\right)$, where

$$I_{ij} = (L\varphi_i, \varphi_j), \quad f_i = (f, \varphi_i).$$

Here (,) denotes scalar product in $L_2(\Omega)$.

As the dimensions of matrix are large (6673×6673), it takes much time to fill it and to solve the SLAE. We propose an approach involving parallel computations.

At the first stage the task for matrix filling is divided in the following way: each of the processors in cluster fills several matrix lines. After matrix filling is completed it is collected on one of the processors. Finally, the system of linear algebraic equations is solved on this single processor.

The results of computation for plane screens of various shapes are presented. Firstly we represent absolute values of surface currents in the center horizontal section of $\lambda \times \lambda$ square plate. Then we get values of surface currents obtained for H-shaped screen according to subhierarchical approach.

Numerical Analysis of Scattering and Absorption Problems of Electromagnetic Waves of a Mobile Communication Range on Non-uniform Biological Structures

Sergey P. Kulikov and Natalya Y. Voronina
Moscow Institute of Radio Engineering, Electronics and Automation, Russia

Abstract— Questions of development of algorithms and programs for the numerical analysis of interaction of electromagnetic waves of a mobile communication range and other microwaves sources with non-uniform biological bodies and structures are considered in this work. The opportunity of numerical modeling of such practical problems in a resonant range is shown. The analytical research of diffraction problems in this range is inapplicable. The problem is put in the strong formulation on the basis of the electromagnetic volume integral equation and further in the mathematical plan is reduced to the numerical solution of large complex systems of the linear algebraic equations (SLAE) with symmetric complex non-hermith matrix. Application of a method of optimum simple iteration (MOSI) proves for the solution of such SLAE. Successful application of this method is based on knowledge of spectral properties of the integral operator of transition, and also a matrix of transition corresponding it and on the developed algorithms of optimum parameter MOSI definition. The principle of an invariance of optimum parameter MOSI is used at transition from a problem with a rare computing grid in 2–3 units per wavelength in the medium to a problem with large SLAE at sufficient accuracy of a problem approximation in 8–12 units per wavelength. The developed software package can be applied at modeling scattering and absorption processes of electromagnetic waves with sources of a various origin on complex non-uniform dielectric biological structures. The 2D problems of absorption of electromagnetic radiation of a mobile communication range on models of human bodies and structures are numerically solved.

On Singular Integral Equations in the Class of Distributions and Their Appliance to Antennas Theory Issues

A. V. Setuha and A. S. Nenashev
Air Force Academy, Moscow, Russia

Abstract— The present article is focused on the theory and methods of numerical calculations for singular and hypersingular integral equations in the class of distributions and also on some ways of those equations appliance to the boundary value problems.

The present paper introduces the definition of "continuation for integral operators with the special integrals", meaning Cauchy's principal value and Hadamard's final value on the distributions. In this concern the approaches based on spectral decomposition as well as on linear functionals extending by their continuity are employed. Formulas of Cauchy and Hilbert integrals inversion are extended to the distributions. The numerical decision methods of the singular and hypersingular integral equations with distributions in the right parts are calculated. The equations of considered types arise at the decision of boundary value problems for Laplace equation in a class of the functions having singularity on boundary.

In work Neumann boundary value problem in domain with the closed boundary and also Neumann external boundary value problem on the screen is considered. In this case the decision is searched out of the screen (the opened surface) and boundary conditions on both parties of this screen are applied. The concept of generalized boundary values and its normal derivatives on a boundary is entered. Neumann problem for a case when boundary values of a normal derivative are distributions is formulated.

Distributions are entered as continuous linear functionals on some special space of the test functions. It is shown, that considered problem is reduced to the boundary integral equation with singularity in integrals in a class of distributions. Resolvability of boundary problems is proved and numerical schemes of their solving based on a method of discrete vortices frames are constructed.

The attained theoretical results are applied for the development of mathematical models of antenna excitation sources and methods of their entrance resistance defining.

Integral Equations Approach to TM-Electromagnetic Waves Guided by a (Linear/Nonlinear) Dielectric Film with a Spatially Varying Permittivity

V. S. Serov[1], K. A. Yuskaeva[2], and H. W. Schürmann[2]

[1]Department of Mathematical Sciences, University of Oulu, P. O. Box 3000, FIN-90014, Finland
[2]Department of Physics, University of Osnabrueck, D-49069 Osnabrueck, Germany

Abstract— A method is proposed for obtaining solutions of Maxwell's equations describing guided TM-waves in a three-layer structure consisting of a nonlinear dielectric film situated between two linear semi — infinite media. All media are assumed to be lossless and nonmagnetic.

The linear part of the permittivity is modelled by a continuously differentiable real valued function of the transverse coordinate. The problem is reduced to a system of two integral equations. On the basis of the Banach fixed-point theorem it is shown that the solution exists in form of a uniformly convergent sequence of iterations. The dispersion relation is presented. Some results are evaluated numerically.

Session 5P5
Computational Electromagnetics 3

3G Base Station Optimal Positioning for Heterogenous Network with Fixed Sector and Adaptive Antennas

Lajos Nagy, Andrea Farkasvölgyi, and Róbert Dady
Department of Broadband Infocommunications and Electromagnetic Theory
Budapest University of Technology and Economics
H-1111 Budapest, Goldmann György tér 3, Hungary

Abstract— During the planning of UMTS radio network, there is a natural need for a base station positioning procedure. Good coverage at an acceptable level of network installation and maintaining costs, low interference and uniform interface load are the main requirements. In this paper, we present an approach based on simulated annealing for optimization of heterogenous radio network with fixed sector antennas and adaptive antennas.

In our paper, we concentrate on the maximal reachable service level at a pre-defined level of cost. It is known that in 3G in order to optimize the radio subsystem there are different aspects to be dealt with unlike in older systems. This is a consequence of the WCDMA technology and the coherent demodulation. The interferencelimited behavior of an UMTS WCDMA radio network and the technology used cause that positioning problem which interests us is NP-complete. We are considering several different approaches, the goal of which is the evaluation and the comparison of algorithms that solve this problem. One of the possible solutions relies on the heuristic algorithm known as simulated annealing. We present the interference-model built in our program, describe the used annealing parameters and present the simulation results.

Two networks are investigated, the homogenous sectorized base station configuration and the heterogenous with sectorized base station antennas and adaptive antennas. Optimum coverage percentage and optimal base station positions are compared for both radio networks.

REFERENCES

1. Farkas, L., C. Orosz, and L. Nagy, "UTRAN resource planning based on a PTAS using a complex profit function," *URSI 2002*, Maastricht, Netherlands, 2002.

Extension of Exact Evaluation of Retarded Time Potentials from 2D to 3D Source Distributions

H. Arda Ülkü, **Fatih Dikmen**, and **A. Arif Ergin**
Electronics Engineering Department, Gebze Institute of Technology
41400 Çayırova Gebze, Kocaeli, Turkey

Abstract— Exact evaluation of retarded time scalar and vector potentials due to impulsively excited Rao-Wilton-Glisson (RWG) basis functions [1] was presented in [2] and the magnetic field due to these currents were developed in [3], for surface scattering problems. As a consequence of [2, 3], scalar and vector potentials and magnetic fields are related with the intersection of the triangular surface (the support of the RWG basis functions) and a sphere that is centered at the observation point with radius $R = ct$. In detail, the intersection of the sphere and triangle yields an arc. Scalar and vector potentials are related with arc length and bisecting vector of the arc, respectively. Also in [4], it is shown that the marching on-in time (MOT) solutions are more accurate and stable with using exact formulations.

The studies in [2–4] are applicable to surface scattering problems. For volume scattering problems, instead of RWG basis, Schaubert-Wilton-Glisson (SWG) basis functions are used for modeling the scatterers [5]. SWG basis are defined on a pair of tetrahedra, just as the RWG is defined on a pair of triangles. In the present work, the procedure for obtaining the scalar and vector potentials due to impulsively excited RWG functions is extended to SWG functions. Retarded-time potentials are formulated in terms of the intersection of the tetrahedra and a sphere with radius $R = ct$. In particular, it can be shown that the scalar and vector potentials are related with solid angle and area centroid of the intersection surface, respectively.

In order to verify the validity of the proposed approach, the time samples of potentials due to SWG basis are evaluated. A CAD tool such as Rhinoceros can be used to calculate geometric quantities: solid angle and area centroid vector. The validity of the obtained time domain results can be demonstrated through the comparison of the results with those obtained in frequency domain by using numerical quadrature.

REFERENCES

1. Rao, S. M., D. R. Wilton, and A. W. Glisson, "Electromagnetic scattering by surfaces of arbitrary shape," *IEEE Trans. Antennas Propag.*, Vol. 30, 409–418, May 1982.
2. Yücel, A. C. and A. A. Ergin, "Exact evaluation of retarded-time potential integrals for the RWG bases," *IEEE Trans. Antennas Propag.*, Vol. 54, No. 5, 1496–1502, May 2006.
3. Ülkü, H. A. and A. A. Ergin, "Analytical evaluation of transient magnetic fields due to RWG current bases," *IEEE Trans. Antennas Propag.*, Vol. 55, No. 12, 3565–3575, Dec. 2007.
4. Ülkü, H. A. and A. A. Ergin, "Application of analytical expressions of transient potentials to the MOT solution of integral equations," *IEEE International Symposium on Antennas and Propagation and USNC/URSI National Radio Science Meeting*, San Diego, CA, USA, Jul. 5–12, 2008.
5. Schaubert, D. H., D. R. Wilton, and A. W. Glisson, "A tetrahedral modeling method for electromagnetic scattering by arbitrarily shaped inhomogeneous dielectric bodies," *IEEE Trans. Antennas Propag.*, Vol. 32, 77–85, Jan. 1984.

Tuning Microstrip Patch Antennas on Ferrite Substrate Using Simple Ground Plane Structures

M. A. Alsunaidi
King Fahd University of Petroleum & Minerals, Saudi Arabia

Abstract— Microstrip patch antennas on ferrite substrates offer a number of advantages over normal dielectric material. Due to their fairly high dielectric constant, miniaturization is possible. Further, because of the property of frequency tuning by external biasing fields, the radar cross section of such antennas can be reduced. Also, changing the beam width and direction is possible in ferrite-based antenna arrays. However, the analysis of ferrite-based problems is often complex due to the inherent anisotropy and nonlinearity in the material. Analytical solutions are generally inaccurate because they are based on simplifying assumptions. Therefore, the development of accurate numerical techniques is essential. In this paper, a new numerical algorithm based on the finite-difference time-domain (FDTD) method is developed to model the response of microstrip patch antennas on magnetized ferrite substrates. This FDTD model utilizes the Auxiliary Differential Equation (ADE) approach to represent the frequency dependent permeability tensor in the time domain equations. The resulting 3D full-wave numerical model is tested and verified against experimental data showing very good agreement. An additional technique for the efficient tunability of the frequency response of the antenna without varying the applied field is also presented. This technique is based on loading the antenna by simple ground plane structures. The Polder frequency dependent permeability tensor for magnetically saturated ferrites is given by

$$\mu = \begin{bmatrix} \mu_r & jk & 0 \\ -jk & \mu_r & 0 \\ 0 & 0 & \mu_o \end{bmatrix} \text{ with } \mu_r = \mu_o\left[1 + \frac{\omega_m(\omega_o + j\alpha\omega)}{(\omega_o + j\alpha\omega)^2 - \omega^2}\right] \text{ and } jk = \frac{j\mu_o\omega_m\omega}{(\omega_o + j\alpha\omega)^2 - \omega^2} \quad (1)$$

where it has been assumed that the magnetizing DC field is in the z-direction. To test the application of the proposed numerical scheme to microstrip patch antennas, the response of a typical patch antenna is considered. The structure is shown in Figure 1 with the following dimensions: $x_1 = 9$ mm, $x_2 = 5$ mm, $x_3 = 2.5$ mm, $y_1 = 3.1$ mm, $y_2 = 0.7$ mm, $y_3 = 0.3$ mm and $y_4 = 0.9$ mm. The antenna is printed on a ferrite substrate with thickness of 1 mm, dielectric constant of 13.69, loss tangent of 0.0002 and saturation magnetization of 27.85 kA/m. The gyromagnetic ratio is taken as 35.173 kHz m/A. A DC biasing magnetic field of 234 kA/m is applied in the z-direction. Figure 2 shows the simulated return loss parameter for the original patch antenna under investigation with complete ground plane (black line) and the antenna response with ground plane features introduced (red line). The simulated response shows that the response is improved and can be tuned to the desired frequency and bandwidth. Further

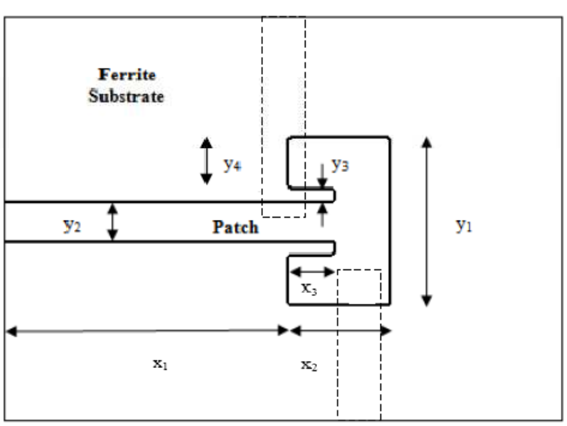

Figure 1: The ferrite-based patch antenna used in the analysis.

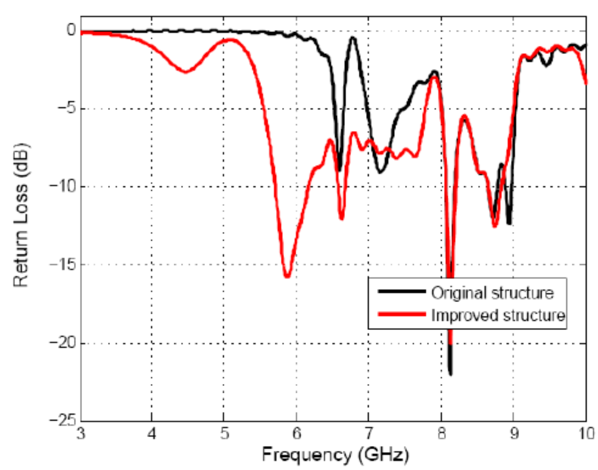

Figure 2: Return loss parameter for the patch antenna as obtained using the FDTD calculations with ground plane features introduced.

results show that tuning is possible by changing the dimensions and orientation of the ground plane features. Experimental results as well as radiation patterns are also collected to support the numerical predictions.

ACKNOWLEDGMENT

The author would like to acknowledge the support of King Fahd University of Petroleum & Minerals.

Regularization of Boundary Integral Equations in a Easy-to-Implement and Efficient Method

E. Korkmaz
Department of Electrical and Electronics Engineering, Fatih University, Turkey

Abstract— The calculation of electromagnetic scattering from arbitrarily shaped perfectly electrical conducting materials find broad applications in RCS calculations. Since analytical solutions are available only for limited geometries numerical techniques has to be used. Usually the scattering from PEC objects are formulated by boundary integral equation formulations. This formulation is based on the calculation of unknown surface current induced on the surface of the scatterer when it is irradiated by an incident wave. This formulation leads to two types of integro-differential equations for the surface current, the electric field integral equation EFIE and the magnetic field integral equation MFIE. From the theoretical point of view both equations are expected to give a solution for an arbitrary scatterer. In MFIE formulation the extra cross product with the unit vector can cause numerical instabilities when it is used for thin bodies or bodies with edges and corners. On the other hand EFIE does not suffer the same limitations and is expected to be capable to solve both for closed and open surfaces. However for arbitrarily shaped objects the regularization of EFIE is more difficult from the presence of derivatives appearing in conjunction with its singular kernel in the integral equation.

The regularization of these integral equations starts with the proper choice of basic functions to represent the induced unknown current on the surface. In the literature Rao-Wilton-Glisson (RWG) functions are the mostly used basis and testing functions. Further, solving the EFIE and MFIE in frequency domain involves the integration of Green's function kernel and its derivatives which possesses singularity when the point of interest coincides with the point of integration. Several techniques have been introduced to cope with the singularity problem. e.g., spherical mean of Green's function and the singularity extraction technique. The singularity extraction method is the most popular one and it is well established for RWG basis function, however, in the application suffers accuracy problems and complexity of the implementation.

In this paper a simple and easy to implement regularization technique will be introduced for both EFIE and MFIE. For the basis and testing functions the barycentric coordinate system is used which is easy to evaluate. The singularity of Green's function is coped by taking the spherical mean over only the singular part of Green's function which is little different than spherical mean of Green's function as a whole. After regularization of integral equations the solutions are obtained by means of conjugate gradient method. The efficiency of the introduced method is demonstrated with the solutions for known objects. Additionally, for the uniqueness of the solution due to the interior cavity resonance problem the efficiency of constrained conjugate gradient method will be discussed. This approach is different than the well known combined field integral equation techniques and yields rigorous solution at resonant frequencies.

Matrix Method for Potential Field Solutions from Quaternion Space

Geert C. Dijkhuis
Convectron N. V., Rotterdam, The Netherlands

Abstract— Planar potential field problems find generic solutions in functions of a complex variable regularized by the Cauchy-Riemann conditions. Their real and imaginary parts define orthogonal net-works for field lines and iso-potentials in the complex plane. As harmonic functions both parts satisfy Laplace equations with Dirichlet- or Neumann-type boundary conditions along their iso-lines. Their inverse functions are also harmonic and regular outside critical points at zeroes of the Jacobian determinant. Successive conformal maps transform uniform field into various patterns with singular points for charge or current density as shown in Fig. 1 for a dipolar field. Ref. [1] gives such plots for a free line source, a doublet source, and a line source confined by a wedge. Hyper-complex quaternion space serves well for tracking purposes and video games, but so far lacks a regularization scheme enabling 3D potential field calculations. Hamilton encoded 4D quaternion symmetries by product rules for three imaginary units, extendable to seven in 8D octavian space treated in Ref. [1]. We avoid all imaginaries by writing (hyper-) complex products in anti-symmetric matrix form. Each coordinate enters once in each row and column, as in Latin squares. Their determinants sum all coordinates in positive squares, enabling matrix inversion as defining property of quaternions as a division algebra. Hereby conjugate pairs of coordinate vectors re-emerge as (hyper-)complex eigenvalues.

For smooth coordinate transformations in complex planes one Cauchy-Riemann equation imposes anti-symmetry on partial derivatives in the matrix of its Jacobian determinant. For regular quaternion and octavian spaces we retain anti-symmetry only in the leading row and column. In the remaining block we impose symmetry on partial derivatives, and likewise for the moments of function components relative to the origin. For closure we write an eigenvalue equation for each imaginary coordinate, reproducing the second Cauchy-Riemann equation upon projection on each of its complex planes.

For polynomials, harmonic, hyperbolic, exponential and logarithmic functions taken from the *Mathematica* library we find full compliance with our real matrix scheme. The same holds for sums, products, quotients and chains of these functions. In 4D quaternion space their real part defines a scalar potential, and three imaginary components give its vector field. The Laplacian of such functions reveals charge distributions just like the Poisson equation does in electrostatics. Fig. 1 shows that quaternion inversion by our matrix method preserves orthogonality of dipolar field lines and iso-potentials plotted on the unit sphere as in stereographic projection.

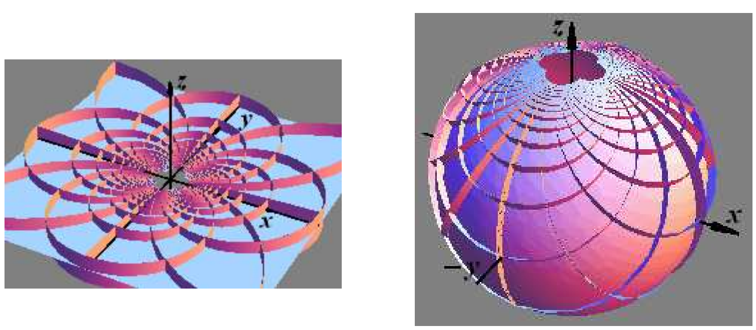

Figure 1: Quaternion inversion maps planar dipole field conformally on the unit sphere.

REFERENCES

1. Conway, J. H. and D. A. Smith, *On Quaternions and Octonions*, A. K. Peters, Wellesley, MA, USA, 2003.
2. Dijkhuis, G. C., "On potential flow solutions from the division algebras," *Proc. 6th European Symposium on Aerothermodynamics for Space Vehicles*, Versailles, France, November 3–6, 2008; ESA SP-659, January 2009.

Computational Modeling of New Kinds of Fractal Antennas and Fractal Frequency-selective Structures Based on Them

E. N. Matveev and A. A. Potapov
Institute of Radio Engineering and Electronics by V. A. Kotelnikov, RAS, Russia

Abstract— Authors' realized modeling of two kinds of fractal antennas with similar structure, but different algorithms of development. The obtained results were analyzed and conclusion of the practical applicability for these antennas was made. The geometry one of the antennas is a figure of "Life Flower", which presents a series of circles crossed in certain order. The geometry of the other one is also a series of crossed circles, according to the authors' algorithm. Both models have a coaxial feeder and modeled over the range of 0.1 GHz to 20 GHz. Moreover, the comparison of both antennas and there features are described in the article. It is notable, that the figure of "Life Flower" is well-known all over the world, but no information about it's application as a geometrical aperture was found by the authors. The obtained theoretical results allow us to conclude that synthesized fractal antennas have multiband and wide-band features. Besides the direct usage, such fractal structures performed on micron-level may reveal an application in a wide class of new fractal frequency-selective materials and surfaces. The applicability sphere of fractal antennas in modern technologies was shown: cellular communication, wireless information transmission and reception, and radar location devices. Also application filed was described for fractal antennas in m.

A General UPML FDTD ABC for Dispersive Media

Bing Wei, **De-Biao Ge**, **Xiao-Yong Li**, **and Fei Wang**
Department of Physics, Xi'dian University, Xi'an 710071, China

Abstract— In recent years, the Finite Difference Time Domain (FDTD) absorbing boundary conditions for dispersive media have been lucubrated. Now, Convolutional Perfect Match Layer (CPML) is an effective absorbing boundary condition applied to dispersive media and quite commonly used in FDTD computation. The parameter of CPML is related to the type of dispersive medium model adjacent to the absorbing boundary. When the medium adjacent to absorbing boundary is the single pole Debye medium, the x component of the Ampere's law in CPML region can be written as

$$\varepsilon_0\varepsilon_\infty\frac{\partial E_x}{\partial t}+\sigma_s E_x+J_{d_x}=\left(\frac{1}{\kappa_y}\frac{\partial H_z}{\partial y}-\frac{1}{\kappa_y}\frac{\partial H_y}{\partial z}\right)+\left(\varsigma_y*\frac{\partial H_z}{\partial y}-\varsigma_z*\frac{\partial H_y}{\partial z}\right) \tag{1}$$

For other kinds of dispersive medium models, such as the Lorentz model, Drude model, etc, the right hand side of Equation (1) maintains the same form, but the left hand side varies with the change of medium type. Owing to this characteristic, we have to compile different programs in dealing with different types of dispersive media while using CPML.

In this paper, a general absorbing boundary condition for dispersive media based on Uniaxial Perfect Match Layer (UPML) and Shift-Operator Finite Difference Time Domain (SO-FDTD) method is given. The dispersive relation of uniaxial anisotropic medium in UPML is obtained by the Maxwell's curl equations and the phase-matching. Then the anisotropic media can become a reflectionless PML layers when the constitutive parameters of the uniaxial medium be selected appropriately. After that, the matching matrix is introduced to deal with the absorption of the edge and angle areas of the UPML region. Combining with the transform relationship of frequency domain to time domain, and the characteristic that the relative permittivity of general dispersive media can be expressed by fractional polynomial with respect to jω, an FDTD absorbing boundary condition for three kinds of general dispersive medium models is deduced. Numerical results show that the absorbing boundary for three typical dispersive models, i.e., Debye model, Lorentz model, Drude model have good absorbing performance. This illustrates the generality and the high effectiveness of presented scheme.

SO-FDTD Applied to the Analysis of EM Scattering by Anisotropic Dispersive Medium

Fei Wang, **De-Biao Ge**, **and Bing Wei**
Department of Physics, Xidian University, Xi'an, Shaanxi 710071, China

Abstract— The finite-difference time-domain (FDTD) method has been widely used to treat a variety of electromagnetic problems, including the computation of wave propagation in dispersive media. In the past decades, there are numerous investigations of FDTD dispersive media formulations, such as the recursive convolution (RC) methods, the auxiliary differential equation (ADE) method and so on, among which the Shift Operator (SO) FDTD in simulating EM scattering by electrically dispersive medium was proposed by Ge et al. in 2003. Considering the complex permittivity of general dispersive medium can be expressed by a rational polynomial fraction in $j\omega$ in frequency domain, a shift operator in discrete time domain is defined, and an unified iterative formulation is then established, which is applicable for commonly used complex permittivity model, including Debye, Lorentz and Drude model.

Plasma and ferrite is a dispersive medium, respectively. Both of them become anisotropic media when an external magnetic field is imposed. The constitutive parameter, i.e., the permittivity of magnetized plasma or the permeability of magnetized ferrite is frequency dependent tensors, and both of them are Hermitian tensors in the principal coordinate system, whose z-axis is related to the direction of external magnetic field. It is worth noting that each element of constitutive parameter tensor is of rational polynomial fraction in $j\omega$ in frequency domain, respectively. The SO-FDTD is then implemented to obtain the advancing formulation in discrete time domain. To treat the electromagnetic scattering by magnetized plasma or magnetized ferrite media in general case, particularly in the case that the direction of external magnetic field is varying in space, it is necessary to perform a transformation from the principal coordinate system to the laboratory coordinate system.

Two examples are given to demonstrate the feasibility of presented SO-FDTD scheme. One is a magnetized plasma or ferrite plate. The reflection and transmission coefficients for left-handed and right-handed circularly polarized (LCP and RCP) waves are computed and compared with the analytical results. Second example is a magnetized plasma or ferrite sphere in an external dc magnetic field of different directions. The co-polarized and cross-polarized RCS is computed and compared with the results given in references. Good agreements are reached in computed examples.

Session 5P6
Biophotonics: Basis and Applications

Biophoton of Sprouts as Indicator of Seed Acclimatization

Cristiano M. Gallep, Samuel R. dos Santos, and Thiago Alexandre Moraes
Applied Photonics Lab — LaFA, DTT/CESET, State University of Campinas
R. Paschoal Marmo, 1888, 13484-370, Limeira, Sao Paulo, Brazil

Abstract— The spontaneous ultra-weak light emission (*biophoton*) of wheat seeds samples germinating simultaneously in Germany and Brazil indicates short-term acclimatization, pointing to further applications of biophoton experiments applied to agriculture.

Introduction: The study of spontaneous light emission during germination is a promise toll for the analyzes of different types of soil and/or fertilization [1]. In the 1950's for the first time Colli presented photon-count measurements in seedlings, indicating that light emission in the visible range should be correlated with the sample's physiological conditions [2]. The day-long measuring of spontaneous emission of cereal seedlings presented a day-like rhythm [3], thing that can be checked by a very simple photomultiplier tube-based apparatus [4].

Experimental Results and Discussion: Photon-count experiments of wheat seedlings were performed simultaneously in Brazil (LaFA, DTT/CESET/ Unicamp, Limeira) and Germany (IIB, Neuss). Two different types of wheat seeds — a Brazilian (standard *MaisVita*, id. FDL-E7C3) and a German (biodynamic *AlNatura*, id. 000 7866 DE), putted to germinated in a closed quartz cuvete (10 seeds with 1 mL of distilled water) at the German lab.

The Brazilian equivalent experiments used the same standard seeds brought to Germany (50 seeds in petri-dish with paper, 10 mL of water). The Brazilian groups, in Brazil and Germany, behave similar up to the Test 2 (10 days after arriving in Germany). Test 3 and 4 are atypical, with any sample going its own way. In Tests 5 and 6 the two samples in Germany go together in time, very different from the sample in Brazil. The data points to further investigation of biophoton emission in seedlings. Acknowledge to FAPESP support (04/10146-3, 07/00431-0). Special thanks to IIB, prof. Fritz-A. Popp and prof. Rajendra Bajpai for their support and collaboration.

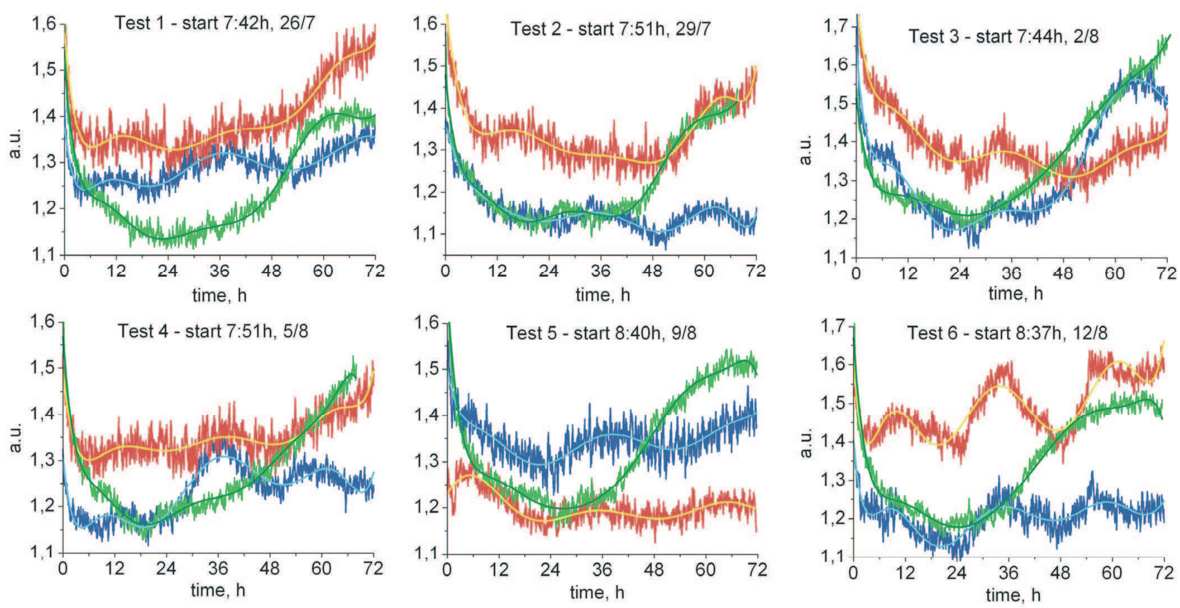

Figure 1: Local average (100 points) and polynomial fit for the photon-counting measurements for 6 tests of simultaneous wheat germination: German (blue, fit in light-blue) and Brazilian (red, fit in yellow) seeds in Germany, Brazilian seeds left in Brazil (green, fit in dark-green).

REFERENCES

1. Gallep, C. M. and S. R. Santos, "Photon-counts during germination of wheat (Triticum aestivum) in wastewater sediment solutions correlated with seedling growth," *Seed Science and Technology*, Vol. 35, 607–614, 2007.
2. Colli, L. and U. Facchini, "Further measurements on the bioluminescence of the seedlings," *Experientia*, Vol. 11, 479–481, 1955.
3. Yan, Y., "Biophoton emission and delayed Luminescence of plants," *Biophotonics — Optics Science and Engineering for the 21st Century*, (eds. X. Shen and R. Van Wijk), 195–204, Springer, New York, 2005.
4. Gallep, C. M., A. M. O. Santos, and E. Conforti, "Low-cost, simplified systems for photon-counting measurements in biological samples," *Proceedings of SBMO/IEEE MTT-S International Conference on Microwave and Optoelectronics*, 188–191, Brasília/Brazil, 2005.

Day- and Month-like Rhythms of Biophoton Emission in Seedlings

Thiago Alexandre Moraes, **Rebeca Tombolato Garofalo**, **Samili Ribeiro Ramos**,
Luciana de Carvalho Martins, and **Cristiano M. Gallep**
Applied Photonics Lab — LaFA, DTT/CESET, State University of Campinas
R. Paschoal Marmo, 1888, 13484-370, Limeira, Sao Paulo, Brazil

Abstract— The study of light spontaneous emission in wheat sprouts identified day- and month-like patterns in the photon-count data, noticing correlation with the germination efficiency and environmental factors and pointing to further uses of biophoton emission.

Introduction: The light emission from living beings has attracted attention of many researchers in Biology, Chemistry and correlated areas. Many species have been tested in a simple photon-counting apparatus connected to a dark-chamber [1], germinating under optimum or stressed conditions [2]. The spontaneous light emission is directly related to physiological and environmental conditions and so can be used in applications such as toxicology, among many.

Experimental Results and Discussion: For each photon-count test six groups of replicates were used to verify the germination efficiency, one half (3) of them exposed to daily rhythms, under indirect sun light, and one half in a controlled chamber, always in dark and fixed temperature (20°C). Each group contains 50 seeds, filter paper and distilled water, in a *petri* dish. The photon-counting (darkcount level $\sim 170\#/10\,\text{s}$) were performed in the 2nd and 3rd days after putting seeds in water, and so be able to measure the first two count-steps that normally occur in these cases, showing periodicities of 12 and 24 hours [2]. Periodicity also appears during the month, as already found in two-month long data of 2007. The rises and falls of the total number of counts in a 48 h-test seem to coincide with the average day-temperature oscillations and also with moon-like and moon-like square cycles. The authors are very grateful to FAPESP (grants 04/10146-3 and 07/50046-6), and International Institute of Biophysics' collaboration.

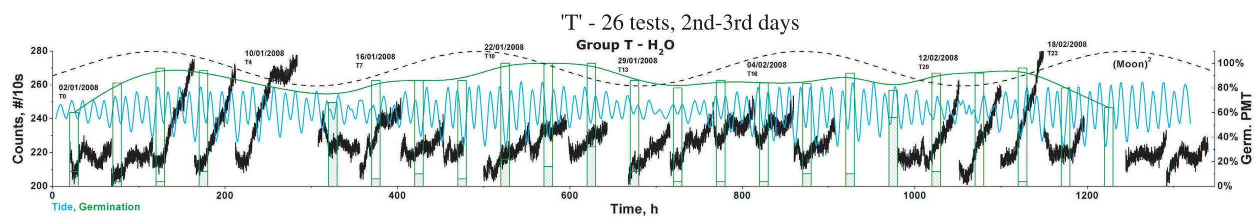

Figure 1: "T" series: Local average (100#) of photon-count data of wheat seedlings in distilled water (black line); germination efficiency (green bars and line); moon phase (dashed line, above); tide level at the local latitude (blue line).

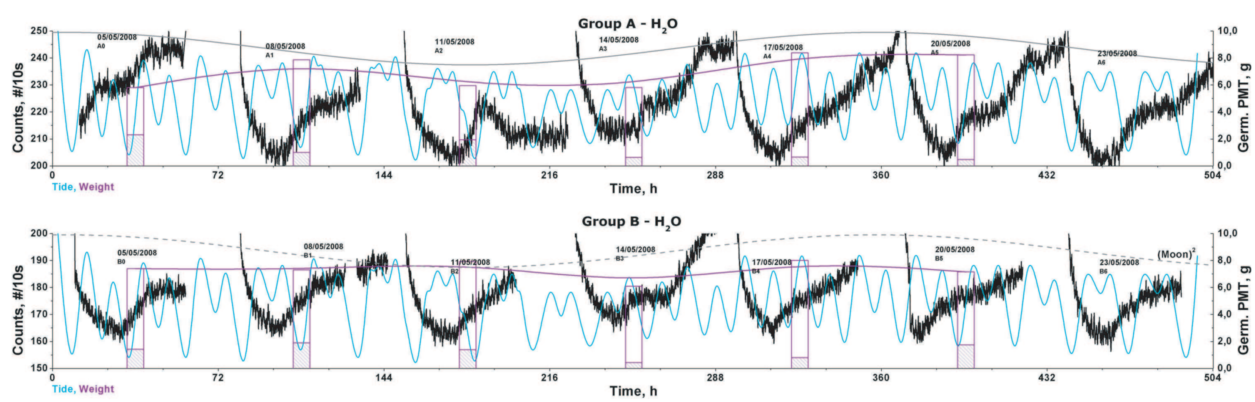

Figure 2: "A" and "B" (simultaneous) series: Local average (100#) of photon-count data of wheat seedlings in distilled water (black line); seedlings weight (purple bars and line); moon phase (dashed line, above); tide level at the local latitude (blue line).

REFERENCES

1. Gallep, C. M., A. M. Santos, and E. Conforti, "Low-cost, simplified systems for photon-counting measurements in biological samples," *Proceed. of International Conference on Microwave and Optoelectronics — IMOC*, 188–191, Brasília/Brazil, 2005.
2. Gallep, C. M. and S. R. Santos, "Photon-counts during germination of wheat (Triticum aestivum) in wastewater sediment solutions correlated with seedling growth," *Seed Science & Technology*, Vol. 35, 607–614, 2007.

Biophoton Emission in Wheat Seedlings with Potassium Dichromate

Thiago Alexandre Moraes, **Rebeca Tombolato Garofalo**, **Samili Ribeiro Ramos**, **Luciana de Carvalho Martins**, **Daniella Cristina Batist**, **and Cristiano M. Gallep**
Applied Photonics Lab — LaFA, DTT/CESET, State University of Campinas
R. Paschoal Marmo, 1888, 13484-370, Limeira, Sao Paulo, Brazil

Abstract— The spontaneous light emission in wheat sprouts series with different dichromate solutions noticed to be very apart, not just in photon-counting intensity but also in the (absence of) time-patterns, that normally occurs in non-stressed samples. The preliminary data prompts indications for further uses of biophotonic techniques.

Introduction: The light emission from living beings has attracted attention of many researchers in Biology, Chemistry and correlated areas. Many species have been tested in a simple photon-counting apparatus connected to a dark-chamber [1], germinating under optimum or stressed conditions [2, 3]. The spontaneous light emission is directly related to physiological and environmental conditions and so can be used in applications such as toxicology, among many

Experimental Results and Discussion: Two separate batteries of tests were conducted (Series F and H, one after the other, in the same equipments) each battery is composed by groups of tests. For each photon-count of test, six replicated tests were used to verify the germination efficiency (25 seeds), one half (3) of them exposed to daily rhythms, under indirect sun light, and one half in a controlled chamber, always in dark and fixed temperature (20°C), termed group. Each photon-count test sample contains 50 seeds over a filter paper in a petri dish. All tests were treated with Potassium Dichromate ($K_2Cr_2O_7$) solutions, of 150 ppm in the F series and of 25 ppm in H series. The photon-counting, took at each 10 s interval (stable background level $\sim 180\#/10\,\mathrm{s}$) were performed in the 3rd day after putting the solution with the seeds, and so be able to measure the emission patterns normally occurring in these cases [3], with 6 and 12 hour cycles, evidencing the influence on the signal intensity and highlight the differences between the two solutions of Potassium Dichromate when interfering in the germination process [3]. The authors are very grateful to FAPESP (grants 04/10146-3 and 07/50046-6), SAE/Unicamp and to the International Institute of Biophysics.

REFERENCES

1. Gallep, C. M., A. M. Santos, and E. Conforti, "Low-cost, simplified systems for photon-counting measurements in biological samples," *Proceeding of International Conference on Microwave and Optoelectronics — IMOC*, 188–191, Brasília/Brazil, 2005.
2. Gallep, C. M. and S. R. Santos, "Photon-counts during germination of wheat (Triticum aestivum) in wastewater sediment solutions correlated with seedling growth," *Seed Science & Technology*, Vol. 35, 607–614, 2007.
3. Moraes, T. A., et al., "Day- and month-like rhythms of biophoton emission in seedlings," *Progress In Electromagnetics Research Symposium*, Moscow, 2009.

Photo-counts in Germination Test with Wheat in Wastewater Sediment Applied in Ecotoxicology Experiments

Samuel R. dos Santos and Cristiano M. Gallep
Applied Photonics Lab — LaFA, DTT/CESET, State University of Campinas
R. Paschoal Marmo, 1888, Limeira 13484-370, Sao Paulo, Brazil

Abstract— The photon-counts of wheat seeds germinating in different wastewater sediment solutions are analyzed and correlated with seedling development. The procedure presented here is based on a very simple photomultiplier tube-based apparatus and constitutes a fast method to evaluate seed germination with real-time response and can help in studies on fertilization evaluation and ecotoxicology studies.

Introduction: The "biophotons" (ultraweak light emission from living systems) is an important research and can be connect with physiology systems, showing as an important tool applied in environmental control. Since the Cooli groups discovery the light emission from seedlings in 1950's indicated that light emission in the visible range should be correlated with the physiological conditions, many research groups in this area applying the photon emission from plants and seeds as indicator of development and metabolic alterations [1]. In this project we study an methodology based on monitoring of photo-counts of wheat seeds (*Triticum aestivum*) in germination tests supplied with diverse wastewater sediment solutions, correlating with seedling development. The further objective is to identify those concentrations of wastewater sediment solutions that promote germination and seedling development because of the nutritive effect without detectable toxic effects. The experimental data confirms the feasibility of a very simple photomultiplier tube (PMT)-based apparatus. More details about this study can be found in [2].

Experimental Results and Discussion: The experimental was develop using solution of wastewater sediment previously submitted to chemical analysis (ammonia, nitrite, nitrate, phosphorous, COD and solid sediment). The germination tests was prepared with 50 wheat seeds (*Triticum aestivum*), disposed in a petri dish (10 cm diameter) with filter paper and 10 mL of solution in the following concentrations: 0% (distiled water), 3%, 6.25%, 12.5%, 25% and 50%. A series containing a range of concentrations bounded was included in the experiment (15%, 17.5%, 20%, 22.5% and 25%). Each test is made in double, been one putted in the dark-chamber for the photon-counting measurements and the other stored in a germination chamber with controlled temperature (21°C) whitout light, for the germination and seedling development. The results show that solutions over 12.5%, combined with high concentrations of ammonia, promoted symptoms of toxicity accompanied by a low rate of photo emission even for the long tests. Since in the series analyzed, the samples contained wastewater solutions, no one presented better development contrasted with the sample control and there was groups with behavior very similar and the differentiated was made using a Boltzmann grow fit-curve. This curve presents great praticality for correlations between photo-emission, developments seedlings and toxic effects (Figures 1(a), 1(b) and 1(c)).

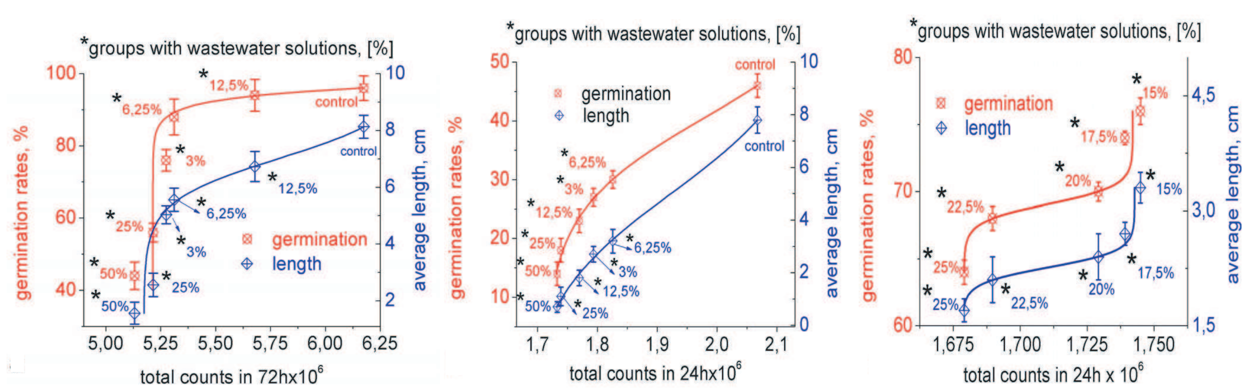

(a) (b) (c)

Figure 1: Photo-counts in germination tests, "Boltzmann grow fit-curve" (germination rates and average length): (a) germination tests in 72 h; (b) germination tests in 24 h with seeds adapted in dark-chamber; (c) range of concentrations.

ACKNOWLEDGMENT

FAPESP support (04/10146-3, 07/50047-2).

REFERENCES

1. Colli, L. and U. Facchini, "Light emission by germinating plants," *Nuovo Cimento*, Vol. 12, 150–153, 1954.
2. Gallep, C. M. and S. R. Santos, "Photon-counts during germination of wheat (*Triticum aestivum*) in wastewater sediment solutions correlated with seedling growth," *Seed Science & Technology*, Vol. 35, 607–614, 2007.

Study of *Daphnia Similis's* Ultra-weak Light Emission When Exposed to Reference Substance $K_2Cr_2O_7$

Daniella Cristina Batista, Natally A. Siqueira, and Cristiano M. Gallep
Applied Photonics Lab., State University of Campinas
R. Paschoal Marmo, 1888, 13484-370, Limeira, Sao Paulo, Brazil

Abstract— The ultra-weak light emission (biophoton) from *Daphnia similis* submitted to different potassium dichromate dilutions were analyzed, presenting notable alteration in the photon-count behavior of stressed groups when compared with the non-stressed control.

The nomenclature "biophoton" was introduced by Fritz A. Popp in 1976 [1], and around the world many research groups have being studying the ultra-weak light emission as the ones leaded by Inaba [2] and Hiramatsu [3] in Japan [4]; Li, Chang and Shen in China; Slawisnki in Poland; A. Gurwitsch, Voeikov and Beloussov in Russia; Mishra e Bajpai in India; Fröhlch, Hyland and Ho in England; VanWijk in Netherlands; Musumeci and Colli in Italy; Fox, Jahn and Puthoff in the USA. In Brazil, the study was approached by Cilento in his "bio-photochemistry without light", where he showed how the excitation to triplet states during enzymatic reaction occurs and discussed the possibility that this should cause other photochemical processes [5, 6].

In this work, we present some eco-toxicology analysis based in ultra-weak light emission's counting from *Daphnia similes*, when exposed to reference substance $K_2Cr_2O_7$. The environmental analysis is an up-to-date area. The pollution detection in aquatic environments by eco-toxicological assays, as standardized by USEPA-821-R-02-012 [7], is the most usual one: it checks the number of immobilized organism in time intervals between 24 h–96 h. The correlation of standard eco-toxicologicals tests with biophoton analysis can decrease the evaluation time, in *quasi* real-time measurements and so enable a rapid decision-making for the problem's remediation or mitigation, in medium term; can also reduce the operational costs since less need of transport, storage, maintenance and disposal of samples and solutions in the laboratory [8].

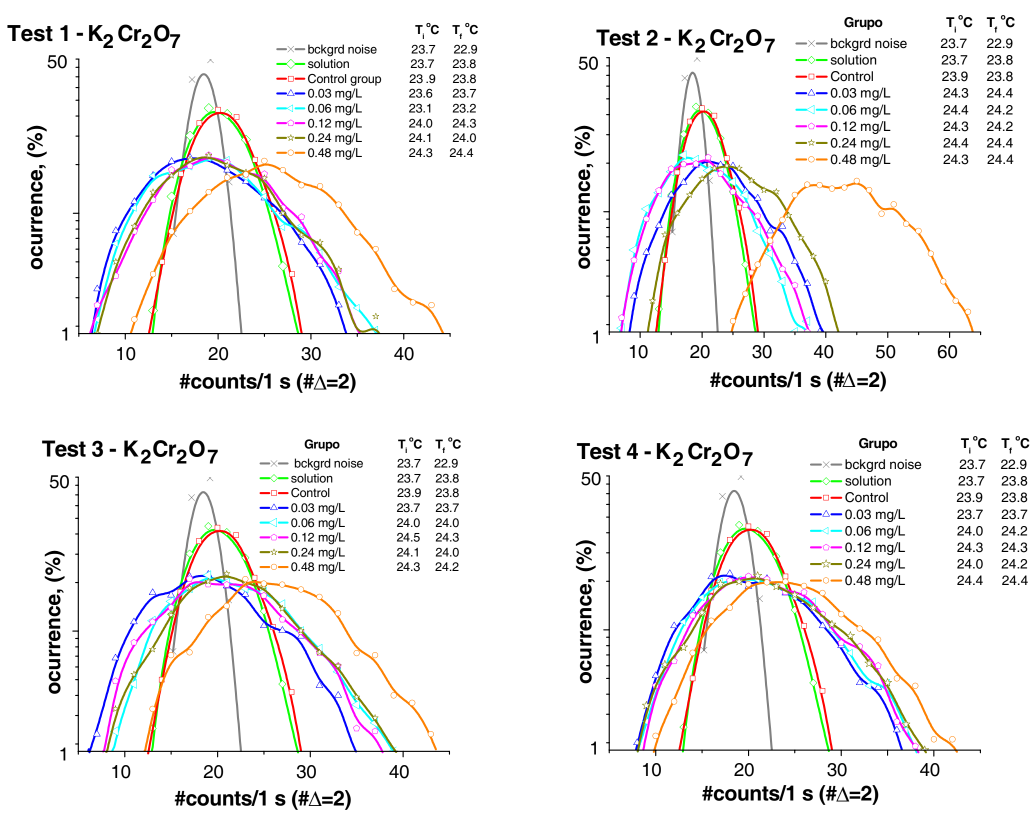

Figure 1: Photon-counting distribution (% occurrence x number of counts/s) for tests 1 to 4: the PMT noise, the control and stressed groups of *D. similes* under $K_2Cr_2O_7$ concentrations from 0.03 to 0.48 mg/L, in the 30-min. after stress.

Tests were carried out in four series using 25 neonates of the test organism *D. similis*. The experimental samples were prepared with 25 neonates (6 h to 24 h hour-old organisms) on Petri dishes (10 cm diameter) with 20 mL of potassium dichromate ($K_2Cr_2O_7$) solution in the concentrations of 0.03, 0.06, 0.12, 0.24 and 0.48 mg/L. These solutions were prepared by *LEAL* [9] considering the organisms' sensibility. The Petri dish so prepared was put inside a dark chamber connected to a photomultiplier tube module (H7360-02, counting board M8784, Hamamatsu K. K.). The photon-counting was initiated after a fixed delay of 5 min. in dark to the avoid delayed luminescence, and with counting-time window of 1 second, taking photon-counts for 30 min. long. A control group was made with organisms and culturing water only, and the dichromate solution was measured too. All the tests were done in triplicate. Meanwhile, the sensibility tests were performed following the ABNT-NBR1273 standards, based in the USEPA [7], for the same $K_2Cr_2O_7$ solutions. The PMT noise was also measured before each experiment.

In the figures, the photon-count distribution for the tests named 1 to 4 are presented. In the test 1, the curve for 0.48 mg/L is strongly deviated from the others solutions, indicating higher counts/s (c/s), this behavior happen again for test 2. In the test 3, the behavior is similar to test 1, and in the test 4 the deviation is the smaller. All tests show counts above 40 c/s for the 0.48 mg/L solution. In the sensibility tests, the EC50 (effective concentration for 50% dead organisms) was 0.34 mg/L, indicating so that the biophotonic approach can indicate the stress threshold, and also that the photon-counting increase a little when the $K_2Cr_2O_7$ concentration starts to immobilize the organisms (> 0.24 mg/L). Acknowledge to FAPESP support (04/10146-3, 07/51025-2).

REFERENCES

1. Popp, F. A., "Biophoton — Background, experimentals results, theorical approach and applications," *Res. Adv. Photochem. & Photobiol.*, Vol. 1, 31–41, 2000.
2. http: //www.jst.go.jp/erato/project/isf_P/isf_P.html.
3. www.lifescientists.de/members/hiramatsu.htm, and www.hpk.co.jp/eng/research/seimeie.htm.
4. http: //www.pref.shizuoka.jp/governor/talk/syoukou1/biophoton.htm.
5. Cilento, G., "Photobiochemistry without light," *Experientia*, Vol. 44, 572–576, 1988.
6. Cilento, G., "Enzymatic generation of electronically excited triplets species: Photobiochemistry without light," *Ciência e Cultura*, Vol. 47, No. 5/6, 312–319, 1995.
7. USEPA-821-R-02-012, *Methods for Measuring the Acute Toxicity of Effluents and Receiving Waters to Freshwater and Marine Organisms*, 5th edition, 2002.
8. Gallep, C. M., et al., "Ultra-weak light emission of *Daphnia similis* stressed by $K_2Cr_2O_7$ solutions," *Proceedings of 2007 SBMO/IEEE MTTS International Microwave and Optoelectronics Conference Salvador*, 241–244, Brasil, 2007.
9. *Lab. Ecotoxicologia Aquática e Liminologia*, CESET, Unicamp.

Daphnia Similis' Ultra-weak Light Emission when Stressed by NaCl

Natally A. Siqueira, Daniella Cristina Batista, and Cristiano M. Gallep
Applied Photonics Lab., State University of Campinas
R. Paschoal Marmo, 1888, Limeira 13484-370, Sao Paulo, Brazil

Abstract— The ultra-weak light emission (*biophoton*) from *Daphnia similis* submitted to different sodium chloride solutions were analyzed, presenting notable alteration in the photon-count behavior of stressed groups when compared with the non-stressed control.

Nowadays the environmental analysis is an up-to-date area. The pollution detection in aquatic environments by eco-toxicological assays as standardized by USEPA-821-R-02-012, is the most usual one [1]: it checks the number of immobilized organism in time intervals between 24–96 h. Some studies showed that it is possible to reduce the time spent in tests like these by using the analysis of the ultra-weak light emission (biophoton) of the organism *Daphnia similis*, comparing groups under chemical stress to the control one [2].

In the work presented here, the experiment was done putting 25 neo-born organisms (daphnias between 6 h to 24 h old) on Petri dish with 20 mL of sodium chloride (NaCl) solution: 0.5, 1.0, 2.0, 4.0 or 8.0 g/L. The Petri dish so prepared was put inside a dark chamber connected to a photomultiplier tube module (H7360-02, counting board M8784, Hamamatsu). The photon-counting was initiated after a fixed delay of 5 min. in dark to avoid delayed luminescence, and with counting-time window of 1 second, taking photon-counts for 30 min. long. A control group was made with organisms and culturing water only. All the tests were done in triplicate. Meanwhile, the sensibility tests were performed following the ABNT-NBR1273 standards, based in the USEPA [1], for the same concentrations of NaCl solutions.

In the figures below the photon-count distribution for tests 1 and 2 are presented. Observing the photon-count distribution curves it is noted different behaviors for the PMT noise, the control group and the groups stressed with NaCl solutions. For the test 1 (Fig. 1(a)) the curve for 0.5 g/L is slightly deviated to the right, indicating higher counts/s, fact that occur for 1.0 g/L for test 2 (Fig. 1(b)). It is noteworthy the decrease in the photon-counts provided by higher NaCl solutions, comparing to the control. Note that in the sensibility tests the EC50 (effective concentration for 50% dead organisms) is 2.24 g/L.

To the control group and the concentration of 0.5 g/L and 1 g/L (whit zero immobilized organisms in the sensibility test) the photon counting sum is the highest and very similar to each other. The photon-counting decrease a little when the NaCl concentration starts to immobilize the organisms (> 1 g/L), decreasing stronger for higher concentrations.

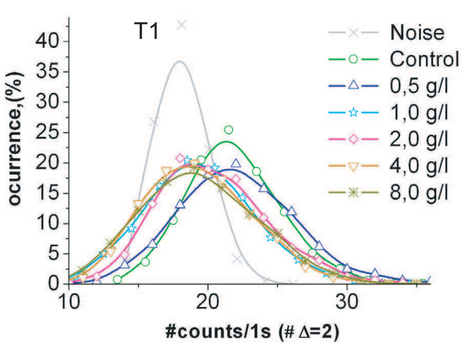

(a)

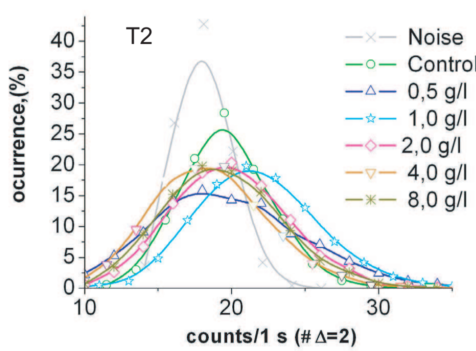

(b)

Figure 1: Photon-counting distribution (% occurrence × number of counts/s) for (a) test 1 and (b) test 2; for PMT noise, control and stressed groups of *D. similis* (NaCl concentrations from 0.5 to 8 g/L), in a 30-min. photon-count experiment.

ACKNOWLEDGMENT

Acknowledge to FAPESP support (04/10146-3, 07/51288-3).

REFERENCES

1. USEPA-821-R-02-012, *Methods for Measuring the Acute Toxicity of Effluents and Receiving Waters to Freshwater and Marine Organisms*, 5th edition, 2002.
2. Gallep, C. M., et al., "Ultra-weak light emission of Daphnia similis stressed by $K_2Cr_2O_7$ solutions," *Proceedings of 2007 SBMO/IEEE MTT-S International Microwave and Optoelectronics Conference Salvador*, 241–244, Brasil, 2007.

Statistical Correlations and Localization-delocalization Transition in DNA Molecules

A. Krokhin[1], **V. M. K. Bagci**[2], **F. Izrailev**[3],
O. Usatenko[4], **and V. Yampol'skii**[4]

[1]Department of Physics, University of North Texas, P. O. Box 311427, Denton, Texas 76203, USA
[2]Research Center for Applied Sciences
Academia Sinica 128, Section 2, Academia Road, Nankang, Taipei 11529, Taiwan
[3]Instituto de Física, Universidad Autónoma de Puebla
Apartado Postal J-48, Puebla 72570, Mexico
[4]A. Ya. Usikov Institute for Radiophysics and Electronics, Ukrainian Academy of Science
12 Proskura Street, Kharkov 61085, Ukraine

Abstract— A DNA molecule is an example of a natural complex system with intriguing properties. One of the fundamental questions is how information is transferred along a sequence of nucleotides. If a mutation occurs in the sequence, it is usually healed. This means that some of physical parameters of the molecule are sufficiently sensitive to detect this mutation. The length of a mutation is relatively short ($\sim$10 base pairs) as compared to the length of a gene ($\sim 10^3$–10^6 base pairs). Because of too small statistical weight of a mutation, the mechanical characteristics are not sensitive enough for its robust detection. Unlike this, the electrical resistance of a DNA molecule fluctuates even if a single nucleotide in a long sequence is replaced (or removed) [1]. This property is a signature of coherent electron transport in mesoscopic samples where local fluctuations of potential do not vanish in the thermodynamic limit. Here we propose a mechanism of information transfer through extended electronic states that accounts for statistical correlations in a double-stranded chain of nucleotides. We analyze electron localization due to randomness of the nucleotide structure in different parts of DNA, namely in exons and introns, and show that exons conduct much better than introns. This is due to a subtle difference in the statistical correlations among nucleotides in exons and introns. Since only the exons store the genetic information we suggest that the information background provides by itself the necessary mechanism for information transfer.

The calculations of the localization length are based on the analytical approach proposed in Refs. [2, 3]. This approach takes into account statistical correlations in two-stranded model of DNA. Unlike previous studies [4, 5], we do not simplify DNA text to a binary sequence. From this point of view our method is much more accurate. The obtained results for randomly selected DNA molecules demonstrate presence of the bands of extended states in the exon regions. At the same time, all the states in the intron regions are well localized.

ACKNOWLEDGMENT

Supported by the US Department of Energy, grant # DE-FG02-06ER46312.

REFERENCES

1. Guo, X., et al., *Nature Nanotech.*, Vol. 3, 163, 2008.
2. Izrailev, F. M. and A. A. Krokhin, *Phys. Rev. Lett.*, Vol. 82, 4062, 1999.
3. Bagci, V. M. K. and A. A. Krokhin, *Phys. Rev. B*, Vol. 76, 134202, 2007.
4. Carpena, P., et al., *Nature*, Vol. 418, 955, 2002.
5. Caetano, R., et al., *Phys. Rev. Lett.*, Vol. 95, 126601, 2005.

Bicarbonate Aqueous Solutions Activated with Hydrogen Peroxide — Long-term Sources of Low-level Photon Emission and Test Systems for the Effects of Ultra-weak Intensity Physical and Chemical Factors

V. L. Voeikov, Do Ming Ha, O. G. Mukhitova, N. D. Vilenskaya, and S. I. Malishenko
Faculty of Biology, Lomonosov Moscow State University, Moscow, Russia

Abstract— It has been shown that addition of H_2O_2 in sub-millimolar concentrations to 1–5 mM Na/K-bicarbonate solutions initiates in these solutions a process accompanied with low-level photon emission amplified with luminol. Photon emission lasts without decay in the samples isolated from air and ambient light for many months. Continuous recording of photon emission from these reaction systems revealed regular (circadian) and irregular rhythms of photon emission intensity. Amplitude of photon emission intensity changes could reach 2-3 fold of the average intensity, especially on periods coinciding with eclipses of Moon and Sun. Intensity of photon emission from the reaction systems could be drastically changed in the presence of ultra-low concentrations of biologically active substances. In particular hydrated fullerenes in dilutions equivalent to their concentrations 10^{-15} and 10^{-20} M stably increased photon emission 2-3-fold while intermediate dilutions did not affect or even diminished it in comparison to control. Addition of human blood lysates in dilutions down to 10^{-13} and lower boosted photon emission from the reaction systems up to 20-fold depending on the particular dilution. We suggest that addition of hydrogen peroxide to aqueous bicarbonate solutions initiates there cyclic reaction chains in which water serves both the source of hydrogen and oxygen and a "fuel" for water oxidation with oxygen. Bicarbonate may serve as a stabilizer of these cyclic reaction due to its ability to participate in free radical reactions. Thus bicarbonate solutions in which cyclic redox processes with water participation are initiated may permanently reside in an excited non-equilibrium state highly sensitive to weak intensity factors. It is notable that bicarbonate is the necessary constituent of cytoplasm of aerobic cells and of important biological liquids, in particular of blood plasma. Ordinary and healing drinking waters as a rule represent bicarbonate solutions.

A Verification of the Mitogenetic Effect on Yeast Culture

I. V. Volodyaev, **R. N. Ivanovsky**, **A. S. Bogachuk**, **N. D. Vilenskaya**,
S. I. Malyshenko, **K. N. Novikov**, **V. L. Voeikov**, **and L. V. Beloussov**
Biological Faculty of the M. V. Lomonosov Moscow State University, Russia

Abstract— The mitogenetic effect (MGE) was discovered in 1923 by A.G.Gurwitsch and researched in detail at the laboratories of Gurwitsch (USSR), Magrou (France), Wolf and Rass (the Netherlands), Rahn (USA) and others in the subsequent 30 years. The phenomenon lies in acceleration of division of cells potentially capable of division, but either not dividing or dividing in a lower rate in the control culture (plant formative tissue, bacterial or yeast cultures) by optical contact with the so-called inductors of the MGE. Among the strongest inductors of the MGE, growing cultures of microorganisms and blood of a healthy man were named. The MGE was stated to be caused by a special type of ultraweak luminescence from inductors. Still some authors reported of negative results of the MGE verification and promoted general skeptical attitude toward the phenomenon.

At this connection we considered pressing to reproduce some of the main experiments dealing with the MGE and inspect its reality.

The experiments were performed on the *Sachromyces vini* yeast culture on the agarysed nutrient medium. Being inoculated onto fresh medium, yeast start budding only after a certain *lag-period*. In the experiment *S. vini* culture in the lag-period (the MGE "detector") was put in optical contact with various "inductors" of the MGE: *S. vini* culture in the period of exponential growth (induction lasted 15–30 min) and human whole blood stabilized by the citrate (induction lasted 5–90 min). As a result, the lag-period of budding shortened and the whole curve of budding (percentage of budding cells as a function of time passed from inoculation) shifted for 15–30 min towards earlier times, compared to the control culture. This corresponded to the MGE of 100–300% in certain points on the curve of budding.

Hence the MGE caused by a distant influence of the growing culture of *S. vini* and the whole blood of a healthy man on the *S. vini* culture in the lag-period was proved.

Feasibility of Biological Cell as an Infrared Electromagnetic Resonator — Storage of the Infrared Biophotons?

Michal Cifra[1,2] **and Jiří Pokorný**[2]

[1]Department of Electromagnetic Field, Czech Technical University
Technická 2, Prague 166 27, Czech Republic
[2]Institute of Photonics and Electronics, Academy of Sciences of the Czech Republic
Chaberská 57, 182 51, Prague 8, Czech Republic

Abstract— Electromagnetic field is generated in biological systems in broad frequency region. Field excited above certain cut-off frequency will redistribute to eigenmodes according to geometrical and dielectric properties of the structure. Feasibility of eigenmodes existence in living cells is approximated by simple model and critically treated. Eigenmodes of the spherical cavity with conducting shell have been treated analytically. COMSOL Multiphysics is used to model eigenmodes in spherical and elliptical cavity. Cut-off frequencies of the first five eigenmodes are provided. Possible sources for field excitation in infrared region are discussed. Quality of the resonator will strongly depend on the field absorption in water-like cytosol. This is the main obstacle for the hypothesis of cell as the infrared electromagnetic resonator. Only hypothetic possibility left is that cellular water would have drastically different dielectric properties compared to bulk water, namely electromagnetic field absorption in infrared region. This could be fulfilled in a microvolumes (coherent domains) but is questioned on the size of the whole cell.

It is shown that the certain eigenmodes, if excited, may play an important role in the organization of processes in the cell, particularly in centrosome or nucleus positioning. Work of other authors on electromagnetic eigenmodes of cellular structures is briefly reviewed. Biological electromagnetic field may contribute to the spatial and temporal organization of the structures and processes in the living cell.

Photons Production and Communications in Biological Systems

S. N. Mayburov and Ilya Volodyaev
Lebedev Institute of Physics, Russia

Abstract— Possible mechanisms of biophoton production, signalling and induced mitogenetic effect are regarded in the framework of quantum optics and information theory. It's argued that Popp theory of coherent biophoton field contradict to theoretical and experimental results for quantum dissipation in bio-systems [1] which give the coherence life-time less then 10^{-13} sec. We propose that the signalling between distant cells of bio-system performed by the noncoherent excitons, generated in cells nucleus, each exciton corresponds to one bit of information. On the border they are converted into photons leaving bio-system volume. The temporal variations of photon intensity, experimentally observed for fish and frog eggs [2], are analyzed as the communications between computers by means of temporal data encoding. Assuming that the bio-systems can control and variate the temporal parameters of biophoton production by a factor 10^{-1}, it's shown that this correlations correspond to the back-reaction algorithm of optimal tuning of this parameters, eventually, it results in the synchroniszation of bio-photon generation for distant bio-systems.

Fuzzy ordered sets (Fosets) studied as possible basic structure of of quantum space-time and phase space (PS) [1]. It differs from Classical space-time manifold structure which is ordered set of points X, so for any points pair a, b strong order relation $R : a < b$ (or $b < a$) holds corresponding to verity values $V = 0$ or 1. Foset M permit generalized or fuzzy order relations R between its elements — fuzzy points a, b, so that R set mapped to real $V = w\ (a, b)$; $0 < w < 1$; for example V about 0.5 means a, b are approximately equal. Thus relative to ordered coordinates axe X fuzzy point b characterized by positive function $w(x)$ which describe b principal position uncertainty dx [1]. If Ω_x is initial m state $w_a(x, t_0)$ support, then for the arbitrary small interval $\Delta x_j \in \Omega_x$ and FP $a_0(t_0)$ it follows: $\forall \Delta x_j$; $a_0 \notin \Delta x_j \cup a_0 \in \Omega_x$; i.e., FP a_0 can't be located in any Δx_j; for $t > t_0$ it means that m source coordinate x is principally uncertain. It corresponds to QM superposition principle in FG; also, due to this effect.

REFERENCES

1. Engel, G. S., et al., *Nature*, Vol. 446, 782, 2008.
2. Belousov, L. V., et al., *Onthogenesis*, Vol. 34, 453, 2003.

Session 5P7
Electromagnetics and its Application in the Advanced Manufacturing Technology

Computer Simulation of Electromagnetic Force Effect on Melting Pool in Layer-laminated Deposition Process

Haiou Zhang[1], Chao Wang[1], and Guilan Wang[2]

[1]School of Mechanical Engineering, Huazhong University of Science and Technology
Wuhan, China
[2]School of Materials Science and Engineering, Huazhong University of Science and Technology
Wuhan, China

Abstract— A new computer simulation was carried out for investigating the electromagnetic force effect on melting pool in layer-laminated deposition process. Because of the gravity and the fluid motion of molten metal in melting pool during the layer-laminated deposition process without supporting, it will difficult to form complex shape parts. So a new scheme which using the magnetic field to restrict the melting metal flow was proposed. The method designed a restricted equipment of magnetic field in order to prevent and reduce the fluid flow and collapse of the melting pool. Compared with traditional method, as the height of the deposition shape increased, the process restricted with electromagnetic force can make the shape of parts more complex and more accurate. The changes of the electromagnetic force field were simulated with the finite element analysis, while the effects of electromagnetic force on forming process were discussed. Simulation and experimental results show that the control system is feasible and practicable. The electromagnetic force will decrease the post-treatment procedure and could contribute to the process of layer-laminated deposition shaping.

Voxel Model-based FGM Metal Part Manufacturing by Plasma Deposition

Bangyou Hu, **Haiou Zhang**, **Ye Chen**, **Yan Huang**, **Chao Wang**, **and Guilan Wang**
Huazhong University of Scince and Technology, China

Abstract— With specific character and new industry requirement, FGM attract the attention of large amount of researchers. Increase manufacturing technologies support these FGM research in different application. As one of them, atmospheric plasma arc has very high manufacture efficiency and economy value in the increase manufacturing technology because of its high energy density as well very low cost. Many researches about FGM coating by plasma spray have been presented, but plasma deposition technology employed to directly manufacture the FGM metal part are seldom reported. In the field of high temperature resistant FGM manufacturing, especially, plasma deposition win advantage because of the high temperature and energy density of plasma arc. In this paper, voxel model was introduced into plasma deposition manufacturing technology for building FGM model. The principle of voxel model is discretizing the target part by selecting geometrical features in surface as a gradient source. Therefore, this model can automatically adapt to the geometrical features in the surface of the target FGM metal part. And then, the FGM layers can be built from complicated 3D geometrical model by slicing. According to the actual technology process of directly manufacturing FGM metal part by plasma deposition, frequent change of material component influence the technology stability in manufacturing process. In order to reduce the change frequency of material component in the process, a path planning method based on iso-composition line is proposed in this paper. For actual manufacturing FGM metal part, a five-axis plasma deposition machine system with multi-powder feed device was designed with which the nearly net shape FGM metal part can be manufactured.

Modeling of Heat Transfer, Fluid Flow and Solute Diffusion in the Plasma Deposition Manufacturing Functionally Gradient Materials

Fanrong Kong[1,2], **Haiou Zhang**[1], **and Guilan Wang**[3]

[1]College of Mechanical Science and Engineering, Huazhong University of Science and Technology
Wuhan 430074, China
[2]Research Center for Advanced Manufacturing, Southern Methodist University
3101 Dyer Street, Dallas, Texas 75205, USA
[3]College of Material Science and Engineering, Huazhong University of Science and Technology
Wuhan 430074, China

Abstract— A solid/liquid/gas unified mathematical model was developed to study heat and mass transfer mechanisms in the plasma deposition manufacturing (PDM) functionally gradient materials (FGM) process. In this model, an enthalpy porosity model combined with level-set method was applied to deal with the solidification and melting at the solid/liquid interface and the evolution of the free surface of the molten pool (liquid/gas interface) and the formed deposited layer profile (solid/gas interface). Moreover, complicated physical phenomena occurring at the liquid (or solid)/gas interface, including heat input due to the plasma arc burning and the heat losses due to the forced convection and heat radiation, have been incorporated into the source terms of governing equations. In the proposed study, a numerical experiment of nickel base alloy K163 powder plus tool steel H13 powder with gradual mass ratio deposited on the tool steel H13 substrate by PDM technology was implemented, in which chemical composition distribution of the deposited materials, temperature field of the deposited layer, and fluid flow in the molten pool were studied in detail. Numerical results show that the geometry of the molten pool and the fluid flow inside directly influence gradient distribution of solute concentration along the thickness of deposited layers and further decide the forming quality of functional gradient materials.

Rapid Manufacturing of FGM Components by Using Electromagnetic Compressed Plasma Deposition

Haiping Zou, **Haiou Zhang**, **Guilan Wang**, **and Jian Li**
Huazhong University of Science and Technology, Wuhan 430074, China

Abstract— Layered Manufacturing (LM) is emerging as a new technology in recent years that enables the fabrication of three-dimensional heterogeneous objects, especially Functionally Graded Materials (FGM) where its composition or the microstructure is locally varied to alter the material properties. To take full advantage of this capability, studies of fabricating FGM materials using laser technologies such as laser engineered net shaping (LENS) and selective laser melting (SLM) have been carried out by researchers. This paper presents a new fabrication method for fabricating FGM component by using electromagnetic compressed Plasma Deposition Manufacturing (PDM) process, which uses a flexible control 3-units synchronous powder feeder delivering proportion form of each powder into the deposition spot during the whole electromagnetic compress PDM fabricating process. Al_2O_3-Fe25 FGM test specimens with continuous gradient transition composition were fabricated in the PDM process and the specimens were analyzed using optical metallography, Microhardness and abrasion testing. It's found that the variation of composition is continuous gradient transition as expected. Microhardness and abrasion testing result indicated the microhardness of the FGM component and the wear resistance of surfacing metal is increasing gradually. The study also found during the electromagnetic compressed Plasma Deposition Manufacturing (PDM) process, the acting of the electromagnetism compress function changes the plasma arc electric arc shape, affects the metal melting and the welded forming; changes welding tub liquid metal crystallization process mass transfer and heat transfer process through electromagnetism agitation, thus changes crystal grain's crystallization direction, refinement one time organization, reduces the segregation, enhances component mechanical properties, reduces flaw and crack sensitivities.

Research on Brushless Doubly-fed Machine with a New Wound Rotor and Its Generating System

Zhongchao Wei, **Xuefan Wang**, **Xia Chen**, **and Chaohao Kan**
Department of Electrical Machines and Drives, Huazhong University of Science and Technology, China

Abstract— The Brushless Doubly-Fed Machine (BDFM) is a new-type of special electrical machine. It solves the structural problems of brushless, combining with the favorable characteristic of the asynchronous motor and synchronous generator.

This paper presents the principle, structure and operation mode of BDFM. Based on the BDFM, A novel BDFM with a new wound rotor structure is proposed according to the tooth harmonic theory. The design of the rotor coil and the basic theory are discussed in detail. Furthermore, aiming to the simulation and practical test research, the 30 kw prototype is developed. Some of experiments of generation have been done. The results prove its application prospect in the field of wind power generation, hydropower and ship.

Study on Offsetting Path Planning for Electromagnetic-compressed Plasma Deposition Manufacturing in Rapid Metal Tooling

Jiang Jiang[1], **Haiou Zhang**[2], **Guilan Wang**[2], **and Jian Li**[1]

[1]State Key Laboratory of Materials Processing and Die & Mould Technology
Huazhong University of Science and Technology, Wuhan 430074, China
[2]State Key Laboratory of Digital Manufacturing and Equipment Technology
Huazhong University of Science and Technology, Wuhan 430074, China

Abstract— Direct metal shaping has been received more and more eyes in rapid manufacturing and plasma Deposition Manufacturing has provided an effective way in fabricating metal parts directly from their digital models. In this paper, the electromagnetic-compressed plasma deposition manufacturing is presented which employs the electromagnetic-compressed plasma arc as the thermal source which is provided with the characteristics of low-cost and high efficiency. The influence of torch path to the performance of metal parts is researched and the algorithms of offsetting path planning are studied including the self-intersection algorithm and across-intersection algorithm between complicated two dimension rings. According to the algorithm, the valid rings are extracted and the redundant ring is eliminated successfully and efficiently in the torch path. The algorithm is verified on path planning of sheet metal stamping mould of wheel fender. The result shows that the crystal grain was greatly refined with the help of electromagnetic and the complicated contour of sheet stamping mould can be fully filled with the help of developed algorithms which suggest an efficient way for virtual manufacturing of rapid metal tooling.

Fabrication of Solid Oxide Fuel Cells with Powder/Suspension Plasma Spraying

Haiou Zhang, Daoman Rui, Kankan Zhang, and Guilan Wang
Huazhong University of Science and Technology, Wuhan 430074, China

Abstract— Solid oxide fuel cells (SOFC) is electrochemical energy conversion device, its high efficiency, pollution-free, all-solid-state structure and a wide range of fuel gas adaptability, and so on, make the SOFC research become a rising hotspot. At present, the reliability and cost competitiveness of the SOFC system are recognized as the key technical barriers that hinder the entry of SOFCs into commercial market. Thermal spray, especially atmospheric plasma spraying (APS) seems to be an economically attractive and effective technique for industrial production of SOFC due to its advantages such as low cost, easy operation, high deposition efficiency, wide selection of materials, etc. In this paper, the current progress and key manufacturing techniques of Positive-Electrolyte-Negative(PEN) and sub-assemblies of SOFC fabricated by plasma spray were over viewed. The work in this paper also focuses on PEN with porous metal-supported of planar SOFC fabricated by multi phases plasma spraying. The influence of the plasma spraying parameters on electrolyte defects and density, electrode porosity and substrate deformation was studied. The process of Atmospheric Plasma Spraying and Suspension Plasma Spraying is discussed, further work is also prospected.

The Digital Simulation System Development for the Electrical Machine

Zhongchao Wei[1], **Xia Chen**[1], **Shuo Liu**[2], **and Jian Li**[1]

[1]Department of Electrical Machines and Drives, Huazhong University of Science and Technology, China
[2]Dongfang Electrial Company, Sichuan, China

Abstract— The conventional electromagnetic computing software for electrical machine is usually restricted to programming and can't associate with the simulation function. While some simulation software such as Matlab/Simulink only can simulate the conventional electrical machine due to the models are not available for public. As for the machine with special structure, a new model has to be established by cumbersome work. To optimize the design of the electrical machine and obtain exact simulating result of its performance, a new model method combining the electromagnetic computing and dynamic characteristic simulation of the machine is put forward in this paper based on the software of Modelica/Mworks, which enables convenient and efficient modeling and simulation of complex, multi-domain physical systems described by differential, algebraic and discrete equation and supports non-causal modeling. The simulation results with 200 kw asynchronous machine validated the feasibility of integrating the machine design with the characteristic simulation to obtain the optimal design parameters.

Modeling and Design of Switched Reluctance Starter/Generator System

Jianbo Sun, **Zhongchao Wei**, **Shuanghong Wang**, **Qionghua Zhan**, **and Zhiyuan Ma**
School of Electrical and Electronics Engineering
Huazhong University of Science and Technology, China

Abstract— Switched Reluctance Motors (SRMs) show great advantages of structural simplicity and high reliability applying to aerial starter/generator. This paper proposes a modeling method of switched reluctance starter/generator system, including switched reluctance machine, power circuit and filter circuit. The simulation model is constructed based on magnetic finite element analysis and electromechanical dynamic equations, which considers magnetic saturation and electromechanical coupling. Through simulations, the performance of the system is evaluated. The control parameters of the controller and component parameters of filter circuit are designed to satisfy the specification performance of the system. The experimental results validate the simulation analysis.

Session 5P8
Asymptotic Methods and Catastrophe Theory

On the Reflection Function Calculation Method in the Problem of Radiowave Propagation

I. I. Orlov, V. I. Kurkin, and A. V. Oinats
Institute of Solar-Terrestrial Physics SB RAS, Russia

Abstract— A reflection function calculation task, which arises in the problem of wave propagation in a stratified inhomogeneous absorbing medium, is considered in the paper. A new method is presented based on combined ordinary differential equations of the first-order that is strictly equivalent to the initial wave equation. The example of the reflection function calculation is presented for the case of radiowave propagation in ionosphere plasma. However the domain of presented method applicability can be vast.

The combined ordinary differential equations obtained earlier by authors [1] can be written in matrix form as

$$\frac{dZ(x,k)}{dx} = ikn(x)I_3Z(x,k) - \frac{S\left(\sqrt{n(x)}\right)}{ikn(x)}I_+Z(x,k), \qquad (1)$$

where $Z(x,k)$ — two-component vector, $S(\sqrt{n(x)})$ — Schwarzian derivative, I_3, I_2 — Pauli's matrices, and $I_+ = I_3 + iI_2$. In the case of radiowave incidence from the left we have usual radiation conditions at infinity in addition to Equation (1).

In the case of small loss the coefficient of the second term of the Equation (1) is concentrated near the turning points. Reflection function defined as a ratio of two components of $Z(x,k)$ matrix sharply changes in the neighborhood of the second term coefficient change.

A special iterative calculation scheme is used for detailed study of the reflection function properties. A variable step of iteration is used due to the essential variability of the second term coefficient of (1). The calculation is carried out from the right to the left since priory conditions are known only at infinity. A feather of the presented numerical scheme is also that a procedure of $Z(x,k)$ matrix renormalization is used. The renormalization doesn't change the reflection function but allows avoiding the loss of calculation accuracy when solutions exponentially increase inside the ionosphere layer.

REFERENCES

1. Orlov, I. I., V. I. Kurkin, and A. V. Oinats, "Wave propagation and geometrical optics," *Optics of Atmosphere and Ocean*, Vol. 19, No. 12, 1016–1020, 2006.

About Strict and Asymptotic Solutions for Focusing of Cylindrical Wave by Veselago Lens with Finite Size and Losses in $kD \gg 1$ Region

A. P. Anyutin
Russian New University, Russia

Abstract— In recent years, one can see that such problem as focusing field by ideal Veselago lens (plane lens with negative refractive index $n_r = -1$) or lens with negative refractive index $n_r < 0$ (or LHM material, or metamaterial) is widely discussed both theoretical and experimental points of view. In 1968 V. Veselago had pointed that flat layer of dielectric with negative refractive index $n = -1$ would focus the field of cylindrical incident wave after the layer. Later in 2000 J. Pendry and D. Smith had made the experimental demonstration of focusing effect in metamaterial (medium with negative refractive index $n_r < 0$)]. Within this time a lot of publications were made. It is important to emphasize that many publication in which the focusing effect were considered by only an asymptotic methods: geometrical optic, some its modifications and Kirchhoffs approximation or strict integral presentation of the scattering field by flat layer. Recently in the first attempts of strict numerical solution of this problem in $kD \sim 1$ region were made.

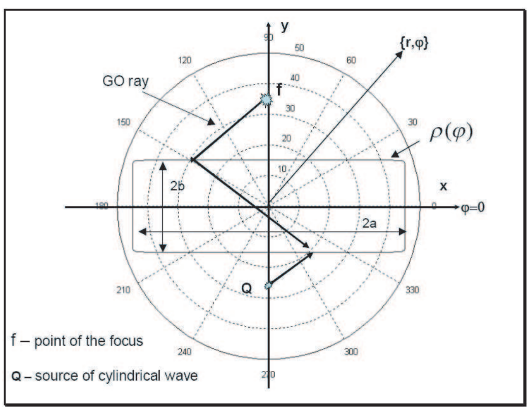

Figure 1: Geometry of the problem.

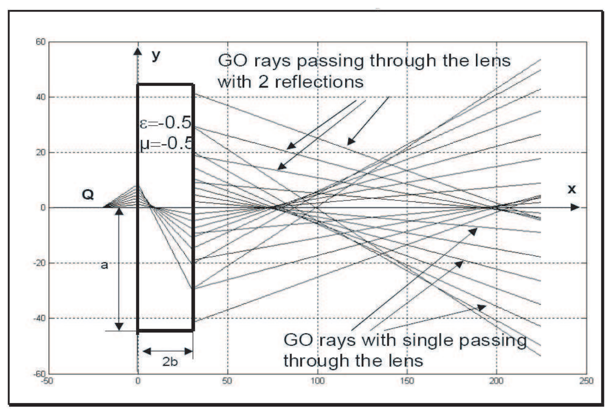

Figure 2: GO ray family for $n_r = -0.5$.

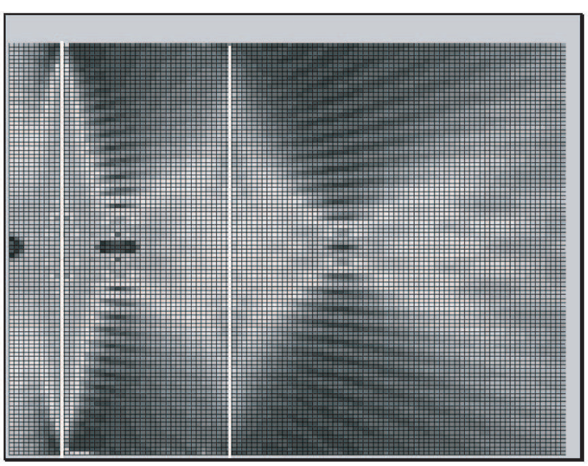

Figure 3: The near field distribution for ideal lens.

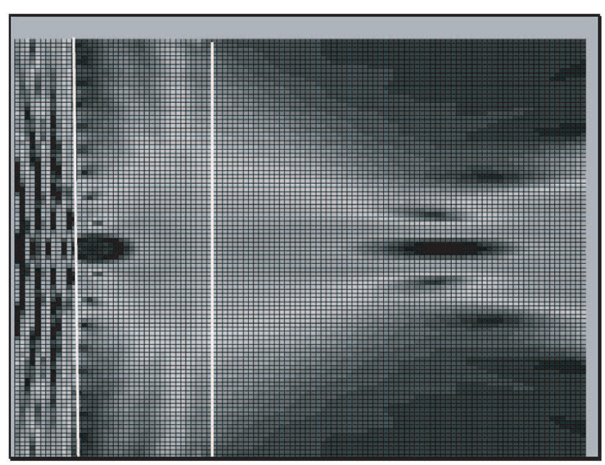

Figure 4: The near field distribution for ideal lens ($n_r = -0.5$).

This paper presents a strict numerical solution and asymptotic (ray) solution for the field in focusing region due to 2D ideal Veselago lens ($n_r \approx -1$) with finite size or flat lens from metamaterial ($n_r < 0$) with losses. The influence of location of the source of cylindrical wave, geometrical sizes of the lens, losses and value of the refractive index $|n_r|$ of metamaterial on focusing process were explored. To explain the results of numerical calculations the geometric optics (GO) ray family was made. The geometry of the problem and some results one can see below at Figs. 1–4.

About 2D Multiple Scattering Problem by Lattice and Its Application for Constructing Metamaterial

A. P. Anyutin
Russian New University, Russia

Abstract— A multiple scattering by 2D cylindrical lattice infinitive structures is the classical problem of the diffraction theory and its fare field has been under discussing since the middle of 20th century. The near field of these structures was not practically investigated. In recent years the problem deal with calculation of near field for lattice has arisen again due to attempts of constructing metamaterial with negative refractive index.

In this paper we has developed 2D modification of the method of discrete sources (MMDS) for scattering E or H polarized cylindrical incident waves from finite 2D lattice structure (finite 2D crystal). The crystal was constructed by array of perfect conducting circular cylinders. Each cylinder has an "electrical" diameter ka (k-wave number for free space). The distance between cylinders was fixed and formed a hexagonal structure with lattice constant kh. The total numbers layers were seven (or nine). The number of cylinders in each layer was 10 (or 9). The example of this structure ($khx = 2\pi/1.54$; $khy = (\sqrt{3}/2)khx$; $ka = 1.697$) illustrates by Fig. 1.

We consider that a source of $H\,(E)$ polarized cylindrical wave Q is located near lattice Fig. 1. The field $u_0(\vec{r})$ of the source Q is given by following expression:

$$u_0(\vec{r}) = H_0^{(2)}\left(k\sqrt{r^2 + R_0^2 - 2rR_0\cos(\varphi - \varphi_0)}\right), \tag{1}$$

where $\{r, \varphi\}$-cylindrical coordinates for point of view, $\{R_0, \varphi_0\}$-coordinates of the source of cylindrical wave Q.

The example of calculated near field distribution for structure Fig. 1 presented at Fig. 2. The result presented at Fig. 2 shows that we have a diffracted maximum for passing field near the lattice only and it is not a ray focusing process. So we can not use such type of structure for constructing metamaterials with negative refraction index.

We also present results of calculation for space near field distribution, field distribution on axis of symmetry of lattice in case of different locations (polarizations) of the source of cylindrical wave Q and the scattering patterns.

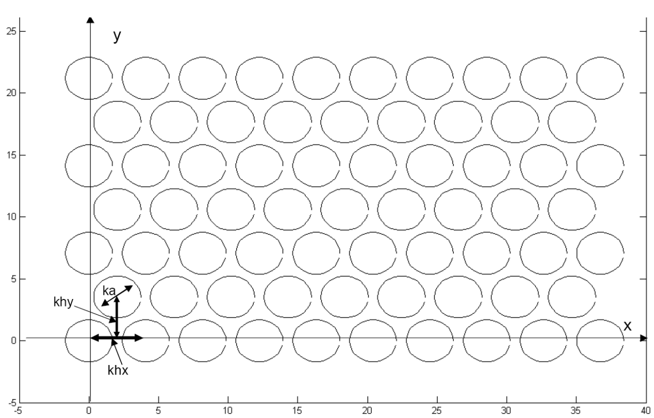

Figure 1: Geometry of the lattice.

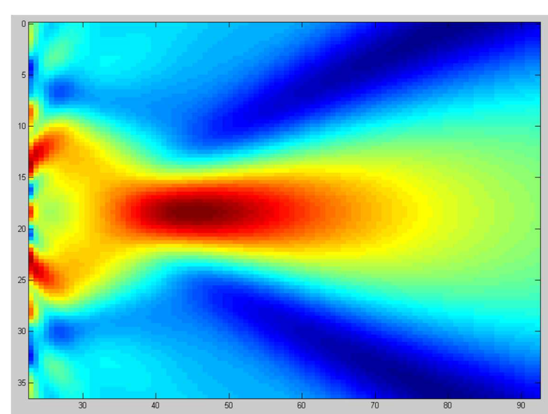

Figure 2: Near field distribution.

About Scattering and 2D Coating Problems by Multilayer Metamaterial Structures

A. P. Anyutin
Department of Science and Information Technology, Russian New University
P. O. 105007, h. 22, Radio Street, Moscow, Russia

Abstract— In this presentation we will tell about strict solution of diffraction problem by 2D multilayer metamaterial structure. The field in near and fare zones of such structure was calculated and presented. It is detected the effect of coating (but not invisible) for some structures.

Caustic Singularities Arising at Propagation of Short Radiowaves in Anisotropic Ionospheric Plasma

A. S. Kryukovsky, **D. S. Lukin**, **and D. V. Rastyagaev**
Dept. of Phys. & Math Problems of Wave, Processes, MIPT
Institutsky per., 9, Dolgoprudny, Moscow Reg. 141700, Russia

Abstract— The modeling of electromagnetic wave propagation in non-uniform ionosphere in view of influence of a magnetic field of the Earth by the bi-characteristic method has been executed. The propagation singularities of ordinary and non-ordinary waves of electromagnetic fields both with the account, and without the account of radial symmetry of a problem on one-reflecting and multi-reflecting traces are considered. One-layer and double-layer models, and also model with a horizontal gradients leading to occurrence of the wave channel at working frequencies as higher, and below critical (plasma) frequency are considered. Caustic singularities of ray structures arising in the basic vertical section, in lateral sections and projection of ray trajectories to a horizontal plane are investigated.

The important effect describing anisotropic media, is the ray going out from a propagation plane with formation caustic singularities, elementary of ones are a smooth caustic and a cusp. Ray and caustic of structure in various cases are considered in detail. In particular, the propagation of an ordinary wave in an ionospheric plasma layer F (with various orientations of a magnetic field) is considered. As the plasma frequency of a layer is chosen a little bit below by worker ones, part of rays at angels of fall close to vertical, pass an ionospheric layer, and others come back to the Earth and form the cusp. The less initial angle of a deviation of a ray from a vertical, the grater it deviates concerning an initial plane of propagation, and then comes back. The rays which are propagating through an ionosphere layer, deviating on certain distance, do not come back more in an initial plane, as it is done by rays reflected from the ionosphere, and, the more initial angle between a ray and vertical, the deviation is more. For a non-ordinary wave the excess of working frequency above plasma up to some meaning does not result in infiltration through an ionosphere layer for any angles of falls. It is considered diffraction and interferential structures of fields formed by combined influence of caustics of ordinary and non-ordinary rays.

Applying the Wave Catastrophe Theory to Solve of Problems of EM Waves Propagation, Diffraction and Focusing in Non-uniform Media

A. S. Kryukovsky, **D. S. Lukin**, **and D. V. Rastyagaev**
Dept. of Phys & Math Problems of Wave, Processes, MIPT
Institutsky per., 9, Dolgoprudny, Moscow Reg. 141700, Russia

Abstract— The review of results of mathematical and numerical modeling for processes of propagation, diffraction, and focusing of electromagnetic waves in non-uniform and dispersive media is resulted on the basis of applying of the wave catastrophe theory. The mathematical means of the solving of problems is developed by methods of the theory of the main, edge and corner catastrophes. As against traditional asymptotical methods (such as, a method of geometrical optics, the geometrical theory of diffraction, physical optics, the physical theory of diffraction, method of the parabolic equation, Gaussian beams summation, etc) the wave catastrophe theory allows to analyze singularities of complex focal and diffraction structures of wave fields. Such structures are not described by traditional asymptotical methods, or their description is extremely complicated or in general it is impossible because of formation of the complex focal areas. The wave catastrophe theory operates in terms of singularities of smooth mapping or catastrophe which physically correspond to steady focusings of wave fields. In essence, the type of wave catastrophe determines the diffraction structure of a field in general. In this work is considered the application of the given approach to the solving of applied problems in which singularities of caustic types such as the main, edge and corner catastrophe take place.

The general rules of the wave catastrophe theory, including classification, indexes and types of focusings, and also methods of uniform asymptotic construction, used for the description of structure of wave fields in such areas, the analysis of amplitude and phase structure of a field are considered. Classes of applied problems in which application of wave catastrophe appeared productive are submitted. The general description of classes of the special functions used for construction uniform asymptotic solving for wave fields, properties of these functions and methods of calculation of one-dimensional, two-dimensional, three-dimensional (space-time) focusings of wave fields is given.

Research an Electromagnetic Field of Edge Waves as "Cusp" and "Butterfly" in the Shadow Region

A. M. Balykina and A. S. Kryukovsky
Russian New University, Russia

Abstract— The mathematical modeling of electromagnetic radiation diffraction on the conductive screen is executed. At first feature of type "cusp" has been considered. The wave field in case of singularity A_3 is calculated at normal falling of a plane wave on the screen. For calculation of an edge wave field behind the screen it is necessary to extract the contribution of edge rays to the integral describing the wave field behind the screen. According to the catastrophe theory in a caustic edge neighborhood a field representation in the form of Pearcey integral and its derivatives is valid. For the further calculations the local asymptotic method was used. From local formulas the space co-ordinates of cusp centre were defined. The method of integration contour turn was used for the calculation of Pearcey integral and its derivatives. The reduction of an angle of integration contour rotation, increasing accuracy, expands a range of parameters at which integrals converge, but increases time of calculations. Further the semi-shadow field on the knife-edge of the screen has been considered. The method of a stationary phase was applied. From these calculations it is possible to receive ray non-uniform asymptotic. The integral has got two critical points: saddle point (if it gets to an integration interval) and edge point. The contribution of the first critical point is defined by the stationary phase method, and the second — by integration by parts. The formula for non-uniform asymptotic was found, carrying out describing transformation. After that all received formulas have been realized by means of the software. Similarly, the singularity of "butterfly" type has been investigated too.

The Application of Tickonov's Regularization Method to Virtual Resonator Problem

P. V. Filonov
Moscow State Technical University of Civil Aviation, Russia

Abstract— In our publication in PIERS in Beijing 2007 we considered the application of embedding method to problem of computing the transparency and reflection coefficients of horn area antenna (HAA). The embedding equations basics on the virtual resonator with "semitransparent" mirror could be written down:

$$\begin{aligned} T_{n+1} &= t_{n+1} M_n^{-1} T_n \\ R_{n+1} &= r_{n+1} + t_{n+1} M_n^{-1} R_n t_{n+1} \\ M_n &= I - R_n r_{n+1} \end{aligned}$$

here, T_n, R_n — transparency and reflection matrices of HAA, t_n, r_n — transparency and reflection matrices of "semitransparent" elemental layer, M_n^{-1} — matrix which describe the virtual resonator. Elementary layer could be consider as grating lattice consist of ideal conductive rectangle section skids with small height. The necessity to consider multi scattering inside a virtual resonator raise the requirements to computing of t_n and r_n.

The modification of Shestopalov's approach with full periodic basis allow us to write down following equations:

$$\begin{aligned} \left[\frac{1}{\Lambda} M(I+E) + \sigma A(I-E)\right] x &= F \\ \left[\frac{1}{\Lambda} M(I-E) + \sigma A(I+E)\right] y &= -F \end{aligned}$$

on x and y. From solutions of this equations we cloud easily get t_n and r_n. In your research we find out what the system of equations become poor conditioned, especially then we increase the dimension of problem. In could be shown what with the small parameter h (lattice height) matrices $(I-E) \to i\sigma h + o(h)$, and $(I+E) \to (2I + i\sigma h + o(h))$. This approximation could be use with Tickonov's regularization method where h could be small parameter.

Such approach could improve conditioned of problem and avoid us to introduce the new parameter (which are specified in Tickonov's method). Also this could help to get some constructive recommendations on value of parameter h.

The Behavior near Focal Points of Asymptotic Solutions to the Cauchy Problem for the Wave Equation with Localized Initial Perturbations

S. Yu. Dobrokhotov, **R. V. Nekrasov**, **S. Ya. Sekerzh-Zenkovich**, **and A. I. Shafarevich**
A. Ishlinski Institute for Problems in Mechanics of Russian Academy of Sciences, Russia

Abstract— We consider the Cauchy problem with localized (but distributed) initial data for the multidimensional wave equation with variable velocity. We suggest a new asymptotic representation for solutions of these problems which is the generalization of the Maslov canonical operator. It is based also on a simple relationship between fast decaying and fast oscillating solutions and on boundary layer ideas. Our main result is the explicit formulas which establish the connection between the initial perturbations and wave profiles near the wave fronts including *the neighborhood of backtracking (focal or turning) and self intersection points*. We show that wave profiles strongly depend on the initial sources. We illustrate our formulas using special initial sources and show that in the neighborhood of the focal points the constructed solutions are crucially different from the fast oscillating ones. In particular, the special functions (like the Airy function) appearing in the fast oscillating case could be changed sometimes by elementary ones. We also discuss the influence of such topological characteristics like the Maslov and Morse indices on metamorphosis of the profiles after crossing the focal points. We apply our results to problems of electromagnetic and water wave propagation.

ACKNOWLEDGMENT

This work was supported by RFBR grant No. 08-01-00726.

Author Index